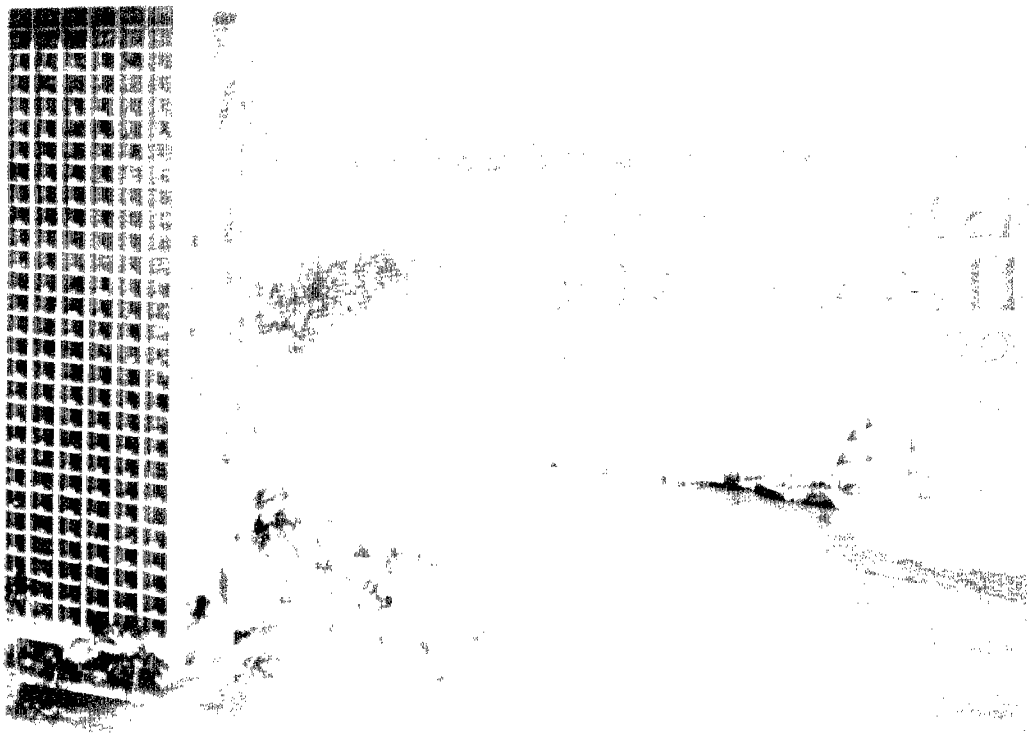
The Second International Conference on Intelligent Processing and Manufacturing of Materials

Volume 1



DISTRIBUTION STATEMENT A
Approved for Public Release
Distribution Unlimited

20000627 118

REPORT DOCUMENTATION PAGE

Form Approved
OMB NO. 0704-0188

Public Reporting burden for this collection of information is estimated to average 1 hour per response, including the time for reviewing instructions, searching existing data sources, gathering and maintaining the data needed, and completing and reviewing the collection of information. Send comment regarding this burden estimates or any other aspect of this collection of information, including suggestions for reducing this burden, to Washington Headquarters Services, Directorate for information Operations and Reports, 1215 Jefferson Davis Highway, Suite 1204, Arlington, VA 22202-4302, and to the Office of Management and Budget, Paperwork Reduction Project (0704-0188,) Washington, DC 20503.

1. AGENCY USE ONLY (Leave Blank)	2. REPORT DATE June 2000	3. REPORT TYPE AND DATES COVERED Final Report

4. TITLE AND SUBTITLE

IPMM'99 The Second International Conference on Intelligent Processing and Manufacturing of Materials, VOLUME 1 AND VOLUME 2

5. FUNDING NUMBERS

DAAD29-99-1-0074

6. AUTHOR(S)

John A. Meech, principal investigator

7. PERFORMING ORGANIZATION NAME(S) AND ADDRESS(ES)

University of British Columbia
Vancouver, BC, V6T-1Z4

8. PERFORMING ORGANIZATION REPORT NUMBER

9. SPONSORING / MONITORING AGENCY NAME(S) AND ADDRESS(ES)

U. S. Army Research Office
P.O. Box 12211
Research Triangle Park, NC 27709-2211

10. SPONSORING / MONITORING AGENCY REPORT NUMBER

ARO 39677.1-RT-CF

11. SUPPLEMENTARY NOTES

The views, opinions and/or findings contained in this report are those of the author(s) and should not be construed as an official Department of the Army position, policy or decision, unless so designated by other documentation.

12 a. DISTRIBUTION / AVAILABILITY STATEMENT

Approved for public release; distribution unlimited.

12 b. DISTRIBUTION CODE

13. ABSTRACT (Maximum 200 words)

The second International Conference on Intelligent Processing and Manufacturing of Materials was held in Honolulu, Hawaii on July 10--15, 1999. IPMM'99 is the second in a series of conferences dealing with the application of Artificial Intelligence and related technologies such as expert systems, fuzzy logic, artificial neural networks, genetic algorithsm, pattern recognition and hybrid systems to the processing and manufacturing of materials and products.

The theme of this year's conference is

"Intelligence in Materials Production - The Competitive Edge!"

14. SUBJECT TERMS

15. NUMBER OF PAGES

16. PRICE CODE

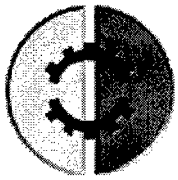
Proceedings

of the Second International Conference

on

Intelligent Processing and Manufacturing of Materials

IPMM'99



Volume 1

Editors:
John A. Meech, Marcello M. Veiga,
Michael H. Smith, Steven R. LeClair

Hilton Hawaiian Village Hotel
Honolulu, Hawaii

July 10 - 15, 1999

DTIC QUALITY INSPECTED 4

IPMM'99

Foreword

It is a great pleasure to welcome you to Hawaii and to the Second International Conference on Intelligent Processing and Manufacturing of Materials.

The theme of this year's conference is

"Intelligence in Materials Production - the Competitive Edge!"

"We are living in a Material World" sings Madonna and throughout the ages, materials have been essential for bettering our standard of living. All materials derive from the Earth's crust, oceans or atmosphere and soon, even from outer space. By applying human intelligence to the properties of matter and the environment of a problem, Mankind has developed countless materials, goods and products to serve Society's needs. Perhaps Madonna's song should refer to an "Intelligent World".

IPMM'99 is the second in a series of conferences dealing with the application of Artificial Intelligence and related technologies such as expert systems, fuzzy logic, artificial neural networks, genetic algorithms, pattern recognition and hybrid systems to the processing and manufacturing of materials and products. The 1st IPMM Conference was held in 1997 in Gold Coast, Australia and attracted over 300 delegates from 37 countries with a diverse set of backgrounds that included computing, mining, metals, materials, manufacturing, etc. The participants found much to share in the "intelligent" methods being used around the world to study, simulate, process or make materials and products. The cross-disciplinary nature of this conference series is a "breath of fresh air" to many of us.

In the production of ores, minerals, metals, ceramics, plastics or food, intelligent methods have become essential to better understand and process materials or to manufacture products. Intelligence is embodied in creative ways to select components, predict properties, control processes or operate plants and factories. Such methods may be software or hardware applications; they may mimic how the human mind processes information; or they may derive from first-principle modeling of the physics and chemistry of matter.

Corporations are increasingly turning to intelligent methods to enhance their competitiveness in today's complex society and so, the technical program at IPMM'99 is focused on research aimed at leading-edge industrial applications and on the identification of newly-evolving technologies.

Intelligence exists all around us. Each of us uses it to conduct our daily lives. As the world becomes increasingly more complex and as communication systems allow massive transfer of information at incredibly reduced time scales, the global community will begin to apply this rapid collection of knowledge through powerful massively-parallel systems that currently exist within our families, communities, towns and cities, states and countries. As computers become more and more predominant in our workplaces and homes, we will begin to consider problems to which previously, we could only apply our imaginations.

Intelligence that exists in humans and other species, is now being placed into machines and materials. We are applying intelligence as we explore outer space and yes, perhaps, one day we will discover new intelligent life forms in the universe.

Conventional approaches to problem solving are becoming more and more integrated into systems that are controlled using fuzzy logic, artificial neural networks, genetic algorithms to create hybrid systems. As these systems become more widely used in industry, the complexity issues will grow as we attempt to find "optimum" solutions to our problems. You will find many papers at IPMM'99 dealing with hybrid systems that combine the attributes of many different methodologies.

The methodologies may mimic the human thought-process either symbolically or structurally. Papers are available describing evolutionary techniques that adapt to changing circumstances and allow solutions to problems to adjust in response to external factors. A number of papers focus on developing instruments that provide artificial senses that mimic the eye, the nose, the ears and yes, even the tongue. Tactile activities are also important in robotic fields and so even, the sense of touch is described in some papers.

As we examine these proceedings and its many fascinating areas of research, I wish to issue a few challenges that we face in developing new products to assist us in our future lives. Some of these ideas came to mind from reading the papers and still others developed from the difficult exercise of putting together this conference and proceedings.

Challenge 1: Can we find a way to put a film onto the surface of eye-glasses that changes its refractive index in response to external light and/or the distance at which the wearer is focusing? Perhaps, the film would have a variable R.I. from top to bottom of the lens.

Challenge 2: Can we develop hearing aids that actually work properly -- which filter out extraneous noise and provide quality hearing to those of us impaired?

Challenge 3: Can we develop a word processing program which always prints out documents the way they were originally designed regardless of the print driver and hardware being used?

The first two challenges can revolutionize the field of hearing and sight aids can improve the quality of life for many, many people. The third challenge probably exists already but is not being marketed in a way to be of widespread use. Much time and effort must be spent by those of who use word processors everyday to reformat documents as we move around our offices or as we move from home to office.

Of course, these challenges are trivial compared to some of the more fundamental (environmental, political and social) issues facing the world today. But it is even such small problems being solved that can have enormous impact on so many people. The opportunity to apply intelligence exists in everything we do or make. It is up to those of us involved in the field to see that the intelligent methods are applied for the good of Mankind.

There are many people who contributed to the success of this conference. For their advice and patience, I would like to thank the following individuals: Marcello Veiga, Mike Smith, Steve LeClair, Tom Zacharia, Guy Nicoletti, Ed Szczerbicki, Madjid Fathi, Malcolm Scoble, Tara Chandra, Lotfi Zadeh, Zoran Bugarinovic, Robert Wagoner, Junichi Endou, Susuma Shima, Debbie McCoy, Iqbal Ahmad, John Atkinson, Scott Meech, Sonia Veiga, Bojan Bugarinovic, Igor Bugarinovic. Special Mahalo (thanks) to Epooni Perkins, Stan Omizo and Lisa Chang of the Hilton Hawaiian Village for their support and patience.

We trust you will find these proceedings of great benefit in your future endeavors and research.

John A. Meech
General Chair, IPMM'99

Honolulu, Hawaii, USA
May 31, 1999.

IPMM'99 Organizing Committee

Honorary Chair:
Lotfi Zadeh, University of California, Berkeley, CA, USA

General Chair:
John A. Meech, University of British Columbia, Vancouver, BC, Canada

Program Co-Chairs:
Michael H. Smith, University of California, Berkeley, CA, USA
Marcello M. Veiga, University of British Columbia, Vancouver, BC, Canada

Vice-Chairs:
N. America: **Thomas Zacharia**, Oak Ridge National Laboratory, TN, USA
Central /S. America: **Marcello Veiga**, University of British Columbia, Canada
Europe: **Madjid Fathi**, University of Dortmund, Germany
Australia: **Edward Szczerbicki,** University of Newcastle, Australia
Japan: **Susuma Shima**, Kyoto University, Japan
Asia: **Tara Chandra**, University of Wollongong, Australia
Special Sessions: **Steven R. LeClair**, Wright-Patterson Air Force Base, OH, US

Workshop Chair:
Guy M. Nicoletti, University of Pittsburgh, Greensburg, PA, USA

Exhibition Chair:
Debbie McCoy, Oak Ridge National Laboratory, Tennessee, USA

Program Committee:

I. Ahmad, USA
H. Asanuma, Japan
M.B. Balachandran, Australia
C.J. Davies, Australia
M.A. Elbestawi, Canada
W. Gruver, Canada
H. Henein, Canada
C.G. Kang, Korea
Y. Kawazoe, Japan
J. Leopold, Germany
W.J. Lui, Canada
J.P. McGeer, Canada
X. Nui, Singapore
J.C. Paschoal, Brasil
J. Pieper, Canada
M. Scoble, Canada
Y. Takefuji, Japan
J.S.L. van Deventer, Aust.
R. Villas Boas, Brasil
D. Yuen, Australia
T. Aizawa, Japan
J.F. Atkinson, USA
J.H. Beynon, U.K.
S. Dolinsek, Slovenia
J. Endou, Japan
J.S. Gunasekera, USA
H. Jalkanen, Finland
R. Kaspar, Germany
A. Kusiak, USA
D.A. Linkens, U.K.
K. Manabe, Japan
B. Mehta, USA
T. Ono, Japan
W. Pedrycz, Canada
Y. Saito, Japan
J. Sestak, Czech Republic
Y. Tamera, Japan
T. Van Le, Australia
R.H. Wagoner, USA
D. Daniel Zhu, USA
A.E. Araujo, Brasil
D. Barschdorff, Germany
L. Cser, Finland
M.A. Duarte-Mermoud, Chile
M. Geiger, Germany
R. Guthrie, Canada
J.J. Jonas, Canada
J. Keller, USA
Y.C. Lam, Australia
R.S. Liu, P.R. China
B. Marett, Australia
L. Monostori, Hungary
P.H. Osanna, Austria
P. Peussa, Finland
T. Sakai, Japan
G.W. Shuy, Taiwan
I.B. Turksen, Canada
B. Verma, Australia
J. Yen, USA
H.J. Zimmerman, Germany

IPMM'99

Affiliated Organizations and Sponsors

Sponsors

The Conference is supported financially by

The Department of the Army[1], US Army Research Office, NC
The US Air Force, Wright-Patterson AF-Base, Dayton, OH; and
Oak Ridge National Laboratory, Oak Ridge, TN

Affiliations

The Organizing Committee is grateful for the affiliation with and cooperation received from the following organizations:

Society for the Advancement of Material & Process Engineering (SAMPE)
The Metallurgical Society (TMS) of AIME
Japan Society for Technology of Plasticity (JSTP)
Australasia Institute of Metals and Materials
Institute of Mining and Metallurgy
Canadian Institute of Mining, Metallurgy and Petroleum (CIM)
North American Fuzzy Information Processing Society
IEEE Systems, Man and Cybernetics (SMC) Society

[1] The views, opinions, and/or findings contained in this report are those of the author(s) and should not be construed as an official Department of the Army position, policy, or decision, unless so designated by other documentation.

About IPMM

Intelligent Processing and Manufacturing of Materials is an informal international community of people interested in intelligent software and hardware applications and solutions to problems that exist in the creation and manufacture of minerals, metals, materials and products. IPMM holds an international conference every two years in July and sponsors a web site for the dissemination of relevant information to workers and researchers in the field.

The first Forum on IPMM took place in the Gold Coast in Australia in July 1997. The technical program consisted of 240 papers on a wide range of topics that included fuzzy systems, artificial neural networks, genetic algorithms, first-principle modeling, finite-element-analysis and thermodynamics. Most papers focused on applications to real-world problems as opposed to theoretical analyses. Over 300 delegates attended from 35 countries and the success of the conference lead to a decision to organize a follow-up conference in 1999.

Hawaii was chosen as the venue for IPMM'99 and the planning of the event began in late August 1997. Over the past two years a numbers of world events have created difficulties in sustaining interest in IPMM. These include the 1998 Asian economic crisis and the late scheduling of several major, related conferences in other parts of the world at the same time as our event.

Despite these difficulties, IPMM'99 has been successful in attracting over 200 papers and about 230 delegates. The list of plenary speakers contains some very important people in the field of soft computing and intelligent methods and we are proud to have their participation. Both financial and logistic support from organizations such as the US Army Research Office, Wright-Patterson Air Force Base, Oak Ridge National Laboratory and IEEE-SMC has been strong and is greatly appreciated. Our Organizing Committee has worked tirelessly to recruit papers and promote the conference and we acknowledge their efforts.

This year, two Awards will be made in memory of two departed colleagues who contributed in many ways to the startup of IPMM -- Dr. J. Keith Brimacombe of the University of British Columbia and Dr. Iqbal Ahmad of the US Army Research Office in North Carolina. The award recipients were chosen by a select committee based on their contributions to IPMM'99. These awards are:

The J. Keith Brimacombe Award for
Excellence in Cross-Disciplinary Research in
Intelligent Processing and Manufacturing of Materials

The Iqbal Ahmad Award for the Best Student Paper in IPMM

We are considering a third conference. IPMM-2001 is being discussed as a possibility to be held in Vancouver, Canada, in Cupertino, California or in Europe. Meetings are scheduled at IPMM'99 to formalize our plans and to make final decisions. Keep up todate about future IPMM activities by visiting our web site at < http://mining.ubc.ca/ipmm/ >

IPMM'99
Special Events

Saturday, July 10, 1999	
Workshop Tutorials	
TW2: Design of Experiments as a Precursor to Neural Networks	900 - 1230
TW4: Using DynaFLeX (DFX) to Create Intelligent Web Sites	Cancelled
TW6: Fuzzy Data Mining and Expert System Development	1400 - 1730
TW8: Artificial Immune Systems: a New Frontier in AI	1400 - 1730
Sunday, July 11, 1999	
Workshop Tutorials	
TW1: Fuzzy Sets and Evolutionary Strategies in Eng. Design	900 - 1230
TW3: Data Mining Using Artificial Neural Networks	Cancelled
TW5: Fuzzy Logic and Data Mining - Methods and Applications	1400 - 1730
TW7: Imaging Procedures for Particles and Particulate Solids	900 - 1230
TW9: Distributed Intelligent Control/Simulation of Large-Scale Systems	1400 - 1730
Organizing Committee Luncheon Meeting	1230 - 1330
Opening Reception	1800 - 1930
Monday, July 12, 1999	
Author's Breakfast	730 - 830
Morning Break	1030 - 1100
Conference Buffet Lunch	1230 - 1330
Afternoon Break	1530 - 1600
Tuesday, July 13, 1999	
Author's Breakfast	730 - 830
Morning Break	1030 - 1100
Conference Buffet Lunch	1230 - 1330
Afternoon Break	1530 - 1600
No-host Reception	1900 - 1930
Conference Banquet	1930 - 2230
Wednesday, July 14, 1999	
Author's Breakfast	730 - 830
Morning Break	1030 - 1050
Free Time	1230 -end of day
Tour of the Hawaiian Electric Co.'s Electric Vehicle Project	1330 - 1630
Additional Workshops	1330 - 1730
Thursday, July 15, 1999	
Author's Breakfast	730 - 830
Morning Break	1010 - 1030
Conference Buffet Lunch	1230 - 1330
Afternoon Break	1500 - 1530
Wrap-up Panel Discussion	1630 - 1700

IPMM'99
Companion's Program

Sunday, July 11, 1999

Opening Reception	1800 - 1930

Monday, July 12, 1999

Sea Life Park (Splash-U optional)	830 - 1530

Tuesday, July 13, 1999

Royal Circle Island Tour of Oahu	730 - 1630
No-host Reception	1900 - 1930
Conference Banquet	1930 - 2230

Wednesday, July 14, 1999

Mai Ta'i Trade Winds Sail	1130 - 1530
Hawaiian Electric Co.'s Electric Vehicle Project (alternate)	1330 - 1630

Thursday, July 15, 1999

Oahu Coastal Cruise into Honolulu and Pearl Harbor	745 - 1230

Additional Individual Tours (not included in Companion Program)

Monday, July 12th	**Three-Star Sunset Dinner Cruise**	1730 - 2030
Monday, July 12th	**Paradise Cove Lu'au - Royal Ali'i**	1615 - 2130
Wednesday, July 14th	**Pacific Splash Barefoot Fun Cruise**	1230 - 1700
Wednesday, July 14th	**Magic of Polynesia Dinner Show**	1700 - 1930

Post-Conference Tours (one day sightseeing trips by air and coach)

Big Island of Hawaii	500 - 2030
Maui	530 - 1930
Kawa'i	530 - 1900

All tours arranged by:

La Rena Saul, Sales Manager,
Classic Destination Management-Hawaii
2255 Kuhio Avenue, Suite 1620,
Honolulu, Hawaii, 96815-2656
Phone: 800-367-2333 ext. 226
Phone: 808-971-2700 ext. 226
FAX: 808-922-2606
Email: saul@classichawaii.com

IPMM'99
The Second International Conference on Intelligent Processing and Manufacturing of Materials

Volume 1

Contents

Plenary Presentations 1

From Computing with Numbers to Computing with Words: From Manipulation of Measurements to Manipulation of Perceptions 3
Lotfi A. Zadeh
Berkeley Initiative in Soft Computing (BISC)
Computer Science Division and the Electronics Research Laboratory,
Department of Electrical Engineering and Computer Science,
The University of California, Berkeley, California, USA

Hybrid Modeling for Testing Intelligent Software for Lunar-Mars Closed Life Support 5
Jane T. Malin
Intelligent Systems Branch, Automation, Robotics and Simulation Division
NASA Johnson Space Center, Houston, Texas, USA

Image Analysis and Vision Systems for Processing Plants 11
Antti J. Niemi[*], Heikki Hyötyniemi[*], and Raimo Ylinen[**]
[*] Helsinki University of Technology, Control Engineering Laboratory
P.O. Box 5400, FIN-02015 HUT, Finland
[**] University of Oulu, Systems Engineering Laboratory,
P.O. Box 4300, FIN-90401 Oulu, Finland

Progress in Japan's Intelligent Manufacturing Systems Research Program 21
Yuji Furukawa
Tokyo Metropolitan University, Minami-Osawa, Hachioji, Tokyo, Japan

Analysis of Processes and Large Data Sets by a Self-Organizing Method 27
Teuvo Kohonen
Helsinki University of Technology, Neural Networks Research Centre,
P.O. Box 2200, FIN-02015 HUT, Finland

Rough Set Theory for Intelligent Industrial Applications 37
Zdzislaw Pawlak
Institute of Theoretical and Applied Informatics,
Polish Academy of Sciences, Poland

From Fuzzy Set Theory to Computational Intelligence – Special European Experiences 45
Hans-Juergen Zimmermann
Aachen University of Technology,
RWTH, Institute of Operations Research, Aachen, Germany

Telemining[tm] Systems Applied to Underground Hard Rock Metal Mining at Inco Limited 53
Gregory R. Baiden
INCO Mines Research, Sudbury, Ontario, Canada

Soft Sensors for Processing Plants 59
Guillermo D. González
Department of Electrical Engineering, University of Chile, Santiago, Chile

J. Keith Brimacombe Memorial Symposium: Intelligence in Materials Engineering 71

In Memory of J. Keith Brimacombe: The Pursuit of Quality in the Casting of Materials 73
Indira V. Samarasekera
The Centre for Metallurgical Process Engineering, The J.K. Brimacombe Advanced Materials and Process Engineering Laboratory (AMPEL),
The University of British Columbia, Vancouver, Canada

Towards Intelligent Steel Processing 75
Rian J. Dippenaar
BHP Institute for Steel Processing and Products,
The University of Wollongong, Wollongong, New South Wales, Australia

Computer Simulation and Information Management Systems for Material Processing 85
Yoshiyuki Nagasaka
Department of Distribution Science, Osaka Sangyo University, Osaka, Japan

Simulation of Springback with the Draw/Bend Test 91
Kaiping Li, Lumin Geng, Robert H. Wagoner
Dep't. Materials Science and Engineering, Ohio State University, Columbus, Ohio

Development of an Integrated System for Designing Steelmaking Aim Compositions 105
P.A. Manohar*, S.S. Shivathaya, M. Ferry*, T. Chandra***
* Dep't. of Materials Engineering., University of Wollongong, NSW, Australia
** Hawker de Havilland Ltd., Bankstown, Australia

A SCADA-based Expert System to Provide Delay Strategies for a Steel Billet Reheat Furnace 111
Clifford Mui*, John A. Meech, Peter Barr****
* Dynapro Systems Inc., Vancouver, B.C., Canada
** The Centre for Metallurgical Process Engineering,
The University of British Columbia, Vancouver, B.C., Canada

Simulation and Analysis of Thin Strip Casting Processes 119
Yogeshwar Sahai, Manish Gupta
Dep't. Materials Science and Engineering, Ohio State University, Columbus, Ohio

Intelligent Manufacturing I 129

Agent-Based Control of Manufacturing Systems 131
László Monostori, B. Kádár
Computer Automation Institute, Hungarian Academy of Sciences,
Budapest, Hungary

Intelligent Database Support for Manufacturing and Processing of Industrial Materials 139
Sylvanus A. Ehikioya, E.G. Truelove, Thomas T. Tran
Brandon University, Brandon, Manitoba, Canada

Intelligent Production Management in Mining Systems 145
Sean Dessureault, Malcolm Scoble, Scott Dunbar
Dep't. of Mining and Mineral Process Engineering,
University of British Columbia, Vancouver, B.C., Canada

Intelligent Quality Control for the Food Industry using a Fuzzy-Fractal Approach 151
Oscar Castillo, Patricia Melin
Tijuana Institute of Technology, Chula Vista, California

Design Tool for Assessing Manufacturing Environments 157
Daniel A. Holder*, Raymond D. Harrell*, Daniel Rochoviak,**
Phillip Farrington, Dawn Russell**, John Rogers**, Sherri Messimer****
* US Army AMCOM, Redstone Arsenal, Alabama, USA
** University of Alabama in Huntsville, Alabama, USA

Models, Algorithms and Decision Support Systems for Letter Mail Logistics 163
Hans-Jürgen Sebastian
RWTH Aachen , Operations Research Group, Aachen, Germany

Intelligent Processes for Production Control 165
Edson Pacheco Paladini
Universidade Federal de Santa Catarina, Florianópolis, SC, Brasil

Fuzzy Systems I 171

Industrial Applications of Fuzzy System Modeling 173
I. Burhan Turksen
University of Toronto, Canada

From Intelligent Models to Smart Ones 179
Heikki Hyötyniemi
Helsinki University of Technology,Espoo, Finland

A Fuzzy Design Evaluation Based on a Taguchi Quality Approach 185
A. Donnarumma*, N. Cappetti*, M. Pappalardo*, Esamuele Santoro **
* Università di Salerno, Italy.
** Università di Napoli, Italy

Non-Traditional Performance Analysis 191
J. Arlen Cooper
Sandia National Laboratories, Albuquerque, New Mexico, USA

Methods of Creating Membership Functions for Fuzzy Rules in Knowledge Bases 195
Cezary Orlowski
Technical University ofGdañsk, Gdañsk, Poland

An Efficient Method for Constructing Fuzzy Rules 201
Bojan Novak
University ofMaribor, Stajerska, Slovenia

Fuzzy Clustering Model Based on Changes in Vagueness 207
Mika Sato-Ilic
University ofTsukuba, Ibaraki, Japan

Thin Films and Surface Processing 213

Modeling and Control of Optical Interference Filters Using Plasma Assisted Chemical Vapor Deposition 215
Derek A. Linkens*, M.F. Abbod*, J. Metcalfe, B. Nichols ****
* University of Sheffield, Sheffield, U.K.
** GEC-Marconi Limited, Caswell, UK.

A Study of Mechanical Properties of Multi-Layered Thin Films 221
T. Hirasawa, H. Kotera, T. Yamamoto, Y. Sakamoto, S. Shima
Kyoto University, Sakyo-ku, Kyoto, Japan

Foundations of Micro-Machining 227
Juergen Leopold
Institute of Tool Engineering and Quality Management,Chemnitz, Germany

Design of Novel Smoothing by Atomic Layer Epitaxy for Microstructure Fabrication 233
S. Hirose*, A. Yoshida, M. Yamaura**, H. Munekata ****
*Mechanical Engineering, AIST, MITI, Tsukuba, Ibaraki, Japan
**Tokyo Institute of Technology, Midori-ku, Yokohama, Japan

Study of the Relationship Between Groove Cross Sectional Area per Pulse of Q-Switched Yag Laser and Strength of Processing Sound 239
T. Kurita, T. Ono
Tokyo Metropolitan Institute of Technology, Tokyo, Japan

Optimization of Thickness Distribution of Micro-Membrane by Genetic Algorithm 245
Hidetoshi Kotera, Y. Sakamoto, T. Hirasawa and S. Shima
Kyoto University, Sakyo-ku, Kyoto, Japan

Manufacturing of Metallic Prototypes and Tools by Laser Cutting and Diffusion Bonding 251
S. Sändig, P. Wiesner
Dep't. of Mechanical Engineering, Technical University ofIlmenau, Germany

Evolutionary Systems and Machine Learning 255

Artificial Immune Systems: a New Frontier in Artificial Intelligence 257
Dipankar Dasgupta*, Stephanie Forrest **
* University of Memphis, Tennessee, USA
** University of New Mexico, Albuquerque, NM, USA

Inductive Learning for Optimization of Simulation Model Output 269
Rainer Barton*, Helena Szczerbicka **
* German Aerospace Center (DLR), Institute for Flight Mechanics, Braunschweig, Germany
** University of Bremen, Bremen, Germany

A Genetically Optimised Fuzzy Parser of Natural Language 277
Olgierd Unold
Wroclaw University of Technology, Wroclaw, Poland

A Genetic Algorithm-based Approach to Solve Process Plan Selection Problems 281
K.M. Tiwari*, S.K. Tiwari*, Debjit Roy*, N.K. Vidyarthi **.
* Manufacturing Engineering, National Institute of Foundry and Forge Technology, Hatia, Ranchi, India
** Mechanical Engineering, NERIST, Nirjuli, Itanagar, India
*** SriVenkateshNagar, Chennai-600092, India

Breeding Policies in Evolutional Approximation of Optimal Subspace 285
H.M. Huang and P.L. Leung
City University of Hong Kong, Kowloon, Hong Kong

Prediction of Cement Paste Mechanical Behaviour from Chemical Composition using Genetic Algorithms and Artificial Neural Networks 291
José C. Cassa, Giovanni Floridia, André R. Souza, Rodrigo T. Oliveira
Universidade Federal da Bahia, Salvador, Bahia, Brazil

Rough Sets-based Machine Learning Using a Binary Discernability Matrix 299
Reynaldo Felix, Toshimitsu Ushio
Systems and Human Science, Osaka University, Toyonaka, Japan

Intelligence in the Design of Materials and Processes I 307

INTELLIGOLD - An Expert System For Gold Plant Process Design 309
Vanessa Torres*, Arthur Torres, John A. Meech *****
*Companhia Vale do Rio Doce, Belo Horizonte, Brazil
**University of Sao Paulo, SP, Brazil
***University of British Columbia, Vancouver, Canada

A Hardware Design for Real-Time Multiple Target Tracking 317
Frederick Ferguson, Chandra Curtis
North Carolina A&T State University, Greensboro, NC, USA

Low-Cost Supersonic Missile Inlet Fabrication Technique 325
C.S. Cornelius, D.A. Gibson
US Army Aviation and Missile Command, Redstone Arsenal, AL

Design of High Performance Missile Structures Utilizing Advanced Composite Material Technologies 331
J.R. Esslinger, R.N. Evans, G.W. Snyder
US Army Aviation and Missile Command, Redstone Arsenal, AL

Modelling the Mechanical Stability of Metal Catalyst Carriers 339
C. Guist, H. Bode
Bergische Universität-Gesamthochschule Wuppertal, Germany

Integration of Newly Developed AI Assembly, Production, and Material Flow Virtual Tools 347
Daniel A. Holder*, Raymond D. Harrell*, Terri L. Calton, John F. Atkinson*, Brandy M. Brasfield***
* US Army AMCOM, Redstone Arsenal, Alabama
** Sandia National Laboratories, Albuquerque, NM

Prediction of Materials Properties 353

How ab-initio Computer Simulation Can Predict Materials Properties Before Experiment 355
Yoshiyuki Kawazoe
Tohoku University, Sendai, Japan

Data Driven Knowledge Extraction of Materials Properties 361
J.S. Kandola*, S.R. Gunn*, I. Sinclair, P.A.S. Reed ****
University of Southampton, U.K.

A Quantum Neural Net: with Applications to Materials Science 367
B. Igelnik*, M. Tabib-Azar*, Y.-H. Pao*, and S. R. LeClair **
*Case Western Reserve University, Cleveland, OH, USA
**Material Directorate, Wright Laboratory, Fairborn, OH, USA

Ontology for Phase Diagram Databases 373
N. Ono, R. Kainuma, H. Ohtani, K. Ishida, M. Kato
Tohoku University, Sendai, Japan

Prediction of Concrete Mechanical Behaviour from Data at Lower Ages using Artificial Neural Networks 381
José C. Cassa, Giovanni Floridia, André R. Souza, Rodrigo T. Oliveira
Universidade Federal da Bahia, Salvador, Bahia, Brazil

Improving the Prediction Accuracy of a Constitutive Model with ANN Models 389
L.X. Kong and P.D. Hodgson
Deakin University, Geelong, Victoria, Australia.

Hybrid Fuzzy Modelling Using Simulated Annealing: Application to Materials Property Prediction 395
Min-You Chen, Derek A. Linkens
The University of Sheffield, Sheffield, UK

Intelligence in Materials Science I 401

Inorganic Glasses: Old and New Structures on the Eve of the 21st Century 403
J. Šesták *, B. Hlavácek +, N. Koga ***
* Czech Academy of Sciences, Prague, Czech Republic
** University of Pardubice, Pardubice, Czech Republic
*** Hiroshima University, Higashi-Hiroshima, Japan

Oxygen Solubility Modeling in Aqueous Solutions 411
Desmond Tromans
University British Columbia, Vancouver, B.C., Canada

On the Oxidation of Steel in CO_2 and Air 417
Gity Samadi Hosseinali, Ainul Akhtar
Powertech Labs Inc., Surrey, British Columbia, Canada

Retardation of Hydrogen Embrittlement by Electrolytic ZrO_2 Coating of AISI 430 Stainless Steel 423
I.B. Huang, S.K. Yen
National Huwei Institute of Technology, Huwei, Taiwan

The Effect of Ca Addition on Viscosity and Electrochemical Properties of Mg-Alloys Produced by Casting 429
H.S. Kim*, Shuji Hanada*, Ha-Guk Jeong*, Dong-Wha Kum **
* Tohoku University, Sendai, Japan
** Korea Institute of Science and Technology, Seoul, Korea

Bio-Compatible Ceramics as Mimetic Material for Bone Tissue Substitution 431
Zdenek Strnad*, Jaroslav Šesták **
*Lab. for Glass and Ceramics (LASAK), Prague, Czech Republic
**Czech Academy of Sciences, Prague, Czech Republic

Intelligent Design of GaSb doped Single Crystals 437
B. Štepánek, J.Šesták, J.J.Mareš, J.Krištofik, V.Šestáková, P.Hubík
Academy of Sciences of the Czech Republic, Semiconductor Department, Prague, Czech Republic,

Intelligent Image Analysis Applications 443

Astronomical Image Processing - Applications To Ultra-Faint Imaging of Small, Moving, Solar System Bodies: Comets and Near-Earth Objects 445
Karen J. Meech
University of Hawaii, Institute for Astronomy, Honolulu, HI, USA

A High Performance Computing Algorithm for Improving In-Line Holography 447
Hesham Eldeib
Electronic Research Inst., National Research Center, Giza, Egypt

Human Face Detection System by KenzanNET with Preprocess Analyzing of Hyperspectral Image 453
Takakazu Chashikawa*, Keizo Fujii, Yoshiyasu Takefuji ***
* Keio University, Kanagawa, Japan.
**NITTAN Co., Ltd., Japan

Using Image Analysis and Partial Least Squares Method to Estimate Mineral Concentrations in Mineral Flotation 459
Jari Hätönen*, Heikki Hyötyniemi*, J. Miettunen, L.-E. Carlsson*****
*Helsinki University of Technology, Espoo, Finland
**Outokumpu Mining Oy, Pyhäsalmi Mine, Pyhäsalmi, Finland
***Boliden Mineral AB, Mineral Processing, Boliden, Sweden

A Combined Morphological and Color-Based Approach to Characterize Flotation Froth Bubbles 465
Giuseppe Bonifazi, Silvia Serranti, F. Volpe, R. Zuco
Università degli Studi di Roma, "La Sapienza", Italia

Robust Bubble Delineation Algorithm for Froth Images 471
Weixing X. Wang, O. Stephansson
Department of Civil and Environmental Engineering,
Royal Institute of Technology, Stockholm, Sweden

The Characterization of Flotation by Colour Information and Selecting the Proper Equipment 477
A.K. Sirén
VTT Information Technology, Espoo, Otaniemi, Finland

Intelligence in Environmental Applications 479

Robust Engineering Approaches to Maximize Results in Business, Cost, Engineering, Human, Quality and System Technologies 481
Roberto C. Villas Bôas
** CYTED - Science and Technology for Development in Iberoamerica, Mineral Technology Sub-Program, Madrid, Spain

Imaging Techniques for Process Optimization and Control in Glass Recycling 485
Giuseppe Bonifazi, Paolo Massacci
Ingegneria Chimica, dei Materiali, Materie Prime e Metallurgia,
Università degli Studi di Roma "La Sapienza", Roma, Italia

Application of Heuristic Modeling in Natural Resource Sciences 491
Steven Mackinson
Fisheries Centre, University of British Columbia,
Vancouver, B.C., Canada

ARDEX - A Fuzzy Expert System for ARD Site Remediation 499
Judita Balcita, John A. Meech
University of British Columbia, Vancouver, B.C., Canada

Modeling of Gold Heap Leaching for Criteria of Sustainability Targets 505
Luiz R. P. De Andrade Lima*, Roberto C. Villas-Bôas**
* Federal University ofBahia, Salvador, BA, Brazil
** Center for Mineral Technology, Rio de Janeiro, RJ, Brazil

Design Optimisation of Aluminium Recycling Using the Taguchi Approach 513
A.R. Khoei , D.T. Gethin, I. Masters
Mechanical Engineering, University of Wales Swansea, UK

Towards a Better Understanding of Environmental Science through Application of Fuzzy Sets 519
Mory M. Ghomshei, John A. Meech
University of British Columbia, Vancouver,B.C., Canada

Intelligence in Rolling Processes 527

Data Mining and State Monitoring in Hot Rolling 529
L. Cser* **, A.S. Korhonen, P.Mäntylä***, O. Simula**, J.Ahola ****
* Bay Zoltan Institute for Logistics and Production Technology, Miskolc-Tapolca, Hungary
** Helsinki University of Technology,Espoo, Finland
*** Rautaruukki Steel, Raahe, Finland

Determination of Thickness Control Parameters of Rolling Processes by the Sensitivity Method, using Neural Networks 537
Luis E. Zárate*, Horacio Helman **
* Departamento de Ciência da Computação, Pontifícia Universidade Católica de Minas Gerais, Belo Horizonte, Brazil
** Departamento de Engenharia Metalúrgica e de Materiais, Universidade Federal deMinas Gerais, Belo Horizonte, Brazil

AI Approach to Modeling Rolling Loads in Design of Cold Rolling Processes 543
J. Kusiak*, J.G. Lenard, K. Dudek***
* Akademia Gorniczo-Hutnicza, Krakow, Poland
** University of Waterloo, Waterloo, Ontario, Canada

Direct Determination of Sequences of Passes for Strip Rolling Process by Means of Fuzzy Logic Rules 549
C.D.M.Pataro, H. Helman
Universidade Federal deMinas Gerais, Belo Horizonte, Brazil

Elongation-Controlled Rolling of H-Shaped Wire 555
H. Utsunomiya, M. Shinkawa, F. Shimaya, Y. Saito
Materials Science and Engineering, Osaka University, Japan.

Application of a Neural Network to Speed Up a Mathematical Model for Calculation of Strip Profiles in Flat Rolling 561
Yukio Shigaki, Horacio Helman
Universidade Federal de Minas Gerais, Belo Horizonte, Brazil

Intelligent Methods in Metal Forming Processes 563

A Fundamental Study of the Incremental Deep Drawing Process 565
S. Shima, H. Kotera, K. Kamitani, S. Nagatomo
Mechanical Engineering, Kyoto University, Kyoto, Japan

Intelligent Design Architecture for Process Control of Deep-Drawing 571
K. Manabe*, H.Koyama*, K.Katoh, S. Yoshihara *****
* Mechanical Engineering, Tokyo Metropolitan University, Japan
** Integrated Systems Japan,Ltd., Tokyo, Japan
*** Tokyo National College of Technology, Tokyo, Japan

An Iterative Approach to Determine Heat-Treatment and Composition from the Mechanical Yield Strength of an Al-Li Alloy 577
James M. Fragomeni,
Ohio University, Mechanical Engineering, Athens, Ohio, USA

A Design of Experiments Statistical Approach to Determine the Effect of Extrusion Process Variables on the Mechanical Properties of a Heat-Treated Al-Li Alloy 585
James M. Fragomeni
Ohio University, Mechanical Engineering, Athens, Ohio, USA

Control of Liquid Segregation of Semi-Solid Al-Alloys during Intelligent Compression Testing 593
C.G. Kang, K.D. Jung, H.K. Jung
Pusan National University, Mechanical Engineering, Korea

Adaptability to Frictional Change of Fuzzy Adaptive Blank Holder Control for Deep Drawing 601
S. Yoshihara*, K. Manabe, H. Nishimura ****
* Tokyo National College of Technology, Mechanical Eng., Japan
** Tokyo Metropolitan University, Tokyo, Japan

An AI Process Control System with Simulation Database and Adaptive Filter for V-Bending 607
M. Yang*, A. Katayama*, K. Manabe*, N. Aikawa **
* Dep't. of Mechanical Engineering, Tokyo Metropolitan University, Japan
** Tokyo Engineering University, Japan

Intelligent Manufacturing II 613

The Distributed Intelligent Control of Complex Systems 615
Wayne J. Davis
University of Illinois at Urbana-Champaign,
Department of General Engineering, Urbana, IL, USA

PDM-based Virtual Enterprises – Bridging the Semantic Gap 623
A. Karcher, J. Wirtz
Dep't. of Mechanical Engineering, Technical University of Munich,
Garching, Germany

A Methodology to Diagnose the Target Cost in a Manufacturing Process 629
A. Arioti, C. Fantozzi, M.Granchi, E. Vettori
Mechanical, Nuclear and Manufacturing Engineering,
University of Pisa, Italy

Resource Allocation for a Fast-Tracked Project 635
Yassiah Bissiri, Scott Dunbar
Department of Mining and Mineral Process Engineering,
University of British Columbia, Vancouver, B.C., Canada

Hybrid Simulation Objects using Fuzzy Set Theory for 641
Simulation of Innovative Process Chains
T. Menzel, M. Geiger
Dep't. of Manufacturing Technology,
University Erlangen-Nuremberg, Erlangen, Germany

Manufacturing Management Improvement through 649
Rapid Production of Budgets
E.J. Colville
School of Engineering, University of Tasmania,
Hobart, Tasmania, Australia

A Connectionist Method to Solve Job Shop Problems 655
Marko Fabiunke, Gerd Kock
GMD Research IT Center,(FIRST) Berlin, Germany

Fuzzy Systems II 661

Designing in Many-Valued Logic 663
A. Donnarumma and Michele Pappalardo
University of Salerno, Mechanical Engineering, Fisciano, Italy

Modulus Genetic Algorithm and its Application to Fuzzy System Optimization 669
Sinn-Cheng Lin
Dep't. of Educational Media and Library Sciences,
Tamkang University, Tamsui, Taipei Hsien Taiwan, PRC

Fuzzy Evolutionary Programming for Portfolio Selection in Investment Decisions 675
T. Van Le
Faculty of Information Sciences and Engineering,
University of Canberra, Belconnen, Australia.

Design of a Region-Wise Fuzzy Sliding Mode Controller with Fuzzy Tuner 681
C.C. Kung, W.C. Lai
Dep't. of Electrical Engineering,
Tatung Institute of Technology, Taipei, Taiwan

A Multi-Input Current-Mode Fuzzy Integrated Circuit for Pattern Recognition 687
Gu Lin, Bingxue Shi
Institute of Microelectronics, Tsinghua University, Beijing, PRC

A Framework for Intelligent Systems based on Vector-Annotated Logic Programs 695
Kazumi Nakamatsu*, Yumi Hasegawa*, Jair Minoro Abe, Atsuyuki Suzuki ***.**
*Himeji Institute of Technology, School of Humanity,
Environment Policy and Technology, Himeji, Hyogo, Japan
**Paulista University, Sao Paulo, Brazil.
***Shizuoka University, Japan

A Fuzzy Logic Assisted Electrodynamic Balance for Unit Operations on Single Levitated Particles 703
M. Pappalardo*, A. Pellegrino*, M. d'Amore,
P. Giordano**, P. Russo ****
* Dep't. of Mechanical Engineering, University of Salerno,
Fisciano, Italy
** Dep't. of Chemical and Food Engineering., University of Salerno,
Fisciano, Italy

Author's Index I-1

IPMM'99
The Second International Conference on Intelligent Processing and Manufacturing of Materials

Volume 2

Contents

Artificial Neural Networks I 711

Artificial Neural Networks (ANN) as Simulators and Emulators: An Analytical Overview 713
Guy M. Nicoletti
University of Pittsburgh at Greensburg, Pennsylvania, USA

Logical Rule Extraction from Data by Maximum Neural Networks 723
T. Saito, Y. Takefuji
Keio University, Fujisawa, Kanagawa, Japan

Iterative RBF Neural Networks as Metamodels of Stochastic Simulations 729
George Meghabghab, George Nasr
Dep't. of Mathematics and Computer Science,
Valdosta State University, Valdosta, Georgia, USA

A Systematic and Reliable Approach to Pattern Classification 735
R.Doraiswami, M.Stevenson, S. Rajan
Department of Electrical Engineering, University of New Brunswick,
Fredericton, New Brunswick, Canada

Dynamic Associative Memory Using Chaotic Neural Networks 743
Yoshihisa Fukuhara, Yoshiyasu Takefuji
Keio University, Graduate School of Media and Governance, Fujisawa,
Kanagawa, Japan

Trends in Intelligent Process Control in the Primary Aluminium Industry 749
R.T. Bui*, L. Tikasz*, J. Perron **
* Université du Québec a Chicoutimi, Chicoutimi, Québec, Canada
** Alcan International Ltd, Jonquiere, Quebec, Canada

Modeling of the Flow Stress Relationship using a BP Network 755
Y. Y. Yang, Derek A. Linkens
University of Sheffield, Sheffield, U.K.

Intelligence in Materials Science II 763

The Heredity and Control of Microstructures of Liquid Metals During Rapid Cooling Processes 765
Rang-su Liu, Ji-yong Li, Hai-rong Liu
*Department of Physics, Hunan University, Changsha, P.R. China
**Department of Chemistry, Hunan University, P.R. China

AI Approach to Internal Variable-based Rheological Model for Steels 773
J. Kusiak, M. Pietrzyk
Department of Metallurgy and Materials Engineering,
Akademia Gorniczo-Hutnicza, Krakow, Poland

Electrolytic ZrO_2 Coating on Co-Cr-Mo Implant Alloys of Hip Prosthesis 779
S.K. Yen, H.Z. Zan, M.J. Guo
National Chung Hsing University, Taichung, Taiwan

Automated Stress Control of Electroplated Nickel-Phosphorus Alloy 785
G.T. Yu, M. Willams
National Huwei Institute of Technology, Materials Eng., Taiwan

Mechanism of Electrolytic Coating of Al_2O_3 on MAR-M247 Superalloy 789
S.K. Yen, C.C. Chang
Dep't. of Material Engineering, National Chung Hsing University,
Taichung, Taiwan

A New Process to Produce Advanced Zirconia-based Ceramic Composites from Low-Value Minerals 797
Sonia M. B.Veiga*, Marcello M. Veiga,**
A.C.D. Chaklader, J. C. Bressiani *.**
* Inst. de Pesquisas Energéticas e Nucleares , São Paulo, Brasil.
** University of British Columbia, Vancouver, BC, Canada

High Temperature Flow Stress Model and Hot Deformation Behaviors for High-Mo Austenitic Stainless Steel 805
Xu Yourong, Chen Liangshen, Jin Lei, Wang Deying
Materials Science and Engineering, Shanghai University,
Jiading, P.R. China.

Intelligent Manufacturing III 811

Information Management of Complex Systems: Perspectives for the New Millennium 813
Z. Gomolka*, E. Szczerbicki **
* University of Szczecin, Szczecin, Poland
** University of Newcastle, Newcastle, Australia

Present Status of Intelligent Machines in Sheet Metal Fabricating and Forming in Japan 817
Junichi Endou
Kanagawa Institute of Technology, Kanagawa, Japan

Design of Enterprise Network Communication Subsystems 823
Adam Grzech
Wroclaw University of Technology, Poland

The Industrial Desktop – Real Time Business and Process Analysis to Increase Productivity in Industrial Plants 829
Osvaldo A. Bascur
OSI Software, Inc., The Woodlands, Texas, USA

Enterprise Staff Scheduling by Genetic Algorithm Search 839
Tiehua Zhang*, William A. Gruver*, Michael H. Smith **
* Simon Fraser University, Burnaby, BC, Canada
**University of California, Berkeley, CA, USA and

Intelligence in Surface Processing of Materials 845

Intelligent AE Sensor for Monitoring of Finish Machining Process 847
Slavko Dolinšek*, J. Kopac*, Z.J. Viharos*, L. Monostori**
* University of Ljubljana, Mechanical Engineering, Slovenia
** Hungarian Academy of Science, Budapest, Hungary

A New Fuzzy-Fractal Approach for Surface Quality Control in Intelligent Manufacturing Of Materials 855
P. Melin, O. Castillo
Tijuana Institute of Technology, Chula Vista, California, USA

A Study on Axisymmetric Indentation by the Rigid-Plastic Finite-Boundary Element Method 861
Yong-Ming Guo, Kenji Nakanishi
Dep't. of Mechanical Engineering, Kagoshima University, Kagoshima, Japan

Design of Intelligent Spindle for High Speed Machining 867
B.L. Zhang, Y.P. Li, B.S. Zhu, P. Ma, Y. Luo
Guangdong University of Technology, Guangzhou, China

Robotics and Intelligent Control I 869

Autonomous Control of Complex Dynamical Systems in Support of a Manned Mission to Mars 871
James A. Kurien, Daniel J. Clancy
NASA Ames MS 269-3, Moffett Field, California, USA

Mining Automation in the Next Millennium: a Tele-Operated LHD Vehicle Model 879
Yeen-Shien Hwang*[1], Neda Farmer*[2], Jason Hart **
*University of British Columbia, Vancouver, B.C., Canada
[1] Huckleberry Mines Ltd., Houston, B.C., Canada
[2] Luscar Coal Mine, Hinton, A.B., Canada
** Nautilus International Limited, Burnaby, B.C., Canada

Dynamic Reconfiguration of Holonic Lower Level Control 887
X. Zhang*, D.H. Norrie*, A. Kusiak **
* University of Calgary, Canada
** University of Iowa, USA

Intelligent Process Monitoring for Paper Machines 895
Janos L. Grantner*, Peter E. Parker, George A. Fodor *****
*Department of Electrical and Computer Engineering,
West Michigan University, Kalamazoo, Michigan, USA.
** Department of Paper and Printing Science and Engineering,
West Michigan University, Kalamazoo, Michigan, USA.
*** ABB Automation Products AB,Vasteras, Sweden

An Integration Design Approach in PID Controller 901
Jen-Yang Chen
China Institute of Technology and Commerce, Taipei, Taiwan

Holonically Object Oriented System 909
Shigeki Sugiyama
Gifu Industry and Technology Research Center, Kasamatsu-Cho,
Hashima-Gun, Gifu-Ken, Japan.

Intelligent Instrumentation and Measurement 919

Pre-Processing of Industrial Process Data for Outlier Detection and Correction 921
Jonathan Tenner*, Derek A. Linkens*, T.J. Bailey **
*University of Sheffield, UK.
**British Steel Engineering Steels U.K. Ltd.

Intelligent Measurement System Confirmation 927
P. H. Osanna, M.N. Durakbasa
Vienna University of Technology, Wien, Austria

Simulation of the Dynamic Properties of Nuclear Meters in Coal Preparation Control Systems 933
Stanislaw Cierpisz
Silesian Technical University, Poland

Acoustic Emission Monitoring of SAG Mill Performance 939
S.J. Spencer, J.J. Campbell, K.R. Weller, Y. Liu
CSIRO Minerals, Queensland, Australia

Novel Polymeric Electrochemical/Chemical Sensors and Display Devices Integrated with Artificial Intelligence 947
A. Talaie*,*, J.Y.Lee***, Y.K. Lee****, J. Jang*,**
D.J. Choo**, S.H. Park****, G. Huh****, J.A. Romagnoli****
* Physics Department, Kyung Hee University, Seoul, Korea
** Chemical Engineering, Sydney University, Sydney, Australia
*** Chemistry Dep't., NSW University, Sydney, Australia
**** Kyung Hee University, Seoul, Korea

Material Properties under Drawing and Extrusion with Cyclic Torsion 953
L.X. Kong, P.D. Hodgson, L. Lin and B. Wang
School of Engineering and Technology, Deakin University,
Geelong, Victoria, Australia

Artificial Neural Networks II 959

Neural Network-based Resistance Spot Welding Quality Prediction 961
N. Ivezic, J.D. Allen, Jr., T. Zacharia
Oak Ridge National Laboratory, Oak Ridge, TN, USA

An Adaptive Artificial Neural Network to Model a Cu/Pb/Zn Flotation Circuit 967
Saiedeh Forouzi, John A. Meech
University of British Columbia, Vancouver, B.C., Canada

Multivariable Predictive Neuronal Control Applied to Grinding Plants 975
Manuel Duarte*, Alejandro Suárez, Danilo Bassi *****
* Dep't. Ing. Eléctrica, Universidad de Chile, Santiago, Chile
** Dep't. de Electrónica, Univ. T.F. Sta. María, Valparaíso, Chile
*** Dep't. de Informática, Univ. de Santiago, Santiago, Chile

Practical Neural Network Applications in the Mining Industry 983
Logan Miller-Tait, Rimas Pakalnis
University of British Columbia, Vancouver, B.C., Canada

Neural Network Model and Model-Based Control of Deformation Processing 989
Nenad Ivezic, John D. Allen, Jr., Thomas Zacharia
Oak Ridge National Laboratory, Oak Ridge, TN, USA

Verifying Detected Facial Parts by Multidirectional Associative Memory 995
Miki Kitabata, Yoshiyasu Takefuji
Keio University, Fujisawa Kanagawa, Japan

A Current-Mode Sorting Circuit for Pattern Recognition 1003
Gu Lin , Bingxue Shi
Microelectronics, Tsinghua University, Beijing, P.R. China

Intelligence in the Design of Materials and Processes II 1009

Intelligent Design Methods for Smart Materials 1011
Madjid Fathi-Torbaghan, L. Hildebrand
Dep't. of Computer Science, University of Dortmund, Dortmund, Germany

Identification of a Model Which Relates Variations in Shape Geometry to Process Control Variables of Shape Forging 1017
B.F. Rolfe*, M.J. Cardew-Hall*, G.A.W. West, S.M. Adballah***
*Australian National University, Canberra, ACT, Australia
**Curtin University of Technology, Perth, Australia

Mechanical Characteristics of HIPed SiC Particulate-Reinforced Al-Alloy MMCs 1023
C.Y. Chung, K.C. Lau
City University of Hong Kong, Kowloon, Hong Kong, P.R. China

Hydrostatic Extrusion of Composite Rod 1029
Ui-Bin Tsai, Chi-Wei Wu, Ray-Quen Hsu
National Chiao-Tung University, Hsin-Chu, Taiwan

Numerical Modelling and Localized Failure Analysis in Metal Powder Forming Processes 1035
A.R. Khoei, R.W. Lewis, D.T. Gethin
Mechanical Engineering, University of Wales Swansea, UK

Microstructure and High Temperature Deformation Behavior of a TiN/Ti_5Si_3Nano-Grain Composite Produced by Non-Equilibrium PM Processing 1041
Kei Ameyama and Yasuhiko Suehiro
Ritsumeikan University, Kusatsu City, Shiga, Japan

Shape Prediction of Growing Billet in Spray Casting using a Scanning Gas Atomizer 1047
Eon-Sik Lee*, Sangho Ahn* and Shinill Kang **
*Research Institute of Industrial Science and Technology,
Advanced Materials Division, Pohang, Kyungbuk, South Korea
**Yonsei University, Seoul, Korea

Intelligence in Concurrent Engineering 1053

Modelling Design Planning in Concurrent Engineering 1055
C. Reidsema and E. Szczerbicki
Dep't. of Mechanical Engineering,
University of Newcastle, NSW, Australia

Computer-Aided Integrated Design for Injection Molding 1061
Yuh-Min Chen*, Rong-Shean Lee*, ChengTer Ted Ho ***
* National Cheng Kung University, Tainan, Taiwan
*** National KaoHsiung Inst. of Science and Technology, Taiwan

Artificial Psychology – an Attainable Scientific Research on the Human Brain 1067
Zhiliang Wang, Lun Xie
University of Science & Technology (USTB), Beijing,P.R. China

Soft-Object Technology for Autonomous Manufacturing Components Control 1073
Ahmed Hambaba
College of Engineering, San Jose State University, San Jose, CA

A Monitoring Framework for Software Project Development 1079
Ho-Leung Tsoi* and Derek Cheung **
* Software Quality Institute, Griffith University, Australia
** Computer Studies, City University of Hong Kong, Hong Kong

Redefining the Web: toward the Creation of Large-Scale Distributed Applications 1087
Guy M. Nicoletti
Engineering Department, University of Pittsburgh at Greensburg,
Pennsylvania, USA

How Can We Form/Expand Conceptions in Workers' Minds According to Their Individualities? 1093
Kumiko Ishino
Konan University, Utsunomiya-City, Kobe, Japan

Robotics and Intelligent Control II 1101

Navigation by Weighted Chance 1103
S. Reimann*, A. Mansour **
*German National Research Center for Information Technology,
Birlinghoven, Germany
** Bio-Mimetic Control Research Center, (RIKEN), Nagoya, Japan

Vehicle Routing Problem Using Clustering Algorithm by Maximum Neural Networks 1109
Noriko Yoshiike, Yoshiyasu Takefuji
Keio University, Fujisawa, Kanagawa, Japan

Acquisition of Communication Protocol for Autonomous Multi-AGVs Driving 1115
Michiko Watanabe, Masashi Furukawa
Asahikawa National College of Technology, Hokkaido, Japan

Heuristic Neuro-Fuzzy Model For Evaluation of Urban Transportation Projects 1123
Marcus Vinicius Quintella Cury, Saul Fuks
Universidade Federal do Rio de Janeiro, UFRJ, Brasil

Optimal Controller Design for Finite Word Length Implementation using a Genetic Learning Algorithm 1125
Wen-Shyong Yu
Tatung Institute of Technology, Taipei, Taiwan

Adaptive Fuzzy Controller for Non-Linear Uncertain Systems 1131
Chiang-Cheng Chiang, Chih-Chien Hu
Tatung Institute of Technology, Taipei, Taiwan, R.O.C.

Hybrid Modeling (view-graphs) 1137

Holistic Strategies for Designing Multistage Material Processes 1139
W.G. Frazier
Air Force Research Laboratories, Wright-Patterson AFB, Ohio

A New Methodology of Using Design of Experiments as a Precursor to Neural Networks for Material Processing: Extrusion Die Design 1151
Bhavin Mehta, Hamza Ghulman, Rick Gerth
Ohio University, Athens, Ohio

Incorporating Hybrid Models into a Framework for Design of Multi-Stage Material Processes 1157
E. Medina
Air Force Research Laboratories, Ohio

Hybrid Modeling for the Interdisciplinary Design of More Affordable Systems 1163
J. Poindexter, Gerald R. Shumaker, Brian A. Stucke
Air Force Research Laboratories, Ohio

Hybrid Modeling for Testing Intelligent Software for Lunar-Mars Closed Life Support 1179
Jane T. Malin
Intelligent Systems Branch, Automation, Robotics and Simulation Division
NASA Johnson Space Center, Houston, Texas, USA

Discrete Modeling via Function Approximation Methods - Towards Bridging Atomic- and Micro-Scales 1185
A.G. Jackson, M. Benedict
Air Force Research Laboratories, Dayton, Ohio, USA

Microstructure Predictions From Atomistic Rule Set Cellular Automata 1197
M.O. Zacate, R.W. Grimes, P.D. Lee
Imperial College, London University, London, England, U.K.

Fuzzy Molecular Modeling 1225
David A. Ress
North Carolina State University, North Carolina, USA

Imaging Studies and Density Functional Analysis of Surfaces and Interfaces: Comparison of Theory and Experiment 1235
John F. Maguire, Steven R. LeClair
Air Force Research Lab, Wright-Patterson AFB, Dayton, Ohio

Modeling Gas Byproducts from MOCVD Thin-Film Depositions 1241
J. G. Jones, P.D. Jero
Air Force Research Lab, Wright-Patterson AFB, Dayton, Ohio

Imaging for Process Optimization and Control (view-graphs) 1247

Nondestructive Imaging of Surface & Sub-Surface Defects in Thin-Films with Super Spatial Resolution using Evanescent Microwave Fields 1249
Massood Tabib-Azar
Case Western Reserve University, Cleveland, Ohio

Investigation of Raman Imaging for Advanced Control of YBCO Cool- Down Processing using Pulsed Laser Deposition 1258
J.D. Busbee *[1], R.R. Biggers*, J.G. Jones*, D.V. Dempsey*[2], G. Kozlowski **
* AFRL, Materials, Wright-Patterson AFB, Dayton, Ohio
** AFRL, PRP, Wright-Patterson AFB, Ohio
[1] Technical Management Concepts, Inc., Beavercreek, Ohio
[2] University of Dayton Research Institute, Dayton, Ohio

Process Control Via Gaze Detection Technology 1263
Jaihie Kim*, Gang Ryung Park*, Steven R. LeClair **
* Yonsei University, Seoul, Korea
** AFRL, Wright-Patterson AFB, Dayton, Ohio

The Third Eye Cameras - Dynamic and Static Hyperspectrum Imaging 1271
Yoshiyasu Takefuji
Environmental Information, Keio University, Fujisawa, Japan

The Third Eye Approach to Innovative Designs and Applications into the 21st Century - Human Recognition System by Nonlinear Oscillations 1277
Souichi Oka, Yoshiyasu Takefuji , William Huang
Environmental Information, Keio University, Fujisawa, Japan

Intelligent Rate Control for MPEG-4 Coders 1285
Gwanh Hoon Park, Jae Hyung Park, Yoon Jin Lee
Yonsei University, Computer Science, Wonju, Kwangwon, Korea

Concept, Development, Mass Production, and Applications of Artificial Retina Chips 1297
Kazuo Kyuma
Mitsubishi Electric Corporation, Japan

Data Reduction via Auto-Associative Neural Networks 1305
Claudia Kropas-Hughes,
Air Force Research Lab, Wright-Patterson AF Base, Dayton, OH

Image Processing Plume Fluence for Superconducting Thin-Film Depositions 1317
J.G. Jones*, R.R. Biggers*, J.D. Busbee*[1], D.V. Dempsey*[2], G. Kozlowski **
* Air Force Research Lab, Materials Direct., WPAFB, Dayton, OH
** Air Force Research Laboratory, PRP, WPAFB, Dayton, OH
[1] Technical Management Concepts, Inc. Beavercreek, OH
[2] University of Dayton Research Institute Dayton, OH

Innovations in Materials Design 1321

Towards the Future: Innovations in Materials Design 1323
Suichi Iwata
RACE, University of Tokyo, Faculty of Eng., Hongo, Japan

Atomic Environments in Relation to Compound Prediction 1339
Jo Daams*, Pierre Villars **
* Phillips Research, The Netherlands
** Materials Phases Data System (MPDS), Vitznau, Switzerland

Analysis and Visualization of Category Membership Distribution in Multivariate Data 1361
Yoh-Han Pao*, B.F. Duan*, Y.L. Zhao*, Steven R. LeClair *
* Case Western Reserve University, Cleveland, Ohio
** Air Force Research Lab, Wright-Patterson AFB, Dayton, OH

Whitney Reduction Networks for Process Discovery 1371
Mark Oxley
Mathematics and Statistics, Air Force Inst. Tech., WPAFB, Ohio

Algorithms for Predicting Properties of Materials from Intelligent Materials Design by Hyperspace Data Mining 1381
Nianyi Chen*, Dongping Daniel Zhu **
* Shanghai Metallurgy Inst. of Chinese Acad. of Sci., P.R. China
** Zaptron Systems, Inc., Mountain View, CA, USA

Data Bases and Semantic Networks for Inorganic Materials Computer Design 1387
N.N. Kiselyova
A.A.Baikov Institute of Metallurgy and Materials Science, Russian Academy of Science, Moscow, Russia

First-Principles Calculations for Materials Science: Their Power and Limitations 1397
Wanda Andreoni
IBM Research Division, Zurich Research Laboratory, Switzerland

Interplay Between Large Materials Databases, Semi-Empirical Approaches, Neuro-Computing and First Principle Calculations 1399
Pierre Villars *, Steven R. LeClair **, Suichi Iwata ***
* Material Phases Data System (MPDS), Vitznau, Switzerland
** Air Force Research Laboratory, Wright-Patterson AFB, Ohio
*** RACE, Faculty of Eng., University of Tokyo, Hongo, Japan

Software Package "MATERIALS DESIGNER" and its Application in Materials Research 1417
Nianyi Chen*, Wencong Lu, Ruiliang Chen*, Pei Qin**
* Shanghai Metallurgy Inst. of Chinese Acad. of Sci., P.R. China
** Department of Chemistry, Shanghai University, P.R. China

Author's Index II-1

Plenary Presentations

From Computing with Numbers to Computing with Words: from Manipulation of Measurements to Manipulation of Perceptions

Lotfi A. Zadeh

* Professor in the Graduate School and Director,
Berkeley Initiative in Soft Computing (BISC)
Computer Science Division and the Electronics Research Laboratory,
Department of Electrical Engineering and Computer Science,
University of California, Berkeley, CA 94720-1776 USA
Tel: 510-642-4959 Fax: 510-642-1712 Email: zadeh@cs.berkeley.edu

Computing, in its usual sense, is centered on manipulation of numbers and symbols. In contrast, computing with words, or CW for short, is a methodology in which the objects of computation are words and propositions drawn from a natural language, e.g., small, large, far, heavy, not very likely, the price of gas is low and declining, Berkeley is near San Francisco, it is very unlikely that there will be a significant increase in the price of oil in the near future, etc.

Computing with words is inspired by the remarkable human capability to perform a wide variety of physical and mental tasks without any measurement and any computation. Familiar examples of such tasks are parking a car, driving in heavy traffic, playing golf, riding a bicycle, understanding speech and summarizing a story. Underlying this remarkable capability is the brain's crucial ability to manipulate perceptions -- perceptions of distance, size, weight, color, speed, time, direction, force, number, truth, likelihood and other characteristics of physical and mental objects. Manipulation of perceptions plays a key role in human recognition, decision and execution processes. As a methodology, computing with words provides a foundation for a computational theory of perceptions -- a theory which may have an important bearing on how humans make -- and machines might make -- perception-based rational decisions in an environment of imprecision, uncertainty and partial truth.

A basic difference between perceptions and measurements is that, in general, measurements are crisp whereas perceptions are fuzzy. One of the fundamental aims of science has been and continues to be that of progressing from perceptions to measurements. Pursuit of this aim has led to brilliant successes. We have sent men to the moon; we can build computers that are capable of performing billions of computations per second; we have constructed telescopes that can explore the far reaches of the universe; and we can date the age of rocks that are millions of years old. But alongside the brilliant successes stand conspicuous underachievements and outright failures. We cannot build robots which can move with the agility of animals or humans; we cannot automate driving in heavy traffic; we cannot translate from one language to another at the level of a human interpreter; we cannot create programs which can summarize non-trivial stories; our ability to model the behavior of economic systems leaves much to be desired; and we cannot build machines that can compete with children in the performance of a wide variety of physical and cognitive tasks.

It may be argued that underlying the underachievements and failures is the unavailability of a methodology for reasoning and computing with perceptions rather than measurements. An outline of such a methodology -- referred to as a computational theory of perceptions is presented in this paper. The computational theory of perceptions, or CTP for short, is based on the methodology of computing with words (CW). In CTP, words play the role of labels of perceptions and, more generally, perceptions are expressed as propositions in a natural language. CW-based techniques are employed to translate propositions expressed in a natural language into what is called the Generalized Constraint Language (GCL). In this language, the meaning of a proposition is expressed as a generalized constraint, X is$_r$ R, where X is the constrained variable, R is the constraining relation and is$_r$ is a variable copula in which r is a variable whose value defines the way in which R constrains X. Among the basic types of constraints are: possibilistic, veristic, probabilistic,

0-7803-5489-3/99/$10.00 ©1999 IEEE.

random set, Pawlak set, fuzzy graph and usuality. The wide variety of constraints in GCL makes GCL a much more expressive language than the language of predicate logic.

In CW, the initial and terminal data sets, IDS and TDS, are assumed to consist of propositions expressed in a natural language. These propositions are translated, respectively, into antecedent and consequent constraints. Consequent constraints are derived from antecedent constraints through the use of rules of constraint propagation. The principal constraint propagation rule is the generalized extension principle. The derived constraints are re-translated into a natural language, yielding the terminal data set (TDS). The rules of constraint propagation in CW coincide with the rules of inference in fuzzy logic. A basic problem in CW is that of explicitation of X, R and r in a generalized constraint, X isr R, which represents the meaning of a proposition, p, in a natural language.

There are two major imperatives for computing with words. First, computing with words is a necessity when the available information is too imprecise to justify the use of numbers; and second, when there is a tolerance for imprecision which can be exploited to achieve tractability, robustness, low solution cost and better rapport with reality. Exploitation of the tolerance for imprecision is an issue of central importance in CW and CTP. At this juncture, the computational theory of perceptions -- which is based on CW -- is in its initial stages of development. In time, it may come to play an important role in the conception, design and utilization of information/intelligent systems. The role model for CW and CTP is the human mind.

Research supported in part by NASA Grant NAC2-1177, ONR Grant N00014-96-1-0556,
ARO Grant DAAH 04-961-0341 and the BISC Program of UC Berkeley.

Hybrid Modeling for Testing Intelligent Software for Lunar-Mars Closed Life Support

Jane T. Malin
Intelligent Systems Branch, Mail Code ER2
Automation, Robotics and Simulation Division
NASA Johnson Space Center
Houston, Texas, USA 77058-3696
Email: malin@jsc.nasa.gov

ABSTRACT

Intelligent software is being developed for closed life support systems with biological components, for human exploration of the moon and Mars. The intelligent software functions include planning/scheduling, reactive discrete control and sequencing, management of continuous control, and fault detection, diagnosis, and management of failures and errors. To develop and test the software and to provide operational model-based what-if analyses, four types of modeling information have been essential to system modeling and simulation: 1) discrete component operational and failure modes, 2) continuous dynamic performance within component modes, modeled qualitatively or quantitatively, 3) configuration of flows and power among components in the system, and 4) operations activities and scenarios. The CONFIG modeling and simulation tool has been used to model components and systems involved in production and transfer of oxygen and carbon dioxide gas in a plant growth chamber and between that chamber and a habitation chamber with physico-chemical systems for gas processing. CONFIG is a multi-purpose discrete event simulation tool that integrates all four types of models, for use throughout the engineering and operations life cycle. Within CONFIG, continuous algebraic quantitative models are used within an abstract discrete event qualitative modeling framework of component modes and activity phases. Component modes and activity phases are embedded in transition digraphs. Flows and flow reconfigurations are efficiently analyzed during simulations. Modeled systems for the Life Support Testbed have included biological plants (using algebraic quantitative models) and crew members, oxygen concentrators and an oxygen transfer control subsystem, and injectors and flow controllers in a carbon dioxide control subsystem. To test the discrete control software, some elements of the lower level control layer and higher level planning layer of the intelligent software architecture are modeled, using CONFIG activity models. CONFIG simulations show effects of events on a system, including control action or failures, local and remote effects, and behavioral and functional effects, the time course of effects, and how effects may be detected. The CONFIG models are interfaced to the discrete control software layer and used to perform dynamic interactive testing of the software in nominal and off-nominal scenarios.

INTRODUCTION

Consumables production plants and closed life support systems with biological components are being developed for human exploration of the moon and Mars. Hierarchical intelligent control software is being designed for autonomous operations of these systems of processors that convert resources to products. The intelligent control systems are made up of layers of functions including planning/scheduling, reactive discrete control and sequencing, management of continuous control, and management of failures and errors. These systems accomplish four broad types of systems management: 1) planning and scheduling for storage and transport of resources and products, 2) discrete or continuous control of processes, or performance of processors, 3) execution of procedures and sequences for discrete control of operational configurations and modes of processors and other components, and 4) management of instrumentation and control subsystems. Whether a system goal can be achieved or a hazard can be avoided, within some time and within some resources, depends on capability both to establish an operating mode (often in the context of a supporting flow or power configuration), and to process or perform at a predicted rate within that target mode.

0-7803-5489-3/99/$10.00 ©1999 IEEE.

INTELLIGENT SOFTWARE FOR CONTROL OF LIFE SUPPORT SYSTEMS

In NASA's Lunar Mars Life Support Test Program (LMLSTP) Phase III 90-day manned test, a three-tiered (3T) hierarchical autonomous control architecture was tested [1]. The 3T software provided integrated monitoring and control (IMC) of product gas transfer between a plant growth chamber, a crew chamber and an incinerator [11]. The basic configuration of chambers for the test is shown in Figure 1. Four crew members lived in the 20 Foot Chamber for 90 days. A physico-chemical air revitalization system (ARS) in the 20 Foot Chamber included a four-bed molecular sieve (4BMS) to remove CO_2 from the chamber, and a CO_2 Removal System (CRS) and O_2 Generation System (OGS) that worked together to add O_2 to the chamber. The variable pressure growth chamber (VPGC) housed plant trays for growing staged crops of wheat. The airlock was connected to the VPGC and the incinerator. The incinerator periodically converted human waste and paper products from the 20 Foot Chamber into CO_2 and H_20. The IMC software managed the configuration of the CO_2 supply for transfer to the VPGC for plant photosynthesis and O_2 production, and managed the systems for concentrating, storing and transferring the O_2 produced by the plants. The IMC software managed the configuration of the O_2 supply for transfer to the airlock for incineration or to the crew chamber. The software flexibly reconfigured and transferred gas among multiple reservoirs in response to predicted needs, observed usage and problem with elements of the system.

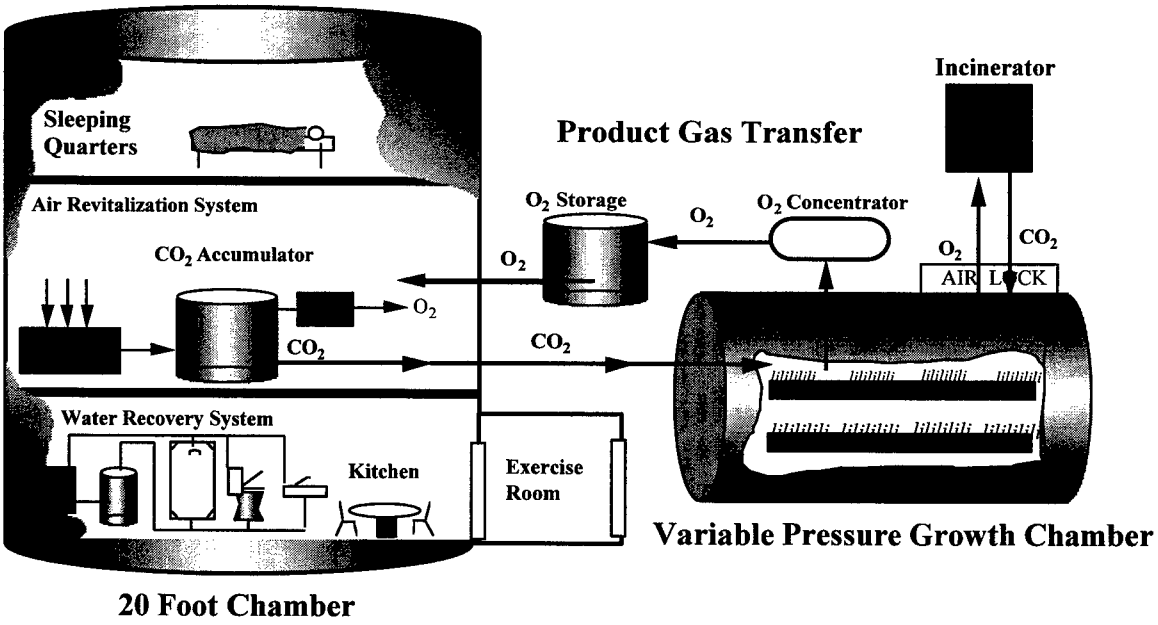


Fig. 1. Product Gas Transfer in the Phase III Test

The uppermost tier of 3T is a planner that handles management of resources and products, and the middle tier is a sequencer. The sequencer provides a reactive discrete control layer that handles event-based control, sequencing and procedures for managing operational configurations and phases of operation [2]. The planner can alter the sequencer's task agenda. The lowest tier, the skill manager, handles low level control. The skill manager interfaces with both the sequencer and the hardware, and manages continuous performance of processors and the continuous control systems themselves. The discrete and continuous control layers and a user interface layer can manage instrumentation and control subsystems.

HETEROGENEOUS MODELS

The layered approach provides several advantages, including modularity, separation of concerns, and support for multiple levels of intervention. However, these layers relate to distinct engineering approaches associated with the four types of system management goals, and a conceptual framework is needed to

integrate the diverse approaches. The system-management framework helps bridge the gap between conventional continuous models and analyses and discrete symbolic models for autonomous systems control [5]. In the LMLSTP case, the *resources and products* are CO_2 and O_2. To support planning and scheduling, systems of simplified processing-rate models are typically used for analysis of resources and balances in scenarios. The LMLSTP *processors* are wheat plants, crew, CRS/OGS, and the incinerator. To support control and sizing analysis, differential and algebraic models are used, based on analytic or empirical data. The LMLSTP *configurations* include flow paths, valves, pumps, fans, injectors, chambers, tanks and processors. To support managing configurations for operations, models are typically systems of connected state transition models. The *instrumentation and control* subsystem includes gas concentration control, processor control, flow and pressure control and valve control. To support managing instrumentation and control subsystems, state transition models are used for modes of control or control regimes.

Four heterogeneous types of models have been essential to develop, test and maintain intelligent control software for space life support systems and to provide operational model-based what-if analyses: 1) discrete functional operational and failure modes of components, 2) continuous dynamic performance within component modes, modeled qualitatively or quantitatively, 3) configuration of flows and power among components in the system, and 4) operations activities, schedules and scenarios. The CONFIG simulation tool has provided the necessary integration of all four types of models [6, 8, 9, 10], making it a suitable testbed, for dynamic interactive simulation-based testing of the LMLSTP IMC application of the 3T layered control software [7].

CONFIG HYBRID DISCRETE EVENT SIMULATION

CONFIG was developed to support analysis of designs for systems and their operations. CONFIG extends discrete event simulation with capabilities for continuous system modeling. The purpose of these enhancements has been to make it possible to apply discrete event technology for model-based prediction, to support design and evaluation of intelligent software for control and fault management. Although discrete event simulation has typically been used for stochastic analyses of scenarios, CONFIG simulations are deterministic, for specific states and inputs.

CONFIG uses a state transition system formalism in a system model made up of a set of connected components, or "devices" structured within a configuration or "flow path". The direction of physical flows and the effects of flow reconfigurations are efficiently analyzed during simulations. Two of the basic building blocks of a CONFIG model are devices and activities. Devices model the behavior of system hardware components and activities model actions in procedures or software. Examples of system devices are pumps, valves, tanks and condensers. Device relations represent the connections between system components. Activity-device relations are used to relate activities to system components for control and monitoring purposes.

The modular discrete event modeling approach provides a framework for organizing and managing the application of more detailed knowledge. In device models, time-related behavior models are embedded within modes, and these modes are within state-transition systems. Two modes of a simple valve, for example, might be open and closed. The way a device interacts with connected devices can depend on the current mode. Failures can be modeled as modes or as factors that precipitate or prevent transitions. Transitions between device modes can be determined by control variables, variable changes propagated through inter-device connections, or by changes in system flows. Model structure can be "recomposed" during a simulation, as the direction and activation of interconnections changes.

Activity models are also state-transition models. Several levels of control can be modeled as activities. An activity might be used to control the positioning of a set of valves, for example. States of activity models, called activity phases, have embedded control behaviors. These behaviors can represent discrete or continuous control regimes, or elements of schedules or simulation scenarios.

Life support system applications require accurate accounting of resource inventories transferred by continuous flow at variable rates to various locations within the modeled system. In CONFIG, two operators, Integrate and Apply-When, are used to periodically compute states or time advances that depend on continuous changes. The Apply-When operator calls external algebraic functions to determine the time advance for a rate-dependent event. The Integrate operator uses a discrete-time approach, providing periodic updates of variables based on a rate, which may be changed dynamically by external inputs. Complex behavior emerges from the interaction of devices that have simple models of internal continuous processes.

CONFIG provides an object-oriented and graphical environment for building models and managing simulation tests. This environment supports incremental model development, maintenance and reuse.

CONFIG Application for Validating Autonomous Control Software

CONFIG simulations were used to validate IMC software that provided control during the LMLSTP Phase III 90-day manned test. IMC sequencer software monitored and controlled the model rather than the skills layer and hardware. The model included diverse components and systems for processing O_2 and CO_2 gases in a plant growth chamber, crew chamber and incinerator, and for storing gases and transferring them between chambers [3]. Figure 2 shows the Product Gas Transfer (PGT) system model during a simulation. The arrowheads along relations indicate the directions of active gas flows. The default graphic representations are rectangles for devices and elongated ovals for activities. Modes are indicated by the text in the rectangles and ovals, or by appearances of icons that indicate device modes.

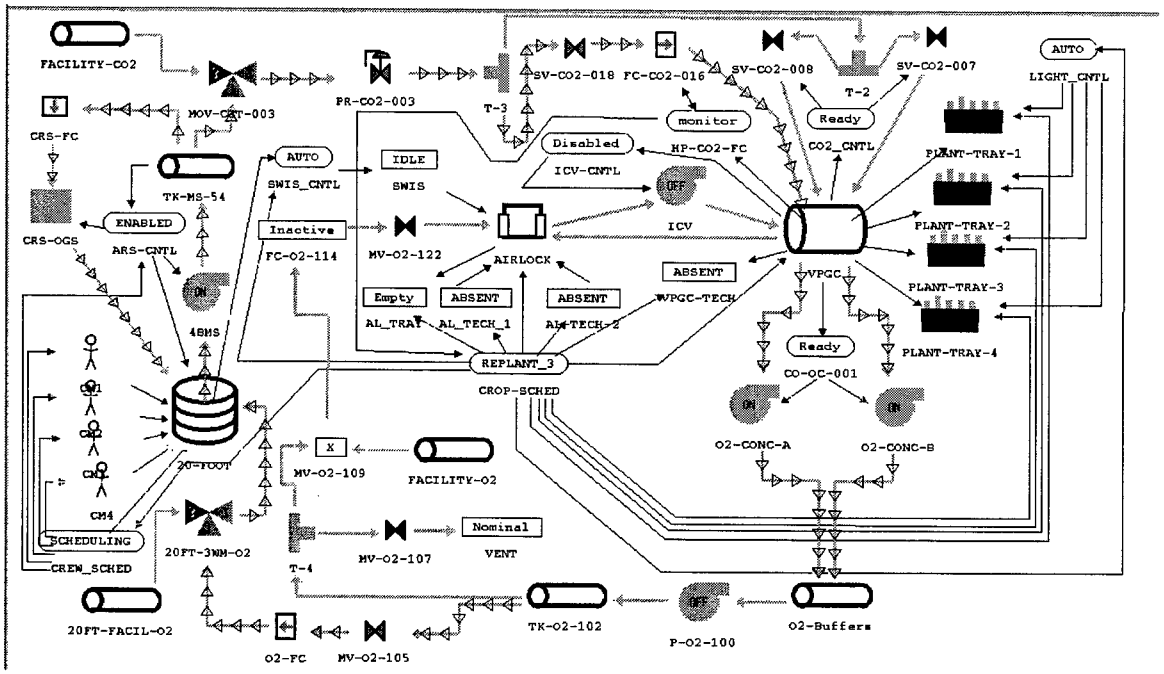


Fig. 2. Product Gas Transfer System Model

The modeled devices include the chambers, various gas processors that convert O_2 to CO_2 or vice versa, gas concentrators, and PGT hardware that directs and regulates flow and pressure. The modeled activities include discrete and continuous control of the hardware that directs and regulates flow and pressure, schedules for crops and human activities, and some manual procedures. The activity models represent control by the 3T planning or skills tiers, local controllers or human operators. There are only two continuous feedback controllers in the 3T skills tier. The rest of the control is discrete, based on deadbands and schedules.

Simulation-based testing followed unit testing and hardware integration testing by the software developers. The interactive simulation-based testing used multiple "batch" long-duration scenarios, running at about 20 times real time. The testing verified software activities during nominal operations in a system context, and tested software response to hardware problems and imbalances. The test results are documented in [4] and [7]. The testing uncovered some software bugs and some issues concerning software requirements. The most interesting issue was observed in the context of a complex interaction including elements of the crew chamber and the plant growth chamber. It is unlikely that this type of software problem would have been found during conventional software testing since it involved a sequence of interactions of multiple devices and controllers in the system that would be difficult to conceive of or emulate in conventional software testing.

During simulation tests, when the CO_2 accumulator was depleted the IMC software switched the source of CO_2 from the accumulator to the facility supply as intended, except when the plant chamber CO_2 concentration was between the alert-low and alarm-low thresholds. When the plant chamber CO_2 concentration was below the alert-low level (1000 ppm) and the CO_2 accumulator on the crew chamber side was also at its alert-low limit (12 psi), the IMC software failed to switch to the facility CO_2 supply. The IMC software disabled continuous flow into the plant chamber and handed over control to the local CO_2 controller in the plant chamber. The local controller then switched to the backup pulse injection system to raise the CO_2 level in the plant chamber. Because the IMC software had failed to switch the CO_2 source from the accumulator to the facility supply, the backup system drew CO_2 from the depleted accumulator. The CO_2 level in the plant chamber continued to drop even with the backup system on.

CONCLUSION

The CONFIG models successfully represented the heterogeneous set of model types that were required for testing intelligent reactive control software. The full range of model representations was necessary for the test, especially for control and reconfiguration. For future programs, simulation-based validation testing will include more complete coverage of off-nominal scenarios. The strength of this type of simulation-based validation is in production of cascaded effects of events in a complex system, to produce novel operational scenarios that intelligent software must handle. In a system as complex as the Phase III testbed, even a seemingly innocuous deviation from normal operating conditions may have more serious consequences than expected. This same type of simulation should also be used to support analysis of operational scenarios to support requirements development. Reliability and safety engineers remind us that software problems are more often associated with lack of system understanding or requirements errors than with coding errors. Dynamic interactive simulation of this type can help get the requirements right for management of complex systems.

Current work includes CONFIG extensions to support interactive operator-in-the-loop evaluations of strategies for adjustable autonomy, which supports operator intervention at multiple levels when appropriate. An interface has been developed between CONFIG and the lowest skills layer of the autonomy software, to support testing of all layers of the architecture. More models are being developed, to support engineering and operation of autonomous production plants for consumables on Mars.

REFERENCES

1. P. Bonasso , R.J. Firby, E. Gat, D. Kortenkamp, D. Miller and M. Slack, 1997. Experiences with an architecture for intelligent, reactive agents. *J. Experimental and Theoretical AI*, 9, 237-256.
2. R. J. Firby, 1997. *The RAP Language Manual*. Neodesic Corporation.
3. L. Fleming, T. Hatfield and J. Malin, 1998. *Simulation-Based Test of Gas Transfer Control Software: CONFIG Model of Product Gas Transfer System*. Automation, Robotics and Simulation Division Report, AR&SD-98-017, NASA Johnson Space Center.
4. L. Fleming, T. Hatfield and J. Malin, 1998. *Simulation-Based Test of Gas Transfer Control Software: Software Validation Test Results*. Automation, Robotics and Simulation Division Report, AR&SD-98-018, NASA Johnson Space Center.
5. J. T. Malin, 1998. Some Roles of Models in Monitoring and Control for BIO-Plex. SAE Paper No. 981727. SAE 28th International Conference on Environmental Systems, Danvers, Mass.

6. J. T. Malin, B. D. Basham and R. A. Harris, 1990. Use of qualitative models in discrete event simulation for analysis of malfunctions in continuous processing systems. In Mavrovouniotis, M. ed., *Artificial Intelligence in Process Engineering.* San Diego, Calif.: Academic Press, 37-79.
7. J. T. Malin, L. Fleming and T. Hatfield, 1998. Interactive simulation-based testing of product gas transfer integrated monitoring and control software for the Lunar Mars Life Support Phase III Test. SAE Paper No. 981769. SAE 28th International Conference on Environmental Systems, Danvers Mass.
8. J. T. Malin and D. B. Leifker, 1991. Functional modeling with goal-oriented activities for analysis of effects of failures on functions and operations. *Informatics & Telematics* 8(4), 353-364.
9. J. T. Malin, D. Ryan and L. Fleming, 1993. CONFIG - Integrated engineering of systems and their operation. In *Proc. Fourth National Technology Transfer Conference*, NASA Conference Publication CP-3249, 97-104.
10. J. T. Malin, D. Ryan and L. Fleming, 1994. Computer-aided operations engineering with integrated models of systems and operations. In *Proc. Dual Use Space Technology Transfer Conference and Exhibition*, NASA Conference Publication CP-3263, 455-461.
11. D. Schreckenghost, P. Bonasso, D. Kortenkamp and D. Ryan, 1998. Three tier architecture for controlling space life support systems. In *Proc. IEEE Symposium on Intelligence in Automation and Robotics*.

Image Analysis and Vision Systems for Processing Plants

Antti J. Niemi*, Heikki Hyötyniemi*, and Raimo Ylinen**

* Helsinki University of Technology
Control Engineering Laboratory
P.O. Box 5400, FIN-02015 HUT, Finland

** University of Oulu
Systems Engineering Laboratory
P.O. Box 4300, FIN-90401 Oulu, Finland

ABSTRACT

Material flowing in a processing plant may be visually observable, but its characterization by physical and computational means of analysis can prove difficult. Problems are encountered in practice both at optical imaging and at extraction of features that characterize the material or its stage of processing, and at related control of the process. Intelligent analysis of the vast amount of data provided by process vision systems is discussed in the paper, in the light of two continuous flow processes, i.e. the froth flotation of minerals and the wet end control of the paper machine.

INTRODUCTION

Visible features of moving and flowing materials are in the process industries traditionally monitored by human operator. His visual observations are subjective and inaccurate, and cannot be directly converted to standard physical transmission signals, but suitable devices for instrumentation of imaging and visual observation had to be waited up to the advent of modern television technology. The classical TV camera was then used for closed circuit monitoring of processes, until the semiconductor camera proved in 1970's more able to operate under industrial conditions, in transmission of sequences of image signals that could then be memorized, processed by computer, reproduced at remote locations and used to control of industrial processes in real time. In fact, it turned out that a one-dimensional, repeatedly scanned array of sensor elements was sufficient to formation of a continuous 2-D image of materials and objects which were steadily carried past a sensor array camera, e.g. on a conveyor belt.

However, despite of the development of electronics, the interfaces of the vision systems with process environments have often proved problematic retarding the development of their applications. An industrial material or object cannot be especially prepared for the needs of on-line image analysis, and the problems of its presentation for viewing have to be solved together with those of the analysis. Problems are created e.g. by unevenness of material surface, variable transparency and reflectance of the often large object surface which may include specularly reflecting elements or parts, scales and dust on surfaces, vapors or particles in the atmosphere etc. These require case specific arrangements of homogeneous or structured illumination of a large surface and direction of viewing in relation to it. Successful imaging requires that they favour the distinction of such features of the object which relate to the interesting characteristics of its composition or structure, but it may be geometrically constrained by the dimensions of the process machinery and shadows cast by it. Deficiencies in presentation or imaging can be partly compensated for by intelligent processing of the data recorded, but it is generally advisable to remove or reduce them at their source, as far as possible.

The imaging of industrial processes is usually not aimed only to analysis of the object and display of its output to the operator, but to control, preferably automatic control, of the imaged or a downstream process. Problems of other kind are met here. They are connected with controllable inputs of the process and with

0-7803-5489-3/99/$10.00 ©1999 IEEE.

their effects on the process variables including those which are measured or evaluated by the image analyzer. Intelligent control algorithms and choices of control inputs are needed also here, in order to reach an optimal control of the process.

If the quantities that are to be extracted from the images are known *a priori*, and if the process structure is known, a closed-loop control can, in principle, be implemented based on the information that is obtained through image analysis. However, if the process structure is not known, visual inspection can be applied to acquire new intuition: *features* can be extracted based on the correlations observed in the data. Hopefully, these features capture the characteristic behavioral patterns of the process, revealing some hidden structure underlying the data. Construction of the features is a mathematically involved task, and a specialized framework is needed.

Problems of imaging, image analysis and related process control are discussed in the present paper in the light of two example cases that illustrate the level reached in their solution. They relate to analysis of flotation in mineral industry and to analysis of the dry line of a paper machine.

THEORETICAL FRAMEWORK

The goal of data modelling is *compression of data*, so that a large number of process measurements could be expressed in terms of only a few parameters. Sometimes, however, the primary goal is *reconstruction* of the original source signals when only their mixtures can be observed. Both of these goals can be expressed as *clever recombination* of the measurements.

In what follows, assume that the measurement data consist of *clusters* characterized by linear subspaces (or linear varieties) in the data space. The observations are results of various (at least locally) linearly additive *features* visible simultaneously in the different information sources. Furthermore, assume that the observed high-dimensional data vector y can be expressed as a linear combination, a weighted sum of N distinct features θ_i so that

$$y = \sum_{i=1}^{N} \phi_i \theta_i . \qquad 1.$$

The features span a relatively low-dimensional *feature space* where all of the observed data patterns can approximately be presented using the domain-oriented feature coordinates.

There are different approaches to defining the features characterizing the process; most of them are rather *mathematically oriented*. They are often based on different kinds of local artificial features, e.g., *splines* or *wavelets*, or other orthogonal function families. The problem with these methods is that the new parameterization in terms of the artificial features does not offer new intuition in what kind of *physical* phenomena are present in the observations. To reach "smart" representations of the process state, the features have to be domain-oriented.

A traditional approach to find data-oriented features is to use, for example, the *principal components* or the eigenvectors of the data correlation matrix as features (*Principal Component Analysis, PCA*; see [1]). The principal components corresponding to largest eigenvalues are the most important ones, capturing the directions of maximum variance in the data, and the other principal components can perhaps be neglected.

The problem with PCA is that it tries to explain all of the N possible features *simultaneously* using only $m < N$ memory units, resulting in a model consisting of some kind of "average" features. If an observation includes some subset of m features out of all available N feature candidates, it is evident that being able to exactly detect these m domain-oriented features the error variance will be zero. This kind of *sparse feature model* does not minimize the number of memory units to achieve the same level of accuracy as the mathematically optimal principal component model. Instead, it minimizes the number of *active* units which means that a minimum number of data transfer is needed.

There are various methods for sparse coding, most notably perhaps the *anti-Hebbian learning* (for example, see [2], [3], and [4]). In what follows, an approach that is specially tailored for practical applications is presented (see [5] and [6]).

Learning algorithm

The sparsity of the data representation [1] means that the overall or global model is *nonlinear* but *locally linear*. In order to get the features linearly better separable, the data preprocessing phase is important. First, all information sources must be made *structureless*. This also means that, in addition to process measurements, the *a priori* information also has to be coded as a set of real-valued (sometimes binary) variables. The following algorithm is based on assumption that the features can be found from the *dependencies* or *correlations* between the data units.

The "feature map", an extension of a self- organizing maps, consists of *nodes i*, $1 \le i \le N$, with *prototype (feature estimate) vectors* $\hat{\theta}_i$. The adaptation of the estimates is carried out as follows [7]:

1. Take the next data vector sample y.
2. Select the prototype vector with index c having the best (positive or negative) correlation with the vector y:

$$c = \text{argmax}_{1 \le i \le N} \left| \hat{\phi}_i \right| = \text{argmax}_{1 \le i \le N} \left| \hat{\theta}_i^T y \right| \qquad 2.$$

3. For each of the nodes i, apply the Kohonen type learning (or adaptation) algorithm [8] using the vector $\hat{\phi}_c y$ as input:

$$\hat{\theta}_i \leftarrow \hat{\theta}_i + \gamma h(i,c)(\hat{\phi}_c y - \hat{\theta}_i) \qquad 3.$$

   where the parameter $h(i,c)$ defines the *neighborhood relation* between the nodes i and c, and γ defines the *adaptation rate* .

4. Normalize the prototype vectors:

$$\hat{\theta}_i \leftarrow \frac{1}{\sqrt{\hat{\theta}_i^T \hat{\theta}_i}} \hat{\theta}_i \qquad 4.$$

5. Eliminate the contribution of the prototype number c by setting

$$y \leftarrow y - \hat{\phi}_c \hat{\theta}_c \qquad 5.$$

6. If the iteration limit m has not been reached, go back to Step 2, otherwise go back to Step 1.

After the features have converged, the algorithm can be used for clustering, i.e., for finding the actual operation regime, together with the fine structure or the feature weights within the clusters.

The algorithm is closely related to the *Generalized Hebbian Algorithm (GHA)* that can be used for calculation of the principal components of $E\{yy^T\}$ [9]. Whereas GHA always results in orthogonal set of features, the presented algorithm can lead to nonorthogonal ones. The algorithm could be called *Generalized Generalized Hebbian Algorithm (GGHA)*. The operation of the algorithm can be described as a *self-organizing algorithm* of Kohonen type, which combines the *principal component analysis* and *cluster analysis* methods. It can also be considered as a non-orthogonal *factor analysis* method.

VISUAL FEATURES AND HIDDEN VARIABLES OF FROTHS IN FLOTATION OF MINERALS

Flotation is used in mineral processing industries for separation of grains of valuable minerals from those of side minerals. In the continuous flow flotation cell (Fig. 1), air is introduced into the agitated suspension of ore and water.

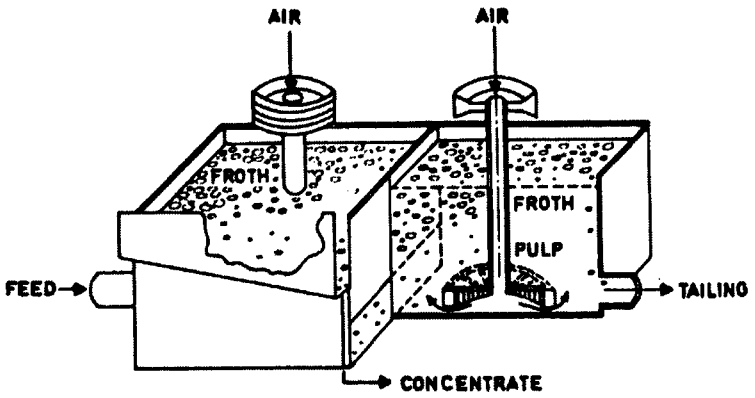


Fig.1. Flotation cell

The desired mineral tends to adhere to air bubbles and to rise to the froth layer that is removed as the product of the cell, while the main part of the slurry exits from its lower part. The separation of minerals requires that the desired mineral is provided with a water-repellent property which is produced by selective adsorption of chemicals at a preceding process stage. – A flotation plant comprises always a high number of cells in the form of a network.

The process operators inspect the froth by eye, in order to make observations on its individual characteristics or general appearance, and to use these as a background of their manual control actions. Various types of froths have been characterized by qualitative terms, like: watery, stiff, polyhedral, shiny, porridge type, flat, stormy etc., in addition to characterization by colour. Instrumental methods have been developed more recently for imaging and more quantitative analysis of scenes of froth.

Some instrument systems that consist of a black-and-white or colour video camera followed by computer have been tested on line in flotation plants [10,11]. They are reported to apply to classification of froths or to extraction of physical features, like average bubble size, size distribution and shape parameters of the bubbles, speed of froth and colour parameters. On the basis of the data displayed, the user may decide how to use such information e.g. to control of froth or flotation.

The methods applied for textural characterization and classification of froths are based on well-known statistical signal processing techniques like histograms, Fourier transforms, power spectra [12] and grey level dependence matrices [13]. They produce either phenomenological or artificial features for classification. The classification is carried out by standard statistical techniques or by use of soft computing methods like machine learning or neural networks.

Another study of industrial flotation froths indicated i.a. that an optimal illumination for distinction of the froth structure may differ from that for distinction of colours [14]. It was shown that e.g. in a bank of apatite flotation cells, the colour of froth changes parallel to the decrease of the apatite content of froth. The froth structure was a central point of interest in sphalerite flotation, in which a collapse of froth may sometimes unexpectedly occur. In addition to the characterization of this phenomenon by means of quantities which can be evaluated directly from the black-and-white image information, a neurocomputing method was applied [15]; for a PCA approach to the same process, see [16].

Process experiments

The data were recorded in the flotation plant of Pyhäsalmi Mine of Outokumpu Finnmines Oy, where an ore containing sphalerite and pyrite minerals is processed. The froth surface was recorded using a monochrome camera once every 20 seconds for about 30 minutes. Originally, the process was in the steady state, but at 15 minutes from the beginning an extra amount of copper sulphate $CuSO_4$ was fed into the conditioner preceding the tested cell, and the response was recorded.

Normally, an increase in $CuSO_4$ makes sphalerite more floatable, but excessive amounts of this conditioning chemical leads to an abrupt collapse, or "poisoning", of the froth surface. This means a shut-

down of the production so that it is extremely important to detect the collapse as fast as possible. At this experiment the poisoning was visually seen to start at 20 minutes but the level dropped down later, completely at 27 minutes. After that the process was returned to normal operation by an extra amount of another chemical.

Figure 2 reveals that the recognition of the collapse situation can be based on the froth outlook — however, defining the features characterizing the exceptional situation in mathematical terms is by no means straightforward.

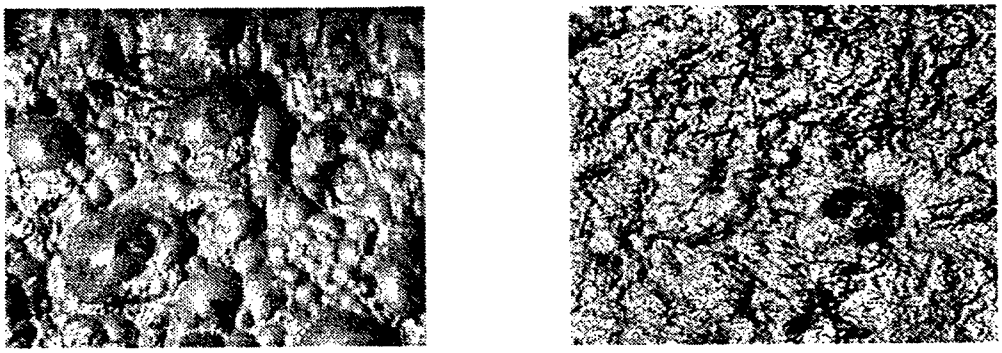


Fig. 2. Typical view of a normal froth surface (left), and of a collapsed surface (right)

The image data were processed off-line using the Matlab software. The GGHA algorithm was applied first by using only the *intensity histogram* information of the images in the data vector (Fig. 3). No external information or classification knowledge was used (see [15]).

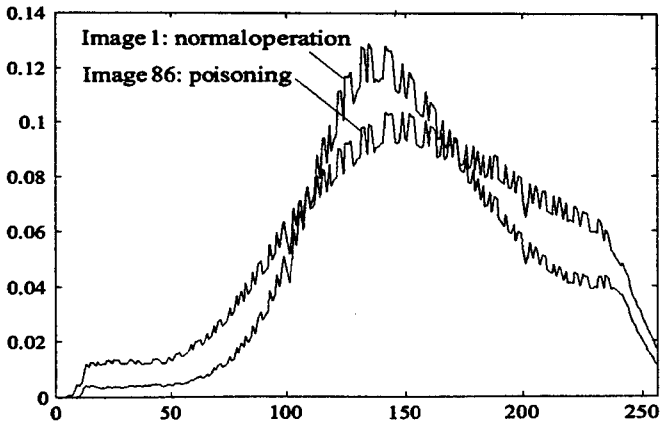


Fig. 3. Typical intensity histograms of the normal surface and the collapsed one

Next, the histogram data were augmented with the *power spectrum* data. The concentric rings on the frequency domain image were regarded as single data units. The zero frequency component was eliminated and base 10 logarithms were calculated, to make the spectral components with largely varying numerical values better compatible. In this way the spectral data were presented as a real-valued vector of only 256 elements (see Fig. 4).

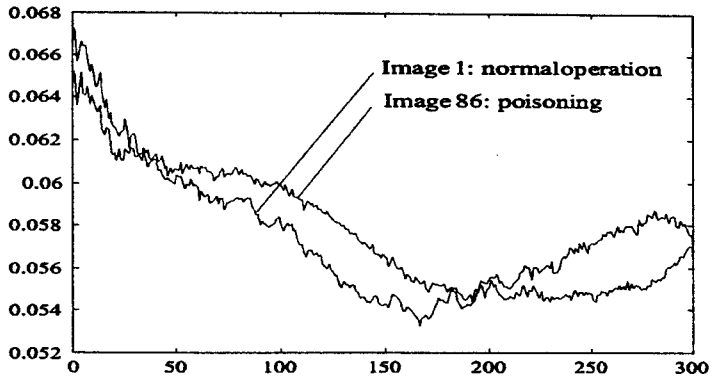


Fig. 4. Typical power spectra of a normal surface and a collapsed one

The algorithm was set to search for four distinct features ($N = 4$) using both the histogram and spectrum data. Two meaningful features, called "typical operation" and "rate of poisoning" were found, the other two having no interpretation (see Fig. 5).

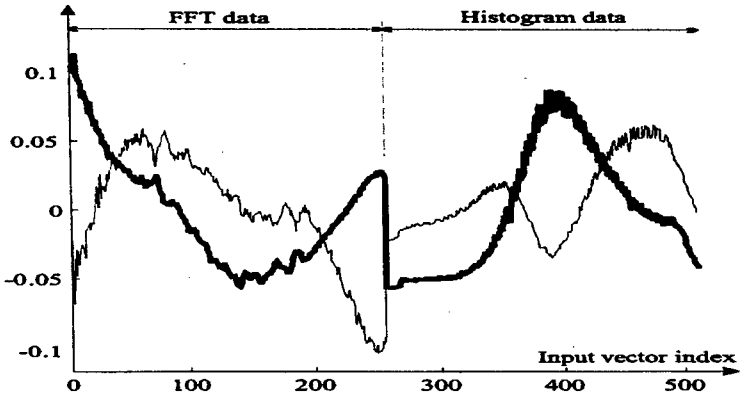


Fig. 5. The two most significant of the extracted features (normalized)

The weight for the feature representing the poisoning state is shown in Fig. 6 as a function of time. The collapse is clearly visible. It can be argued that the algorithm has been capable of automatically extracting relevant information from the process; it must be recognized, however, that the features only reflect dependencies between data units. The analysis of the results has to be carried out by a domain area expert.

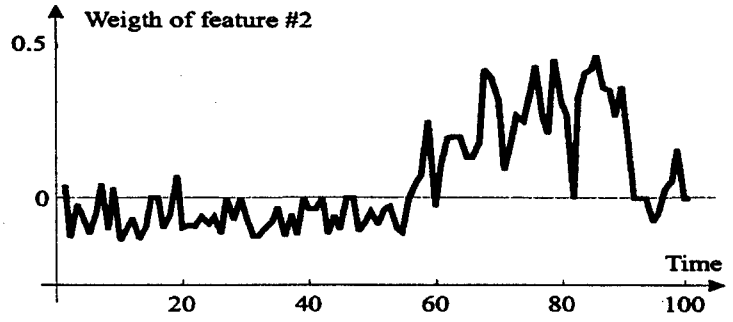


Fig. 6. Weight for poisoning (image index 60 corresponds to run of 20 minutes)

IMAGING, CHARACTERIZATION AND CONTROL OF THE "DRY LINE" IN A PAPER MACHINE

Raw material input to a paper machine is dilute wood fibre pulp. This is fed onto a plane, broad wire on which it settles as a layer. The main part of the water content of the pulp is removed through a multitude of holes in the wire, as it transports the pulp toward the pressing and drying sections of the machine.

The disappearance of the liquid water from the surface of the pulp on the wire is manifested by a "dry line" (Fig. 7). Its location and form have always been a special object of the operator's interest, although an unaided eye finds at most only a part or parts of it. Substitution of the human eye by a regular or opto-electric camera has, as of yet, not improved its observation.

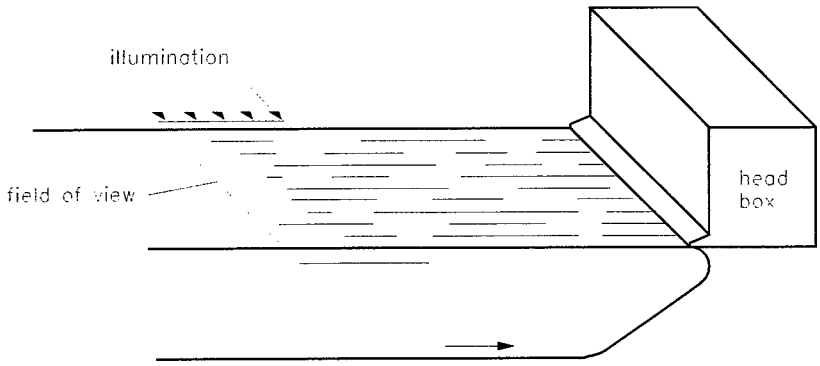


Fig. 7. Illustration of the dry line monitoring setup

The dry line can be reproduced successfully by two new methods which take the optical requirements of illumination, viewing and image formation of the dry line range properly into account [17,18]. They provide the video camera with a wire view which consists of two fields of different, homogeneous luminosities, one preceding and the other following the dry line, while such bright areas are not produced which would effect a blinding or blooming of the detector. The computer which receives the image signal is then able to extract the complete dry line by means of an edge detection algorithm, as the borderline of the two fields, and to reproduce it on a graphical display.

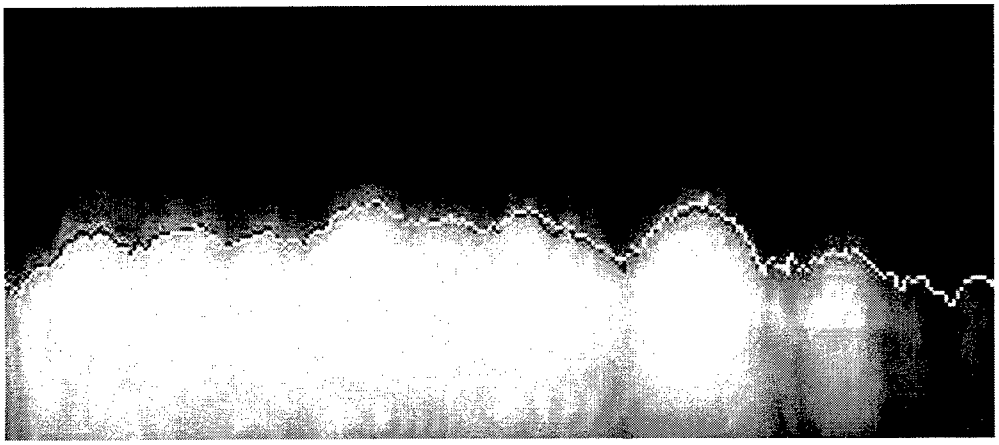


Fig. 8. Digitally reproduced dry line displayed on a monitor.

Both methods have been installed and tested in industrial paper machines. Fig. 8 shows the geometrically rectified wire image together with the digitally extracted dry line, displayed repeatedly in the control room of a large paper board machine at Imatra mills of Stora Enso Company in Finland. The average location of the dry line is counted and shown on the monitor after each measurement, and also brought to a controller for automatic control. – The methods of dry line measurement and control have been patented in several countries.

The closed loop control of the dry line location is accomplished through the headbox slice which regulates the feed of pulp onto the wire, as instructed by the controller. The benefit of this control method is its fast reaction to disturbance inputs entering the head end of the machine, while the conventional controllers which rely on measurements at the dry end of the machine only, are handicapped by a long process delay. Under the control described, the dry line follows fast the changes of setpoint, and keeps the dry line close to its setpoint, both in presence of disturbances and during transitions between different product grades [18,19,20].

Changes of the form of dry line can be effected by one or more of the slice screws, an array of which is available for adjustment of the crosswise distribution of the feed flow of pulp. The control of the form or profile of the dry line requires that the response of the dry line to the change of setting of a single screw is known. Fig. 9 shows the experimentally obtained response of the dry line to the adjustment of a single actuator [18]. The response is similar to the single actuator responses of the dry basis weight of the final product reported in the literature by several authors. It appears that changes in the latter can be predicted on the basis of the dry line measurement, immediately after a disturbance enters from the headbox.

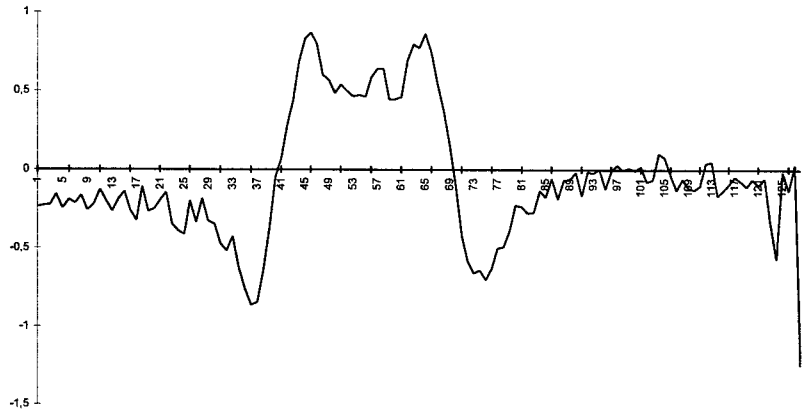


Fig. 9. Typical actuator (location 57 in cross direction) response in dry line profile

Feature extraction

The feature extraction methodology that was discussed above can be applied directly to analyse the dry line profiles. The dry line vectors of length 128 determining the instantaneous profile outlook were used as input data in the algorithm. There is just one "cluster center", representing the average position and profile of the dry line; four additive features were extracted in the experiment (see Fig. 10). No *a priori* information about the process was utilized, the features were determined by the statistical dependencies between dry line measurements only.

This approach may reveal some underlying structure that gives valuable insight to the process operator. Often encountered characteristic variations in the dry line profile are reflected in the extracted features; later on, it is up to the human experts to somehow react and compensate for the unwanted phenomena. For example, note that the last feature (lower right corner in Fig. 10) can probably be interpreted in terms of variations in the flow around the actuator location 32 (cf. Fig. 9) – should the corresponding slice screw or screws perhaps be checked?

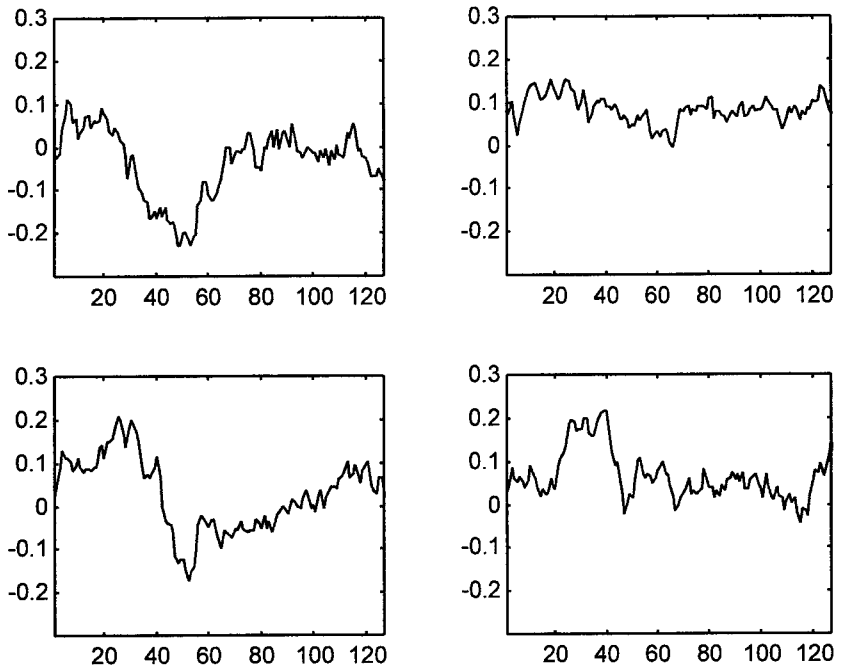


Fig. 10. The four extracted "dry line" features

CONCLUSION

Image analysis of industrial processes is a new field of technology. Its practical implementations are variable depending on the particular process, and new applications keep on appearing. Although a generality cannot be reached, some conclusions can be made on the basis of the applications elaborated above and of other cases described in the literature, such as analysis of defects on surface of steel plate in rolling mill [21], flame in the combustion chamber of a boiler [22], cross-section and defects of wooden board in saw-mill [23], etc.

Thus it has turned out that whenever the human eye and mind are able to distinguish and define such features of a scene which characterize the material observed or the stage of its processing, these can be measured also by physical vision systems, even quantitatively. New types of illumination and viewing are then often needed, in order to establish a successful imaging of the moving and variable, industrial material. Even if such features have not been defined by the human vision, they may be found by intelligent processing of the abundant data provided by a single image or a succession of images. An intelligent analysis of the detected features may also be needed, whenever it is not known, which ones of the available actuators are to be manipulated, and to which extent each, in order to establish a successful control of such material properties which relate to those features.

ACKNOWLEDGEMENT

The authors are grateful to Mr. Jouko Berndtson, M.Sc., for the paper machine data material. This research has been partly financed by the Academy of Finland.

REFERENCES

1. A. Basilevsky, 1994: Statistical Factor Analysis and Related Methods. John Wiley & Sons, New York.
2. F. Palmieri, J. Zhu, and C. Chang, 1993: Anti-Hebbian learning in topologically constrained linear networks: A tutorial. IEEE Trans. on Neural Networks, **4** (5), 748-761.
3. P. Földiàk, 1990: Forming sparse representations by local anti-Hebbian learning. Bio.Cybernetics, **64** (2), 165-170.
4. E. Saund, 1995: A multiple cause mixture model for unsupervised learning. Neural Computation, **7**, 51-71.
5. H. Hyötyniemi, 1998: Automatic Structuring of Unknown Dynamic Systems. In Soft Computing in Engineering Design and Manufacturing (P.K. Chawdhry, R. Roy, and R.K. Pant, R, eds.), Springer-Verlag, London, pp. 410-419. Available at http://Saato014.hut.fi/Hyotyniemi/publications/97_wsc2.htm.

6. H. Hyötyniemi, 1998: Structure from Data: AI Approaches to Systems Modeling. Proc. 8th Finnish AI Conference STeP'98 (P. Koikkalainen and S. Puuronen, eds.), Finnish Artificial Intelligence Society (FAIS), Helsinki, pp. 31-40. Available at http://Saato014.hut.fi/Hyotyniemi/publications/98_step_1.htm.
7. H. Hyötyniemi, 1996: Constructing non-orthogonal feature bases. IEEE Int. Conf. on Neural Networks ICNN'96, Washington, DC. Available at http://Saato014.hut.fi/Hyotyniemi/publications/96_icnn.htm.
8. T. Kohonen, 1995. Self-Organizing Maps. Springer-Verlag, Berlin.
9. S. Haykin, 1994: Neural Networks – Comprehensive Foundation. Macmillan College Publishing, New York.
10. A. Cipriano, M. Guarini, R. Vidal, A. Soto, C. Sepúlveda, D. Mery, and H. Briseño, 1998: A real time visual sensor for supervision of flotation cells. Minerals Engineering, **11** (6), 489-499.
11. D.W. Moolman, C. Aldrich, J.S.J. van Deventer, J.J. Eksteen, W.W. Stange, P. Marais, C. Goodall, and R.S. Veitch,1995: On-line image analysis to improve industrial flotation plant performance. Preprints of the 8th IFAC Int. Symp. on Automation in Min. Met. Processing, Sun City, South Africa, 367-371.
12. D.W. Moolman, C. Aldrich, J.S.J. van Deventer, and W.W. Stange, 1994: Digital image processing as a tool for on-line monitoring of froth in flotation plants. Minerals Engineering, **7**, 1149-1164.
13. D.W. Moolman, C. Aldrich, J.S.J. van Deventer, and D.J. Bradshaw, 1995: The interpretation of flotation froth surfaces by using digital image analysis and neural networks. Chemical Engineering Science, **50**, 3501-3513.
14. A.J. Niemi, R. Ylinen, and H. Hyötyniemi, 1997: On characterization of pulp and froth in cells of flotation plant. Int. J. of Mineral Processing, **51**, 51-65.
15. H. Hyötyniemi and R. Ylinen, 1998: Modeling of Visual Froth Data. Preprints of the IFAC Symposium on Automation in Mining, Mineral and Metal Processing (J. Heidepriem, ed.), International Federation of Automatic Control, pp. 309-314. Available at http://Saato014.hut.fi/Hyotyniemi/publications/98_mmm.htm.
16. J. Hätönen, H. Hyötyniemi, G. Bonifazi, S. Serranti, F. Volpe, and L.-E. Carlsson, 1999: Using PCA in controller strategy design for a flotation process. Preprints of the 14th IFAC World Congress, July 5-9, Beijing, P.R. China.
17. A.J. Niemi and C. Bäckström, 1992: Automatic observation of dry line on wire for wet end control of the paper machine. Proc. of Control Systems '92, CPPA, Canada, pp. 261-265. Also in Pulp and Paper Canada, **95** (2): 27 (1994), T55-58.
18. A.J. Niemi, J. Berndtson, and S. Karine, 1998: Improved wet end control of the paper machine. Proc. Of Control Systems '98 (September 1-3, Porvoo, Finland), Finnish Soc. of Automation, 371-378.
19. A.J. Niemi, J. Berndtson, and S. Karine, 1999: Feedback control of the dry line on wire of paper machine. Preprints of the 14th IFAC World Congress, July 5-9, Beijing, P.R. China.
20. J.E. Larsson, T. Gustafsson, and S. Rönnbäck, 1998: Paper machine dry line positioning system. Proc. Of Control Systems '98 (September 1-3, Porvoo, Finland), Finnish Soc. of Automation, 355-362.
21. E. Kiuru, E. Keränen, and T. Piironen, 1993: Improving overall performance of automatic systems for metal surface inspection. Proc. 1st Int. Conf. Measurement and Instruments in the Metallurgical Industry, Shenyang, P.R. China, 24-29.
22. J. Hirvonen, R. Lilja, K. Ikonen, and J. Nihtinen, 1996: Image processing in combustion control. Int. Journal of Pattern Recognition and Artificial Intelligence, **10** (2), 129-137.
23. M. Pietikäinen and L.F. Pau (eds.), 1996: Machine Vision for Advanced Production. Series in Machine Perception and Artificial Intelligence (Vol. 22), World Scientific Publishing.

Progress in Japan's Intelligent Manufacturing Systems Research Program

Yuji Furukawa

Tokyo Metropolitan University, Minami-Osawa, Hachioji, Tokyo, 192-0364 Japan
Email: furukawa-yuji@c.metro-u.ac.jp

ABSTRACT

The IMS Program aims at improving the circumstances around manufacturing industries and developing the next generation manufacturing technologies and systems. It is a very unique and unprecedented mechanism supported by industry, academia as well as governments, challenging to undertake industry-led international collaborative R&D among six participant regions; Australia, Canada, the EU, Japan, Switzerland (EFTA) and the USA.

The IMS Program now sees it's selected 13 international projects implemented and tries to increase the number of projects more than a hundred. With increasing number of projects and proposals actively proposed by member regions, this initiative will further expand its effective network and enhance global manufacturing cooperation as expected.

Keywords: IMS(Intelligent Manufacturing Systems); mega competition, global manufacturing, environmentally-conscious manufacturing

HISTORY OF IMS (Figure 1)

At the end of 1989, Japan proposed the IMS Program as a framework for international collaboration by industry, academia and governments whose aim would be the resolution of many problems shared by the world's manufacturers. In response, a feasibility study began in 1992 with participants from Japan, Europe, USA, Australia and Canada. The final report, released in 1994, stated that "the IMS Program is feasible and a full-scale Program should start as soon as possible." April 1995 saw ISC1 (the first meeting of the International Steering Committee) and the announcement of the IMS Program's official start. Since then, some projects have been endorsed and are steadily underway. In January 1997, the EU became an official member of the IMS Program. The six current participants include Australia, Canada, the EU, Japan, Switzerland (EFTA) and the USA. In November 1997, South Korea is also participating on an experimental basis.

BACKGROUND OF IMS

Recently, manufacturing industries faced radical changes in their business environment. First is **Globalization of Manufacturing**. Production units are being shifted overseas and procurement is crossing international borders. Lack of uniform standards and human-interface difference have resulted in numerous problems. Second is **Changing Market Environment**. Consumer needs are becoming more diverse, and product life-cycles are shrinking. This leads to creation of production systems that are flexible enough and to shortened R&D cycles. Third is **Changing Labor Environment**. With experienced technicians in short supply and young engineers leaving production, retaining talented staff requires improvement in job content and the production environment. Forth is **Response to Environment Issues**. It has become common sense that recycling and efficient use of nonrenewable resources are essential to protect and improve the global environment. These problems can not and/or should not be solved by a single organization or country because they have become so big in scale and so complicated. It seems that a way must be found to solve these problems by international collaboration among industries, governments and academia. The IMS Program is the first trial to realize this collaboration of R & D in manufacturing.

0-7803-5489-3/99/$10.00 ©1999 IEEE.

OBJECTIVES OF IMS

Under today's globalized economy, every private company is forced to compete against others, hence it has to develop more competitive products. Therefore, it seems difficult to collaborate among the competing companies together. However, looking the manufacturing technology development carefully, we realize a circulation of technological knowledges, that is, companies are competing in the current technological level, however, they fall in cooperation in the standardized level, as can be seen in ISO activities, which can be nominated as a post-competitive knowledge and also in the basic/enabling level, as can be seen in development of environmentally conscious combustion engines in automobile industry, which can be called as a pre-competitive knowledge. The IMS Program aims to develop many independent projects which remain in either in post-competitive or in pre-competitive level.

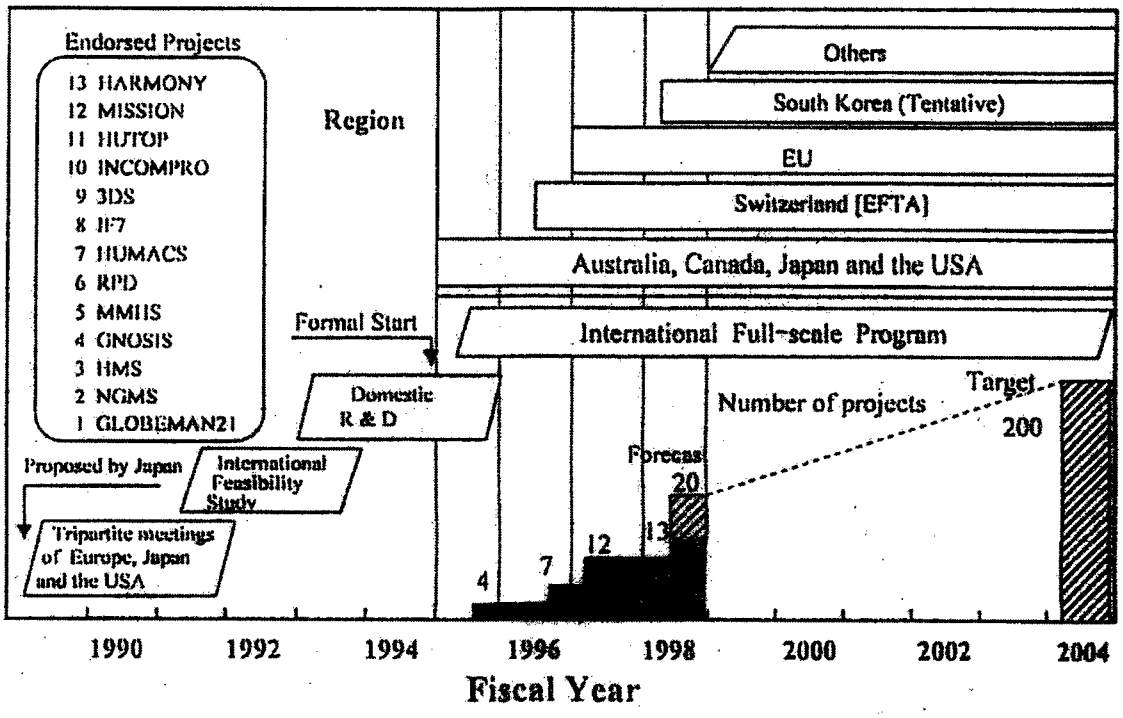


Fig. 1. Evolution of the IMS Program.

CURRENT STATUS OF IMS

The current status of the IMS projects as of May 1999 is as follows:

Projects fully endorsed	13
Projects conditionally endorsed	1
Proposal under revision	4
Abstracts endorsed	30
Abstracts under review or revision	11
Outline proposals	5

During the period from ISC6 (the sixth meeting of the International Steering Committee) held in November 1997, to 1 May 1999, 41 abstracts were submitted from the participating regions, mostly from EU. Those are currently awaiting development into full proposals. Five outline proposals are waiting for development into abstracts and subsequently, into full proposals. These have been circulated among the participating regions for appropriate action.

Figure 2 shows the status of participation made by 14 projects for which full proposals were submitted to date. Those projects include 13 endorsed projects and 1 project which is awaiting endorsement. For the full proposals, origins were identified with the domiciles of their respective first ICPs.(International

Coordinating Partners). The numbers of participating organizations from all regions are 418 in total. Of those participating, 177 organizations are from academia and 241 organizations are from private corporations. Each region has several participants. Figure 2 also shows a comparison of the regions.

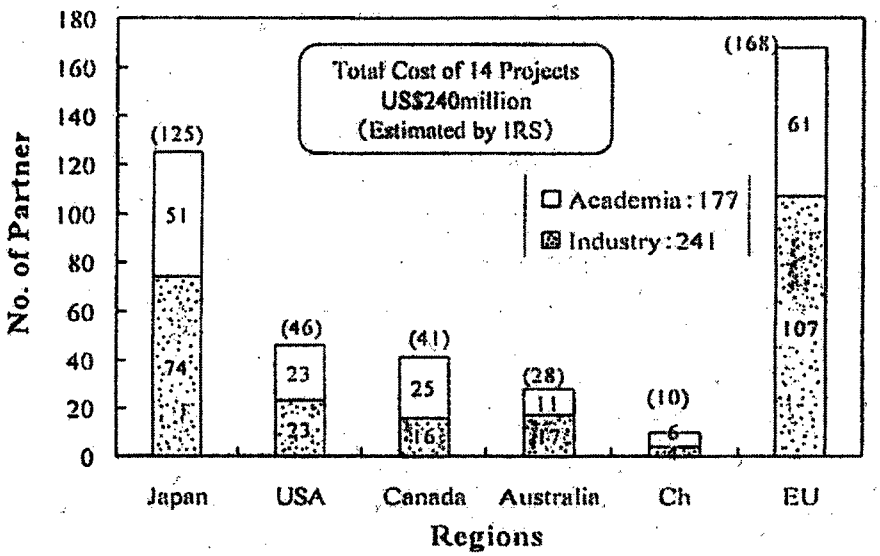


Fig. 2. Current Project Status and Comparison of the Different Participating Countries.

Although Australia, Canada and Switzerland enjoy a fair share, the originating region is heavily weighted in favor of the EU and Japan, reflecting the number of countries, which consist of the former region and the fact that the latter has had a head start. The balance between academia and industry is now becoming better, especially in Japan and the EU, the portfolio in those regions shows that the IMS Program is an industrial-led program aimed at both pre-competitive and post-competitive research in the manufacturing industry.

The commitments made by each project were estimated by valuing each person year at US $100,000 and adding to that any other costs as stated. In Figure 2, there are the estimated total commitments by all the 14 projects for which full proposals were submitted to date. The total commitments are US$ 240 million. We are expecting big growth in the future, because a large number of abstracts are ready for development into full proposals.

TECHNICAL TREND OF ON-GOING PROJECTS

With a view to providing a general picture of how the IMS projects are covering various areas of manufacturing technology, all the full projects and abstracts in the current portfolio were roughly sorted into a number of categories.

Figure 3 shows their distribution over the topics suggested by TTWG (Technical Themes Working Group), which is one of the most important committees under ISC and led by Y. Furukawa, in their report submitted to ISC5 (held in May 1997) as Key Seed Technologies for IMS. In order to provide a general picture in the simplest form, each of the projects and abstracts was identified with a single topic for simplicity's sake.

Assuming that the full projects indicate the current trend, the most popular themes are understandably enough **"Advanced processing and assembling technologies", "Virtual manufacturing"** and **"Advanced design technologies"** at present as well as in the foreseeable future. On the other hand, assuming that the abstracts indicate the future trend, **"Remote monitoring and control technologies"** seems to be an expanding topic. There are no full projects addressing **"STEP and CALS"** and a small number of projects will cover this topic considering the abstracts submitted to date.

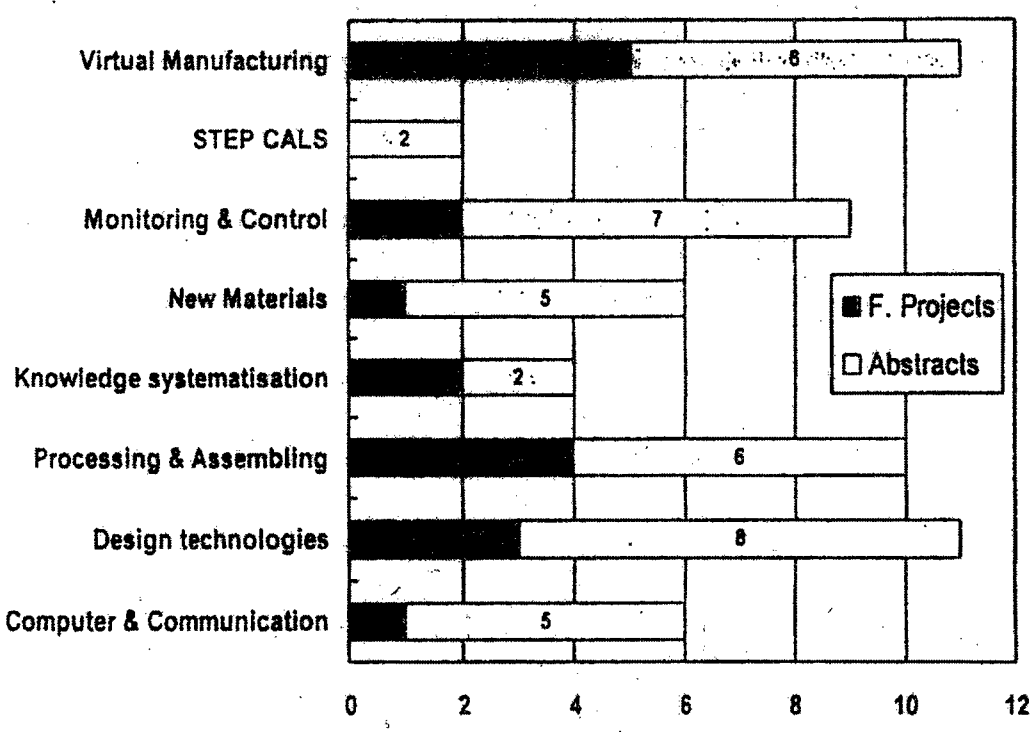


Fig. 3. Project Categories in the IMS Program.

Figure 4-1 indicates all the projects classified by size, i.e. number of partners. Projects appear to have become smaller in size as the average number of partners decreased from 39 in 95 series to 26 in 97 series. Future projects are likely to be even smaller as the abstracts develop into full proposals.

On the other hand, Figure 4-2 shows the distribution of project size in terms of cost for full proposals in 95, 96 and 97 series, as well as for the 20 recent abstracts on which data were available. Project size has undergone a steady decrease and will continue to decrease in terms of cost as well.

Note should be taken, however, that the forecast may not match the reality as data from abstracts are not reliable as most of them are at too premature a stage of formation.

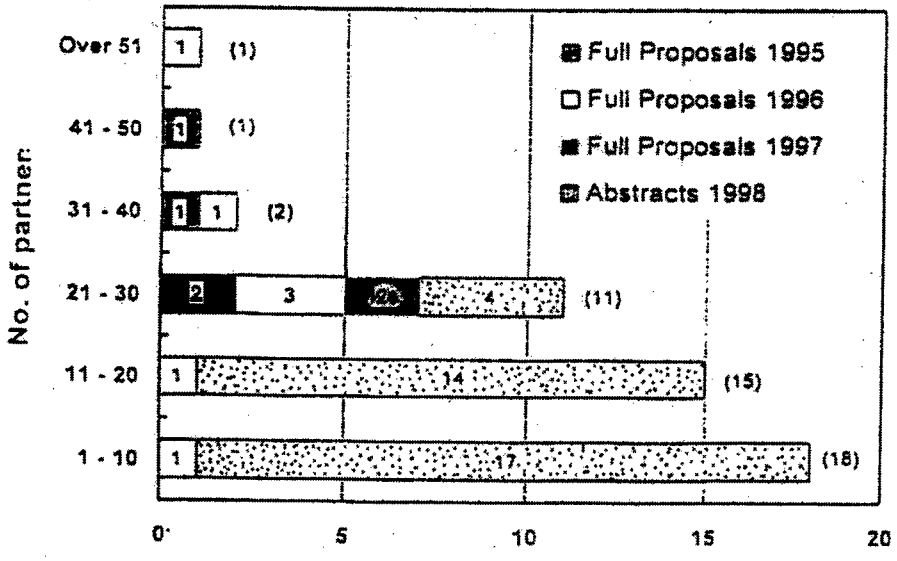


Fig. 4-1. Project Size by Number of Partners.

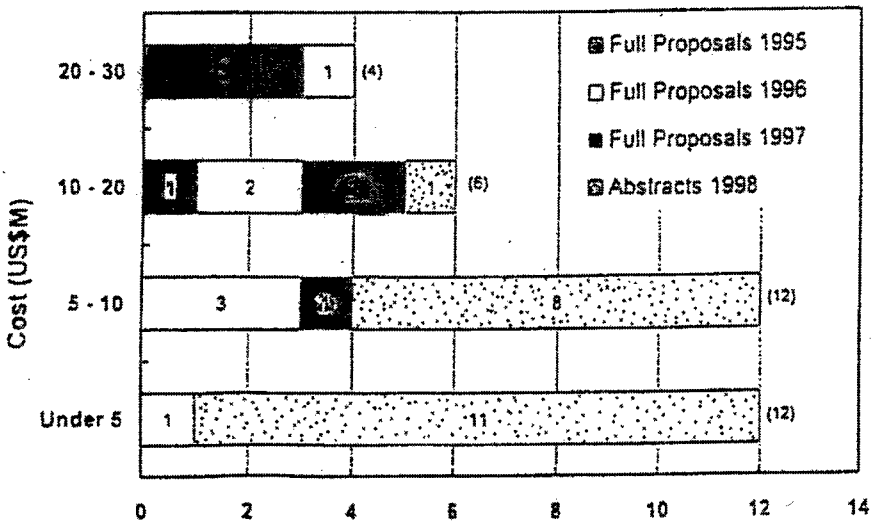


Fig. 4-2. Project Size by Cost.

FUTURE DEMANDS OF MANUFACTURING INDUSTRIES

Manufacturers must meet not only various and varying demands from users at a reasonable price but the chief requirement now is to minimize adverse environmental effects arising from their activities. It is not always possible however, for manufacturers to meet all demands including those of the environment.

By taking the foregoing into consideration, demands on manufacturers can be summarized as follows: provide users with products that best meet their needs including servicing such products; have the highest possible quality; have the lowest possible cost; minimize the load on the natural environment. How to meet these demands is the basic question for manufacturers to answer. Demands arising from these changes in the manufacturing environment are summarized and the fundamental measures are considered as follows:

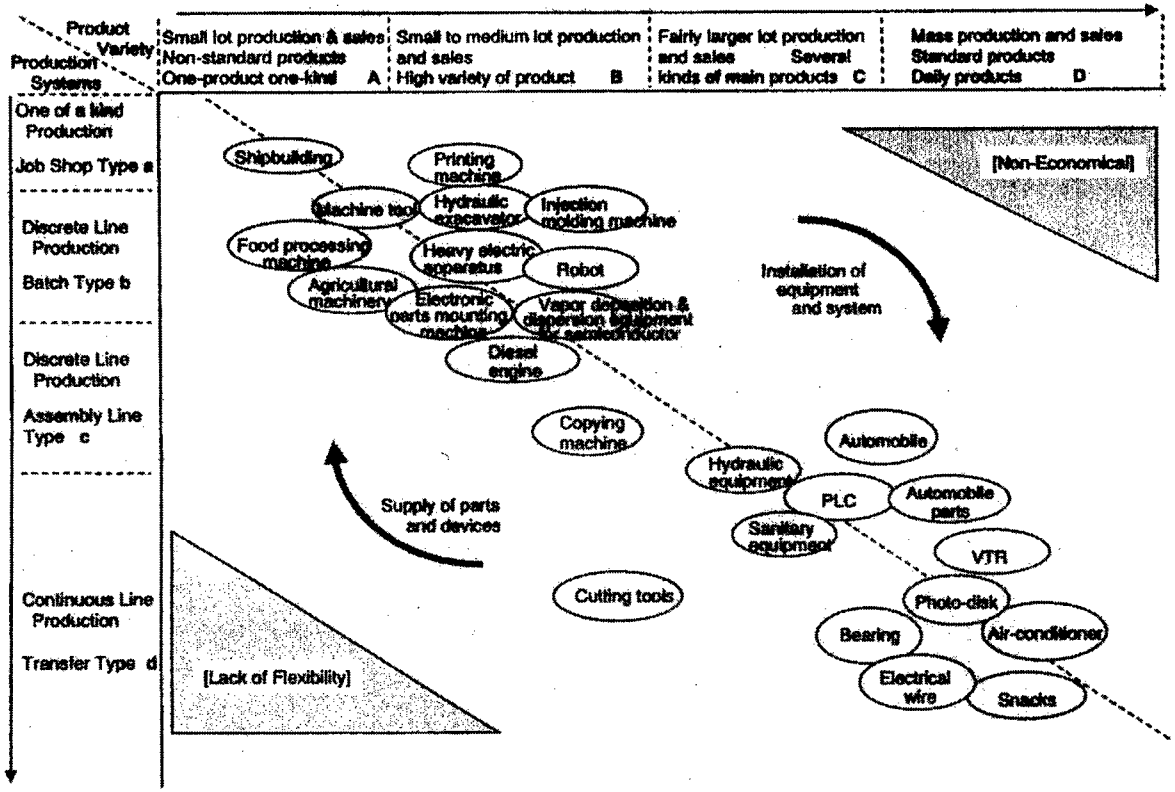
- Mega-competition
  - Overseas implant for manufacturing low value-added products. Concentrating efforts on competitive products. De-facto standards. Optimal automation. High-speed manufacturing.
- Globalized operation
  - Optimal resource and effort distribution. Material and component acquisition and out-sourcing.
- Global environment and material recycling
  - Design for recyclable and clean products. Clean manufacturing. Energy and resource efficient manufacturing. Disassembling and sorting-out technology. Waste collection systems.
- Manufacturing culture and workers
  - Enhanced awareness of manufacturing activities. Education/training of manufacturing workers. Professional qualification.

FUTURE TECHNICAL AREAS OF IMS

The TTWG (Technical Themes Working Group chaired by Y. Furukawa) surveyed and proposed possible technical themes taking these demands into consideration. The report summarizes the problems associated with many industrial sectors and products accounting for both product variety and production systems, and proposes R&D themes in manufacturing technology, systems and possible management ones as shown in Figure 5. These themes should be referenced when a new candidate research consortium is formed.

CONCLUSION

The present paper has introduced the state of the art of the IMS Program which is now conducted by the six participating countries/areas aimed at solving problems encountered in manufacturing in these times of a global economy. The paper has stressed the Program technologies, introducing the state of current projects as well as forecasting future directions. It is hoped that other authors will refer to this report to recognize the position of their individual research compared to the worldwide trend of manufacturing projects.



R&D Themes in Manufacturing Technology and Systems

*Automation : 3D Automatic Welding and Painting or other Casting Processes
*Improved Capability for Production Systems Design

*Concurrent One-of-the-Kind Production *Reducing Bottle-Necks at Shopfloor *One of the Kind Production *Manufacturing-load Simulation *Process Synchronization *Double-production at single Shopfloor *Real- time LAN *Open Type NC Systems
*Information Exchange via Communications Network *Flexible Production on a Product-to-Product Basis *Plastic-state Metal Casting Processes *Reduced Cycle-time

*Human-Machine Co-existent/Cooperative System *Human Skill supporting System *Documentation of Knowledge & Ability of Skilled Workers & its Applications *Reduced Bottlenecks at Shopfloors
*In-situ Cleaning of Hydraulic Fluid *Self-Growing Production System
*Product distribution Concurrent Production Systems *Improved Chip-Monitoring & Removal System *Recovery of Useful Materials from Metallic Wastes *Recovery of Plastics for Insulation Inclusion

*Super-Automated Production Lines: easy start, flexible, equipped with an automatic material-supply, products-retrieval and waste-removal system, an in-line measuring as well as remote control system and capable of changing line setup by itself and work with trackless AGV with an autonomous navigation system *Automated and Intelligent Inspection System *Failure forecasting and Remote Diagnostic System
*Super-Precision Production Systems : Super-high-speed (e.g. 500m/s), Super-Precision Machining (with errors within sub-micron order), Grinding, Polishing and other similar processes *Processing Technology for New, Advanced Materials *Automated Wiring and Piping Systems *Open-type Protocol and Interface for High-Speed LANs Capable of Handling Image Information *Self-Growing Production Systems *Technology to recover useful Materials from Metallic Waste *Standardization of Graphics User Interface *Automatic Selection and Setting of Tools and Cutting / Grinding and other Processing Conditions *Design for Reverse Manufacturing

Management Themes

*Difference between Japanese and foreign prices / Costdown
*Competition of manufacturing techniques
*Lack of labor force/ Education
*Automation based on economic effectiveness (Automation in accordance with cost performance)

*Difference between Japanese and foreign prices/Costdown *Development of highly value-added product *Speed up of delivery *Inevitable overseas implants *Decision on what to remain and not to remain in Japan *Optimized production and production at the right place *Balance between labor saving and automation *Effective response to aging society *Unit parts and their common use *Automatmated distribution *Automation during night *Workers with much skill to develop new product *Early automation of mass-production *Active response to frequent setup and build

*Inevitable overseas implants and procurement
*Optimized production and production at the right place
*Needs for skilled workers albeit automation
*Improvement of product distribution
*High-speed data exchange

*Human-machine coexisting automated manufacturing systems
*Cell-type systems capable of manufacturing tailor-made products on demands
*Optimized production and production at the right place *Sales-concurrent manufacturing / Integrating sales into manufacturing *De facto standards
*Fully-automated systems to manufacture products with high added values
*Advanced quality control & assurance
*Reducing material handling processes
*Reduced lead-time *Networking with overseas facilities *Multi-purpose machine tools *Automation and labor saving of inspection and packaging

Future Development

*Manufacturers shifting their major activities from traditional hard-products production to softer services providing → Development of virtual manufacturing
*Manufacturing systems undergoing a differentiation into fully automated mode and human-centered mode with machines assisting operators
*Development of manufacturing networks on a global scale
*A great leap forward in simulation technology for designing production lines
*Downsizing of component parts
*Increase common use of standardized parts (more than 50%)
*Large manufacturers transforming themselves into vendors of components, certain key devices in particular

Analysis of Processes and Large Data Sets by a Self-Organizing Method

Teuvo Kohonen

Helsinki University of Technology, Neural Networks Research Centre,
P.O. Box 2200, FIN-02015 HUT, Finland

ABSTRACT

Frequently one must deal with natural processes and data for which no known models can be derived from classical systems theory. Examples are discrete measurements from distributed processes that are not identifiable, and data generated by human actions such as speech, text, and financial time-series. A recent solution is that relationships between the elements are described by nonlinear functional expansions called "neural networks." The most familiar neural-network models make use of supervised learning, which means that the data used for identification must be verified, validated, and preclassified. Such data, however, is very expensive and sometimes even impossible to acquire. A different approach altogether is unsupervised learning that uses raw data, usually available on mass. In this presentation, the most widespread unsupervised-learning method, the Self-Organizing Map (SOM) algorithm is described. The central idea in this algorithm and in self organization in general, is to use a large number of relatively simple and structurally similar, interacting, statistical submodels. Each submodel describes only a limited domain of observations, but since the submodels can communicate, they can mutually decide what and how large a domain belongs to each submodel. By virtue of such collective interactions it becomes possible to span the whole data space nonlinearly, thereby minimizing the average overall modeling error. As the SOM implements a characteristic nonlinear projection from the input space to a visual display, it can be used, e.g., to reveal process states that otherwise would escape notice. Applications to industry and "data mining" in general are surveyed. A recently implemented curiosity of self-organizing maps, the mapping of all electronically available patent abstracts in the world onto a visual display will also be reported.

INTRODUCTION

With the increasing computing power, it has become possible to process and classify masses of natural data, such as statistical information, images, speech, as well as other kinds of signals and measurements coming from very different sources. Such tasks occur in industry, remote sensing, medicine, finance, and natural sciences, to mention only a few main fields. For financial, medical, administrative, and other databases, one needs efficient tools for *visualization*, *prediction*, *clustering*, and *profiling*. In industrial problems, it is essential to build empirical data based models of complex systems in order to be able to *monitor*, *predict*, *diagnose faults*, and *control* the systems.

Natural information has properties that have not been taken into account in the classical mathematical statistics, not even in traditional multivariate analyses. The dimensionalities of such data tend to be immense, a priori statististics are not available, parametric density functions cannot be found, and the mutual statistical dependencies between the data elements are usually nonlinear and dynamic.

In the early 1980s a new line of computational approaches based on simple models of biological neurons was launched. The insight was that although nonlinear and dynamical statistical descriptions are not available in analytical form, the intrinsic features of the observations and their interrelations can nonetheless be *learned* from the input and output data using a *great number of simultaneously cooperating submodels*. This approach was not possible until the computers became so effective that high-dimensional submodels, which learned their structures from the collective interactions between the data elements, could be set up. There have also existed attempts to develop special massively parallel computers for such *artificial neural networks*, but at least for the time being the hardware has not brought about any breakthroughs in natural computing.

0-7803-5489-3/99/$10.00 ©1999 IEEE.

Among the many neural-network architectures and algorithms, the Self-Organizing Map (SOM) [1] is in a special position, because it is able to form *abstract, but ordered images* of large and often high-dimensional data sets. It converts complex, nonlinear statistical relationships between high-dimensional data elements into simple geometric relationships between points on a low-dimensional display. As it thereby compresses information while preserving the most important topological and metric relationships of the primary data elements on the display, it may be thought to produce some kinds of abstraction. These two aspects, visualization and abstraction, can be utilized in a number of ways in complex tasks such as process analysis, machine perception, control, and communication.

THE BASIC PRINCIPLE OF THE SELF-ORGANIZING MAP (SOM)

The self-organizing process may be realized in any set of elements, schematically illustrated in Figure 1, where only a few basic operational conditions are assumed. For simplicity, let the elements (often signified as "neurons") form a regular planar array and let each element represent a set of numerical values M_i which we call a *model*. We further assume that each model is modified by the messages the element receives.

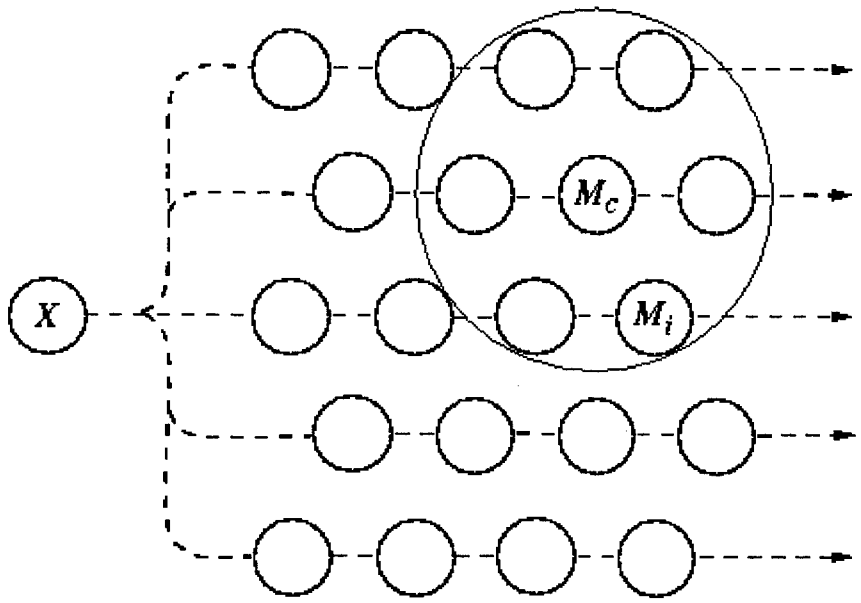


Fig.1. A self-organizing model set. An input message X is broadcast to a set of models M_i, of which M_c best matches to X according to some criterion. All models that lie in the vicinity of M_c (larger circle) improve their matching with X. Note that M_c differs from one message to another.

Let there exist some mechanism by which an ingoing message X, a set of parallel signal values, can be compared with all models M_i. It is customary to speak of "competition" between the models, when they receive common input, and the model, whose parameters are fittest to this input, is selected for the further steps of the process. This element is called the "winner" denoted by M_c. Another requirement for self-organization is that the models shall be modified only in the local vicinity of the winner(s) and that all the modified models shall then resemble the prevailing message better than before this step.

When the models in the neighborhood of the winner are made to resemble the prevailing message X better, they also tend to mutually become more similar, i.e., the difference between all models in the neighborhood of M_c are smoothed. Different messages at different times affect different parts of the set of models, and thus the models M_i, after many learning steps, start to acquire values that relate to each other smoothly over the whole array, in the same way as the various messages X in the "signal space" do; in other words, maps related topologically to the set of messages start to emerge as can be proven mathematically [2].

These three subprocesses — broadcasting of the input, selection of the winner, and adaptation of the models in the spatial neighborhood of the winner — seem to be sufficient, in the general case, to define a self-organization process that then results in the emergence of the topographically organized "maps".

The SOM usually consists of a 2-D regular grid of nodes. The SOM algorithms described below compute the models so they optimally describe the domain of (discrete or continuously-distributed) observations. The models are organized in a meaningful two-dimensional order such that similar models become closer to each other in the grid than the more dissimilar ones. In this sense the resulting SOM is also a *similarity graph*, and a clustering diagram, too. Its computation is a nonparametric, recursive regression process.

THE INCREMENTAL-LEARNING SOM ALGORITHM

In the majority of practical applications, the input messages X are represented by sets of values that constitute real vectors $\mathbf{x}$. Similarly, the models M_i are represented as real vectors $\mathbf{m}_i$. Regression of a set of model vectors $\mathbf{m}_i \in \Re^n$ into the space of observation vectors $\mathbf{x} \in \Re^n$ is often made by the following sequential process, which takes care of that the resulting models will become ordered:

$$\mathbf{m}_i(t+1) = \mathbf{m}_i(t) + h_{c(\mathbf{x}),i}(\mathbf{x}(t) - \mathbf{m}_i(t)) \quad , \tag{1.}$$

where t is the sample index of the regression step, whereupon the regression is performed recursively for each presentation of a sample of $\mathbf{x} = \mathbf{x}(t)$. Index c ("winner") is defined by the condition

$$\forall i, \|\mathbf{x}(t) - \mathbf{m}_c(t)\| \leq \|\mathbf{x}(t) - \mathbf{m}_i(t)\| \quad . \tag{2.}$$

Here $h_{c(\mathbf{x}),i}$ is called the *neighborhood function*, and it is like a smoothing kernel that is time-variable and its location depends on condition (2). It is a decreasing function of the distance between the ith and cth models on the map grid. The norm is usually assumed as Euclidean.

The neighborhood function is often taken to be the Gaussian

$$h_{c(\mathbf{x}),i} = \alpha(t) \exp\left(-\frac{\|\mathbf{r}_i - \mathbf{r}_c\|^2}{2\sigma^2(t)}\right) \quad , \tag{3.}$$

where $0 < \alpha(t) < 1$ is the learning-rate factor, which decreases monotonically with the regression steps, $\mathbf{r}_i \in \Re^2$ and $\mathbf{r}_c \in \Re^2$ are the vectorial locations in the display grid, and $\sigma(t)$ corresponds to the width of the neighborhood function, which is also decreasing monotonically with the regression steps.

A simpler definition of $h_{c(\mathbf{x}),i}$ is the "bubble neighborhood" defined as in the following: $h_{c(\mathbf{x}),i} = \alpha(t)$ if $\|\mathbf{r}_i - \mathbf{r}_c\|$ is smaller than a given radius around node c (whereupon this radius is a monotonically decreasing function of the regression steps, too), but otherwise $h_{c(\mathbf{x}),i} = 0$. In this case we shall call the set of nodes that lie within the given radius the *neighborhood set* N_c.

Some mathematicians may be more familiar with the so-called "principal curves" of Hastie and Stuetzle [3] and see a relationship between them and the SOM. However, the SOM was introduced eight years earlier than the "principal curves." It can be computed much more conveniently and effectively than the latter. There are also other differences, for instance, the SOM can be generalized in many ways, which are not possible for the principal curves.

Another principal alternative to the SOM is the *generative topological mapping (GTM)* [4], in which the mapping directly tends to preserve the topological-metric relations on the output array. It has turned out, however, that numerous shortcut computations can be applied to make very large SOMs, while these methods are not applicable to the GTM.

Due to the many stages in the development of the SOM method and its variations, there is often useless historical ballast in the computations.

For instance, an old ineffective principle is random initialization of the model vectors $\mathbf{m}_i$. Random initialization was originally used to show that there exists a strong self-organizing tendency in the SOM, so that the order can even emerge when starting from a completely unordered state, but this need not be demonstrated every time. On the contrary, if the initial values for the model vectors are selected as a regular array of vectorial values that lie on the subspace spanned by the eigenvectors corresponding to the two largest principal components of input data, computation of the SOM can be made orders of magnitude faster, since (i) the SOM is then already approximately organized in the beginning, (ii) one can start with a narrower and even time-constant neighborhood function and smaller learning-rate factor.

Many computational aspects like this and the selection of proper parameter values have been discussed in the software package SOM_PAK [5], as well as the book [1].

More General SOMs

Above the models consisted of ordered sets of real numbers (feature values or descriptors), regarded as real vectors in the Euclidean space. The same philosophy, however, applies to many other entities that are then ordered on a SOM array. For instance, the models can be *strings of symbols*, *filters*, *operators* with a finite number of parameters, or *manifolds* in the space defined, e.g., by a set of basis vectors. For the construction of an ordered map, the following requirements are sufficient:

1. There must be definable a *distance measure* between any two items (input items and/or models), on the basis of which any input item can be compared with all the model items, and the "winner" is identified.
2. The models must be updatable, such that the new value of each model in the "neighborhood" has a smaller or equal distance from the input.

A yet more general SOM is obtained when no distance measure is definable between the input items. Assuming that there exists a set of possible models, and a fitness function between each model and each input can be defined, the models can be ordered according to their functional similarity [6].

THE BATCH VERSION OF THE SOM

The incremental regression process defined by (1) and (2) can often be replaced by the following batch computation version of the SOM, which is significantly faster and does not require specification of any learning-rate factor $\alpha(t)$.

Assuming that the convergence to some ordered state is true, we require that the expectation values of $\mathbf{m}_i(t+1)$ and $\mathbf{m}_i(t)$ for $t \to \infty$ must be equal, even if $h_{ci}(t)$ were then selected nonzero. In other words, in the stationary state the values $\mathbf{m}_i^*$ must satisfy the equilibrium equation

$$\forall i,\ \mathrm{E}_t\left\{h_{c(\mathbf{x}),i}(x-\mathbf{m}_i^*)\right\}=0\ . \qquad 4.$$

In the special case where we have a finite number (batch) of the $\mathbf{x}(t)$ with respect to which (4) has to be solved for the $\mathbf{m}_i^*$, and $h_{c(\mathbf{x}),i}$ represents the kernels used during the last phases of the learning process, we can write Equation 4. as

$$\mathbf{m}_i^* = \frac{\sum_t h_{c(\mathbf{x}),i}\mathbf{x}(t)}{\sum_t h_{c(\mathbf{x}),i}}\ . \qquad 5.$$

This, however, is not yet an explicit solution for $\mathbf{m}_i^*$, because the subscript $c(\mathbf{x})$ on the right-hand side still depends on $\mathbf{x}(t)$ *and all the* $\mathbf{m}_i^*$. The way of writing (5), however, allows us to apply the *contractive mapping method* known from the theory of nonlinear equations: starting with even coarse approximations for the $\mathbf{m}_i^*$, (2) is first utilized to find the indices $c(\mathbf{x})$ for all the $\mathbf{x}(t)$. On the basis of the approximate $h_{c(\mathbf{x}),i}$ values, the improved approximations for the $\mathbf{m}_i^*$ are computed from (5), which are then applied to

(2), whereafter the computed $c(\mathbf{x})$ are substituted into (5), and so on. The optimal solutions $\mathbf{m}_i^*$ are usually obtained in a few iteration cycles, after the discrete-valued indices $c(\mathbf{x})$ have settled down and are no longer changed in further iterations. This procedure is called the *Batch Map* principle.

An even simpler Batch Map principle is obtained if $h_{c(\mathbf{x}),i}$ is defined in terms of the neighborhood set N_c. Further we need the concept of the *Voronoi set*. It means a domain V_i in the $\mathbf{x}$ space, or actually the set of those samples $\mathbf{x}(t)$ that lie closest to $\mathbf{m}_i^*$. Let us recall that we defined N_i as the set of nodes that lie up to a certain radius from node i in the array. The union of Voronoi sets V_i corresponding to the nodes in N_i shall be denoted by U_i. Then (5) can be written

$$\mathbf{m}_i^* = \frac{\sum_{x(t)\in U_i} \mathbf{x}(t)}{n(U_i)} \quad , \tag{6.}$$

where $n(U_i)$ means the number of samples $\mathbf{x}(t)$ that belong to U_i.

Notice again that the U_i depend on the $\mathbf{m}_i^*$, and therefore (6) must be solved iteratively. The procedure can be described as the following steps:

1. Initialize the values of the $\mathbf{m}_i^*$ in some proper way. (Even random values for the $\mathbf{m}_i^*$ will usually do.)
2. Input all the $\mathbf{x}(t)$, one at a time, and list each of them under the model $\mathbf{m}_i^*$ that is closest to $\mathbf{x}(t)$ according to (2).
3. Let U_i denote the union of the above lists at model $\mathbf{m}_i^*$ and its neighbors that constitute the neighborhood N_i. Compute the means of the vectors $\mathbf{x}(t)$ in each U_i, and replace the old values of $\mathbf{m}_i^*$ by the respective means.
4. Repeat from 2 a few times until the solutions can be regarded as steady.

For the case in which neighborhood sets N_i are used,

$$\mathbf{m}_i^* = \frac{\sum_{j\in N_i} n_j \bar{\mathbf{x}}_j}{\sum_{j\in N} n_j} \quad , \tag{7.}$$

A further acceleration of computation results if one notes that for the different nodes i, the same addends occur a great number of times. It is advisable to first compute the mean $\bar{\mathbf{x}}_j$ of the $\mathbf{x}(t)$ in each Voronoi set V_j and then weight it by the number n_j of samples in V_j and the neighborhood function. Now we obtain

$$\mathbf{m}_i^* = \frac{\sum_j n_j h_{ji} \bar{\mathbf{x}}_j}{\sum_j n_j h_{ji}} \quad , \tag{8.}$$

where the sum over j is taken for all units of the SOM. A convergence and ordering proof of the Batch Map has been presented in [7].

There is a Matlab SOM Toolbox program package available on the Internet at the address http://www.cis.hut.fi/projects/somtoolbox/, which involves the Batch Map method.

A BRIEF OVERVIEW OF SOM APPLICATIONS

The four most promising application areas of the SOM are:

- analysis and control of industrial processes and machines
- various tasks in telecommunications
- exploratory data analysis and knowledge discovery in databases (KDD)
- biomedical analyses and applications.

Analysis of Processes and Machines

An industrial plant or complex machine is traditionally described in terms of physical, chemical, or other state variables, which are usually related in a highly nonlinear way. The system model, which is usually distributed, may then not be identifiable from measurements. Nonetheless there may exist much fewer characteristic states or state clusters in the system that determine its general behavior and are somehow reflected in the measurements. As the SOM is a nonlinear projection method, such characteristic states or clusters can often be made visible in the self-organizing map, without explicit modeling of the system.

Consider a system from which several discrete measurements relating to the system itself as well as to its environment are taken. These measurements and the values of the control variables may be regarded to constitute the data vector **x** used in the training of the SOM. The scale of each variable can be normalized so that either the maximum and minimum of each variable, respectively, are equal, or the variance of every variable is the same. Assume that the model vectors are $\mathbf{m}_i = [\mu_{i1}, \mu_{i2}, \ldots, \mu_{in}]^T$. The *component plane j* of the SOM is defined as the array of values μ_{ij} that represent the *j*th components of all the model vectors $\mathbf{m}_i$. The component plane can be displayed as an array of squares in the same format as the SOM array, colored with shades of gray or pseudocolors according to the values μ_{ij}.

A practical example of the use of the SOM is shown in Figure 2, where a power transformer has been analyzed [8]. In this example, the states relating to the measurements of ten variables (voltages, currents, temperatures, hydrogen content of the insulating coolant) have been followed during a period of 24 hours. The trajectory has been drawn on the component plane that displays the load current of the transformer. Dark gray tones correspond to small and light tones to heavy loads, respectively. It can be seen that the operating point has moved from dark to light areas and back again corresponding to the daytime operation of the system, when the load was switched on and off, respectively.

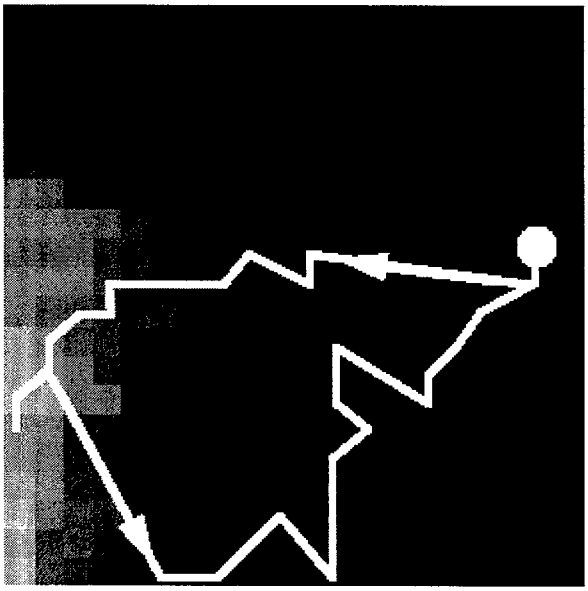


Fig. 2. Each small square represents the value of one component *j* of some model vector $\mathbf{m}_i$, in gray scale. The trajectory drawn in white describes the sequence of "winner" units on the SOM, in response to a sequence of input vectors {**x**(t)} taken over some period of time. This picture describes the load current (white: high, black: low), whereby its values can be read as a function of time from the gray-shade values along the trajectory. The form of the trajectory is defined by the sequence of states of the transformer, as a function of switching the load on and off, during 24 h of operation.

In addition to visualizing the normal operating conditions by the SOM, it would be desirable to be able to visualize *fault states*, too. The main problem thereby is where to get abnormal but still typical measurements from, in order to use them in the training of the SOM. The faults may be rare and true

measurements thus not available. In some cases, fault situations can be produced during the development and testing of the equipment, but especially in the case of industrial processes and big machines, production of a sufficient number of severe faults might be too costly. Then the faults must be simulated, and the simulated input vectors **x** used for training.

Semi-automatic Control of Industrial Processes

Traditionally, in order to be able to control a process, a global system model ought to be available, and it must be possible to place a sufficient number of transducers to places where they measure essential process variables. Typical problems are thus that the most relevant places in the process are frequently not accessible, and the most essential properties of the product may only be measurable off-line. Therefore, estimation of process or signal states is frequently made indirectly. For instance, elaborate methods such as multivariable analyses or computation of cross correlations and power spectra have been used; long series of measurements are thereby needed, and still the statistical dependencies may only be obtainable in the linear approximation.

When using the SOM, a physically or chemically definable process model is not necessary. The map is computed from normalized measurements over a training period (the map can also be made to adapt to new measurements continuously). When the display is labeled by calibration measurements, it will be possible to monitor the process state by following the trajectory of the operating point on the map. The SOM display then facilitates direct semiautomatic control of the process: the operating personnel will easily learn to spot the most effective control variables in each situation and to adjust them in such a direction that the trajectory will be guided to the allowed region in the shortest way.

Miscellaneous process applications are reported in the review article [9].

Applications to Material Science

The following stray examples have a bearing on material science studies: identification of car body steel [10], composite damage assessment [11], grading of beer quality [12], operation guidance in a blast furnace [13], shear velocity estimation [14], flow regime identification and flow rate measurement [15, 16], analysis of particle jets [17], and intrusion detection [18].

Various Tasks in Telecommunications

In *telecommunications*, one may monitor, e.g., *telephone traffic* and *communication networks* by the SOM on the basis of their statistics, but there also exist numerous tasks in the telecommunications technology for which the SOM would bring about viable solutions. One of them is the *quadrature-amplitude modulation (QAM)* in *digital communications*, especially adaptive demodulation, equalization, and intersymbol and interchannel noise cancellation in high-definition television (HDTV). Another task for which SOM solutions have so far only been demonstrated by simulation is efficient *encoding and decoding of images* by a pair of SOMs, which tolerate transmission errors much better than the more traditional vector quantization methods.

Maps of Document Collections (WEBSOM)

The basic SOM carries out a clustering in the Euclidean vector space. Surprisingly, the same vector-space clustering methods sometimes apply even to entities that are basically symbolic by their nature. We shall show in the following that it is possible to perform the clustering of free-text, natural-language documents, if their contents are described statistically by using different words in them. Document word statistics can be shown to be very powerful for the discrimination between different documents and their topic areas.

A rather old idea is to use word histograms to characterize texts. With the increasing number of documents and if no restrictions are set to their language, the vocabulary to be taken into account can be huge, e.g., in Internet documents its size may be over a million. A trivial method would be to consider histograms of the most important words only, but this requires plenty of manual work, and the discriminatory power of such representations remains low. Nonetheless it will always be a good strategy to omit the words that occur most seldom, and then it is possible to reduce the vocabulary to, say, 100 000 items. But such histograms would still correspond to real vectors of dimensionality 100 000, which is computationally very heavy.

The histograms, however, are usually very sparsely occupied: in one document one may use only, say, a few dozen to a couple hundreds of different words, depending on its length. Therefore a simple but still effective method to reduce the dimensionality of the representation vectors, without essentially decreasing their discriminatory power, is to project them randomly onto a much lower-dimensional Euclidean space. If the original histogram is denoted by vector **n**, and **R** is a rectangular matrix with random but normalized columns, the vectors $\mathbf{x} = \mathbf{Rn}$ can then have a dimensionality of, say, a couple of hundreds, and be used in place of the **n** as input data vectors to the SOM, without noticeably reducing the classification accuracy.

Without going into all computational details, the document-clustering SOM called the *WEBSOM* produces the visual display of the document collection in the following steps: 1. Some preprocessing of the texts is first carried out, removing nontextual symbols and very rare words. Eventually, a stemmer is used to transform all word forms into their most probable stem words. 2. The word histogram of each document is projected randomly onto a space of dimensionality 300 to 500, thereby obtaining a representation vector **x** for each document. 3. A SOM is formed using the **x** as input data. 4. The models $\mathbf{m}_i$ formed at the nodes of the SOM are labeled by all those documents that are mapped onto the said node. In practice, the nodes are linked to the proper document data base by address pointers (indexing). 5. Standard browsing software tools are used to read the documents mapped to the SOM nodes.

It is possible to use a "key document," or alternatively, a set of keywords as a search argument to find the best-matching node of the SOM, where browsing may begin.

An example of HTML pages found in browsing is given in Fig. 3.

We have already implemented WEBSOM systems for the following applications:

- Internet Usenet newsgroups; the largest experiment consisted of 85 newsgroups, with a total of over 1 million documents. The size of the SOM was thereby 104 448 nodes.
- News bulletins (in Finnish) of the Finnish News Agency (Finnish Reuter).
- Patent abstracts (English) that are available in electronic form. The largest demonstration, being finished during the writing of this report, consists of seven million patent abstracts from the U.S., Japan and European patent offices and the SOM array consists of 1 002 240 nodes.

Demonstrations of various WEBSOM displays are available on the Internet at the address http://websom.hut.fi/websom/, where they can be browsed with standard www browsers.

Other Major Application Areas of the SOM

Applications to *medicine* have barely started to spread. In the analysis of *brain signals*, EEG and MEG, it has been possible to classify various waking and sleep states on the SOM. Various *biochemical analyses* and interpretation of results in *clinical chemistry* already use SOM methods that have been transferred to practice. An important mode of use of the SOM is the *profiling of patients* for their diagnosis and treatment.

In addition to the four main areas mentioned above, one may report numerous tasks in *finance*, ranging from the analysis and prediction of time series to the classification and evaluation of macroeconomic systems. We have cooperated with the World Bank, analyzing their socioeconomic data in many ways [19]. Analyses of financial performance [20] and bankrupts [21] of companies are being made using the SOM method. The reform of the Finnish *forest taxation* in 1992, i.e., an option given to the owners to choose between two taxation policies, was based on a cluster analysis made by the SOM method.

One also ought to mention the following examples from other fields of science. The Finnish meteorological institute has used the SOM to *classify clouds* [22] from infra-red satellite images (especially at nighttime), and in the USA, astronomical data produced by the *Hubble space telescope* [23] have been analyzed; an earlier unknown classification of thousands of galaxies at moderate red shifts has thereby emerged.

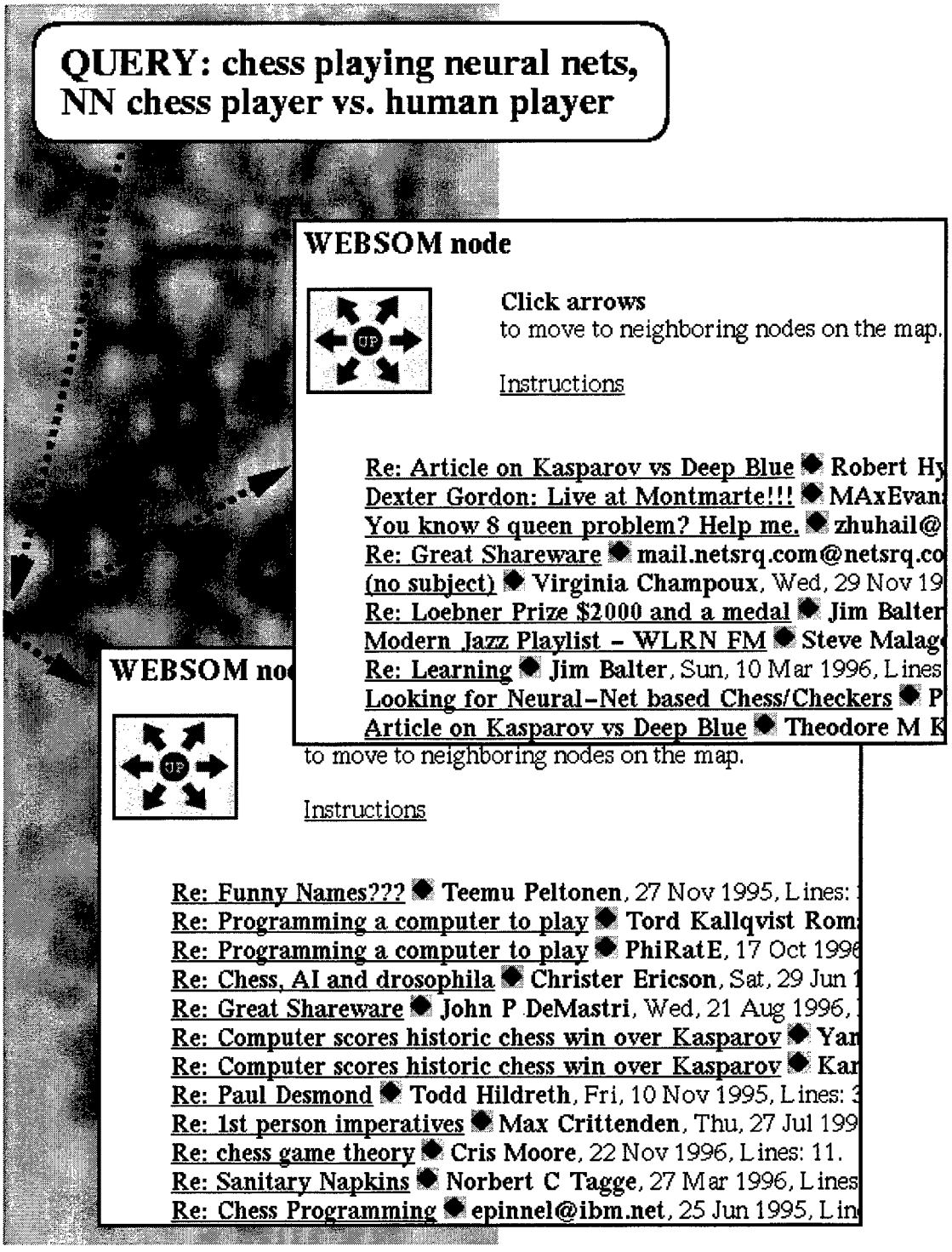


Fig. 3. Content-addressable search from a 1 124 134-document WEBSOM. The contents of two adjacent nodes are shown.

It is not possible to survey the whole range of applications of the SOM method in more detail in this paper. Let it suffice to refer to the list of 3343 research papers on the SOM [24] that is also available at the Internet address http://www.icsi.berkeley.edu/~jagota/NCS/vol1.html.

REFERENCES

1. T. Kohonen, 1995. *Self-organizing maps*. Series in Information Sci., 30. Springer, Heidelberg. 2nd Ed. 1997.
2. M. Cottrell, J. C. Fort, and G. Pagès, 1997. Theoretical aspects of the SOM algorithm. *Proc. WSOM97, Workshop on Self-Organizing Maps* , Espoo, Finland, 246-267.
3. T. Hastie and W. Stuetzle, 1989. Principal curves. *J. Am. Stat. Assoc.*, 84, 502-516.
4. C. Bishop, M. Svensen, and C. Williams, 1996. GTM: a principled alternative to the self-organizing map. In *Artificial Neural Networks - ICANN 96, 1996 Int. Conf. Proc.*, C. v.d. Malsburg, W. von Seelen, J. Vorbruggen, and B. Sendhoff, Eds., pp. 165-7. Springer-Verlag, Berlin.
5. T. Kohonen, J. Hynninen, J. Kangas, and J. Laaksonen, 1996. SOM_PAK: The self-organizing map program package. Helsinki University of Technology, Laboratory of Computer and Information Science, Espoo, Finland, Report A31.
6. T. Kohonen, 1999. Fast evolutionary learning with batch-type self-organizing maps. *Neural Process. Lett.*, in press.
7. Y. Cheng, 1997. Convergence and ordering of Kohonen's batch map. *Neural Comput.*, 9, 1667-1676.
8. M. Kasslin, J. Kangas, and O. Simula, 1992. Process state monitoring using self-organizing maps. in *Artificial Neural Networks*, I. Aleksander, J. Taylor, Eds., 2, 1532-1534. North-Holland, Amsterdam.
9. T. Kohonen, E. Oja, O. Simula, A. Visa, and J. Kangas, 1996. Engineering applications of the self-organizing map. *Proc. IEEE*, 84(10), 1358-1384.
10. W. Kessler, D. Ende, R.W. Kessler, and W. Rosenstiel, 1993. Identification of car body steel by an optical on line system and Kohonen's self-organizing map. *Proc. ICANN93, Int. Conf. on Artificial Neural Networks*, S. Gielen and B. Kappen, Eds., p. 860. Springer, London.
11. B. Grossman, X. Gao, and M. Thursby, 1991. Composite damage assessment employing an optical neural network processor and an embedded fiber optic sensor array. *Proc. SPIE - Int. Soc. for Opt. Eng.*, 1588, 64-75.
12. Y. Cai, 1994. The application of the artificial neural network in the grading of beer quality. *Proc. WCNN94* , 1, 516-520. Lawrence Erlbaum, Hillsdale, NJ.
13. M. Konishi, Y. Otsuka, K. Matsuda, N. Tamura, A. Fuki, and K. Kadoguchi, 1990. Application of neural network to operation guidance in blast furnace. *Third European Seminar on Neural Computing: The Marketplace*, 13. IBC Tech. Services, London.
14. P. Burrascano, P. Lucci, G. Martinelli, and R. Perfetti, 1990. Shear velocity estimation by the combined use of supervised and unsupervised neural networks. *Proc. ICASSP-90, Int. Conf. on Acoustics, Speech and Signal Processing*, IV, 1921-1924. IEEE, Piscataway, NJ.
15. S. Cai, H. Toral, and J. Qiu, 1993. Flow regime identification by a self-organizing neural network. *Proc. ICANN93, Int. Conf. on ANNs* , S. Gielen, B. Kappen, Eds., 868. Springer, London.
16. S. Cai and H. Toral, 1993. Flowrate measurement in air-water horizontal pipeline by neural network. *Proc. IJCNN-93, Int. Joint Conf. on Neural Nets, Nagoya*, II, 2013-2016. IEEE, Piscataway, NJ.
17. K.H. Becks, J. Dahm, and F. Seidel, 1992. Analysing particle jets with artificial neural networks. *Industrial and Engineering Applications of Artificial Intelligence and Expert Systems, 5th Int. Conf. IEA/AIE-92*, F. Belli and F.J. Radermacher, Eds., 109-112. Springer, Berlin, Heidelberg.
18. K.L. Fox, R.R. Henning, J.H. Reed, and R.P. Simonian, 1990. A neural network approach towards intrusion detection. *Proc. 13th National Computer Security Conference. Information Systems Security. Standards - The Key to the Future*, I, 124-134. NIST, Gaithesburg, MD.
19. G. Deboeck and T. Kohonen, Eds. 1998. *Visual Exploration in Finance with Self-Organizing Maps*. Springer-Verlag, London.
20. B. Back, K. Sere, and H. Vanharanta, 1997. Analyzing financial performance with self-organizing maps. *Proc. WSOM97, Workshop on Self-Organizing Maps* , Espoo, Finland, 356-361.
21. K. Kiviluoto, 1998. Predicting bankruptcies with the self-organizing map. *Neurocomput.*, 21, 191-201.
22. A. Visa, K. Valkealahti, J. Iivarinen, and O. Simula, 1991. Experiences from operational cloud classifier based on self-organizing map. In *Proc. SPIE - The Int. Society for Optical Engineering, Applications of Artificial Neural Networks V*, 2243, 484-495.
23. A. Naim, K. U. Ratnatunga, and R. E. Griffiths, 1997. Galaxy morphology without classification: Self-organizing maps. *Astrophys. J. Suppl. Series*, 111, 357-367.
24. S. Kaski, J. Kangas, and T. Kohonen, 1998. Bibliography of self-organizing map (SOM) papers: 1981-1997. *Neural Computing Surveys*, 1(3&4), 1-176. http://www.icsi.berkeley.edu/~jagota/NCS/vol1.html

Rough Set Theory for Intelligent Industrial Applications

Zdzislaw Pawlak

Institute of Theoretical and Applied Informatics,
Polish Academy of Sciences, Poland
Email: zpw@ii.pw.edu.pl

ABSTRACT

Application of intelligent methods in industry has become a very challenging issue nowadays and will be of extreme importance in the future. Intelligent methods include fuzzy sets, neural networks, genetic algorithms and other techniques known as soft computing. No doubt, rough set theory can also contribute to this domain. In this paper basic ideas of rough set theory are presented and some possible intelligent industrial applications outlined.

INTRODUCTION

Rough set theory is a new mathematical approach to data analysis. The basic idea of this method hinges on classifying objects of interest into similarity classes (clusters) containing objects which are indiscernible with respect to some features, e.g., color, temperature, etc. which form basic building blocks of knowledge about reality and are employed to find hidden patterns in data. The basis of rough set theory is found in [20,22,26].

Rough set theory has some overlap with other methods of data analysis, e.g., statistics, cluster analysis, fuzzy sets, evidence theory and others, but it can be viewed in its own right as an independent discipline. The rough set approach seems to be fundamental to AI and cognitive sciences, especially in the areas of machine learning, knowledge acquisition, decision analysis, knowledge discovery from databases, expert systems, inductive reasoning and pattern recognition. It seems particularly important in decision support systems and data mining.

Rough set theory has been successfully applied to solve many real-life problems in medicine, pharmacology, engineering, banking, financial and market analysis and others. More about applications of rough set theory can be found in [9,17,19,26,28,35,40] and others. Very promising areas of new applications for rough sets are expected to emerge in the near future. These include rough control, rough data bases, rough information retrieval, rough neural networks and others.

ROUGH SETS AND INTELLIGENT INDUSTRIAL APPLICATIONS

Artificial intelligence approach to industrial processes is real challenge for industry in the years to come. Rough set theory seems to be particularly suited for problem solving in this area. Some examples are:

1) Material sciences. Application of rough sets to new materials design and investigating material properties has already shown the usefulness of the theory in this area. Pioneer work in this domain is due to Jackson et al [4,5,6]. It is also interesting to note the work on applying rough sets to investigate the relationship between structure and activity of drugs [28]. The method used can be also applied to any other type of materials.
2) Intelligent control. Industrial process control in many cases, especially highly non-linear systems, cannot be treated successfully with classical control theory methods. It turns out that in this case fuzzy sets, neural networks, genetic algorithms offer very good solutions. Also rough sets can be used here in many cases. Cement kiln control algorithms obtained from observation of stoker actions and blast furnace control in iron and steel works are exemplary applications of rough set techniques in intelligent industrial control [11]. Satellite attitude control [25] is another non-trivial example of the application of rough set theory in

0-7803-5489-3/99/$10.00 ©1999 IEEE.

intelligent control. More on applications of this theory in control can be found in [3,8,12,13,17,23,33,34,39, 41,42,43]. The rough set approach in control offers simple and fast algorithms, which can be obtained either from observation of the controlled process or mathematical model of the process or a knowledgeable expert.

3) Decision support systems. Rough set based decision support systems can be used for many kinds of industrial decision-making on various levels, from specific industrial processes to management and business decisions [28,29,30].
4) Machine diagnosis. The rough set approach has been used to provide technical diagnosis of mechanical objects by analysing vibroacoustics symptoms [14,15,16,31,32].
5) Neural networks. Neural networks have found many interesting applications in intelligent control of industrial processes. Combining neural networks with fuzzy sets adds new dimension to this domain. Rough sets and neural networks can be also linked together and give better results and greater speed than the classical neural network approach alone. Besides, an interesting idea of *rough neural network* has been proposed in [10]. More about rough sets and neural networks can be found in references given in [26].
6) Varia. Besides the above domains of intelligent industrial applications of rough sets there are many other fields where rough set approach can be useful [1,2,7,19,26,35,37,38,43].

The above discussed list of possible applications of rough sets is of course not exhaustive but shows areas where application of rough set has already proved to be of use.

The rough set approach has many advantages. The most important ones are listed below.

- Provides efficient algorithms for finding hidden patterns in data.
- Identifies relationships that would not be found while using statistical methods.
- Allows both qualitative and quantitative data.
- Finds minimal sets of data (data reduction).
- Evaluates significance of data.
- Generates sets of decision rules from data.
- It is easy to understand.
- Offers straightforward interpretation of obtained results.

No doubt rough set theory can be used in many branches of intelligent industrial applications as an independent, complementary approach or combined with other areas of soft computing, e.g. fuzzy sets, neural networks, etc.

APPROXIMATIONS – BASIC CONCEPTS OF ROUGH SET THEORY

Data are usually given in a form of a *data table*, called also *attribute-value table, information table or database*. A database is a table, rows of which are labeled by *objects*, whereas columns are labeled by *attributes*. Entries of the table are *attribute values*. An example of a database is shown in Table 1.

Table 1. An attribute-value table of data.

Store	*E*	*Q*	*L*	*P*
1	*high*	*good*	*no*	*profit*
2	*med.*	*good*	*no*	*loss*
3	*med.*	*good*	*no*	*profit*
4	*no*	*avg.*	*no*	*loss*
5	*med.*	*avg.*	*yes*	*loss*
6	*high*	*avg.*	*yes*	*profit*

In the database six stores are characterized by four attributes:

E – empowerment of sales personnel,
Q – perceived quality of merchandises,
L – high traffic location,
P – store profit or loss.

Each subset of attributes in the database determines a partition of all objects into clusters having the same attribute values, i.e., displaying the same features expressed in terms of attribute values. In other words, all objects revealing the same features are *indiscernible* (*similar*) in view of the available information and they form blocks, which can be understood as elementary granules of knowledge. These granules are called *elementary sets* or *concepts*, and can be considered as elementary building blocks (atoms) of our knowledge about the reality we are interested in. Elementary concepts can be combined into *compound concepts*, i.e., concepts that are uniquely defined in terms of elementary concepts. Any union of elementary sets is called a *crisp set*, and any other set is referred to as *rough* (*vague*, *imprecise*).

With every set X we can associate two crisp sets, called the *lower* and the *upper approximation* of X. The lower approximation of X is the union of all elementary sets which are included in X, whereas the upper approximation of X is the union of all elementary sets which have non-empty intersection with X. In other words, the lower approximation of a set is the set of all elements that *surely* belong to X, whereas the upper approximation of X is the set of all elements that *possibly* belong to X. The difference between the upper and the lower approximations of X is its *boundary region*. Obviously a set is rough if it has non-empty boundary regions; otherwise the set is crisp. Elements of the boundary region cannot be classified employing the available knowledge, either to the set or its complement. Approximations of sets are basic operations in rough set theory and are used as main tools to deal with vague and uncertain data. Let us illustrate the above ideas by means of data given in Table 1.

Each store has a different description in terms of attributes E, Q, L and P, thus all stores are discernible when employing information provided by all attributes. However, stores 2 and 3 are indiscernible in terms of attributes E, Q and L, since they have the same attribute values. Similarly, stores 1, 2 and 3 are indiscernible with respect to attributes Q and L, etc.

Each subset of attributes determines a partition (classification) of all objects into classes having the same description in terms of these attributes. For example, attributes Q and L aggregate all stores into the following classes $\{1, 2, 3\}$, $\{4\}$, $\{5, 6\}$. Thus, each database determines a family of classification patterns which are used for further considerations.

Let us consider the following problem: what are the characteristic features of stores making a profit (or having a loss) in view of information available in Table 1, i.e., we want to describe a set (concept) $\{1, 3, 6\}$ (or $\{2, 4, 5\}$) in terms of attributes E, Q and L. Of course this question cannot be answered uniquely since stores 2 and 3 have the same values of attributes E, Q and L, but store 2 makes a profit, whereas store 3 has a loss. Hence in view of information contained in Table 1, we can say for sure that stores 1 and 6 make a profit, stores 4 and 5 have a loss, whereas stores 2 and 3 cannot be classified as making a profit or having a loss. That is, employing attributes E, Q and L, we can say that stores 1 and 6 *surely* make a profit, i.e., *surely* belong to the set $\{1, 3, 6\}$, whereas stores 1, 2, 3 and 6 *possibly* make a profit, i.e., *possibly* belong to the set$\{1, 3, 6\}$. We say that the set $\{1, 6\}$ is the *lower approximation* of the set (concept) $\{1, 3, 6\}$, and the set $\{1, 2, 3, 6\}$ is the *upper approximation* of the set $\{1, 3, 6\}$. The set $\{2, 3\}$, being the difference between the upper approximation and the lower approximation is referred to as the *boundary region* of the set $\{1, 3, 6\}$.

Now let us give some formal notations and definitions.

By a *database*, we understand a pair $S = (U, A)$, where U and A, are finite, non-empty sets called the *universe*, and a set of *attributes* respectively. With every attribute $a \in A$, we associate a set V_a of its *values*, called the *domain* of a. Any subset B of A determines a binary relation $I(B)$ on U, which is called an *indiscernibility relation*, defined as follows:

$$(x, y) \in I(B) \text{ if and only if } a(x) = a(y)$$

for every $a \in A$, where $a(x)$ denotes the value of an attribute a of element x.

It can easily be seen that $I(B)$ is an equivalence relation. The family of all equivalence classes of $I(B)$, i.e., the partition determined by B, is denoted by $U/I(B)$, or simple U/B; an equivalence class of $I(B)$, i.e., the block of the partition U/B containing x is denoted by $B(x)$.

If (x, y) belongs to $I(B)$ we say that x and y are *B-indiscernible*. Equivalence classes of the relation $I(B)$ (or blocks of the partition U/B) are referred to as *B-elementary sets* or *B-granules*.

Next, the indiscernibility relation is used to define two basic operations in rough set theory as follows:

$$B_*(X) = \bigcup_{x \in U} \{B(x) : B(x) \subseteq X\},$$

$$B^*(X) = \bigcup_{x \in U} \{B(x) : B(x) \cap X \neq \emptyset\},$$

and are called the *B-lower* and the *B-upper approximation* of X, respectively.

The set

$$BN_B(X) = B^*(X) - B_*(X)$$

is referred to as the *B-boundary region* of X. If the boundary region of X is the empty set, i.e., $BN_B(X) = \emptyset$, then the set X is *crisp* (*exact*) with respect to B; in the opposite case, i.e., if $BN_B(X) \neq \emptyset$, the set X is referred to as *rough* (*inexact*) with respect to B.

DEPENDENCY ATTRIBUTES

Approximations of sets are strictly related with the concept of dependency (total or partial) of attributes.

Suppose the set of attributes A is partitioned into two disjoint subsets C and D called *condition* and *decision* attributes, respectively. Databases with distinguished condition and decision attributes are referred to as *decision tables*.

Intuitively, a set of decision attributes D *depends totally* on a set of condition attributes C, denoted $C \Rightarrow D$, if all values of decision attributes are uniquely determined by values of condition attributes. In other words, D depends totally on C, if there exists a functional dependency between values of C and D.

We also need a more general concept of dependency of attributes, called the *partial dependency* of attributes. Partial dependency means that only some values of D are determined by values of C. Formally dependency can be defined in the following way:

Let C and D be subsets of A, such that $D \cap C \neq \emptyset$ and $D \cup C = A$.

We say that D *depends on C in a degree* $k\ (0 \leq k \leq 1)$, denoted $C \Rightarrow_k D$, if

$$k = \gamma(C, D) = \sum_{X \in U/D} \frac{card(C_*(X))}{card(U)},$$

where *card* (X) is the cardinality of X.

If $k = 1$ we say that D *depends totally* on C, and if $k < 1$, we say that D *depends partially* (*in a degree k*) on C.

The coefficient k expresses the ratio of all elements of the universe, which can be properly classified to the block of the partition U/D employing attributes C and is called the *degree of the dependency*.

For example, the attribute P depends on the set of attributes $\{E, Q, L\}$ in the degree 2/3. That means that only four of six stores can be identified exactly by means of attributes E, Q and L as having a loss or making a profit.

REDUCTION OF ATTRIBUTES

We often face the question of whether we can remove some data from a database preserving its basic properties, i.e., whether a table contains some superfluous data.

Let us express this idea more precisely:

Let $C, D \subseteq A$, be sets of condition and decision attributes, respectively. We say that $C' \subseteq C$ is a *D-reduct* (reduct with *respect* to *D*) of *C*, if C' is a minimal subset of *C* such that

$$\gamma\left(C,D\right)=\gamma\left(C',D\right).$$

Hence any reduct enables us to reduce condition attributes in such a way that the degree of dependency between condition and decision attributes is preserved. In other words reduction of condition attributes gives the minimal number of conditions necessary to make specified decisions.

In the database presented in Table 1 $\{E, Q\}$ and $\{E, L\}$ are the only two reducts of condition attributes with respect to *P*, i.e., either the set $\{E, Q\}$ or the set $\{E, L\}$ can be used to classify stores instead of the whole set of condition attributes $\{E, Q, L\}$.

For large databases finding reducts on the basis of the definition given above is rather difficult because the definition leads to inefficient algorithms. Therefore more efficient methods of reduct computation have been proposed. For details see references in [26].

DECISION RULES

Every dependency $C \Rightarrow_k D$ can be described by a set of decision rules in the form *"If ... then"*, written $\Phi \rightarrow \Psi$, where Φ and Ψ are logical formulas describing *conditions* and *decisions* of the rule respectively, and are built up from elementary formulas (*attribute, value*) combined together by means of propositional connectives *"and"*, *"or"* and *"not"* in the standard way.

An example of a decision rule is given below:

if (*E,med.*) *and* (*Q, good*) *and* (*L,no*) *then* (*P,loss*).

With every decision rule $\Phi \rightarrow \Psi$, we associate a conditional probability that Ψ is true in *S*, given Φ is true in *S* with the probability $\pi_S(\Phi)$ called a *certainty factor* and defined as follows:

$$\pi_S\left(\Psi \mid \Phi\right)=\frac{card\left(|\Phi \wedge \Psi|_S\right)}{card\left(|\Phi|_S\right)},$$

where $|\Phi|_S$ denotes the set of all objects satisfying Φ in *S*.

As well, we need a *coverage factor* [36]

$$\pi_S(\Phi \mid \Psi)=\frac{card\left(|\Phi \wedge \Psi|_S\right)}{card\left(|\Psi|_S\right)},$$

which is the conditional probability that Φ is true in *S*, given Ψ is true in *S* with the probability $\pi_S(\Psi)$.

For the decision rule given above the certainty and coverage factors are 1/2 and 1/3, respectively, i.e., the probability that the decision made by the decision rule is correct equals 1/2 and the rule covers one of the three decisions indicated by the rule.

Let $\{\Phi_i \rightarrow \Psi\}_n$ be a set of decision rules such that all conditions Φ_i are pairwise mutually exclusive, i.e., $|\Phi_i \wedge \Phi_j|_S = \varnothing$, for any $1 \leq i,j \leq n$, $i \neq j$, and

$$\sum_{i=1}^{n} \pi_S(\Phi_i|\Psi) = 1.$$

For any decision rule $\Phi \rightarrow \Psi$ the following is true:

$$\pi_S(\Phi|\Psi) = \frac{\pi_S(\Psi|\Phi) \cdot \pi_S(\Phi)}{\sum_{i=1}^{n} \pi_S(\Psi|\Phi_i) \cdot \pi_S(\Phi_i)}.$$

The relationship between the certainty factor and the coverage factor, expressed by this formula is the Bayes' theorem. The formula shows that any decision table satisfies Bayes' theorem. This property gives a new dimension to Baysian reasoning methods and enables us to discover relationships in data without referring to prior and posterior probabilities inherently associated with Bayesian philosophy. The above result is of special value for large databases.

CONCLUSION

Rough set theory proves to be a very well suited candidate, besides fuzzy sets, neural networks and other soft computing methods, for intelligent industrial applications. Particularly challenging areas of applications of rough sets in industrial environment are material science, intelligent control, machine diagnosis and decision support.

The rough set approach has many advantages, e.g., it identifies relationships that would not be found using statistical methods, allows both qualitative and quantitative data and offers straightforward interpretation of obtained results. Despite many successful applications of rough sets in industry, there are still problems which require further research. In particular, development of suitable, widely-accessible software dedicated to industrial applications as well as microprocessors based on rough set theory are badly needed.

REFERENCES

1. A. An, C. Chan, N. Shan, N. Cercone, W. Ziarko, 1997. Applying knowledge discovery to predict water-supply consumption. IEEE Expert, 12(4), 72-78.
2. T. Arciszewski, W. Ziarko, 1990. Inductive learning in civil engineering: rough sets approach. Microcomputers and Civil Engineering, 5(1).
3. E. Czogala, A. Mrozek, Z. Pawlak, 1995. The idea of rough-fuzzy controller. International Journal of Fuzzy Sets and Systems, 72, 61-63.
4. A.G. Jackson, M. Ohmer, H. Al-Kamhawi, 1994. Rough sets analysis of chalcopyrite semiconductor band gap data. In: T. Y. Lin (ed.), The Third International Workshop on Rough Sets and Soft Computing Proceedings (RSSC'94), November 10-12, San Jose State University, San Jose, California, USA, 408-417.
5. A.G. Jackson, S.R. Leclair, M.C. Ohmer, W. Ziarko, H. Al-Kamhwi, 1996. Rough sets applied to material data. Acta Metallurgica et Materialia, 4475.
6. A.G. Jackson, Z. Pawlak, S.R. Leclair, Rough set and discovery of new materials. J. of Alloys and Comp. (in press).
7. W. Kowalczyk, 1996. Analyzing temporal patterns with rough sets. In: EUFIT-96: The fourth European Congress on Intelligent Techniques and Soft Computing, September 2-5, Aachen, 139-143.
8. T.Y. Lin, 1997. Fuzzy controllers: an integrated approach based on fuzzy logic, rough sets, and evolutionary computing. in: T. Y. Lin and N. Cercone (eds.), Rough Sets and Data Mining. Analysis for Imprecise Data, Kluwer Academic Publishers, Boston, London, Dordrecht, 123-138.
9. T.Y. Lin, N. Cercone, (eds.), 1997. Rough Sets and Data Mining – Analysis of Imperfect Data, Kluwer Academic Publishers, Boston, London, Dordrecht, 430.

10. P. Lingras, 1996. Rough neural networks. Sixth International Conferences, InformationProcesing and Management of Uncertainty in Knowledge-Based Systems, Proceedings (IPMU'96), Volume II, July 1-5, Grenada, 1445-1450.
11. A. Mrozek, 1992. Rough sets in computer implementation of rule-based control of industrial processes. In: R. Slowinski (ed.), Intelligent Decision Support. Handbook of Applications and Advances of the Rough Set Theory. Kluwer Academic Publishers, Boston, London, Dordrecht, 19-31.
12. T. Munakata, 1997. Rough control: a perspective. In: T. Y. Lin and N. Cercone (eds.), Rough Sets and Data Mining. Analysis for Imprecise Data. Kluwer Academic Pub., Boston, London, Dordrecht, 77-88.
13. T. Munakata, 1998. Fundamentals of the New Artificial Intelligence. Springer, 231.
14. R. Nowicki R. Slowinski, J. Stefanowski, 1990. Possibilities of appling the rough sets theory to technical diagnostics. In: Proceedings of the IXth National Symposium on Vibration Techniques and Vibroacoustics, December 12-14, AGH University Press, Kraków, 149-152.
15. R. Nowicki, R. Slowinski, J. Stefanowski, 1992. Rough sets analysis of diagnostic capacity of vibroacoustic symptoms. Journal of Computers and Mathematics with Applications, 24(2), 109-123.
16. R. Nowicki, R. Slowinski, J. Stefanowski, 1992. Evaluation of vibroacoustic diagnostic symptoms by means of the rough sets theory. Journal of Computers in Industry, 20, 141-152.
17. A. Oehrn, 1993. Rough logic control. In: (Project), Technical Report. Knowledge Systems Group, The Norwegian University of Science and Technology, Trondheim, Norway.
18. E. Orlowska (ed.), 1997. Incomplete Information: Rough Set Analysis. Physica-Verlag, Heidelberg.
19. S.K. Pal, A. Skowron (eds.): Fuzzy Sets, Rough Sets and Decision Making Processes.Springer--Verlag, Singapore (in preparation)
20. Z. Pawlak, 1991. Rough Sets - Theoretical Aspects of Reasoning about Data. Kluwer Academic Publishers, Boston, London, Dordrecht, 229.
21. Z. Pawlak, 1998. Rough set theory and its applications to data analysis. Cybernetics & Syst., 29, 661-688.
22. Z. Pawlak, J, Grzymala-Busse, R. Slowinski, W. Ziarko, 1995. Rough sets. Commun. of ACM, 38, 88-95.
23. Z. Pawlak, T. Munakata, 1996. Rough control application of rough set theory to control. Fourth European Congress on Intelligent Techniques and Soft Computing, Proceedings EUFIT'96, I, 209-218.
24. Z. Pawlak, 1998. Reasoning about data – a rough set perspective. In: L. Polkowski, A. Skowron (eds.), Rough Sets and Current Trends in Computing, Lecture Notes in Artificial Intelligence, 1424 Springer, First International Conference, RSCTC' 98, Warsaw, Poland, June, Proceedings, 25-34.
25. J.F. Peters, K. Ziaei, S. Ramanna, 1998. Approximate time rough control: Concepts and application to satellite attitude control. In: L. Polkowski, A. Skowron (eds.), Rough Sets and Current Trends in Computing, Lecture Notes in Artificial Intelligence, 1424 Springer, First International Conference, RSCTC' 98, Warsaw, Poland, June, Proceedings, 491-498.
26. L. Polkowski, A. Skowron (eds.), 1998. Rough Sets in Knowledge Discovery, Physica-Verlag, 1(2).
27. L. Polkowski, A. Skowron (eds.), 1998. Rough Sets and Current Trends in Computing, Lecture Notes in Artificial Intelligence, 1424 Springer, Proc..1st International Conference, RSCTC'98, Warsaw.
28. R. Slowinski, 1992. Intelligent Decision Support. Handbook of Applications and Advances of the Rough Set Theory. Kluwer Academic Publishers, Boston, London, Dordrecht.
29. R. Slowinski, 1995. Rough set approach to decision analysis. AI Expert, 10, 18-25.
30. R. Slowinski, 1995. Rough set theory and its applications to decision aid. Belgian Journal of Operation Research, Special Issue Francoro, 35(3-4), 81-90.
31. R. Slowinski, J. Stefanowski, R. Susmaga, 1996. Rough set analysis of attribute dependencies in technical diagnostics. In: S. Tsumoto, S. Kobayashi, T. Yokomori, H. Tanaka and A. Nakamura (eds.), The fourth International Workshop on Rough Sets, Fuzzy Sets, and Machnine Discovery, Proceedings (RS96FD), November 6-8, The University of Tokyo, 284-291.
32. J. Stefanowski, R. Slowinski, R. Nowicki, 1992. The rough sets approach to knowledge analysis for classification support in technical diagnostics of mechanical objects. In: F. Belli and F. J. Radermacher (eds.), Industrial & Engineering Applications of Artificial Intelligence and Expert Systems. Lecture Notes in Economics and Mathematical Systems 604, Springer-Verlag, Berlin, 324-334.
33. A. Szladow, W. Ziarko, 1993. Adaptive process control using rough sets. Proceedings of the International Conference of Instrument Society of America, ISA/93, Chicago, 1421-1430.
34. A. Szladow, W. Ziarko, 1993. Application of rough sets theory to process control. Proceedings of Calgary 93 Symposium of Instrument Society of America, Calgary.

35. S. Tsumoto, S. Kobayashi, T. Yokomori, H. Tanaka, A. Nakamura, (eds.), 1996. The Fourth Internal Workshop on Rough Sets, Fuzzy Sets and Machine Discovery, Proceedings. The University of Tokyo.
36. S. Tsumoto, 1998. Modelling medical diagnostic rules based on rough sets. In: L. Polkowski, A. Skowron (eds.), Rough Sets and Current Trends in Computing, Lecture Notes in Artificial Intelligence, 1424 Springer, First International Conference, RSCTC' 98, Warsaw, Poland, June, Proceedings, 475-482.
37. P.P. Wang, (ed.), 1995. Second Annual Joint Conference on Information Sciences, Proceedings. Wrightsville Beach, North Carolina, USA.
38. P. Wang, (ed.), 1997. Joint Conference of Information Sciences, Vol. 3. Rough Sets and Computer Sciences, Duke University, Ga., USA.
39. W. Ziarko, 1992. Acquisition of control algorithms from operation data. In: R. Slowinski (ed.), Intelligent Decision Support, Handbook of Applications and Advances of the Rough Set Theory, Kluwer Academic Publishers, Boston, London, Dordrecht, 61-75.
40. W. Ziarko, (ed.), 1993. Rough Sets, Fuzzy Sets and Knowledge Discovery. Proceedings of the International Workshop on Rough Sets and Knowledge Discovery (RSKD'93), Banff, Alberta, Canada, October 12-15, Springer-Verlag, Berlin.
41. W. Ziarko, J. Katzberg, 1989. Control algorithms acquisition, analysis and reduction: machine learning approach. in: Knowledge-Based Systems Diagnosis, Supervision & Control, Plenum Press, Oxford, 167-78.
42. W. Ziarko, J. Katzberg, 1993. Rough sets approach to system modelling and control algorithm acquisition. Proceedings of IEEE WESCANEX 93 Conference, Saskatoon, 154-163.
43. J. Zak, J. Stefanowski, 1994. Determining maintenance activities of motor vehicles using rough sets aproach. in: Proceedings of Euromaintenance'94 Conference, Amsterdam, 39-42.

From Fuzzy Set Theory to Computational Intelligence – Special European Experiences

H.-J. Zimmermann

Aachen University of Technology, Institute of Operations Research, Aachen, Germany

ABSTRACT

Even though the first publication in the area of Fuzzy Set Theory (FST) appeared already in 1965, the development of this theory for almost 20 years remained in the academic realm. Almost all basic concepts, theories and methods were, however, developed during this period.

Fuzzy Control opened the gate to real applications for FST. Particularly in Japan the applications of the fuzzy control principle in consumer goods made FST known in the public and made it commercially interesting for industry. This lead to two developments: since the development of fuzzy applicational systems had to be efficient, fuzzy CASE tools and expert system shells were developed making FST to Fuzzy Technology. The success in Japan could draw the attention of the media and started – first in Germany – the "Fuzzy Booms", which lead to an unprecedented growth in publications, university teaching and other industrial applications in many countries.

Around 1993 FST, Neural Nets and Evolutionary Computing joint forces and were soon considered to be one area called Soft Computing or Computational Intelligence. Applications in Engineering as well as in Management will be described during the presentation. Of particular interest for Europe might also be the development of ERUDIT (European Network of Excellence for Fuzzy Sets and Uncertainty Modeling), a network which grew from 15 nodes in 1995 to 250 nodes in 1997 and which has just been extended for another two years by the European Commission. Details about possibilities in the framework of ERUDIT will also be described in more detail.

HISTORICAL DEVELOPMENT

Fuzzy Set Theory, Fuzzy Technology and Computational Intelligence

Fuzzy Set Theory was conceived in 1965 as a formal theory which could be considered as a generalization of either classical set theory or of classical dual logic. In spite of the fact that Prof. Zadeh when publishing his first contribution had already some applications in mind Fuzzy Set Theory for several reasons kept inside the academic sphere for more than 20 years. During these 20 years most of the basic concepts which are nowadays used very successfully have already been invented. Starting at the beginning of the 80s Japan was the leader in using a smaller part of Fuzzy Set Theory - namely fuzzy control - for practical applications. Particularly improved consumer goods such as video cameras with fuzzy stabilizers, washing machines including fuzzy control, rice-cookers etc. caught the interest of the media which led around 1989/1990 to the first "fuzzy boom" in Germany. Many attractive practical applications - not so much in the area of consumer goods but rather in automation and industrial control - led to the insight that the efficient and affordable use of this approach could only be achieved via CASE-tools. Hence, since the late 80s a large number of very user-friendly tools for fuzzy control, fuzzy expert systems, fuzzy data analysis etc. has emerged. This really changed the character of this area and started to my mind the area of **"Fuzzy Technology"**. The next - and so far the last - large step in the development occurred in 1992 when almost independently in Europe, Japan and the USA the three areas of Fuzzy Technology, artificial neural nets and genetic algorithms joined forces under the title of **"computational intelligence"** or **"soft computing"**. The synergies which were possible between these three areas have been exploited since very successfully. The figure 1 shows these developments as a summary.

0-7803-5489-3/99/$10.00 ©1999 IEEE.

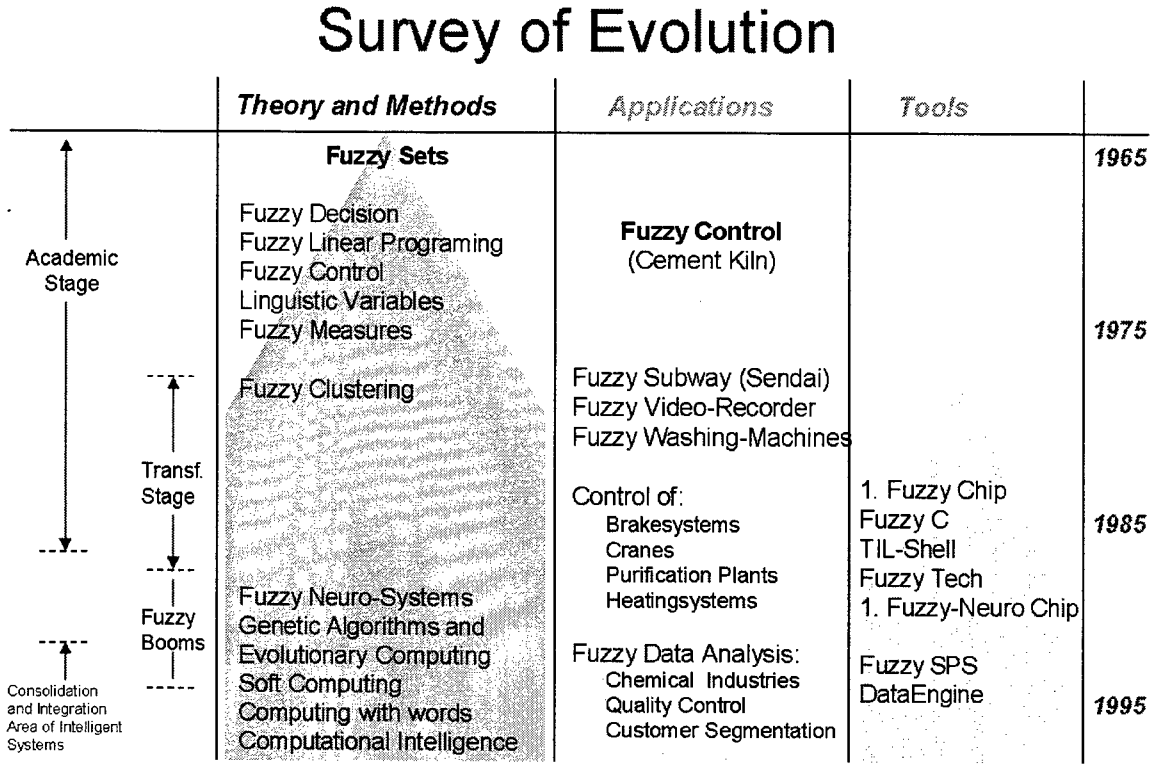


Fig. 1. From Fuzzy Set Theory to computational intelligence

Management, engineering and other areas can be supported by computational intelligence in many ways. This support can refer to information processing as well as to data mining, choice or evaluation activities or to other types of optimization. Classical decision support systems consist of data bank systems for the information processing part and algorithms for the optimization part. If, however, efficient algorithms are unavailable or if decisions must be made in ill-structured environments, knowledge-based components are added to supplement or substitute algorithms. In both cases Fuzzy Technology can be useful. In this context it may be useful to cite and comment on the *major goals* of this technology and to correct the very common view that Fuzzy Set Theory or Fuzzy Technology is exclusively or primarily useful to model uncertainty:

a) Modeling of uncertainty

This is certainly the best known and oldest goal. I am not sure, however, whether it can (still) be considered to be the most important goal of Fuzzy Set Theory. Uncertainty has been a very important topic for several centuries. There are numerous methods and theories which claim to be the only proper tool to model uncertainties. In general, however, they do not even define sufficiently or only in a very specific and limited sense what is meant by "uncertainty". I believe that uncertainty, if considered as a subjective phenomenon, can and ought to be modeled by very different theories, depending on other causes of uncertainty, the type and quantity of available information, the requirements of the observer etc. In this sense Fuzzy Set Theory is certainly also one of the theories which can be used to model specific types of uncertainty under specific types of circumstances. It might then compete with other theories, but it might also be the most appropriate way to model this phenomenon for well-specified situations. It would certainly exceed the scope of this article to discuss this question in detail here [6].

b) Relaxation

Classical models and methods are normally based on dual logic. They, therefore, distinguish between feasible and infeasible, belonging to a cluster or not, optimal or suboptimal etc. Often this view does not capture reality adequately. Fuzzy Set Theory has been used extensively to relax or generalize classical

methods from a dichotomous to a gradual character. Examples of this are fuzzy mathematical programming [5], fuzzy clustering [2], fuzzy Petri Nets [3], fuzzy multi criteria analysis [4].

c) Compactification
Due to the limited capacity of the human short term memory or of technical systems it is often not possible to either store all relevant data, or to present masses of data to a human observer in such a way, that he or she can perceive the information contained in these data. Fuzzy Technology has been used to reduce the complexity of data to an acceptably degree usually either via linguistic variables or via fuzzy data analysis (fuzzy clustering etc.).

d) Meaning Preserving Reasoning
Expert System Technology has already been used since two decades and has led in many cases to disappointment. One of the reasons for this might be, that expert systems in their inference engines, when they are based on dual logic, perform symbol processing (truth values true or false) rather than knowledge processing. In Approximate Reasoning meanings are attached to words and sentences via linguistic variables. Inference engines then have to be able to process meaningful linguistic expressions, rather than symbols, and arrive at membership functions of fuzzy sets, which can then be retranslated into words and sentences via linguistic approximation.

e) Efficient Determination of Approximate Solutions
Already in the 70s Prof. Zadeh expressed his intention to have Fuzzy Set Theory considered as a tool to determine approximate solutions of real problems in an efficient or affordable way. This goal has never really been achieved successfully. In the recent past, however, cases have become known which are very good examples for this goal. Bardossy [1], for instance, showed in the context of water flow modeling that it can be much more efficient to use fuzzy rule based systems to solve the problems than systems of differential equations. Comparing the results achieved by these two alternative approaches showed that the accuracy of the results was almost the same for all practical purposes. This is particularly true if one considers the inaccuracies and uncertainties contained in the input data.

The development of Fuzzy Technology during the last 30 years has, roughly speaking, led to the following application oriented classes of approaches:

- Model-based (algorithmic) Applications
- fuzzy optimization (fuzzy linear progr. etc.)
- fuzzy clustering (hierarchical and obj. function)
- fuzzy Petri Nets
- fuzzy multi criteria analysis

- Knowledge-based Applications
- fuzzy expert systems
- fuzzy control
- fuzzy data analysis

- Information Processing
- fuzzy data banks and query languages
- fuzzy programming languages
- fuzzy library systems.

For almost all classes of application mentioned above tools (software and/or hardware) are available to allow efficient modeling. Institutionally Fuzzy Set Theory developed very differently in the different areas of the world. The first European Working Group for Fuzzy Sets was started in 1975, at a time at which Fuzzy Sets became visible in international conferences, such as NOAK (Scandinavian Operations Research Conference, IFORS-Conference in Toronto, and the 1st USA-Japan Symposium in Berkeley.

At the beginning of the 80s, national societies were founded in the USA (NAFIPS) and Japan (Soft) and almost at the same time a worldwide society IFSA was started.

When the 3rd World Congress of IFSA took place in Tokyo, Fuzzy Technology was already well-known in the Japanese economy where it had been successfully applied to consumer goods (washing machines, video cameras, rice cookers) but also to the industrial processes (cranes etc.) and to public transportation (subway system in Sendai). In the rest of the world it was still very little known and primarily considered as an academic area.

The European Development

By contrast to Japan and the USA Europe is very heterogeneous economically, culturally and scientifically. When in 1989/90 the "Fuzzy Boom" was triggered by the media, that had observed the fast development of this technology in Japan, there existed in different European countries approximately ten research groups in the area of Fuzzy Sets but they hardly communicated with each other, even hardly knew of each other. They were working on an international level but were not very application-oriented.

In this situation the fear grew that Europe would again lose one of the major market potentials to Japan. What seemed to be needed most was communication and cooperation between European countries and between science and economy. Neither a company nor a university seemed to have the standing to bring this about. Hence, a foundation (ELITE = European Laboratory for Intelligent Techniques Engineering) was founded. It was much smaller and had much less public support than LIFE in Japan, which had very similar objectives. The Media and the strong public interest had strong influences on the universities and within one to two years the European Commission could be convinced of the economic importance of this area. Via a European Working Group on Fuzzy Control one of the European Networks of Excellence was dedicated to Fuzzy Technology (ERUDIT). It became a European framework in which new theoretical and practical developments were and are methodically and interdisciplinary triggered, supported and advanced. Some of its important features are

- its structure,
- its growth,
- its orientation, and
- its services.

These are depicted in the following figures. The structure is a matrix organization with the functions and methods horizontally intersecting all sectors of the economy.

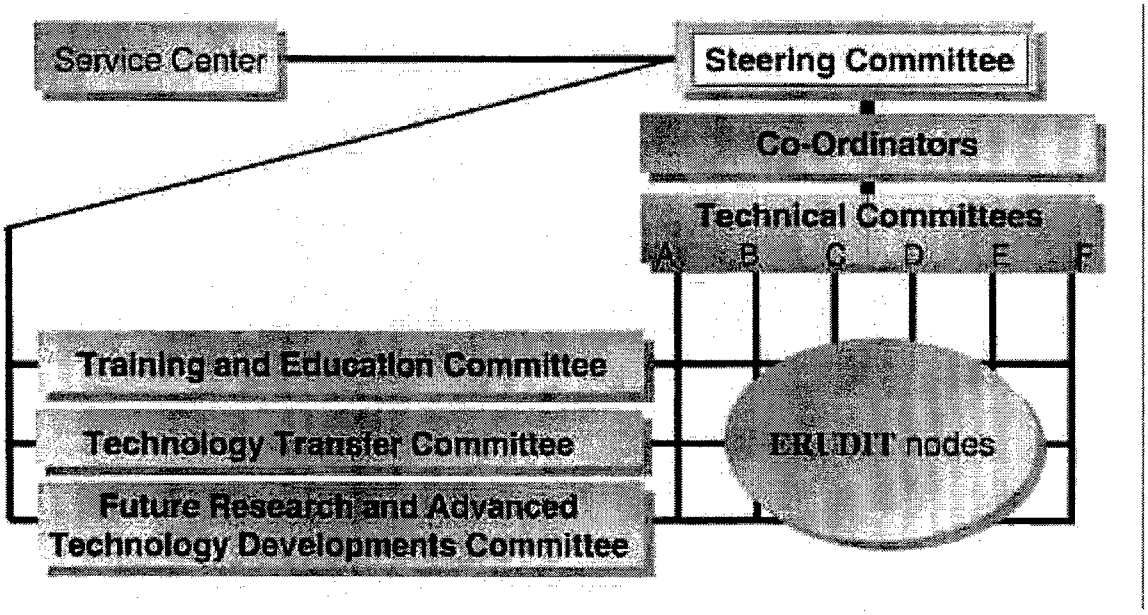


Fig. 2. ERUDIT – Structure

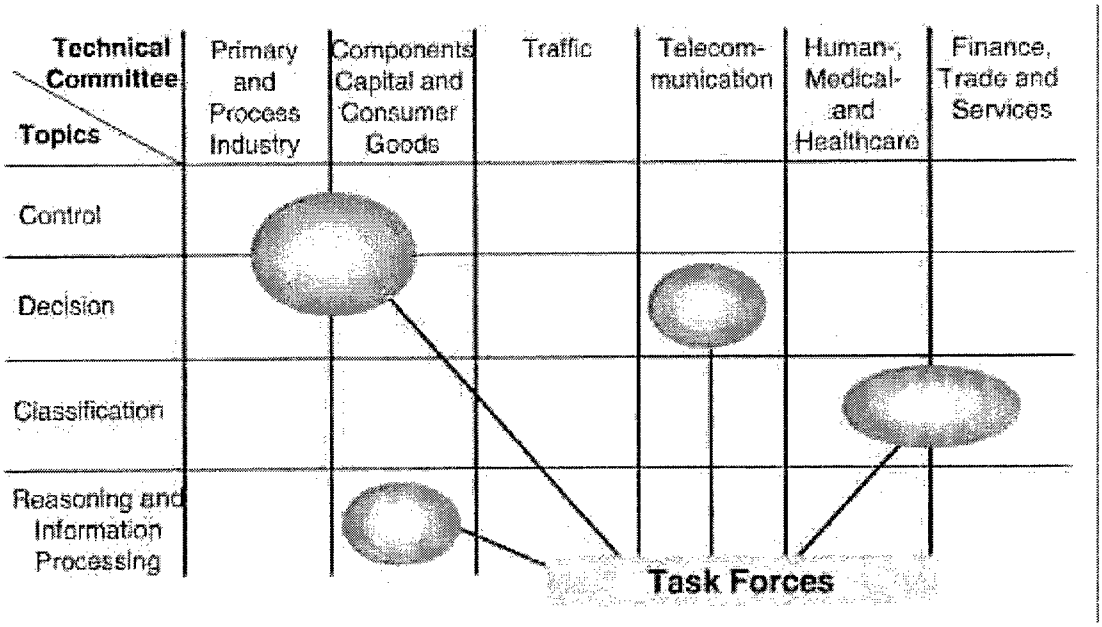


Fig. 3. Committee Structure.

Its growth and orientation are shown in Figure 4. A self-imposed constraint ensures the application orientation and focussed activities in several directions lead to a steady growth.

	Industry				University				Total			
	1.1.95	1.1.96	1.1.97	30.11.98	1.1.95	1.1.96	1.1.97	30.6.97	1.1.95	1.1.96	1.1.97	30.6.97
Active Nodes	8	26	29	32	6	23	31	44	14	49	60	76
Pending Active						18	20	9		18	20	9
Nodes		26	61	58		48	109	108		74	170	166
Information/ Mailing List		1208	1519	1584		1260	1414	1436		2468	2933	3020
Total Nodes	8	52	90	90	6	89	160	161	14	141	250	251

Fig. 4. Composition and growth of ERUDIT

Services offered are geared to the requests of the nodes as shown in Figure 5.

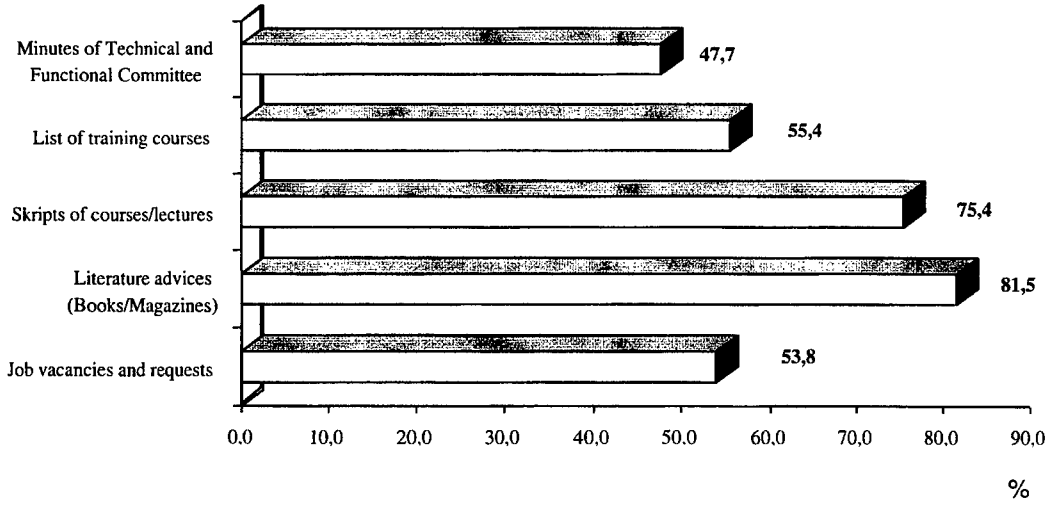


Fig. 5. Requested Services

Extensive surveys also allow very focussed activities to advance the area in scope and depth. Figures 6 and 7 sketch results from these surveys.

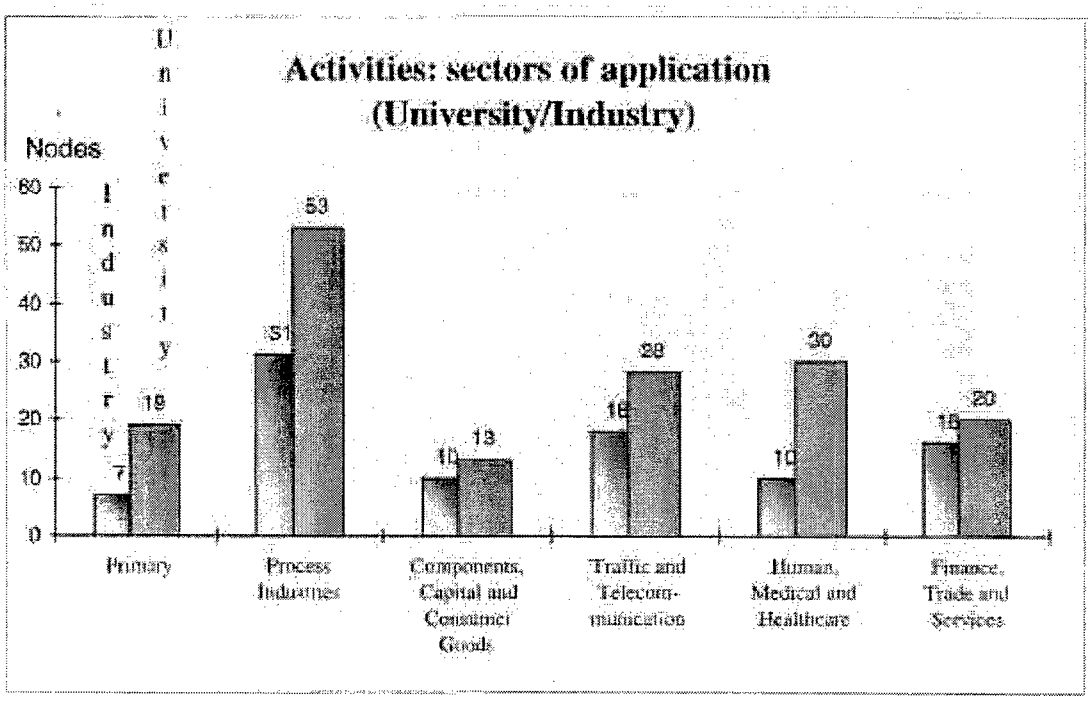


Fig. 6. Activities by sector of the economy.

At present a merger of the Networks of Excellence for Fuzzy Sets, Neural Nets, Evolutionary Computing and Machine Learning is being implemented and a very extensive survey is to be executed. The results of this will be ready by June 1999 and will be reported at IPM'99 in Hawaii in July 1999.

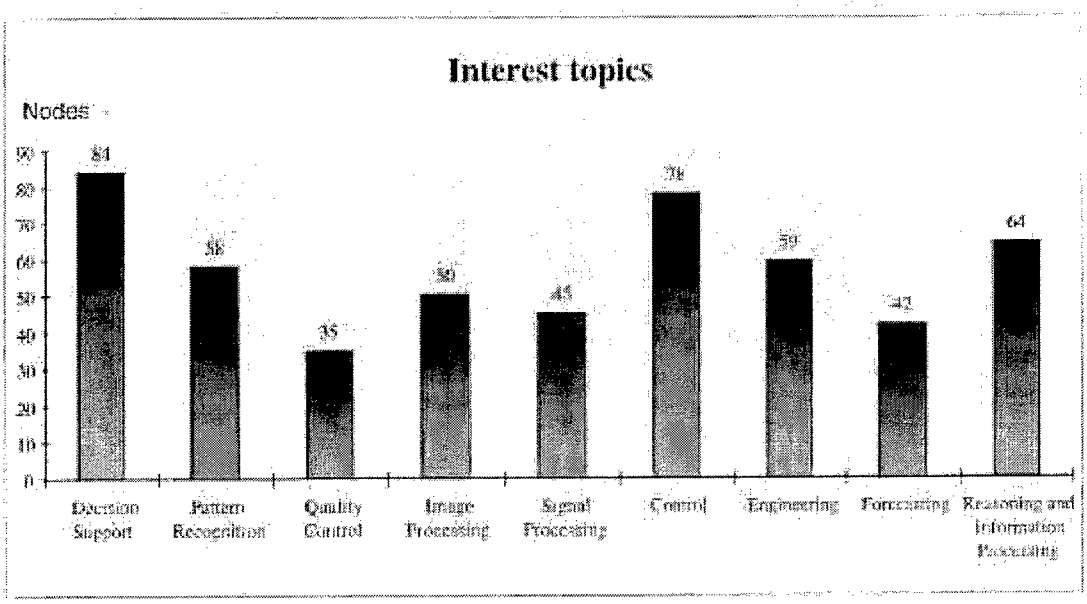


Fig. 7. Application Areas.

Which conclusions can be drawn from the European experience described above? Maybe that a strong and steady growth of a technology, even in difficult conditions as in Europe, can be achieved if the media are intensively included in the promoting activities and if the development is not left to chance but if communication, initialization, support and technology transfer are improved systematically and steadily.

REFERENCES

1. A. Bardossy, 1996. The Use of Fuzzy Rules for the Description of Elements of the Hydrological Cycle *Ecological Modelling,* 85, 59 - 65.
2. J. C. Bezdek and S. K. Pal, 1992. Fuzzy Models for Pattern Recognition. New York.
3. H.-P. Lipp, R. Günther and P. Sonntag, 1989. Unscharfe Petri Netze - Ein Basiskonzept für Computerunterstützte Entscheidungssysteme in Komplexen Systemen. *Wissenschaftliche Schriftenreihe der TU Chemnitz,* 7.
4. H.-J. Zimmermann, 1986. Multi Criteria Decision Making in Crisp and Fuzzy Environments. in: Zimmermann, Jones and Kaufman (edtrs.). Fuzzy Set Theory and Applications. Dodrecht, 233 - 256.
5. H.-J. Zimmermann, 1996. Fuzzy Set Theory - and Its Applications. 3rd rev. edit. Boston.
6. H.-J. Zimmermann, 1997. A Fresh Perspective on Uncertainty Modeling: Uncertainty vs. Uncertainty Modeling. in: B. M. Ayyub and M. M. Gupta (edtrs.). Uncertainty Analysis in Engineering and Sciences: Fuzzy Logic, Statistics, and Neural Network Approach. *International Series in Intelligent Technologies*, Kluwer Academic Publishers,. 353 – 364.

Telemining[tm] Systems Applied to Underground Hard Rock Metal Mining at Inco Limited

Gregory R. Baiden

INCO Mines Research, Sudbury, Ontario, Canada
Email: gbaiden@inco.com

ABSTRACT

The introduction of intelligent systems to the underground mining of nickel, copper, cobalt and precious metals can provide significant improvement in the performance of a mine when compared with conventional mining techniques. This paper presents the concepts of Telemining in an actual case study showing how the systems work and the competitive advantage they provide for Inco's underground metal mining operations today and into the future.

INTRODUCTION

Inco Limited is a metal processing company that produces 17 minerals and chemicals from raw ore in the form of sulphides and laterites deposits. Sulphide deposits have enjoyed a competitive advantage over laterites to date primarily due to the cost of metal processing. Recent advances in the processing of laterite deposits have put considerable pressure on sulphide producers to lower costs to be competitive. The main different between sulphide producers and laterite producers is the cost of mining. Laterite producers enjoy low mining costs due to the utilization of open pit mining techniques while underground sulphide producers have higher mining costs because of underground extraction techniques. This paper describes Telemining techniques that can potentially close the gap between the mining costs of laterite and sulphide producers.

TELEMINING[tm]

Telemining is the application of remote sensing and remote control of mining equipment and systems. The main technical ingredients are:

- Advanced underground mobile computer networks
- Underground positioning systems
- Mining process monitoring and control software systems
- Mining methods designed specifically for Telemining
- Advanced mining equipment

These ingredients are shown in Figure 1.

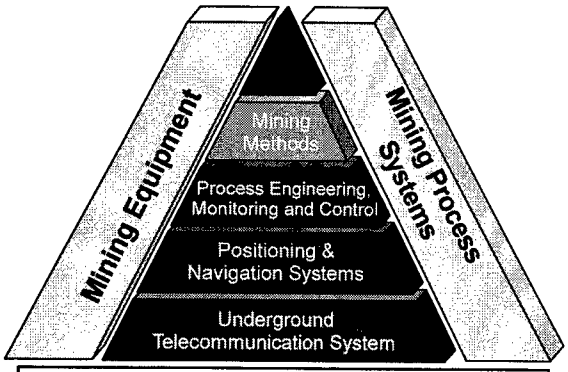


Fig. 1. Core Technologies for Telemining.

0-7803-5489-3/99/$10.00 ©1999 IEEE.

Advanced underground mobile computer networks allow the mining process to be connected to Operations Centers for the running of the mining process. Inco, in conjunction with IBM and Ainsworth Electric, developed this advanced mobile computer network in the early 1990s. It consists of a high capacity CATV network linked to radio cells that are located in central areas in the levels of the mine. The capacity of the system was designed to provide 2.4 GHz of bandwidth allowing operation of mobile telephones, handheld computers, mobile computers on board machines and multiple video channels to run multiple pieces of mining equipment. These systems have the capacity to fulfill all the needs of an individual mine for operation from a surface control room.

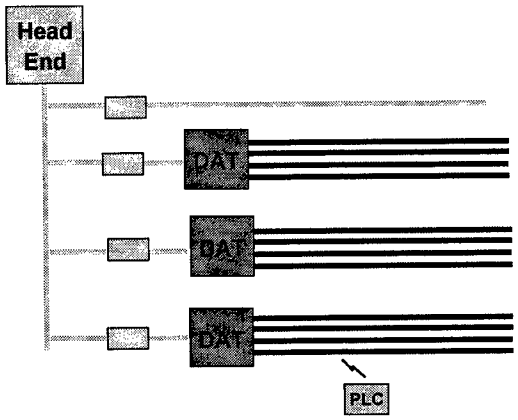


Fig. 2. Underground Telecommunication System.

Underground positioning systems have been established that provide enough accuracy to locate the mobile equipment in real-time. The ability to perform this function provides a number of practical uses including machines set up, hole location and remote surveying. The systems that have been developed function similar to Global Positioning Systems (GPS). The positioning equipment used consists of a Ring-Laser-Gyro. These units will be mounted on all drilling machines that so surface operators can position the equipment without needing to go underground. The test bed machine for trying these systems is shown below. This unit is capable of surveying a 1km drift (tunnel) in a few hours while current work practices require several days. The output of this work is the ability to develop "virtual reality" as-builds of the mine.

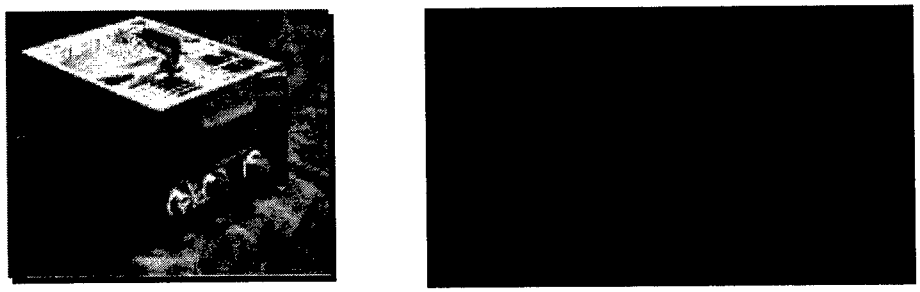


Fig. 3. Underground Positioning Unit and Surveying Machine.

Mine Planning, Simulation and Process Control Systems are the next advance to be made. The linking of engineering directly with operations is key to the proper application of telemining. Present mine planning systems provide visualization of the mineralization available for mining. It is not until the method has been simulated that a true idea of the output of an operation in a given timeframe can occur. Since the speed of planning and simulation has now been accelerated, an interative approach can now be less onerous thus freeing time for optimizing the plan. The output of this high level plan now becomes the input for a more detailed plan using an MRP III (Manufacturing Resource Planning) system. This establishes schedules for individual work tasks that are fed directly to the mining machines connected over the network. Feedback is done with a base data collection system residing in a Spatial Database.

The technologies discussed here will be applied to the processes of exploration, drifting and stoping. These process systems will allow the teleremote capability of mining machinery. The main process machinery will be diamond drills, drifting drills, explosives loading machines, Load-Haul-Dump machines and ground support units.

RESEARCH MINE

Let us now use the Inco Limited Research Mine – 175 ore body as a case study to describe how this plan will work. Key to improving the value of a mineralized area is the speed with which we mine the ore and the cost of doing the actual work. By far the driving factor to increase mine value is the reduction of cycle time. Given that the 175 area has a total mineralization of approximately 8 million tons (see Figure 4) grading 0.5 %Cu and %Ni combined, the challenge is to use the techniques to bring the ore production forward.

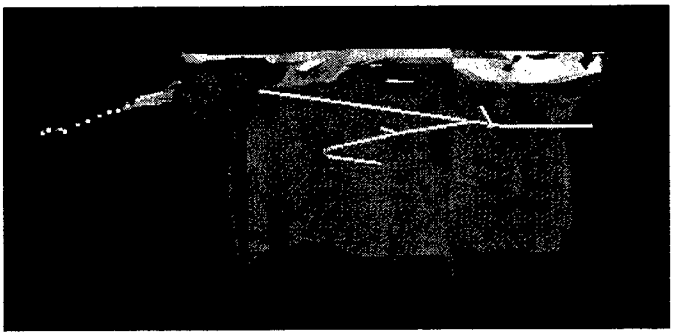


Fig. 4. Research Mine Mineralization.

The process of mining consists of four overall components: delineation, development, production and materials handling. Delineation is the continuous proving of the ore grade quality to locate the closed mineral resources. Delineation today consists of a geologist making a request for tonnage and grade information. This request is sent to a diamond drilling and/or geologic probing group. In this group the reduction in cycle through surface operation allows on-line information to be available for faster turnaround times in the continuous planning and redefinition of the ore body to dynamically alter planning where possible. Today turnaround times on information are about 3 months. Surface teledelineation with probes will reduce this cycle time to minutes through introduction of Spatial Information Systems linked to teledrilling machines that probe as they go.

Today development times are typically 24 hours for total cycle in our industry. This is using conventional tools such as the 2-boom electric/hydraulic jumbo, hand explosives loading, mucking and ground support. Teledevelopment will provide a compressed development cycle time, as the available time for work will be increased by 30%. This will occur through teleoperation of a computer controlled telejumbo, a computer controlled explosives loader, a teleoperated LHD and the use of more expensive but faster-setting ground support coatings. Synchronization of the development cycle will provide a 100% improvement in the rate of development while the utilization of people will be enhanced through on-surface teleoperation of the machinery. A 100% improvement in rate or a doubling, significantly changes the cash flow of the entire mine. The can be seen in the results of the simulator comparison below, based on projections for the teledevelopment process under study.

Production cycle time is less significant to the cash flow than is speeding up development but each reduction in cycle times will help. The real challenge is to control drilling and blasting so as to avoid slowing the process. Today we use longhole drills, explosives loaders (typically AN/FO) and LHDs followed by backfilling with rock or tailings, if required. Teleproduction at the research mine will be done with Tamrock Datasolo drills specifically designed for reliability and teleoperation, Dyno Nobel's latest emulsion explosive loader using microprocessor-based caps, and LHDs and Trucks for material handling.

Simulation of the research mine shows that with blasting techniques such as those described, the mine is able to process under-grade ore profitability since it can be mined faster, thus increasing its value.

The keys to synchronizing the process are software tools that become the mine control system. Just-in-time techniques that balance mine development and stope inventory against the acceleration of the mining rate provide a cost savings while still achieving value enhancement by reducing the overall mine cycle time. A KANBAN production order processing system with direct links to the mining machines, will improve the efficiency of mining well in excess of the results already demonstrated by manufacturers such as Toyota.

FIELD TEST WORK

Initial test work at Inco has been completed in the processes of delineation, development and production. Preliminary results are shown in the following examples including Teledelineation, Teledevelopment and Teleproduction.

Teledelineation combines diamond drilling technology with teleremote operation and on-line grade collection. Work todate has seen process automation of the drilling together with rod changing, a prototype SIS and new infrared probes. A conceptual picture is shown in Figure 5. The work completed in machine reliability todate significantly enhances the reliability of the drill through addition of computer control packages and a rod-handling package. Control improvements have reduced consumables. Todate our testing shows:

- bit life has improved on average by 300% with some results as high as 400%.
- rod life has improved by 100%.

Both results exhibit better consistency and reliability that is absolutely necessary for teleoperation. Spatial database development has been a key ingredient to compressing cycle times. Probing results can go directly into the database where geologists and engineering have the latest information to use in planning all of the time. Database development has been an off-shoot of oceanographic work. A drill hole database that links directly to mine planning systems is now available today.

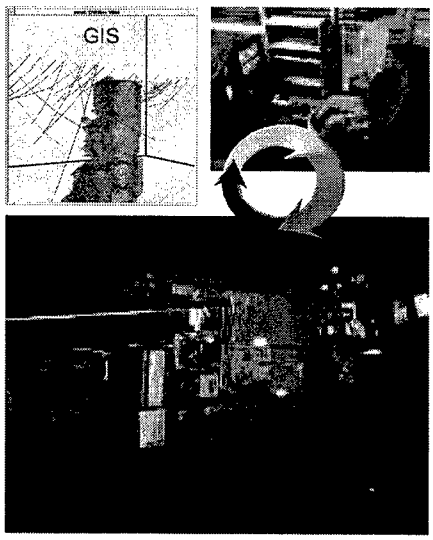


Fig. 5. Delineation Drilling System combined with a Real-Time Software System.

Teledevelopment comprises four machines at present. These include a teleremote horizontal-drilling machine, an explosives-loading unit, a materials-handling machine (LHD) and a ground-support machine. The drilling machine requires a change in the drilling pattern to provide consistency. New patterns have been developed to improve the reliability of the tunneling process as part of the teledevelopment strategy.

The computerized horizontal drill (jumbo) has a computer system that is linked to the underground network to provide on-line engineering information to drill the pattern. The underground positioning system provides location coordinates of a machine for rapid setup and accurate drilling. These types of control systems are a must in teleremote. Automated explosives loaders are beginning to be developed and teleoperated LHDs are working in the field achieving significant production improvements today.

Teleproduction combines three machines that must interact in stoping. These units are a longhole production drill, explosive loader and an LHD. The machines running teleremotely will reduce cycle times and cost. Today, testing is underway on the drilling and LHDs for production. The results of this work are quite promising. Drilling performance has seen teledrilling with 3 drills and 3 operators with 3 rovers achieve the same production as a conventional mining scenario of 5 drills with 20 operators. These improvements remove 2 drills and reduce the need for 14 operators. As well, these drills operate for 7.5 hours of a current 8-hour shift in comparison to manual drills that only run 5 hours for the same 8-hour shift. The LHD performances are similar. The LHDs are moving material at the same rate as current LHDs with highlights of a single machine operating 23 hours out of a 24 hour day in comparison to a normal production unit that would work 15 hours out of a 24 hour day.

MINE OPERATION CENTER

A Mine Operation Center connected to multiple mines offers the opportunity to enhance further the utilization of people and equipment. An MOC connects to the individual headframes allowing control of geographically dispersed equipment. An example that is currently running as a prototype at Inco is shown in Figure 6. This prototype has been put in place to test the technical and financial feasibility. Some of the questions being answered are:

- How many pieces of machinery can a single operator run?
- What are the logistics issues of operating this way?
- How should the Operations Center be organized?

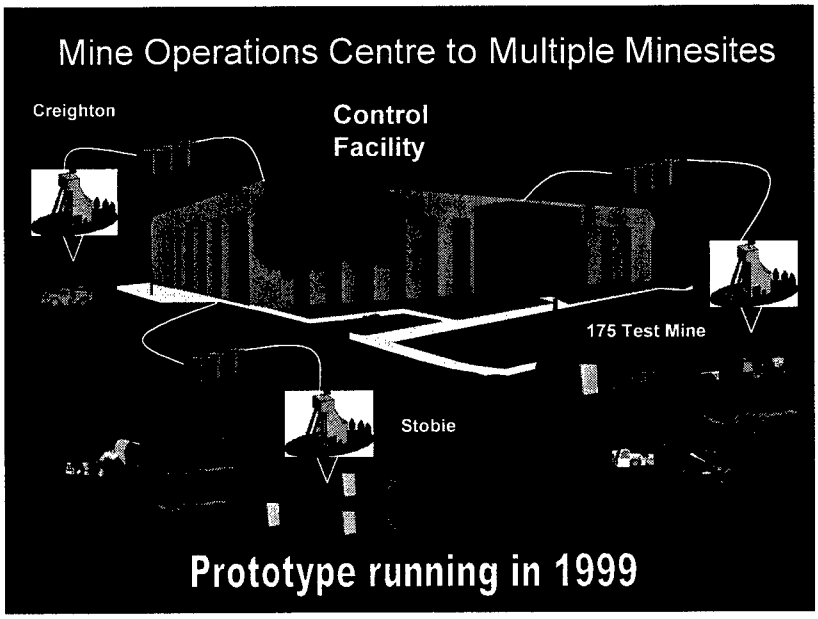


Fig. 6. Mine Operations Center Concept.

BENEFITS

The main benefits of this style of operation are improvements in safety, productivity, value-added time and cycle time. Safety improves since an operator has less time underground. Productivity shifts from one person per machine to one person per three machines. Value-added time has been demonstrated by having

23 continuous hours of operation in a 24-hour period. These results reduce the time of the development and production cycles.

To determine these benefits, several telemining simulators of the Research Mine have been created. These simulators compare the timing of conventional mining processes to telemining for the Sub-Level Retreat mining method (see Figure 7). The benefits of this style of underground mine operation are significant. Recent results show improvements in project life reduction of one year and a change in net cash flow of $3 million or –25% to + 30% (see Figure 8) for telemining over conventional mining techniques. Taken one step further to a central Mine Operation Center (MOC) that runs three equivalent mines indicates returns and cash flow changes of +130% and +$35 million.

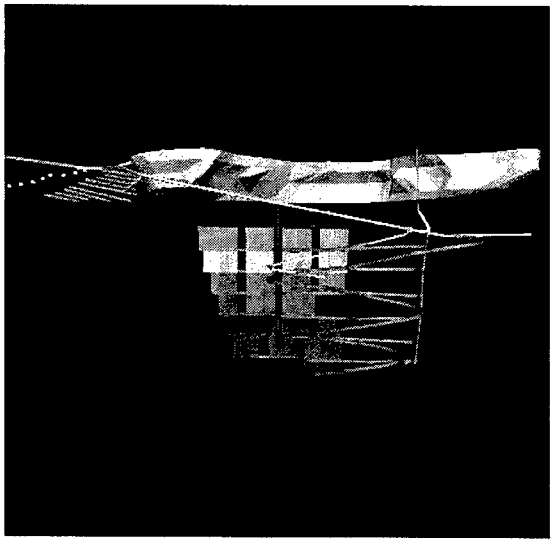


Fig. 7. Research Mine Sublevel Retreat Design.

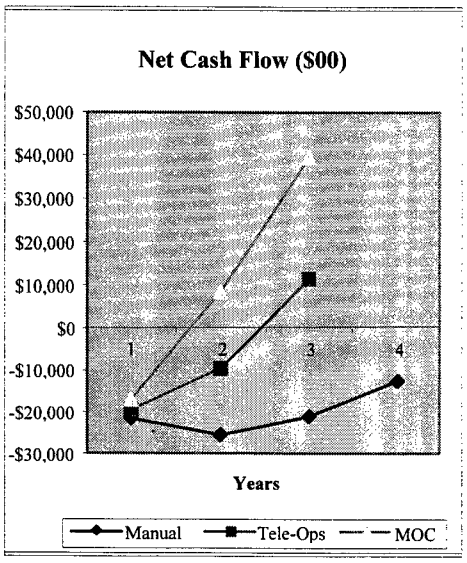


Fig. 8. Financial Comparison of Operating Methods.

SUMMARY

Telemining is a direction in which underground mining companies must head if they intend to continue operating in the ever-tightening base-metal commodity business. The techniques shown in this paper are similar to Computer Integrated Manufacturing (CIM) methods that provide a consumer with a continuous supply of cheap products. Application of these advanced manufacturing techniques to mining will allow sulphide deposits to significantly reduce production costs to remain competitive with laterite deposits.

Soft Sensors for Processing Plants

G.D. González

Department of Electrical Engineering, University of Chile,
Santiago, Chile

ABSTRACT

Soft-sensors assist in solving the problem created by the unavailability of a sensor by providing a software backup for it, thus allowing a reduction of losses in plant performance. Similarly, the use of a soft sensor to estimate a plant variable for which no sensor is installed, provides an occasion for improving the performance of a plant. The core of a soft-sensor is a partial model of a plant allowing the generation of a estimated measurement to replace missing actual measurements. Coupled with the model there is a problem of signal estimation, interpolation and prediction. Modes considered here are black box models (e.g., ARMAX, NARMAX, Neural Network, Cluster Analysis) and gray models which include phenomenological knowledge. Also, comparisons are made concerning the requirements for soft-sensor models and for models used in model based control. An approach to an integrated view of the various soft-sensor modeling methods is attempted. Among other aspects considered are: (i) how a soft-sensor may be used for interpolation and prediction of measurements having a sampling rate which is too low, (ii) performance of a control loop when a sensor is replaced by a soft-sensor, (iii) performance of the soft-sensor indication in the period following the removal of the actual sensor by a soft-sensor as plant characteristics change (iv) complementary considerations for ensuring the availability of soft-sensors in industrial environments and (v) problems related to the use of soft-sensors in automatic control loops. A review made of a sample of the technical literature on applications as well as of research and development in this field, is commented in the text and summarized in a table.

INTRODUCTION

Sensors are the eyes through which the behavior of a plant is seen and information about its performance is obtained. But the measurements from a sensor may become unavailable because of failure, removal for maintenance or repairs. Also, it may happen that the sampling is infrequent, i.e., the plant variable to be measured is not sampled at a fast enough rate, so that the samples do not represent the actual evolution of such variable, because of a violation of Shannon's sampling theorem [1]. This happens when a sensor is time shared for performing measurements at different points. It is also the case when no sensor is installed (e.g., because it has not yet been developed or placed in the market, or because of its high cost) and laboratory analyses are required. In addition, it may be that a sensor is not very robust so that, instead of having it always on-line, it is used to take infrequent samples [2]. Then due to the fact that a set of measurements is totally missing or incomplete during a certain period of time, the plant performance will almost surely be impaired. Soft-sensors may provide a convenient solution to eliminate or at least palliate this problem [1, 3, 4, 5, 6, 7, 8], even in cases when the sampling rate is inadequate, if certain conditions are met [2, 9, 10, 11, 12] (see Table 1 below).

In general soft-sensors supply the estimation of the missing measurements by using a model that relates the corresponding variable with other measurements that are correlated with it (Fig. 1). The fact that the model is implemented by means of software (hence the name *soft*(ware)-*sensor*) means that soft-sensors provide a software back-up for unavailable sensors, as an alternative to a hardware back-up using spare sensors.

Two are the main topics related with the problem of maintaining the availability of measurements in a plant by means of soft-sensors :

i) The soft-sensor model, and
ii) The detection that a sensor has failed together with the identification of which is the failing sensor out of a set of sensors.

0-7803-5489-3/99/$10.00 ©1999 IEEE.

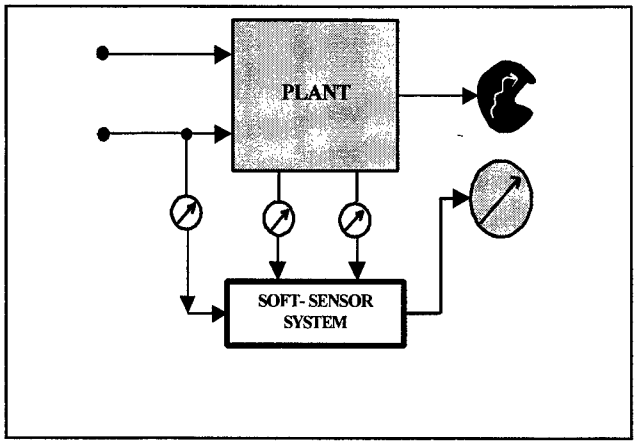


Fig. 1. Soft-sensor system replacing failed sensor with model having correlated secondary measurements as inputs.

Concerning the models, some authors define soft-sensors only on the basis of neural network models (e.g., [12]), but a broader point of view should be adopted, since soft-sensor models are also obtained using regression or correlation techniques, as well as fuzzy logic or first principles models, or combinations of them. But developments seem to have followed independent paths, and as a result, different names are given to the same concepts, e.g.: parameters = weights, parameter estimation = training, new data tests = generalization

Other subjects of interest concerning soft-sensors are:

a) Performance of a control loop when a sensor is replaced by a soft-sensor [13, 14].
b) Performance of the soft-sensor indication in the period following the removal of the actual sensor by a soft-sensor as plant characteristics change [13, 14, 15].
c) Complementary considerations for ensuring the availability of soft-sensors in industrial environments [3, 4, 16, 17].

This paper deals mainly with the subject of the soft-sensor by itself. Although fault detection and identification is an important and interesting associated subject, closely connected with soft-sensor modeling as witnessed in [6, 7, 8], lack of space prevents an adequate treatment of this matter here.

MODELS

The core of a soft-sensor is a partial model of a plant allowing the generation of a virtual measurement to replace a real sensor measurement. Coupled with the model there is a problem of signal estimation, interpolation and prediction. The model must generate the missing measurements in terms of other measured variables with which these measurements are correlated. This process is well stated paralleling the definition of identification given by L. Zadeh. Here a class of models, a class of input signals, and a criterion are defined in order to determine the best model (Fig. 2). The problem consists of finding which model belonging to the class of models (e.g., a subset of ARMAX models, a subset of neural network models) is best, according to the chosen criterion (usually defined in terms of the mean square error between the model output or prediction and the measured plant variable to be represented by the soft-sensor), for the specified class of signals. For this purpose only measured input and output variables of the plant or process may be used. The modeling process depicted by Fig. 2, applies whether the models be based in neural networks, regression, fuzzy logic, first principles (phenomenological), combinations of them, etc. In general, models based only on input output measurements will be called black box models, those based on first principles will be termed phenomenological models, while those using not only the input-output measurements but incorporating some phenomenological knowledge about the plant will be called gray box models.

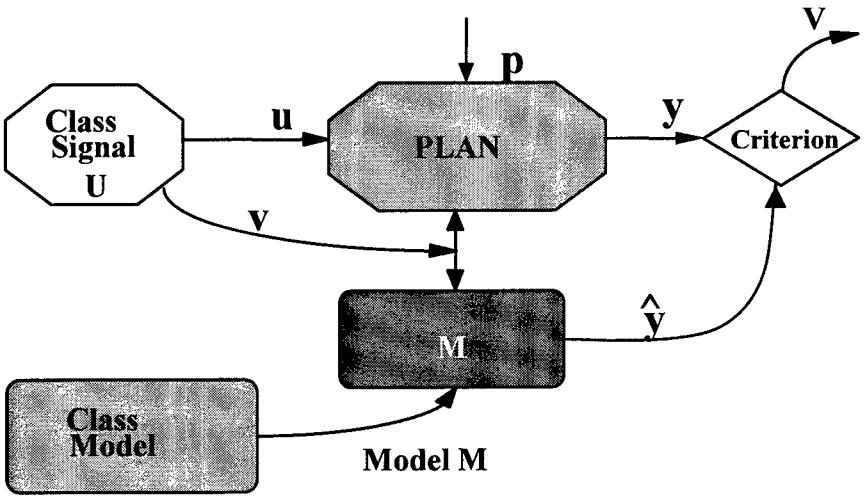


Fig. 2. Choosing the best model. Here **u** is a vector of command (manipulated) variables, **v** is a vector or measured disturbances, **p** is a vector of unmeasured disturbances, **y** is the plant output and $\hat{y}$ the model output. The instantaneous error is $e(t) = y(t) - \hat{y}(t)$.

It is convenient to distinguish two stages in this process of finding the best model:

- Structure determination and
- Parameter (weight) estimation

Both structure determination and parameter estimation should be done with one set of data – the training set – and tested with a different set: the test set.

Structure

The model structure stage is concerned with finding a form for the soft-sensor model. For example, in the ARMAX class of models this entails finding the most significant components correlated with the soft-sensor signal which will be used as inputs signals to the model.. A component is a term in the model having an associated parameter, and may be a measurement or an appropriate combinations of measurements (composite components). In the neural network case, the structure comprises the type of network, the network topology, the most significant measurements to be used as inputs, the number of layers, the selection of the activation functions, and the number of nodes in each layer. Composite components may also be considered as suitable inputs to a neural network. A given structure may be valid for a large operating region of a process, while its parameters (weights) may need to be updated as the operating point undergoes small or large changes. Some usual structure determination methods follow.

Regression Based Models

Model structures of the ARMAX [28] and NARMAX [5] class are determined using regression techniques. In order to find the components that determine the model structure all the relevant information is used, including measurements of inputs, internal plant variables, and measured disturbances. Phenomenological knowledge of the plant may be of great use [1, 3, 4, 18]. Delays associated with the different measurements are included in this determination. The structure determination consists then in finding which are the components most correlated with the soft-sensor variable. In order to do this, methods such as Piecewise Regression may be used. In this way the model is simplified, since no highly correlated components are included in the resulting model. In addition it turns out that the standard deviation of the error in the determination of the model parameters is reduced. An example of an ARMAX structure having both kinds of components is given in (1).

$$y(t) = \theta_1 y(t-1) + \theta_2 x_1(t-1) + \theta_3 \frac{x_2}{x_5} + \theta_4 \sqrt{x_7} + \theta_5 \qquad 1.$$

where the secondary measurements are $x_j(t)$, $j = 1, \ldots, m$, and the sampling times are t.

Stepwise Regression. This is one of the methods used to find which are the most significant components associated with the soft-sensor variable. It begins by selecting that component from a list of candidate components which is most closely correlated with the variable to be modeled , i.e., the soft-sensor variable. In this way a first partial model is determined. The residue of this model is then correlated with the remainder candidate components. In each following stage, the component to be included is the particular component that gives the largest partial correlation with the previous step residue, calculated after a multilinear regression is performed with the previously selected components. With this procedure, the model structure increases through the addition of one component at a time, such that the added component is the one that contributes the greatest improvement in the goodness of fit to the model. Before each new component is included in the model, though, the components to be included are tested for their statistical significance. Each model parameter estimate has an estimated error standard deviation The ratio between this standard deviation and the coefficient value, is used to decide the inclusion of every new component. If for any component the ratio exceeds a given threshold then the corresponding component is not included, or excluded if it had been previously included. This procedure is repeated until no component from the list of candidate components is either deleted or included in the model being determined. Then the determination of the model structure has been completed [29].

Using this method, with data gathered during experimental runs, several soft-sensors have been designed for industrial grinding and flotation plants in an off-line [1, 3, 4, 18]. The list of candidate components included single measurements, as well as composite components combining various measurements to produce components having physical significance. In order to determine the composite components a phenomenological model of the plant has been used for finding the general form of the relation between the soft-sensor variable and other measurements in the plant. It turned out that the majority of the components selected by the stepwise regression method are of the composite type - i.e., having some physical significance - instead of the single measurement linear components. In the case of the particle size soft-sensor for a grinding plant [3] the result is given by

$$F_{65}^{O}(t) = \theta_0 + \theta_1 F_{65}^{O}(t-1) + \theta_2 J_B(t-1)\left[S_w^F(t)\right]^3 + \theta_3 J_B(t-3) S_w^F(t-3) + \theta_4 \frac{\left[G_{L1}(t)\right]^2}{G_{SF}(t-2) P_S(t-3)} \qquad 2.$$

where the autoregressed soft-sensor measurement is

F_{65}^{O}(t-i) = % in weight over the 65 mesh, in the final product of a section of the grinding plant,

and the secondary measurements are

J_B(t-i) = Total power of the three ball mills in the grinding section.
S_w^F(t-i) = Average solids concentration in the section (% by weight) in the hydrocyclones feed, considering the three grinding circuits of the section.
G_{L1}(t-i) = Rod mill water feedrate; P_S(t-i) = Sum of the three sump pumps speeds;
S_W(t-i) = Solids concentration, % by weight;
G_{L2}(t-i) = Sump water addition rate; PS(t-i) = Sump pump speed; G_{SF}(t-i) = Fresh ore feedrate.

All variables were placed in the candidate component list including various delays, along with the composite component candidates including their delays. The result was that all selected components depending on secondary measurements, were composite types. The performance of this soft-sensor was appreciably better than the model based on only single measurement components in the candidate list [7].

Principal Components

In the Principal Component modeling methods [30] an $n*m$ sample measurement matrix X is formed in which each row is a vector x^T (j) containing the m measurements performed in the plant at sample times j = *1 .... n.*. The m eigenvalues $\lambda_{\lambda p}$ and eigenvectors $\boldsymbol{p}^i$ of the symmetrical correlation matrix $X^T X$ are found. Of the m eigenvectors a subset is selected that explain most of the variation of the data, e.g. by choosing those having the largest eigenvalues. This subset spans the principal component space (PCS), while the remaining eigenvectors span the Residual Space (RS). Since $X^T X$ is symmetric, all eigenvalues are

orthogonal to each other, and if they are normalized to Euclidean length 1, an orthonormal basis for the PCS as well as for the RS space is obtained. The measurement vectors x(j) are projected onto the PCS, $\hat{x}$ being the projection. The components of vector $\hat{x}$ are called the principal components, and are mutually orthogonal (uncorrelated).

In the Principal Component Analysis method a missing measurement may be reconstructed [6, 7, 8]. But more than one measurement may be reconstructed, depending on the dimension s of the PCS and the number m of the sensors. Hence several soft-sensors are implicit in the PCA modeling method and the set of secondary measurements for any of them depends on which of the m measurements are missing. Therefore the PCA method may be viewed as a system of soft-sensor models. Here the model structure is contained in the principal component space and is determined form the sample correlation matrix X^TX.

In Principal Component Regression [24, 30] a regression model is determined by regressing the soft-sensor variable on the principal components of the secondary measurements. Here matrix X is similar to the one in PCA, but contains only the secondary measurements used to model the soft-sensor.

Clustering

The advantages of dealing with a simple -. parsimonious - model may sometimes be retained by means of separating the operation range in clusters, each of which has good simple model. Then if the operating point is identified as belonging to a given cluster, the corresponding model is used. Such a procedure has been used in building a soft-sensor for concentrate grade measurement in a rougher flotation plant [21]. Much better results were obtained with clustering as compared with the case of a single model determined for the complete operating range. Clustering has also been used in a soft-sensor for estimating a variable for which there is no on-line measurement in a distillation column [16, 19]. The models are based on radial basis function neural networks that are determined for each of the clusters into which the secondary measurement space is divided. Then, for a given operating point – given by a set of secondary variables at a given sampling instant – the outputs of the neural networks are combined using fuzzy logic, according to the membership grade of the set of secondary measurements to each of the clusters. Clustering has also been used for a soft-sensor designed to model an event and the proximity to the occurrence of such event [M6]. In this case the objective was to give early warning for the event defined by the overload of a ball mill in an industrial grinding plant. C-means clustering was used to group operating points of the plant. Later developments led to retain two clusters representing two different types of overload. The distance of the operating point to the center of these clusters was computed on-line and the distance to each of them was an indication of how far the operation was from reaching one of the two overload conditions. Different corrective actions could then be taken according to the distance to the nearest cluster.

Kalman Filter

Soft-sensor models using Kalman Filters have been used when the phenomenological knowledge about the plant allows a convenient state-state/output model to be stated. Such is the case of a soft-sensor for the fiber rate in a sugar cane mill [10]. A soft-sensor has been tested using data from a pilot semiautogenous grinding mill, with aid of phenomenological model [20]. In this case an Extended (nonlinear) Kalman Filter had to be used, since a linearized state model had a very small region of validity (see below). The estimated variables were water, ore and fine ore mill contents. In addition the ginding rate, water and ore discharge rates were estimated.

PARAMETER ESTIMATION (TRAINING)

For a given model structure, the model parameters (weights) are estimated (training in the case of neural networks) for an operating region, normally employing gradient techniques to minimize a function of an error measuring the discrepancy between the plant measurement and the estimated measurement obtained using the model. A model structure may be valid for a large region, but the model parameters have to be updated as the operating point moves within the region. The result being sought is an optimal set of model parameters (weights) for the selected model structure. The scheme of Fig. 2 may also be used here, considering now that the model structure is given and that models change due to the change in the parameter (weight) set. Parameter estimation is performed on-line or off line, depending on the case. If the

change in operating point - within a specified time span - is such that the soft-sensor model parameters (weights) undergo important changes while the plant is in normal operation, then they must be updated on-line using available on-line measurements. This is an adaptive process. In this case the region of validity of the model for a fixed set of parameters (i.e., the region in which the error criterion function is less than a specified value) is small. This situation is found when a linear model is used in the case of an appreciably non linear-plant. On the other hand, if a set of model parameters is valid through most of the normal operating points of a plant within the specified time span, parameter estimation may be performed off-line. In the case of non-linear plants, this requires the models to be of the NARMAX Class (preferably with components having physical meaning), of the Neural Network Class or of the Phenomenological Class. According to the availability of on-line measurements, two basic cases may be distinguished:

PE1 - Parameter estimation (training) using on-line measurements at each sampling time. This is the usual case where recursive parameter estimation is employed but batch estimation may be used as well.

PE2 - Parameter estimation (training) using on-line or off-line measurements (e.g., analysis of samples in a laboratory) at infrequent (relatively long) sampling periods for the variable being modeled.

A model based on the slow sampling rate will in general be a bad model, since it is derived using samples that do not represent the actual evolution of the involved variable. Instead, a model must built using a sampling rate that is sufficiently fast so that the sampling theorem is satisfied. If there are other correlated secondary measurements that are sampled at an appropriately fast rate there is a solution. A model is built based on the fast sampling rate, notwithstanding which its parameters (weights) may be found using the infrequent samples provided by the measurement of the modeled variable as well as the fast rate samples of the correlated (secondary) measurements. For example, an instrumentation system for measuring grades in a flotation plant is used in a time sharing mode to assay 14 samples piped to an X-ray analyzer. If the analyzer takes 30 seconds to measure each mineral sample, the sampling rate for any of the 14 measured grades is 7 minutes. In a similar case there is a laboratory analysis performed infrequently on the modeled variable but due to the dynamics of the process a faster rate is required for good manual or automatic control [2, 9, 10, 11, 12, 22] (see Table 1 below).

This method has been used for ARMAX type models in a stirred tank fermenter, and in a distillation column [9]. Applications using this scheme with neural network soft-sensor models are reported in [12]. Another application of this method is found in composition soft-sensors in a distillation column using as models radial basis function neural networks [19]. See also Table 1 below.

Region of validity.- Once a sensor fails, the parameter updating must cease, since it is no longer possible to determine the error between the soft-sensor output and the actual measurement. The soft-sensor signal then begins to perform its job, providing a virtual measurement of the missing one, using the secondary measurements and or composite components as inputs. It is usual to freeze the model parameter (weight) set at some value determined before the sensor failure. But plant characteristics may change during the period after the sensor failure, e.g. because the operation point moves due to disturbances or control actions. If the model involves a simplification of reality, as it is often the case, it may be expected that , except in very simple instances, the model will not be able to represent the part of the actual plant to be modeled for all possible operating points or operating trajectories. This is clearly the situation when for the sake of having a simple model, a class of linear models is selected containing the candidates to represent a nonlinear plant (or sub-plant). As the operating point changes the optimal parameter set changes so that a frequent updating of the model parameters may be required. But since the sensor signal is no longer available this updating is no longer possible, and the soft-sensor error becomes unacceptable since its region of validity has been surpassed. On way to palliate this degradation of performance is to increase the region of validity of the soft-sensor model by incorporating more structure into it, e.g., using NARMAX or neural networks models having physically significant components or inputs (gray models), sufficiently complex neural networks, and models incorporating phenomenological structure [1, 3, 10, 20].

Another way to extend the validity of the soft-sensor model after it becomes unavailable at t_f is by predicting the future value of its parameters using a parameter evolution sub-model, whenever appropriate conditions are met so that the sub-model parameters may be estimated while the soft-sensor is working. The sub-model is then used to give an optimal prediction of the future value of the soft-sensor model

parameters for $t > t_f$. The optimal prediction for a given parameter is its conditional expectation given its value prior to the time of failure t_f. [15]. As an example a first order sub-model for each parameter of a soft-sensor for particle size measurement in an industrial grinding plant has been used. The prediction evolves exponentially from the initial value at t_f to its unconditional expected value for $t >> t_f$. As should be expected the frozen parameter choice gives better prediction for time near the fault, and the unconditional expected value parameters give a better prediction for $t >> t_f$ [15].

CONTROL ASPECTS

Soft-sensors in control loops

Soft-sensors are used mainly in the manual or automatic control of a plant. But partial modeling involved in soft-sensor design may cause unexpected control performance when soft-sensors are used in automatic control loops because of two circumstances: (a) change of the plant-controller model structure introduced because of the soft-sensor model and (b) parameter coupling between the unmodeled and modeled part of the plant: (i) inherent coupling of input/output model parameters due to changes in parameters of the sate/state-output plant model, and (ii) a common disturbance causing changes of parameters both of the modeled and the unmodeled part of the plant. Among the components selected by the structure determination method there usually appear measurements that are not necessarily inputs to the plant (controls or measured disturbances), but also other measurements of intermediate variables that are measured by sensors which are close to the real sensor to be replaced. In this way, only a part of the plant is modeled, so that a control loop using the soft-sensor contains a modeled and an unmodeled part of the pant. Coupling between the modeled and the unmodeled part of the plant may lead to off specification control performance – even instability – unless the fact that a soft-sensor is eventually going to replace the actual sensor is considered in the design of the control loop [13, 14].

Differences between soft-sensor and control models

In order for a control model to be useful in control, it is required to predict the future values of the controlled variable within a relatively short time interval, e.g. several setting times in General Predictive Control (GPC) strategies [31], or in shorter periods for other control strategies, e.g., adaptive PID+Feedforward control. Then the time span used to determine the model needs not to be very large. On the other hand, soft-sensors are required to predict the absent sensor signal for periods that may be relatively long, until the real sensor signal is again available. Therefore, the time span used for the determination of soft-sensor models may be much larger than in the control model case. In this way different models may be obtained. For example, a slowly varying measured disturbance may be considered constant during the time span of a control model, so that it becomes part of the constant component of the model. But in the case of the larger time span needed for the soft-sensor model, it may well happen that the disturbance changes, and cannot be considered to be constant. Then it is liable to become included in the model , while it does not become included in the control model [23].

INDUSTRIAL ASPECTS

There is clearly a question of economics in deciding whether the back-up for a sensor is to a spare sensor or a soft-sensor. Justification for a soft-sensor depends, on the one hand, on the relative cost of a real back-up sensor. For example, as a back–up for a wattmeter a spare wattmeter may be best, while for backing-up other complex sensors, a soft-sensor may be a best choice. Such would be the case in the replacement of a particle size analyzer used in the minerals industry. On the other hand, a wattmeter may be directly replaced by its spare, while other in other cases – e.g. that of the particle size analyzer - an undue period of time and effort may be required and, in the worst cases, even a shut down of a unit could be necessary.

From an industrial point of view a soft-sensor must be reliable and robust, otherwise its main purpose, i.e., of serving as an alternative for obtaining a measurement when a real sensor is not available, is not fulfilled. Therefore in an industrial application the soft-sensor models must be imbedded in systems that ensure robustness of the soft sensor performance. Before the measurements are used, signal conditioning (scaling, filtering) , data reconciliation including elimination of outliers, etc. [16, 17, 32, 33]. Also, as in [3]

it may be convenient to have several soft-sensor models for the same soft-sensor signal, in case one of the secondary measurements also fails. While the actual sensor is available, the error between the sensor and soft-sensor signals should be monitored. If some index of this error exceeds a certain threshold, a system must decide whether the cause is the sensor is faulty or the plant has changed its characteristics [6, 7, 8, 32, 33]. If the cause is the changing of plant characteristics, e.g., because the operating point has exceeded the region of validity of the current set of model parameters, then the plant must undergo some excitation of its inputs in order to estimate the new optimal parameter set. Having the plant under excitation conditions at all times would be frowned upon by the operators, so that this action should be resorted to only when it is indispensable.

SUMMARY OF RESEARCH AND APPLICATIONS

Soft-sensors are being increasingly applied in the process industries because their ability to solve the problem of the unavailability of sensors for any of the reasons already considered. Paralleling these growing applications, there is a quite a number of research results and ongoing research leading to the design of soft-sensors themselves, as well as to fault detection and identification. Table 1 contains a summary of a sample of the published literature concerning soft-sensors. Acronym used in table 1 are:
NN = Neural Network; RBF = Radial Basis Function; PCR = Principal Component Regression; PCA = Principal Component Analysis; ARMAX = Autoregressive Moving Average with eXogenuos input; NARMAX = Nonlinear ARMAX;

Table 1. Summary of Relevant Literature on Soft Sensors.

Ref..	Model Class	Main features	Applications
1	NARMAX	Stepwise regression. Comparison between gray and black box (linear) soft sensor models. Effects due to improper sampling period.	Tests in industrial grinding plant density and particle size. Sampling period effects tested in simulated simple plant.
2	Neural Network	Infrequent sampling. System implementation basics. General modeling approach	Naphtha end boiling point for a residual fluidic cracking unit
3	NARMAX	Stepwise Regression. Robustness to secondary measurements failures. Grey models using phenomenological components	Tests in particle size distribution in industrial grinding plant
4	NARMAX	Stepwise regression. Grey models. Availability Index increased through a system of soft-sensors	Tests in pulp density in industrial grinding plant
5	Neural Network	RBF properties. RBF polynomial expansions. Correlated noise. Validity tests.	Liquid level. Diesel engine speed
6	PCA	Missing measurement reconstruction (soft-sensing) for sensors within a set of sensors. Types of faults. Fault detection . Identification of failed sensor through s sensor validity index. Effect of filtering . Separating sensor fault detection from plant changes.	Data from boiler process with a 9-sensor set.
7	PCA	Geometric approach of subjects in FD3 and FD6 provides intuitive, although rigorous, point of view.	
8	PCA	Abridged version of [8]	
9	ARMAX	Infrequent sampling Adaptation	Biomass concentration, distillation tower top product composition, melt flow index in polymerization reactor
10	Kalman Filter	Infrequent sampling. Use of phenomenological knowledge	Fiber rate in sugar cane mill.
11	Neural Network	Infrequent (4 day) sampling. From ARMAX and NARMAX to Radial basis functions NN models. Determination of network topology and placement of RBF centers.	Biomass estimation in industrial process
12	Neural Network	Increasing use of soft-sensors in industrial applications reported.	Distillation column kerosene flash point and distillate flash point. Polymer melt index in industrial plant. Cardboard strength and porosity test for a liner board machine. pH for neutralization circuit in gold extraction.
13		Effect of plant parameter changes when the control loop includes a soft sensor	
14		Design problem when soft-sensor replaces sensor in control loop	
15	ARMAX	Comparison of soft-sensors with frozen, optimal and average parameters	Density in industrial grinding plant

Ref.	Model	Main features	Applications
16	Neural Network	Clustering. Infrequent sampling. System design features. Sensor selection by Singular Value Decomposition.	Compositions in distillation column top and bottom
17	Expert System	System implementation details	Cooking time and kappa number in batch pulping process in pulp mill.
18	NARMAX	Stepwise regression. Grey model.	Test for solids concentration in hydrocyclone overflow in industrial grinding plant
19	Neural Network	Radial basis NN. Infrequent sampling. Clustering, with fuzzy combination of outputs of cluster models.	Propylene and propone composition in distillation column
20	Kalman Filter	Extended Kalman Filter. Nonlinear state model based on phenomenological knowledge. Improvement over linear model using linear Kalman Filter.	Pilot SAG mill with aid of phenomenological model. Water, ore and fine ore content. Estimated parameters: ginding rate, water and ore discharge rates.
21	ARMAX	Stepwise regression. Comparison of soft-sensors with and without clustering. Soft sensor based exclusively on clustering	Tests in industrial rougher flotation plant grades. Tests of mill overload in industrial grinding plant.
22	NN	Infrequent sampling. Recurrent NN.	Simulation tests in simple plant
23	NARMAX	Stepwise Regression. Grey models Comparison between soft-sensor and control models	Tests in industrial rougher flotation plant concentrate grade
25	PCA, PCR, NN	Fault detection and identification of the set of sensors using sensor validity index. Actual and reconstructed measurements used as input to model.	Test in gas emission monitoring of industrial boiler
26	Neural Network	Recurrent Neural Networks Influence of noise on model and training algorithms	Tests using simulated abstract nonlinear plant
27	Neural Network	Identity NN used for estimating faulty measurements followed by soft-sensor model. Comparisons in terms of missing data	Recovery of light component in bottom of distillation column.

CONCLUSIONS

Soft-sensors are being increasingly applied in process industries. At the same time there is an appreciable deal of research and development in the modeling aspect and in the associated subject of fault detection and identification, sometimes with tests performed in pilot plants, and with tests and permanent applications in industrial plants. All classes of models are being used: regression and multivariable correlation models, neural network models, fuzzy logic models, and combinations between them, including the incorporation of phenomenological knowledge.

Concerning modeling, a unified point of view to consider under a common point of view several aspects concerning modeling with regression or correlation models, neural networks, etc. , appears to be lacking. One consequence of this is that different names are given to the same concepts, e.g.: parameters = weights, parameter estimation = training, prediction ability = generalization, etc. Even sometimes confusion arises because variables are give the name of "parameters" , most probably because parameters are already called weights in the neural network literature. In addition, some results which have already common knowledge in the case of ARMAX and NARMAX type models may be extended to the case of neural networks, e.g., in the case of the dependence of training and parameter estimation algorithms on whether the disturbances are white or colored noise [5, 26]. It would be useful to develop the unified approach initially attempted in this paper .

Although the published literature shows quite a deal of effort devoted to soft-sensor modeling and to fault detection and identification, not much is being done in the area of the effects produced by the substitution of a sensor by a soft –sensor. The fact that the soft-sensor model may result in a partial model of the plant using intermediate plant measurements, introduces problems in the overall control loop, which should be further investigated.

Good results obtained by introducing phenomenological components as inputs to regression models, suggest research in using a similar approach in other modeling methods, such as neural networks and principal component analysis models.

AKNOWLEDGEMENTS

The author is most grateful for the contribution of Aldo Casali, Gianna Vallebuona (Mining Eng. Dept., U. of Chile) and Ricardo Barrera (Electrical Eng. Dept., U. of Chile) for his work in soft-sensors.

REFFERENCES

1. González, G.D., Odgers, R., Barrera, R., Casali, A., Torres, F., Castelli, L., Giménez, P (1995) Soft-sensor design considering composite measurements and the effect of sampling periods. Proc. Copper 95, International Conference, Santiago, Chile, II, 213 - 224.
2. J.C. Wang and S.Q. Wang. Neural soft-sensor for the RFCCU's fractionator naphtha endpoint, 1996. INCONIP '96, Hong-Kong, 2, 1164-1168.
3. A. Casali, G. González, F. Torres, G. Vallebuona, L. Castelli, P. Giménez, 1998. "Particle size distribution soft-sensor for a grinding circuit". Powder Technology ,Vol. 99, pp 15 – 20.
4. Casali, A., González, G., Torres F., Cerda I., Castelli L., and Giménez P.,1995. Pulp density soft-sensor for a grinding circuit", Proc. XXV APCOM, Brisbane, Australia, 371-376.
5. S. Chen, S.A. Billings, 1990. Practical identification of NARMAX models using radial basis functions. Int. J. Control, 52(6), 1327-1350.
6. R. Dunia, S.J. Qin, T.F. Edgar, T.J. McAvoy,1996. Identification of faulty sensor using principal component analysis. AIChE Journal 42(10), 2797-2812.
7. R. Dunia and S.J. Qin, 1998. A unified geometric approach to process and sensor fault identification and reconstruction: the unidimensional fault case. Computers Chem. Eng. 22 (7-8), 927 – 943.
8. R. Dunia, S.J. Qin, T.F. Edgar, and T.J. McAvoy, 1996. Sensor fault identification and reconstruction using principal components. Proc. 13th Triennial IFAC World Congress, San Francisco, N, 259-264.
9. M.T. Tham, G.A. Montague, A.J. Morris, and P.A. Lant, 1991. Soft-sensors for process estimation and inferential control, J. Proc. Control, 1, 3-14.
10. S. Crisafulli, R.D. Pierce, G.A. Dumont, M.S. Ingegneri, J.E. Seldon, and C.B. Baade, 1996. Estimating sugar cane fibber rate using Kalman filtering techniques. Proc. 13th IFAC Triennial World Congress, San Francisco, USA. , 361-366.
11. A.G. Hofland, A.J. Morris and G.A. Montague, 1992. Radial basis function networks applied to process control. Proc. American Control Conf., 1, 480-483.
12. G. Martin, 1997. Soft-sensors get the process data you really want. Control & Instrument., K , Jan., 45
13. G:D: Gonzalez, R. Odgers. Issues in the design of control loops using soft-sensors, 1996. Proc. 13th IFAC Triennial World Congress, San Francisco, USA. A, 499-504.
14. G. González, M. González P., J.C. Cartes., Control problems due to replacement of sensors by soft - sensors. Advances in Instrumentation and Control, Proc. ISA/92 International Conference and Exhibition, Houston, USA., Oct. 1992, v. 47, part 2, 1193-1200.
15. G.D. González, M.A. Aguilera and L. Castelli, 1993. Development of a density soft-sensor for a mineral grinding plan Prepr. 12th IFAC World Congress, Sydney, Australia, 5, 355-358.
16. Fuzzy neural nets based soft sensor and its applications, 1994. Int. Conf. on Data and Knowledge Systems for Manufacturing and Engineering, 2, 503-508.
17. M. Rao, J. Corbin and Q. Wang, 1993. Soft sensor for quality prediction in batch chemical pulping process. Proc. IEEE Int. Symp. on Intelligent Control, 150-155.
18. A. Casali, G. Vallebuona, M. Bustos, G. González, P. Giménez, 1998. A soft-sensor for solids concentration in hydrocyclones. Minerals Engineering 11(4), 375-383.
19. X. Wang, R. Luo and H. Shao, 1996. Designing a soft sensor for a distillation column with the fuzzy distributed radial basis function neural network. Proc. IEEE 35th Conf. on Decision and Control, Kobe, Japan, 1714-1719.
20. R. Améstica, G. González, J. Menacho and J. Barría , 1993. On-line estimation of fine and coarse ore, water, grinding rate and discharge rates in semiautogenous grinding mills. Proc. XVIII International Mineral Processing Congress, Sydney, Australia, 1, 109-115.
21. Espinoza, P.A., G. D. González, A. Casali, C. Ardiles, 1995. Design of soft-sensors using cluster techniques. Proc. International Mineral Processing Congress, Oct. 22-27, San Francisco, 1, 261-265
22. Y. Yang and T. Chai, 1997. Soft sensing based on artificial neural networks, Proc. American Control Conference, Albuquerque, New Mexico, 1, 674-678.
23. G.D. González and J.P. Redard, 1994. Adaptive models for soft-sensors and control for a rougher

flotation plant, 1994. Proc. of ISA '94 Conference and Exhibit, Anaheim, CA, Oct. 3, 1143-1152.
24. R.H. Myers, 1990. Classical and modern regression with applications, 2nd Edition, Duxbury Press, Belmont, California.
25. S.J. Qin, H Yue and R. Dunia, 1997. A Self-validating inferential soft-sensor for emission monitoring. Proc. American Control Conf., Albuquerque, NM, 473-477.
26. O. Nerrand, P. Roussel-Ragot, D. Urbani, L. Personnaz and G. Dreyfus. Training recurrent neural networks: Why and how? An illustration of dynamic process modeling, 1994. IEEE Trans. On Neural Networks, 5(2), 178-184.
27. K. Meert, 1996. A real – time recurrent learning network structure for dealing with missing sensor data. IEEE, 1600-1605.
28. L. Ljung, 1987. System Identification: Theory for the User, P.T.R. Prentice Hall, Information and System Sciences Series, New Jersey.
29. R. Harber and H. Unbehauen, 1990. Structure identification of nonlinear dynamic systems –A survey on input-output approaches, Automatica, 26(4), 651-677.
30. J.E. Jackson, 1991. A user's guide to principal components, John Wiley, New York.
31. R. Bitmead, M. Gevers and V Wertz, 1990. Adaptive Optimal Control: The Thinking Man's GPC, Prentice Hall International Series in Systems and Control Engineering, New Jersey.
32. R. Barrera, G. Gonzalez, A. Casali, G. Vallebuona, 1996. SENVIR: A soft-sensor system for industrial applications (In Spanish). Project FONDEF MI-17, Dept. of Elect. Eng., University of Chile.
33. R. Issermann, 1994. Integration of fault detection and diagnosis methods, Prepr. IFAC Symposium on Fault Detection, Supervision and Safety for Technical Processes: SAFEPROCESS, 2, 597-612.

J. Keith Brimacombe Memorial Symposium: Intelligence in Materials Process Engineering

In Memory of J. Keith Brimacombe: The Pursuit of Quality in the Casting of Materials

I.V. Samarasekera

The Centre for Metallurgical Process Engineering
Advanced Materials and Process Engineering Laboratory
2355 East Mall, University of British Columbia. Vancouver, B.C. Canada
Email: indira@cmpe.ubc.ca

There are few of us who have impacted the field of metallurgical process engineering in the 20th Century to the extent of the late Keith Brimacombe. In a remarkable career, that spanned three decades, he changed the field irrevocably. Dr. Keith Brimacombe applied the power of combining mathematical models, sophisticated laboratory measurements and ingenious plant trials to analyse complex processes in both the non-ferrous and steel industries. Of his many contributions to the discipline, his work in the pursuit of quality in commercial casting processes stands out. It transformed our understanding of many processes and illustrated the importance of an interdisciplinary approach. Keith Brimacombe was passionate about the need to break down walls that exist between industries, between universities and industry, and between the scientist or engineer in the laboratory and the shop floor worker in whose hands lies the challenge of transforming knowledge into wealth.

This paper traces Dr. Brimacombe's contribution to the continuous casting of steel, the D.C. casting of zinc and aluminum, the static casting of fused cast refractories, and ingot casting. The paper also seeks to illustrate his philosophy of cross-fertilization of knowledge between industries, and of the power to apply lessons learned from one field to solve real-life problems in another. Through the use of mathematical models and judicious in-plant measurements, Keith Brimacombe and his students elucidated the formation mechanism of numerous defects in these casting processes and prescribed measures to eliminate them. Not content to simply publish his findings in journals, he went further by spearheading measures to transfer technology to the shop floor, through short courses, through in-plant trials which implemented his ideas, and through the development of expert systems. It was his dream to build an "intelligent continuous casting process" equipped with sensors and a "smart" system to monitor the formation of defects and prescribe corrective measures on line. These ideas are being pursued vigorously world wide and it is up to those of us who follow in his foot-steps to make them realities.

0-7803-5489-3/99/$10.00 ©1999 IEEE.

Towards Intelligent Steel Processing

Rian Dippenaar

BHP Institute for Steel Processing and Products, University of Wollongong, Northfields Avenue, Wollongong, NSW 2522, Australia

ABSTRACT

In recent times there has been a rapid increase in the use of dynamic models and artificial intelligence to control steelmaking processes. These developments have created a heightened awareness of the importance of developing diagnostic sensors to provide input into, or to validate process models. Of fundamental importance in various steelmaking processing steps is the control of the oxygen potential. Reliable and accurate sensing of the oxygen potential is a mandatory requirement if intelligent processing techniques are to be used. The late Keith Brimacombe pioneered the validation of many mathematical models and sensing devices designed for metallurgical process control by experimental measurement in the laboratory and on production plants. I have elected to honour him by emphasising the importance of the accurate measurement of the oxygen potential in liquid steel. The significance and experimental measurement of electronic conduction in electrochemical sensors will be highlighted, with special reference to the small zirconia sensors used in commercial practice.

INTRODUCTION

The late Keith Brimacombe passionately pursued the development of quantified links between process and product. He argued that measurements of processes give us understanding and knowledge, while mathematical models provide the framework to assemble the knowledge and to apply it quantitatively to link process behaviour and product properties. His refrain that validation of mathematical and computer models by experimental measurement is at the core of the success of intelligent processing, will always remain with me. Hence, I have elected to honour him in this special session of the Conference by concentrating on validation. In this instance not on the validation of a mathematical model as such, but on the validation of the measurement of the oxygen potential in liquid iron and steel. This measurement and the validation thereof is important, especially because many decisions made in the course of the various steelmaking processes hinge on a proper knowledge of the oxygen potential in the steel melt which, in turn, is pivotal information required for the effective use of mathematical process models employed as elements of the larger artificial intelligent systems.

Following the revolution in the engineering world brought about by Henry Bessemer's invention of a pneumatic steelmaking process in 1856, great strides have been made in process efficiency and product quality. Modern oxygen steelmaking processes are capable of producing 1000 tons of steel per hour and by the use of secondary processing techniques the impurity content can be reduced to less than 50 ppm. Suspension bridge cables with a tensile strength of 1.8 GPa have been used while the tensile strength of steel tyre chord is in excess of 3.5 GPa and steel sheet is drawn down to thicknesses of less than 0.1mm for the large scale production of beverage cans. These major achievements have been brought about by the integration of knowledge rooted in thermodynamics, reaction kinetics, fluid dynamics and a multitude of other disciplines.

Recently, great strides have been made towards the development of intelligent processing techniques, leading to yet further improvements in processing efficiency and product quality. The availability of high speed personal computers has led to the rapid development of computerised mathematical models with an emphasis on describing rigorously either individual process steps or integrating the process-product interrelationships. These models incorporate the basics of conservation and the laws of physics and chemistry mathematically and, once properly formulated and validated, predict product properties reliably and quantitatively as a function of process conditions [1]. In a related but different kind of approach we have seen the development of dynamic process models which combine heuristic and current process data

0-7803-5489-3/99/$10.00 ©1999 IEEE.

with fundamental knowledge to describe individual process steps and then employing artificial intelligence to integrate all of this into a unified whole.

This drive towards quantitative analysis and control of steelmaking processes has created a heightened awareness of the importance of developing diagnostic sensors to provide input into or to validate process models. Of fundamental importance in various steelmaking processing steps is the control of the oxygen potential. Not only does the oxygen potential determine the behaviour of various alloying elements, but it also impacts directly on the carbon, phosphorous sulphur, nitrogen and hydrogen contents of the steel product. It is therefore not surprising that considerable attention has been dedicated to the measurement of the oxygen potential in liquid steel, to the extent that instantaneous oxygen sensing has become an indispensable tool for process control. Moreover, in pursuit of modernisation and automation of continuous casting and ladle processing operations, it is not only the instantaneous measurement that is important but also the on line monitoring and control of the oxygen potential. Consequently, much effort had been expended to increase the lifetime and reliability of oxygen sensors. Reliable and accurate sensing of the oxygen potential is a mandatory requirement if intelligent processing techniques are to be used for the control of modern and advanced steelmaking processes. It is therefore of the utmost importance to assess the validity and accuracy of such oxygen activity measurements and the extent to which this information can be used in our quest to quantify and automate steelmaking processes.

THE PRACTICAL USE OF OXYGEN SENSORS

Steelmaking is an oxidation process in which the oxidisable elements in the melt are selectively transferred to the slag whilst decarburisation occurs at the same time. The transfer of silicon from the metal to the slag may be expressed as:

$$[Si]+2[O]=(SiO_2) \qquad 1.$$

Where [x] signifies an element in infinite dilute solution and (y) a compound in the slag.

or by the thermodynamically equivalent expression:

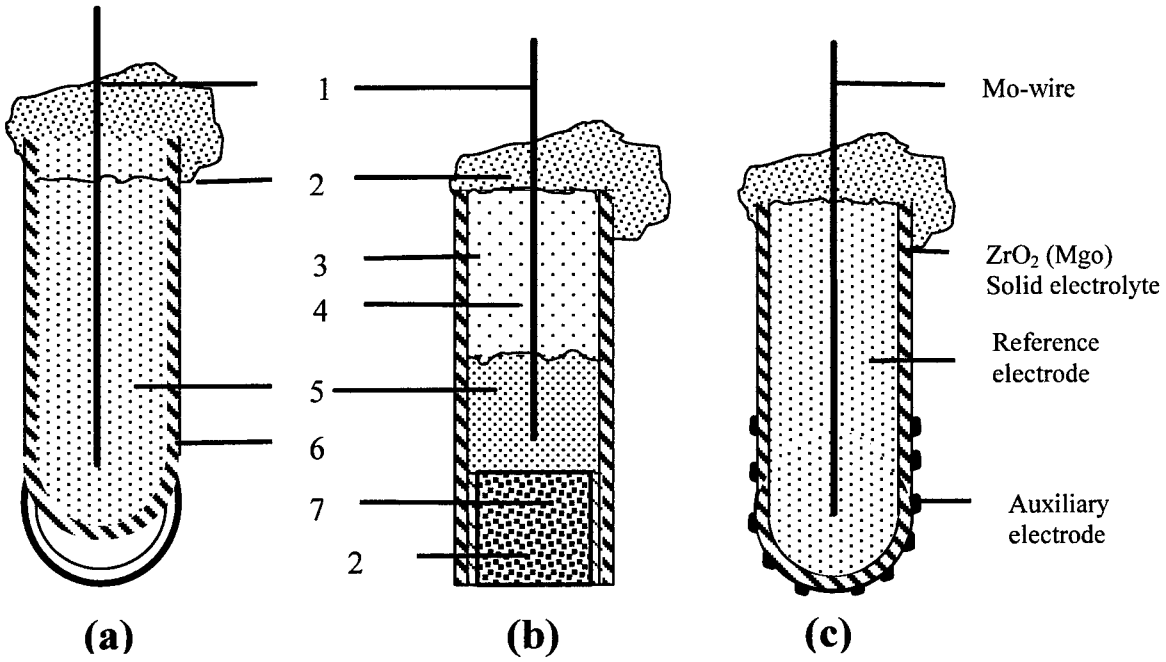
$$[Si]+(FeO)=(SiO_2)+Fe_l \qquad 2.$$

and similar equations apply to the oxidation of other elements.

From a fundamental point of view, the progress of such multi-component slag-metal equations can be described by incorporating the thermodynamics and process dynamics of the system. For example, Oeters and Xie [2] have shown that in a reaction such as Reaction 2, the thermodynamic equilibrium needs to be established, four flux equations need to be developed and three continuity equations need to be complied with. As the equalibrium constant is a function of the slag composition, this dependence also needs to be known before the kinetic analysis can be done. When the flux equations are integrated over time, an equation system for each component is obtained which yields the concentration versus time curves for each component in the bulk phases.

The silicon oxidation reaction is only one of many oxidation reactions occurring simultaneously in the steel bath and each one of these reactions has to be analysed in this fashion. However, a common denominator in all these reactions is the oxygen potential in the liquid pool as indicated in Equation 1, so that a knowledge of the oxygen potential of the liquid metal is a prerequisite for a proper understanding of the progress of these reactions and hence, for process control. For this reason oxygen sensors have been developed which can measure the oxygen potential of the steel bath instantaneously. A vast amount of work has been done on the development and application of such oxygen sensors and many literature reviews have been compiled. For example McLean [3], Iwase [4] and Janke [5]. No attempt will be made to review the literature, the vast portfolio of techniques employed, or the underpinning theory, save to put the current discussion into context.

The use of oxygen sensors employing stabilised zirconia solid electrolytes to measure the oxygen activity in molten steel in the various stages of steelmaking, has become standard practice. The tube design, shown in Figure 1a is typically used for instantaneous measurements while plug-type designs, such as shown in Figure 1b are employed for long term measurements in an attempt to minimise polarisation. Tu and Janke [6] used an even more advanced sensor to monitor the oxygen potential continuously during vacuum treatment of liquid steel for periods of longer than three hours. More recently, oxygen concentration cells have also been used to measure the activity of components other than oxygen in molten steel. For example silicon, chromium, titanium, phosphorous [4, 5, 7], Such measurements have been made possible by the incorporation of an auxiliary electrode in the sensor. An example of such an auxiliary electrode is shown in Figure 1c, the details of which will be discussed below.



1. Molybdenum wire
2. Alumina cement
3. Alumina tube
4. Alumina powder
5. Reference powder
6. Solid electrolyte tube
7. Solid electrolyte rod

Fig. 1. Schematic diagrams of oxygen concentration cells.
(a) ZrO_2-tube type; (b) Plug type; (c) Auxiliary type

THE THEORETICAL FRAMEWORK

Ideal electrochemical cells

The oxygen sensor which is widely used in the steel industry is essentially an electrochemical oxygen concentration cell, such as shown in Figure 1a, and which may be expressed as:

$$p_{O_2}(ref) \,|\, (solid\ electrolyte) \,|\, p_{O_2}(slag) \qquad 3.$$

Such a cell usually comprises a reference electrode of known oxygen potential, a solid electrolyte, for instance magnesia stabilised zirconia, and a liquid metal electrode, the oxygen potential of which is to be determined. The output signal of such an electrochemical cell is electrical voltage, which is related to the oxygen activity through the Nernst equation as follows:

$$E = \frac{RT}{nF} \ln \left[\frac{p'O_2}{p''O_2} \right] \quad 4.$$

where p'_{O2} and p''_{O2} are the oxygen partial pressures at the two electrolytes respectively, E is the Open-circuit emf of the galvanic cell, R is the Gas Constant, T the Temperature (K), n the number of electrons participating in the exchange reaction and F is Faraday's constant.

The partial pressure of the oxygen in the liquid metal is related to the oxygen activity through the thermodynamic equilibrium constant and hence, the oxygen activity in the liquid metal can be determined directly from the open-circuit potential of the cell.

By using a solid state zirconia electrolyte in conjunction with an auxiliary electrode, it has also been possible to measure the activity of alloying elements in liquid steel. For example, the activity of silicon in the liquid hot-metal product of the blast furnace can be measured by the addition of an auxiliary electrode firstly painted and then sintered onto a zirconia tube in the fashion shown in Figure 1c [4,7,8].

The electrochemical cell may be expressed as:

$$Mo \left| (Mo + MoO_2) \right| ZrO_2 (MgO) \left| (SiO_2)_{aux} \right| Si_{(in\,Fe)} \left| Fe \right. \quad 5.$$

The oxygen potential at the three-phase boundary (electrolyte + molten iron + auxiliary electrode) is established by the equilibrium reaction

$$ZrO_2(s) + Si(in\,Fe) + O_2(g) \Leftrightarrow ZrSiO_4(s) \quad 6.$$

for which

$$\ln K = -\ln h_{Si} - \ln p_{O_2} \quad 7.$$

where h_{Si} is the silicon activity in molten iron referred to a 1 mass % solution.

Substitution of the value of p_{O2} from this equation into Equation 4 yields the open-circuit cell potential as

$$E = \frac{RT}{4F} \ln \left[\frac{p'O_2}{K\, h_{Si}} \right] \quad 8.$$

Hence the activity of silicon, and in similar fashion that of other alloying elements in liquid metal, can be determined directly.

Practical electrochemical cells

The Nernst Equation above relates the true emf of the galvanic cell to the oxygen concentration difference across the solid electrolyte only in the ideal case when the solid electrolyte exhibits pure ionic conduction. In practice zirconia solid electrolytes exhibit ionic as well as n-type electronic conduction when used at high temperature and low oxygen potential. Wagner [9], in appreciation of this difficulty, developed a relationship between the emf and the oxygen potential of an electrochemical cell containing a solid

electrolyte which exhibits mixed ionic and electronic conduction. He had shown that the oxygen potential at the two electrodes μ'_{O2} and μ''_{O2} respectively, are related to the emf as follows:

$$E = \frac{1}{zF}\int_{\mu'_{O_2}}^{\mu''_{O_2}} t(ion)\,d\mu_{02} \qquad 9.$$

where z is the number of electrons required to ionise an oxygen molecule according to the reaction

$$O_2 = 4e^- = 2O^{2-} \qquad 10.$$

F is the Faraday Constant and $t_{(ion)}$ is the ionic transport number.

Since μ_{O2} can be related to the oxygen partial pressure, this equation simplifies to the Nernst equation (4) when $t_{(ion)} = 1$. In other words, when the solid electrolyte exhibits pure ionic conduction. Since the ionic conductivity is a function of the prevailing oxygen pressure, it is important to define a parameter which describes the electrical characteristics of the solid electrolyte irrespective of the partial pressure of oxygen. Schmalzried [10], carefully analysing Wagner's model and proposed such a parameter which he called P_e and which characterises the electronic conductivity of a solid electrolyte. P_e is defined as the partial pressure of oxygen at which $t_{(ion)} = 0.5$. In mathematical terms this statement may be expressed as:

$$t_{(ion)} = \frac{1}{1 + \left[\frac{p_{O_2}}{Pe}\right]^{-\frac{1}{4}}} \qquad 11.$$

Substitution of this criterion into Wagner's equation leads to the following relationship:

$$E = \frac{RT}{4F}\ln\left[\frac{(p''_{O_2})^{\frac{1}{4}} + (Pe)^{\frac{1}{4}}}{(p'_{O_2})^{\frac{1}{4}} + (Pe)^{\frac{1}{4}}}\right] \qquad 12.$$

Thus, if the extent of electronic conduction of a solid electrolyte, characterised by the P_e value is known, and accurate measure of the prevailing oxygen potential in liquid metals or slags can be obtained from a measurement of the emf of the electrochemical cell. It is consequently of great importance to assess to what extent accurate values of P_e can be obtained experimentally and also to determine what material properties and processing parameters have an influence of the electronic conductivity. Hence, the P_e-value of a particular solid electrolyte ought to be determined before its use. It is also important to be aware that an erroneous emf may be measured if electronic conduction in the solid electrolyte causes transportation of ions which, in turn, will cause polarisation. Also, if chemical interaction between the melt and electrolyte influences the electrical characteristics thereof. In addition, mass transport of oxygen in the melt may influence the absolute value of the emf measured. Mass transport becomes important, especially in those cases where multi-phase equilibria need to be established.

A single example will illustrate the importance of knowing precisely the P_e-value of the solid electrolyte used in an electrochemical cell which is used to determine the oxygen potential of a liquid metal. As background it is of some significance to refer to requirements in the stainless steel industry. The amount of alloying additions, the optimum slag composition required to ensure efficient refining and the details of the process route to be followed are usually determined by the use of mathematical models and artificial intelligence systems. Of critical importance to calculate these requirements, is a knowledge of the activity of chromium in the melt, simply because it is the prevailing activity of chromium which dominates the

slag/metal equilibria of importance. Hence, the intelligent processing aids employed in process control are of little value if the activity of chromium as a function of alloy content of the molten bath is not known to a high degree of accuracy. Experimentally, the chromium activity can be calculated from a knowledge of the oxygen potential in a liquid iron-chromium alloy which is in equilibrium with a Cr_2O_3-saturated slag. This value in turn, is determined by an electrochemical sensing techniques as described above, employing a zirconia solid electrolyte as the core component.

About thirty years ago Fruehan, in pursuit of optimising process control, measured the chromium activity in iron using such an oxygen probe [11]. Many years later, Geldenhuis [12,13] repeated these same measurements for different reasons but, interestingly enough, found a discrepancy of some 30% in the chromium activities at chromium compositions of commercial interest. It was possible to resolve this discrepancy by consideration of the properties of the solid electrolytes used in the different experiments. At the time Fruehan did his experiments, the electric characteristics of zirconia electrolytes were not known and he was forced to assume that the solid electrolyte is an ideal ionic conductor. Geldenhuis on the other hand, measured the P_e-value of the solid electrolyte he was using. Fortunately, Fisher and Pieper [14] had by then measured the P_e-value of an electrolyte similar to that used by Fruehan and when the activities Fruehan measured were recalculated using this P_e-value, the recalculated activities agreed with those of Geldenhuis. This example is important because it shows that a 30% error in the experimentally determined values of the chromium activity in liquid iron can result from a lack of knowledge of the P_e-value of the solid electrolyte used in the sensor, emphasising the need to know the P_e-value exactly.

Experimental measurement of the P_e value

The P_e-value of a solid electrolyte can be determined most effectively by measuring the cell emf of type:

$$p'_{O_2} \left| (solid\ electrolyte) \right| p''_{O_2}$$

where

$$p'_{O_2} << Pe << p''_{O_2}$$

By imposing this condition, equation 12 becomes:

$$E = \frac{RT}{4F} \ln\left[\frac{p''_{O_2}}{Pe}\right] \qquad 13.$$

The value of P_e can therefore be determined directly if the value of p''_{O2} is known.

The so-called coulometric titration method [15] embodies these principles and is usually used to measure the P_e-value of solid electrolytes. A typical cell arrangement for such a measurement is shown in Figure 2.

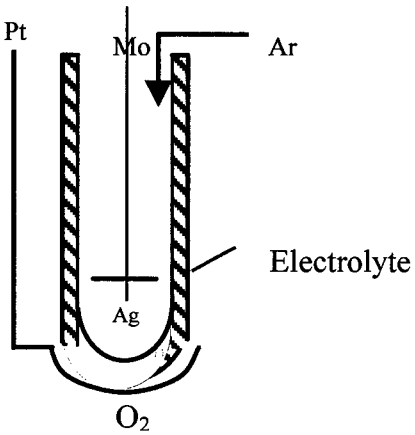


Fig. 2. Cell arrangement for Coulometric Titration

Experimentally, the condition $p'_{O2} << P_e$ is imposed by passing a direct electrical current under an applied potential of approximately 5V through the cell so as to remove oxygen electrolytically from the silver, transporting it to the Pt/Ag electrode and thereby polarising the silver interface of the electrolyte. Since the Pt/O_2-electrode is essentially non-polarisable, the partial pressure at this interface of the electrolyte remains atmospheric, hence maintaining the condition $P_e << p''_{O2}$. As soon as the polarising current is interrupted, a stable open-circuit emf plateau is obtained for about 4 seconds after which the potential decays slowly. However, it is only possible to obtain a stable plateau if there is no leakage of O_2 back into the molten Ag and so, a gas-tight experimental assembly is a prerequisite if reliable P_e measurements are to be made. An example of the P_e-values of a long MgO-stabilised zirconia tube, as a function of temperature, is shown in Figure 3.

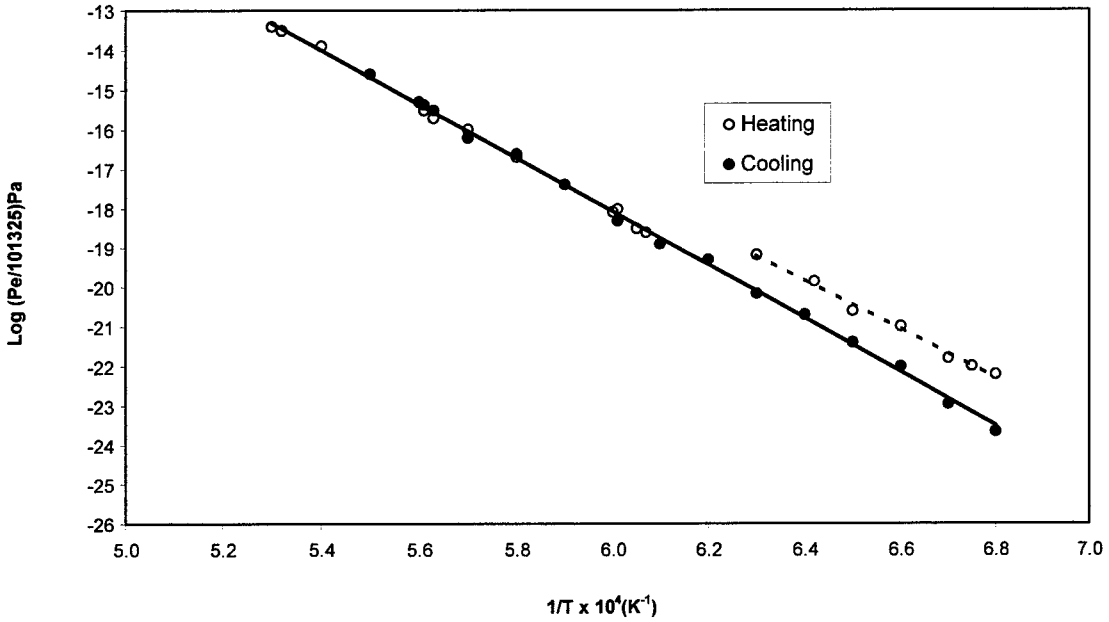


Fig. 3. P_e-values of a long magnesia stabilised zirconia solid electrolyte tube as a function of temperature

It is interesting to note that the solid electrolyte displays different P_e-values on heating and cooling below a temperature of 1400 °C and furthermore, that this behaviour is irreversible. However, the P_e-value measured above 1400 °C is the same whether a heating or cooling cycle is used. This behaviour is related to the phase composition in the ZrO_2-MgO-system and it does indicate that phase equilibrium in the solid electrolyte is to be ensured before reliable measurements can be made.

Because the electrical characteristics of a solid oxygen electrolyte are dependent not only on the bulk chemical composition but also on the manufacturing technique, heat treatment and phase composition, the P_e-values of the small solid electrolyte tubes which are actually being used in the commercial oxygen sensors need to be determined. In the past it was not possible to use the coulometric titration technique for this purpose because of the difficulties encountered in constructing a gas tight seal between the small electrolyte tubes and the extension tube which is required to position the small tube in the hot-zone of the furnace. Recourse had to be had to measurements on long tubes which were manufactured to simulate the properties of the tubes actually used in the commercial sensors. However, a couple of years ago, researchers in the University of Pretoria overcame this problem by the construction of a gas-tight seal which enabled the positioning of the small tubes in the hot-zone of the furnace [16,17]. It is the construction and use of this seal which has led to the accurate measurement of the P_e-values of the solid electrolytes which are used in commercially available oxygen probes.

The construction of such a gas-tight seal is schematically shown in Figure 4.

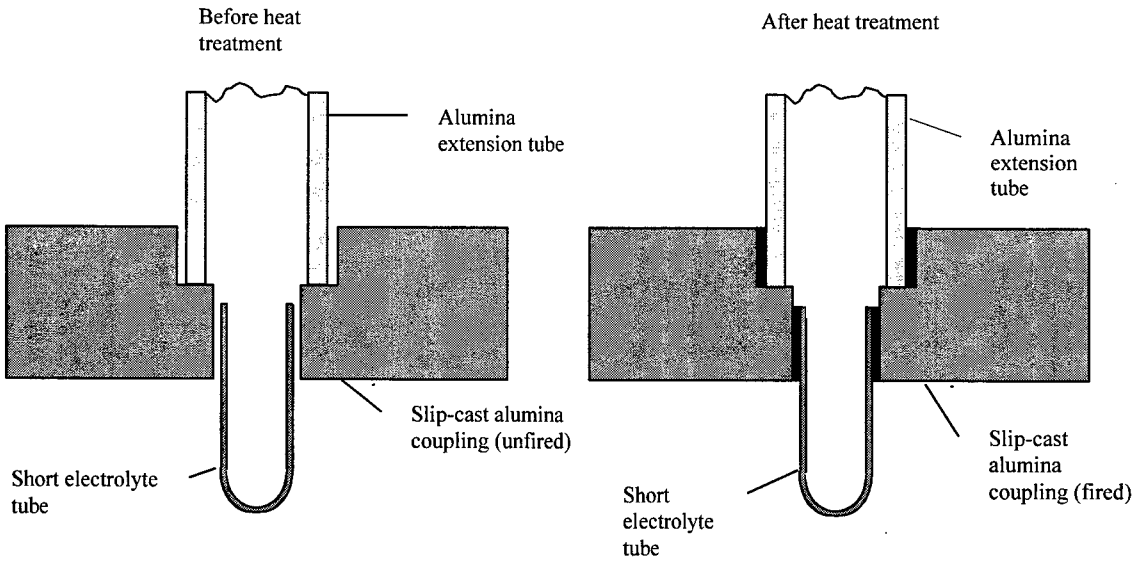


Fig. 4. Schematic illustration of the construction of a gas-tight ceramic seal

In principle, a short electrolyte tube is coupled onto an alumina extension tube by means of a slip-cast alumina coupling. Experimentally, a slip-cast alumina disc was presintered at 900 °C to strengthen it, followed by machining of the appropriate holes. The small electrolyte tube, alumina extension tube and the alumina coupling were assembled and slowly heated to 1500 °C, held for 2 h and slowly cooled to room temperature. During the heat treatment the slip-cast alumina disc shrinks and forms a strong gas-tight seal round the surfaces of the electrolyte and the alumina tube. Using such seals, the P_e-values of short solid zirconia electrolytes could be measured and the results of such experiments are shown in Figure 5.

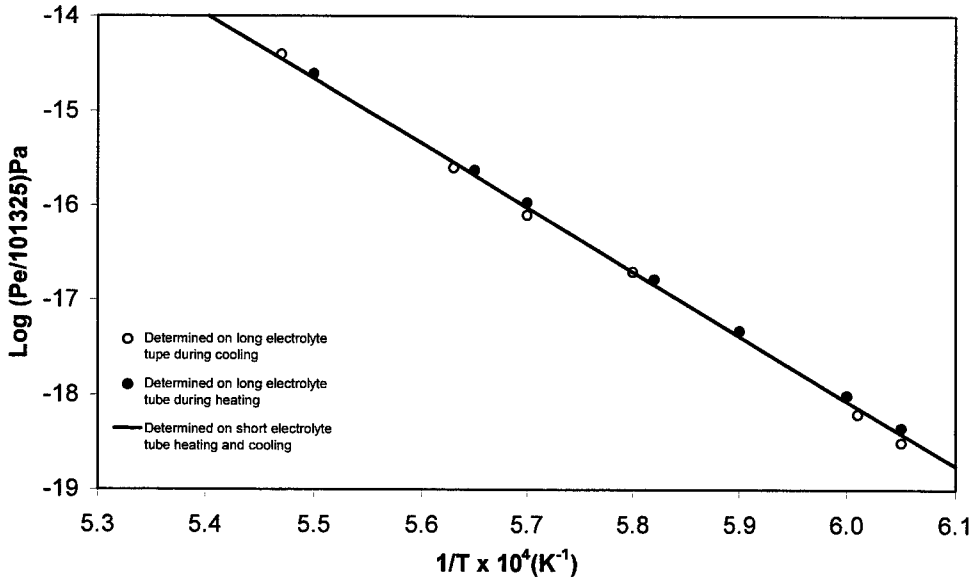


Fig. 5. P_e-values of short magnesia stabilised zirconia solid electrolyte tubes, of the type used in industrial practice, as a function of temperature

DISCUSSION

The late Keith Brimacombe had a passion to quantify the linkage between process and product. He developed as well as implemented mathematical models and artificial intelligence at a time when other

process metallurgist still feared to tread. Another passion was to validate such models and many examples of careful experimental measurements in the laboratory and pioneering measurements on the plant are to be found in his work. However, he not only emphasised the validation of models but also the validation of the data which are used as input to these models. I have attempted to illustrate the great importance of the validation of such data, in this instance the electronic properties of solid electrolytes which are used daily in most steel plants. That brings me to the third of Keith's many passions: the interaction between university and industry. He impressed industry and the scientific community alike with his remarkable talent to nurture collaboration and has as a consequence received wide recognition for these efforts. I am glad to say that the work on the experimental measurement of the oxygen potential, conducted in the University of Pretoria, was done in close collaboration with the steel industry as well as the ceramics industry and

Thus the engine of knowledge generation
(was) coupled with the engine of wealth creation

J Keith Brimacombe (1993) [18]

The development of the gas-tight ceramic seal has made it possible to measure the P_e-value of the small electrolytes used in commercially available oxygen sensors. This means that the prevailing oxygen potential can be determined to a high degree of accuracy and consequently, the equilibrium distribution of oxidisable elements between the liquid metal and the slag can be calculated much more reliably. Because the prevailing oxygen potential in the liquid metal/liquid slag system plays such a pivotal role in the mathematical models which in turn, form an integral part of the intelligent process control systems used in steel processing, a proper knowledge of the oxygen potential should enhance effective process control.

I should like to conclude with reference to the well-known words of Henry Longfellow which I thought apply to our gathering here today:

Lives of great men all remind us
We can make our lives sublime,
And, departing, leave behind us
Footprints on the sands of time.

Let us pay tribute to our dear departed friend by striving to achieve those ideals he so passionately fought for. Let us, like him, relentlessly labour in pursuit of the truth and

Let us, then, up and doing,
With a heart for any fate;
Still achieving, still pursuing,
Learn to labour and to wait.

A Psalm of Life (1838)
Henry Wadsworth Longfellow

REFERENCES

1 J.K. Brimacombe, 1989. The extractive metallurgist in an emerging world of materials. *Metall. Trans. B.,* 20B, June, 291-313.

2. F. Oeters and H. Xie, 1995. A contribution to the tehoretical description of metal-slag reaction kinetics. *Steel Research,* 66(10), 409-415.

3. A. McLean, 1990. Sensor aided process control in iron and steelmaking. *Solid State Ionics* 40/41, 737-742.

4. M. Iwase, 1992. Developments in Zirconia Sensors during the 1980's – Laboratory and in-plant applications in iron and steelmaking. *INFACON 6, Proc. of the 1st Chromium Steel and Alloys Congress, Cape Town,* V.2, Johannesburg, SAIMM, 49-61.

5. D. Janke, 1990. Recent developments of solid ionic sensors to control iron and steel bath composition. *Solid State Ionics* 40/41, 764-769.

6. S. Tu and D. Janke, 1995. EMF Sensor Control in vacuum decarburization and deoxidation of steel melts. *ISIJ Int.* 35(11), 1362-1367.
7. S. Tu, V. Burzev and D. Janke, 1995. EMF Sensing of Al, Ti and Cr dissolved in pure iron melts. *Trans. ISS*, Nov, 61-68.
8. M. Iwase and A. Mclean, 1990. Sensors for iron and steelmaking. Proc. of the 6th International Iron and Steel Congress, Nagoya, Japan, *ISIJ*, 521-528.
9. C. Wagner, 1993, Theory of Tarnishing Process, *Z. Physic. Chem*, Abt. B, 21, 25-41.
10. H. Schmalzried, 1962. Uber Zircon dioxid als Electrolyte für electrochemische Untersuchungen bei hoheren Temperaturen. *Electrochemie*, 66, 572-576.
11. R. J. Fruehan, 1969. Activities in the liquid Fe-Cr-O system. *Trans. Met. Soc. AIME*, 245, 1215-1218.
12. J.M.A. Geldenhuis, 1991. Development of electrochemical sensing techniques for the determination of activity-composition relations in liquid alloys and slags at 1873K. *PhD thesis, University of Pretoria.*
13. J.M.A. Geldenhuis and R.J. Dippenaar, 1991. A reassessment of the activity of chromium in the Fe-Cr-O system at 1873K. *Metall. Trans. B.,* Vol 22B, Dec, 915-917.
14. W.A Fisher and C. Pieper, 1973, Die elektrische Leitfâhigkeit und Thermokraft von reinem und mit Calciumoxid stabilisation Zirkonoxid bel Termperaturen zwischer 1000 und 1700°C und Sauerstoffpartiel drücken zwischen 1 und 10^{-16} atm *Arch. Eisenhüttenwes,* V.44, 251-259.
15. D.A.J. Swinkels, 1970. Rapid determination of electronic conductivity limits of solid electrolyte. *J. Applied Electrochemistry,* 1297-1298.
16. J.M.A. Geldenhuis, 1988. The quantitative determination of certain electrical characteristics of commercial zirconia solid electrolytes (in Afrikaans), University of Pretoria.
17. M.J.U.T. van Wijngaarden, J.M.A. Geldenhuis and R.J. Dippenaar, 1988. An experimental technique employing a high-temperature gas-tight alumina seal for the assessment of the electrical properties of solid electrolytes. *J. Applied Electrochemistry,* 1998, 18, 724-730.
18. J.K. Brimacombe, 1993. Prosperity into the next millenium built on the process engineering of materials. *1st Int. Conf. On Processing Materials for Properties, Eds. Henein and Oki, The Minerals, Metals and Materials Soc.,* 7-15.

Computer Simulation and Information Management Systems for Material Processing

Yoshiyuki Nagasaka

Department of Distribution Science, Osaka Sangyo University
3-1-1 Nakagaito, Daito, Osaka, 574-8530, Japan

ABSTRACT

Several computer simulation and information systems for machinery industries have been studied. The objective is to construct a virtual manufacturing environment for concurrent engineering. For the environment, three types of models, which are geometry model for a product, mathematical model for physical phenomena and activity model for human operations, should be considered. In this study, computer simulation systems for casting and heat treatment processes as tools of a virtual manufacturing environment have been developed considering the interface of geometry model from a three-dimensional CAD system. These computer simulations can predict the quality and productivity quantitatively. As well, an information management system for pre-production material processes based on activity models has been developed. Background data for decision-making is stored and related to foreground information such as multimedia data. A summary of the system is shown and several examples are presented.

INTRODUCTION

If the manufacturing conditions can be optimized in the design stage before actual trials, the total cost and lead-time can be reduced drastically. Generally speaking mechanical designers should consider functions and productivity simultaneously, but it is not easy. However they must indicate which processing is good for each part in a drawing definitely. For example, it is very important to select proper material and heat treatment process for gear production. The problem is that manufacturing engineers have no generic method to show quantitative data to the designers before actual trials so far. It is thought that VME (Virtual Manufacturing Environment) is one of the most effective technologies to solve this problem. In this study, several computer simulations and information systems have been developed to construct a virtual manufacturing environment of materials processing.

For a virtual manufacturing environment, geometry model and mathematical models for physical phenomena should be considered as well as activity models for operations. Recently some three-dimensional CAD systems have come into wide use to handle geometry models easily. In practice many pre-production processes are performed considering the geometry. Activity models for pre-production processes are useful to inherit and improve the skillful operations. Computer simulation based on mathematical models is also useful to predict productivity and quality for the materials processing. These tools are valid by harmonizing with practical works.

Although several commercial software packages for material processing are available, we sometimes want to develop an original computer simulation system because these packages are not satisfied very much for the practical operation. However it is not easy to develop such a sophisticated system by only one company. For this problem it may be a good way to construct a consortium. The consortium can consist of some companies, universities as well as organizations of the government for specific objective. A computer simulation system for casting processes has been developed by a Japanese consortium and named "JS-CAST". Mold filling and solidification phenomena can be simulated to predict shrinkage cavities and optimize mold design. The architecture of "JS-CAST" is open to users. Namely, it is possible to develop other unique solvers and combine them with "JS-CAST". This function is helpful to make the CAE system grow up. In addition, another computer simulation system for heat treatment named "GRANTAS" has been developed. It is based on a mathematical model of phase transformations and elasto-plastic stresses. Hardness and residual stress distribution can be predicted.

0-7803-5489-3/99/$10.00 ©1999 IEEE.

Furthermore, an information management system for material pre-production processes named "JCAP" has been developed based on activity model by considering the requirements of practical engineers. The objectives of the system are to achieve more efficient and reasonable pre-production design as well as to inherit traditional technologies. A methodology has been developed to implement the activity model in a computer. The activity model includes task models which are structured as a tree and related with a data model including background information. Documents, drawings and computer files are created through several tasks. We can know the foreground information by looking at the results. But, it is usually very difficult to know the reason why the value was fixed. Namely, the background information is important to know how the engineer made a decision. For example, a drawing is not enough to know why and how the dimension is determined. The design background information is stored and linked to each object in the drawing in this system. It helps us to verify design conditions.

VIRTUAL MANUFACTURING ENVIRONMENT FOR MATERIAL PROCESSING

Most companies continue to make effort to utilize information technologies to improve quality and productivity. Actually each computer system has been developed and used to optimize each process. CAD is powerful to achieve efficient drawing and CAM is popular to produce metal molds with very accurate dimensions. PDM is useful to store and control lots of data related to a product. Recently integration of each system is progressed to optimize enterprise resources totally. ERP is considered as a representative system to control stock and to manage human operation and manufacturing procedures depending on demand. Moreover, the concept of virtual manufacturing environment is accepted to put into practical use. Digital manufacturing or digital engineering has similar meaning. The relation of these computer systems and business processes is shown schematically in Figure 1.

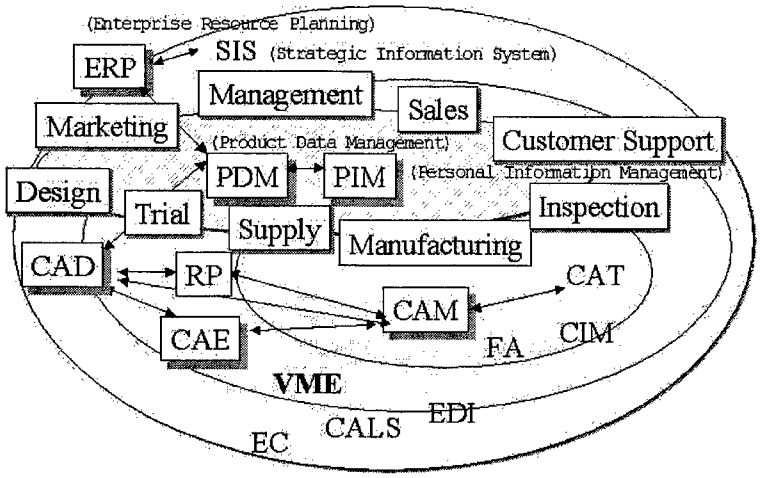


Fig.1. The relation of information systems and business processes.

Concurrent engineering approach can be performed efficiently and powerfully in a virtual manufacturing environment. Namely, a virtual prototype is generated and examined by common consent in network computers. A designer generates a geometry model. The model is the origin of a virtual prototype. The prototype is transferred to manufacturing designers, cost estimation engineers, supply division workers and so on. A lot of examinations can be performed simultaneously. At the same time, lots of explicit data such as weight, cost, supplier's name and delivery date is attached to the prototype. During these processes, requirements to modify the design must occur many times because productivity and reliability are checked from several different views. For example, a virtual environment for assembly is very useful to check interference problems and to estimate assembly time. If some problems are found out, the original geometry may be changed. Off line teaching system for industrial robots is also very powerful to set up NC data in a short time without inconsistency. Each CAE system for each process has been developed for specific purpose as shown in Table.1.

Recently, these CAE systems are used in an integrated virtual manufacturing environment. The common geometry model, which can be applicable to all tools in the environment, should be prepared. In addition, not only explicit simulation such as geometry check but also mathematical models to predict quality of a product such as fatigue strength and residual stresses are very important. For instance, scattering range of mechanical properties such as hardness distribution usually depends on the character of material processing and the original quality of material. The designer should consider the substantial strength essentially. For these problems, several computer simulations of material processing are useful. Although several commercial software packages are available, they cannot sometimes satisfy us very much for practical operations. However it is difficult to develop and improve such a sophisticated system by only one company. For this problem it may be a good way to construct a consortium which consists of some companies, universities and organizations of the government. A consortium in Japan has developed a simulation system for casting processes as shown later. Furthermore, computer simulations for heat treatment developed by us is ready to be grown up by another consortium. Not only computer simulations but also information management systems are necessary to construct a virtual manufacturing environment. An information management system for material pre-production processes has been developed based on activity model by a consortium as shown later. It is important that we should have tools which can show clear quantitative data and rationale of material processing to mechanical designers and others who don't know the processing very much. Those tools are important parts of a virtual manufacturing environment.

Table 1: Processes for machinery production and applicable CAE for VME

Process		Objective	CAE
Design	Planning	Design	Design CAD
		Layout, Vision	Geometric Simulation
	Parts	Elastic stress	stress analysis
		Fatigue life	Fatigue analysis
		Contact	Contact stress analysis
		Vibration	Vibration analysis
	Behavior	Collision	Collision analysis
		Noise	Noise analysis
		Comfortableness	Vibration analysis
	Engine	Power	Combustion analysis
		Efficiency	Thermal fluid flow analysis
	Piping, Harness	Layout	Geometric Simulation
		Assembly efficiency	Geometric Simulation
Material processing	Casting	Defect, Microstructure, Strength	Mold filing, solidification analysis
	Forging	Defect, Productivity	Plastic deformation analysis
	Powder metallurgy	Deformation, Productivity	Distinct Element analysis
	Plastic forming	Productivity, Quality	Plastic deformation analysis
	Polymer processing	Injection condition, Quality	Mold flow analysis
	Electric device processing	Productivity, Quality	Molecular dynamics
Manufacturing processing	Welding	Nesting, Deformation	Thermal stress analysis
	Robot teaching	Off-line teaching	Robotics simulation
	Machining	Process planning	Machining simulation
	Heat treatment	Condition, Microstructure, Strength	Phase transformation, Thermal stress analysis
	Surface treatment	Condition, Strength	Chemical phenomena simulation
	Component	Assembly efficiency	Geometric Simulation
	Sub-assembly	Assembly efficiency	Geometric Simulation
	Total assembly	Assembly efficiency	Geometric Simulation
	Scheduling	Optimum scheduling	Operation research
	Supply management	Optimum supplement	Operation research

DEVELOPED COMPUTER SIMULATION SYSTEMS FOR MATERIAL PROCESSING

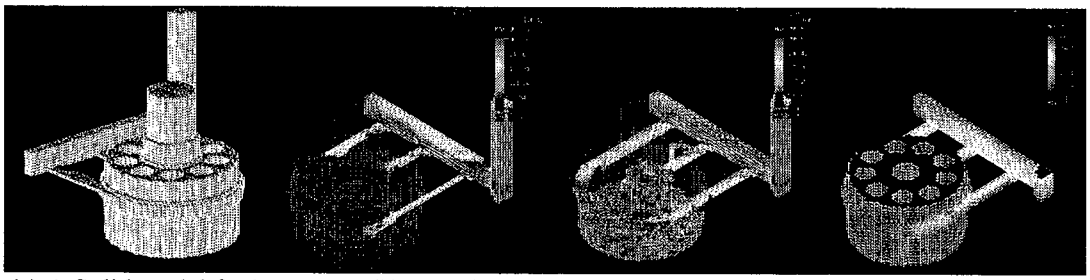
Mold Filling and Solidification Simulation for Casting Processes

Research Committee of Casting CAE (Chairman: I.Ohnaka) was established at the Materials Process Technology Center in Japan to propose a suitable basic design of a new CAE system for casting processes in 1992. The proposal was adopted as a development project of 1993 by Japan Small Business Corporation, which is one of the government organizations. Then, a CAE system of casting processes named "JS-CAST" has been completed as a result of many people's effort for three years. At first, the know-how and basic technology of "SOLDIA" [1] developed by Komatsu Ltd., which is one of the most popular packages for foundries in Japan, has been succeeded to by "JS-CAST"[2]. Then, the results of research performed in Osaka University were added to the CAE system. This approach could reduce the development time and cost. For development, the necessary conditions mentioned below were fully considered.

1. Clear objectives of CAE System and low computation cost
2. Accurate predictions and user friendly operation
3. Open architecture and enough support service

The CAE system consists of pre-, main-, post-processor, CAD data interfaces and a weight calculation module [2]. Mold filling and solidification phenomena can be simulated with rectangular elements for DFDM (Direct Finite Difference Method). The CAE system is available on UNIX or Windows. Project Manager has been developed to supply more user-friendly operation. Once "JS-CAST" is executed, Project Manager is displayed and small windows are prepared to show three-dimensional shapes of several projects indicating each progress. If a project's window is chosen, the menus that should be selected next are highlighted for easy operation.

For three dimensional geometry construction, digitizing of a drawing and utilizing a two-dimensional CAD data of IGES as well as direct input of coordinates are possible. Primitive shapes such as polyhedron, cylinders and solids of revolutions are created and combined by rotating, copying and moving. STL data can be utilized as direct input data, too. A rectangular mesh in xyz is generated automatically keeping in mind the maximum and the minimum dimensions of casting along the x, y and z directions. Furthermore, the operator can edit the generated mesh easily. After these operations, the system automatically creates a solid model of the casting including its mold. The mold-filling solver calculates transient fluid flow with free surfaces and heat transfer phenomena. The temperature distribution after pouring is used as initial conditions of the solidification solver. Solidification time and parameters to characterize shrinkage defects are stored as calculated results. Post-processing by using multi-windows is very useful to compare several results. Any sections of the casting and mold can be scanned simply with a mouse operation. An operator can check filling time, velocity, temperature, pressure, solidification time and temperature gradient of any desired section from any three-dimensional view. An example is shown in Figure 2.



(a) A Solid model for DFDM (b) Velocity distribution (c) Temperature distribution

Fig. 2. A mold filling calculation of a casting

Phase Transformations and Elasto-Plastic Stress Simulation for Heat Treatment Processes

Mathematical models for thermo-elasto-plastic behaviors during material processing have been studied by J.K.Brimacombe 's group vigorously [3]. then, a practical computer simulation system using FEM (finite-element technique), named "GRANTAS", for heat treatment processes was born based on the research[4]. The objective is to predict microstructure and hardness distribution, as well as distortion and residual stresses quantitatively in practical use. The linkages among temperature, stress, carbon distribution and microstructure, which a model of carburizing and quenching must be able to predict, are shown in Figure 3. Thus, the four sub-models which comprise the overall model should be coupled, because the microstructure is determined by the thermal history while the heat generated by the phase transformation influences the temperature distribution; the volume changes produced by phase transformations and variations in temperature result in thermal stresses. An elasto-plastic model is needed to compute stresses, because normally, the yield stress is exceeded during quenching to cause residual stresses and distortion of some magnitude.

Hardness distribution is one of the most important properties that mechanical designers want to know. In order to estimate the hardness, the following procedure can be adopted. First, an equivalent Jominy distance is obtained from the calculated cooling rate at each point by applying the experimental relations; then, the hardness is calculated based on experimentally obtained Jominy curves. If the experimental data can be obtained easily and generally, a mathematical model for practical purpose should use them positively.

"GRANTAS" has pre-, main-, post-processor and properties database. Meshing for FEM is semi-automatically generated based on CAD data. After meshing, the operator must select material and heat treatment conditions. Finally, calculated results are obtained as shown in Figure 4 and 5.

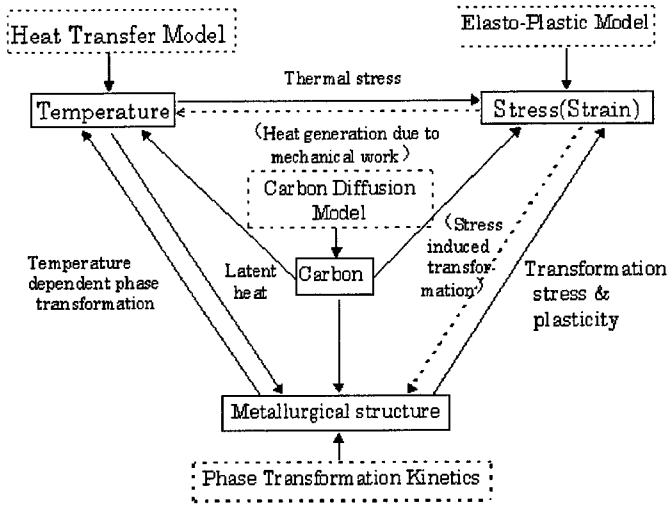
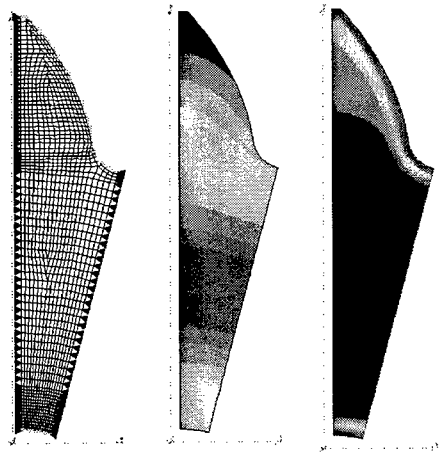


Fig.3. The linkages among temperature, stress, carbon distribution and microstructure.



(a) FEM mesh (b) Temperature (c)Hardness

Fig.4. A simulation of quenching (1/2 tooth of a gear)

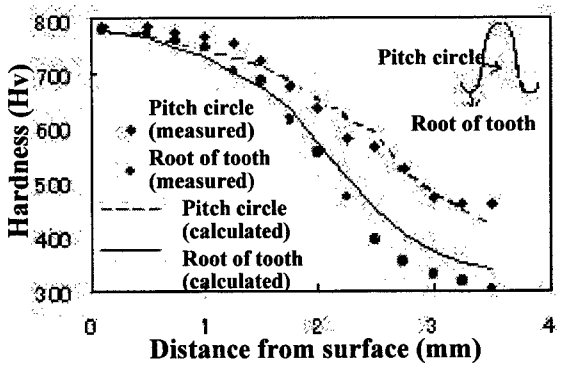


Fig.5. Comparison of predicted and measured hardness distribution in a gear

An Information Management System for Material Pre-Production Processes based on Activity Model
In general, pre-production work is a non-routine work and much depends upon inherent technologies of the person in charge. It is necessary to share and inherit important information in natural form [5]. Here, methodology has been reviewed to register background information for decision making in addition to formal information as a database and relate it to activity model and CAD system. Requirements for pre-production supporting information system are summarized as follows. (1) Complete data management with which data in various forms like figures, pictures or CAD drawings can be easily accumulated and retrieved. (2) Clear modeling of pre-production work and link to database of background information relating to each process. (3) A system to accumulate data with less load operation. (4) A system that can manage information that should be unitarily and centrally controlled for the company and other types of information that should be accumulated and distributed for individual person in charge or small groups.

Activity model is a model of entire production activity which include various elements of working procedure or person in charge, negotiation, environment, background of decision making and so forth. Here, activity model is considered to implement for practical use and an infrastructure-like software named "J-CAP" has been developed. The activity model can be loaded in the combination of three elements such as hierarchical task model, design items to be determined in each work level (like shape, working condition or specification) and background information related to each design item. These three elements are arranged in the manner where they can be freely registered or changed and their mutual relationship can be modified or dynamically constructed as shown in Figure 6. Thus, an integrated system was developed in which this activity model and multi-media database and further, CAD are combined. All contents of operation are accumulated as log information and determined values are accumulated as a part of product information. Through the above arrangement, it became possible to select effective background information like frequently used information or the basis to obtain reliable quality. Relationship between the determined value and the applied background information used to determine it is referenced when the ground of the production design is perused while it is also used to check whether determined value contains any error. It should be possible to revise and improve production design standard using this system.

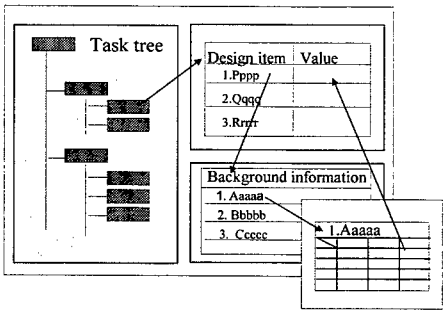


Fig.6. Man-machine interface for activity model

SUMMARY AND CONCLUSIONS

The concept of virtual manufacturing environment has been discussed and summarized. In order to construct the environment, practical simulation systems for casting and heat treatment processes have been developed and introduced. It is found that developed information management system for material pre-production processes based on activity model is also useful in practice.

REFERENCES

1. Y.Nagasaka, S.Kiguchi, M.Nachi and J.K.Brimacombe .1989. *Three Dimensional Computer Simulation of Casting Processes.* AFS Transactions,89-117, 553-564.
2. I. Ohnaka, Y.Nagasaka and T.Murakami, 1996. *A Computer Simulation System of Casting Processes for Concurrent Engineering Approach.* Proc. of MCS3-96, 46-51.
3. Y.Nagasaka, J.K.Brimacombe, E.B.Hawbolt, I.V.Samarasekera, B.Hernandez-Morales and S.E.Chidiac, 1993. *Mathematical Model of Phase Transformations and Elastoplastic Stress in the Water Spray Quenching of Steel Bars.* Matallurgical Trans.A 24A, 795-808.
4. H.Shichino, Y.Nagasaka, T.Takahashi and N.Hamasaka. 1992. *Computer Simulation For Heat Treatment of Gears.* Proc. Of the8 th Int. Heat Treatment of Materials Conf., 597-600
5. Y.Nagasaka I.Ohnaka and T.Murakami. 1997. *An Intelligent Casting CAD system based on multi-media database.* Proc. of IPMM97, 490-496

Simulation of Springback with the Draw/Bend Test

K.P. Li, L.M. Geng and R.H. Wagoner

Dept. Materials Science and Engineering, The Ohio State University,
Columbus OH 43210 USA

ABSTRACT

This paper summarizes a length analysis of springback of the draw/bend test, conducted using three sheet materials, several friction coefficients, die radii, and draw-in restraining forces. In 1997, at the last IPMM early results were presented that showed large discrepancies between experiments and simulations for some conditions. The simulations have been optimized since that time and their sensitivity to a variety of numerical parameters and, more recently, to the choice of finite element and material model, have been examined. The finite element analysis (FEA) of springback is shown to be very sensitive to numerical parameters, including the number of through-thickness integration points, the angle of contact per shell element, and the tolerances for equilibrium and contact. With the help of numerical sensitivity studies, guidelines are provided for choosing these values effectively. Good agreement between experimental and simulated (3-D FEM modeling) springback has now been obtained for a range of process parameters. From this further analysis, it is concluded that the presence of 3-D bending (anticlastic curvature) effects dominate the discrepancies, with smaller errors caused by the material model.

INTRODUCTION

Springback describes the change of shape of a formed part upon removal from the tooling after forming. Sheet metals are particularly prone to springback because of their weak bending resistance, especially for materials with high strength-to-modulus ratios (aluminum and high strength steel, for example). These materials are becoming more important in the automotive industry to reduce vehicle mass and increase fuel efficiency. Springback causes difficulty in the die design process because the final part shape does not conform to the tool geometry. In order to compensate for springback, die tryout is required in the current automotive die development and construction process. Accurate prediction of springback is critical to reduce the lead time of tool design, thereby saving time and money. Finite element analysis, which has been demonstrated successfully for many complex industrial forming operations, has not yet shown the same reliability or accuracy for sheet springback applications [1-4].

In the literature there are few papers dealing systematically with springback prediction. The role of work-hardening for plane-strain has been investigated [5-7] and springback can be reduced for tensile loads greater than yield [7]. Other work has focused on the change of elastic modulus with plastic strain [8] and the presence of the Bauschinger Effect [9-11]. Use of isotropic hardening (i.e. without Bauschinger Effect) has been identified [8,16] as a cause of inaccurate springback simulation.

Parametric studies, either experimental [12-15] or numerical [1-3], have been conducted. Numerical effects in treating bending accuracy were addressed in a limited manner. Based on a chordal deviation analysis, Frey and Wenner [16] studied the mesh size limitation at the die corner and proposed that the number of contacting finite elements should be at least one per each 10° contact angle. The role of element size and hardening law in numerical problems with combined explicit loading and implicit unloading was studied [17], and springback of the wrong sign when simulations are carried out with large elements was reported. Stability problems with explicit simulations prior to springback analysis were identified for particular program combinations [18].

The magnitude of springback depends on the geometry of the deformed sheet and the distribution of the bending moment, in the plane of the sheet at the end of stamping operations. Most codes can give an accurate prediction of the geometry, even dynamic explicit codes with numerical acceleration schemes. However, the

0-7803-5489-3/99/$10.00 ©1999 IEEE.

correct prediction of stress distribution in the structure is sensitive to a range of variables. The physical sensitivity depends on material properties, hardening laws, friction coefficient and possibly, the unloading procedure. Numerical sensitivity depends on the number of integration points through the thickness, the type of element (plane strain, plane stress, 3-D shell and 3-D solid, etc.), the mesh size, and convergence tolerance.

The lack of springback measurements under carefully-controlled conditions in the literature motivated carrying out a series of draw/bend tests [14,19-20]. A set of central values of process parameters was chosen to represent typical automotive panel forming. The "central" variable values and ranges were as follows:

Sheet thickness: 1mm
Tool radius: 9.5mm (3.2mm - 25.4mm)
R/t (tool radius/sheet thickness): 10 (3 - 25)
Back force: 0.9 (0.5 - 1.3) tensile yield force
Friction condition: draw lubricant (dry, rolling)

The friction coefficients were not determined consistently from the test, but values in the range of 0 to 0.25 were adopted from the literature for comparison simulations. These measurements allow evaluation of the dependence of springback on process parameters, under conditions approximating sheet forming practice.

In early studies [19,21], simulations corresponding to the physical tests were carried out [22] to verify the sensitivity of springback to these process parameters without confounding changes of other aspects. It became apparent during that work that the simulations exhibited considerable non-physical scatter that made meaningful comparison problematic. The simulations have since been optimized, and their sensitivity to a variety of numerical parameters examined. The more recent examination of sensitivity to the choice of finite element and material model will be presented in this paper.

Section 2 describes the draw/bend test and material properties. Section 3 presents the 2-D numerical sensitivity studies of springback prediction, 2-D being used since 3-D simulations are CPU intensive, making their numerical sensitivity study prohibitive. The conclusion is so general for beam/shell type elements that it can be extended to 3-D shell analysis without concern. Section 4 addresses the discrepancies between experiments and 2-D simulations, and shows good springback prediction from optimized 3-D models. However special care for choosing shell (or solid) elements must be taken if the R/t ratio (Ratio of curvature/sheet thickness) is too small (i.e., ~5). Section 5 shows the influence of the Bauschinger Effect on springback prediction by 3-D shell elements with the help of the bending/unbending and tensile/compression tests. A brief discussion is given in Section 6 while Section 7 presents the conclusions.

THE DRAW/BEND TEST

The draw/bend test [14,19-20], Figure 1, consists of two hydraulic actuators oriented at a 90° angle, and a fixed or rolling cylinder to simulate a tooling radius over which the strip sample (50mm wide) is drawn. The upper actuator is programmed to provide a constant restraining force, F_b. The lower actuator is set to displace at constant speed, v, thus drawing, bending/unbending, and possibly, stretching the sample over the cylinder. When the test is over, the sample is allowed to springback by removing it from the grips.

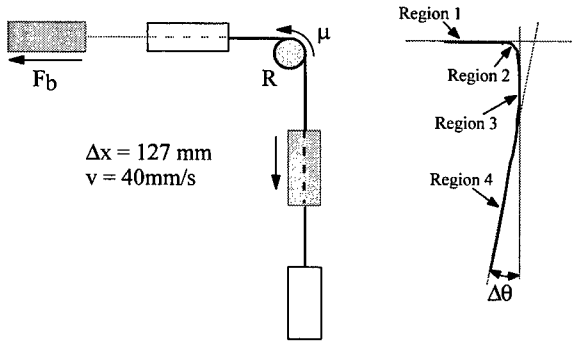


Fig.1. Schematic of the draw/bend test (left) and unloaded specimen shape after testing (right).

This test achieves steady-state after a small initial displacement, and is mechanically similar to the die sidewall region of a stamping operation. Three materials were tested: DQSK (draw-quality, silicon-killed) steel, a common material for automotive stamping; HSLA (high-strength, low-alloy) steel; and 6022-T4 aluminum. The last two materials are of interest for weight savings. For reasons of space, only the results with 6022-T4 and DQSK will be studied in the current presentation.

A series of tensile tests were used to obtain the uniaxial strain-hardening material properties [19,20], as follows:

6022-T4: Young's Modulus, E = 69 GPA; Poisson's Ratio, ν=0.3; The thickness of the sheet is 0.9mm. The true stress and true strain curve is:

$$\sigma = A[1 - B\exp(-C\varepsilon) - D\exp(-F\varepsilon)] \qquad \varepsilon \geq 0.002$$

where A = 389MPa, B = 0.566, C = 8.44, D = 1.20, F = 1120.

DQSK: Young's Modulus, E= 212 GPA; Poisson's Ratio, ν=0.3; The thickness of the sheet is 1.5mm. The true stress and true strain curve is:

$$\sigma = A(B + \varepsilon)^C - D\exp(-F\varepsilon) \qquad \varepsilon \geq 0.0035$$

where A = 540 MPa, B = 0.00965, C = 0.274, D = 150 MPa, F = 1700.

2-D SIMULATIONS

Because the ratio of strip width to thickness (w/t) for the draw/bend specimens is about 50 for 6022-T4 and 30 for DQSK, the plane strain model was expected to be appropriate. Therefore our original analyses concentrated on 2-D modeling, carried out using ABAQUS [23] and SHEET-S [21,22,24,25]. In ABAQUS, there is no plane strain model for 2-D beam elements. Hence, new developments were required in our SHEET-S program.

SHEET-S developments

With this in mind, SHEET-S [21,24,25] was modified to simulate springback. Two co-rotational 2D beam elements [26] were implemented with an elasto-plastic formulation. These elements have two nodes with three degrees of freedom per node. One is based on the Bernoulli formulation (without shear) and the other is formulated with the Timoshenko theory (with shear correction). Only results obtained with the Timoshenko element are presented here, although it should be noted that there was no significant difference in the results for most simulations, even for R/t as small as 3. All finite element simulations in this section were performed for the 6022-T4 using an isotropic hardening law. Step size was found to have little or no effect on simulated springback angle.

State of stress and strain

Based on the geometry (w/t of 50 for 6022-T4), plane strain should give a good approximation of the strain state in the draw/bend test. However, the plane stress model always produced results in closer agreement with experiments (Fig.2), especially for low back forces. The difference between springback angles of these two models is almost constant regardless of the applied back force (~10°-15°). In the remaining simulations for the numerical sensitivity studies, the plane stress model was chosen, although the results are similar for either condition.

The principal effect (and reason for better plane stress results) lies in the occurrence of the anticlastic curvature which arises during forming, and, in some cases, persists after springback. The presence of this secondary curvature greatly increases the section moment and reduces principal springback accordingly. This will be discussed in Section 4.

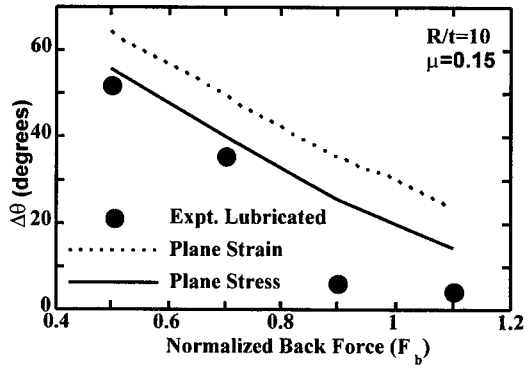


Fig. 2. $\Delta\theta$ for plane stress vs. strain models.

Unloading procedure

In order to simplify the problem, springback is often considered to be a purely elastic unloading (for example, see [27-28] and many others). However, during springback, plastic deformation may occur (Fig.3), and pure elastic unloading is not appropriate. Purely elastic unloading overstates the springback angle relative to the elasto-plastic case. The amount of overestimation depends on applied back force, although the maximum difference can exceed 1/3 of the total (10° for a $\Delta\theta$ equal to 25°, Fig. 3).

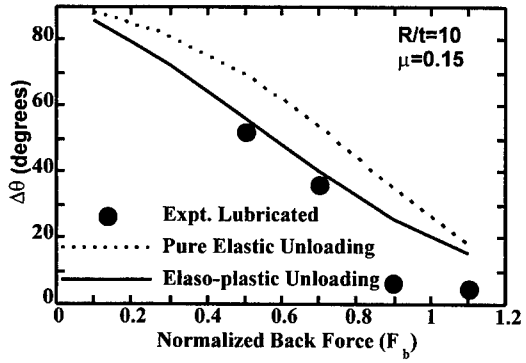


Fig. 3. The influence of unloading: elastic vs. elasto-plastic unloading cases.

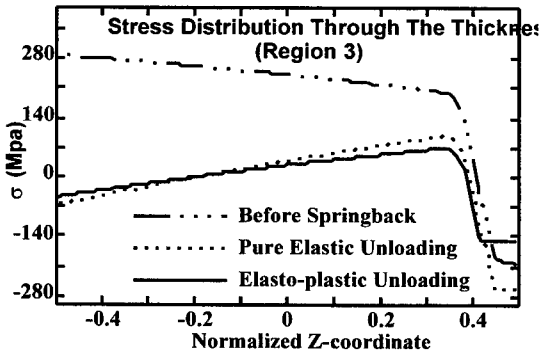


Fig. 4. Stress distribution along the thickness of sheet before and after springback for unloading case 2.

Figure 4 shows through-thickness stress distribution for elastic versus elasto-plastic unloading. The drawn/bent/unbent section (Region 3) exhibits the elasto-plastic unloading that occurs at the outer fiber of the sheet (normalized z coordinate is equal to 0.5).

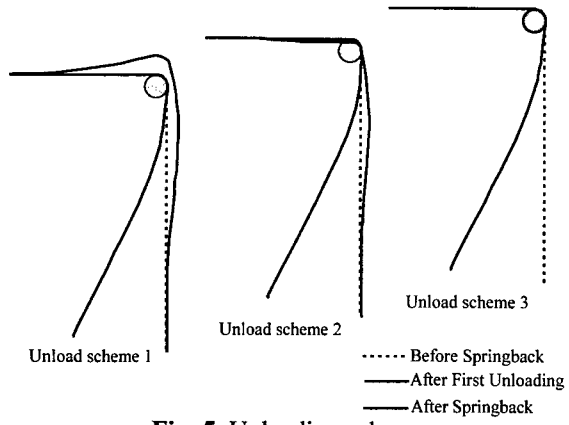


Fig. 5. Unloading schemes.

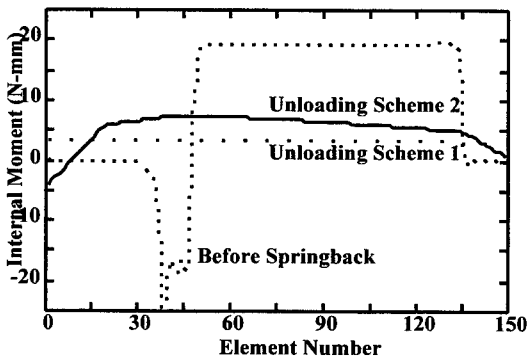


Fig. 6. Moment distribution following the first unloading step for Schemes 1 and 2.

Since elasto-plastic unloading is path dependent, three unloading "schemes" were compared for consistency of results. Schemes 1 and 2 consist of two steps while Scheme 3 is accomplished in one step. The specimen shapes for the steps in these schemes are shown in Figure 5.

For Scheme 1, the stretching force at the end node of the sheet is released first with the tool contact in place. The contact between the sheet and the cylinder disappears at the end of this step. A nearly constant moment distribution is obtained at this moment (Fig.6). The second step consists of releasing the end node by reducing the nodal forces to zero. For Scheme 2, the contact is removed by replacing the contact boundary condition by equivalent nodal forces and reducing these forces to zero. During this step, there is no real contact treatment: the process is a purely mechanical one. The moment distribution along the sheet at the end of this step is quite different (Fig.6). In the final unloading, the end node is freed by reducing the nodal forces to zero. For Scheme 3, the contact equivalent forces and the nodal forces are proportionally reduced to zero, with no contact treatment. For these three unloading paths, Scheme 1 is very CPU intensive because of the concurrent contact treatment, whereas Scheme 2 is more efficient than Scheme 3. $\Delta\theta$ for these three unloading cases is 26.42°, 26.45°, 26.26° for Schemes 1, 2, and 3 respectively. As will be shown later, these differences, in the range of 0.2°, are inconsequential as compared with numerical scatter. Thus, the choice of loading scheme is immaterial, in spite of the elastic-plastic path.

Numerical Sensitivity

Early simulations of the draw/bend test revealed that careful attention to numerical parameters of the simulation was required. Values for these parameters that have been established for forming simulations were no longer suitable for springback analysis, and unacceptable scatter was obtained. The source of numerical errors come from the number of integration points through the thickness, the number of elements contacting with the tools, convergence tolerances, material hardening laws and 2-D and 3-D modeling. In this section, only the effect from the number of integration points, the number of elements in contact with die radius and convergence tolerance will be discussed. Other parameters, for example, material hardening law and 3-D modeling, will be presented later in this paper.

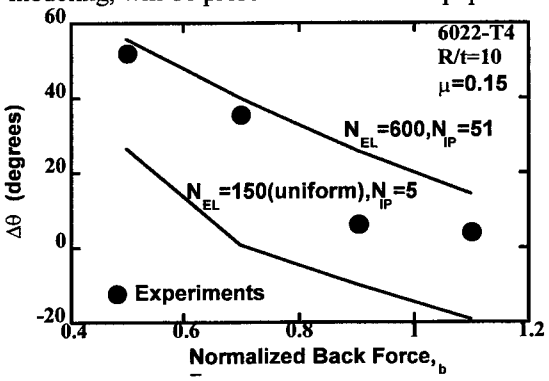


Fig. 7. Effect of the number of elements (N_{EL}) and integration points (N_{IP}).

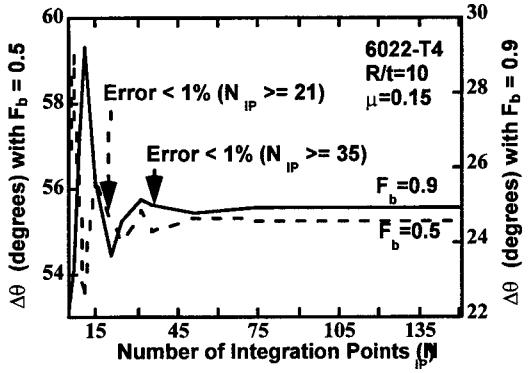


Fig. 8. Effect of the number of integration points on simulated springback angle.

Figure 7 illustrates the dramatic combined sensitivity of springback simulation to numerical aspects. To represent a typical forming simulation, a mesh of 150 equal-size elements (4 in contact with the tool) and 5 integration points through the thickness was employed, compared with 600 non-unequal-size elements (50 in contact with the tool) and 51 integration points. The springback predictions given by the 150 element mesh are clearly incorrect, and for larger back forces have the wrong sign.

In order to isolate the effects of these various parameters, we carried out a sensitivity study using values that we found to be sufficient (600 elements, 51 integration points, and contact/equilibrium tolerance of one part in 10^{-4}), then varied each parameter independently.

Number of integration points

Most shell elements require numerical integration of stress through the thickness to obtain the internal force vector, moments and tensile forces. This brings numerical error in the results. For sheet forming processes, 5 integration points are commonly specified [23,29] and good results are usually reported. However, our results show that springback is very sensitive to the number of integration points, and many more, by nearly an order of magnitude, are required because of the need to locate precisely the elastic core in the sheet.

Figure 8 shows the effect of the number of integration point through the thickness (N_{IP}) for R/t=10, and F_b=0.5 or 0.9 [21]. For a given R/t and F_b, if a percentage error less than, for example, 1%, is required, N_{IP} depends strongly on the overall springback angle. For F_b=0.5 ($\Delta\theta$=55°), $N_{IP}\geq 21$ and for F_b=0.9 ($\Delta\theta$=25°), $N_{IP}\geq 35$. If the error of springback angles is required to be less than 1 degree, then $N_{IP}\geq 15$ is sufficient for both cases. For a total $\Delta\theta$ of about 25° (R/t=10, F_b=0.9), the numerical error caused by an insufficient number of integration points can be as high as 5° (by comparing 5 to 151 integration points), or about 1/5 (20%) of the total $\Delta\theta$. An even larger scatter (about 7°) occurs as the number of integration points is varied in the normally-recommended range of 5 to 9.

Number of elements

The extreme case of the influence of number of elements on springback prediction is shown in Figure 7, which used a mesh of 150 equal-size elements, N_{IP}=5 for R/t=10 and F_b=0.9. The wrong springback prediction happened again with a mesh of 300 equal-size elements for R/t=4. This wrong-sign springback prediction, which in this case is an example of extreme numerical scatter, has also been observed by others [17,26]. In both cases, the number of nodes in contact with the tooling (cylinder), N_{CN} is less than 5 (about 4 nodes for R/t=10 and about 3 nodes for R/t=4).

Table 1. Typical mesh parameters for R/t=10.

	Part 2 L_2=140mm		
N_{EL}	N_2	l_2	$\Delta\Phi/N_{El.}$
150	106	1.3	7.8°
300	221	0.63	3.8°
600	452	0.31	1.9°
900	684	0.2	1.2°
1200	914	0.15	0.9°
2400	1838	0.08	0.5°

In order to examine numerical error for a variety of simulations more systematically, we defined a "reference" simulation result for a given physical problem, and defined error as deviation of simulated $\Delta\theta$ from this result. The error may be expressed more compactly either in terms of absolute angle, $|\Delta\theta|$ or absolute percent, $|\Delta\theta/\Delta\theta_{ref}| \times 100$, without specifying whether the simulation over- or under- estimates the reference result.

To study of the influence of element size, the unequal-size meshes listed in Table 1 were constructed (here only the mesh parameters for the part 2 are listed, for more details of other parts, see [21]). In the regions 1 and 4 (originally flat and remains so after springback), coarse meshes are used. The turning angles and lengths of Part 2, including Regions 2 and 3 (originally flat and makes contact during the draw) refer to the standard tooling radius of 9.5mm. For other cases, the turning angles can be scaled from the standard case. For the region initially in contact with the die, the number of elements is fixed at 10 for all cases. The length of each element is thus 1.5mm for R/t=10, and the lengths for other tool radii can be obtained proportionally.

Figure 9 illustrates the combined effect of the number of elements and the number of integration points through the thickness for R/t=10, F_b=0.9 and R/t=28, F_b=0.9, respectively. In all cases, a 900-element mesh with N_{IP}=51 was used as reference, with the choice of R/t= 10 or 28 distinguishing the two reference calculations. From Figure 9, the following remarks can be make:

a) the errors settle down to variations of less than 1° (for a fixed number of elements) with $N_{IP}\geq 25$, approximately independent of springback angle.

b) It is obviously difficulty or even impossible to achieve an error under 1% tolerance, especially for small springback cases.

c) In terms of the number of elements required, all the meshes are able to achieve 1° accuracy for the cases presented, whereas for percentage error, the results vary widely. The high springback case (Figure 9a, $\Delta\theta_{ref}$=24.7°) requires 600 elements to achieve 1% error, whereas the low springback case (Figure 9b, $\Delta\theta_{ref}$=3°) cannot reduce error to 1% even with 600 element mesh. (Thus, it may be argued that a mesh of more than 900 elements should be used as the reference here).

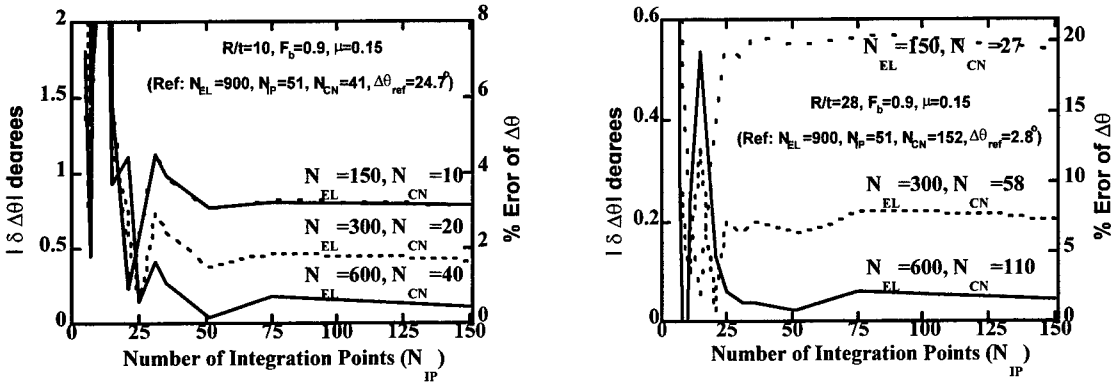


Fig. 9. Dependence of numerical simulation error (from reference calculation) on simulation parameters.

When there are enough elements in contact with the tool, (approximately 10 elements in the worst case shown here), $|\delta\Delta\theta|$ is always less than 1 degree. If we only require that the error in $\Delta\theta$ be less than 1°, then for R/t=10, the mesh with 150 elements is sufficient. However, for tighter angular tolerance specified as a percentage of total springback, the small springback cases may require more than 900 elements, or many times more contact elements. Clearly, it is simpler and more consistent to specify error in terms of angle rather than percentage.

Numerical tolerances

In SHEET programs, each step solution is converged if both equilibrium and contact conditions are satisfied. Equilibrium is achieved if the total unbalanced force norm over the total force norm, and the iterative incremental displacement norm over the incremental displacement norm, are below the prescribed tolerances.

$$\frac{\|F_{int} - F_{ext}\|}{\|F_{ext}\|} \le T_F \quad \text{and} \quad \frac{\|\delta\Delta u_n\|}{\|\Delta u\|} \le T_u \qquad 1.$$

where $\|\cdot\|$ denotes the Euclidean norm of a vector and T_F, T_u are the tolerances.

The contact conditions are satisfied if, for each contact node, both the contact force over the force norm, and the penetration distance ($d_{penetration}$), defined by the penetration distance along the mesh normal [23,24], over a normalized norm (either the element length or the nodal displacement norm), are below the imposed tolerances.

$$\frac{F_{contact}}{\|F_{ext}\|} \ge -T_{CF} \quad \text{and} \quad \frac{d_{penetration}}{\|D_{norm}\|} \le T_{CD} \qquad 2.$$

where T_{CF} and T_{CD} are the tolerances for contact force and penetration distance, respectively.

In the simulations presented here, identical values for T_F, T_u, T_{CF}, and T_{CD} are enforced, with typical results shown in Figure 10. For convergence tolerances ranging from 10^{-3} to 10^{-8}, the %error is less than 1%, which is negligible compared to the error induced by insufficient N_{IP} and N_{EL}. The value adopted in the simulations presented is 10^{-4}, chosen to avoid any significant error caused by tolerance in convergence or contact.

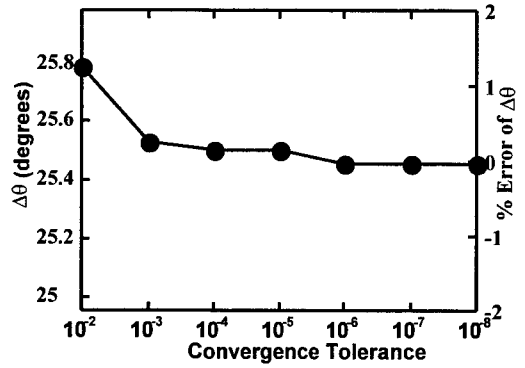


Fig. 10. Influence of tolerances on Δθ and % error.

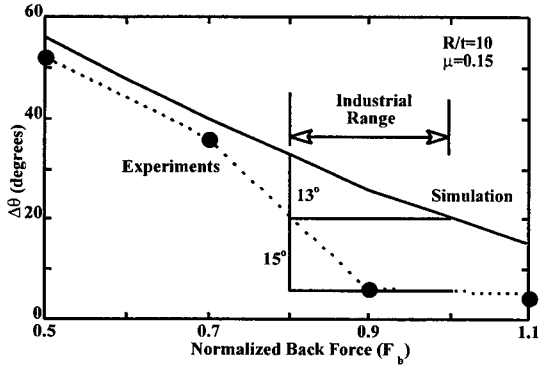


Fig. 11. Effect of restraining force on springback.

Sensitivity To Process Parameters

In the sensitivity studies of the process parameters, the following base values were used: 600 unequal-size elements, 51 integration points through the thickness, and 10^{-4} tolerances. These values were found to be sufficient for numerical error limited to less than 1°. In order to reduce springback, the most common and effective strategy in practice is to increase tensile stress in the sheet. In sheet forming applications, the typical applied F_b is in the range of 0.5-1.1 of the tensile yield force. A normalized back force of F_b = 1.1 was found to be the upper limit to avoid strain localization with 6022-T4 aluminum.

Figure 11 shows the predicted springback angles versus back restraining force, as compared to the experimental data. Springback reduces steadily with the increase of restraining force. But the experimental data show a rapid decrease as the normalized back force approaches 0.9, while the numerical results are nearly linear. This discrepancy is because of the occurrence of anticlastic curvature developed during unbending and persisting after springback, which will be presented in 3-D simulation thereafter.

Friction

The role of friction on springback was investigated under three experimental conditions: 1) low friction - lubricated / free rolling die cylinder; 2) medium friction - lubricated fixed die; 3) high friction - unlubricated fixed die. Parco 404 [30], a standard industrial forming lubricant, was used for the lubricated cases [19,22].

A common method to determine the friction coefficient is called the rope formula, which uses the front and back force values measured during the tests [31]. But values obtained in this way are very scattered. Instead, in the simulations, the friction coefficients were estimated by past experience as follows: μ=0 for the lubricated free roller, μ=0.15 for the lubricated case, and μ=0.25 for the dry case. (Note: these estimates only affect the placement of the experimental results, and small errors are not very significant in springback determination.)

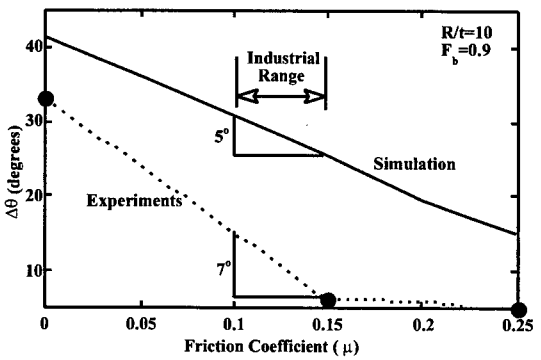


Fig. 12. Experimental [18,19] and simulated sensitivity of springback angle to friction coefficient.

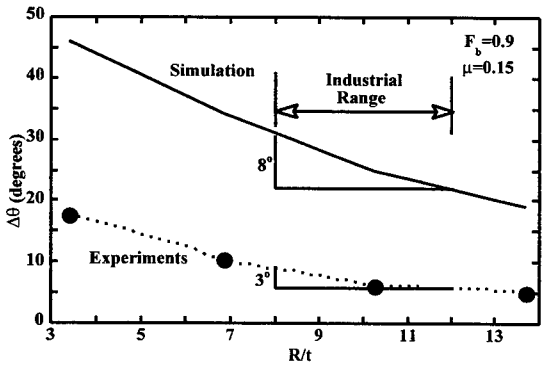


Fig. 13. Influence of R/t on springback.

Figure 12 illustrates the effect of friction coefficients for simulations and experimental data. Springback decreases as friction increases, and the role of friction increases considerably as back force is increased.

Normalized bending ratio (R/t)

The influence of the R/t ratio on springback has been studied by many authors [9,11,26,31,32], who have been nearly equally divided about the direction of the effect. Four R/t cases were simulated for a fixed, normalized back force (F_b=0.9) with lubricated tooling (μ=0.15).

In a typical sheet forming range, R/t has a modest effect on springback for this combined stretch and draw condition (Figure 13). The direction of the R/t effect is contrary to some reports in the literature [12,27,32] and consistent with others [10,33]. In the experiments and simulations with steel cases described in Section 4, the effect for R/t was seen to reverse below a critical value near R/t = 5.

3-D SIMULATIONS

In the 2-D simulations (Figures 11-12), the predicted springback decreases nearly linearly with an increase of restraining force, but the experimental data show a rapid decrease as the normalized back force approaches 0.9. The error for Fb=0.9, ($\Delta\theta$=6° experiment vs. $\Delta\theta$=26° simulation) is nearly 400%. In order to understand this discrepancy, 3-D shell and solid elements were employed. 4-node shell elements were used with a mesh of 4×300 elements (4 elements in the width, 300 unequal-size elements in the length), with 51 through-thickness integration points; and 8-node solid elements (C3D8R [23]) with a mesh of 4×300×6 elements (4 elements in the width, 150 unequal-size elements in the length and 6 elements in the thickness).

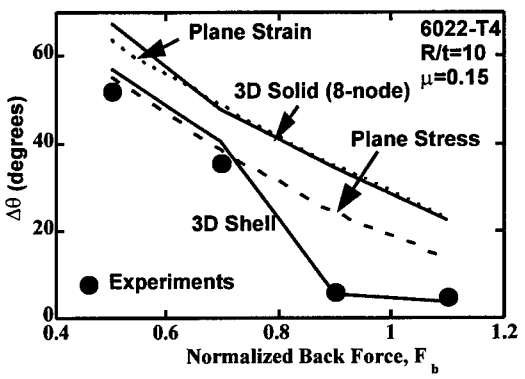


Fig. 14. Effect of restraining force on $\Delta\theta$ for various FEA models.

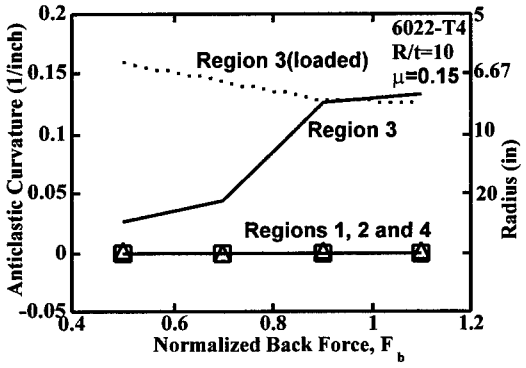


Fig. 15. The anticlastic curvature of Regions 1 to 4.

Figure 14 shows the springback angles versus back restraining forces for R/t=10. It is evident that the results given by shell elements agree with experimental data, while the answers given from the 8-node solid are very similar to the results obtained by the plane strain model.

The origin of the differences between 2-D simulations and the experiments for normalized back forces greater than 0.9 can be understood in terms of anticlastic curvature, the secondary curvature that occurs normal to principal bending in thin sheets. In the elastic case, it is a product of Poisson contraction.

Although anticlastic curvature is usually described as a result of bending under plane stress [34] (e.g., w/t=10), Figure 15 shows that cross-sections in Region 2 (Fig.1), the bending region, along with Regions 1 and 4, remain nearly flat. Region 2 is presumably constrained by the tensile stress and high contact pressure with the tooling. Region 3, the unbending region of the sheet or "sidewall curl" area, exhibits anticlastic curvature approaching the principal curvature of Region 3 (after unbending). The unloaded Region 3 principal curvature is 0.009 mm^{-1} (0.23 in^{-1}) for the F_b=0.5 case and 0.002 mm^{-1} (0.05 in^{-1}) for the F_b=0.9 case.

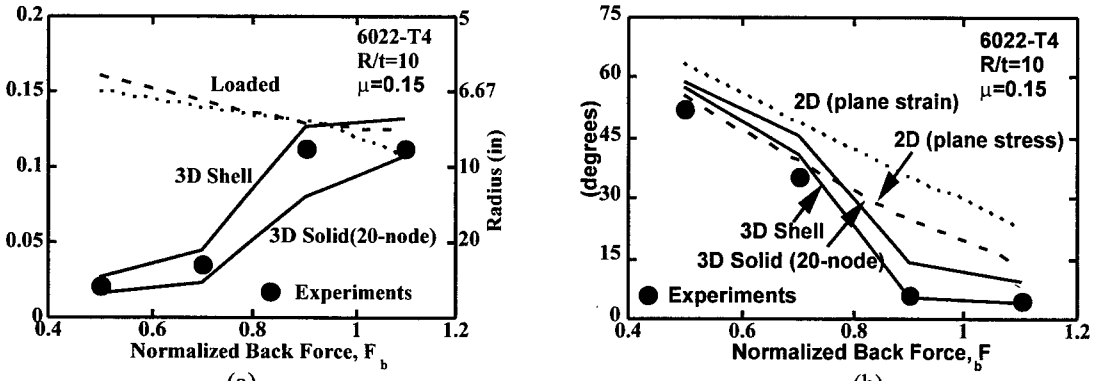


Fig. 16. $\Delta\theta$ vs. F_b for various FEA models with R/t=6.35 (t_0=1.5mm)

Figure 16a shows that the anticlastic curvature in Region 3 is high and nearly insensitive to back force during loading, but after unloading it takes a sudden jump at F_b greater than or equal to 0.9. This jump matches closely the experimentally measured values. Furthermore, this jump in anticlastic curvature is matched precisely by a sudden decrease in springback angle (Fig.16b), for 3-D simulations and experiments. Thus, the origin of the sudden decrease of springback angle for F_b above 0.9 lies with the persistence of anticlastic curvature following unbending. The persistence of this curvature increases the effective section modulus for principal bending and, for a fixed applied moment, reduces the springback angle correspondingly.

Note that in Figure 14, the 3-D solid simulation did not show the presence of persistent anticlastic curvature, nor the accompanying sudden change of springback angle. The results were essentially the same as for plane strain simulation. Since 8-node solid elements, which have linear shape functions, are very stiff in bending modes, the simulations were repeated with 20-node nonlinear 3-D solid elements (C3D20 [23]). Because of the large CPU times involved (15-20 hours), a mesh of 2×150×3 (2 in the width, 150 in the length, and 3 in the thickness) was used. The results, also shown in Figure 16b, reproduce the main features of the 3-D shell simulation. Subsequent results (Figures 17-20) are shown for both kinds of elements and meshes.

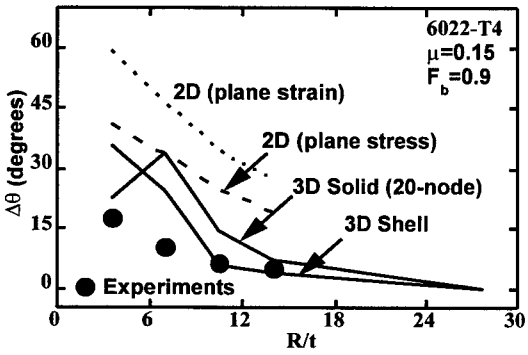


Fig. 17. $\Delta\theta$ vs. R/t for various FEA models with F_b=0.9.

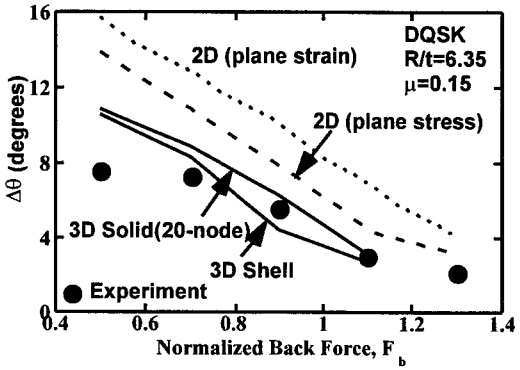


Fig. 18. $\Delta\theta$ vs. F_b for various FEA models with R/t=6.35 (t_0=1.5mm).

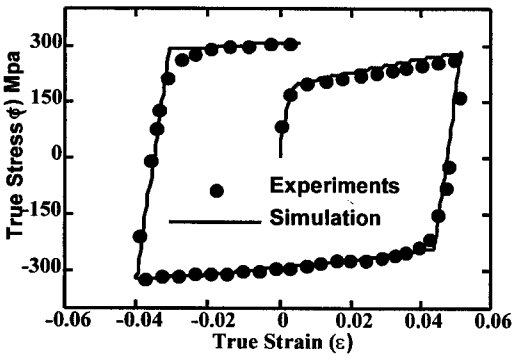


Fig. 19. Dependence of anticlastic curvature on back force.

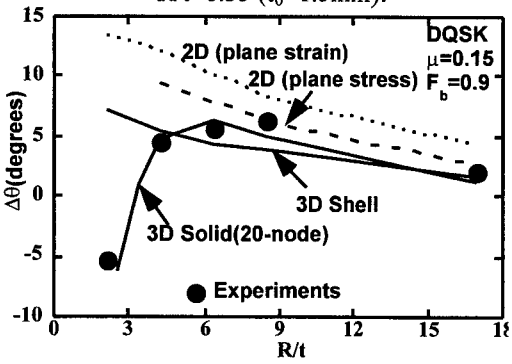


Fig. 20. $\Delta\theta$ vs. R/t for various FEA models with F_b=0.9.

Figures 17-20 show that good agreement between experiments and simulations with both elements (3-D shell, 3-D/20-node solid) is obtained for the larger R/t ratios tested. However, for the DQSK material (Fig.20), there is a clear departure of experimental results from the shell simulations at R/t less than 6. As R/t is decreased below 6, the springback angle decreases rapidly, contrary to the shell simulations. The 3-D solid elements, however, reproduce this change well. The difference presumably lies in the basic shell element theory upon which the shell elements are based. That is, the bending strain is assumed to be distributed linearly through the thickness.

BAUSCHINGER EFFECT

As shown in Figures 14 and 16, the simulated springback angles are very close to the experimental ones for high back forces, while more difference is apparent for low back restraining forces. A possible source of error in the simulation lies in the use of the anisotropic hardening law, which may be inadequate to approximate the real material strain-hardening behavior for some alloys. In the draw/bend test (and in real sheet forming), reverse loading occurs because bending and unbending occurs when the sheet strip is pulled over the radius and straightened back after leaving the radius. For materials which exhibit a Bauschinger effect, yield stress in reverse loading is usually lower than for continuous loading, while the isotropic hardening model offers a reasonable fit to material hardening for proportional loading path, but may not account for this effect. Because springback is very sensitive to the moment/stress at the end of the forming, for material that exhibits a Bauschinger effect, using an anisotropic hardening law instead of the isotropic one could give more realistic stress/moment distribution for bending and unbending processes, improving the accuracy of the prediction.

Two kinematic type of hardening laws were implemented into finite element code to account for Bauschinger effect. One is the mixed hardening law presented in [26], in which a scalar m is defined to divide total plastic strain into isotropic part and kinematic part. This hardening law is very well in reproducing the lower reverse yield stress and permanent softening, however, it can not show the smooth elastic-plastic transition. On the other hand, nonlinear-kinematic hardening law proposed by Chaboche [35] does show this gradual transition on the reverse loading, however, it needs advanced modification to reproduce the permanent softening. The simulated springback angles with these two kinematic types of hardening laws are very material parameter sensitive. Depending on the choice of material parameters, the springback angle could vary significantly.

To determine the material parameters needed for describing the Bauschinger effect, direct in-plane tension-compression tests were performed [36]. In this test, the sheet specimen is sandwiched between the two sets of forks. Clamping force is applied on the sides of the fork to prevent the buckling of the sheet sample during compression, and axial force is applied using a standard tensile testing machine. The stress-strain data obtained directly from the device were corrected to account for the friction between the sheet specimen and the fork surface, and for the biaxial stress state caused by the clamping force normal to the sheet surface. Preliminary experiments were carried on with three stages: tension-compression-tension, or compression-tension-compression. The results show the lower yield stress and permanent softening on the reversed loading curve for PNGV material HSLA, AL6022-T4 and DQSK (Fig.21). The mixed hardening model and nonlinear-kinematic model were used to fit the experimental tension-compression curve, material parameters were determined by trial and error. The results (Fig.22) show that material parameters (such as mixed factor m) have to be functions of effective strain in order to reproduce the experimental result reasonably well.

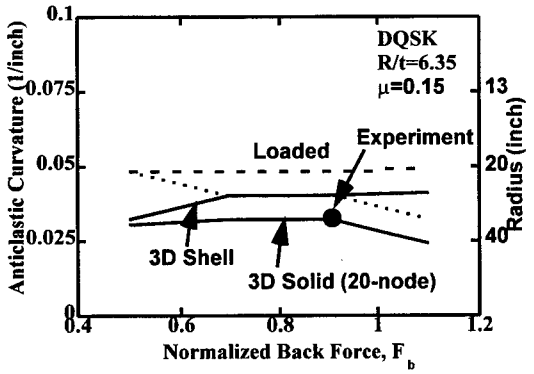


Fig. 21. True stress vs. true strain curve for tensile/ compression test: experiment and simulation.

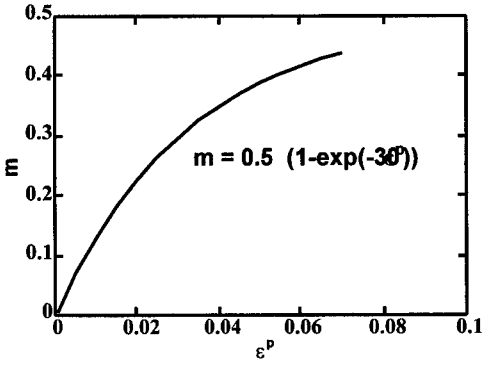


Fig. 22. Curve of mixed hardening control parameter m vs. plastic strain.

With the experimental data available from the tension/compression tests, the mixed hardening law was modeled to simulate the draw/bend test of 6022-T4 (Fig. 23). For low back restraining forces, the simulated springback angles are considerably closer to the experimental data, while for high back restraining forces, they move slightly away from the test results. While definitive conclusions are difficult at this preliminary stage, it appears the remaining discrepancies are attributable to material law complexity under reverse loading.

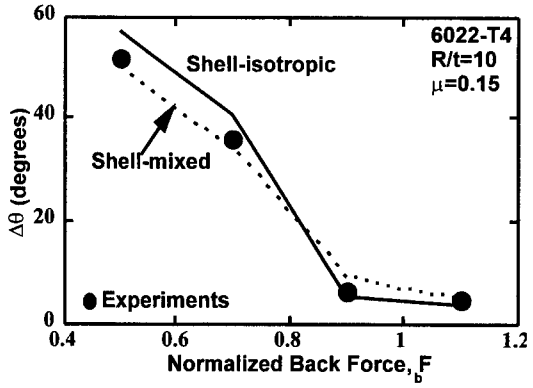


Fig. 23. Effect of hardening law on the simulated springback angle

DISCUSSION

The numerical sensitivity studies indicate that stable, reproducible numerical results can be obtained if the mesh size, contact and equilibrium tolerance, and through-thickness integration scheme are chosen properly. Furthermore, the variation of springback angle with typical physical process variables (friction coefficient, bending ratio, and tensile force) is consistent between simulations and measurements. Thus it appears that, with care, FEA can be used to predict systematic springback effects consistently and accurately.

With this in mind, it is necessary to note that if the element isn't chosen properly, the simulated springback angles can differ greatly from measured ones (the extreme case is shown in Figure 2-3,7,11-12, 14, and 20). Anticlastic curvature appears during unbending of the sheet after drawing over the die radius even when w/t is over 50. For higher back forces (F_b>0.9), this secondary curvature persists after unloading and the increased section moment greatly reduces springback. 3-D shell elements or 3-D nonlinear solid elements are needed to simulate this effect.

For small R/t values (less than about 5), shell elements are no longer valid for springback analysis and solid elements are required. Mixed solid/shell elements may be a promising approach to analyse springback [37].

CONCLUSIONS

Simulations and experiments of draw-bending of 6022-T4 aluminum over a typical range of process variables were carried out. The following conclusions can be made.

In terms of numerical sensitivity:

- Whereas typical forming simulations are acceptably accurate with 5 to 9 points, springback analysis requires up to 51 points, and more typically 25 points.
- A sufficient number of contact nodes is also critical, approximately one node per 5-10° of turn angle. When nodes are separated by 20° of turn angle or more, simulated springback can occur in the opposite direction.
- Convergence and contact tolerances must be enforced carefully, but values of one part in 10,000, which are typical of implicit forming simulations, are sufficient.
- 3-D shell and non-linear solid elements are preferred in springback prediction even for large w/t ratio (in our case greater than 50) because of the presence of the anticlastic curvature.
- For small R/t ratio (about 5), only 3-D non-linear solid elements can accurately predict springback.

In terms of physical sensitivity:

- Springback decreases with increasing tensile stress, up to about 90% or 50°. This effect dominates.

- Springback decreases significantly (3-7°, approximately 25%) with increasing R/t ratio, for R/t greater than approximately 3.
- Friction has a modest but measurable effect on springback in a typical industrial range (3-7°, or 5-20%), larger for low tensile stress.

ACKNOWLEDGMENTS

The financial support of a PNGV subcontract via NIST/ATP and the Center for Advanced Materials and Manufacturing of Automotive Components (CAMMAC) is gratefully acknowledged. Experimental data and early simulations for draw/bend tests were provided by William Carden, D. K. Matlock and Wendy P. Carden. Experimental data for Bauschinger Effect were provided by Y. Shen and V. Balakrishnan. Computer time was provided by the Ohio Supercomputer Center (PAS 080).

REFERENCES

1. Proceedings of the 2nd International Conference NUMISHEET'93 - Numerical Simulation of 3-D Sheet Metal Forming Processes, 1993.
2. Proceedings of the 5th International Conference on Numerical Methods in Industrial Forming Processes NUMIFOR' 95 - Simulation of Materials Processing: Theory, Methods and Applications, 1995.
3. Proceedings of the 3rd International Conference NUMISHEET'96 - Numerical Simulation of 3-D Sheet Metal Forming Processes, 1996.
4. Proceedings of the 6th International Conference on Numerical Methods in Industrial Forming Processes, NUMIFORM'98 - Simulation of Materials Processing: Theory, Methods and Applications, 1998.
5. Zhang, D. Lee, 1995. Effect of Process Variables and Material Properties on the Springback Behavior of 2_D Draw Bending Parts, Automotive Stamping Technology, 11-18.
6. M.K. Mickalich, M.L. Wenner, 1988. Calculation of Springback and its Variation in Channel Forming Operations, Symp. Proc. for the March 3, Soc. of Automotive Engineers Meeting.
7. M.L. Wenner, 1983. On Work Hardening and Springback in Plane Strain Draw Forming. J. Applied Metal Working, 2(4).
8. F. Morestin, M. Boivin, "On the necessity of taking into account the variation in the Young Modulus with plastic strain in elastic-plastic software", Nuclear Engineering and design, 162, 1996, 107-116
9. S.C. Tang, "Application of an anisotropic hardening rule to springback prediction", Advanced Technology of Plasticity, (1996) 719-722
10. Kuwabara, S. Takahashi and K. Ito, 1996. Springback Analysis of Sheet Metal Subjected to Bending-Unbending under Tension, Part I and II, Advanced Technology of Plasticity, 743-750.
11. Kunio Miyauchi, 1992. Deformation path effect on stress-strain relation in sheet metals, J. Materials Processing Technology, 34, 195-200.
12. M.L. Wenner, 1982. An Analysis of Springback on the Punch Corner Radius in Channel Forming, (General Motors Research Report), May 19, 1982.
13. M. Sunseri, J. Cao, A.P. Karafillis, M.C. Boyce, "Accommodation of Springback Error in Channel Forming Using Active Binder Force Control: Numerical Simulations and Experiments", Transactions of ASME, vol. 118, July, 1996.
14. Vallance and D. K. Matlock, 1992. Application of the Bending-Under-Tension Friction Test to Coated Sheet Steels. J. Material Engineering and Performance, 1(5), 685-693.
15. L.C. Zhang, G. Lu and S.C. Leong, 1997. V-shaped sheet forming by deformable punches. J. of Materials Processing Technology, 63, 134-139
16. W. H. Frey, M.L. Wenner, 1987. Development and Applications of a One-dimensional Finite Element Code for Sheet Metal Forming Analysis", (General Motors Research Report), September.
17. Mattiasson, A. Strange, P. Thilderkvist, A. Samuelsson, 1995. Simulation of springback in sheet metal forming. 5th International Conf. on Numerical Methods in Industrial Forming Process, NY, 115-124
18. N. He, R.H. Wagoner, 1996. Springback Simulation in Sheet Metal Forming. NUMISHEET 96, eds. J. K. Lee, G. L. Kinzel, R. H. Wagoner, Ohio State University, 308-315.
    a) R.H. Wagoner, W.D. Carden, W.P. Carden, D.K. Matlock, 1997. Springback after drawing and bending of metal sheets, THERMEC '97, Australia.
    b) W.D. Carden, 1997. Springback after drawing and bending of metal sheets. MS thesis, MSE/OSU.
21. K. Li and R.H. Wagoner, 1998. Simulation of springback. NUMIFORM'98, 21-31.

22. W.P. Carden, 1997. Analysis of Springback in Draw-bending Forming, MS Thesis, MSE/OSU.
23. ABAQUS User Manual, version 5.5
24. M.J. Saran, R.H. Wagoner, 1991. "A Consistent Implicit Formulation for Nonlinear Finite Element Modeling with Contact and Friction, Pt. 1 - Theory", ASME Trans. - J. Appl. Mech., 58, 499-506.
25. D.J. Zhou, R.H. Wagoner, 1995. Development and application of Sheet-Forming Simulation", J. of Materials Processing Technology, 50, 1-16.
26. M.A. Crisfield, 1991. Non-linear Finite Element Analysis of Solids and Structures, J. Wiley & Sons, England.
27. Wang, G. Kinzel and T. Altan, 1993. Mechanical Modeling of Plane-Strain Bending of Sheet and Plate. J. Materials Processing Technology, 39, 279-304.
28. Hosford, and R. Caddell, 1993. Metal Forming: Mechanics and Metallurgy. Englewood Cliffs, Prentice-Hall.
29. C.J. Burgoyne, M.A. Crisfield, 1990. Numerical integration strategy for plates and shells. Int. J. Num. Meth. Engng., 29, 105-121.
30. M.J. Wenner, 1996. private communication, General Motors Corporation, March.
31. R.H. Wagoner, J.L. Chenot, 1997. Fundamentals of Metal Forming, New York, NY, J Wiley & Sons.
32. Huang, J.C. Gerdeen, 1994. Springback of Double Curved Developable Sheet Metal Surface. Analysis of Autobody Stamping Technology , (Society of Automotive Engineers), 125-138.
33. F. Pourboghrat, E. Chu, 1995. Prediction of Springback and Side-Wall Curl in 2-D Draw Bending. J. of Materials Processing Technology, 50, 361-374.
34. T.X. Yu, L.C. Zhang, 1996. Plastic bending, theory and applications. World Scientific.
35. Chaboche, J. L., 1986, Time-independent constitutive theories for cyclic plasticity, International Journal of Plasticity, 2, 2, 149-188.
36. V. Balakrishnan, 1999. Measurement of in-plane Bauschinger effect in metal sheets. MS thesis, MSE/OSU.
37. Z.C. Xia, S.C. Tang, J.C. Carnes, 1998. Accurate springback prediction with mixed solid/shell elements", NUMIFORM'98, 813-818.

Development of an Integrated System for Designing Steelmaking Aim Compositions

P. A. Manohar*, S. S. Shivathaya, M. Ferry* and T. Chandra***

* Department of Materials Engineering, University of Wollongong, Northfields Avenue, Wollongong, NSW - 2522, Australia.

**Hawker de Havilland Ltd., 361 Milperra Road, Bankstown, NSW - 2200, Australia.

(Author was with the Department of Mechanical Engineering, University of Wollongong when work was carried out.)

ABSTRACT

A new integrated approach is proposed in this paper to generate and evaluate the alternative steelmaking aim compositions which not only meet the customer requirements but also suit the established rolling schedules. The methodology developed is based on hybrid approach combining knowledge-bases as well as mathematical modelling and is applicable for C - Mn steel grades. The system consists of two modules. The first module utilises various empirical models for the relationship between mechanical properties and the elements in steelmaking aim compositions, along with knowledge bases containing expert and heuristic knowledge of expert metallurgists to generate a list of alternative steelmaking aim compositions. The second module uses the output of the first module and computes the microstructural evolution during processing depending on steel composition and known processing conditions such as strain, strain rate, temperature, interpass time and plate cooling rate. Calculated values of the metallurgical parameters are then used to estimate the achievable mechanical properties in the final hot rolled product using knowledge-bases. System output is expected to assist product development metallurgists in the selection of appropriate steelmaking aim compositions for any combination of property specifications required by the customer.

INTRODUCTION

The steel industry is currently facing a number of challenges such as being more flexible and responsive, less capital intensive, energy efficient and environmentally "greener". Competition from non-ferrous metals and non-metallic materials is intensifying. Relentless pressure is applied by ever-increasing quality demands from the customer. The need for cost reduction is driving the industry towards increased automation to produce higher quality steels at reasonable cost. To deal with these challenges and for efficient management of the uncertainties involved, it has become imperative to apply artificial intelligence (AI) techniques by developing expert systems in almost all areas of steelmaking practice. In the past three decades, a number of systems have been developed around the world for more efficient solutions to problem areas of diagnostics, design, planning, scheduling, process control, and quality control [1-3]. Application of a knowledge-based approach to steel composition design has been considered by several researchers [4-5]. Development of such systems is a complex task because the material design process is ill-structured, difficult to systematise and involves a large number of rules. In addition, the relationships between composition and process parameters and product properties is nonlinear. The knowledge of steel composition design is largely intuitive and heuristic.

On the other hand, hot rolling of steels has been investigated intensively and several mathematical models and computer systems have been developed. Several major objectives of the mathematical models have been reported which include improving the efficiency of mill trials to establish optimum compositions and rolling schedules [6], prediction of microstructure and mechanical properties during rolling [7], development of new steel grades and rolling processes [8-9] increase productivity and quality, reduce manufacturing cost through the use as an off-line prediction, on-line prediction, on-line control or off-line alloy and process design tool [10-11], ability for flexible manufacturing [12], control of size, shape, quality and stability of steel products, more responsive for product development [13], betterment of understanding of the processes [14], a useful "what - if" tool which provides directions for further fundamental research along with problem investigation, schedule development, design or redesign of mill configuration and enhancement of understanding [15].

0-7803-5489-3/99/$10.00 ©1999 IEEE.

In the current work, a new integrated approach is proposed which combines the above two approaches to generate and evaluate the alternative steelmaking aim compositions which meet the customer requirements. The system consists of two modules. The first module uses both mathematical (iterative) and knowledge-based approaches and utilises both interview and non-interview techniques for knowledge elicitation (KEL). KEL is also characterised by a 3-character codification scheme to record customer's special requirements. The codification scheme is coupled with a decision table-based knowledge representation tool "TABLEAUX" for incorporation within knowledge-based systems. The system generates a list of alternative aim composition which may meet the property requirements. The compositions are then evaluated by using the second module which consists of mathematical modelling approach to calculate the microstructural evolution during hot rolling of the steel. The estimated values of metallurgical parameters are then converted to prediction of the mechanical properties of the steel products using empirical relationships, thus enabling more realistic assessment of the designed compositions. The system is developed in C language on an IBM PC in a windows environment. User interface is developed utilising a commercial package, 'PROTOGEN+', to make the system user friendly. The system is expected to assist the product development metallurgists in the selection of appropriate steelmaking aim composition and for hot rolling process optimisation.

KNOWLEDGE ELICITATION

The process for knowledge elicitation (KEL) adopted in this work has been reported elsewhere [16], however a brief summary is given here. The KEL is characterised by a three-character codification scheme having a hybrid structure to codify all the customer's special requirements based on the initial structured and unstructured interviews. The customer special requirement codes (CSRCs) are given by the equation:

$$\text{Customer Special Requirement Code} = X_i Y_j Z_k$$

The first character in the code is X_i called the major group code, which is the i^{th} property of a steel grade (eg. tensile strength, yield strength, elongation etc.). The second character in the CSRC is called the subgroup code and it represents the j^{th} type of steel (eg. structural, pressure vessel, line pipe steel etc.). Z_k is the value code which represents the k^{th} value of the properties relating to each combination of X_i's and Y_j's. Z_k has a hierarchical structure while X_i and Y_j are chain type structures. Figure 1 illustrates the codification scheme along with major codes, subgroup codes and value codes. A total of 238 328 CSRCs are possible using this codification scheme.

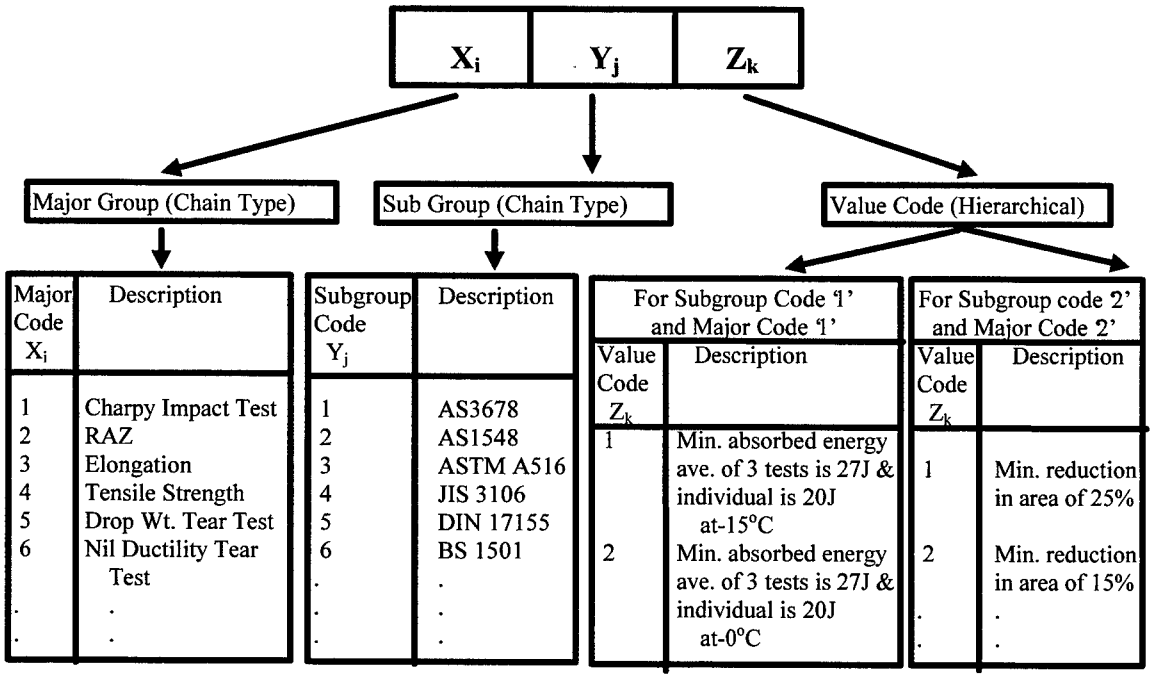


Fig. 1. Codification scheme for the Customer's Special Requirement Codes (CSRCs).

DETERMINING AIM COMPOSITION

The approach adopted in this work for the design of steelmaking aim composition is represented in the form of a flow chart shown in Figure 2.

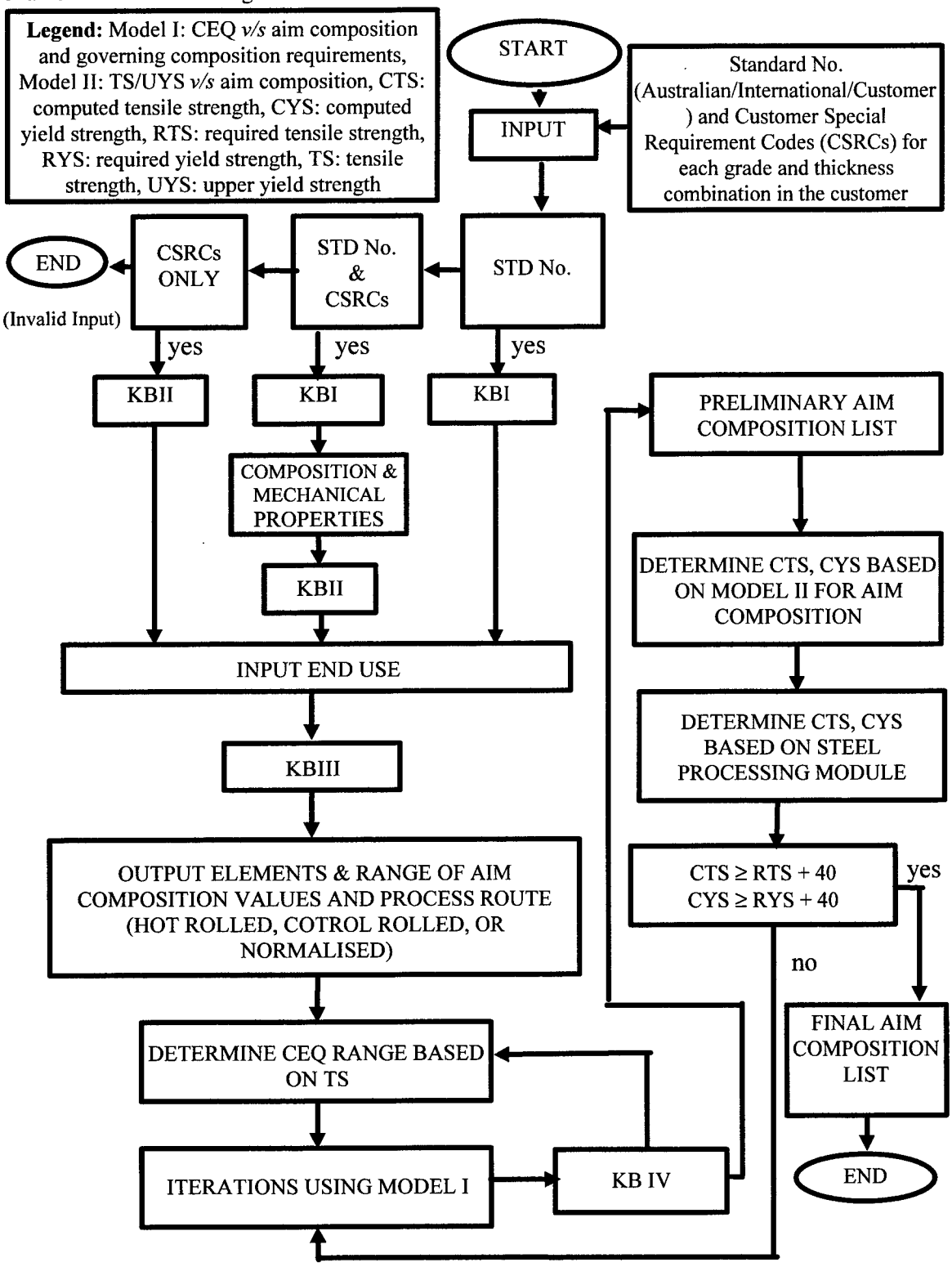


Fig. 2. Flow chart for determining steelmaking aim compositions.

A list of alternative steel making aim compositions is generated using four knowledge bases, two iterative models and one steel processing module as shown in Figure 2. Input information from the user regarding the material enquired or ordered is obtained through interactive sessions. Information on the material standard, its size, quantity, weight, end use, and customer's special requirements, if any, is the input to the system through the dialogue sessions. Depending on the type of inputs, the knowledge base KB I is accessed which consists of information on properties and composition corresponding to relevant material standards. The material standards include Australian standards and other overseas standards transformed into a form which is similar to the Australian standards. Customer special requirements are also included in KB I. Based on the customer special requirements, the composition and mechanical properties from the existing steels need to be modified. This is achieved through the 'knowledge rules' contained in the second knowledge base, KB II. The knowledge representation in KB II is done in the form of IF-THEN rules which relate to main categories: composition and processing. An example of rules in the composition category is given below:

IF Type of steel is structural **AND** Testing requested is RAZ **AND** Value of RAZ is 25% minimum
THEN Maximum S is 0.005% **AND** Maximum H is 0.00019% **AND** Maximum Ca is 0.010%.

Input information about the end use of the steel or the intended application of the steel alongwith information in KB I and KB II dictates a set of rules regarding elements to be included in the aim composition and the basic process route to be followed. The process routes could be hot rolled, controlled rolled, or normalised. These rules are included in the third knowledge base, KBIII. Upper and lower values of aim composition determined by KB III are based on the assumption that a tolerance could be applied to the certification limit values (CLIM) to obtain the minimum and maximum values of aim composition. In the case of carbon the minimum and maximum values are given by

$$C_{min} = \text{lower CLIM} + 0.02 \qquad C_{max} = \text{upper CLIM} - 0.02.$$

Iterative Model I subsequent to KB III calculates the initial aim values of the CLIM using the information from KB III and combining it with expert and heuristic knowledge. The model calculates carbon equivalent (CEQ) for each CLIM, uses empirical formulae to convert these CEQ values to mechanical properties and then finds out a range of CLIM values which are close to the required CEQ, mechanical properties, steel grade and thickness combination. Some values of aim composition, in spite of being within the range of values obtained through KB III, are infeasible due to practical difficulties faced by either the plate mill or the slab caster in using the above aim values. In addition, based on the end use and the mechanical properties required, certain strategies need to be adopted in the design of the aim compositions. Such strategies impose further restrictions on the aim composition values. Thus the rules regarding process limitation and design strategies are contained in the fourth knowledge base, KB IV. Some examples of such rules are:

increment in C (ΔC) = 0.005%, ΔNb = 0.001%, ΔB = 0.0001%, Cu:Ni $\leq$ 2.0, Ti:N $\leq$ 3.42, Mn:C $\geq$3.

The output from KB IV and the process details given in KB III are combined in steel processing module which calculates the metallurgical structure evolution as a function of composition and process sequence. Details of the steel processing module is given in the following section.

STEEL PROCESSING MODULE

The flow chart for the steel processing module is given in Figure 3.

Mathematical modelling of microstructural evolution during hot rolling of steels has received a great deal of attention over the past two decades and a number of models which describe metallurgical phenomena during steel processing have been published for different steel compositions (eg. C-Mn, Nb-/Ti-/Nb-Ti/Nb-V microalloyed steels) and a variety of steel processing routes (eg. conventional, conventional controlled rolling, recrystallization controlled rolling, hot direct rolling etc.). These models have been reviewed by Sellars [17] and Kwon [11]. The basic equations employed in the current work are given in Table 1. Iterative Model II calculates the mechanical properties for each steelmaking aim composition (SAC) based on the output from KB IV and the steel processing module. Empirical models derived from the statistical data are utilised for this process. The empirical models are characterised by an error of about $\pm$ 20 MPa in

the prediction of tensile strength and upper yield strength, a factor of safety of 40 MPa is added to the required values of tensile and upper yield strength while comparing with the corresponding computed values. Thus the final aim composition list is generated which has alternative aim compositions that are feasible for any inquiry or order.

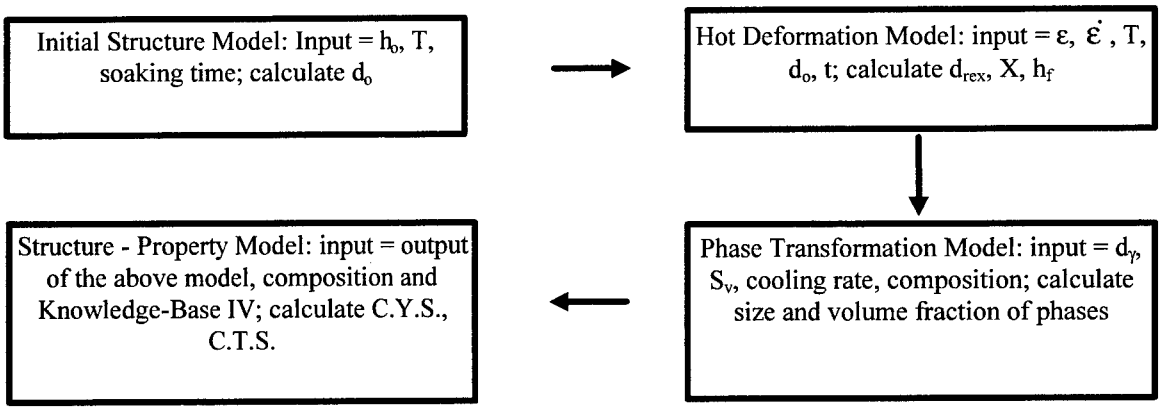


Fig. 3. Flow chart for the steel processing module.

Table 1. Summary of the basic equations used in the computer model for processing a C-Mn steel.

Parameter	Equation	Reference
pass strain ε	$1.155 \ln(h_o/h_f)$	[15]
pass strain rate $\dot{\varepsilon}$	$\varepsilon V_R/\sqrt{RR(h_o - h_f)}$	as above
time for 50% recrystallization $t_{0.5}$	$2.5 \times 10^{-19} \times d_o^2 \times \varepsilon^{-4} \times \exp(300000/RT)$	as above
volume fraction recrystallized X	$1 - \exp(-0.693(t/t_{0.5})^{1.5})$	[8]
recrystallized grain size d_{rex}	$0.763 d_o^{0.67}/\varepsilon$	[15]
Zener - Hollomon parameter Z	$\dot{\varepsilon} \times \exp(312000/RT)$	[18]
time for 95% recrystallization ($t_{0.95}$)	$3.54 \times 10^{-21} \times \varepsilon^{-4} Z^{-3/8} \times d_o^2 \exp(480000/RT)$	as above
Grain growth during interpass time	$d^7 - d_o^7 = 1.45 \times 10^{27} \times \exp(-400000/RT) \times t_{eff}$; $t_{eff} = t - t_{0.95}$	[19]
grain size estimation when X < 0.95 (partially recrystallized austenite)	$\varepsilon_{eff} = \varepsilon_{pass} + \Delta\varepsilon$ $\Delta\varepsilon = \text{const.} \times \varepsilon_{previous} \times (1-X)$ const. = 1 if X < 0.1; 0.5 if X ≥ 0.1; $d_{eff} = 0.5 \times d_o^{0.67} \times \varepsilon_{eff}^{-0.67}$ $\bar{d} = X^{4/3} \times d_{rex} + (1-X)\, d_{eff}$	[20] [15]

h_o = original slab thickness, h_f = final slab thickness, T = pass temperature, t = interpass time, V_R = peripheral roll speed (mm/s), RR = roll radius (mm), R = gas constant (8.31 J/mol-°K), d_o = initial grain size.

SUMMARY

The new integrated system for material design proposed in this work combines both mathematical modelling and knowledge-based approaches. Mathematical modelling enables iterations involving enormous computations while the knowledge-based approach enables utilisation of the expert as well as the heuristic knowledge from a group of experts to successfully determine the steelmaking aim compositions. The procedure involved in this approach is to identify the possible customer requirements with regard to composition, mechanical properties and testing requirements, then to codify them, coupled with processing schedules used in the industry and finally to direct the KEL to acquire knowledge to deal with these special customer requirements. The quality of the output of this system is depends mainly on the quality of the rules

in knowledge bases and mathematical models. As the knowledge base grows richer by experience and the mathematical models refined further through research, it is always possible to incorporate more rules into knowledge bases to improve the output of the system. The system is expected to assist metallurgists to choose an existing composition or to design a new steel composition so that the customer requirement are satisfies in an economical way. The prototype material design system has been fully implemented by developing a software module for generating alternative steelmaking aim compositions that are practically feasible for the slab caster and plate mill. Implementation of the process optimisation module is currently under development.

REFERENCES

1. H. Kominami, S. Naitoh, N. Kamada, C. Hamaguchi, T. Tanaka, H. Endo, 1991. Neural network system for breakout prediction in continuous casting process. Nippon Steel Tech. Report, 49(4), 34-38.
2. H. Yasuda, Y. Nakatsuka, A. Yamamoto, I. Takeuchi, T. Hashimoto, 1992. An expert system for the material design of large-diameter steel pipe. The Sumitomo Search, 50(7), 3-10.
3. R.S.H. Mah, K.D. Schnelle, A.N. Patel, 1991. A plant-wide quality expert system for steel mills. Computers in Chemical Engineering, 15(6), 445-450.
4. S.S. Shivathaya, 1997. Material design in steelmaking utilising mathematical modelling, knowledge-based and fuzzy logic approaches. Ph. D. Thesis, University of Wollongong, Australia.
5. F.J. Vasko, F.E. Wolf, K.L. Stott, 1989. A set covering approach to metallurgical grade assignment. European Journal of Operational Research, 38, 27-34.
6. T. Abe, T. Honda, S. Ishizaki, H. Wada, N. Shikanai, T. Okita, 1990. Application of computer modelling of thermo-mechanical processing on steel plate production. proc. int. symp. on Mathematical Modelling of Hot Rolling of Steel, ed. by S. Yue, Hamilton, Canada, 66-75.
7. P. Choquet, A. Le Bon, Ch. Perdrix, 1985. Mathematical model for prediction of austenite and ferrite microstructures in hot rolling processes. proc. int. conf. on Strength of Metals and Alloys (ICSMA 7), 2, ed. by H. J. McQueen *et al.*, Montreal, Canada, 1025-1030.
8. P.D. Hodgson, R.K. Gibbs, 1990. A mathematical model to predict the final properties of hot rolled C-Mn and microalloyed steels. proc. int. symp. on Mathematical Modelling of Hot Rolling of Steel, ed. by S. Yue, Hamilton, Canada, 76-85.
9. A. Laasraoui, J.J. Jonas, 1991. Recrystallization of austenite after deformation at high temperatures and strain rates - analysis and modelling. Met. Trans. ASM, 22A, 151-160.
10. O. Kwon, 1995. Modelling of austenite evolution and transformation for MA strips. proc. int. conf. Microalloying 95, ed. by M. Korchynski *et al.*, ISS, Pittsburgh, USA, 251-261.
11. O. Kwon, 1992. Technology for the prediction and control of microstructural changes and mechanical properties in steel. ISIJ International, 32, 350-358.
12. M. Suehiro, K. Sato, Y. Tsukano, H. Yada, T. Senuma, Y. Matsumura, 1987. Computer modelling of microstructure change and strength of low carbon steel in hot strip rolling. Trans. ISIJ, 27, 439-445.
13. N. Komatsubara, K. Kunishige, S. Okaguchi, T. Hashimoto, K. Ohshima, I. Tamura, 1990. Computer modelling for the prediction and control of mechanical properties in plate and sheet steel production. The Sumitomo Search, 44, 159-168.
14. M. Pietrzyk, C. Roucoules, P.D. Hodgson 1995. Modelling the thermomechanical and microstructural evolution during rolling of a Nb HSLA steel. ISIJ International, 35, 531-541.
15. J.H. Beynon, C.M. Sellars, 1992. Modelling microstructure and its effects during multipass hot rolling. ISIJ International, 32, 359-367.
16. X.D. Fang, S.S. Shivathaya, 1995. Eliciting knowledge for material design in steelmaking using paper models and codification scheme. Engineering Applications of Artificial Intelligence, 8(1), 15-24.
17. M. Sellars, 1990. Modelling - an interdisciplinary activity. proc. int. symp. on Mathematical Modelling of Hot Rolling of Steel, ed. by S. Yue, Hamilton, Canada, 1-18.
18. M. Sellars, J. Whiteman, 1979. Recrystallization and grain growth in hot rolling. Met. Sci., 13, 187-194.
19. P.D. Hodgson, R.K. Gibbs, 1992. A mathematical model to predict the mechanical properties of hot rolled C-Mn and microalloyed steels. ISIJ International, 32, 1329-1338.
20. A. Laasraoui, J.J. Jonas, 1991. Prediction of temperature distribution, flow stress and microstructure during multipass hot rolling of steel plate and strip. ISIJ International, 31, 95-105.

A SCADA-based Expert System To Provide Delay Strategies for a Steel Billet Reheat Furnace

Clifford Mui*, Edmund Osinski, John A. Meech**, Peter V. Barr****

*DynaMotive Technologies Corporation, Vancouver, B.C., Canada
Email: cliff_mui@bc.sympatico.ca
**Centre for Metallurgical Process Engineering,
University of British Columbia,Vancouver, B.C., Canada
Email: jam@mining.ubc.ca, pvbarr@interchange.ubc.ca

ABSTRACT

The manufacturing of steel bar products in mini-mills involves continuous casting of billet sections, cooling of the billets, reheating to rolling temperatures and final shaping and size reduction in rolling mills. The operation of the reheat furnaces is a significant challenge due to the dynamic nature of both the reheating and rolling processes. The operation of a furnace was analyzed with the use of a SCADA data collection system, and with both steady state and transient mathematical models. The new knowledge gathered in this way was complimented by knowledge from experienced mill personnel to form the basis for an expert system designed to offer timely advice to furnace operators. The result was development of an industrial expert system leading to an increase in furnace and rolling mill productivity [1].

INTRODUCTION

In a typical mini-mill steelmaking plant, the reheat furnace is situated between the caster which produces steel billets, and the rolling mill which shapes the billets into finished products. The operation of a steel billet reheat furnace located in Alberta, Canada has been utilized in our analysis. Production of material such as construction rebar or rail sections involves conversion of raw billets into hot rolled products. Billets must be heated in the furnace in order to bring average billet temperature to a point at which the billets can be rolled with reasonably low force and with a proper microstructure at the end of rolling.

In an ideal world, all processes would run at steady state and no problems would occur to disturb this perfect equilibrium. In this perfect world, steel billets are charged cold into the furnace, heated for a set time until they can be removed in a hot state at regular intervals, and all billets are heated homogeneously prior to rolling in the downstream mill rolls. The furnace, of course, would be operated at optimal steady-state conditions at all times and would never require adjustment. The rolling mill would be able to accept these billets in a timely fashion and would shape all of the bars successfully into rolled products. Unfortunately, this ideal world does not exist.

In the real world, furnaces routinely experience transient conditions. For example, scheduled delays due to regular downstream roll changes or unscheduled delays due to unexpected cobbles are a few of the conditions that may be encountered during initial charging of cold billets. Furnaces have large thermal inertia - things change slowly and errors take time to recover from. Control of furnace temperatures is critical if the desired result is to produce a homogeneously-heated billet at the proper time and proper temperature. The consequences of improperly controlled delays may include unnecessary rolling mill idle time, uneven rolling of unevenly heated billets, center-line cracking or product downgrading due to excessive heating time within the furnace. Intelligent control of this process is the responsibility of experienced furnace operators who base their decisions on a myriad of different factors. Consistency of such operator-based control can be poor at the best of times especially when new employees enter the situation and require training. So a systematic, computerized approach seems to be the solution.

Artificial Intelligence is defined as "a collection of computer-based techniques which manipulate symbols rather than numbers to enable computers to produce behavior resembling that previously only seen in

0-7803-5489-3/99/$10.00 ©1999 IEEE.

humans" [2]. Expert Systems involve the application of Artificial Intelligence concepts to real world problems. Expert Systems operate very differently from conventional computer programs in that the problem solving techniques, or "heuristics" mimic human-problem-solving. Expert systems would therefore have a distinct advantage over conventional control schemes in experience-laden applications such as steel reheating furnaces. The ultimate goal of this exercise was to improve product consistency and lower mill operating costs.

THE STEEL REHEAT FURNACE

The facility chosen to implement this expert system was a mini-mill located in Alberta, Canada. The mill buys scrap steel on the open market, melts the raw material in an electric arc furnace and makes metallurgical adjustments to composition prior to a continuous casting process to produce square steel billets. These billets are taken to a storage yard where they are cooled prior to scheduled charging into a natural gas-fired reheat furnace. The billets are heated in the furnace to obtain a homogeneous temperature prior to hot forming. The hot billets from the furnace are then shaped in a rolling mill to produce bar products such as grinding stock, rebar and structural stock.

The natural gas fired furnace utilizes a combination of stationary and walking beams which carry the billets into and out of the heating zones. The furnace is controlled as three distinct zones in which individual PLCs (programmable logic controllers) control zone temperatures in accordance with set-points chosen by the shift furnace operators. Operators follow general guidelines for control but they rely mainly on experience and "know how" to select appropriate measures during both steady state and transient operating conditions. Figure 1 illustrates a side cut-away view of the reheating furnace.

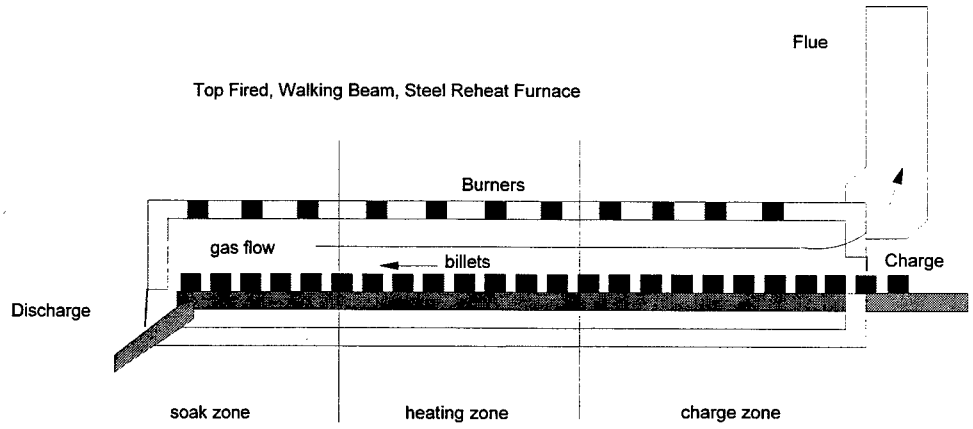


Fig. 1 Side View of the Reheat Furnace.

Developed in conjunction with the expert system initiative, the operation of the furnace was examined thoroughly using mathematical models. A steady-state model was originally developed by Barr [3] to study the efficiency of steady-state operating procedures. A plant trial in 1995 produced data to assist in the evolution of a 3-D transient model which was later verified at two Canadian reheat furnaces by Scholey [4]. These models along with control-scenario development by Osinski [3] became integral in the development of this project.

BUILDING OF THE KNOWLEDGE BASE

The operational knowledge used to control the furnace in the form of operator experience should be a valuable starting point in building a knowledge base. Unfortunately, furnace operators have created many different approaches to deal with transient conditions and their experience under similar circumstances, while useful, was too inconsistent to allow collection of the "best" knowledge. This "episodic" knowledge was disjointed and often clouded by "process lore" [6]. Therefore these ideas were not used directly in the knowledge acquisition phase. However, a set of "Standard Operating Practices" (SOP) was created by the

plant combustion engineer and from discussions with the operators to provide congruency in operating strategy. This agreement in the required furnace operating practices provided a good degree of procedural consensus [5]. The majority of this knowledge is in the form of "declarative" and "procedural" knowledge and is considered significant because it was scrutinized by the combustion engineer and untainted by Process Lore. The SOP became the basis for creation of a reheat furnace control knowledge base and was incorporated into the Expert SCADA System as an on-line hypertext help document.

The expert system was designed to allow its basic knowledge to be maintained as well as the addition of newly developed or acquired knowledge. The expert system is able to provide timely, online knowledge-based advice through a user-friendly man-machine interface. In addition, the system created a way for mill management to introduce a standardized methodology to handle the majority of furnace transients.

ACQUIRING PROCESS INFORMATION

The SCADA package chosen to implement this expert system was ProcessVision and Comdale/C operating on a PC in a QNX operating system environment. The Comdale/C application can be separated into a series of separate modules each given specific tasks. Although these modules all operate independently in QNX, they are linked to influence the operation of each other. The Comdale system was originally designed to operate efficiently with processes in which reaction times are relatively slow. The inference engine operates with a one second or greater cycle time which is adequate for moderately-paced supervisory control situations on continuous processes. The cycle times of such systems must be fast enough to sample critical events accurately. The reheat furnace system has a myriad of slow response inputs but also, one very-fast output.

This latter signal is generated from an optical pyrometer which provides a continuous analog measurement of the temperature profile of a billet discharged from the furnace. This process is a batch occurrence taking place on a regular basis every 1 to 2 minutes depending on the production level. A billet passes in front of the instrument within a 2 second time interval. An existing data collection system at the time this project was commenced recorded about 2000 temperature points along the billet, i.e., at a rate of one record every millisecond. In order to link such high frequency, intermittent data to the intelligent supervisory control and data-acquisition system (I-SCADA) a set of high speed Computational Intelligence (CI) modules were designed to operate in parallel with the Man-Machine Interface (MMI) [7,8]. These data collection drivers intelligently samples input signals until an event is detected. After the driver has buffered the record of the event internally, the data are processed and uploaded into the inference engine at a rate equivalent to the current billet production rate of 1-2 minutes.

APPROACH TO THE REHEAT PROBLEM

The furnace had been operating reasonably satisfactorily in preparing billets for the rolling mill but there was a strong desire to improve certain aspects of the process. Delays in production of hot billets result in loss of useful rolling mill time and a subsequent monetary loss. As well, poor procedural operation results in low recovery rates or product yields due to billet rejection as well as product downgrading. One goal of the project was to reduce both of these factors as well as fuel consumption. Part of this goal can be achieved by having the operators use standardization procedures in response to delay situations. The expert system provided direct access to all of the mill's standardized settings and procedures.

A secondary objective of the expert system was to collect as much static knowledge on the operation of the furnace as well as make timely assessments of transients based on the "best guess" of furnace operators. The system contains logic rules to provide automatic detection of a delay situation which allows the system to flag the operator with an initial estimate of the delay duration. This estimate is made in linguistic terms as a short, medium, or long delay. The range of each of these terms is assigned from the knowledge base depending on the type of product being heated. The system issues an advisory based on this input as well as information provided by the knowledge base (SOP) with respect to the delay category. The category

determined causes the system to make specific recommendations regarding burner settings to attempt to reduce energy consumption and avoid overheating of the billets held within the furnace.

As a delay progresses, the system tracks the actual delay length to determine if the initial estimate was correct. If the delay terminates prematurely or the delay is longer than initially estimated, the advice that was originally issued about burner settings is now likely unsuitable. Table 1 illustrates the possible outcomes of an initial delay estimates and a variety of actual delay times. The system is able to determine quickly this aberration and issue a revised advisory. This advice will dynamically change based on the new estimated delay time as well as the actual progressive time. Table 2 shows how the system can adjust to meet the requirements of a correction in the actual delay duration.

Table 1. Possible Outcomes of Delay Time Estimation and Error Consequences.

	Predicted Short Delay	Predicted Medium Delay	Predicted Long Delay
Actual Delay is Short	Accurate delay estimate	Furnace too cold, delay in heating back to temperature	Furnace much too cold, delay in heating
Actual Delay is Medium	Furnace not cooled enough, billets may overheat	Accurate delay estimate	Furnace too cold, delay in heating back to temperature
Actual Delay is Long	Furnace not cooled enough, billets may overheat and spend too much time at high temperatures	Furnace not cooled enough, billets may overheat, possibly long time at high temperatures	Accurate delay estimate

Table 2. Possible Outcomes of Delay Time Estimation and Control Responses.

	Predicted Short Delay	Predicted Medium Delay	Predicted Long Delay
Actual Delay is Short	Well understood and simple control	Furnace too cold, advise heating regiment	Furnace much too cold, advise a rapid heating regiment
Actual Delay is Medium	Furnace not cooled enough, advise lower zones set points	Well understood and simple control	Furnace too cold, advise a heating regiment
Actual Delay is Long	Furnace not cooled enough, advise lower zone set points, track overheat times	Furnace not cooled enough, advise lower zones set points	Well understood and simple control

IMPLEMENTATION OF THE EXPERT SYSTEM

System implementation was divided into two distinct phases. The first phase was long-term data collection and logging. In this stage, inputs from the furnace controllers were recorded along with some inputs normally seen only by furnace operators. The data were compiled into daily log files and subsequently into the cumulative collection of files into the plant database. These files along with hard copies of schedules were remotely retrieved and analyzed both by plant engineers at the mill and by personnel at UBC. The second phase involved construction of the knowledge base and insertion into a man/machine interface designed to look similar to that which the operators were already familiar. The system could detect transient conditions and provide timely advice to the operator in both steady-state and transient operating conditions.

Phase I of the system implementation involved installation of a data-logger to facilitate long term collection of furnace control knowledge. Developing the man-machine interface was considered of utmost importance due to the need for operator acceptance [5] and the creation of a method to verify the expert system.

The billets are scanned for their temperature profile to retrieve information for the Expert System and to display to the operators. Information such as maximum and minimum temperatures as well as the profile shape characteristics decide the fate of a billet. A billet that is not up to standard for a particular job may be rejected prior to rolling or the rolled product is held for quality control assessment. The user interface was created to display the most important operating data on a "main" screen and supplementary information on secondary screens accessible by "clicking" a button on the main screen. Figure 2 illustrates the main screen which provides a large amount of information to be available to the operator in a high-density graphical form as noted by the billet temperature profile and the historical profile limits in the lower portion of the display. Also included in this display are a billet heat-tracking and operating status message strip.

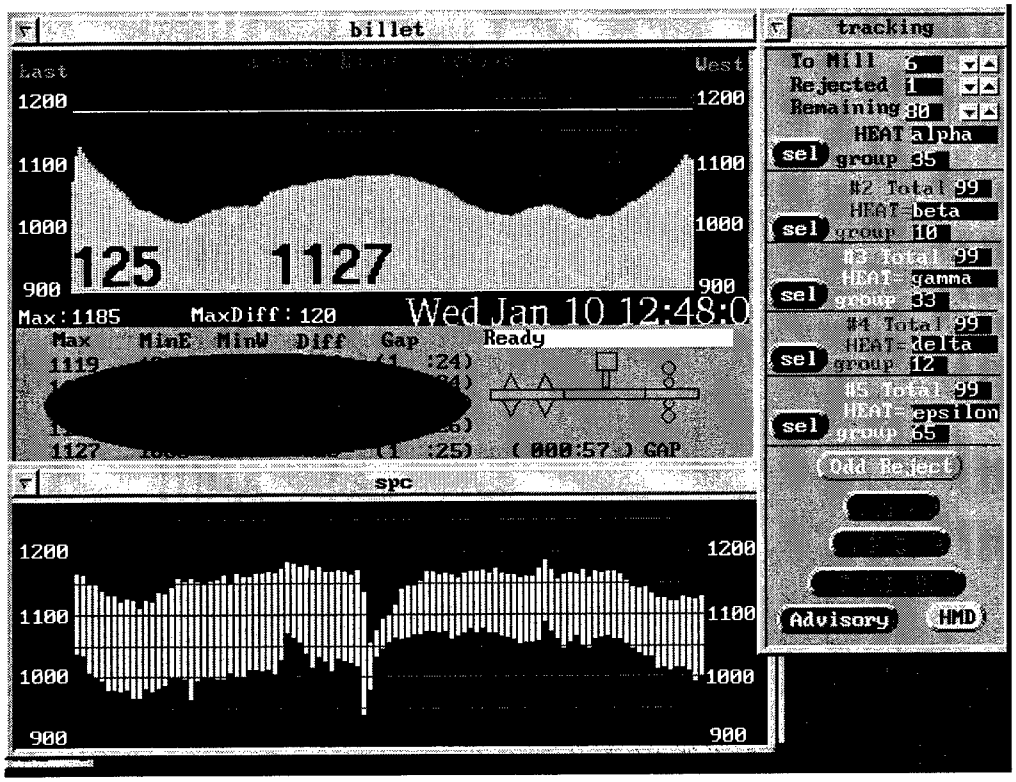


Fig. 2 Main Screen of the Expert System.

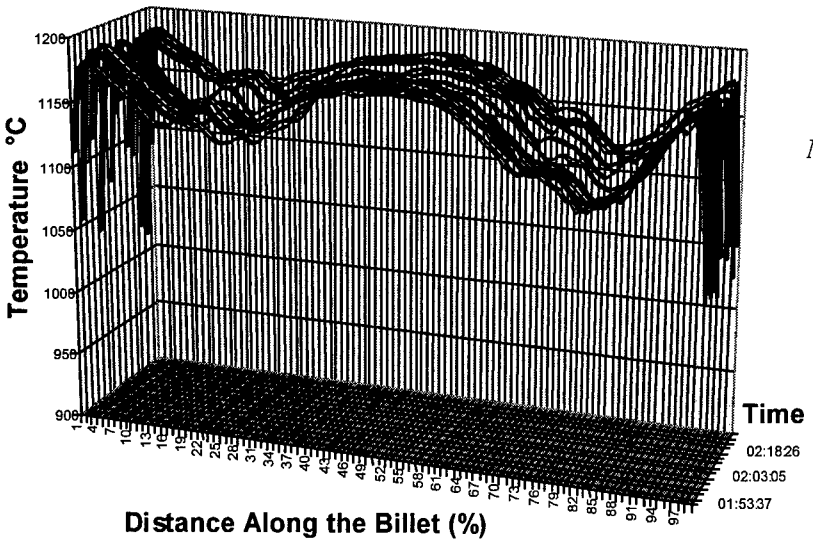
The second phase of the project included installation of a knowledge base containing plant procedures and the development of an advisory screen which prompts the operator to read during transition or transient-operating events. The expert system provides static advice as well as advice based on delay conditions. If the operator provides an estimate of the delay length, the system will present appropriate information to handle the situation. If the actual delay time is longer or shorter than the prediction, the advice changes to suit the situation based on information contained within the knowledge base.

RESULTS AND DISCUSSION

The system is stocked with declarative and procedural knowledge from the Standard Operating Practices as well as new knowledge from scenario "role playing" using the UBC transient furnace model. This knowledge forms the basis for the expert system in terms of providing an operator with knowledge gathered and refined from years of experience and from recent scenario development. When the knowledge base is applied to complex delay situations, the system can offer timely advice for a myriad of transient conditions

The system records and archives time-stamped temperature profiles of the billets for scrutinization. Furnace operating data was also made available to the modeling experts. The zone temperature records can be correlated with the billet temperature data. In addition to these traces, gas flows, air flows, and total furnace pressure stemming from operator control of the PLCs were also available for analysis. An example of a billet temperature profile is illustrated in Figure 2. This example illustrates the change in temperature profile which can occur during a short delay. The dip in temperature of the billets is due to the change in thermal history prior to discharge as a result of operator response and manipulation of burner controls.

These responses can then be analyzed via a 3D mathematical model to determine the efficiency of the operator's response as well as the possibility of creating better response without needing to experiment with the actual furnace controls. The analysis can then be expanded to include theoretical responses to incorrect initial responses based on inaccurate initial operator delay estimates. This information can then be placed into the expert system to provide timely new advice for an initially misdiagnosed delay progresses.



Note: This example contains a 7.5 minute delay midway along the time sequence.

Fig. 3. Sequence Plot of Billet Temperature Profiles.

During the final phase of furnace modeling, we were able to create some general response scenarios with respect to nominal operator control as well as developed control schemes of varying complexity. Several new procedures were postulated and tested for a number of variations. The result was a set of new post delay procedures which the model deemed to be more effective. We assembled a set of results from the modeling efforts which included examination of the effectiveness of three delay strategies as follows:

1. null strategy - no action is taken during or after this delay
2. basic strategy - as is currently prescribed
3. fine strategy - fine adjustments to the operation during and after the delay

The firing strategies noted above are summarized in Table 3 and Table 4 [3]. The modeled outcomes of these strategies are summarized in Figure 4 and Figure 5 [3]. It is clear from these results that the null strategy as expected produces greatly overheated billets and that the fine control strategy produced billets with much lower standard deviation in temperature. These procedures were presented to the mill for validation prior to assimilation into the mill SOP.

Table 3. Basic Post-Delay Firing Strategy.

	Charge Zone [Nm3/h]	Heat Zone [Nm3/h]	Soak Zone [Nm3/h]
delay (70 min)	280	280	280
1st 10 min. after delay (70-80 min)	280	280	150
next 20 min. after delay (80-100 min)	1850	280	150
next 5 min after delay (100-105 min)	1850	280	400
steady state	1850	900	400

Table 4. Fine Post-Delay Firing Strategy.

	Charge Zone [Nm^3/h]	Heat Zone [Nm^3/h]	Soak Zone [Nm^3/h]
delay (70 min)	280	280	280
1^{st} 10 min. after delay (70-80 min)	280	280	150
2^{nd} 10 min. after delay (80-90 min)	1850	280	200
3^{rd} 10 min. after delay (90-100 min)	1850	280	200
4^{th} 10 min. after delay (100-105 min)	1850	280	300
105-140 min	1850	900	300
140-150 min	1850	900	400
150-155 min	1850	900	600
steady state	1850	900	400

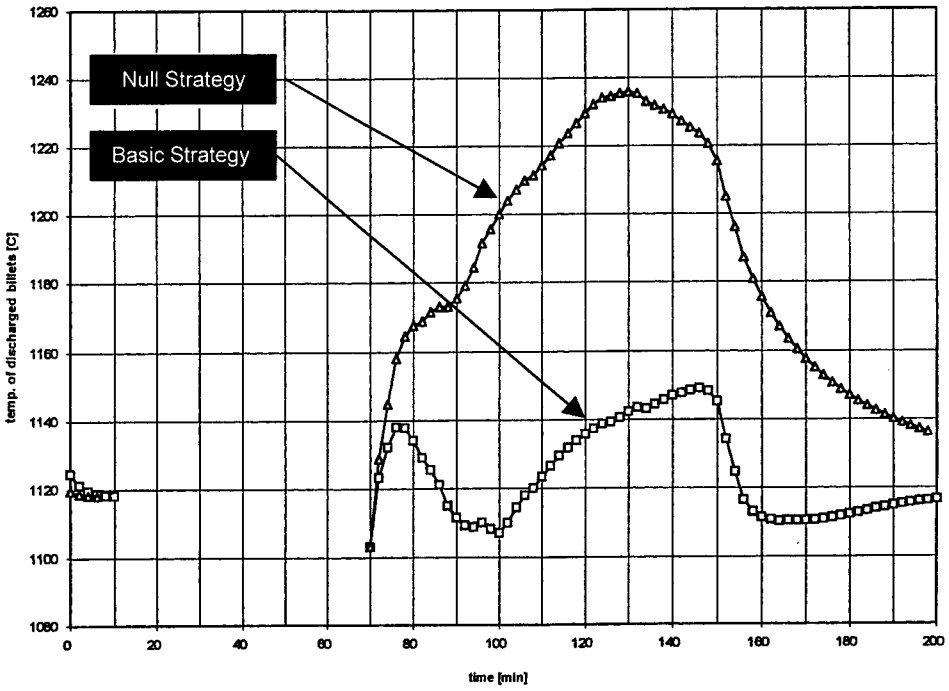


Figure 5 Comparison of a Basic Fine Control Strategy with a Null Strategy.

It had been believed that about 40% of the production is constrained by rolling mill delays, leaving the remaining 60% of the billets in the furnace at full burner capacity. Logged furnace data used for model development showed that this was not that case since not all of the furnace zones were maintained under heavy firing conditions with large 8" billets. In fact, the manner in which the furnace was operated may have affected throughput. Further examination of these procedures is required to assess the feasibility of increasing furnace throughput by altering the ingrained operating procedures with this new knowledge. It is clear from this example of mathematically-modeled delay response strategies, that the expert system can be more effective with addition of externally generated knowledge.

The initial response to Phase I of the installation showed great reluctance on the part of the operators as they were suspicious that mill management intended to replace furnace operators with a computer control system. This is consistent with the "Feigenbaum Bottleneck" which includes reluctance from experts due to the fear of "loss of work" from AI technology and automation. [2,9]. These fears were alleviated by carefully demonstrating and explaining the system to the operators to clarify our objectives and to explain that our goal was to supplement the operators' "toolbox" with on-line presentation of the appropriate operating procedures. Following these discussions, this initial phase was successfully completed.

Phase II was essentially a seamless addition to the interface. All interface screens from Phase I remained intact with the addition of an advisory screen to provide on-line advice, based on the knowledge within the newly installed knowledge base and delay-detection rules. As expected, this phase was the portion of the project most difficult to obtain general acceptance from furnace operators. This reluctance was due mainly to the past nature of furnace control in which operators were allowed to implement any control procedure in order to produce billets with minimal mill delay. Unfortunately, these decisions often produced billets at the expense of product quality or total overall production. However, since the expert system goals are being championed by the supervising combustion engineer, this reluctance will eventually be overcome.

CONCLUSION

This project has examined problems involved in controlling a steel reheat furnace at an Alberta mini-mill. On completion of the work, the following conclusions can be made:

- Control of billet reheating furnaces has proven to be well-suited to an expert system approach due to the heuristic nature of the process.
- An Expert System consisting of a data collection module and advisory module was developed and successfully installed at an Alberta mill. The system is still in operation 3 years after installation. This implementation can be considered a success because of the continued use by the mill personnel.
- An on-line and off-line statistical process database was created for forensic analysis of operations.
- The static and transient furnace models developed during this project were effectively used to study control conditions and procedures leading to new knowledge which increased mill efficiency. This knowledge was assimilated into the SCADA system for on-line use.
- The system allows creation of an operating standard in which inexperienced or undisciplined operators must use proven procedures designed to increase productivity and decrease operating losses.
- The system has become an integral tool for operators who benefit from a man-machine interface as well as the mill managers as they attempt to improve the operating bottom line via process efficiency.

ACKNOWLEDGEMENTS

CM would like to express his appreciation to Dr. Peter Barr and Dr. John Meech for their support and guidance towards the completion of this project and to thank the late Dr. J. Keith Brimacombe, Dr. Indira Samarasekera, the Centre for Metallurgical Process Engineering and NSERC for financial and moral support in this endeavor. A debt of gratitude to Vladimir Rakocevic is expressed for his invaluable assistance in creating the hardware drivers. Ken Scholey and Edmund Osinski are acknowledged for their modeling work as well as the assistance of personnel at Alta Steel: Bob Pugh, Doug Ostafichuk, Dennis Gutknecht, Mark Burrough, Ed Duchesne and the furnace operators.

We wish to acknowledge the financial and in-kind support of the following sponsors of this research: Alta Steel, Manitoba Rolling Mills, Accumold Ltd., Comdale Technologies (Canada) Inc., and the Natural Sciences and Engineering Research Council of Canada.

REFERENCES

1. C.L.B.Mui, 1998. Thesis. Steel Billet Reheating: An Expert Approach. UBC MASc.
2. J.Efstathiou, 1989. Expert Systems in Process Control, 114-138.
3. P.V.Barr, K.E.Scholey, E.Osinski, 1997. Unpublished work in progress, Modeling of Steady-State and Transient Billet Furnace Operation.
4. K.E.Scholey, 1996. A Transient, Three-Dimensional, Thermal Model of a Billet Reheating Furnace. UBC PhD Thesis,
5. L.Boullert, A Krigsman, R.A. Vingerhoeds, 1992. Application of Artificial Intelligence in Process Control: Lecture Notes Erasmus Intensive Course, 127-141
6. J.K.Brimacombe, 1993. Towards the Intelligent Mould for the Continuous Casting of Steel Billets. 76th Steelmaking Conference, Iron and Steel Society, Empowerment with Knowledge:, 3-27.
7. V.Rakocevic, J.A.Meech, 1995. Computational Intelligence in a real-time SCADA system to monitor and control continuous casting of steel billets. IFSA '95 Sao Paulo, Brazil, July 22-28,
8. J.C.Bezdek, 1994. Computational Intelligence -Imitating life. IEEE World Congress on Computational Intelligence (WCCI), What is computational intelligence?, 1-12
9. J.A.Meech, 1995. AI Applications in the Mining Industry into the 21st Century, APCOM XXV Conference, Brisbane May 9-14, 95-96.

Simulation and Analysis of Thin Strip Casting Processes

Yogeshwar Sahai and Manish Gupta

Department of Materials Science and Engineering
The Ohio State University, Columbus OH, USA.

ABSTRACT

An overview of the thin strip casting processes for steel and aluminum is presented in this work. A two-dimensional finite element mathematical model, capable of simulating the turbulent fluid flow, heat transfer and solidification, and thermally induced stresses, is presented.

INTRODUCTION

Thin strip casting processes for casting molten metal directly into thin strips of desired thickness and width are currently being developed around the world. These processes have the following advantages over conventional continuous casting processes:

1) Energy savings in heating and deformation in hot and cold rolling.
2) Reduced production time, which increases the efficiency of the process.
3) Reduced segregation due to decreased solidification time.
4) Refined microstructure due to faster cooling.

Three thin strip casting processes have shown the potential for industrial production of thin strips of steel. These are melt drag process, twin-roll process, and two-roll melt drag method.

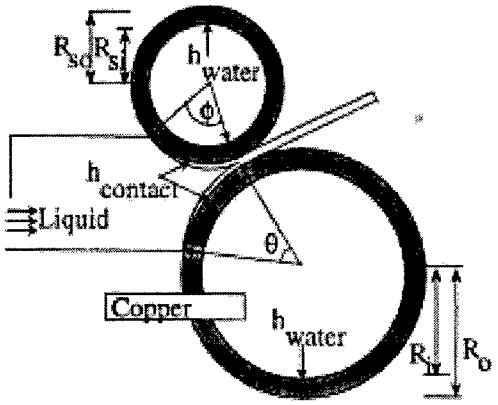


Fig. 1. Schematic of a two-roll melt drag thin strip caster.

In melt drag process only one side of the strip solidifies on the roller while the other side solidifies in the open atmosphere and thus results in poor surface finish. In order to get better surface finish on both sides, the twin-roller caster is used. In this process, both sides of strip solidify in contact with roller surface. In two-roll melt drag process, as shown in Fig. 1, a roller of small or equal diameter is placed on the top free surface which improves the quality of the top cast surface. Generally, the melt drag process is most suitable for casting strips upto 2 mm thickness, while the two-roller melt drag and twin-roll strip casting processes are preferable for casting of strips upto 7 mm. Fig. 2 shows the typical velocity vectors in the melt pool and rolls for a two-roll melt drag caster.

For industrial production of thin strips of Aluminum, twin roll casters have proven to be the most economical and efficient machines. In a horizontal type twin roll caster, molten aluminum is fed from a refractory feed tip into the gap between two counter rotating, water-cooled cylindrical steel rolls. The

0-7803-5489-3/99/$10.00 ©1999 IEEE.

schematic of this caster is shown in Fig. 3. Unlike thin strip casting of steel, the solidification gets over well before the kissing point during casting of aluminum sheets and the material undergoes a considerable amount of rolling before it leaves the rolls. Also, there is relative velocity between the cast strip and the rolls, which results in shear stresses at the metal/roll interface

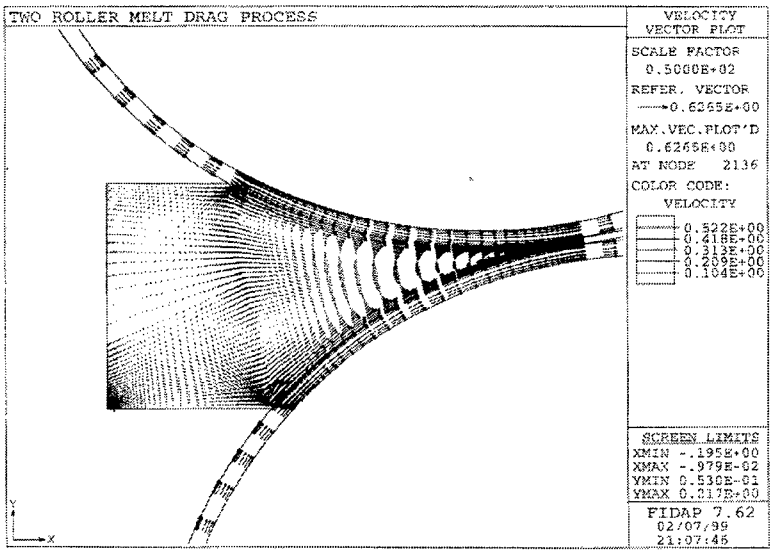


Fig. 2. Typical velocity vectors in the melt pool and rolls for a two-roll melt drag thin strip caster.

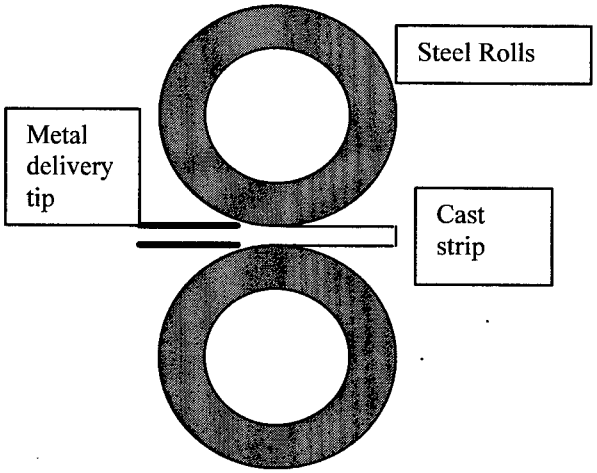


Fig. 3. Schematic of a horizontal type twin-roll thin strip aluminum caster.

A significant amount of work has been done by Gupta and Sahai [1] to mathematically model these thin strip casting processes. In their work, they simulated melt drag, twin roll and two roll melt drag thin strip casting processes.

Strip casting process involves solidification of liquid metal and, in case of aluminum, solidified metal undergoes considerable amount of rolling before it leaves the kissing point. Solidification of molten metal starts at the point of first metal-roll contact and is over at or before the kissing point. During the process, molten metal experiences a very high rate of heat extraction, which results in very high thermal stresses in the material. These stresses arise due to thermal gradients in the material, rolling action, metallostatic pressure of the unsolidified melt pool and friction between roller and strip. These stresses can have a deleterious effect on the quality of the cast product. Stresses, tensile in nature can lead to the formation of a variety of surface and internal cracks. Hence, it is of great importance to understand the development and nature of thermal stresses. The modeling of stresses in thin strip casting processes has received very little

attention of the researchers in past. During the thin strip casting of aluminum, the major problems in the industry today are the various defects in the cast product. Various casting defects like centerline segregation [2], heat line formation [3], and sticking problems occur during strip casting.

This paper presents some results of two-dimensional mathematical model of heat transfer, turbulent fluid flow, solidification and thermally induced stress simulation. Two casting processes, two-roll melt drag method for thin strip casting of steels and a horizontal type twin-roll casting process for aluminum, are presented in detail. In aluminum strip casting, it has been observed that the extent of centerline segregation increases with the length of solidification interval, or the *sump depth.* Effect of process variables on the sump depth and thermal stresses is presented for a typical twin-roll aluminum caster. For two-roll melt drag casting of steel, effect of process variables on the cast strip thickness, flow profile and thermal stresses is presented. Fluid flow and heat transfer calculations are performed using a commercial software, FIDAP, and the temperature profiles obtained at steady state are imposed as thermal load to the mechanical system. Stress analysis calculations are performed using another commercial software, ANSYS. The stress analysis model uses viscoplastic constitutive equation to describe the material behavior at temperatures close to melting point.

MATHEMATICAL MODEL

A general mathematical model is described here and its details can be found elsewhere [4]. This model is capable of simulating all thin strip casting processes for steel and aluminum, with some differences, such as velocity and load boundary conditions.

The mathematical model involves the following assumptions:

1) The process is at steady state. After a small initial transient period, process parameters do not change with time.
2) By taking into account the fact that width/thickness ratio is very large and ignoring the end effects, the geometry of the process can be approximated as two-dimensional.
3) Liquid metal is incompressible and is a Newtonian fluid.
4) Material is assumed to be isotropic in nature.
5) The elastic strains are small relative to plastic strains.
6) The plastic flow of material is assumed to be isochoric.
7) Material properties (except viscosity and specific heat) are temperature independent.
8) Heat losses by radiation are negligible.

Under the above assumptions, the following equations are solved in the calculation domain,

- Continuity equation
- Turbulent Navier-Stokes equation
- Equation for conservation of thermal energy
- Two equations for k and ε to model turbulence.
- Equation for mechanical equilibrium

The above equations are solved with appropriate boundary conditions. The strip velocity in aluminum thin strip caster is about 10% higher than the rolls.

RESULTS AND DISCUSSION

Two-roll melt drag process for strip casting of steels

Process variables that affect the thickness of cast strip significantly were identified as:

(i) Roller speed
(ii) Gap heat transfer coefficient
(iii) Melt superheat

Effect of roller speed on cast strip thickness

Fig. 4 shows the variation in strip thickness with roller speed. It can be seen that the strip thickness decreases with increase in roller speed. This is because, at higher casting speed contact time of melt with roller is less,

hence the time provided for solidification of liquid metal is also less, which results in thinner strips. From Fig. 4, it also evident that the growth rate for low roller speed is higher than that for high roller speeds.

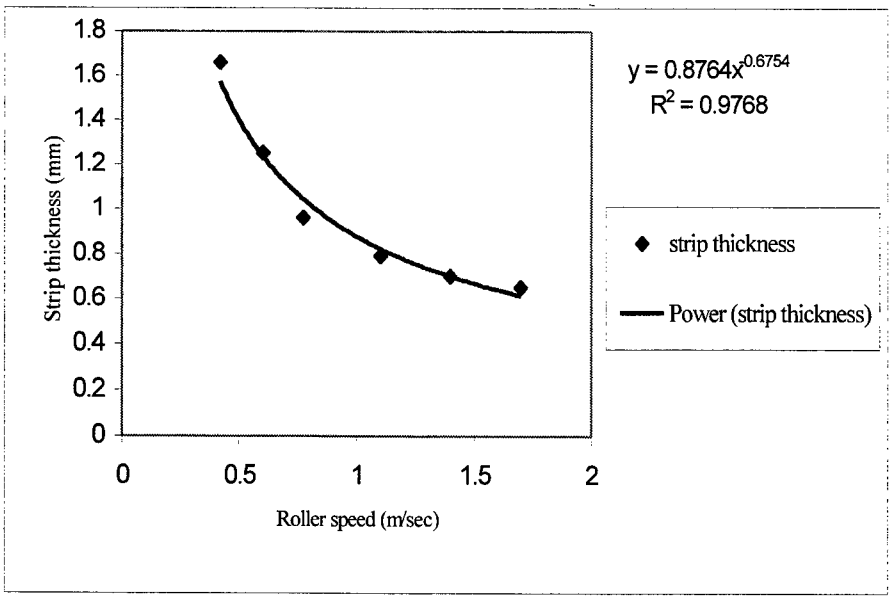


Fig.4. Strip thickness as a function of roller speed.

Effect of gap heat transfer coefficient on cast strip thickness

Gap heat transfer coefficient governs the rate of heat transfer from melt pool to roller. Fig. 5 shows the variation in strip thickness with gap heat transfer coefficient. It can be seen from the figure that as the value of gap heat transfer coefficient increases thickness of cast strip increases.

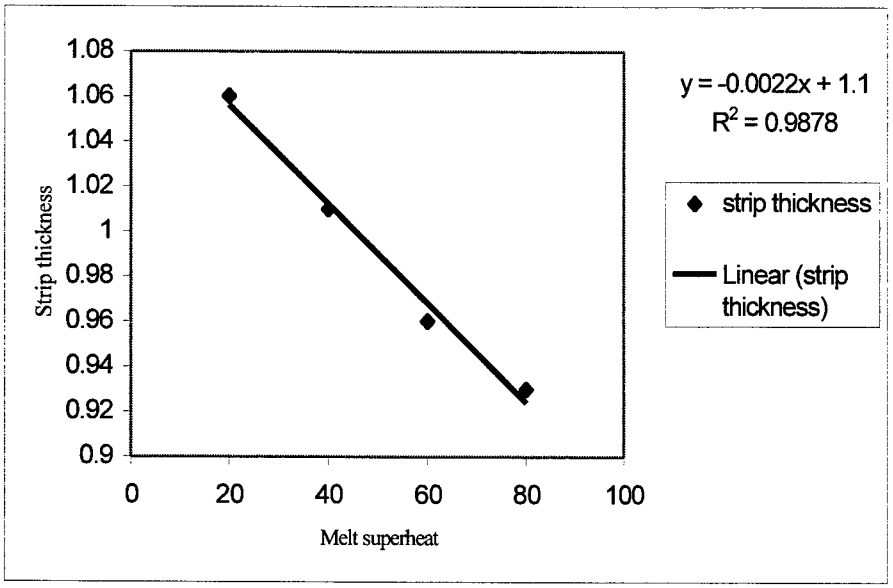


Fig. 5. Strip thickness as a function of gap heat transfer coefficient.

Effect of melt superheat on cast strip thickness

Fig. 6 shows the variation in strip thickness with the melt superheat. Larger amount of heat is to be removed through the solidifying strip in case of liquid steel with higher superheat. This, in turn reduces the solidification rate. It can be seen that, increase in superheat of liquid steel reduces the solidified thickness of the shell. The effect of superheat of strip thickness does not seem to be significant because the major part

of heat is coming from the release of latent heat of fusion and not from the superheat. Sensible heat due to superheat is very less compared to latent heat of fusion.

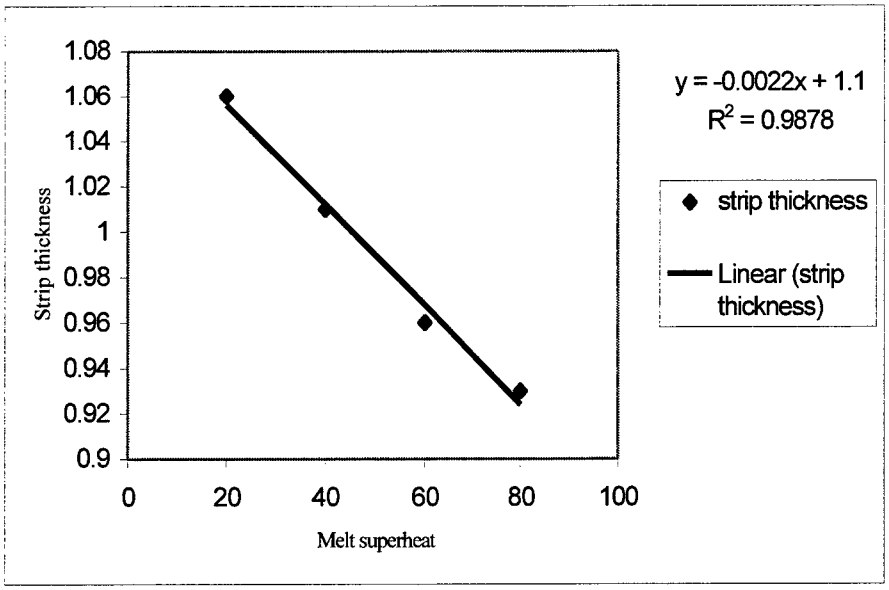


Fig. 6. Strip thickness as a function of melt superheat.

Stress model's predictions

The stress model can be used to evaluate conditions under which cracks may appear in the solidifying body. In this study, the cracking criterion proposed by Ramacciotti [5] is employed, in which a temperature dependent ultimate strength is used as a reference for cracking criterion:

$$\sigma_R = C(T_{sol} - T)^{0.5} \text{ (MPa)} \qquad 1.$$

where, $C = 1.2^{-0.5}$ (MPa K)$^{-0.5}$.

A cracking index was defined based on the principal stress as C.I. = $(\sigma_p/\sigma_R)_{max}$ where, σ_p is the magnitude of the principal stress.

A positive cracking index at a point means that the material is subjected to tensile stresses at that point whereas a negative cracking index would mean the material is subjected to compressive stresses. Cracks can appear at points with C.I. greater than one, i.e. the points subjected to tensile stresses, while cracks will not appear at the points under the compressive stresses.

Fig. 7 represents the variation in the cracking index, across the width of cast strip at the point where it leaves the rolls, in a two-roll melt drag thin strip casting under three different casting conditions. In the finite element mesh, there are 45 nodes along the width of the strip. Point 1 represents the node at the point of contact between the strip and upper roller and point 45 represents the node at the point of contact between the cast strip and lower roller. It is evident from Fig.7 that the susceptibility of material to fail due to thermal stresses is highest at points, which are close to two rolls and is lowest at locations in the middle of the cast strip. The magnitude of thermal stresses in the cast strip increases as the casting speed decreases. This is due to the fact that at low casting speed, shell thickness of solidified metal on the rolls is more which reduces the rate of heat transfer from the melt pool to the rolls (effective thermal conductivity of liquid metal is much higher than that of solidified metal). This leads to higher thermal gradients in the material and consequently higher thermal stresses are generated.

Horizontal type twin-roll thin strip casting of aluminum

The cause of centerline segregation is the interdendritic fluid motion through the partly solid region, which arises because of the pressure gradient in the roll gap. The intensity of segregation or the liquid motion between the dendritic arms is influenced by the *local solidification time,* which is defined as the time at a

given location in a casting between initiation and completion of solidification. The length of solidification interval or the sump depth increases as solidification time increases. Sump depth is a function of alloy freezing range, casting speed, strip/roll gap heat transfer coefficient and inlet temperature of liquid metal.

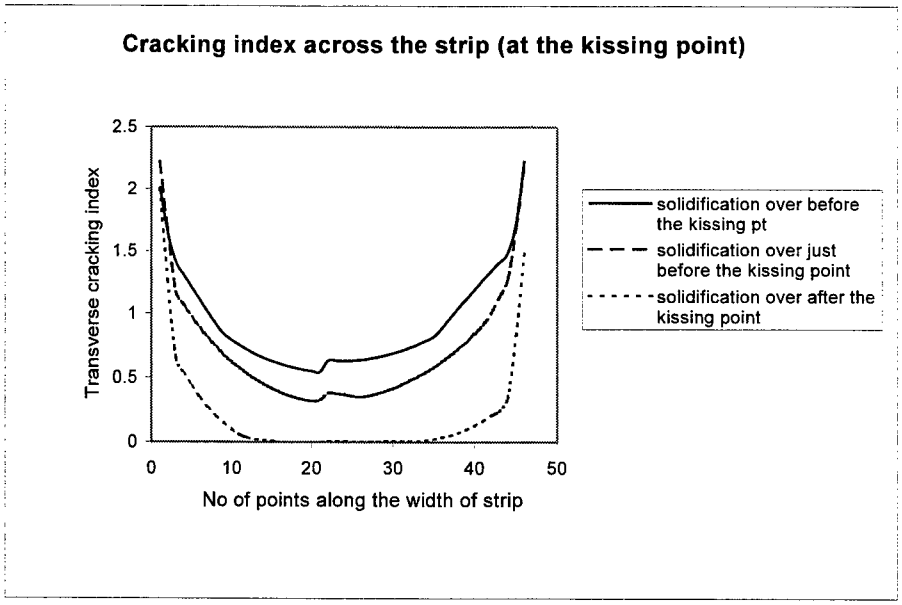


Fig. 7. Variation in cracking index across the cast strip in a two-roll melt drag thin strip caster.

The liquidus and solidus temperatures of the alloy are 660°C and 640°C respectively. It is assumed that the alloy behaves as solid at temperatures above the mean of liquidus and solidus temperature, which is 650°C, and as liquid at temperatures below 650°C.

The position of the solid/liquid interface is shown in Fig. 8. The distance between the nozzle and the completion of solidification is defined as the sump depth. Fig. 9, 10, and 11, show the effect of casting speed, slab/roll gap heat transfer coefficient and melt superheat, respectively on the sump depth.

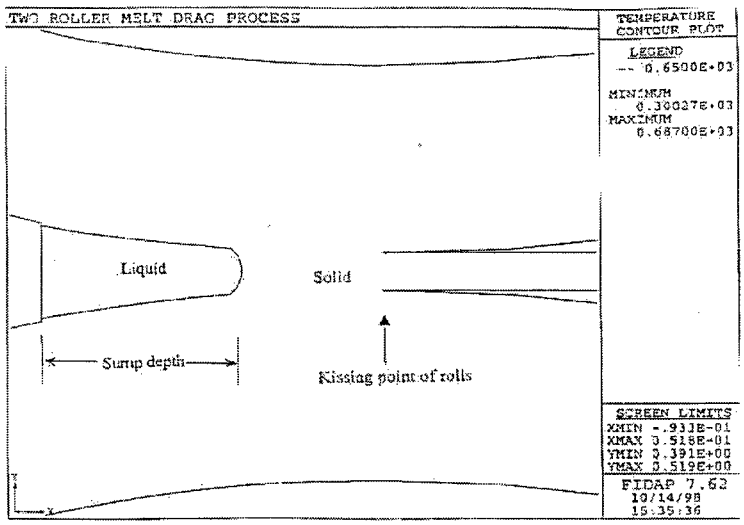


Fig. 8. Solid-liquid interface in the melt pool for a twin-roll aluminum thin strip caster.

Of these parameters, variation in casting speed has the largest influence on the process. Higher casting speed gives less time for solidification and hence allows greater motion of liquid between the dendritic arms. From Fig. 9, it can be seen that for casting speed of 5mm/sec, the sump depth is around 18 mm and

this becomes 35 mm for casting speed of 25 mm/sec. This effect of casting speed seriously limits the strip casting process to relatively short freezing range alloys and relatively low production rates.

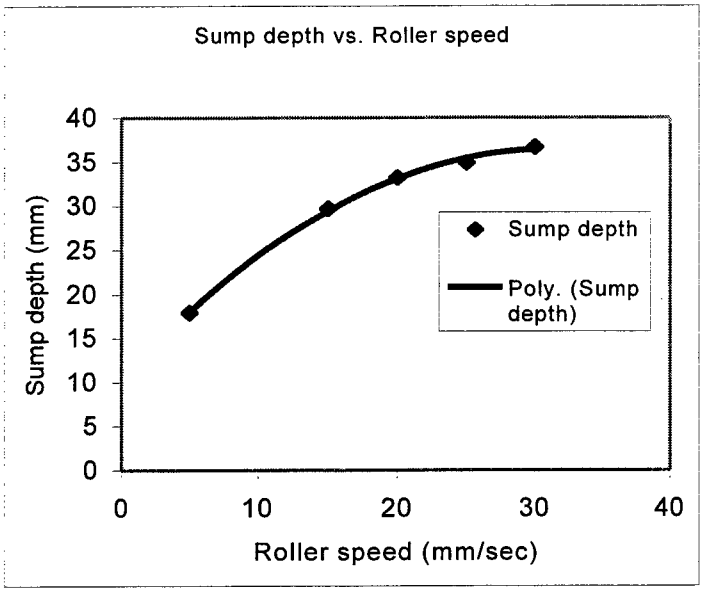


Fig. 9. Sump depth as a function of roller speed.

The gap heat transfer coefficient controls the removal of heat from the aluminum strip into the steel roll. Fig. 10, shows that below ~ 7000 kW/m^2 K, changes in the heat transfer coefficient due to non-uniformity of the roll surface for example, can significantly affect sump depth. This may be responsible for the periodic variation in the amount of centerline segregation, which is often seen in the cast strip.

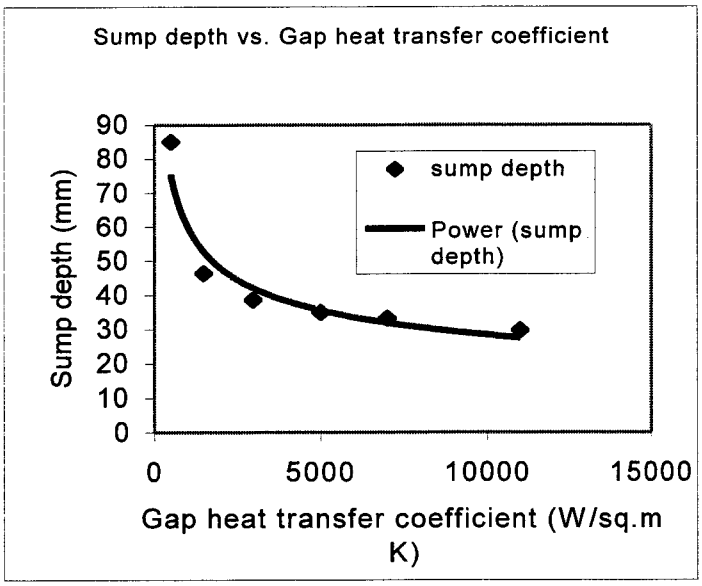


Fig. 10. Sump depth as a function of gap heat transfer coefficient.

Fig. 11 shows the increase in sump depth with increases in melt superheat. The sump depth increases with superheat because the required time for molten metal to solidify increases with the superheat in the metal. But this effect is not very significant, as the heat released from solidification is much higher than the heat due to superheat in the metal.

It is evident that a long solidification interval and hence, strong segregation can be expected for high casting speed, low heat transfer rate and high melt superheat. This is supported by experimental studies on centerline segregation in Al-Mg and Al-Fe alloys by Jin et al. [2]. They studied the appearance of centerline segregates in Al-4.0%Mg-1.0%Cu alloy during twin roll strip casting and observed centerline segregation increasing as solute content increased at a given speed and as casting speed increased for a given alloy.

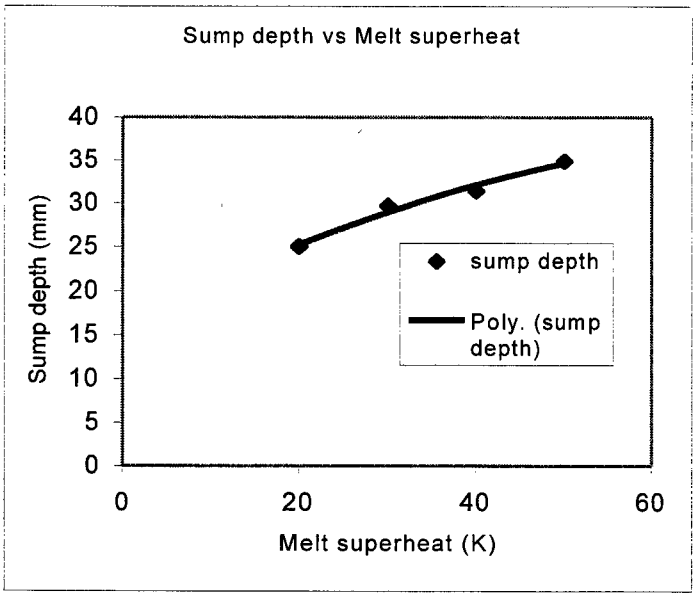


Fig. 11. Sump depth as a function of melt superheat.

During the course of thin strip casting, stresses develop in the solidified material primarily due to the thermal gradient which exist in the solid metal and the pressure exerted by the rolls. Fig. 12 shows the maximum principal stress across the cast strip, for different casting speeds, at the point where strip leaves the rolls. Surface of the strip experiences maximum stress due to the roll force and chilling action of rolls.

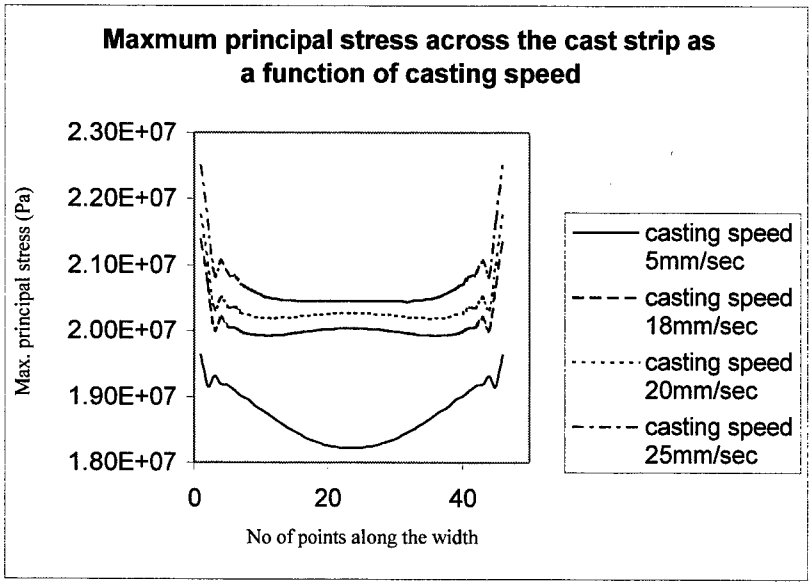


Fig. 12. Maximum principal stress across the strip for different casting conditions.

It can be seen that as the casting speed increases, magnitude of stresses in the solidified material also increases. This is due to the fact that at higher casting speeds, contact time of metal with rolls is less hence it gets less time for homogenization of temperature. Consequently, high temperature gradients exist in the material when the casting speed is high, resulting in higher stresses in the material.

SUMMARY

In this paper, an overview of the thin strip casting processes for steel and aluminum is presented. More detailed analysis of two casting processes, one for steel and one for aluminum is given. A two-dimensional mathematical model is presented to simulate the turbulent fluid flow, heat transfer and solidification in two roll melt drag process. Relationship between various operating parameters like roller speed, gap heat transfer coefficient and melt superheat and cast strip thickness was obtained from the model.

From the stress analysis of the two-roll melt drag process for thin strip casting of steels it can be concluded that the position of solid-liquid interface in the melt pool determines the magnitude of thermally induced stresses in the material. Hence, operating parameters such as casting speed, temperature or roll coolant, melt superheat and gap heat transfer coefficient should be strictly controlled to avoid situations where solidification gets over much before or much after the kissing point.

During thin strip casting of aluminum using horizontal type twin-roll caster, the extent of centerline segregation and thermally induced stresses increases with process parameters like casting speed and melt superheat and decreases for higher heat transfer rate across slab/roll interface. Hence a low casting speed would be desirable for smooth casting operation but that would reduce the productivity. High productivity can be achieved by increasing the casting speed and offsetting the effect of higher casting speed by insuring a higher rate of heat withdrawal from the melt pool through the rollers.

REFERENCES

1. Gupta, Shailesh, 1998. Mathematical modeling of thin strip casting processes, M.S. thesis, Department of Materials Science and Engineering, Ohio State University, Columbus, Ohio.
2. Jin, I., Morris, L.R., Hunt, J.D., 1982. Light Metals, TMS, p.873.
3. Bagshaw, M.J., Hunt, J.D., Jordan, R.M., 1988. Cast Metals, 1(1), p.16.
4 Gupta, Manish, 1999. M.S. thesis, Department of Materials Science and Engineering, Ohio State University, Columbus, Ohio.
5. Ramacciotti, A, 1988. Steel Research. 59(10), 438-448.

Intelligent Manufacturing I

Agent-based Control of Manufacturing Systems

L. Monostori, B. Kádár

Computer and Automation Research Institute, Hungarian Academy of Sciences
Kende u. 13-17, Budapest, POB 63, H-1518, Hungary

ABSTRACT

Management of complexity, changes and disturbances is one of the key issues in production today. Distributed, agent-based (holonic) structures represent viable alternatives to hierarchical systems provided with reactive / proactive capabilities. The paper outlines the difficulties which hinder their industrial acceptance. Several approaches to overcome these barriers are introduced, i.e. the use of simulation techniques for developing and testing agent-based control architectures, the holonification of existing resources and traditional (centralized / hierarchical) manufacturing systems. Finally, the cooperative use of agent-based distributed control structures and the more centralized (e.g. GA-based) schedulers is proposed aiming at systems which can handle critical complexity, reactivity, disturbance and optimality issues at the same time.

INTRODUCTION

Attempts were made to develop novel manufacturing architectures that can deal with the problems indicated in the abstract, i.e. growing complexity, changes, disturbances, uncertainties. The most known approaches are as follows: *fractal manufacturing* [1], *bionic manufacturing* [2, 3], *random manufacturing* [4], and *holonic manufacturing* [5].

Over the past years significant research efforts have been devoted to the development and use of *Distributed Artificial Intelligence* (*DAI*) techniques (e.g. [6]). An *agent* is a real or virtual entity able to act on itself and on the surrounding world, generally populated by other agents. Its behavior is based on its observations, knowledge and interactions with the world of other agents. An agent has several important features. It has capabilities of perception and a partial representation of the environment, can communicate with other agents, can reproduce child agents, and has own objectives and an autonomous behavior [7]. A *multi-agent system* (*MAS*) is an artificial system composed of a population of autonomous agents, which cooperate with each other to reach common goals, while simultaneously pursuing individual objectives [7].

Holonic manufacturing systems (HMSs), as one of the new paradigms in manufacturing, consist of autonomous, intelligent, flexible, distributed, cooperative agents or *holons* [5]. Three types of basic holons, namely *resource holons*, *product holons* and *order holons*, together with the main information flows between them are defined in [8]. These basic entities are structured by using object-oriented concepts such as *aggregation* and *specialization*. *Staff holons* are also foreseen to assist the basic holons in performing their work. *Reference architecture* for holonic manufacturing systems is given in [8]. Other authors refer only to two types of basic building blocks, e.g. order and machine agents in [9], job and resource agents in [10] order and machine (resource) holons in [11]. A common feature of these approaches is that the functions of the order and product holons are somehow integrated in one basic type. One of the most promising features of the holonic approach is that it represents a transition between fully hierarchical and heterarchical systems [5, 12].

The main questions concerning agent-based manufacturing architectures are as follows [11]:

- *Agents'structure:* internal structure of agents and the level of their self-containment.
- *Communication:* communication protocol, common interchange language.
- *Group formation:* negotiation, suitable communication protocol, persuasion of machines to participate in a group, reward / penalty systems, market mechanisms, agents'objective function.
- *Reconfigurability*: system openness (machine addition, deletion, substitution).

0-7803-5489-3/99/$10.00 ©1999 IEEE.

- *Scalability:* potential appropriateness for scaling up to the level of the extended enterprise [13].
- *Global versus local optima:* how to reach global optima with selfish agents pursuing their own goals; which is the optimal ratio of hierarchy and heterarchy in a given situation; how to tune the system; how to accomplish learning at system and agent levels?

Distributed, holonic-like systems represent viable alternatives to hierarchical and heterarchical structures and the corresponding reactive scheduling approaches [14]. The industrial acceptance of holonics, however, is relatively low among others things by reasons of

- the relative *crudeness* of the agent theory and its manufacturing applications,
- the *insufficient communication and decision making capabilities* of present numerical controls,
- the *high investment costs* of a production system working according to the agent principles,
- the seemingly insurmountable difficulties in their *stepwise integration* into existing production systems [15].

Several approaches are introduced and treated in the paper to overcome the above difficulties:

- the use of the *simulation technique* for the development of agent-based control architectures,
- the *holonification of existing resources*,
- the *holonification of traditional systems* by using the *virtual manufacturing* (*VM*) concept.

DEVELOPMENT OF AGENT-BASED ARCHITECTURES BY SIMULATION

Simulation is usually an efficient technique to make difficult problems more tractable, i.e. to illustrate the feasibility of related approaches. In respect to the scope of the paper, simulation technique can contribute to: answering at least the first part of the questions enumerated above, elaborating new algorithms, decreasing the risk in investments, developing the (virtual) information system of the HMS by using the virtual manufacturing (VM) concept introduced in [16].

The questions enumerated above can be answered by extensive simulation only. The object-oriented framework for the development and evaluation of distributed manufacturing architectures described in [11] provides a root model that represents a plant and can contain different agents. The object library incorporates two main agent types: *resource agent* and *order agent*. A plant in the model will contain only one order agent which is responsible for order processing, job announcements and job dispatching between different resources or groups (Figure 1). A model may incorporate several resource objects which can be initialized during construction (giving the name of the resource, process-capabilities of the resource, etc.).

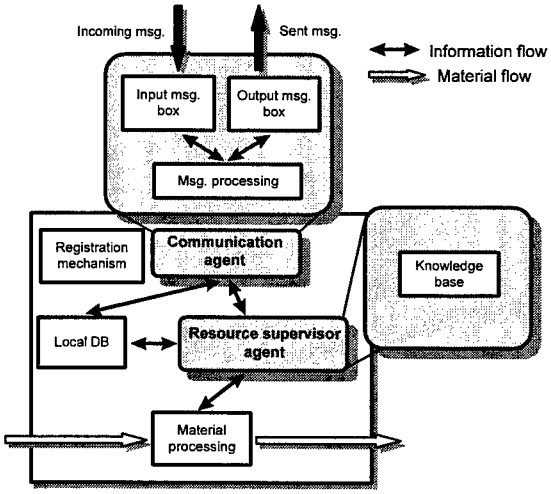


Fig. 1. Structure of a resource agent [11].

Agent objects contain different, functionally separated subagents. Each agent in the framework incorporates a communication subagent, through which it can send and receive messages, by using a modified version of

the contract net protocol [17]. Each resource agent involves a resource supervisor subagent which controls its actions. All agents contain a registration mechanism through which they register and unregister themselves. Each agent has local knowledge and databases. Information about machine capability, allocated time intervals for different jobs, groups in which the agent is interested, etc. are stored there. Any information concerning the agent itself can be accessed only through the communication subagent by a request message. Only one information provider, i.e. the registration book, is treated centrally in the system.

The framework is intensively used for research purposes. A new approach to agent-based scheduling developed and tested by the framework is described in [14].

HOLONIFICATION OF EXISTING RESOURCES

The above simulation framework is appropriate to support the realization of holonic manufacturing systems in green field, i.e. from resources (e.g. CNC controlled machines) which are able to function in a holonic way. Unfortunately, still on good grounds, firms are interested in using - at least partly - their existing resources or resources available on the market. There are some severe barriers, however, which raise difficulties in this respect:

- no computer numerical controls (CNCs) which satisfy the requirements of functioning in a holonic way are on the market,
- the available CNCs provide communication facilities on different levels and their autonomy is rather limited, the heterogeneity of the system makes the realization of the communication-intensive holonic approach more difficult.

In this section an approach to the holonification of existing resources (i.e. converting existing resources into holons) is suggested, based on the solutions frequently used in *agent-based software engineering*.

Agent-based software engineering was invented to facilitate software that is inter-operable. The questions raised by software engineers are similar to those of holonification of existing manufacturing resources: what about programs that have already been written, the so-called *legacy software*?

Techniques applicable for converting a legacy software into software agents [18] can also be used for holonification as follows:

- Implementation of *transducers* which mediate between an existing program and other agents. This is especially useful for situation in which the code for the program is unavailable or too delicate to modify. *Transducers* can be implemented by the developers of HMSs or even by independent organizations, supposing that the CNC in question provides two-directional communication facilities.
- *Wrapping*, i.e. injecting code into the program to allow it to communicate in ACL. This effective solution, however, requires that the code for the program should be available. *Wrapping* is a feasible solution not only for CNC manufacturers but also for users having CNCs with appropriate openness.
- *Rewrite* the whole program which is only applicable in the case of whole possession of the original program. *Rewrite* can be applied only by CNC manufacturers as the only owners of the source code, but usually only in the case when the experts, e.g. the former programmers are available.

It is important to note that manufacturing agents (holons) can include not only information processing, but also material processing activities.

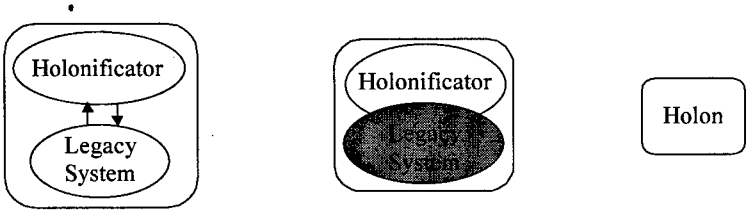


Fig. 2. Approaches to holonification of existing resources

Holonification of existing resources requires a *holonificator* (Figure 2) which realizes all the functions needed by the resource to be able to act as a holon (communication, autonomy). Depending on the realization of the coupling between the legacy system (resource) and the holonificator, *loosely* and *tightly coupled holonification approaches* can be distinguished bearing a resemblance to the *transducer* and *wrapper* concepts of software agentification.

Holonification of existing resources is an effective technology for the *stepwise realization of HMSs*, i.e. in cases when the systems' resources - fully or partly - are of traditional ones, i.e. without the autonomy and cooperation facilities required by the holonic concept. Figure 3 illustrates a heterogeneous system where 'real' and holonificated resource holons form a HMS. (The holonificated resource holons can be substituted by "real" holonic ones in a stepwise manner.)

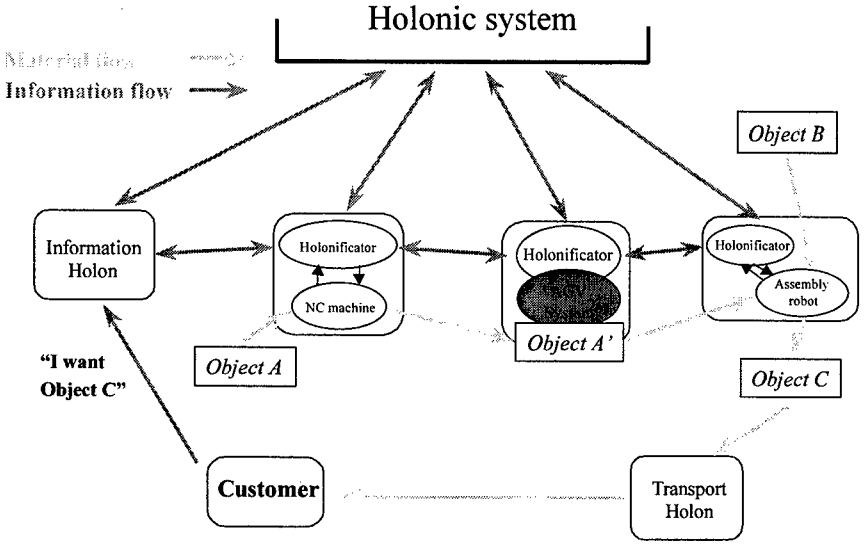


Fig. 3. Heterogeneous HMS consisting of 'real' resource holons and resources holonificated by different approaches

However, holonification of existing resources and development of the whole information system, constitute a large assignment, and, taking the open questions of holonics into account, seems to be a bit premature.

HOLONIFICATION OF TRADITIONAL SYSTEMS BY USING THE VM-CONCEPT

In this Section a novel approach to holonisation of whole manufacturing systems is introduced based on an extension of the *Virtual Manufacturing* (*VM*) concept. *Virtual manufacturing* is a relatively new concept of executing manufacturing processes in computers as well as in the real world [16]. Manufacturing sub-systems can be classified into four categories: Real Physical System (RPS), Real Informational System (RIS), Virtual Physical System (VPS), Virtual Informational System (VIS). VM enables to simulate manufacturing processes previously, without using real facilities, and by this way to accelerate the design and re-design of real manufacturing systems [19].

A fundamental feature of the VM concept is that it realizes a one-to-one mapping between the real and virtual systems, i.e. VIS and VPS try to simulate RIS and RPS, respectively, as exactly as possible. In this section an extension of VM concept is suggested and illustrated. The main novelty of the approach is the break with the above one-to-one mapping, more exactly the use of the VM concept to control a traditional (centralized / hierarchical) manufacturing system in a holonic way.

Suppose there is a central control unit in the traditional system, the fundamental requirements for holonisation of this system by the above approach are as follows. The ability to communicate with the

outside world, the transfer of control information to the resources, the capture of state information and the transfer of these to the central unit, the interruption of the functioning of resources at given periods, the stopping or modifying of processes started previously.

The virtual part of the system (Figure 4) runs in a holonic way and incorporates order management, scheduling and control issues. To realize the virtual part, approaches such as the framework for developing and testing agent-based manufacturing architectures described earlier in this paper can be advantageously used. Resource agents which, from technological point of view, correspond to the real resources of the traditional system can be easily constructed by using the object library of the framework [11]. Order management proceeds fully in the virtual system.

Decisions are taken in the virtual, holonic system and conveyed to the VIS of the traditional system. The real production situation is sensed by the RPS and forwarded to the VIS, which initiates appropriate measures in a holonic way. In summary, the traditional system shows holonic behavior. Naturally, requirements like those enumerated here are important prerequisites for the approach. The holonic information system (VIS) tested in a virtual environment has the potential of to be used in a real holonic system.

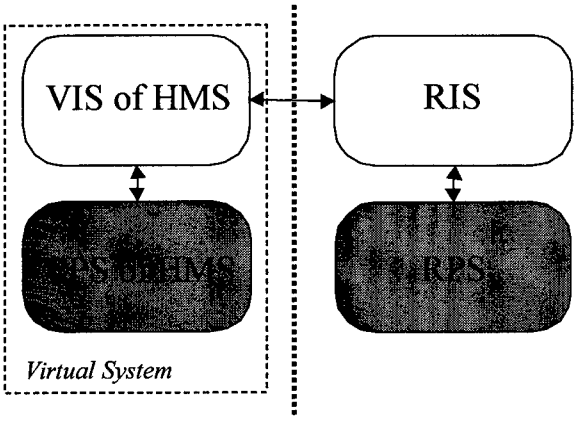


Fig. 4. Concept for holonification of traditional manufacturing systems by using the VM technology

CONCLUSIONS AND FUTURE ISSUES

Distributed, holonic-like systems represent viable alternatives to hierarchical and heterarchical structures and the corresponding reactive scheduling approaches.

Both of these - apparently distinct - lines can be advantageously used in rapidly changing production environments, however none of them can be regarded as a universal tool. Even the application of such powerful global optimization techniques as GAs [20, 21] are not appropriate for very large problems, and as centralized approaches, are not totally devoid of all the known drawbacks of centralized / hierarchical control systems. The multi-agent approach also becomes unrealistic beyond a given problem size, first of all due to the rapidly increasing communication burden. Consequently, both directions crave for some kind of *aggregation* [8]. There is a scope for *temporal or permanent hierarchies* also in holonic architectures [12].

A fundamental issue in distributed systems is how to ensure global performance with selfish agents pursuing their own goals [22]. The integration of scheduling agents as a kind of *staff holons* [8] into the architecture, can contribute to achieving global coherence in distributed systems. This enhancement of the basic, heterarchically dominant structure can be accomplished in several ways:

- There is one *central scheduling agent* in the system, which in normal, static conditions can ensure global performance if other agents follow its command or accept its advice. In changing conditions, however, through increased autonomy of agents, a more dynamic behavior can be reached.

- The opportunity to incorporate a *scheduling agent into any aggregated holon*, i.e., to introduce some hierarchy in temporal or static coalitions, is expected to result in systems with a more balanced operation and to resolve the questionable scalability of the approaches investigated in the paper. In this way, the amount of necessary communication can be decreased, and the holonic concept can be expanded to the level of *extended* or *virtual enterprises*.

The object-oriented simulation framework described in the paper, is expected to provide the necessary framework for further research addressing such fundamental issues of distributed manufacturing as agent structures, communication protocols, group formation, negotiation, global versus local optima, scalability, system tuning, agents'behavior, learning at system and agent level [23].

ACKNOWLEDGEMENT

This work was partially supported by the *National Research Foundation, Hungary,* Grant Nos. T026486 and F023628. A part of the work was covered by the *National Committee for Technological Development, Hungary* Grants (EU-96-B4-025 and EU-97-A3-099) promoting Hungarian research activity related to the *ESPRIT LTR Working Groups* (IiMB 21108 and IMS 21995).

REFERENCES

1. H.J. Warnecke, 1993. The Fractal Company, a revolution in corporate culture, Springer-Verlag.
2. N. Okino, 1993. Bionic manufacturing systems. in CIRP, Flexible Manufacturing Systems Past-Present-Future, Peklenik, J. (ed), 73-95.
3. K. Ueda, 1993. A genetic approach toward future manufacturing systems. In CIRP, Flexible Manufacturing Systems Past-Present-Future, Peklenik, J. (ed), 211-228.
4. K. Iwata, M. Onosato, M. Koike, 1994. Random manufacturing system: a new concept of manufacturing systems for production to order. CIRP Annals, 43(1), 379-383.
5. P. Valckenaers, F. Bonneville, H. Van Brussel, L. Bongaerts, J. Wyns, 1994. Results of the holonic system benchmark at KULeuven, Proc. of the Fourth Int. Conf. on Computer Integrated Manufacturing and Automation Technology, Oct. 10-12, Troy, New York, 128-133.
6. A.H. Bond, L. Gasser, (Eds.), 1988. Readings in DAI, Morgan-Kaufmann.
7. K. Koussis, H. Pierreval, N. Mebarki, 1997. Using multi-agent architecture in FMS for dynamic scheduling, Journal of Intelligent Manufacturing, 16(8), 41-47.
8. H. Van Brussel, J. Wyns, P. Valckenaers, L. Bongaerts, P. Peeters, 1998. Reference architecture for holonic manufacturing systems, Computers in Industry, Special Issue on IMS, 37(3), 255-276.
9. H.-P. Wiendahl, V. Ahrens, 1997. Agent-based control of self-organized production systems, CIRP Annals, 46(1) 365-368.
10. M.M. Tseng, M. Lei,C. Su, 1997. A collaborative control system for mass customization manufacturing, CIRP Annals, 46(1), 373-376.
11. B. Kádár, L. Monostori,. E. Szelke, 1997. An object oriented framework for developing distributed manufacturing architectures, Proc. of the Second World Congress on Intelligent Manufacturing Processes and Systems, Budapest, Hungary, 548-554., and in J. Intel. Manu., 9(2), 1998, 173-179.
12. L. Bongaerts, L. Monostori, D. McFarlane, B. Kádár, 1998. Hierarchy in distributed shop floor control Proc. of 1st Inter. Workshop on Intel. Manu. Sys., IMS Europe 1988, Lausanne, Switzerland, 97 - 113.
13. H. Van Brussel, P. Valckenaers, J. Wyns, L. Bongaerts, J. Detand, 1996. Holonic manufacturing systems and IiM. in: IT and Manufacturing Partnerships, Conf. on Integration in Manu., Galway, Ireland, 185-196.
14. L. Monostori, B. Kádár, J. Hornyák, 1998. Approaches to manage changes and uncertainties in manufacturing, CIRP Annals, 47(1), 365-368.
15. B. Kádár, L. Monostori, 1998. Agent based control of novel and traditional production systems, Proc. ICME98, CIRP Inter. Sem. on Intel. Comp. in Manu. Eng., Capri, Italy, 31 - 38. (key-note paper)
16. M. Onosato, K. Iwata, 1993. Development of a virtual manufacturing system by integrating product models and factory models, CIRP Annals, 42(1), 475-478.
17. R.G. Smith,. 1980. The Contract Net Protocol: High-level communication and control in a distributed problem solver, IEEE Trans. on Computers, Vol. C-29, 12, Dec., 1104-1113.
18. M.R. Genesereth, S.P. Ketchpel, 1994. Software agents, Communications of the ACM, 37(7), 48-53.

19. K. Iwata, M. Onosato, M.K. Teramoto, S. Osaki, 1995. A modeling and simulation architecture for virtual manufacturing systems, CIRP Annals, 44(1), 399-402.
20. H.P. Wiendahl, R. Garlihcs, 1994. Decentral production scheduling of assembly systems with genetic algorithm, CIRP Annals, 43(1), 389-395.
21. J. Hornyák, L. Monostori, 1998. Genetic algorithms for predictive and reactive scheduling of manufacturing systems, Proc. ICME98, CIRP Int. Sem. on Intel. Comp. in Manu. Eng., Capri, Italy, 213-220.
22. J. Hatvany, 1985. Intelligence and cooperation in heterarchic manufacturing systems, Robotics & CIM, 2(2), 101-104.
23. L. Monostori, A. Márkus, H. Van Brussel, E. Westkämper, 1996. Machine learning approaches to manufacturing, CIRP Annals, 45(2), 675-712.

Intelligent Database Support for Manufacturing and Processing of Industrial Materials

S.A. Ehikioya, E.G. Truelove, and T.T. Tran

Department of Mathematics and Computer Science,
Brandon University,
Brandon, MB, Canada, R7A 6A9

ABSTRACT

This paper describes the framework and characteristics of an Intelligent Database System that supports and satisfies business needs and requirements of industrial materials manufacturing and processing. We also examine the methods to design and build such systems and discuss the issues and technologies that require attention. We focus on intelligent database systems support for a reasoned choice among alternatives, and the manner in which their capabilities can be extended to create an effective decision support tool.

INTRODUCTION

Businesses collect and use data regularly, to help make important decisions. Almost all decisions rely on data in some way and the quality of data affects the quality of decisions, sometimes drastically [1]. Today businesses are in a global competition where success does not only depend on a long-term strategy, but also on how well a business supports decision-making that is unpredictable in advance. With development of the computer, data storage and processing have become much more efficient. An organisation's decision-makers must decide how to use and interpret data. With a large volume of data to be interpreted, it can be difficult to extract the specific data needed for each decision. As technology advanced, Management Information Systems emerged to provide periodic reports containing static, descriptive knowledge. Since these reports were only produced periodically, they had limited use to support dynamic business decisions. This has necessitated Decision Support Systems (DSS) to help management with critical decision-making. A DSS is a "computer-based information system that provides the user with decision-oriented information whenever decision-making situations arise" [2]. In other words, a DSS uses computer technologies to process and refine data, and present the correct information to the decision-maker to assist in solving unstructured problems. A DSS aids the decision-maker to make informed decisions by allowing for better decisions, increasing the efficiency, productivity, and effectiveness of decisions, helping manage stored data, and supplementing the decision-maker's abilities. A DSS broadens the scope of decisions, particularly semi-structured and unstructured decisions, and so, increases business productivity.

The shift in focus from transaction processing to knowledge processing in work done by business managers requires an intelligent DSS to process knowledge for sophisticated managerial decision-making. The human decision-maker still makes the decisions, so these systems are really support-systems. DSS designers must understand human decision-making and the domain of the application. Decision-making is knowledge intensive. An intelligent DSS can combine and synthesize solutions of sub-problems into the solution of a larger problem thereby enhancing the process. Since a DSS does not typically make decisions, a successful DSS must provide sufficient, accurate information in a useful, efficient way. To achieve this, the DSS must be built on a robust data delivery architecture that addresses all end-user requirements.

Businesses and organizations now recognize the value of DSS, substantially increasing demand for efficient, fully functional, well-designed DSSs. Many systems lack an Intelligent Database System (IDBS) architecture that integrates the data warehouse, metadata, and a graphical user interface to give advanced DSS features. Without an architectural blueprint, it is not possible to define and develop fundamental DSS components, which combine to provide a full suite of DSS capabilities such as multi-dimensional data viewing, data mining, fast query processing, and elegant reporting. Data mining is "the extraction of hidden predictive information from large databases" [3]. Data mining extracts information quickly and efficiently and uses existing information to model unknown situations. See [3] for an array of data mining techniques.

0-7803-5489-3/99/$10.00 ©1999 IEEE.

In this paper, we focus our attention on development issues of an IDBS using Relational On-line Analytical Processing (Relational OLAP) technology. We also discuss how such a system ensures success of its DSS counterpart. In particular, we detail the end-user requirements, the main features that an IDBS must offer to address these requirements, the design issues, as well as techniques and tools used to obtain these features. The described architecture consists of components, each with a distinct purpose in the delivery of data. This architecture: (i) provides seamless access to existing, normalized data models and a variety of performance-optimized data models including data warehouses, and (ii) enables an organisation to use information as a strategic asset by applying their databases to support decision-making. We utilize workflow design methodology and fuzzy logic/set theory to formalize the correctness of our underlying IDBS for the DSS.

Relational OLAP, a flexible and general architecture that meets a wide variety of DSS and OLAP needs. allows multidimensional analysis of relational data. It is our preferred architecture. See [4] for details of our choice over multidimensional OLAP architectures. This framework directly provides the functionality to support an intelligent DSS. Decisions in manufacturing and processing of industrial materials are akin to those in most manufacturing companies. They can be very complex and can include scheduling of plants, downsizing operations, maintaining market share, supplier information, inventory analyses, sales analyses, and customer relations. The framework is applicable across many organisational settings.

CHARACTERISTICS AND FRAMEWORK

The characteristics and framework of a DSS as well as the nature of decisions must be understood before beginning system design. Decision problems can be very complex since the business world is dynamic. So quite often, there are situations for which the information needed is not ideal, i.e., they may be either *semi-structured*, or *unstructured*. In a *semi-structured* situation, there are some unknowns, or some areas where knowledge is incomplete or unavailable. The task may not be completely understood. In an *unstructured* situation, there is little relevant knowledge available, no experience with the task, and many unknown, un-reproducible cases leading to a highly uncertain environment. Problem-structuring is important to the overall system performance. The issues and implications of the problem must be identified, in the belief that better understanding will lead to better support from a computerized system. An intelligent DSS must support many cases of unstructured decisions. The DSS must provide alternatives, or when given a set of alternatives, be able to decide upon the best possible decision in a timely and efficient manner.

Features common to most DSSs are: (a) a large knowledge base which is both historical and immediate in nature; (b) the ability to respond to many different questions, e.g., what-if scenarios and queries; (c) the ability to interact with users and provide flexible decision-making choices; (d) the ability to acquire new information, which may be descriptive in nature, and (e) the ability to maintain data and other kinds of knowledge. In addition, other key features include: (a) a multidimensional conceptual view of data; (b) an ability to create complex criteria sets that establish both pattern and dimensions in the data, (c) support for hierarchical consolidation of data, and the ability to drill down into detail to mine relevant sub-facts; (d) support for rapid responses and elegant reporting systems; (e) seamless integration of the system with other desktop productivity tools; (f) support for interpretation of query results and facilities to automate transaction initiations, e.g., change product prices; and (g) automation of common tasks, e.g., requests for detailed information about a decision-support inquiry. The DSS allows managers to make strategic and tactical decisions using corporate data. The system allows complex analysis of large input data sets from different perspectives. Managers can manipulate and analyse data intuitively, quickly, and flexibly.

To fulfill the above user requirements, the underlying IDBS must provide the following key features:

- A Criteria Builder Manager to allow a user to specify, save, and reuse filters to retrieve data from the data warehouse. This item enables a user to specify constraints, data source domains, specific needs in relation to the current decision, and various confidence measures and similarity functions used to assess the recommendations. The degree of inclusion is also specified here by constructing a set of values and conditions to create dynamic SQL statements used to retrieve relevant data. This item provides configurable functionality, i.e., the ability to customize data sources [5].
- The Presentation View Manager that offers facilities to customize the output templates, by specifying the format e.g., tabular, graphical, in which to present query results.

- The Data Rotation Manager that allows the specification of how query results are presented on x-y axes. This provides an advanced transform module to create integrated views of important information.
- The Intelligent Agent Manager that enables the creation of customized data analyses, the mining of data using predefined criteria sets and data extraction techniques, the differentiation of retrieved data into various degrees of relevance, and the reporting of the data to the user.
- The Knowledge System is the data that a business has stored, quite often in the form of large databases (both operational data and data warehouses) on stable storage media such as a hard disk. Relevant operational data is extracted from the operational database, cleansed and summarized. The resulting data is formatted for decision-support before uploading it into the data warehouse.
- The Problem-Processing System, the engine of the DSS, processes information and recognizes and solves problems. It consists of modules for data mining, OLAP, and fast, dynamic query processing. Data mining provides trends, influence factors and relationships in data, e.g., what impacts sale of rod in Toronto. OLAP provides multidimensional processing of data, e.g., sales performance for rod by state by month and by brand. Query processing allows a user to ask questions. The Problem-Processing System can use the contents of the Knowledge System to acquire information to solve problems. The system uses fast-query processing to access data. The activity is RAM-based to enhance performance.
- The Metadata System that provides logical linkage between data and applications; identifies the contents and location of data and includes definitions from a decision-support perspective. Since Metadata provides decision-oriented pointers to enterprise [warehouse] data, it acts as a bridge between enterprise data and the decision-support application.. When combined with the DSS engine, this module enables pinpoint access to information across the entire data warehouse.

The data cleansing activity of the underlying intelligent database, which is the process of ensuring all values in a data set are consistent and correctly recorded, should be robust and efficient. That clearly addresses the Metadata preparation and storage needs, thereby creating a clear, clean integrated view of the data distributed effectively for decision-making. This increases/improves the accuracy of data and provides the most cost-effective way to retrieve data. During analysis, the retrieved metadata are fuzzified to provide additional information about the strength of various attributes to resolve any expressive deficiencies of the original Metadata sets. We associate a fuzzy measure with each attribute to provide measurement of its relevance to the decision. This is similar to assigning a probability value ranging from 0 to 1. Fuzziness allows greater flexibility in classifying decision variables.

To be intelligent, a database system must efficiently process user queries, and allow a wide variety of options for querying. The ability to extract the most relevant attributes to discriminate among decisions is key to a successful IDBS to improve decision support. Various techniques are used to optimize the retrieval of relevant data. These techniques will be discussed in a later section. Figure 1 illustrates the architecture of our IDBS. The criteria builder, presentation view, and data rotation managers are the underlying layers of the user interface which consists of the language and report systems.

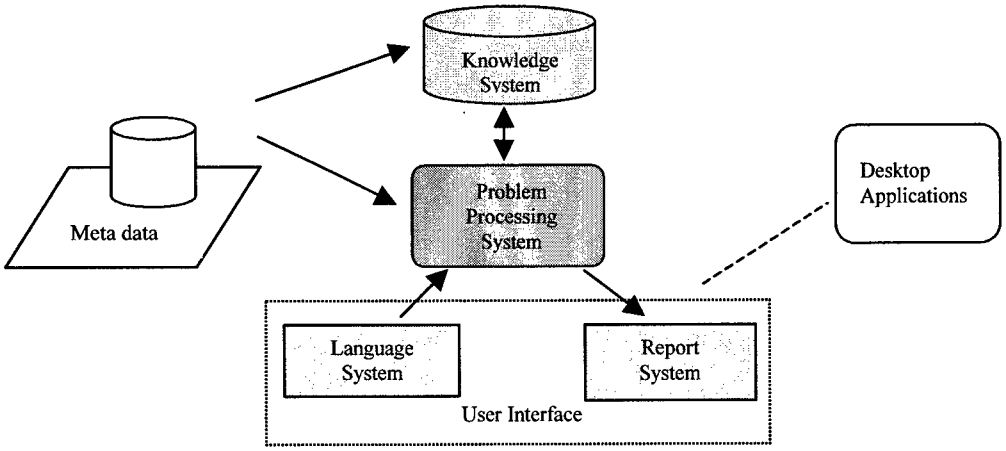


Fig. 1. The Generic IDBS Framework

Many techniques can be used to support DSS: mathematical modeling, such as, discriminant analysis, rough and fuzzy sets analysis, and artificial neural networks [6]. These techniques enhance a DSS's capabilities, so it can apply a greater degree of intelligence to support a manager's decisions. The methodologies and tools needed to build a DSS are discussed in the following section. Note that intelligent database support for quality control is essential in all database applications, to ensure the integrity of the data on which critical decisions are based.

METHODOLOGIES

Design of a DSS can be done in several ways; some are formal approaches that apply a specific methodology while other are informal approaches that do not require strict adherence to specific steps. We highly recommend the formal approaches because of the benefits (see [7] for details) associated with their use. A system development life cycle (SDLC) [2] is a common formal approach, which comes in many flavours, but usually incorporates the steps shown in Figure 2.

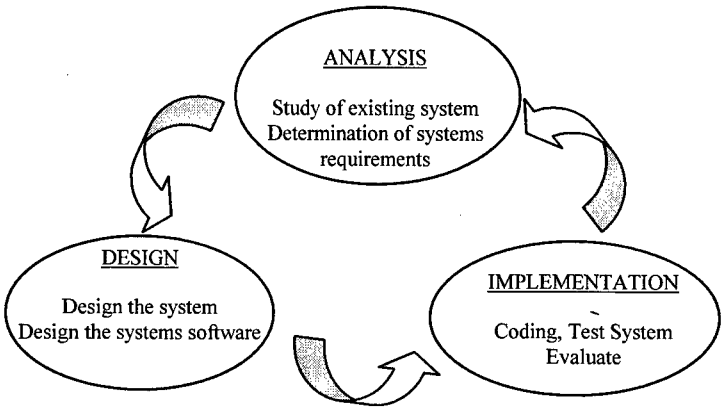


Fig. 2. The Systems Development Life Cycle

Various methodologies follow the above approach but only "structured analysis" will be discussed along with its applicability to design of a DSS. Structured analysis is primarily based on the representation of systems-essential processes with a variety of models, including data models, logical data flow diagrams, and physical data flow diagrams. One of the first steps in any analysis is to determine the system requirements. For a DSS, this involves several things.

- *What are the kinds of data for which the knowledge system will be responsible?* It is not necessary to plan the database itself at this point, but a general idea, of the data to be stored, is an asset. Data models can be drawn to show the types of data and the relationships between them.
- *Who will be using the DSS?* It is very important to have end-user participation to successfully model the language and presentation systems so that the DSS is easy to understand andaccessible. Interface models can be drawn to represent communication with the user.
- *What type of decisions will the system be required to support?* When analyzing the problem-processing system, relevant problem recognition and solving means, the knowledge used in decision-making, the organization context in which the system will be used, and the behavior and inclination of the decision-makers should be taken into consideration. [8]
- *What processes are required and how do they relate to each other?* This is where the data flow diagrams are designed. The processes needed for the functioning of the DSS must be identified and a logical data-flow diagram can be drawn so show what the system should do.

To design the language system and report system, it is necessary to model the user interface. The problem-processing system uses data-flow diagrams with process control and workflow diagrams. Design of the knowledge system includes modeling of the database structure itself, and deciding on the best format to store the data. Implementation involves putting the knowledge system on some type of storage medium, and organizing the other pieces of the DSS to create an operational system. Extensive tests must be performed on the new system to ensure that it runs to satisfaction.

The formal approach prescribed by structured analysis ensures that all proper steps are followed so that all requirements are discovered and modeled correctly. A structured analysis also gives the end-users of the system a great deal of input into how the system will behave.

TOOLS

Information System developers use a variety of tools to create DSSs, including 3rd and 4th generation language application development tools. Although these tools provide valuable development functionality, they are often used outside the context of an integrated, decision-support architecture. This leads to development of unreliable and brittle applications that cannot guarantee the desired functionality. The choice of tool has great impact on the final system. These tools can aid in identifying analysis requirements or producing design specifications [8]. There are many types of tools which can be used in many different combinations. Different tools can be used for certain aspects, interface design, graphics design, etc. It is possible to delay the decision on which tool to use until after initial design so that design is not constrained by using a particular tool. However, the system may be difficult to implement.

A tool such as System Architect ™ can aid greatly in the analysis phase of structured analysis because it provides the ability to create the necessary models. Models can still be "hand drawn" but CASE-based programs like System Architect allow greater flexibility and their ease of use make them a good choice. Microsoft ® Project is a good tool for building Gantt and PERT charts that help plan and monitor the progression of the phases of the system development. Various database tools, such as Oracle, Microsoft ® ACCESS, SQL Server, and PowerBuilder, can facilitate building the knowledge system in the form of a relational database. The relational database model is an excellent choice for storing data because of its fast data access, support for multiple-user views, and its built-in querying language.

The user interface may be the most important aspect as it is the user's point of contact with the DSS. Some issues in designing the user interface include whether to use a natural, non-procedural language to make the interface as user-friendly as possible; and how to present the results of a query. Microsoft ® ACCESS, Visual Basic, Delphi, and Visual C++, Oracle Forms, all allow design of forms that can be tied to database tables. These forms display information in an understandable format. Other options are a menu-based interface where a user selects commands, or a question and answer-based interface where a user asks one question at a time. A rising technology is voice recognition software. There are other classes of tools that include specialized data mining, OLAP, AI, and web-based DSS tools. See [3] for a comprehensive listing.

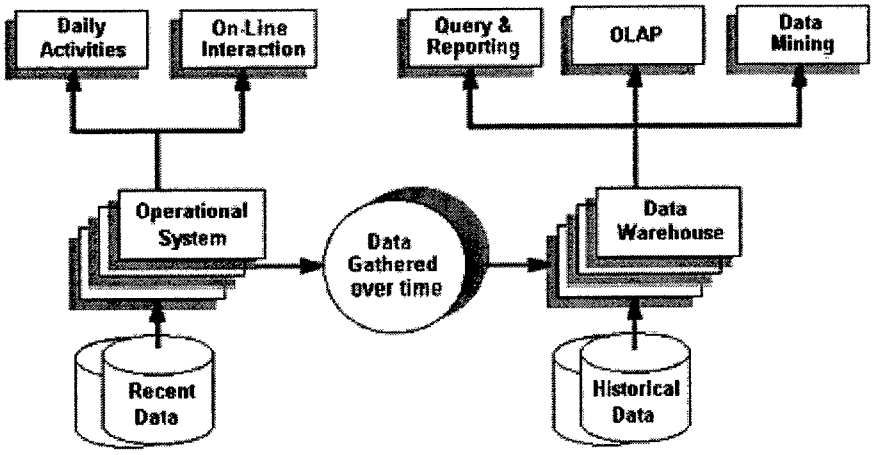


Fig. 3. Data Mining in the DSS Context [9]

Figure 3 shows the relationship between data mining and other techniques as applied to the historical data warehouse. Data mining helps a DSS to be more intelligent as it can recognize patterns of data that managers never thought to look for. This data can help predict what might happen in the future, allowing for more informed decisions.

OLAP "enables better decision-making by giving business-users quick, unlimited views of multiple relationships in large quantities of summarized data." [10]. OLAP helps DSSs to be more intelligent since a greater depth of query is allowed. The results of these queries can be used to forecast trends in business and can support management decisions.

SOME DESIGN ISSUES

Some design issues deserve attention. Creation of a robust data delivery architecture that seamlessly supports DSS is difficult due to problems associated with metadata definitions. In an IDBS, metadata must map a users' familiar entities, e.g., dimensions and attributes to tables and columns within the database. So, design specification must include: (a) dimension, attribute and metric definitions; (b) attribute hierarchies that indicate parent-child relationships; (c) metric–attribute mapping, including physical mapping.

The user interface is an important component of the IDBS. Since the Criteria Builder allows a user to specify subsets of data retrieved from the data warehouse by constructing condition clauses of dynamic SQL SELECT statements. It provides facilities that guarantee reliability and correctness. The interface should be friendly to use and able to create complex component sets while abstracting away the mathematics underlying SQL statements. The DSS engine should provide multiple analyses from a single data set by varying presentation and rotation options.

Although we adopt the framework discussed in this paper to build an IDBS prototype with advanced features for improved DSS, some problems still persist. Data uncertaintity is a prevalent occurrence in most organisations. We cannot vouch in some cases about the quality of the data upon which decisions are based. So we need a robust data-quality module to improve the data before they are used in the system. The best idea is to incorporate quality criteria in the acceptance of operational data into the databases.

CONCLUSION

There have been great strides made in the area of DSS. The use of data mining, OLAP, AI, and web-based tools and techniques have increased the degree of intelligence in supporting the complex decisions of management. Despite all the advances, one thing is certain: there is no way to predict the future, but a well-designed DSS can help management make decisions for the growth and improvement of the company. While some problems persist, the IDBS discussed here can play an important role in satisfying business requirements of various industries, e.g., materials manufacturing and processing. Our design is practical and scalable, and applicable to environments that require semi-structured or unstructured decisions.

REFERENCES

1. Parsaye K. and Chignell M.H., 1994. *Quality Unbound*, Database Programming and Design, November. (also at: http://www.datamining.com/datamine/quality.htm)
2. Whitten, J.L. Bentley, L.D., 1998. *Systems Analysis and Design Methods* ." 4th ed., McGraw-Hill,
3. Pilot Software, 1998. *Introduction to Data Mining: Discover Hidden Value in Your Data Warehouse*, Pilot Software, Inc., Cambridge, MA., (also at: http://www.pilotsw.com/dmpaper/dmindex.htm)
4. MicroStrategy Inc., 1995. *The Case for Relational OLAP*, Data Warehouse DSSs, MicroStrategy Inc. (also at: http://www.strategy.com/DW_Forum/WhitePapers/Case4Rolap)
5. Ehikioya S.A, 1999. "A Formal Model for the Reuse of Software Specifications". *1999 IEEE Canadian Conf. on Electrical and Computer Engineering*, Edmonton, Alberta, Canada, May 9-12.
6. Michalowski, D. "Intelligent Decision Support: Knowledge Discovery and Applications". (see: http://www.iiasa.ac.at/research/DAS/res98/node10.html)
7. Ehikioya S.A., 1997. *Specification of Transaction Systems Protocols.* Ph.D Thesis, Dept. of Computer Science, University of Manitoba, Winnipeg, Manitoba, Canada.
8. Holsapple C.W., Whinston A.B., 1996. *Decision Support Systems: A Knowledge-Based Approach*, West Publishing Company.
9. Information Discovery Inc., 1997. Perspective on Data Mining: Reaping Benefits from Your Data, A White Paper, Information Discovery Inc., (also at http://www.datamining.com/datamine/dm-ka.htm)
10. Business Intelligence / OLAP, *SAS*, (also at: http://www.sas.com/software/olap)

Intelligent Production Management in Mining Systems

Sean Dessureault, Malcolm Scoble, Scott Dunbar

Department of Mining and Mineral Process Engineering,
University of British Columbia,
Vancouver, British Columbia, Canada

ABSTRACT

This paper attempts to characterize the mining process and the principles of mine production management. It considers the integration of decision support and information technologies into new intelligent systems for mine production management. A case study is examined which considers the production planning and control procedures at an open pit copper mine. This is used to demonstrate an approach to short term planning based on optimizing profit, using spreadsheet software and linear programming. This work shows that with little cost and time, a spreadsheet tool can be developed in-house for more scientific and cost effective mine production management. Such tools enable more constraints to be considered and management performance to be evaluated.

INTRODUCTION

Decision support tools have evolved in scope, efficacy and availability faster than the mining industry's ability to absorb them. Empirical criteria, past procedure and intuition still represent the foundations for mine production planning and control. Although most mines have access to linear programming and simulation software, few use such tools to improve production management. This paper will demonstrate, through a case study, how software can be used to support the formulation of mining plans and production control in a more effective and intelligent way. The case study is based on a large open-pit copper mine in British Columbia, operating trucks and shovels as its primary materials handling system. A ten-year-old truck management (dispatch) system is used to optimize the productivity of the trucks. The dispatch system is linked via radio to the trucks whose position is determined using passive transponders at key locations along the haul routes. The mine is looking to implement global positioning systems for its mobile equipment within the mine.

MINING SYSTEMS

Surface mines are typically very large in scale and low in grade. They represent a complex materials handling system which is challenging in terms of production management. The first component process in the system consists of drilling and blasting in order to fragment the ore and waste for subsequent handling. Then the primary loading equipment, either cable or hydraulic shovels, load the material onto hauling equipment, which are usually very large haul trucks. The second process is usually based on stationary equipment such as in-pit crushers and conveyor belts, aiming to deliver the material to the mineral processing plant (mill). The high capital and operating costs of any fleet of mobile equipment make its proper management a critical component in mining. The frequent scheduling of excavation from different locations, due to the variable nature of a mine's geology, results in a very dynamic production planning. When drills, shovels and trucks move to different locations often on a daily basis, then planning in terms of truck allocations and shovel positions becomes challenging. The daily plan must account for the required mine outputs, such as ore quality (grade), as well as ore and waste rock tonnages in order to maintain the required progress in excavation and feed to the mill. Quality control over the mill feed would generally be achieved according to grade, hardness and size distribution.

ISSUES IN MINE PRODUCTION CONTROL

Fleet management is one of the most important issues in large open pit mines using a truck and shovel network. Planners must ensure that the trucks are allocated according to the long term plans for the mine, the variability of the mineralogical and physico-mechanical characteristics of the material handled, and the

0-7803-5489-3/99/$10.00 ©1999 IEEE.

needs of the mill. This sets the sources, tonnages and destinations of rock (ore and waste) to be drilled, blasted and moved over time. It also accounts for preventative maintenance (PM) activity. Daily plans are typically formed using empirical criteria and past experience.

The first main issue is how the dispatch system is used. Most dispatch systems (certainly the older systems) for truck-shovel fleets are based on the optimization of productivity. When such systems were designed, it was assumed that with optimum productivity comes optimal profit. With homogeneous shovel costs and a static number and capacity of trucks, this may be the case; however, considering variable shovel costs and flexible truck fleet size, designing for increased profitability may be more lucrative. Through economies of scale, it has been proven that larger shovels can usually move ore at a fraction of the cost of smaller shovels. Working the larger shovels more than the smaller shovels therefore should result in lower cost per ton of rock moved. Dispatch systems, however, typically maximize the productivity of the truck fleet instead of minimizing the overall costs of that step in the production cycle. The assumption that maximizing truck productivity will lead to optimum plan in terms of profit is not always valid. This assumption also assumes that all the shovels should be used. The overhead and operating costs of working a shovel for an entire shift when there is no need to utilize that particular shovel can make the mine plan sub-optimal.

The second main issue is that the benefits of blending the mill feed material according to its hardness are rarely recognized. In the case study discussed in this paper, the benefit of accounting for processing variables in the daily plan is recognized. It is assumed that certain blends of ore hardness will maximize the recovery of the mineral processing. This blending issue is not addressed directly by the truck dispatch system. It is addressed in the daily planning through rule-of-thumb procedures, unproven assumptions and experience. A more automated manner of blending based on scientific measurements and optimization algorithms may be a better solution in the long term and will ensure consistent quality. Blending is a common problem that can be easily solved using linear programming [1], yet no scientific management procedures are used in mining to take this important variable into account.

This paper examines a simple optimization approach developed to address these issues in terms of the truck-shovel system in use at an open pit.

PRODUCT BLENDING ISSUES

Hardness has always been a concern at this open pit due to the strength of the ore and the high throughput demand of the mill that offsets the low grade of the ore feed. Hardness, until recently, had only been taken into account by visual examination in the field by mine geologists. A hardness index was developed to predict the particular ore's throughput when milled. A single hardness value was awarded to an entire blasted ore bench. Recently acquired drill performance monitoring technologyhas revealed that hardness can vary dramatically within a single ore bench. This new technology can enable hardness to be integrated into planning in a more consistent and scientific manner.

EQUIPMENT ISSUES

The open pit currently owns and operates 35 trucks. Generally, 25-30 trucks are used every day, while the rest of the fleet is either under PM or idle. On average, thirty truck drivers are used every shift. Many operators are trained for other types of equipment such as graders or dozers. Extra truck drivers usually operate service equipment.

The mine operates 7 shovels: 3 of which are ore shovels and the rest are used in waste (this parameter can alternate, depending on which shovel is closest to the source of blasted rock). Due to the PM schedule, at least one shovel is down for maintenance, therefore only 6 shovels are usually in operation at a single point in time. The shovels differ in size and therefore have different costs per ton. The most cost-effective shovels should be those with the highest utilization. This is not the case, for several reasons. Firstly, the production constraints may require that a particular bench be cleared to maintain the long-term plan.

Secondly, hardness and grade constraints imposed by the mill sometimes take precedence; thirdly, the dispatch system optimizes the truck allocation based on truck productivity, not shovel costs.

The simple optimization approach adopted as a spreadsheet tool indicated that too many shovels were used in the daily operations. The mine employs 6 shovel operators per shift, yet does not have the flexibility (due to union constraints) to change the shovel allocation or operator requirements on an hourly basis. Some shovel operators, however, could be used on service equipment, similar to extra truck operators.

PRODUCTION CONSTRAINTS

The mine production plan must fulfill daily targets in terms of stripping waste and milling ore. The mill was designed to operate most efficiently at a particular hardness and grade of feed, therefore the daily requirements for the ore's grade is also a production requirement. The numerical values of the daily requirements used in the model are shown at the lower left side of the spreadsheet screen capture shown in figure 1, at the end of this document. The table entitled 'Production Requirements' shows variables such as 'ore +' and 'ore-'. These values represent the possible upper and lower limits of ore. For example, the highest quantity of ore that can be produced is 144000 tons/day (140000 tons/day + (2000 tons/shift x 2 shifts/day)). The production constraints and key variables are also listed in the lower left corner of the screen capture.

DEVELOPING A MINE PRODUCTION MODEL

Since the production model is graphically large, in order to facilitate comprehension and to avoid accidental formulae elimination within a cell, the fonts and some cells can be color-coded. Red numbers can appear as those for manual input, whilst black letters are for variable values calculated from previous tables. The spreadsheet model for this problem was developed as follows:

Inputs

All key variables were entered in the 'Constraints' and 'Production Statistics' tables viewed at the bottom left corner of the spreadsheet. These key variables are used in the spreadsheet for various calculations and as constraints. The following also explains some of the important aspects of the model. Specific functions or equations within the software are not discussed since such a model could be developed using any modern spreadsheet or other software tools with linear programming abilities.

The top five rows (cells B3:C7) are values that must be entered according to the current situation in the pit. These can be entered automatically through a macro, within the spreadsheet software, that reads these statistics directly from the dispatch computer. The top row is the identification number of a particular shovel. The number of the shovel is inversely representative of its age. For example, shovel 12 is the oldest while shovel 18 is the newest (largest and cheapest to operate). The next row is the location of the shovel. The third row indicates the hardness index of the current volume of blasted material available to the particular shovel. As discussed previously, hardness can be included in the model; however, it will not be explored in this version since the mine currently has no direct policy governing blending objectives. This model will deal only with grade and production requirements as its planning constraints.

The operating costs per hour are listed in the range C8:P8. The shovel load time and truck rates in tons/hour are input using the macro that takes the variables directly off the dispatch computer. These rates can be used to design the next day's daily plan if the general statistics are expected to be the same. For example, if shovel 12 moves to another location, the truck productivity may change, therefore the optimum plan is no longer the same. These values can also be used to determine the efficiency of the planning procedure. For example, the resulting truck allocations for that day can be input into the changing cells, to be compared with the spreadsheet tool's optimized allocation, based on the previous day's production variables.

The changing variables are allocated to cell range C11:P12. These are the cells that the linear program solver, imbedded within Excel, changes in order to achieve the optimal solution. Rows 18 and 19 show the

constraint that limits the number of truck loads per hour that are allocated to a particular shovel. The algorithm can be presented by the equation 1.

$$\text{max loads/hr./truck} \geq \text{actual loads/hr./trk} \rightarrow \frac{\text{shovel load time (min)}}{60\,\text{(min/hour)}} \geq \frac{\text{trucks allocated} \times \text{truck rate (t/hr)}}{\text{truck capacity}} \qquad 1.$$

It is recognized that a shovel may spend half a day loading ore, and the rest of the day loading waste. This would result in two different 'maximum truck loads' per hour. It was assumed the highest truckloads per hour would be the maximum of the two possibilities .

Results

Basic and array multiplication equations are used to calculate values such as dry metric tons of ore and waste. These values are also used as constraints since the mine wants to maximize ore recovery while maintaining the stripping ratio. Average grade is calculated using the weighted average and recovery is calculated using a macro developed by the milling department (developed several years ago using empirical data). The variables used in the macro are the hardness values and grade of that particular ore. The revenue is calculated by equation 2.

$$\text{dry metric tons/day} \times \text{grade (\%Cu)} \times \text{recovery} \times \$/\text{ton of concentrate} = \text{revenue to mine} \qquad 2.$$

Truck, shovel and milling costs are calculated using the operating and milling costs (per hour) already developed by the mine. Therefore total profit is simply the revenue less the costs.

Solver Setup

To solve the linear problem, the solver imbedded within Microsoft Excel was used. The main steps involved in using the solver are discussed here. The main elements of any linear programming tool (objective, changing variable, and constraints) will be very similar to what follows:

1. Objective. Maximize profit by selecting the profit solution (cell P34)
2. Changing Cells. For this particular model, the number of trucks allocated to the shovels are the changing variables. (C11 to P11 are the changing cells)
3. The following constraints are required for this model:

- Maximum number of truck loads per hour
- Maximum dry metric tons of our per day
- Minimum waste stripping in tons per day
- Ideal grade.
- Maximum number of trucks available

DISCUSSION

The case study implies that the mine should allocate only 20 trucks and 4 shovels for this particular mining sequence. Although not obvious, fractions of a truck per hour can be considered in the daily plan. For example, if a single truck alternates between shovel 12 and 15 then the 0.6 and 0.5 fractions can be accounted for. Major financial savings could accrue by disregarding the traditionally held assumption that all shovels must be used. Secondary benefits, such as better services due to the increased staffing of extra shovel and truck operators on service duty, may add further savings that cannot be calculated directly.

Certain available blasted material at different locations may need to be prioritized by the mine plan if required. A constraint can be added that ensures the shovel at a particular ore bench loads out the required amount. The solution shows that the copper output is maximized and that the cheapest shovels to operate are fully utilized. This can be accounted for in the automatic dispatch system by increasing the allowable average queue time for the most productive shovels. This will insure their preferred utilization.

As monitoring technology is introduced into the mine, the ore characteristics obtained can be used to improve the mine design. If computerized daily planning is further developed, then the planning software may be able to account for blending for optimum mill throughput.

A great deal of emphasis is currently being placed on 4D CAD coupled with economic models[2]. The long range-planning engineer currently uses these tools at this mine. A short-term planning tool should be developed to allow optimized daily plans. The spreadsheet solver described in this paper was developed in under four hours. The previous shift's truck allocation decision was entered into the spreadsheet and revealed that cost savings of $350,000 would have been possible if the optimum schedule was implemented. It should be noted that no bench clearing constraints were input, therefore the true cost savings may have been less. From this spreadsheet tool, the mine has identified the likely over-capacity of equipment and personnel being employed daily, although the impact on production flexibility of reducing labor is not known. This work shows that with little cost and time, a spreadsheet tool can be developed in-house for more scientific and cost effective mine production management. This work has also shown that the assumption that the mine should use all shovels for this production phase is false. The optimum solution does calls for using only 5 shovels. This would allow the mine to avoid the operating, maintenance and overhead costs involved in operating that particular shovel.

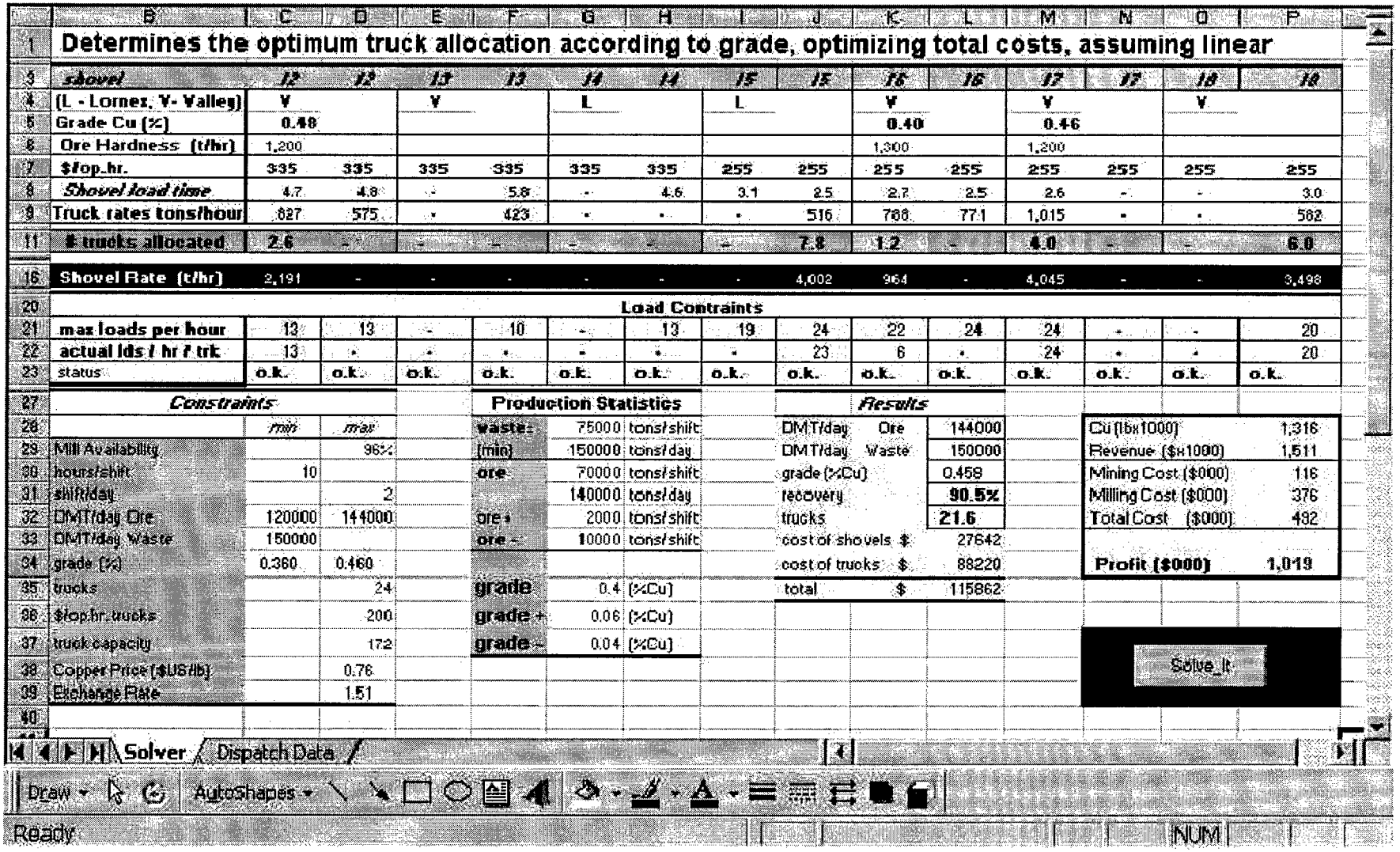
CONCLUSION

Scientific methods of planning have been advocated since the early part of this century[3]. Mines have used queuing theory and other operations management tools during the initial design phase; however, very little is used in daily operations. The availability of modern spreadsheet software and user-friendly management texts (many that directly involve spreadsheet software) [1,4] make intelligent production management accessible to even the smallest mines. Questioning long held assumption would also allow mines to identify other sources of cost savings.

REFERENCES

1. Wayne L. Winston and S. Christian Albright, 1998. Practical Management Science: Spreadsheet Modeling and Applications, New York: Duxbury Press
2. Adam Wheeler, 1997. The Shape of Things to come at Bjorkdal. *Mining Magazine*, August, 128-130
3. Frederick Winslow Taylor, 1967. The Principles of Scientific Management. New York: W. W. Norton & Company, (first published in 1911 by Taylor)
4. Jeffery D. Camm and James R. Evans, 1996. Management Science; Modeling, Analysis and Interpretation., South-Western College Publishing,

Fig. 1. Solver Worksheet and Solution.



Determines the optimum truck allocation according to grade, optimizing total costs, assuming linear

shovel	12	12	13	13	14	14	15	15	16	16	17	17	18	18
(L - Lornex, V- Valley)	V		V		L		L		V		V		V	
Grade Cu (%)	0.48								0.40		0.46			
Ore Hardness (t/hr)	1,200								1,300		1,200			
$/op.hr.	335	335	335	335	335	335	255	255	255	255	255	255	255	255
Shovel load time	4.7	4.8	-	5.8	-	4.6	3.1	2.5	2.7	2.5	2.6	-	-	3.0
Truck rates tons/hour	827	575	-	423	-	-	-	516	766	771	1,015	-	-	582
# trucks allocated	2.6	-	-	-	-	-	-	7.8	1.2	-	4.0	-	-	6.0
Shovel Rate (t/hr)	2,191	-	-	-	-	-	-	4,002	964	-	4,045	-	-	3,498

Load Contraints

max loads per hour	13	13	-	10	-	13	19	24	22	24	24	-	-	20
actual lds / hr / trk	13	-	-	-	-	-	-	23	6	-	24	-	-	20
status	o.k.	o.k.	o.k.	o.k.	o.k.	o.k.	o.k.	o.k.	o.k.	o.k.	o.k.	o.k.	o.k.	o.k.

Constraints	min	max
Mill Availability		96%
hours/shift	10	
shift/day		2
DMT/day Ore	120000	144000
DMT/day Waste	150000	
grade (%)	0.360	0.460
trucks		24
$/op.hr. trucks		200
truck capacity		172
Copper Price ($US/lb)		0.76
Exchange Rate		1.51

Production Statistics		
waste:	75000	tons/shift
(min)	150000	tons/day
ore:	70000	tons/shift
	140000	tons/day
ore +	2000	tons/shift
ore -	10000	tons/shift
grade	0.4	(%Cu)
grade +	0.06	(%Cu)
grade -	0.04	(%Cu)

Results		
DMT/day Ore		144000
DMT/day Waste		150000
grade (%Cu)		0.458
recovery		90.5%
trucks		21.6
cost of shovels	$	27642
cost of trucks	$	88220
total	$	115862

Cu (lbx1000)	1,316
Revenue ($x1000)	1,511
Mining Cost ($000)	116
Milling Cost ($000)	376
Total Cost ($000)	492
Profit ($000)	**1,019**

Solve It

Solver | Dispatch Data

Draw | AutoShapes

Ready | NUM

Intelligent Quality Control for Manufacturing in the Food Industry using a New Fuzzy-Fractal Approach

Oscar Castillo and Patricia Melin

Computer Science Department, Tijuana Institute of Technology,
P.O. Box 4207, Chula Vista CA 91909, USA,
Email: ocastillo@mail.tij.cetys.mx emelin@mail.tij.cetys.mx

ABSTRACT

In this paper we describe a new method to perform automated quality control in the food industry, based on the use of a new fuzzy-fractal approach. Traditional quality control in the food industry consists mainly of microbiological and chemical techniques performed on samples of food extracted from production lines. Traditionally, the goal of the quality control department in the food industry has been the application of the minimal number of microbiological and chemical techniques to the samples of food, so as to have a decision on the quality of the production as quickly as possible. The main idea in this paper is to combine the use of the fractal dimension as a measure of classification of microorganisms and chemicals with the use of fuzzy logic to simulate the expert evaluation/decision process of production's quality. We have developed an intelligent system that is able to perform automated quality control in the food industry.

INTRODUCTION

Traditional quality control in the food industry consists of a long sequence of microbiological and chemical lab techniques that have to be performed on samples of food extracted from production lines. Traditionally, the goal of the quality control department has been the application of the minimal number of microbiological and chemical techniques to the samples of food, so as to have a decision on the quality of the production as soon as possible. The goal of the microbiological and chemical techniques is the identification of possible harmful microorganisms and toxic chemicals for the final consumers of the food [11, 12]. This is the information that is evaluated at the end, by the human experts in quality control, to make the final decision about the quality of the production.

In this paper we describe a new method to perform automated quality control in the food industry, using fuzzy logic techniques [1, 8] and fractal theory [10]. We also show in this paper how to implement this new method as a computer program to really achieve the goal of automated quality control in practice. We use fractal theory in our new method to minimize the number of microbiological and chemical techniques that are needed to make the identifications of harmful microorganisms and toxic chemicals. We use a method for the identification of microorganisms based on the use of the fractal dimension, developed by the authors [3], to eliminate the need of applying a long sequence of microbiological techniques to the samples of food.

This method of identification uses the fractal dimension as a measure of classification of the microorganisms and can greatly reduce the time needed to identify possible harmful microorganisms for the consumers. The computer program contains a module to perform this fractal identification, which in turn enables automated identification of microorganisms minimizing the use of microbiological techniques. On the other hand, we use fuzzy logic techniques to simulate the expert evaluation/decision process to obtain the quality of the production. The process of quality evaluation is simulated in the computer program using as input the information about the identifications of microorganisms and chemicals, and then by applying heuristics and statistical calculations to decide on the degree of quality of the production. The computer program contains an "intelligent" module to perform this "expert" simulation, which in turn results in automated evaluation of production quality. In conclusion, we can say that combining the use of

0-7803-5489-3/99/$10.00 ©1999 IEEE.

both fuzzy logic techniques and fractal theory in a computer program we can achieve the desired goal of Automated Quality Control in the Food Industry (AQCFI).

The use of fuzzy logic and fractal theory increases the efficiency (in accuracy and in time) of the quality control, because the computer program has the mathematical algorithms (for the fractal dimension) needed to identify possible harmful microorganisms and toxic chemicals minimizing the use of microbiological or chemical techniques for the identification, and also because the computer program has the knowledge to decide at the end on the final quality of the food production. In this paper the authors have successfully generalized their previous work on this matter [5, 6], by using a Fractal Module to perform automated identification of microorganisms and chemicals and by developing an Expert Module for evaluation of the quality of the production using fuzzy logic techniques.

DESCRIPTION OF THE NEW METHOD FOR AUTOMATED QUALITY CONTROL

The new method for automated quality control in the food industry consists mainly of two parts: one part performs the automated identification of microorganisms and chemicals by using the fractal dimension, and the second part performs an automated evaluation on the quality of the production by using SC techniques and the information obtained in part one. We show in Figure 1 how the new method works, beginning with the samples of food extracted from production lines and ending with the final evaluation of the production quality. We describe below in more detail the two main parts of the new method for AQCFI.

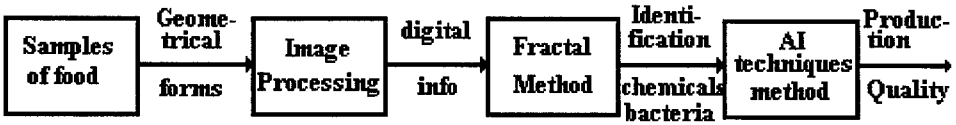


Fig. 1. New Method for Automated Quality Control in the Food Industry.

The samples of food are extracted randomly from production lines (this is the only part that is not automated) and prepared for identification. Then a Laser Scan Microscope is used to digitize the geometrical forms of bacteria colonies. The digitized information is then used as input for the method of identification (using the fractal dimension). Finally, the identifications of bacteria and chemicals are used as information by a knowledge base to decide on the general quality of the production.

DESCRIPTION OF THE METHOD FOR IDENTIFICATION OF MICRO-ORGANISMS AND CHEMICALS USING THE FRACTAL DIMENSION

We describe briefly in this section a new method for the identification of microorganisms for the food industry, developed by the authors [2], that is based on the use of the fractal dimension [10]. This method uses the fractal dimension to make a unique classification of the different types of microorganisms, because it is a known experimental fact that the colonies of different types of bacteria have different geometrical forms. The problem is then of finding a one to one map between the different types of bacteria and their corresponding fractal dimension, in this way obtaining a unique method of identification of microorganisms for the food industry. The first step in obtaining this map is to find experimentally (in the microbiological lab) the different geometrical forms for the bacteria. The second step is to calculate the corresponding fractal dimensions for the different types of bacteria. This fractal dimension can be calculated for a selected type of bacteria with several samples, to obtain as a result a statistical estimation of the dimension and the corresponding error of the estimation.

The method for identification of microorganisms using the fractal dimension can be stated mathematically in the following form: let M_m be a one to one map between the sets I_m and D_m, where the set I_m can be called set of identifications of microorganisms and the set D_m can be called set of fractal dimensions. The set of identifications can be as follows:

$$I_m = \{ \text{Staphylococcus}_{aureus}, \text{Streptococcus}_{fecalis}, \text{Pseudomona}_{aureoginosa}, ...\}$$

and the set of fractal dimensions can be as follows:

$$D_m = \{ D_{sa}, D_{sf}, D_{pa}, ...\}$$

where D_{sa} is the fractal dimension of the Staphylococcus aureus bacteria, D_{sf} is the fractal dimension of the Streptococcus fecalis bacteria, D_{pa} is the fractal dimension of the Pseudomona aureoginosa bacteria and so on. The fractal dimension of an object can be defined approximately as follows:

$$d = [\ln N(r)] / [\ln(1/r)]$$

where N(r) is the number of boxes covering the object and r is the size of the box. In this case, the object is the colony for a particular bacteria. An approximation of the fractal dimension can be obtained by counting the number of boxes covering the object for different r sizes and then performing a logarithmic regression to obtain d (box counting algorithm).

DESCRIPTION OF THE METHOD TO PERFORM AUTOMATED EVALUATION OF PRODUCTION QUALITY

We describe briefly in this section the method to perform the evaluation of production quality using SC techniques. This method simulates the expert evaluation/decision process involved in obtaining the degree of quality of the production. This method uses as input the information obtained by the "Fractal Method", i.e. the identification of microorganisms and chemicals, and then applies heuristics and statistical calculations (implemented as fuzzy rules) to decide on the quality of the production. This method uses expert knowledge to decide if a microorganism can be harmful to the consumer or if a chemical can be toxic to the consumer. Also, the method uses expert knowledge to decide on the degree of quality of the production. Both kinds of expert knowledge can be implemented in MATLAB as a set of fuzzy rules (knowledge base) for the computer program. The choice of MATLAB is because of its symbolic and numeric manipulation features and also because it is a good language for developing prototypes.

The use of fuzzy logic in manufacturing applications has been well recognized [1, 9] and many applications have been developed. In this case, we came to the conclusion that the best way to convey the information about the quality level of a manufactured food product was using fuzzy sets [8]. Also, we think that the best way to reason with uncertainty in this case is using fuzzy logic. In a prior prototype developed by the authors [5] we didn't consider using fuzzy logic in the simulation of the expert decision process. However, when we considered expanding the number of microorganisms and chemicals for the system, then we run into problems with the consistency of the knowledge base. We realized then, the need to consider the use of reasoning with uncertainty and also as a result of this using a rule base consistent with this approach. Our choice for reasoning with uncertainty was fuzzy logic, considering the success that this theory has achieve in the fields of manufacturing and engineering.

DESCRIPTION OF THE INTELLIGENT SYSTEM

The modules of the intelligent system are: the Expert Module, the Fractal Module, the Interface and the Inference Engine. The description of the Expert Module and the Fractal Module is given below, because it is very interesting from the point of view of the application to manufacturing in the food industry. We also give a description of the implementation strategies used in developing the computer system.

DESCRIPTION OF THE FRACTAL MODULE

The Fractal Module consists of a computer program that is an implementation of the method for the identification of microorganisms and chemicals using the fractal dimension described before. This computer program uses the geometrical forms of the colonies of microorganisms, obtained by the Interface of the system from the samples of food to estimate the fractal dimension (box dimension) using a known algorithm [10], and then compares this value with the data base of known fractal dimensions and their corresponding identifications, to arrive to the conclusion of which microorganisms are present in the samples of food. This computer program also uses the geometrical forms of the spectrums of unknown chemical compounds in the samples of food, to estimate their fractal dimensions and then compares this value with the data base of known chemical identifications, to arrive to the conclusion of which chemical compounds are present in the samples. In Table 1 we show part of the data base of fractal dimensions for different types of microorganisms obtained by extensive prior experimental microbiological work done by the authors [2].

Table 1. Data base for the classification of microorganisms

Number	Fractal Dimension	Microorganism Identification
1	$D_{sa} \pm e_{sa}$	Staphylococcus aureus
2	$D_{sf} \pm e_{sf}$	Streptococcus fecalis
3	$D_{pa} \pm e_{pa}$	Pseudomona aureoginosa
4	$D_{st} \pm e_{st}$	Salmonella typhi
5	$D_{ec} \pm e_{ec}$	Echerichia coli

In this table D_i denotes the average fractal dimension expected for a particular type of microorganism and e_i denotes the corresponding statistical error associated with the identification. We can interpret then the value $D_i \pm e_i$ as the confidence interval for each particular identification shown in the table.

DESCRIPTION OF THE EXPERT MODULE

The Expert Module of the computer system is an implementation of the method to perform automated evaluation of production quality described before. The Expert Module uses the information given by the Fractal Module to obtain the quality of the production, i.e., the Expert Module uses the identifications of microorganisms and chemicals found in the samples of food to decide if the quality of the production meets the requirements of acceptance. The knowledge base of the Expert Module consists of a set of fuzzy rules containing the knowledge of the human experts for the domain of quality control in the food industry. The knowledge base consists of two parts: one part contains the knowledge to decide if a microorganism is harmful to the consumer or if a chemical is toxic to the consumer, the second part contains the knowledge to decide on the degree of quality of the production.

Suppose that n samples of food are extracted from production lines during the manufacturing process, and that the Fractal Module makes the corresponding identifications of microorganisms and chemicals found in the samples. The output of the Fractal Module will be a list of microorganisms and the percentages of the samples that they were found in and the same for the chemicals. For example, in the case that only three bacteria were found the output can be written as follows:

Output = {(BacteriaX, %samplesX), (BacteriaY, %samplesY), (BacteriaZ, %samplesZ)}

With the percentage of samples for each Bacteria, we can calculate the Total Percentage of Bacteria that can cause Infection or that can cause Intoxication. For example, if in the above case only Bacteria X and Bacteria Y can cause infection, then:

%Bacteria_Infection = %samplesX + %samplesY

Using as variables the Total Percentage of Bacteria that can cause Infection and the Total Percentage that can cause Intoxication, we can classify the "Microbiological Evaluation of the Production" as one of the three following fuzzy sets: GOOD, REGULAR and BAD. A similar classification can be done with the "Chemical Evaluation of the Production", using the fuzzy sets: GOOD, REGULAR and BAD. In our implementation the membership functions were found using heuristics from the experts in microbiology and chemistry for the food industry.

We classify "Production Quality" using four fuzzy sets: EXCELLENT, GOOD, REGULAR and BAD. This classification depends on two variables: Microbiological Evaluation and Chemical Evaluation. We show in Figure 2 the membership functions for the values of the "Quality" linguistic variable. The membership functions were defined in the membership function editor of the Fuzzy Logic Toolbox.

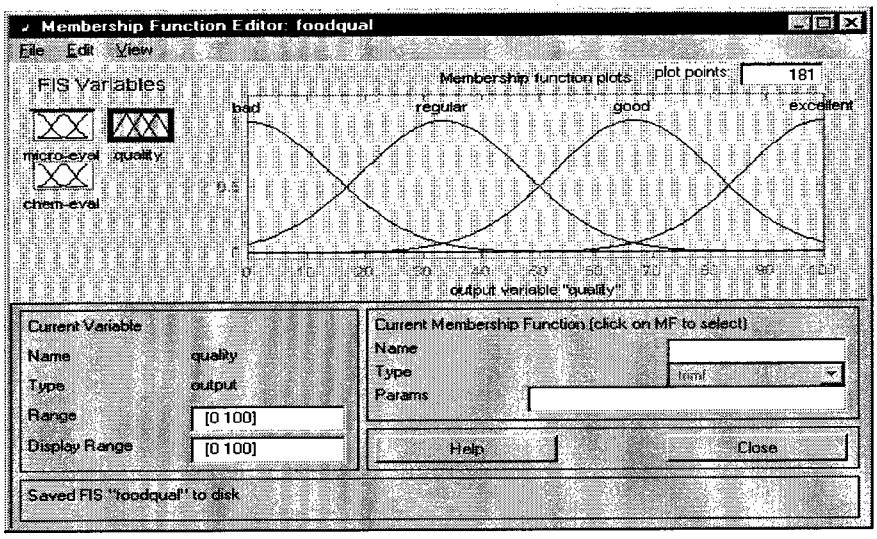


Fig. 2. Membership functions for the linguistic values of the quality variable.

We show in Figure 3 the fuzzy rule base for the prototype intelligent system developed in the Fuzzy Logic Toolbox of the MATLAB programming language.

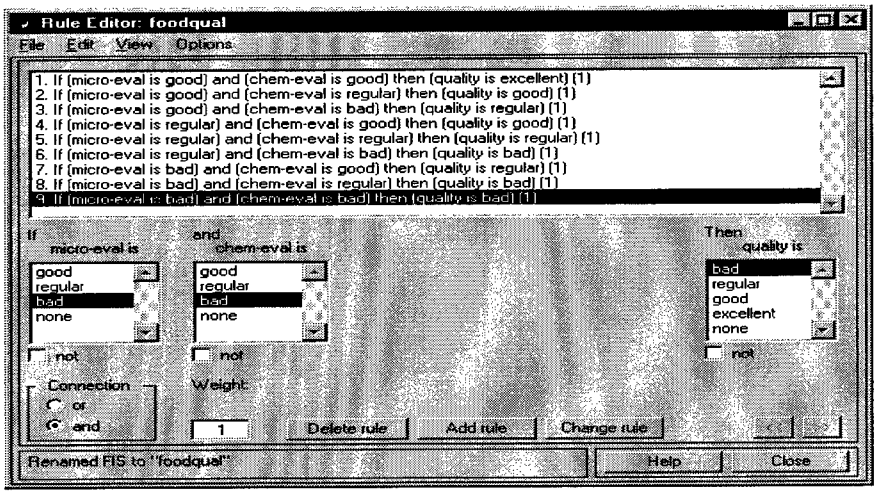


Fig. 3. Fuzzy rule base in the rule editor of fuzzy logic toolbox.

We show in Figure 4 the non-linear surface for the problem of quality evaluation using as input variables: microbiological evaluation and chemical evaluation. The three-dimensional surface represents the non-linear fuzzy model for the problem.

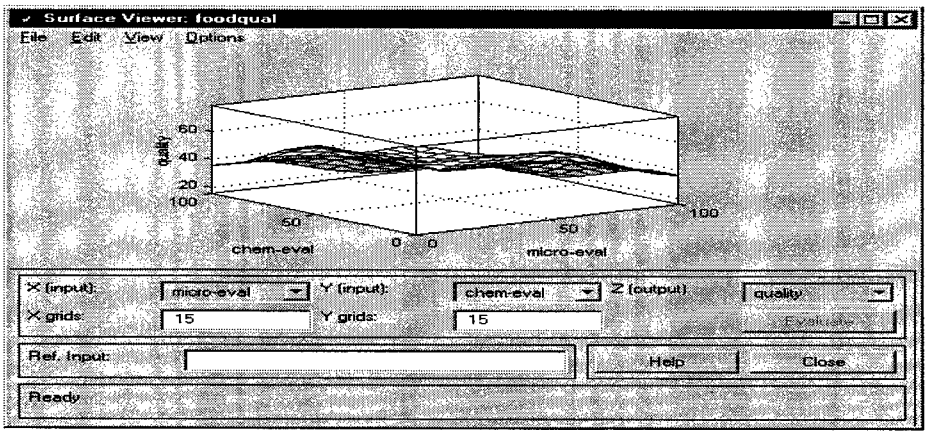


Fig. 4. Non-linear surface for quality evaluation.

CONCLUSIONS

We have developed a computer system for automated quality control of the manufacturing process for the food industry. The computer system is an implementation of a new method developed by the authors for automated quality control, based on the use of SC techniques and fractal theory. In a prior prototype system developed by the authors [3] the use of SC was only for the selection of the microbiological techniques needed to identify the microorganisms present in the samples of food and this is only part of the problem in quality control. Then in other prototypes developed by the authors [4, 5, 6] we introduced the fractal theory method to help in the identification of microorganisms. In the computer system presented now in this paper, the Fractal Module eliminates the need of using microbiological techniques for the identification of microorganisms. Also, the Fractal Module identifies chemicals present in the samples of food. In the system described in this paper, the use of SC techniques is for the simulation of the decision process of finding if a microorganism can be harmful or a chemical can be toxic for the consumers. Also, the system uses fuzzy logic techniques for the simulation of the evaluation process of the quality of the production using the information given by the Fractal Module.

REFERENCES

1. Badiru, A.B., 1992. *Expert Systems Applications in Engineering and Manufacturing*, Prentice-Hall.
2. Castillo, O., Melin, P., 1994. Developing a new method for the identification of microorganisms for the food industry using the fractal dimension, *Journal of Fractals*, 2(3), 457-460.
3. Castillo, O., Melin, P., 1994. An Intelligent System for the Identification of microorganisms for quality control in the food industry, *Proceedings of the Ninth International Conference on Applications of Artificial Intelligence in Engineering*, Wessex Institute of Technology, U.K. 133-140.
4. Castillo, O., Melin, P., 1995. Automated Quality Control in the Food Industry combining Artificial Intelligence Techniques and Fractal Theory, *Proceedings of the Tenth International Conference on Applications of Artificial Intelligence in Engineering*, Wessex Institute of Technology, U.K., 109-118.
5. Castillo, O., Melin, P., 1995. QUACONTRA: Quality Control Training in the Food Industry using an Intelligent Tutor, *Proceedings of the Ninth International Conference on Industrial an Engineering Applications of Artificial Intelligence and Expert Systems*, Gordon and Breach Publishers, Australia, 835-844.
6. Castillo, O., Melin, P., 1996. Automated Quality Control for Manufacturing in the Food Industry using Fuzzy Logic and Fractal Theory, *Proceedings of DKSME'96*, Tempe, Arizona, USA, 349-360.
7. Castillo, O., Melin, P., 1997. Intelligent Quality Control for Manufacturing in the Food Industry using Fuzzy Logic Techniques and Fractal Theory, Proceedings AISC'97,Acta Press, Banff, Canada, 100-103.
8. Kosko, B., 1992. *Neural Networks and Fuzzy Systems*, Prentice-Hall.
9. Kusiak, A., 1992. *Intelligent Design in Manufacturing*, John Wiley and Sons.
10. Mandelbrot, B., 1983. *The Fractal Geometry of Nature*, W. H. Freeman and Company.
11. Pelczar, M.J. , Reid, R.D., 1982. *Microbiology*, McGraw Hill.
12. Pettipher, G.L., Rodriguez, M.V., 1987. Rapid Enumeration of Microorganisms in Food by the Direct Epifluorescent Filter Technique, *Applied and Environmental Microbiology*, 52(3), 115-117.

Design Tool for Assessing Manufacturing and Environmental Impact

Daniel Rochowiak[1], Sherri Messimer[2], Phillip A. Farrington[2], Dawn Russell[2], Raymond D. Harrell[3] and Daniel A. Holder[3].

[1]Department of Computer Science
Department of Industrial and Systems Engineering
and [2]Engineering Management
The University of Alabama in Huntsville
[3]US Army AMCOM, Redstone Arsenal, Alabama, USA

ABSTRACT

This paper outlines a design tool that incorporates environmental and quality concerns into a traditional simulation environment. The Design Tool for Assessing Manufacturing Environmental Impact (DTAME) allows a user to concurrently consider the impact of environmental, quality, cost and production attributes early in the product life cycle. DTAME aids in making environmentally conscious decisions and allows designers to understand the consequences of their decisions regarding manufacturing options.

INTRODUCTION

As the DoD undergoes reshaping and resizing to achieve a more affordable defense capability, it is also important that weapon systems be developed and manufactured in an environmentally conscious manner. To achieve this goal requires that a change occur in the paradigm that is used to view the weapon system life cycle. In today's paradigm, the addressing of environmental concerns occurs as de facto activities after the product, process, and manufacturing plan have been established. Many studies have shown that this reactive approach is not effective. Currently, the DoD and its contractors are in the process of "cleaning up" their facilities and weapon system designs due to inadequate environmental planning.

The drive for improved performance at a lower cost often results in the use of new and emerging materials and manufacturing processes. Since these processes and materials are typically not well understood, opportunities for applying a life-cycle approach to the detection of manufacturing and environmental problems early in the product's life cycle are difficult. For instance, many designers are encouraged to utilize polymer-based composite materials in their design due to such noted properties as corrosion resistance and high strength to weight ratios although many design engineers often misunderstand the repercussions of the associated composites manufacturing processes.

Currently, Program Management Office personnel do not have the expertise to address the environmental impacts of design decisions made during the design process. This paradigm change requires that environmental concerns be viewed as an important factor in the trade-off decision making that must occur during the early development phases. Assessing pollution impacts and energy consumption during early product development will result in long-term savings and a significant reduction in pollution and hazardous waste generation [1,2].

Discrete event simulation provides an effective tool for evaluating system configurations and new processing strategies; in fact, simulation is often the only viable choice for analysis of complex manufacturing systems. Advances in simulation software have led to the design of user-oriented modular simulation packages thereby decreasing the time needed to build a simulation model. However, these tools have not directly addressed the issues of simulation in the context of environmental concerns and multiple

0-7803-5489-3/99/$10.00 ©1999 IEEE.

performance metrics. The typical tool concentrates on providing throughput and capacity information for assessing the impact of an individual station's speed and reliability on overall system performance. By combining modular simulation software techniques and life cycle design with the domain knowledge of a specific manufacturing technology, a simulation system can be provided that not only generates traditional production output but also integrates environmental, quality, and cost criteria into the simulation.

The Design Tool for Assessing Manufacturing Environmental Impact (DTAME) was developed in order to merge the concepts of life cycle design with modular simulation techniques. The simulation models can be used to generate a complete material balance around a particular manufacturing process and can be made available to design engineers to aid in life cycle design assessment. The output of the DTAME simulation model provides design engineers, program managers and integrated product teams with information on energy usage and a complete material balance. This information includes the types and quantities of scrap and hazardous material produced, as well as the more traditional system analysis results including queue lengths and production lead times. The goal is to develop the tools that allow users to make decisions with a high degree of confidence about whether a proposed system meets design constraints and is environmentally and economically preferable.

The targeted domain of the DTAME system is polymer-based composite materials and their associated processes. The basic steps for fabricating composite material parts are: begin with a plastic matrix and reinforcement, co-mingle the matrix and reinforcement, form the co-mingled composite into the part geometry, cure or heat the composite, and finally, perform any required finishing or joining operations. While typical finished composite parts are chemically benign and pose little ecological threat, environmental concerns and issues arise in the basic manufacturing steps [3]. Environmental regulatory acts that establish materials that constitute hazardous waste, that regulate treatment and disposal, and that establish reporting requirements for chemical release, waste reduction, recycling and energy recovery, impact on the manufacture of composite parts. Ignorance of these regulations can lead to severe penalties. Hence, composite manufacturers are sensitive to these regulations and must be apprised of revisions.

DTAME SYSTEM ARCHITECTURE

Figure 1 illustrates the architecture of the DTAME system. It is composed of three major modules, in addition to the supporting modules for communication and integration. The analysis of a proposed system begins with the CDMCS, a critiquing system designed to provide high level expertise in determining whether a particular process is appropriate for the specified design. The next stage is the simulation environment, called SimBuilder, where information regarding environmental and production parameters is collected and exercised through discrete event simulation. Finally, the simulation output is submitted for optimization. The interface is designed to facilitate the entry of information into the DTAME system. This is accomplished by providing the user with a set of specially designed input screens and menu selections that are tailored for the manufacturing process being evaluated.

CDMCS

The Composite Design and Manufacturing Critiquing System (CDMCS), assists a design engineer by critiquing the proposed manufacturing methods for a particular design [4]. The critique is intended to aid the decision by providing evaluative information based on domain knowledge. The critique provided by CDMCS is built by comparing the design parameters for a specified part against a set of design rules and parametric relationships that govern the acceptability of individual composite part manufacturing processes. The rules and metrics that qualitatively simulate an expert's knowledge are divided into three categories: requisite metrics, core metrics and enabling metrics. Requisite metrics are Boolean in nature and must be satisfied. Core metrics must be satisfied to a high degree. Finally, enabling metrics are those metrics that are not vital to the acceptability of a candidate process, but enhance or detract from its desirability. An aggregate score for the candidate process is obtained by analyzing each of the metrics that apply to a specified candidate process. The success values for the metrics are compiled into an overall score. The aggregate score for the process is then mapped to a qualitative rating from *very poor* to *highly acceptable*. The qualitative rating is used to produce both explanatory text and graphical representations. The system also provides suggestions for improving the aggregate score.

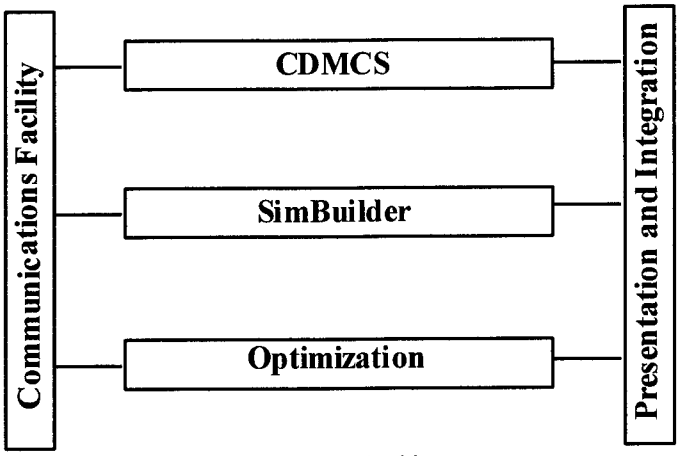


Fig. 1. DTAME Architecture

The use of a critiquing system is a central feature of DTAME as it provides guidance about the evolving simulation definition and allows a user to choose an appropriate manufacturing process to meet the design specifications. A graphical user interface allows the user to operate the system and observe results. Network links connect the system to remote databases that allow for the most current selections of materials and other parameter values.

SimBuilder

Whether maintaining and improving existing production lines or designing new lines, simulations are employed to evaluate and compare alternatives. Simulation is often the only viable choice for analysis of complex manufacturing systems especially where there is a high degree of interdependence between design, process equipment, and process control. Simulation provides an effective tool for evaluating system configurations and new processing strategies. If properly constructed and maintained, a simulation model of an existing production line can be used to:

- evaluate the impact of product mix changes,
- evaluate the impact an individual station's speed and reliability on overall system performance,
- compare the system throughput and capacity with different process configurations,
- provide environmental data that can be integrated with process cost information to develop more detailed and accurate models of processing, and
- compare the performance of different system configurations required by competing design technologies.

The SimBuilder module is used to rapidly define, model, and evaluate a proposed manufacturing system once a manufacturing process has been specified in CDMCS. This tool supports rapid prototyping and concurrent engineering by creating a modeling environment that improves the clarity of the model, increases productivity, reduces the modeler's need to know the details of a simulation language, and provides for easier maintenance and improved documentation. The SimBuilder simulation system is composed of three subsystems, the input system, the simulation, and the output system.

The purpose of the input system is to ensure that all required information is obtained from the user and available for use within the system. Icons, which represent the various equipment elements, can be placed anywhere in a two-dimensional graphical workspace. The user interactively responds to questions about the process and environmental factors. Certain databases were developed to store information, which were not directly used to populate the simulation but were needed for the output analysis. Most importantly, the material database, consists of 1) a general section which contains general information about the materials being used including the name, cost, and Material Safety Data Sheet (MSDS) environmental information, and 2) the option specific section which includes information required for each simulation experiment. This includes, for example, the amount of material used for the original part and the percentage of the part discarded during certain operations. All of the information required for the material database is captured from the interface questions developed for the submodels.

The second subsystem is the simulation. The simulation subsystem uses information obtained from the user to develop and run the simulation model and to generate information needed for the output subsystem. This includes developing submodels for all process steps and creating system variables, which track the required information. Once the user has completed the data input and is satisfied with the model, the simulation code is generated and executed using the WITNESS [Lanner Group] simulation environment. SimBuilder builds the simulation code from a library of submodels. The simulation can now be optimized using a Genetic Algorithm (GA) approach as presented below in the discussion on the Optimization module.

The output subsystem utilizes information from the user and the simulation to generate material, environmental, quality, cost, production, and energy reports. Six basic output reports were developed to effectively communicate information to the user. The reports developed were: 1) the material report which includes the amount of each material that enters the system, exits the system in each output stream (good parts, mandrel prep scrap, etc.) and remains in the system as work in process, 2) the process report (from WITNESS) which includes traditional simulation output, 3) the quality report which includes the amount and cost of all scrapped materials by processing station and type of material, 4) the environmental report which includes the amount and cost of all materials discarded as waste, 5) the energy report which includes the amount and cost of the energy used to produce the parts, and 6) the cost report which includes material, energy, and labor costs to produce the parts. Fig. 2. provides a sample output report on environmental criteria. This report lists both material waste and scrap and provides an average cost per finished part for each category. In particular, amounts of hazardous waste can be easily tracked and documented.

Environmental Report	Wt/Finished part	Wt/Week	Cost/Finished part	
Waste Type	Avg	Avg	Avg	
Discarded RM's	0.98	18.04	$0.50	
Total Amount of Mat'l in Scrap	5.99	164.31	$5.56	
Machine Waste	0.00	0.00	$0.00	
Cuttings	0.00	0.00	$0.00	
Waste Resin	0.72	19.74	$0.72	
Solvent Bottoms	1.92	52.60	$1.92	
Air	2.40	65.71	$2.40	
Discarded Mat'ls used for good parts or	2.58	70.62	$2.03	
Mandrel Mat'ls	1.00	27.52	$1.00	
Bag Mat'ls	0.42	11.54	$0.01	
Mold Release	1.00	27.52	$1.00	
Mandrels	0.15	4.04	$0.00	
Total	14.58	391.02	$13.12	
Environmental Categories	Waste/Finished Part	Waste/Week	Usage/Finished Part	Usage/Week
Ext Haz Sub-Rep Quantity	0.00	0.00	0.00	0.00
Ext Haz Sub-TPQ	0.00	0.00	0.00	0.00
Toxic Chemical	0.00	0.00	0.00	0.00
TRI Chemical	0.00	0.00	0.00	0.00
SARA H-1	0.34	9.23	11.15	305.68
SARA H-2	0.00	0.00	0.00	0.00
SARA P-3	0.00	0.00	0.00	0.00
SARA P-4	0.00	0.00	0.00	0.00
SARA P-5	0.00	0.00	0.00	0.00
Hazardous				
Non-hazardous				

Fig. 2. Environmental Report

Once a production line has been defined and before committing to a simulation model, the user is given the option of performing a static analysis. A static analysis is a high level quantitative analysis based on simplifying assumptions that quickly produces results for the following information on each of the manufacturing operations: Production Cycle Time, Percent Down time, Effective Cycle Time, and Shift Capacity. The static analysis of the manufacturing system can be generated using the processing times for each component to generate a maximum throughput for the line and identify bottlenecks.

Optimization

The third module, Optimization, is used to improve the manufacturing system configuration. Several studies have shown that optimization, in conjunction with simulation, is the best way to obtain the maximum amount of information while minimizing the amount of resources utilized [5]. A Genetic Algorithm approach has been used in conjunction with the WITNESS simulation model. The optimization component takes as input a WITNESS simulation model. The genetic algorithm adjusts the down times (the frequency of a machine being taken off-line for maintenance or breakdown), number of machines, and cycle times in the WITNESS model in order to achieve better results over time. The genetic algorithm takes the results of the simulation run and evaluates the results in light of a predefined fitness function. The user can modify the fitness function associated with the algorithm; one example is a weighted average of profit, average flow, and average work in process. Once WITNESS receives the necessary data from the genetic algorithm, it runs a simulation of the manufacturing line for a pre-determined amount of simulation time (including a warm-up period).

CONCLUSIONS

The DTAME has been developed to aid designers in evaluating the incorporation of composite materials in their design. DTAME accomplishes this goal by consolidating material and process knowledge in a simulation environment that integrates environmental, cost, quality and production factors.

The primary modules of DTAME provide for a consistent methodology while allowing continuous improvement of the tools that implement it. The critiquing module, CDMCS, assists the user in determining the viability of a manufacturing process for a particular design. The simulation module, SimBuilder, models a wide variety of manufacturing options through the incorporation of reusable simulation submodels. Furthermore, the simulation integrates material usage, environmental impact and direct costs in addition to production criteria. The user can select from a variety of post simulation data displays and analysis options allowing quality, environmental, cost and production reports for use by the design engineer when considering manufacturing alternatives. Once the simulation models are created in the SimBuilder system, they serve as input to the genetic algorithm module. This module attempts to generate an optimal solution from each generation can then be simulated to provide a more detailed evaluation.

Research is currently being conducted on data, information and knowledge version and case control. The goal of this effort is to provide a consistent environment for archiving, searching and tracking the decision process for particular cases. Ideally this evolving enterprise knowledge base will be used both to refine the knowledge incorporated into the modules and to provide additional information that will allow the user to make more informed and better decisions.

REFERENCES

Keoleian, G.A. and Menerey, D. (1993) Life Cycle Design Guidance Manual. Ohio Environmental Protection Agency (EPA 600/R-92/226).

U.S. Environmental Protection Agency. Guide to Pollution Prevention, (1991). The Fiberglass-Reinforced and Composite Plastics Industry (EPA/625/7-91/015).

Russell, D. (1997). Methodology for Designing Modular Multi-Criteria Discrete Event Simulations. Dissertation. The University of Alabama in Huntsville.

Messimer, S., Henshaw, J., Montgomery, J., and Rogers, J. (1996) Composites Design and Manufacturing Critiquing Assistant. *Artificial Intelligence in Engineering Design and Manufacturing* 10, 65-69.

Hall J. and Bowden, R. (1996). Simulation Optimization for a Manufacturing Problem. *Proceedings of the 1996 Southeastern Simulation Conference*, 135-140.

Models, Algorithms and Decision Support Systems for Letter Mail Logistics

Hans-Jürgen Sebastian

RWTH Aachen , Operations Research Group, Aachen, Germany

ABSTRACT

The reorganization of the Deutsche Post AG imposed massive structural and organizational changes. These changes strongly influence the design and operations of the logistic network. Here we will focus on the so-called main transportation network. It consists of the network connecting 83 letter mail centers distributed throughout Germany as well as the international letter mail center at the Frankfurt am Main airport. The planners have to decide how an average of about 1,500 tons of letter mail is transported between the letter mail centers each night. Moreover the system should be able to deal with special situations, such as the strong quantity increases before Christmas.

The Deutsche Post AG and the ELITE Foundation are implementing a Decision Support System for this specific planning task in cooperation with the RWTH Aachen. The system is currently running at the Deutsche Post AG's branch in Bonn and is simultaneously being extended and improved. It is based on a client-server architecture, including a Geographical Information System (GIS), a relational data-base system, a Graphical User Interface (GUI), and a number of optimization algorithms for different planning tasks.

In order to reduce the complexity of the planning problem, it was decided to divide the problem into sub-problems, which are solved sequentially. There is, of course, always the possibility to backtrack to an earlier planning stage, if necessary. The sub-problems include the night airmail network, the ground-feeding transportation design, the road network and hub design problem, hub vehicle scheduling, and the direct loading vehicle scheduling problem.

The process of letter mail collection can be roughly divided into five sub-processes: first, the letter mail is collected from the mailboxes at each letter mail center. It is then sorted according to the destination letter mail center. This process finishes at about 2115 hours. In the third step, the letter mail is transported between the letter mail centers. This process has to be finished no later than 415 the next morning, resulting in a transportation time window of about 7 hours. However, because of sorting capacities, it must be guaranteed that the letter mail arrives almost continuously during the 7-hour period, effectively making the problem an inventory-routing design problem.

The incoming letters are sorted in correspondence to their local destination at every letter mail center. Eventually, the letter mail is transported to pick-up points where it is collected by the postman. The tight time window constraint forces a fraction of about 20% of the letter mail to be transported using the so-called night airmail network. However, it might be better to increase this fraction in order to save road transportation costs. The assignment of letter mail to either the night airmail network or the road network is in itself an optimization problem, which can only be solved by consideration of the entire transportation network.

For a given quantity of letter mail, optimization of the night airmail network consists of assigning the letter mail for each origin-destination pair to a flight. A flight is defined by its take-off and landing airport, the take-off time, and the type of aircraft. It can be shown that only a limited number of take-off times have to be considered, thus reducing the number of possible flights. This observation leads to a model that is similar to a warehouse-location (or facility-location, plant-location) model. However, its size (several thousands of warehouses and customers) requires heuristic methods to be used effectively. We have developed a Tabu Search algorithm, which iteratively calls the commercial mixed-integer solver CPLEX. The results indicate strong potential for savings compared to the existing solution.

0-7803-5489-3/99/$10.00 ©1999 IEEE.

Ground-feeding of the night airmail network is performed by vehicles of different size and speed. The objective is to design vehicle trips from the letter mail centers to the airport and back, so that on-time delivery of letter mail at the airport is guaranteed.

There is the possibility of by-passing other letter mail centers on the way to the airport and/or picking-up additional mail in order to save transportation costs. The number of additional pick-ups is limited however, to two or three due to the time-window constraints.

We have chosen to generate a large number of tours and to model the problem as a set-covering problem. The model is solved by a Lagrangean heuristic for set-covering. Most letter mail quantities between the different letter mail centers are rather small. Therefore, it is desirable to consolidate the letter mail into a hub system. On the other hand, hub consolidation is time-consuming and rather costly due to sorting costs - especially since the sorting process is performed manually. Due to the requirement of almost continuous input, it is only feasible to delay a fraction of the mail by hub consolidation. Moreover, process feasibility can only be checked if the entire system is considered simultaneously. We have developed an Evolutionary Algorithm which performs this optimization, i.e., whether to transport by hub consolidation or direct loads, based on modification of vehicle schedules. Letter mail is then re-assigned to the modified schedules in the algorithm. The algorithm is able to improve initial solutions considerably.

The hub and direct loading vehicle scheduling problems are similar to the ground-feeding problems and can again be solved by a set-covering approach. However, due to the size of the problem, heuristic preprocessing methods have to be employed.

The Decision Support System also contains a large number of methods for cost and resource analysis, which support manual modification of the computer-generated plans. These methods have increased the user-acceptance of the system and enable users to gain an impression of the system-wide consequences of their decisions.

Intelligent Processes for Production Control

Edson Pacheco Paladini

Universidade Federal de Santa Catarina
EPS / CTC – CP 476 – Trindade
88040-970 , Florianópolis, SC, Brazil

ABSTRACT

This paper presents an intelligent system which makes possible to control raw material flow (a typical production control problem) automatically. The system is supported by Artificial Intelligence devices, more specifically by two Expert Systems which determine on a case-by-case basis whether raw material must be allowed straight into the factory without inspection or, otherwise, it must go through any kind of inspection. Should the material be inspected, it must be sent either to a reposition department, where perfect pieces will replace defective ones, or to a general lot analysis department, where in case of lot rejection, the material must be re-inspected or returned to suppliers. An experimental use of this system is reported and the preliminary results are analyzed.

INTRODUCTION

This paper presents a system applied to wall tile factories and deals with an automatic process for raw material flow organization in those companies. Due to its nature and generality, however, this study can be extended to other companies, since the problems analyzed here are rather frequently observed.

In general terms, this paper refers to an automatic system of decisions about the factory's incoming raw material. Two areas are structured and in each of them automatic decisions are made about the flow of raw material arriving at the factory. Expert Systems are used as basic decision modules.

GENERAL INSPECTION PROCEDURES OF RAW MATERIAL

Organization of the raw material reception area in a factory is usually divided into two areas. In the first one, all of the raw material arriving at the factory undergoes a preliminary analysis called *Inspection Control*. Here one decides whether the raw material ought to be inspected or not. Raw material not requiring inspection is allowed straight into the factory. Raw material which requires inspection follow on to the second area. In this second area, called *Inspection Selection,* one decides if the lot must be inspected, so that defective pieces are replaced by perfect ones (*rectifying inspection*), or if the lot analysis is to decide only whether the lot will be released for use or returned to its supplier (*inspection for acceptance*).

For the purpose of this study, quality inspection is regarded as the process aimed at determining whether a given piece, sample or lot complies with pre-established quality specifications [1]. Thus, inspection evaluates the quality level of a certain part or a set of pieces, comparing each piece or each piece with a pre-determined standard. The inspection aims essentially at providing a diagnosis of the product in terms of its quality level [2]. Such a diagnosis is always centered upon the quality characteristic, which consists of each and every elementary property that the product must possess in order allow it to work at full compliance with its project as well as with the function it was designed to perform.

It can be seen that in both areas there are decisions related to raw materials flow. In the first case, such decisions have to do with sending the raw material straight to the assembly line or to an inspection process. In the second case, these decisions involve (1) allowing the lot in the assembly line, now as the result of an inspection process, or (2) returning it to the supplier. For each case, we have developed and applied an Expert System to make the decision required.

0-7803-5489-3/99/$10.00 ©1999 IEEE.

INSPECTION CONTROL AREA

The basic decision in the first raw material reception area involves the establishment (or not) of the necessity of a given raw material that has just arrived to be inspected. In order to make decisions in this area; a Decision Support Expert System was developed which determines the most suitable choice as regards whether or not the development of inspection procedures for materials received is in fact necessary.

The Expert System in question makes use of a basic study previously developed to determine if inspection is really justifiable for some pieces or specific situations. This question stems, first and foremost, from what the inspection is intended to – fundamentally, it provides a diagnosis of the process, detecting defects, identifying situations of non-compliance, analyzing cases of non-fulfillment of basic functioning requisites and also carrying out particular evaluations of the product's quality characteristics along its different manufacturing stages.

The concept underlying the Expert System is simple. In general terms, inspection is deemed justifiable if fits within a broader process, being thus seen as a simple support activity. Rendering it adequate to control strategies or to the process evaluation methodologies will then be essential to determine whether it must be carried out or not.

Carrying out an inspection is justifiable only after the criterion exposed above has been attended to, e.g., that the inspection fits within a broad quality evaluation process, so that its results can be analyzed and taken into consideration when the general actions of the Quality System are defined.

The objectives of the inspection ought to be simultaneously considered with this general criterion. If what we seek is only suppliers' quality evaluation, inspection may not be the most appropriate means of obtaining such information, since it provides more specific considerations and emphasizes particular aspects of pieces. However, a whole group of inspections duly put together and analyzed could serve that purpose – which would not be true for individual inspections.

Together with these broad guidelines, sometimes rather generic, other more specific aspects can be taken into account. Such considerations, in complete accord with the general criteria described above, show well-characterized practical situations, although likely to be found in a large number of products and processes in which inspection is highly recommended and others where it simply is not reasonable to carry it out.

Inspection costs in view of the importance of a given piece is one of such aspects. If inspection cost is too high, inspection is not justifiable. In this case, control could be carried out by some activity subsequent in the productive process or by testing a given set including the piece in question. A combined analysis would thus compensate high inspection costs of individual items.

A related aspect has to do with the cost of the unsatisfactory product. If this cost is exaggerated, inspection should be carried out. Otherwise, it should probably not. Whenever the raw material immediate use phases involve covering operations or alterations on face or external features of the piece, inspection is justified. In more general terms, if the following operation in the process is of extreme importance for the product, inspection is required.

There are cases where inspection is necessary to perform essential tasks related to raw material analysis. This happens when inspection is used for classifying pieces, for instance. The same situation takes place if the product has many characteristics to be controlled. On the other hand, inspection ceases to be relevant if rejection of the product does not interfere with the disposition of using it. In this case, testing the product is not justifiable if such an evaluation results in no change on its effective utilization. It is practically the same as making no use of the inspection results. If such results are not taken into consideration, there is no reason for us to get them and, hence, no reason for us to carry out the inspection.

The inspection can still be considered within the context of the productive process as a whole. We may choose not to proceed with an inspection where the supplier's history shows a high performance or where

techniques of Statistical Control of Processes determine that the productive process is under control, having full compliance with the specifications of the project [3]. In such cases, if the capability value of the process is reliable and meets the specifications of the piece, inspection may, at least, be mitigated. However, if the evaluation of a supplier's previous data reveals a proneness to produce defects that become more serious in the following phases or simply propagate along them, inspection is then recommended.

In view of the specificity observed, we have detected the need of designing a Decision Support Expert System which makes possible to determine the best option to be adopted in a given situation, where it becomes necessary to decide effectively whether or not an inspection should be carried out. This is the aim of the present system, which compares the benefits and restraints of carrying out an inspection at this point in the process and defines the posture to be adopted. It is noteworthy the fact that in other areas of Quality Management, Expert Systems have been used successfully [4,5].

FLOW CONTROL SYSTEM 1

This is an Expert System based on rules, having 66 rules and 30 qualifiers. The system can list all the qualifiers as well as the rules in which the choices were used. In this case, the choices appear in all the rules used for the decision. The decision of the Expert System has to do with carrying out or not the inspection. The scale of values used by the system is made up of (integer) values ranging from 0 to 10. The adequacy of the option chosen is made evident when values close to 10 are given to it; its inadequacy is characterized by values close to 0. All the rules possible are deployed in deriving data for the selection of the most suitable choice. The system does not show the rules while they are being used. Notwithstanding, the user may alter this option. As an example of a rule we have:

(Rule 24)
IF rejection of a product precludes its use,
THEN Inspection should be carried out – Probability: 9/10.
THEN Inspection should not be carried out – Probability: 1/10

As an example of a qualifier we have:

(Qualifier 21)
The immediate phase of use of raw material
(1) is costly because it uses expensive materials;
(2) is irreversible;
(3) implies high execution costs;
(4) does not have special characteristics

Most of the rules have bibliographical references, providing them with a conceptual background. Some rules also have explanatory notes as to their formulation or concepts therein included. The system is made up of 5 basic areas involving analyses related to the nature of the inspection, of the product, of the process and of the lots, as well as a quality level analysis of the process. In broad terms, each area involves the following aspects, amongst others: (a) As to the nature of the inspection: inspection cost levels in view of the importance of the piece; inspection efficacy level; general objectives of the inspection; nature of the tests for carrying out the inspection; effects of the inspection on specific phases of the process; defect occurrence possibility; necessity or convenience of classifying the pieces; (b) as to the nature of the product: characteristics of the product to be controlled; consequences of rejecting a defective product; cost of products non-compliant with the project; relation between defect occurrence and manufacturing phases of the product (e.g. probability).

INSPECTION SELECTION AREA

The raw materials which Area 1 Expert System released will be forwarded straight to the assembly lines without inspection. The others will be submitted to a new Decision Support Expert System which determines the most suitable choice in the case of a decision between quality inspection only for acceptance (or rejection) of raw material lots, and quality inspection for lot rectification.

It is worth pointing out that the decision here involves the purpose of the inspection, i.e., it can be sorted out into two types: lot inspection exclusively for acceptance (or rejection) and inspection for correction for upgrading the quality level of a given lot, therefore altering its value. The first case consists of inspection for acceptance – inspection is aimed only at detecting defective pieces in a lot to determine whether the lot should be accepted in its completeness or rejected, considering thereto maximum values of those defective pieces. Thus, this type of inspection is limited to accepting or rejecting the lot based on the analysis of a sample taken from it. Acceptance implies releasing the lot for use; rejection means that it should be returned to the supplier. This type of inspection is called 'inspection for acceptance', since it consists only of an evaluation in order to determine what to do with the lot – accept it (which means its habilitation for effective use in the factory) or reject it (which means returning it to its origin, i.e., returning the lot to the supplier).

The second type involves rectifying inspection. If we do not want to return the whole lot, we may carry out an inspection aiming at replacing defective pieces by perfect ones. In this case, we work on a sample of the lot initially. Each defective piece found in the sample is replaced by a perfect piece. If the number of defective pieces is lower than a given limit, the lot is then accepted and released for use. Here, only those defective pieces from the sample were replaced. If, however, the number of defective pieces should exceed of a pre-established limit, then the whole lot will be inspected with replacement of all the defective pieces by perfect ones. This is what we call *rectifying inspection.*

There is a fundamental difference between these two types of inspection. Inspection for acceptance determines the quality level of the lot, but it does not go any further than that, whereas rectifying inspection, in addition to determining the quality level, makes it better by means of replacement of defective pieces by perfect pieces. Of course rectifying inspection shows the same problems as a complete inspection, i.e., there is no guarantee that all the defective pieces, whether from the sample or, in case of rejection of this sample, from the whole lot, will be effectively detected and replaced.

Therefore, it is said that rectifying inspection tends to improve lot quality, although it is not guaranteed that at the end of the rectifying process the lot will have a 0% rate of defective pieces. This happens because of both considering the situation in which the samples were accepted (in this case the rest of the lot has not been analyzed), and observing the natural practical difficulty to detect all of the defective pieces of the lot (in those cases of rejection of the original sample).

FLOW CONTROL SYSTEM 2

It consists of an Expert System based on rules, having 47 rules and 22 qualifiers. The characteristics of the system are the same as those of system 1. Thus, for instance, the system can list all the qualifiers as well as the rules where they are being used. It can also show all the rules in which the choices were used. In this case, the choices appear in all the rules used for making the decision. There are two options for decisions here: Inspection for Acceptance or Rectifying Inspection. Here too the adequacy of the option chosen is made evident when values close to 10 are given to it; its inadequacy is characterized by values close to 0. As an example of a rule we have: ***IF*** there are perfect pieces in stock and at low cost, ***THEN*** Inspection for acceptance – Probability: 2/10; Rectifying Inspection – Probability: 7/10 (Rule 25). As an example of a qualifier we have: The inspection is carried out in terms of (1) raw material from various suppliers and easily available; (2) raw material from various suppliers and of difficult availability; (3) raw material from exclusive suppliers (Qualifier 28). Like the previous system, most of the rules have bibliographical references, providing them with a conceptual background. Some rules also have explanatory notes as to their formulation or concepts therein included.

The system is made up of 4 basic areas involving analyses related to the nature of the inspection, of the process and of the lots, and it also takes into account the suppliers and raw materials. In broad terms, each area involves the following aspects, amongst others: (1) As to the nature of the inspection: role played by the inspection in the quality of the process; actions resulting from the inspection; general objectives and emphasis given by the inspection; scope of the inspection in relation the productive process; areas of action

of the inspection; (2) as to the nature of the process: evaluation of the supplier's average quality level; general characteristics of production planning and control; stocking structure; (3) as to the nature of the lots: relation between lots and samples; use of lots of pieces after the quality evaluation decision; (4) as to suppliers and raw materials: relationship with suppliers in terms of quality control of the lots purchased and raw material reposition levels.

PRACTICAL APPLICATION

The Expert Systems were deployed in four wall tile factories in 24 material reception situations. Altogether, 56 decisions had to be made. A group of *'experts'* monitored the decisions made by the system (these experts were in fact 5 students from of the graduation programs participating in a technical training at the company and 7 employees of the company working as supervisors and involved with raw material reception). They considered 53 decisions to be correct, 2 mistaken decisions were make in system 1, which did not come to be problematic, since the system requested an inspection and this decision could be left out – costs were raised, however without problems to the use of raw material in the factory. There was still 1 mistaken decision in system 2 where, according to the cost of the stock of perfect pieces, inspection for acceptance would have been more appropriate.

CONCLUSION

In view of the results obtained with the experimental implementation of the systems, they were considered to be adequate to the various cases studied. It is important to remark that in some situations the systems were tested at specific moments where, due to the characteristics considered, a certain result from the processing was expected. The decision previously determined was the same made by the system in all the cases studied (there were 14 cases within this context and 14 correct decisions).

According to the results of the application of the Expert Systems, a list could be drawn of a series of actions complementary to the inspection, which make possible to optimize the operation of the quality evaluation system as a whole. Such operations are determined by results reached in the two systems described above.

Evaluation of the application of the system can still be carried out by monitoring the results of their successive applications. Experimental implementations show that their decisions alter according to well-defined factors. The change in the results is, thus, always due to such alterations, which can and must be monitored, because they indicate situations requiring control – almost always preventive.

Tests carried out on the operation of the system showed that their sensitivity is high and that their results can be altered with slight changes in the decisions made as an answer of the qualifiers. This approach, however, could be impaired, should the whole system be reprocessed, which would result in efficiency loss. But it does not happen, since in the operation of the system there are devices which allow to alter only some qualifiers. The systems stores the previous result as well as all the decisions made. The system shows the new results, making possible to compare both sets of solutions. From the evaluation of the answers offered in the twofold processing and the comparative analysis of the results come the information to determine the actions to be taken. Additionally, by using the *WHY'* device the direction being given to the analysis by the system can be observed and so can the elements being stressed.

Shortly, the testing of the effect that changes on the entry data have on the results is thus developed: selections in some qualifiers are altered and the others remain unchanged. Next, data are processed according to this new situation and the effect of the changes is observed in the final result. The value of the previous decisions is kept in a record for comparison purposes with the new values. This procedure has yet an extra advantage: decisions taken in the qualifiers can be created and analyzed based on the results obtained. We can, thus, determine the relevance (relative weight) of a decision in obtaining a result and give it more or less emphasis, according to its influence on the processing of the system.

Here is a simple example. In the operation of System 2, inspection for acceptance is indicated for lots of a certain supplier. In this case, having reposition stocks is unfeasible and, by applying rule two of the system, building such stocks is deemed costly. This factor, together with others, determines inspection for acceptance. A change of supplier was, however, processed and now the pieces are bought from a place much close to the company. In accordance with a legal contract, the new supplier keeps available stocks of reposition pieces. So the defective pieces are quickly replaced. Additionally, it is worth mentioning that, based on this, it is possible to equip control procedures with means to change the final quality of the lots inspected. Thus, rules 1, 3 and 12 have their options altered, i.e., new decisions are made for the corresponding qualifiers. The system then starts to recommend rectifying inspection, altering its original proposal. It becomes clear that the new situation offers undeniable advantages over the previous one; nevertheless, its use was convenient only because some working conditions of the productive process varied.

The monitoring of these alterations by the Expert System allowed the change of lot evaluation procedures with evident benefits for the company. It also highlighted the benefits of the application of intelligent processes of decision for the control of the raw material flow of the company.

REFERENCES

1. Aft, L. S. 1996. Industrial Quality Control. Reading, Addison-Wesley.
2. Cullen J. & Hollingum, J. 1987. Implementing Total Quality. IFS Publications. NY, Springer-Verlag.
3. Tenner, A. R. & DeToro, I. J. 1992. Total Quality Management. Reading, Mass. Addison- Wesley.
4. Dagli, C. H. 1990. Expert Systems for Selecting Quality Control Charts. USF Report. P. 325-343.
5. Dagli, C. H. & Stacey, R. 1988. A Prototype Expert System for Selecting Control Charts. Int. Journal of Production Research. 26(2), 987-996.

Fuzzy Systems I

Industrial Applications of Fuzzy System Modeling

I.B. Turksen

Information Intelligent Systems,
Department of Mechanical and Industrial Engineering,
University of Toronto, Toronto, Ontario, M5S 3G8 Canada
Email: turksen@mie.utoronto.ca

ABSTRACT

Aggregate industrial system behaviour models can be built with fuzzy data mining provided historical system behaviour data is available from system databases. Given the input-output data vectors, a unified system modeling approach can be used to extract "hidden rules" of system behaviour using fuzzy technology. In particular, fuzzy cluster analysis could be used with unsupervised learning to extract fuzzy set membership function and the fuzzy rule structures. A parametric reasoning method combined with supervised learning with minimum error criteria could determine combination operators. This eliminates the arbitrary choice of t-norms and t-conorms that are required in the execution of approximate reasoning algorithms. Examples include continuous caster scheduling in steel making with criteria of minimum tardiness and minimum mixed grade steel production. As well as, this methodology could be applied to pharmacological analysis of experimental data for alcohol dependence, lithium retention and sertraline influence on alprazolam, etc.

INTRODUCTION

The motivation of this paper centers on the need to provide a management team of experts with an aggregate system modeling, analysis diagnosis prediction, and decision support and hence an overall view of the operating conditions for an industrial system and its behaviour patterns under the current structure of operating procedures. The *hypothesis* is that generally the actual structure of the operating rules are **hidden** due to complex interactions of a large number of variables and various procedures implemented by managers that affect the performance measure(s).

Furthermore, it is *hypothesized* that such interactions are not well describable in a crisp way and that such interactions generally demonstrate highly non-linear and fuzzy patterns that can be elicited via fuzzy system structure identification. It should be noted that in complex systems there are at least two categories of variables: (1) those that are objectively measurable and have a direct impact on the operations, for example, once a schedule is fixed in a steel plant, width of continuous casting strand must be adjusted to various customer order specifications, etc., and (2) those that are subjectively measurable and have an indirect but definite influence on the system activities such as the sequence of operations, for example, the priority of the customer orders, etc. Hence, the interactions of these two categories of variables together with the procedures with which they are implemented by the managers are rather complex and appear to be highly non-linear.

Therefore, for the analysis of systems, our *goal* is to propose a fuzzy system modeling approach that would identify the structure of **hidden** rules which would select important variables and their fuzzy patterns as well as their connectives that affect system performance measure(s) via supervised and unsupervised learning techniques where appropriate. Such system models would serve two purposes: (1) an identification and an assessment of critical bottle-neck variables that may be subject to change and modification to improve the efficiency and effectiveness of a given capacity of productive activity, and (2) prediction(s) of a performance measure indicator(s) for given customer orders under the current operating rules of scheduling procedures., and (3) managerial short and long term policy analysis and potential re-engineering suggestions to improve system performance measures. Naturally one would ask whether such system models might not be developed by classical statistical partitioning methods such as principle component analysis, multi-variate regression analysis, etc. Clearly, the advantage of fuzzy system modeling to be

0-7803-5489-3/99/$10.00 ©1999 IEEE.

proposed here are that: (1) fuzzy knowledge representation techniques allow the extraction of highly complex interactions of input variables and their effect on the output variables. That is, fuzzy information granules and their fuzzy membership functions provide us with many-to-many correspondence with varying gradations which can represent complex fuzzy patterns of interaction amongst input variables and their effects on the output variables; and (2) fuzzy inference techniques allow reasoning with fuzzy knowledge representation for crisp or fuzzy input patterns via forms of generalized reasoning methods such as generalized modus ponens, etc., and hence an assessment and prediction or forecasting of system performance measures for new customer orders.

On the other hand, it should be noted that there are certain disadvantages to, for example, multi-variate regression models which require certain assumptions, such as: (1) linearity and additivity, (2) model structure, i.e., the order of the polynomial, (3) normality and same variance, etc. Fuzzy system models do not require such assumptions to be made at all.

That is, fuzzy system models would depict and demonstrate non-linear and complex interactions in a flexible and robust manner amongst system variables and represent their trade offs more clearly as well as forecast performance measure indicators under current operating conditions.

In Section 2, the theoretical and technical aspects of the structure of fuzzy rule base is outlined briefly. In Section 3, we present the aggregate scheduling analysis in continuous casting, with its rules, and fuzzy patterns of variables in the rules in order to highlight the analyses of complex interactions of variables that affect the performance measures, of a caster scheduling such as (1) customer order's tardiness (2) mixed zone tonnage productions which is complementary to the tardiness measure and (3) a higher order performance measure that attempts to balance the interaction of tardiness and mixed zone.
Conclusions are presented in Section 4.

FUZZY SYSTEM MODELING PARADIGM

The proposed fuzzy system modeling approach has two main modules: (1) knowledge representation and (2) approximate reasoning. The knowledge representation module is based on a modified and improved fuzzy c-means algorithm which is an extension of classical FCM algorithm in several respects. The knowledge representation is developed with an unsupervised learning with respect to a given input- output data set and three parameters of fuzzy clustering. The approximate reasoning module contains four reasoning parameters that are subject to supervised learning for a given input-output data set and error minimization criteria.

Knowledge representation is formulated with a structure identification technique that first elicits output patterns in terms of fuzzy clusters, then relates them to the input variables' fuzzy clusters and hence leads to the formation of fuzzy rules in **IF...THEN** patterns [13-18]. Fuzzy clustering algorithm has three parameters: (1) Order or **level** of fuzziness, m 0 [1, 4] that identifies the optimal level of fuzziness between the crisp and infinitely fuzzy representation; (2) the number of fuzzy clusters, c 0 [2, ..., 20]; and (3) the location of fuzzy cluster centres. As a result, the structure identification consists of the rule generation activity which has three sub-modules: (1) output and input clustering, (2) input and output membership function assignments, and (3) input selection.

The approximate reasoning module has four parameters (1) two parameters p and q are associated with (a) the t-norm for the **AND** connective of the antecedents, i.e., input variable clusters, and (b) the t-norm or t-conorm of the **IMPLICATION** connective, depending on the type of implication that is to be chosen, that dictates the impact of inputs on the output variable, i.e., the consequent, respectively; and (2) two other parameters β and α are associated with: (a) the combination of alternative reasoning methods, and (b) the power of the generalized defuzzification method, respectively. These four parameters are identified with a supervised learning algorithm based on a training data set in order to minimize the error of the model with respect to either the actual system output measure or a desired system output measure. These four parameters will be discussed further in detail in the subsection below. The technology is based on our theoretical studies [13-18].

Therefore, it should be noted that fuzzy system modeling depends on (1) unsupervised learning with an input-output data set without requiring the acquisition of human expert knowledge and (2) supervised learning of the **AND**, conjunction, and **IMPLICATION**, IF .. THEN, operators with respect to an error minimization of a performance measure indicator without any requirement of the selection of these operators *a priori*.

In summary, training data determines: (1) the structure of the system knowledge, via the extraction of **hidden** patterns with unsupervised learning, and (2) the interaction of these **hidden** patterns by specifying the parameters of connectives and weighting of alternate reasoning methods and alternate defuzzification techniques with supervised learning.

AGGREGATE SYSTEM ANALYSIS

In this section, we present, the key issues of aggregate system analysis of a continuous caster scheduling system in a conceptual framework based on the technical foundation of fuzzy system modeling **paradigm** outlined in Section 2 above.

In this framework, we deal with, very briefly; (i) representation of the system, (ii) analysis and diagnosis of it, and (iii) prediction of performance.

The representation of system is made with structure identification techniques which include (i) fuzzy cluster analyses of the output, (ii) projection of the output clusters into input space, (iii) identification of input clusters, (iv) formation of input and output membership functions, (v) selection of significant input variables and their clusters, and finally (vi) the determination of **IF... THEN** fuzzy rules that expose the **hidden** behaviour of the system.

Essential to this is the identification of fuzzy information granules. As depicted in Figure 1, given a scatter diagram, we have the option of determining fuzzy information granules with fuzzy clustering techniques or fitting a non-linear curve with multi-variate regression techniques. We choose to represent our knowledge about a scatter diagram with fuzzy information granules simply because as pointed out earlier, we do not have to make assumptions of linearity, additivity, normality, same variance, etc.

In this manner, we identify fuzzy information granules of each variable that affect the performance measure in combination with all input variables and their information granules.

As a result, four major **hidden** rules were discovered for the tardiness measure. For example, one of the rules shows how **low** tardiness measure may be obtained when the indicated information granules of the input variables interact in a non-linear manner. The analysis of this rule, for example, indicates that the tardiness of customer order delivery due dates will be **low** when **low to moderate** priority and **very low to moderate** grade transition penalty and **somewhat high** customer order widths and **somewhat high** minimum slab widths and **somewhat average** maximum slab widths and **more or less average** qualities and **very low and low** customer order widths and **very low and low** number of slabs that are required per order and **average to large** slab weights interact together.

Further analysis show that the critical variables in the investigation of tardiness measure.are:

(i) maximum width of slabs
(ii) quality of products
(iii) customer order weights
(iv) weights of the slabs

In a similar manner, five major rules were discovered for the mixed zone tonnage production. In the mixed zone tonnage analysis, the critical variables are:

(1) *phosphors*, (2) *sulfur*, (3) *aluminum*, (4) *nitrogen*, (5) *tundish start weight*, (6) *tundish end weight*, and (7) *average casting speed.*

Finally a combined analysis of tardiness and mixed zone measures produced eight **hidden** rules. The investigation of the rules show that **low** cost of balancing tardiness versus mixed zone production could be achieved when **very low to somewhat low** grade transition penalties are combined with **average to somewhat large** maximum slab widths and **high** quality and **low** customer order weights and **low** number of slabs and **somewhat low** carbon and **very low to low** *Mn* and **very low** *P* and **somewhat low** *S* and **low to high** *Si* and **low** *Ti* and **average** tundish start weights and **average** of average casting speeds.

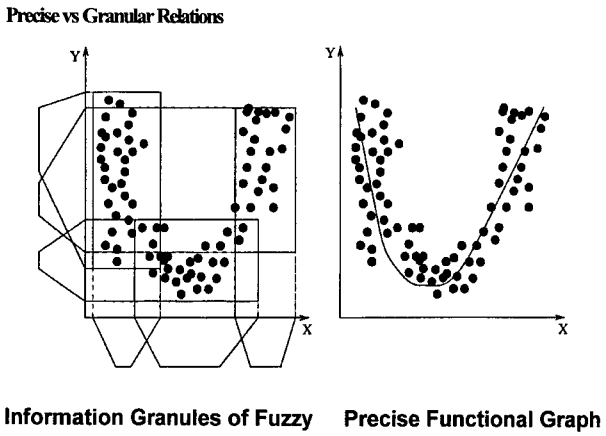


Figure 1. Formation of Fuzzy Information Granules, vs., multi-variate regression-curve fitting

COMPARISON WITH REGRESSION MODELS

In order to compare fuzzy system model, we modeled the same data sets with multi-variate regression techniques It is to be observed that in the tardiness regression model customer order widths and minimum slab widths are excluded from the model. In the mixed zone regression model no variable is considered to be significant. Further analysis of the results reveal that the standard deviation of residuals (errors) of multiple regressions is 14.69 that the fuzzy model is 3.9 in the tardiness model analyses. In the mixed zone tonnage analyses, while the standard deviation of residuals (errors) of multiple regression is 14.86 that of the fuzzy model is 4.33.

On the basis of these results, it is concluded that fuzzy system modeling gives low prediction errors, hence fuzzy system models are better representation of **hidden** system behaviour.

REFERENCES

1. Bezdek, J.C., Windham, M.P., Ehrlich, R., 1980. Statistical parameters of cluster validity functional. International Journal of Computer Information Science, 9(4): 324-336.
2. Bezdek, J.C., 1981. Pattern recognition with fuzzy objective function algorithms. Plenum Press, NY.
3. Duda, R.O., Hart, P.E., 1973. Pattern classification and scene analysis. John Wiley and Sons, Inc.
4. Emami, M.R., Türksen, I.B., Goldenberg, A.A., (1996) An improved fuzzy modeling algorithm, Pt. I: inference mechanisms. Proc. NAFIPS'96, Berkeley, CA: 289-293.
5. Emami, M.R., Türksen, I.B., Goldenberg, A.A., 1996. An improved fuzzy modeling algorithm, part II: system identification. Proceedings of 1996 Biennial Conference of the North American Fuzzy Information Processing Society-NAFIPS: 294-298.
6. Fukuyama, Y., Sugeno, M., 1989. A new method of choosing the number of clusters for fuzzy c-means method. Proc. 5th Fuzzy Systems Symposium (in Japanese) 247-250.
7. Kandel, A., 1982. Fuzzy techniques in pattern recognition. Wiley, New York.
8. Kaufman, L., Rousseeuw, P.J., (1990) Finding groups in data. Wiley, New York.
9. Keller, J.M., Gray, M.R., Givens, J.A., 1985. A fuzzy k-nearest algorithm. IEEE Trans. Systems, Man. and Cybernetics SMC-15(4): 580-585.
10. Kosko, B., 1997. Fuzzy engineering. Prentice Hall, New Jersey, U.S.A.
11. Nakanishi, H.,Türksen, I.B., Sugeno, M., 1993. A review and comparison of six reasoning methods, fuzzy sets and systems 57: 257-295.

12. Slany, W., 1996. Scheduling as a fuzzy multiple criteria optimization problem. Fuzzy Sets and Systems, 78: 197-222.
13. Sugeno, M, Yasukawa, T., 1993. A fuzzy-logic based approach to qualitative modeling. IEEE Trans. Fuzzy Systems 1(1): 7-31.
14. Türksen, I.B., 1986. Interval-valued fuzzy sets based on normal forms, Fuzzy Sets and Systems, 20(2): 191-210.
15. Türksen, I.B., 1995. Fuzzy normal forms, fuzzy sets and systems 69: 319-346.
16. Türksen, I.B., 1995. Type 1 and interval-valued Type II fuzzy sets and logics, in: P.P. Wang, Advances in Fuzzy Theory and Technology, Bookright Press, Raleigh, NC 3:31-82.
17. Türksen, I.B., 1996. Fuzzy truth tables and normal forms. Proceedings of BOFL'96, December 15-18, 1996, TIT, Nagatsuta, Yokohama, Japan: 7-12.
18. Türksen, I.B., 1996. Type I and Type II fuzzy system models. Special Issue, FSS.
19. Ward, J.H., 1963. Hierarchical grouping to optimize an objective function. J. Amer. Stat. Assoc. 58: 236-244.
20. Yager, R.R., Filev, D.P., 1994. Essentials of fuzzy modeling and control. John Wiley and Sons.

From Intelligent Models To Smart Ones

Heikki Hyötyniemi

Helsinki University of Technology
Control Engineering Laboratory
P.O. Box 5400, FIN-02015 HUT, Finland

ABSTRACT

The "intelligent" modelling methods may perhaps not be the ultimate solution. This paper discusses the new questions that have emerged after the introduction of the modern soft computing methods, and proposes a framework for attacking the new problems.

INTRODUCTION

The field of "computational intelligence" can today be seen in a perspective. It seems that the new modelling methods, neural networks or fuzzy systems, are sometimes applied without even thinking of the other, more traditional alternatives. The tool has become more important than the application itself. However, in modelling, the primary task is to capture the properties of the real-life process in the best possible way; the tool for accomplishing this should be selected accordingly.

The "intelligent" techniques promise to make the modelling task transparent to the user, and that is why they have been eagerly waited for by practitioners tackling with complex processes. When applying the new methodologies, the normal procedure that is followed is to take one of the general-purpose soft-computing algorithms and apply it as any of the other "off-the-shelf" tools. Multi-layered feedforward perceptron networks, for example, have been shown to be capable of representing any smooth function – assumedly they can be used also as a model for the process at hand. However, from the point of view of process modelling, there are two main problems with the concurrent soft-computing methodologies:

- First, they seem to be *too* powerful; to constrain the number of alternative behavioural patterns in the network the number of training data samples that is needed grows exponentially as a function of the free parameters (the models do not "scale up"; whereas modelling in a toy domain can be carried out, in a more complex environment problems soon become overwhelming).
- Second, no *structure* emerges in the training process; the trained network (or the conventional compiled fuzzy rule set) is just a numerical mapping from input signals to output signals.

he role of structure is of utmost importance in intelligent modelling. When huge industrial processes with thousands of simultaneous measurement signals are being monitored, a tool that is capable of extracting the underlying relationships between the data samples may help the human expert to gain some intuition or understanding of the process structure. This "understanding" is the key towards truly intelligent-looking modelling results.

In this paper, the current modelling paradigms are reviewed from the above points of view. As a conclusion, a unified framework is proposed.

ABOUT "SMART MODELS"

The role of a model is to capture system behaviour in a compact form to facilitate analyses and applications. This dual role is a delicate matter: constraints come from two directions, and compromises are needed (see Fig. 1).

0-7803-5489-3/99/$10.00 ©1999 IEEE.

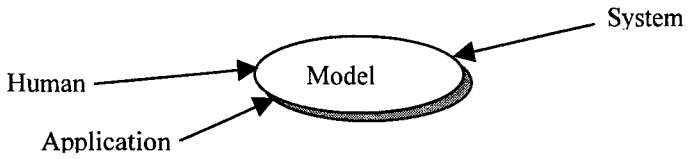


Fig. 1. The role of the model as an "interface" between the system and the outside world. The model should match the properties of the system, and, simultaneously, it should match the needs of the humans (or further applications) that use the model.

Constraints *From Below*

First, study the boundary conditions that are determined by the system to be modelled. To look even remotely smart, the modelling tool must support the structure of the system. There is a problem, though – to support the structure of a specific application, the model should be tailor-made, and so, the generality has to be sacrificed. The solution to this problem is to exclude system structure in the kernel of the model, and rather, to design the model structure so that structural properties of the system can be easily implemented in that framework. The question then arises, "what kind of structural features are to be supported?" We want to restrict ourselves, to the absolute minimum complexity to achieve easy use (trainability and analysability, as discussed later). Loosely speaking, this can be expressed as: the structural properties to be supported need to be "enumerated" or "parameterised".

It is clear that as a starting point, *linearity* of the model structure is a good first approximation: Often linear models are at least locally valid and they have strong theory.

In addition to selecting a linear model structure as the general framework, the domain-specific system structure must be captured. To reach this, families of functional nonlinearities that are encountered in a complex process must be detected. There are also nuances to be recognised also in what is apparent in strictly linear systems. It is assumed that the *basic types of behavioural patterns* that are typically found in complex real systems are the following:

- *Data clusters* are caused by the underlying system alternating between essentially different internal structures each of them having a local dependency structure between the variables. Take the *flotation process* (for example, see [1]) as an example: ore coming from different mines have varying mineral contents, and the process behaviour changes accordingly. Similarly, different control strategies may result in different clusters in the data. There is no real continuum between the clusters.
- *Continuous nonlinearities* are common in practical systems. However, the nonlinearities are normally smooth, so they are locally linearisable. This way the need to cover an infinite number of non-linear behaviours can be avoided.
- *Independent components* are hidden variables that define mutually non-orthogonal subspace directions within linear data. In flotation data for example, the independent subspace directions in the data can be determined by the different process inputs: control actions result in characteristic responses in the process variables. The different control signals may have partially overlapping effects; that is why the subspace axes are not orthogonal.

It should to be mentioned that modelling problems only become acute in really large systems. In toy domains, all methods can be made to work, however fancy they are and no matter how high their computational complexity. In real environments, the data are *high dimensional*. This high dimensionality is, of course, caused by the large number of measurements, but this is only one part of the story. When complex phenomena are recorded, the information is often delivered in different formats – there may be image data, qualitative measurements, etc. When this kind of *multimodal* information is processed, it first must be coded as real numbers so the problem of data heterogeneity is converted to one of high dimensionality. The modelling tool must be insensitive to the large quantity of data and the high amount of poorly-preprocessed data also means that some are badly conditioned – there may exist collinearity among the measurements, and irrelevant data may exist.

It turns out that the above assumptions about *data ontology* offer powerful conceptual tools to mastering complex systems.

Constraints *From Above*

An equally important aspect about the value of a model is how it looks from the outside. There are also various aspects to take care of – for example:

- *Model applicability* is important if something such as prediction or control is to be implemented. The model structure should be flexible; from a control engineering point of view, for example. A very basic need is that input-output relationships can be represented.
- *Efficiency* in terms of training time needed to fix the model parameters is an essential practical factor. Another practical value of the model is its *robustness* or *consistency*, i.e., how reliable is the training method; will the results be the same if the training process is repeated?
- *Comprehensibility* reveals how well the model and the training results can be interpreted in a form that is understandable to a human. A*nalysability* is another facet of the same transparency objective: a good model makes it easy for mathematical tools to operate on the data structures.

Whereas most of the above criteria are strictly technical, the comprehensibility objective is crucial from the point of view of artificial intelligence (AI). To be called truly intelligent, the created model must offer some added value such as new intuition to the user. Automatically-created constructs should offer a bridge from the numeric level to the conceptual level. This may sound unrealistic – but all "intelligent" methods that do not address this question, are deficient by definition!

TODAYS TOOLS

Here, some of the prototypical data modelling methods are reviewed in the above perspective. None of them fulfils all of the presented needs. What is more – none of them can be regarded as truly "intelligent".

Principal component analysis, PCA, (and its related regression method, PCR) is based on multivariate linear systems theory [2], results in an orthogonal set of mathematically-motivated hidden variables. On the other hand, independent component analysis, ICA, is a novel method developed especially to find the independent component structure [3]. The self-organising map, SOM, is a neuron-motivated clustering method that makes relationships within the data nicely visible [4]. The feed-forward perceptron networks [5] and fuzzy systems [6], denoted here as NN and FS, respectively, are perhaps the most common representatives of computational intelligence and they are also included in the comparison below.

Table 1. How the different methods address the properties of the systems to be modelled.

System property	PCA	ICA	SOM	NN	FS
Local nature of representations	−−	−	++	−	++
Continuous nonlinearities	−−	−−	+	++	++
Independent components	−	++	(−)	(−)	(−)
High dimensionality	++	−	+	−−	−−

Table 2. How the different methods address the practical issues

Objective	PCA	ICA	SOM	NN	FS
Model applicability	++	++	−	+	+
Efficiency, trainability	++	+	−	−	(−)
Robustness, consistency	++	+	−	−	(−)
Comprehensibility and analysability	++	++	++	−−	(+)

Tables 1 and 2 summarise the pros and cons of the different modelling approaches. In many cases the comparisons are difficult because the methods are tailored for different kinds of applications. However, they are sometimes advertised as a *panacea*, so perhaps some criticism is justified, after all. The parentheses in the tables mean that the properties cannot be evaluated: for example, fuzzy rule bases are normally explicitly determined, so that the criteria concerning automatic generation of the models cannot be applied. Only methods that are explicitly based on linear theory can be used for modelling independent components in the data. One '+' or '–' sign instead of two is used if only a partial solution is offered by the method; for example, SOM is especially tailored for visualising high-dimensional data, but it is necessary that there be only a few degrees of freedom, the data being distributed on a 2-dimensional manifold, etc.

SPARSITY – THE KEY?

The question that arises is how the objectives can be combined in the same framework. It turns out that a technique called *sparse coding* offers a very potential alternative. Sparsity means that the model consists of a set of simple constituents; at any time only a *subset* of all available constructs is utilised. In the sparse coding framework, it is not the total number of memory elements that are to be minimised; it is the number of simultaneously *active* elements that are minimised [7].

Assume that the underlying substructures are defined as vectors spanning *feature dimensions* in the data space, so the model becomes piecewise linear, the observation data vector f being presented as a weighted sum of the features φ_i:

$$f = \sum_{i=1}^{n} \varsigma_i \varphi_i \qquad 1.$$

To better match the data modelling needs, the purely mathematical sparse coding formulation can be slightly refined. Separate one of the selected features, so that it stands for the *operating point*, and let the other features represent "fine-tuning" around this cluster centre vector. Assume there exists n_1 alternative operating points, and out of the n_2 additional features only N are utilised:

$$f = \phi_{i\in[1,n_1]} + \underbrace{\xi_j \cdot \varphi_{j\in[1,n_2]} + \cdots + \xi_{j'} \cdot \phi_{j'\in[1,n_1]}}_{N} \qquad 2.$$

Examples

To gain some intuition, the different system properties are implemented in the sparse coding framework. In Figs. 2, 3, and 4, examples of data clusters, nonlinearities, and independent components are shown. It needs to be recognised that the low-dimensional projections of the assumedly very high-dimensional data give a trivialised view of the problem complexity.

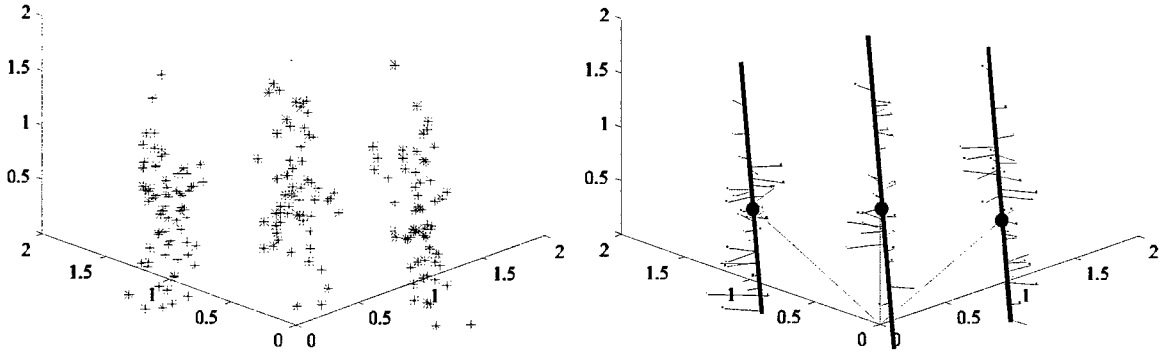


Figure 2. Clustered data; sparse model with $n_1 = 3$, $n_2 = 1$, and $N = 1$.

Let us study Fig. 2 a bit closer. If the clustered data are studied as a whole, no PCA-like data compression scheme can be applied: the data are genuinely 3-dimensional, the data covariance matrix having three approximately equal eigenvalues. The sparse model now contains four constructs ($n = n_1 + n_2$) – more than

the dimensions of the data! Seen from a traditional modelling point of view, this "inflation" of the representation is intolerable. All individual data points can, however, be represented rather accurately using only *two* constructs: the appropriate cluster centre vector and the single fine-tuning parameter.

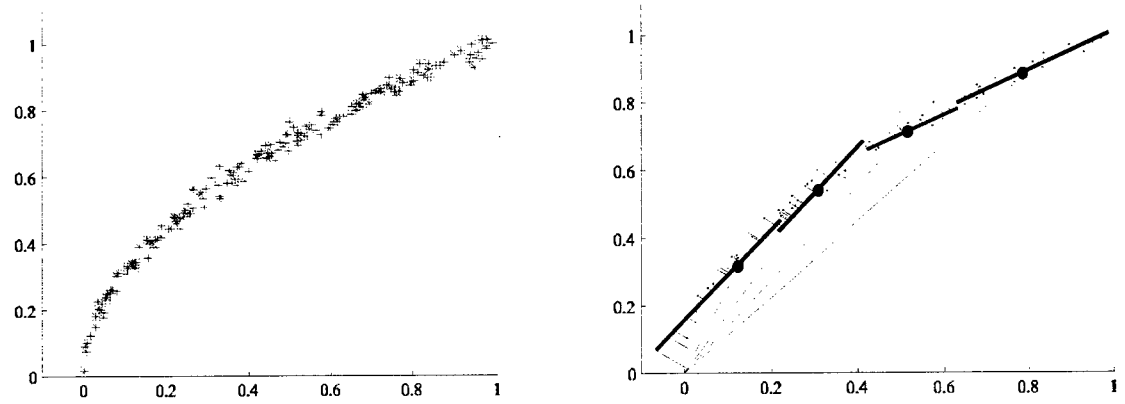


Figure 3. Nonlinear behaviour; sparse model with $n_1 = 4$, $n_2 = 2$, and $N = 1$

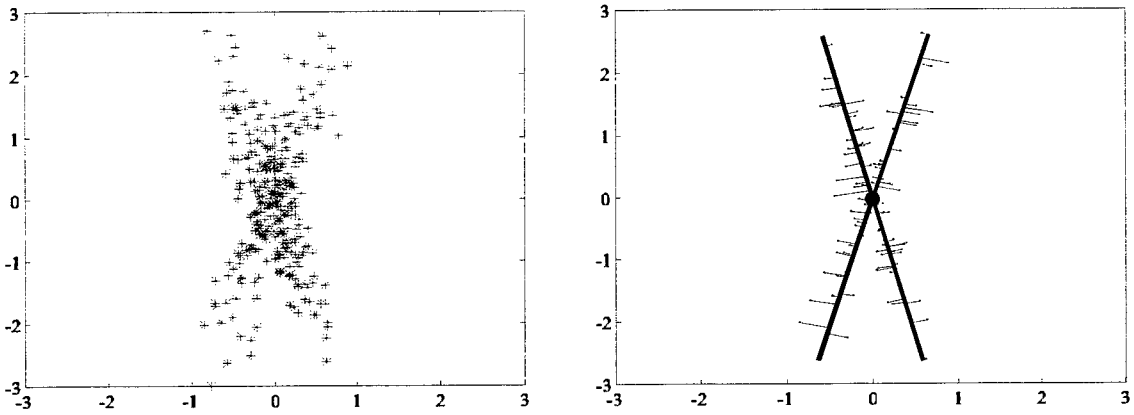


Figure 4. Independent components; sparse model with $n_1 = 1$, $n_2 = 2$, and $N = 1$

It can be said that the sparsity results in an *emergent structure*. The constructs that facilitate compact representations tell something fundamental about the underlying system. It can even be claimed that one step towards the truly intelligent model has been taken: the sparse representation of a system is "symbolic but not labelled" – the interpretation of the extracted dependency structures must be carried out separately by the human domain area expert.

DISCUSSION

Even though the sparse model is "almost" linear, it incorporates all of the assumed nonlinear phenomena; the operation of the model is linear only after the appropriate constructs have been selected. After the sparse structure is fixed, the model can be written in a matrix form

$$f = \phi_f + \Phi_f \cdot \xi(f), \qquad 3.$$

where the operating point (the cluster centre) vector ϕ_f and the matrix Φ_f containing the feature vectors are somehow, determined by the current measurement data vector f. The "generalized state" vector $\xi(f)$ can be determined in the least squares sense, as:

$$\xi(f) = (\Phi_f^T W \Phi_f)^{-1} \Phi_f^T W \cdot (f - \phi_f) \qquad 4.$$

Above, the diagonal weighting matrix W is essential: the key to generality. Formally, no output has been defined in Equations 1 to 4; all signals, no matter what their role, are coded in the data vector f. When the model is used for prediction purposes, for example, the nature of the vector elements becomes clear: the output signals are unknown, whereas the inputs can be measured. Setting the entries in W that correspond to the unknown variables to zero, they are not used for matching measurements against the model. The reconstructed f, calculated from Equation 3, reveals the "best guesses" for the unknowns; so that, *associative regression* can readily be implemented using the general model framework. The generality of the model formulation makes it possible to apply it in very different applications – for example, pattern recognition can be implemented, and *associative reasoning* systems have also been experimented with. Technical applications include, for example, feature extraction in a visual images of a flotation process [8].

A straightforward implementation of the above view is an algorithm called GGHA (Generalised GHA). This algorithm can be interpreted as an extension of PCA, being based on self-organisation and explicit sparse coding of the data [9,10]. The sparsity property makes it also possible to capture independent components (having positive kurtosis). The models in the examples of the previous section were calculated using this algorithm and the parameters n_1, n_2, and N were explicitly given.

So, finally, how well have we reached our objectives? The first class of constraints, those related to the ability to represent the system structure, are all rather nicely satisfied (this is natural since these objectives were explicitly taken as targets). Being based on linear constructs, the model structure can also meet the needs "from above" rather well. One of the weakest points is the lack of robustness; the model does not always converge in the same way. Actually, this cannot be avoided since the distinction between a cluster and a feature is not exact (this phenomenon is fundamental: when it comes to *mental categories*, we have noticed that the boundaries between classes are not clear-cut, but, rather, determined by *relevance*). For this reason the algorithms implementing the proposed view must be iterative and this may cause efficiency problems in practice.

REFERENCES

1. A. J. Niemi, R. Ylinen, H. Hyötyniemi, 1997. On characterization of pulp and froth in cells of flotation plant. Int. J. of Mineral Processing, 51, 51–65.
2. A. Basilevsky, 1994. Statistical Factor Analysis and Related Methods. John Wiley & Sons, New York.
3. T.-W. Lee, 1998. Independent Component Analysis – Theory and Applications. Kluwer Academic Publishers, Boston.
4. T. Kohonen, 1995. Self-Organizing Maps. Springer-Verlag, Berlin.
5. S. Haykin, 1994. Neural Networks – Comprehensive Foundation. Macmillan College Publishing, NY.
6. L.-X. Wang, 1997. A Course in Fuzzy Systems and Control. Prentice-Hall International, London.
7. E. Saund, 1995. Multiple cause mixture model for unsupervised learning. Neural Computation, 7, 51-71.
8. A. J. Niemi, H. Hyötyniemi, R. Ylinen, 1999. Image analysis and vision systems for processing plants. Proc. 2nd Intl. Conf. on Intelligent Processing and Manufacturing of Materials, IPMM99, Honolulu, HI.
9. H. Hyötyniemi, 1998. Automatic Structuring of Unknown Dynamic Systems. In Soft Computing in Engineering Design and Manufacturing (P.K. Chawdhry, R. Roy, and R.K. Pant, eds.), Springer-Verlag, London, 410–419. available at http://Saato014.hut.fi/Hyotyniemi/publications/97_wsc2.htm.
10. H. Hyötyniemi, 1998. Structure from Data: AI Approaches to Systems Modeling. Proc. 8th Finnish AI Conference STeP'98 (P. Koikkalainen and S. Puuronen, eds.), Finnish Artificial Intelligence Society (FAIS), Helsinki, 31–40. available at http://Saato014.hut.fi/Hyotyniemi/publications/98_step_1.htm.

A Fuzzy Design Evaluation Based on Taguchi Quality Approach

A. Donnarumma *, N. Cappetti*, M. Pappalardo *, E. Santoro **

* Dipartimento Ingegneria Meccanica , Università di Salerno, Italy
** Dipartim. di Progettazione e Gestione Industriale, Università di Napoli Fed. II, Italy

ABSTRACT

A fuzzy method to handle vagueness and imprecision in the description of requirements for multi-attribute decision making (MADM) problem is presented. This method is applied to design of an apron conveyors to collect and transfer scraps. The aggregation function for the overall evaluation is obtained utilising the Taguchi loss functions.

INTRODUCTION

The design process is essentially a decision process where a choice between different design alternatives must be performed on the basis of evaluations obtained analysing assigned characteristics, requirement, performances, etc.

In most design situation the description of some requirements, etc. is imprecise, vague or expressed in terms of linguistic concepts (expensive, heavy, reliable, etc.), therefore under such conditions it is convenient utilise the fuzzy sets for representing and manipulating such imprecision and vagueness [1,2,3].

Two important problems involve the fuzzy sets in the design process: the choice of an aggregation function for computing the overall evaluation and the construction of membership functions (m.f.) for each imprecise requirement [4].

The above problem are strongly related since both require the designer's experience and expert'judgement and their solution are high subjective.

In fact, the construction of membership functions is based on the expert'judgement and may be classified into direct and indirect methods [5]. When the designer assigns a membership value equal to one that means that there is a full degree of satisfaction of the requirement. Therefore considering the value one as target value, a deviation from a such value may be interpreted as a reduction of the design product quality. This basic idea will be utilised in this paper for defining an aggregation function which combining the deviations of each requirement will hold to compute an overall evaluation of each design alternatives.

This approach is not new since also Taguchi proposed a similar approach [6] introducing some very simple concepts, for quality control in the manufacturing industries, which should guide the designer along the design process.

He emphasised that quality is directly related to deviation of given design parameter from target or desirable values and developed more then 68 loss functions. Besides, he believed that the target value can be elicited only utilising designer experience and preference, expert'judgement, etc..

The Taguchi "loss functions" don't regard only the design parameters but also any characteristics, requirements that contribute to the designer conception of quality, since the product quality begins to gradually deteriorate as their effective parameter and requirement values deviate from the corresponding desirable (target) values.

0-7803-5489-3/99/$10.00 ©1999 IEEE.

In general many situations are described by the following quadratic loss function [7] which is called the nominal-the best

$$L_R(x) = k(Y - Y_0)^2 \tag{1}$$

where Y is the quality characteristic, Y_0 is the corresponding target value and k a quality loss coefficient. Other common loss functions are the smaller-the better and larger-the better. .

Substituting to Y_0 and Y respectively 1 and the membership value and for k=1, Eq. (1) becomes

$$L_R(x) = [1 - \mu_R(x)]^2 \tag{2}$$

which is a fuzzy complement operation, in fact $L_R(x)$ can be interpreted as the degree to which x does not belong to R.

In general the design process involves many requirements R_i i=1,..,m having unequal preference, therefore can be useful associate to each requirement R_i a weight $w_j \in [0,1]$. In a such condition an aggregation function based on the Eq. (2) for compute the overall evaluation is

$$P(x) = \frac{\sum w_i L_{Ri}(x)}{\sum w_i} = \frac{\sum w_i [1 - \mu_{Ri}(x)]^2}{\sum w_i} \tag{3}$$

The above function can be very useful for solving a fuzzy multi-attribute decision making (MADM) problem, since the design alternative with the lowest overall value will be the most "efficient" solution.

FUZZY PROPERTIES OF LOSS FUNCTION

A fuzzy complement of fuzzy set A with respect to the universe set X is defined by the function

$$c(\mu_A(x)) : [0,1] \rightarrow [0,1] \tag{4}$$

For any $x \in X$ the $c(\mu_A(x))$ value may be interpreted as the degree to which x does not belong to X. An example of fuzzy complement is the well-known standard fuzzy complement function $c(\mu_A(x)) = 1 - \mu_A(x)$. Obviously function (4) is independent of X and to produce a meaningful complements of given fuzzy set, A must possess at least the following boundary and monotonicity properties

$$c(\mu_A(x) = 1) = 0 \qquad c(\mu_A(x) = 0) = 1$$
$$\forall \ \mu_A(x_i) \le \mu_A(x_j) \quad c(\mu_A(x_j) \ge c(\mu_A(x_i)$$

An element of X for which $c(\mu_A(x)) = \mu_A(x)$ is called equilibrium point and obviously for standard complement function the equilibrium point is that for which $\mu_A(x) = 0.5$.

If a complement function satisfies also the property $c(c(\mu_A(x))) = \mu_A(x)$ is said involutive. An example of involutive fuzzy complement is the Sugeno function

$$c_\lambda(\mu(x)) = \frac{1 - \mu(x)}{1 + \lambda\mu(x)} \qquad \text{for } \lambda \in [-1, \infty[$$

We observe that the quadratic loss function (2) is a fuzzy complement function which satisfies the boundary and monotonicity properties, but it is not involutive and besides its equilibrium point has $\mu_A(x) = 0.382$.

In Fig. 1 is shown a graphical representation of a triangular membership function and the corresponding fuzzy loss function.

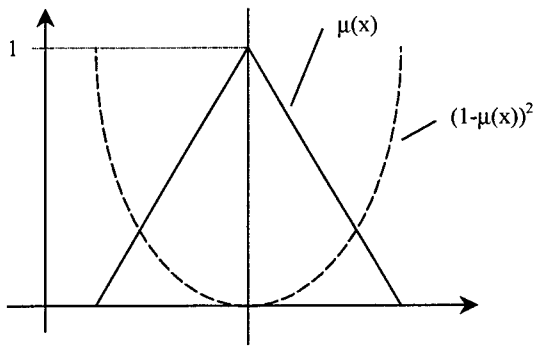


Fig. 1. Triangular membership function and corresponding loss function

APPLICATION

A metal stamping industry need some apron conveyors to collect and transfer scraps [8]. Three alternative systems with different form of conveyor plates are analysed. The systems are:

x_1 - a modular stamped plates conveyor. Two borders of the plates are bend to obtain pivot seats for joining plates and the chains. Lateral plates are welded to prevent scrap loss.

x_2 - a modular plates conveyor with welded tubes. The same of x_1 but pivot seats are welded tubes.

x_3 - a modular stamped plates conveyor. The plates are not joined between themselves but one is leaned on the following. Lateral plates are fixed with screws to prevent scrap loss. The same screws join plates to chains.

These systems are different not only for plate typology, but also for processing, materials and geometric characteristic. However all systems must work properly and satisfy, at least a bit, some functional requirements. Defining the requirements by fuzzy sets, the problem is to assign membership values to each requirement R_i. To achieve this, some industry experts were carefully selected and for each requirement the following membership functions were suggested:

R_1 - **Investment costs**: this represents the economic value of a process and the assemble of conveyor equipment. For costs within [0-50M] the m.f. is linear decreasing in [1,0.5], where 50M is the maximum value.

R_2 - **Working costs**: this represents economic operating cost of conveyor process and assembling. The membership function is defined by the an indirect method with one expert.

R_3 - **Simplicity of maintenance**: the simplicity and speed of maintenance operations are important for this requirement. The m.f. is $M(\Delta_t, \Delta_i) = p_t M_{\Delta t} + p_i M_{\Delta i}$, where $M_{\Delta t}$ and $M_{\Delta i}$ are, respectively, *the time to operation* score and *the time of operation* score, while p_i, and p_t are corresponding weights. The m.f. is expressed by an expert and shown in Table 1 (indirect method with one expert).

R_4 - **Loss of Scraps**: the main reason for scrap loss is the nominal gap G between plates since a minimal thickness of produced scrap is 0.8mm and the tolerance for all systems is ±0.2. The m.f. is 1 for $G < 0.6$, and decreases to 0 for $G = [0.6, 1.0]$ and is 0 for $G > 1$.

R_5 - **Reliability**: this m.f. is defined by an expert and shown on Tab. 2 for *attribute* = reliable.

R_6 - **Assembly simplicity**: the m.f. is defined by an expert and shown on Tab. 2 for *attribute* = simple. This requirement represents the simplicity of assembling operations.

R_7 - **Availability of materials**: the m.f. is a linear-decreasing function with respect to unavailable components since time and cost of realisation are reduced when materials to construct the system are already available.

Table. 1. :Maintenance scores $M_{\Delta t}$ and $M_{\Delta i}$

$M_{\Delta t}$	$M_{\Delta i}$	μ_3
30 days	7 minutes	1
25 days	30 minutes	0.9
20 days	1 hour	0.8
15 days	2 hours	0.7
10 days	5 hours	0.6
7 days	8 hours	0.5
5 days	1 day	0.4
2 days	2 days	0.3
1 day	3 days	0.2
Few hours	5 days	0.1
Immediately	7 days	0

Table.2. Scores for R_5 and R_6

	$\mu_{5\text{-}6}$
Very *attribute*	1
More than *attr.te*	0.9
Normally *attr.te*	0.8
Enough *attr.te*	0.7
Almost *attr.te*	0.6
Little *attr.te*	0.5
Not almost *attr.te*	0.4
Not enough *attr.te*	0.3
Not *attr.te*	0.2
Hardly ever *attr.te*	0.1
Very not *attr.te*	0

R_8 - Weight of plates: the m.f. is defined by indirect method with one expert, it is a decreasing function versus weight. When the weight of plates is high we have a big and heavy supporting structure, a high current drain of motors and consequently an increasing of costs.

R_9 - Safety: it represents the behaviour of the system when an unforeseen event occur i.e. chain block because of scrap locking or accidental load. The m.f. is $S(t, p) = p_t S_t + p_p S_p$, where S_t and S_p are traction and vertical loads scores, and p_t e p_p the corresponding weights.

Table 3. S_p and S_t scores.

No deformations	1
Elastic deformations	0.8
Plastic deformations	0.6
Probably dangerous deformation	0.4
Dangerous deformation	0.2
Fault	0

Examination of each design alternative by an expert allows the assignment of a membership value to each requirement. Moreover the experts establish the relative importance of each requirement assigning a weight in the global evaluation. Tab. 4 shows the membership values and the weights w_i. for the three alternatives.

Table4. Membership values & weights.

	x_1	x_2	x_3	W_i
R_1	0.81	0.92	0.91	0.70
R_2	0.47	0.37	1.00	0.80
R_3	0.68	0.70	0.86	1.00
R_4	1.00	0.75	0.75	0.75
R_5	0.80	0.80	0.60	1.00
R_6	0.50	0.80	0.80	0.60
R_7	0.50	0.50	0.70	0.40
R_8	0.55	0.68	1.00	0.90
R_9	0.52	0.72	0.56	1.00

Values shown in Table 4 are composed through Eq. (3) for computing the overall evaluation of the design alternative x_i to the industry target. The results of first row of Table 5 indicate that x_3 has the minimum value, therefore it is better than x_1 and x_2. Obviously, the choice could be influenced by assigned weights and corresponding requirements. For verifying that in the other rows are calculated the overall evaluation when the weight of one requirement is posed to 0, that means ignore the corresponding requirement. For this application we note that the design alternative x_3 is always better than x_1 and x_2.

In the fifth column of Table 5 the fuzziness index of set $X = \{x_1, x_2, x_3\}$ is shown where 0 indicate the certainty of choice and 1 is total indecision. The index allows evaluation of the goodness of problem definition. The requirement that yields much more indecision is R_5 because $I_s(w_5 = 0) = 0.78$, i.e., if we do not consider R_5, the fuzziness decreases whereas for R_8, the fuzziness index increases to $I_s(R_8 = 0) = 0.87$.

Table 5. Scores and influence of every requirement.

	x_1	x_2	x_3	I_s
$P(x_i)$	0.15	0.11	0.07	0.83
for w_1=0	0.16	0.12	0.07	0.83
for w_2=0	0.13	0.07	0.08	0.82
for w_3=0	0.15	0.11	0.08	0.84
for w_4=0	0.16	0.12	0.07	0.81
for w_5=0	0.17	0.12	0.05	0.78
for w_6=0	0.14	0.12	0.07	0.86
for w_7=0	0.14	0.10	0.07	0.83
for w_8=0	0.14	0.11	0.08	0.87
for w_9=0	0.13	0.12	0.05	0.82

Table 6 shows the domination degree matrix [dij] which indicates haw much a design alternative x_i is better/worse than x_j . For dij > 0.5, we know that alternative x_i is better than x_j, vice versa for dij< 0.5.

Table 6. Dominance degree matrix.

	r_1	r_2	r_3
r_1	0.50	0.57	0.68
r_2	0.43	0.50	0.62
r_3	0.32	0.38	0.50

CONCLUSION

The decision between available design alternatives presupposes an overall evaluation of the different alternatives with respect to assigned requirements. For vague and subjective requirements the fuzzy approach is very useful for representing and manipulating such requirements. But in this approach an expert's knowledge is particularly important either to obtain the m.f. for each requirement or for selecting an aggregation function to compute the overall evaluation. This paper has demonstrated the usefulness of the fuzzy approach for solving a practical design problem utilising an aggregation function which is derived from Taguchi philosophy. As well we note that the presented application is a real case of choice involved by an Italian mechanical company.

REFERENCES

1. J.D. Jones, Y. Hua, 1998. A Fuzzy Knowledge base to support routine engineering design. Fuzzy sets and System, Nr. 98, 267-278.
2. E. K. Antonsson, K.N. Otto, 1995. Imprecision in Engineering Design. ASME Jour. of Mechanical Design, Vol. 117, S.25-31.
3. N. Cappetti, E. Santoro, 1998. An Application of Computer Visualisation for Solving a Mechanical Design by Fuzzy Set. IEEE Inter. Conf. on Inform. Visualisation, London, S. 60-75
4. M.J. Scott, E.K. Antonsson, 1998. Aggregation functions for engineering design trade-off. Fuzzy Set and Systems, Vol. 99, S. 253-264
5. G.J. Klir, B. Yuan, 1995. Fuzzy sets and Fuzzy Logic. Prentice Hall.
6. R. Ranjit, 1990. A primer on the Taguchi Method. Van Nostrand Reinhold Book
7. A. Donnarumma, M. Pappalardo, A. Pellegrino, 1998. Classification and information using fuzzy design. APE 98, Warsaw (Poland).
8. N. Cappetti, A. Donnarumma, E. Santoro, 1998. A fuzzy approach to design evaluation of an apron conveyor for a mechanical industry. 7th Int. Sci. Conference "Achiev. Mech. & Mat. Engineering, Ed. L.A. Dobrzanski, Poland, S. 59-62.

Non-Traditional Performance Analysis

J. Arlen Cooper

Sandia National Laboratories,*
Albuquerque, NM 87185-0490, USA
Email: acooper@sandia.gov

ABSTRACT

Traditional performance analysis methods are applicable to many standard problems, including those examples illustrated in most formal courses. However, there are many real-world situations for which non-traditional methods appear to be more appropriate, mainly because most practical problems involve substantial subjectivity about the inputs and models used. This paper surveys some of the most applicable approaches found in a recent research study. Each approach is developed individually and is illuminated by selecting example situations of apparent applicability. Then, the combinational blending of the approaches with each other and with traditional methodology is discussed.

* Sandia is a multiprogram laboratory operated by Sandia Corporation, a Lockheed Martin Company, for the United States Department of Energy under Contract DE-ACO4-94AL85000

INTRODUCTION

In most analyses, conventional approaches are typically employed, even where they may not match the problem parameters very well. For example, most people frequently express their thoughts probabilistically, even when actually thinking possibilistically. To illustrate, one might be tempted to use a high school transcript showing half As and half Bs for forecasting a "probability" of a student getting an A in a university course as 50%. This associates a frequentist concept with a possibilistic event (it is judged equally possible that the grade will or will not be A, where "not A" = {B,C,D,F} and there is positive weight only for B). There is no direct evidence prior to receiving college course grades.

Carrying this a step further, it is often necessary to associate an "extreme" prognosis with an event that might cause an unexpected safety or reliability problem. As an analogy, one might forecast the probability of the student above getting five As in five courses as 1/32. In practice, there is a strong possibility that this perception is misleading.

For example, the student may place high importance on university grades and be inspired to work very hard, getting straight As. This might help explain why historical examination of accident histories has shown a tendency of prior traditional safety analyses to be overly optimistic, and why possibilistic mathematical approaches are currently receiving considerable attention. In this paper, we consider a number of non-traditional methods, each of which can be used to advantage in particular classes of problems. Subsequently, we describe a hybrid technique that can be applied to problems corresponding to diverse models

FUZZY MATHEMATICS

Fuzzy mathematics is a form of possibilistic processing. The difference between fuzzy logic and fuzzy mathematics is roughly analogous to the difference between Boolean algebra and the algebra of real numbers. Like probabilistic calculus, Fuzzy mathematics also can be applied to introduce variability to fixed parameters. For example, a subjective parameter can have some of the characteristics of more than one number (e.g., "approximately" five may indicate a range of real numbers including, but not limited to, five). Fuzzy models can therefore be applied to describe parameters in analyses (e.g., probability analysis),

0-7803-5489-3/99/$10.00 ©1999 IEEE.

and this has some similarity to strictly conventional descriptions. However, fuzzy algebra differs from conventional mathematics both formally and in concept.

Since fuzzy mathematics does not assume the precise relationships inherent in probability distributions, it appears to be more appropriate for the subjective inputs applicable to vaguely defined environments.

A fuzzy number (formally a convex and normal fuzzy set) can be represented mathematically [1] as:

$$A_{\mu}(x) = A_{\mu} = [a_1(\mu), a_2(\mu)] \qquad 1.$$

where the a_1 and a_2 values on x represent the lower and upper limits, respectively, of the variation possible for the parameter as a function of μ, and μ is a "level of presumption." The level of presumption represents a collection of subjective judgments[1] about the range specified.

One must be more presumptuous in order to specify monotonically decreasing variable ranges (maximum level of presumption is presumption of minimum uncertainty).

This is associated with the convexity property. The "normal" restriction fixes the maximum level of presumption at 1 and the minimum to 0. If a particular value of presumption, a, is selected, a horizontal line can be drawn that intersects the ordinate at μ = a. The two points where the line intersects the function represent the lower and upper bounds for the parameter at the specified presumption level. No information is implied within the limits.

In contrast to fuzzy logic, fuzzy mathematics treats operands as fuzzy (subjectively known) numbers with uncertainty along the abscissa, and computes in terms of abscissa values rather than ordinate values. The mathematical basis for combining fuzzy numbers is based on Zadeh's Extension Principle [2]. For addition and multiplication (basic to fault tree and event tree computations), this produces:

$$\mu_{A+B}(z) = \bigvee_{z=x+y} (\mu_A(x) \wedge \mu_B(y)) \qquad 2.$$

$$\mu_{A\times B}(z) = \bigvee_{z=x\times y} (\mu_A(x) \wedge \mu_B(y)) \qquad 3.$$

These are convolutions basically constructed like those used in probabilistic calculus, but without the "independent" abscissa valuations. This is because the above fuzzy-algebra operations utilize only ranges of values, and make no use of or assumptions about relationships between probability parameters, or of independence between probability parameters.[2] The operations shown above are directly useful for parameters for which relative probabilities and independence are not well known (a common situation). On the other hand, probabilistic operations are limited to parameters for which these characteristics are well known (a less common situation).

MODIFIED DEMPSTER-SHAFER THEORY

Another concept under examination is an "enhanced" Dempster-Shafer theory. Dempster-Shafer theory represents both frequentist and Bayesian concepts, separating supportive evidence and contrary evidence for particular situations. The supplement we are pursuing is to represent the amount of subjectivity in the two components, which allows decision-makers (looking at analysis results) to track more precisely how much subjectivity was included. An illustration of the use of this technique is shown in Figure 1.

Here, we postulate the projection of a final "average" based on partial data. It is further postulated that the supporting evidence and contrary evidence are partially applicable, so that with a higher degree of

[1]Preferably from "experts," preferably based on data (even if limited), and possibly weighted according to expertise

[2]However, treatment of independence/dependence properties is not precluded [3].

subjectivity, tighter bounds are derived. This has the value of not only indicating the bounds supported by the evidence, but also indicating how much subjectivity was used in applying the bounds.

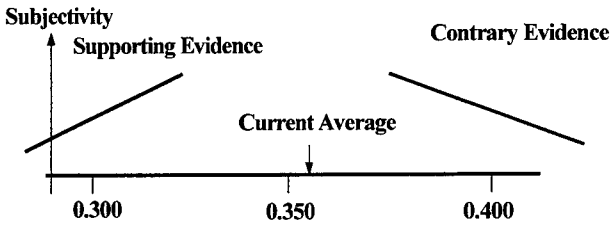


Fig. 1. Subjective/Dempster-Shafer Model.

SOFT MATHEMATICAL AGGREGATION

Soft mathematical aggregation is useful in a significant number of applications. Inputs may contribute to the output without being related to linear, Boolean, or possibilistic mathematics. For example, a production line employee who is disgruntled or unmotivated, or a training program that is not done skillfully might not directly contribute to an accident, but the presence of such situations projects safety concerns and potential contributors to an accident, if other unfavorable events occur.

As another example, a medical doctor may accumulate weighted health information combined non-linearly (weight/height, blood pressure, temperature, pulse rate, blood test parameters, reflexes). Safety indicators are similar. The potential effectiveness of protective measures (e.g., medicine) is also weighed. In these and similar applications, there is a particular need for contributions that push toward a limit (e.g., "unsafe" or "safe") without ever being assured of reaching the limit. Our model for these situations is exponential, as shown in Figure 2. Safety protective measures are aggregated up the ordinate and threats are aggregated down the ordinate. The abscissa indicates a weighted "rating" function that is subjectively obtained and based on expert judgment. The equation used is:

$$f = \left[1 - e^{-\sum_{i=1}^{n} k w_i x_i}\right] e^{-\sum_{j=1}^{m} k v_j y_j} \qquad 4.$$

The w_i and v_j indicate "weights" on the importance of the protective measure and threat aggregates, respectively (m in number). The weights are normalized so that $\sum_{i=1}^{n} w_i x_i = 1$ and. $\sum_{j=1}^{m} v_j y_j = 1$. The x_i and y_j are ratings of how bad the hazards are on a scale of 0 to 1. The constant k is a variable dependent on the number of aggregate constituents. Figure 2 shows an example aggregation of threats and controls. The aggregation can be carried out with the parameters combined in any order; or the aggregation can be carried out for the entire system.

Figure 2 shows growth of the aggregate attribute with three contributing controls and three types of concerns. Also shown is a "threshold of concern", which is conceptually a fuzzy threshold, and below which system concern becomes greater.

MULTI-PARAMETER DECISION ANALYSIS

Multi-parameter decision analysis is also an important tool, because system designers choose components under cost, performance, size, safety, and reliability constraints. System usage, modification, and control are determined by multiple parameters. System analysts also weigh all of the above factors and select mathematical models. The high degree of subjectivity and the mathematical constraints involved have made this a target for subjective mathematical tool development [4]. A few of the many techniques that are commonly used are: weighted sum, threshold logic, propositional logic, and ordered weighted averaging.

The process we have developed is a weighted sum that can be either linear or softly aggregated. The method also includes uncertainty characteristics. An example is shown below in Table 1. The scenario shown demonstrates how two different viewpoints of the same data set can yield different conclusions.

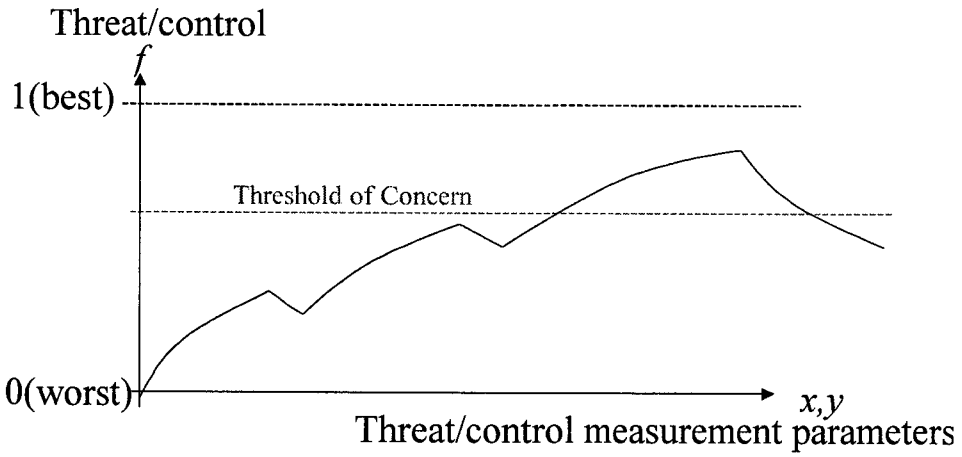


Fig. 2. Exponential Aggregation

HYBRID COMBINATION

The above approaches, numerous others under study, and traditional analyses could be appropriate individually for a particular part of a system analysis. However, it is more likely that combinations might generally be necessary. For this reason, a hybrid mathematical structure has been developed that allows the models (traditional and non-traditional) to be combined while tracking the amount of subjectivity involved and portraying its source. Our solution treats each part of a problem as a subsystem, and each subsystem can have an objective and a subjective constituent. Initially, each subsystem is addressed separately. Then, we then carry along the analysis to combine subsystems by processing objective and subjective portions separately to derive a two-part result. The solutions are currently being incorporated into software tools [4].

Table 1. Combining Parameter Importance and Quality to Reach an Aggregate Decision.

Example factors	safety weighting	system weighting	attribute score
Safety contribution	**0.3-0.4**	**0.1-0.2**	**0.6-0.9**
bypass potential	**0.3-0.4**	**0.1-0.2**	**0.5-0.8**
synergism with other features	**0.03-0.07**	**0.1-0.2**	**0.4-0.6**
lifetime stability	**0.1-0.2**	**0.05-0.15**	**0.2-0.5**
produceability	**0.01-0.03**	**0.05-0.15**	**0.9-1.0**
reliability	**0.01-0.03**	**0.05-0.15**	**0.9-1.0**
size	**0.01-0.03**	**0.05-0.15**	**0.9-1.0**
cost	**0.05-0.15**	**0.05-0.15**	**0.8-1.0**
operability	**0.05-0.15**	**0.05-0.15**	**0.8-1.0**

Safety weighted score: 0.62-0.73
Systems weighted score: 0.74-0.85

REFERENCES

1. A. Kaufmann and M. Gupta, 1991. Introduction to Fuzzy Arithmetic, Van Nostrand Reinhold, NY, NY.
2. L. Zadeh, 1965. Fuzzy Sets, Information Control, 338-353.
3. J. Cooper, 1994. Fuzzy-Algebra Uncertainty Analysis, Journal of Intelligent & Fuzzy Systems, 2(4).
4. J. Cooper and T. Ross, 1997. An Investigation of New Mathematical Structures for Safety Analysis, Sandia National Laboratories Report SAND97-2695, November.

Methods to Create Membership Functions in Fuzzy-Rules in Knowledge-based Systems

Cezary Orlowski

Faculty of Management and Economics
Technical University of Gdansk
Ul. Narutowicza 11/12, 80-952 Gdansk, Poland
+ 48 58 347 24 55 cor@sunrise.pg.gda.pl.

ABSTRACT

The paper aims to present the author's experiences in building complex systems with knowledge bases. The systems were worked out using the author's own method based on concurrent engineering philosophies with elements of fuzzy logic in the net environment.

The accepted method ensures the following:

- ease of creation and verification of membership functions in situations where engineers co-operate with experts.
- efficiency of creating the rules in concurrent engineering.
- reduced number of errors in testing the discussions path in the graphic work environment.

The examples of domains and ways of creating the system with the special emphasis on the membership function are presented in the paper.

INTRODUCTION

Computer-aided decisions in systems with knowledge bases require the application of techniques enabling to employ implementation of the decisions presented in form of a semantic network and a natural language in terms of multi-valued logic.

It has been assumed that the description of the rules will be based on linguistic models applied by Zadech [8] and modified later by Tong and Gupta [3]. To elaborate the method the linguistic models were constructed by use of rules of the knowledge bases in form of IF-THEN, which were consequently formed on the basis of semantic networks. There has been proposed a linguistic model making use of inference of Madami type: IF U is B_i, THEN V is D, where fuzzy relation R_i is based on the product of fuzzy sets B_i and D_i.

PROPOSED SOLUTION

There has been elaborated a solution of qualitative type taking advantage of the phenomenological approach to solve the problem of constructing the membership function for projecting the hybrid systems.

The induction approach, which has been defined before, is taken into consideration. An attempt has been made to apply the deduction method utilising the Mesarovic approach [4]. It has been proved that the acquired experience was in favour of the Weinberg approach [7] suggesting the researcher's intuition as a cognitive tool helping to work out the method. Making use of both the descending and the ascending approach and assuming the performance of the task according to some rules governing the creation of complex systems it was possible to define, on one side the objective of carrying out the system, and on the other to determine the method for its realisation. Hence also to carry out the task it has been suggested to employ a multi-level system assessment of the tasks and processes taking into consideration:

- separation of tasks necessary to attain the objective in view of the requirements of the system;

0-7803-5489-3/99/$10.00 ©1999 IEEE.

- determination of the system processes related to the accomplishment of some particular task;
- determination of requirements necessary for the existence of the processes resulting from tasks leading to the attainment of the aim of the hybrid system. The aim of the system is determined during the phase dealing with analysis of informal requirements.

The work presents an alternative approach to creating hybrid systems. The method is the result of a search for system methods of building intelligent systems based on knowledge processing. It consists of the following models of:

- Multiplane division of the project cycle comprising: project management , projecting tools, sources of knowledge and assisting techniques.
- Multilevel division into project ranges.
- Decomposition of projecting processes for the sake of acquiring knowledge using parallel solutions at the knowledge base level and serial ones at the level of the processes feedback controlled by external domain experts and their usage for multilevel assessment.
- Management of the process with the specified scopes of project solutions and the selection of solutions for those scopes based on the processes.
- Integration of technical, institutional and organisational functions of the projecting team for the model of team management defined as the working team.
- Serial projecting processes with feedback in the parallel projecting areas and at the specified levels.
- Groups of products together with the method of defining them by the projecting team.

The elaboration of the method has been encouraged by Rattray's definition [114] of the projecting cycle division and its modification to separate out the various ranges of the investigations carried out. Use has also been made of theoretical models [80,85,118,119,144] in the elaboration of the method. The ranges related to the processes of constructing the system have been defined. Range I is related to transformation of knowledge by synthesis and analysis, whereas Range II refers to the projecting processes. The synthesis and analysis processes as well as the projecting processes occur on four parallel planes (Fig. 1).

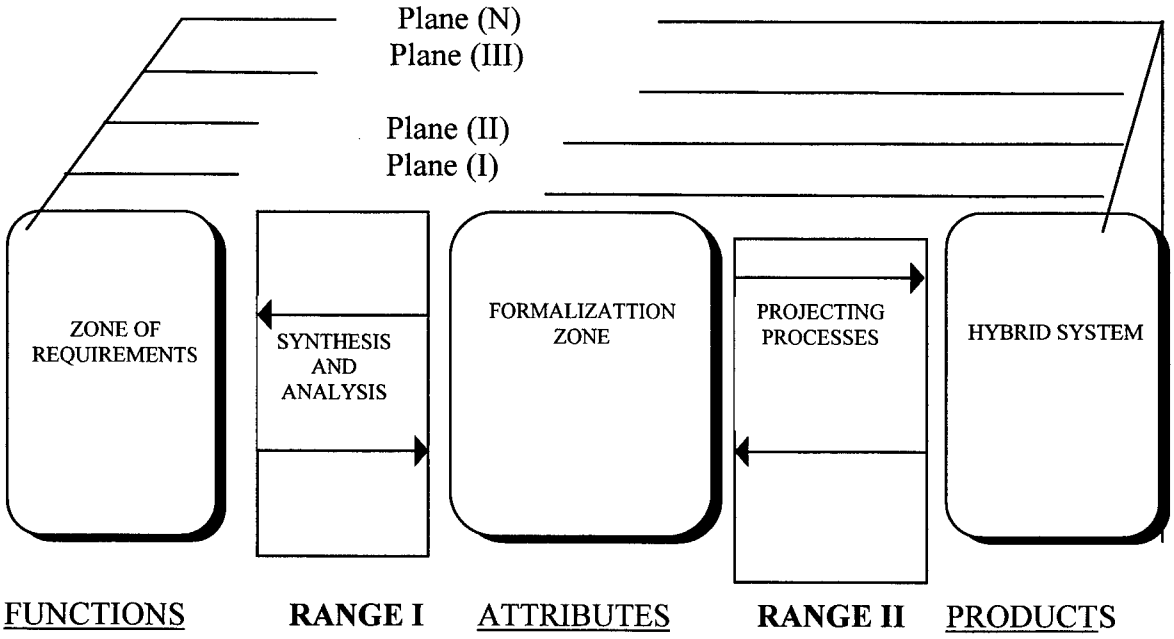


Fig.1. Model of division of projecting cycle into parallel planes and design ranges [own elaboration]

RANGE I

Range I includes synthesis and analysis processes using the denotations expressed by equations 1 and 2

Synthesis = (functions_ of the system) 1.

Analysis = (attributes_ of the system) 2.

The processes of synthesis and analysis include events connected with transformation of expert's knowledge into formulated expression. It is suggested to apply knowledge engineers to the control process of the knowledge transformation process. Fig. 2 presents a model of knowledge acquisition, where:

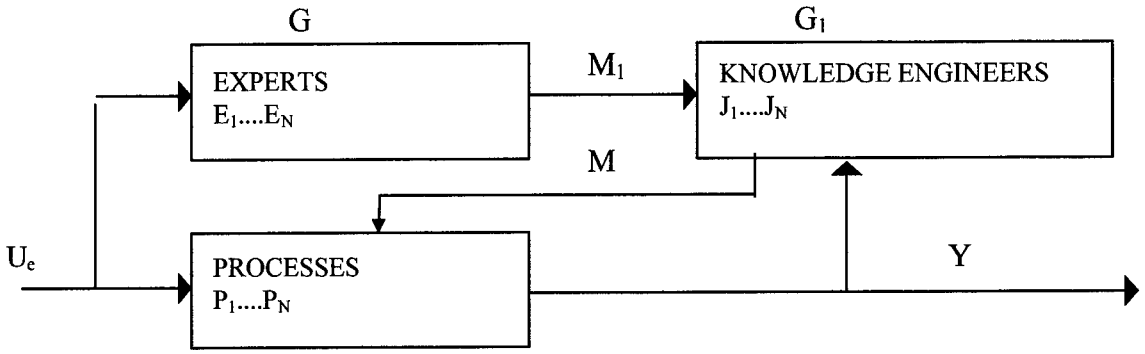


Fig. 2. Model of knowledge acquisition during formalisation processes [own elaboration]

Where G – group of branch experts,
G_1 – group of knowledge engineers,
M_1 – serial process of transferring knowledge between an expert and a knowledge engineer,
M – process of transferring formalised knowledge,
U_e – input data,
Y – output data,
$P_1 – P_n$ –projecting processes

Acquisition of knowledge is defined as set D made up of the following elements:

$$D = < M, M_1, U_e, Y, P, G, G_1 > \quad 3.$$

The process of acquiring knowledge P is defined as:

$$P : (M + M_1) \times U_e \rightarrow Y \quad 4.$$

and depends directly on value $M+M_1$, i.e., on the way it is transformed by knowledge experts and engineers.

RANGE II

The projecting processes are defined as serial processes involving feedback occurring in parallel design areas;

$$\text{Projecting processes} = (P_{11} ..... P_{MN}) \quad 5.$$

The matrix of the serial processes (13) comprises processes taking place independent of $P_{11}.....P_{nm}$ in areas $O_1.....O_m$ defined by vector O. Products $p_{r1}.....p_m$ are the result of these processes. A parallel transformation process is illustrated in Fig.3.

$$P=\begin{vmatrix} p_{11} & p_{12} & p_{13} & \cdots & p_{1n} \\ p_{21} & p_{22} & p_{23} & \cdots & p_{2n} \\ p_{31} & p_{32} & p_{33} & \cdots & p_{3n} \\ p_{m1} & p_{m2} & p_{m3} & \cdots & p_{mn} \end{vmatrix} \quad O=\begin{vmatrix} O_1 \\ O_2 \\ O_3 \\ \cdots \\ O_m \end{vmatrix} \quad P_r=\begin{vmatrix} P_{r1} \\ P_{r2} \\ P_{r3} \\ \cdots \\ P_{rm} \end{vmatrix} \qquad 6.$$

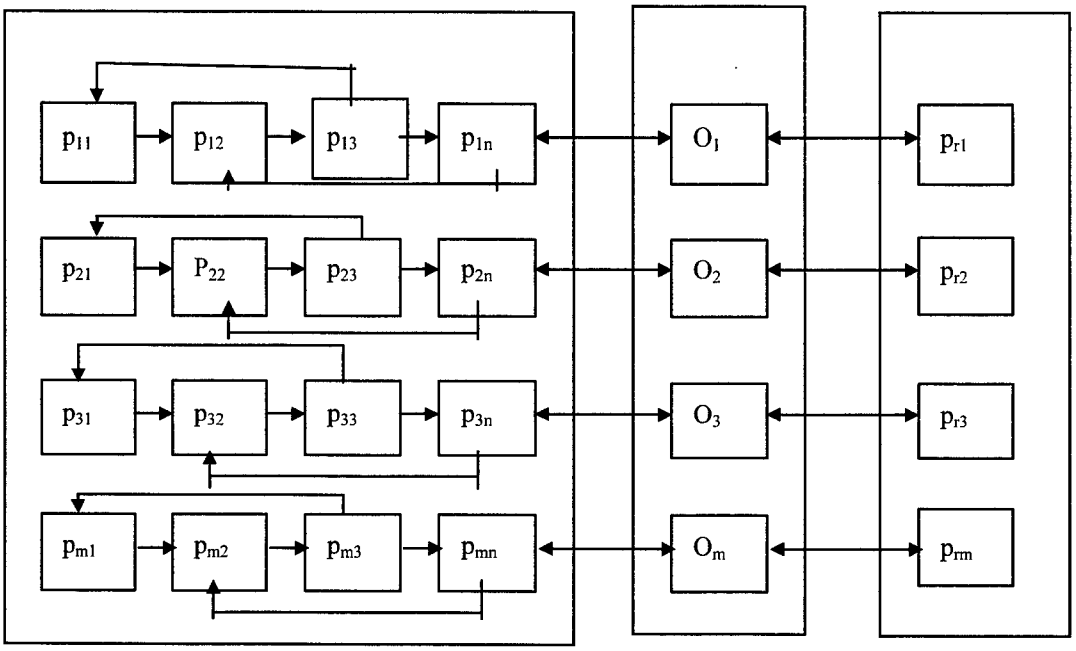


Fig. 3. Model of serial projecting processes accompanied by feedback generated in the parallel projecting areas [own elaboration].

The production of the final product is based on producing successively the following groups of products in compliance with Fig. 4.

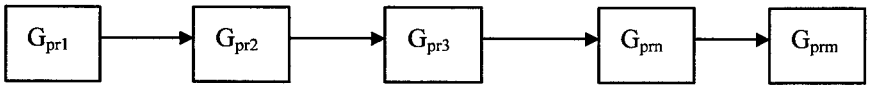


Fig. 4. Model of groups of products [own elaboration]

where $G_{pr1} = p_{r1} = p_{r2} + \ldots\ldots + p_{rm}$
$G_{pr2} = p_{r2} + p_{r3} + \ldots\ldots + p_{rm}$ 7.
$G_{prm} = G_p$
G_p is the final product

EXAMPLE OF APPLICATION

The way of rule implementation making use of the fuzzy logic technique for the method proposed is presented in Fig. 5. The method makes it possible to define the membership function at the stage of setting up the formal requirements for the system designed. According to the criteria set out in the description of the method, which are related to the accomplishment of the project, advantage has been taken of the fuzzy logic technique. The values let into the system are identified with a group of fuzzy magnitudes and assigned to a given set by membership function, by assignment of values determined by experts. In order to carry out the right "fuzzification" process, assignment of fuzzy values to input magnitudes, use is made of

various membership functions, most frequently defined by the designer of the system. An example of the membership functions applied to the project is given by fig. 6.

In the case of constructing a system with knowledge bases using object techniques, conditions and operation of rules have been verified by unclear (fuzzy) values. On completing the session and obtaining some specified fuzzy magnitudes, the problem of their change into output values was carried out in the defuzzification process.

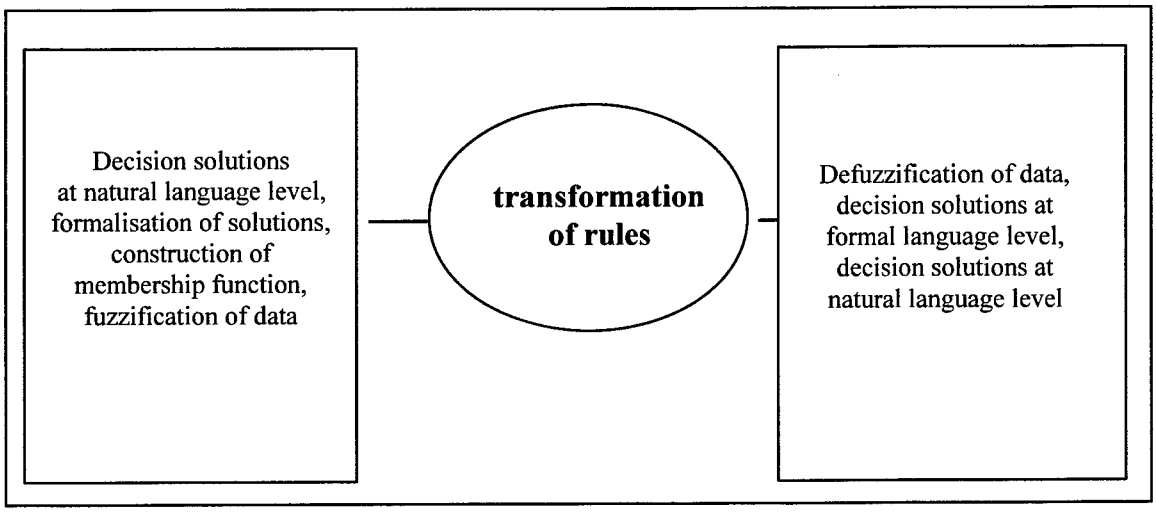


Fig. 5. Rule implementation by use of the fuzzy logic techniques [own elaboration].

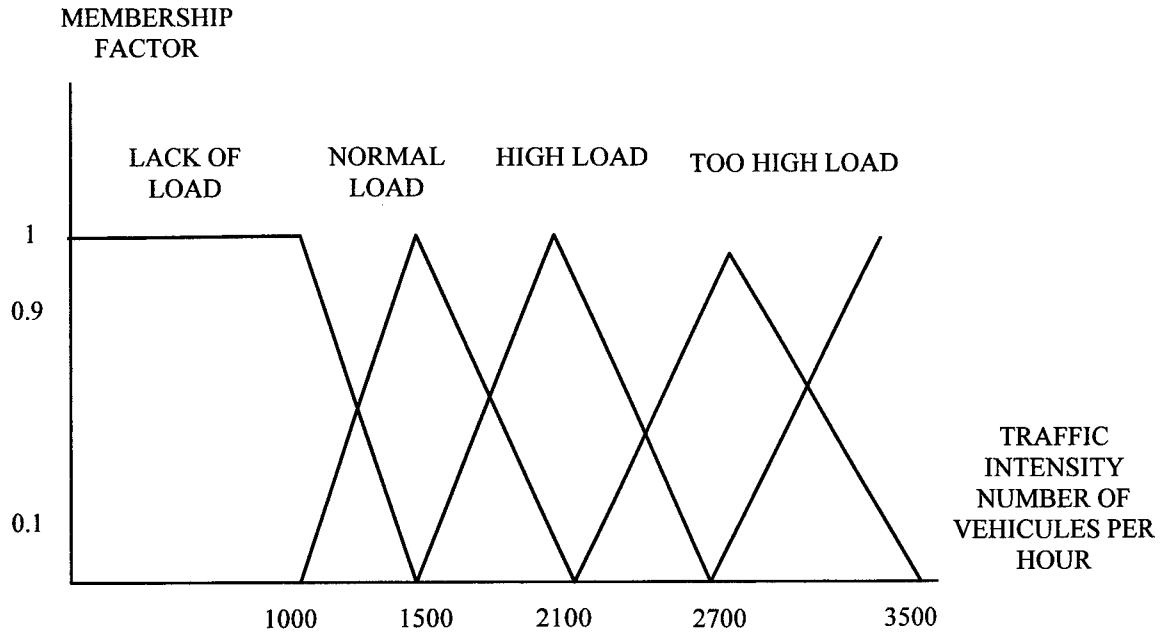


Fig. 6. Example of rule implementation using fuzzy logic techniques [own elaboration].

Advantage has been made of the centre of mass technique consisting of the following steps [4]:

- for output, the membership functions are defined by calculating the centroids;
- for the output function, a reducing procedure is used to decrease the value to a level at which it was produced;
- calculation is made of the surface area of the reduced membership function.

The output values have been calculated in terms of the weighted mean of coordinate x of the centroid and the newly calculated field with the fields of the weights.

The application of the method has made it possible to use fuzzy values (conditions or actions) in the creation of rules , which in the circumstances of expert-knowledge engineer cooperation allows for a more effective acquisition of knowledge.

REFERENCES

1. Ceri, S.,Fraternali, P., 1997. Database Applications with Objects and Rules, Addison-Wesley, Harlow.
2. Coad, P., Yourdon, E., 1991. Object Oriented Design, Prentice-Hall, Engl. Cliffs.
3. Gupta, M.M., Kiszka, J.B., Trojan G.J., 1986. Multivariable structure of fuzzy systems, IEEE Transactions and Systems, Man and Cybernetics, SMC-16, 7, 638-656.
4. Mesarovic, M., Takahara, Y., 1989. Abstract Systems Theory, Lecture Notes in Control and Information Science, Springer.
5. Mesarovic, M., Takahara, Y., 1970. General Systems Theory: Mathematical Foundation , Acad. Press.
6. Rattray, C., 1996. "Identification and Recognition through Shape in Complex Systems", Computer Aided Systems Theory – EUROCAST'95 (eds. F. Fichler, R. Moreno Dfaz, R. Albrecht), LNCS 1030, Springer-Verlag.
7. Weinberg, G., 1979. Myslenie systemowe., Warszawa.
8. Zadeh, L.A., 1978. Fuzzy sets as a basis for theory of possibility. Fuzzy Sets and Systems 1, 3-28.

An Efficient Method for Constructing Fuzzy Rules

Bojan Novak, Ivan Rozman

University of Maribor, Faculty of Electrical Engineering and Computer Science,
Smetanova 17, 2000 Maribor,
Email: novakb@uni-mb.si

ABSTRACT

Recent advances have merged artificial neural networks (ANNs) with fuzzy logic to generate automatically and to tune membership functions, rules and inference systems. Unfortunately these tools are not simple and can generate very complicated error surfaces with multiple local optimums that are traps for the learning algorithm. If the structure of the ANN (the number of neurons in the hidden layer) is not properly defined, the actual error will remain high despite a low training error, i.e., over-fitting. These troubles can be avoided through the selection of adequate input variables and proper ANN structure. With the clustering methods automatic rule generation and optimal shape of membership functions can be generated. In this paper a different approach is considered. Instead of generating cluster centers, some vectors are chosen by using certain described criteria. The structure of the learning machine is defined during training. The Vapnik Chervonenkis (VC) dimension is introduced as a measure of the capacity of the learning machine. A prediction of the expected error on the yet unseen examples can be estimated with the help of the VC dimension. The structural risk minimization principle is introduced to construct a machine with the lowest expected error.

INTRODUCTION

Recent advances have merged artificial neural networks (ANNs) with fuzzy logic to generate automatically and to tune membership functions, rules and inference systems. Three basic combinations exist:

- neural-based fuzzy systems
- fuzzy-based neural networks
- fuzzy-neural hybrid systems.

In the third approach, the best properties from both techniques are used. To this category belongs adaptive controllers such as the FALCON (Fuzzy Adaptive Learning Control Network) and the ANFIS (Adaptive Neural Fuzzy Inference System). They are implemented in the form of the radial basis function network (RBFN). The idea results from the theory of function approximations and as well, from the biologically inspired theory of locally tuned and overlapping receptive fields which are a well-known structure in regions of the cerebral cortex and the visual cortex. Between RBFN and fuzzy inference systems there exists functional equivalence. This principle is applied in fuzzy-neural hybrid systems. Backpropagation and recurrent ANN are the most often used ANN for the task of non-linear modeling. Unfortunately these tools are not simple and can generate very complicated error surfaces with multiple local optimums that are traps for the learning algorithm. If the structure of the ANN (the number of neurons in the hidden layer) is not properly defined, the actual error will remain high despite a low training error, i.e., over-fitting. These troubles can be avoided through the selection of adequate input variables and proper ANN structure. In defining an optimal structure, different time-consuming methods exist such as pruning. But the problem of complicated error surfaces with multiple error surfaces still remains. With the addition of clustering methods, automatic rule generation and optimal shape of membership functions can be generated. Basically the idea of clustering is to generate new vectors - cluster centers, in the center of the areas where a cluster of data exists. The cluster centers are the basis for a decision about rule generation. Another important fact is that in practical applications, very limited sources of the data are available for learning. An ANN is capable of learning on a data set that is large enough. Different validation techniques exist to construct the ANN with a minimal actual error. These methods must extract a significant amount of data into the validation set, so the training set becomes even smaller which significantly affects the quality of the ANN performance.

0-7803-5489-3/99/$10.00 ©1999 IEEE.

In this paper a different approach is considered. Instead of generating cluster centers, some vectors are chosen by using certain described criteria. The structure of the learning machine is defined during training. The Vapnik Chervonenkis (VC) dimension is introduced as a measure of the capacity of the learning machine. A prediction of the expected error on the yet unseen examples can be estimated with the help of the VC dimension. The structural risk minimization principle is introduced to construct a machine with the lowest expected error. The result is that validation is unnecessary since a reliable formulation of the upper bound on the actual error is formulated based on the VC dimension. This is particularly important when the data set is small.

The problem is transformed in the reproducing kernel Hilbert space which is a very efficient method to transform a non-linear problem to the linear form.

MATHEMATICAL MODEL

For a given k observations each consists of a pair: $\mathbf{x}_i$, y_i , where $\mathbf{x}_i$? R^n, i=1,... k is input vector and y_i is associated output. Learning a machine is actually building up a mapping ability $\mathbf{x}$? f($\mathbf{x}$,a) where the functions f($\mathbf{x}$,a) themselves are labeled by adjustable parameters a. For the artificial neural networks (ANN) a represents weights and biases. The expectation of test error for the trained machine is:

$$R(\alpha) = \int \frac{1}{2} |y - f(\mathbf{x},\alpha) dP(\mathbf{x},\alpha)| \qquad 1.$$

R(a) is the expected risk. P is a probability. The measured mean error rate on the finite number of observations is "empirical risk":

$$R_{emp}(\alpha) = \frac{1}{2k} \sum_{i=1}^{k} |y - f(\mathbf{x}_i,\alpha)| \qquad 2.$$

R_{emp}(a) is fixed for a particular choice of a and for a particular training set {$\mathbf{x}_i$, a} and the probability is not included in the equation. The quantity ½ | y_i – f($\mathbf{x}_i$, a)| is loss function. But empirical risk minimization does not imply small error on the test set if the number of examples in the training data set is limited. The structural risk minimization is one of new techniques for handling efficiently limited amount of data. For a chosen ?: 0 = ? = 1 the bound holds:

$$R(\alpha) \le R_{emp}(\alpha) + \Phi(\frac{h}{k}, \frac{\log(\eta)}{k}) \qquad 3.$$

where F is defined as :

$$\Phi(\frac{h}{k}, \frac{\log(\eta)}{k}) = \sqrt{\frac{h(\log\frac{2k}{h} + 1) - \log(\frac{\eta}{4})}{k}} \qquad 4,$$

The parameter h is Vapnik Chervonenkis (VC) dimension [2,3,4]. It describes the capacity of a set of functions implemented on the learning machine.

According to Equation 3., risk can be controlled by two quantities: R_{emp} (a) and h({f($\mathbf{x}$,a) : a ? k_{sub}}), where k_{sub} is some subset of index set k. The empirical risk R_{emp} depends on the choice of optimal function (a) applied in the learning machine. The VC dimension h depends on the set of functions {f($\mathbf{x}$,a) : a ? k_{sub} } . The parameter h is controlled by introducing structure of nested subsets S_n :={f(x,a) : a ? k_n } of {f($\mathbf{x}$,a) : a ? k },

$$S_1 \subset S_2 \subset S_3 \subset .... \subset S_n \subset .... \quad (5)$$

with the adequate VC dimensions satisfying:

$h_1 = h_2 = ... \ ... h_n =$ (6)

The structural minimization principle chooses the function $f(x,a^*)$ in the subset $\{f(\mathbf{x},a)$: a? $k_n\}$ with the minimal right hand side of the eq. 3. The guaranteed risk bound is minimal.

For the nonlinear tasks such as regression, identification, control, fuzzy system modeling a non-linear support vector approach is applied. A non-linear mapping is applied to map data in higher dimension feature space where a linear regression is applied. This is possible with the kernel functions. This functions have origin in theory of Reproducing Kernel Hilbert Spaces [1,2,3,4] .An inner product in feature space has an equivalent kernel input space:

$$K(\mathbf{x},\mathbf{y}) = k(\mathbf{x}) \cdot k(\mathbf{y}) \quad 7.$$

If K is positive definite function, satisfying Mercer's conditions:

$$K(\mathbf{x},\mathbf{y}) = \sum_{m=1}^{\infty} \alpha_m \psi(\mathbf{x}) \psi(\mathbf{y}), \quad \alpha_m \geq 0 \quad 8.$$

$$\int K(\mathbf{x},\mathbf{y}) g(\mathbf{x}) g(\mathbf{y}) d\mathbf{x} d\mathbf{y} > 0, \quad \int g^2(\mathbf{x}) d\mathbf{x} < \infty \quad 9.$$

Then kernel is legitimate product in feature space.

There are different functions satisfying Mercer's condition: polynomial, splines, B-splines, radial basis functions, etc. In present work the Gaussian radial basis function will be used:

$$K(\mathbf{x},\mathbf{y}) = \exp[-\frac{(\mathbf{x}-\mathbf{y})^2}{2\sigma^2}] \quad 10.$$

The support vector technique places in each support vector one local Gaussian function. This means that no clustering method is needed. The basis width s can be selected using the structural minimization principle defined in Equation 5.

A special from of the loss function described in Equation 2 is the e-insensitive loss function and does not penalize the errors below some small positive value for the e:

$$|y - f(\mathbf{x}_i,\alpha)|_\varepsilon = \max\{0, |y - f(\mathbf{x}) - \varepsilon|\} \quad 11.$$

The estimation of a function is:

$$f(x) = \mathbf{w}^{\mathrm{T}}\mathbf{x} + b, \quad \mathbf{w},\mathbf{x} \in \mathbf{R}^n, b \in \mathbf{R} \quad 12.$$

With the application of the e-insensitive loss function following quadratic optimization problem can be defined:

$$\min \Phi(x,\xi^*,\xi) = \frac{1}{2}(\mathbf{w}^T\mathbf{w}) + C(\sum_{i=1}^{k}\xi_i^* + \sum_{i=1}^{k}\xi_i) \quad 13.$$

with the respect to the following constraints:

$$\mathbf{w}^{\mathbf{T}}\mathbf{x}_i + b - y_i \le \varepsilon + \xi_i$$

$$y_i - \mathbf{w}^{\mathbf{T}}\mathbf{x}_i - b \le \varepsilon + \xi_i^*$$

$$\xi_i, \xi_i^* \ge 0$$

Where ?, ?* are slack variables. Some small subset of the training data called support vectors (SV) is extracted from the data and the optimal separation is found that is equivalent to the optimal separation for the entire data set. Optimal separation means that the minimal distance for the closes point to the separating hyperplane between the two different classes is maximal. If hyperplane is described by the equation $y = \mathbf{w}\mathbf{x}_i + b$ then finding optimal hyperplane means minimizing $\|\mathbf{w}\|^2$ subject to the constraints defined in 13 [2,3,4]. In general it can be solved as dual quadratic problem and this form is referred to as support vector machine SVM technique. The scalar *C* controls the trade-off between complexity and proportion of non-separable sample points [3]. In Equation 13 the first term $\| \mathbf{w} \|^2$ expresses the model complexity of the e-insensitive loss function described in Equation 11.

The following dual problem can be developed from Equation 13 including the property from Equation 7:

$$\max \Phi(,\alpha^*,\alpha) = -\varepsilon(\sum_{i=1}^{k}(a_i^* + \alpha_i) + \sum_{i=1}^{k}(a_i^* - \alpha_i)y_i - \frac{1}{2}\sum_{i,j=1}^{k}(a_i^* - \alpha_i)(a_j^* - \alpha_j)K(\mathbf{x}_i\mathbf{x}_j) \quad 14.$$

with the respect to the following constraints:

$$\sum_{i=1}^{k}(a_i^* - \alpha_i) = 0$$

$$a_i^*, \alpha_i \in \left[0, \frac{C}{k}\right]$$

and **w** is defined as:

$$\mathbf{w} = \sum_{i=1}^{k}(a_i^* - \alpha_i)\mathbf{x}_i = 0 \quad 15.$$

APPLICATION

For illustration, the model described in Equation 14 was applied to the simple example of identifying a noisy sine curve – Figure 1.

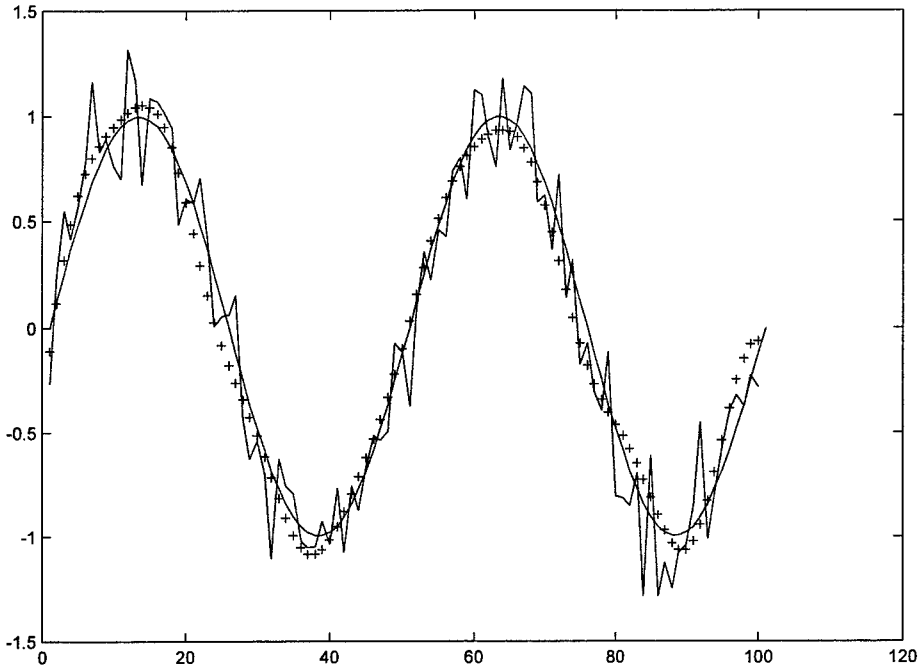


Fig. 1. Noisy data identification, + prediction, - actual data, -- sine curve

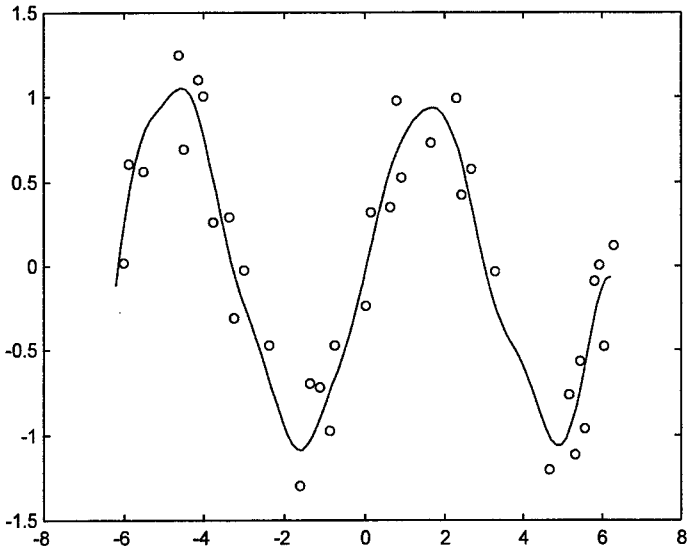


Fig. 2. Support vectors (circles) for the noisy data problem from Fig.1. Dashed lines define 2? area.

The parameters were the following: C = 100, s = 1, ? = 0.2. The Support vectors found by the SVM are presented in Figure 2. In the proposed model, the Sugeno-type fuzzy inference system was applied. The membership functions were Gaussian radial basis functions (Equation 10). From Figure 1, it is evident that the prediction is close to the sine curve. The even data were the training set and the odd data were the testing set. Some practical applications of the SVM can be found in [4,5,6].

CONCLUSION

An alternative approach for fuzzy rules generation is described. Instead of generating the cluster centers, some vectors are chosen by using certain described criteria. The structure of the learning machine is defined during training. The Vapnik Chervonenkis (VC) dimension is introduced as a measure of the capacity of the learning machine. A prediction of the expected error on the yet unseen examples can be estimated with the help of the VC dimension.

The structural risk minimization principle is introduced to construct a machine with the lowest expected error. The result is that validation is unnecessary since a reliable formulation of the upper bound on the actual error is formulated based on the VC dimension. This is particularly important when the data set is small.

The problem is transformed in the reproducing kernel Hilbert space which is a very efficient method to transform a non-linear problem to the linear form. Advantages over other fuzzy-neural hybrid systems are: the architecture of the system doesn't have to be determined before training., solution of the optimization problem is unique, whereas conventional ANNs have multiple local minimum error surface.

REFERENCES

1. A. Aizerman, E. M. Braverman, L. I. Rozoner, 1964. Theoretical foundations of the potential method in pattern recognition learning, Automation and Remote Control, 25, 821-837.
2. B. Schölkopf, C. Burges, V. Vapnik, 1995. Extracting Support Data for a Given Task, in U. M. Fayyad and R. Uthurusamy, eds., First International Conference on Knowledge Discovery and Data Mining, Proceedings, AAAI Press, Menlo Park, CA.
3. V. N. Vapnik, S. E. Golowich and A. Smola, Support vector method for function approximation, regression and signal processing in Advances in Neural Information Processing Systems. Vol. 9 MIT Press, Cambridge MA., USA.
4. V. N. Vapnik, 1998. Statistical Learning Theory, John Wiley and Sons.
5. B. Novak, 1999. Application of support vectors machines for the non-linear identification in the electrical power systems, submitted to the Trans. on Neural Networks, IEEE.
6. B. Novak, 1999. Computer Supported Medical Diagnosis, MIE 99, in print.

Fuzzy Clustering Model based on Changes in Vagueness

Mika Sato-Ilic

University of Tsukuba
Inst. of Policy and Planning Sciences
Tenodai 1-1-1, Tsukuba, Ibaraki 305-8573, Japan
Email: mika@sk.tsukuba.ac.jp

ABSTRACT

This paper proposes a fuzzy clustering model to extract the exact changes of vagueness in data, which are observed as similarities of objects over time. That is, the objective data is assumed to have vagueness, which changes over time. I regard this data as 3-way data. For such 3-way data, the most difficult problem has been that the optimal solutions at different times are in conflict with one another. In order to solve this problem, conventional methods have used parameters to represent the weights of clusters at different times.

However, in such a case, we cannot see the exact change in vagueness. So, in this paper, I propose a clustering model for defining situations of dynamic change. The vagueness of an observation is defined by convex and normal fuzzy sets (CNF sets). I define a conical membership function to represent the CNF sets. The dissimilarity between two observations is defined as a fuzzy asymmetric dissimilarity. In order to deal with the asymmetry of this fuzzy dissimilarity, I use an asymmetric aggregation operator which is similar to the asymmetric metric. Finally, I present numerical results from an application of the proposed model, which will show the validity of the model.

INTRODUCTION

In conventional cluster analysis vagueness has not been considered, even with observational error, when defining a similarity (or dissimilarity) between objects. However, in a real situation, there are many cases where the data involves subject or linguistic vagueness. For instance, the dissimilarity based on human relationships or perceptual confusion, is considered to have some fuzziness. To represent such a dissimilarity, I propose a fuzzy dissimilarity between a pair of fuzzy observations which is an extension of the fuzzy distance. A fuzzy distance between two fuzzy data O_i and O_j is defined by the use of two α-level sets $O_i(\alpha)$, $O_j(\alpha)$. In usual set theory, there are many definitions of the distance between two sets. Here I employ a kind of asymmetric dissimilarity between $O_i(\alpha)$ and $O_j(\alpha)$. The dissimilarity d_{ij}^{α}, from $O_i(\alpha)$ to $O_j(\alpha)$, is defined as the maximum distance from the point of $O_i(\alpha)$ to the set $O_j(\alpha)$, and d_{ji}^{α} is defined from the point of $O_j(\alpha)$ to the set $O_i(\alpha)$. (defined in the subsequent section in detail).

In order to get the fuzzy distance or fuzzy dissimilarity, it is natural to assume that the classified object is observed as fuzzy data which has been defined by several researchers ([1,4,7]). The fuzzy data in this paper is represented by a fuzzy set with a conical membership function in which the boundaries of α-level surfaces are hyperellipsoids in R^n. This means that the direction of the hyperellipsoid shows a correlation with the vagueness of the observed attributes and the size of the hyperellipsoid is considered the degree of vagueness. From the definition of fuzzy dissimilarity, I can find that this dissimilarity varies with the shape of the hyperellipsoid which is determined by the degree of the fuzziness and its correlation. Then I can employ such a dissimilarity. To deal with the asymmetry of this fuzzy dissimilarity, I use an asymmetric aggregation operator [8] which is similar to the asymmetric metric.

This paper focuses on data which is observed by three ways, i.e., the dissimilarities of data over time. According to the times, the vagueness of a relationship among observations changes. Real situations may have such data, e.g., diagnostic data on the system or illness in medical care or biological sciences etc. To treat such data, I have proposed a dynamic clustering model which can extract changes in the vagueness over time [8]. In conventional methods for such 3-way data, INDSCAL [2] and INDCLUS [3] are well-known for dealing with data types which consist of similarities in objects over time (or context). In the above conventional methods, the differences at different times are represented by parameters which show the weights of clusters for each time. However, in such cases, we can not obtain a result which shows the

0-7803-5489-3/99/$10.00 ©1999 IEEE.

exact changes of the clustering situations. So, I propose a model that can show the exact changes over time using the idea to fix the clusters at different times, i.e., the model gets solutions about clusters based on a fixed space. Then it is possible to find solutions which can be compared to each other over time. In order to construct the model, I use the idea of a fuzzy additive clustering model [8].

FUZZY DATA

Fuzzy data in R^n are defined by membership functions $\mu(\boldsymbol{x})$, $\boldsymbol{x} \in R^n$. I assume that membership functions are conical, and defined as follows using a vector and a matrix. A position vector corresponding to fuzzy object O_i, i=1,...,N is denoted by $\boldsymbol{o}_i \in R^n$, i=1,...,N and P_{Oi} is a positive semidefinite $n \times n$ matrix. I denote by? ·? $_{\alpha}$ the following elliptical norm of the distance between an arbitrary $\boldsymbol{x} \in R^n$ and $\boldsymbol{o}_i$:

$$\|\boldsymbol{x}-\boldsymbol{o}_i\|_{o_i} = \begin{cases} \left[(\boldsymbol{x}-\boldsymbol{o}_i)^T P_{O_i}^{-1}(\boldsymbol{x}-\boldsymbol{o}_i)\right]^{1/2}, & \text{if} \quad \boldsymbol{x}-\boldsymbol{o}_i \in X_{O_i} \\ +\infty \quad \text{otherwise}, \end{cases}$$

where P_O^{-1} is the Moore-Penrose generalized inverse of P_{Oi}, and $X_{Oi} \subseteq R^n$ is the linear space spanned by the columns of P_{Oi}, The conical membership function of O_i is

$$\mu_{O_i}(\boldsymbol{x}) = 1 - \min\left\{1, \|\boldsymbol{x}-\boldsymbol{o}_i\|_{O_i}\right\}. \qquad 1.$$

The property is such that $\mu_{Oi}(\boldsymbol{x}) > 0$ is satisfied. If the matrix P_{Oi}, is positive definite, then Equation 1 defines a cone in R^n, and the boundaries of the support of μ_{Oi} and of other level surfaces μ_{Oi} = constant are hyperellipsoids in R^n. The conical membership function μ_{Oi} is normalized to $0 \le \mu_{oi} \le 1$, and the fuzzy set with a conical membership function is a convex, normal fuzzy set [9]. In R^1, the conical membership function is the triangular function

$$\mu_{O_i}(x) = 1 - \min\left\{1, |x - O_i| / s_{O_i}\right\},$$

where $s_{Oi} = P_{Oi}^{1/2}$ is the spread of the function. Therefore, the diagonal elements of P_{Oi} denote the fuzziness corresponding to each variable x_t, t=1,..., p, and off-diagonal elements of P_{Oi} indicate possible interactions between the components of fuzzy membership functions, namely they describe the tendency of a correlation of vagueness among the variables. Figure 1 shows the conical membership function of the fuzzy objects O_i, i=1,2 in R^2, where $O_i(\alpha)$ are α-level surfaces of these conical membership functions.

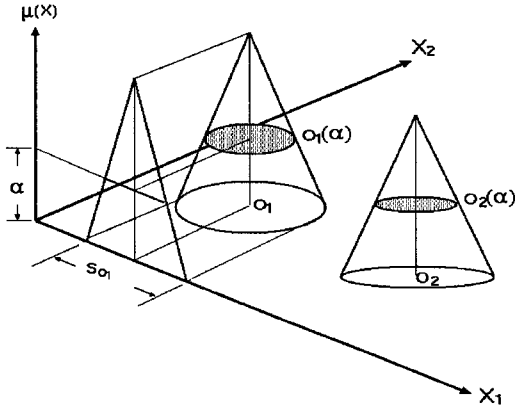


Fig. 1. Conical membership functions.

FUZZY DISSIMILARITY

In order to measure the dissimilarity among the above fuzzy objects, I introduce the fuzzy dissimilarity shown in figure 2. This figure shows the simplification of this fuzzy dissimilarity in R^2, $O_i(\alpha)$, i=1,2 are α-level surfaces of the conical membership functions, and x_t, t=1,2 are variables. The fuzzy dissimilarities at α-level between i-th and j-th fuzzy objects are defined as follows:

$$d^{\alpha}_{L(ij)} = \sup\left\{d(\boldsymbol{x}, O_j(\alpha)) \middle| \boldsymbol{x} \in O_i(\alpha)\right\}, \quad d^{\alpha}_{R(ij)} = \sup\left\{d(O_i(\alpha), \boldsymbol{x}) \middle| \boldsymbol{x} \in O_j(\alpha)\right\},$$
$$d(\boldsymbol{x}, O_j(\alpha)) = \min\left\{d(\boldsymbol{x}, \boldsymbol{y}) \middle| \boldsymbol{y} \in O_j(\alpha)\right\}.$$

where $d(\boldsymbol{x}, O_i(\alpha))$, i=1,...,N is a distance between a point $\boldsymbol{x}$ and a set $O_i(\alpha)$ in a usual sense, namely

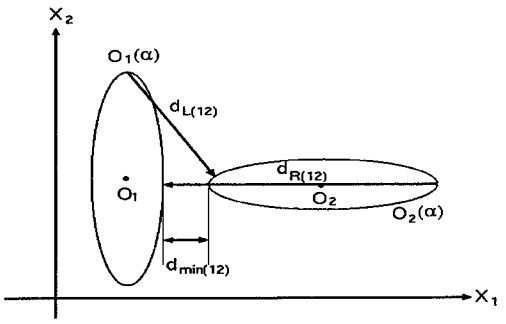


Fig. 2. Fuzzy distance (α-level).

In Figure 2, $d_{min(ij)}$ (i,j=1,2, i?j) shows an ordinal distance between the two sets, if I assume that $O_i(\alpha)$, i=1,2 are conventional sets. $d_{min(ij)}$ is invariant for the shape and the direction of the sets, and it holds $d_{min(ij)} = d_{min(ji)}$. On the other hand, the fuzzy dissimilarities, $d_{L(ij)}$ and $d_{R(ij)}$, vary with the shape and direction of the sets, and clearly, it holds that $d_{L(ij)}$?$d_{R(ij)}$. If x? R^1, then $d_{L(ij)}$ and $d_{R(ij)}$ are lower and upper fuzzy distances, respectively [6], so if I define

$$d_{(ij)} = \max\left(d_{L(ij)}, d_{R(ij)}\right),$$

then $d_{(ij)}$ satisfies the condition of a Hausedorff distance.

ADDITIVE FUZZY CLUSTERING MODEL

The main purpose of unsupervised clustering of a set of objects is to detect natural subgroups(clusters) based on the similarity between the pair of objects. According to the definition of a fuzzy set or interpretation of natural subgroups, I have proposed an additive fuzzy clustering model. I define the additive fuzzy clustering model as follows:

$$s_{ij} = \sum_{k=1}^{K} \rho\left(u_{ik}, u_{jk}\right) + \varepsilon_{ij}, \qquad 2.$$

where the similarity s_{ij} has a ratio scale and $0 \le s_{ij} \le 1$. u_{ik} is a fuzzy grade which represents the degree of belongingness of object i to cluster k. Generally, u_{ik} are denoted by using the matrix representation U=(u_{ik}) called a partition matrix, which satisfy the following condition:

$$u_{ik} \ge 0, \quad \sum_{k=1}^{K} u_{ik} = 1. \qquad 3.$$

The function ρ (u_{ik}, u_{jk}) is the degree of simultaneous belonging of objects i and j to cluster k. That is, the function denotes the degree of sharing of common properties. ε_{ij} (= ε_{ji}) is an error term. The aggregation function is assumed to satisfy the following conditions:

1. $0 \le \rho\left(u_{ik}, u_{jl}\right) \le 1, \quad \rho\left(u_{ik}, 0\right) = 0, \quad \rho\left(u_{ik}, 1\right) = u_{ik},$
2. $\rho\left(u_{ik}, u_{jl}\right) \le \rho\left(u_{sk}, u_{tl}\right)$ *whenever* $u_{ik} \le u_{sk}, \; u_{jl} \le u_{tl},$
3. $\rho\left(u_{ik}, u_{jl}\right) = \rho\left(u_{jl}, u_{ik}\right),$

where i,j,s,t are suffixes for objects, k,l are suffixes for clusters, and they satisfy $1 \le i,j,s,t \le n$, $1 \le k,l \le K$. The method of fuzzy clustering based on this model is to find the partition matrix U=(u_{ik}) which satisfies condition 3 and has the best fitness for model 2. Then, I find U which minimize the following sum of square error η^2 under condition 3,

$$\eta^2 = \frac{\sum_{i \ne j=1}^{N} \left(s_{ij} - \sum_{k=1}^{K} \rho\left(u_{ik}, u_{jk}\right) \right)^2}{\sum_{i \ne j=1}^{N} \left(s_{ij} - \bar{s}\right)^2}, \qquad \bar{s} = \frac{1}{N(N-1)} \sum_{i \ne j=1}^{N} s_{ij}.$$

ASYMMETRIC ADDITIVE FUZZY CLUSTERING MODEL

In practical applications, similar data s_{ij} is not always symmetric. For such asymmetric similar data, the additive fuzzy clustering model 2 is extended using an asymmetric aggregation function which is defined as a function satisfying the above conditions (1 and 2 in the above section.) Denoting the asymmetric aggregation function by γ (x, y), this is defined as follows:

Suppose that $f(x)$ is a generating function of t-norm and $\phi(x)$ is a continuous decreasing monotone satisfying ϕ: $[0,1] \rightarrow [1, \infty]$, $\phi(1) = 1$. Then we define the asymmetric aggregation operator $\gamma(x, y)$ as:

$$\gamma(x,y) = f^{[-1]}(f(x)+\phi(x)f(y)). \quad 4.$$

Using the asymmetric aggregation functions, we define the additive fuzzy clustering model for asymmetric similarity data as follows:

$$s_{ij} = \sum_{k=1}^{K} \gamma(u_{ik}, u_{jk}) + \varepsilon_{ij}, \quad 5.$$

where $\gamma(u_{ik}, u_{jk}) \neq \gamma(u_{jk}, u_{ik})$. This model expects to find clusters in which the objects are not only similar to each other but also asymmetrically related.

DYNAMIC ADDITIVE FUZZY CLUSTERING MODEL

The data are observed by the values of similarity with respect to n objects for T times, and the similarity matrix of t-th time is shown by $S^{(t)} = \{ s_{ij}^{(t)} \}$. Then a super-matrix is defined as follows:

$$S' = \begin{bmatrix} S^{(1)} & S^{(12)} & S^{(13)} & \cdots & S^{(1t)} \\ S^{(21)} & S^{(2)} & S^{(23)} & \cdots & S^{(2T)} \\ \vdots & \vdots & \vdots & \vdots & \vdots \\ S^{(T1)} & S^{(T2)} & S^{(T3)} & \cdots & S^{(T)} \end{bmatrix}, \quad 6.$$

where, $S^{(t)}$ is an asymmetric similarity matrix for t-th time and $S^{(t)} = \{ s_{ij}^{(t)} \}$, $s_{ij}^{(t)} \neq s_{ji}^{(t)}$. $S^{(rt)}$ is defined by $S^{(r)}$ and $S^{(t)}$ as follows:

$$s_{ij}^{(rt)} \equiv \gamma(s_{ij}^{(r)}, s_{ij}^{(t)}), \quad \gamma(s_{ij}^{(r)}, s_{ij}^{(t)}) \neq \gamma(s_{ij}^{(t)}, s_{ij}^{(r)}),$$

where $\gamma(\cdot,\cdot)$ is the asymmetric aggregation operator shown above. Then the model is as follows:

$$s'_{ij} = \sum_{k=1}^{K} \gamma(u_{i(t)k}, u_{j(t)k}), \quad 1 \le i, j \le Tn, \quad i = (n-1)t + i^{(t)}, \quad 7.$$

where, $1 \le i^{(t)} \le n$, $1 \le t \le T$. $u_{ik}^{(t)}$ is a degree of belongingness in t-th time of an object i to a cluster k and s'_{ij} is (i,j)-th element of the matrix S' in 6.

NUMERICAL EXAMPLE

I shall show a numerical experiment using artificial data shown in Figures 3 and 4. These diagrams denote the α-level surfaces of conical fuzzy membership functions of 8 fuzzy objects at two different times. From Figure 3 to Figure 4, the 4th object changes in vagueness, i.e., the object changes from a fuzzy observation to a crisp one. In this case, the value of α is 0.5. The proposed model uses similarity, so I transformed from similarity data to dissimilarity data using the following linear transformation in the unit interval:

$$s_{L(ij)} = 1 - \frac{d_{L(ij)}}{d_{L(\max)}}, \quad d_{L(\max)} \equiv \max_{i,j} d_{L(ij)}, \quad s_{R(ij)} = 1 - \frac{d_{R(ij)}}{d_{R(\max)}}, \quad d_{R(\max)} \equiv \max_{i,j} d_{R(ij)}.$$

Tables 1 and 2 show fuzzy dissimilarity matrixes for these fuzzy objects (Figs. 3 and 4), in particular, the upper triangular matrix denotes $d_{L(ij)}$, while the lower triangular matrix is $d_{R(ij)}$. Table 3 shows the results of model 2 using the fuzzy dissimilarity shown in Table 1, in which the similarities are $s_{L(ij)}$, $s_{R(ij)}$, -- the transformed Hausedorff distances, respectively. I use the algebraic product as ρ. In this table, C_1, C_2 represent two clusters, and each value denotes the fuzzy grade that a fuzzy object belongs to in each cluster. η^2 shows the value of fitness for the method. From this table, I can find the difference of the 4th and 5th fuzzy objects for belonging to the clusters. Namely, if the classification is based on $s_{R(ij)}$, then the 4th and 5th fuzzy objects are combined with the 1st - 3rd fuzzy objects, otherwise they belong to a cluster whose components are the 6th - 8th fuzzy objects by $s_{L(ij)}$. This difference is caused by a feature of fuzzy dissimilarities, that is, these dissimilarities depend on the direction and the size of the hyperellipsoids. The results of $s_{L(ij)}$ and the Hausedorff distance are almost same. However, in the case of the Hausedorff distances, the value of fitness is worse than the case of $s_{L(ij)}$.

Figure 5 shows the results of model 7 using data shown in Tables 1 and 2. The asymmetric aggregation operator in model 7 is $\gamma(x,y) = (x^2y)/(1-y+xy)$ which is created by a generating function of the Hamacher product [5], $f(x) = (1-x)/x$ and $\phi(x)=1/x^2$. In this figure, the abscissa shows the numbers of objects and the ordinate shows the degree of belonging of objects to clusters: (a) shows the degree of belonging to cluster 1 while (b) shows the degree of belonging to cluster 2. From this figure, I can see changes in the situation of object 4. Moreover, we can see movement in object 7. This shows the large change in dissimilarity between objects 4 and 7 from the 1st time to the 2nd time, by comparing other dissimilarities between the objects.

Table 1: Fuzzy distance matrix at 1st time ($\alpha = 0.5$).

No	1	2	3	4	5	6	7	8
1	0	8	9	21	22	63	63	71
2	9	0	9	24	25	57	73	57
3	11	8	0	14	16	56	54	63
4	50	42	39	0	9	78	86	75
5	51	53	40	9	0	75	71	83
6	62	55	51	13	13	0	8	7
7	66	65	55	22	25	8	0	10
8	72	59	62	23	25	14	12	0

Table 2: Fuzzy distance matrix at 2nd time ($\alpha = 0.5$).

No	1	2	3	4	5	6	7	8
1	0	8	9	26	22	63	63	71
2	9	0	9	27	25	57	73	57
3	11	8	0	19	16	56	54	63
4	18	16	10	0	5	37	43	34
5	51	53	40	5	0	75	71	83
6	62	55	51	41	13	0	8	7
7	66	65	55	49	25	8	0	10
8	72	59	62	40	25	14	12	0

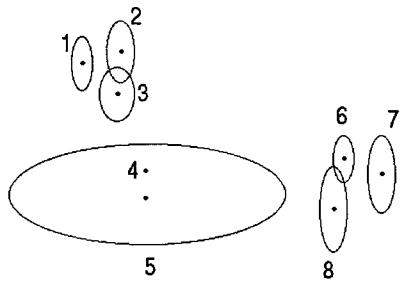


Fig. 3. α-level surfaces of conical membership functions at 1st time ($\alpha = 0.5$).

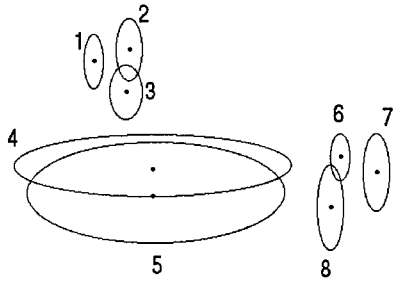
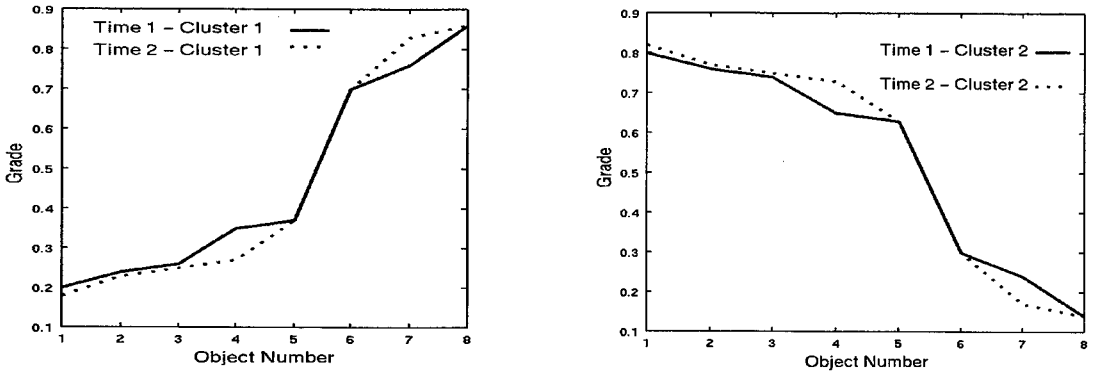


Fig. 4. α-level surfaces of conical membership functions at 2nd time ($\alpha = 0.5$).

Table 3: Fuzzy Clustering at 1st time ($\alpha = 0.5$).

	$S_{L(ij)}$		HD		$S_{R(ij)}$	
No.	C_1	C_2	C_1	C_2	C_1	C_2
1	.16	.84	.24	.76	.01	.99
2	.20	.80	.26	.74	.09	.91
3	.19	.81	.27	.73	.16	.84
4	.06	.94	.10	.90	.72	.28
5	.08	.91	.15	.85	.74	.26
6	.90	.10	.94	.06	.88	.12
7	.93	.07	1.0	.00	.91	.09
8	.94	.06	.98	.02	.91	.09
η^2	.0343		.1969		.0326	

HD = Hausedorff distance



(a) Clustering for cluster 1. **(b)** Clustering for cluster 2.

Fig. 5. Dynamic fuzzy clustering ($\alpha = 0.5$ and $\eta = 0.0015$).

CONCLUSION

This paper proposed a clustering model which can extract changes in vagueness involved in observations. This can be possible by obtaining solutions on the same coordinate, in other words, this model can obtain clustering results using the same clusters throughout time. Concerning the representation of vagueness for real data this is now under consideration.

REFERENCE

1. H. Bandemer and W. Näther, 1992. Fuzzy Data Analysis. Kluwer Academic Publishers.
2. J.D. Carroll and J.J. Chang, 1970. Analysis of Individual Differences in Multidimensional Scaling via an N-way Generalization of ``Eckart-Young" Decomposition. Psychometrika, 35, 283-319.
3. J.D. Carroll and P. Arabie, 1983. INDCLUS: An Individual Differences Generalization of the ADCLUS Model and MAPCLUS Algorithm. Psychometrika, 48, 157-169.
4. A. Celminš, 1992. Nonlinear Least-Squares Regression in Fuzzy Vector Spaces. Fuzzy Regression Analysis, (J. Kacprzyk et al. eds.), 153-168.
5. R. Fullér, 1991. On Hamacher-sum of Triangular Fuzzy Numbers. Fuzzy Sets and Systems, 42, 205-212.
6. L.T. Kóczy and K. Hirota, 1993. Ordering, distance and closeness of fuzzy sets. Fuzzy Sets and Systems, 59, 281-293.
7. T. Okuda, Y. Kodono and K. Asai, 1992. Approximate Maximum Likelihood Estimates in Regression Models for Fuzzy Observation Data. Fuzzy Regression Analysis, (J. Kacprzyk et al. eds.), 169-180.
8. M. Sato-Ilic, 1999. On Dynamic Clustering Models for 3-way Data. J. of Advanced Computational Intelligence, 3(1), 28-35.
9. L.A. Zadeh, 1965. Fuzzy Sets. Information and Control, 8, 338-353.

Thin Films and Surface Processing

Modelling and Control of Optical Interference Filters Using Plasma Assisted Chemical Vapour Deposition

D.A. Linkens*, M.F. Abbod*, J.G. Metcalfe and B. Nichols****

* Department of Automatic Control and Systems Engineering,
University of Sheffield, Sheffield, England, U.K.
** GEC-Marconi Materials Technology Limited, Caswell, Towcester, UK.

ABSTRACT

Optical interference filters with continuously modulated refractive indices throughout their thickness (rugates) are designed and fabricated using microwave plasma-assisted chemical vapour deposition techniques. Intelligent modelling and control techniques are used to model the process and improve the reproducibility of reflection filters.

INTRODUCTION

Dielectric optical interference filters are made by depositing a sequence of discrete layers of transparent materials that have different refractive indices. Different filters with different optical performances can be made by depositing high and low refractive indices in multiple-layers. One of the most significant recent advances in optical filters has been the realisation of rugate type filter designs. A rugate filter (Latin: *rugosus* = wrinkled) is an interference filter in which the refractive index varies periodically as a smooth continuous function of optical thickness, the simplest example being that the variation is sinusoidal. The implementation of the most advanced rugate type designs should achieve optical performances that would have been impossible using conventional design. The realisation of rugate filters requires both the availability of an optical material whose refractive index can be varied significantly by varying its composition and a means of depositing the material uniformly over a surface while controlling its index continuously to a high accuracy.

A model was developed for a similar process (semiconductor manufacturing) to predict the thickness of the deposited polysilicon films using a fuzzy inference system [1]. In the present paper, a neuro-fuzzy model is presented to model the process of depositing thin films on a transparent substrate. The model is based on experimental data obtained from a microwave plasma-assisted chemical vapour deposition (MPACVD) process, utilising different inputs such as gas flow rates, pressure, microwave power and temperature. The model output is the predicted growth rate for each deposited layer and its refractive index. This output is fed to the rugate filter design to obtain the final characteristics of the filter, i.e., wavelength and stop band.

Based on the model, a control technique is under development to set up the inputs and calculate the number and length of material-depositing cycles. Utilising the growth characteristics of the rugate filter, an on-line correction procedure is used in each cycle to yield consistent, required filter characteristics. In this paper we discuss issues of concern in designing a rugate fabrication process. We present control and monitoring methods that have been investigated, and suggest areas where improved process capability in controllers based on intelligent principles would aid development of this emerging technology.

DEPOSITION PROCESSES

The specific rugate coatings are optical interference films where the refractive index of the film continuously and periodically varies as a function of the film's optical thickness. The index variation is typically achieved by co-depositing two materials of different index. Co-deposition complicates process monitoring and control. Bleed gas rates for reactive deposition and microwave beam parameters must be actively controlled as the constituent material rates are varied to ensure good process quality. Blended material systems are more sensitive to temperature and source plume distributions than are discrete stack filters. Deviation in the

0-7803-5489-3/99/$10.00 ©1999 IEEE.

controller settings for source flow rates and in temperature can cause an increase in out-of-band transmission in the filters. The challenge of fabricating rugate filters is not so much filter design as process control.

Since a large RI variation is needed in the filter deposition, silicon oxynitride was used, which retains a glassy phase throughout its composition from silica (refractive index 1.46) to silicon nitride (refractive index 2.04), the index varying smoothly with composition. The precursors used are silicon tetrachloride ($SiCl_4$), O_2 and N_2 gases. The $SiCl_4$ is contained in a constant temperature bubbler and transported on a carrier gas, normally nitrogen. The argon affects the power density of the microwave plasma but does not take part in deposition. Silicon oxynitride films deposited by MPACVD are remarkably durable and highly resistant to scratching. They resist acid attack and can be handled and cleaned without taking special precautions.

DEPOSITION EQUIPMENT

Microwave plasma-assisted chemical vapour deposition (MPACVD) is a new technique being applied to fabricate hard, dielectric optical coatings. The method is currently being developed within GEC-Marconi [2]. The deposition equipment is shown schematically in Figure 1. It consists of a plasma chamber made of fused silica and contained in a furnace designed to operate up to 1000°C. The chamber is evacuated by a pump to maintain a working pressure in the chamber of about 1 mbar for the required gas flow. Microwave power is coupled to the chamber by a tuned launcher enclosing the gas inlet limb. The waveguide feed incorporates a cross-coupler with attenuators so that forward and reflected power is continuously monitored. Typically, a net microwave power of 1 kW is supplied to the plasma. All gases supplied to the chamber are controlled using precision mass-flow controllers. A computer program calculates the flow parameters to achieve the required RI modulation against optical thickness during each rugate cycle based on known calibration data.

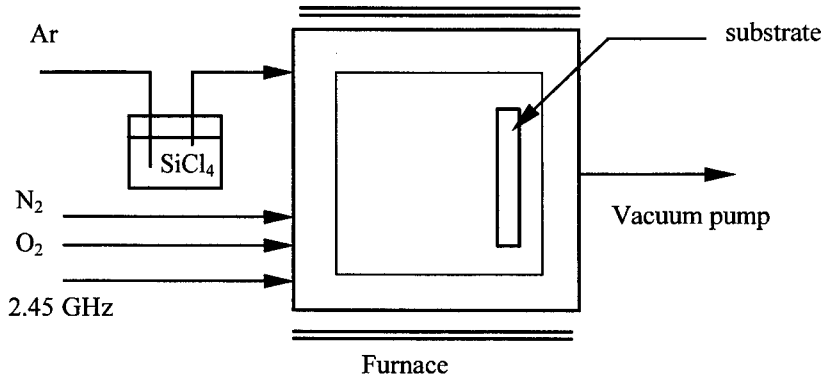


Fig. 1. Schematic diagram of the depositions apparatus.

PROCESS MODELING

Neurofuzzy Modeling (ANFIS)

The Adaptive Network-based Fuzzy Inference System (ANFIS) architecture is based on a fuzzy inference system implemented in the framework of an adaptive network [3]. Using a hybrid learning procedure, ANFIS can learn an I/O mapping related to human knowledge (in the form of fuzzy if-then rules). The ANFIS architecture has been employed by various researchers to model non-linear functions, identify non-linear components on-line in a control system, and predict chaotic time series etc.

ANFIS identifies an I/O mapping, available in the form of a set of N input-output examples, with a fuzzy architecture, inspired by the Takagi-Sugeno modeling approach. The fuzzy architecture is characterised by a set of rules, which are properly initialised and tuned by a learning algorithm. The rules are in the form:

1. if input 1 is A_{11} and input 2 is A_{12} then output = f_1(input 1, input 2)
2. if input 1 is A_{21} and input 2 is A_{22} then output = f_2(input 1, input 2)

where A_{ij} are parametric membership functions.

Process Model

The experimental results obtained from the process consist of a set of input data for each variable, and its corresponding output in terms of the layer growth rate (GR) and the refractive index (RI). A set of 18 data points was used to train. Seven inputs were selected: temperature, microwave power, pressure and O_2, Ar, $SiCl_4$ and N_2 flow rates. Neural network training would require many more data points for the training process to generate a good model, unlike ANFIS which can produce a good model with little data. Since ANFIS can generate a model for one output only, two models were generated representing the GR and RI. Figure 2 shows a block diagram of the neurofuzzy inference system for the MPACVD model.

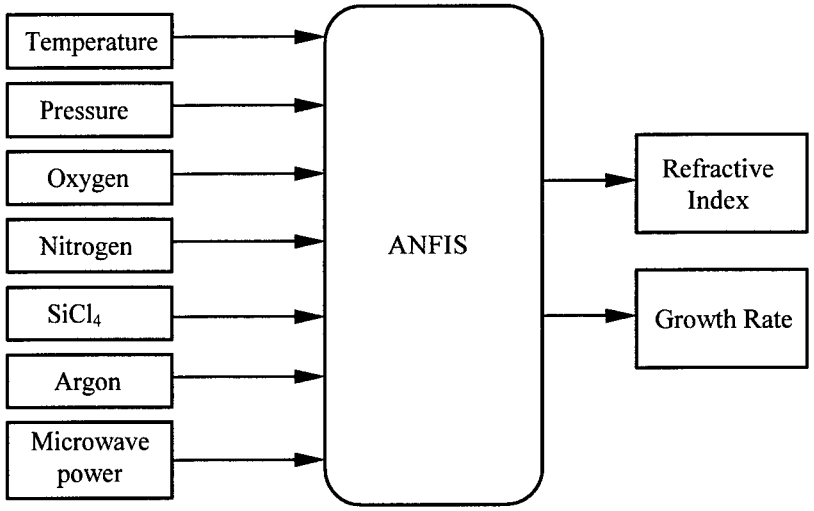


Fig. 2. Block diagram of fuzzy inference system.

The two outputs from the process model are fed into a model to calculate the spectral characteristics of the filter [4]. A typical growth record is shown in Figure 3. The filter output is calculated by feeding the operating conditions into a neuro-fuzzy model to obtain RI and GR. Then the output of the growing process is calculated by feeding the Optical Thickness (OT) and RI into the optical filter equations to obtain the frequency response during each depositing cycle. Optical thickness is the result of combining RI with GR.

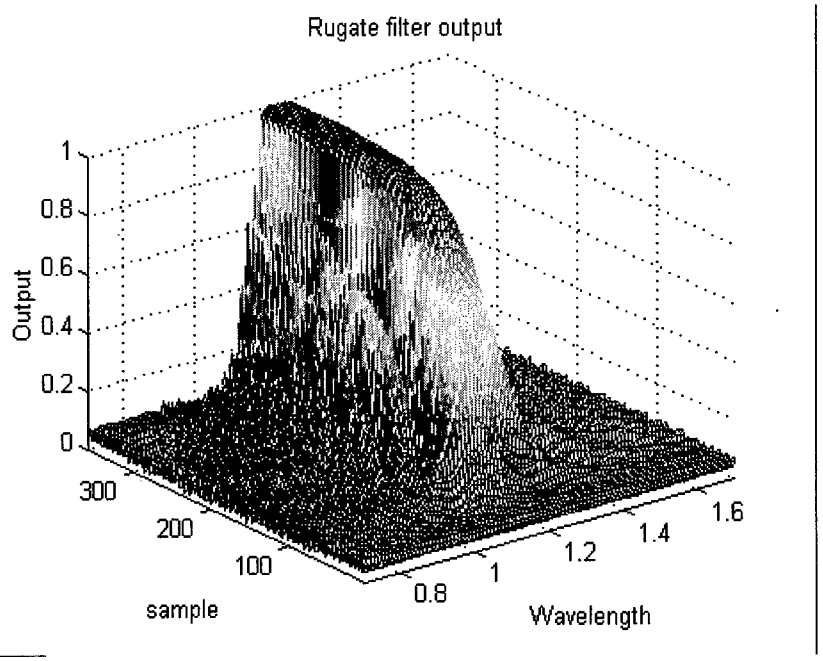
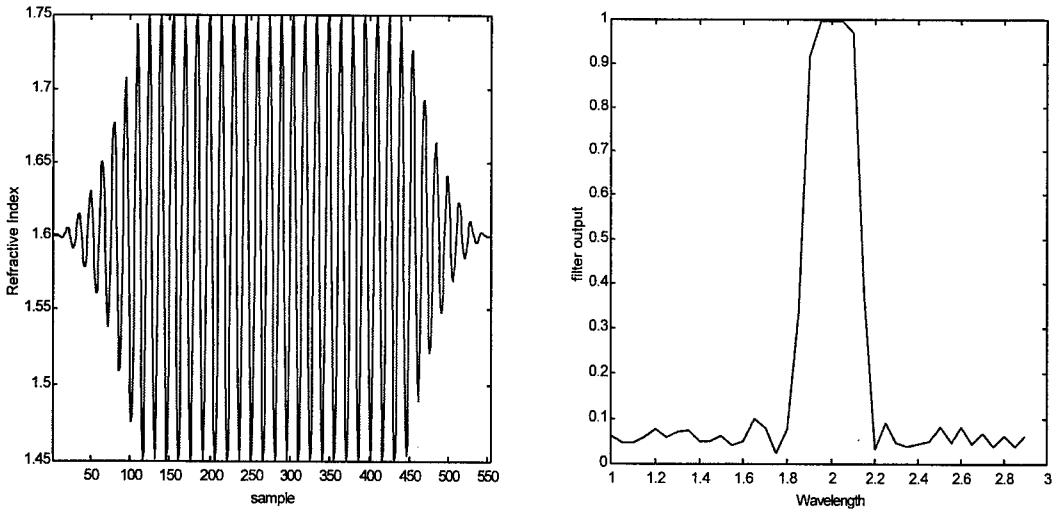


Fig. 3. Rugate filter response to using the process model.

Rugate Filter

Figure 4 shows the refractive index for a 37 layer filter and its modelled spectral characteristics. An apodising envelope modulated sinusoidal refractive index layer can produce a suppressed side band rugate filter [5].



(a) Refractive index (b) wavelength response

Fig. 4. Refractive index profile and wavelength response for a 37 cycle filter.

The refractive index is varied smoothly between two limits in a sinusoidal manner by varying the oxygen gas flow smoothly in the same manner. The application of MPACVD to the deposition of a variable index material such as silicon oxynitride allows these theoretical models to be realised in practice without the complexity of the approximation techniques involving constant index layers.

CONTROLLER DESIGN

The process of making filters starts with calibrating the apparatus under standard operating conditions in terms of refractive index versus oxygen flow rates. This also allows the determination of deposition rate as a function of flow rates, which is also required.

Initially the number of growing cycles and refractive index (RI) range is calculated based on the required reflectivity and bandwidth. Then the cycle length is calculated based on the growth rate obtained from the model. Depending to the deposited materials, operating conditions and filter design, the RI will vary between two limits. In our case the limits will be between the RIs of silica (1.46) and silicon nitride (2.04). Based on the cycle number, length and RI variation, sinusoidal cycles of RI are generated. The RI cycles are then fed into an inverse model of the process which utilises the RI and the other input variables as inputs, and predicts the oxygen level required for achieving the input RI. This neurofuzzy model was developed using ANFIS which was trained using the same operating data but in a different format.

In order to obtain a uniform sinusoid in optical thickness during the growing process and modulation of the RI, the oxygen cycle has to be modified to ensure that the growth rate variation with oxygen flow rate is taken into account. The modified oxygen cycles are then fed to the process to start deposition of materials.

During the growing process, the filter response is monitored so that adjustments may be made to the growth conditions to counter any developing defects. Figure 5 shows a block diagram of the system including the model and controller.

SIMULATION RESULTS

The system has been simulated using Matlab. A filter was simulated to achieve a reflectivity of 0.996 at a wavelength of 2.0 microns and a bandwidth of 9%. This resulted in a design with 37 growth cycles and, after adjusting the oxygen cycle, the cycle length was 12 min. This means the growing process takes 444 min.

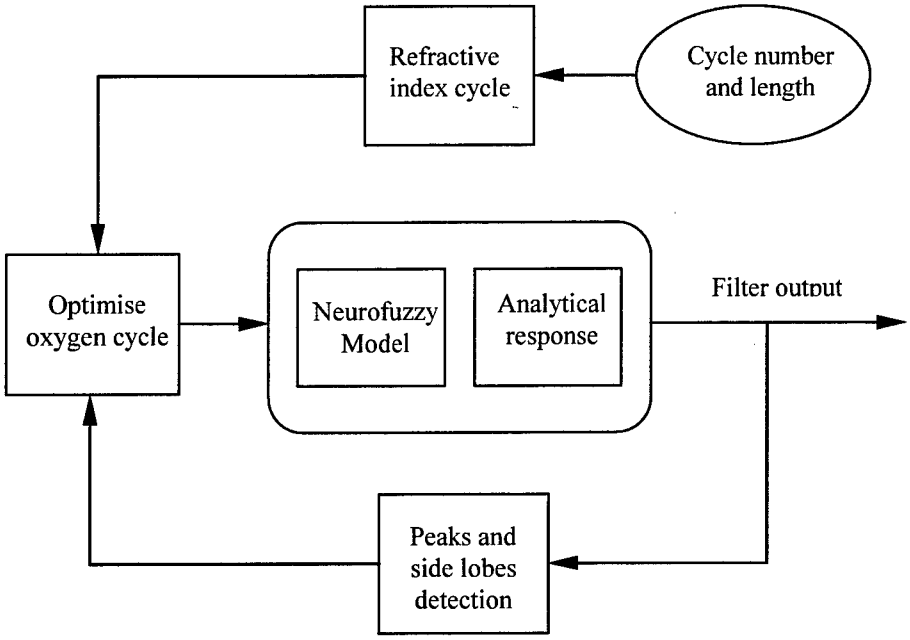
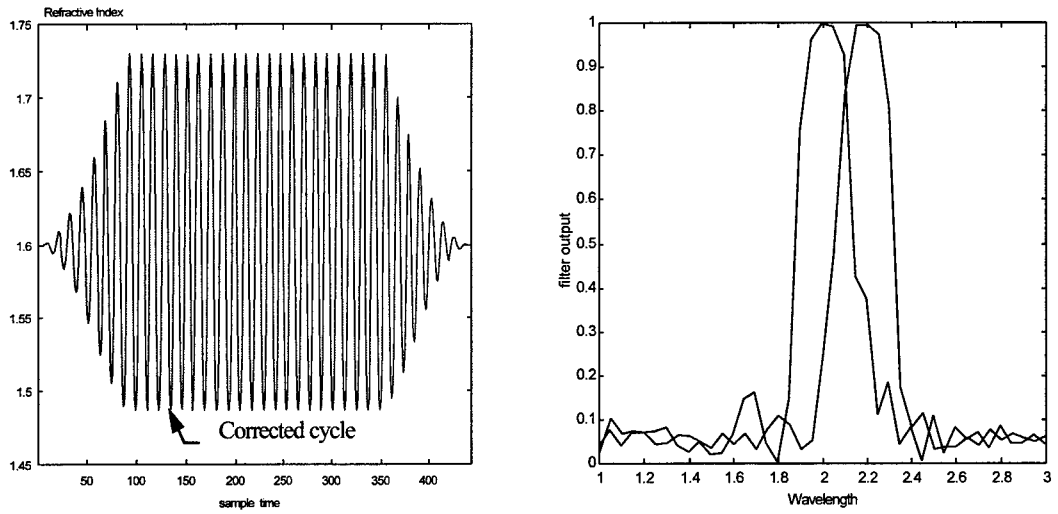


Fig. 5. Block diagram of the PMACVD control system.

During the simulation of the growing process, a defect was introduced, at cycle 11. To counter this the software reduced the growth time for this cycle to 11, then the cycle length was set back to normal length until the end of the deposition process. Without correction, the filter output would have ended up with an erroneous bandwidth. In figure 6(a) the refractive index profile of an apodised 37 sinusoidal rugate cycles is shown. The final filter spectral response is shown in figure 6(b). The solid line represents the filter response with the correction procedure, while the dotted line represents the filter response without correction procedure.



(a) Refractive index cycle (b) Filter spectral response

Fig. 5. 37 cycle rugate filter.

CONCLUSION

MPACVD has been successfully applied to the fabrication control of continuously modulated refractive index dielectric interference filters of rugate design. The process has been modelled using a neurofuzzy technique. The model interprets the input-output relationships captured by means of fuzzy sets and inference rules trained using the neurofuzzy technique. The model can be used to simulate the behaviour of the process and to design the control algorithm for achieving the required response.

ACKNOWLEDGEMENT

Two of the authors (from Sheffield University) gratefully acknowledge the UK EPSRC (Engineering and Physical Sciences Research Council) for their financial support.

Two of the authors (from GEC-Marconi) gratefully acknowledge the support of the European Commission under Brite-EuRam project BE-96-3059, OPTICOM.

REFERENCES

1. R.L. Chen, C.J. Spanos, 1992. Self-learning fuzzy modelling of semiconductor processing equipment. IEEE/SEMI Advanced Semiconductors Manufacturing Conference.
2. A.C. Greenham, B.A. Nichols, R.M. Wood, N. Nourshargh, L.L. Kewis, 1993. Optical interference filters with continuous refractive index modulations by microwave plasma-assisted chemical vapour deposition. Optical Eng., 32(5), 1018-1023.
3. J.R. Jang, 1993. ANFIS: adaptive-network, based fuzzy inference system. IEEE transaction on Systems, Man, and Cybernetics, 23(3), 665-685.
4. H.A. Macleod, 1986. Thin film optical filters. Adam Hilger Ltd, 2nd edition.
5. W.H. Southwell, R.L. Hall, 1989. Rugate filter side-lobe suppression using quantic and rugated quantic rugated layers. Appl. Opt., 28(4), 2949-2951.

A Study of Mechanical Properties of Multi-layered Thin Films

T. Hirasawa, H. Kotera, S.Tawa, S. Shima

Department of Mechanical Engineering, Kyoto University
Yoshidahonmachi, Sakyou-ku, Kyoto, 606-8501, Japan

ABSTRACT

It is of great importance to investigate mechanical properties of a multi-layered thin film in designing and realizing micro-electro-mechanical systems (MEMS). A new tensile test method is proposed to measure mechanical properties of a multi-layered thin film, which are used in MEMS. In this method, we develop a prefabricated test substrate of gage portion. After measuring Young's modulus of prefabricated test substrate, a thin film is deposited on the test substrate and tensile test is carried out. Young's modulus of the thin film can be measured by subtracting the effect of Young's modulus of the prefabricated test substrate. As an example, Young's modulus of a tungsten thin film deposited by sputtering is measured. We discuss the viability of this method for measuring the mechanical properties of deposited thin film.

INTRODUCTION

There have been a number of studies of micro-electro-mechanical systems (MEMS), such as pressure micro sensor [1], micro motor [2], micro switch [3] etc. In fabrication of MEMS, in general, materials are deposited on other materials by sputtering, CVD or vapor deposition; the MEMS are thus composed of multi-layered thin films. They must behave in a desired manner under external forces or support applied loads in practice, and therefore the mechanical properties of the multi-layered deposited materials should be clarified in designing the MEMS devices.

Several methods have been proposed to measure the mechanical properties of thin films. Tabata et al. measured Young's modulus and Poison's ratio of silicon nitride thin film by a bulge test [4]. Weihs et al. measured Young's modulus of Au and SiO_2 by a bending test of cantilever microbeams [5] and Hashimoto et al. measured a Co-Ta-Zr film by a three-point bending procedure [6], while Kieseweter et al. employed the resonance method for a silicon nitride thin film [7].

In these studies, the specimens are subjected to bending. In the calculation, it is assumed that Young's modulus of the deposited thin film in tensile direction is equal to that in the compresive direction. However, it is common knowledge that the internal structure of the deposited thin film made by sputtering or CVD is granular or porous, and that the mechanical properties of the deposited thin film may be different from those of the bulk material. For example, piezo-electric films such as PZT or ZnO, are of an oriented structure [8], which results in highly anisotropic properties. Therefore, to clarify the mechanical properties of the thin film, test methods that cause a stress distribution such as in bending may be inappropriate.

Conventionally, the tensile test is a most familiar and straightforward test. Sharpe et al. and Ando et al. proposed an on-chip tensile test [9,10]. They measured Young's modulus of silicon films fabricated on silicon substrates. By their methods, the gage portion is fabricated by a surface micro-machining process, and then the material is subjected to wet or dry etching. This can have an unpredictable effect on the mechanical properties of the specimen. Also, the internal structure of the film is affected by the fabrication process. A scatter of more than ±20% in their measured results may have been caused by these factors. It is necessary to develop a test system in which the effects of the above factors are eliminated.

In this study, we propose a new tensile test method. A prefabricated test substrate on which a thin film is deposited is developed. The concept of our method is shown in Fig.1. First, on a silicon substrate, the gage portion is prefabricated by surface micro-machining such as photolithography and wet-etching. After fabricating the test substrate, a tensile test is performed to measure Young's modulus of the test substrate. Secondly, the thin film we are concerned with is deposited on the prefabricated test substrate. Finally, the

0-7803-5489-3/99/$10.00 ©1999 IEEE.

tensile test is again performed. Young's modulus of the thin film can be measured by subtracting the Young's modulus of the prefabricated test substrate. For the purpose of this, we also developed a new tensile test equipment and a test substrate holder. As an example, we measure Young's modulus of a tungsten film deposited on a prefabricated test substrate by sputtering. We discuss the viability of this method for measuring the mechanical properties of deposited thin films.

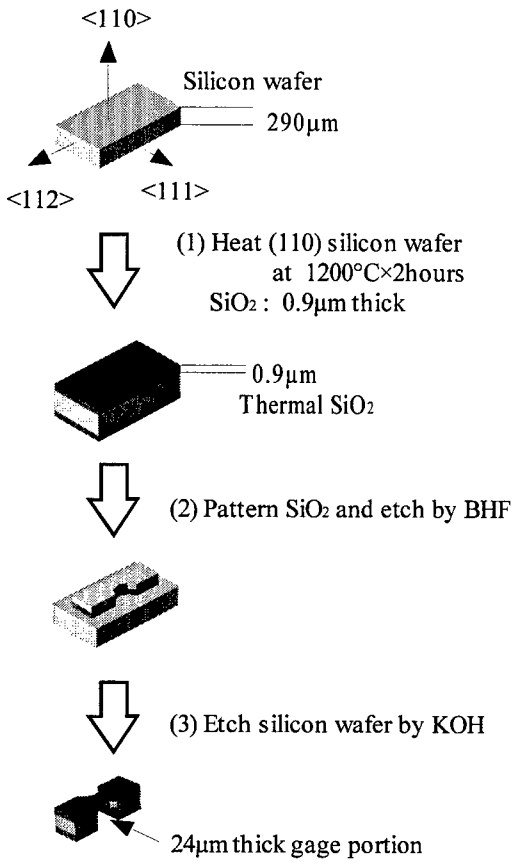


Fig. 1. Concept of test method.

EXPERIMENT

Prefabricated Test Substrate

Figure 2 shows a schematic drawing of the prefabricated test substrate. The gage length was 1955μm, the width 962μm and the thickness of the gage portion is 24μm. To fix the test substrate, a pair of through holes are drilled in the test substrate. The test substrate is fabricated using the steps shown in Figure 1.

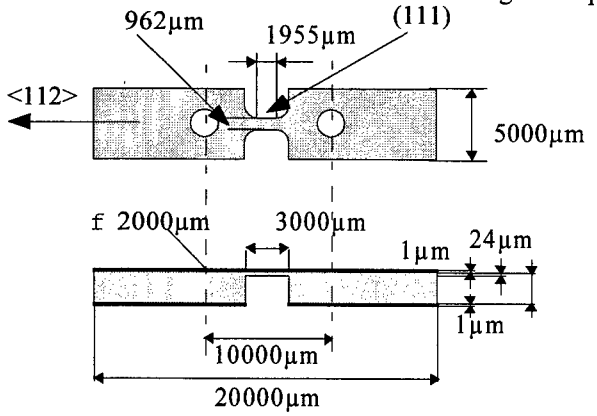
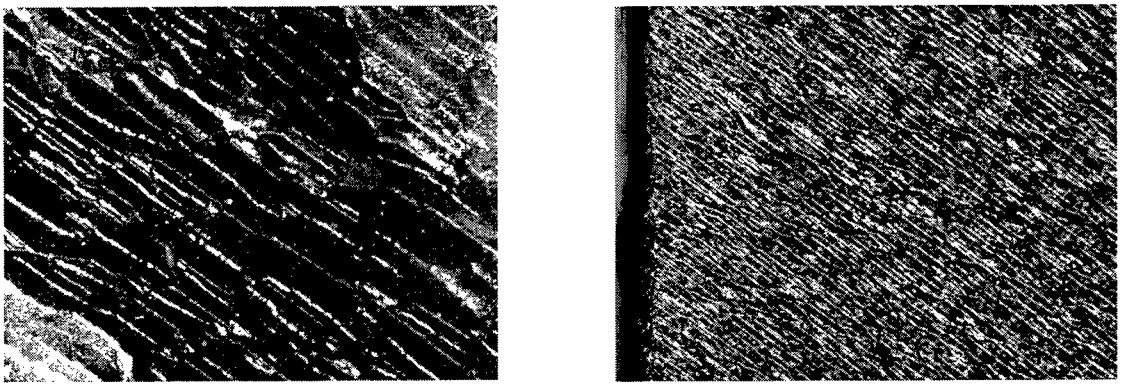


Fig. 2. Schematic drawing of prefabricated test substrate.

1. A 0.9μm thick thermal SiO_2 is produced as a mask by heating a (110) silicon wafer at 1200°C×2hour.
2. The mask pattern is set so that the gage length direction is parallel to the (111) plane, that is, the side-edge surfaces of the gage portion consist of (111) planes. Then SiO_2 is etched by BHF (NH_3F 50wt% : HF 49% = 10:1).
3. The gage portion is anisotropically etched by KOH.

The etching conditions are summarized in Table 1. Figure 3.a. shows a photograph of the surface etched by 24wt% KOH. The mean surface roughness is ~10μm. Figure 3.b. shows the surface of the gage portion etched by 40wt% KOH. In this case, the mean roughness was below 2μm. As seen in these photographs, surface roughness is affected by the etching conditions. So, we chose 40wt% KOH at 80°C for Si-etching.

Since the gage portion of the test substrate is rather weak and is likely to be broken during KOH etching, we employed a test substrate holder made of Polytetrafluorethylene (PTFE) as shown in Figure 4.a. The holder is composed of two parts: upper holder and lower holder. The test substrate was sandwiched between these two parts. The lower holder has a guide recess to prevent the test substrate from twisting or bending. There is a through hole in these holders so that we are able to etch and observe the gage portion of the sandwiched test substrate. Before we deposit the thin film on the prefabricated test substrate, we replace the PTFE holder by a glass one. The tensile test is carried out on the glass holder.



a. Surface etched by 24wt% KOH
Roughness : 10 μm

b. Surface etched by 40wt% KOH
Roughness : 2 μm

Fig. 3. Photograph of etched surface of test substrate.

Table 1: Conditions of KOH Etching Process

Solution	24wt% ,40wt%
Temperature	80°C
etching time	1.5-2hours

Tensile Test Equipment

Figure 5 shows a schematic drawing of the test equipment. The prefabricated test substrate was fixed on the dual axial stage by a pin. The test substrate was subjected to tensile load when pulling the claw. The displacement of the claw was measured by a differential transformer; it was attached on the triaxial stage to align the claw with that of the differential transformer. The claw part was pulled through a 9.8N load cell mounted at the end of a micrometer. The micrometer was controlled by a reduction gear. The claw part was suspended by a pair of plate springs. It was long enough so that the claw part moved in parallel to the gage portion, and therefore, the tensile load was not affected by the spring.

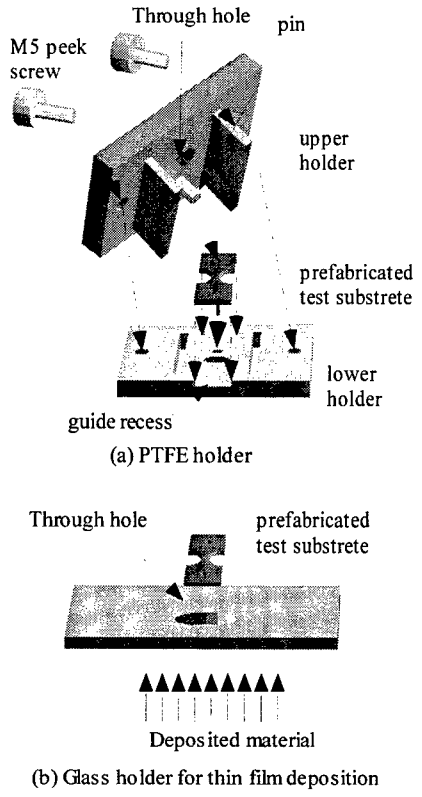


Fig. 4. Schematic drawing of test substrate holder.

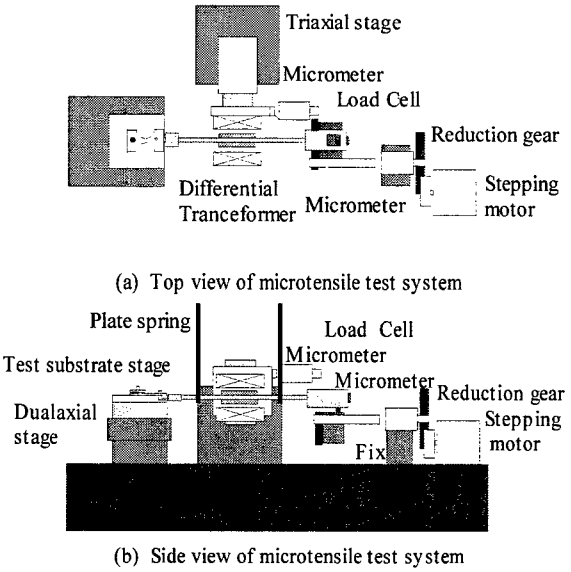


Fig. 5. Schematic of micro-tensile test equipment.

RESULTS and DISCUSSION

As an example, we made an attempt to measure Young's modulus of a tungsten thin film by the proposed system. Prior to the measurement of Young's modulus of the deposited material, we measured the stress-strain curve of the prefabricated test substrate. This is shown in Figure 6. The relationship between stress and strain is linear and Young's modulus of the prefabricated test substrate is 129.7GPa. The test substrate did not break up to 250MPa.

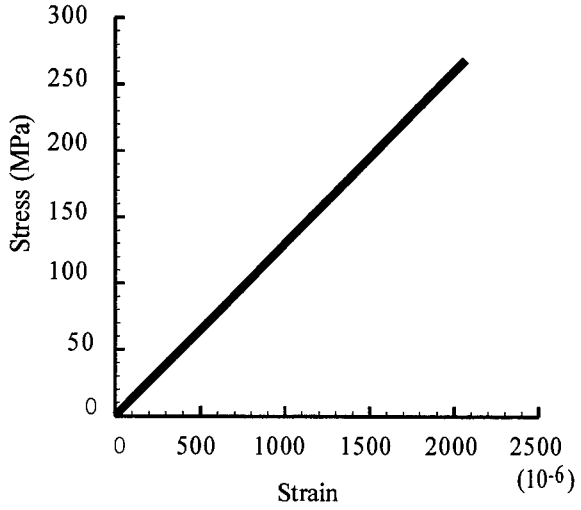


Fig. 6. Typical stress-strain curve for test substrate.

A 0.6μm thick tungsten film was deposited on the test substrate by sputtering. The sputtering conditions are shown in Table 2. After the tungsten was deposited, a tensile test was performed again. The stress/strain curve is also liner and so, Young's modulus was obtained as 132.7 GPa. Since the tungsten was deposited on the silicon wafer, no diffusion has occurred. The measured Young's modulus of the tungsten film is 246 GPa, while that of bulk tungsten is reported as 352 GPa; the former being ~30% lower than the latter. This may be attributed to the difference in internal structure, i.e, porosity. Figure 7 shows AFM images for a 0.3 μm thick tungsten film with a mean surface roughness of 2.3 nm and of a 0.6 μm thick tungsten film with a mean surface roughness of 4.5nm. From these images, the structure seems to be composed of granular material; the grain size is about 40 nm diameter for the former film and about 8 nm for the latter. If the film is porous, Young's modulus is lower than that of the fully dense material. Both the mean roughness and the grain size increase with increased thickness or sputtering time. Since the internal structure of the tungsten film may grow toward its thickness direction, the properties in-the plane direction may be inferior to those of the isotropic bulk material.

Table 2: Sputtering condition for tungsten

RF power	60w
Ar pressure	6.7 10^{-1}Pa
Sputtering rate	0.6μm/hour

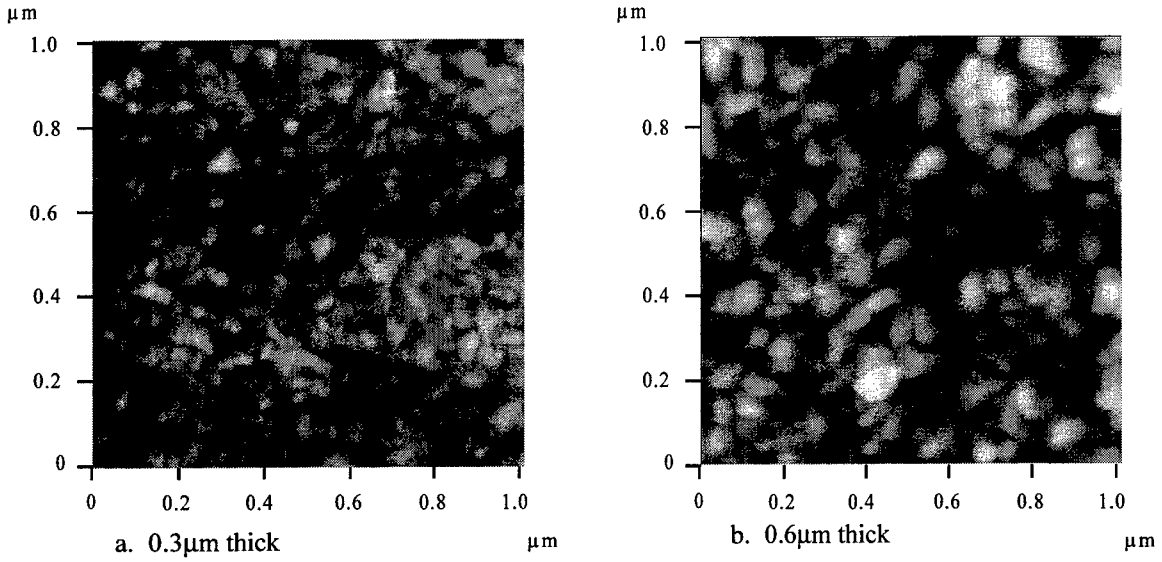


Fig. 8. AFM surface image of tungsten.

In layered thin films, diffusion may occur affecting the mechanical properties as shown in our previous work [11]. Furthermore, it is well-known that the internal structure of the thin film is affected by its substrate or by a pre-deposited film. In the proposed test method, if we repeat the tensile test and deposition of the thin film alternately, then we can accurately measure Young's modulus of each film and of the multi-layered film. The effects of the above factors on the mechanical properties of a single layered or multi-layered film can thus be investigated.

CONCLUSION

A method to measure Young's modulus of thin films using a prefabricated test substrate was proposed. To confirm the viability of the method, a tungsten film deposited on the test substrate was measured. We therefore have shown the potential of this method to measure precisely the mechanical properties of thin films.

ACKNOWLEDGEMENT

This work was supported by a Grant-in-Aid for Scientific Research (C)(No. 10650258) by the Ministry of Education, Science, Sports and Culture.

REFERENCES

1. Mastrangelo, C.H. et al., 1996. Surface-Micromachined Capacitive Differential Pressure Sensor with Lithographically Defined Silicon Diaphragm. Journal of Micromechanical Systems, 5(2), 98-105.
2. Tai, Y. et al., 1989. IC-processed Electrostatic Synchronous Micromotors. Sensors & Actuators, 20, 49-55.
3. Zavracky, P.M. et al., 1997, Micromechanical Switches Fabricated Using Nickel Surface Micro machining. Journal of Microelectromechanical Systems, 6(1), 3-9.
4. Tabata, O. et al., 1989. Mechanical Property Measurements of Thin Films Using Load-Deflection of Composite Rectangular Membranes. Sensors and Actuators, 20, 135-141.
5. Weihs T.P. et al., 1988. Mechanical deflection of cantilever microbeams: A new technique for testing the mechanical properties of thin films. J,Mater,Res., 3(5) Sep/Oct, 931-942.
6. Hashimoto, K. et al., 1994. Development of Precision Three-Points Bending Machine for Measuring Young's Modulus of Thin Films for Electronic Devices. J. Soc. Mat. Sci. Japan, 43(489), 703-709.
7. Kiesewetter L. et al., 1992. Determination of Young's moduli of micromechanical thin films using the resonance method. Sensors and Actuators A, 35, 153-159.
8. Kotera, H., 1999. Piezoelectric Property of CVD ZnO Film for Pressure Micro Sensor. Advances in Information Storage Systems (AISS), 9, in press.
9. Sharpe, W.N. et al., 1997. Measurements of Young's Modulus, Poisson's ratio, and Tensile Strength of Polysilicon. Journal of Microelectromechanical Systems, 6(3), 193-199.
10. Ando Taeko et al., 1999. Measurement of Stress and Stran of Single-Crystal-Silicon Thin Film during On-Chip Tensile Test. T. IEE Japan, 119-E(2), 67-72.
11. Hirasara, T. et al., 1999. A study of the effect of the fabrication process on the diffusion in a layered thin film. Microsystem Technologies 26, in press.

Fast 3D - Surface Quality Control

Jürgen Leopold

Society for Production Engineering and Development
Department for Calculation and Testing
Lassallestr. 14
D - 09117 Chemnitz; Germany
Email: 100536.1232@compuserve.com

ABSTRACT

Inspection is the process of determining if a product deviates from a given set of specifications. Fast Inspection usually involves measurement of specific part features such as assembly integrity, *geometric dimensions and surface finish.* It is a quality control task, but is distinguished from testing tasks. The visual inspection of 3D - parts (bulk materials and also thin-film) is a special task within manufacturing that has been automated at a comparatively slow pace up to this time. Different optical methods, applied for 3D - Measuring of microscopically and macroscopically bulk parts and thin-films based on the Laser Scanning Technique (LST), the Projected Fringes Method (PFM), the Electronic Speckle Interferometry (ESPI), White-Light-Interferometry (WLI) and also on SEM- and AFM- Methods. In addition, stylus instruments and also colorimeter measurements will be included. The physical characterization of the surface topography is the scientific basis for the next step, the intelligent interpretation. Advantages and disadvantages of different contemporary intelligent methods : Neural Net based Classification; Fuzzy - Clustering; Fractal Analysis and some industrial applications will be discussed.

Keywords
Surface Characterization, Bulk and Thin-Film Inspection, Laser Scanning, Projected Fringes Method, Photogrammetric Method, Electronic Speckle Pattern Interferometry, AFM, SEM, Fractal Analysis; Neural Net

INTRODUCTION

In different companies Quality Assurance policy is established in order to guarantee the best quality products and technical support for its clients. In this way, in-process inspections must cover all levels of production to meet the requirements of ISO 9000.

The surface of a solid is that part of the solid that represents the boundaries between the solid body and its environment. Surfaces as physical entities possess many attributes, geometry being one of them. Surface geometry by nature is three-dimensional and the detailed features are termed topography. In engineering, topography represents the main external features of a surface.

In practice, the notion of a surface extends to sub-layers of solid boundaries and the surface assumes certain internal features. These internal features, e.g. hardness, residual stress, deformation, chemical composition and reactions, microstructure, are often of foremost concern in an application and surface topography often interrelates with these features, in complicated manners and in three dimensions, to manifest certain engineering properties. Surface topography is, therefore, significant for surface performance and the importance of surface topography measurement as a means of functional analysis and prediction is indisputable. Engineering surfaces are created in various way, typically by machining, surface treatment and coating. Surface topography modification is therefore performed by material removal, transformation or addition. Most often a combination of various machining, treatment and coating operations are employed to produce surfaces with characteristics that are desirable for a particular application. Each surface generation process produces surface topography characteristic of the process and process variables used. Surface topography, therefore, contains signatures of the surface generation process and as such can be

0-7803-5489-3/99/$10.00 ©1999 IEEE.

used to diagnose, monitor and control the manufacturing process. In an engineering sense, the ultimate objective of surface topography measurement, as a means of control and knowledge, is to establish a correspondence between an engineering surface phenomenon (e.g. wear, chatter, etc.) and its topographical characteristics (e.g. bearing area and oil retention volume, waviness power and periodicity, etc.). Surface topography measurement, therefore; serves as a vital link between manufacturing, functional performance analysis and prediction, and surface design.

The relationships between surface design, function, manufacturing and assessment based on the measuring techniques, the physical characterization and intelligent interpretation are schematically shown in Fig. 1.It is well known, that the geometrical topography of tools and sheet metal parts depends on its manufacturing conditions. On the other hand the functional performance of the 3D-geometry and the quality is strongly related to the geometrical characteristics of the surface topography. Additional the demands of high-productivity manufacturing require that advanced process control balance between functional properties, 3D-topography and the surface characterization. There are different optical, non-contact methods to investigate surface structures and morphologies[1].

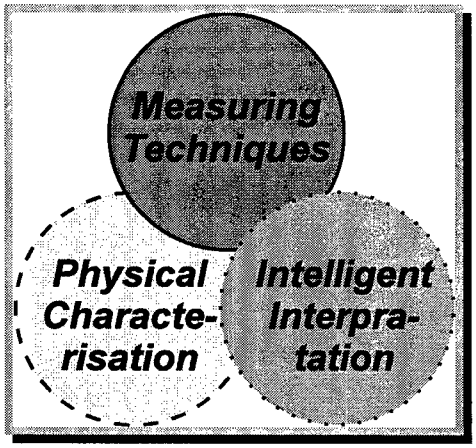


Fig. 1: Foundations of a Intelligent Surface Characterization

SPECKLE MEASUREMENT

Two speckle patterns of the same surface but recorded at different laser illumination angles are correlated. The degree of the correlation depends on the surface roughness and is expressed by the correlation coefficient $\rho_{1,2}$ that is given by the relation of the covariance of the intensities in the two speckle patterns and the variance. Now it is this correlation coefficient that is related to the surface roughness. The angular correlation of the speckle phase images is used to get the desired 3D information of the investigated object surface.

Butters and Leendertz [1] developed the Electronic Speckle Pattern Interferometry (ESPI) as a non-destructive testing technique to determine the full displacement field of a diffuse reflecting object in 1969 . But it was 1984 when the introduction of phase-shifting techniques in speckle interferometry automated the quantitative analysis of the speckle fringe pattern . During the last ten years, the progress in computer technology and image processing has made speckle interferometry additionally more and more attractive for research work as well as for the first industrial applications.

Whereas in holographic interferometry two electromagnetic waves interfere, the interference mechanism in the similar ESPI is different. Here two laser waves illuminate a surface of interest, and two speckle fields are produced in space by the well known speckle effect of the optically rough surface and Huygens' s principle to interfere with each other.

There are mainly three different techniques to measure the 3D-shape or contour of an object in speckle interferometry: the angular, spectral and refractive speckle contouring techniques. In the angular speckle contouring technique, the illumination geometry, that means the object illumination angles, are changed between two subsequent phase image recordings .Butters, Jones and Wykes have carried out the initial research work of contouring the optically rough surface of an object using the dual illumination approach . A ESPI contouring technique has been proposed first by S. Winther and Slettemoen in 1984 .The spectral speckle contouring technique uses two different laser wavelengths between two subsequent phase image recordings , whereas the surface of interest can also be illuminated by two waves of different wavelengths simultaneously, and only one phase image is recorded.

In the refractive speckle contouring technique, the refractive index of the medium between CCD chip and object surface has to be changed between the two needed recordings of the phase fringe patterns .But also the speckle shearing interferometry has been used to determine the slope and shape of a surface. Ganesan and Sirohi proposed a new method of speckle contouring using digital speckle pattern interferometry (DSPI) in 1988 to get the 3D contour of an object in real-time . The technique makes use of DSPI with an in-plane sensitive optical set-up. The main difference of Ganesan's and Sirohi's method to ours is that the object is tilted whereas in our contouring method only the illuminating angles are changed, and the object surface remains fixed. Furthermore they do not use the incremental addition of phase images. The usefulness of the contouring technique in ESPI is demonstrated, for example, in combination with displacement field measurements of curved surfaces to be able to identify the displacement vector with the corresponding surface point which is impossible if the shape of the surface is unknown. In one of the first practical applications, Paoletti and Spagnolo demonstrate a speckle contouring technique by DSPI for surface inspection, where they developed an interferometer for the investigation of surface defects in deterioration studies in 1991 .

EXPERIMENTAL SET-UP FOR ANGULAR SPECKLE CONTOURING MEASUREMENT

The optical set-up of the two-beam angular speckle contouring interferometer shown in Fig. 1 consists of an optical head, containing a laser diode, a phase-shifting device and a standard CCD camera, a driver unit for diode, shutter and CCD camera, a VME-bus for data transfer, a PC for image processing, a TV monitor for real-time control, two plane mirrors on turntables with scanning motors and a corresponding driver unit.

The laser diode has a power of 32 mW and produces light with a wavelength of about 828 nm in the near infrared. The phase-shifting device is a piezo-transducer element (PZT). The camera produces 512 × 512 × 8 bit images [2].

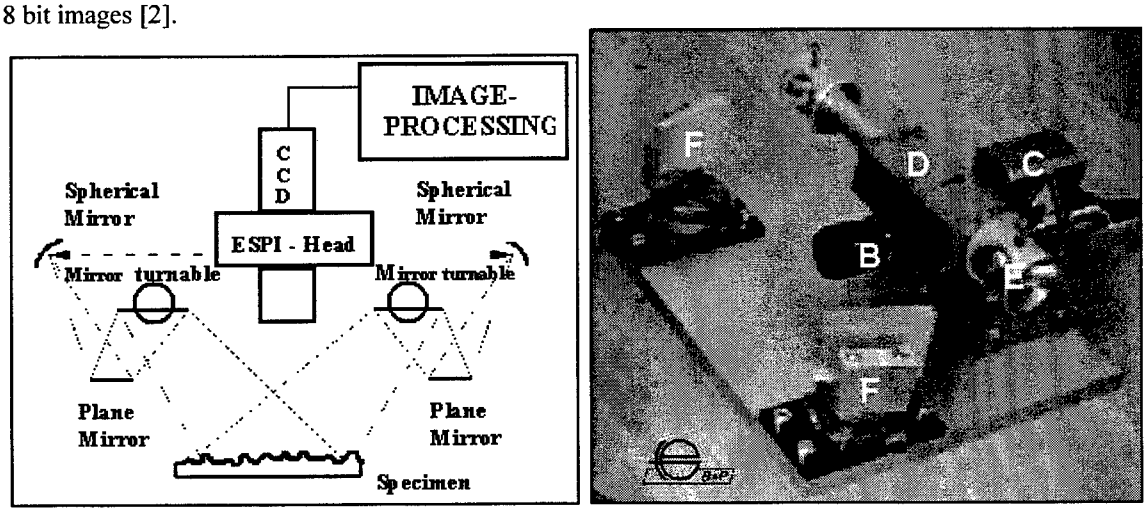


Fig. 1. Angular speckle contouring set-up

Speckle contouring measurements and according roughness evaluations have been performed on milled Rugo test surfaces [3]. The measurement range is characterized by an average mean roughness R_a = 12.5 µm down to 1.6 µm. Here it is clearly demonstrated that the used speckle interferometric technique resolves surface structures in the µm-range with the advantage of a full-field method. (Fig. 2 to Fig.4)

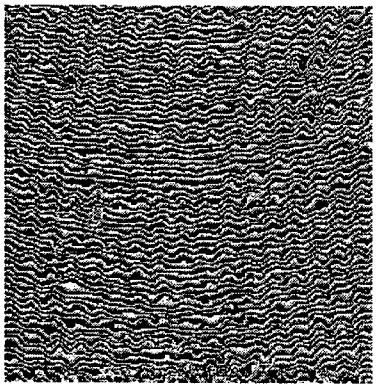


Fig. 2. Phase-map of the surface

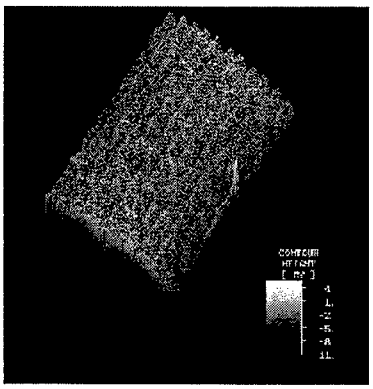


Fig. 3. Pseudo 3D- map

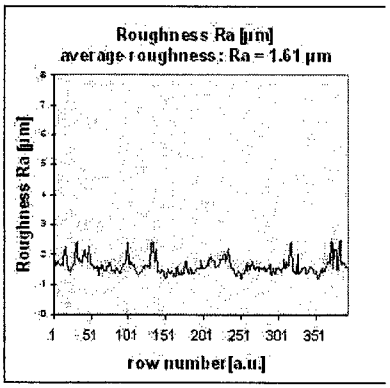


Fig. 4. Roughness evaluation

Table 1 gives the measured and averaged speckle roughness values R_a in comparison with stylus profilometric reference results. The 1D profilometric reference measurements were carried out with a Talystep profilometer with diamond stylus. To get a comparable speckle value, R_a has been averaged over all measured rows. The profile lengths were chosen according to the ISO-normed cut-off wavelengths.

Table : Comparison of average mean roughness

R_a [µm]	
speckle contouring	**stylus reference**
12.75	12.50
6.25	6.30
3.07	3.20
1.61	1.60

NEW SYSTEM FOR FAST 3D-SURFACE CHARACTERIZATION

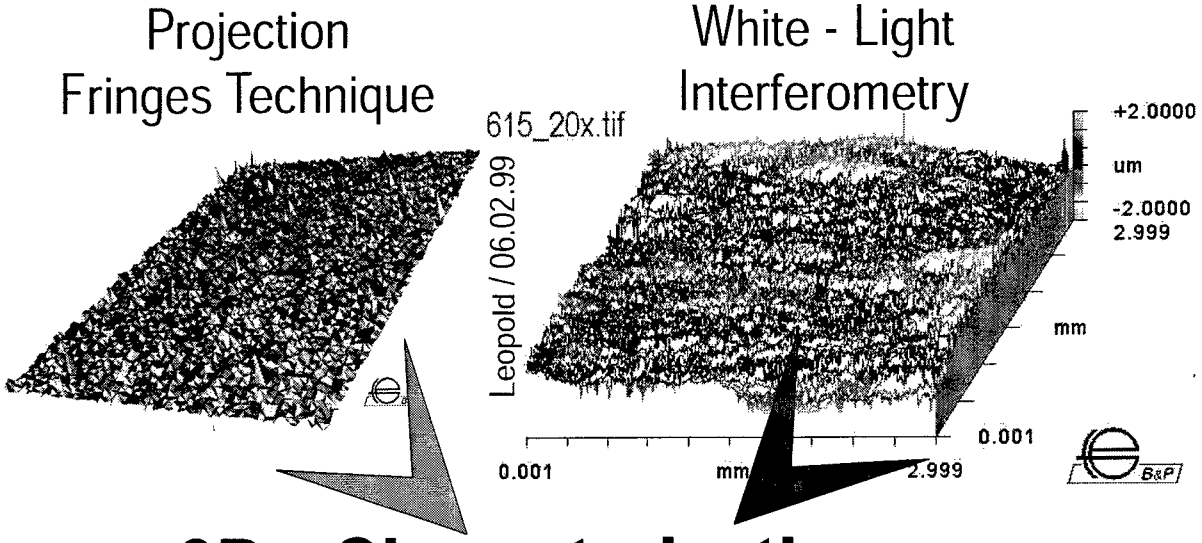
The new developed system for fast 3D surface characterization is based on Figures 5 and 6. Using projected fringe methods, angular speckle correlation techniques, white light interferometry and atomic force microscopy, the 3D-structure of an technical surface (bulk or thin layers) may be determined. The software tool LAYERS (Fig. 5) was developed to characterize the material structure of the surfaces. Based on Intelligent Methods (Fast Fourier Transformation; Neural Nets; Fractal Analysis, Wavelet Transforms and Power Spectra) an real-time system for bulk and thin-film inspection of surfaces has been developed (Fig. 6.). Applications for sheet metal parts and surface characterizations of surfaces will be discussed.

ACKNOWLEDGMENT

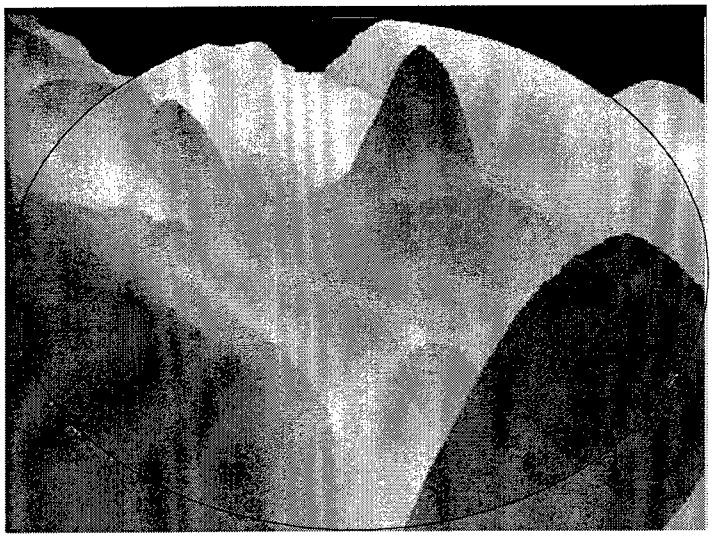
The investigations were partly sponsored by the German Research Council, the German Ministry of Economy and the Foundation for Promotion of Advanced Automation Technology / Japan.

REFERENCES

1. J.Leopold, H.Günther, R.Leopold, 1998. Metrology Based Surface Quality Control. Proceedings 6th ISMQC IMEKO Symp.,Metrology for Quality Control in Production, Vienna/Austria; 401-408
2. J.Leopold, H.Günther, 1998. Fast Characterization of Glossy Surfaces by Means of Coherent Radiation; Proc. 3 rd. Inter. Kongreß und Fachausstellung für Optische Sensorik, Meßtechnik & Elektrotechnik, Erfurt, 18.-20. Mai, 179 - 184
3. J.Leopold, M. Hertwig, H. Günther, B. Staeger, 1996. 3D-Measurement of Macro- and Microdomains using optical methods; Proceedings of the IX. Int. Oberflächenkolloquium, Chemnitz,Germany



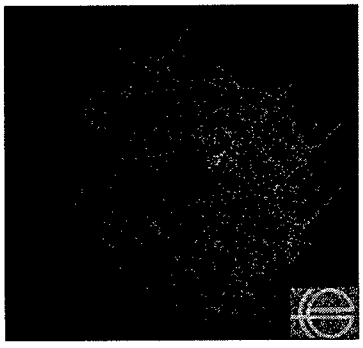
3D - Characterization



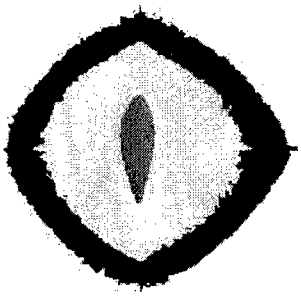
AFM

Fast - Characterization

FFT



Speckle - Gloss



Speckle Image



Fig. 5 : Experimental methods for Fast 3D - Surface Characterization

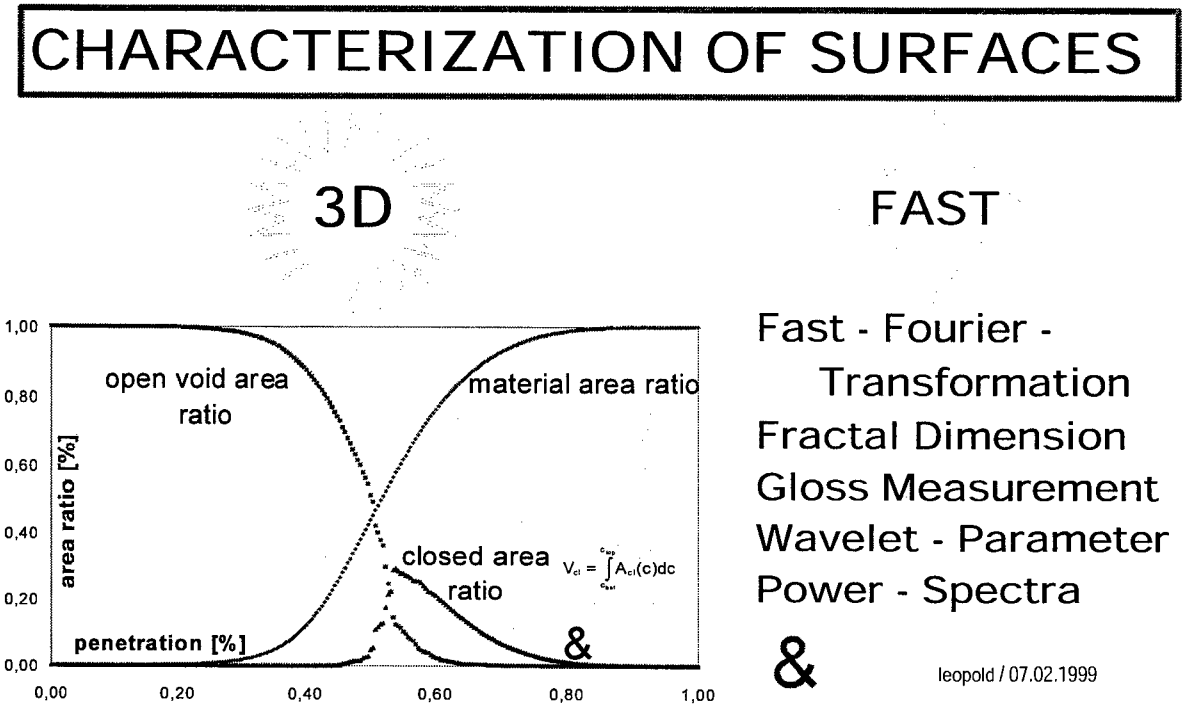


Fig. 6 : Results of different methods for surface quality control.

A Study on a Novel Smoothing Method by Atomic Layer Epitaxy for Microstructure Fabrication

S. Hirose*, A. Yoshida, M. Yamaura** and H. Munekata****

*Mechanical Engineering Laboratory, AIST, MITI,
1-2 Namiki, Tsukuba, Ibaraki 305-8564, Japan
**Imaging Science and Engineering Laboratory, Tokyo Institute of Technology,
4259 Nagatsuda, Midori-ku, Yokohama 226-8503, Japan

ABSTRACT

We prove that atomic layer epitaxy (ALE) provides a novel technique to smooth a relatively rough GaAs surface. The method has been applied successfully to smooth chemically etched V-grooved GaAs structures and selectively grown GaAs stripe structures The key advantage is that ALE is governed by two-dimensional island growth mode.

INTRODUCTION

Microstructure formation of semiconductor devices has been developed primarily using photolithography and etching [1]. Surface roughness, being unavoidable in the nano-/micro-structure processing, is a key problem which leads to degradation in physical properties and device performance. One typical example is that the edge roughness of mask layers formed by the etching process results in striations on side facets. Smoothing of damaged surfaces is required for fabrication of high quality advanced semiconductor microstructures. This paper investigates the application of ALE to the final smoothing process.

THE CONCEPT OF SURFACE SMOOTHING

ALE of GaAs has been studied for the last decade and is expected to realize nano-structures with thickness controllability at the monolayer (ML) level. The ALE growth is controlled at just 1-ML per source supply cycle by supplying trimethyl gallium [$(CH_3)_3Ga$] and arsine [AsH_3] alternatively, which means that alkyl radicals on the surface prevent further Ga adsorption. The advantages of ALE are: (i) self-limiting growth [2], (ii) good thickness controllability and uniformity [3], and (iii) excellent selectivity on different surfaces [4]. We have found an additional specific feature of ALE in this study in that the ALE growth is dominated by a two-dimensional island growth mode. We have inferred that these qualities may be applicable to the smoothing of damaged surfaces of microstructures without significantly changing the shape and size of the original structures.

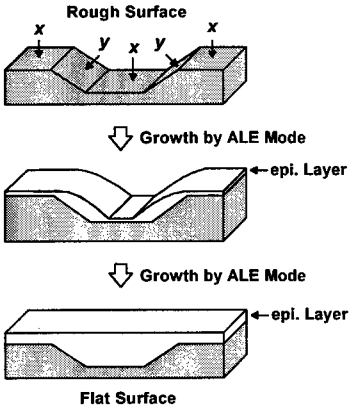


Fig. 1. Schematic illustration showing the method to smooth the rough surface by using ALE growth mode.

0-7803-5489-3/99/$10.00 ©1999 IEEE.

The concept of the surface smoothing method is schematically illustrated in Fig. 1. For simplicity, let us assume that the rough surface consists of x and y planes. We then choose the specific ALE growth conditions such that the growth rate on the x surface is much lower than that on the y surface. Then, the growth on the x surface proceeds very slowly relative to that on the y surface, automatically creating a flat x surface. The growth on the x surface is improved by the formation of self-limiting two-dimensional (2D) formation. When the ALE growth process is completed, the result will be a smooth surface.

SMOOTHING FOR V-GROOVED GaAs STRUCTURE

We will first describe an experiment to smooth the (111)A surfaces in V-grooved GaAs structures. The patterning of V-grooved structures were formed by chemical vapor deposition (CVD) with the method of SiO_2 mask and photolithography. Figure 2 (a) shows the bottom part of the as-etched structures in which we can clearly observe a number of etch-pits and line-shaped striations on the (111)A side walls. The striations are attributed to edge roughness of a patterned conventional photoresist polymer layer.

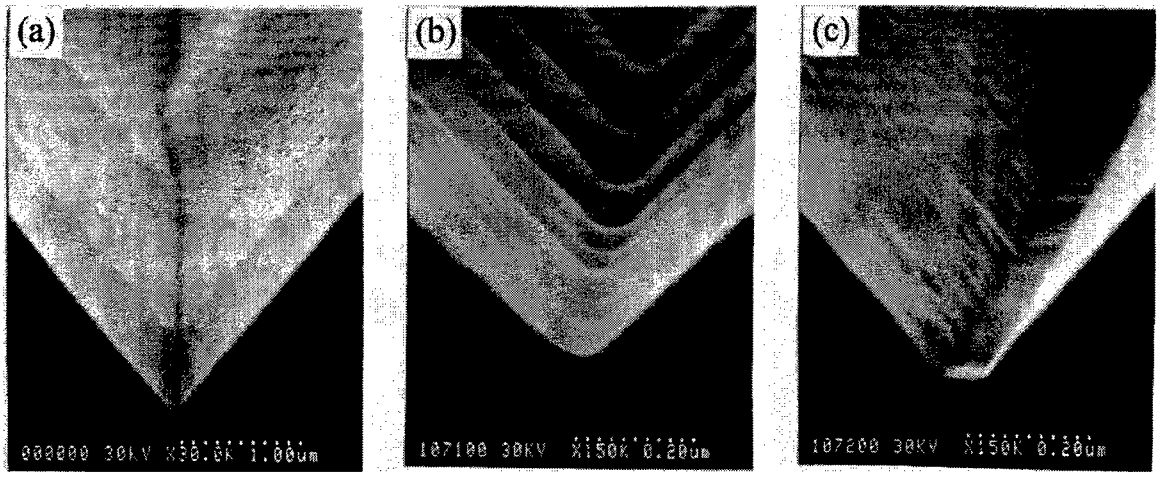
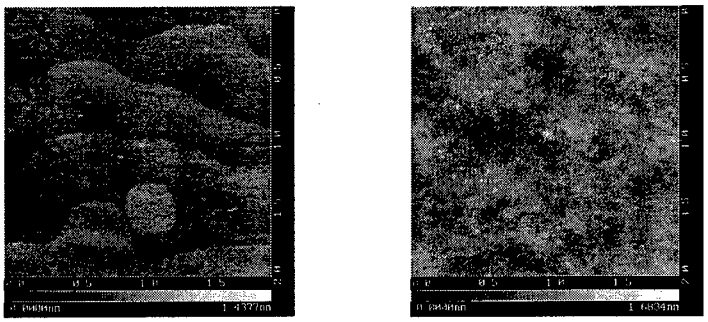


Fig. 2. SEM images of V-grooved GaAs surfaces after (a) wet chemical etching, (b) growth by MOVPE, and (c) growth by ALE.

Figure 2 (b) shows the bottom part of the V-groove after growing a thin GaAs layer by conventional metal organic vapor phase epitaxy (MOVPE) process. To make a good comparison between MOVPE and ALE, the total layer thickness on the (001) GaAs surface was kept constant at 200 nm. When MOVPE growth was performed to smooth the V-grooved surface, the initial surface striations were emphasized, reflecting the unevenness of under layer (Fig. 2 (b)). This is likely a natural consequence of the step-flow mode in the MOVPE process (Fig. 3 (a)). Another problem in MOVPE sample is that the sharp bottom profile of the V-groove is rounded, which signifies variations in surface orientation.

In contrast to the results obtained by MOVPE, the smoothness of surfaces of V-grooved structures is clearly improved through application of the ALE process, as shown in Fig. 2 (c). Figure 4 shows the dependence of the GaAs growth rate on substrate temperature (T_s) for (001) and (111)A surfaces. The ALE conditions used for this experiment were T_s = 480 °C, TMG and AsH_3 supplied at 1.5×10^{-1} μmol/s and 3.0×10^{1} μmol/s for 3 and 10 s, respectively, with 3 s of hydrogen purge between each source supply. The ALE growth rate on the (001) plane saturates at 1-ML per cycle, indicating self-limiting behavior. On the other hand, the growth rate on the (111)A plane is relatively slow. On the basis of these data, we have chosen the specific substrate temperature T_s = 480 °C.

In Fig. 2 (c), we can clearly see that the ridges appearing in Fig. 2 (a) vanish almost completely after ALE processing. Also, a (001) plane is spontaneously developed at the bottom of the V-groove. Furthermore, sharp edges are clearly developed at the intersection of the (001) and (111)A surfaces. This is probably explained in terms of the difference in the nucleation mechanism between MOVPE and ALE. Atomic force microscopy (AFM) observations have verified that ALE is primarily driven by formation of 2D islands (Fig. 3 (b)). We have concluded that the ALE growth process achieves smooth GaAs surfaces.



(a) MOVPE (b) ALE

Fig. 3. AFM plan-view image of the GaAs on the (001) surface grown by (a) MOVPE and (b) ALE.

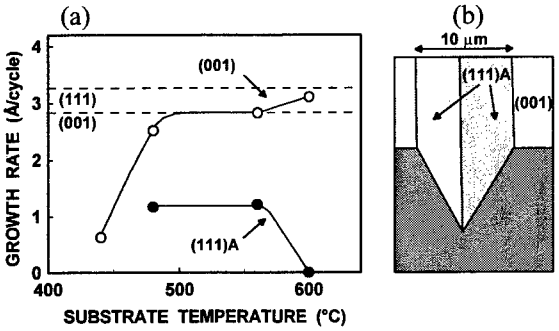


Fig. 4. (a) Growth rates on (001) and (111)A GaAs surfaces as a function of substrate temperature. (b) Schematic illustration of a V-grooved structure.

SMOOTHING FOR RIDGE GaAs STRUCTURE

We then applied ALE to smooth the ridge structure, containing (110) and (111)B surfaces, which was grown selectively by conventional MOVPE at T_s = 700 °C. As can be seen in Fig .5 (a), many wavy striations exist on the (110) surface, and moreover, the (111)B surface was not flat, having irregular holes particularly at the top of the ridge.

In order to eliminate these defects, we applied ALE to smooth the (110) surface in which the growth rate on the (110) surface is relatively slower than on the other surfaces. Figure 6 shows the dependence of the GaAs growth rate on T_s for (001), (111)B and (110) surfaces. T_s = 480 °C satisfies this condition in that 1-ML self-limiting ALE growth mode is almost realized on the (001) surface while the growth rate on the (110) surface is less than 1 Å per cycle. The growth rate on the (111)B plane is inbetween those on the (001) and (110) surfaces.

After applying the ALE smoothing process, the wavy surface features on the (110) surface, formed originally by the MOVPE process, are almost repaired as shown in Fig. 5 (b). Also, (111)B and (001) surfaces have a degree of smoothness equivalent to surfaces formed by crystal cleavage. However, the

inner (111)B plane still remains somewhat rough. We infer that the roughness of these defective structures were too large to smooth out completely by a single smoothing process. Applying another ALE process with different conditions would result in further improvements in the surface roughness.

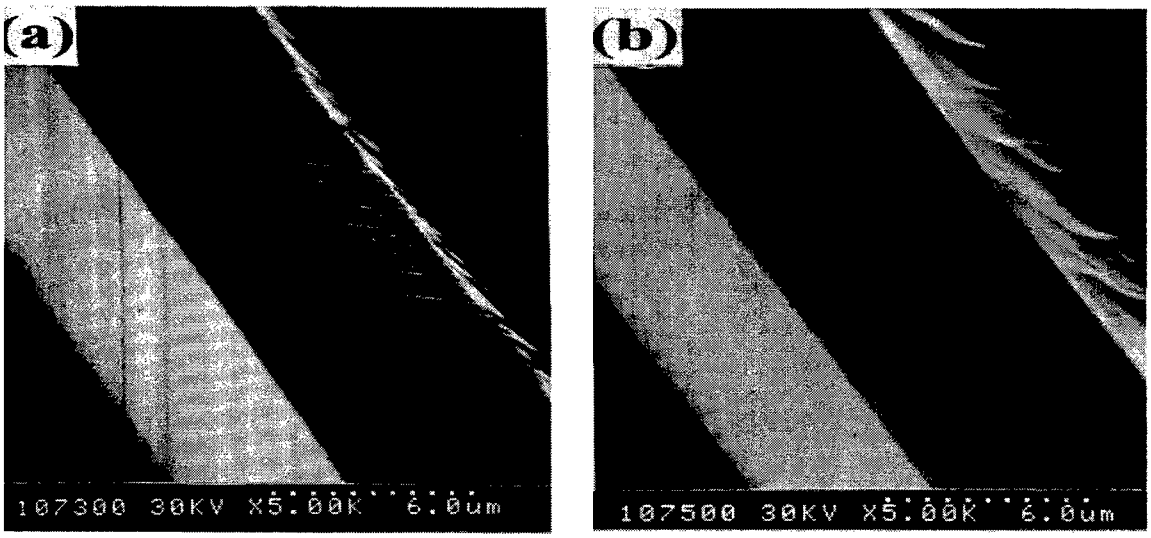


Fig. 5. (a) SEM image of a side wall of a GaAs stripe structure grown by selective area MOVPE. (b) SEM image of the structure after ALE smoothing method.

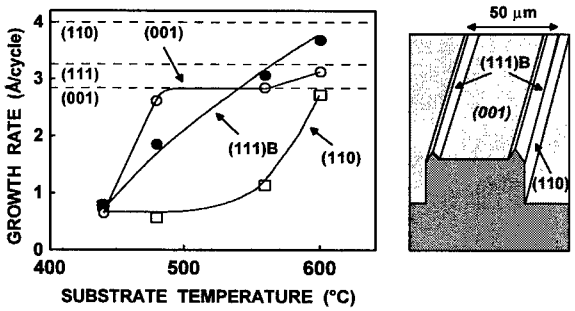


Fig. 6. (a) Growth rates on (001), (111)B and (110) GaAs surfaces as a function of substrate temperature (b) Schematic illustration of a ridge structure.

CONCLUSION

We have proposed and demonstrated a novel method to smooth the surface of GaAs microstructures using atomic layer epitaxy (ALE) and keeping film thickness controllability at the monolayer level. It has been demonstrated that ALE makes it possible to form surfaces with smoothness equivalent to those formed by crystal cleavage because the growth is characterized by 2D-island nucleation.

This result is much superior to that from metal organic vapor phase epitaxy wich is a more traditional processing technique. When MOVPE growth was performed, initial surface striations became emphasized, reflecting the unevenness of the under layer, a natural consequence of the step-flow mode in the MOVPE process.). Variations in surface orientation is also a significant problem with MOVPE processing.

ACKNOWLEDGEMENT

The authors gratefully acknowledge Taiyo-Toyo Sanso Co., Ltd for supplying highly pure AsH_3 gas. This work was partially supported by Research Fellowships of the Japan Society for the Promotion of Science for Young Scientists.

REFERENCES

1. R. Bhat, E. Kapon, S. Simhony, E. Colas, D. M. Hwang, N. G. Stoffel, M. A. Koza, 1991. J. Cryst. Growth 107, 716-721.
2. T. Suntola, 1994. Handbook of Crystal Growth, ed. D.T.J. Hurle (Elsevier, Tokyo,) 3, Ch. 14, 601.
3. S. Hirose, N. Kano, K. Hara, and H. Munekata, 1997. J. Crystal Growth 172,13-17.
4. H. Isshiki, Y. Aoyagi, T. Sugano, S. Iwai, T. Meguro, 1993. Appl. Phys. Lett. 63 1528-1530.

Relationship between groove cross-sectional area per pulse of YAG laser and strength of processing sound

Tsuneo Kurita*, Tomohiko Ono, Tsuyoshi Nakai**, Noboru Morita*****

** Japan Science and Technology Corporation*
MEL, 1-2 Namiki, Tsukuba, Ibaraki, JAPAN
***Tokyo Metropolitan Institute of Technology,*
6-6 Asahigaoka, Hino, Tokyo, JAPAN
****Faculty of Engineering, Chiba University,*
1-33 Yayoi-cho, Inage-ku, Chiba, JAPAN

ABSTRACT

Laser processing is an important manufacturing technology in machining difficult-to-cut materials. A sound generates when a laser processing is carried out, and the intensity of a sound changes according to processing conditions. The goal of the research is to construct a laser processing system for the manufacture of free form surface. In order to achieve this goal, this study aims to clarify the relationship between the strength of laser processing sound and groove cross-sectional area per pulse when Q-switched YAG laser beam was applied for laser grooving.

INTRODUCTION

Laser processing is characterized that various types of material such as hard metals and ceramics can be processed in a high speed condition, because it is possible to concentrate an input laser energy to a small area. On the other hand, heating, melting and vaporization of material occur continuously when a high power laser energy is applied, and such phenomena make difficult to monitor laser processing characteristics. In the case of a material removal process, for instance, it is very difficult to keep a removal depth of a material and a processed accuracy at a constant level without applying a laser process control. When considering these technological backgrounds, it may be necessary to realize a high accuracy control system for a laser processing, in which a processing information is monitored and is transferred to a laser machine controller to construct a feed back system. In order to achieve these technologies, the utilization of the laser processing sound has been tried [1]-[6]. The final goal of the research is to construct a laser processing system for the manufacture of free form surface or stepped groove. In order to control the laser processing characteristic, various types of condition should be manipulated. For the monitoring of the characteristics of laser processing by utilizing the generated sound, it is very important to clarify the fundamental relationship between laser processing sound and processing characteristics which is not affected by laser processing conditions. The authors have clarified the relationship between the cross-sectional area of processed hole and sound pressure level at the specified frequency experimentally, and it may be possible to express both relationship by the straight line when a low frequency laser beam is used [7]. The purposes of the research are to clarify the accurate relationship between material removal cross-sectional area per laser pulse and the strength of processed sound at various

0-7803-5489-3/99/$10.00 ©1999 IEEE.

processing conditions, and also to clarify the effect of work material on the both relationship when a high frequency Q-switched YAG laser beam is applied.

EXPERIMENTAL SETUP

Fig.1 shows the experimental setup for the sensing and for the frequency analysis of a laser processing sound. A work material was set on the numerically controlled table, and a TEM_{00} single mode Q-switched YAG laser beam (500Hz~50kHz) was irradiated to the pre-determined position. Generated sound was detected by a condenser microphone which was set at the distance of 40 mm from the incident position of a laser beam with the inclination of 30 deg., and was recorded by a DAT (Digital Audio Tape) data recorder through an amplifier. The strength of detected sound versus processing time was measured by using an FFT. The photos of cross-sectional area of processed groove were taken by SEM (Scanning Electron Microscope) in order to measure the cross-sectional area of grooves after groove was ground by #1000 diamond grinding wheel.

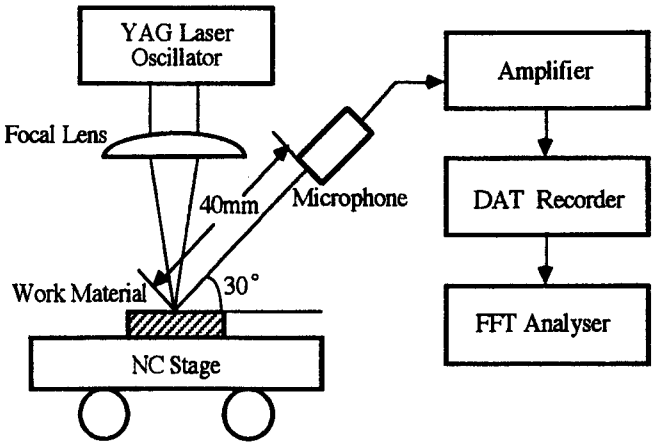


Fig. 1. Experimental setup for a detection and an analysis of laser processing sound

EXPERIMENTAL RESULTS

The measurement of strength of processing sound

Fig.2 shows the relationship between groove volume increase rate (mm^3/s) and sound pressure level at specified frequencies of processing sound. Where, work material was (Al_2O_3+TiC) ceramic, Q-switch frequency was 2kHz, laser energy was 1.10J/s and processing speeds were from 0.01 to 4.0mm/s. It was cleared that the relationships of two variables at frequencies of 4 steps could be expressed by straight lines. This experimental results show that it is not necessary to select a specified frequency in order to express the relationship with material removal volume and the strength of processing sound. Fig.3 shows the variation pattern of the strength of processing sound versus processing time at 1mm/s processing speed, 3kHz Q-switch frequency and 1.40J/s laser energy. In the experiments, (Al_2O_3+TiC) ceramic (a) and a (WC+Co) sintered carbide (b) were selected as work materials. As shown in Fig.3, signals having the same pattern were detected repeatedly when a high frequency Q-switched YAG laser beam was used for a laser grooving. It can be assumed that these signals coincide with incidence of Q-switched laser beam because the time duration of a signal is equal to the inverse value of Q-switch

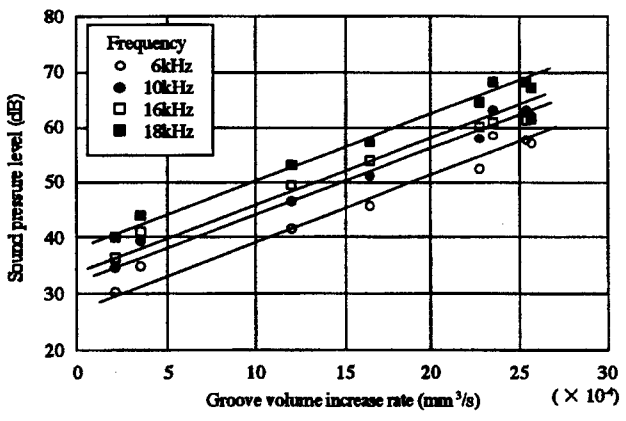


Fig. 2. Relationship between groove volume increase rate and sound pressure level

frequency. In this report, the maximum value of the amplitude of a signal is defined as the strength of processing sound.

The measurement of cross-sectional area of groove

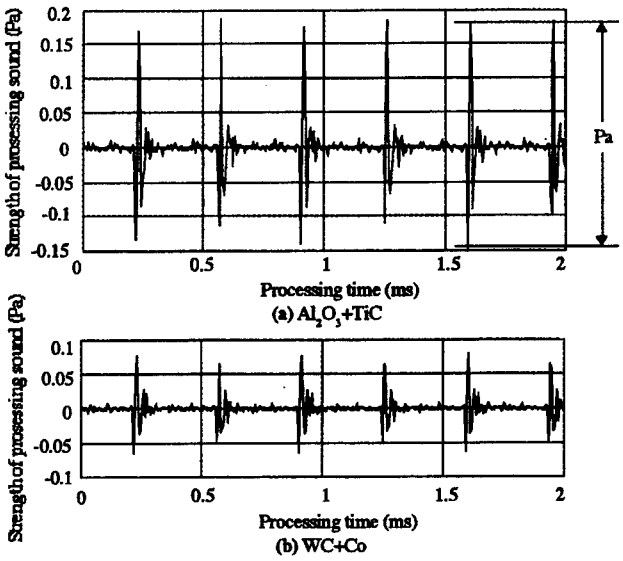
A circle, which diameter d(μm) is equal to the focused spot of laser beam, is imagined on the surface of work material. The number of incidence of laser beam across the circle of laser beam can be calculated by the equation (d · q)/v, where q(kHz) is Q-switch frequency and v(mm/s) is processing speed. The maximum value of the incidence is called " Maximum Incident Times (MIT)" in this report. Fig.4 shows the relationship between cross section of processed groove and MIT. As shown in these figures, the depth of groove changes according to both the number of incidence and work materials.

The relationship between cross-sectional area and the strength of sound

Fig.5 shows the strength of processing sound and cross-sectional area versus MIT when an (Al_2O_3+TiC) and a (WC+Co) were used as work materials. In case of an (Al_2O_3+TiC), cross sectional area increases rapidly until MIT of about 3000, and after that value, the inclination of increase becomes moderate. On the other hand, the strength of processing sound decreases as the increase of MIT. For a (WC+Co), the changes of the strength of processing sound and cross sectional area are similar to the case of an (Al_2O_3+TiC), but both values are smaller than those of an (Al_2O_3+TiC). These phenomena indicate that the strength of processing sound and cross sectional area versus MIT differ by changing work materials.

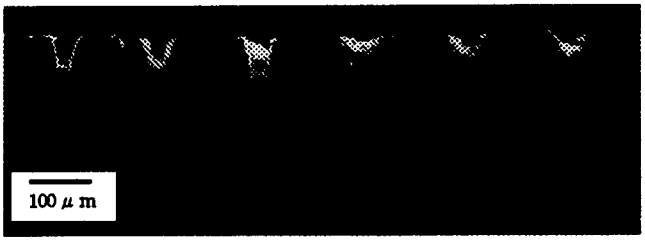
INVESTIGATION AND DISCUSSION

The purpose of this research is to clarify experimentally the relationship between the strength of laser processing sound and removed cross-sectional area per a pulse of laser beam when Q-switch YAG laser is used for a grooving. The authors have revealed that there exists the linear relationship between the sound pressure level at the



Laser energy: 1.40J/s, Stage travel speed: 1 mm/s,
Q-sw. frequency: 3kHz

Fig. 3. Distribution pattern of the strength of processing sound versus processing time



240 (1) 480 (0.5) 800 (0.3) 1200 (0.2) 2400 (0.1) 12000 (0.02)

Maximum incident times
(Stage travel speed (mm/s))

(a) Al_2O_3+TiC



240 (1) 480 (0.5) 800 (0.3) 1200 (0.2) 2400 (0.1) 12000 (0.02)

Maximum incident times
(Stage travel speed (mm/s))

(b) WC+Co

Laser energy: 1.40J/s, Initial width of groove: 80 μ m,
Stage travel speed: 0.01~1.5mm/s, Q-sw. frequency: 3kHz

Fig. 4. SEM images of processed groove

specified frequency and cross sectional area per a single pulse laser beam in a laser drilling. Where, laser beam is controlled by the outer electric circuit. But there were the following problems in these procedures

①It was not easy to detect the deepest position of hole because of the difficulty of grinding. So, there is a possibility the occurrence of measuring error in the calculation of the cross sectional area of processed hole.

②A lot of times are necessary to repeat the experiment many times in order to assure the accuracy under the same processing condition.

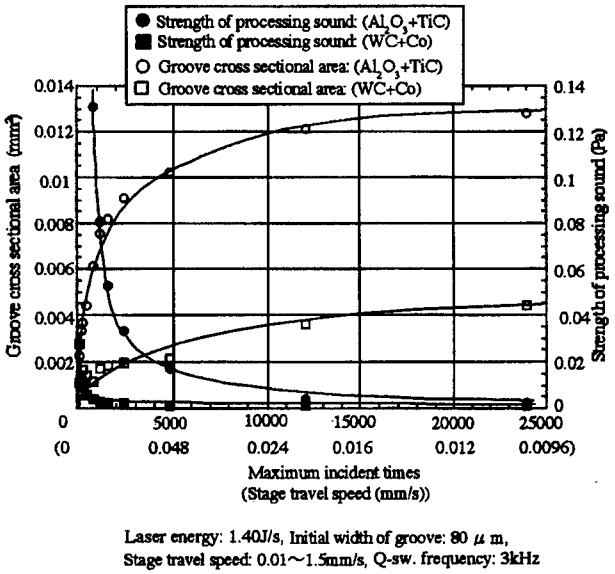
Because of these reasons, the relationship between cross sectional area of processed groove and sound pressure level was obliged to express by a straight line with distributed values. The most difficult thing in the experiment is to calculate the accurate cross sectional area of processed groove. In this report, the values of cross sectional area was calculated based on the SEM images of Fig. 4, and the relationship between sound pressure level and processed cross sectional area per one pulse irradiation of Q-switched YAG laser beam was indicated. This procedure make possible to heighten the accuracy of experimental data.

Fig. 5 shows the relationship between MIT and groove sectional area, and also the relationship between MIT and the strength of processing sound. The cross sectional area of processed groove per a laser pulse was calculated based on Fig. 4.

A cross sectional area of a processed groove per a laser pulse V_P at the maximum incident time N can be calculated by the following equation.

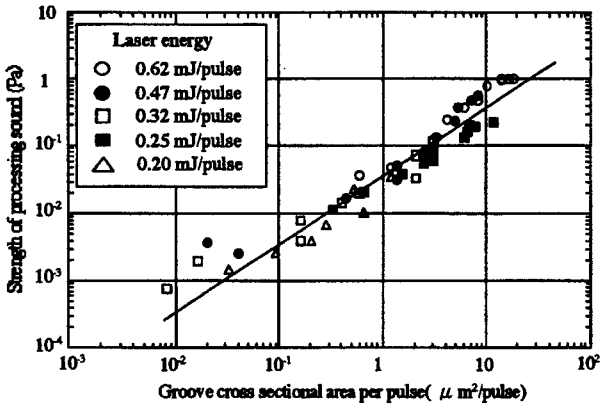
$$V_P=(V-V_0)/(N-N_0)_{(N>N0)}$$

Where, V and V_0 are the cross sectional area of processed groove at the maximum incident time of N and N_0. And the value of sound pressure level at Nth irradiation was used to indicate the correlation with a cross sectional area per a laser pulse.



Laser energy: 1.40J/s, Initial width of groove: 80 μ m,
Stage travel speed: 0.01～1.5mm/s, Q-sw. frequency: 3kHz

Fig. 5. Strength of processing sound and groove cross sectional area versus maximum incident times of laser beam



Stage travel speed: 0.01～1.5mm/s, Work material: Al_2O_3+TiC

Fig.6. Relationship between groove cross sectional area per pulse and strength of processing sound

The effect of processing condition on the relationship between cross sectional area and strength of processing sound

Fig. 6 shows the relationship between groove cross sectional area per pulse and strength of processing sound when an (Al_2O_3+TiC) is used as a work material. In this figure, laser energy was changed from 0.2 to 0.62 mJ/pulse. It is cleared that the relationship of both variables can be expressed by a straight line on a log-log chart, and the gradient of the line is not

affected by the applied laser energy. These phenomena mean that the calculation of the cross sectional area of groove per a laser pulse is possible only by measuring the strength of laser processing sound when applied average laser energy and processing speed are changed under the constant work material.

The effect of work material on the relationship between cross sectional area and strength of processing sound

Fig. 7 shows the results of qualitative analysis of work materials used for the experiment. Two types of work material,

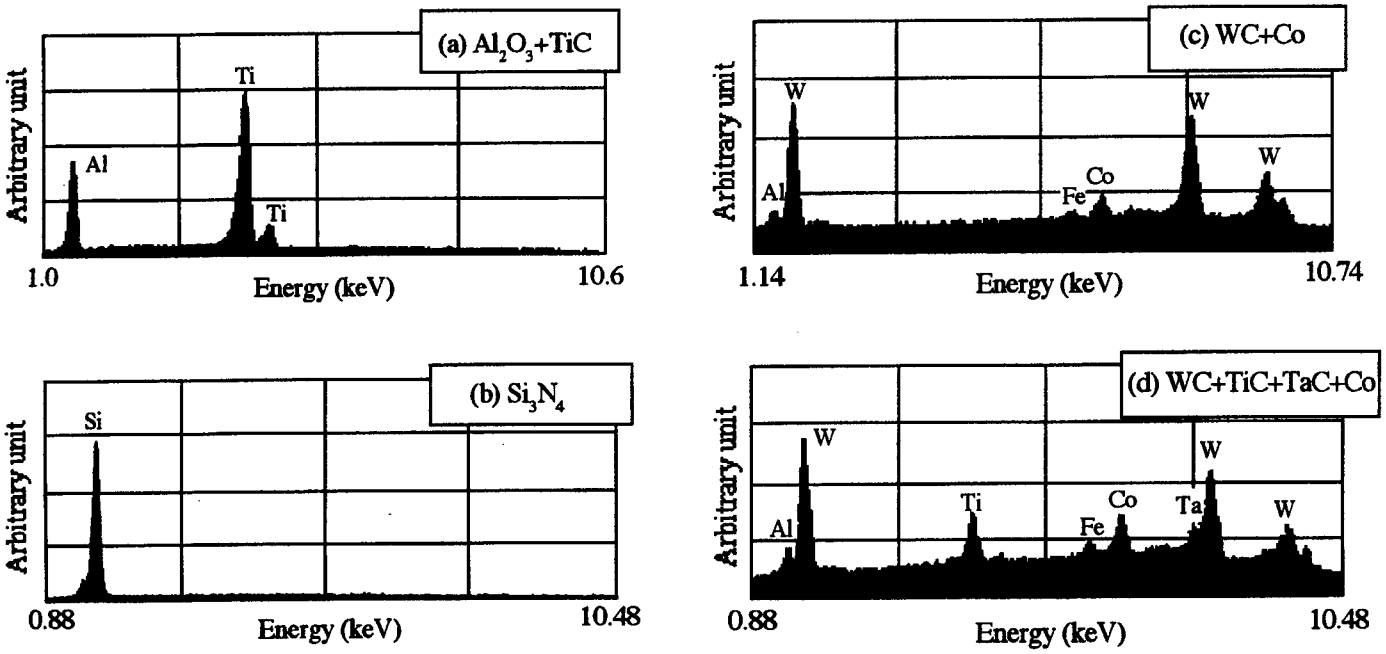


Fig. 7. Qualitative analysis of work material with EDS

ceramics (a and b) and sintered carbides (c and d), were used. Fig. 8 shows the relationship between strength of processing sound and groove cross sectional area per a pulse laser beam for four kinds of work material. Where, applied laser energy was 1.4J/s, Q-switch frequency was 3kHz and processing speed were 0.01 ~ 1.5mm/s. Experimental data were separated into two groups, one was for ceramics and the other was for sintered carbides, and the gradient of straight line of ceramic materials showed the bigger value than that of sintered carbides. This means that strong sound generates when ceramic material is selected as a work material than sintered carbide at the same cross sectional area per a pulse laser beam. Fig. 9 shows the SEM images of processed groove of ceramic (a) and sintered carbide (b) at the 800 irradiations of laser beam. The appearance of the inside of groove of both materials are very differ. In case of

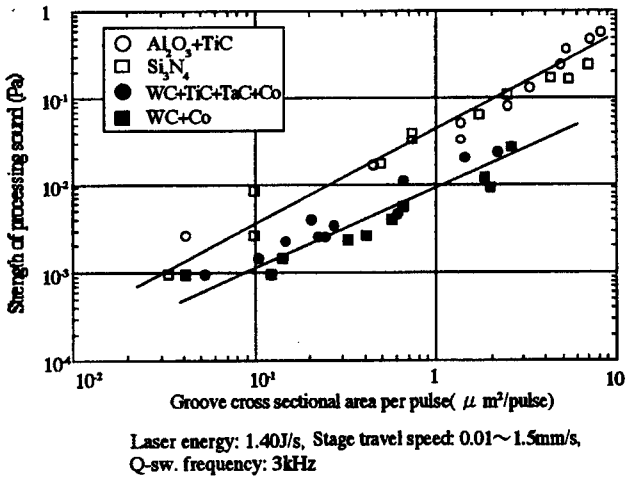
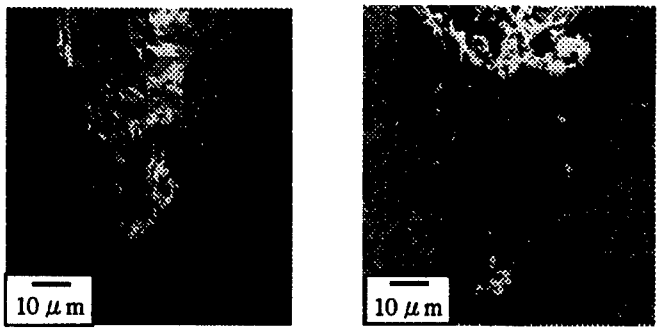


Fig. 8. Relationship between strength of processing sound and groove cross sectional area per pulse

sintered carbide, there exist resolidified material in the groove, and the generation of groove is not normal. In case of ceramic material, on the other hand, a part of material is removed by sublimation of material. From these SEM images, it is cleared that more work material is removed at a ceramic than a sintered carbide even if the depth of grooves is same for both two materials. It can be concluded by observing these SEM images that the defference in the manner of evapration of matrix material effects on the gradient values of two straight lines of Fig. 8.



(a) Al_2O_3+TiC (b) WC+Co

Laser energy: 1.40J/s, Q-sw. frequency: 3kHz
Stage travel speed: 0.3mm/s

Fig. 9. SEM images of cross sections of processed groove

CONCLUSIONS

The conclusions of this research are as follows.

1) The cross sectional area of groove increases rapidly until the certain value of incident times of laser beam, and increases monotonously after the constant value as the increase of incidence of laser beam. The strength of processing sound changes with inverse inclination of the described phenomenon as the increase of incident times. These phenomena could be observed for two kinds of work material, ceramics and sintered carbides.

2) The relationship between the strength of processing sound and the cross sectional area per a laser pulse could be expressed by straight lines on a log-log chart when applied laser energy was changed.

3) The gradient of straight line was changed when two kinds of work material were used. This phenomenon depends on the laser material removal characteristic.

4) It was cleared experimentally that calculation of material removal volume with Q-switch YAG laser was possible only by measuring the strength of processing sound.

REFERENCES

1. G.V.Arbach, R.L.Melcher and C.E.Scranton, 1983, Combined Acoustic and Pyroelectric Laser, IBM Tech. *Disclosure Bull.*25, 5092
2. C.E.Yeack, R.L.Melcher and H.E.Klauser, Transient Photoacoustic Monitoring of Pulsed Laser Drilling, *App;.Phys.Lett.* 44, 1043
3. T.Miyazaki, T.Uyemura and Y.Yamamoto, 1973, A Study on the Mechanism of Laser Piercing, *Ann.CIRP*, 22, 67
4. M.T.Brienza and A.J.DeMaria, 1967, Laser-Induced Microwave Sound by Surface Heating, *Appl.Phys.Lett.* 11, 44
5. P.Sheng and G.Chryssolouris, 1994, Investigation of Acoustic sensing for Laser Machining Processes, Part 1: Laser Drilling, *J.MaterProcess.Technol.* 43, 125
6. P.Sheng and G.Chryssolouris, 1994, Investigation of Acoustic sensing for Laser Machining Processes, Part 2: Laser Grooving and Cutting, *J.MaterProcess.Technol.* 43, 145
7. T. Ono, T. kurita and N. Morita, 1997, Study on the relationship between material removal volume and sound pressure level in laser processing, *IPMM 97*, 1045

Optimization of Thickness Distribution of Micro-Membrane by Genetic Algorithm

Hidetoshi Kotera, Masatoshi Senga, Taku Hirasawa, Susumu Shima

Department of Mechanical Engineering, Kyoto University
Yoshida Honmachi, Sakyo-ku, Kyoto, 606-8501, Japan

ABSTRACT

A simulation method for optimizing dynamic motion of micro-electro-mechanical devices and systems (MEMS) is proposed. A series of equations of electrostatic field, fluid dynamics and deflection of micro-membrane are coupled and solved simultaneously. Since the genetic algorithm is appropriate to reduce the searching space of solution, □□ is used to optimize the thickness distribution of a micro-membrane. As an application of the developed method, the thickness distribution of the micro-membrane of a micro air pump is optimized. The prescribed performance of the micro-air-pump can be calculated.

INTRODUCTION

A few types of micro-electro-mechnical system (MEMS), e.g., micro optical mirrors, micro valves and micro actuators, have been developed and used in practice. These devices are actuated by electrostatic force and/or fluid pressure. To simulate the motion or deformation of the micro devices, computational algorithms have been studied [1,2,3]. In the present study, the air pressure field is expressed by the modified Reynolds equation considering first-order slip on the surface of the material. We couple the fluid equation with the membrane deflection equations that incorporate in-plane stress. The coupled equations are solved by the finite element method, where the electrostatic force is considered as an external force. Since the electric field changes according to the membrane deflection, the equation of electric field, expressed by the Laplace equation, is solved by the boundary element method. The fluid, membrane deflection and the electric field equations are coupled to solve in the scheme of calculation based on our previous work [4].

The numerical simulation is intended to characterize the motion of the devices and to design the shape of the mechanism to realize the prescribed functions. There have been studies using such numerical methods as design sensitivity analysis and genetic algorithm [5] to find the optimum shape or mechanism that realizes the prescribed functions. To produce a mechanical element of conventional scale, it is difficult to distribute the thickness of, say, sheet metal to realize a prescribed performance. In the field of MEMS, the components are produced by physical vapor deposition or by chemical deposition, i.e., a thin film is deposited by CVD or sputtering. By these processes, it is easy to distribute the thickness of the deposited thin films. It may thus be possible to develop a new mechanical structure for the desired performance.

The purpose of this work is to develop a simulation method to calculate the optimum thickness distribution of a micro-membrane actuated by an electrostatic force. Since a genetic algorithm is appropriate to reduce the solution search space, we used it to find an optimum shape. As an example, the thickness distribution of the micro-membrane of a micro-air-pump actuated by an electrostatic force is optimized to realize the prescribed response. We will show a numerical optimization method based on a genetic algorithm and discuss the convergence of the solution and efficacy of the developed method.

COUPLING ANALYSIS SYSTEM

As an example of a micro-actuator forced to be moved by the electrostatic force, Figure 1 shows a model of a micro-air-pump. The micro-membrane is the upper electrode and the bottom of the micro-pump is the lower electrode The air is pumped out according to the deflection of the micro-membrane actuated by the electrostatic force.

0-7803-5489-3/99/$10.00 ©1999 IEEE.

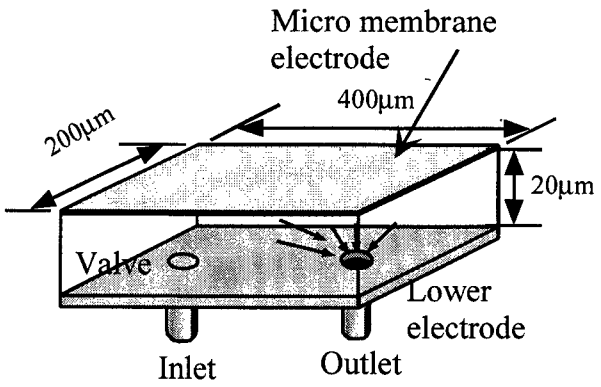


Fig. 1. Schematic view of micro pump.

Pulled by the electrostatic force, the micro membrane undergoes deformation in both in-plane and out-of-plane directions. Therefore, stress equilibrium equations of in-plane stress and bending are used. As the micro membrane deflects, the distance from the lower electrode changes. Thus, the change of actuation force due to the micro-membrane deflection should be considered. We used the following equations:

1) Electric field

The Laplace equation for electrostatic field where a space charge between the upper and lower electrode does not exist is written as

$$\nabla^2\phi = 0 \tag{1.}$$

where ϕ is an electrostatic potential. The strength of electrostatic field E is given by

$$E = -\nabla\phi = -\frac{\partial\phi}{\partial n} \tag{2.}$$

where n is the outward normal to the surface of the area concerned. The electrostatic stress is written as

$$f_e = -\varepsilon\frac{E^2}{2} \tag{3.}$$

where ε is dielectric constant of the fluid.

2) Stress equilibrium

The stress equilibrium equation for in-plane deformation is written as

$$\frac{\partial\sigma_x}{\partial x}+\frac{\partial\tau_{xy}}{\partial y}+f_x=0, \qquad \frac{\partial\sigma_y}{\partial y}+\frac{\partial\tau_{yx}}{\partial x}+f_y=0 \tag{4.}$$

where f_x and f_y are body forces in x and y directions, respectively.

The membrane is bent by dynamic pressure of fluid, and electrostatic force. The stress equilibrium equation for bending is expressed by

$$D_{xx}\frac{\partial^4 w}{\partial x^4}+2\left(D_{xy}+D_{ss}\right)\frac{\partial^4 w}{\partial x^2\partial y^2}+D_{yy}\frac{\partial^4 w}{\partial y^4}-t_m\sigma_x\frac{\partial^2 w}{\partial x^2}-t_m\sigma_y\frac{\partial^2 w}{\partial y^2}=p-p_a+f_e+t_m\rho\frac{\partial^2 w}{\partial t^2} \tag{5.}$$

where

$$D_{yy}=\frac{E_y t_m^{\,3}}{12(1-\nu_x\nu_y)},\ D_{xx}=\frac{E_x t_m^{\,3}}{12(1-\nu_x\nu_y)},\ D_{xy}=\frac{\left(\nu_y E_x+\nu_x E_y\right)t_m^{\,3}}{24(1-\nu_x\nu_y)},\ D_{ss}=\frac{G_{xy}t_m^{\,3}}{6},\ G_{xy}=\frac{E_x E_y}{(1+2\nu_y)E_x+(1+2\nu_x)E_y}$$

where w is membrane deflection, D_{xx}, D_{xy}, D_{yy}, D_{ss} are flexural rigidity, t_m is the thickness of the micro membrane, p is the pressure of fluid, p_a is atmospheric pressure, ρ is density of micro membrane, f_e is electrostatic stress, E_x and E_y are Young's moduli of micro-membrane in x and y direction respectively, ν_x and ν_y are Poisson's ratio. Since the micro-membrane is composed of a layered thin film deposited as a physical and/or chemical deposition, such as CVD, sputtering and vapor deposition, the mechanical property is assumed to be anisotropic as in Equation 5.

3) Fluid equation

The fluid in the pump is squeezed out by the micro-membrane deflection. To simulate the fluid flow and the pressure distribution in the micro-pump accurately, it is necessary to consider the fluid flow, a pressure loss and blowout of the fluid at the outlet. To do this, the Navier-Stokes equation should be solved. However, considering that the aspect ratio of the micro-pump cavity is more than ten and the height is in the order of 20 μm, we may estimate the performance of the micro-pump from the pressure distribution on the deflected micro-membrane and from the volume change of the pump cavity without taking account of these factors. Therefore, we use the modified Reynolds equation as the fluid equation. The outlet is a hypothetical one without a through hole. The compressible fluid-pressure is expressed by the modified Reynolds equation considering slip on the material surface as

$$\left\{\frac{\partial}{\partial x}\left(ph^2\frac{\partial p}{\partial x}\right)+\frac{\partial}{\partial y}\left(ph^2\frac{\partial p}{\partial y}\right)\right\}+6\lambda_a p_a\left\{\frac{\partial}{\partial x}\left(ph^2\frac{\partial p}{\partial x}\right)+\frac{\partial}{\partial y}\left(ph^2\frac{\partial p}{\partial y}\right)\right\}$$
$$=6\ a\left\{V_x\frac{\partial(ph)}{\partial x}+V_y\frac{\partial(ph)}{\partial y}\right\}+12\ a\frac{\partial(ph)}{\partial t} \qquad (6.)$$

where h is the distance between the micro membrane and the lower electrode, λ_a is molecular mean free path of the air, t refers to time, V_x and V_y are velocities of the micro-membrane surface in x and y directions, respectively, and μ_a is viscosity of air. h is given by $h = h_0 + w$, where h_0 is the initial gap between the micro-membrane and the lower electrode. V_x and V_y are calculated by the velocity of the deflection.

Equations (4), (5) and (6) must be solved simultaneously to analyze the deflection of the micro-membrane [4]. The distance between the micro-membrane and the lower electrode is large enough so that the effect of molecular mean free path of the air may be negligibly small.

In the coupled analysis, first, the electric field equation is solved by the Boundary Element Method. Secondly, derivatives with respect to time involved in (5) and (6) are calculated by the implicit method. Finally, stress equilibrium equations (4) and (5) and the modified Reynolds equation (6) are solved until the deflection w becomes unchanged. These steps are calculated iteratively. According to the deflection of the micro-membrane, the boundary elements of the electrostatic field are modified.

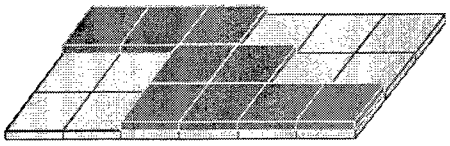
CODING AND DE-CODING OF THE MEMBRANE FOR OPTIMIZATION

We used the genetic algorithm to determine the optimum thickness distribution of the micro-membrane so that the pressure of the fluid in the vicinity of the outlet is maximized.

In the genetic algorithm, the thickness of the micro-membrane must be coded to 0 or 1. As an example, the coded genes are as follows,

11100000110000111100000110000111100000110000111100000110000111100000110000111100000110000
01111

Each component of the gene refers to the thickness of of a finite element of the membrane; "1" means t_1 and "0" means t_2, as shown in Fig.2. The thickness of the neighboring four meshes is of the same value.



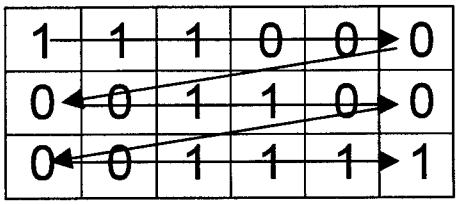


Fig. 2. Coding method of thickness distribution.

For optimization by a genetic algorithm, a fitness function for each population must be calculated and verified for all population in each generation. The fitness function should be defined in a way that is proper to express the characteristics of the phenomena for optimization. As a demonstration of the proposed

method, we optimized the thickness distribution of micro-membrane used for the micro-air-pump as shown in Figure 1. If the thickness of the micro-membrane actuated by the electrostatic force is uniform, the deflection of the micro-membrane is the largest at the center. The fluid pressure at the center also becomes a maximum. Although the volume change of the micro-pump cavity is large enough, the pressure at the outlet is low. Therefore, the performance of the micro-pump composed of a micro-membrane of a uniform thickness may be low. The maximum deflection point would change according to the thickness distribution of the micro-membrane. Since the pressure distribution depends on the distance between the micro-membrane and the lower electrode, we utilized the distance at the outlet as a fitness function. Furthermore, in order to increase the flow at the outlet, we considered the volume change in the pump cavity due to the micro-membrane deflection. The fitness function f is defined as:

$$f = 0.7\sqrt{\frac{(x_p - x_h)^2 + (y_p - y_h)^2}{(x_c - x_h)^2 + (y_c - y_h)^2}} + 0.3\left|\frac{V_{init} - V_{def}}{V_{init}}\right| \qquad 8.$$

where (x_h,y_h) is the outlet position, (x_p,y_p) is the maximum deflection point, (x_c,y_c) is the center of the membrane, V_{def} is the internal volume of the micro-pump cavity after deflection, and V_{init} is the initial volume of the pump cavity.

We used "one point" mutation for crossover and elite strategies with crossover and mutation rates of 0.9 and 0.005 respectively. The tournament method was used to select populations of 20 up to the 40th generation. In each generation, deflection was calculated by the coupled analysis for 20 populations. The thickness distribution of each population for the next generation was based on results of the previous one.

RESULTS and DISCUSSION

The size of the micro-pump is 400μm long, 200μm wide and 20μm high. The material of the micro-membrane is aluminum. The material constants for calculation are summarized in Table 1. In the calculation, the outlet is assumed to be located 150μm apart from the center of the micro-pump and 100μm from the side-wall. As a first demonstration of optimization, 2μm and 3μm thick elements were distributed. Figure 3 shows the initial thickness distribution of the micro-membrane for optimization. The initial distribution thickness is decided in a random manner for 20 populations. Since the thickness is distributed randomly, the deflection of the membrane is maximum at the center.

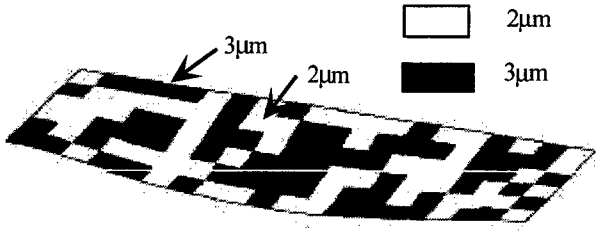


Fig.3. Thickness distribution of initial generation.

Table 1: Material of micro-membrane and geometrical properties for analysis.

Length (μm)	400
Width (μm)	200
Height (μm)	20
Thickness of the membrane (μm)	2 or 3
Mass density of the membrane (kg/m^3)	2330
Young's modulus(GPa) E_x , E_y	150
Poisson's ratio	0.3
Viscosity (μPa.s)	17.6
Molecular mean free path(μm)	0.064
Atmospheric pressure(MPa)	0.101
Permittivity(F/m)	8.854E-12

The fitness value of each population decreases with increasing generation as shown in Figure 4. After the 15th generation, the best fitness for 20 populations decreases to 0.55. The average fitness also decreases to

about 0.6. The best fitness does not change after 20 generations. At the 10th generation, the number of elements of 2μm thick increases around the outlet. On the other hand, the number of elements of 3μm thick increases in the middle area of the micro-pump. The flow volume rate increases with increasing generation.

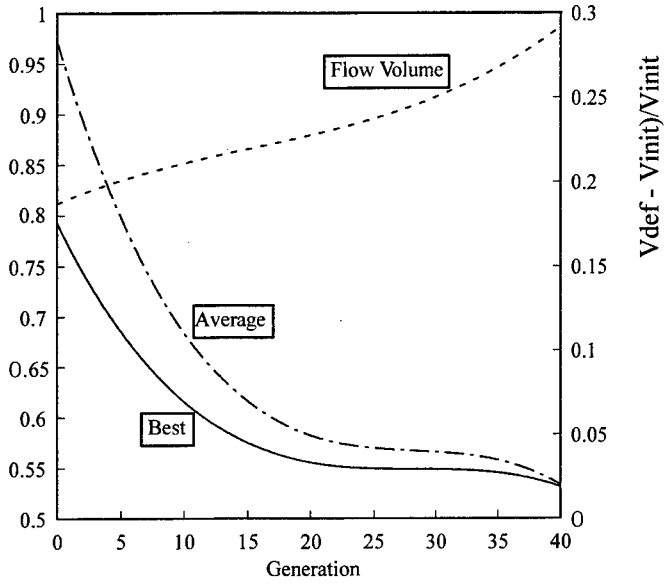


Fig. 4. Fitness and flow volume in each generation.

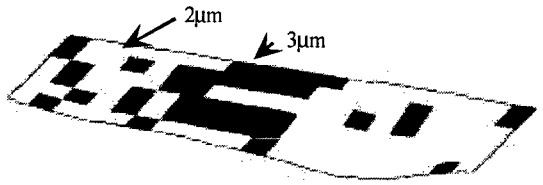
Figure 5.a. shows the thickness distribution of the best fitness individual in the 40th generation. The maximum deflection point of the micro-membrane has approached 90μm to the outlet, see Figure 5.b. At the outlet, the pressure of the air becomes a maximum. The bending angle of the micro-membrane is plotted in Figure 5.c. The area with 2μm thick elements coincides with that where the bending angle is relatively large. It seems that the bending performance of the micro-membrane is dominant as it deflects. In the genetic algorithm, populations that bend more easily in the vicinity of the outlet are selected as being better. This may be due to the limited geometry and configuration of the membrane and the pump.

As a second demonstration, we optimized cases with elements of 2μm and 4μm thick. Figure 6(a) shows the thickness distribution of the best fitness population in the 40th generation. The maximum deflection point, see Figure 6(b), shifts ~40μm from the result for elements of 2μm and 3μm thick but it is still ~20μm from the outlet point.

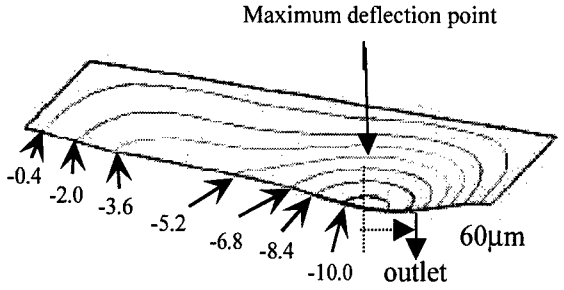
In the second example, the maximum deflection point moved toward the outlet point in comparison with that in the first example. However, the pump-out volume rate decreased about 10% (see Figure 4). It is a common knowledge that it is easy to reduce the searching space by using the genetic algorithm, however, it is difficult to discover the best solution. To achieve the optimum, we must combine the genetic algorithm with other searching algorithm, such as hill-climbing and/or steepest descent. Nevertheless, we have hereby shown that by giving a thickness distribution in the membrane we are able to obtain better or even, optimum performance.

CONCLUDING REMARKS

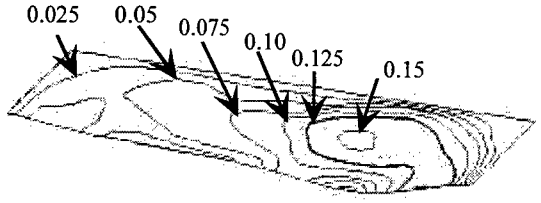
We have developed an analytical method to simulate the deflection of a micro-membrane. We also have developed a method which attempts to optimize the thickness distribution in the micro-membrane actuated by an electric force to perform a desired deflection. As an application example of our developed method, we optimized the thickness distribution of the micro-membrane actuated by the electrostatic force. It was shown that the deflection pattern strongly depends on the thickness distribution. By using a genetic algorithm, the thickness distribution that realizes the prescribed performance is obtained after the 40th generation in three hours calculation on a small EWS. However, the maximum deflection point is still 60μm separated from the outlet. The optimization method must be studied further to seek out improvement.



(a) Thickness distribution of micro-membrane

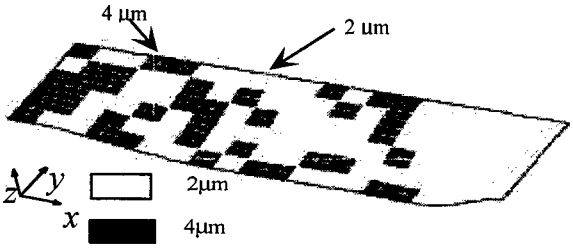


(b) Membrane deflection

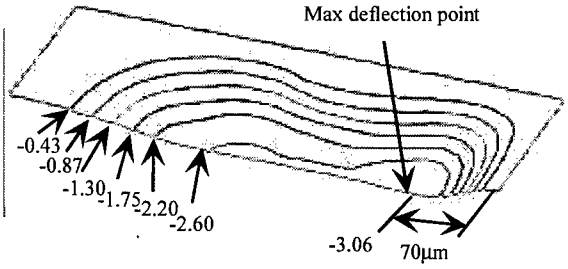


(c) Magnitude of bending angle (radians)

Fig. 5. Deflection of 2 and 3μm thick elements in the 40th generation.



(a) Thickness distribution of micro-membrane



(b) Membrane deflection

Fig. 6. Deflection of 2 and 4μm thick elements in the 40th generation.

ACKNOWLEDGEMENT

This work was supported by a Grant-in-Aid for Scientific Research (C)(No. 10650258) by the Ministry of Education, Science, Sports and Culture.

REFERENCES

1. H. Kotera, H. Kita, H. Yoshida, Y. Mizoh, 1992. A Scheme for Finite Element Analysis of an Interface Phenomena of VCR Drum, Head and Tape. IEEE Trans. on Consumer Electronics, 38(3).
2. G.K. Ananthasuresh, R.K. Gupta, S.D. Senturia, 1996. An Approach to Macro-modeling of MEMS for Nonlinear Dynamic Simulation. Microelectromechanical Systems(MEMS) ASME, DSC-59.
3. F. Shi, P. Ramesh, S. Mukherjee, 1996. Dynamic Analysis of Micro-Electro-Mechanical Systems. International Journal for Numerical Methods in Engineering, 39, 4119-4139.
4. H. Kotera, Y. Sakamoto, T. Hirasawa, S. Shima, R.W. Dutton, 1998. Dynamic simulation of MEMS coupling electrostatic field, fluid dynamics & membrane deflection. Micro System Tech., 491-496.
5. D.E. Goldberg, 1989. GAs in Search Optimization and Machine Learning. Addison Wesley.

Manufacturing of Metallic Prototypes and Tools by Laser Cutting and Diffusion Bonding

S. Sändig, P. Wiesner

Faculty of Mechanical Engineering, Technical University of Ilmenau, Germany

ABSTRACT

This paper presents a new rapid metal prototyping technology. The direct production of metallic structures is accomplished by laser cutting of metal sheet and subsequently forming a component by diffusion-welding the sheets. The combination of this two flexible manufacturing techniques with a special computer-aided design process offers excellent means of producing fully functional metallic parts as well as tooling inserts from sheet metal in a short time.

INTRODUCTION

Today manufacturing processes must fulfill several requirements. A process must be flexible, with few intermediate stages, capable of automatisation, integration and environmentally acceptable, with no harmful by-products and low energy consumption. The first of the requirements mentioned above are most important due to the competitive situation. The rate of development is so rapid that today's technologies are soon out of date. A company must respond to the market forces in the shortest time possible.

Up to 50% of development time is required for the manufacture of prototypes and models. In some cases the lifetime of the new product is shorter than the design time. This necessitates a drastic reduction in the product development cycle. Rapid prototyping and rapid tooling techniques offer a way of achieving this.

Rapid Prototyping and Rapid Tooling are terms reserved for a new group of computer-based design and manufacture processes able to produce parts or tools directly from computer images. Stereo-lithography is the best known technique. Traditional application of rapid prototyping techniques are for non-metallic parts (polymers and paper). Often these parts can only be used for applications not requiring component strength and durability. In addition to tolerances, shape and aesthetic evaluation, the requirement of functional testing necessitates material properties close to those encountered in actual use. There is growing demand for functional prototype parts and prototype tools which accurately represent the characteristics of production components. It is clear that a prototype matching the chemical, mechanical and thermal properties of the end-product is a much more valuable prototype. For that reason, development of new flexible manufacturing methods to produce metallic parts and tools is one of the objectives of recent research.

Generating a complex metal prototype part or tool for industrial application is difficult. Basically there are two main ways to produce truly-metallic parts by rapid-prototyping. Indirect methods such as metal investment casting using stereo-lithography-based moulds, or selective-laser sintering of moulds directly in foundry sand, work well, but they are very time-consuming due to secondary tooling. Therefore, present research activities are focussed on developing direct methods. Many research institutes are examining direct-laser sintering of metal powders and laser-cladding as well. RP-components produced with metal powder techniques are porous and must be furnace-sintered or infiltrated with a lower-melting-point alloy to consolidate the objects. All of these techniques using metal powder are at an early stage of development and at present are limited to small components. In many cases they are unsuitable to produce tools.

Therefore we prefer a different approach -- combination of laser cutting and diffusion bonding. This offers an excellent way to produce fully-functional metallic parts and tool inserts from sheet metal in a short time.

MANUFACTURING PROCESS

0-7803-5489-3/99/$10.00 ©1999 IEEE.

The key idea is based on the concept of the Laminated Object Manufacturing (LOM) techniques, originally developed for manufacturing of "wood-like" paper models. In our case the initial material consists of metal sheets. The metal is cut to the required shape just as for paper parts. Cutting the metal sheets is possible with CO_2-laser or Nd:YAG-lasers but also, water-jet or electrical discharge machining can be used. Laser-cutting was one of the first uses of lasers in material processing and apart from laser marking, it represents the most common field of application in production technology today [1]. Laser-cutting has established itself as a highly flexible and precise process for internal and external contours in components.

The main problem arising with metal sheets is to develop a process to join them together. Several possibilities are laser-welding sheet edges, bonding and of course mechanical joining such as threaded joints, rivets or clamps [2]. The disadvantage of all these solutions is that the mechanical stability and density of these prototypes do not correspond to the properties of the conventional metallic part.

If the metal sheets are to be joined over the entire contact surface, diffusion bonding is a excellent method. This is a special joining method which enables matched joining of metallic, silicate and ceramic material completely in the solid state. Metals such as copper, steel-copper, titanium-nickel, combinations of iron and sapphire, corundum and aluminium, in total, more than 600 different material combinations, can be joined by solid phase diffusion (movement of atoms across the interface) without addition of any material. Unlike other pressure welding processes there is little or no macroscopic distortion. The bonded interface has essentially the same physical and mechanical properties as the base material. The surfaces to be joined are pressed together and maintained in contact over the entire surface so a bond can be formed by solid-state diffusion. Diffusion is carried out at a temperature, dependent on the metal, at which the diffusion rate is high and at a pressure conducive to forming a good bond. Diffusion-welded bonds can be thermally and mechanically loaded and, furthermore, they are vacuum-tight. The strength of the bond is of the same order of magnitude as that of the basic material. Thus, high functionality of the prototype can be realised.

The specific conditions of diffusion welding must be taken into account when designing and constructing the prototype, but basically, the process is very simple. It begins with component and tool design on a 3D-CAD system. The design is done using any CAD software suitable for complex geometry. On completion of the design, an industry-standard file is output which describes the surface of the model. A software program slices the complex 3D model into simple 2-D cross sections and converts the file into a format compatible with the postprocessor (e.g., DXF). The outer surface of each layer maintains the 3D-geometry of the original model. Then the postprocessor generates the corresponding NC data for the handling unit (i.e., the laser cutting path) and provides specific information required by the laser. A CO_2 or Nd:YAG-laser is used to cut sheets of the desired material, usually steel. The thickness of the metal sheet, as well as the required alloy must be selected carefully, as these features influence cutting accuracy and final properties of the part. It is not unusual that the optimal thickness varies according to the cross-section of the part. Beam quality, process parameters and the positioning unit, all influence the quality of the cut and affect the accuracy of the prototype. After cutting, the sheets are stapled and positioned in a vacuum chamber. The sheets are then joined over their entire surface by diffusion bonding to form the required part or tool. Fig. 1 summarizes the specific manufacturing process.

BENEFITS

The process enables fully functional parts or tools (moulds and dies) to be produced. In contrast to material removal using conventional CNC machining operations, such as turning and milling, any 3-D internal contours can be shaped due to the sandwich construction. An example is mould inserts with optimally positioned cooling pipes for heat diversion. With sheet metal, it is possible to combine thin and/or thick sheets of the same or different material into one part. Therefore it is possible to optimise part properties.
Components produced in this manner can be used directly in functional testing and in-field applications, so shorter iterative development steps are possible. Potential manufacturing problems can be eliminated at an earlier stage of development when changes are not so costly. The suggested technology is a further example of the benefits obtainable if conventional manufacturing techniques, such as laser cutting and diffusion

of the benefits obtainable if conventional manufacturing techniques, such as laser cutting and diffusion welding, are combined together with computer-aided design and engineering in a continuous process chain. In the presentation several examples will be provided to demonstrate the potentials of this new technique.

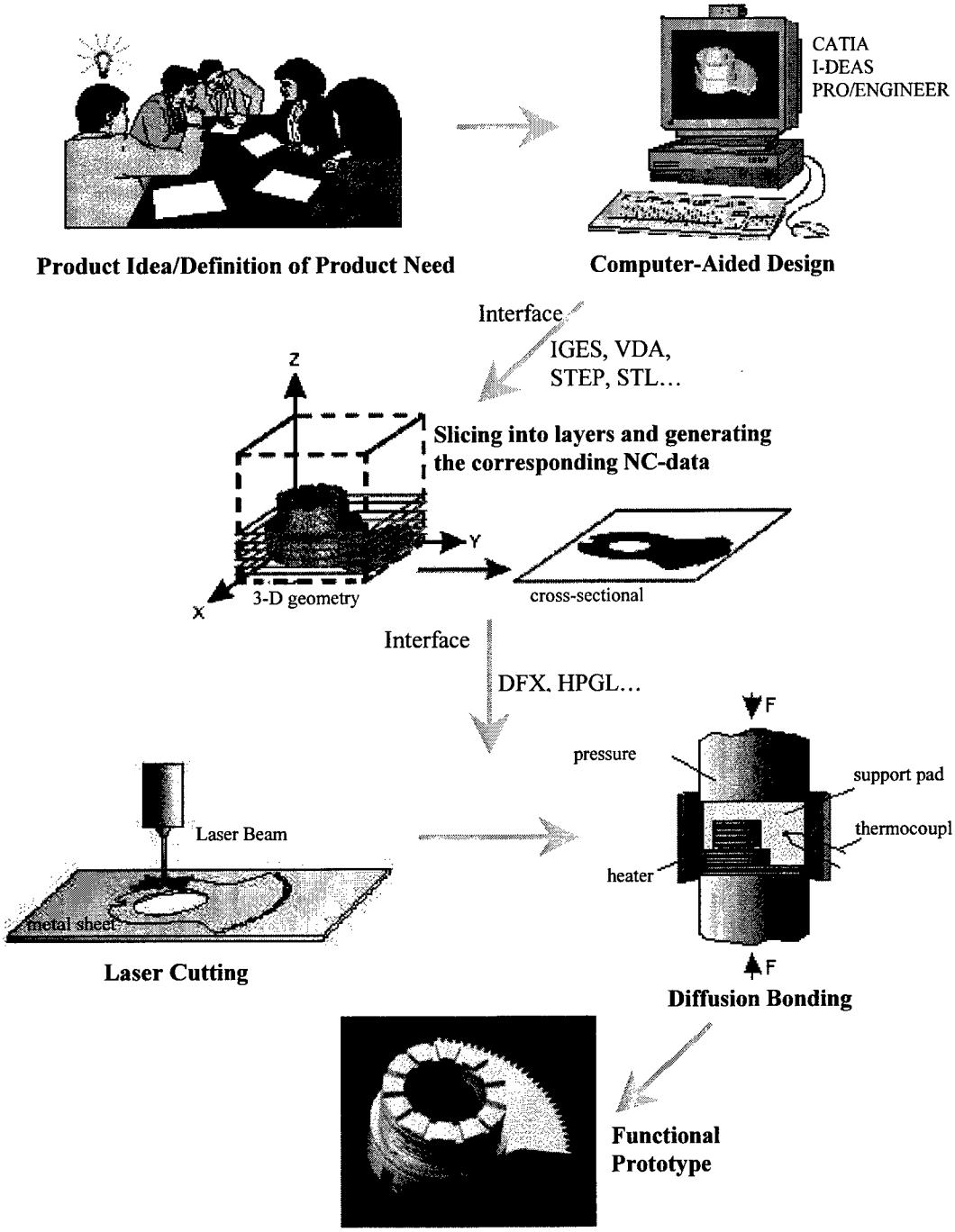


Fig.1. Schematic illustration of the various process steps

REFERENCES

1. H.K. Tönshoff, 1997. Laser-based manufacturing - competition or ideal complement to conventional production technologies. Proc. LANE'97, 3-30
2. J.-P. Kruth, J. Bonse, I. Meyvaert and B. Morren, 1997. Laser-based Rapid Prototyping a Decade after its Introduction. Proc. LANE'97, 93 - 113

Evolutionary Systems and Machine Learning

Artificial Immune Systems in Industrial Applications

Dipankar Dasgupta* and Stephanie Forrest**

* Dept. of Mathematical Sciences, The University of Memphis,
Memphis, TN 38119
** Dept. of Computer Science, The University of New Mexico
Albuquerque,NM 87131

ABSTRACT

Artificial Immune System (AIS) is a new intelligent problem-solving technique that is being used in some industrial applications. This paper presents an immunity-based algorithm for tool breakage detection. The method is inspired by the negative-selection mechanism of the immune system, which is able to discriminate between the self (body elements) and the non-self (foreign pathogens). However, in our industrial application, the self is defined to be *normal* cutting operations and the non-self is any deviation beyond allowable variations of the cutting force. The proposed algorithm is illustrated with a simulation study of milling operations. The performance of the algorithm in detecting the occurrence of tool breakage is reported. The results show that the negative-selection algorithm detected tool breakage in all test cases.

INTRODUCTION

Manufacturers are always looking for ways to improve productivity without compromising on quality of manufacturing processes. To this end, much attention has been directed towards automated manufacturing. In drilling or high-speed milling industries, on-line monitoring of tool breakage is a key component in unmanned machining operations.

In most milling industries, a reliable and effective tool breakage detection technique is required to respond to unexpected tool failure [1]. In particular, such a monitoring technique is necessary to prevent possible damage to the workpiece and the machine tool or to avoid production of defective parts and possible overloading of tools. The normal operation of a milling cutter is often characterized from the measurements of some parameters that are correlated with tool wear. It is essential to detect the occurrence of abnormal events as quickly as possible before any significant performance degradation results. This can be done by continuous monitoring of the system for changes from the normal behavior patterns.

Thus, a signal may be sent to the machine controller/operator for triggering an emergency stop of the machine and the tool can be changed. Several techniques have been suggested for monitoring tool breakage in different machining operations [1]. Recent efforts include time-series analysis [2], Artificial Intelligence (AI) techniques [3], pattern recognition methods [4], fuzzy set theory [5], and neural networks [6] applied to the problem of recognizing the cutting states and detecting tool breakage. Among these, neural network-based techniques have been used to detect tool breakage in milling and monitoring manufacturing processes [7].

Most methods require prior knowledge about various fault conditions [8] or tool breakage patterns [7]. It is difficult to obtain a variety of good tool breakage patterns in an industrial environment. A robust method should detect any unacceptable (unseen) change rather than looking for specific known activity patterns. This paper proposes a new detection algorithm for tool condition monitoring in milling operations. The algorithm is based on ideas from the immune system. It is a probabilistic method that notices changes in force pattern of tools without requiring prior knowledge of what changes to look for. In this way, it resembles the approach to novelty detection taken by ART neural architectures [9]. Both neural networks and our immune system-based algorithm are biologically-inspired techniques that have the capability of identifying patterns of interest. However, they use different mechanisms for recognition and learning.

0-7803-5489-3/99/$10.00 ©1999 IEEE.

In the next section, the basic immunity-based detection algorithm is described. The problem, simulated cutting force dynamics in a milling process, is then discussed following which the proposed method is demonstrated for tool breakage detection by monitoring (simulated) cutting force patterns. This includes the preprocessing of sensory data and the implementation details of generating detector sets for monitoring tool conditions. The results of different experiments and our evaluation of performance are given followed by final conclusions.

IMMUNITY-BASED CHANGE DETECTION ALGORITHM

This detection algorithm is inspired by the information-processing properties of the natural immune system [10]. The immune system uses learning, memory, and associative retrieval to solve pattern recognition problems. Vertebrate immune systems are capable of distinguishing virtually any foreign cell or molecule from the body's own cells which are created and circulated internally. This is known as the self-nonself discrimination problem [11]. In the immune system, T cells have receptors on their surface that can detect foreign proteins (antigens). During the generation of T cells, receptors are made by a pseudo-random genetic rearrangement process. Then they undergo a censoring process, called negative selection, in the thymus where T cells that react against self-proteins are destroyed, so only those that do not bind to self-proteins are allowed to leave the thymus. This censoring process is very important in self-nonself discrimination. Our artificial immune system [10] is a simplification of the complex chemistry of antibody/antigen recognition in natural immune systems. The basic principle of our negative-selection algorithm is as follows:

- Define *self* as a multiset S of strings of length l over a finite alphabet, a collection that we wish to protect or monitor. For example, S may be a segmented file, or a normal pattern of activity of some system or process.
- Generate a set R of *detectors*, each of which fails to match any string in S. We use a partial matching rule, in which two strings match if and only if they are identical at least r contiguous positions, where r is a suitably chosen parameter [10].
- Monitor S for changes by continually matching the detectors against S. If any detector ever matches, a change (or deviation) must have occurred.

Matching Rule

We adopted a partial-matching rule based on a prespecified degree of similarity. To measure this similarity, we are currently using an r contiguous matching rule between two strings of equal length. Thus, for any two strings x and y, *match(x, y)* is true if x and y agree (match) on at least r contiguous locations (*r less than or equal to l*), as illustrated in Fig. 1.

$$X: \quad bcabcbad$$
$$Y: \quad dcabdcba$$

Fig. 1. Illustration of Matching Rule:
x and y are two strings defined over the four-letter alphabet *a, b, c, d.*
X and Y match at 3 contiguous locations (underlined).
Thus, *match(x, y)* is true for $r \leq 3$ and false for $r > 3$.

A partial-matching rule provides a detector with its ability to detect sample strings in its neighborhood according to the threshold value, r. This is demonstrated in Fig. 2, for a binary string. The graphs in Fig. 2 illustrate that the coverage of a string of defined length increases exponentially with a decrease in r. Although maximum coverage can be achieved with $r = 1$, the generated detectors will probably match many self strings resulting in false detection. On the other hand, a perfect matching (for $r = l$) implies that the symbols are identical at each location in two strings; accordingly, a very large number of detectors are needed to detect patterns in the non-self space. An optimal r value estimates a reasonably-sized detector set for the success of this method.

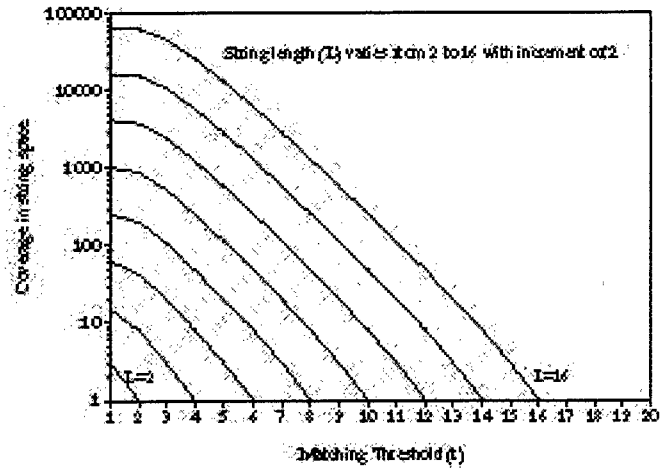


Fig. 2. The number of points that can be covered by each binary string (of defined length in its string space) is seen to vary with different matching threshold.

When a non-overlapping set of detectors is generated with a suitable matching threshold, each one can serve as a distinct novelty pattern class in the non-self space. However, in the case of overlapping detectors, multiple detectors may be activated for a sample (abnormal) pattern, and more are needed to provide sufficient coverage in the non-self space.

Generating Detectors

There are many possible ways to generate detectors in the non-self space. These approaches generally have different computational complexities dependent on the choice of matching rule. In the original description of the negative-selection algorithm [10], candidate detectors are generated *randomly* and then tested (censored) to see if they match any self string. If a match is found, the candidate is rejected. This process is repeated until the desired number of detectors is generated. A probabilistic analysis is used to estimate the number of detectors that are required to provide a given level of reliability. The major limitation of the random generation approach appears to be computational difficulty of generating valid detectors, which grows exponentially with the size of self. Also for many choices of l and r, and compositions of self, the random generation of strings for detectors may be prohibitive.

In this paper, we generate detector sets using an improved algorithm proposed by [12] which runs in linear time with the size of self. The algorithm has two phases; first it employs a dynamic programming technique to count recurrences in order to define an enumeration of all unmatched strings (i.e., all feasible detectors). Second, a random subset of this enumeration is chosen to generate a detector set. In other words, given a collection of self strings S and matching threshold r, the first phase of the algorithm determines the total number of unmatched strings that exist for the defined self (S). Then in the second phase, some of these are selected to generate detectors for monitoring self (normal patterns).

SIMULATION OF CUTTING TOOL DYNAMICS

The dynamics of a machining process can generally be monitored when it operates in a defined environment [1]. Usually, the methods for monitoring a milling process utilize measurements of cutting parameters correlated with tool breakage [13]. These cutting parameters include temperature [14], cutting force [13], vibration [15], torque [16], acoustic emission [17], etc. Of these parameters, cutting forces are widely used for tool breakage detection [13, 18, 19] for several reasons:

- Cutting force signals are much less dependent on structure.
- Cutting force signals can be simulated easily and more accurately than acceleration and acoustic emission signals.
- The cutting force is a very good indicator of the vibration between the tool and workpiece because of their higher sensitivity and more rapid response to changes in cutting state.

The cutting force variation characteristics of normal and broken tools are different. Under normal (stable) cutting conditions, the cutting force periodically varies with tooth frequency, Ω_t that depends on the spindle speed:

$$\Omega_t = \frac{NP}{60} \tag{1}$$

where N is the spindle speed in *rpm* and P is the number of teeth on the cutter.

If the tool is broken, it can not remove the same amount of material as the other teeth. Accordingly, the number of tooth periods deviating from the stable cutting pattern depends on the number of teeth that are actively involved in the cutting zone.

Some approaches for tool breakage detection are based on an analysis of signal spectra obtained from prior FFT signal preprocessing where signal magnitude at specific frequencies increases when tool fractures occur. However, Moore and Reif [15] demonstrated that tool breakage can be more reliably monitored in the time-domain than in the frequency-domain.

We prepared simulated data for cutting operations using the vibratory model described in [13, 20]. This model has been used by many other investigators for tool breakage detection [2, 18].

To generate data, the spindle was represented by a vibratory system with two degrees of freedom in the two orthogonal directions X and Y. We considered a four-tooth cutter with uniform pitch, performing an end-milling, half immersion cut in the X-direction. In this model, the instantaneous cutting force at angle φ is assumed to be proportional to the chip thickness, h. Forces acting on a tooth are the tangential force, F_t and radial force, F_r. The instantaneous tangential force F_t can be approximated by considering the tool displacement as:

$$F_t = K_c\, b\, h \tag{2}$$

subject to the condition that if $F_t \leq 0$ then $F_t = 0$.

In Eq. 2, K_c is the dynamic cutting force coefficient, b is the axial depth of cut, and h is the chip thickness. The instantaneous chip thickness is obtained from:

$$h = f_t \sin\varphi - z + z_{\min}$$

where f_t is the feed rate per tooth, and z is the displacement of the tool normal to the machined surface which is derived from vibratory displacements in the X and Y directions; z_{min} is the minimum undulation left behind in preceding cuts at the angle φ.

Now the displacement, z in the direction normal to the cut surface is given by:

$$z = x\sin\varphi + y\cos\varphi \tag{3}$$

The corresponding instantaneous radial component of the cutting force

$$F_r = K_r F_t \tag{4}$$

In previous studies [13, 20], the value of K_r was assumed to be 0.3.

For non-helical teeth, the instantaneous cutting force in the X and Y directions can be obtained by decomposing the cutting forces F_t and F_r into the X and Y directions:

$$F_x = F_t \cos\varphi + F_r \sin\varphi = F_t(\cos\varphi + K_r \sin\varphi)$$
$$F_y = -F_t \sin\varphi + F_r \cos\varphi = F_t(-\sin\varphi + K_r \cos\varphi) \quad (5)$$

In the case of multi-tooth milling, instantaneous cutting forces in the X and Y directions is expressed as:

$$FX = \sum_{i=1}^{P} \delta(i) F_x(\varphi_i)$$
$$FY = \sum_{i=1}^{P} \delta(i) F_y(\varphi_i) \quad (6)$$

and

$$\delta(i) = \begin{matrix} 1 & if \varphi_s \le \varphi_i \le \varphi_e \\ 0 & otherwise. \end{matrix} \quad (7)$$

In Eq. 7, φ_s,and φ_e are the start and exit cutting angles, and φ_i is the cutting edge rotation angle of the i^{th} tooth.

Now, the instantaneous resultant cutting force,

$$F = (FX^2 + FY^2)^{1/2} \quad (8)$$

At every angle φ, the vibration amplitude induced by cutting forces are used where the force components of F (F_x and F_y) excite vibrations in X and Y directions which can be determined from the equations of motion for the system:

$$F_x = m_x \ddot{x} + c_x \dot{x} + k_x x$$
$$F_y = m_y \ddot{y} + c_y \dot{y} + k_y y. \quad (9)$$

In Eq. 9, the structural parameters of two modes of vibration are m is the mass, c is the damping coefficient, and k is the stiffness. At time step t, the cutter has rotated by the angle φ_t from the reference axis Y. The F_x and F_y components of the cutting force excite vibrations in the x and y directions. The cutting force profiles were simulated using forth-order Runge-Kutta method for every time step (δt = 0.0001 sec), where displacements at step, $t+1$ are calculated from the cutting force data at step t. So the computation loop is repeated for every time step δt, then as a whole cycle per tooth period. The deflections are used to determine the uncut chip thickness for each tooth in cut (in the direction normal to the cut surface, z). Once the uncut chip thickness is determined, its value is used to determine instantaneous cutting forces.

In our experiments, one tooth is engaged in the cut at an angle φ, where the cutting angle varies from 0 to $\pi/2$ for every tooth engagement. The complete breakage of one tooth was simulated where the broken tooth did not remove any material or started to remove less material than the other teeth that gave periodic amplitude fluctuations in cutting force.

For detailed analysis of the vibratory model, and calculation of the cutting force and vibration, the reader is referred to [13, 20]. The parameters used in our simulation are:

Damping coeff., $c_x = c_y = 471.9$ kg/s; Mass, $m_x = m_y = 10$ kg;
Spring constant, $k_x = k_y = 8.1 * 10^6$ N/m; Feed rate/tooth, $f_t = 0.2$ mm;
Cutting coefficient, $K_c = 6.67 * 10^6$ N/m; Depth of cut, $b = 0.508$ mm;
Spindle speed, $N_s = 600$ rpm; Spindle diameter, $D = 40$ mm.

TOOL BREAKAGE MONITORING

We formulated the tool breakage detection problem in terms of the problem of detecting temporal changes (or abnormal patterns) in cutting force patterns resulting from the broken cutter. The patterns are encoded as strings and are monitored for whether or not the current strings are different (matched using negative selection), where a change (or match) implies a shift in the normal behavior in cutting force patterns.

Data Preprocessing

We preprocess sensory data into a form suitable for the detection algorithm. Preprocessing can be viewed as constructing an alternative representation to try to capture the regularities of the data while preserving the information content. Furthermore, any change that exceeds allowable variation in the data pattern should ideally be reflected in the representation space. This can be a problem when very small changes in real-valued data need to be monitored. To handle this, we use an approach that maps close real-valued data into a discrete form: an analog value is normalized with respect to a defined range and discretized into bins (or intervals). Each datum is assigned the integer corresponding to the bin into which it falls.

The integer is then encoded using binary representation. However, if an observed value falls outside the specified range, it is mapped to all 0's or all 1's depending on which side of the range it crossed. The number of bits used in the discretization thus determines the size of the bins. If each datum is encoded by n bits (which may be chosen according to the desired precision), then there are $2^n - 2$ different bins between the maximum *(MAX)* and minimum *(MIN)* ranges of data (see Fig. 3).

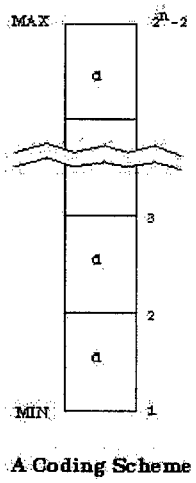


Fig. 3. Illustration of a mapping technique for encoding close analog values into a discrete form. For binary encoding with n bits/data, the number of intervals and the size of each interval (d) are shown here.

Implementation Details

In our implementation, raw sensory data are sampled from a moving time window and mapped to binary form. Each window, therefore, is the concatenation of a fixed number (called *Win_size*) of data points. We collect the bit strings from a succession of windows, sliding along the time series in discrete steps (*Win_shift*) for the normal data set. As long as the time series data pattern maintains similar behavior, these collected strings are sufficient to define normal behavior of the system. This collection of strings for windows is our self set (S). We then generate strings that do not match any of the strings in S to be members of the detector set. The generation of detectors in this detection algorithm is usually performed off-line, as in the case of neural networks (supervised) training for fault detection [7] or developing rule-based expert-systems for detecting faults/anomalies etc. [21]. Overall, our approach can be summarized as shown in Fig. 4.

The steps in the method are as follows:

1. Collect time series (sensor) data that sufficiently exhibit the normal behavior of a system (these may be raw data at each time step, or average values over a longer time interval).

2. Examine the data series to determine the range of variation (*MAX, MIN* values) of data and choose the data encoding parameter (n) according to the desired precision.
3. Encode each value in binary form using the above coding scheme.
4. Consider a suitable window size that can capture the semantics in data pattern.
5. Slide the window along the time series and store the encoded string for each window as *self* for processing by the negative-selection algorithm.
6. Generate a set of detectors that do not match any of the self strings according to the partial matching rule with suitably chosen r. It is desirable that the detectors are spread enough to cover the unmatched string (non-self) space. Also an estimate for the size of the detector set is needed to ensure a certain level of reliability in detecting changes [10].
7. Once a unique set of detectors is generated from the normal database, it can probabilistically detect any change (or abnormality) in patterns of monitoring sensory data.
8. When monitoring the system, we used the same preprocessing parameters as in steps 3 and 4 to encode new data patterns (moving window). If a detector is activated (matched with the current pattern), a change in behavior is known to have occurred and an alarm signal is generated regarding the abnormality. We use the same matching rule to monitor the system as was used to generate detectors.

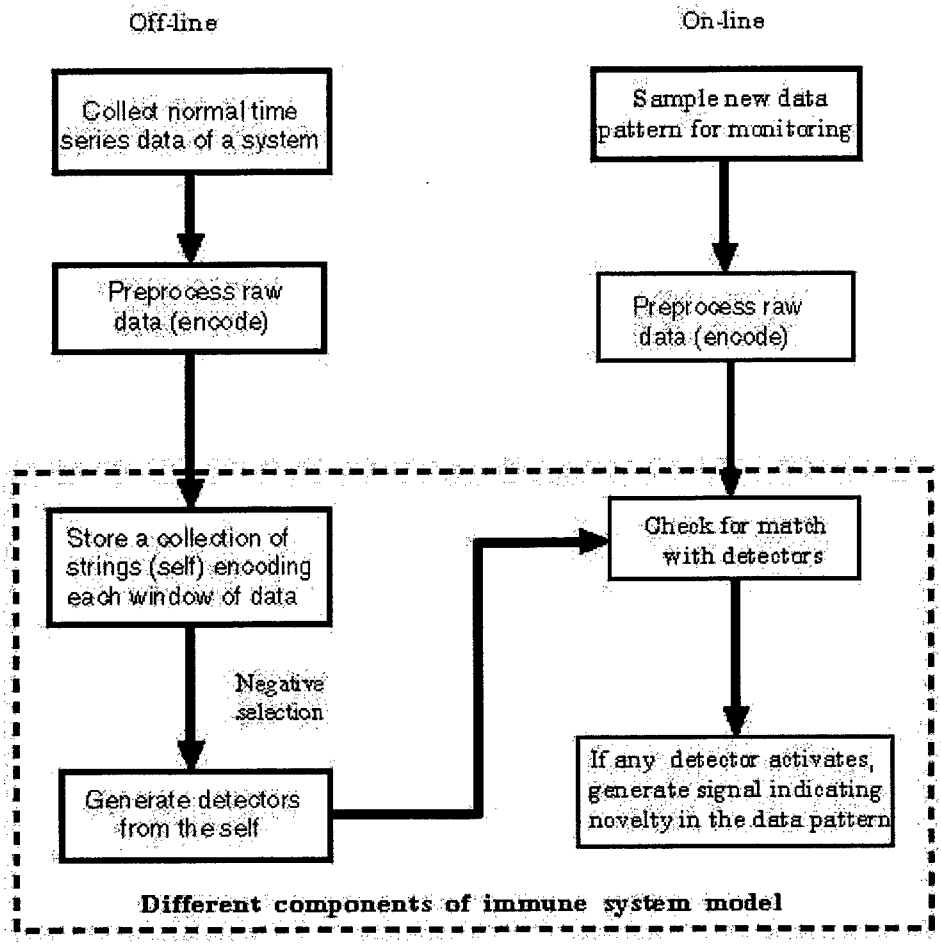


Fig. 4. Schematic diagram showing the processing stages of immune system-based fault detection.

The encoding parameters that affect preprocessing are:

BITS_PER_DATA (n) - this will dictate the degree of numerical precision with which real numbers are represented in binary form. For example, 5-bit data encoding gives 30 intervals into which the range *[MIN, MAX]* of data is divided.

WINDOW_SIZE (w) - the number of samples encoded in a single pattern (each string in self).

WINDOW_SHIFT - the number of samples by which one pattern is shifted from the previous one in a moving window. For example, if WIN_SHIFT = 1 with a window size w, the patterns will be $\{x_1, x_2, ..., x_w\}$, $\{x_2, x_3, ..., x_{(w+1)}\}$ .... etc.

EXPERIMENTAL RESULTS

We simulated several test cases of the milling cutter dynamics to carry out a set of experiments with the proposed detection algorithm. The purpose was to detect tool breakage in different cutting environment.

Fig. 5 shows typical cutting force patterns with and without tool breakage in a simulated milling operation. In this simulation, the tool was in normal cutting operation for 1500 time steps and then one tooth was broken, causing changes in cutting force signals at the corresponding tooth periods. In our experiments, we used the first 1000 data points as the self set, S for generating detectors and the rest of the data series are used for testing. Results of the experiments are shown in Table 1 and in Fig. 6. Table 1 shows the various parameters used for preprocessing data and for generating detectors. We tried several different parameter values and found the reported values most suitable. We generated the diverse set of detectors in such a way that they do not match each other by r-contiguous bit rule. In these experiments, we set $n = 6$ for binary encoding of data and two different window sizes are considered. Detection results (columns 4 and 5) show that the mean number of times detectors activated and the average detection rate in each case.

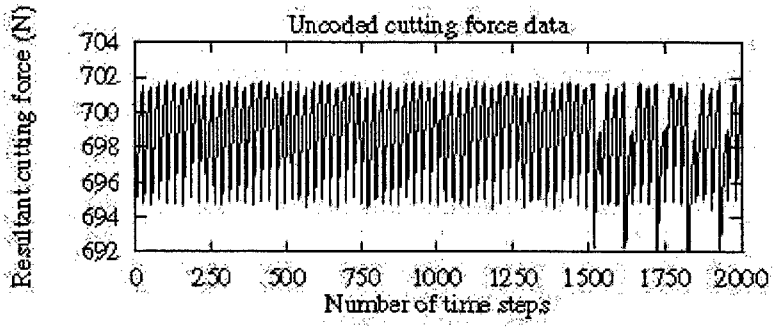


Fig. 5. Simulated cutting force signals of normal operation and with tool breakage in a milling operation. Here, one tooth of the cutter is broken after 1500 time steps.

In all test runs, the generated detectors could detect the tooth periods in which the changes in the force pattern occurred. Fig. 6 shows a typical run and the number of activated detectors (novel patterns encountered) at different time steps. In this example, a maximum of three detectors is activated (out of 20) when there are significant changes. Note that the detectors remain inactive during the normal operating period, in particular, between 1000 and 1500 time steps where the data exhibit a normal pattern, thus avoiding false positives. Also all broken tooth periods can easily be detected.

Further experiments were conducted with various cutting parameters to simulate cutting forces for normal and broken tool condition as summarized in Table 2. In each case, first 1500 data were considered as the measurement of normal cutting and the rest were for the broken tool. In all experiments, the encoding parameter n was set to 5. Two different window sizes were considered with different parameter settings. Experiments were repeated (10 times) for each cutting condition, where a small set of detectors were generated from 1000 initial data and used for monitoring the rest. Results of the experiments are shown in Table 3. These experiments indicate that our algorithm can easily detect tool breakage in all test cases.

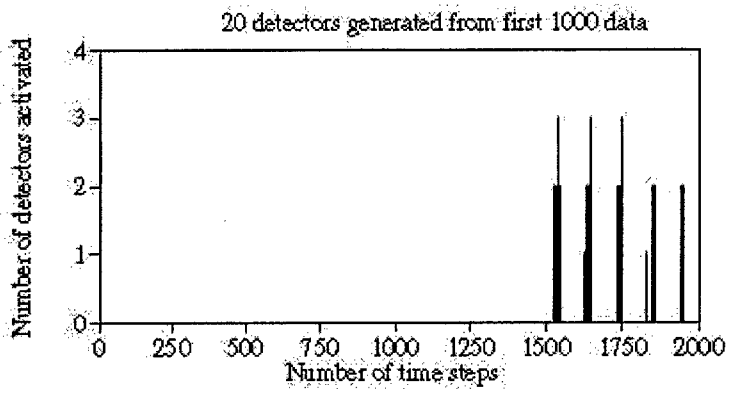


Fig. 6. The height of vertical lines in the graph corresponds to the number of detectors activated when novel patterns are found.

The results agree with our theory that performance is a function of the matching threshold (r). With larger r, the generated detectors become sensitive to any particular novelty in data patterns, so more detectors are needed to achieve a desired level of reliability. On the other hand, if r is too small, it may be impossible to generate a detector set of reasonable size from the available self, since no unmatched strings (non-self) may not exist. This suggests that r can be used to tune detection reliability against the risk of false positives.

Table 1.

Tool breakage detection results, averaged over 50 runs. Column 4 shows the mean number of detections. The standard deviations are shown in parentheses. The detection rate is shown in column 5. This is the ratio of the average detection to the number of actual novel data patterns.

Encoding parameters	Matching Threshold (r)	Number of Detectors (R)	Breakage detection	
			Mean (Std. Dev.)	Detection Rate (%)
Win_size=5	10	50	14.30(2.32)	59.58
Win_shift=5	9	40	17.57(2.25)	74.32
l =30, S=200	8	30	22.16(2.57)	91.64
Win_size=7	12	40	10.36(3.36)	62.78
Win_shift=7	10	30	20.38(5.57)	75.56
l =42, S=142	9	20	30.75(7.91)	93.28

Table 2. Use of various cutting parameters for generating cutting force signals.

Experiment Number	Axial Depth Cut (mm)	Feed Rate (m/min)	Spindle Speed(rpm)	Spindle Diameter(mm)
1	1.34	90.6	800	50
2	1.016	125.4	500	40
3	1.524	50.8	700	40

Table 3.
Results of tool breakage detection under different cutting conditions. Column 5 shows the number of detectors (as %) activated when novel patterns were encountered in periods corresponding to a broken tooth. Column 6 shows detection rates. Note that detection rates are high (95 - 100 %) when monitoring broken tooth periods.

Encoding Parameters	Experiment Number	Matching Threshold (r)	Total Number Of Detectors Generated	Detectors Activated (%)	Broken Periods Detected (%)
Win_size = 6	1	8	30	75	98
Win_shift =6	2	8	40	72	100
l=30, N_s=166	3	9	50	63	96
Win_size = 8	1	9	40	78	99
Win_shift =8	2	10	50	73	98
l=40, N_s=125	3	11	70	67	95

CONCLUSION

In this paper, we have proposed a method for tool breakage detection based on principles inspired by the natural immune system. The objective of this work is to develop an efficient detection algorithm that can be used to alert an operator to any changes in steady-state characteristics of milling cutter dynamics. The results demonstrated that the proposed algorithm could successfully detect the tooth breakage from dynamic variation of the cutting force signals. It is to be noted that our approach relies on a large enough samples of normal sensory data to generate a diverse set of detectors that probabilistically notice any deviation from the normal operation. Because it does not look for any particular (or known) fault, rather indicate that these patterns are novel with respect to the normal behavior pattern, this algorithm could be incorporated into existing diagnostic tools for further classification.

The detection system can be updated quickly by generating a new set of detectors as the normal milling operation is modified by tool-workpiece geometry, change in cutting conditions, etc. Forrest et al. [10] show that even a small set of detectors have a high probability of noticing changes in the original data set.

In most monitoring systems, detection of spurious changes in sensor measurements is not as important as the gradual change in pattern over a period of time, so our probabilistic detection algorithm is a promising alternative to such problems. It may be necessary to choose a fault-detection threshold that allows instantaneous variations or spikes from the established normal patterns while monitoring real sensor data.

There are a number of parameters that are tunable in both preprocessing and detector generation. During preprocessing, the desired precision can be achieved by grouping similar analog data in the same bin, and a suitable window size can be chosen to capture regularities in the data patterns. Note that the system can monitor using different time scales simultaneously. Instead of directly encoding time-series data, it may be necessary to transform data (e.g., by Fourier transform) depending on the data properties. It is also possible to combine several sensor signals (sensor fusion) to improve system reliability [22], particularly, when a single sensor does not correlate well with all the anomalies to be detected. Decisions based on multiple sensors provide more information simultaneously with higher quality than decisions from a single sensor.

One simple data fusion method is weighted addition of sensor signals. A desired detection reliability can be achieved by changing window size, matching threshold, or the number of detectors. The probability of a match at r contiguous positions and the impact of different r vslues on overall computational behavior of the algorithm are reported in [10]. Theoretical analysis and empirical experiments suggest the algorithm is highly sensitive to r. We are currently investigating other matching rules and generation algorithms [23].

We have tested the feasibility of this detection algorithm on a number of data sets, including the Mackey Glass series [9], and some real sensor data. The experiments suggest this detection algorithm can be useful for many other similar problems, including fault detection, anomaly detection, machine monitoring,

signature verification, noise detection, patient's condition monitoring and so on. The idea of using immune system principles in fault detection was also studied by others [24, 25], however, they have chosen a different set of principles to emulate process fault diagnosis. The remarkable detection ability of biological immune systems suggest negative-selection algorithms are well worth exploring in industrial applications.

REFERENCES

1. Altintas, Y. and Yellowley, I., 1989. In-Process Detection of Tool Failure in Milling using Cutting Force Models. J. Eng. for Ind., 111, 149-157.
2. Tansel, I.N., McLaughlin, C., 1993. Detection of tool breakage in milling operations-I. The time series analysis approach. Int. J. Mach. Tools & Manu., 33(4), 531-544.
3. Chryssolouris, G., Guillot, M., 1990. A comparison of statistical and AI approaches to the selection of process parameters in intelligent machining. Trans. ASME; J. Eng. for Ind., 112, 122-130.
4. Li, C.J., Wu, S.M., 1989. On-line Detection of Localized defects in bearings by pattern recognition analysis. Transactions of the ASME; Journal of Engineering for Industry, 112, 331-336.
5. Du, R.X., Elbestawi, M.A., Li, S., 1992. Tool condition monitoring in turning using fuzzy set theory. In Int. J. Mach. Tools & Manu., 32(6), 781-796.
6. Tansel, I.N., McLaughlin, C., 1993. Detection of tool breakage in milling operations-II. The neural network approach. Int. J. Mach. Tools & Manu., 33(4), 545-558.
7. Guillot, M., Ouafi, A.E., 1991. On-line Identification of Tool Breakage in Metal Cutting Processes by use of Neural Networks. Intelligent Engineering Systems through Artificial Neural Networks, ASME Press, New York , I, 701-709.
8. Kozma, R., Kitamura, M., Sakuma, M., Yokoyama, Y., 1994. Anomaly Detection by neural network models and statistical time series analysis. Proc. IEEE Int. Conf. Neural Networks, Orlando, FL.
9. Caudell, T.P., Newman, D.S., 1993. An Adaptive Resonance Architecture to Define Normality and Detect Novelties in Time Series and Databases. IEEE World Cong. Neural Networks, Portland, IV, 166-176.
10. Forrest, S., Perelson, A.S., Allen, L., Cherukuri, R., 1994. Self-Nonself Discrimination in a Computer. Proc. IEEE Symp. Research in Security and Privacy, Oakland, CA, 202-212.
11. Percus, J.K., Percus, O., Person, A.S., 1993. Predicting the size of the antibody combining region from consideration of efficient self/non-self discrimination. Proc. Nat. Acad. Sci., 60, 1691-1695.
12. Helman, P., Forrest, S., 1994. An Efficient Algorithm for Generating Random Antibody Strings. Technical Report Technical Report No. CS94-7, Dep't. Comp. Sci., University of New Mexico.
13. Elbestawi, M.A., Ismail, F., Du, R., Ullagaddi, B.C., 1994. Modelling machining dynamics including damping in the tool-workpiece interface. J. Eng. for Ind., 116, 435-439.
14. Palmai, Z., 1987. Cutting Temperature in Intermittent Cutting. Int. J. Mach. Tools & Manu. 27(2), 261-274.
15. Moore, T., Reif, Z., 1992. Detection of Tool Breakage using Vibration Data. Proc. N.A.. Manu. Res. Conf. (13th NAMRC); SME Trans. Manu. Eng. 45-50.
16. Takata, S., Ogawa, M., Bertok, P., Ootsuka, J., Matushima, K., Sata, T., 1985. Real-Time Monitoring System of Tool Breakage using Kalman Filtering. Robotics & Computer-Integrated Manu., 2(1), 33-40.
17. Liang, S.Y., Dornfeld, D.A., 1989. Tool wear detection using time series analysis of acoustic emission. In Journal of Engineering for Industry, 111, 199-205.
18. Tarng, Y.S. Lee, B.Y., 1992. Use of model-based cutting simulation system for tool breakage monitoring in milling. In International Journal of Machine Tools & Manufacturing,32(5), 641-649.
19. Li, G.S., Lau, W.S., Zhang, Y.Z., 1992. In-Process Drill wear and breakage monitoring for a machining centre based on cutting force parameters. Int. J. Mach. Tools & Manu., 32(6), 855-867.
20. Tlusty, J., Ismail, F., 1983. Special aspects of chatter in milling. Trans. ASME; Journal of Vibration, Acoustics, Stress, and Reliability in Design, 105, 24-31.
21. Frank, P.M., 1990. Fault diagnosis in dynamic systems using analytical and knowledge-based redundancy - A survey and some new results. Automatica, 26(3), 459-474.
22. Dornfeld, D.A., 1990. Neural network sensor fusion for tool condition monitoring. Annals CIRP, 24, 101-105.
23. Dasgupta, D., Forrest, S., 1996. Novelty detection in time series data using ideas from immunology. ISCA 5th Int. Conf. Intelligent Systems, Reno, Nevada.
24. Ishida, Y., Mizessyn, F., 1992. Learning Algorithms on an Immune Network Model: Application to Sensor Diagnosis. Proc. Int. Joint Conf. Neural Networks, China, I, 33--38.
25. Ishida, Y., 1993. An Immune Network Model and its Applications to Process Diagnosis. Systems and Computers in Japan, 24(6), 38-45.

Inductive Learning for Optimization of Simulation Model Output

Rainer Barton [*], **Helena Szczerbicka** [**]

[*] German Aerospace Center (DLR), Institute for Flight Mechanics, Lilienthalplatz 7, 38108 Braunschweig, Germany, Email: barton@informatik.uni-bremen.de

[**] Department of Computer Science and Mathematics - FB3, University of Bremen, 28334 Bremen, Germany, Email: helena@informatik.uni-bremen.de

ABSTRACT

In this article we present the optimization approach, 'ML-Opt', which approximates the structure of an unknown goal function by analyzing functional dependency between search points. The functional dependency is determined by an inductive learning algorithm, which generates a classifier used as a control structure in the optimization process. A numerical example and discussions are presented.

INTRODUCTION

Parameter optimization is one of the most important issues in a simulation study. In terms of these methods optimization is a kind of blind-directed stochastic search in a solution space. Direct optimization strategies are normally used to solve an optimization problem $f^+ : R^n \rightarrow R^m$ given by a simulation model with n input parameter. Therefore the m-dimensional model output is transformed by a problem dependent goal function $f^* : R^m \rightarrow R$. In the following paper we will concentrate on the optimization of the function $f : R^n \rightarrow R$ with $f(\vec{x}) = f^*(f^+(\vec{x}))$. Then the optimization task is to find a parameter vector $\vec{x} = (x_1, x_2, \ldots, x_n)$ which yields the global or at least a local extremum of the goal function f.

To optimize simulation models, only direct methods not using gradient information are applicable. These methods can be divided into global and local optimization strategies. Today the most common direct methods for global optimization are Genetic Algorithms [1], Evolution Strategies [1] and Simulated Annealing [2]. For local optimization the most common strategy is hill climbing [3]. Generally, optimization methods work iteratively only requiring goal function values $f(\vec{x}) = y$ to determine a parameter vector of an extremum. However, the user is often interested in alternate solutions close to the extremum, e.g., to reduce costs, increase flexible performance of a single subtask or reconfigure a system.

After studying direct optimization algorithms, we have noticed that common optimization strategies either apply a functional dependency between the recently found search points to locate an extremum (e.g. hill climbing) or they combine information between single search points to explore the search space (e.g. Genetic Algorithms). We thought it might be possible to exploit more information than only that given by the evaluations of the recently found search points. Indeed, we developed a global optimization method ML-Opt (machine learning optimization) which learns the structure of the goal function and applies this information to generate new search points.

In our approach, an inductive learning algorithm generates of a set of search points (population) a classifier which divides the search space into regions. Some of these regions might contain a local extremum. For this reason we use the classifier to decide which regions should be investigated particularly by generating and evaluating new parameter settings of the goal function in these regions. The extended population is the base for a further iteration of ML-Opt, in which the search space is partitioned again. Thus, the strategy ML-Opt yields two important answers of the optimization problem: First, it locates a near optimal solution itself. Second, it determines regions in which alternative near-optimal solutions may be located.

0-7803-5489-3/99/$10.00 ©1999 IEEE.

In section two of this paper, inductive learning and the algorithm *C4.5* are briefly discussed. In the next section the approach ML-Opt is presented. Section four reports some numerical results. The last section comments upon the approach and discusses some further improvements of the algorithm.

INDUCTIVE LEARNING

Machine learning is primarily devoted to represent knowledge or to drawing conclusions out of data. One field in machine learning is inductive learning which is based on generalization of example knowledge. Let us briefly discuss an application of inductive learning for classification. A data set $X = \{\vec{x}^1, \vec{x}^2, \ldots, \vec{x}^k\}$ with $\vec{x}^i = (x_1^i, x_2^i, \ldots, x_n^i)$, a set of examples $E \subseteq X$ and a set of classes $C = \{c^1, c^2, \ldots, c^s\}$ are the basic inputs of an inductive learning algorithm. Additional for every example a relation $\approx$ is known a priori with a class:

$$\forall \vec{e}^i \in E \; \exists c^j \in C : \vec{e}^i \approx c^j \qquad 1.$$

Together with their related classes, the examples are the initial information base for a learning process (see Figure 1). The learning process builds a knowledge base out of the information base by means of generalization. This knowledge base is applied to an interpretation process to classify elements of the data set. Here classification is the process of attaching a particular class to a data set element. The task of inductive learning is the construction of the classification function $\phi : X \rightarrow C$. It has to map all examples correctly regarding the relation $\approx$ and it has to map every element of the data set into a class.

For the purpose of classification there are many different inductive algorithms such as neural network, statistical and symbolic approaches [4]. Requirements on an inductive learning algorithm concern learning time, classification time, quality of generalization, classification accuracy and usability.

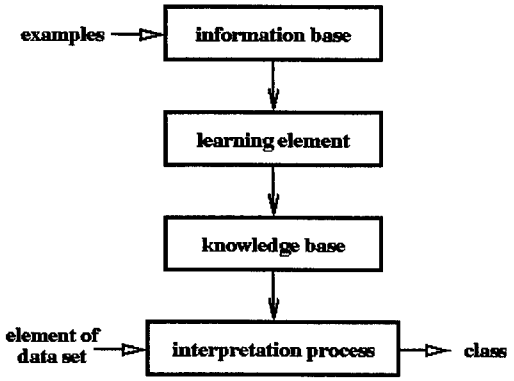


Fig. 1. Inductive Learning.

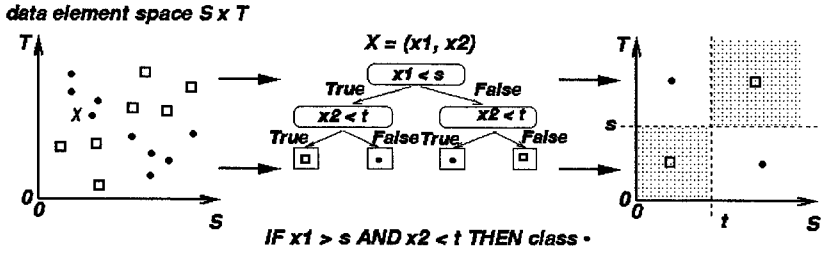


Fig. 2. *C4.5* Classification Example.

In our approach we use *C4.5* [4], [5] one of the most widely used inductive learning algorithms due to its good performance and transparent description of the relations between attribute values and the classes. The

algorithm partitions examples by the gain and gain ratio criterion. *C4.5* generates a classification function in form of a decision tree, e.g., the left side of Figure 2 represents a set of two-dimensional examples belonging either to the class • or to the class □. *C4.5* partitions the data space in regions related to two classes. The middle of the Figure displays its classifier and an extracted rule to classify a new element in the data space. The right side shows the partitioning of the data space generated by the classifier.

OPTIMIZATION WITH ML-Opt

The central idea of ML-Opt is to apply a machine learning algorithm as a control element in the optimization process. For a detailed description of the algorithm we present its control structure in pseudo code in Figure 3. In the following subsection the different tasks and their internal parameters are described.

Initialization Task

At the beginning a initial population is generated. Its size depends on the dimension of the input vector $\vec{x}$ and the modeling of the goal function f if earlier information about the goal function is available. The classification criterion τ reflects the relevancy of search points in an iteration of ML-Opt. It separates the population elements $(\vec{x}, f(\vec{x}))$ in at least two classes according to a classification criterion. For a maximization process we apply the following classification criterion:

$$\forall(\vec{x}, f(\vec{x})) \in points : \tau(\vec{x}, f(\vec{x})) = \begin{cases} \square & \text{if } f(\vec{x}) < limit \\ \bullet & \text{else} \end{cases} \qquad 2.$$

The class □ reflects relative low values of the goal function and the class • reflects relative high values of the goal function. The threshhold value *limit* is defined as the *k*-highest value of the goal function in the population. Alternatively, the median or arithmetic average could be applied.

```
PROCEDURE ML-Opt ( FUNCTION f  )
VAR
      points, newPoints : BAG OF POINT;
      τ : RELATION OF POINT;
      rules : SET OF RULES;
      regions : SET OF REGIONS;
BEGIN
      points := initializePopulation( f  );
      REPEAT
τ  := defineClassCriterium( points );
      rules := machineLearning( points, τ  );
      regions := regionGeneration( rules );
      newPoints := exploreRegion( regions );
      points := points ∪ newPoints;
      UNTIL ( terminationCondition( points, regions ) )
      RETURN( findExtremum( points ) );
END;
```

Fig. 3. ML-Opt in Pseudo Code

Learning Task

In every optimization step a new classification function is generated by an inductive learning process in order to find a new partitioning of the search space. Therefore examples of the inductive learning process are created by the points of the actual population and the classification criterion τ. Thereby the example set E is defined as:

$$E = \{(\vec{x}, \tau(\vec{x}, f(\vec{x}))) \mid (\vec{x}, f(\vec{x})) \in points\} \qquad 3.$$

In the approach, we use *C4.5* as inductive learning algorithm to classify the whole example set E. Its parameters are set in that way that *C4.5* does not prune the calculated decision tree and a leaf of the

decision tree can cover at least one example. A set of rules is generated in the learning process. It is derived from the resulting decision tree.

Each rule covers a particular region in the search space of the goal function. Due to the classification criterion only regions covering elements of the class • are interesting for a maximization process (called 'high regions'). In every high region new search points are generated. In the next iteration of the optimization process the additional points support a more accurate partition of the search space. For the generation of new search points many different algorithms, e.g. Latin Hypercube sampling or equidistant distance sampling, can be used. We prefer Monte Carlo sampling.

Region Generation

Any high region corresponding to the 'high' values of f may cover a local extremum. However, the probability that an extremum is located outside a high region is not zero. That is why by generating search points only inside a high region, the position of an extremum lying outside would never be discovered. In order to avoid this case we extend high regions in the direction of the growing (descending) value of the goal function (see Fig. 4). Therefore the point with the highest evaluated value of the goal function in a region is called the critical point of a region. If the critical point is in a ε -neighborhood of a high region boundary then the region is extended in order to contain a $d \cdot \varepsilon$ -neighborhood of the critical point ($d \in N$).

Termination Condition

The termination condition is built out of two stop criteria dealing with the average value (called 'fitness') of the $N_{Fitness}$ -best values of the goal function in the actual population. ML -Opt checks whether the fitness belongs to the δ -neighborhood of the extremum found in the actual iteration step. The second termination requirement regarding whether ML-Opt can improve the δ -neighborhood within h iterations.

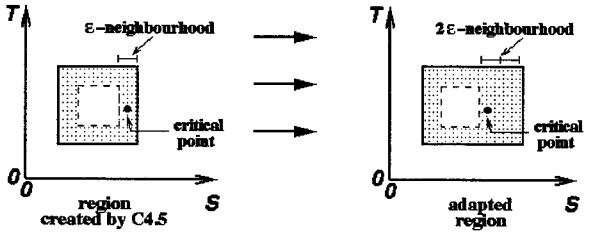


Fig. 4. Extension of a Region $d=2$.

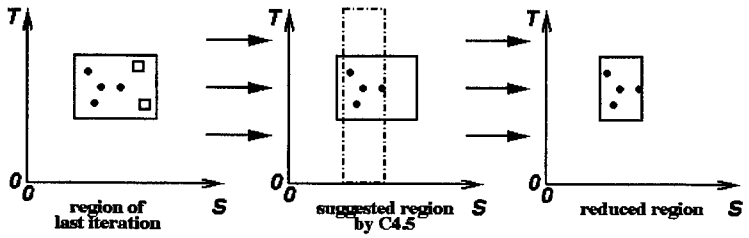


Fig. 5. Reduction of a Region.

Region Reduction

Classification with *C4.5* may result in regions which cover additional parts of search space dealing with to regions of the last iteration (see Figure 5). On the one hand, these parts could be an extension of regions in direction of a possible extremum. On the other hand, these parts were not classified in the previous iterations. Carefully analyzing the behavior of *C4.5* we notice the additional search space results from a classification problem. That is why we reduce every region by calculating its intersection with the convex hull of all high regions of the last iteration. After this, the region is extended in the direction of an extremum if necessary.

Example of Execution

The dynamic behavior of ML-Opt is visualized in Figure 6. The start population of ML-Opt has ten search points and in the next iteration in every high region two additional new search points are evaluated. For definition of the two classes • and □ see equation 2. Its value *limit* is set to the fourth-best value of the goal function dependent on the search points in the actual population. In the first iteration ML-Opt investigates three regions and terminates in one region in its last iteration. Notice that in every iteration classification of examples by the classifier changes due to increasing knowledge about behavior of the goal function.

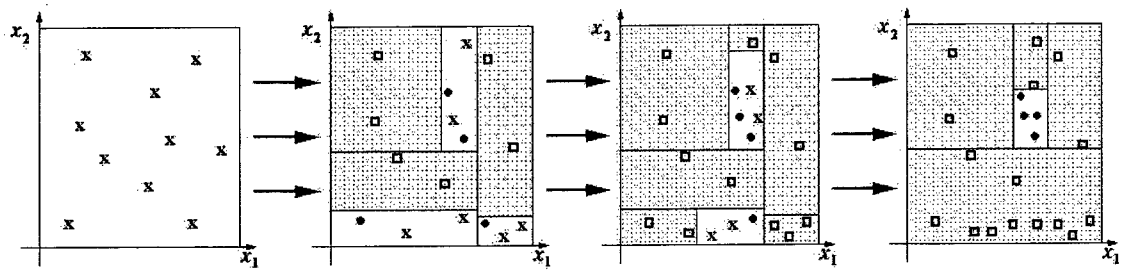


Fig. 6. Dynamic Behavior of ML-Opt

NUMERICAL EXAMPLE

The developed optimization approach has been already applied to several simulation models as well as to a diversity set of mathematical test functions. Let us consider the following numerical test function (see Table 1) which defines a multimodal function used for maximization (see Figure 7 for a two-dimensional case). For all dimensions it comprises exactly one global maximum point $\vec{x}$ =(7.98,7.98,...,7.98). The number of local maximum points raises exponentially with an increase of the dimension n. We performed experiments for n=1 to n=10.

With this test function we compare several results of ML-Opt (average accuracy of the located optimum, average evaluation number and average number of iterations) with other strategies. One thousend independent runs have been performed for every experiment entry. For the experiments different control parameter settings are used. Table 2 lists values of ML-Opt parameters: the size of the start population N_{MC} generated with Monte Carlo sampling, the influence of the trashhold variable *limit* defined by the value of the goal function of the *four*-best element, the number of exploring evaluations in a single rule $N_{Explore}$ and the number of the fitness elements $N_{Fitness}$ are given. The δ -neighborhood is set to be 0.05% of the located extremum in the actual iteration.

Table 1. Mathematical Test Function

Search space	$\{\vec{x} \in R^n \mid 0 \le x_i \le 3 \cdot \pi \wedge i \in N_1^n\}$
Goal function	$f(\vec{x}) = \left\lvert \prod_{i=1}^{n} x_i \cdot \sin(x_i) \right\rvert$

Table 2. Settings of ML-Opt

Exp.	N	N_{MC}	$N_{Explore}$	$N_{Fitness}$
1	1,2,...,10	$10+N \cdot 10$	4	4
2	6	20	4,6,...,12	4,6, ...,12

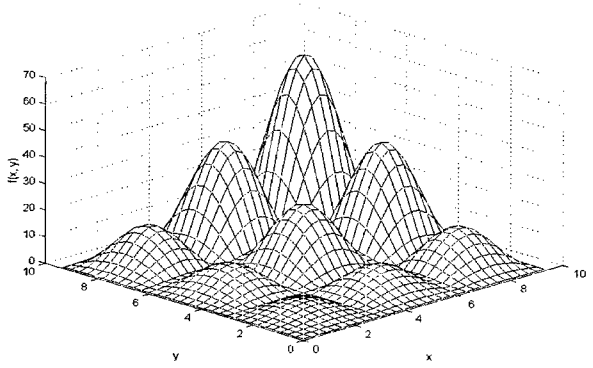


Fig. 7. Graphical Representation.

Since we are dealing with a heuristic algorithm we validate its behavior by comparing with Genetic Algorithms. For Genetic Algorithms we used the software tool REMO [6] with standard control parameter settings recommended in the literature. In the following the most important control parameter values are presented: The cross-over rate is set to 0.75% and the mutation rate is set to 0.075%. The length of a parameter segment in the fixed-length binary strings representing parameter vectors is set to 10 bit. For the experiment the size of the initialization population is set to 40 elements and the termination condition is defined whether the Genetic Algorithm cannot improve the goal function by 0.05% within 20 generations. The population size is set to 10 elements.

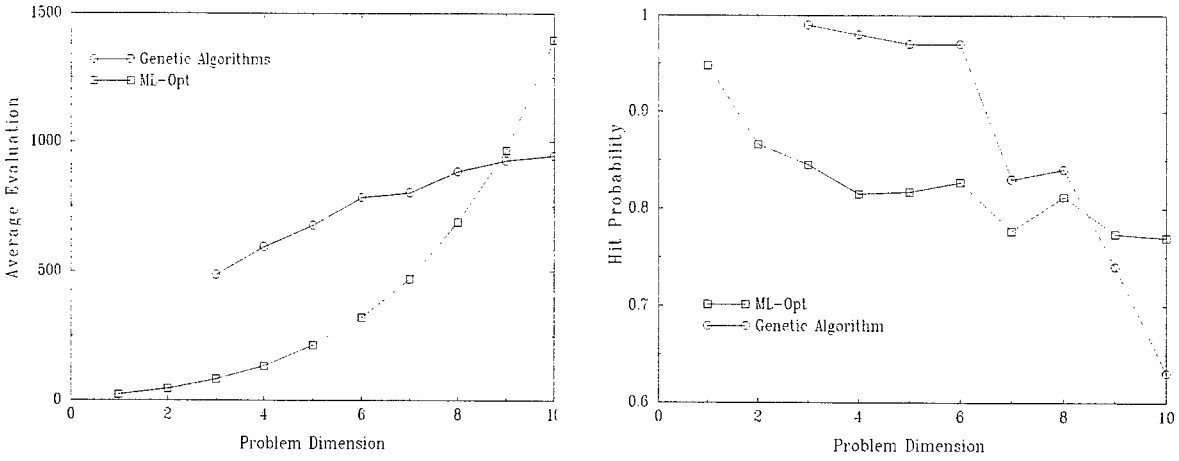


Fig. 8. Comparing ML-Opt with Genetic Algorithms.

The strategies correctly located the global extremum with an accuracy corresponding to $\frac{\Pi}{2}$-neighborhood.

In the first experiment (see Fig. 8) the probability of locating the global extremum (called 'hit probability') decreases in both optimization algorithms for increasing problem dimension. The lower hit probability of ML-Opt results out of the small number of investigations in a region and considering maximal four high regions for further analysis. By changing the parameters of ML-Opt we are able to improve its hit probability (see experiment two). From $N=2$ to $N=6$ the average evaluation number of ML-Opt increases constantly by a dimension dependent offset: $eval_N - eval_{N-1} \cong 20 * N$. The non smooth trajectories can be explained by the small experiment size of one thousand independent experiment runs.

In Figure 9 some results of the second experiment are presented for $N=6$. The hit probability and the average evaluations in a single experiment increase if either $N_{Explore}$ or $N_{Fitness}$ increase. An interpretation for the influence of $N_{Explore}$ is a more detailed exploration of regions. The second parameter

influences the termination condition leading to a more detailed search in the latest regions. So, both results in a higher probability of detecting parameter settings near to the global extremum by a higher sampling size in interesting regions.

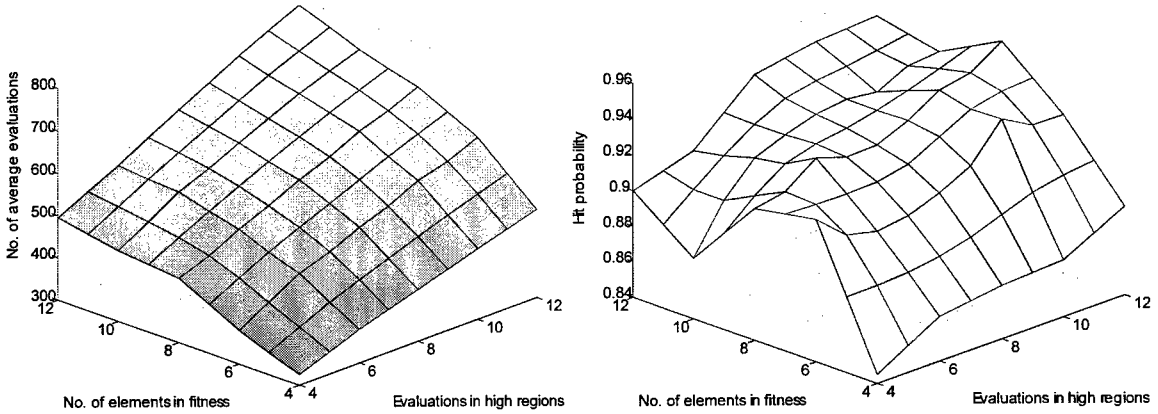


Fig. 9. Variation of Internal Parameter.

Due to the limited space of this article, we can only briefly refer here to other methods to improve the hit probability. By changing the influence of the threshold variable *limit* to the value of the *k*-highest element in a population (k>4) more high regions can be defined by the learning algorithm. This results in a more detailed analysis of the search space.

CONCLUSIONS

Our approach directly integrates methods of machine learning in the optimization process. In this paper the basic structure of the optimization algorithm ML-Opt was presented. It applies the inductive learning algorithm *C4.5* as a control in an optimization process. The optimization differs regarding existing direct methods in building and using a metamodel of the goal function generated by a classifier and learning out of history information. We are aware that regarding to the free lunch theorem it is not possible to make any general statement about the quality of behavior of search algorithms.

The topics for our future work will concern integration of other inductive learning algorithms in ML-Opt, improving the Monte Carlo search in high regions via Latin hypercube search (or other methods out of experimental design) and the definition of the classification criterion which learns the slope of the goal function as well. By using more than two classes a more carefull analysis of the search space might be possible. Other topics concern methods for generation of additional new search points in the whole search space, parallelism of single tasks, analyzing termination conditions, which depend on the volume of the regions, and criteria for the applicability of ML-Opt prior to direct optimization algorithms.

REFERENCES

1. Z. Michakewicz, 1996. Genetic algorithms + data structures = evolution programs. Springer-Verlag Berlin Heidelberg
2. E. Aarts and J. Korst, 1990. Simulated annealing and boltzmann machines. Wiley
3. R. Hooke and T. A. Jeeves, 1961. Direct search solution of numerical and statistical problems. Communications of the ACM, 8, 212-221
4. T. M. Mitchell, 1997. Machine Learning. McGraw Hill
5. J. R. Quilan, 1993. C4.5: Programs for machine learning. Morgan Kaufmann Publishers, Inc.
6. M. Syrjakow and H. Szczerbicka, 1994. Optimization of simulation models with REMO. Proceedings of the European Simulation Multiconference ESM'94, Barcelona, Spain, June 1-3, 274-281

A Genetically-Optimised Fuzzy Parser of Natural Language

Olgierd Unold

Institute of Engineering Cybernetics, Wroclaw University of Technology
Wyb. Wyspianskiego 27, 50-370 Wroclaw, Poland
Email: unold@ci.pwr.wroc.pl Web sitez; http://www.ict.pwr.wroc.pl/~unold

ABSTRACT

This paper presents a genetic approach to inductive learning of natural language parser. The parser is based on a fuzzy automaton and works in the stratificational knowledge representation system.

INTRODUCTION

The goal of our research is to design a computer system with the same capability of language and knowledge acquistion as human being. To this end, we have to first equip the natural language processing system with the "smart" parser, which can be taught while working. . We have proposed a self-learning parser of a dialog system, which can in fact learn the grammatical rules from the gained sentences.

When developing the architecture of adaptable analyzer, we should use a powerful global optimization method for the problem with a large search space, which contains possible difficulties like noise. Due to their population-based approach, genetic methods are ideally suited for implementation in searching the architecture of self-learning analyzer. The problem of inducing parsers from actual sentences of the language, also known as grammatical inference, is a very hard machine learning problem. Many researchers have attacked this problem [1, 4, 6, 8]. To author's knowledge, the problem of infering fuzzy automaton-driven analyzer has not yet been considered.

This paper describes a genetic approach to infer the architecture of natural language parser based on a kind of fuzzy automaton, which works in the stratificational knowledge representation system (SKRS).

STRATIFICATIONAL KNOWLEDGE REPRESENTATION SYSTEM

In [10-12] we have proposed a fuzzy analyzer of natural language texts (so-called fPDMAS - fuzzy nondeterministic pushdown automaton with associative memory access) which works in the stratificational knowledge representation system [9].

Stratificational knowledge representation system is an attempt at formalizing the multilayer structure of natural language. The SKRS is based on a multistratum semantic network whose nodes contain particular linguistic units (single words, the so-called structural-semantic components, sentences). The node-to-node links correspond to relations between particular linguistic units.

If a natural language text representing the acquired knowledge is to be mapped onto the stratificational semantic network, the particular linguistic units must be isolated in the analysed text, such as word groups and sentences. If we decide to limit our input texts to isolated clauses, we can limit the sentence decomposition task to two subtasks: one of word group decomposition into the particular words and one of sentence decomposition into word groups. In order to increase both knowledge integrity in the knowledge base and the efficiency of the search algorithm, an assumption has been made that it is not phrases, but the structural-semantic components (the components) that are the objective of the sentence decomposition, the components being word groups constituting semantic units which can no longer be decomposed, each of which has its own syntax characteristics. Sentence decomposition into structural-semantic components in the SKRS is performed by a fuzzy automaton-driven analyzer fPDAMS. An automaton decomposition model in the SKRS can be used due to the reduction of the process of sentence decomposition into

0-7803-5489-3/99/$10.00 ©1999 IEEE.

structural-semantic components to the process isolating appropriate substrings of symbols in the string of symbols representing lexical categories.

FUZZY AUTOMATON-DRIVEN PARSER

The construction of the proposed analyzer is based on a fuzzy automaton [3]. The recent application of finite-state approach in NLP show the usefulness of automata in this area of AI [7]. The basic advantage of applying a fuzzy automaton to process natural language lies in the existence of an established algorithm for the next state selection based on values of the characteristic functions, allowing the characteristic functions value to change with time. In that case fuzzy automaton-driven parser "gets accustomed" to the input syntax constructions, imitating human behavior.

Figure 1 shows a graph of a subautomaton $fA(l_1)$ that isolates from the string of the lexical categories of the words a substring having a syntactical category of the nominal group. There is another subautomaton, $fA(l_3)$, incorporated into the $fA(l_1)$ subautomaton structure, which accepts a substring having a syntactical category of the adjectival group. The subautomaton $fA(l_3)$ is represented by the subgraph $fG(l_3)$ in the transition graph. The label $w_p i_s$ means that a transition along the edge is possible when w_p (standing for the lexical categorie of the word from the analysed sentence) is the input symbol that is being read. During the transition the instruction i_s is performed. The label $w_p i_s q_t l_u$ means that during the transition, the instruction i_s is performed with the parameters q_t l_u. The symbol r_k denotes a specific set of type w symbols; an edge marked with a label that contains the r_k symbol represents a bundle of edges each of which is marked with one of the symbols belonging the r_k set.

The transition from the state q_i to q_j at the input signal w_p has some degree of membership (usually denoted as $\mu_{ij} \in [0,1]$). There is the following role for the characteristic function μ_{ij} which describes the transition relation of the fPDAMS automaton: for a given state q_i and input w_p of the automaton, the next state q_j of the automaton is determined so that to maximize the characteristic function value corresponding to the transition. By the way, note that the fuzzy automaton is similar to the stochastic automaton. Both fuzzy and stochastic automata are examples of the acceptors of weighted languages. However, in stochastic automata the transitions are applied according to a probability distribution, there exists no uncertainty about the generated string. In fuzzy automata all applicable transitions are executed to some degree and transtions weights, in contrary to stochastic automaton, do not need to sum to 1, if there exist several alternative transitions at any state.

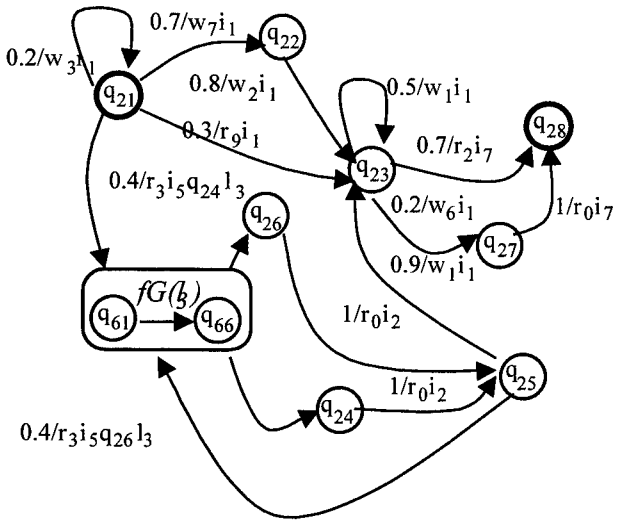


Fig. 1. The transition subgraph $fG(l_1)$ of the fuzzy subautomaton $fA(l_1)$

The transition subgraph $fG(l_1)$ of the fuzzy subautomaton $fA(l_1)$ is described by a symbolic expression $fG^{-}(l_1)$ as follows:

$$fG^{-}(l_1) = (q_{21}(0.2/w_3i_1q_{21},\ 0.7/w_7i_1q_{22}(0.8/w_2i_1q_{23}(0.5/w_1i_1q_{23},\ 0.2/w_6i_1q_{27}(1/r0i_7q_{28}),\ 0.7/r_2i_7q_{28})),$$
$$0.3/r_9i_1q_{23},\ 0.4/r_3i_5q_{24}l_3q_{61}),\ q_{24}(1/r_0i_2q_{25}(0.9/w_1i_1q_{23},\ 0.4/r_3i_5q_{61}l_3q_{61})),\ q_{26}(1/r_0i_2q_{25})) \quad 1.$$

The graph transition represents an analysis of a fragment of the input string of the lexical categories, the analysis result being stored on one of the six stacks of the fPDAMS automaton. The automaton operation is determined by a finite number of instructions. These instructions constitute the transition rules to allow the automaton to transit from one configuration to another. Limited number of instructions, straight rules of activity permit to use fPDAMS as a kind of linguistic tool. The formal definition of the fPDMAS was presented in [12].

A GENETICALLY OPTIMISED fPDMAS

Genetic algorithms (GA) operates on a space of chromosomes, which are the representatives of the corresponding elements in the search space. The algorithm of evolutionary scheme is simply and can be presented by the selfexplanatory pseudocode as follows (P(t) stands for a family of elements forming the GA search space in evolution t) [5]:

```
begin
        iteration: =0
        initiate population P(0)
        evaluate population P(0)
        while (not termination criterion) do
        begin
                selection P(iteration) from P(iteration-1)
                alter P(iteration)
                evaluate P(iteration)
        end
end
```

In one of the first approaches to an evolutionary scheme, that is evolutionary programming [2], finite state machines was used. Evolutionary programming can operate on fPDMAS's as follows:

1) Initially a population of parent fPDMAS's is randomly or by hand constructed. The fPDMAS is represented by its transition graph (coded by the symbolic expression).

2) The parents are tested in the environment, that is for each parent fPDMAS the collection of positive and negative examples of sentences is offered. The fitness of the automaton can be measured on the basis of the fraction of correctly analyzed sentences.

3) Offsprings fPDAMS's are created by mutating each parent automaton. Mutation can change both the topology and the connection weights. The topology-modifying operators can change the topology of the fPDMAS by: adding new state to the transition graph or removing the existing state. The operators changing the connection weigths operate on the terms $w_p i_s q_t l_u$ modifing the individual elements.

4) The offsprings are evaluated over the existing environment in the same manner as their parents.

5) Those fPDMAS's that provide the best fitness are retained to become parents of the next generation.

6) Steps 3)-5) are repeated until the end condition is reached.

When modeling evolutionary processes using evolutionary programming, it is necessary to use a fitness function to evaluate the performance or fitness of an inidividual chromosome (i.e. the fPDMAS). Those chromosomes that are most fit are most likely to survive, with less fit chromosomes dying off, being replaced by the fitter chromosomes. Several possible functions may be used in determining the fitness and efficacy of the fPDMAS.

Following [6] the evaluation function can in fact count only the number of sentences incorrectly classified and the number of words incorrectly accepted by the analyzer. According to [4] the fitness of the fPDAMS can be measured on the basis of the fraction of correctly analyzed sentences or can be extended to credit also correctly analyzed substrings of each positive training sentence.

CONCLUSIONS

We have proposed the concept of using the genetic approach to inference of natural language analyzer fPDAMS. The theoretical bases for the use of evolutionary programming that supports automated designed of the architecture of the fPDAMS were provided. Fuzzification of the parser and its evolutionary developing are the first steps toward the self-learning, "smart" analyzer of the natural language texts. The presented adaptable sentence analyzer, which can be taught while working, can be part of various NLP systems.

REFERENCES

1. Brave S., 1996. Evolving Deterministic Finite Automata using Cellular Encoding, [in:] Koza J.R., Goldberg D.E. Fogel D.B., Riolo R.L. (eds.) Proc. of the First Annual Conference Genetic Programming 1996, Stanford University, CA, USA, MIT Press., 28-31.
2. Fogel L.J., Owens A.J., Walsh M.J., 1996. Artificial Intelligence through Simulated Evolution, J.Wiley, Chichester.
3. Kandel A., Lee S.C., 1979. Fuzzy Switching and Automata: Theory and Applications, Crane Russak, New York.
4. Lankhorst M.M., 1994. Grammatical Inference with a Genetic Algorithm, [in:] Dekke L., Smit W., Zuidervaart J.C. (eds.) Proc. 1994 EUROSIM Conf. on Massively Parallel Procesing Applications and Development, Elsevier, Amsterdam, 423-430.
5. Michalewicz Z., 1992. Genetic Algorithms+Data Structures=Evolution Programs, Springer Verlag, Berlin.
6. Poli R., 1996. Evolution of Recursive Transition Networks for Natural Language Recognition with Parallel Distributed Genetic Programming, Technical Report CSRP-96-19, School of Computer Science, The University of Birmingham.
7. Roche E., Schabes Y., 1997. Finite-State Language Processing, A Bradford Book, The MIT Press, Cambridge, Massachusetts.
8. Schwehm M., A Massively Parallel Genetic Algorithm on the MasPar MP-1, [in:] Albrecht R.F., Reeves C.R., Steele N.C. (eds.) Proc. Int. Conf. Artificial Neural Nets and Genetic Algorithms, Wien, Springer, 502-507.
9. Unold O., 1996. A Stratificational Knowledge Representation System, [in:] Vetulani Z., Abramowicz W. (ed.) Language and Technology, Academic Printing House PLJ, Warszwa, 177-181 (in Polish).
10. Unold O., 1997. Automatic Analysis of Natural Language Texts in Man-Machine Communication [in:] Wojtkowski G. at al (ed.), Systems Development Methods for the Next Century, Plenum Publishing Corp., New York, 185-193.
11. Unold O., 1998. A Fuzzy Automaton Approach to Dialog Systems, Proc. of the IASTED International Conference-ASC'98, Cancun, Mexico, May, 215-218.
12. Unold O., 1998. Application of Fuzzy Sets in Natural Language Processing, Proc. of the 6th Congress on Intelligent Techniques and Soft Computing EUFIT'98, Aachen, Germany, September, 1262-1266.

A Genetic Algorithm Based Approach to Solve Process Plan Selection Problems

M.K.Tiwari*, S.K.Tiwari*, D. Roy*, N.K.Vidyarthi and S.Kameshwaran*****

* Department of Manufacturing Engineering,
National Institute of Foundry and Forge Technology,
Hatia, Ranchi-834 003,India.
** Department of Mechanical Engineering
NERIST, Nirjuli, Itanagar-791 109,India.
***SriVenkateshNagar, Chennai-600092, India.

ABSTRACT

Selection of a process plan is a crucial decision making problem in manufacturing systems due to the presence of alternative plans arising from the availability of several machines, tools, fixtures etc. Because of its impact on the performance of a manufacturing system, several researchers have addressed the plan selection problem in recent years. Selecting an optimal set of plans for a given set of parts becomes a NP complete problem under multiobjective and fairly restrictive conditions. In this paper, a Genetic Algorithm (GA) is used to obtain a set of feasible plans, for given part types and production volume, to minimize the processing time, setup time and materials-handling time constrained by not overloading the machines. Obtaining near optimal solutions by using different weights for different objectives in GA, is also studied.

INTRODUCTION

Process planning is the systematic organization of detailed methods by which parts are manufactured from raw material to finished product. With the possibility of alternate machines, setups, and processes to manufacture a particular part, plan selection in a manufacturing environment has become a crucial problem. Moreover, modern manufacturing systems may require a part to be produced simultaneously with any combination of part types and volume, and to be re-routed adaptively to alternative machines in case of breakdown or overloading of the pre-assigned machine. Because of it has a vital impact on manufacturing system performance, several researchers have examined the plan selection problem in recent years. Kusiak and Finke [1] developed a model to select a set of process plans with minimum cost of removing material and minimum number of machine tools and other devices. Bhaskaran [2] provided a model to account for factors such as, flow rate, processing time and processing steps. Zhang and Huang [3] extended the Bhaskaran [2] model using a fuzzy approach due to imprecise, conflicting objectives in plan selection. Seo and Egbelu [4] used Tabu search to select a plan based on product mix and production volume. Tiwari and Vidyarthi [5] addressed plan selection by accounting for similarity measures among the plans of the parts.

In this paper, we use Genetic Algorithm (GA) to obtain a set of process plans for a given set of parts and production volume. GAs are search and optimization algorithms based on the mechanics of natural genetics and natural selection. It has been recognised as a powerful method to obtain near optimal solutions for combinatorial optimization problem. (Davis [6], Goldberg [7], Deb [8]). We have used GA to obtain a set of process plans for a given variety of parts and production volume with the objective of minimizing the total processing time, setup time and material handling time constrained by not overloading the machines.

PROBLEM DESCRIPTION

The analytical model for the process plan selection in our approach, consider the following parameters – processing time, setup time and material handling time. The objective is to minimize the above parameters. But these objectives may overload a few workstations shared by most process plan and cause a system bottleneck. Hence a constraint function which caters the needs of not overloading any workstations is used to obtain a practically feasible optimal solution. The notations used in this problem are:

0-7803-5489-3/99/$10.00 ©1999 IEEE.

a	1, 2, ... N parts
b_a	batch size of part a
P_{aj}	set of process plans for part type a, $P = \{P_{a1}, P_{a2}, .. P_{an}\}$ where P_{aj} is the jth process plan for part a, $n = \| P_a \|$
K	1, 2,.. K work stations
t_{ajk}	processing time on work station k for the process plan P_{aj}
mt_{aj}	material handling time for part a associated with process plan jth process plan of part a
s_{ai}	total setup time for P_{aj} for a batch size of b_a
ws_k	maximum allowable time on workstation k
o	objectives of minimizing processing time (1), setup time (2) and material handling time (3).
w_o	Weight of objective o. $\sum w_o = 1$
x_{ai}	1-if P_{aj} is selected for part a, 0-otherwise

The weighted cost of a process plan for P_{aj} is defined as

$$T_{aj} = w_1 \sum_k t_{ajk} b_a + w_2 s_{aj} + w_3 mt_{aj} b_a$$

The objective is to minimize the total weighted process plan cost (T) for a set of process plans, given by,

$$T = \sum_a T_{aj} x_{aj} \quad 1.$$

subject to the constraints

$$[\sum_a t_{ajk} b_a x_{aj}] <= ws_k, \ \forall k = 1, 2, .. K \quad 2.$$

and

$$\sum_j x_{aj} = 1 \ \forall a = 1, 2,.. N \quad 3.$$

Constraint (2) prevents the occurrence of an overloaded machines and constraint (3) ensures that only one process plan per part is selected.

GA BASED SOLUTION METHODOLOGY

For a given set of N parts with na process plans for part a, the number of feasible solutions is given by $\prod^N$na. Thus for 6 parts with 5 process plans each, 15625 solutions need to be exhaustively searched to find the optimal solution and the search space increases combinatorially for further increase in the number of parts. Genetic algorithms are found to be potential search and optimization algorithms (Deb, [8]) for complex engineering optimization problems. They mimic the principles of natural selection (reproduction) and natural genetics (crossover and mutation) to constitute search and optimization procedures. Sets of initial feasible solutions are selected randomly and fitness values proportionate to their objective function are evaluated. The solutions with higher fitness values are selected with higher probability for next generation to perform crossover and mutation, thus conserving the Darwin's theory of fittest of survival. Since, GAs start with a set of initial points in the search space, the near optimal solutions are obtained in the increasing generations. The objective function to be minimized in our algorithm is:

$$OB = \sum_i T_{aj} x_{aj} + (mc * M)$$

where mc = number of workstations that are overloaded and M is a high scalar value that penalizes the OB by increasing it to higher values.

The fitness function evaluated for a solution in GA is given by:

$$F = S/(1+OB)$$

where S is a suitable scalar such that $0<F\leq100$.

EXPERIMENT AND RESULTS

For solving the process plan selection problem by our proposed GA approach, we considered the problem given in Table 1. A part mix of 8 different parts was considered each with different batch sizes and a set of process plans. The shop floor has 4 workstations and each was allowed a maximum machining time of 1000 units. The objective is to select an optimal set of process plans with the minimum objective function OB, from the solution space of 139,968,000. Weights, w_o ={0.6,0.2,0.2}, were used for the objectives. GA was then applied to the problem with a population size of 10 for 30 generations. Single point crossover was used and mutation was performed over each crossovered string with the given mutation probability. The convergence of the GA to the optimum solution for different sets of GA operators is shown in Figure 1. GA1 with crossover (0.6) and mutation probability (0.1) converges faster to the optimal than GA2 with crossover (0.1) and mutation probability (0.8). The set of process plans selected by GA1 and GA2 are {3,3,2,4,2,3,2,3} and {2,3,2,4,2,2,4,3} respectively. The convergence of GA1 to the optimal is due to the fact that higher crossover rates result in better solutions. When all objectives were given equal weights, w_k={0.33,0.33,0.33}, the optimal set of process plans selected was {2,3,2,4,2,3,4,3}.

Table 1. Data for the process plan selection problem.

Part No	Batch Size	Process Plan	WS1	WS2	WS3	WS4	Setup Time	Material Handling Time
1	15	1	0	24	18	0	60	5
		2	10	10	8	9	90	15
		3	15	0	10	14	75	9
2	12	1	8	10	9	10	100	16
		2	0	12	10	17	70	12
		3	15	0	5	10	80	10
3	18	1	13	16	0	16	85	18
		2	0	15	11	12	65	14
4	8	1	10	10	10	10	100	16
		2	12	12	10	0	88	10
		3	0	12	12	10	75	12
		4	12	0	8	10	65	14
5	15	1	14	12	8	0	89	15
		2	15	0	16	0	80	10
		3	13	0	9	10	90	11
6	6	1	7	0	3	13	75	11
		2	9	5	0	7	70	13
		3	0	8	4	4	65	12
7	12	1	3	8	12	0	55	12
		2	4	6	0	7	64	14
		3	8	11	0	0	50	12
		4	0	4	7	6	55	11
8	5	1	0	4	8	12	65	11
		2	0	9	11	0	60	9
		3	6	4	3	0	68	13

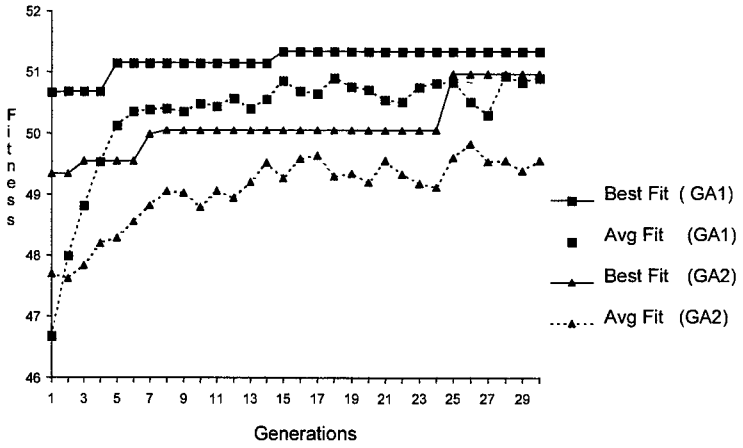


Fig. 1. Performance of the proposed GA Algorithm.
(GA1 - *Cr. Prob = 0.6, Mutt. Prob = 0.1* , GA2 - *Cr.Prob = 0.1, Mut. Prob = 0.8*)

CONCLUSION

Process Plan selection is a crucial problem in an automated manufacturing environment. Further, selecting a set of optimal process plans for a variety of parts with different production volume is a combinatorial

optimization problem, which makes the exhaustive search technique a practically infeasible solution. Various researchers have attempted the problem using heuristics and other optimization techniques like Tabu Search and Simulated Annealing. In our approach, we used GA to find a optimal set of process plans that minimizes the total processing time, setup time and material handling time, meanwhile avoiding system bottleneck by not overloading the workstations .GA, which starts with different initial points in the search space, ultimately finds a near optimal solution for the complex combinatorial problem of process plan selection .By varying the weights of the different objective function, different set of optimal solutions were obtained which eases the post design issues following process plan selection in the automated manufacturing systems.

REFERENCES

1. A. Kusiak, G.Finke, 1998. Selection of Process Plans in Automated Manufacturing Systems, IEEE J. of Robotics and Automation. 4 (4), 397-402.
2. K. Bhaskaran, 1990. Process Plan Selection. Inter. J. of Production Research. 28 (8), 1527-1547.
3. H.C. Zhang, S.H. Huang, 1994. A Fuzzy Approach to Process Plan Selection. Inter. J. of Production Research. 32 (6), 1265-1279.
4. Y. Seo, P.J. Egbelu, 1996. Process Plan Selection Based on Product mix and Production Volume. Inter. J. of Production Research. 34 (9), 2369-2655.
5. M. K. Tiwari, and N. K. Vidyarthi, 1998. An Integrated Approach to Solving the Process Plan Selection problem in an Automated Manufacturing System. Inter. J. of Production Research. 36 (8), 2167-2184.
6. L. Davis, 1991. Handbook of Genetic Algorithm, Van Nostrand, Reinhold.
7. D. E. Goldberg, 1989. Genetic Algorithm in Search. Optimization and Machine Learning, Addision Welsey, Reading, MA.
8. K. Dev, 1996. Optimization for Engineering Design. Algorithms and Examples, Prentice Hall, New Delhi, India.

Breeding Policies in Evolutionary Approximation of Optimal Subspace

H.M. Huang and P.L. Leung

City University of Hong Kong, Kowloon, Hong Kong, P.R.China

ABSTRACT

In very high dimension variable space(e.g. 30 or more), huge computations evenly hinder investigators to conduct any direct meaningful analysis. A traditional trick is firstly to conduct single variable analysis, then combinie several top most single-fittest variables to approximate the optimal subspace. In this investigation, an evolutionary method[1,2] for optimal subspace approximation is proposed. The breeding policies of this evolutionary approximation, its scalability and generalization have been intensively investigated. The studied object is a 30-D variable space which contains 6000 artificial individuals. In this data, except for 3 variables containing two donut-type data distributions, each with 3000 individuals, the remaining 27 variables only contain quasi-random data with the same value range as the donut data distributions. The donut distribution consist of two toroidal distributions(classes) which are interlocked like links in a chain. The cross-section of each distribution is a Gaussian function distributed with standard deviation delta. Even the Donut problem which possesses a variety of pathological traits can invalidate many non-complex analyses for classification. The goal of this investigation was to find the 3 donut variables within the optimal subspace of 30-D variable space in which most quasi-random variables emerge as noise variables. In order to reach this goal, various breeding policies were implemented and compared. Although no perfect solution for the approximation was found, various breeding policies and their impact on decreasing the error were studied. These were found to be relatively usable for reference and might be improved when used in a practical application.

INTRODUCTION

In high-dimension space, statistical analysis of the distribution characteristics of variables is a widely applied and popular technique. For statistical pattern classification[3], different patterns are usually discriminated by their respective statistical characteristic, such as mean difference, variance, etc.. Before any practical data is fed to a pattern recognition system, plentiful relative data must be collected and comprehensive analyses must be performed on the data. Among all the techniques to design an appropriate pattern classifier, feature selection and extraction [4] are at the core.

Feature extraction is a technique to project samples in high-dimension space to lower dimensions, especially a plane. In a plane or a 3D space, sample distribution configurations can be visually depicted. So, feature extraction techniques are the quintessence for high-dimension space data visualisation. When exerting feature extraction, the final low-dimension variables usually carry all the information of each original variable in high-dimension space. But for feature selection, only part of the original variables are kept, unrelated variables are just neglected. The approximation of optimal subspace include the meaning of both feature extraction and selection.

Genetic algorithm is an advanced technique which are applied in optimal problems, abstract and real object recognition, pattern classification, etc. They have received intensive attention in recent years. Different phases such as evolutionary algorithms, evolutionary strategies, evolutionary programming have been devised by investigator with different backgrounds. These phases have carried almost the same meaning as genetic algorithms because they all are born from the idea of biological evolutionary theory.

In this paper, an evolutionary approximation method for optimal subspace selection is coined from the combined derivative of the schemes of genetic algorithms (GA) and basic event generation (BEG). The

0-7803-5489-3/99/$10.00 ©1999 IEEE.

BEG method is a non-parametric pattern classifier. This evolutionary method is applied to feature selection for 30D samples and is used as a classifier for 2 interlocked 3-d doughnuts.

SAMPLE DISTRIBUTION CHARACTERISTICS

The order of space under investigation is assumed to be 30 dimensions. In this paper, the samples are artificial data which are composed of 6000 individuals. In this data, 3 variables contain two donut type distribution data each containing 3000 individuals, all other 27 variables contain quasi-random data with the same value range as the donut distribution data. The samples in the two donut distribution are designated as class A and class B respectively. The mean centres of class A and class B are at points MeanA (3.0, 3.0, 3.0) and MeanB (4.5, 3.0, 3.0), but the distributions of A and B are centred on two interlocked circles:

$$\text{Distribution centre of class A}: \begin{cases} (x_A - 3.0)^2 + (y_A - 3.0)^2 = 2.25 \\ z_A = 3.0 \end{cases} \quad 1$$

$$\text{Distribution centre of class B}: \begin{cases} (x_B - 4.5)^2 + (z_B - 3.0)^2 = 2.25 \\ y_B = 3.0 \end{cases} \quad 2$$

The distribution of class A or B is Gaussian distributed with standard deviation delta($\sigma = 0.30$). The distribution functions for samples of class A and B were respectively:

$$f_A(r_A(x,y,z)) = \frac{1}{\sqrt{2\pi}\sigma} e^{-\frac{(r_A)^2}{2\sigma^2}} = \frac{1}{\sqrt{2\pi} \times 0.3} e^{-\frac{(z-3.0)^2 + \left(1.5 - \sqrt{(x-3.0)^2 + (y-3.0)^2}\right)^2}{2\times 0.3^2}} \quad 3$$

$$= 0.728 e^{-5.56\left((x-3.0)^2 + (y-3.0)^2 + (z-3.0)^2 - 3\bullet\sqrt{(x-3.0)^2 + (y-3.0)^2} + 2.25\right)}$$

$$f_B(r_B(x,y,z)) = 0.728 e^{-5.56\left((x-4.5)^2 + (y-3.0)^2 + (z-3.0)^2 - 3\bullet\sqrt{(x-4.5)^2 + (z-3.0)^2} + 2.25\right)} \quad 4$$

where (x,y,z) is a sample point, $r_A(x,y,z)$ and $r_B(x,y,z)$ are distances between point(x,y,z) and the points on the distribution centres of class A and B which with minimal distance to (x,y,z).

The distance between the means of class A and class B is 1.5. Within the extension $1.5/2 = 0.75 = 2.5\sigma$, these classes samples are not overlapped. By the characteristic of Gaussian distribution, it is clear that the overlapped rate is about 1.24%, so an ideal classifier should achieve a maximum correct recognized rate of 98.76%.

EVOLUTIONARY STRATEGY

Suppose there exist N *(N=6000)* individuals each containing m *(m=30)* variances, in which the *ith* individual can be expressed as $X_i = (x_{1i}, x_{2i}, \cdots, x_{mi})$, $i = 1,2,\cdots,N$, or more simply as $X_i = (x_i)^m, i=1,2,\cdots,N$. Then the $N(individuals) \times m(\text{var}iables)$ data can be expressed as a matrix $X = (x_{ij})^{m\times N}$. These N sample evenly come from class A and B, i.e., the numbers of class A and B samples are N_A *and* N_B, $N_A = N_B = \frac{1}{2}N$.

For $m=30$, in order to search optimal subspaces for each class, each variable should at least be divided into two parts, so the number of subspace in one dimension is at least 3, then the number of probable subspaces for 30 variables is at least $3^{30} \approx 2.1\times 10^{14}$. Clearly, an exhaustive strategy is impossible. The

proposed evolutionary approximation method of the optimal subspace is intended to circumvent this highly computational requirement. A traditional trick is to first conducting single variable analysis, then combine several top-most single-fittest variables to approximate an optimal subspace. This strategy sometimes may achieve a solution, but more often, becomes trapped in local optimum.

This algorithm generates subspaces populations according to the scheme of BEG, and approximates optimal subspaces by the scheme of GA.

1. **Random generation of initial subspace population** G_0 : The initial generation or seed generation which includes P_0 individuals that represent P_0 subspaces, denoted as $I_1, I_2, \cdots, I_i, \cdots, I_{P_0}$, where I_i is a triad of three measures (Variable selector(SL), Centre of subspace(CT) and Suburb of subspace(SU)). Variable selector SL is a binary (0-1) string, $SL_i = (b_1 b_2 \cdots b_j \cdots b_m)_i$, where m is the number of variables and $b_j = 0$ *or* 1 . If $b_j \neq 0$, the *j-th* variable is included as a component of the *i-th* subspace. The Centre of subspace, CT, is a high-order point in the subspace under consideration (order <= m). The Suburb of subspace, SU, is a range for each valid variable. The subspace I_i can represent any high-dimension simple continuum, such as super-cuboid, super-ellipsoid, etc. In this work, only super-cuboid is considered.

2. **Approximation of optimal subspace**: In the seed generation G_0 and any subsequent generation $G_l, l = 0,1,2,\cdots$, the subspace I_i can be called a classifier since just these evolutionary subspaces classify sample space into an appropriate class. In addition to the three measures for subspace I_i, there exist two properties for I_i, the correct rate and error rate. The evolutionary strategy is:

   (a) At $G_l, l = 0,1,2,\cdots$, judge the **validation of each subspace** I_i and calculate a correct rate and error rate for each validate subspace I_i. Suppose I_i contains a total of Q_i samples in which Q_{iA} samples come from class A and $Q_{iB} = Q_i - Q_{iA}$ samples come from class B, if $Q_i \geq \tau_0 N (e.g., \tau_0 = 0.05)$ which means subspace I_i contains at least τ_0 (e.g., 5%) of the total samples, subspace I_i is a valid candidate as an optimal subspace. If I_i is a valid candidate subspace and if $Q_{iA} > \tau_1 Q_{iB}$, $(e.g., \tau_1 = 10)$, I_i is a valid subspace whose correct rate is Q_{iA} / N_A and error rate is Q_{iB} / N_B; else if $Q_{iB} > \tau_1 Q_{iA}$, I_i is also a valid subspace whose correct rate is Q_{iB} / N_B and error rate is Q_{iA} / NA; otherwise, I_i should be excluded as a valid subspace. In subsequent evolutions, we can validate subspaces only by one of three GA operators: reproduction, crossover and mutation. The invalid subspaces operate only by mutation.

   (b) For a subspace I_i, the **reproduction operator** does nothing on I_i, only copies and transfers it to the next generation. The **crossover operator** for I_i firstly selects another subspace $I_j (j = 1,2,\cdots P_0, j \neq i)$ from the same generation and then randomly selects the crossover point $k (k = 1,2,\cdots m)$, next it divides I_i, I_j at point k and then crosses over these four sub-strings to formulate two new offspring I_i^1, I_j^1, finally it replaces the old I_i, I_j by new I_i^1, I_j^1 in the next generation. The **mutation operator** for I_i is somewhat more complex since it applies to both valid and invalid subspaces. For valid subspaces, the mutation operator enlarges or shrinks the suburb of the subspace SU; for invalid subspaces, the mutation operator used one of four sub-operators, (i)one-bit mutation in variable selector (SL), (ii)one co-ordinate shift in the centre of subspace CT, (iii) one-co-ordinate enlargement or shrinkage in the suburb of subspace SU or (iv) random initialization of a new subspace.

(c) **Determination of evolutionary termination condition.** Because samples in class A and B are distributed as two interlocked doughnuts and each evolutionary subspace is a simple continuum, it can't be counted on to classify class A and B perfectly using any single evolutionary subspace. So the overall evaluation of all valid subspaces should consider the determination of the evolutionary termination condition. At the learning stage, suppose for a sample X_i, J_A subspaces (i.e., classifiers) classify it as class A, and J_B classifiers classify it as class B, then if $J_A > \tau_3 J_B$, X_i is classified as class A and if $J_B > \tau_3 J_A$, $X_i$is classified as class B, otherwise X_i is indeterminate. So that the overall correct rate, error rate and unknown rate are now available. When the overall recognition rate (= overall correct rate - overall error rate) reach a predefined value, the evolutionary process terminates.

At different stages of evolution, selection of a breeding policy can significantly affect the final outcome.

RESULTS AND DISCUSSION

Various evolutionary breeding policies were assumed and implemented. The resulting total fitness (correct recognition rate, %) and the number of variables in the optimal subspace were intensively correlated with the selected breeding policy, such as the selection of initial population, determination of classifier resolution, formation of mutation operator and crossover operator etc. For example, if the resolution of a classifier (minimal sample number to judge the validation of a classifier) is too small, the resulting number of variable in the optimal subspace will oscillate far away from the theoretical-known value, otherwise if it is too large, the analysis will achieve nothing!

The evolutionary process up to the 2784th epoch for total fitness and number of variables in the optimal subspace are illustrated in Fig.1 and Fig.2. Although the theoretical optimal fitness (98.76%) hasn't been reached even after 2784 epochs, from a start of less than 10 epochs, the number of variable in optimal subspace is very stable at 3, with rare exceptions of 2 and 4. The number 3 represents the doughnut dimensions which carry sufficient information to discriminate the two 3D doughnuts.

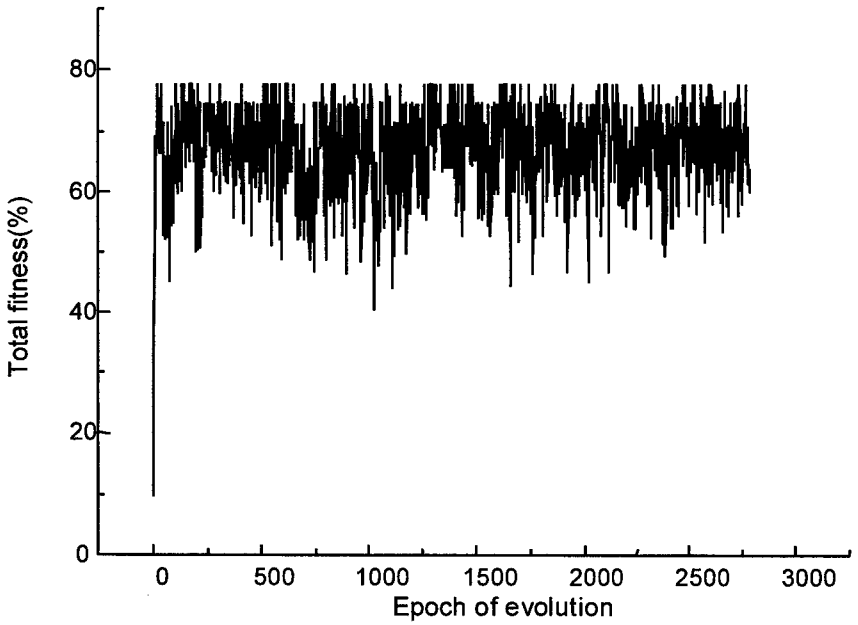


Fig.1. Total fitness (correct recognition rate, %) of distributed interlocked donuts

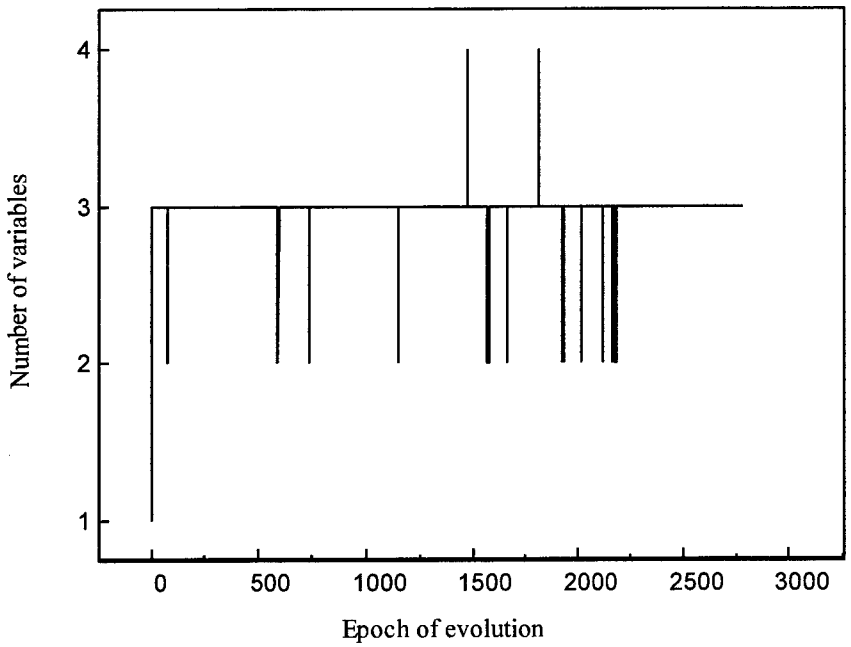


Fig.2. Number of variables in optimal subspace

In practical applications of high-dimension feature extraction and selection, such as complex medical data analysis, abstract object recognition, high-dimension variables and huge computation may hinder complete searching of the solution space. Traditional technique often reach sub-optimal solutions. By careful design and prudent selection of evolutionary breeding policies, evolutionary scheme may perfectly approximate the optimal subspace.

REFERENCES

1. Thomas Back, 1996. Evolutionary algorithms in theory and practice: evolution strategies, evolutionary programming, genetic algorithms , Oxford University Press, New York.
2. Michalewicz and Zbigniew, 1996. Genetic algorithms + data structures = evolution programs, Springer-Verlag, New York,.
3. Robert Schalkoff, 1992. Pattern Recognition---Statistical, Structural and Neural Approaches, John Wiley & Sons, Inc.
4. Keinosuke Fukunaga, 1990. Introduction to Pattern Recognition, 2nd Edition, Academic Press,.
5. Perambur S. Neelakanta, Dolores F. De Groff, 1994. Neural Network Modeling---Statistical Mechanics and Cybernetic Perspectives, CRC Press, Inc.
6. Clifford Lau(edited by),1992. Neural networks---Theoretical Foundations and Analysis, IEEE Press,
7. Brian D. Ripley, 1996. University of Oxford), Pattern Recognition and Neural Networks, Cambridge University Press, Great Britain,,
8. Paolo Antognetti and Veljko Milutinovic, Eds., 1991. Neural Networks, Concepts, Applications and Implementations, Vol. I, Prentice Hall Inc., Simon & Schuster, Englewood Cliffs, New Jersey, USA.

Prediction of Cement Paste Mechanical Behaviour From Chemical Compositon using Genetic Algorithms and Artificial Neural Networks

José C. Cassa, Giovanni Floridia, André R. Souza, Rodrigo T. Oliveira

Grupo de Estudos em Inteligência Computacional Aplicada (GEICAP)
DTCM - Escola Politécnica - Universidade Federal da Bahia
Rua Aristides Novis, 02 - Federação, 40210-630 Salvador, Bahia, Brazil
e-mail: jccassa@ufba.br

ABSTRACT

Computational Intelligence (CI) techniques have attracted the interest of some engineers as valid tools for the representation of complex systems. A growing number of works are showing that they are also effective in optimisation. Building materials, such as concrete and mortars, usually display a complex behaviour hard to model and seems to be an interesting area to explore the application of CI as modelling technique. This paper describes how CI can be used to model the performance of cement paste. The specific objective was to develop models able to predict the mechanical behaviour of this material using only data available from chemical composition of cement. The developed models showed the advantage of CI with respect to conventional techniques leading rapidly to useful results with reasonable precision and accuracy.

INTRODUCTION

The technology of cement has had significant advances in the last two centuries. The success of engineering techniques using intensively this material is a clear demonstration of the achieved progress as well as an alert to the building construction industry for the need of new developments. Although the commercial value of this technology is huge, the scientific basis today are far from complete and it is possible to identify spaces and opportunities for new scientific developments.

In other work [1] the authors showed the validity of the use of artificial neural networks (ANN) as modelling technique to predict the concrete mechanical behaviour. Three different neural network main architectures were used: the Multi-Layer Perceptron (MLP), the General Regression Neural Network (GRNN) and the polynomial network known as Group Method of Data Handling (GMDH). The key question is how to choose the best ANN architecture.

Even in a known architecture like MLP there are many possibilities giving different MLP structures: one can change the number of layers, the transfer function of each neuron, and the connections between neurons. If one allow also to "jump" a layer and freely connect neurons, the MLP name itself makes little sense, because there are no more clear layers. The compromise can be to use a modified MLP that accepts different "slabs" in the same layer [2,3]. There are many possibilities to choose the best neural network architecture. In order to automate this search for best network configuration genetic algorithms can be used. This work shows a simple application of this technique.

COMPUTATIONAL INTELLIGENCE

In the last decades the great majority of works on modelling using **computational intelligence (CI)** is characterised mainly by the search of methods inspired in nature where a large number of live systems can be regarded as intelligent. Although it is not possible to assure that all solutions in nature are optimised and/or intelligent there is no doubt that they are well designed and suitable to survive in their environment. For this reason some of these systems have been adopted as new paradigms for engineers, scientists, and

0-7803-5489-3/99/$10.00 ©1999 IEEE.

mathematicians in order to model, simulate and/or control complex systems. These professionals search new ideas that can be copied or imitated in a computer and then applied for the solution of hard problems that science and engineering cannot yet solve satisfactorily using classical mathematical approach (phenomenological or others). For example, the central nervous systems of superior animals and the natural evolution processes gave the inspiration for the development of new CI techniques called **artificial neural networks** [2,3] and **genetic algorithms** [4], respectively.

Artificial Neural Networks

Many different ANN structures and training techniques are described in the literature [3], but multi-layer perceptrons **(MLP)** seem suitable to model complex systems. In simple terms, this type of ANN works like a non-linear regression approach. As with any curve-fitting technique, model parameters can be found by least squares optimisation. With multi-layer perceptron networks, processing elements are arranged into inter-connected layers. There is an input layer to receive data, one or more hidden layers, and finally, an output layer to transmit the result of network calculations. The hidden layer is essential to represent non-linear processes.

Although MLP neural networks can solve many modelling problems, other ANN architectures [3] such as General Regression Neural Networks (GRNN), Probabilistic Neural Networks (PNN), and Polynomial Networks (GMDH) can often do the same job easier [1].

The ANN designer must specify the number of hidden layers (usually one), the number of nodes in each layer, and the transfer function of each layer. This is called the ANN "architecture". Expertise, judgement and trial-and-error as in regression methods are used to define the suitable architecture. Once the ANN architecture is selected, the weights have to be adjusted by finding the values that minimise for example the sum of square deviations of the ANN and process outputs.

The main problem for engineers and scientists unfamiliar with non-linear modelling is to apply and understand ANN concepts that require reasonable investment in software, training and developing the heuristics of neural programming. For many end users this situation looks impracticable. So it would be very useful if an automatic computer system could represent the knowledge of a neural programmer in order to find acceptable ANN solutions. Recent progress in Evolutionary Computing made it possible through Genetic Algorithms [4].

Genetic Algorithms

Genetic Algorithms **(GAs)** are search algorithms based on the mechanics of natural selection and natural genetics [4]. They combine survival of the fittest among string structures with a structured but randomised information exchange to form a search algorithm with some characteristics of human search. . It is necessary to represent any possible solution as a string of bits called "chromosome" in a clear metaphor of the in biological counterpart. One also calls these strings "individuals" or "artificial creatures". There is a clear coding schema in this process and each "creature" is a candidate solution under that schema. The procedure is to create a population of candidates that will compete: well-adapted individuals will grow in number, bad ones will vanish.

In every generation, a new set of artificial creatures (strings) is generated using bits and pieces of the fittest of the old and occasionally new parts are tried for good measure. The efficiency exploit historical information to speculate on new search points with expected improved performance.

GAs are different from more normal optimisation and search procedures in four ways, they:

a) work with a coding of the parameters, not the parameter themselves
b) search from a population of points, not a single point
c) use objective function information, not derivatives
d) use probabilistic transition rules, not deterministic rules.

A simple GA that yields good results in many practical problems is composed of three operators: reproduction, crossover and mutation.

Reproduction is a process in which individual strings are copied according to their objective function values (the fitness function). This function f can be some measure of profit, utility or goodness that we want to

maximise or minimise. Copying strings according to their fitness values means that strings with a higher probability of contributing to one or more offspring will be kept in the next generation. This operator is an artificial version of natural selection, the survival of the fittest among string creatures. How crossover and mutation operators work will be illustrated in the following example. A classic problem of model optimisation is the search for the best regression equation to represent a system. As an example, suppose that a model relates an output z to two inputs x and y, so that

$$z = F(x,y) \qquad 1.$$

where F is any linear or non-linear function or transformation of original variables x and y that can be useful in the model, such as:

$$z = G(x, y, x^2, y^2, x^3, y^3, xy, ...) \qquad 2.$$

where G is a linear weighting of the terms (in this case we are seeking a model that is linear in the parameters). Once all possible terms in the model are chosen it is possible to produce a random population of models in binary form where 1 indicates inclusion of the corresponding term and 0 indicates that the term is not used. For instance, the following strings correspond to three members in the population derived from terms in Eq. 2.:

1101001 => x, y, y2 and xy
0110010 => y, x2 and y3
1110010 => x, y, x2 and y3

Each of these models can be fit to part of a data set by least squares and the ability of the model's predictive can be tested with the remaining data. The models are then ranked based on their prediction error (some criterion is adopted, i.e., R2 or MSE).

It is possible to create a GA strategy where half of the population of models is allowed to live and breed at each step (generation). Pairs of these models are randomly selected for breeding. A randomly selected crossover point is chosen for each pair of models and genes are twisted. Suppose that the first and second model were chosen for breeding and the crossover point selected as indicated. The result would be

1101001 => **1101**010
0110010 => 0110**001**

where two new members of the population are shown at right. Other breeding schemes can be adopted[5].

A similar process used by the crossover operator is used for the mutation operator. This operator is applied to some selected individual that belongs to the new generation that can be the result of the crossover operator application. A random number either 0 and 1 is generated and at the same time it is set the position of a bit. If the mutation probability is greater than the random number generated, the value of bit change (from 0 to 1 or from 1 to 0). This process is made until the end of the bit strings. As example, a mutation operator in the third member of population described before operating as indicating

11<u>1</u>0<u>0</u>10 => 11<u>0</u>0<u>1</u>10

The overall process stops when there is no more improvement after several generations. Then, it is assumed that optimum conditions were reached. Using this approach is possible to define a search algorithm based on GAs in order to optimise a defined objective function f = f(s), such as ANN architecture (the type of ANN architecture, the number of hidden layers, the number of neurons in the hidden layer, the most suitable transfer function in each layer and the weights/connections between neurons) by using suitable objective functions.

THE CONSIDERED PROBLEM

Predicting the flexural mechanical strength of cement pastes

Several researchers attempted to predict mechanical properties of cement paste and/or concrete from the chemical composition. Unfortunately, the results were not encouraging and the mathematical models developed did not show the reliability and precision required in this type of work.

Dragicevic and Rsumovic [6] using D-Optimal Design and regression analysis proposed a statistical model for this purpose. But, primary mistakes of overfitting (perfect adjusting due to zero degree of freedom) invalidate any usefulness of the developed model as it has no ability of generalisation (the model was only educated to repeat the original training set of data). Although, there are some mistakes in the modelling approach of the paper, the experimental results are believed to be consistent and reliable, and were used in this paper to demonstrate the application of computational intelligence.

In the original work, one area of interest was defined where four types of cements were used (z1, z2, z3 and z4) and the mineralogical composition estimated from the chemical composition of cements (Bogue formulae), as shown in Table 1.

Table 1: Potential mineralogical composition of cements used.

	z1	z2	z3	z4
X1-C_3S	73.04	40.95	73.73	53.34
X2-C_2S	6.89	41.05	7.43	21.04
x3-C_3A	10.05	4.82	5.89	13.59
x4-C_4AF	10.02	13.18	12.95	12.03

An experimental data base relating different mixtures of cements (z1, z2, z3 and z4) and flexural mechanical strength of cement pastes at the 28th day of age was developed by using a design of experiments technique called "D-Optimal Design" from information extracted from [6].

The value of potential mineralogical composition of another cement (x1, x2, x3 and x4) can be calculated from its composition or measured directly using X-ray techniques, microscopy or other quantitative mineralogical method. By using matrix algebra, the values of potential mineralogical composition (x1, x2, x3 and x4) can be converted into equivalent mixtures of cement used in this study (z1, z2, z3 and z4) from the equations:

$$z1 = 5.517x1 + 5.600x2 + 0.484x3 - 34.660x4 \quad (4.1.)$$
$$z2 = 1.300x1 + 4.051x2 - 0.627x3 - 7.623x4 \quad (4.2.)$$
$$z3 = -2.295x1 - 5.481x2 - 5.811x3 + 26.324x4 \quad (4.3.)$$
$$z4 = -3.523x1 - 3.203x2 + 10.921x3 + 16.926x4 \quad (4.4.)$$

The major objective is to develop a prediction model based on ANN that allows the calculation of flexural mechanical strength (FS) at 28th day from the knowledge of its chemical / mineralogical composition, so that

$$FS = f(x1, x2, x3, x4) \quad (5.)$$

TRAINING THE NETWORK

Using Backpropagation

The architecture of a Multi-Layer Perceptron (**MLP**) has to be adapted to the problem to be solved. The number of network inputs to the network is constrained by the problem, and the number of neurons in the output layer is constrained by the number of outputs required by the problem. Backpropagation (**BP**) training follows gradient descent on the error surface to minimise network error. Local minima may trap the network. The more neurons in intermediate layers the more freedom a network has and more variables to optimise. Hecht-Nielsen demonstrated that a hidden layer with ($2\mathbf{n} + 1$) neurons, where **n** is the number of input variables, can represent any mathematical continuous function [2].

The best network scored 2,77% MSE, using a simple full-connected MLP. Often in polynomial regression the best generalisation can be achieved with not full polynomials. In ANN regression we can have a similar behaviour: best generalisation can be achieved with not full-connected MLP. Genetic Algorithms can be a good tool to manage the difficulty to find such architectures

Using Genetic Algorithms

It is quite obvious that training an MLP network using backpropagation is time-consuming even with fast computers as well as requiring some heuristic knowledge of neural programming. GAs offer the possibility of automatic searching to ease the work of finding an acceptable ANN solution. NeuroGenetic Optimizer (**NGO**) [7] is a commercial software based on this principle. The NGO process consists of:

a) Creating an initial population of genotypes
   (genetic representations of the neural networks able to solve the problem of interest)
b) Building neural networks (phenotypes) based on the genotypes
c) Training and testing the neural networks to determine how fit they are
d) Comparing the fitness of the networks and keeping the best (Top 10)
e) Selecting those networks in the population that are better, discarding those which are not
f) Refilling the population back to the defined size
g) Pairing up the genotypes of the neural networks
h) Mating the genotypes by exchanging genes (features) of the networks
i) Mutating the genotypes in some random fashion.

Then returning back to step b) and continuing this process until some stopping criteria is reached or the process is stopped manually.

Through this process, the better networks survive and their features carried forward into future generations and/or combined with others to find better networks for the desired application. This genetic search capability is much more effective than random searching, as the genetic process of recombining features vastly improves the speed of identifying highly fit networks. It also has a potential advantage over just using personal experience in building neural networks, as new and potentially better solutions may be found through this process than might be found using the nearly unavoidable assumptions made by the user.

Neural network fitness is computed by the application of the neural node influence (**NNI**) factors and optionally, Learning Ability Compensation to the networks test accuracy. When using NNI, the networks test accuracy is adjusted by this factor according to the equation:

Net_Fitness = Test_Accuracy * (1 +/- 0.5 *((Input_Node_Influence*(1-Nbr_Inputs / Nbr_Possible_Inputs))
+ (Hidden_Node_Influence*(1-Nbr_Hiddens / Max_Hiddens)))) 6.

Accordingly, smaller networks are rewarded by an amount proportional to the input and hidden node influence. The NGO formula for Learning Ability Compensation is proprietary and confidential.

General Regression Neural Networks

General regression neural networks (**GRNN**) are feedforward networks based in probability density functions. GRNN train fast showing good performance provided enough experimental data are available. This network was developed in the statistical literature as kernel regression and rediscovered later as a new ANN architecture [11]. Its topology consists of four layers: the input layer, a hidden layer working as classifier, addition neurons and the output layer. Training is processed in one step when the training set is copied in the hidden layer. The addition neurons process the kernel function. The network approximates any new input to the nearest one available in the classifier and then presents the output response. The weights are a smoothness factor that can be trained and calibrated using GAs.

Polynomial Neural Networks

Polynomial neural networks also called Group Method of Data Handling (**GMDH**) was invented by Ivakhnenko in Russia but later used as neural networks and enhanced by others.

GMDH works by building successive layers with complex links (or connections) that are individual terms of a polynomial. These polynomial terms are created by using linear or non-linear regression. The initial layer

is simply the input layer. The first layer created is made by computing regressions of the input variables and then choosing the best ones. The second layer is created by computing regressions of the values in the first layer along with the input variables. Once again, the best are chosen using a convenient algorithm (i.e., GAs). They are called survivors. This process continues until the network stops getting better (according to a specified criterion).

The resulting network can be represented as a complex polynomial description of the model. In some respects, it is like using regression analysis but is far more powerful. GMDH can build very complex models while avoiding overfitting problems.

NEUROSHELL GMDH [11] can recognise the most significant variables as it trains, and will display a list of them. This software has also facilities to select the degree of expected model non-linearity (off, low, medium and high) as well as the model diversity by using the maximum number of survivors (low, medium and high). The length of the model is associated to complexity (low, medium and high). The final model can be also optimised eliminating the less significant parameters.

RESULTS

Different types of ANN architecture were performed using MLP combined with GAs. The idea was to investigate all possible combinations such as the number of hidden layers, the number of neurons in each layer, and the type of transfer functions in each neuron (including free allocation of these transfer functions in any neuron). The best combination for the considered problem was a network with one hidden layer (twelve logistic functions) and one output layer (logistic function) with MSE = 1,59%. It can be seen that only small improvements were obtained indicating the goodness of traditional approach (simple MLP).

Other more advanced networks suitable to represent the studied problems were also considered giving the results summarised in Table 2. These networks correspond to the best architecture found for each case considered. This application was developed using MATLAB [9,10], NEUROGENETIC OPTIMIZER [7] and NEUROSHELL [11]. Two types of ANN gave good results: GRNN and GMDH. GRNN works as interpolating polynomials where the training set is copied in the hidden layer. This type of network will lead to satisfactory results when enough reliable data are available. Table 3 shows the main results for GMDH networks. It is interesting to note that this type of ANN looks as regression models that are familiar to researcher and engineers. The complexity necessary in any case will depend on the desired precision and accuracy. In the studied cases, even simple models gave good results.

Table 2: Summary of results of best fitting some ANN.

MODEL	MSE (%)
MLP simple	2,77
MLP / GAs	1,59
GRNN / GAs	3,21
GMDH simple / GAs	2,27
GMDH interm. / GAs	2,17
GMDH complex / GAs	1,95

The final evaluation of the usefulness of the systems developed can be assessed in figures 1 to 4 when calculated and experimental values are compared for the considered problems. It can be seen that in all cases good agreement was found indicating reasonable solutions for all proposed models.

Table 3: Main results for GMDH networks.

Normalisation of input / output values

X1=2.*(x1-.41)/.33-1.

X2=2.*(x2-.07)/.34-1.

X3=2.*(x3-.05)/.09-1.

X4=2.*(x4-.1)/.03-1.

$Y = 2.*(y_{exp} - 7.)/2.-1.$

GMDH simple:

Y= 0.61 + 1.8*X1 + 1.3*X2 - 0.65*X1^2 + 2.2*X1*X3 + 2*X2*X3

GMDH intermediate:

Y= 0.33*X3 + 2.2*X1 + 2*X2 + 0.64 + 2.1*X2^2 + 0.36*X3^2 + 2.6*X1*X2 + 3.7*X1*X3 + 4*X2*X3 + 0.44*X1^2 + 0.39*X1*X4 - 0.46*X1^3 + 0.15*X1*X4^2 – 0.42*X1^2*X4

GMDH complex:

Y= 2.1*X1 + 0.58 + 1.9*X2 + 0.33*X3 + 2.1*X2^2 + 0.35*X3^2 + 2.6*X1*X2 + 3.7*X1*X3 + 3.9*X2*X3 + 0.95*X1^2 + 0.46*X1*X4 - 0.49*X1^3 + 0.21*X1*X4^2 - 0.45*X1^4 - 0.47*X1^2*X4

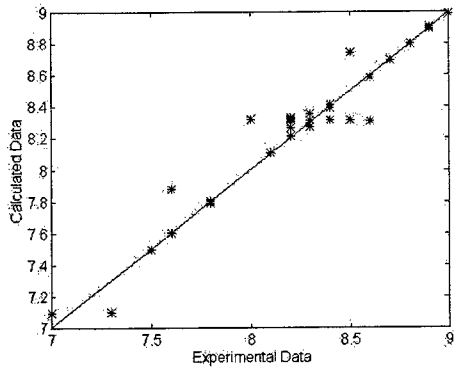


Fig. 1. Calculated vs. Experimental Data for best MLP / GAs (MSE = 1,59 %).

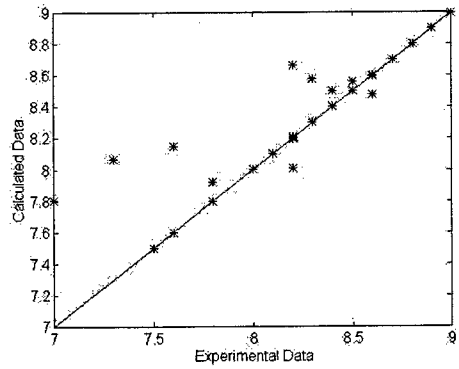


Fig. 2. Calculated vs. Experimental Data for best GRNN (MSE = 3,21%).

CONCLUSIONS

The analysed problem shows the applicability of artificial neural networks combined with genetic algorithms as modelling tool for prediction of concrete mechanical behaviour. It is hoped that this paper will encourage other applications of computational intelligence for the prediction of mechanical performance of other complex materials, specially those materials that do not have any model available or the traditional models do not offer the desired precision.

The combination of artificial neural networks and genetic algorithms is extremely powerful as modelling technique for complex hard problems. The automation of model developing process makes the application quite simple even for end users not familiar with neural programming and non-linear modelling.

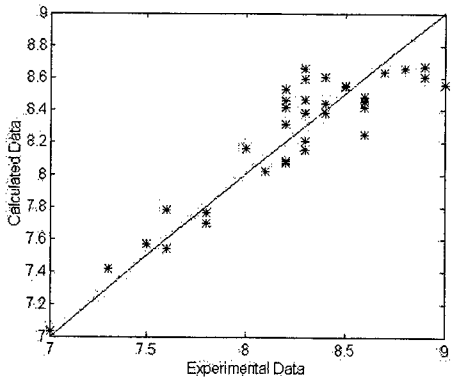


Fig. 3. Calculated vs. Experimental Data for best simple GMDH (MSE = 2,27 %).

REFERENCES

1. J. C. S. Cassa, et al., 1998. Prediction of Concrete Mechanical Behaviour from Data at Lower Ages Using Artificial Neural Networks. IPMM 99 – The Second International Conference on Intelligent Processing and Manufacturing of Materials – Honolulu, Hawaii, July 10 – 15, 1999.
2. R. Hecht-Nielsen, 1990. Neurocomputing. Addison-Wesley.
3. S. Haykin, 1994. Neural Networks - A comprehensive foundation. Prentice Hall
4. D.E. Goldberg, 1997. Genetic Algorithms in Search, Optimisation & Machine Learning. Addison Wesley.
5. J.C. Bean, 1994. Genetic Algorithms and Random Keys for Sequencing and Optimisation. ORSA Journal of Computing, 6(2), 154-160
6. L.M. Dragicevic and M. M. Rsumovic, 1987. Prognosis of characteristics of multicomponent materials on the example of flexural strength of Portland cement. Cement and Concrete Research, 17, .47-54.
7. BIOCOMP, 1997. NeuroGenetic Optimizer. Biocomp Systems Inc.
8. M. Hagan , H. Demuth and M. Beale, 1996. Neural Network Design. PWS Publishing Company.
9. MATLAB, 1992. MATLAB High Performance Numeric Computation Software. The Mathworks.
10. MATLAB, 1993. MATLAB Neural Network Toolbox. The Mathworks.
11. NEUROSHELL, 1996. NeuroShell 2. Ward System Group Inc.
12. C.E.S. Tango, 1991. Um estudo do desenvolvimento da resistência a compressão do concreto de cimento Portland até 50 anos. Boletim 160 - IPT.
13. C.E.S. Tango, et al., 1995. Planilha eletrônica para previsão da resistência do concreto. Anais do 37º REIBRAC - IBRACOM, 785-797).

Rough Sets-based Machine Learning Using a Binary Discernibility Matrix

Reynaldo Félix, Toshimitsu Ushio

Department of Systems and Human Science
Graduate School of Science and Engineering
Osaka University, Japan

ABSTRACT

This paper presents an approach with two methods to obtain minimal coverings in Rough Sets based Machine Learning, both methods are based on the definition of a *binary discernibility matrix*. The first method is an exhaustive search of coverings and the second uses a genetic algorithm (GA) based search. The approach represents the discernibility of two examples by a condition attribute of an information system in a single bit. Thus, operations that usually are performed with a set approach are redefined in order to use bit-wise logical operations. The algorithms for both methods are presented and discussed.

INTRODUCTION

Rough sets theory is a mathematical approach to imprecision, vagueness and uncertainty in data analysis [1]. The starting point of rough sets is the assumption that with every object of interest we associate some information, also called knowledge. With this knowledge we can perform classifications and this is the key issue in reasoning, learning and decision making. Such classifications can be done not only in objects, but also in abstract ideas or concepts, processes, moments of time, states, etc.

The knowledge can be irrelevant, redundant, uncertain, imprecise or incomplete and usually is obtained from experience or from querying an expert about what action to take depending on different conditions. This knowledge can be represented in an information system as examples described for condition attributes and decision attributes. Then rough sets theory is used to: remove superfluous data through measurement of dependencies between attributes and deal with inconsistencies through the definition of lower and upper approximation [1]. The depurate and consistent data is used to define sets of decision rules (i.e. decision table), where each rule is also described for condition and decision attributes.

The characteristics described above, support the applicability of rough sets theory in machine learning considering that data in real applications is often vague and has many inconsistencies. The use of the theory in methods of learning from examples and inductive learning was first proposed in [1] and developed in several works as pointed in [4]. Nowadays there are many approaches to machine learning based on the rough sets. The theory has been used at different stages of the process of rule induction and data preprocessing. This work is focused in the learning from examples approach. We first use the theory for data preprocessing to deal with inconsistencies in data and remove superfluous attributes and then in the rule induction stage to obtain the coverings for the basic concepts.

The problem in finding minimal coverings is proven to be NP-hard, so the importance of developing more efficient computational methods for rough sets applications is discussed in several works [2][3][8]. In this paper, the proposed approach to find minimal coverings is based on a binary representation of discernibility between pairs of examples in a table, called the "*binary discernibility matrix*" and a binary representation of sets of condition attributes, thus implicit parallel processing up to 64 bits (condition attributes) is used.

The binary discernibility matrix enables us to detect inconsistent examples, irrelevant attributes and indispensable attributes; to measure the capability of an attribute to classify objects and mainly to find the

0-7803-5489-3/99/$10.00 ©1999 IEEE.

minimal coverings. In this representation, the coverings finding is done by testing which sets of condition attributes can discern all the pairs of examples in the table. Two methods for this search are proposed, the first is an exhaustive search while the second uses a genetic algorithm (GA) based search.

PRELIMINARIES AND NOTATIONS

We consider an *information system* with a finite non-empty set (the universe) of objects that we are interested in, denoted by $\mathbf{U}=\{e_1,e_2,..,e_m\}$, each object e_i of **U** is called an example or an instance. Those objects are described by a finite non-empty set of *condition attributes* $\mathbf{A}=\{a_1,a_2,..,a_n\}$, and a finite non-empty set of *decision attributes* $\mathbf{C}=\{c_1,c_2,..,c_p\}$. Thus we can say that by using the description in **A**, the examples in **U** can be classified in concepts or categories of **C**. We define **B** as a subset of the whole set of condition attributes **A**, and $\mathbf{B}_k$ as a subset composed just for the condition attribute a_k.

The *decision attributes* define the categories or *equivalence classes* [1], representing the family of concepts in the information system (see Table 1). A concept or equivalence class will contain all the examples with the same condition attributes values, thus $[e_i]_C$ is the concept c to which the example e_i belong. In its simplest form a decision attribute can take only two values: *belong to the concept* or *not* (yes, no), thus it represents a *basic concept*. The set of examples of **U** that has the decision attribute "yes" is called the *set of examples positives*. Nevertheless, even if most of the cases include multi-valued decision attributes that define several basic concepts, in our approach we will split any multi-valued decision attribute into several binary decision attribute in order to define all the basic concepts.

Table 1. Information system: Computer buying criteria

	Condition attributes				Decision attributes							
					Multi-valued Concept	Basic Concepts for Buy			Concept Yes approximations		Concept No approximations	
Examples	Speed (MHz)	Price	Software installed	Memory (MB)	Buy	Yes+ dec.*	No+	Not	Lower*	Upper*	Lower*	Upper*
e_1	200~300	Medium	Yes	128	Yes	Yes	No	No	Yes	Yes	No	No
e_2	200~300	Low	Yes	64	No	No	Yes	No	No	No	Yes	Yes
e_3	~200	Low	Yes	80	No	No	Yes	No	No	No	Yes	Yes
e_4	300~	High	Yes	64	Yes	Yes	No	No	No	Yes	No	Yes
e_5	300~	Medium	Yes	64	Not decided	No	No	Yes	No	No	No	No
e_6	300~	High	Yes	64	No	No	Yes	No	No	Yes	No	Yes
e_7	200~300	High	No	80	Not decided	No	No	Yes	No	No	No	No
e_8	~200	Low	No	128	No	No	Yes	No	No	No	Yes	Yes

Note: examples 4 and 6 are inconsistent. +Inconsistent basic concepts *Consistent basic concepts.

Inconsistent representation of examples is a kind of uncertainty frequently found in knowledge bases. When inconsistent examples exist (i.e. examples with the same condition attributes but belonging to different concepts), we use a lower and upper approximation, as defined in [1] to obtain concepts defined by consistent examples (i.e. examples with the same condition attributes and belonging to the same concept). In general, the lower approximation includes all objects that can be certainly classified as while the upper approximation includes all those that can be probably classified as elements of a concept.

Let $\mathbf{E}_C=\{e_1, e_2,..e_q\}$ be a subset including all examples of **U** belonging to the concept C, and $[e]_C$ is the concept to which e belongs, then the lower approximation $\underline{C}\mathbf{E}_C$ and the upper approximation $\overline{C}\mathbf{E}_C$ are:

$$\underline{C}\mathbf{E}_C = \{e \in \mathbf{U} : [e]_C \subseteq \mathbf{E}_C\} \quad 1.$$

$$\overline{C}\mathbf{E}_C = \{e \in \mathbf{U} : [e]_C \cap \mathbf{E}_C \neq \phi\} \quad 2.$$

When the concept has inconsistent examples, we obtain the lower approximation and the upper approximation which correspond to the sets of *certain rules* and *possible rules*, respectively [8].

Knowledge bases sometimes contain redundant or irrelevant information. So, to simplify data without losing information, it is necessary to reduce the knowledge base by obtaining its *reducts*.

Pawlak [1] defines a *reduct* (also called covering) as "the minimal subset of attributes that discerns all objects discernible by the whole set of attributes". In this definition, the whole set of attributes includes condition attributes and decision attributes. When we consider only *condition attributes*, this concept turns into that of *relative reduct*. A relative reduct is the minimal subset of condition attributes that can discern all the examples belonging to different concepts (positive and negative examples for a basic concept), examples belonging to the same concept are not considered because they do not need to be discerned . It is noted that all the supersets of a reduct are also a reduct [1]. We are mainly interested in the minimal reducts (i.e. coverings containing as few attributes as possible). We will refer to a (minimal) relative reduct as a (minimal) *covering*, a condition attribute as an *attribute*, and a decision attribute as a *concept*.

BINARY REPRESENTATION

The problem of finding minimal coverings has been proved to be NP hard, thus the importance of developing more efficient computational methods for rough sets based applications has been discussed in several works [2][3][4]. In our approach, we take advantage of bit-wise operations that are performed in a computer in parallel for groups of 8, 16, 32 or 64 bits. For bigger groups, we divide the attributes into groups and process them sequentially. A binary representation of the information system and a set of condition attributes $\mathbf{B} \subset \mathbf{A}$ is defined below.

Binary Discernibility Matrix

The proposed method is based on the construction of a binary table to represent discernibility between pairs of examples, called the *binary discernibility matrix*.

Table 2. a) Binary discernibility matrix for the information system in Table 1. b) Pairs considered in each basic concept for analysis.

a)

Pairs	Attributes a_1	a_2	a_3	a_4
$e_1\ e_2$	0	1	0	1
$e_1\ e_3$	1	1	0	1
$e_1\ e_4$	1	1	0	1
$e_1\ e_5$	1	0	0	1
$e_1\ e_6$	1	1	0	0
$e_1\ e_7$	0	1	1	1
$e_1\ e_8$	1	1	1	0
$e_2\ e_3$	1	0	0	1
$e_2\ e_4$	1	1	0	0
$e_2\ e_5$	1	1	0	0
$e_2\ e_6$	1	1	0	1
$e_2\ e_7$	0	1	1	1
$e_2 e_8$	1	0	1	1
$e_3\ e_4$	1	1	0	1
$e_3\ e_5$	1	1	0	1
$e_3\ e_6$	1	1	0	1
$e_3\ e_7$	1	1	1	0
$e_3\ e_8$	0	0	1	1
$e_4\ e_5$	0	1	0	0
$e_4\ e_6$	0	0	0	1
$e_4\ e_7$	1	0	1	1
$e_4\ e_8$	1	1	1	1
$e_5\ e_6$	0	1	0	1
$e_5\ e_7$	1	1	1	1
$e_5\ e_8$	1	1	1	1
$e_6\ e_7$	1	0	1	1
$e_6\ e_8$	1	1	1	0
$e_7\ e_8$	1	1	0	1

b)

Basic concepts				
Pending	L-Accept	U-Accept	L-Reject	U-Reject
	+	+	+	+
	+	+	+	+
	+			+
+	+	+		
	+			+
+	+	+		
	+	+	+	+
		+	+	
+			+	+
		+	+	
+			+	+
		+	+	
+			+	+
		+	+	
+			+	+
+		+		+
+		+		+
		+	+	
+		+		+
+			+	+
+		+		+
		+	+	
+			+	+

+ denotes pairs of examples involved in the basic concept, i.e. those pairs where one example belongs to the concept but not the other.

The discernibility $d_{Bk}(e_i,e_j)$ between two examples e_i and e_j by using a single condition attributes $\mathbf{B}_k$, $\forall\, i \neq j$ and $[e_i]_C \neq [e_j]_C$ can be given in a binary representation (i.e. {1,0} = {yes, no}), such that

$$d_{Bk}(e_i,e_j) = \begin{cases} 1 & \text{if } e_i \text{ is discernible of } e_j \text{ by } \mathbf{B}_k \\ 0 & \text{otherwise} \end{cases} \quad 3.$$

Such binary representation of discernibility let us determine if a pair of examples is discernible by **B** with a single bit. In the binary discernibility matrix, columns are single condition attributes and rows are example pairs belonging to different concepts.

The number of condition attributes determine the length of the binary string, the number of rows in the matrix for an information system with m_e examples is

$$\mathrm{BDM}_{\mathrm{rows}} = m_e\,(m_e\text{-}1)/2 \quad 4.$$

and the number of rows of the matrix involved in a basic concept which has n_e examples is

$$\mathrm{BDM}_{\mathrm{Ci}} = n_e\,(n_e\text{-}m_e) \quad 5.$$

The rows involved in a basic concept form a partial discernibility matrix for the concept. This matrix has the following main patterns:

- If a row is all 0's, it means that the corresponding pair of examples are indiscernible even when using the whole set of condition attributes, then the examples are inconsistent because they belong to different concepts while having the same condition attribute values. In that case, the lower and upper approximations for the concept should be used in order to deal with such inconsistencies.
- If a column is all 1's, then the attribute is capable of distinguishing all the pairs of examples that are discernible by the whole set of attributes, and that is the definition of a covering. In such a case, a covering was found, and since it has only one attribute, we can say that it is a minimal covering.
- If a column is all 0's, then the attribute is completely irrelevant to the concept because it is unable to distinguish any pair of examples by itself.
- If a row in the matrix has only one "1" in the bit string, then the corresponding attribute is the only one able to distinguish that pair of examples and so it is indispensable to the concept.
- The *rate of ones* in a column over the number of pairs in the discernibility matrix is a measure of the approximation of that attribute (or combination of attributes) to a covering, it is called the discernibility degree and is a part of the fitness function in the GA-based search method proposed later.

Binary representation of sets

We define a bit string with length n (the number of condition attributes), where each bit corresponds to a condition attribute. Figure 1 shows conventional notation for bits and attributes, where the LSB b_0 corresponds to the first attribute.

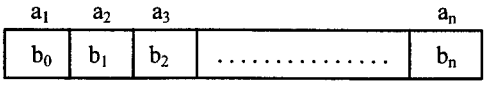


Fig. 1. Location of the condition attributes in a binary string.

Given a set $\mathbf{B} \subset \mathbf{A}$, each bit of the bit string is set to "1" if the corresponding attribute is a member of the combination; otherwise it is set to "0". For simplicity, we use the same symbol for both a set and its representation in a binary string.

Bit-wise sets operations

It is well known that a computer processes in parallel bit strings in standard lengths (e.g. 8, 16, 32 or 64 bits) and also the function of the Boolean operations. Thus given the sets $\mathbf{B}, \mathbf{D} \subset \mathbf{A}$ represented in bit strings as shown in Fig. 1, we use the following operations:

- AND, **B** & **D**. The result preserves only those attributes that are members of both sets. In a sets point of view this operation is equivalent to $\mathbf{B} \cap \mathbf{D}$.

- INCLUSIVE OR, $\mathbf{B} \vee \mathbf{D}$. The result preserves those attributes that are members of any of the sets, i.e., $\mathbf{B} \cup \mathbf{D}$.
- EXCLUSIVE OR, $\mathbf{B} \underline{\vee} \mathbf{D}$. The result preserves those attributes that are members of one set but not of the other, i.e. $(\mathbf{B} \cup \mathbf{D}) - (\mathbf{B} \cap \mathbf{D})$.
- NOT, !**B**. This operand involves only one set, the result will have as members only those attributes that are not members in the set before the operation, then $\mathbf{B} \cup !\mathbf{B} = \mathbf{A}$ or $!\mathbf{B} = \mathbf{A} - \mathbf{B}$.

Now we will use these operations to make sets operations such as equality and inclusion of sets that are used in rough sets analysis to eliminate superfluous attributes and search for coverings.

- Equality of sets, even when this operation does not require a logical operation, we can outline that

$$\mathbf{B} \underline{\vee} \mathbf{D} = \phi \qquad \text{if } \mathbf{B} = \mathbf{D} \tag{6.}$$

- Inclusion of sets. The test is performed as follows: $\mathbf{B} \underline{\vee} \mathbf{D}$ will show us those attributes in which the sets differ, if $\mathbf{B} \subseteq \mathbf{D}$ then only those attributes members of **D** but no-members of **B** will be included in the result; then $\mathbf{D} \vee \mathbf{B} \underline{\vee} \mathbf{D}$ will preserve members of both, the original **D** and the previous operation, thus if $\mathbf{B} \subseteq \mathbf{D}$ only the members of **D** will remain in the result.

$$\mathbf{B} \vee (\mathbf{B} \underline{\vee} \mathbf{D}) = \mathbf{D} \quad \text{if } \mathbf{B} \subseteq \mathbf{D} \tag{7.}$$

- Add elements to the set **B**. Given **D** a set whose members are those elements that will be added to the set **B**. **B'** will include elements in set **B** plus the new elements.

$$\mathbf{B'} = \mathbf{B} \vee \mathbf{D} \tag{8.}$$

- Remove elements from the set **B**. In a similar way the elements of **D** will be removed from **B** by using:

$$\mathbf{B''} = \mathbf{B} \,\&\, (!\mathbf{D}) \tag{9.}$$

- Calculate discernibility degree by **B**. Lets suppose a pair of examples i,j where the discernibility for **A** is described in $P_{i,j}$ (a row in the binary discernibility matrix) and a set of attributes $\mathbf{B} \subset \mathbf{A}$:

$$P_{i,j} \text{ is discernible by } \mathbf{B} \text{ if } \quad \mathbf{B} \,\&\, P_{i,j} \neq \phi \tag{10.}$$

  Now if we apply this operation with all the pairs of examples included in the concept (denoted $\mathbf{P_C}$), we can define the *discernibility degree* as the number of pairs of examples in $\mathbf{P_C}$ that the set **B** can distinguish, and is denoted as $dd_{\mathbf{B}}$.

- Find dispensable and indispensable attributes. Given $\mathbf{P_C}$ (all the pairs involved in the concept C) and a set $\mathbf{B_k} \subset \mathbf{B}$, such that $\forall\, P_{i,j} \in \mathbf{P_C}$, $(P_{i,j} \,\&\, \mathbf{B}) \neq 0$, we have
  - if $\forall\, P_{i,j} \in \mathbf{P_C}$, $P_{i,j} \,\&\, (\mathbf{B} \,\&\, !\mathbf{B_k}) \neq \phi$ then a_k is *dispensable* in **B** to discern pairs in concept C. (11.)
  - if $\forall\, P_{i,j} \in \mathbf{P_C}$, $P_{i,j} \,\&\, (\mathbf{B} \,\&\, !\mathbf{B_k}) = \phi$ then a_k is *indispensable* in **B** to discern pairs in concept C. (12.)
- Find coverings of the concept. Given a $\mathbf{B} \subset \mathbf{A}$, **B** is a covering if

$$\forall\, P_{i,j} \in \mathbf{P_C}, \quad (P_{i,j} \,\&\, \mathbf{B}) \neq \phi \tag{13.}$$

  and is considered a minimal covering if all $\mathbf{D} \subset \mathbf{B}$ are not coverings.

MINIMAL COVERINGS FINDING ALGORITHMS

Exhaustive search method

This method is a direct search starting from a single attribute and afterwards using combinations of two attributes, three and so on. Analysis of a given combination of attributes **B** is performed until the combination cannot distinguish a pair of examples (i.e. until a zero results from ANDing **B** and the rows in

the binary discernibility matrix). If all pairs are analyzed without obtaining zeros, then **B** is a covering. As the search begins from the simplest combinations, we know **B** is a minimal covering.

When a covering is found, all the supersets should be eliminated from the search space. Hence for each succeeding combination, we test if the covering is its subset. If so, the combination is not a minimal covering. The search finishes when all possible combinations are analyzed. Our problem is not reduced to find only one covering but *all minimal coverings*, or at least a *set of best coverings*. So we use a *covering pool* to save all the found coverings, and we use it also as a reference to skip analyzing supersets of existing coverings in the pool.

It is important to outline here that when inconsistent examples are found in a concept C and the lower and upper approximations were generated (i.e. $\underline{C}$ and $\overline{C}$), given the characteristics of these approximations, it is possible to search coverings for only the upper approximation of the basic concept. Then, in order to obtain the minimal coverings of the lower approximation, it is sufficient to test which elements of the covering pool for the upper concept are also coverings of the lower concept.

GA based method

The main stages of a GA-based method are described below and some important considerations for its implementation are mentioned [5].

In a GA, a population of *individuals* is used, each represents in a binary string a combination of attributes ($\mathbf{B} \subset \mathbf{A}$) which is considered a *possible covering*, then we evaluate each individual to determine if in fact it is a covering or, if not, how near it is from being one. Individuals are then selected by a polarized random process and recombined to produce new individuals which are expected to be better approximations, the process finishes when the stop criteria is satisfied, therefore the *coverings finding process* is expected to be faster than the exhaustive search.

Representation. Individuals in the GA population will be sets of attributes as presented before (see Fig.1), thus the length of individuals depends on the number of attributes. In this case it is also recommendable to have a covering pool besides the population and to use results stored in the pool instead of using the individuals of the last generation.

GA uses the first generation produced randomly, but a first generation composed of sets with just one attribute seems a better option in our problem, thus the first generation will analyze all single attribute combinations, this fact would save computational time. This single attribute sets evaluation will also assure a well oriented search of more complex combinations.

Evaluation. This stage is very important because a good evaluation of individuals will lead the search to good results. The evaluation of individuals is done through a fitness function and would be quite time consuming. We evaluate the fitness of a set B using the following fitness function, where $dd_{\mathbf{B}}$ is the degree of discernibility of **B**, $\mathrm{BDM}_{\mathrm{Ci}}$ is the numbers of pairs involved in the concept, n is the number of attributes and *length* is the set length measured as the number of members (ones) in the set (bit string).

$$f(\mathbf{B}) = \frac{dd_{\mathbf{B}}}{\mathrm{BDM}_{\mathrm{C_i}}} + \frac{n - length}{n-1} \qquad 14.$$

Selection. Once the population is evaluated, a polarized random selection should be done. We implemented two random sampling methods with similar results (i.e. roulette wheel method and SUS method [6]).

Crossover. After selecting the parents of the next generation, it is necessary to recombine them into new individuals. There are several methods proposed [5][7], the procedures are relatively easy and it is strongly recommended to implement some of them and evaluate their performance in a given problem, then we can use the best for a specific type of problem.

Mutation. An additional but important stage in the GA is the mutation of individuals which would be done at very low rates. We mutate a random individual complementing a random bit.

Stop criteria. The desired stop criteria to be used is when all minimal coverings were founded, it avoids waste of time or obtaining a sub-optimal solution, nevertheless in our case this criteria is difficult to implement and we do not have a method to prove it yet. Besides the traditional stop criteria at the n_g^{th} generation we stop when n_c coverings were found, this criteria lets us establish a size for the covering pool. Nevertheless, depending on the information system under analysis it may give non-minimal coverings. Based on the measures given in rough sets theory, we can use the accuracy of approximation or the quality of approximation as stop criteria [1], guaranteeing a minimal performance of classifications.

We have implemented this method for coverings finding but it has not been completely tested or evaluated.

CONCLUSIONS

The use of a matrix containing a binary representation for discernibility has been proposed and its characteristics and properties discussed. Some operations oriented to sets analysis in this representation are also presented.

This representation takes advantage of the implicit parallel processing over groups up to 64 bits to analyze groups of attributes at one time. A drawback of the method is the matrix size, then the approach is advantageous when solving problems with many attributes but relatively few examples.

We have tested and implemented the data preprocessing and covering finding stages, but the validation and comparison of this approach with traditional methods of Machine Learning is left for future work. Another important task is its implementation in an inductive learning approach which will enable us to update the rule set adding new knowledge.

REFERENCES

1. Z. Pawlak, 1989. Rough sets, theoretical aspects of reasoning about data. Kluwer Academic Publishers, 1991.
2. J. Wroblewsky, 1998. GA in decomposition and classification problems. In "Rough sets in knowledge discovery, v.2", L. Polkowski and A. Skowron. Physica-Verlag. 471-487.
3. J.W. Guan and D.A. Bell, 1998. Rough computational methods for information systems. Artificial Intelligence 105, 77-103.
4. J.W. Grzymala-Busse, J. Stefanowsky, W. Ziarko, 1996. Rough sets: facts versus misconceptions. Informatica 20, 455-464.
5. David E. Goldberg. Genetic algorithms in search, optimization and machine learning. Addison-Wesley Publishing Co. Inc.
6. Peter J.B. Hancock, 1995. Selection methods for Evolutionary Algorithms. In "Practical handbook of genetic algorithms, Volume II, New Frontiers". CRC Press. 67-92.
7. M.A. Pawlowsky, 1995. Crossover operators. In "Practical handbook of GA, Volume I, Applications". CRC Press. 101-141.
8. C.C.Chan, J.W. Grzymala-Busse, 1998. On the lower boundaries in learning rules from examples. In "Incomplete information: rough sets analysis". Physica-Verlag. 58-74.

Intelligence in the Design of Materials and Processes I

Intelligold - an Expert System for Gold Plant Process Design

Vanessa M. Torres* , Arthur P. Chaves, John A. Meech*****

* Companhia Vale do Rio Doce, Belo Horizonte, MG, Brazil
** Escola Politécnica da Universidade de São Paulo, São Paulo, Brazil
*** University of British Columbia, Vancouver, BC, Canada

ABSTRACT

Gold mining projects are a rare opportunity in the minerals industry. They require relatively small capital and give high profitability and fast return on investment compared with other mineral projects. To expand or maintain gold production, continuous development of new deposits and fast implementation of new mining sites are needed. Process design is one of the major issues. As simple and easily extractable ores are almost all exhausted, there is a need for a consistent approach to deal with increasing complexity and decreasing or stagnant gold prices. Process design must consider ore genesis, mineralogical characteristics, ore behaviour in available metallurgical processes, linkage with the mining method, environmental impact, and economic issues. The type of work and environment involved makes this application ideal for using AI tools such as Expert Systems, Fuzzy Logic and Neural Networks.

This paper presents **Intelligold**, an expert system for project development teams to use at the preliminary evaluation and conceptual project stages. Information and knowledge from geology/mineralogy, processing and economics are organized, and recommendations on process options and estimated costs and revenue are given. The "knowledge building" method is described, together with implementation and verification. Success in building this system suggests application to other ores such as copper and complex base metals.

INTRODUCTION

Evolution of a gold project is a dynamic activity [1]. To expand or maintain production, continued discovery of deposits and fast implementation of new mines are needed. After the rapid growth in gold production in the 80's, following significant price increases in the late 70's, the industry is now faced with low grade and/or complex ores [2]. We must optimise development from geological exploration through to production and commercialisation to reduce risk in making a poor decision. From the time of discovery until the first bar is poured, careful work and thought are needed. Input from the geology, engineering, architecture, economics, sociology and biology are needed over many years until start-up can occur.

There is a need for consistency to deal with the paradox of making a profit despite increased complexity and decreased or stagnant gold prices. Plant design must consider ore genesis, mineralogical characteristics, ore behaviour in available metallurgical processes, mining method, environmental impact, and economics. Uncertainty makes this environment ideal for Expert Systems, Fuzzy Logic and Neural Networks [3].

PROJECT DEVELOPMENT: IMPRECISION, RISK AND DECISION-MAKING

Success of a new mine depends on many factors. The answer to a simple question is key, "is it a 'good project'?" Unfortunately, the answer is far from simple, especially at the preliminary stages. The search for an answer is termed a "feasibility study": an interactive process to gather and evaluate information. Development is performed in gradual stages as follows:

- geological assessment
- mineralogical assessment
- ore behaviour assessment
- process and flowsheet selection
- equipment selection and sizing
- economic analysis

0-7803-5489-3/99/$10.00 ©1999 IEEE.

In the preliminary stages, information may be sufficient to classify the project as a bad one, but it is almost never extensive enough to ensure the project will be profitable. The boundary between a poor prospect and a good one is fuzzy: the prospect can be clearly poor (e.g. there is no gold in the ore, grade is too low, etc), possibly poor, possibly good and clearly good. Figure 1 illustrates these fuzzy concepts.

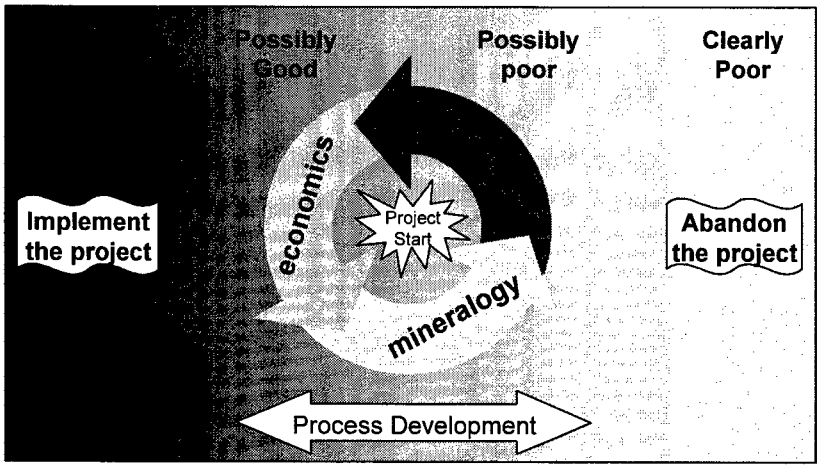


Fig. 1. Uncertainty of project development.

Technical feasibility with maximum precision is only possible when detailed engineering is complete. From the early stages of research, investment is needed and decisions are made to move on to the next development stage. Table 1 illustrates the characteristics of the development stages of a gold project.

Table 1. Development stages of a mineral project.

Phase of development	**Accumulated cost** (% total capital cost)	**Information available**	**Error in capital cost estimation** (estimated - actual)
Preliminary evaluation	negligible	very uncertain, "order of magnitude" evaluation	from +40 to –20%
Conceptual project	**0,6 to 1%**	**uncertain, yet sufficient to outline the main characteristics**	**from +20 to –12%**
Basic engineering	~ 10%	reliable geological and metallurgical data, basic layout and equipment sizing	from +15 to –10%
Detailed engineering	~ 100%	final geological and metallurgical reports, detailed layout and equipment specification	from + 7 to –5%

THE USE OF DIAGNOSTIC TOOLS FOR GOLD PROCESS PLANT DESIGN

The need to evaluate potential gold resources with increased accuracy in a timely fashion has lead to the development of diagnostic methods at many laboratories using standard procedures for cyanidation, flotation, gravity recovery and various leaching options [4]. Because of these efforts together with the evolution of new processes for refractory ores, gold processing can be considered a separate subject within the field of mineral processing. Good textbooks are available [5,6] and many papers appear each year describing technological breakthroughs. As process design is only one step in project evaluation, we have integrated relevant testwork with data from geology, mineralogy, economics and environmental issues. Our system is intended for multidisciplinary teams from the very beginnings of a new discovery.

AN EXPERT SYSTEM FOR GOLD ORES

An expert system for gold ores, **IntelliGold**, has been developed as a tool for project development teams to use at both the preliminary evaluation and conceptual project stages. Data and knowledge from geology, mineralogy, processing and economics are co-ordinated in the analysis. The two main system features are:

- an inference system able to suggest processing options for a specific ore and estimate costs and revenue even when the data are uncertain. The system establishes the main risk factors in each recommendation to point out areas for additional research. By using this tool, a development team can be directed towards solutions that are more likely to increase profitability and decrease risk of failure;

- a hypertext document containing state-of-the-art knowledge on gold processing and case studies for different ores and existing plant flowsheets, to provide easy access to the material and references.

The system is aimed at geologists, research engineers, project engineers and mineral economists involved in gold projects. It can provide feedback to each area individually, and assist an entire team when working together in a workshop. It can help evaluate prospect acquisition or joint ventures. Finally, the system can help train new professionals to the field.

From ore and deposit features collected during initial geological work, decision rules choose processing options. Unit operations are assembled and sized. With process routes defined, cost and revenue are calculated from existing models and/or historical data. Options are sorted as to their potential return and associated risk. The hypertext document can retrieve information on existing similar mines. The user decides which process to investigate further, or to abandon, hold or implement the project (see Figure 2).

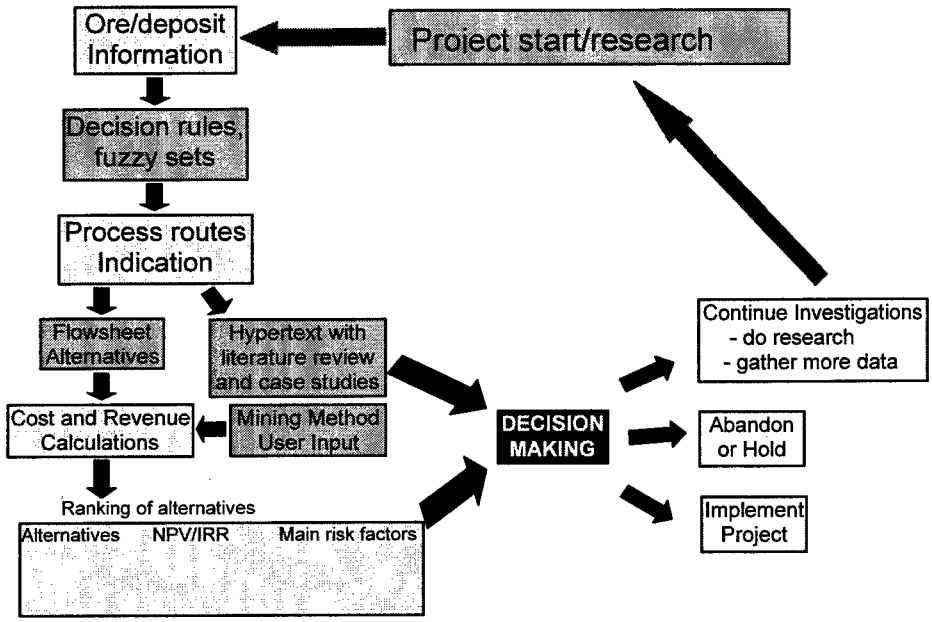


Fig. 2. System structure as perceived by the user.

We chose to use Comdale/X as the development tool for this project. This software tool defines variables as "keyword triplets", characterised by 3 elements: object, attribute and data type. Triplets are grouped into classes, which are organised hierarchically. Triplets can be numeric, string or fuzzy. Fuzzy triplets transform a numerical measurement into a facet called Degree of Belief (DoB) which varies between 0 (F) and 100 (T). Rules in the form of IF-AND-OR-THEN-ELSE are used to conduct inferencing [7].

IntelliGold has been developed as a series of modules, so the system naturally expands as new modules are developed and added. This approach allows future application to deal with other ores, such as copper, iron, lead/zinc and nickel.

Even if data are missing, the system can inference results from knowledge derived in a prior stage. As data enters the system, the DoB in a conclusion improves and the options decrease to 1 or 2 flowsheets.

Knowledge Building Structure

To provide a flowsheet based on ore mineralogical and metallurgical data, the system links information and knowledge in a way similar to human-reasoning. Information is represented by variables and knowledge by rules. The system contains ~1300 variables and 600 rules. Different information classes are identified:

- deposit type and geology;
- mineralogy;
- metallurgical behaviour;
- response of the ore for various processes;
- combination of processes into a process route.

Ultimately, ore behaviour defines the process to be used. Ideally, we would like to have all ore processing information, with all variables and scale-up factors pre-defined. To achieve this in the early development stages, we must infer, approximate, or, even guess, the process from geology, mineralogy, or preliminary testwork. The knowledge base rules that suggest unit operations and select process routes try to correlate aspects of geology, mineralogy and ore behaviour with the many processes available for gold ores.

The rules that link several aspects in each class are structured into layers, since many geological premises can indicate mineralogical characteristics, which in turn infers process behaviour, which then defines the processes to be tested. As more information is generated, more accurate predictions are derived. As testing progresses through ore behaviour and process determination, the system ultimately determines if the prospect is **poor** or **good** with reasonable belief. Figure 3 depicts the knowledge-building structure.

Inference and Feedback

As can be seen in Figure 3, each variable is a combination of inferencing and interpretation of experimental data. The system works from geology upward to process route selection accumulating and weighting information at each level. The weights used to combine inferred and measured variables are derived from the conditions under which the tests were done such as sample quality. The following situations can occur:

- **There is only an inferred certainty for a variable**: in this case, the combined belief is the average of the inferred value (which is different from 50) and default value (which is 50), and so, confidence in the variable is diminished since there is no measure to verify it;
- **There is only a measured certainty for a variable**: in the same way, belief is diminished because of a lack of reason for the measurement. However, the degree of amortisation is low if the weight of the measurement is high such as a good analysis on a representative sample;
- **The certainties of the measured and inferred variables are either both true or false**: combined belief lies between the measured and inferred triplets, depending on their respective weights;
- **The certainties of the measured and inferred variables are discordant:** -- combined belief tends toward that fact with the higher weight. The system alerts the user to the disagreement, which may be due to poor sampling, analysis error, incorrect grouping, etc., or an unusual deposit or ore.

Management of incompatible data is only one way the system feeds back variables. Feedback also comes from the economic analysis which is applied after the flowsheet design stage.

Geology to Mineralogy Inference

Mineralogical inferencing is based on the characteristics of most common gold deposits. The classification of Marsden [5] was used for ore types while, for deposit types that proposed by Paterson [8] was chosen.

Classification of deposit types is driven by ore genesis, i.e., geological issues. On the other hand, ore types are classified by mixed geological/mineralogical characteristics of the ore and, in the case of "free-milling" ores, behaviour during cyanidation is determinant. The term **deposit type** is the terminology of field geologists while **ore type** is the language of petrographic geologists or mineralogists. A literature review on gold deposits and projects was performed to derive common ore characteristics for a given **ore type** or **deposit type**, resulting in typical ores for each classification. Of course, there are deposit types in which several ore types may occur. In these cases, the system gives several options, but with low belief. Inferred mineralogy is combined with experimental observations using the weighting method described above.

Mineralogy to Behaviour Inference

The inference of ore behaviour aims to correlate mineralogical variables and ore metallurgy. The approach is consistent since the objective of all processing plants is to modify ore mineral properties to effect separation and then, to perform selective destruction to extract valuable elements (gold). The system uses rules derived from interviews with experts, the authors' experience and a literature review to instantiate inferred behaviour variables. An important issue is metallurgical testwork. **IntelliGold** interprets numerical data into linguistic expressions that characterize process behaviour. The system uses interpretation rules for laboratory/pilot tests on major unit operations such as comminution, gravity processing, cyanidation, flotation, diagnostic-leaching, pre-oxidation and solution purification/Au recovery.

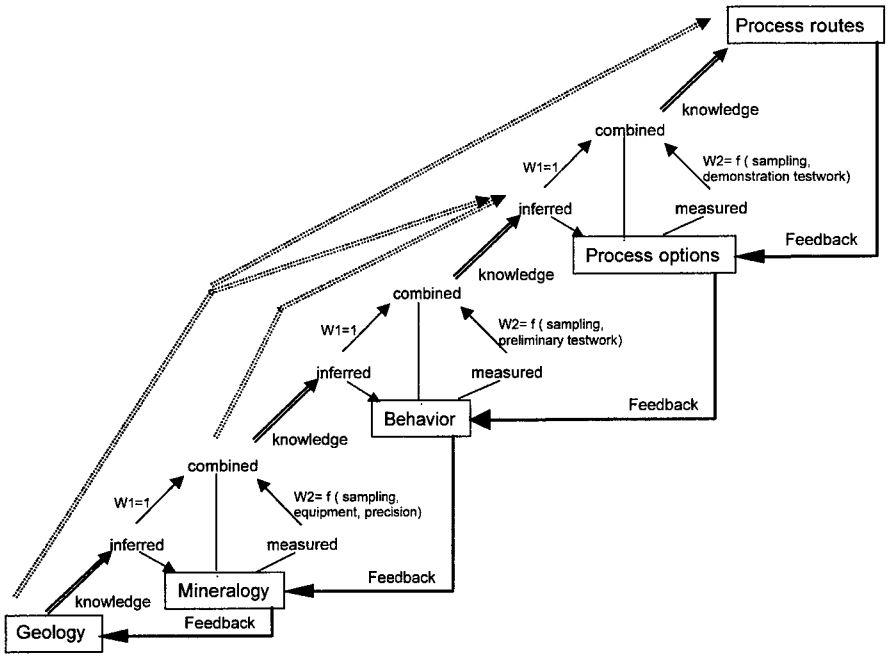


Fig. 3. Knowledge-Building Structure.

Selection of Industrial Processes

Once basic ore behaviour is established, the system selects the industrial processes to be applied to the ore. The selection of industrial processes considers metallurgical behaviour together with general guidelines such as typical gold recovery, throughput and head grade ranges.

Selection of Process Routes and Flowsheet Design

IntelliGold continues its consultation by building flowsheet options. To accomplish this, the system uses a combination of rules and default values to select unit operations from primary comminution through to gold smelting. The system defines different flowsheet "options" since more than one alternative may be possible.

It is important to enter the economic evaluation module with more than one flowsheet, since final choice depends on economic, political and environmental factors. The user must be shown more than one feasible option, since site-specific factors unknown to the system may add more certainty to one specific flowsheet.

Metallurgical Report and Flowsheet Drawing

The final step in the process selection module is the report generation and flowsheet drawing procedure. All input data and results generated during the consultation are arranged within a hypertext report. The user can browse through the report, go to a specific page or print the report. Using rules and graphical files, the system is able to draw a flowsheet representing each possible ore process selected by the system. The flowsheet is designed as a series of block diagrams, each of which represent a specific unit operation. By clicking on a unit operation, users can search the hypertext document for details on each unit operation, equipment sizes, possible problems, and a picture of an actual unit. Flowsheets are generated as in Figure 4.

Economic Evaluation of Process Routes

Recommended processes are input to the economic module. The module calculates capital and operating costs for each unit operation, using actual costs and adjustment factors to correct for inflation (using the M&S index), location, tonnage rate or plant size, availability of salvaged equipment, etc.

The system determines project revenue from reserve size, estimated throughput, gold grade and recovery. Net Present Value and Internal Rate of Return are generated from the cost and revenue data. The main source of uncertainty and project risk are identified and the user is shown which testwork parameters must be confirmed, optimised or reviewed. This provides feedback on process behaviour and flowsheet design.

Management of Contradictions
An important feature involves management of contradictions. A contradiction is found when inferred and measured conclusions are discordant, or, using a fuzzy logic definition, when the difference between their DoBs exceeds 50%. A contradiction occurs when:

- facts cause rules to fire that give two or more possible scenarios. Then, when the system considers measured data, only one or some of these conclusions are confirmed;
- facts cause rules to fire which give a single possibility that is denied by measured information.

In the first case, there is no need to adapt the system, since narrowing existing possibilities using additional data is an expected, natural outcome of the reasoning process. In the second case, it is important to manage such a contradiction, especially if it involves key elements. This type of contradiction occurs when:

- the information available is inconsistent for a wide variety of reasons;
- the rules that instantiate the inferred variable are incorrect or incomplete;
- the specific ore is an exception to the rules because of incomplete knowledge in the system.

Users can review the measured data. If a contradiction exists after this "correction", the system examines how and why an inference was made, providing another opportunity to adjust the model. If conflict still persists then the rule base is incomplete or the case is an exception. The system allows data weights to be changed to prioritize more reliable data. Such adjustments are noted to allow a developer to study the likelihood of new knowledge about certain data combinations. Contradiction management is done for "key" process selection facts, such as "the ore is refractory" or "free gold is available for gravity concentration".

Justification for Process Choice
Justification of each process choice is also important as it pinpoints the reasons and factors that lead the system to its conclusions. This was implemented by adding reasons why each rule fires in the form of text variable. At the end of a consultation, the main factors used and concluded at each level of inference are presented to the user in a hypertext report with output and the appropriate rationale for each conclusion.

System Validation
Case studies of existing plants and simulated cases analysed separately by experts show the system can identify different deposit types and the effect of mineralogy on metallurgical behaviour (see Table 1). Inferred behaviour is refined with added data, as seen for Fazenda Brasileiro mine and the Carlin-type deposit. The Witswatersrand case shows two inferred options which can be verified later through testwork.

CASE STUDY: FAZENDA BRASILEIRO MINE

System verification was also performed by simulating a complete feasibility study on an existing mine. Fazenda Brasileiro is one of the major gold mines operating in Brazil, with an annual production of 5 tons of gold. It started operation in 1985. To simulate the design process, only geological and metallurgical preliminary reports dated 1982 were used to provide system input. The input data is presented below:

With these inputs, the system generated the flowsheet depicted in Figure 4. The suggested process route is very similar to the actual flowsheet at Fazenda Brasileiro mine. In fact, the process implemented in 1985 initially used Cyanidation and CIP instead of CIL to extract the gold but, in 1995, the plant was converted to CIL after comparative testwork showed CIL gave higher Au recovery. The grinding circuit is also different as it uses finer crushing with more stages to feed a ball mill directly which, at the time of implementation, was a more conservative and appropriate approach. Today, with the evolution and success of SAG grinding, this would be the preferred choice.

CONCLUSION

Development of an expert system to design processes for gold ores is justified for the following reasons:

- process design is an important issue in gold projects as it affects both technical and economic feasibility of exploiting an ore. Co-ordination of data and people needed to conduct the design is often difficult since information is uncertain and not all "experts" are available at one time and place;

- knowledge of gold processing options can be critical in providing input to the early decision-making to continue to explore and to evaluate the prospect.

IntelliGold was developed to provide a consistent methodology to integrate information from different areas of project development and to estimates and infer possible process options. The system aims to give a basis for decision-making during the initial project stages even if information is incomplete or unavailable.

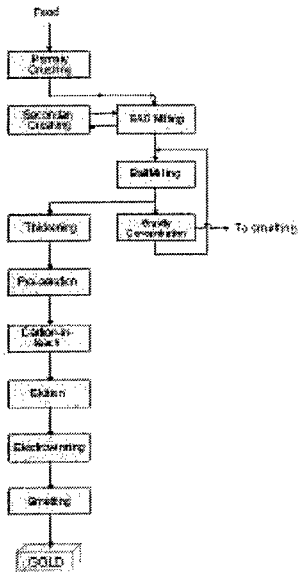


Fig. 4. Flowsheet generated for Fazenda Brasileiro by **Intelligold**.

ACKNOWLEDGEMENT

The authors would like to thank their supporting institutions and organisations: The University of British Columbia, Escola Politécnica da Universidade de São Paulo and Companhia Vale do Rio Doce.

REFERENCES

1. Nardi, R.P., 1996. Revisão crítica do circuito de cianetação de Fazenda Brasileiro. São Paulo, Escola Politécnica da Universidade de São Paulo, (Qualifying examination).
2. Torres, V. M., 1996. Diagnóstico de Lixiviação para Minérios de Ouro. São Paulo, Escola Politécnica da Universidade de São Paulo, dissertation (M.Sc.).
3. Meech, J.A., 1992. Managing uncertainty in expert systems - a fuzzy logic approach. in: 31st CIM MetSoc. Conf. Proc., Edmonton, 77-85.
4. Lorenzen, L., 1995. Guidelines for designing a diagnostic leach experiment. Min. Eng., 8(3), 247-256.
5. Marsden, J., House, I., 1992. The chemistry of gold extraction. London, Ellis Horwood Limited.
6. Yannopolous, J.C., 1991. The extractive metallurgy of gold. New York, Van Norstrand Reinhold.
7. Meech J.A., Kumar, S., 1996. A hyper-manual on expert systems v. 5.0. CANMET, (electronic book).
8. Paterson, C.J., 1990. Ore deposits for gold and silver. Min. Process. & Extract. Met. Rev. 6, 43-66.

Table 1. Input Data for Case Study on Fazenda Brasileiro.

Input information	
Geology	Probable type of deposit: archean greenstone belt gold-quartz veins (100%) Probable type of ore: Free milling (70%); Fe and As sulphide bearing (90%)
Mineralogy	Chemical analysis: 2% As, 10% Fe, 2% S, 8.4 ppm gold Mineralogical analysis: 2% Arsenopyrite, 30% Oxides, 1% Pyrite, 60% Quartz Au characterisation: equipment: optical microscopy/electron microprobe; particle size (d_{95}) = 37 μm; particle location: border (70%), fractures (100%), encapsulated (20%); shape: amorphous; association: Fe/As sulphides/quartz.
Metallurgical Testing	Gravity concentration test with ground sample (d_{80} = 0.090 mm): 55% recovery using a Knelson-type Concentrator; Cyanidation testwork with ground sample (d_{80} = 0.090 mm): 95% recovery with 800 g/t NaCN, 6 hr. pre-aeration, 24 hr. leaching; Flotation testwork with ground sample (d_{80} = 0.090 mm): 95% gold recovery and 10% weight recovery
Throughput and Grade	Estimated gold grade of 5 g/t and plant throughput of 3200 t/day

Table 2. Case studies used to validate the inference of process behavior from mineralogy.

Case Study	Input - geology	Input – mineralogy	Inferred behaviour
Fazenda Brasileiro (real case without mineralogical information)	**Deposit type:** archean greenstone belt, quartz veins **Ore type:** Fe-sulphide bearing (80%) As-sulphide bearing (80%)	None	**gold is cyanidable if ground (78%)** floatable for preconcentration (78%) gravity recoverable if ground (61%) high cyanide consumption (75%) **some gold refractoriness (67%)** refractory types: encapsulation As- and Fe-sulphides (100%) pyrrhotite/oxides/carbonates (75%)
Fazenda Brasileiro (real case with mineralogical information)	**Deposit type:** archean greenstone belt, quartz veins **Ore type:** Fe-sulphide bearing (80%) As-sulphide bearing (80%)	Sample is representative (80%) **Chemical analysis:** 2 %As, 10 %Fe, 2 % S, 8.4 g/t Au (S.D. =0.2) **Gangue mineralogy:** 1% pyrite; 2% arsenopyrite; 30% quartz; 60% oxides **Equipment used for mineralogy:** optical microscopy + microprobe **Gold Mineralogy:** particle size (d_{95}): 37 μm; gold in fractures, borders (70%); encapsulated (20%); individual (50%); with sulphides and quartz (70%) amorphous shape;	**gold cyanidable if ground (true)** floatable for preconcentration (True) gravity recoverable if ground (57%) high cyanide consumption (69%)
Carlin-type deposit (hypothetical case with carbonaceous ore)	**Deposit type:** epithermal gold-silver sediment hosted **Ore-type:** carbonaceous	None	**gold cyanidable if ground (64%)** high cyanide consumption (75%) weak preg-robbing effect (70%) floatable for preconcentration (64%) **some gold refractoriness (70%)** refractory types: carbonaceous, pyrite, arsenopyrite
Carlin-type deposit with carbonaceous ore type and information that Au is encapsulated	**Deposit type:** epithermal gold-silver sediment hosted **Ore-type:** carbonaceous	Sample is representative (80%) **Gold Mineralogy:** encapsulated gold (100%), no gold in borders, fractures or individual particles	**gold cyanidable if ground (59%)** high cyanide consumption (69%) weak preg-robbing effect (65%) floatable for preconcentration (59%) **total gold refractoriness (92%)** partial gold refractoriness (65%) refractory types carbonaceous, pyrite, arsenopyrite
Witswatersrand type deposit	**Deposit type:** paleoplacer quartz-pebble conglomerate **Ore type:** free milling	None	**gold cyanidable if ground (79%)** **gold is gravity-recoverable (78%)**

(Note: if no measured behaviour is available, the combined degree of belief will be the average of the DoB in brackets and 50%)

A Hardware Design for Real-Time Multiple Target Tracking

Frederick Ferguson and Chandra Curtis

Center for Aerospace Research, North Carolina A&T State University
Greensboro, NC 27411

ABSTRACT

This paper describes the use of a simulated real time system of a feed-forward neural network, a recurrent neural network and a set of expert rules in solving the problem of Multiple Target Tracking. It is assumed that data is provided in the from of blips, taken off 3 consecutive focal plane arrays, operating at visible or infrared wavelengths. In this paper, the task of multiple target tracking is transformed from one of blip-frame data association to one of target clustering, which in turn is broken down and solved in four stages. Each stage is described and mapped with the use of a feed-forward, a recurrent neural network or a set of fuzzy rules. The first and second stages of the solution procedure involve the use of two feed-forward neural network modules, while the third and forth stages use a recurrent neural network module and a set of expert rules module. The Multiple Target Tracking solution procedure is simulated through use of a FORTRAN Code. In principle the number of targets that can be tracked with the routine is unlimited. However, in reality, the number of targets is dictated by the number of neurons, which in turn is constrained by hardware requirements. Software simulation results shows that the Multiple Target Tracking code is capable of tracking an arbitrary number of targets very efficiently. The program was tested and debugged for use in the tracking of sets of multiple targets; ranging from 2 to 14. Results indicated that once the average acceleration of the targets is adequately evaluated, track files could be developed with 100% accuracy.

INTRODUCTION

Air and Missile Defense, and Battlefield Awareness face unprecedented challenges in target detection and tracking. Traditional single-sensor systems experience unacceptable performance degradation when dealing with multiple targets in the highly mobile environment in which today's forces must operate. New developments in multiple sensor data fusion are addressing many of these issues and advanced techniques, such as pre-detection tracking, context-sensitive data association and tracking, adaptive data fusion and tightly-coupled fusion and sensor management, are under development.

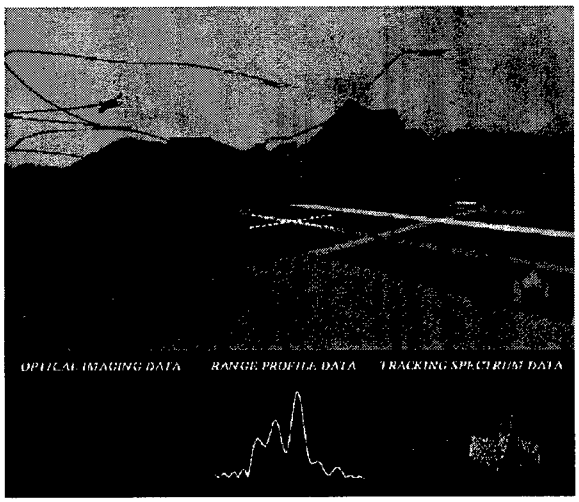


Fig. 1. A Typical Multiple Target Problem [1-3].

0-7803-5489-3/99/$10.00 ©1999 IEEE.

One of the key functions performed by a surveillance system is to keep track of all targets of interest within the coverage region of its sensors. For military surveillance systems, the coverage region generally involves several thousand cubic miles containing several hundred targets. The sensors available for use in these surveillance systems operate at visible or infrared wavelengths, and cannot provide perfect information about all targets. In general, sensor measurements of targets tend to be ambiguous, (lack of knowledge as to which target was reported), incorrect (reports of false targets), and imprecise (random errors in the measurements) [4]. A typical multiple target-tracking scenario of interest to our defense forces is illustrated in Figure 1.

A BRIEF REVIEW OF MULTIPLE TARGET TRACKING RESEARCH

Multiple target tracking (MTT) is an essential requirement for surveillance systems employing one or more sensors together with computer subsystems in order to interpret an environment that includes both true targets and false alarms. The objective of MTT [1-6] is to partition the sensor data into sets of observations or tracks produced by the same source. The crux of MTT is to carry out data association process of measurements whose origin is uncertain due to one or all of the following reasons:

i. random false alarms in the detection process;
ii. clutter due to spurious reflectors or radiators near the target of interest;
iii. interfering targets;
iv. decoys or other counter measures.

The three basic methods for data association are as follows [1-8]:

i. Nearest Neighbor (NN) method, which is computationally efficient but unreliable for tracking targets in a highly cluttered environment.
ii. Joint Probabilistic Data association (JPDA), which has its own shortcomings. In tracking closely spaced targets, JPDA delivers poor performance because of the persistent interference from neighboring targets. Also, when the problem size increases, the required computation increases exponentially.
iii. Multiple Hypotheses Tracking (MHT), which is a multiple scan method and both the memory and computation requirement of which increase exponentially with problem size.

At the Center of Aerospace Research at North Carolina A&T State University research in MTT has been focused on the NN method. Sensor data is provided in the form of blips, taken off three consecutive focal plane arrays, operating at visible or infrared wavelengths. A typical RF-communication unit capable of providing the required data and currently used to characterize sea and surface targets, is illustrated in Figure 2. Our goal is to develop an algorithm that simultaneously traces the paths described by multiple targets in

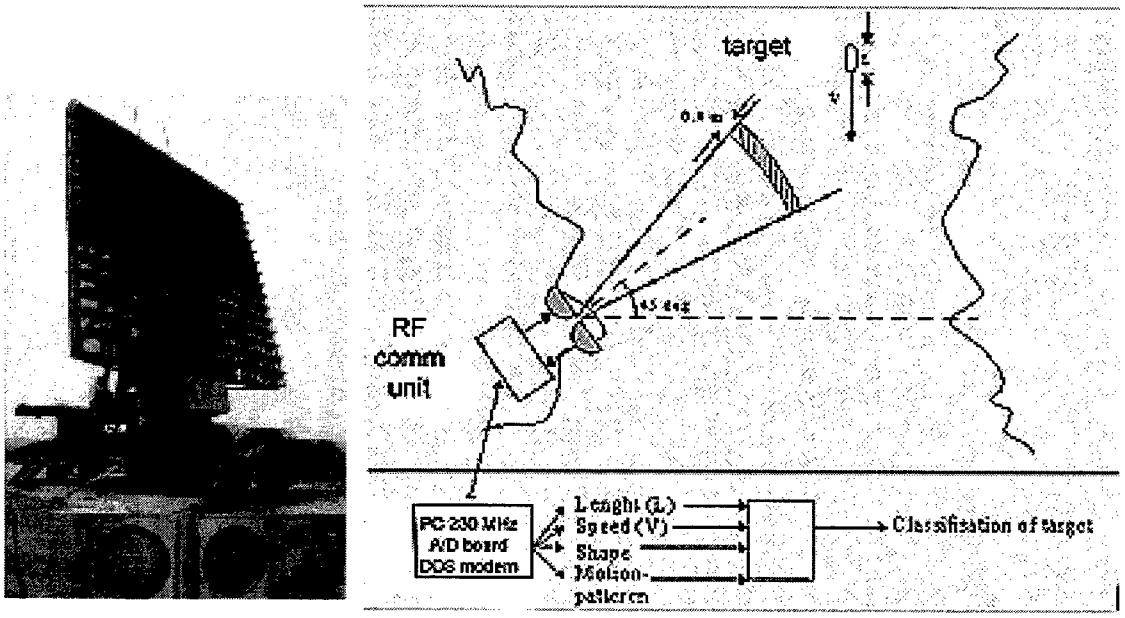


Fig. 2. A typical RF-communication unit used to characterize sea and surface targets.

real time as they traverse a given domain. The algorithm of interest to this study involves the use of the following paradigms; a feed-forward neural network, a recurrent neural network, and a set of fuzzy rules. An interesting advantage of this algorithm is the fact that it can be configured on Digital Signal Processors and used in real time applications.

REAL-TIME MULTIPLE TARGET TRACKING

In a multiple target environment surveillance systems are faced with the prospect of identifying and tracking individual targets, based on models developed from sensor reports and target kinematics. The best choice of target and sensor models will depend on specified missions or applications. Nevertheless, regardless of the choice of sensors and target models, the bottom line capability of any reasonable multiple target tracking algorithm is its ability to trace the appropriate location of all objects of interest over specified time intervals. In general, a simplification of the problem of multiple target tracking can be described as shown in Figure 1.

Over time, target indications move across the field of view of the sensor, and it is required the targets be clustered by their location. To accomplish this task, any multiple target-tracking algorithm must identify, discriminate and locate all targets of interest at specified time instances. However, sensors can only provide focal plane array data of ambiguous targets or blips, i.e., the lack of specific knowledge as to which target was reported, at discreet time intervals. In this analysis, it is also assumed that information on the target location (x, y, z) and target speed with a time resolution of 1/50 second. Available systems [1-4], as illustrated in Figures 1 and 2, capable of delivering these requirements are available off the shelf. Moreover, the surveillance system illustrated in Figure 2 can deliver information on target length, shape, speed, internal motion, sea spectrum and estimated weight. The most common sensors of this type are focal plane arrays, operating at visible or infrared wavelengths. In this paper, it is assumed that each target will be tracked in a 256x256 focal plane array, which can be represented by the Cartesian system of coordinates in the form of blips. A proposed field of view, which includes hardware assembly and data frame, is illustrated in Figure 3.

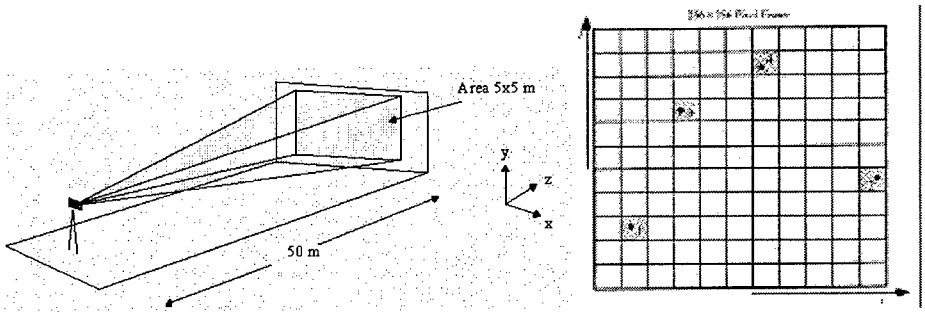


Fig. 3. Illustration of Observation Domain.

The type of preprocessing that is necessary depends greatly on whether the input blip data is already ordered in some fashion. Typical focal plane imagers come out in row scan order. In this paper it is assumed that blip data is extracted and labeled from each pixel, based on the rule of fixed row with varying columns. Only the pixels containing objects are labeled. Results of the blip/frame data extraction using this method are illustrated in Table 1.

Table 1: Typical Ambiguous Data Clusters

Blip Label	Blip_x Location	Blip_y Location
1	X_1	Y_1
2	X_2	Y_2
...	...	...
n	X_n	Y_n

DATA PROCESSING DURING MULTIPLE TARGET TRACKING

The task of real time multiple target tracking is equivalent to the re-organization of the input blip/frame data into track files. The mapping of input to output is based on the use of three very important mathematical paradigms, namely, the feed-forward neural network, the recurrent neural networks, and a set of fuzzy rules. The uses of these paradigms in the multiple target tracking algorithm presented herein is described in the following five sub-sections. The mapping of the input data to track files, and the details of the mapping process are illustrated in Figure 4.

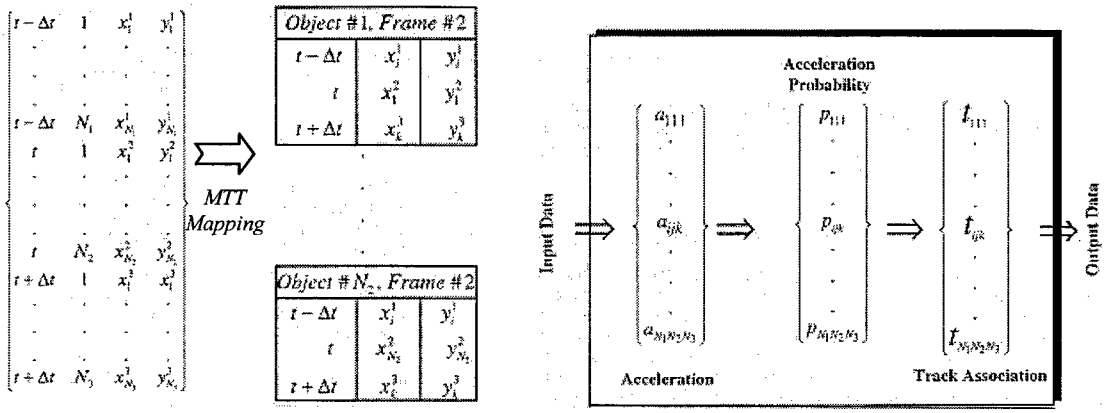


Fig. 4. The three stages of input to output MTT data mapping.

Elementary Data Unit for Multiple Target Tracking

The algorithm described herein is based on 3 frames of data, which is provided by a sensor capable of mapping a two-dimensional image of the observation. No depth information is needed, only speed and/or acceleration. Figure 5 illustrates a single data plane, and its use with a previous and past neighbors forming a basic unit of three consecutive data frames from which appropriate track files are developed.

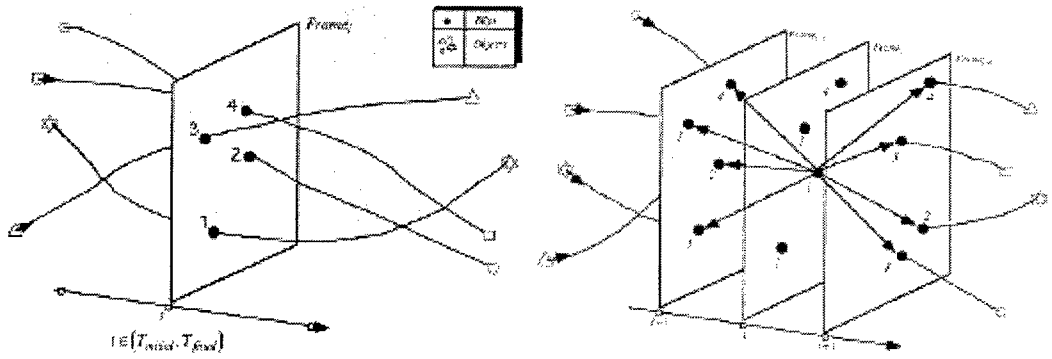


Fig. 5. Consecutive arrays of ambiguous targets.

Track files contains information about the targets and their location history. The successful tracking of a given target specified by the i^{th} blip in frame^2, involves the identification of two corresponding blips located in frame^1 and frame^3 respectively. When i^{th} blip in frame^2 combines with the identified blips in frame^1 and frame^3 the result is the most likely path of the target for the duration of time, *t-dt,* through time, *t+dt.*

Notation Convention for the Multiple Target Tracking Process

In figure 5, and through out this paper a convention on the use the indices *i, j,* and *k* is adopted. The indices *i, j,* and *k* are such, that, *i, i = 1, N_1;* represents any blip in frame[1], at time *t-dt; k, k = 1, N_2* represents any blip in frame[2], at time *t;* and *j, j = 1, N_3,* represents the blips in frame[3], at time *t+dt.* Besides, the indices, *i, j,* and *k* carry a special implication when used with the coordinate of a vector. Under the terms of this convention any parameter or variable labeled by the indices, *i, j,* and *k,* refers to all of the possible combination of the three indices as they vary independently from their minimum to maximum values. As a result any parameter labeled by the indices, *i, j,* and *k,* refers to a vector of $n_1n_2n_3$ coordinates. A coordinate of the vector described by the indices, *i, j,* and *k,* will be described by the expression, $P_{m;ijk}$, where the index *m* varies from *1* through $n_1n_2n_3$.

The notations adopted in this analysis are outlined as follows:

***Convention # 1**: P_{ijk} = vector of $n_1n_2n_3$ coordinates*

Convention # 2: $P_{m;ijk}$ = m^{th} coordinate of vector P_{ijk}

Acceleration and Probability Mapping with Feed-Forward Neural Networks

In this analysis it is assumed that the time interval between frames is uniform, and moreover, that the frame rate is high enough so that differentiation can be conducted by finite differences. With these assumption, the velocity vector, V, can be evaluated with any two consecutive frames, using the expression,

$$\mathrm{V}_{jk} = \mathrm{L}_k - \mathrm{L}_j \qquad 1.$$

Vector, **L**, represents the two dimensional blip coordinates, *x* and *y*. The indices *i, j,* and *k* represents the appropriate frames in which the coordinates are taken. On the other hand, the acceleration vector, $\mathbf{A}_{ijk}$, is evaluated with three frames, using the expression,

$$\begin{aligned} \mathrm{A}_{ijk} &= \mathrm{V}_{jk} - \mathrm{V}_{ij} \\ &= \mathrm{L}_k - 2\mathrm{L}_j - \mathrm{L}_i \end{aligned} \qquad 2.$$

In the expressions given in equations (1 - 2), the notation convention adopted earlier is used. The acceleration vector, $\mathbf{A}_{ijk}$, consists of $n_1n_2n_3$ coordinates, each of which is evaluated using one of the possible combinations of the indices, i, j and *k.* It is of interest to note that the vectors, **L, V** and **A**, are described by 1, 2, and 3, subscripts, respectively. This fact indicates that whereas, the velocity vector can be described by only 2 frames, the acceleration vector must be described with the use of 3 frames.

Since this analysis deals with the 'angle-only' or the two dimensional model for target tracking, the acceleration vector, **A**, has two components, one along each axis in the Cartesian system of coordinates. As a result, the evaluation of the acceleration vector, $\mathbf{A}_{ijk}$, can be conducted with the aid of two feed-forward neural network modules, as follows

$$\mathrm{A}_{ijk} = \sqrt{\left(\mathrm{a}^{x}_{ijk}\right)^2 + \left(\mathrm{a}^{y}_{ijk}\right)^2} \qquad 3.$$

Parameters, $\mathbf{a}^{x}_{ijk}$ and $\mathbf{a}^{y}_{ijk}$, represent the components of the acceleration vector. Equation (3) can be evaluated with the use of a single feed-forward neural networks. However, for real time on board analysis, two neural networks module are recommended.

Probability Mapping with Feed-Forward Neural Networks

The kinetic model used in this analysis is based on the acceleration association probability. Having a priori determined a mean acceleration value, $\overline{\mathrm{A}}$, for the targets of interest, the normal probability density function for the acceleration vector gives,

$$P = e^{-(A-\bar{A})^2} \qquad 4.$$

The vector **P** will be referred to as the acceleration association probability vector. Again, in expression (4), the notation convention adopted earlier is used. The acceleration association probability vector **P**, consists of $n_1n_2n_3$ coordinates P_{ijk}, each of which is evaluated using one of the possible combinations of the indices, *i, j* and *k*. Evaluating the acceleration association probability coordinates can be accomplished real time with the aid of a feed-forward neural network module.

Track Association using Recurrent Neural Networks

The recurrent neural network is merely a single layer feed-forward network with feedback connections of the network output channels bridging its input channels. The dynamics of the recurrent network is equivalent to the evaluation of an equation of the type, described by the following equation:

$$t_{ijk}^{s+1} = g\left(\sum_{l=1}^{n_1n_2n_3} w_{lm} t_{m;ijk}^{s}\right) + p_{ijk} \qquad 5.$$

where the variables; w_{lm} represents the network weights, $P_{m;ijk}$ the input acceleration probabilities, t^s_{ijk} the track association vector and the function, g, represents the nonlinear activation or threshold function used in this analysis. Once again, the notation convention adopted earlier is used in equation (5). In this report the threshold function takes the form of a piecewise linear sigmoid function.

The very first thing to be defined when using the recurrent neural network is the network weights. Typically, the network weights are determined by differentiating the network energy, *E,* or cost function with respects to the acceleration association probability. The shape and state of this energy function is determined by the network initial input and the interconnection constraints and strengths of its neurons, as follows:

$$E = \beta \sum_{ijk} \sum_{i'j'k'} t_{ijk} t_{i'j'k'} \chi\left(\delta_{ii'} \delta_{jij} \delta_{ki'}\right) + \alpha \sum_{ijk} p_{ijk} t_{ij'k'} \qquad 6.$$

Here t_{ijk} represents the tracks, p_{ijk} defines the probability of the *ijk* track, δ_{jj} is the Kronecker Delta function, α and β are the optimization parameters and χ is the Exclusive OR function. The Exclusive OR function, χ, is defined as follows

$$\chi(x,y,z) = \begin{cases} 1; & if \begin{cases} x,y=1, & z \neq 1 \\ x,z=1, & y \neq 1 \\ y,z=1, & x \neq 1 \end{cases} \\ 0; & otherwise \end{cases} \qquad 7.$$

When equation (7) is twice differentiated with respect to $t_{m;ijk}$, the appropriate weights to the recurrent neural network is found in the form,

$$w_{lm} = -\beta \left[\chi\left(\delta_{ii'}, \delta_{jj'}, \delta_{kki'}\right)\right]_{l;ijk}^{m,i'j'k'} \qquad 8.$$

The range of values for β used in this analysis is: $0 < \beta < 0.50$. Once activated the network converges toward a minimum of the energy function in which some neurons are on and others are off. The set of neurons that are on at convergence represents the group of tracks that are part of a final solution. Within the context of the multiple target tracking problem, the network weights also enforces the constraints of having one corresponding blip per frame per track.

Association Probabilities to Track Files Mapping

Once activated the recurrent neural network converges toward a minimum of the energy function, *E*, in which some neurons are on and others are off. The set of neurons that are on at convergence represents the

group of tracks that are part of a final solution. At convergence the track vector, t_{ijk}, of $n_1n_2n_3$ coordinates will have values clustered around the values of zero and one. Only the coordinates with values that are clustered in the upper range are of interest. The next step in the evaluation process is to identify the coordinates with values that are clustered in the region of unity and represents these tracks in terms of targets located in frames 1, 2, and 3.

TECHNICAL RESULTS

When properly initiated the simulated real time multiple target tracking accepts data in the form of 3 consecutive blip-frame data sets. The data is processed and track files are developed. A FORTRAN Code was developed to simulated the functions of the two feed-forward neural networks, the recurrent neural network and the set of expert rules modules. The code for multiple target tracking is program according to the flow chart illustrated in Figure 4. Results from observing the tracking algorithm at work with four objects on a 256x256 focal array plane over 30 frames are illustrated in Figures 6. As indicated by these results the multiple target-tracking algorithm is capable of tracing very complex movements, even when there are crossover in motions.

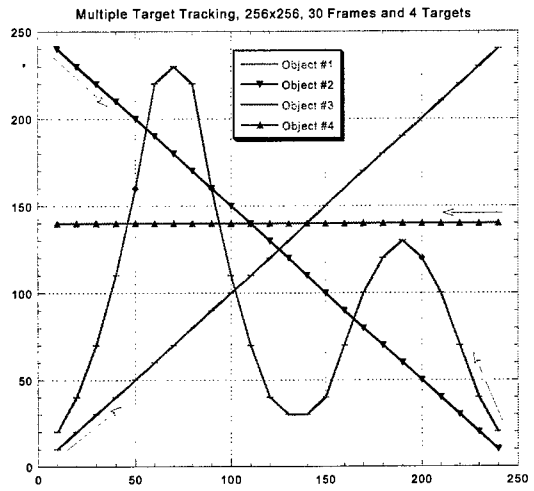


Fig. 6. Results from tracking four targets.

In principle the number of targets that can be tracked with this algorithm is unlimited. However, in reality, the number of targets is dictated by the number of neurons, which in turn is constrained by hardware requirements. Software simulation results showed that the MTT algorithm is capable of tracking an arbitrary number of targets very efficiently. The program was tested and debugged for use in the tracking of sets of multiple targets; ranging from 3 to 14. Preliminary results indicated that once the average acceleration of the targets is adequately evaluated, track files can be developed with 100% accuracy.

REFERENCES

1. R.E. Bethel, and G.J. Paras, A PDF Multisensor Multitarget Tracker. *IEEE Log No. T-AES/34/1/00185*
2. D.R. Zahirniak, D.L. Sharpin and T.W. Fields, A Hardware-Efficient, Multirate, Digital Channelized Receiver Architecture. *IEEE Log No. T AES/34/1/00184*
3. P.E. Pace, B.H. Nishimura, W.M. Morris and R.E. Surratt, Effectiveness Calculations in Captive-Carry HIL Missile Simulator Experiments. *IEEE Log No. T-AES/34/1/00183*
4. E. Mazor, A. Averbuch, Y. Bar-Shalom and J. Dayan, Interacting Multiple Model Methods in Target Tracking: A Survey. *IEEE Log No. T-AES/34/1/00182*
5. B. Armstrong and B.S. Holeman, Target Tracking with a Network of Doppler Radars. *IEEE Log No. T-AES/34/1/00176*
6. R. K. Saha and K. C. Chang, An Efficient Algorithm for Multisensor Track Fusion. *IEEE Log No. T-AES/34/1/00189*

7. I Ishii, Y. Nakabo and M. Ishikawa, Target Tracking Algorithm for 1ms Visual Feedback System Using Massively Parallel Processing. *IEEE Int. Conf. Robotics and Automation (Minneapolis, 1996.4.25)/Proc. IEEE Int. Conf. Robotics and Automation*, pp.2309-2314
8. J.F. Pusztaszeri, P.E. Rensing and T.M. Liebling, 1996. Tracking elementary particles near their primary vertex: a combinatorial approach. *Journal of Global Optimization,* 9: 41-64.

Low-Cost Supersonic Missile Inlet Fabrication Technique

C.S. Cornelius*, D.A. Gibson**

*U.S. Army Aviation and Missile Command
Missile Research, Development, and Engineering Center
Redstone Arsenal, Alabama USA
**Nichols Research Corporation, Huntsville, Alabama USA

ABSTRACT

This paper presents a technique that allows for the fabrication of complex shapes to high accuracy without the expense of conventional machining. The savings associated with using this new approach over conventional fabrication methods directly resulted in an 85% reduction in fabrication costs. This technique was demonstrated in the fabrication of supersonic inlets for a ramjet engine missile. A single computer aided design (CAD) model was used for design and hardware integration, generation of the rapid prototyping computer file for producing a mandrel, finite element modeling of the inlet, development of the final machining tools paths and inspection of the mandrels and finished inlets. The development of this integrated single master model and stereolithography plating process is a major step forward in the area of missile component prototyping and frees the designer to approach component design and fabrication with a new, accurate and relatively inexpensive tool. The savings realized from the use of this technique are directly applicable to the manufacturing of other complex-shaped components both for military and commercial applications.

INTRODUCTION

Design requirements and goals for any future Army surface-to-surface or surface-to-air missile systems may include extended range and enhanced payload capabilities that can be satisfied only by air-breathing missiles. In general, supersonic air-breathing missiles are much more expensive than traditional all-solid motor missiles due to increases in integration complexity and high tolerances required for the air and fuel handling subsystems. Inlets for supersonic air-breathing missiles are normally built to wind tunnel standards; with high accuracy and extremely fine surface finishes. Highly accurate components are critical during the system development process to ensure that the data acquired during testing is relatively unaffected by normal fabrication uncertainties. However, if a future supersonic air-breathing missile system is to be fielded, the costs associated with the model-shop precision employed during development becomes unsupportable even for moderate rate production. It has become apparent that low cost methods for fabrication of high tolerance components, such as inlets, are needed and that low cost should have as much emphasis as high performance early in the missile development cycle.

SINGLE MASTER MODEL DEVELOPMENT

To incorporate design features that are consistent with low-cost manufacturing techniques early in a development, it is crucial that the designer understand the computer design and analysis tools available and make efficient use of a single model for many purposes. In the development of the low-cost inlet, a single parameter based, three-dimensional computer aided design model was used to design the inlet interior and exterior configuration. For the application studied, the inlet design was a conformal 3-D geometry that wrapped around the exterior of the missile fuselage for increased launcher packaging density. The inlet shape was therefore extremely complex and afforded no real opportunities for fabrication by normal machining methods. The inlet would have to operate in Mach 3 sea-level airflow conditions necessitating careful analysis of material and joining methods for multiple inlet pieces. Since the geometry of the inlet interior was a non-reentry shape and because of the high operating temperatures, it was decided that the entire inlet should be built as a single part.

0-7803-5489-3/99/$10.00 ©1999 IEEE.

THE TECHNIQUE

A novel fabrication technique was developed to utilize in-house rapid prototyping capabilities. A summary of the technique is shown in Figure 2. A computer-generated model of the inlet was created and used to construct a mandrel based on the inside surfaces of the inlet. Due to the dimensional limitations of the stereolithography equipment and length of the mandrel required for the inlet, the mandrel model was divided into three interconnecting pieces and a .STL file of each of section was produced. The .STL file is the format needed to provide the stereolithography equipment with the data necessary to create the model. The three-mandrel pieces were then aligned, joined, faired and smoothed to the required interior surface finish. The completed mandrels were then checked by automated inspection equipment against the mandrel computer file for acceptance.

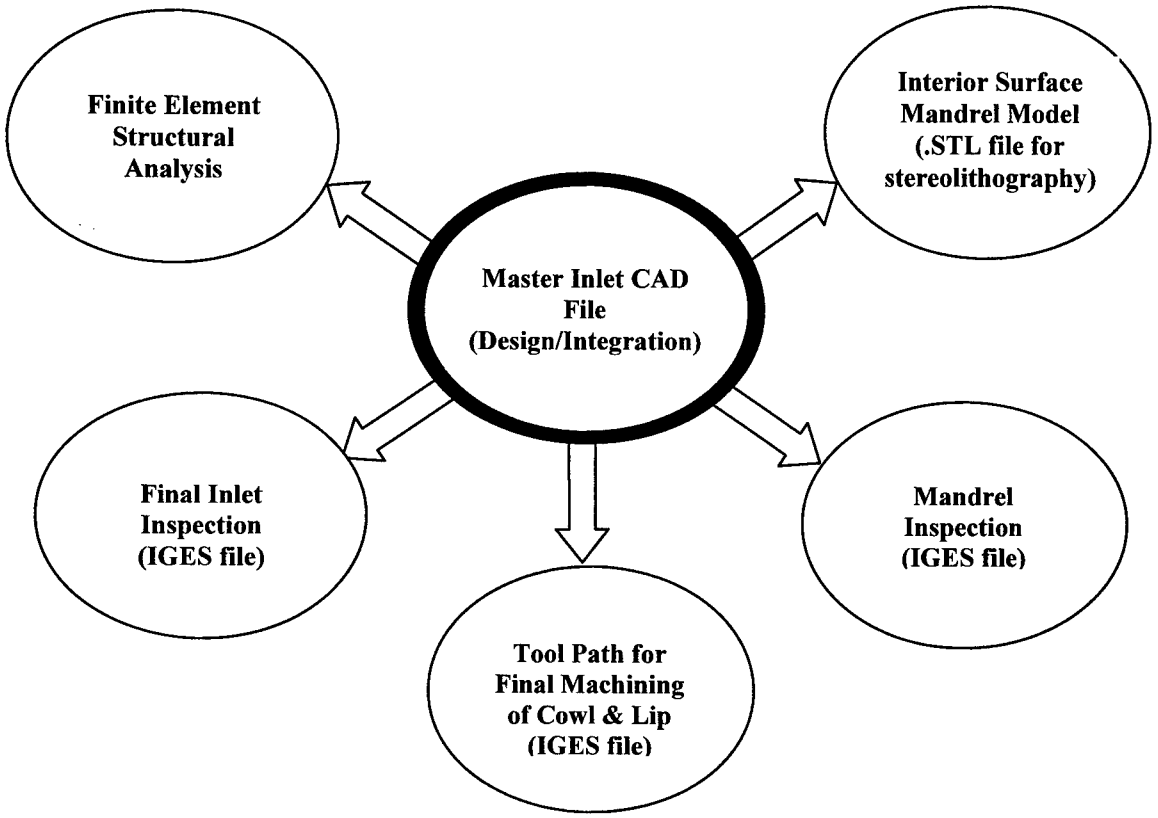


Fig. 1. Single master computer aided design model was used for many purposes.

The master inlet computer model was also used to define the inlet structure and interfaces with the missile and test equipment. A file of the inlet model was exported to a finite element program for structural analysis of the inlet. The structural analysis was used to determine the minimum inlet thickness required to withstand the test conditions with an appropriate margin of safety.

The plastic mandrels were surface-coated with a thin silver paint and allowed to cure. Electrical connections were integrated onto the mandrel base and pure nickel was electrically deposited on the mandrel surface. The individual inlet platings were monitored periodically to determine shell thickness. The plating process was continued until the minimum required thickness to withstand the flight conditions was achieved.

Based on the information from the master inlet model, the rough inlets were then machined on one end to establish the missile attachment flange interface. An attachment flange was welded to the inlet using specially designed welding fixtures to ensure proper flange and inlet alignment. An IGES file generated from the master inlet computer model was used to provide the tool paths for a 5-axis CNC milling machine to machine the flange, exterior inlet cowl shape and leading edges. Minimal hand fairing of the cowl and

lip was required. The IGES file was then used by automated inspection equipment to check the completed cowl and leading edge location, shape and dimensions. The surface finish of the interior surfaces ranged between 16 and 23 micro-inches.

Views of the assembled three-piece stereolithography inlet mandrel, the mandrel prepared for plating and the completed supersonic inlet are shown in Figures 3 through 5.

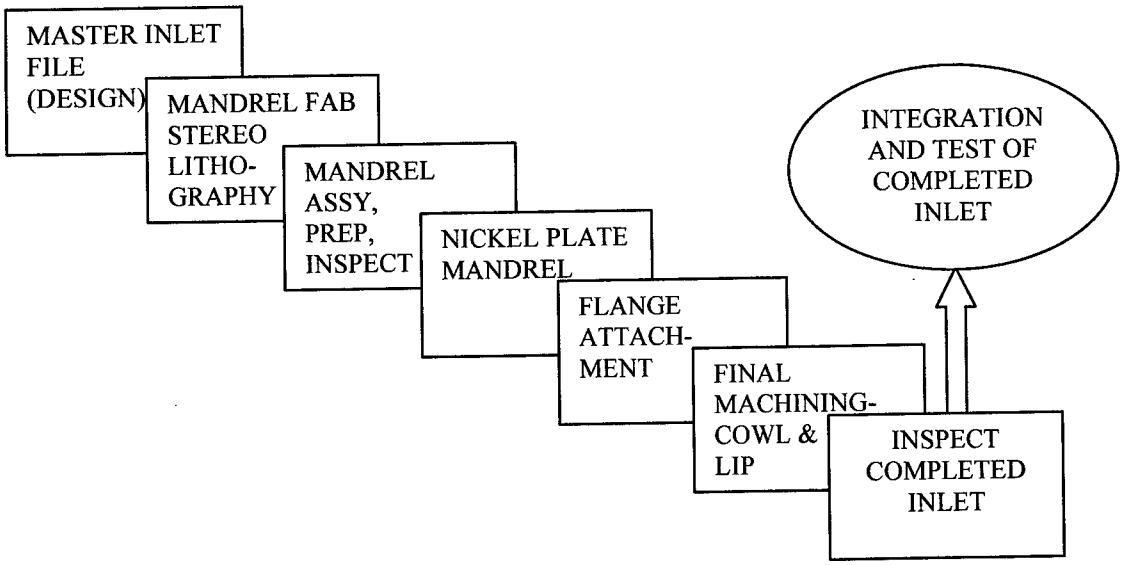


Fig. 2. Low-cost inlet fabrication process.

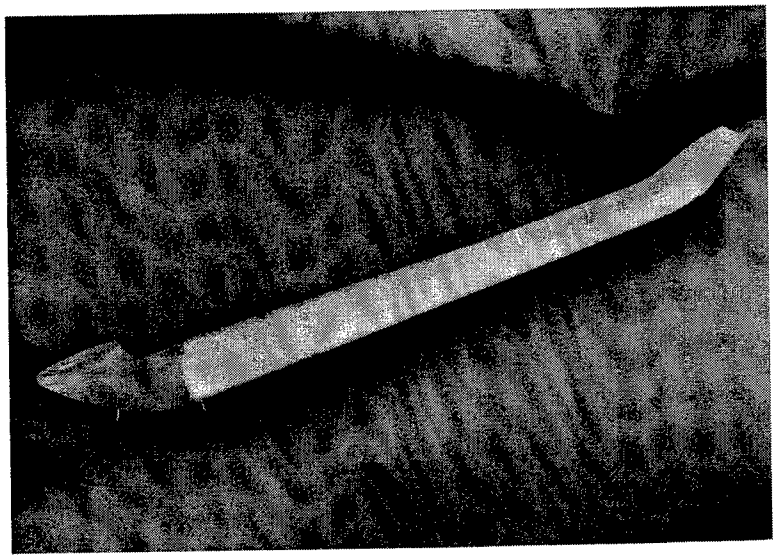


Fig. 3. Assembled mandrel with integrated pressure instrumentation features.

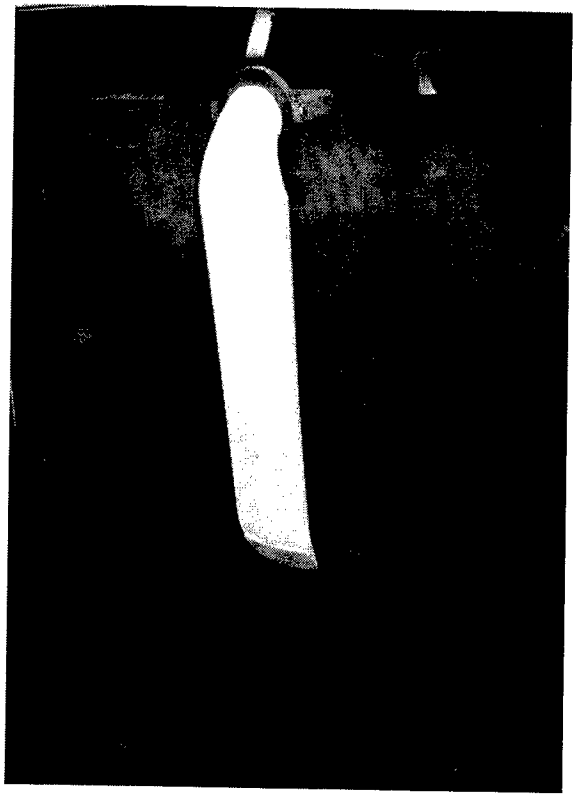


Fig. 4. Mandrel preparation prior to plating.

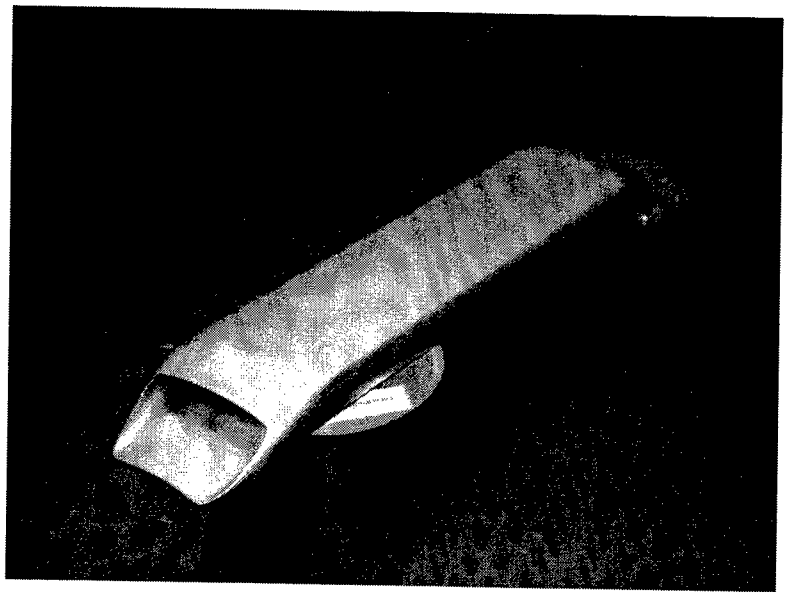


Fig. 5. Completed supersonic conformal inlet.

TESTING OF COMPLETED HARDWARE

The completed inlets were installed on a full-scale ramjet missile and subjected to flight conditions. The inlets operated as designed under extremely harsh temperature and loading and met all design and performance requirements. Performance of the inlets was compared to wind tunnel inlets built in a model-shop. The data indicated the performance of the "low cost" inlets and the expensive wind tunnel model were essentially the same.

PROGRAM COST SAVINGS

The inlets fabricated using the low-cost technique performed essentially as well as the very expensive wind tunnel model inlets at a much lower cost. The cost of an instrumented wind tunnel inlet was approximately $100K when built using conventional high precision fabrication techniques. The total cost, including mandrel preparation, plating and final machining for the low-cost inlet was $15K each - a savings of 85% without a significant reduction in overall performance.

CONCLUSION

This was the first time that this or a similar rapid prototyping technique was used to fabricate a supersonic inlet or structural element of a missile and subjected to supersonic flight loads. This technique employed a single master inlet computer aided design (CAD) model for design and test hardware integration purposes, generation of the rapid prototyping computer file for producing a mandrel, finite element modeling, determining the tools paths for final machining and for inspection of the mandrels and finished inlets. The development of this process is a major step forward in the area of missile component prototyping and frees the designer to approach mechanical and electrical component design and fabrication with a new, accurate and relatively inexpensive tool. The savings realized from the use of this technique are directly applicable to the manufacturing of other complex-shaped components both for military and commercial applications.

Design of High Performance Missile Structures Utilizing Advanced Composite Material Technologies

J. R. Esslinger, R. N. Evans, and G. W. Snyder

Propulsion and Structures Directorate,
Missile Research, Development and Engineering Center
U.S. Army Aviation & Missile Command, Redstone Arsenal, Alabama

ABSTRACT

The U.S. Army Aviation and Missile Command (AMCOM) has demonstrated the ability to develop and utilize advanced composite material technologies for the design and fabrication of hypervelocity kinetic energy missiles for the next generation of Army air defense and anti-tank applications. Future kinetic energy missiles must be small, fast, lethal, and maneuverable, which requires the delivery vehicles to operate in a severe loading environment. Innovative designs and manufacturing techniques have been developed to provide an avenue for enhancing propulsion system performance while significantly reducing the missile size and mass requirements. Propulsion units with high strength–to-density ratio filament wound composite motorcases are stronger, stiffer, and more readily producible than their metallic counterparts; however, these structures are susceptible to manufacturing variability and are more easily damaged during handling and storage. This paper will discuss the AMCOM motorcase fabrication approach and its applications as well as development efforts in the area of embedded sensor technology for in-process monitoring, structural characterization, damage detection, and service life monitoring of filament wound composite motorcases. The advanced composite material applications have enabled major improvements in System Applications for Hypervelocity Missile concepts and integration to multiple lightweight launch platforms.

SYSTEM DESIGN AND DEVELOPMENT CONSIDERATIONS

The goals and factors influencing future U.S. Armed Forces stress the need for rapidly deployable continental United States (CONUS) based forces to engage regional threats promptly in decisive combat on a global basis. Size and weight are paramount factors for weapon systems supporting this future force structure. Hypervelocity kinetic energy (KE) missiles offer a highly viable means of maintaining weapon effectiveness at substantially lower weight and reduced length while achieving essentially double the range of KE tank gun projectiles. These characteristics are particularly important for missiles fired from both armored vehicles and air vehicles (helicopters). Some of the systems technology requirements and developments to achieve the required reductions in weight and size are briefly addressed. The weapon system development objective is directly linked to a potential future lightweight armored vehicle weapon system that utilizes a hypervelocity kinetic energy missile system as opposed to a gun launched KE projectile for its primary kill mechanism. It is important to emphasize the need for well planned and executed system development efforts which start with coordinated technology advancements in all supporting disciplines; however, the major thrust of this paper is the utilization of advanced lightweight composite materials technology for the development of next generation hypervelocity missile concepts.

Lethality

The primary lethality challenge is to demonstrate the perforation of advanced tank armor, such as composite steel/ceramic armor covered with increasingly sophisticated explosive and nonexplosive reactive armor. An additional challenge is to establish or prove the lethality of a range of reasonably sized Kinetic Energy Penetrators impacting targets with more than 25 MJ of kinetic energy. The tradeoff between penetrator weight and impact velocity has a profound effect on the total missile weight as these are the primary variables influencing the design of the propulsion sub-system.

Propulsion

Solution of several propulsion technical challenges are crucial to developing future operational hypervelocity missiles which would represent significant advances over current state-of-the-art. The desire

0-7803-5489-3/99/$10.00 ©1999 IEEE.

for small takeoff weights and volume, drive the need for high specific impulse and energy density, while maximizing the propellant weight fraction (PWF). Very short burn times and high mass flow rates are required to compete with the minimum range of tank-launched kinetic energy penetrators and to decrease velocity loss due to drag. Hypervelocity missile solid rocket propulsion research and development has focused on simultaneously achieving four goals which are widely perceived to be mutually conflicting. The four goals are:

1) high specific impulse (>250 lbf-s/lbm)
2) very high burn rate propellants (~3 inches/second)
3) non-detonable propellants
4) minimum smoke propellants

Structures

The challenge to provide increased kinetic energy lethality against advanced tank armors, at minimum and extended ranges, requires a high performance propulsion unit and a control system able to survive the hypervelocity boost and coast phases. Filament-wound carbon-reinforced composite motor cases using high strength to density ratio fibers and high performance propellant technology provide a baseline for achieving the desired MACH 6.5 velocity at a range below 500 m. in 0.6 seconds. Remarkable advances have been made with carbon reinforced materials in filament wound or braided motor cases. Propellant Weight Fractions (PWF) in excess of 80 % have been demonstrated in a motor which provides 30,000 pounds of thrust for 0.6 seconds. Even greater PWF designs appear to be feasible for these high pressure rocket motors. A major challenge is to increase the maximum service temperature of processable resin materials from the neighborhood of 190 °C up to the neighborhood of steel (~400 °C). Success would significantly reduce the amount of thermal protection material in the centerbody case, thus reducing total missile mass. The composite motor PWF is also enhanced by using lightweight composite nozzles and/or nozzle inserts.

PROPULSION SYSTEM OBJECTIVES

The U.S. Army Aviation and Missile Command has developed multi-mission kinetic energy missile concepts which impact their targets with 4-6 times the energy of conventional tank fired projectiles. These kinetic energy missiles fulfill a close combat mission role, which generally includes line of sight targets at ranges from 200 meters to 5000 meters. AMCOM's kinetic energy missiles reach a peak velocity of over 2 km/s at a range less than 500 meters, and can be launched from multiple light platforms. Peak velocity goals are based on maximizing the penetration performance of continuous long rod kinetic energy penetrators. The additional energy and improved penetration performance provides increased hole volume in armored targets, which relates to higher system lethality from the behind armor debris spallation and collateral damage to the vehicle.

The kinetic energy mission pushes propulsion system design to the limit. High chamber pressures (>3000 psi) combined with short burn times (< 1sec) improve performance, but place significant stresses on the structure. High strength composite materials offer the potential for surviving the severe operational loading environment while reducing the inert mass. The minimization of inert mass is critical for kinetic energy missiles so that propulsive energy can be placed into lethal mechanism impact energy rather than into carrying parasitic weight that adds little or no effect to lethality. In addition to being high performance, line of sight kinetic energy propulsion systems must have minimum signature and must be non detonable to meet insensitive munitions requirements.

The effectiveness and feasibility of the hypervelocity kinetic energy concept was conducted as part of an AMCOM Missile Research, Development and Engineering Center technology demonstration program for the Advanced Kinetic Energy Missile (ADKEM). ADKEM utilized a four-clustered booster concept in which boost motors were discarded upon burnout, and a low-drag penetrator delivery vehicle was guided to the target under coast. A flight test of the ADKEM concept is shown in Fig. 1.

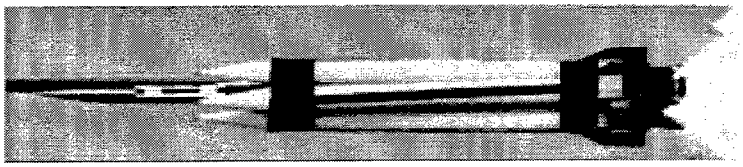


Fig. 1. Advanced Kinetic Energy Missile (ADKEM) Concept

MOTORCASE OPTIMIZATION

In developing the propulsion units for the ADKEM, AMCOM selected the ambitious design goal of a reduced smoke solid fueled motor with a propellant weight fraction (PWF) of 0.85. PWF is the ratio of propellant weight to total propulsion system weight and is an important measure of motorcase design efficiency. For meeting PWF goals and operating at a nominal chamber pressure of 3400 psi, a filament wound composite case utilizing carbon fiber and an epoxy matrix offered the best material solution.

Attachment and interface structures present a challenge to achieving an efficient motorcase design. AMCOM investigated methods to eliminate or reduce the weight of nozzle and motor closure attachment mechanisms. AMCOM has adopted the practice of integrally winding a composite nozzle insulator to eliminate an aft interface structure and reduce nozzle weight. Head closures for tactical composite motorcases are traditionally mechanically fastened inside a full diameter opening at the forward end of the case. In previous AMCOM filament wound motorcases with full diameter forward openings and integrally wound nozzles, the highest PWF obtianed was 0.80. The ADKEM design replaced the traditional forward joint with an integrally wound polar boss. The resulting 3.75 inch diameter unitary motorcase design, shown in Fig. 2, achieved a PWF of 0.84.

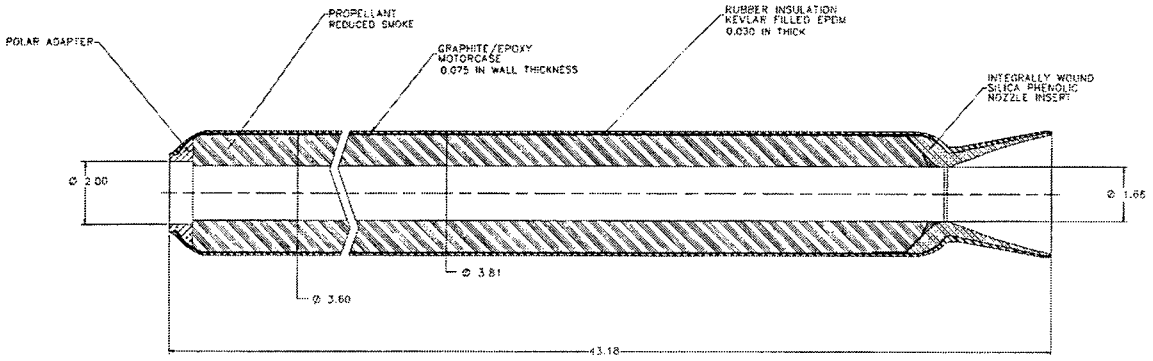


Fig. 2. ADKEM Motor Design Layout

The fabrication techniques developed for ADKEM are unique in that they provide precision alignments about the centerline of the motor and eliminate post processes such as application of internal insulation and joining. The issues of tooling for the closed geometry of ADKEM was addressed through an expendable filament winding tool and a collapsible tool for propellant casting. Kevlar filled polyisoprene was selected for use as internal insulation between the propellant grain and carbon/epoxy case. The insulation was applied to the mandrel before winding and was co-cured with the motorcase. The case was fabricated using 90 degree hoop layers to carry radial pressure and 40 degree helical layers to carry axial loads and to retain the forward polar boss and the nozzle insulator. Fig. 3 shows insulation application, the winding of a helical layer over the polar boss, a compression molded silica phenolic nozzle with non-eroding insert, and the integration of the nozzle with the case structure.



Fig. 3. ADKEM Motorcase Fabrication

INNOVATIVE MATERIAL SOLUTIONS

Filament wound composites offer design flexibility unattainable with conventional materials. AMCOM has used this flexibility to implement innovative approaches that address critical issues related to tactical missiles. One of these critical areas is the improvement of missile and launch platform integration by reducing the missile envelope to increase the number of stowed kills, the number of missiles that can be stowed on a given launch platform.

Since tactical missiles are likely to be subjected to various environmental and handling extremes and composite structures face the effects of manufacturing variability, another critical area is service life monitoring. The Army is currently researching the use of embedded fiber optic sensor arrays for monitoring filament wound structures from manufacturing to final use.

Annular Motorcase Development

In an effort to mitigate certain risk areas and more efficiently package the ADKEM, the UNICORN alternate propulsion unit was envisioned. The 4 ADKEM boost motors were replaced with a single motor with a rod and tube propellant grain configuration. Fig. 4 shows a sketch of the UNICORN missile concept.

UNICORN offers several advantages over the clustered ADKEM configuration. The missile base diameter was reduced from 10.6 inched to 8.6 inches, representing a 33 percent reduction in missile frontal cross sectional area and an increased number of stowed kills. The unitary booster concept also reduces the effects of thrust misalignment and aerodynamic instabilities associated with the original four cluster booster design. In ADKEM there were also concerns with simultaneously igniting four motors; however, the UNICORN single booster concept eliminates this issue.

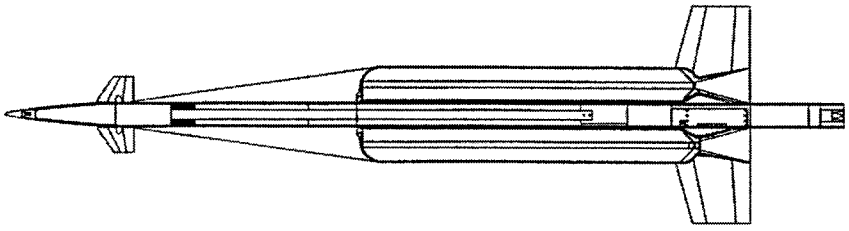


Fig. 4. UNICORN Alternate Propulsion Concept for ADKEM

The UNICORN rod and tube motor configuration, shown in Fig. 5, consists of outer and inner structural shells with an annular nozzle throat. The ADKEM lethal centerbody is submerged within the inner shell and egresses from the motor after boost. For solid-fueled motors, a rod and tube grain offers performance characteristics that are advantageous for systems that require high burn rates. In the past, these advantages have been offset by the lack of an efficient means to support the inner grain inside the motor chamber. AMCOM addressed this problem by developing an inner shell support structure at the nozzle throat.

The UNICORN motorcase incorporates many of the fabrication techniques used in ADKEM. Both outer and inner shells are filament wound using carbon fiber and an epoxy matrix. The outer shell utilizes a silica phenolic nozzle and an aluminum forward polar boss that are integrally wound with the motorcase. The inner shell presented significant design challenges because it is subjected to external pressure combined

with the large axial force resulting from pressure acting on the inner portion of the annular nozzle. The primary risk areas for the inner shell were in designing a lightweght composite structure to withstand the external buckling loads and in developing effective forward and aft joints. The forward joint is an integrally wound stainless steel cylindrical adapter with locking grooves. The aft joint is accomplished via an external version of the integrally wound nozzle concept. The silica phenolic nozzle components, shown in Fig. 6, have integral supports that maintain alignment between the outer and inner shells.

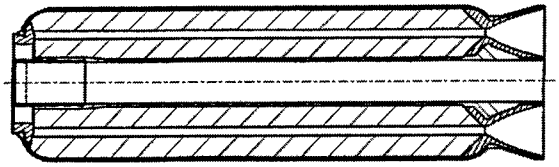


Fig. 5. UNICORN Motor.



Fig. 6. UNICORN Flightweight Hardware.

The UNICORN motor was designed to a 4700 psi maximum expected operating pressure, a 7050 psi design burst pressure, and a 350 ms burn time. A successful static firing of the UNICORN motor demonstrated that the concept could meet the ADKEM propulsion requirements.

Structural Health Monitoring

The small size of optical fibers and fiber optic based sensors make them ideal candidates for building embedded sensor networks within a filament wound structure. The Army is currently sponsoring research through a Small Business Innovative Research (SBIR) agreement with Technology Development Associates, Inc. The research focuses on several critical areas related to embedded fiber optics in filament wound structures. These areas include automated embedding of sensor arrays, development of ingress/egress techniques, and assessment of the effects of embedded sensors on structural integrity.

The issue of automated embedding is being addressed by utilizing a modified carbon fiber delivery eye that locates the optical fiber directly beneath the carbon fiber tow as it contacts the part. The modified fiber delivery eye is shown in Fig. 7. During the early phases of the program several fiber optic based sensors were investigated; however, Bragg Grating sensors offered the most promising results. Multiple Bragg Gratings can be applied to a single fiber. Multiplexing techniques can then be used to query the various gratings along the fibers to obtain strain and temperature measurements. Sensors may be automatically embedded along both helical and hoop directions. Fig. 8 shows a 5.75 inch diameter pressure vessel with embedded fiber optic sensors and surface mounted strain gages for correlation of strain measurement data.

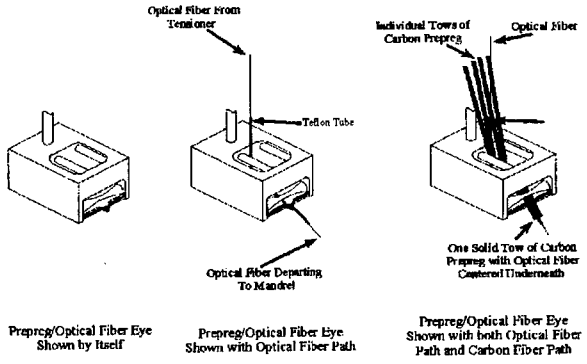


Fig. 7. Automated Embedding of Fiber Optics.

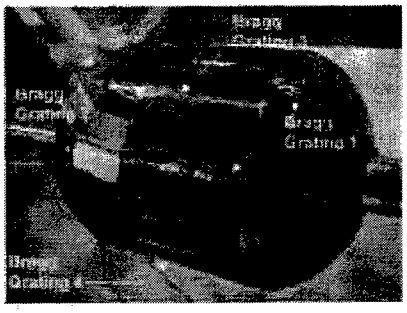


Fig. 8. Instrumented 5.75 inch Bottle.

Hydrostatic testing of pressure vessels with embedded optical fibers has shown that the embedded fibers have little effect on the structural integrity of the pressure vessel. In order to demonstrate the capabilities of the fiber optic sensor array, the sensors were used to monitor the vessel during cure and hydrostatic testing. Fig. 9 shows strain measurements during a typical 150 °C cure cycle. Strain peaks can be seen during matrix polymerization and mechanical cross-linking. The residual strain present in the structure after cure is

readily evident. Fig. 10 shows a high correlation between Bragg Grating and surface mounted strain gage data taken during a hydrostatic pressurization experiment.

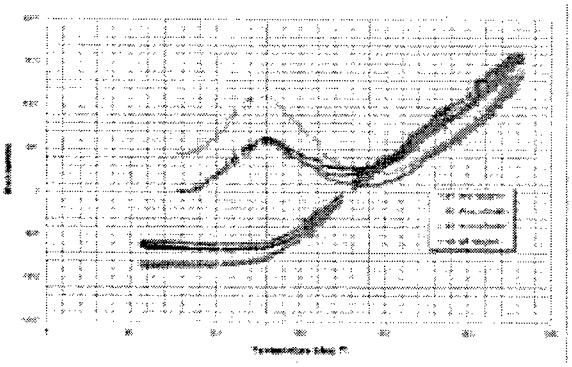


Fig. 9. Cure Monitoring Experiment

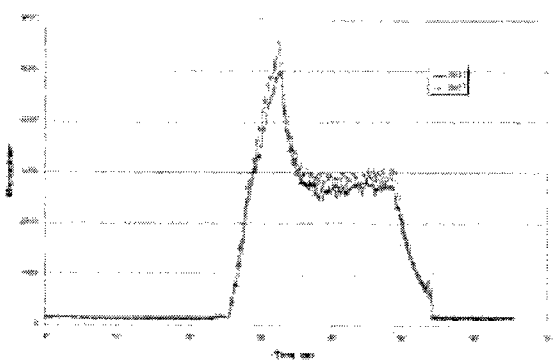


Fig. 10. Pressurization Experiment

Results to date indicate fiber optic sensors offer a useful and practical tool for structural health monitoring of filament wound composite missile structures. The Army's research in this area is an ongoing effort.

MATERIALS TECHNOLOGY FOR FUTURE MISSILE SYSTEMS

The AMCOM Missile Research, Development and Engineering Center is actively pursuing technology for the Army After Next (AAN) initiative, which focuses on developing warfighting capabilities for the 2025 timeframe. One of the primary AAN goals is to create a highly mobile land force that can be rapidly deployed across the globe. The Future Combat System (FCS) or Multi-Mission Combat System (MMCS) is the yet-to-be defined compliment to the Legacy force for the Army After Next. The FCS/MMCS will be fast, lightweight and capable of engaging heavily armored ground vehicles. One possible scenario is to reduce the vehicle's profile and weight by replacing the traditional cannon with both line of sight kinetic energy missiles and beyond line of sight missiles that can defeat the next generation of armored targets.

The AMCOM envisions advancements of technology for the FCS requirements to include a missile concept that represents the evolution of kinetic energy missile technology developed for ADKEM and UNICORN. The Compact Kinetic Energy Missile technology program offers lethality against hardened and reactive armored targets at a minimum range of 400 meters and a maximum range of 4 kilometers. The propulsion unit and airframe act as the delivery vehicle for a long rod penetrator that is embedded in the motor chamber. A line sketch of the CKEM Technology Testbed configuration is shown in Fig. 11.

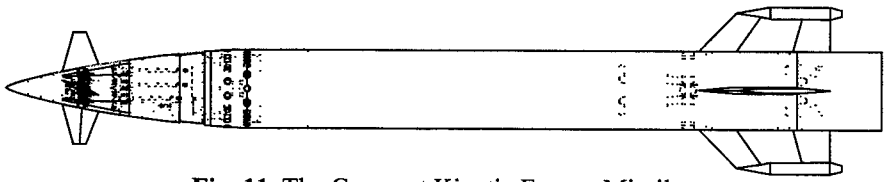


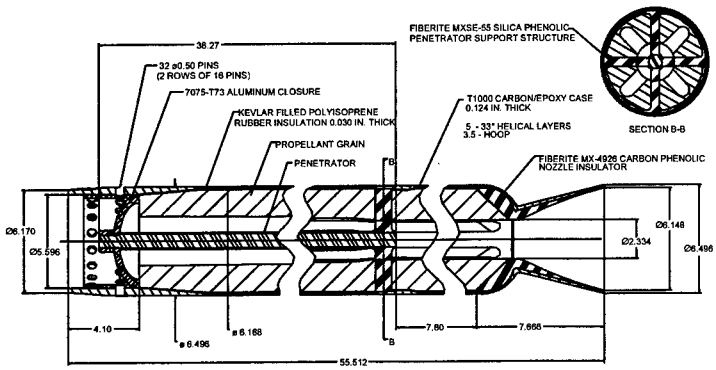
Fig. 11. The Compact Kinetic Energy Missile

The system goals call for a robust propulsion system that is high performance, minimum signature, and non-detonable. To best meet these goals a modification of the ADKEM/UNICORN high rate reduced smoke propellant has been formulated. To enable a large number of missiles to be stored inside a low profile ground vehicle, substantial restrictions on missile envelope and weight are necessary. Parametric trade studies were initiated with the assumption that the overall missile length could not exceed 6 feet, launch weight would be no more than 110 pounds, and missile diameter would be kept to a minimum.

Trade study results showed that an increase in the propellant burn time along with a reduction in the payload weight results in a reduction in the motor length and weight. An increase in the motor diameter yields a reduction in the motor length but results in an increase in the motor weight. Inert weight was reduced by utilizing lightweight composite materials and by eliminating the weight of an inner shell/centerbody by embedding the penetrator inside the motor chamber. Burn time was lengthened from

350 ms for ADKEM/UNICORN to 600 ms for CKEM. Longer burn times resulted in an inability to meet minimum range requirements. As with ADKEM and UNICORN, the CKEM round is 6 feet long; however, the missile base diameter has been reduced to 6.5 inches. CKEM offers a 62 percent reduction and a 43 percent reduction in missile frontal area as compared to ADKEM and UNICORN, respectively.

The CKEM motorcase consists of a filament wound T-1000 carbon/epoxy composite motorcase with an integrally-wound carbon phenolic nozzle insulator and a pinned forward closure. The practice of integrally winding the carbon phenolic nozzle reduces thrust misalignment and parasitic weight. The embedded penetrator is supported at its forward end by the motor closure and at its aft end by a four-spoked silica phenolic support structure. The motorcase forward opening is a near open end design to allow for penetrator assembly. The composite lay-up in the forward joint region consists of a hybrid laminate comprised of T-1000 carbon/epoxy and fiberglass/epoxy for bearing strength. The forward joint has been tested to 10,500 psi, (72.4 MPa) which is 121% of the design burst pressure. The final flightweight design resulted in a propellant weight fraction of 0.82. The configuration is shown in Fig. 12.



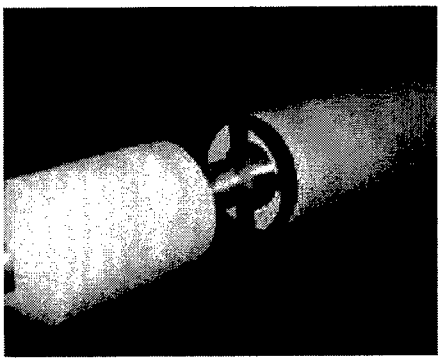


Fig. 12. CKEM Motor Layout.

Fig. 13. Penetrator Support Integration.

The CKEM geometry requires a collapsible filament winding tool. MARCORE polyisocyanurate foam tooling material developed by Lockheed Martin at NASA Marshall Space Flight Center was used as an expendable winding tool. MARCORE foam is compatible with epoxy resin systems, is easily machined, and is unaffected by typical oven and autoclave cure cycles. Fig. 13 shows integration of the penetrator support structure with the winding tool. After cure, the foam is removed with a high pressure water jet.

The design point selected for the CKEM has given rise to critical design issues that are currently being addressed. Concern has been raised regarding the effects of the high velocity flow region on the penetrator support structure, penetrator support structure survivability, and nozzle performance. An extensive experimental test program using full-scale flightweight hardware, currently in fabrication, is planned for the evaluation of the nozzle components, the penetrator support structure, and the motor performance.

CONCLUSION

The technical issues and challenges associated with demonstration and development of the next generation hypervelocity KE missile at half the current mass and size, but with increased lethality characteristics are difficult to solve and require cutting edge missile technology advancements. The solution of these technical challenges should be accomplished in a missile system context. This should be done even if the entire missile system will never be flown and will only be used to investigate the interaction of the components in a virtual prototype. The tradeoff between hypervelocity missile component performance and missile system performance and cost requirements is perhaps the greatest technical challenge of all. The pursuit of component performance, independent of system constraints, is simply inappropriate. The U.S. Army Aviation and Missile Command has utilized advanced composite materials, unique fabrication techniques, and innovative attachments and interfaces to provide light weight, high performance structures to meet the requirements of current and future missile systems. Innovative concepts developed by AMCOM provide enabling technologies for significantly enhancing missile operational and life cycle performance. Demonstrations of the propulsion unit relative to system constraints are the backbone for realizing the potential for achieving the desired requirements of the next generation hypervelocity KE weapon system.

Modelling the Mechanical Stability of Metal Catalyst Carriers

C. Guist, H. Bode

Bergische Universität-Gesamthochschule Wuppertal, Germany

ABSTRACT

To be sure about an efficient and flexible design for technical systems, instrumentation is required which will assist in assessing and predicting reliability. Simulation is of increasing value in this respect. With simulations, it is the translation of a technical system to a virtual plane, the modelling process, that is the factor that determines success. This factor can be seen from the example that simulates mechanical stability of metal catalyst carriers.

INTRODUCTION

Function of a catalytic converter and generel description of the product

Catalytic converters are installed in exhaust systems of internal combusion engines so that harmful gases like CO, HC and NO_x are transformed into less harmful gases such as CO_2, H_2O and N_2. Platinum, rhodium and palladium are examples of elements that act as catalysts. They are placed inside a porous, ceramic layer known as the wash-out. The wash-out in turn lies on a substrate either made of ceramic (cordierite) or a high alloy steel containing Cr (~ 20%), Al (5-6%), and reactive elements (~ 0.03-0.1%) [1].

Figure 1 shows a converter with ceramic carrier and a metal carrier respectively. This report concentrates on metallic substrates and the products derived from them.

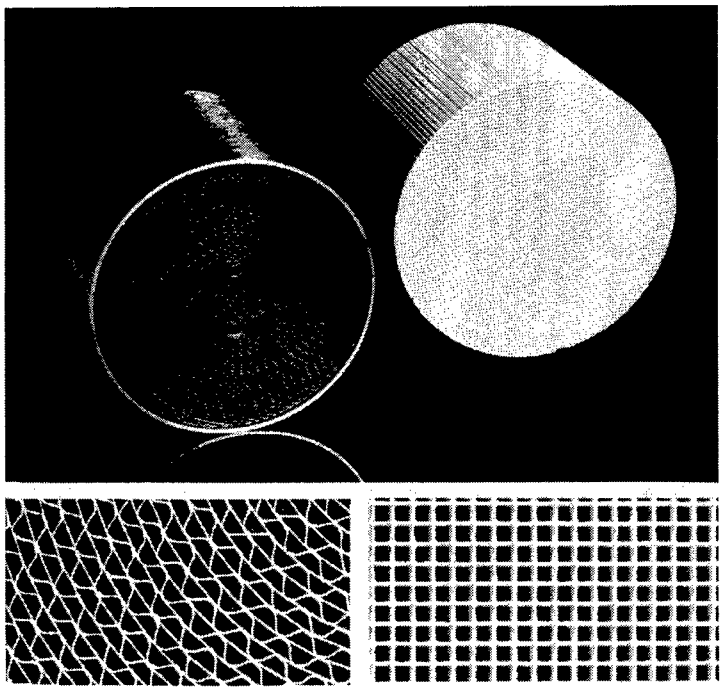


Fig. 1. Catalyst support systems (left) metal based and (right) ceramic based [Courtesy of EMITEC GmbH]

0-7803-5489-3/99/$10.00 ©1999 IEEE.

The product generally used with a metal carrier, as shown on the left-hand side of Figure 1, consists of smooth and corrugated pieces of foil moslty 50μm thick and a so-called jacket. The foil is usually soldered to the points of the contract in the frontal area and is also jointed to the jacket at previously designated places by one more soldered joints. Partial soldering of foil at defined points in the axial depth is also possible and may be specified depending on application.

The number of cells made in this way depends on the type of vehicle, i.e., its application, and there may be 100 to 600 cells per inch^2. When the metal carrier has been coated, it is installed in the exhaust system by welding.

Former and future product developments

The transformation of harmful gases is almost complete with the use of optimised products, i.e., catalysts, in an equally, optimised exhaust system. Until now, the requirement was for metal carriers to have high oxidation and form stability, i.e., a sufficiently high resistance to high-temperature corrosion during the entire lifetime of the product. This requirement is necessary because of the prevailing temperature load of ~900 °C during continous operation. In the event of malfunction, the temperature may even exceed 1100°C. These temperatures can be tolerated by steel foil but not by the porous wash-out layer which becomes a dense layer at such high temperatures - hindering access of exhaust gas to the catalyst elements.

Temperature distribution is generally uneven. Results of development work in the field of high-temperature corrosion resistance were compiled in 1997 [2].

Due to specific advantages of metal carriers over ceramic ones [4], further new development of modern production technology in producing catalyst carriers, as shown for example in [4] and foil [5,6], and also stricter emission tolerance limits [7], the application potential of metal carriers have greatly increased. Their production today is about 10% (in comparison with 90% ceramic carriers) and is growing annually at two-figure rates.

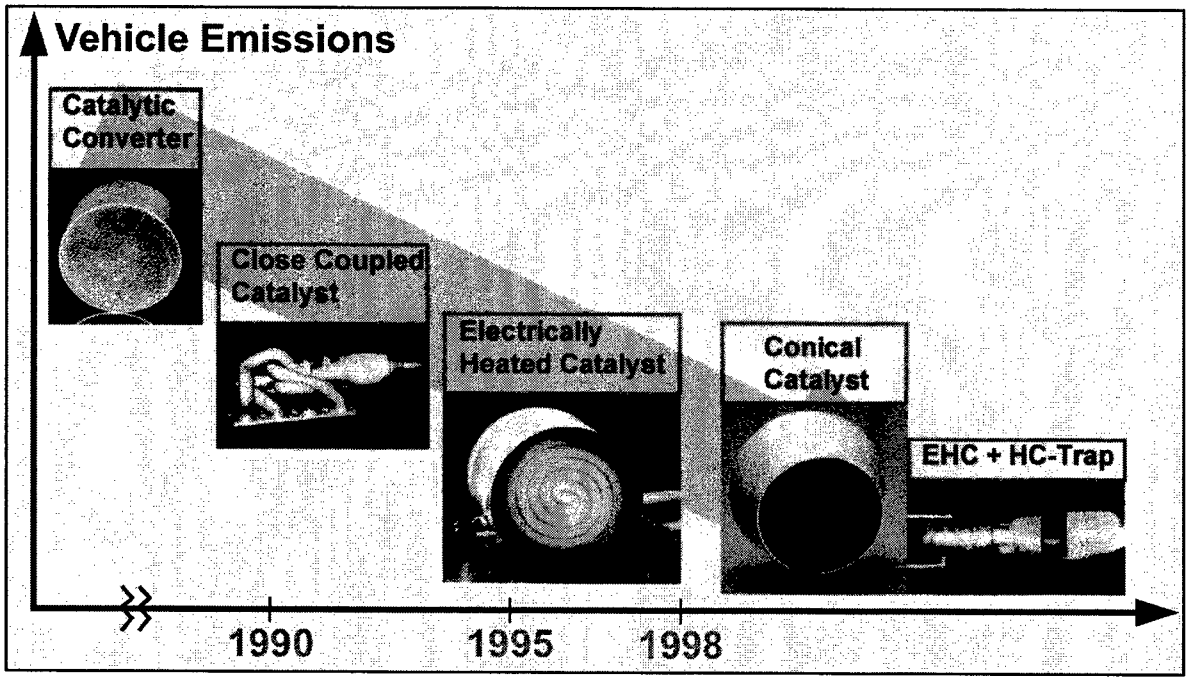


Fig. 2. Technical Progress in Exhaust Gas After-treatment for Low-Emission Vehicles

Figure 2, updated from [8], shows some stages in product development. Although lower emission tolerance values have been achieved, this has been accompanied by greater requirements of mechanical stability and resistance to oxidation which have been achieved by:

- placing the catalyst near the motors, and/or
- using a catalyst that can be heated by electricity; or
- combining a electrically-heated catalyst with an HC-trap; or
- using a cone catalyst, etc.

The production stages require application of computer-supported construction tools and implementation of results from further development in processing technology. It must be stressed that:

- foil thickness of 30μm instead of 50μm is possible [9].
- Al content of 8% (and perhaps higher) can be used [5,6], to provide improved oxidation resistance.
- the use of microwaved foil instead of a smooth foil is possible [10]
- structured foil can be made to produce local turbulence in the exhaust stream [11]
- cell density of a maximum of 600 cells/inch^2 can be increased to 1200 cells/inch^2 [12].

Former and future requirements of the product life span

Earlier demands of the product life span were 100,000 km. This minimum life expectancy will be increased to 180,000 km in the future. The specified reduced emission limits mentioned above have triggered product development which along with demand for extended product life span, have meant very exacting development tasks for catalyst and vehicle manufacturers and for their product suppliers. Among other things, there is a need to test further processing developments, e.g., by making 30μm thick foil instead of 50μm foil without conflicting with the need for a simultaneous increase in the life span of the product.

Former procedure in product design

Oxidative and mechanical requirements of catalysts are specific to vehicles. Securing the highest product protection against malfunction means that with respect to product design, apart from applying generally valid procedures in construction, e.g., applying finite element methods and know-how, vehicle-specific tests are also necessary. These include large-scale, expensive experiments with engine test stands, exhaust gas simulation tests and vehicle endurance runs. Details about such tests may be found in the literature [13].

Proposal for application of modelling for future procedure in product design

Subject to

- a sharp increase in new applications and
- the required protection against malfunction, in particular in new applications and
- the above mentioned future development of products

simulation of vehicle-dependent loads, with load variants or with different engines within one type of vehicle, and also the comparison of materials and product features can greatly reduce development time. They may even be more cost effective and display the required protection against product malfunction. Preliminary research in this area has been carried out at the Bergisch University, GH Wuppertal in the Department of Materials.

The following exposition focuses on investigating mechanical strength, since modelling is only possible when material and component characteristics are known for the conditions present in a vehicle. Essential observations concerning load are in the forefront of our investigation. Afterwards there will be a short explanation as to the procedure for assessing mechanical stability where a reference system is used with a researched load profile. Further information on the modelling method appears in [14].

ANALYSIS OF INFLUENCING PARAMETERS AND MODELLING

During the driving operation the catalyst is subjected to an extremely high load. This load is made up of a variety of types of influence. These include the built-in circumstances (vehicle, engine, exhaust system, etc.) and the driving operation (distance covered, way of driving, etc.).
At the same time the catalyst itself affects these types of influence. These and the catalyst together determine the boundary conditions under which the catalyst must carry out its function.

This mechanism can be described as follows (see Figure3):

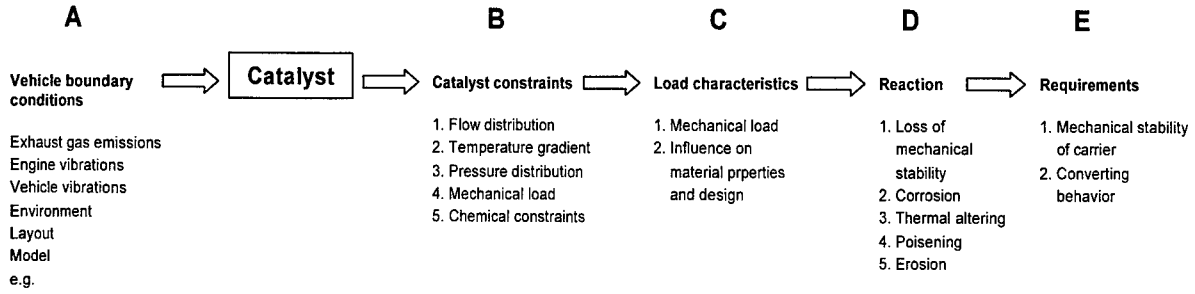


Fig. 3. Process chart of exhaust system

The *boundary conditions* produce a load profile that affects the catalyst, e.g., the exhaust system produces a specific emission which has an effect upon the *catalyst*. This triggers certain reactions in the catalyst. The type and extent of these reactions establish whether catalyst demands are being met.

If a balance shell is laid around the system boundaries of the catalyst (simplified in Figure 4 as represented on an engine-related, dual-flow, catalytic system of a 6-cylinder engine), then the catalyst's boundary conditions are found as described in row B with respect to: distribution of flow, temperature gradients, pressure distribution, mechanical load, chemically-active environment.

The *load profile* emerges from interactions with the described parameters (areas) of the catalyst. This consists of mechanical load, influence of material characteristics and product construction. The catalyst's *reaction* results from the relationship between load and strength. One reaction of the catalyst is *mechanical stability* response, e.g., in the sense of fatigue durability. The connections shown in Figure 3 are to be interpreted in such a way that each subsequent link is a function of all preceding links.

QUALITATIVE RESULTS OF AN INVESTIGATION INTO STRESS

Reference system and indication of construction variable

The reference system consisting of a first and a second catalyst can be seen in Figure 4.

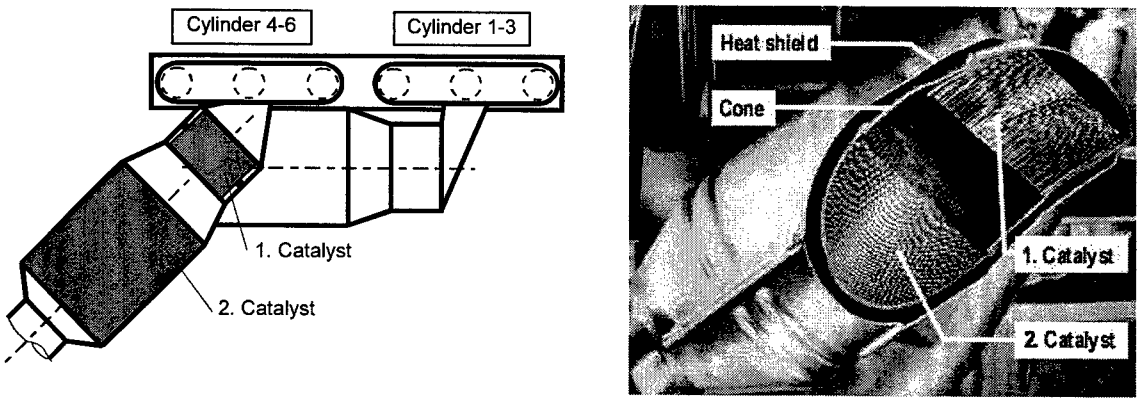


Fig. 4: Schematic graph of reference exhaust system.

Table 1 provides data about the reference system. Differences between the components used should be noted, such as diameter, length, length of soldering, cell density, foil thickness and design.

Table 1: Specifications of Reference-Catalysts

	Diameter [mm]	Length [mm]	Brazed Length [mm]	Cell density [cpsi]	Foil thickness [mm]	Design
1. Catalyst	80	50.8	2 - 15	300	0.065	SM, W3
2. Catalyst	98.4	90	2 - 25	400	0.05	S, W5

Load components with influence on mechanical stability (fatigue durability)
The procedure used will be described in [14] for investigating load components that have an influence on mechanical stability (fatigue durability). The qualitative results are shown in Table 2. Accordingly the following must be observed more closely:

- vibration loads,
- thermal loads and
- flow loads.

This entails indicating their extent in tension and expansion values by experimental methods or through simulation of loads and comparing them with material and component characteristics that are also related to tension and expansion values.

Table 2: Fatigue load components

	Vibration Load		Thermal Load	Gas Flow Load
axial / high frequency		Inertia forces		Flow forces
axial / high frequency	Natural frequency			
radial / low frequency			Deformation due to thermal load	

RESULTS OF INVESTIGATIONS INTO STRENGTH

Material and component strength
On the basis of applied production technology which includes for example the identified high-temperature soldering process and local soldering, it must be noted that reference to foil characteristics is not sufficient when studying mechanical stability; it is necessary rather to refer to component characteristics as well (see also the details about the reference system).

Stress on the catalyst is caused by processes occurring at high frequency in the engine (forces of mass, change in load) and by low-frequency processes from the transient driving operation (thermally-related tensions). This mainly dynamic load influences the catalyst's behaviour as regards strength.

Dynamic strength characteristics were established by carrying out fatigue tests. High-frequency load occurs as a result of inertial and flow forces which act from outside. Fatigue tests were carried out analogous to this load while controlling the force.

Static strength characteristics are needed to be able to assess load from transient driving operation, i.e. thermally-related tensile strength and pressure tension regarding component stability. The following limitation should be noted in that the influence of time with respect to load is not taken into account in this report, i.e. creep and creep fatigue are not considered for assessment.

Tension tests
The limit of elasticity decreases as a function of temperature in the presence of static load. This means the transition from elastic cell to plastic cell deformation greatly depends on temperature. Quantitative values may be found in the chart included in the section "Procedure in defining mechanical stability".

Pressure tests
Figure 5 demonstrates the development of pressure as a function of course covered. In this case cube samples were used made from smooth and corrugated foil pieces soldered together at contact points. The number of layers, i.e., the number of corrugated foil layers between smooth layers varied up to 22. An elasticity module defined for this application may be derived from the almost linear rise in force in the area of elasticity (the area of proportionality). This depends on the number of layers. As cell density increases so does resistance to elastic deformation. This relationship must also be taken into account in the respective model that should have an overall valid character.

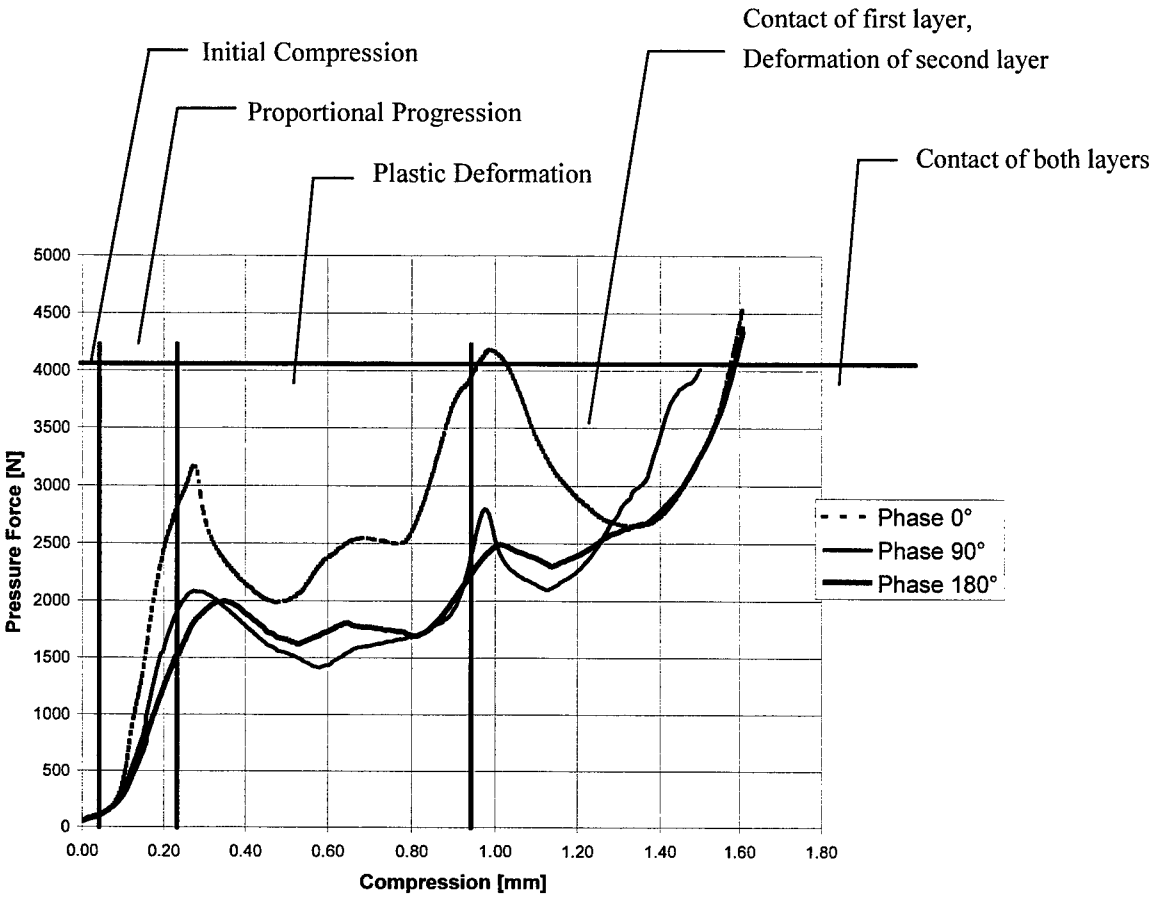


Fig. 5: Graph of Pressure versus Compression (Specimen: 2 Layers. 400 cpsi, 0,05 mm)

Dynamic tests

Figure 6 shows a result from dynamic tests done on soldered samples in the tension-pressure alternating field at room temperature and 600 °C. It can be seen here that only very small tension deflections in the elastic area can be tolerated at 900 °C.

Investigation into allowable expansion

A mathematical model is described in [14] that provides evidence that the occurrence of expansion depends on radial catalyst dimensions. Accordingly near the jacket, the maximum allowed expansion of 0.06 mm/mm at room temperature and 0.048 mm/mm at the tested 800 °C takes place as shown in Figure 7.

Comparison Between Temperature-Related Mechanical Load and Limit of Elasticity and Expansion

In Figure 7 shown below load and strength are compared in the upper right-hand part. It may be seen from here that mechanical load contributed by the temperature profile in the outer layers (comparative tension) is greater than the temperature-related limit of elasticity that is also evident at this point. In these areas plastic deformation can be expected. In the same diagram evidence as to the extent of expansion occurring in the reference system may be found in relation to the maximum allowed expansion. The procedure for investigating comparative tension and maximum allowed expansion is described in [14].

PROCEDURE FOR DEFINING MECHANICAL STABILITY

The main procedure for defining mechanical stability can also be seen in Figure 7. This diagram shows not only characteristic material and component features, but also quantitative data that have been taken from the reference system by appropriate analysis [14]. According to this analysis, temperature-related tension is of the greatest importance.

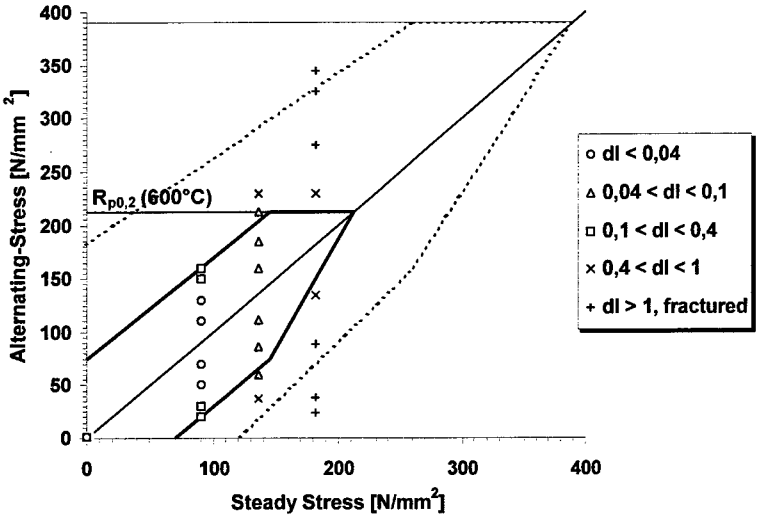


Fig. 6: Fatigue diagram for foil-specimen (600°C) [4].

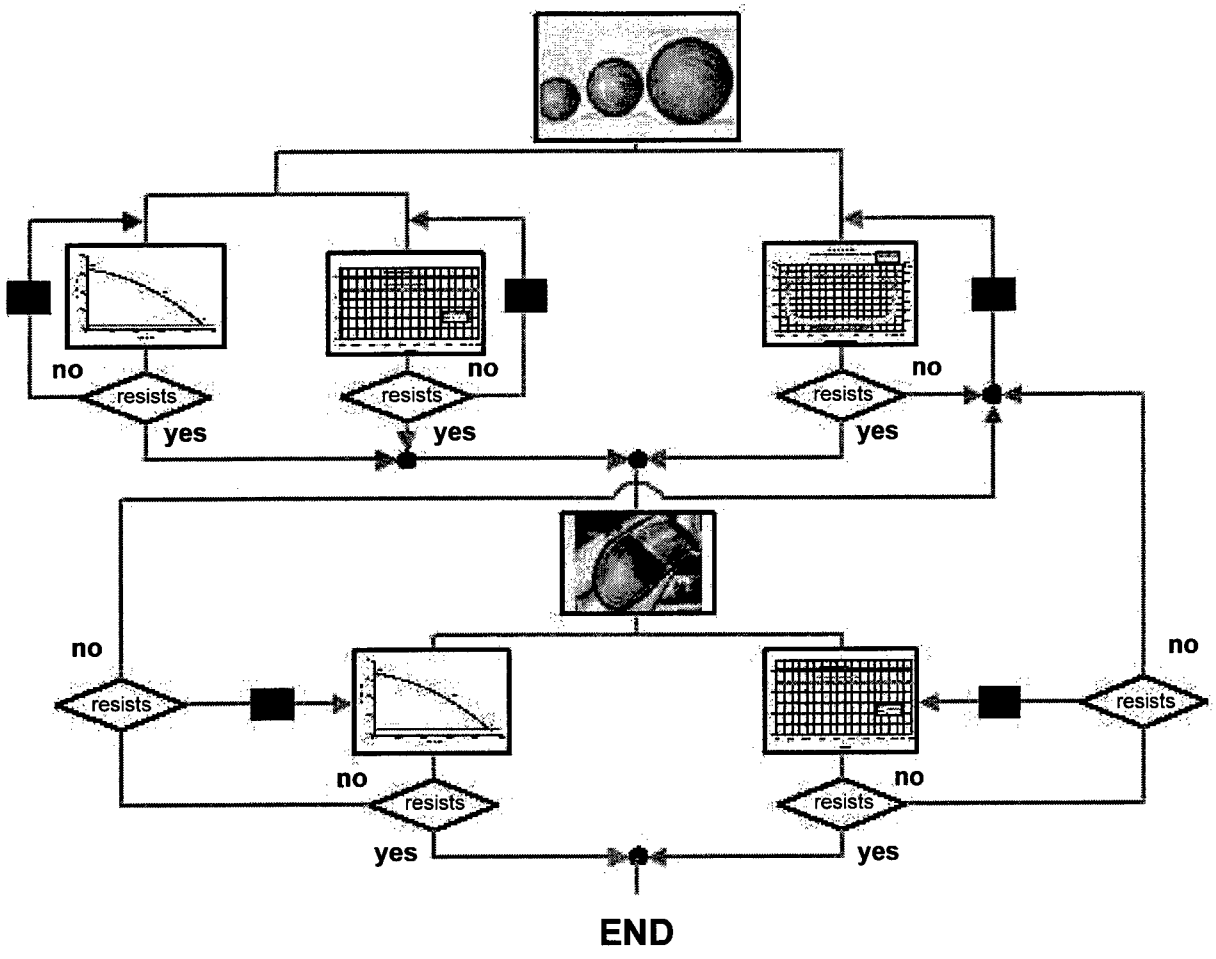


Fig. 7. Model for Calculation of Mechanical Stability

According to the present state of modelling an individual assessment concerning mechanical stability must be made. The aim of an overall valid model will be to compare one or two stress values, e.g., tension and expansion with the actual values of the material and component characteristics. This comparison must also take into account the time of the stress: This indeed illustrates the complexity of the modelling process.

REFERENCES

1. H. Bode, 1997. Developmental status of materials for metal supported automotive catalysts. in [3], 17-31.
2. H. Bode, ed., 1997. Metal-Supported Automotive Catalytic Converters. Wiley-VCH, ISBN 3-883555-254-2.
3. G. Faltermeier, B. Pfalzgraf, R. Brück, C. Kruse, W. Maus, A. Donnerstag, 1996. Katalysatorkonzepte für zukünftige Abgasgesetzgebungen am Beispiel eines 1,8 l 5V-Motors. 17, Inter. Motor. Symp., 25-26, Wien, Vienna.
4. W. Maus, R. Brück, 1998. The Conical Catalytic Converter-Potential for Improvement of Catalytic Effectiveness. SAE Paper 98 2633
5. I.M. Subkonnik, S. Chang, B. Jha, 1997. DuraFoil ICR-a New Material for Catalytic Converter substrates. published in [3], 93-97.
6. A. Kolb-Telieps, J. Klöwer, R. Hojda, U.Heubner, 1997. A New Production Technique for Fe-Cr-Al. published in [3], 99-104.
7. H. Oetting, editor, 1996 and 1998. Future Emission Legislation in Europe and USA: Technical Solutions, Petrol Engines. Haus der Technik e.V., Essen, Germany, 1996 :No. 30-918-056-6.
8. W. Maus, 1997. Mobility, Prosperity and Environmental Protection - the catalytic converter is indispensable. in [3], 3-13.
9. J. Klöwer, H. Bode, M. Brede, R. Brück, A. Kolb-Telieps, L. Wieres, 1998. Development of High-Temperature Resistant Fe-Cr-Al-Alloys for Metal Exhaust Gas Catalysts. Materials Week 1998, Munich, Section 2, ISBN 3-527-29955-6.
10. U. Martin, 1994. Research into Flow Relationships in the Cell Channels of an Exhaust Catalyst with Metal Substrate by Simulation on a Model. M.Sc. Thesis, Bergische University-GH Wuppertal, Dept. Mech. Eng.
11. R. Brück, J. Diringer, U. Martin, W. Maus, 1995. Flow improved efficiency by new cell structures in metallic substrates. SAE Paper 95 0788
12. W. Maus, R. Brück, P. Hirth, 1998. Theoretische Auslegung eines Abgasnachbehandlungssystems zur Einhaltung der kalifornischen SULEV-Grenzwerte. 2nd Paper, given at 4th Symposium "Entwicklungstendenzen bei Ottomotoren", TAE-Symposium 23956/64.153, Esslingen, Germany.
13. T. Nagel, W. Maus, J. Breuer, 1997. Development of more Exacting Test Conditions for Close-Coupled Converter Applications. in [3], 107-126.
14. C. Guist, 1998. Dauerhaltbarkeit von bestehenden Abgassystemen mit metallischen Katalysatorträgern und Möglichkeiten der Zuverlässigkeitserhöhung. to be published, Bergische Univ. Wuppertal, FB 14, D 468

Integration of Newly Developed AI Assembly, Production, and Material Flow Virtual Tools

Daniel A. Holder*, Raymond D. Harrell*, Terri L. Calton, John F. Atkinson*, Brandy M. Brasfield***

*US Army AMCOM, Redstone Arsenal, Alabama, USA
Intelligent Systems and Robotics Center, Sandia National Laboratories*, Albuquerque, NM 87185-1008, USA
***Sandia is a multiprogram laboratory operated by Sandia Corporation, a Lockheed Martin company, for the United States Department of Energy under contract DE-AC04-94-AL85000.)

ABSTRACT

In this paper we discuss the applicability of artificial intelligence virtual tools in addressing real world design for manufacturing issues and the lessons learned from experimenting with this approach. A current project that has predicted a 70% reduction in scheduling as achievable is addressed. Operation of the real production line of the project will be discussed with a comparison of predicted values versus actual.

INTRODUCTION

The integration of production process modeling and material flow software with newly developed Artificial Intelligence (AI) assembly software provides a critical link in creating a seamless virtual manufacturing environment from solid model designs through manufacturing issues to facility planning and layout.

Production simulation modeling based on AI has been proven in the United States Army over the last several years as providing greater insight into the cost, schedule and efficiency of building and maintaining weapon systems. In every case when applied properly has provided additional unexpected benefits from healing contractual disputes to aiding in reengineering business processes. Adding material flow software to this capability allows the optimization of facility planning.

The capabilities above are currently commercial off the shelf software tools. Historically, providing production simulation assumed that the assembly order was known. No consideration had been given as to whether the assembly was optimal or even possible. A method of performing constraint based "What-if" analysis on assembly planning in conjunction with production and material flow planning was needed. Recently, Archimedes, under continued development at Sandia National Laboratories has demonstrated that constraint-based interactive assembly planning software has come of age. Archimedes has demonstrated success in planning, optimizing, simulating, visualizing, and documenting sequences of assembly. Given a CAD model of the product, Archimedes automatically finds part to part contacts, generates collision free insertion motions and chooses an assembly order. Combined with an Engineer's knowledge of application specific assembly process requirements allows systematic exploration of the alternative assembly sequences. Archimedes implements AI in the planning, geometric reasoning, and search algorithms, the constraint-based implementation heuristics, and the graphical-user-interface.

AI ASSEMBLY SOFTWARE

Manufacturing companies throughout the world are rapidly changing in order to survive in today's highly competitive market environments. Some examples of coping with changing environments are manufacturing globalization, automated and intelligent manufacturing, virtual manufacturing, and agile

0-7803-5489-3/99/$10.00 ©1999 IEEE.

manufacturing. The objective of this movement in manufacturing is to improve flexibility, reliability and productivity, and to achieve competition-based technology development.

Accordingly, the main focus of Sandia's automated assembly analysis and planning research and development program is to provide intelligent software tools which automate many of the manufacturing processes that have traditionally been known to be the most costly, the most time-consuming, and the most error-prone. Some of these include part-level assembly planning, fixture planning, grasp planning, motion planning, tools planning, and cost analysis. Sandia's overall strategy to reduce these costs is to push the breadth of application and depth of analysis and to find an appropriate balance between human and machine planning. Figure 1 helps illustrate this concept. The ultimate goal is to improve profitability of operations by developing smart software. The developers of the Archimedes software focus on the limitations of the commercially available software packages and the needs of the manufacturing community to provide better solutions quicker.

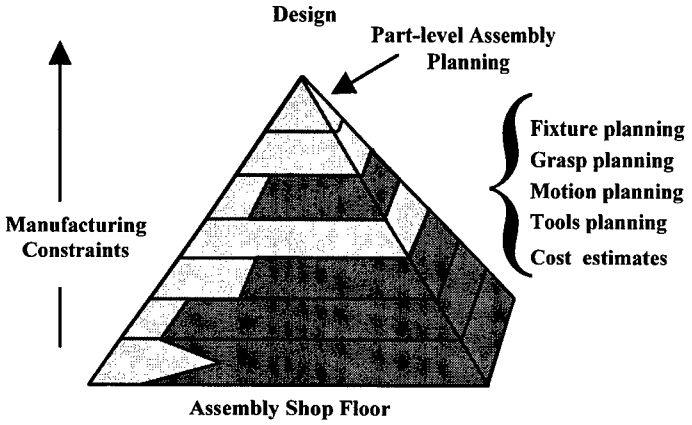


Fig. 1. Geometric-reasoning for manufacturing processes.

The Archimedes 4.0 system is a constraint-based interactive assembly planning software tool used to plan, optimize, simulate, visualize, and document sequences of assembly. Given a CAD model (ACIS® representation) of the product, the program automatically finds part-to-part contacts, generates collision-free insertion motions, and chooses assembly order. The engineer specifies a quality metric in terms of application-specific costs for standard assembly process steps, such as part insertion, fastening, and subassembly inversion. Combined with an engineer's knowledge of application-specific assembly process requirements, Archimedes allows systematic exploration of the space of possible assembly sequences. The engineer uses a simple graphical interface to place constraints on the valid assembly sequences, such as defining subassemblies, requiring that certain parts be placed consecutively with or before other parts, declaring preferred directions, etc.

The system considers thousands of combinations of ordering and operation choices in its search for the best assembly sequences and ranks the valid sequences by the quality metric. Graphical visualization enables the engineer to easily identify process requirements to add as sequence constraints. Planning is fast, enabling an iterative constrain-plan-view-constrain cycle. For some restricted classes of products, it determines plans that optimize a given cost function, graphically illustrates those plans with simulated robots, and facilitates the generation of robotic programs to carry out those plans in a robotic workcell.
Figure 2 represents the overall structure of the system. At the top-middle and on the left-hand side are the design and constraint modules, which capture and represent the geometric, mechanical, and other information about the product required for analysis. These constraints come from a wide variety of sources: design requirements, part and tool accessibility, assembly line and workcell layout, requirements of special operations, and even supplier relationships; they can drive the choice of a feasible or preferred assembly sequence.

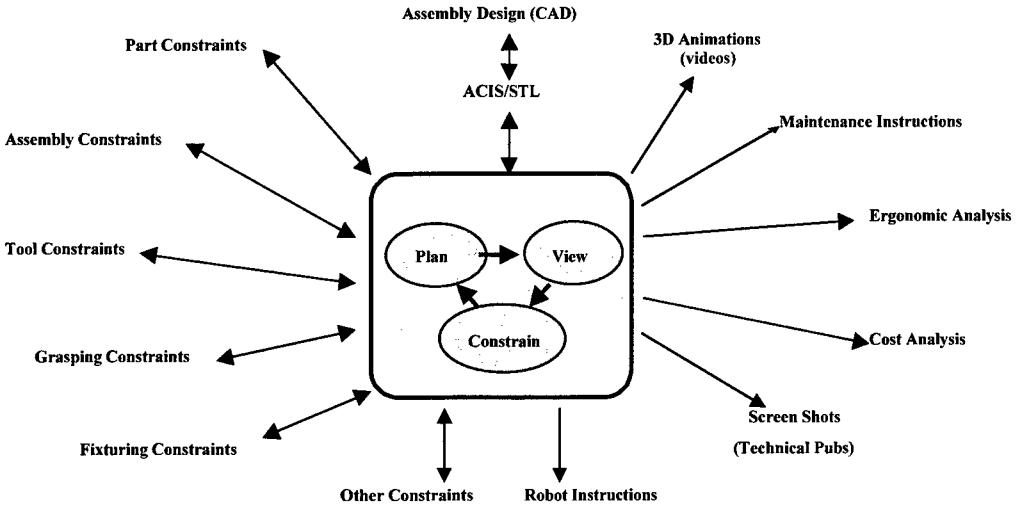


Fig. 2. The Archimedes 4.0 Assembly Analysis and Planning Software System.

The modules listed on the right-hand side are the output modules. They include options to capture the sequences in the form of 3D-animations and videos, textual scripts and snap-shots that can be used for maintenance instructions and technical publications. The system also generates skeleton scripts to run robots, cost analysis information, and ergonomic analysis information.

Throughout the development the system has been applied to a wide variety of products from industry and government and has been tested on over 100 assemblies. Assembly part-count ranges from 5 to 1500. ACIS® data sizes range from 0.2 MB to 212 MB where the data for each distinct part is counted only once, regardless of the number of times that part appears in the assembly. Planning times vary from 4 seconds up to approximately 6 hours. Planning times given are those required to load in the pre-facetted data, identify all contacts in the assembly, and find a single geometrically valid part-level assembly sequence. Times were reported using an SGI Indigo Extreme workstation.

Statistical results indicate savings in both time and money. Early reports by some users show more than a 75% reduction in time schedules, and a 25% reduction in prototype-fabrications cost.

PRODUCTION PROCESS MODELING

Once a assembly process has been defined and optimized using Archimedes the next step is to introduce and test the process inside a manufacturing facility. This step introduces several more constraints outside the scope of Archimedes that can have a dramatic impact on cost and schedule. Some of these constraints can include throughput requirements, multi-manufacturing lines sharing common resources, availability and shifts of labor, pre- and post-processing of assembly parts such as environmental testing and oven curing, sub-assembly part availability, power outages, machine breakdown and repair, yields, bottlenecks, rework, lot sizes, part starts/day, and quantity of tooling and fixture availability. Additional constraints to include contractual agreements, business process and safety and environmental regulations can have dramatic and pivotal impacts upon the assembly times. The most effective means for accounting for these constraints is to use production process modeling.

Production modeling has been available commercially within the last two decades. However, only in the last couple of years has production process modeling become the versatile tool it is today. Object Linking and Embedding (OLE), Open Database Connectivity (ODBC), Multimedia, and Component Object Model (COM) standards and others have been adopted enabling easier integration of other software tools.

The multimedia capability is what has currently been determined the best way to tie the Archimedes output to the process model. The simulation has the ability to run the video files within the simulation to visually demonstrate the assembly procedures at various stages of the process simulation. Combining these two visual elements allows the user a unique perspective and an opportunity to modify assembly procedures as a result of process imposed constraints. The iteration of assembly process to manufacturing process can continue until a reasonable amount of satisfaction has been achieved.

MATERIAL FLOW SOFTWARE

Assembly sequence and process simulation have now provided a solution to the majority of issues surrounding successful manufacturing planning and implementation. The few that remain involve the actual placement of machines, personnel, walkways and material handling routes and storage. These can be accomplished with material flow software.

This software requires the process simulation information, physical size, quantity, and space required to access the machine or workstations, the physical layout of the facility with doors, walls, and any other physical constraints of the building structure. The software then searches for the optimal placement of machines based on the process flow information attempting to arrange major and minor flow of production in a manner that minimizes congestion of material handling and crossover of personnel movements. This software is not limited to inside a facility but can be used for multi-building configuration where material handling must be performed between the buildings.

This kind of analysis can give insight into alternative approaches to assembly and process optimization particularly where shared resources and limited production spaces are involved. Once again an iterative approach is used in order to optimize design to process simulation to material flow.

APPLICATION

A U.S. Army missile wing and probe assembly is being analyzed to determine the optimal assembly sequence, the number of operators required to ramp up production, and the optimal allocation of labor, to affect an overall reduction in process lead times.

The current process for the wing and probe assembly proposes that all assemblies be performed by one operator at an assembly workstation. The wing and probe are both made separately at the same workstation and are not assembled together. The current workflow consists of five first order assemblies preceding a series of additional assemblies and seven oven cures. The current production facility contains four assembly workstations with one operator to man each workstation. There is an additional employee who works as a material handler and is responsible for ensuring that the operators are supplied with assembly kits, placing subassemblies in the oven, keeping the oven login sheet updated, removing cured assemblies from the oven and distributing them back to the operator. There is currently one oven with the capacity to handle the seven oven curing processes. According to the contractor, there is additional space for three additional ovens and six additional workstations each to be manned by one operator. These additional workstations will be utilized when production ramps up to higher volumes.

A baseline simulation model of the current process was set up using WITNESS simulation software. To determine the most effective way of utilizing the current process, a series of variations was made to the baseline model. The variations included changing shift schedules, increasing number of workstations and operators, changing which subassembly was performed first, and incorporating a learning curve into the process. The variations did not show a significant difference in throughput, however starting subassemblies according to the longest remaining assembly time showed a significant decrease in work in process. All variations to the model showed that the work in process was at least twice the throughput. The work in process is attributed to the fact that operators continue to start new subassemblies during the oven cures, the oven cures are so long that the operator has time to start numerous new subassemblies.

From the baseline model results it was also determined that the current process could not meet future production requirements. If the additional operators, workstations, and ovens are utilized during full rate production the process can only produce approximately 30% of demand. To increase throughput and meet demand, product will have to be produced ahead of schedule or process improvements will have to be made.

To aid in determining the optimal assembly sequence, the use of Archimedes will be implemented. While the current assembly sequence may be optimal, Archimedes should conclude what the optimal sequence is. If the optimal assembly sequence is currently being utilized, alternative solutions such as changing the process to an assembly line verses an assembly cell will be made. The process is currently being simulated as an assembly line to determine if there is an increase in throughput and a decrease in work in process. Since the operator will work on a smaller number of subassemblies, he should become more efficient and thus improve the overall process. Preliminary analysis has shown that one of the assembly line ideas could reduce the number of operators from 4 to 3 and increase throughput by 26%. A plan has been made to maintain the fourth operator in hopes to gain a greater throughput increase.

A material flow analysis has not yet been performed. This analysis will be done following the assembly line model completion.

CONCLUSIONS

The contractor producing the wing and probe for the Army could not provide drawings needed for Archimedes assembly order analysis. The drawings are in the process of being converted to the solid model representations needed for this purpose. There are approximately 84 parts that will need to be redrawn. Varying sequence of assembly of the wings and probes are possible. However, only one process has been traditionally used. Once the drawings are available to Archimedes, alternative assembly orders can be experimented with. Parallel assembly processes are also possible allowing for a greater savings in overall process time reduction that has been predicted. The process modeling has been able to demonstrate a 30% increase in throughput with one less labor allocation. The assembly line approach versus a single person assembly work cell is responsible for this increase in throughput. In addition, the process modeling has provided insight into the scheduling of new kit starts, thereby decreasing the amount of work in process. The high amount of work in process can have a detrimental effect on the efficiency of the process both in quality of workmanship that goes into each assembly and the time needed to accurately maintain a higher than necessary number of partially completed assemblies. Hard benefits such as increased throughput and soft benefits such as the effects of substantially high work in process and the number of operations an operator performs are all benefits that come from the use of a new application of artificial intelligence technology. The concept of performing and verifying assembly processes prior to developing process simulation and then followed by material flow software is considered to be a sound one. Additional amount of research and work will need to be performed to integrate these tools at a higher level. The currently used standards do not allow a smooth flow between software packages and the iterations that must occur between them can be time consuming. With this in mind this type of analysis and verification has not been possible until now. The next step will be the integration of design to assembly and the material flow to near real-time data visualization and control. Thereby creating a completely virtual environment that can then become reality with a high degree of confidence in a products ability to be designed, built and perform as intended.

Prediction of Materials Properties

How *Ab initio* Computer Simulation can Predict Materials Properties before Experiment

Yoshiyuki Kawazoe

Institute for Materials Research (IMR), Tohoku University,
Sendai, 980-8577, Japan
Email: Kawazoe@imr.edu

ABSTRACT

Ab initio simulation is now possible to predict materials properties without experimental parameters. To this aim, it is important to avoid any parameters which depend on experiments in calculation. As a fundamentally new all electron formulation, mixed-basis approach is introduced which is completely free from experimental data and several typical examples of numerical simulation using it are shown. It is shown that *ab initio* simulation to be effectively applied to real materials,hierarchical approaches are fundamentally necessary.

INTRODUCTION

To achieve fundamental progress in industrial development, new materials arealways the basis to realize such progress. However, most simple binary and ternary alloys have already been studied and it becomes more and more difficult, time consuming, and costly to create useful new materials only by experimental studies. To overcome this difficulty, it has long been a dream to predict material properties theoretically without experimentation. Because of the rapid progress in supercomputer power, it is now possible to determine physical and chemical properties of materials by*ab initio* simulation. Material properties can be estimated theoretically, since fundamentally the system in which we are interested contains atoms consisting of nucleus and electrons that interact with Coulomb force and obey the quantum mechanical Schrödinger equation. The only difficulty to solve the equation lies in the large number of atoms(10^{23}) to be treated and the many-body interactions.[1] *(From ancient times, the three-body problem has been a synonym for difficult problems.)*

However, to study the vast variety of mechanical, electrical, and magnetic properties, it is only necessary to solve the equation for the ground state. The local density approximation (LDA) is a practical method to eliminate the many-body interactions and is known to be able to reproduce the ground state properties correctly. To avoid time consuming calculations, normally pseudo-potentials are used with plane wave expansion of the system wave function. Although this method has been used widely, it contains arbitrary parameters (how to construct pseud-opotentials, etc.). We have developed one of the most accurate formulations based on LDA adopting all-electron full-potential mixed-basis wave functions[2, 3] The computer code based on this formulation can predict the structure of materials (Complete structure optimization is only possible by our method, and it is impossible by any methodsthat assume "muffin tins") and a wide range of material properties. Some typical numerical results obtained by the program onthe dynamic behavior of clusters, surfaces, and bulk materials will be introduced to indicate that new materials that have properties required by industry can actually be predicted by computer simulation.

It is not possible to analyze interesting experimental data simply by applying *ab initio* calculations, since real materials are very complex and this complexity can not be handled even by present-day highest-speed and largest-memory supercomputing systems. To overcome this difficulty, several methods have been developed and used. The first one is to use simple classical molecular dynamics, which extracts potential parameters from the *ab initio* results. Although this method is powerful for simulating large size systems, it can only be applied under conditions in which the potential parameters are determined [4] The next technique is the tight binding (TB) method, which also fits TB parameters to the*ab initio* results. [5] This method is far better than classical-molecular dynamics, since it recalculates electronic charge density for different structures. An example of TB simulation isshown in the next section for carbon nano-tubes. [6]

The third method is cluster-variation, which can estimate free energy and has beenused in material science for a long time, starting with empirical parameterization. At present, with the cluster variation method, *ab initio* total energy results are used. [7,8] Lastly a new method called the direct method has been introduced to treat phonon dispersion. Several groups have developed this method and we are one of these. Below is given an example of numerical result by using the direct method [9]

As mentioned above, LDA is a good approximation for the ground state. To simulate material properties related to excited states, it is necessary to introduce better approximations. *(Basically all experiments are performed including excited states; it is only possible to observe materials properties by exciting the system!)* Therefore, we have added a new computer code to our all-electron program to be allow treatment of excited states. The approximation is known as GW (Green function + vertex). It was developed almost half a century ago! Unfortunatley, it has not been able to be computed numerically, because computer resources have been limited. Recently, rapid progress of computer power has made it possible to calculate realistic materials with the GW approximation. We have already simulated several important physical properties, like band gap in typical semiconductors and microclusters.[10]

This paper is organized as follows: In the next section, several examples of the application of all-electron mixed-basis code are shown with the TB calculation and cluster variation method (CVM). Concerning the direct method, simulated results on structural phase transitions are shown.

SIMULATION RESULTS BY ALL ELECTRON-MIXED BASIS-APPROACH

Carbon nanotube diode

Present day state-of-the-art large-scale, integrated-circuits (LSI) technology uses the order of 0.1μm fabrication sizes It is desirable to make more and more high-density devices to realize larger memory size to store high-quality video and allow higher speed scientific and engineering calculations. For these aims, it is not possible to only play within the photo-etching technology. To overcome this level of density fundamentally, we propose a new nano-scale device based on the carbon nanotube. [6]

By doping both positive and negative ions into a nanotube, it is possible to make an N-P junction. Using this junction as a building block, we can fabricate nano-scale transistors and nano-scale electric devices. In the simulation, we have used a zigzag nanotube of radius 7.7Å and length of ~ 50Å with 480 carbon atoms simulated by the tight binding model. A periodic boundary condition is applied to the tube direction. It is a semiconductor having 0.6eV gap. By doping 6 pairs of ions, donor and acceptor bands appear and the gap becomes very small at 0.1eV, and the behavior of nanotube is almost metallic The transport properties are estimated by assuming the nanotube as a simple cylinder. The I-V curve is calculated by using Landauer's formula, and this confirms that the doped nanotube behaves as a nano-scale diode.

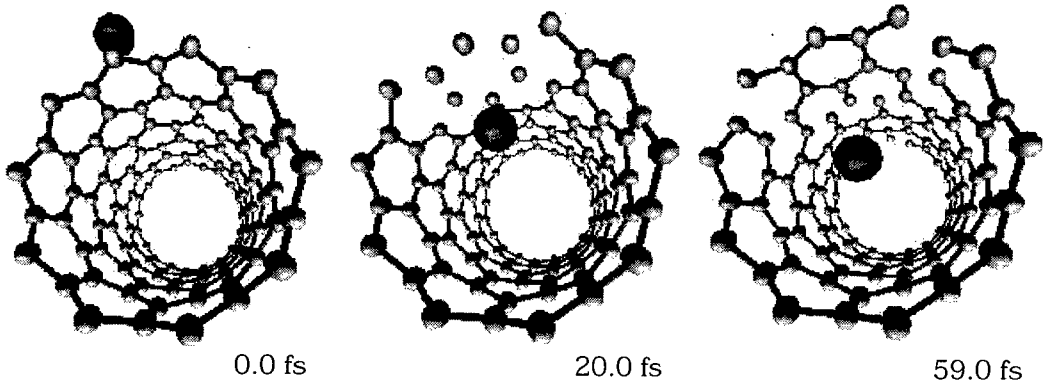


Fig. 1. Ion insertion into a carbon nanotube simulated by all-electron mixed-basis molecular dynamics.

Although we have proposed the carbon nanotube diode, at the moment, experimentally it is very difficult to pick it up to dope ions. Especially, it seems impossible to insert ions from the tube edge. The only

plausible way to insert positive and negative ions into thenanotube is to strike them through the wall. Even the hexagon seems too small to pass ions through. We have performed an all-electron mixed-basis molecular dynamics simulation and confirmed that this process is possibleWhen the ion comes close to the nanotube, the hexagon or pentagon in the wall of the nanotube opens and the ion shrinks because of charge transfer, and so, finally, inclusion is realized. The initial kinetic energy to achieve this process is around 40eV. Lower kinetic energy is insufficient for an ion to penetrate into the nanotube, and higher energy damages the wall and the ion passes through the nanotube but then goes away. Figure 1 shows the process of ion insertion into the nanotube. It takes about 40 fsec for this process. [11]

Defect in bulk iron

It is an important subject to estimate the effect of defects in crystals generally in materials science. Among these, defects in iron have been a central theme in nuclear reactor studies. We have applied our all-electron formulation to analyze this phenomenon. An all-electron full-potential mixed-basis simulation is performed using a bcc unit cell with an experimental nearest neighbor lattice constant of 2.48Å. The atomic orbitals used in this calculation are 1s, 2s, 2p, and 3s orbitals, together with 3,151 PW's corresponding to 178 Ry cutoff energy. The number of $\boldsymbol{k}$-points is 40 inside the irreducible part of the first Brillouin zone. The resulting magnetic moment is 2.19μ_B, which is closer to the experimental value than previous results. In the present calculation, not only do we calculate Hellmann-Feynman forces but also the variational forces are determined explicitly in the molecular dynamics simulation. Although *ab initio* total energy calculations and *ab initio* molecular dynamics simulations can be applied to determine the energetics and locally stable structures of metallic systems with vacancies and interstitial atoms, it is very difficult to estimate them, since there is no translational symmetry.

The numerical results of our simulation areshown below for a bcc iron crystal.[12] The vacancy formation energy of the crystal is estimated as the difference of total energies of perfect crystal and a system with a single vacancy. For the perfect system, we put 16 atoms inside a cubic unit cell of size, 5.73x 5.73 x 5.73 Å, while for the system with a vacancy we put 15 atoms inside the same unit cell. Although this system is not large enough, atomic displacements surrounding the vacancy are notso important in comparison to the interstitial case. Comparing the total energies of the 15-atom defect system with that of the 16-atom perfect system, we obtain the vacancy formation energy of 1.8 eV by using the LDA pseudo-potential approach and 1.2±0.2 eV by using the all-electron full-potential mixed-basis approach with the local spin density approximation, which are comparable to the reported experimental value of 1.8 eV. In the calculation performed with the all-electron full-potential mixed-basis approach, the number of $\boldsymbol{k}$-points in the irreducible Brillouin zone is set to 4 and the PW cut-off energy is 16.5Ry (the number ofPW's is 1,419). The present results stillhave room to be modified by expanding the size of the simulation cell, which needs more computer resources.

Cluster variation method

The standard *ab initio* LDA calculation gives us information on the ground state total energy and stable structure of the materials with physicochemical properties. It is necessary to study thermodynamic properties to reveal dynamic behaviors of materials at finite temperature. To this aim,the cluster variation method (CVM) was used to determine the phase diagram by estimating the free energy by using the energy parameters for clusters in complex systems estimated by*ab initio* calculation.

CVM can also be applied to determine site preference of ternary additions in alloys. We have studied the site preferences of transition metals in Ni_3Al and other important alloy systems to analyze and predict, for example, phase stability at low temperature for high temperature materials. [7] Another application of CVM is to study the dynamic behavior of the interface. The Al-Al_2Li system has been studied as an example [8]. We have used a supercell consisting of 38 fcc cubes in the calculation includinga (100) interface boundary (IPB). A part of the obtained results is shown in Figure 2. It clearly shows that at the IPB the Li concentration varies from one phase to another. At 400 K the thickness of this variation is about 4 lattice constants and is a linear function of temperature.

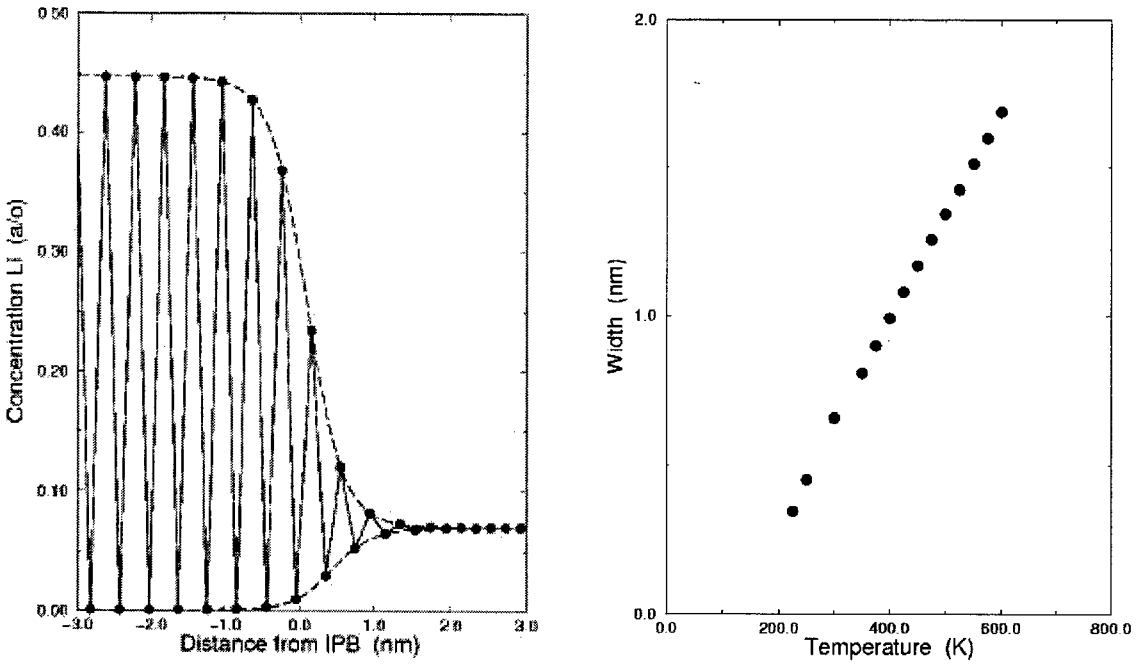


Fig. 2. (left) Li concentration averaged over (100) planes parallel to the IPB as a function of distance (in units of the lattice constant) at 400 K. The solid and dotted lines are drawn for the eye. **(right)** Estimated width of the IPB as a function of temperature.

Direct method

Ab initio calculations have mainly been applied to estimate electro-magnetic properties in solids. On the contrary, it has been very difficult to analyze mechanical properties based on first-principles simulations. The direct method was recently invented to study phonon dispersions and phase transitions in crystalline solids based on *ab initio* calculations [9] This approach is one of the first attempts to simulate mechanical properties in crystals. The calculation of phonon frequencies of the crystal is one of the fundamental elements required to study phase stability, phase transition, and thermodynamics. Another *ab initio* calculation, the linear response method, has difficulty in determining phonon dispersions, since the dielectric matrix must be calculated in terms of electronic eigen-functions of perfect crystal [13]. In the direct method, the dynamical matrix is constructed using cumulant force constants determined numerically by the Hellman-Fynman force and this is solved to obtain phonon dispersions.

We have successfully applied the direct method to study structural phase transition in cubic ZrO_2. The force constants are determined from the Hellman-Fynman forces induced by displacement of atoms in a 2 x 2 x 2 fcc supercell. The calculated phonon dispersions in Figure 3 show clearly a soft mode at point X, which corresponds to the experimentally confirmed cubic to tetragonal structural phase transition.

CONCLUSIONS

In this paper, it is discussed and some examples are indicated to show the present possibility of predicting materials properties without any arbitrary and/or experimental parameters. It is ***not*** a dream already to numerically solve the basic quantum mechanical equations for realistic materials industrially interested in.

ACKNOWLEDGEMENTS

The author thanks all his collaborators who have contributed to this work. Especially, Profs. K. Parlinski, K. Ohno, and M. Sluiter, Drs. K. Esfarjani, Y. Maruyama, H. Kamiyama and Z-Q. Li, and Mrs. A. Farajian and K. Shiga, are the researchers who provided the new concepts and numerical simulations presented in

this paper. He is also grateful to the crew of the Information Science Group at the Institute for Materials Research, Tohoku University for their continued support of the HITAC S-3800/380 supercomputer system.

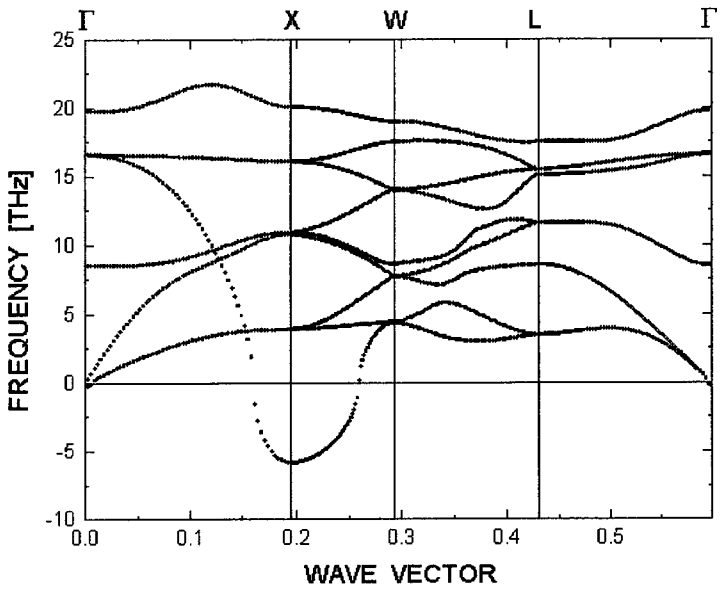


Fig. 3. Phonon dispersion of ZrO_2 in the cubic structure estimated by the direct method.

REFERENCES

1. Y. Kawazoe, K. Ohno, and K. Esfarjani, 1999. "Materials Science - Molecular Dynamics and Monte Carlo Simulation", Springer-Verlag, (in press).
2. K. Ohno, Y. Maruyama, K. Esfarjani, Y. Kawazoe, N. Sato, R. Hatakeyama, T. Hirata, M. Niwano,1996. Phys. Rev. Lett. 76, 3590.
3. Y. Maruyama, K. Ohno, Y. Kawazoe, 2000. to be published.
4. T. Aihara and Y. Kawazoe, 1997. Prog. Theor. Phys. S126, 355.
5. K. Esfarjani, Y. Hashi, J. Onoe, K. Takeuchi, Y. Kawazoe, 1998. Phs. Rev. B 57, 223.
6. K. Esfarjani, Y. Hashi, A. A. Farajian, Y. Kawazoe, 1997. Proc. of IPMM97, 171.
7. M. Sluiter Y. Kawazoe, 1996. Phys. Rev. B 54, 10381.
8. M. Sluiter, M. Asta, Y. Kawazoe, 1996. Sci. Rep. RITU A 41, 97.
9. K. Parlinski, Z-Q. Li, Y. Kawazoe, 1997. Phys. Rev. Lett. 78, 4063.
10. M. Ishii, K. Ohno, Y. Kawazoe, 2000. to be published.
11. A. A. Farajian, K. Ohno, K. Esfarjani, Y. Maruyama, Y. Kawazoe, 2000. to be published.
12. K. Ohno, Y. Maruyama, H. Kamiyama, E. Bei, K. Shiga, Z.-Q. Li, K. Esfarjani, Y. Kawazoe, 1999. in `Mesoscopic Dynamics of Fracture: Computational Materials Design' edited by HKitagawa, T. Aihara, Jr., and Y. Kawazoe, Vol.1 of Advances in Materials Research Springer-Verlag.
13. R. D. King-Smith, R. J., 1990. Needs, J. Phys.: Condensed Matter 2, 3431.

Data Driven Knowledge Extraction of Materials Properties

J.S. Kandola*, S.R. Gunn*, I. Sinclair, P.A.S. Reed****

* ISIS Research Group, Department of Electronics and Computer Science,
** Engineering Materials Research Group,
School of Engineering Sciences, University of Southampton, U.K.

ABSTRACT

In this paper the problem of modelling a large commercial materials dataset using advanced adaptive numeric methods is described. The various approaches are outlined, emphasising their characteristics with respect to generalisation, performance and transparency. A highly novel Support Vector Machine (SVM) approach is taken incorporating a high degree of transparency via a full ANalysis Of VAriance (ANOVA) expansion. Using an example which predicts 0.2% proof stress from a set of materials features, different modelling techniques are compared by benchmarking against independent test data.

INTRODUCTION

The development of empirical models is fundamental to understanding complex materials properties within the field of materials science [1,2]. Models may then be used to discern the physical relationships that exist and enable optimisation of materials production. Empirical modelling is the extraction of system relationships from observational data, to produce a model of the system, from which it is possible to predict responses of that system. Ultimately the quantity and quality of the observations govern the performance of the empirical model. Often only partial knowledge is available about the physical processes involved, although significant amounts of 'raw' data may be accessible from production and product release records, which may then be used to construct a data-driven model.

The empirical study of materials phenomena through statistical models has a number of limiting characteristics. Consider a dataset $D_N = \{x_i, y_i\}^N_{i=1}$, drawn from an unknown probability distribution, F, where x_i represents a set of inputs (e.g. alloy composition and thermomechanical processing information), y_i represents a set of outputs, (e.g. mechanical properties) and N represents the number of data-points. The empirical modelling problem is to find any underlying mapping $x \rightarrow y$ consistent with the dataset D. Due to their observational nature, the data obtained are finite. Typically, this sampling is non-uniform and, due to the high dimensional nature of the problems of interest (i.e., large numbers of inputs), the data only forms a sparse distribution in input space. Consequently the problem is nearly always ill-posed in the sense of Hadamard [3]. To address this ill-posed nature, it is necessary to convert the problem to one that is well-posed. To be well-posed, a unique solution must exist that varies continuously with the data. We consider various modelling approaches intended to transform the problem to one that is well-posed. A further limitation of any empirical modelling technique is its ability to resolve the problem of highly correlated inputs; if two inputs are highly correlated it is difficult to identify individual effects on the output.

The work presented in this paper compares and contrasts common empirical models, and state of the art approaches, on the basis of their generalisation ability and transparency. This paper advocates a transparent approach to the modelling problem, which enables understanding of the underlying relationships between inputs and outputs. This knowledge can then be used to enhance model validation through comparison with prior physical knowledge. Generalisation performance is the assessment of model predictions to new and unseen data. Traditional empirical modelling approaches may suffer in terms of generalisation, producing models that can overfit the data. Typically, this is a consequence of the model selection procedure which controls the complexity of the model. For a given learning task, with a finite amount of training data, the best generalisation performance will be achieved if the "capacity" of the model is matched to the complexity of the underlying process.

0-7803-5489-3/99/$10.00 ©1999 IEEE.

THE MATERIALS DATASET

In this paper we consider an extensive commercial dataset for Aluminium alloy 2024 in a T351 temper, with the objective being to predict 0.2% proof stress. The "raw" dataset consists of 35 input variables and 2870 data pairs covering various compositional and thermomechanical processing parameters, as well as containing "shop floor" information such as plate numbers and date of alloy manufacture.

For a physically amenable model to be constructed, the original data set was decomposed into a smaller subset based on a single tensile direction (LT), thickness position (C), and a width position (0.5). All of the major alloying elements and the major impurities were retained as inputs to the model, however the minor compositional information was removed. The "shop floor" information was also removed since it was not expected to contribute directly to proof stress, but does provide a valuable check for changes in processing methods, equipment *etc.* Assessment of the slab dimensional information revealed the majority of the slab width and the slab gauges to be fixed; as a consequence the dataset which was used for modelling contained information for a single slab width/gauge combination. The initial scalped slab gauges on inspection were found to be equal, and as such the total reduction of each plate is entirely defined by the final gauge. The hot-rolled width and length were used to define reduction in the longitudinal and transverse directions; hence a "reduction-ratio" was computed as the ratio of engineering strain in the long and transverse directions between the slab and the final plate. This stage of data pre-processing left a reduced size dataset: the input variables comprised ten characteristics; the final gauge (FG), Cu, Fe, Mg, Mn, Si (in weight percent), slab length (SL), solution treatment time (STT), percentage stretch (%st.), and reduction ratio (RR). After removing the entries with missing and repeated values, 290 data points remained. Before any of the modelling techniques were used to predict the proof stress, the dataset was normalised to have a mean of zero and unit variance.

MODELLING TECHNIQUES

This section considers the adaptive numeric methods used to predict proof stress based on a dataset described in the previous section. Three techniques were considered: (i) Multivariate Linear model, (ii) Bayesian multi-layer perceptron, (iii) Support Vector Machine. Data structure was also examined using a graphical Gaussian model. Each of these models (except the graphical Gaussian model) are assessed against each other quantitatively using the MSE test statistic, and qualitatively in terms of transparency.

Graphical Gaussian Models

As the dimensionality of the problem domain increases graphical models and graphical representations are playing an increasingly important role in statistics, and empirical modelling in particular. Relationships between variables in a model can be represented graphically by edges in a graph where the nodes represent the data variables. Such graphs provide qualitative representations of the conditional independence structure of the model, as well as simplifying inference in highly structured stochastic systems.

Let X be a k-dimensional vector of random variables. A conditional independence graph [4], $G = (V,E)$ describes the association structure of X by means of a graph, specified by the vertex set V, and the edge set E. Conditional independence is an attractive method to generalise the relation between two variables. A graphical model is then a family of probability distributions P_G that is a Markov distribution over G. A graphical Gaussian model is obtained when only continuous random variables are considered. If we can assume that the data has been drawn from a Gaussian distribution, then there is no loss of information by condensing the data into the sample mean vector, and the sample variance-covariance matrix. A symmetric correlation coefficient matrix can then be obtained from this matrix. To construct the graphical model it is necessary to test for the presence or otherwise of dependencies between the variables. Using a scaled inverse correlation matrix, a second deviance matrix can be computed using equation 1, where X_a and X_b represent the variables against for which conditional independence is being tested for given the other variables in the dataset X_C. This test statistic has an asymptotic chi-squared distribution with one degree of freedom.

$$dev(X_b \| X_c | X_a) = -N \ln(1 - corr_N^2(X_b, X_c \mid X_a)) \qquad 1.$$

This second matrix, the deviance matrix, measures the overall goodness of fit of a graphical model by carrying out a hypothesis at a 95% confidence interval of the chi-squared distribution. Figure 1 illustrates the graphical model obtained for the materials dataset.

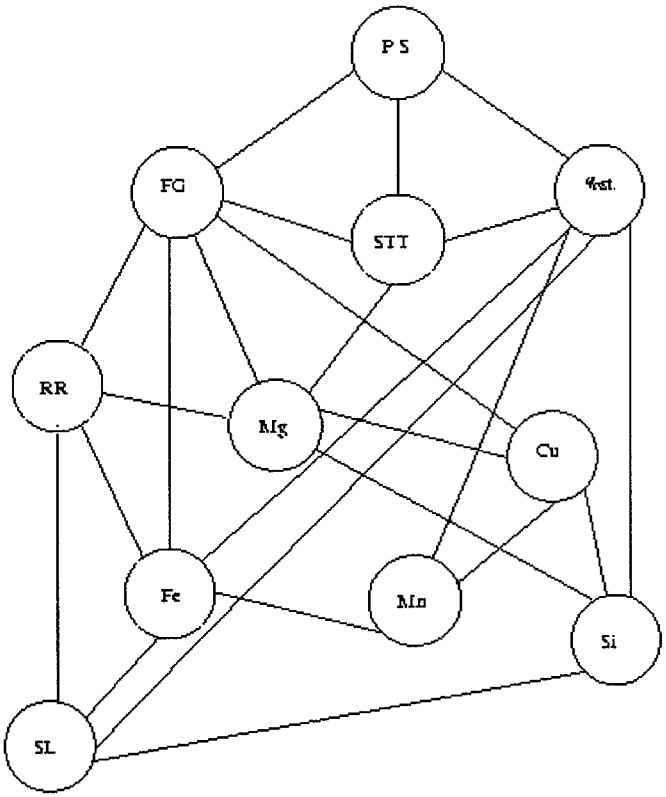


Fig. 1. Graphical Gaussian model for the materials dataset.

This figure provides a powerful tool to visualise the complex interactions between different data variables. For a 10 input dataset, a total of 45 relations are possible, however approximately 50% of the relations are deemed to be significant at the 95% confidence level. The graphical model suggests that proof stress (PS) could only be directly predicted from final gauge (FG), solution treatment time (STT) and percentage stretch (%st.) since these are the only variables with which proof stress has direct links. However, the representation shows that there is a large complex hierarchy between the different data variables. The links which are established could represent true physical dependencies between the different variables, as well as representing manufacturing artefacts (for example the use of master alloys in altering composition).

The Multivariate Linear Model

A multivariate linear model is given by equation 2:

$$y = w_0 + w_1 x_1 + w_2 x_2 + \cdots + w_n x_n \qquad 2.$$

where $x_1, \ldots, x_n$ is the models input vector, $w_1, \ldots, w_n$ are unknown parameters to be estimated, and w_0 is a bias term. The unknown vector of parameters, w, can be estimated together with the associated parametric uncertainty in the standard least squares sense [5].

Low parametric uncertainty standard deviation values, relative to the parameter values, are desirable since they imply more confidence in these parameter values, and hence more significance in the inputs. The parameter values and their associated uncertainty are given in Table 1.

Table 1: Weight gains and parametric uncertainty values for the materials dataset.

	Bias	FG	Cu	Fe	Mg	Mn	Si	SL	STT	%st.	RR
w	360.0	-18.1	5.30	4.50	-0.58	4.86	-8.01	-0.41	24.4	21.5	-2.1
σ	4.85	3.45	5.05	3.39	6.12	3.80	3.64	3.37	8.20	3.98	5.68

Since the data are normalised, the size of the weight gains can be directly interpreted to show the first order importance of these variables in affecting the output. The bias term, the final gauge, solution treatment time and percentage stretch show the biggest values with lowest uncertainty. Selection of these variables is consistent with the graphical model dependencies and the expected physical behaviour. However, it must be borne in mind that the graphical model suggests that a complex system of interdependencies exist in this dataset. The MSE obtained for the linear model was 144.13(MPa^2), which represents a tolerance of 12MPa on the proof stress (one standard deviation in the errors between target and predictions).

Bayesian Multi-layer Perceptron

A Bayesian multi-layer perceptron (MLP) encompasses all of the key features of the classical MLP, but differs in that network training takes place using Bayesian learning [6,7]. The result of Bayesian learning is a probability distribution over model parameters that expresses our degrees of belief regarding how likely the different parameter values are. Initially a wide prior distribution, is defined which might express some rather general properties such as smoothness of the network function, but will otherwise leave the weight values fairly unconstrained. Upon observation of the data, this wide prior distribution is converted to a narrower posterior distribution by using Bayes' theorem. This illustrates the fact that we have learned something about the extent to which different weight values are consistent with the observed data.

Following the work of MacKay [8] a Gaussian prior was chosen for the initial weight values (including bias), corresponding to the use of weight decay regularisation which controls the network capacity. Bayesian learning in an MLP simplifies to finding the weight vector, w, which minimises the cost function,

$$E(w) = \frac{\beta}{2}\sum_{n=1}^{N}\{y(x^n;w) - t^n\}^2 + \frac{\alpha}{2}\sum_{i=1}^{W} w_i^2 \qquad 6.$$

This cost function was minimised using the scaled conjugate gradient algorithm [6] while α and β were continuously re-estimated using the evidence framework. Automatic Relevance Determination (ARD) [8] was also used as a form of input selection. A single hidden layer with varying numbers of nodes was used to model the relationship between inputs and outputs. For assessment, cross-validation was used. A plot of the MSE for both training and test data sets is shown in Figure 2 for increasing numbers of hidden nodes.

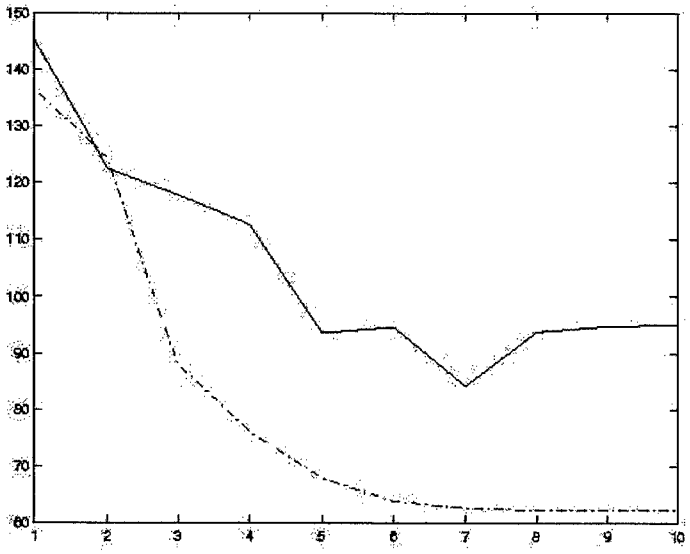


Fig. 2. Varying MSE (training data '-.'; test data '-') for increasing numbers of hidden nodes.

An increase in the number of hidden nodes corresponds to an increase in complexity. The initial MSE values for the test set show a consistent decrease as the number of hidden nodes increases up to a maximum of 7 hidden nodes, after which the MSE increases suggesting that overfitting of the data has started to occur. The MSE for the training set shows a decreasing error for increasing hidden nodes, a manifestation of the fact that increasing complexity corresponds to an increase in regularisation. The training data showed a MSE of 65.0 whilst the test error showed a MSE of 84.2 corresponding to an effective standard deviation of 8MPa on the training data and 9MPa on the test data.

Support Vector Machines (SVMs)

SVMs have recently received intensified research effort, due to many attractive features and promising empirical performance. The formulation embodies the principle of structural risk minimisation (SRM) developed by Vapnik [9]. SRM differs from the common empirical risk minimisation (ERM), by trying to minimise an upper bound on the expected risk, rather than minimising the training set error. If the VC dimension is low, the potential to overfit is low, enabling good generalisation. SVMs nonlinearly transform the original input space into a higher dimensional feature space by using reproducing kernels. The only way the data appears in the training problem is in the form of dot products. The use of a kernel function enables operations to be performed in the input space rather than the potentially high-dimensional feature space.

SVMs, like the Bayesian MLP, are essentially black box models, however transparency can be introduced by use of the SUPANOVA framework [10]. The SUPANOVA promotes a sparse representation within an ANOVA (Analysis Of VAriance) representation. The ANalysis Of VAriance (ANOVA) representation provides a transparent approach to modelling. It describes the decomposition of the function into additive components, with the objective being to represent this function by a subset of terms from an expansion,

$$f(x) = f_0 + \sum_{i=1}^{N} f_i(x_i) + \sum_{i=1}^{N} \sum_{j=i+1}^{N} f_{i,j}(x_i, x_j) + \cdots + f_{1,2,\cdots N}(x) \qquad 7.$$

The solution to this problem is represented by a sum of univariate, bivariate and trivariate ANOVA terms. For this dataset 1024 different terms were possible, however only 20 terms were chosen as being significant. Figure 3 shows a selection of the regression surfaces for the univariate and bivariate ANOVA terms. The MSE for the training set was 61.6 whilst the generalisation MSE was 79.8 a tolerance of 8.9 MPa on the proof stress values.

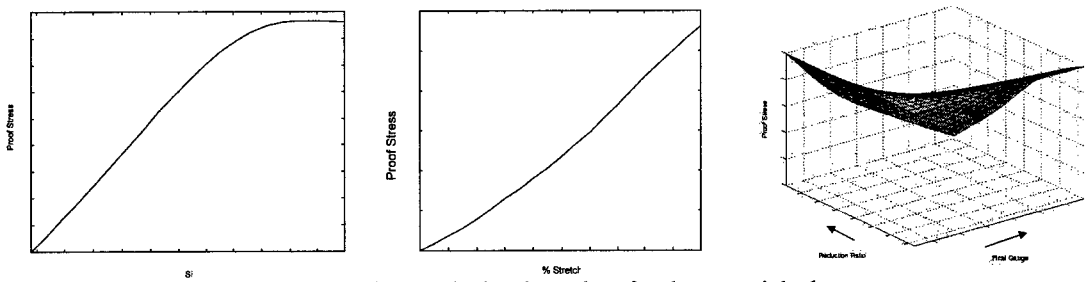


Fig. 3. Univariate and Bivariate plots for the materials dataset.

These regression surfaces represent interaction terms: to be interpretable the terms which appear in the univariate plots, must be added across the relevant dimension should they occur in the bivariate (or higher order) regression surfaces. The regressions may be compared with physical trends, with those shown in Figure 3 showing increasing strength with increasing silicon concentration and percentage stretch, but decreasing with final gauge.

DISCUSSION

This paper has described the modelling of proof stress using advanced adaptive numeric methods. In the context of this example the key empirical modelling themes of model validation, model transparency and model generalisation were illustrated. Table 2 shows the MSE values for each of the quantitative modelling techniques used.

Table 2. MSE values for the empirical models.

	Linear	Bayesian MLP	SVM
MSE Train	94.1	65.0	61.4
MSE Test	145.0	84.2	80.8

The graphical model, through its highly transparent nature, shows that a complex hierarchy of interactions are prevalent in this dataset, as such the separation of a particular variables influence on the output is made difficult. The linear model provided a benchmark against which all of the other techniques were compared. As a consequence of its simple inflexible nature, and inability to adapt to more complex scenarios, it exhibited the worst performance in terms of MSE. However it does provide an indication of variable influence through its transparent nature. The Bayesian MLP showed better performance over the simple linear model, a consequence of its advanced features such as incorporation of input selection via ARD and ability to prevent overfitting through regularisation. A limitation of the Bayesian MLP is that it lacks transparency, the parameters in the network are not directly interpretable in the same way as the linear model. Very local transparency can be introduced by testing the model using artificial datasets, where an input is varied between its maximum and minimum values whilst setting the other variables to be at their means. However, this process is very limited in high dimensional problems. The support vector approach showed the best generalisation ability. The SUPANOVA framework incorporates transparency, and the trends depicted in figure 2 are consistent with expected theories of physical behaviour. This illustrates that a fully transparent modelling approach does not affect generalisation performance, but provides a means for validating the model constructed. SVM's prevent overfitting of the data by zero order regularisation in the nonlinear feature space. A major problem with any empirical modelling approach is the extent to which each of the data variables are correlated with each other. Further work will try to assess the applicability of data preprocessing techniques to resolve this problem.

ACKNOWLEDGEMENT

The authors would like to thank the EPSRC and British Aluminium Plate for their financial support of this work.

REFERENCES

1. H. Fujii, D.J.C. MacKay, H.D.K.H Bhadeshia, 1996. Bayesian neural network analysis of fatigue crack growth rate in Ni-base superalloys. ISIJ International, 36, 1373-1382.
2. A.F. Karr, 1994. Statistics and Materials Science – Report of a Workshop. National Institute of Statistical Sciences.
3. J. Hadamard, 1923. Lectures on the Cauchy Problem in Linear Partial Differential Equations. Yale University Press.
4. J. Whittaker, 1990. Graphical Gaussian Models in Applied Multivariate Statistics. Wiley Publishers.
5. J. Neter, M.H. Kutner, C.J. Nachtsheim, W. Wasserman, 1996. Applied Linear Statistical Models 4th Edition. Irwin Publishers.
6. C.M. Bishop, 1995. Neural Networks for Pattern Recognition. Oxford University Press.
7. R.M. Neal, 1995. Bayesian Learning for Neural Networks. Springer-Verlag Publishers.
8. D.J.C. MacKay, 1994. Bayesian Non-linear Modelling for the Prediction Competition. ASHRAE Transactions: Symposia, OR-94-17-1, 1053-1062.
9. V. Vapnik, 1995. The Nature of Statistical Learning Theory. Springer-Verlag Publishers.
10. S.R. Gunn, 1999. SUPANOVA – A Sparse Transparent Modelling Approach. submitted to NNSP'99. USA.

A Quantum Neural Net: with Applications to Materials Science

B. Igelnik*, M. Tabib-Azar*, Y.-H. Pao*, and S. R. LeClair**

*Electrical Engineering and Computer Science Department
Case Western Reserve University, Cleveland, OH, USA
**Material Directorate, Wright Laboratory, Fairborn, OH, USA

ABSTRACT

In this article a new neural network architecture suitable for learning and generalization is discussed and developed. The architecture is inspired and modeled after quantum electronic devices and circuits where coherent electronic wavefunctions traveling through different parts of the circuit are combined together and result in interferences at detection nodes. These wavefunctions, represented by complex numbers, are implemented as complex weights in our neural net architecture to efficiently and accurately facilitate certain computations. Although similar to the radial basis function (RBF) net, our computational model called quantum net (QN) has demonstrated a considerable gain in performance and efficiency in number of applications compared to RBF net. Its better performance in classification tasks is explained by the cross-product terms in internal representation of its basis functions introduced parsimoniously. These cross-products are the results of interferences naturally occurring in coherent electronic systems. Although we primarily discuss the software implementation of QN on Von Neuman computers, its hardware implementation is also briefly discussed. A number of examples, solved using QN and other networks, are used to illustrate the desirable characteristics of QN.

INTRODUCTION

We explore a new computation method that we call "quantum network" (QN) that uses complex weights in a neural network lattice and can be constructed using quantum wires, dots, and other quantum electronic components. Using coherent electrons or other quantum particles to perform calculations, QN takes advantage of "interferences" that take place between these particles traveling through different paths in the circuit. These interferences are very well known in quantum mechanics and are basis of many physical phenomena such as conductivity of solids, tunnelings in quantum layers, optical properties of clusters, etc. Our QN is the subset of a more general class of computational models and techniques called quantum computers and quantum computing that has received a renewed interest in recent years [1]–[8].

The mathematical model, considered here, is an expansion in basis functions, that is, it connects the multivariate system input x and output y (which without loss of generality can be assumed univariate) by the equation

$$y \doteq f_{N,E_T}(x) = \sum_{n=1}^{N} a_n g_n(x, b_n),$$

where a_n, b_n are adjustable real parameters, g_n are called basis functions. The types and the number of basis functions determine the architecture of the model, its accuracy and efficiency. The basis functions usually have the same structure for any n =1, N and constitute a superposition of a simple multivariate function φ of x and b_n (internal function) and a univariate function g (external function), as shown in the equation

$$g_n(x, b_n) = g(\varphi(x, b_n)).$$

In neural networks and RBF networks the internal function φ is a linear sum of univariate functions

0-7803-5489-3/99/$10.00 ©1999 IEEE.

$$\varphi(x,b_n)=\sum_{i=1}^{d} w_{ni}\psi_i(x_i,c_{ni}),$$

where $x=(x_1,...x_d),\psi_i(x_i,c_{ni})=x_i-c_{ni}$ for neural networks, $\psi_i(x_i,c_{ni})=(x_i-c_{ni})^2$ for RBF networks, and w_{ni},c_{ni} are adjustable parameters. The QN architecture constitutes a model of the following form

$$y=a_0+\sum_{n=1}^{N} a_n g\left[(x-d_n)^T\circ c_n\cdot(\bar{c}_n)^T\circ(x-d_n)\right], \qquad 1.$$

where the parameters $a_n, n=0,...N$ are real numbers, while the parameters $c_n, n=1,...N$ are complex vectors, $\bar{c}_n$ means complex conjugate of c_n, and $\circ$ stands for inner product of two vectors. Unlike the neural, or RBF net, the internal representation in a basis function is not a weighted sum of univariate functions but constitutes a quadratic function of d variables with cross-product terms of special form. This form of internal representation, as we show in next two sections, has both "hardware" and "software" implementations.

MOTIVATION

We were intrigued by the ability of QN to solve some interesting problems, such as XOR problem, in a very simple and straightforward manner. While the neural or RBF networks with one nonlinear basis function cannot solve the XOR problem, the "quantum net" can do it with only one node. As will be shown below, this ability is due to the specific construction of internal representation of a basis function in 'quantum net'. This fact suggests that in some applications QN will work better than neural or RBF networks, at least for classification tasks. Several examples confirm this guess. The number of parameters in a basis function of a 'quantum' net is roughly twice that of similar neural or RBF networks. However, savings in the number of basis functions may exceed losses in the number of parameters. Even relatively small decrease in the number of basis functions can compensate increase in the number of parameters since computational time grows as a quadratic function of the number of basis functions. Another rationale for developing the 'quantum net' is its universal approximation capability.

To illustrate the concept of quantum computing, we examine the well-known double-slit interference experiment shown in Figure 1.

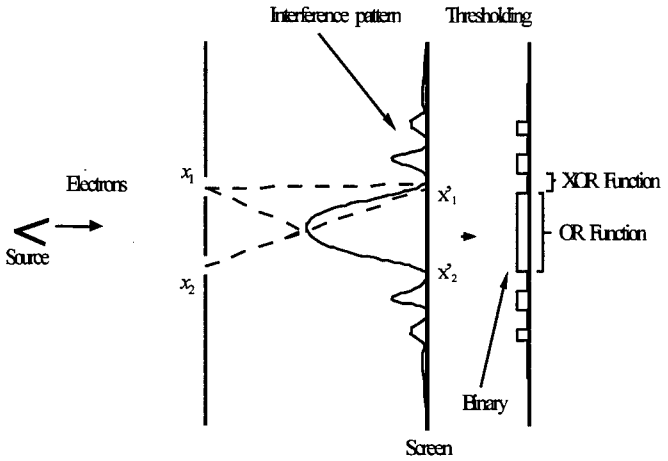


Fig. 1. Schematic of the double-slit interference experiment to illustrate the concept of quantum computing.

We note that the double-slit apparatus can be used to perform both OR and XOR functions depending on the location of the detector on the screen. To perform the OR function the light intensity on the screen is integrated from x_1' to x_2'. Hence, when only one of the slits is open there is enough light at the detector to

exceed the threshold for "1". If both slits are open, the light at the detector almost doubles and after thresholding, a logic one is detected. In the regions where the XOR function is performed, the light intensity is zero when both slits are open (due to destructive interference between lights coming through different slits) or when both of them are closed. The light intensity in this region is high when only one of the slits is open. By choosing an appropriate function for thresholding, this system can be made relatively immune to noise and variations to slit size and other parameters.

Quantum devices in particular and "wave-mechanical" devices in general, can be readily used to perform the following operations: attenuation and amplification, phase change, and detection. Mathematically, attenuation and amplification of an electronic wavefunction (ψ) amounts to multiplication by a real number (A,ψ) while changing its phase $(\psi e^{i\theta})$ is accomplished by multiplication of a complex number. Detection of the electronic wavefunction is accomplished by integration of the square modulus of the wavefunction over a region in space corresponding to the detector's active volume V:

$$\text{Probability of Detection} = \iiint_V \psi(v) * \overline{\psi}(v) dv .$$

When ψ is a slowly-varying function of position and for a unit active volume of the detector, the probability of detection is approximately proportional to the square modulus of the wavefunction:

$$\text{Probability of Detection} = \propto \alpha |\psi|^2 .$$

XOR PROBLEM

The XOR problem is to find a curve $f(x,y)=t$ that separates the points $A(0,0), C(1,1)$ from the points $B(1,0)$ and $D(0,1)$ as shown in Figure 2. That means that there exists a real number t and a model $z=f(x,y)$ such that the points A and C are on the one side of the curve $f(x,y)=t$ and the points B and D are on another side of the curve. Obviously we can take $t=0$. Then we can prove the following propositions [9]

Proposition 1.
Any net of the form

$$f(x,y)=g(\psi_1(x)+\psi_2(y)), \qquad 2.$$

where g is a monotonic, fixed univariate function, ψ_1,ψ_2 are arbitrary fixed-shape univariate functions cannot solve XOR *problem.*

Proposition 2.
There exists a net f of the form (2) with fixed monotonic univariate function g and adaptive-shape differentiable functions ψ_1,ψ_2, formed from polynomials, which solves XOR problem. Any such net should have at least 8 parameters.

Proposition 3.
There exists a quantum net with one node and 4 parameters which solves XOR problem.

Proof. The equation of separating curve for QN with one node is

$$(x-0.5)^2 + 2(x-0.5)(y-0.5)\cos(\theta_2-\theta_1) + (y-0.5) = a^2 . \qquad 3.$$

Transform the variables x and y to new variables u and v by the turn of coordinate axes on the angle $\pi/4$

$$\begin{aligned} x-0.5 &= u\sqrt{2}/2 - v\sqrt{2}/2, \\ y-0.5 &= u\sqrt{2}/2 - v\sqrt{2}/2. \end{aligned} \qquad 4.$$

Substituting (4) into (3), one obtains

$$2u^2 \cos^2 \frac{\theta_2-\theta_1}{2} + 2v^2 \sin^2 \frac{\theta_2-\theta_1}{2} - a^2 = 0 , \qquad 5.$$

which is the equation of an ellipse with axes parallel to coordinate axes. Therefore, in coordinates x and y the equation (5) also constitutes an equation of ellipse with the angle between axes of the ellipse and coordinate axes equal $\pi/4$. This is shown in Figure 2.

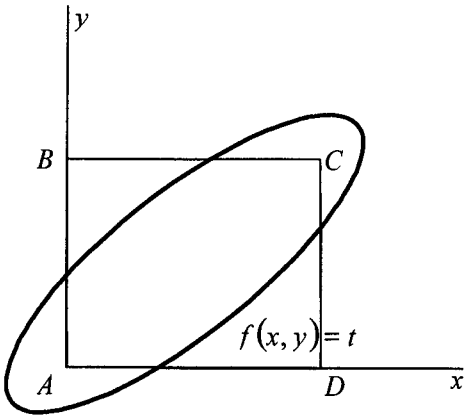


Fig. 2. Geometric illustration of the solution of the XOR problem by quantum net

Substitution of the coordinates of the points A, B, C, and D in the left-hand side of the equation (5) yields

$$\cos^2(\theta_2 - \theta_1) - a^2 > 0, \sin^2(\theta_2 - \theta_1) - a^2 < 0. \qquad 6.$$

The simultaneous inequalities (6) are satisfied, for example if

$$a^2 = 0.5, 0 < \theta_2 - \theta_1 < \pi/4.$$

Therefore, there exists a quantum net with only one basis function, which solves the XOR problem. This net requires not more than 4 parameters if we make position of the center of the ellipse adjustable.

SOFTWARE IMPLEMENTATION

For practical consideration the quantum net should be written in the form

$$y = \tilde{f}(x_1,...x_d) = a_0 + \sum_{n=1}^{N} a_n g\left[\sqrt{w^2 \sum_{j=1}^{d} e^{i\theta_{nj}}(x_j - c_{nj}) \sum_{j=1}^{d} e^{-i\theta_{nj}}(x_j - c_{nj})}\right],$$

where the model is in the coordinate form, all the parameters $a_0, a_n, c_{nj}, \theta_{nj}, w$ are real, w is the absolute value and θ_{nj} is the argument (phase) of a complex parameter. We assume that the input variables $x_1,...x_d$ are scaled so that $0 \le x_j \le 1$. For certainty we assume that the external function g is the Gaussian

$$g(t) = e^{-t^2/2}.$$

The values of the internal parameters are specified by the following inequalities

$$0 \le c_{nj} \le 1, 0 \le \theta_{nj} \le \pi - \Delta, \pi + \Delta \le \theta_{nj} \le 2\pi,$$

where $\Delta > 0$ is any number small compared to π. We divide all data that are available for learning, into two sets, the training set E_T and the generalization set E_G. The ensemble approach [10], [11] is used for training and testing. It constitutes a further development of ideas of the Functional-Link net [12]. The training set is used to adjust the parameters $a_0, a_n, c_{nj}, \theta_{nj}$ on the criteria of the minimal training error, while the testing set is used to determine the number of basis functions N. The parameter w can be adjusted manually. The learning of the model is made by the ensemble approach. The main features of this approach are as follows. The algorithm of learning is sequential. That means that only one node is learned at a time.

The learning starts with a simplest net of the form (node 0) $y = a_0$ and then grows net node by node. Next, consider the best net that can be chosen from the ensemble. This is done by the process of adaptive stochastic optimization. The whole ensemble of K possible choices of the parameters c_{nj}, θ_{nj} is divided in M groups each having L members so that $K = ML$. In first group the parameters c_{nj}, θ_{nj} are generated from the intervals $[0,1]$ and $[0.2\pi] - [\pi - \Delta, \pi + \Delta]$ uniformly. After the first group of the parameters c_{nj}, θ_{nj} have been chosen, the parameters $a_0, a_1, \ldots a_n$, net output, and the training error have been calculated, the net with the minimal training error is identified. The internal parameters $c_{njopt}, \theta_{njopt}$ of this optimal net are kept in memory and used to correct the distribution of the parameters in the groups 2,3,...M. For these groups, instead of the uniform distribution, we use the triangle distribution.

UNIVERSAL APPROXIMATION CAPABILITY OF THE QUANTUM NET

The universal approximation capability of the quantum net was proved [9] in the following theorem

Theorem.(The universal approximation capability of the quantum net).

Suppose the external function g satisfy the conditions

$$0 \neq \int_{-\infty}^{\infty} \ldots \int_{-\infty}^{\infty} \left| g\left(\sum_{j=1}^{d} t_j^2 \right) \right| dt_1 \ldots dt_d < \infty . \qquad 7.$$

Define a distance between a function f, defined and continuous on I^d, *and a quantum net* f_N

$$f_N(x) = a_0 + \sum_{n=1}^{N} a_n g\left[w^2 \sum_{j=1}^{d} e^{i\theta_{nj}} (x_j - c_{nj}) \sum_{i=1}^{d} e^{-i\theta_{nj}} (x_j - c_{nj}) \right] \qquad 8.$$

as

$$\rho(f, f_N) = \sqrt{E \int [f(x) - f_N(x)]^2 dx} . \qquad 9.$$

Thus for any $\varepsilon > 0$ *and any function f, defined and continuous on* I^d, *there exists a quantum net* f_N, *such that*

$$\rho(f, f_N) < \varepsilon . \qquad 10.$$

EXAMPLES OF APPLICATIONS IN MATERIALS SCIENCE

Example 1.

The comparison between quantum net and RBF net was made also on real data [13]. A body of data constitutes 6431 patterns of ternary systems (systems of 3 chemical elements) with 15 features of the elements in the system, 5 for each element. For each system it is known if it can or cannot form a compound. This information is available through long and expensive experimentation and lengthy calculations. The task is to build a neural net, which can accurately predict possible formation of a compound for a new system, not available in the database. The quantum net and the RBF net were applied to this data, both using the ensemble approach for learning and generalization. With RBF net the results are: 72 (95.5% correct) misclassifications in a testing set of 1607 patterns, using 44 nodes, with quantum net 60 misclassifications (96.2% correct) are obtained with 30 nodes and 49 misclassifications (97.0% correct) with 70 nodes. Our experiments have indicated that the activation function for the quantum net can be chosen from the same set of functions as for RBF net. In particular the minimum of generalization error is achieved with the "thin plate" activation function $f(t) = t^2 \log(t)$. These results are shown in Figure 3.

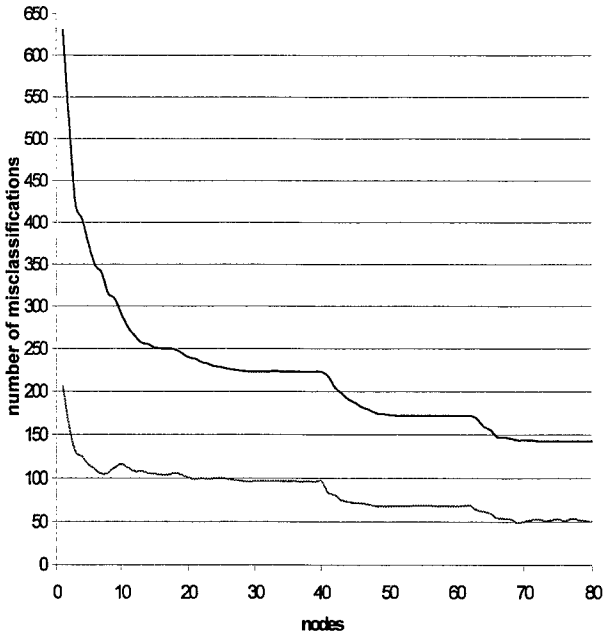


Fig. 3. Training error (upper) and testing error (lower) versus number of nodes for QN -- Villars' data.

Example 2.
A quantum net and an RBF net are compared in the task of building a cellular automata (CA) based model of thin film growth [14]. The atoms of types A and B are sent to the substrate by two heated sources. Those atoms which bond between each other or/and with the substrate, form a surface film. The geometric features of the surface, such as average roughness, are of great importance to the quality of the film. Depending on the current state of the surface and substrate, an incoming atom can form different types of bonding with the surface or remain as a vapor. For the current state of the model, 6 possible states of an atom are assumed. These are AA bond, AB bond, adsorbed, wall-adsorbed, cliff-adsorbed, and vapor. In the CA model it is supposed that the actual state of an atom depends not on the entire substrate and surface but only on the states of atoms in the neighborhood of the incoming atom. The neighborhood constitutes 26 cells that together with the incoming atom form a cube with the incoming atom at the center. Surrounding cells are filled by atoms of type A or B, or they are empty. The state of an incoming atom can be predicted given the state of the neighborhood, temperature and some probabilities calculated by using laws of statistical physics. It is impossible for such a model to operate in a reasonable time given that calculations must be carried out for millions of atoms. That is why a neural net is used. After training on a number of known examples, the net can predict the current state of the incoming atom.

In the current model, we used two discrete variables to characterize each of the neighborhood, the temperature, and 3 probabilities -- altogether 6 variables -- as inputs to the net, and one discrete output taking 6 possible values. The number of training patterns was 3208, and the number of testing patterns was 1069. Comparison of the RBF and quantum net is made in terms of the number of misclassifications of the output and the time required to predict the state of an incoming atom. Results are shown in Table 1.

Table 1: Comparison between RBF and quantum nets in terms of time and accuracy.

Type of net	# training patterns	# testing patterns	# misclassed patterns.	% correct test patterns	Time/ test pattern
RBF	3208	1069	70	93.4	14 μsec
QN	3208	1069	60	94.4	12 μsec

Example 3.
The data set consisted of 676 points describing dependency of the optical thickness of a thin film (output) on its spectral pattern (input) [15]. The input constituted a 33-dimensional vector. The output values were

uniformly distributed in the range [0.5,5.5] with the average value equal to 3. Thus, 1% of error corresponds to 0.03 or 0.0009 MSE. Three quarters of the data (507 patterns) were used for training and one quarter (169 patterns) was used for testing. This is an example of learning a continuous function with a large number of variables. The results of training and testing for a quantum net are shown in Figure 4.

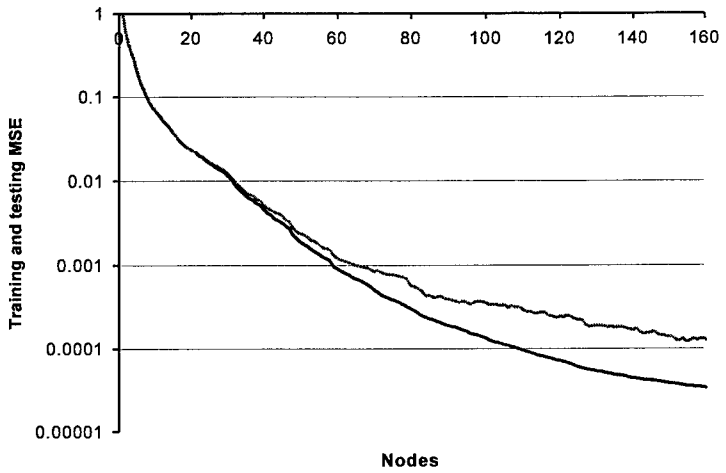


Fig. 4. Training MSE (lower) and testing MSE (upper) versus number of nodes for quantum net.

The level of 1% of testing error was achieved with a net of 68 nodes (0.000895 MSE), while the training error was 0.8% (0.000597 MSE). The best results were obtained with a net of 170 nodes: testing error 0.37% (0.000121 MSE), training error 0.16% (0.000031 MSE). The corresponding results for RBF net of the same size were : testing error 0.5% (0.000225 MSE), training error 0.27% (0.000063 MSE). These examples confirm that the quantum net has a visible advantage in accuracy and efficiency of learning and generalization compared with the RBF net. These advantages will become even more when the quantum computers will make calculations with complex numbers much faster than now.

HARDWARE IMPLEMENTATION

To demonstrate the practicality of the hardware implementation of QNs, we discuss a specific example below involving the XOR function. A QN capable of performing XOR is shown in Figure 5 where an Aharanov-Bohm ring is used with two FET switches. The magnetic field perpendicular to the ring is chosen so that when both the FETs are on (conducting) the current through the ring is zero (i.e., destructive interference case) and when either of the FETs are closed, the current is non-zero. It should be noted that this structure is very similar to the regular microwave waveguide structure (with angstrom dimensions) and that the reflection paths should be properly terminated /matched to prevent unwanted interferences.

Only the magnetic field is varied as the adjustable parameter to train this QN. The output is monitored while the magnetic field is varied to ensure zero output when both FETs are on. A small feedback circuitry can be devised to automate the training (very much like the Hopfild net). This hardware implementation is shown schematically in Figure 5.

CONCLUSION AND FUTURE WORK

The new architecture of neural network, suggested in this paper, has a solid motivation and has proved a considerable and measurable advantage over the RBF net in performance and efficiency in a number of applications. Our future work will be concentrated both on applications of this architecture, in particularly in the area of smart sensors, and on theoretical development of a new, completely adaptive architecture.

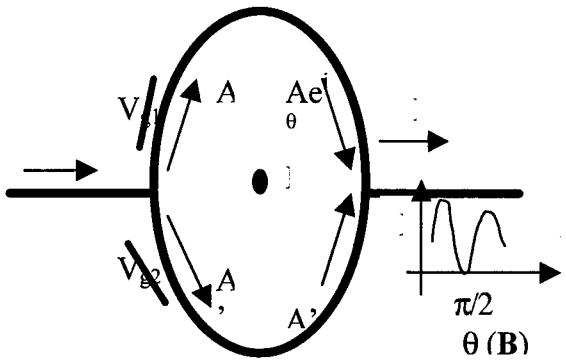


Fig. 5. An example of hardware implementation of QN using an Aharonov-Bohm ring. The ring, schematically shown here, is composed of a high-quality gold or AlGaAs/GaAs 2-D gas layer. The gates are used to raise or lower the potential barrier and control the current flow through a given arm. The magnetic field, **B**, is perpendicular to the ring's plane and it causes the phase difference of 2θ between the electronic wavefunction flowing through the two arms. The value of θ depends on the strength of the magnetic field.

REFERENCES

1. A. Garcia and M. Tabib-Azar, 1995. Sensing Means and Sensor Shells: A New Method of Comparative Study of Piezoelectric, Piezoresistive, Electrostatic, Magnetic, and Optical Sensors. Sensors and Actuators A. Physical, 48(2), 87-100.
2. M. Tabib-Azar, 1998. Microactuators; Electrical, Magnetic, Thermal, Optical, Mechanical, Chemical and Smart Structures. Boston, MA: Kluwer Academic Publishers.
3. P.W. Shor, 1994. Algorithm for Quantum Computation: Discrete Logarithms and Factoring. In Proceedings of 35th Annual IEEE Symposium on Foundations of Computer Science, 124-137.
4. D. P. DiVincenzo, 1995. Two-bit gates are universal for quantum computation. Phys. Rev. A, 51(2), 1015-1022.
5. C. H. Bennett, 1973. The Fundamental Physical Limits of Computation. IBM J. Res.Dev., 17, 525.
6. D. Deutsch and R. Joszsa, 1992. Rapid Solution of Problems by Quantum Computation. Proc. Royal Soc., A 439, 553-558.
7. D. Deutsch, 1985. Quantum theory, the Church-Turing principle and the universal quantum computer. Proc. Royal Soc., A 400, 97-117.
8. S. Lloyd, 1993. A Potentially Realizable Quantum Computer. Science, 261(17) 1569-1571.
9. B. Igelnik, M. Tabib-Azar, S. R. LeClair,, 1999. Quantum net: a net with complex coefficients. Submitted to IEEE Transactions in Neural Networks.
10. B. Igelnik and Y.-H. Pao, 1995. Stochastic choice of basis functions and adaptive function approximation. IEEE Transactions on Neural Networks, 6(6), 1320-1329.
11. B. Igelnik, Y.-H. Pao, S. R. LeClair, and C.-Y. Shen, 1999. The ensemble approach to neural network learning and generalization. IEEE Transactions on Neural Networks, 10(1), 19-30.
12. Pao, Y-H, 1989. Adaptive pattern recognition and neural networks. Reading, MA: Addison-Wesley.
13. P. Villars. 1998. Private communication.
14. A. Jackson, M. Benedict, 1997. Private Communication.
15. S. Fairchild, 1998. Private Communication.

Ontology for Phase Diagram Databases

N. Ono*, R. Kainuma*, H. Ohtani, K. Ishida*** and M. Kato***

*Graduate School of Engineering, Tohoku University, Sendai, Japan
**Center for Interdisciplinary Research, Tohoku University, Sendai, Japan,
***New Industry Creation Hatchery Center, Tohoku University, Sendai, Japan

ABSTRACT

Due to close similarity between the common forms of ontology specification and classes in object-oriented systems, a set of object-oriented classes in a domain may provide the skeleton of the ontology of the domain. An object-oriented design for phase diagram database has been made with special attention to this. Through the description of the analysis and coding of phase diagrams, the nature of the task of ontology construction is illustrated.

INTRODUCTION

It has been emphasized in recent years that an ontology provides a common foundation for the development of intelligent systems such as databases, data mining systems, expert systems, etc. in a field of expertise [1]. An ontology as such is expected to facilitate not only the development of individual systems but also their maintenance and integration. The same should apply to the field of materials science and engineering. It is to be noted here that an ontology is a form of representation of knowledge in a field. When the field is a professional discipline such as materials science and engineering, therefore, contribution from experts in the field is indispensable in the compilation of an ontology.

The present authors currently attempt to construct a phase diagram database by the use of MOOD-SX that is an object-oriented database system (OODBS) developed by Ono [2]. As typically seen in ASM phase diagram handbook [3], information on phase diagrams includes not only diagrams but also descriptions of phases and their structures, invariant reactions, bibliographic data and so on. In the course of examination of contents of these items as a basis for our database schema design, it has been noticed that the design of an object-oriented system has close similarity with ontology construction [1,4,5,6]. In both cases, we need to encode entities and relations among them in the domain of interest and further the way of encoding generally used in the current ontology study resembles that in the object-oriented system development. From this and also from the significance of ontology as above described, it is considered worthwhile to extend the scope of our work in the phase diagram database from providing containers for data items to contributing to the construction of an ontology for materials science and engineering.

In the following, similarity between the ontology compilation and object-oriented database design will be examined. It will be shown that a set of object-oriented classes can provide the skeleton of an ontology of the domain. Following these, entities involved in the description of phase diagrams are examined and a set of codes to capture them and relations among them will be proposed and discussed.

ONTOLOGY AND MOOD-SX

The Free On-line Dictionary of Computing [7] defines ontology as follows:

> *An explicit formal specification of how to represent the objects, concepts and other entities that are assumed to exist in some area of interest and the relationships that hold among them.*

The examination of two currently common ontology specification languages, Ontolingua [8] and Cyc [9], indicates that *the relationships* are generally categorized into the following three kinds:

0-7803-5489-3/99/$10.00 ©1999 IEEE.

1. *Is-a relationships*
2. *A-kind-of relationships*
3. *A-part-of relationships*:

In the statement "sodium is an alkaline metal", "alkaline metal" is a collection of things. "Sodium" is a member of the collection. This is called an *is-a relationship*. Collection as such is called also *class*. It is often said that "sodium" is *an instance of* the class "alkaline metal". When all members of the class "alkaline metal" are also members of another class "metal", "alkaline metal" is *a kind of* "metal". Entities of interest are captured as either classes or instances and arranged in a hierarchical classification tree. We generally assign specific names to these entities so that an ontology is often compared with the collection of these names such as thesaurus and electronic dictionary. The third ones, *a-part-of relationships*, are not incorporated in these items.

For example, metals have certain crystal structures. Here, a crystal structure type, say, A2 appears in the description of many metals. A2, thus, is an entity separate from metal. It is related to metals and constitutes a part of them, e.g., "Sodium has a structure, A2". This link between sodium and A2, or the link between the class, metal, and the class, crystal structure type, in general is expressed usually by stating that the class, metal, has an attribute, "crystal structure type", and the value of the attribute is constrained to the class, crystal structure type. Attributes of a class as such are inherited by its subclasses with their constraints.

It is apparent that the constitution of ontology, or the mechanism for explicit formal specification of entities and relationships so far described above is basically the same as the date structure of object-oriented systems. Programming-oriented systems like C++, Java and Smalltalk and OODBS based on these are more restricted from this. For example, these systems do not support naming of individual instances. Java and Smalltalk do not allow a class to have more than one superclasses. Some OODBSs such as O_2 [10] and MOOD-SX support both of these. Object-oriented systems as such are capable of capturing so far described aspects of ontology.

Ontology languages have features other than these. Cyc expresses a-part-of relationships with binary predicates and those predicates are classified according to their nature in a variety of aspects. For example, methods to handle particular attributes and their values are inherited along the classification of attributes. This classification facilitates implementation of functions in application programs based on the ontology and it will be beneficial in database services that include user interfaces. MOOD-SX and Ontolingua do not support this classification in general. However, a basic classification of attributes, i.e., if their values should be a unique value or a collection of values, is supported in all of these. In MOOD-SX, a collection of things (A, B) is expressed very explicitly as:

```
#list
 |-with
   =A
   =B
```

In the convention used in the description of MOOD, this is an instance of a class `list` (indicated by its name following `#`) that has an attribute, `with` (indicated with leading `|-`) whose values are `A` and `B` (indicated with `=`). For collections, distinction is made in regard to if their elements are ordered or not, to if each element is unique or not, and also to the cardinality. MOOD-SX does not support the last two of these. The following features may be further enumerated:

1. Constrains on attributes inherited from superclasses may be made more restrictive in subclasses. This is allowed in MOOD-SX, but not in common object-oriented systems.
2. Codes in Cyc and Ontolingua are written in LISP and various functions either to infer or to calculate attribute values can be implemented with LISP. MOOD-SX is equipped with a few kinds of default reasoning mechanisms but it does not yet support linkage with a full programming language.
3. A set of classes can be declared mutually disjoint in Cyc and Ontolingua but not in MOOD-SX.

As seen from these, the power of MOOD-SX in the ontology specification is the subset of those of Cyc and Ontolingua. It is not possible, therefore, to convert classes and instance objects stored in the MOOD-SX system to these codes automatically. It is still capable of capturing basic elements of ontology, entities in the field of interest and essential relationships among them. To identify these elements and to encode them are the starting point of an ontology construction and call for the most intensive contributions from domain experts. Domain knowledge encoded with classes and instance objects in MOOD-SX can, therefore, play the role of the intermediate expression that is ready for the more intensive formalization.

ONTOLOGY FOR PHASE DIAGRAMS

Because our primary aim is to provide a good phase diagram database service, the ontological analysis, i.e., the enumeration of entities and relationships will be made most appropriately in the top-down manner starting from phase diagram. This and other entities which appear as components of the description of phase diagrams such as the elements, phases, crystal structures and so on should be related to upper ontological structures. More specifically, we need to have at least one superclass for each of these classes and it is desirable that the superclass is smoothly linked to yet higher hierarchy such as the Cyc upper ontology. It is also desired that the specifications of individual components are not only suitable for the description of phase diagrams but also valid in more general contexts in science.

Phase diagrams are in fact diagrams, and lines and regions drawn in them should convey significant pieces of information. In spite of this, study of the semantics of these drawings is left for the future work. For the moment, then, we confine ourselves to the representation of the descriptions of features found in those diagrams as well as various notes that generally accompany phase diagrams.

Identification of Sections: Issues

To begin with, we need to establish a way to identify individual phase diagrams. This starts with such a naive question as follows: Suppose that our system stores an Al-Fe binary phase diagram and a user asked for a Fe-Al phase diagram. How would our system know that it is appropriate here to report the Al-Fe phase diagram? In handbooks such as [3], this problem is handled by enforcing a rule that two components of binary phase diagrams are enlisted in alphabetical order. This rule, however, becomes more difficult to adhere to in the description of pseudo-binary diagrams, i.e., the temperature-concentration(T-C) sections of ternary systems and those with more components. Fe-10%Ni - Fe-20%Cr diagram, for example, should be written as Cr-80%Fe - Fe-10%Ni.

It is desirable, therefore, that our system is intelligent enough to know that the above two expressions are equivalent with each other and thus to save us from the trouble of this rewriting. To achieve this, it is first needed to let the system acknowledge that a description of a section, *A-B*, is equivalent to *B-A*. In MOOD-SX, this is expressed with an instance of a system intrinsic class `pair` as follows:

```
#pair
 |-of=A
 |-and=B
```

The `pair` as such is the MOOD implementation of the more general notion: "a set (in which the order of appearance is insignificant) of cardinality 2".

Another issue is the equivalence of Fe-20%Cr and Cr-80%Fe. Because this is the problem common to all descriptions of composition, it will be discussed elsewhere in more general context. Yet another problem envisaged in the description of T-C sections of phase diagrams is if it is permissible to assume that the entities `A` and `B` in the above pair are always compositions. For example, binary phase diagrams may be specified with two pure substances like alumina-silica binary phase diagram. However, it is not surprising that, when you have asked an intelligent agent (such as a graduate student) to find alumina-silica phase diagram, the agent comes up with an Al_2O_3-SiO_2 pseudo-binary section found in a ternary phase diagram handbook. Because the formal ontology is not flexible like any other computer system, we need a little trick

to let our system behave as intelligent as this. Namely, suppose that we have implemented binary phase diagram as a class that has an attribute that holds a pair of pure substances. The corresponding attribute of the class, pseudo-binary phase diagram takes a pair of compositions. Because of this, these two classes become mutually disjoint.

In the first sight, pseudo-binary phase diagram appears to be an extension of binary phase diagram. One may, therefore, make this a subclass of binary phase diagram. The attribute, section, of binary phase diagram is inherited to pseudo-binary phase diagram. The constraint on its value, a pair of pure substances, is irrelevant in pseudo-binary phase diagram. To override the constraint with a pair of compositions is not allowed due to the nature of the formal system. When we tell the system that pseudo-binary phase diagram is a subclass of binary phase diagram, we permit the system to treat an instance of the former as that of the latter. The system may, therefore, try to manipulate a composition in the instance of pseudo-binary phase diagram as a pure substance and go into trouble. Vise-versa is the case when binary phase diagram is made a subclass of pseudo-binary phase diagram. These two classes, therefore, should not be placed in a thread of inheritance and thus should be made mutually disjoint. Database search and data mining based on an ontology generally rely on the class hierarchy. A query on alumina-silica binary phase diagram cannot find those represented with instances of a disjoint class, pseudo-binary phase diagrams.

Identification of Sections: Proposed Solution

A solution to remove this limitation is as follows. Let us start with the fact that alumina and silica are instances of compound that is a kind of pure substance while neither Fe-20%Cr nor Fe-10%Ni are considered to be a substance. Note that it is still appropriate to mention composition for all of Fe-20%Cr, alumina, and so on. These things are, therefore, something that is commonly characterized with composition. It is possible to mention composition of simple substances, e.g., "pure substance, aluminum, consists of 100% single element, aluminum". These things, therefore, can include simple substances. Unfortunately, we do not have a name to call these things for which mentioning composition is relevant so that we need to invent one. Let us call them, temporarily, *pseudo-substance*.

The classification of pseudo-substance as such is a big issue that involves the examination of all forms of existing stuffs. The following may be the briefest and most agreeable one:

```
pseudo-substance
  pure substance
    simple substance
    compound
  mixture
    alloy
```

Here, mixture includes stuffs like Fe-20%Cr while alumina is an instance of compound. However, the distinction of compound from mixture is not always clear. An intermetallic compound Ni_3Al, for example, is generally considered as not a pure substance but as a phase that appears among a series of Ni-Al alloys. We may argue the same for Al_2O_3. It is, therefore, considered permissible to adopt a more relaxed attitude on the difference between compound and mixture at least in the interpretation of phase diagrams as described in the following.

Corresponding to pseudo-substance, let us assume a concept, T-C phase diagram, that includes both binary and pseudo-binary phase diagrams. This concept is convenient to distinguish these diagrams from isothermal phase diagrams that are omitted from the present consideration:

```
phase diagram
  isothermal phase diagram
  T-C phase diagram
    binary phase diagram
    pseudo-binary phase diagram
```

This class, T-C phase diagram, is characterized with an attribute, section, whose value is constrained to a pair of pseudo-substances:

```
#T-C phase diagram
 |-section=#pair
             |-of=#pseudo-substance
             |-and=#pseudo-substance
```

Binary phase diagram inherits this attribute but the constraint is made more restrictive there. Its section must be specified with a pair of pure substances. Alumina-silica phase diagram is thus represented as follows:

```
#binary phase diagram
 |-section=#pair
             |-of=alumina
             |-and=silica
```

In pseudo-binary phase diagram, this restriction is not possible because it includes sections from a pure substance to a mixture like Fe vs. Ni-50%Cr. Alumina-silica pseudo-binary phase diagram may be represented equally well with the following two:

```
#pseudo-binary phase diagram
 |-section=#pair
             |-of=alumina
             |-and=silica

#pseudo-binary phase diagram
 |-section=#pair
             |-of=#mixture
             |       |-composition=Al-60mol%O
             |-and=#mixture
                     |-composition=Si-66.7mol%O
```

Our intelligent system should have been instructed that, or a method to infer that, alumina is a pseudo-substance with a composition Al-60mol%O and so on. When these representations are compared with each other, therefore, it is possible to let the system *up-cast* all of these instances to a common representation as follows and find that they all mean the same thing:

```
#T-C phase diagram
 |-section=#pair
             |-of=#pseudo-substance
             |       |-composition=Al-60mol%O
             |-and=#pseudo-substance
                     |-composition=Si-66.7mol%O
```

Phases and Their Appearances

A record of a piece of phase diagram is accompanied by the description of the section as discussed above. It should have a pointer to an image data for the diagram. The diagram will be composed of curves delineating regions and the regions will be accompanied by the names of phases stable there. The diagram will also contain insets that show temperatures of invariant reactions. Although phase diagrams should be universal truth like the Plank constant, those we have currently are artifacts that are well guessed through elaborated work. It is, therefore, appropriate to mention the method of construction and bibliography for the more detailed information on the construction process. Although each of these things has its own details and deserves closer inspection, comments will be made only on phases and only briefly here.

It should be noted that phases or phase names in phase diagrams do not directly indicate phases but they are considered to be labels that relate individual regions to their descriptions made separately from the diagrams. The reason for this remark is as follows. For example, in Cu-Fe system, (Cu) and (γ-Fe) are separate, distinct regions. However, in isothermal section of Cu-Fe-Ni phase diagram, (Cu) and (γ-Fe) form one region through (Ni) region. Cu and γ-Fe phases are, therefore, the same phase in fact. This is true in a physical point of view. We postulate the thermodynamic stability of the same, say, fcc phase which is contiguous through out the multi-dimensional concentration-temperature-pressure space. (Cu), (Ni), (γ-Fe) and many other fcc regions are regions where this single fcc phase happens to exist as the most stable one

among many other structures. We need to distinguish each appearance of this phase to discuss (Cu) and (γ-Fe) in Cu-Fe phase diagram individually as we are doing here, but the names (Cu), (γ-Fe), etc. do not necessarily designate different phases.

CONCLUDING REMARKS

Those items described in the previous section may well illustrate the nature of the tasks needed in the process of examination and encoding of items in our domain for the construction of an ontology. The previous section does not cover many other important entities such as crystal structures, elements and so on. We need to carry out a similar analysis for all these things.

One may have an impression that formality required in ontology coding is too rigid to capture the complexity in the core of materials science and engineering. Although this is in a way true, to pursue analysis as such is considered still worthwhile since at least we can foresee in the light of the analysis how much we could expect from intelligent information services. Practical systems may be designed by curtailing some part of the complexity. The consultation of the results of these analyses will be beneficial in providing a basis on which the designers of the systems overview what they are capturing as well as what they are missing.

On the other hand, the impression may be totally wrong and, however complex, essential concepts in a rational science should be well encoded in an equally rational way. Further study is needed to see which expression is correct.

ACKNOWLEDGEMENT

Thanks are due to Mr. T. Kawaminami and T. Hanayama for their help in carrying out this work. Financial support by the Grant-in-Aids for Scientific Research from the Ministry of Education, Science and Culture, Japan is gratefully acknowledged.

REFERENCES

1. N. Guarino. 1998, Some Ontological Principles for Designing Upper Level Lexical Resources. First International Conference on Language Resources and Evaluation, Granada, Spain.
2. N. Ono: MOOD-SX system program package, `http://mood.mech.tohoku.ac.jp/`.
3. H. Okamoto, P. Villars and A. Prince, 1997. Handbook of Ternary Alloy Phase Diagrams, Version 1.0. ASM International.
4. S. Borgo, N. Guarino and C. Masolo, 1996. Stratified Ontologies: The Case of Physical Objects. Proceedings of ECAI-96 Workshop on Ontological Engineering, Budapest.
5. A. Gomez-Perez, M. Fernandez and A. J. de Vicente, 1996. Towards a Method to Conceptualize Domain Ontologies, Proceedings of ECAI-96 Workshop on Ontological Engineering, Budapest.
6. P.E. van der Vet and N.J.I. Mars, 1998. Bottom-Up Construction of Ontologies. IEEE Trans. Knowledge and Data Eng., 10, 513-526.
7. Free On-Line Dictionary of Computing. http://wombat.doc.ic.ac.uk/
8. T.R. Gruber, 1992. Ontolingua: A Mechanism to Support Portable Ontologies. Technical Report KSL 91-66, Stanford University .
9. Cycorp, Inc. 1999. The Upper Cyc Ontology. http://www.cyc.com/publication.html
10. O. Deux et al., 1990. The Story of O_2. IEEE Trans. On Data and Knowledge Engineering, 2.

Prediction of Concrete Mechanical Behaviour from Data at Lower Ages using Artificial Neural Networks

José C. Cassa, Giovanni Floridia, André R. Souza, Rodrigo T. Oliveira

Grupo de Estudos em Inteligência Computacional Aplicada (GEICAP)
DCTM - Escola Politécnica - Universidade Federal da Bahia
Rua Aristides Novis, 02 - Federação 40210-630 Salvador, Bahia, Brazil
Email: jccassa@ufba.br

ABSTRACT

The complex mechanical behaviour of concrete is hard to model with traditional mathematical tools. This paper shows how artificial neural networks can be used to predict concrete mechanical strength at 28^{th} day by using experimental results from 1^{st} and 7^{th} days.

INTRODUCTION

The material science of cementitious materials has not developed as far as the science of other materials (metals, polymers, ceramics and others) but there is the perception in the academic community that computing may be able to help overcome some of the difficulties. One major challenge of concrete technology is the development of a system to predict the mechanical behaviour of material. The developments so far have been based on empirical experience valid only under special situations. Many engineers and scientists believe that one possible way to represent the performance of concrete is through reference models that can explain its behaviour.

This reference model must relate the organised knowledge by using a set of mathematical equations or other equivalent methods such as a simulation model or alternative techniques suitable for complex phenomena. Simulation models probably are the most viable way to represent the material science and technology of concrete. In traditional mathematical models, equations based on first-principles or derived-empirically from experiments, demonstrate the concepts included in the model. But questions related to concrete are normally complex such as:

a) Which factors influence the behaviour of this material due to variation of one or more components, mixing proportion and cure conditions?
b) Which paths are possible to find the desired end conditions?

Many of the phenomena involved are hard (or impossible) to describe using deterministic or stochastic models. In other cases, the level of available knowledge is not yet complete for its representation with the precision and reliability required. For these cases, neural network modelling can be a good approach for reliable predictions.

ARTIFICIAL NEURAL NETWORKS

The concept of artificial neural networks (ANN) was inspired by the hope to reproduce artificially some of the flexibility and power of the human brain. Humans can recognise complex patterns although there is not always a complete understanding of the involved phenomena. The application of ANN for modelling systems that are hard to be represented by phenomenological explanation may looks difficult at first but it is easy to understand for those who are familiar with least-square modelling and optimisation.

A computer ANN is composed of single elements called nodes, neurons or processing elements. These elements receive several inputs through weighted connections, multiplies each input by its respective weight, totals the results, and performs some type of transfer function on the input sum. Once the transfer function has acted, the result is forwarded to the next processing element.

0-7803-5489-3/99/$10.00 ©1999 IEEE.

In the multi-layer perceptrons networks (MLP) the processing elements are arranged in interconnected layers. Usually there is an input layer to receive data, one or more hidden layers, and finally, the output layer that transmits the result of the network calculations. The hidden layer is essential to represent non-linear processes. Another feature of the MLP is the bias vector that can be regarded as an additional degree of freedom that can be adjusted to obtain the desired network performance. Although many different ANN structures and training techniques have been described in the literature [1] multi-layer perceptrons **(MLP)** seem to be suitable to model complex systems. In simple terms, this type of ANN works like a non-linear regression approach. As any curve fitting technique, model parameters can be found by least square optimisation.

The MLP designer must specify the number of hidden layers (usually one), the number of nodes in each layer, and the transfer function of each layer. This is the MLP "architecture". Expertise, judgement and trial-and-error as in regression methods are used to define the suitable architecture. Once the MLP architecture is selected, the weights have to be adjusted by finding the values of weights that minimise the sum of square deviations of the ANN and process outputs. The traditional training approach is called backpropagation and usually works, but in some cases non-linear optimisation may be necessary. In order to speed the convergence of backpropagation training some complementary techniques are available such as using better initial conditions, variable learning rate and to avoid traps at local minimum conditions in the error function - the impulse function [2,3].

The main advantages of MLP are:

a) Its ability to grasp very complex relationships and to learn the process behaviour by adjusting to real data with no need of previous basic understanding of the process or the definition of a number of rules or equations. So, complex systems can be modelled with little specialist knowledge.
b) Once MLP has completed training, it can predict useful results in spite of presence of some faulty information. This robust behaviour allows MLP to compute noisy data, partial data and even foreign data and still perform acceptably.
c) There is no need of prior screening the most important variables, as the trained network will learn the relationship between responses and input variables finding out automatically which inputs and connections are important. If the training reduces the interaction between processing elements by assigning low weights, irrelevant parameters can be eliminated through the assignment of null weights to these connections (pruning techniques). This property makes ANN a more realistic approach with no need of simplification beforehand and is particularly helpful in multivariable models.
d) It is computationally efficient. This characteristic allows ANN to replace models that are computationally intensive making real-time model-based applications practicable.

Although MLP neural networks can solve many problems of modelling, other ANN architectures [1] such as General Regression Neural Networks (GRNN), Probabilistic Neural Networks (PNN), and Polynomial Networks (GMDH) may be able to do same job easier as it will be showed in this paper. The previous MLP advantages are also present in these ANN architectures.

PREDICTING THE MECHANICAL STRENGTH OF CONCRETE

The mechanical strength of concrete increases continuously as a function of time due to the evolution of the hydration reaction of cement. The determination of mechanical strength of concrete in quality control technological tests is performed at 28th day accordingly most national standards (ABNT, ASTM, DIN, BS and others). In large concrete works (i. e., bridges and dams) it is also useful the knowledge of expected strength in the long term (01 to 50 years old). The traditional procedure for strength determination at any age consists in the preparation of concrete specimens with standard geometry followed by mechanical testing as described in the technical literature. Under this scenario, prediction models that are able to anticipate the quality of produced materials are very useful in order to check if conditions designed in the project will be achieved or if not, to indicate the need some action to satisfy the specifications.

Usually this prediction is carried out by using some methods based in a set of characteristics of the cement or concrete under study. These methods can be grouped as

a) Methods based in the strength obtained under conditions of accelerated hydration/ cure
b) Methods based on the strength at normal cure conditions at low ages
c) Methods of correlation with other characteristics of cement or concrete (i. e., chemical composition and fineness of cement, hydration heat developed in the concrete mixture or other characteristics).

The validity and limitation of these methods are described in the literature[4,5], [6].

In the perception of the authors, the main difficulty for the application of any method mentioned before is the identification of a suitable mathematical equation. The complexity of the physicochemical phenomena involved in concrete formation is an inherent difficulty to the application of any computer model. The traditional models available are

a) Empirical models - obtained by best fitting equations to experimental data using techniques such as regression analysis. These models are relatively simple and thier application is limited to the experimental conditions tested
b) Phenomenological models - based on fundamental equations of fluid flow in porous media and kinetic equations to represent solid-fluid reactions and the energy conservation laws. These models are complex which require some simplifying hypotheses to lead to viable numeric solutions. The usefulness of any of these models depends on its completeness and how realistic are the assumed operating conditions.

The main objective of this paper is to show a model free technique in order to help those professionals working in concrete technology with interest in the anticipated knowledge of mechanical strength by using systems based on ANN. These systems must use only data available from the technological quality control of cement or concrete production and should be able to predict with reasonable precision the mechanical behaviour under expected conditions (higher ages).

THE CONSIDERED PROBLEM

Prediction of mechanical strength of concrete at traditional age of control (28th day)
In order to illustrate the applicability of ANN for the prediction of concrete mechanical properties, a simple problem was chosen. This problem has been solved satisfactorily before by using conventional statistical techniques so that the efficiency of ANN methods can be compared and evaluated.

Tango et al. [4,5] suggest the AMEBA method for the prediction of concrete strength at the 28th day by using experimental results at low (01 day) and middle (07 days) ages. The technical reasoning is well described in the literature. Basically, the method assumes that there is a mathematical model suitable to represent the mechanical strength of concrete as a function of time. In this case, there is a continuous mathematical function, differentiable, exact, so that

$$r(t_3) = f[r(t_1), r(t_2)] \qquad 1.$$

where r(t1), r(t2), r(t3), ... are strength r(ti) at some age (high = Alta, middle = MEdia and low = BAixa ages forming the acronym AMEBA in Portuguese).

The model adopted in the AMEBA method is just an approximation of the exact mathematical model. The usual mathematical models proposed in the literature contain intrinsically inadequacies derived from simplifications in the original physical model and/or in the linearization of involved equations in order to find a viable solution. This discrepancy with the exact model can be evaluated by comparison of experimental and calculated results using mean square error (MSE) as model discriminator and then, allowing the ranking of proposed/ available models.

Prediction models at other ages (i.e., 01 and up to 50 years) can be developed from available database. In this cases, mechanical strengths at 07 and 28 days can be used to predict results at 01 year and experimental data at 28 days and 01 year to predict at 05, 10, 20 and 50 years (work in this direction is in progress at GEICAP - UFBA). Few databases displaying such mechanical strengths of concrete up to 50 years of age are available in

the world. One of those is available at IPT (São Paulo - Brazil) for cements produced in Brazil [4]. The experimental data for this problem were taken from [5] for concretes produced during a tunnel construction in São Paulo, where 40 results were used for training and another 40 for testing the proposed systems.

TRAINING THE NETWORK

Using Backpropagation

The architecture of a Multi-Layer Perceptron (**MLP**) has to be adapted to the problem to be solved. The number of network inputs to the network is constrained by the problem, and the number of neurons in the output layer is constrained by the number of outputs required by the problem. Backpropagation (**BP**) training follows gradient descent on the error surface to minimise network error. Local minima may trap the network. The more neurons in intermediate layers the more freedom a network has and more variables to optimise. Hecht-Nielsen [7] demonstrated that a hidden layer with ($2\mathbf{n}$ + 1) neurons, where $\mathbf{n}$ is the number of input variables, can represent any mathematical continuous function. It is known that networks with biases and at least one sigmoid neuron layer are capable of approximating any reasonable differentiable function[2,3].

The backpropagation learning rules are used to adjust the weights and biases of networks so as to minimise the squared error of the network. This is done by continually changing the values of the network weights and biases in the direction of steepest descent with respect to error. Trained BP tends to give reasonable answers when presented with inputs that they have never seen. Unfortunately, plain BP is slow because of low learning rates and the large number of variables in multilayered networks, and suffers from other difficulties in addition.

Methods of improving backpropagation include techniques such as momentum and variable learning rate. These improvements can be used to make BP more reliable and faster by a factor of 10-20 on small problems and perhaps more on larger problems. Momentum allows a network to respond not only to the local gradient, but also to recent trends in the error surface and allows the network to ignore small features in the error surface sliding through local minimum. Training time can also be decreased by the use of an adaptive learning rate which attempts to keep the learning step size as large as possible while keeping learning stable. The learning rate is made to vary with the complexity of the local error surface.

Backpropagation can be also improved by using more favourably initial conditions than purely random numbers. Ngyen and Widrow [8] demonstrated that a hidden layer with sigmoid / linear functions can be viewed as performing a piecewise linear approximation of any learned function. It is shown that weights and biases generated with certain constraints will result in an initial network better able to form a function approximates to the respect of any arbitrary function. Use of Ngyen-Widrow (instead of purely random) initial conditions shortens training time by more than an order of magnitude.

General Regression Neural Networks

General regression neural networks (**GRNN**) are feedforward networks based on probability density functions. GRNNs train fast showing good performance provided enough experimental data are available. This network was developed in the statistical literature as kernel regression and rediscovered later[9] as a new ANN architecture. Its topology consists of four layers: the input layer, a hidden layer working as classifier, addition neurons and the output layer. Training is processed in one step when the training set is copied into the hidden layer. The addition neurons process the kernel function. The network approximates any new input to the nearest one available in the classifier and then presents the output response. The weights are a smoothness factor that must be trained and calibrated using some optimisation algorithm.

Polynomial Neural Networks

Polynomial neural networks also called Group Method of Data Handling (**GMDH**) was invented by Ivakhnenko in Russia but later used as neural networks and enhanced by others[9].

GMDH works by building successive layers with complex links (or connections) that are individual terms of a polynomial. These polynomial terms are created by using linear or non-linear regression. The initial

layer is simply the input layer. The first layer created is made by computing regressions of the input variables and then choosing the best ones. The second layer is created by computing regressions of the values in the first layer along with the input variables. Once again, the best are chosen using a convenient algorithm. This process continues until the network stops getting better (according to a specified criterion). Note this way the architecture of the network is not previously chosen but developed iteration by iteration.

The resulting network can be represented as a complex polynomial description of the model. In some respects, it is like using regression analysis but is far more powerful. GMDH can build very complex models while avoiding overfitting problems.

NEUROSHELL GMDH [9] can recognise the most significant variables as it trains, and will display a list of them. This software has also facilities to select the degree of expected model non-linearity (off, low, medium and high) as well as the model diversity by using the maximum number of survivors (low, medium and high). The length of the model is associated to complexity (low, medium and high). The final model can be also optimised eliminating the less significant parameters.

RESULTS

The considered problems were firstly modelled using simple MLP with one hidden layer trained by backpropagation. After several trials it was found that hyperbolic tangent functions in the hidden layer and linear function in the output layer gave the best predictions. Figure 1 represents graphically the optimised MLP network. The predicted results (MSE = 6,62 %) were compared with the performance of AMEBA method (MSE = 10,10 %) indicating the advantage of MLP. The solutions correspond to the first approach when using ANN indicating clearly the power of this technique.

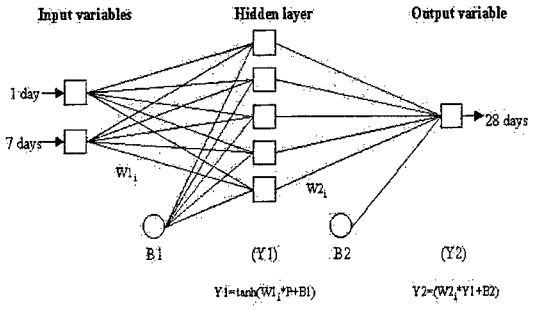


Fig. 1. Best simple MLP architecture for the problem.

In order to improve previous predictions search of new types of ANN architecture were performed. The idea was to investigate all possible combinations such as the number of hidden layers, the number of neurons in each layer, and the type of transfer functions in each neuron (including free allocation of these transfer functions in any neuron). The best combination for the considered problem was a network with two hidden layers (three tangent functions/ three linear functions for layer one and three linear functions/ four tangent functions for layer two) and one output layer (linear function) with MSE = 5,47%. It can be seen that only small improvements were obtained indicating the goodness of traditional approach (simple MLP).

Other more advanced networks suitable to represent the studied problems were also considered giving the results summarised in Table 1. These networks correspond to the best architecture found for each case considered. These applications were developed using MATLAB [2,3], NEUROGENETIC OPTIMIZER [10] and NEUROSHELL [9]. In these cases two types of ANN gave good results: GRNN and GMDH. GRNN works as interpolating polynomials where the training set is copied in the hidden layer. This type of network will lead to satisfactory results when enough reliable data are available. The authors have worked with problems where GRNN were the best choice. It is interesting to note that GMDH looks as regression models that are familiar to researchers and engineers. The complexity necessary in any case will depend on the desired precision and accuracy. In the studied cases, even simple models gave good results.

Table 1: Summary of results of best fitting some ANN architectures

MODEL	Mean Squared Error (MSE) - %
AMEBA*	10,10
MLP (simple)	5,47
GRNN	5,70
GMDH	4,11

(*) statistical model

The final evaluation of the usefulness of the systems developed can be assessed in figures 2 to 4 when calculated and experimental values are compared for the considered problem. It can be seen that in all cases good agreement was found indicating reasonable solutions for all proposed models.

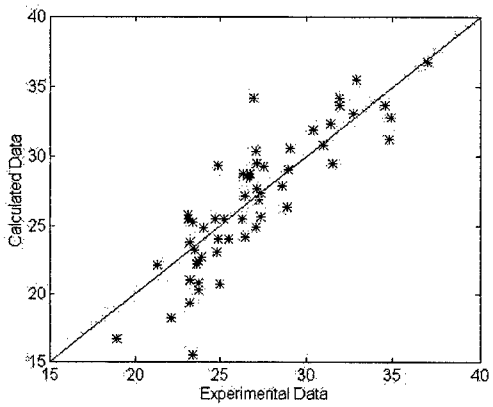


Fig. 2. Calculated vs. Experimental Data for AMEBA method (statistical) - (MSE = 10,10%).

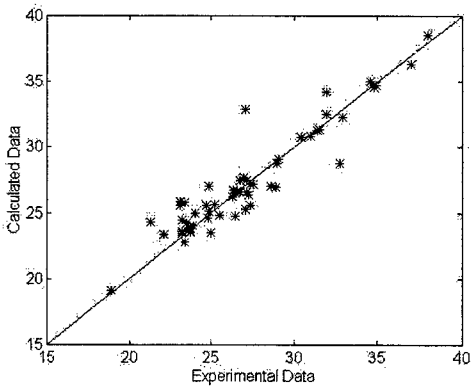


Fig. 3. Calculated vs. Experimental Data for best MLP (MSE = 5,47 %).

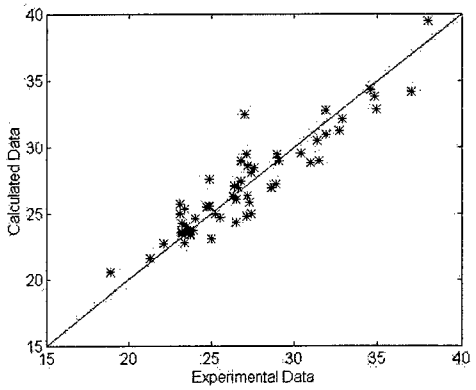


Fig. 4. Calculated vs. Experimental Data for simple GMDH - Problem 1 (MSE = 4,11 %).

CONCLUSIONS

Building materials of complex mechanical behaviour, such as concrete, can be easily modelled using artificial neural network techniques even if few experimental data points are available. The analysed problem show clearly the potential and usefulness of artificial neural networks. It is hoped that this paper will encourage other applications of artificial neural networks for the prediction of mechanical performance of other complex materials, specially those materials that do not have any model available or the traditional models do not offer the desired precision.

In another work [11] the authors discuss the use of genetic algorithms in automatic selection of neural network architecture. The automation of model developing process makes the application quite simple even for end users not familiar with neural programming and non-linear modelling.

REFERENCES

1. S. Haykin, 1994. Neural Networks - A comprehensive foundation. Prentice Hall
2. MATLAB, 1992. MATLAB High Performance Numeric Computation Software. The Mathworks.
3. MATLAB, 1993. MATLAB Neural Network Toolbox. The Mathworks.
4. C. E. S. Tango, 1991. Um estudo do desenvolvimento da resistência a compressão do concreto de cimento Portland até 50 anos. Boletim 160 - IPT.
5. C. E. S. Tango, et al., 1995. Planilha eletrônica para previsão da resistência do concreto. Anais do 37º REIBRAC - IBRACOM, 785-797).
6. L. M. Dragicevic and M. M. Rsumovic, 1987. Prognosis of characteristics of multicomponent materials on the example of flexural strength of Portland cement. Cement and Concrete Research, 17, .47-54.
7. R. Hecht-Nielsen, 1990. Neurocomputing. Addison-Wesley.
8. M. Hagan, H. Demuth and M. Beale, 1996. Neural Network Design. PWS Publishing Company.
9. NEUROSHELL, 1996. NeuroShell 2. Ward System Group Inc
10. BIOCOMP, 1997. NeuroGenetic Optimizer. Biocomp Systems Inc.
11. J. C. Cassa, et allii, 1999. Prediction of Cement Paste Mechanical Behaviour from Chemical Composition Using Genetic Algorithms and Artificial Neural Networks. IPMM 99 – The Second International Conference on Intelligent Processing and Manufacturing of Materials – Honolulu, Hawaii, July 10–15.

IMPROVING THE PREDICTION ACCURACY OF CONSTITUTIVE MODEL WITH ANN MODELS

L.X. Kong and P.D. Hodgson

School of Engineering and Technology, Deakin University,
Geelong, Vic 3217, Australia.

ABSTRACT

The unified constitutive model developed by Estrin and Mecking has successfully been used in hot rolling to provide information for the control of strip thickness. It has presented a high accuracy in predicting the hot strength of austenitic steels. However, the materials can show quite different properties under different deformation conditions and the constitutive models are not able to be generalised to cover a wide range of compositions and deformation conditions, therefore, the potential of those model is limited. In this work, the robustness of the unified constitutive model is enhanced by incorporating an artificial neural network model to predict the flow strength of austenitic steels with carbon content ranging from 0.0037 to 0.79%.

INTRODUCTION

Collinson et al [1] experimentally studied the effect of carbon content on the flow strength, static and dynamic recrystallisation behaviour of C-Mn steels with carbon contents ranging from 0.0037 to 0.79 wt.%. It was observed that the carbon content had a complex effect on the flow strength of austenite. Under single peak dynamicrecrystallisation conditions, the low carbon steel showed a continuous increase in the critical strain for the initiation of dynamicrecrystallisation as the strain rate of testing was increased and the temperature reduced. For the high carbon steel the critical strain for dynamic recrystallisation increased up to a strain of 0.7 and then remained constant, despite further reductions in the temperature or increases in the strain rate. Attempts to predict the strength with a universal model gave high prediction errors for both high and low carbon steels.

Kong et al [2] studied the stress-strain behaviour of these austenitic steels with a modified artificial neural network (ANN) model. In this model, three parameters - work hardening rate, square product of work hardening rate and stress, and logarithm Zener-Hollomon parameter, Z ($Z = \varepsilon \exp(Q_{def} / RT)$, Q_{def} is the activation energy), - developed from phenomenological and empirical models were used as inputs to train the model in conjunction with deformation conditions and carbon content. The modified model significantly improved the prediction of stress with a reduction in both the average and standard errors. However, the ANN model has limited capability of extrapolation which is required for industrial implementation as has been discussed in[3].

In the current work, the Estrin Mecking model was used to predict the hot strength of low carbon, high carbon steels and the whole range of steels, respectively. The constitutive predictions were then compared with those of an ANN model. As both constitutive and ANN models were advantageous in some aspects, a combined model was then developed.

ESTRIN MECKING MODEL AND PREDICTIONS

The modified Estrin and Mecking model, which incorporated dynamicrecrystallisation (DRX) is [3]:

$$\begin{aligned} \sigma^{EM} &= [\sigma_s^2 + (\sigma_0^2 - \sigma_s^2)\exp(-2B\varepsilon)]^{1/2} && \varepsilon < \varepsilon_c \\ \sigma &= \sigma^{EM} - X(\sigma^{EM} - \sigma_{ss}) && \varepsilon \geq \varepsilon_c \end{aligned} \qquad 1.$$

0-7803-5489-3/99/$10.00 ©1999 IEEE.

and $$X = \frac{\sigma_{EM} - \sigma}{\sigma_s - \sigma_{ss}} = 1 - \exp(-a(\varepsilon - \varepsilon_c)^b) \quad 2.$$

where ε_c is the critical strain. When the strain is smaller than critical strain, ie, within the work hardening region, the stress is predicted with EM model. TheAvrami equation [4] was incorporated with EM model if the strain was larger than critical strain. During the development of the modified EM model, the constants in Eq. 1 such as B, saturation stress σ_s, steady state stress σ_{ss}, critical strain ε_c and constants a and b in Eq. 2 were determined from experimental data.

The evaluation of the constants in Eqs. 1 and 2 has been discussed in [3]. For a steel deformed under certain conditions, Eq. 1 was to predict the hot strength in the work hardening regime. Generally, the Estrin and Mecking model [5] is used to obtain saturation stress σ_s and the constant B,

$$\theta\sigma = A - B\sigma^2 \quad 3.$$

where θ is work hardening rate. And saturation stress

$$\sigma_s = \sqrt{A/B} \quad 4.$$

To obtain constants a and b, Eq. 2 is rewritten as,

$$\ln a + b\ln(\varepsilon - \varepsilon_c) = \ln(-\ln(1 - X)) \quad 5.$$

The constants obtained with the above analysis are optimised to predict the hot strength of the specific steel under specific deformation conditions tested. The Estrin and Mecking approach provides a good constitutive understanding of the metals deformed at elevated temperatures and wide range of strain rate, for example stainless steel[6] and austentic carbon steel [2].

Using the Estrin and Mecking model, steels with carbon content ranging from 0.0037 to 0.79% were analysed. Fig. 1 shows the prediction with the optimum constants (ie different constants for each curve) for steels of carbon constant of 0.065 and 0.58% which represents the two regions with markedly different strain stress behaviours [1]. As only the optimum value for the constants was used, the Estrin and Mecking model can accurately predict the strain stress behaviourof both low and higher carbon steel.

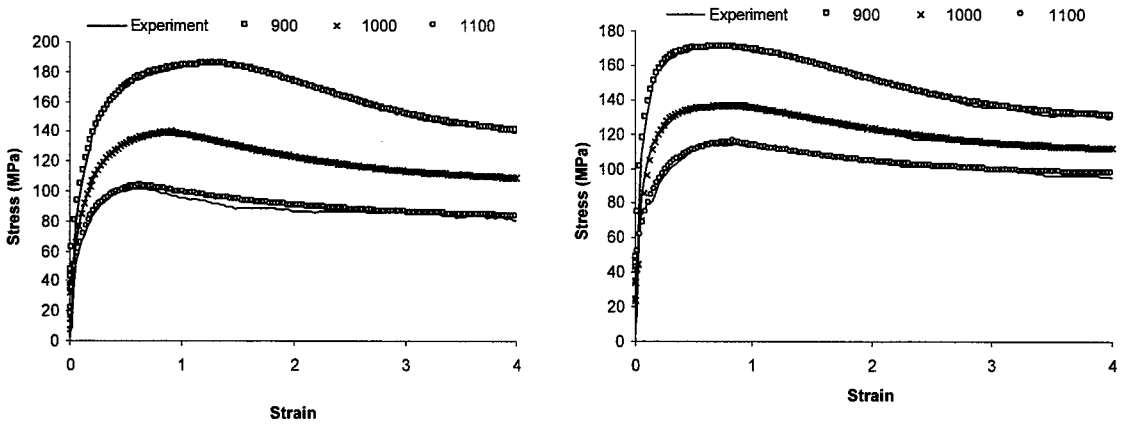


Fig. 1. Comparison between EM prediction with optimum constants and experimental results deformed at a strain rate of $10s^{-1}$ for two steels: (a) 0.065%C (b) 0.58%C

Although the modified Estrin and Mecking modelling with optimum constants can predict the hot strength with very high accuracy, it cannot predict the strain-stress behaviour of other steels or the same steel deformed at different conditions. This requires generalisation. The application of the Estrin and

Mecking model using constants optimised over the entire data set to predict steels with lower and high carbon content is shown in Fig. 2. The peak stress and strain for both steels deformed at a strain rate of $10s^{-1}$ and temperatures from 900 to 1100°C were accurately predicted with the accuracy for steel 0.065% being higher than that of the steel 0.58%. A large error occurred in predicting the saturation and steady state stresses for steel with carbon of 0.58% deformed at temperatures of 900 and 1100°C.

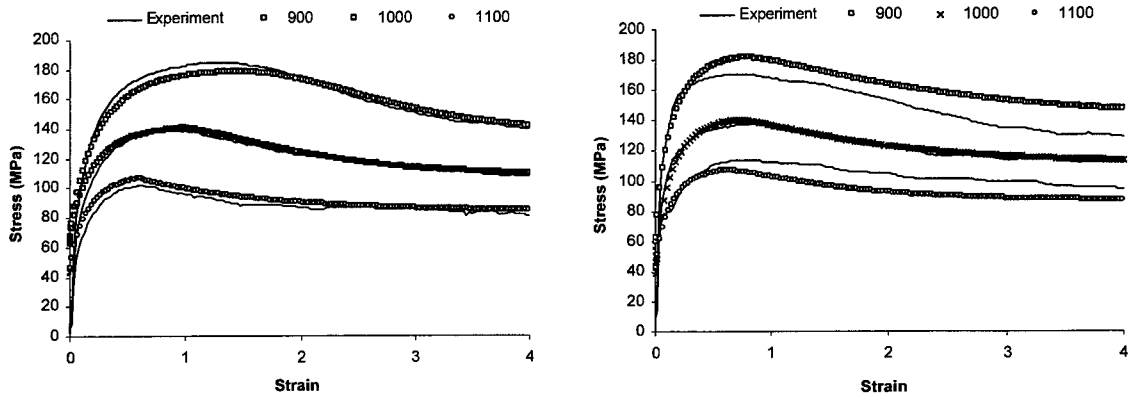


Fig. 2. EM prediction for two steels: (a) 0.065%C (b) 0.58%C

As the peak strain of those steels varies with deformation conditions in a complex way[1], the generalised model is particularly unable to precisely predict such a complexity (Fig. 3). For the steel with a carbon content of 0.065%, the prediction of hot strength at temperatures of 1000 and 1100°C and strain rate of $10s^{-1}$ is very accurate, but the peak strain for temperature of 1100°C is significantly underestimated. However, although the model generalisation sacrifices the prediction accuracy for some conditions, it provides accurate prediction for other conditions. For example, for the steel with a carbon content of 0.58% deformed at a strain rate of $10s^{-1}$, the prediction at temperatures from 900 to 1100°C gave a high accuracy (Fig. 3(b)). As the steel of 0.58%C is in the transition area of the two distinguishing regimes where peak strain changed in different ways[1], the characteristics of the constants varying in either the lower carbon or high carbon steel regions are not well developed. It has been observed that if the generalised model was used, the accuracy of the prediction for steel with carbon content of 0.79% was poor and the peak strain at lower temperatures was significantly overestimated[7].

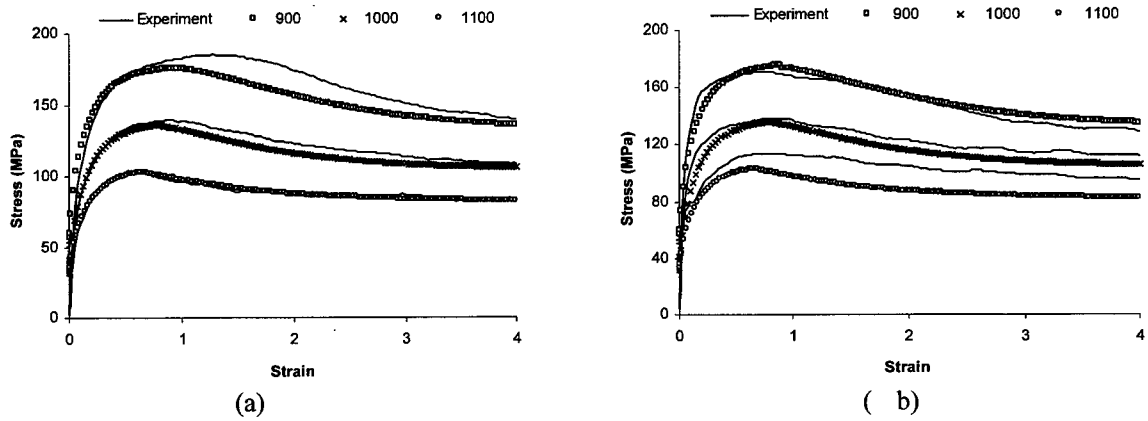
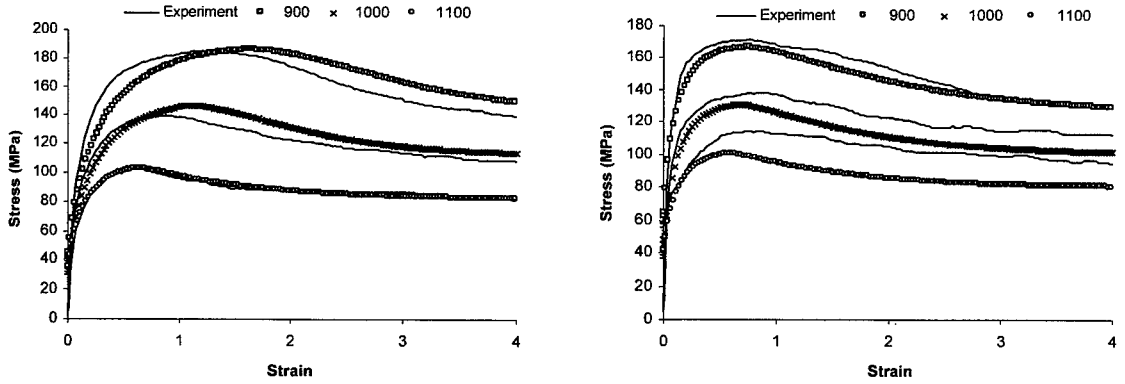


Fig. 3. Generalised EM prediction: (a) 0.065%C (b) 0.58%C

Since the steels of low carbon content performed in a different way to the high carbon steels, the Estrin and Mecking model can be used separately for those two regimes to improve the prediction. This is particularly encouraging as many constants inEqs. 1 and 2 have a similar trend to that of peak strain and vary in two regions. The prediction of those separate models on two steels of 0.0065% and 0.58% is shown in Fig. 4. The peak stress and peak strain are accurately predicted in comparison with the prediction of the generalised model for all steels (Fig. 3).



(a) (b)

Fig. 4. Separate EM prediction: (a) 0.065%C (b) 0.58%C

Using the Estrin and Mecking constitutive model, the prediction of the hot strength on steels with a wide range of carbon content can be in different modes. Generally, there is a conflict between the model accuracy and the level of the model generalisation. If the model is used to predicta specific steel, the prediction is very accurate. However, with the extension of the model to predict a wider range, the accuracy becomes poorer. Hence the constitutive prediction shows a similar trend to the prediction using artificial neural network [2] in that the more generalised the model, the less accurate is the model. The prediction can be described from Fig. 5 where the different levels of model generalisation were used. For the peak strain of all steels, the linear fitting in all three cases presented a very high error. For the generalised Estrin and Mecking model to predict all steels with carbon content from 0.0037 to 0.79%, the lower peak strain corresponding to lower Zener-Hollomon parameter, Z, was predicted with a high accuracy. However, for the high Zener-Hollomon parameter, the peak strain of the high carbon steels was overestimated while an underestimation of the peak strain for lower carbon steel occurred. If separate models were used for low and high carbon steels, higher prediction accuracy was achieved compared to the generalised model. It is also observed that the prediction of the peak strain on the high carbon steels is more accurate than steels with lower carbon content. A higher accuracy of the prediction on one constant does not guarantee the accuracy of the prediction on the strain stress behaviour. This can be seen from Fig. 4 which the inaccurate prediction of the steady state stress for both steels led to a high prediction error in dynamic recrystallisation regime although the peak strain was more accurately predicted than the generalised model for all steels.

INTEGRATION OF ANN MODEL WITH EM CONSTITUTIVE MODEL

From the analyses in previous section, it is found that all variables need to be accurately predicted to improve the prediction accuracy in both work hardening and dynamicrecrystallisation regions. Although the employment of separate constitutive models (Fig. 4) improved the prediction of constants such as peak strain, it was not able to accurately predict the constants such as B as they varied in a more complex way (Fig. 6). For both low and high carbon steels, linear fitting of those constants gave a high error. As the development of a universal model is difficult, the prediction of the constants in Estrin and Mecking model with other techniques needs to be explored.

Artificial Neural Networks have successfully been used to predict thenonlinear relationship between inputs and outputs. Although a direct mathematical description cannot be given, an ANN model is able to predict complex relations such as strain stress behaviours ofaustenitic steels [2] if appropriate training strategies and training and test data set are employed. To provide a more accurate prediction to constants in Eqs. 1 and 2, a multilayer ANN perceptron was used. The supervised feedforward network was trained with the standard backpropagation algorithm. In the three layers used, the inputs were carbon content (C), temperature (T), strain rate ($\dot{\varepsilon}$), Zener-Hollomon parameter (Z) and activation energy (Q_{def}), and the outputs were the constants in Eqs. 1 and 2. One hidden layer was used with 15 hidden nodes.

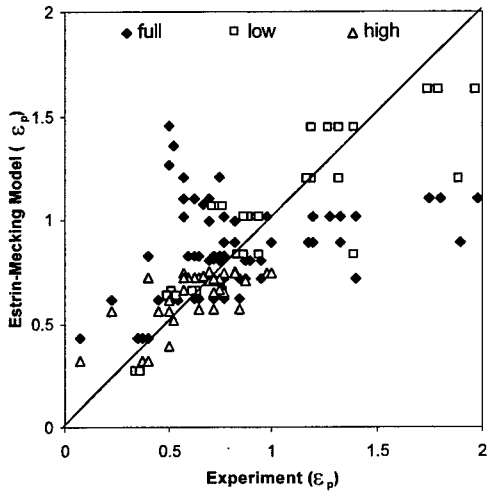


Fig. 5. Linear fitting of peak strain with different models

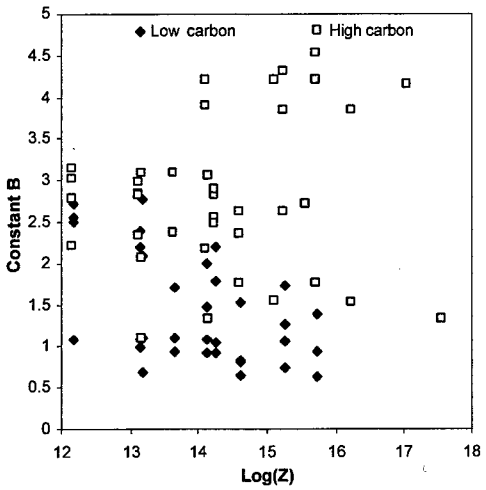
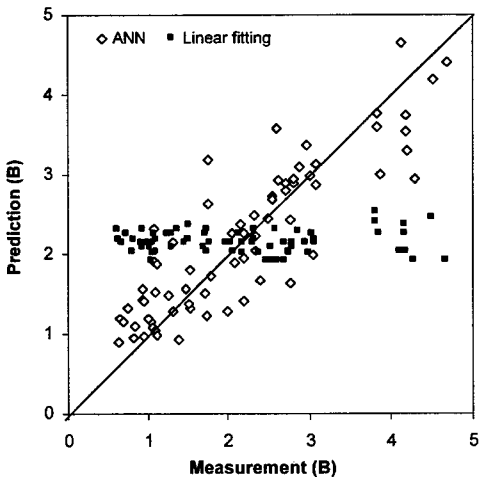
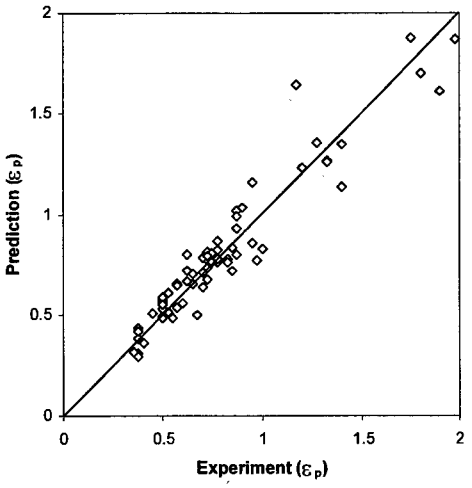


Fig. 6. variation of constant B with log(Z)

The prediction of the constant B and peak strain using ANN model is shown in Fig. 7. For constant B, the ANN prediction is much more accurate than the Estrin and Mecking model with the Pearson's correlation coefficient of 0.88 and 0.032 for ANN and EM model, respectively. As it was hardly able to employ a mathematical function to fit the constant B (Fig. 6) then it is not supposing that linear fitting presented such a low accuracy. For peak strain ε_p, both linear fitting and ANN prediction presented a higher accuracy with the Pearson's correlation coefficient for linear fitting of 0.40 and of 0.96 for ANN as a trend can be developed for both high and low carbon steels. However, the prediction of ANN model is still much more accurate than the linear fitting (Figs. 6 and 7(b)).

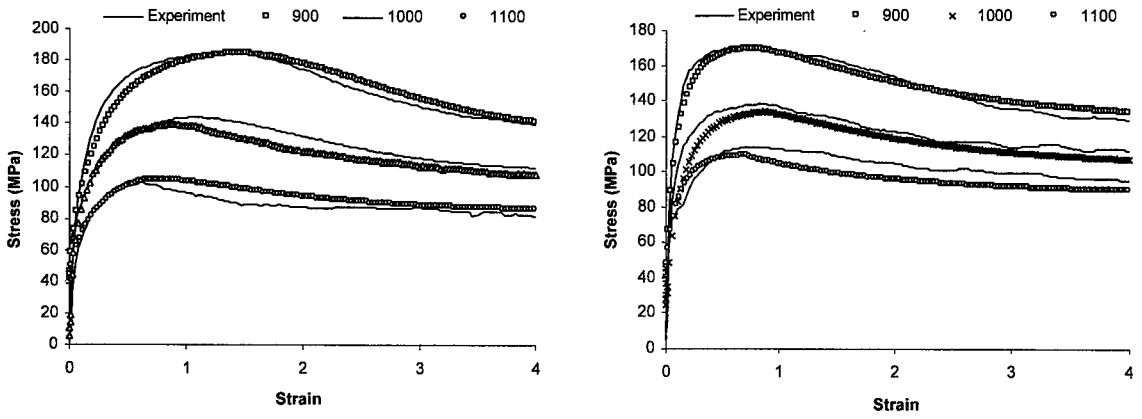


(a)



(b)

Fig. 7. ANN prediction of constants: (a) Constant B (b) Peak strain



(a) (b)

Fig. 8. Comparison between EM prediction with optimum constants and experimental results: (a) 0.065% (b) 0.58%

Due to the improvement of the prediction accuracy with the ANN model on the constants, the prediction on the strain stress behaviour significantly improves (Fig. 8). Every aspect of both the work hardening and dynamic recyrstallisation regimes is accurately presented. Unlike the linear fitting of the constants in Estrin and Mecking model, the ANN provides precise information on peak strain, saturation stress and steady state stress for low and high carbon steels which leads to the accurate prediction of the hot strength.

CONCLUSION

The strain stress behaviour of the austenitic steels with carbon content ranging from 0.0037 to 0.79% was studied using Estrin and Mecking unified constitutive model. Due the complex influence of the chemical composition, the constitutive model was not able to accurately predict the behaviour in both the work hardening and dynamic recrystallisation regions. With the incorporation of the ANN model into a modified Estrin-Mecking phenomenological model to predict the variables in the constitutive model, both the work hardening and dynamic recrystallisation regimes were accurately predicted. As the integrated constitutive ANN model also accurately predicts the materialproperties [2], the integration of constitutive and artificial neural network models provides an excellent approach to enhance the capability of the constitutive model.

REFERENCES

1. D. C. Collinson, P. D. Hodgson, B. A. Parker, 1993. Modelling the Effect of Carbon Content on the Hot Strength of Steel. *Modelling of metal rolling processes*, pp. 283-295, London.
2. L. X. Kong, P. D. Hodgson, D. C. Collinson,. 1998. Modelling the Effect of Carbon Content on Hot Strength of Steels Using a Modified Artificial Neural Network.*ISIJ International*, **38**, 1121-1129.
3. L. X. Kong, P. D. Hodgson, D. C. Collinson,. 1998. Application of an Integrated Phenomenological Neural Network Model to Extrapolatively Predict the Hot Strength of Austenitic Steels.*Steel Rolling'98*, Tokyo, pp.540-545.
4. M. Avrami. 1939. Kinetics of phase change. Pt.I: general theory. *J. Chemical Physics*, **7**, 1103-1112.
5. Y. Estrin and H. Mecking,. 1984. A unified phenomenological description of work hardening and creep based on one-parameter models. *Acta Metall.*, vol. **32**, pp. 57-70.
6. P. D. Hodgson, L. X. Kong, and C. H. J. Davies,. 1999. Prediction of the Hot Strength in Steels with an Integrated Phenomenological and Neural Networks Model. *J. Ma.. Proc. Techn.*, **87**, 132-139.
7. L. X. Kong and P. D. Hodgson. 1999. Constitutive Analysis of Flow Strength of Austenitic Steels with the Integration of ANN models. *8th Inter. Conf. on Mech. Behaviour of Materials* , Canada.

Hybrid Fuzzy Modelling Using Simulated Annealing and Application to Materials Property Prediction

Min-You Chen and D. A. Linkens

Department of Automatic Control and Systems Engineering
The University of Sheffield, UK
Email: Minyou.Chen@shef.ac.uk D.Linkens@shef.ac.uk

ABSTRACT

This paper proposes a hybrid fuzzy modelling approach using a self-organising network and simulated annealing algorithm for self-constructing and optimising fuzzy rule-based models. The proposed fuzzy modelling procedure consists of two stages. Firstly, a fuzzy competitive neural network is exploited as a data pre-processor to extract a number of clusters which can be viewed as an initial fuzzy model from engineering data. This step is used to perform fuzzy classification with the objective of obtaining a self-generating fuzzy rule base. Secondly, simulated annealing (SA), a combinatorial optimisation technique, is used to optimise the fuzzy membership functions. The application of this approach to the mechanical property prediction for C-Mn-Nb steels is given as an illustrative example.

INTRODUCTION

Fuzzy modelling has become an important subject in engineering because the if-then rule mechanism is easy to manipulate, understand and, to a certain extent, is domain independent. Also, the rapid development of hybrid approaches based on fuzzy logic, neural networks and genetic algorithms enhances the fuzzy modelling technology significantly. A variety of different fuzzy modelling approaches have been developed and applied in system identification, control, prediction and pattern recognition[1-5]. However, many existing methods using gradient-descent learning to design and optimise the fuzzy rule-based model encounter some problems such as local minima, slow learning speed and requirement of large memory as they are applied to engineering practice. In material engineering, it is important to establish an appropriate composition-microstructure-property model for materials development.

Much research has been done on developing models which will predict the final properties of the steel after rolling and cooling to room temperature as a function of the processing conditions and steel composition[6-8]. This kind of model usually consists of quite a number of input variables, such as the contents of different kind of chemical elements, microstructural parameters and process variables. Commonly used neural network models and neuro-fuzzy models based on gradient-descent learning algorithms may become trapped in local minima and they are computational inefficient for multivariable approximation problems.

To remedy the above problems, this paper proposes a hybrid fuzzy- modelling approach using a self-organising network and simulated annealing algorithm to self-construct and optimise the fuzzy-rule-base and increase the computational efficiency of the modelling process. The proposed fuzzy model is built in two stages. First, a competitive neural network is exploited to extract a number of clusters which can be viewed as an initial fuzzy model from engineering data. This step performs fuzzy classification with the object to obtain a self-generated fuzzy rule base. Domain knowledge is used for structure determination, i.e., to determine relevant inputs, number of membership functions for each input, number of rules, types of fuzzy models, etc.). Second, simulated annealing (SA), a combinatorial optimisation technique, is used to optimise the parameters in the antecedent and consequent parts of the fuzzy rules. The proposed approach allows construction of a mechanical property prediction model for structural steels.

GENERATING THE FUZZY RULE-BASED MODEL

A fuzzy reasoning model is considered as a set of rules in an IF-THEN form to describe the I/O relationship of a complex system. Consider a collection of N data points $\{\boldsymbol{P}_1, \boldsymbol{P}_2, ..., \boldsymbol{P}_N\}$ in a $n+1$ dimensional space

0-7803-5489-3/99/$10.00 ©1999 IEEE.

combining both input and output dimensions. Without loss of generality, a multi-input and single-output (MISO) model is used as a generic representation of a fuzzy system. Thus, the I/O data pair can be represented as:

$$\boldsymbol{P_k} = (\boldsymbol{x}_{1k}, \boldsymbol{x}_{2k}, ..., \boldsymbol{x}_{nk}, y_k),\ P_k \in R^{n-1},\ k=1,2, ..., N.$$

Let $\boldsymbol{x} = (x_1, x_2, ..., x_n) \in R^n$, be inputs and $y \in R$ be the output. The modelling problem is to identify the non-linear function $y = f(x)$: $R^n \rightarrow R$ with the given N input/output data pairs. A generic fuzzy model is presented as a collection of fuzzy rules in the following form:

$$R_i:\ \text{IF } x_1 \text{ is } A_{1i} \text{ and } x_2 \text{ is } A_{2i} \ ... \text{ and } x_n \text{ is } A_{ni} \ \text{ THEN } y \text{ is } f_i(\boldsymbol{x})$$

where $\boldsymbol{x} = (x_1, x_2, ..., x_n)$ and y are linguistic input and output variables respectively, A_{ji} are fuzzy sets of the universes of discourse of $U_j \in R$ (j=1,2,...,n), and R_i represents the ith rule, i=1,2,..., p. Typically, $f_i(\boldsymbol{x})$ takes one of the following three forms: singleton, fuzzy set or linear function of the input variables. To obtain the fuzzy rules requires defining the types and parameters of the membership functions for all fuzzy sets. Specifically, we chose singleton consequences and a Gaussian function as the form of the membership functions. Fuzzy logic systems with centre-average defuzzification, product-inference rule and singleton fuzzifier are of the following form:

$$y = \sum_{i=1}^{p} f_i(\prod_{j=1}^{n} \mu_{ij}(x_j)) \Big/ \sum_{i=1}^{p} (\prod_{j=1}^{n} \mu_{ij}(x_j)) \qquad 1.$$

where $\mu_{ij}(x)$ denotes the membership function of x_j belonging to the ith rule. i.e.,

$$\mu_{ij}(x_j) = \exp[-(\frac{x_j - a_{ij}}{\sigma_{ij}})^2] \qquad 2.$$

where σ_{ij} and a_{ij} are the width and centre of the fuzzy membership function $\mu_{ij}(x_j)$ respectively.

Creating the initial fuzzy model is a clustering process which groups the data scattered in space R^{n+1} into a collection of clusters. Since the goal is to minimise the objective function and the centres and widths are adjustable later in the parameter-learning phase, it is unnecessary to spend much time to assign centres and widths for the perfect cluster. Hence, we simply use a competitive learning network [9] to produce the clusters. The purpose of this stage is to classify the given training data into a small number, say $p << N$, clusters using competitive learning. The network classifies vectors into one of the specified number of p categories according to the clusters detected in the training data set. The training is performed in an unsupervised mode, and the network undergoes a self-organising process. During training, dissimilar vectors are rejected, and only the most similar, is accepted for weight-building. The procedure of rule generation via competitive learning is as follows.

Assume that the input vector is $\mathbf{x} = (x_1, x_2, ..., x_n)^t$, and we have a set of training data $\{\mathbf{x}_1, \mathbf{x}_2, ..., \mathbf{x}_N\}$. The learning algorithm treats the set of p weight vectors as variable vectors that need to be learned. The weight adjustment criterion for this mode of training is the selection of $\hat{\mathrm{W}}_i$ such that:

$$\| \mathrm{x} - \hat{\mathrm{W}}_{\mathrm{m}} \| = \min_{i=1,2,...,p} \{ \| \mathrm{x} - \hat{\mathrm{W}}_{\mathrm{i}} \| \} \qquad 3.$$

The index m denotes the winning neuron number corresponding to the vector $\hat{\mathrm{W}}_m$, which is the closest approximation to the current input $\mathbf{x}$. Note that the left side of Equation 3. can be rearranged as:

$$\| \mathrm{x} - \hat{\mathrm{W}}_m \| = (\mathbf{x}^t \mathbf{x} - 2\, \hat{\mathrm{W}}_m^t \mathbf{x} - 1)^{1/2} \qquad 4.$$

It is obvious from Equation 4. that searching for the minimum of p distances as on the right side of the equation corresponds to finding the maximum among the p scalar products:

$$\hat{\mathrm{W}}_m^t \mathbf{x} = \max_{i=1,2,...,p} (\hat{\mathrm{W}}_i^t \mathbf{x}) \qquad 5.$$

The left side of Equation 5. is the activation value of the "winning" neuron. After the winning neuron has been identified and declared a winner, its weights must be adjusted so that the distance calculated in Equation 3. is reduced in the current training step. It seems reasonable to reward the weights of the winning

neuron with an incremental change in weight in the negative gradient direction. Thus we have:

$$\nabla_{w_m} \|\mathbf{x}-\mathbf{w}_m\|^2 = -2(\mathbf{x}-\mathbf{w}_m) \quad 6.$$

$$\Delta \hat{\mathrm{W}}_m = \alpha(\mathbf{x} - \hat{\mathrm{W}}_m) \quad 7.$$

where $\alpha \in (0,1)$ is the learning rate selected heuristically. The remaining weights $\hat{\mathrm{W}}_i^t$, $i \neq m$, remain unaffected. The learning rule in Equation 7. in the kth step is rewritten in a more formal way as follows:

$$\hat{\mathrm{W}}_m^{k+1} = \hat{\mathrm{W}}_m^k + \alpha(\mathbf{x} - \hat{\mathrm{W}}_m^k) \quad 8.a.$$

$$\hat{\mathrm{W}}_i^{k+1} = \hat{\mathrm{W}}_i^k, \qquad \text{for } i \neq m \quad 8.b.$$

Learning according to Equations 7. and 8. is called the "*winner-take-all*" method -- a common competitive and unsupervised learning technique. As learning continues and clusters develop, the network weights acquire similarity to input data within clusters. In contrast to the standard competitive learning algorithm, we define the activation value of an output node as:

$$o_i = \mathbf{w}_i; \quad i = 1, 2, ..., p,$$

where $\mathbf{w}_I = (w_{i1}, w_{i2}, ..., w_{in})^T$ represents the prototype of the ith fuzzy cluster in I/O space.

After competitive learning, the produced p nodes in the competitive layer can be viewed as p data clusters centred at $\boldsymbol{W} = \{\boldsymbol{w}_1, \boldsymbol{w}_2, ..., \boldsymbol{w}_p\}$. Each cluster centre $\boldsymbol{w}_I = (w_{i1}, w_{i2}, ..., w_{in}, w_{i,n+1})$ is in essence, a prototypical data point that exemplifies a characteristic I/O behaviour of the system we wish to model. Hence each cluster centre can be used as the basis of a rule that describes the system behaviour. Each vector $\boldsymbol{w}_i$ can be decomposed into two component vectors x_i^* and y_i^* The cluster centre vector can be denoted as: $\boldsymbol{w}_i = (x_i^* \; y_i^*)$, where $x_i^* = (x_{i1}^*, x_{i2}^*, \cdots, x_{in}^*) = (w_{i1}, w_{i2}, ..., w_{in})$, $y_i^* = w_{i,n+1}$. Thus, each cluster centre $\boldsymbol{w}_i = (x_i^* \; y_i^*)$ can be viewed as a fuzzy rule that describes the system's local behaviour. Intuitively, cluster centre $\boldsymbol{w}_i$ represents the rule "IF input is around x_i^* THEN output is around y_i^*". Hence, the initial rule-base consisting of p rules is created by this competitive learning. The deviation parameter of cluster i, $\sigma_I = \sigma_{ji}$, is selected by using the average distance to the nearest m-cluster centres:

$$\sigma_i = \left(\sum_{j=1}^{m} \|\boldsymbol{c}_i - \boldsymbol{c}_j\|/m\right)^{1/2} \quad 9.$$

where $\boldsymbol{c}_j$ is the centre of the jth cluster nearest to cluster i. The obtained p prototypes are used to construct the parameters of the fuzzy rule-base. So, the rule-base, composed of c fuzzy rules, is represented as:

R_j: IF x_1 is A_{j1} and x_2 is A_{j2} ... and x_n is A_{jn} THEN y is f_j

where R_j denotes the jth rule, $j = 1,2,..., c$; A_{ji} is the fuzzy set defined by the Gaussian membership function centred at a_{ji}; and $f_j = \sum_{i=0}^{n} b_{ji} x_i$ is the jth rule output with respect to the TSK model, where $x_0 = 1$. Thus, the fuzzy inference model shown in Equation 1. is obtained:

OPTIMISING THE FUZZY MODEL USING SIMULATED ANNEALING

After structure identification, the fuzzy rule-based model must be trained for model optimisation via parameter-learning. The Simulated Annealing (SA) algorithm [10] is introduced as a combinatorial optimisation technique to find the optimal parameters of the membership functions in the fuzzy rules. SA comes from the similarity between mathematical optimisation procedures and the way a metal cools into a minimum energy crystalline microstructure called annealing. The optimisation process starts with an initial set of membership function parameters. The fuzzy model corresponding to this set of parameters is used in

a simulation for the test disturbance signal to evaluate the cost for these parameters. Then a new solution is selected randomly on a hyper-sphere with a certain radius around the previous solution. The cost for the new solution is evaluated in a similar fashion, and the costs of each solutions are compared. Optimal seeking starts at high temperatures resulting in acceptance of both cost-increasing and cost-decreasing solutions. The search is terminated when a certain degree of improvement is achieved in the cost function, or ended at a pre-set lower temperature. The SA method has a major advantage over other optimisation methods in its ability to avoid local minima. However, the standard SA algorithm suffers from very slow convergent process due to its slow cooling. To improve the computational efficiency, the fast SA approach proposed by Kirkpatrick [11] was adopted. The training procedure using the SA algorithm is as follows.

Step 1. Initialisation

Set up the initial temperature T_0, minimum temperature T_{min}, and cooling rate β. Define the cost function $E(\boldsymbol{x})$ as the *Root Mean Squared Error* (RMSE) of the model output. The SA algorithm starts with the initial state vector $\boldsymbol{x}_0$, produced by the competitive network. Set the iteration number $k = 1$.

Step 2. Generation of a new solution

A new solution based on the existing solution is generated as the following formula:

$$\boldsymbol{x}(k+1) = \boldsymbol{x}(k) + \gamma D$$

where γ is a random vector whose elements are in the range [-1 to +1], and D is a diagonal matrix that represents the maximum allowable change in search parameters.

Step 3. Make decision of acceptance

Calculate the cost function $E(\boldsymbol{x}(k))$, $E(\boldsymbol{x}(k+1))$, and the acceptance probability $P = min\{1, \exp(-\Delta E/T)\}$, where $\Delta E = E(\boldsymbol{x}(k+1)) - E(\boldsymbol{x}(k))$, T is the current temperature. If $P > \lambda$, where $\lambda \in [0, 1]$ is a random number, then go to Step 4, otherwise back to Step 2.

Obviously, the method not only accepts solutions that decrease the cost but also accepts solutions that increase the cost with a probability given by $P = \exp(-\Delta E/T)$.

Step 4. Temperature scheduling

Decrease the temperature using the following expression: $T(k+1) = \beta\, T(k)$;

Step 5. Termination judgement.

If $T(k) < T_{min}$, or $E(\boldsymbol{x}(k)) < \varepsilon$; Then stop the search; otherwise repeat from Step 2

APPLICATION TO MATERIAL PROPERTY PREDICTION

The problem with modelling hot-rolled metal materials can be stated broadly as: given a certain material which undergoes a specified heat treatment process, what are the final properties of this material? Typical final properties of interest are mechanical properties such as tensile strength, yield strength, elongation, etc.. A trial-and-error approach to solve this problem is often taken in the materials industry, with many different hot working conditions attempted to achieve a given final product. The obvious drawbacks of this approach are large time and financial costs and a lack of reliable predictive capability. By using the proposed hybrid fuzzy-modelling approach, we have developed composition-microstructure-property models for hot rolled *C-Mn-Nb* steels. The experimental data of more than 300 different steels with normalized heat treatment were used to train and test the fuzzy models which relates composition and microstructure to mechanical properties. Simulation for two typical prediction models are given as follows:

Structure-Property Model

In this model, Grain size ($D^{-1/2}$), Pearlite(%) and the percentage content of Nb (Nb%) are chosen as the model inputs, and Ultimate Tensile Strength (UTS) is the model output. 340 experimental data records of different steels are used for modelling. Half of the data set was used for training, the other half for testing. Through self-organised learning and parameter optimisation using the SA algorithm, a 2-rule fuzzy model was developed as shown in Figure 1.

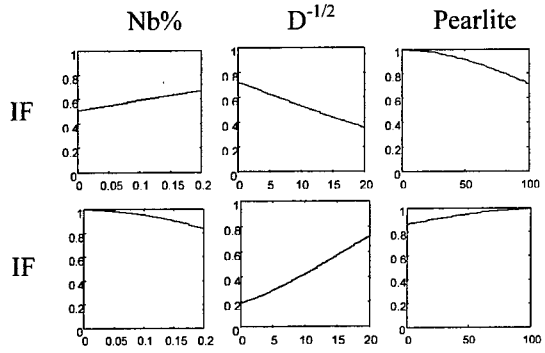


Fig. 1. The final fuzzy rule-based model for property prediction

The simulation results with 6% average prediction error of the UTS from the trained fuzzy model is shown in Figure 2(a) and (b). The predicted UTS versus measured UTS is plotted in Fig.2(c). The graph shows good agreement between measured and model-predicted values.

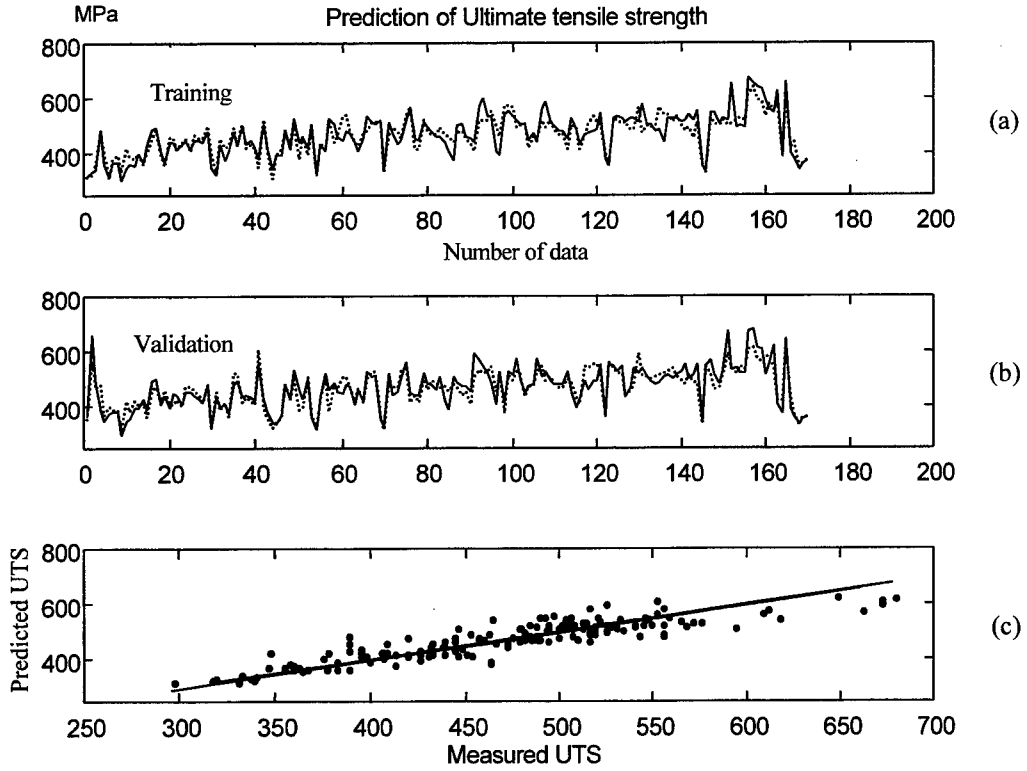


Fig. 2. Simulation results of the structure-property model.
in (a) and (b) : solid line: measured UTS. dotted line: predicted UTS

Composition-Microstructure-Property Model

The inputs to this model include the main chemical composition C%, Si%, Mn%, N%, Nb% and grain size $D^{-1/2}$. The model output is Lower Yield Strength (LYS). Using the proposed hybrid fuzzy-modelling approach, a final fuzzy model with 2 rules was constructed. The simulation results with 5.3% average prediction error is shown in Figure 3. A direct comparison of the measured LYS values versus predicted values over a wide range of samples is shown in Figure 3(c). The scatter of the points indicates that the predictions and generality of the obtained fuzzy model are good.

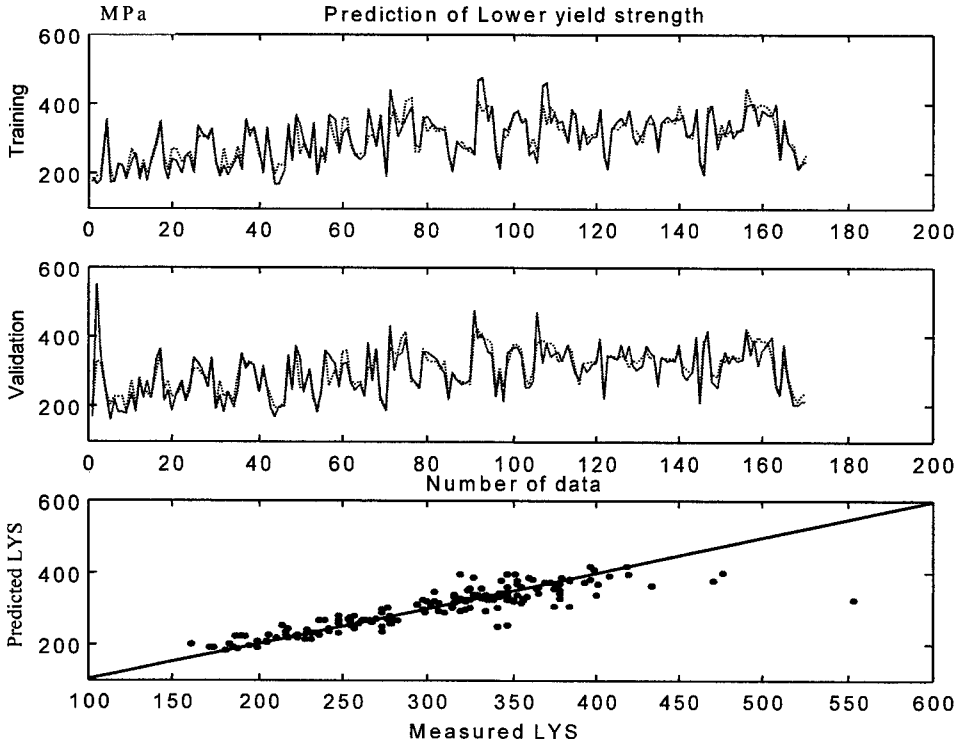


Fig. 3. Simulation results of the composition-microstructure-property model. in (a) and (b) : solid line: measured UTS. dotted line: predicted UTS

DISCUSSION AND CONCLUSION

A hybrid fuzzy-modelling approach using simulated annealing has been presented and applied to the task of predicting material properties. The main characteristics of this modelling approach are: (1) the fuzzy rule-base can be generated and optimised automatically from training data through a proposed hybrid fuzzy modelling procedure; (2) by using simulated annealing, the local minima problem is averted, thus global optimisation of the membership functions is possible; (3) the acquired fuzzy model has a simple structure and is fast to compute. Simulation shows predicted mechanical properties agree well with experimental data by using an optimised two-rule model. This work presents early work in development of fuzzy models for materials property prediction. Future work will be done to improve modelling accuracy, incorporate linguistic information with numerical data, and apply to microstructure modelling and property prediction.

REFERENCES

1. M. Sugeno, G.T. Kang, 1988. Structure identification of fuzzy model. Fuzzy Sets & Sys., 28, 15-33.
2. M. Sugeno, T. Yasukawa, 1993. A fuzzy-logic-based approach to qualitative modeling. IEEE Trans. Fuzzy Systems, 1(1), 7-31.
3. L.X. Wang, 1994. Modelling and control of hierarchical systems with fuzzy systems. Automatica, 33(6), 1041-1053.
4. J.R. Jang, 1992. Self-learning fuzzy controllers based on temporal back propagation. IEEE Trans. on Neural Networks, 3(5), 714-723.
5. S. Marsili-Libelli, A. Muller, 1996. Adaptive fuzzy pattern recognition in the anaerobic digestion process. Pattern Recognition Letters, 17(6), 651-659.
6. P.D. Hodgson, 1996. Microstructure modeling for property prediction and control. J. Mat. Proc. Tech., 60, 27-33.
7. C. Chen, Y. Cao, S.R. LeClair, 1998. Materials structure-property prediction using a self-architecturing neural network. J. Alloys and Compounds, 279(1), 30-38.
8. C.A.L. Bailer-Jones, T.J. Sabin, D.J. Mackay, P.J. Withers, 1998. Prediction of deformed annealed microstructures using Bayesian networks and Gaussian processes. Proc. Int. Conf. on Forging and Related Technology, Birmingham, U.K., 913-919.
9. T. Kohonen, 1984. Self-organization and associative memory, Springer-Verlag, Berlin.
10. S.Kirkpatrck, C.D. Gelatt, M.P. Vecchi, 1983. Optimization by simulated annealing, Sci. 220, 671-680.
11. S.Kirkpatrck, 1984. Optimization by simulated annealing: quantitative studies, J. Stat. Phys., 34, 975-986.

Intelligence in Materials Science I

Inorganic Glasses: Old and New Structures on the Eve of the 21st Century

J. Šesták * , B. Hlavácek + and N. Koga #

* Institute of Physics, Czech Academy of Sciences, Praha, Czech Republic
+ Dept. of Polymers, University of Pardubice, Pardubice, Czech Republic
# Chemistry Laboratory, Faculty School Education, Hiroshima University, Higashi-Hiroshima, Japan

ABSTRACT

History has shown that glass is a remarkable noncrystalline substance, usually made naturally or artificially from the simplest raw materials. Mimicking evolution however, mankind has been responsible for the creation of new families of a wide variety of glasses which gradually appeared through creative-thinking particularly during last hundred years. The process of rapid extraction of heat turned out to be successful in providing quenching treatments to assist physicists in preparing glassy states from different types of materials (metals) in contradiction to the previously traditional chemical approach which sought an appropriate composition to vitrify under self-cooling (silicates). The most discussed issue is the thermodynamic stability of the glassy state as a special form of matter with its low-dimensional organisational structure, as well as its classification within the hierarchy level of noncrystalline solids. In this respect the most important is entropy. We can say that the major part of the entropy under *Vogels* temperature, T_v , has its origin in the thermal entropy contribution, W_{th}. When the temperature becomes higher than T_v , the configurational part of the entropy, W_{cf} , starts to play a role. This W_{cf} part is mainly connected to the micro-configurational displacements of particles. At and above, the glass transition temperature, T_g , the conformational part of entropy, W_{conf} , which is connected to the displacements of particles through diffusion in the macro-sample is involved. It seems that liquids above the T_g transition are formed by two mechanically distinct "species". Under the T_g temperature, a matrix system is formed, in vast majority, by particles excited just to the lower level of the amplitude of an anharmonic oscillator. Above T_g , the second "species" starts to appear which is formed by thermally-excited particles able to overcome viscous and elastic forces of the matrix in their vicinity and bring the particles, through thermal excitement and interactions within their vicinity, to the upper amplitude levels of a non-linear oscillator. The thermally excited particles thus form the active and ephemeral vacancy spaces. These vacancies have very high expansion coefficient and are responsible for high expansion coefficient of liquids in general.

INTRODUCTION: A SHORT HISTORY OF GLASS MAKING

Advancement of tailored material engineering involves exploitation of relationships among the four basic elements: structure and composition; properties; performance; synthesis and processing. A common element that links the great diversity of work in materials science of both inorganic and organic engineering is thus the controlled combination of atoms and molecules in large segregation in ways that endow resulting compounds with desirable properties. This depends not only on the chemical nature of atomic and molecular constituents but also on the degree of their interactions, organisation and freeze-in phenomena with the greatest flexibility in the field of glasses. This depends on reshaping the concept of what material science is and what role it plays in analysing modern ordering and/or disordering phenomena functional in rigid states under our observation. The formation of new states long customary in nature but also aided by intelligent creatures is also of importance. In this respect, glass is a remarkable noncrystalline [1,2] substance, usually made from the simplest of raw materials. Mimicking evolution, however, Man has become responsible for the creation of a whole new family of a wide variety of glasses which gradually appeared through human creativity particularly during last hundred years where the process of rapid extraction of heat turned out to be responsible for successful quenching treatments to assist physicists in preparing glassy states from different

0-7803-5489-3/99/$10.00 ©1999 IEEE.

sorts of materials in contradiction to the previously traditional chemical approach which sought an appropriate composition to vitrify under self-cooling.

The first natural glasses were formed as the earth cooled and therefore, they pre-date the creation of living organisms by about 1.5 billion years. Such primordial glasses were limited in composition and versatility as were the first primitive unicellular organisms (bacteria), however, some compositions (in an unstable state of glass) have survived unchanged for enormously long periods (similarly to certain strains of bacteria). The diversity of glasses has been known since humans learned how to control fire, roughly a few hundred thousand years ago. The first man-made glasses were synthesized unintentionally by the fortuitous smelting of sand and alkaline plant flux by fire about ten thousand years ago. Some glasses were created by accidental action of spark and, particularly, tektites (natural acidic silicate glasses [3] with a high melting point), were formed by terrestrial impact and volcanism. They have attracted the attention of men since prehistoric times, having been used as cutting instruments, amulets or cult objects. It is also worth noting that the extent of natural glass on earth is in the range of a tenth of a percent with a ratio of about 3450 minerals versus 5 types of natural glass while on the moon (and possibly also other planets) it is possible to find merely 60 minerals against 35 glasses. So, the frequency of glass deposits is at least one order of magnitude higher than that on Earth.

Several notable milestones of modern science depended on the availability of new glass as a preeminent choice of alchemist for their apparatus. Relatively unstable and fragile glass was always essential for many chemical operations in early times. Dissatisfied with the chemical durability of glass, glass properties were modified by adjusting composition; however, this could not yet have been done properly as chemistry was still on a mystical basis, and the techniques of analysis did not exist. An important cornerstone was Galileo's work on the motion of planets based on glass lenses in astronomical telescopes, as well as Newton's pioneering work in optics (1666) requiring prisms and mirrors. Other basic investigations required specific glass apparatus to describe the properties of gases, to introduce thermometry, barometry and to develop microscopy. The first reasonably documented description of glass-making procedures is associated with the invention of lead glass around 1676. The most influential books appear to be Neril's " L'Arte Vetraria" (1612) and Kuncel's "Ars Vitraria Experimentalis" (1679) which were translated into other languages (as well as many others such as the Encyclopedia in 1765, etc.) all of them remained simple recipe manuals. In the middle of the seventeenth century, a proper understanding of heat was yet lacking, recognizing only three degrees of heat (calor, fervor, and ardor) and cold (frigus, algor and one unnamed) sensed more as a kind of chemical element and even treated with a negative mass. From the Bohemian Comenius (~1592) until the Scottish Black (~1728), temperature and heat were not distinguished, so that melting, solidification and glass formation could not be understood properly. The only important glass properties easily measured were density and refractive index.

Since medieval times, manual skill allowed the making of window glass by the crown process (forming a shallow bowl and, after reheating, spinning to make it open up into an almost-flat circular disc) and by the cylinder process (blowing a cylinder, cutting off the ends and cracking it longitudinally) often mentioned as "procede de Boheme". The nineteenth century showed an enormous progress in optical glasses [4] through effective stirring and later by fruitful investigation of property versus composition relationships. The tank furnace made possible continuous large scale production, as well as, machines for automated production of containers which essentially revolutionized the glass industry. By the turn of the century, Owens produced a successful six arm rotary machine which differed from most others in the way it was supplied with glass, and it remained almost unchanged until the 1960s when it was supplanted by gob feeders. Patents for sheet glass production date back to the 1850s but with little success. The invention of mechanically-drawing sheet glass was made by the Belgian, Fourcault, in 1914, but was not finalized due to the war. The original serial pulling was later improved by a system called "Bohemian cross", but the most important large scale production took place in the 1950s by a rather expensive redundant plate process.

The production of foam glass and fused basalts is also worthy of mention in the same period. The large scale production of glass fibers for insulation and for textiles was another important twentieth century development as well as less known advances in high quality, dimensionally-accurate pressing or optical fibers, gradient index glasses , etc. One of the most significant scientific achievements was Graffiti's theory of the strength of brittle materials (1920). X-ray diffraction analysis was a particularly exciting field having enormous impact on glass science in the first quarter of the century. It led Zachariesen to consider his principles on how bonding

requirements were met and nearest neighbor coordination maintained without imposing an exact long range order.

Since the thirties conferences on oxide glasses started their regular series followed by a search for novel glasses with properties not previously known or studied. This resulted in introduction of novel families of unconventional glasses; such as the non-oxide glasses of chalcogenides which exhibited many general features shared with oxide glasses. Serial conferences began to take place in the fifties and the most widespread ones came later with the development of xerography, electropholarography and lithography. Afterwards there appeared quite unexpected inorganic systems of which halide and metallic glasses are the most notable with those researchers specializing in the latter starting their regular meetings in the sixties.

Halide glasses have the potential for application as ultra-low loss optical fibers operating in the mid-IR and nonlinear optical ranges, while "metglasses" and nowadays, nanocrystalline "finemetals" have already found their place in various magnetics. It is worth noting as well, the preparation of glass-like carbon achieved by solid carbonization of thermosetting resins in the 1960s (once used for inert bio-implants) which appeared in the same year as the first Au-Si alloy glass. However, there was almost parallel development of the individual description of vitrification and crystallization based on the theories of nucleation and crystal growth which was also true for another separate group, the organic and polymeric glasses. Nowadays the theories have been unified.

GLASS TRANSITION AND PREVIOUS THOUGHTS

Terminology consensus has not been agreed to on the meaning of glassy and often synonymous amorphous states [5] (of solids), the latter frequently employed by physicists to describe highly, non-equilibrated structures of quenched metals and semiconductors while the first is preferred by chemists in the traditional field of silicates and related oxide and other anionic melts. Amorphous solids can be prepared by any generalized process of chemical and/or physical disordering to exhibit an overlap of premature crystallization with glass transformation. This is somewhat different from a "more thermodynamically-stable state" of glasses attainable by repeated vitrification through duplicated (often rapid) liquid cooling which should always be accompanied by a more or less discriminative region of glass transformation, which is assumed to be a general characteristic of the glassy state.

The physical appearance of a glassy and/or amorphous solid looks, however, more stable than that of an udercooled liquid, the latter being more easily convertible to the nearest stable state of a crystalline solid. Consequently we also come to the discussion of the term "solid" in view of vitroids within the framework of rheology. This would be more appropriate for glass since such a vitroid changes with time and the observation time is involved in detecting the extent of change. Three types of glasses can be distinguished by the previous idea to be ranked as glassy liquids, glassy (molecular) crystals and glassy liquid crystals characterized by their own transformation regions related to dissipation of a certain "freedom". In this view, amorphous solids actually belong to a fourth limiting case depending on execution of the disordering process itself. In this light we can also consider formation of low-dimensional structures and sol-gels, the latter being particularly, subjected to further classification due to the inability to clearly involve the glass transformation phenomenon. Correlation between the characteristic temperatures and glass forming ability has been anticipated in the form of reduced quantities. The ratio between T_g and T (= T_{gr}) melt should be roughly 2/3. A similar behaviour relates to the ratio T_o/T_{melt} (= T_{or}).

Let us repeat some traditional energy considerations [5,6]. At the melting point, the liquid and solid have equal Gibbs energies but differ in the enthalpy and entropy contents. Upon cooling below the melting point the entropy of the undercooled liquid decreases more rapidly than that of a stable solid . Examining these different rates of entropy loss, we can determine a point where the entire entropy of melting would be diminished, resulting in the entropy of both phases becoming identical at a temperature called the Kauzmann "pseudo-critical" temperature, still lying above absolute zero. This means that the liquid loses its entropy at a faster rate than the solid and if the liquid maintains configurational equilibrium on very slow cooling to the region where it attains high viscosity, it would have a lower entropy than the solid. Such a

state, however, is unattainable and the equilibrium-like liquid must therefore transform into rigid glass at a pseudo-second order transformation. Such a critical trend of entropy is not always sufficiently understood since such a prior intersection by liquid vitrification causes the heat capacity of the liquid to change abruptly to a value close to that of a corresponding solid. However, an unsolved question remains as to what would happened if such an isoentropy-temperature of the so-called ideal glass transformation is nevertheless attained by hypothetical infinitesimal-slowing of the cooling rate, thereby avoiding the irreversible freeze-in. Although this is an imagination game, there would appear to be a kind of higher order transition wherein the heat capacity of the undercooled liquid changes to that of the congruous stable crystalline solid and could be regarded as a "fourth state of matter".

The viscosity of liquid can be regarded as a reflection of the relation between the thermal energy available at a given temperature and the strength of the forces pulling the species together and restructuring their position in a given volume within which molecular rearrangement can occur. The possible rate of these rearrangements rapidly decreases with decreasing volume within which the species are packed. The volume is determined by the strength of the attractive forces and is reflected in the characteristic temperatures (melting, critical points, etc.). The more strongly the components interact, the more rapidly the freezing point of the solvent is depressed and the viscosity is increased, consequently slowing perturbing nucleation, but this should not be so strong as to generate a new competing crystalline phase. Zachariesen rules can thus be understood to predict low melting points relative to the forces acting between the species, although some newly developed glasses violate these predictions.

ANHARMONICITY VIBRATIONAL APPROACH TOWARDS THE CREATION OF FREE VOLUME IN THE VICINITY OF GLASS TRANSITION

Entropy Considerations

As shown above, the problem of explaining T_g (glass transition) for a long time was presumed to be mainly related to the configurational or conformational changes of entropy. Therefore we would like to concentrate our effort on the clarification of T_g transition through anharmonic vibrations [7,8] and drastic amplitude changes in the vicinity of T_g . Such an isolated non-linear oscillator can reveal double frequencies and pulses. If the individual oscillators can interact on similar frequencies, then the individual particles can undergo a discontinuity in amplitudes (so-called amplitude jump). In the liquid state, such an amplitude jump of a monomer or dimer unit would push aside particles in the vicinity forming an opening for a vacancy space. Enlargement of the amplitude can be detected by means of methods of neutron-scattering which can provide the information about average vibrational amplitude (the Debye-Waller factor). Occasional misapprehension passed on in early work with T_g transitions had its source in the disregard of two facts: (1) omission of a proper definition of "α" known in studies in solid state physics and (2) over-emphasis of the meaning of the configurational and/or conformational part of entropy in the following equation as found in the vast majority of cases:

$$S = k \ln W_{conf} + k \ln W_{therm} \qquad 1.$$

where k stands for the Boltzmann constant. In our theory, we suppose that the T_g transition is connected to the release of vibrational motion of monomer or dimer units in the rotational sense as, e.g., the spinning of a benzene ring around vinyl groups in a polystyrene chain. Above the T_g region, the vacancy thus created can occupy a volume larger than 10 L^3 . For inorganic glasses, the substructure of the SiO_4 tetrahedron is reputed to be released in the vicinity of T_g . Under the temperature ($T_g \approx 52$ K), only a very small part of the particles can undergo a finite displacement. About 10^{-5} tunnelling states per atom and about 10^{-3} states connected to boson peak at very low temperatures can be presumed if we disregard the motion of side chains. Below T_g , Equation 1 becomes :

$$S = k \ln W_{therm} \qquad 2.$$

as a consequence of $W_{conf} = 1$. The Kauzman paradox of negative entropy (the so-called entropy crisis) can thus never occur, because one part of entropy which should participate under T_g just disappears. For

polymers the value of c_p (heat capacity) per atom is approximately "k" to "2k" forming a sort of analogy to the Dulong-Petit rule for metals. The potential valley, in which the individual particle is supposed to undergo vibrational motion, can be written as follows:

$$U - U_o = \frac{1}{2}kT = \frac{1}{2}f^2\xi \text{ , where } kT/f = \xi^2 \qquad 3.$$

In Equation 3, U_0 is the reference energy level which can be taken as equal to zero and $\xi = r - r_0$ is the deviation from the bottom of potential valleys while k is the Boltzman constant and f is related to the bulk compressibility modulus $K = f/r_0$.

For the non-linear form of a potential valley, the relationship becomes:

$$U - U_0 = -\frac{1}{2}f\xi^2 - \frac{1}{3}g\xi^3 \qquad 4.$$

The non-zero coefficient of thermal expansion can be defined as:

$$a = \frac{1}{r_0}\frac{g}{f^2}k = \frac{1}{f_0}\frac{d\bar{\xi}}{dT} \qquad 5.$$

It is evident that this definition does not need to be perfect. However, as it has already been shown that the inclusion of a higher term in the power series development, analogous to Equation 4, would not bring any difference into the definition of, α, or

$$U - U_0 = \frac{1}{2}f\xi^2 - \frac{1}{3}g\xi^3 - \frac{c}{4}\xi^4 \qquad 6.$$

This type of potential valley is generally considered in the basic physics of inorganic glasses. Usually the authors do not consider possible interactions of particles with particles located in the neighbourhood. Such interactions with a nearby resident can bring the isolated particle to a completely different level of $\bar{\xi}$ for which the particle, if left subsequently isolated, must associate with a different anharmonicity level characterised through a completely different ratio of g/f^2 functions. This stems from Equations 3 and 5 as well as from the expression for the average force acting on the isolated particle:

$$(F_{AV} = f\bar{\xi} - g\overline{\xi^2} = 0 \text{ and } \bar{\xi} = \frac{g}{f}\overline{\xi^2}) \qquad 7.$$

The non-linearity can also accounted for through the variation coefficients of the second order differential equation together with the addition of the right-hand side to yield Equation 8. A variety of particle interactions can be considered. For particle motion in the potential valley, we get:

$$m\frac{d^2\xi}{dt^2} + F\left(\xi;\frac{d\xi}{dt}\right)\frac{d\xi}{dt} + \frac{dU}{d\xi} = A\left(\xi;\frac{d\xi}{dt}\right)\cos pt \qquad 8.$$

where the angular frequency , "p" is presumed to be close to the characteristic "eigen" frequency "ω" of free vibrations. The right hand side of the equation stands for particle interactions with its neighbours. By using mathematical methods, the non-linear system of the second order differential equation can be turned into two separate first order differential equations with variables A_1 and A_2 (corresponding for example to $A = d\xi/dt$ and $A_2 = \xi = f(A_1; t; \alpha; ...\text{etc.})$; and subsequently even the time dependence can be eliminated. We can get:

$$\frac{dA_1}{dt} = \alpha_{11}A_1 + \alpha_{12}A_2 \ , \quad \frac{dA_2}{dt} = \alpha_{21}A_1 + \alpha_{22}A_2 \qquad 9.$$

and choosing, e.g., $-a_1 = -\alpha_{11} + \alpha_{22}$ we can arrive at the time-independent amplitude representation of the problem [8] where the type of motion is defined through different ratios of constants a_1 and a_2. The neutron scattering data [9] present the most convincing evidence of the average amplitude rise in T_g vicinity. The average amplitude of vibrations starts to rise slowly at Vogel's temperature and at $T = T_{cr}$ (the so-called crossover temperature $T_{cr} \approx 1{,}2T_g$), the constant slope of the average amplitude rise is established (for area of $T \geq T_{cr}$). We assume that vacancies are created in the liquid matrix through the

high amplitude motion of the particles. In such a case a vibrating particle is able to push aside neighbouring particles as experimentally evidenced with cis-1,4-poly(butadiene) [10]. The basic conclusion of the theory is that the amplitude change would play a governing role in the definition of a liquid state and in its transition into the solid or the glassy state. The rise in vibrational amplitude is the major reason for solid and/or liquid volume enlargement. These expansions proceed either through continuous changes or through a sharp discontinuity. In such a way the non-linear, mutually interactive, oscillator system can successfully cope with the first order as well as with the second order transitions which take place in the liquid state.

THE SCIENCE AND HORIZON OF NONCRYSTALLINE STATES

Yet more study [6,11] must be directed to ascertain near-glass-transformations and pseudo-glass-transformations in order to study intermediate states between amorphous and glassy solids in the sub-glass transformation region. Among these should be order/disorder changes of deposited tetrahedral and amorphous carbon or a pronounced short and\or medium ordering in the as-quenched and amorphised alloys. Progressive study of vibrational states of silicon in the crystalline and amorphous forms as well as the associated void formation seems to be of no-less importance for a better understanding of the higher density of amorphous forms. Inelastic neutron scattering will assist in observing the nature of hydrogenated amorphous silicon when investigating, e.g., the bond type (so far single, double, but not triple) of hydrogenated and deuterated samples as well as the effect of hydroxylation. An attempt at forming a nanocrystalline theory of photoluminescence is also foreseen to guide technologists in preparing a comparable material by controlled nucleation of laser glazed surfaces or even sol-gel precursor samples. There is a certain hope of tailoring the multilayer silicon-silica sandwiches instead of using conventional electrolysis of high voltage discharging.

Interesting attention is still to be expected in the study of intermediate states between glass, liquid and crystal, i.e., the architecture of ordered crystallites at a submicron scale relevant to the medium-range order that exists in the glassy state and which become prenucleation stages in generalized precursor liquids. This will be continued by studying the anomalous small/wide angle x-ray diffraction (ASAXS and AWAXS) using an NMR insight into the medium-range ordering and microscopic mechanism of diffusion and viscous flow in precursor melts for a better understanding of bonds between cations and anions, the spectroscopy of substructures using, e.g., the still traditional concept of bridging, half- and non-bridging oxygen (regarding e.g. biocompatibility) or interaction of metallic and metalloid species in metglasses to possibly explain the role of thermal history, recreated medium-range order and the effects of modifying admixtures. The successful assistance of theoretical treatises based on classical molecular dynamics and dynamic stimulation of electronic ground states and of topological restructuring (low temperature annealing process) remains inevitable (ab-initio molecular dynamic techniques, reverse Monte Carlo, etc.).

For a progressive tailoring of magnetic as well as of mechanical, ferroelectric and dielectric properties, attention is paid again to the medium ordering states because, e.g., the extent of magnetic exchange interactions is effective across a given width of magnetic domain walls, and the disordered nanocrystallites of a subcritical domain size ('finemetals') would thus appear as magnetically disordered in a similar way as trulynoncrystalline, yet classical, 'metglasses'. Similarly, this may bring new dimensions to nonlinear optoelectronics where again noncrystallite waveguides can eventually play an important role in infrared optics. Silica glass fibers could cause the frequency doubling of infrared laser beams suggesting that even a noncrystalline solid can have large second-order susceptibilities. Oxide glasses also serve as useful transparent matrices for semiconductor microcrystallites to form nanocomposites with large third-order susceptibilities. Controlled uniform size distribution of quantum dots is needed for such nonlinear devices and soliton switching as well as waveguide lasers while nonuniformity is required in applications of optical data storage. Submicron crystallites of halides in composite glassy electrolytes essentially increase ionic conductivity, and nanometric pinning centers improve superconductivity of complex cuprates. Nanocrystallization of porous silicon plays an important role in better managing of photoluminiscence when taking into account the properties of silica, as the separating interfaces of silicon grains were recently shown to be responsible for blue photoluminescence, their quality dependent on the nano-sized separating layers which should remain, according to early studies carried out on inorganic and organic silanes.

To speak of another important area, that of superalloys, we can briefly cite the importance of inhibition of any subcritical nuclei formation in such diverse fields as biology, to mention cryo-preservation of viruses and/or growth of faults (diseases, e.g., cancer) in preventative medicine. Self-protection of plants against freezing is another example taking place by the process of drying (fluid concentrational changes). Oxide gels and organically-modified silica gels (ormosils) should not be forgotten as well-known hosts for nanocrystallites which, in combination with optically-active polymers, can provide high third-order optical materials.

Order/disorder phenomena in systems with lower dimensions are separate emerging fields providing new boundary problems such as nanometer range phase separation in thin amorphous films prepared by CVD as known for germanium. It touches as remote a material area as non-stoichiometric semiconductors prepared via nonequilibrium MBE or MOCVD, e.g., semiisolating GaAs where Ga, substituted in As-regular sites, produces As-vacancies acting as deep-level electron traps. These matrices are generally understood as submerged disordered systems of defects with nanocrystalline dimensions. When one characteristic dimension is of the order of the electron wave-length, quantum electron phenomena (i.e. dimensional absence of electron resistance) become important. These are known as quantum wells, wires and/or dots. If for an appropriate thickness of a semiconductor layer, disorder of the interface is controlled by remote doping, a high mobility transistor (HEMT) function is achieved on the basis of the quantum well. A comparable but almost zero dimensional fluctuation can be created across the dividing insulating layer by formation of quantum dot arrays prepared either by semiconductor layer etching or by random chemisorption (chemical FET). Quantum dots can also be conventionally formed by dispersion in a suitable matrix, their optimum size is estimated from the ratio of material permittivity to effective mass. Such a field, apparently remote from the traditional glass field, may become a boundary area for theoreticians when assuming during slow cooling of a single crystal, that non-equilibrium and relatively large-scale fluctuations are created. Thus even highly ordered structures with a low dopant concentration show positioning comparable to nanometric, medium ordered, modulated structures.

The functional utility of such newly ranked materials need not be appreciated right away before their properties are adequately characterized. Already common rapid solidification has played a key role in the discovery of quasicrystals, a class of materials neither exactly crystalline nor noncrystalline, and in the ongoing reexamination of the basic principles of crystallography. Closely related stereochemical models, where so-called order within disorder is a reliable approach considering modulus as a probable measure of structural order, question the classical models of crystallography versus noncrystallography. Breakthroughs, such as the recent discovery of the Hall-quantum effect or high-temperature-superconductivity cannot be predicted or planned for the next millennium. The case is similar for any possible prospect of the above discussed branches of material science related to the discussed glasses and noncrystalline and low-dimensional structure in general.

ACKNOWLEDGEMENT

This study was carried out under the financial support of the Grant Agency of Czech Republic 106/97/0589

REFERENCES

1. Barrington-Haynes, E., 1948. Glass through the Ages, Penguin, Harmondsworth.
2. Phillips, C.J., 1948. Glass the Miracle Maker, Pitman & Sons, London.
3. Bouska, V., 1993. Natural Glasses, Academia, Praha.
4. Zarzycki, J. (ed.), 1991. Material Science and Technology: Glasses and Amorphous Materials, VCH-Weinheim
5. Sestak, J., 1985, Thermochim. Acta 95, 459.
6. Sestak, J., 1997, Glastech. Ber. Glass. Sci. Tech. 70C, 153.
7. Hlavácek, B., Kresálek, V., Soucek, J., 1997, J. Chem. Phys., 107, 4658 & 1996, Thermochimica Acta, 280/281, 417.
8. Hlavacek, B., Sestak, J., 1999. Theory of anharmonicity vibrational approach towards the creation of free volume in the vicinity of glass transition, Keynote Lecture at Glass'99, Prague, (in press).
9. Buchenau, U., Zorn, M., 1992, Europhysics. Letters. 18, 523.
10. Bartos, J., at al., 1997, Macromolecules 30, 6912 & Physica B 234/236, 435.
11. Sestak, J., in the book by Chvoj, Z., Sestak, J., Triska, A., (eds.) 1991. Kinetic Phase Diagrams; Non-equilibrium phase transformations, Elsevier, Amsterdam.

Oxygen Solubility Modeling in Aqueous Solutions

Desmond Tromans

Department of Metals and Materials Engineering, and Pulp and Paper Centre,
University of British Columbia, Vancouver, BC V6T 1Z4, Canada.

ABSTRACT

Oxygen dissolved in the aqueous phase $(O_2)_{aq}$ is an important oxidant in many industrial processes, ranging from pressure leaching and heap leaching of metals from minerals to the bleaching of wood fibers in the pulp and paper industry. Frequently, $(O_2)_{aq}$ is a prime agent promoting corrosion of metals in aqueous systems. This study presents a general solubility model for estimating oxygen solubility in aqueous inorganic solutions over a wide range of conditions. These include changes in oxygen partial pressure P_{O_2} (atm), variations in the process temperature T (K), and changing concentrations C_I of dissociated inorganic solute I. The model is based on a thermodynamic analysis showing that the concentration c_{aq} of $(O_2)_{aq}$ in pure water is dependent upon P_{O_2} and T via an equation of the form $c_{aq} = P_{O_2} f(T)$, where $f(T)$ is a T-dependent function related to the chemical potential, entropy, and partial molar heat capacity of the gaseous oxygen $(O_2)_g$ and dissolved $(O_2)_{aq}$ species. In the presence of a single I, this equation is modified by a ϕ-factor such that the new oxygen solubility, $(c_{aq})_I$, becomes $(c_{aq})_I = \phi c_{aq} = \phi P_{O_2} f(T)$, where ϕ is an I-dependent function of C_I. Inorganic solutes of similar stoichiometry, composed of a common anion and having cations from the same Group in the Periodic Table, tend to exhibit a similar ϕ-factor and $(c_{aq})_I$ value, provided all concentrations, c_{aq}, $(c_{aq})_I$, and C_I, are reported in molal (m) units (mol/kg H_2O). Methods for incorporating the effect of multiple I on ϕ are presented and discussed.

INTRODUCTION

Many industrial oxidation processes rely upon the presence of dissolved oxygen $(O_2)_{aq}$, to accomplish oxidation, including leaching of minerals from ores and oxygen bleaching of pulp. In other situations $(O_2)_{aq}$ may have undesirable effects, such as corrosion of metals. Frequently, these processes fall under mass transport control of $(O_2)_{aq}$ to the reacting surface. Consequently, higher oxygen solubility enhances mass transport and increases oxidation rates. Thus, a quantitative and predictive knowledge of oxygen solubility is desirable, particularly as it is affected by such process variables as temperature T (K), partial pressure P_{O_2} of oxygen in the gas phase $(O_2)_g$ and the concentration C_I of inorganic solutes I.

Measurements of oxygen solubility in water and aqueous solutions have been made for many decades [1]. Until recently, little progress was made towards the development of a unifying and predictive equation (model) that combined the conjoint effects of T, P_{O_2}, and C_I. This was due partly to the variety of different oxygen and solute solubility units used that were used and to considerable empiricism in reported relationships. Recent analytical modeling studies by the author [2] have shown that a rigorous thermodynamics-based approach leads to a unifying equation for the concentration c_{aq} of $(O_2)_{aq}$ in pure water. Good agreement between the unifying equation and published data were evident when such data were converted to the same set of thermodynamic units as those used in the model. This model was then modified to incorporate the effects of different I and shown to have the potential for predicting (estimating) oxygen solubility $(c_{aq})_I$ in I-containing solutions of industrial relevance [3]. Predictive capabilities are necessary for the utility of any model for process development, in order to avoid the prohibitive time and costs involved in the measurement of $(O_2)_{aq}$ solubility for different combinations of T, P_{O_2} and C_I.

The oxygen solubility model for pure water will be outlined first, followed by a modification to account for the effects of I. Subsequently, examples of the predictive capability of the model will be presented and discussed. All thermodynamic units are consistent with those recommended by the International Union of Pure and Applied Chemistry (IUPAC), *e.g.* molal (m) units (mol/kg H_2O) for the concentrations c_{aq}, $(c_{aq})_I$, and C_I; degrees Kelvin (K) for T; and atmospheres (atm), for P_{O_2}, where 1 atm = 101.325 kPa. Methods

0-7803-5489-3/99/$10.00 ©1999 IEEE.

for converting concentrations of $(O_2)_{aq}$ and I from other units to m are described previously [2,3], including use of the International Critical Tables [4] to convert molar (M) units (mol/liter of solution) to m.

OXYGEN IN PURE WATER

Equilibrium between $(O_2)_g$ and $(O_2)_{aq}$ is given by Eq. 1,

$$(O_2)_g = (O_2)_{aq}, \quad k = [O_2]_{aq}/[O_2]_g = [\alpha c_{aq}]/[\gamma P_{O_2}] \qquad 1.$$

where k is the equilibrium constant, square brackets [ ] denote activity, α is the activity coefficient of $(O_2)_{aq}$, and γ is the fugacity coefficient of $(O_2)_g$.

The value of k at any T is related to the standard molar chemical potentials μ^o_{aq} and μ^o_g of the $(O_2)_{aq}$ and $(O_2)_g$ species, respectively, at that temperature and the overall change in chemical free energy of the reaction ΔG^o via Eq. 2 leading to Eq. 3,

$$\Delta G^o = \mu^o_{aq} - \mu^o_g = -RT \ln k \qquad 2.$$

$$k = \exp(-\Delta G^o / RT) = \exp\{(\mu^o_g - \mu^o_{aq})/RT\} \qquad 3.$$

where R is the gas constant (8.3144 J.mol^{-1}.K).

The T-dependence of k (and c_{aq}) is controlled by the effect of T on the exponential function in Eq.3. The value of μ^o for a single species at T_2 is related to that at a reference T_1 by Eq. 4[2],

$$(\mu^o)_{T_2} = (\mu^o)_{T_1} + \int_{T_1}^{T_2} C_P \partial T - T_2 \int_{T_1}^{T_2} \frac{C_P}{T} \partial T - S^o_{T_1}(T_2 - T_1) \qquad 4.$$

where C_P is the molar heat capacity of the species at constant pressure and $S^o_{T_1}$ is its standard entropy at T_1.

Hence from known μ^o and S^o data at T_1 the new chemical potentials of each species may be calculated at T_2 to give the new equilibrium constant k_{T_2} at T_2,

$$k_{T_2} = \exp\left(\frac{(-\Delta G^o)_{T_2}}{RT_2}\right) = \exp\left(\frac{(\mu^o_g)_{T_2} - (\mu^o_{aq})_{T_2}}{RT_2}\right) \qquad 5.$$

The most common reference T_1 for which considerable thermodynamic data have been determined is 298K (25°C). Standard μ^o and S^o values for the gaseous and dissolved oxygen species at 298 K are listed in Table 1, together with the data sources [2.5].

Table 1. Standard Thermodynamic data at 298 K

Species	μ^o (kJ.mol^{-1})	S^o (J.mol^{-1}.K^{-1})	Reference
$(O_2)_g$	0	205.028	Hoare [5]
$(O_2)_{aq}$	+16.506	+109	Tromans [2]

Based on the reported T-dependent variation in the molar heat capacity $(C_P)_g$ of $(O_2)_g$ [6,7], it was found that $(C_P)_g$ could be represented by a linear function of T in the range 273-650 K [2],

$$(C_P)_g = +26.65 + (9\times10^{-3})T, \text{ J.mol}^{-1}\text{.K}^{-1} \qquad 6.$$

Also, analysis of reported oxygen solubility behavior by the author [2] showed that the molar heat capacity $(C_P)_{aq}$ of $(O_2)_{aq}$ could be represented by a linear function of T

$$(C_P)_{aq} = +230 - (8.3\times10^{-2})T, \text{ J.mol}^{-1}\text{.K}^{-1} \qquad 7.$$

The much higher value of $(C_P)_{aq}$ relative to $(C_P)_g$ indicates that changes in molecular rotations and bond vibrations have been caused by interactions (disturbances) between $(O_2)_{aq}$ molecules and the surrounding water molecules. The decreasing $(C_P)_{aq}$ with increasing T is then seen to be consistent with the decreasing interactions between water molecules (*i.e.* diminishing hydrogen bonding) with increasing T, as revealed by the decrease in activation energies of viscosity and self diffusion of water with increasing T [8].

From Eqs.4 to 7, together with the data in Table 1 and using a reference temperature T_1 of 298 K, it is a straightforward arithmetical exercise to show [2] that the value of k at any arbitrary value of T (equivalent to T_2) is given by the function of T, $f(T)$, shown in Eq. 8 [2],

$$k = f(T) = \exp\left(\frac{0.046T^2 + 203.35T\ln(T/298) - (299.378 + 0.092T)(T - 298) - 20.591\times10^3}{(8.3144)T}\right) \quad 8.$$

Combining Eqs. 1 and 8,

$$c_{aq}(\alpha/\gamma) = P_{O_2}k = P_{O_2}f(T) \quad 9.$$

Furthermore, it was shown previously [2] that for P_{O_2} to ~60 atm and T from 273 to 616 K that α/γ may be closely approximated to unity so that the final model equation for oxygen solubility becomes,

$$c_{aq} = P_{O_2}k = P_{O_2}f(T) \quad \text{or} \quad c_{aq}/P_{O_2} = k = f(T) \quad 10.$$

where $f(T)$ is given by Eq. 8.

The predictions of Eq. 10 compare very favorably with published solubility data [9-14] in Fig.1, after converting all data to molal (m) concentrations). The data include P_{O_2} to ~60 atm and T to 616 K

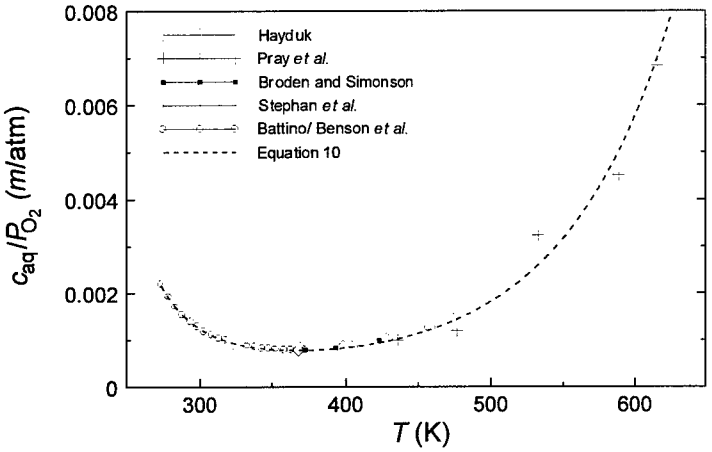


Fig. 1. Comparison of model Equation 10 with published oxygen solubility data in water.

SOLUTIONS CONTAINING SINGLE INORGANIC SOLUTES (DISSOCIATED)

The effect of dissociated (ionized) inorganic solutes, I, on oxygen solubility is modeled by assuming that only a fraction ϕ of the water is available for the dissolution of $(O_2)_{aq}$, the remaining fraction (1-ϕ) being unavailable due to near and distant interactions between the solute ions (cations and anions) and water molecules [3]. This concept arose from similarities in the difference between C_P values of the $(O_2)_{aq}$ and $(O_2)_g$ species and the difference between the C_P values of metals and their corresponding cation [2]. Thus the oxygen solubility $(c_{aq})_I$ in the presence of a single I is given by Eq. 11,

$$(c_{aq})_I = \phi c_{aq} = \phi P_{O_2}k \quad 11.$$

where k and c_{aq} have the same values as those in Eqs. 8 and 10, respectively.

For modeling purposes, it is sufficient to treat the dependence of ϕ on C_I in terms of an empirical function, $\phi = f(C_I)$, where $\phi \to 1$ as $C_I \to 0$ and $\phi \to 0$ as $C_I >> 1$. A suitable function requiring positive values for the coefficient κ and exponents y and η is given by Eq. 12, leading to Eq 13 after combining with Eq. 11.

$$\phi = \left\langle 1 + \kappa(C_I)^y \right\rangle^{-\eta} \quad 12.$$

$$(c_{aq})_I = P_{O_2}k\left\langle 1 + \kappa(C_I)^y \right\rangle^{-\eta} \quad 13.$$

Values of κ, y and η have been calculated for 26 I at 298 K and 1 atm P_{O_2} [3,15,16], using published oxygen solubility data. They are listed in Table 2.

The shape of the C_I - ϕ curves based on the data in Table 2 are shown in Figures 2(a) to 2(c). Curves for, HCl and the halide salts are included in 2(a), H_2SO_4 and sulfates in 2(b), and alkaline hydroxides and other salts in 2(c). The behavior of aqueous ammonia $(NH_3)_{aq}$, shown in Fig. 2(c), will be discussed later.

Considering a common anion, Fig. 2 suggests the effect of a metal salt on ϕ is related to the position of the metal in the Periodic Table. For chlorides, Fig. 2(a), ϕ decreases in the order Group IA metals (Na, K)>Group IIA (Mg, Ca, Ba)>Group IIIA (Al). For sulfates, Fig. 2(b), the trend is transition metals (Co, Ni, Cu)>Group IA (Na, K)≥Group IIA (Mg) and IIB (Zn)>Group IIIA (Al). Similarly, for nitrates in Fig. 2(c), Group IA (Na)> Group IIA (Ca). Additionally, Figure 2 suggests that 1:1 and 2:1 salts (cation:anion ratio) having a common anion with cations from the same Periodic Group tend to exhibit similar ϕ-fractions. Thus, ϕ-fractions of salts for which there are no data may be estimated from similar salts in Fig. 2 and inserted in Eq.13.

Table 2. Values of κ, y and η for dissociated (ionized) solutes, Eq. 12, at 298 K and 1atm P_{O_2}.

Solute I	κ	y	η	Solute I	κ	y	η
HCl	0.305514	1.092174	0.232093	$NiSO_4$	2.23207	1.115617	0.222794
H_2SO_4	2.01628	1.253475	0.168954	$CuSO_4$	2.23207	1.115617	0.222794
NaOH	0.102078	1.00044	4.308933	$MgCl_2$	0.179714	0.984502	2.71142
KOH	0.102078	1.00044	4.308933	$CaCl_2$	0.179714	0.984502	2.71142
NaBr	0.034541	0.925947	7.095218	$BaCl_2$	0.179714	0.984502	2.71142
KBr	0.034541	0.925947	7.095218	$AlCl_3$	0.38142	0.804022	1.683714
NaCl	0.075502	1.009502	4.223927	$Al_2(SO_4)_3$	0.641163	0.954719	3.033594
KCl	0.407374	1.116089	0.842095	$NaNO_3$	0.314	1.084	0.883
Na_2SO_4	0.629498	0.911841	1.440175	$Ca(NO_3)_2$	0.020554	0.946932	21.04
K_2SO_4	0.55	0.911841	1.440175	Na_2CO_3	0.34	1.1	3.13
$MgSO_4$	0.119674	1.107738	5.455537	Na_2SO_3	0.332	1.03	2.67
$ZnSO_4$	0.232671	1.010428	2.655655	NH_4Cl	0.57	1.2	0.278
$CoSO_4$	2.23207	1.115617	0.222794	$(NH_4)_2SO_4$	0.69	1.11	0.749

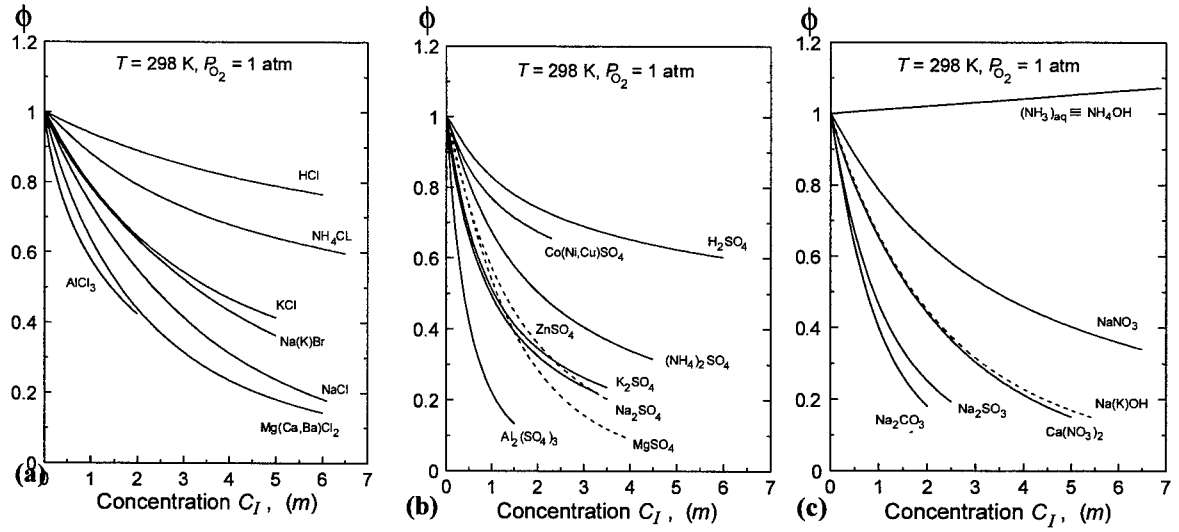


Figure 2. Effect of concentration of inorganic solute C_I on the ϕ-fraction (m is mol/kg H_2O).

The ϕ-function of Eq. 12 becomes a very useful modeling parameter if it is assumed to be independent of T; at least as far as first approximation treatments are concerned. In this event, values of κ, y and η obtained under a known set of conditions, such as 298 K and 1 atm P_{O_2} in Table 2, may be used under all other conditions in Eq.13. An examination of this assumption, using limited data relating to the effects of I at different T in H_2SO_4, KOH, NaOH, NaCl and $CuSO_4$ solutions, suggests it is reasonably justified [3]. An example is shown for $CuSO_4$ solutions [3] in Fig. 3 where predicted behaviors from Eq. 13 and Table 2 compare favorably with experimental data obtained from the studies of Bruhn *et al.* [17]. Hence, Eq. 13 becomes the unifying model equation for describing oxygen solubility behavior in the presence of a single I, where k is the only T-dependent parameter.

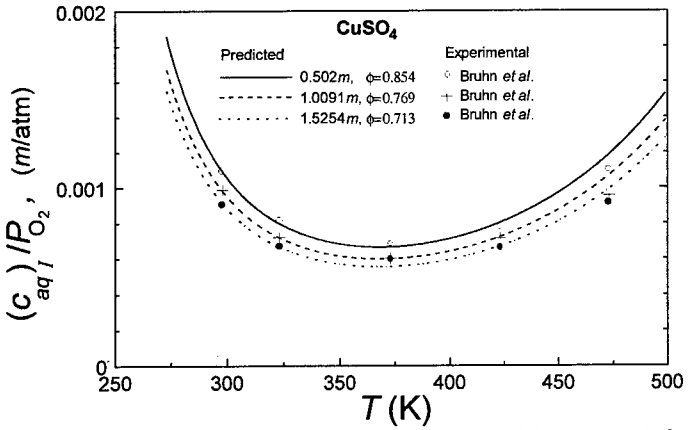


Fig. 3. Measured (experimental) and predicted oxygen solubility (Eq. 13) for single I, $CuSO_4$

MULTIPLE INORGANIC SOLUTES (DISSOCIATED)

Multiple I is the more common situation for industrial oxygenated solutions. In the presence of z different solutes I_1, I_2,.....I_z, with ϕ-factors ϕ_1, ϕ_2,..... ϕ_z, arranged so that $\phi_1<\phi_2<.....\phi_z$, the overall effective value ϕ_{eff} will be dominated by ϕ_1. The remaining factors will then exert a multiplying effect on ϕ_1 to produce a ϕ_{eff}. Under these circumstances, ϕ_{eff} may be reasonably represented by a function such as Eq.14 [3],

$$\phi_{eff} = \phi_1 \left(\prod_{2}^{z} \phi_i \right)^q \qquad 14.$$

where $\prod_{2}^{z} \phi_i$ represents the product $\phi_2 \times \phi_3 \times .....\phi_z$ and q is an empirical exponent, $1>q>0$, that has been shown to have a value close to 0.8 [3].

After substituting ϕ_{eff} for ϕ in Eq. 11, and $q = 0.8$, the solubility model for multiple I becomes

$$(c_{aq})_I = P_{O_2} k \phi_{eff} = P_{O_2} k \phi_1 \left(\prod_{2}^{z} \phi_i \right)^{0.8} \qquad 15.$$

where k is given by Eq. 8.

The predictions of Eq.15 compare satisfactorily with oxygen solubility measured by Cramer [18] in a brine solution in Fig. 3(a) and with measurements by Hayduk [9] in two $H_2SO_4/ZnSO_4$ solutions characteristic of Zn pressure leaching in Fig 3(b). Cramer's [18] measurements in pure water are included in Fig.3(a) and compare very favorably with with predicted values (Eq. 10). Cramer's data are a good test of the model because P_{O_2} ranged between 42.4 and 51.3 atm.

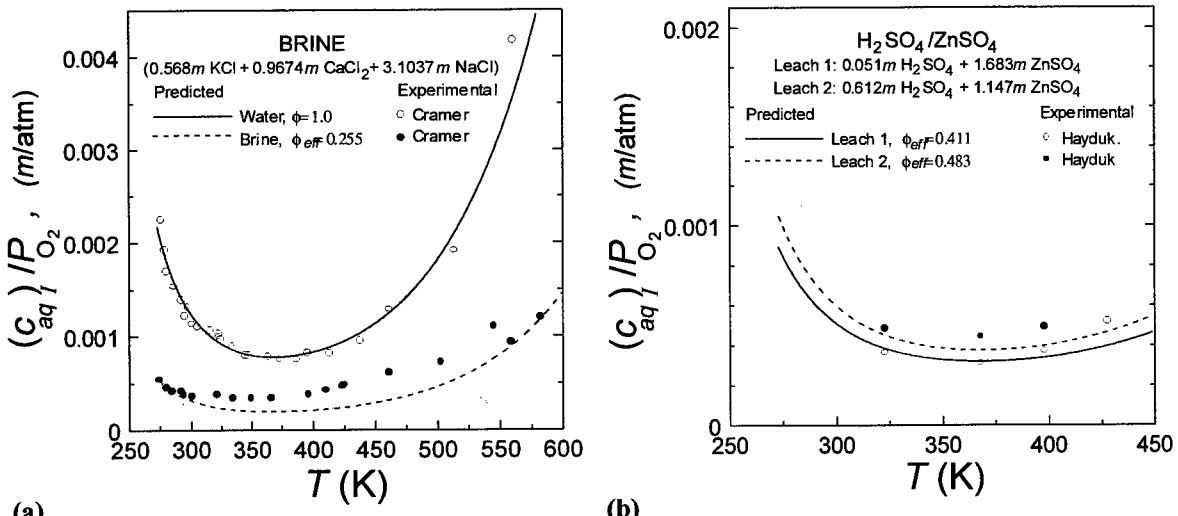


Figure 3. Measured (experimental) and predicted oxygen solubility (Equation 15) for multiple I.

UNDISSOCIATED INORGANIC SOLUTES (MIXED SOLVENT EFFECT)

Ammoniacal sulfate solutions are used for oxygen pressure leaching of Ni-based sulfide ores [19]. They contain undissociated "free ammonia" $(NH_3)_{aq}$. Ammonia has a dipole moment and is a polar solvent in the liquid state, analogous to water [16,20]. Thus $(NH_3)_{aq}$ and H_2O molecules are expected to behave similarly and produce a mixed oxygen solvent effect. Hence oxygen solubility in simple aqueous ammonia solutions ("NH_4OH"), where the dissolved species is almost entirely "free ammonia" $(NH_3)_{aq}$ and not the NH_4^+ ion [16], should increase with ammonia concentration. Analysis [16] of oxygen data for "NH_4OH" solutions [17,21] between 298 and 423 K showed that ϕ increased linearly with the molal concentration of $(NH_3)_{aq}$ at constant oxygen pressure, as indicated in Figure 2(c),

$$\phi_{NH_3} = 1 + C_{NH_3}(0.0105) \qquad 16.$$

Thus, in a solution containing z dissociated I solutes and "free ammonia" $(NH_3)_{aq}$, the overall final value of the ϕ-factor ϕ_f is best represented by $\phi_f = \phi_{NH_3} \times \phi_{eff}$, where ϕ_{eff} is calculated from the z solutes (Eq. 14).

Hence, from Eq. 15, oxygen solubility $(c_{aq})_{I+NH_3}$ in the presence of $(NH_3)_{aq}$ and dissociated I becomes,

$$(c_{aq})_{I+NH_3} = P_{O_2} k\phi_f = P_{O_2} k\phi_{NH_3}\phi_{eff} = P_{O_2} k\phi_{NH_3}\phi_I\left(\prod_2^z \phi_i\right)^{0.8} \qquad 17$$

Using a representative leaching solution containing 0.876 m $NiSO_4$, 0.108 m $CuSO_4$, 0.108 m $CuSO_4$, 1.752 m $(NH_4)_2SO_4$ and 3.84 m $(NH_3)_{aq}$ [18], together with Eqs. 14 and 16, and Table 2, it is seen that ϕ_f is 0.447 (*i.e.* 1.04 x 0.43), which may then be inserted in Eq. 17 to obtain the estimated oxygen solubility.

CONCLUSION

A unified model has been developed to estimate oxygen solubility in simple and relatively complex industrial solutions where the oxidizing characteristics of dissolved oxygen are important.

REFERENCES

1. Oxygen and Ozone, 1981, R. Battino (Ed.),IUPAC Solubility Data Series, **7**, Pergamon, Elmsford, NY.
2. D. Tromans, 1998, Hydrometallurgy, **48**, 327-342.
3. D. Tromans, 1998, Hydrometallurgy, **50**, 279-296.
4. International Critical Tables of Numerical Data, Physics , Chemistry and Technology, 1928, E.W. Washburn (Ed.), Vol. III, National Research Council, McGraw Hill, New York, 45-171.
5. J.P. Hoare, in Standard Potentials in Aqueous Solutions, 1985, A.J. Bard, R. Parsons and J. Jordan (Eds.), IUPAC, Marcel Dekker, New York, 49-66.
6. H.M. Spencer, 1945, J. Am. Chem. Soc., **67**, 1859-1860.
7. W. Wagner and K.M. de Reuck, Oxygen, IUPAC International Thermodynamic Tables of the Fluid State-9, 1987, Blackwell, Oxford, UK, 84-85.
8. S. Glasstone, K. Laidler and H. Eyring, 1941 Theory of Rate Processes, McGraw-Hill, New York, 504-505, 516-525.
9. W. Hayduk, 1991, Final Report Concerning the Solubility of Oxygen in Sulfuric Acid-Zinc Pressure Leaching Solutions, DDS Contract #UP 23440-8-9073/01-SS, Dept. Chem. Eng., Univ. of Ottawa, ON.
10. H.A. Pray, C.E. Schweickwert and B.H. Minnich, 1952, Ind. Eng. Chem., **44**, 1146-1151.
11. A Broden and R. Simonson, 1978, Sven. Papperstidning, **81**, 541-544.
12. E.I. Stephan, N.S. Hatfield, R.S. Peoples and H.A. Pray, 1956, Rep. BMI 1067, Battelle Memorial Inst.
13. R. Battino, 1981, in Oxygen and Ozone, R. Battino (Ed.), IUPAC Solubility Data Series, Vol.7, Pergamon, Elmsford, NY, 1-5.
14. B.B. Benson, D. Krause and M.A. Peterson, 1970, J. Soln. Chem., **8**, 655-690.
15. D. Tromans, 1998, submitted to Tappi J.
16. D. Tromans, 1999, submitted to Hydrometallurgy.
17. G. Bruhn, J. Gerlach and F. Pawlek, 1965, Z. Anorg. Allgem. Chem., **337**, 68-79.
18. S.D. Cramer, 1980, Ind. Eng. Chem., Process Design Dev., **19**, 300-305.
19. F.A. Forward and V.N. Mackiw, 1955, J. of Metals, **7**, No. 3, 457-463.
20. D. Nicholls, 1979, Inorganic Chemistry in Liquid Ammonia, Elsevier Scientific, Amsterdam, 1-28.
21. E. Narita, F. Lawson and K.N. Han, 1983, Hydrometallurgy, **10**, 21-37.

On the Oxidation of Steel in CO_2 and Air

Gity Samadi Hosseinali and Ainul Akhtar

Powertech Labs Inc.
12388 – 88th Avenue, Surrey,
British Columbia, Canada V3W 7R7

ABSTRACT

Oxidation of a low alloy 0.3% carbon steel (SAE 4130) was investigated using Scanning Electron Microscopy (SEM), X-ray diffraction and optical metallography. Closed cylindrical specimens were treated at 860°C for up to 2h in air and carbon dioxide, under pressure in the range of 0.1- 0.7 MPa. At the initial stage, wüstite grew through the coalescence of small clusters of crystallites. The size of wüstite grains was dependent on the kind of gas and independent of the gas pressure. The time dependence of wüstite grain growth has been studied. It was found that during the initial stage of oxidation wüstite grains grow epitaxially and by grain coalescence. Isothermal transformation of wüstite into magnetite (Fe_3O_4) was studied in the temperature range of 550°C-610°C. The results suggest that it may be possible to have the desired proportion of wüstite and magnetite, which can be controlled by the processing environment.

INTRODUCTION

It is well known that when a steel is heated in flowing air, it oxidizes and forms a scale composed of three kinds of iron oxide, FeO (wüstite), Fe_3O_4 (magnetite) and Fe_2O_3 (hematite). They are formed one above the other, wüstite remaining adjacent to the metal and hematite furthest away from it. The first oxidation stage consists of wüstite crystal growth at 860°C on the substrate. If cooled rapidly to room temperature, wüstite does not decompose to magnetite. Wüstite is converted into magnetite through a subsequent heat-treatment below 570°C. It is generally believed that the wüstite to magnetite transition takes place below 570°C.

The iron oxide is probably formed through a process involving nucleation and growth. Nucleation entails collision of gas molecules and their equilibration on the substrate. A nucleus may grow by either surface diffusion or through direct collision. In the former case, two or more neighboring nuclei coalesce, so the nucleus grows by surface diffusion. The aim of this investigation was to examine the role of different atmospheres on the growth mechanism and morphology of the oxide. Results on the growth of magnetite and other higher oxides will be presented elsewhere.

EXPERIMENTAL

Hollow cylinders of AISI 4130 steel were used in the oxidation experiments. The dimensions of the cylinder were as follows:

Outer diameter: 51mm
Inner diameter: 40mm
Length: 102mm

The inside of each cylinder was grit blasted (alumina) to remove existing scale on the surface. End caps were welded. The cylinders were sealed off at room temperature (a shut off valve was used) and then heated. The furnace temperature was brought to 860°C before inserting the cylinders inside the furnace tube. After steady state was achieved, the cylinder was inserted inside the furnace tube. The specimen attained a temperature of 860°C in approximately 10 minutes.

The austenitizing treatment was carried out for different times. Upon completion of the austenitizing treatment, the specimen was quenched in a water bath. Thereafter, the cylinder was depressurized and cut into small pieces for the characterization of the coating by using SEM (Scanning Electron Microscopy), X-ray diffraction (XRD) and eddy current testing. Cobalt K_α radiation was used for the x-ray diffraction. The oxide coating thickness was measured using a transverse section of the cylinder. The specimen was

0-7803-5489-3/99/$10.00 ©1999 IEEE.

mounted and polished using metallographic preparation techniques. Etching was carried out in 5% Nital before making the scale thickness measurement. Figure 1 shows the experimental setup.

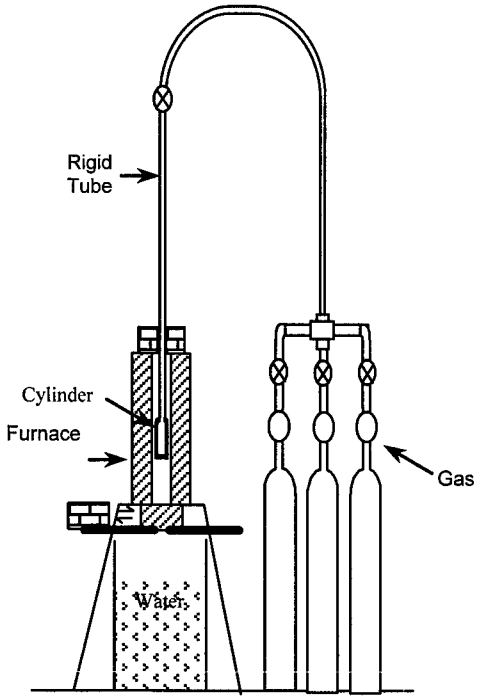


Fig. 1: The experimental setup.

RESULTS

A large number of cylinders were heat-treated with different pressures of air and CO_2. Table 1 shows a summary of samples oxidized in air. Specimens treated with CO_2 are listed in Table 2.

Table 1: Summary of treatment tests carried out in air.
The specimens were treated at 860°C for 1h unless stated otherwise.

Cylinder identification	Air pressure kPa (psig)	X-ray analysis
5A	207 (30)	Only FeO
8A	276 (40) 1 h at 880°C	Only FeO
10A	414 (60)	Only FeO
14A	621 (90)	Only FeO
18A	621 (90) 2 hrs at 860°C	Only FeO

Table2: Summary of treatment tests carried out in carbon dioxide.
The specimens were treated at 860°C for one hour unless stated otherwise.

Cylinder identification	CO_2 pressure kPa (psig)	X-rays analysis
1D	207 (30)	FeO
2D	310 (45)	FeO
7D	552 (80)	FeO
9D	552 (80) 2 h at 860°C	FeO
10D	345 (50) 2 h at 860°C	FeO
12D	345 (50) 30 minutes at 860°C	FeO
13D	345 (50) 15 minutes at 860°C	FeO
14D	345 (50) 5 minutes at 860°C	-
15D	345 (50) 10 minutes at 860°C	FeO
17D	Atmospheric pressure	FeO
19D	345 (50)	FeO

Examination of the as quenched specimens

Features of the specimens oxidized in air are presented first followed by those obtained in carbon dioxide.

The X-ray diffraction patterns obtained from the interior surface of air oxidized cylinders showed only FeO and Fe peaks. This observation suggests that the FeO, which formed at 860°C, does not transform into other oxides of iron upon quenching. The intensity of the FeO (200) reflection was found to be dependent on the time of oxidation and the air pressure. Metallugraphic measurements gave scale thickness values in the range of 15-35μm. SEM examination of the interior surface of any given cylinder showed that the surface grain size did not vary significantly from one region to another. The grains on the surface of the oxide scale were 1-5μm in size and had an equiaxed structure.

Specimens treated with CO_2 also produced reflections in their diffraction patterns which were characteristic of only Fe and FeO. The intensities of FeO peaks were generally higher with CO_2 than with air. Metallugraphic measurements revealed that the coatings with CO_2 were thicker than those obtained with air. The coating thickness ranged between 6μm to 50μm depending on the time of oxidation and the pressure of CO_2. The wüstite grains were at least twice as large with CO_2 than with air.

It may be noted from table 2 that 6 cylinders (10D through 15D and 19D) were treated under a constant pressure of 345 kPa (50 psig). However, the exposure time at 860°C was varied between 5 minutes and 120 minutes. Of these, the specimen exposed at 860°C for 5 minutes (14D) did not have a detectable oxide scale as revealed through x-ray diffraction and SEM examination of the interior surface. Metallographic polishing of a transverse section of the cylinder followed by etching in a 5% Nital solution showed that the steel substrate had a ferrite-pearlite microstructure. This is typical for this steel, when heated to a temperature below (730°C) rather than to the desired oxidation temperature of 860°C. A martensitic structure was observed with the substrate of specimen 15D, which had been kept in the furnace for 10 minutes prior to being quenched. Figure 2 shows a SEM photograph of the interior surface of specimen 15D that was exposed to 860°C for 10 minutes. It may be noted from figure 2 that the grain size remains relatively uniform. Figure 3 shows the morphology of the scale for specimen 10D which had been exposed to a much longer period of 120 minutes at 860°C. This longer exposure under 345 kPa (50 psig) produced a non uniformity in the distribution of the oxide grains in any given region. Some grains were large while others were small, as seen in Figure 3.



Fig.2. Morphology of the oxide after 10 minutes heat treatment under 345 kPa CO_2.

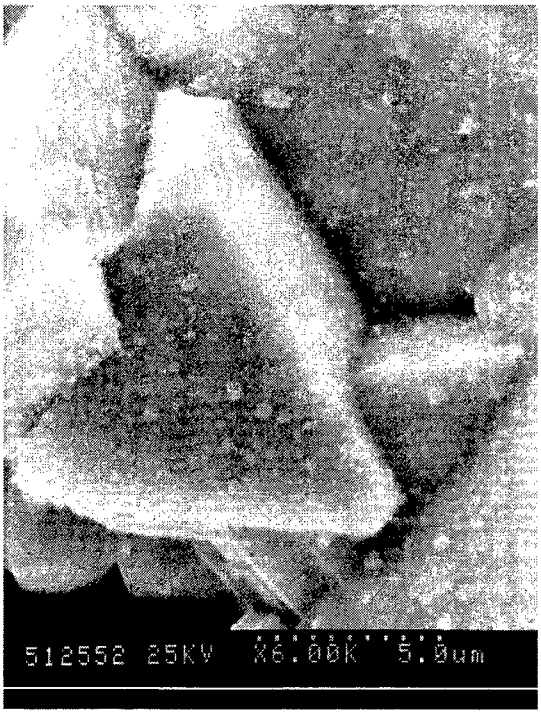


Fig.3. Morphology of the oxide after 2 hours heat treatment under 345 kPa CO_2.

Figure 4 shows the time dependence of scale thickness under a constant pressure of 345 kPa CO_2.

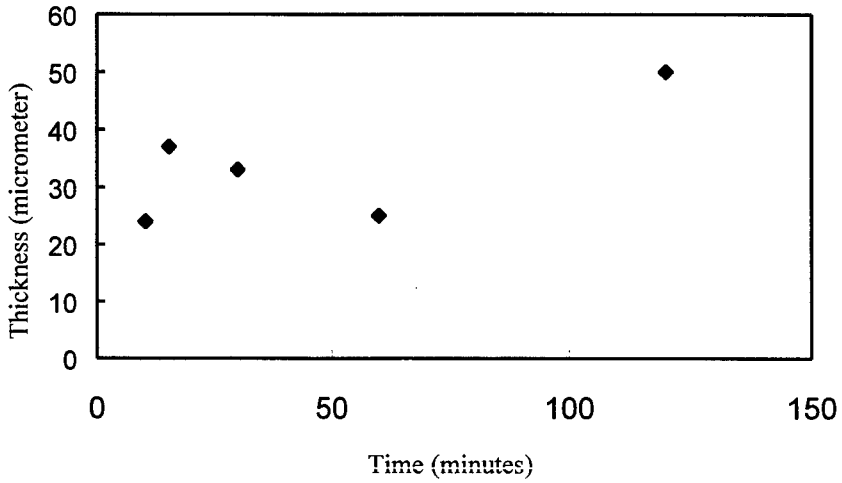


Fig.4: Time dependence of the scale thickness. The atmosphere was 345 kPa (50 psig) CO_2.

Treatment below 570°C

Some of the quenched specimens were tempered at different temperatures (550°C-610°C) and time spans. The X-ray diffraction has indicated that it is possible to obtain a wide range of microstructures of the oxide using appropriate combinations of time and temperature. Desired combinations of wüstite and magnetite may be introduced in this manner into an oxide scale. The kinetics of the transformation of wüstite into magnetite and hematite, as well as the associated microstructural features will be discussed elsewhere.

DISCUSSION

This study made it possible to understand the growth mechanism of wüstite and magnetite. The characteristics of the oxide grain growth are similar to those of subgrain coalescence during the recrystallization of cold worked metals [1, 2]. In the recrystallization process, the boundaries between neighboring subgrains gradually disappear. This process occurs by the gradual migration of dislocations from the disappearing subgrain boundaries into boundaries of neighboring subgrains. The boundary energy increases as the misorientation increases up to 10-20°, where grain boundary structure can no longer be explained simply by an array of lattice dislocations [3].

Energetically, the decrease in grain boundary energy through coalescence of many grains with small misorientations can act as a driving force for elimination of subgrain boundaries. Grain coalescence is more active during the early stages of oxide grain growth, i.e., from oxide grain nucleation through coalescence to the large grains in sizes up to 10μm. Due to the large boundary area available during the early stages of oxidation, the driving force for grain growth is highest with respect to the later stages of growth.

When the oxide scale becomes thicker, grain coalescence does not occur because of the lack of the low angle boundaries, which in turn gives rise to low mobility of dislocations. Consequently, nucleation of a new grain takes place at an area near a grain boundary [4].

Although the simple mechanism of nucleation and growth presented here accounts for some of the observed features, the process of wüstite growth is complex. For instance, the study has also shown that wüstite penetrates well into the austenite grain boundaries. This and other features of the oxide scale growth will be discussed elsewhere.

Another feature, which has been observed in this work, is the difference in the size of wüstite grains grown under different atmospheres. The size of the wüstite grains was found to be larger in CO_2 than in the air atmosphere. This could be due to the slower oxidation occurring under CO_2. Due to the rapid reaction in the air atmosphere, the grains of FeO, which nucleated within a single austenite grain, may contain a high density of lattice defects. Such lattice defects could impede the subsequent coalescence of these FeO grains into larger ones through the process of gradual migration of dislocations discussed above.

The early SEM observation of the tempered specimens showed that magnetite starts to grow on the boundaries of wüstite grains. Tempering for longer times results in the conversion of the wüstite grains into magnetite.

CONCLUSION

In the initial stages of oxidation at 860°C in with either air or CO_2, it appears that discrete wüstite nuclei develop epitaxially on the substrate grains. Once the oxide nuclei grow laterally and impinge, then grain coalescence takes place. Grain coalescence is believed to be the major mode of grain growth. The size of wüstite grains remains smaller in the air atmosphere than in CO_2. This could be due to the rapid oxidation reaction that takes place in air.

Magnetite forms on top of wüstite upon low temperature tempering. The quantity of magnetite can be controlled by varying the temperature and the exposure time.

REFERENCES

1. H.Hu, 1962. Trans. Met. Soc. AIMC, 224, 75-84.
2. J.C.M. Li, 1962. Journal of Applied Physics, 33, 2958-2965.
3. R. Bresdesen, P. Kopfstad, 1990, On the oxidation of iron in CO_2+CO gas mixtures: 1. Scale morphology and reaction kinetics. Oxidation of Metals, 34 (5/6), 361-379.
4. M. Lee, R.A. Rapp, 1987, Coalescence of wüstite grains during iron oxidation in a hot-stage environmental SEM. Oxidation of Metals, 27(3/4), 187-197.

Retardation Effects of Electrolytic ZrO_2 Coating on Hydrogen Embrittlement of AISI 430 Stainless Steel

I. B. Huang and S. K. Yen

Institute of Materials Engineering, National Chung Hsing University,
Taichung, 40227, Taiwan

ABSTRACT

Through Devanthan hydrogen permeation tests and a mathematical analysis, the retarding effect of electrolytic deposition ZrO_2 oxide films on the hydrogen embrittlement or entry has been investigated. The permeation test has indicated that the diffusion coefficient without oxide film D_m($1.46X10^{-8}cm^2/s$) has been reduced to $D_{Zr}(8.81\times10^{-16}cm^2/s)$ with ZrO_2 oxide film and the surface hydrogen concentration C_h^m (2.06×10^{-5} mol/cm^3) has been reduced to C_h^m (0.76×10^{-6} mol/cm^3) by the oxide film and a high concentration ratio constant K (3.5×10^3).

INTRODUCTION

Measurements of the diffusion coefficients and permeation rates of hydrogen through a metal membrane have been widely investigated accounting for not only a sensitive electrochemical method developed by Devanathan[1] but also some mathematical solutions of the pertinent diffusion equation given by McBreen[2], Kiuchi and McLellan[3], and Yen and Shih[4]. On the other hand, a practical mathematical solution of the permeation rate of hydrogen in a metal with an oxide film on it has been found scarcely, since a time-dependent interface boundary condition of metal/oxide makes the mathematical analysis more complex. Although three decades ago Ash, Barrer and Palmer[5] developed a general treatment of time lag for diffusion in a multiple laminate ABCD... where each lamina is composed of different material, the concentration ratio constant K in Henry's law of two adjacent materials is hard to measure independently and makes this method more difficult.

Recently, many results have shown that the metal oxide films have effectively retarded the hydrogen embrittlement of metals, such as sputtered layers of TiO_2 onto 15-5 PH stainless steel [7], sputtered layers of Al_2O_3 or SiO_2 onto 17-4 PH stainless steel [8], and thermally grown oxide film on sea-cure stainless steel[9]. The mechanism on the effects of oxide films on hydrogen entry and/or HE (hydrogen embrittlement) has not been really identified. Swansier and Bastaz[10] indicated that a low hydrogen surface adsorption coefficient plays a leading role in preventing hydrogen entry, while Caskey[11], Piaggott and Siarkowski[12-14] showed very low diffusivities (10^{-12} to 10^{-17} cm^2/s) of hydrogen through oxides. Probably, both factors contribute to the ability of oxide films to retard the hydrogen entry or embrittlement but no confirmed and direct evidence has shown which factor is dominant, up to this time. Although some efforts have been made to model the effect of an oxide film on a metal on hydrogen permeation by Song. Pyun and Oriani[15], they conducted a very low ratio of hydrogen concentration in metal to that in oxide (1.01×10^{-6}) and a very low diffusivity ($6.0\times10^{-19}cm^2$/sec). Probably, this is because the oxide film is too thin (~2nm) to be considered as diffusion controlled. In this study, the retardation of hydrogen embrittlement was also found by electrolytic ZrO_2 coating on AISI 430 stainless steel. The author tried to utilize permeation measurements developed by Devanathan[1], and a mathematical analysis by Yen[6] to find out whether a low hydrogen surface adsorption coefficient, a low diffusivity of the electrolytic ZrO_2 coating and/or a high concentration ratio constant, K of coating to metal, dominates the retardation effect on hydrogen embrittlement directly.

0-7803-5489-3/99/$10.00 ©1999 IEEE.

Nomenclature

t_1^m : the time lag in the metal without an oxide film

t_2^{Zr} : the time lag in the metal with an ZrO_2 film

L_m : the thickness of the metal

L_{Zr} : the thickness of the oxide film

D_m : the diffusivity of hydrogen in metal

D_{Zr} : the diffusivity of hydrogen in the ZrO_2 film

C_h^m : the subsurface concentration of hydrogen on the metal without an oxide film

C_h^{Zr} : the subsurface concentration of hydrogen on the ZrO_2 film

$C_h^{m'}$: the interface concentration of hydrogen in the metal at X=L_{Zr}

$C_h^{Zr'}$: the interface concentration of hydrogen in the oxide at X=L_{Zr}

J_∞^m : the hydrogen flux of the metal without an oxide film at steady state

J_∞^{Zr} : the hydrogen flux of the metal with an ZrO_2 film at steady state

K : the concentration ratio constant of $C_h^{Zr'}$ to $C_h^{m'}$

MATHEMATICAL ANALYSIS

Now consider a metal with a thin ZrO_2 film on its surface prepared for a hydrogen permeation test. Before conducting the mathematical analysis, two assumptions are required, i.e.,

1. The surface concentration of the out-diffusion side is always kept to zero.
2. D_{Zr} and K are constant and independent of the ZrO_2 film thickness.

According to the analysis of R.Ash, R.M.Barrer and D.G.Palmer[5] and S.K.Yen[6]:

$$t_1^m = \frac{L_m^2}{6D_m} \tag{1.}$$

and

$$t_1^{Zr} = \left(\frac{L_{Zr}}{D_{Zr}} + K\frac{L_m}{D_m}\right)^{-1}\left\{\frac{L_{Zr}^2}{D_{Zr}}\left(\frac{L_{Zr}}{6D_{Zr}} + \frac{KL_m}{2D_m}\right) + \frac{L_m^2}{D_m}\left(\frac{KL_m}{6D_m} + \frac{L_{Zr}}{2D_{Zr}}\right)\right\} \tag{2.}$$

After steady state, the hydrogen concentration should be linear both in the oxide film and in the metal membrane but possibly of different slopes, as shown in Fig.1.a. and Fig. 1.b.

Then the flux of hydrogen in metal is determined from:

$$J_\infty^m = D_m\frac{C_h^m}{L_m} \tag{3.}$$

On the other hand, the flux of hydrogen in metal with an oxide film can be explained by:

$$J_\infty^{Zr} = D_{Zr}\frac{C_h^{Zr} - C_h^{Zr'}}{L_{Zr}} = D_m\frac{C_h^{m'}}{L_m} \tag{4.}$$

By taking the ratio of Eq. 3. to Eq. 4., we derive:

$$\frac{J_\infty^{Zr}}{J_\infty^m} = \frac{C_h^{m'}}{C_h^m} \tag{5.}$$

There are still two unknown constants D_{Zr} and K in Eq. 2. which can't be determined by only one experiment. However, if two experiments with the same chemical component but different thickness of oxide films are measured, Eq. 2. becomes:

$$t_{l_1}^{Zr} = \left(L_{Zr1} + KD_{Zr} \frac{L_{m1}}{D_{m1}} \right)^{-1} \left\{ \frac{(L_{Zr1})^2}{D_{Zr}} \left(\frac{L_{Zr1}}{6} + \frac{D_{Zr} K L_{m1}}{2D_{m1}} \right) + \frac{(L_{m1})^2}{D_{m1}} \left(\frac{D_{Zr} K L_{m1}}{6D_{m1}} + \frac{L_{Zr1}}{2} \right) \right\} \quad 2.1.$$

$$t_{l_2}^{Zr} = \left(L_{Zr2} + KD_{Zr} \frac{L_{m2}}{D_{m2}} \right)^{-1} \left\{ \frac{(L_{Zr2})^2}{D_{Zr}} \left(\frac{L_{Zr2}}{6} + \frac{D_{Zr} K L_{m2}}{2D_{m2}} \right) + \frac{(L_{m2})^2}{D_{m2}} \left(\frac{D_{Zr} K L_{m2}}{6D_{m2}} + \frac{L_{Zr2}}{2} \right) \right\} \quad 2.2.$$

In other words, D_{Zr} and K are assumed to be independent of the thickness of L_{Zr}. Combining Eq. 2.1. and Eq. 2.2. derives the following:

$$D_{Zr}^{-1} = \frac{-b \pm \sqrt{b^2 - 4ac}}{2a} \quad 6.$$

where

$$a = \frac{1}{6} \left[\frac{(L_{Zr2})^3 (L_{Zr1})^2 L_{m1}}{2D_{m1}} - \frac{(L_{Zr1})^3 (L_{Zr2})^2 L_{m2}}{2D_{m2}} \right] \quad 6.a.$$

$$b = \left[t_{l_1}^{Zr} L_{Zr1} - \frac{L_{Zr1} (L_{m1})^2}{2D_{m1}} \right] \frac{(L_{Zr2})^2 L_{m2}}{2D_{m2}} - \left[\frac{(L_{m2})^3}{6(D_{m2})^2} - \frac{t_{l_2}^{Zr} L_{m2}}{D_{m2}} \right] \frac{(L_{Zr2})^3}{6} - \left[t_{l_1}^{Zr} L_{Zr2} - \frac{L_{Zr2} (L_{m2})^2}{2D_{m2}} \right] \frac{(L_{Zr1})^2 L_{m1}}{2D_{m1}} \quad 6.b.$$

$$+ \left[\frac{(L_{m1})^3}{6(D_{m1})^2} - \frac{t_{l_1}^{Zr} L_{m1}}{D_{m1}} \right] \frac{(L_{Zr1})^3}{6}$$

$$c = \left[t_{l_1}^{Zr} L_{Zr1} - \frac{L_{Zr1} (L_{m1})^2}{2D_{m1}} \right] \left[\frac{(L_{m2})^3}{6(D_{m2})^2} - \frac{t_{l_2}^{Zr} L_{m2}}{D_{m2}} \right] - \left[t_{l_2}^{Zr} L_{Zr2} - \frac{L_{Zr2} (L_{m2})^2}{2D_{m2}} \right] \left[\frac{(L_{m1})^3}{6(D_{m1})^2} - \frac{t_{l.}^{Zr} L_{m1}}{D_{m1}} \right] \quad 6.c.$$

t_{l_1} or t_{l_2} can be measured by permeation test, L_{m1}, and L_{m2} are known. D_{m1} and D_{m2} can be determined by Eq. 1. and L_{Zr1} or L_{Zr2} can be measured. Consequently, D_{Zr} can be calculated. Substitute the value of D_{Zr} into Eq. 2.1. or Eq. 2.2., K can also be determined.

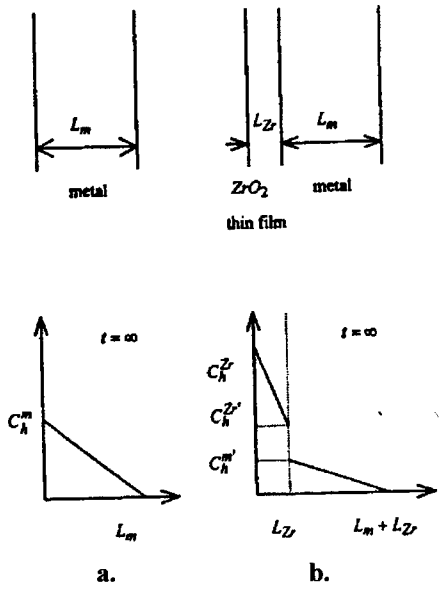


Fig.1. Hydrogen Concentration distribution after Steady State (a)Uncoated (b) Coated Specimens.

EXPERIMENTAL

Sample preparation

An AISI 430 stainless steel sheet, as received, was used as a substrate for the ZrO_2 electrolytic coating. Its nominal chemical component is listed in Table 1. The sheet thickness is 0.8 mm. The sheet was cut into $35\times35mm$. All specimens were polished to a mirror finish with 1μm and 0.05μm Al_2O_3 powder, then degreased by detergent, further ultrasonically cleaned in deionized water and acetone, then dried in air.

Table 1. The chemical component of the AISI 430 stainless steel sheet.

Element	C	Mn	Si	Cr	Ni	P	S	Fe
W_i%	0.045	0.342	0.693	17.82	0.18	0.031	0.015	Balance

Electrolytic deposition and annealing

The electrolytic deposition of ZrO_2 was conducted in a naturally-aerated solution of 0.03125 M $ZrO(NO_3)_2$, at pH=2.7 and a constant cathodic potential of 850mv for 250 and 500s , by using an EG&G M273A potentiostat and M 352 software. The specimen was the cathode, graphite the anode and saturated calomel was the reference electrode. The above electrolytic conditions gave the most efficient deposition in our experiments. The specimens with a $Zr(OH)_4$ gel coating were then naturally-dried in air and annealed in air at 703K for 120 min, respectively.

Hydrogen permeation test and OM observation

Details of the cell and ancillary apparatus used in the permeation measurements have been described in previous papers [16, 17]. The cathodic compartment contained about 1 liter of a solution of 0.2N CH_3COOH - 0.1N CH_3COONa_3-H_2O, a constant current of 500A/m^2 was applied to the cathodic surface of the coated specimen. The anodic compartment contained about 1 liter of a solution of 0.1N NaOH-H_2O. The surface of the specimen was maintained at a constant voltage of 50 mv (SCE) to make the hydrogen concentration on the surface zero. The solutions were de-aerated in both sets of tests by Ar. The cell was thermostatically-controlled at 303$\pm$ 1K. The uncoated specimen was also measured. The surface morphology of the coated specimen after the hydrogen permeation tests was observed by optical microscopy (OM).

RESULTS AND DISCUSSION

The permeation flux of the specimen with electrodeposition ZrO_2 coatings and without coating were recorded. By integrating the flux curve, the time lag can be found as $t_{l_1}^{m}$=73200 sec, $t_{l_1}^{Zr}$=124600 and $t_{l_2}^{Zr}$=130500 sec. From Eq. 1. to Eq. 5., J_∞, D_{tl}^{eff} and C_h^S can be calculated. The corresponding data are listed in Table 2.

Table 2. The data of t_l, I_∞, J_∞, D_{tl}^{eff} (effective diffusion coefficient) and C_h^S (surface hydrogen concentration)

Electrodeposition	t_l (sec)	I_∞ (μA)	J_∞ ($\times10^{-12} mol/cm^2.sec$)	D_{tl}^{eff} ($\times10^{-8} cm^2$)	C_h^s ($\times10^{-5} mol/cm^3$)
250 sec	124600	0.84	2.77	0.856	1.52
500 sec	130500	0.42	1.38	0.817	0.76
Uncoated	73200	1.14	3.76	1.46	2.06

The surface morphologies of specimens for coated and uncoated after hydrogen diffusion can be observed by optical microscope (OM). No blistering was found on the surface of the coated specimens but many blisters were observed on the surface of the uncoated specimen as shown in Figures 2a., 2b. and 2c.

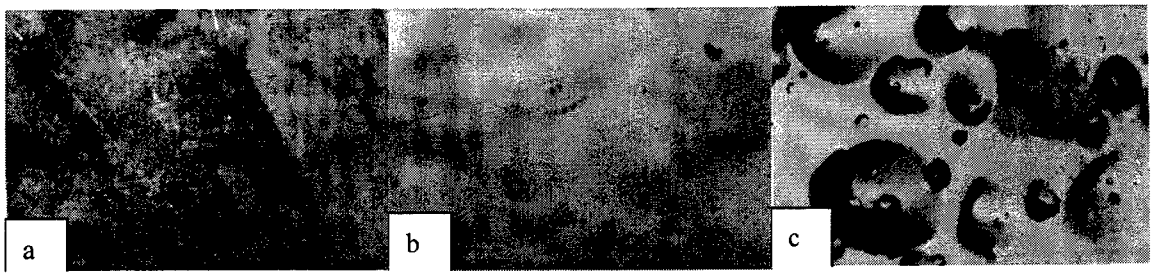


Fig. 2. OM of the specimen after hydrogen permeation
a. ZrO_2 coated for 250 sec. **b.** ZrO_2 coated for 500 sec. **c.** uncoated.

The thickness of the coated specimen, L_{Zr} can be measured by a surface profiler , L_m is already know as the specimen thickness. From Eq. 1. to Eq. 6., D_m, D_{Zr} and K can be calculated. The corresponding data are listed in Table 3.

Table 3. The data of $L_{Zr}, D_m, t_l^{Zr}, D_{Zr}$ and K for AISI 430 stainless steel sheet specimens

Electrodeposition Time	L_{Zr} (cm)	L_m (cm)	D_m (cm^2/sec)	t_l^{Zr} (sec)	D_{Zr} (cm^2/sec)	K
250 sec	6×10^{-6}	8×10^{-2}	1.46×10^{-8}	124600	8.81×10^{-16}	3.5×10^3
500 sec	1.1×10^{-5}	8×10^{-2}	1.46×10^{-8}	130500		

From Table 2, $C_h^{m'}$ (0.76×10^{-6} mol/cm^3) has been reduced to be much lower than that of C_h^m (2.06×10^{-5} mol/cm^3) and that of the critical concentration C_h^C (2.3×10^{-5} mol/cm^3) for brittle transgranular fracture type[17], with time lag calculation. Obviously, the retarding effect of electrolytic ZrO_2 coating on the hydrogen embrittlement of AISI 430 stainless steel is due to the reduction of $C_h^{m'}$ which is much lower than C_h^m and C_h^C. From Table 3.,it is clear that C_h^{Zr} is much larger than C_h^m while C_h^C is much lower than D_m Therefore, the retarding effect due to the low absorption coefficient of oxide film can effectively be excluded. For short duration exposure to hydrogen, the lower D_{Zr} will delay hydrogen diffusion. However, for long exposure times, a high concentration ratio constant K, which reduces $C_h^{m'}$ to a value much lower than the critical concentration C_h^C, is the main factor involved in the retarding effect.

SUMMARY AND CONCLUSIONS

Through Devanathan hydrogen permeation tests, and a mathematical analysis, C_h^m, D_m, $C_h^{m'}$, C_h^{Zr}, $C_h^{Zr'}$, D_{Zr} and K have been determined. This novel method also suggests a way to check whether the low diffusivity D_{Zr}, high concentration ratio constant K and/or the low surface concentration C_h^{Zr} of hydrogen on the ZrO_2 film are dominant in controling the retarding effect on hydrogen embrittlement and entry into the metal. In this study, two conclusions are drawn:

1. The surface morphology of the uncoated specimen after hydrogen diffusion indicates blistering behavior but the coated specimen does not. Obviously, the electrolytic deposition ZrO_2 film on AISI 430 stainless steel has shown a retarding effect on hydrogen entry and hydrogen embrittlement.
2. The retarding effect on hydrogen entry into an electrolytic ZrO_2 coating on AISI 430 stainless steel is mainly due to the high concentration ratio constant K (3.5×10^3) which makes $C_h^{m'}$ (0.76×10^{-6} mol/cm^3) much less than C_h^m (2.06×10^{-5} mol/cm^3) and because of a low diffusivity D_{Zr} (8.81×10^{-16} mol/cm^3), but not a very low C_h^{Zr} which is very high as 4.37×10^{-2} mol/cm^3.

ACKNOWLEDGMENT

The authors are grateful for the support of this research by the National Science Council, Republic of China, under Research Project No. 36358D.

REFERENCES

1. M. A. V. Devanathan and Z. Stachurski, 1962. Proc. R. Soc. , Edingburgh, Sect. A, 270, p.90.
2. J. McBreen, L. Nanis, and W. Beck, 1966. J. Electrochem. Soc. , 113, p.1218.
3. K. Kiuchi and R.B. McLellan, 1988. Acta Met. 31, p.961.
4. S. K. Yen and H. C. Shin, 1988. J. Electrochem. Soc., 135, p.1169.
5. R. Ash, R. M. Barrer and D. G. Palmer, 1965. Brit. J. Appl. Phys., 16, p.873.
6. S.K.Yen, 1999. Retarding Mechanism of Themally Grown Oxide Films on Hydrogen Embrittlement of AISI 430 Stainless Steel, Materials Chemistry and Physics, accepted.
7. J. G. Nelson and G. T. Murray, 1984. Metall. Trans. A, 15A, p.597.
8. G. T. Murray, J. P. Boufard, and D. Briggs, 1987. Metall. Trans. A, 18A, p.162.
9. S. K. Yen and H. C. Shih, 1962. Proceeding of the Annual Conference of the Chinese Society for Material Science, p.646.
10. W. A. Swansiger and R. Bastaz, 1979. J. of Nuclear Materials, 85, p.335.
11. G. R. Caskey, 1974. Material Science and Engineering, 14, p.109.
12. M. R. Piggott and A. C. Siarkowski, 1972. J. Iron and Steel Institute, 210, p.901.
13. M. R. Louthan. Jr. and R. G. Derrick, 1975. Corrosion Science, 15, p.565.
14. R. A. Strehblow and H. C. Savage, 1974. Nuclear Technology, 22, p.127.
15. R. H. Song, S. L. Pyun and R. A. Oriani, J. Electrochem. Soc., 137, p.1703.
16. S. K. Yen and H. C. Shin, 1990. J. Electrochem. Soc. 137, p.2028.
17. S. K. Yen and Y. C. Tsai, 1996. J. Electrochem. Soc. 143, p.2736.

The Effect of Ca Addition on Viscosity and Electrochemical Properties of Mg-alloys Produced by Casting

Hye-Sung Kim*, Shuji Hanada* , Ha-guk Jeong*, and, Dong-Wha Kum**

*Institute of Material Research, Tohoku university, Sendai, 980-8577, Japan
Tel: 81-022-215-2406 Fax: 81-022-215-2116 Email: Kim4385@imr.tohoku.ac.jp
**Division of Metals, Korea Institute of Science and Technology,
P.O. Box 131, Chungang, Seoul, Korea

ABSTRACT

The composition of different Mg alloys is known to affect their current capacity, potential, and anode efficiency. Many alloying elements have been used in attempts to improve the electrochemical properties of magnesium anodes. Significant improvements of electrochemical properties have been achieved by controlling the adverse effects of impurity elements such as Fe, Ni, Cu with alloying elements.

Out of many elements, Ca is considered as a very effective element that can improve the electrochemical properties of Mg-alloys because of its relatively low potential in comparison with specified elements such as Mn, Al, Zn in high Mn alloys or AZ63 alloys with the effect of grain refining. Ca has recently been used as a common inhibitor for the ignition of molten Mg alloys. However, the viscosity of pure Mg is markedly increased with increasing Ca content. Ca is responsible for making the casting of Mg alloys from Mg melt difficult at desirable pouring temperatures.

In the present study, the effect of Ca addition on the viscosity and electrochemical properties of Mg-Ca alloys is investigated. Viscosity as well as electrochemical data will be correlated with chemical composition of impurities, and the microstructural change before and after Ca is added.

0-7803-5489-3/99/$10.00 ©1999 IEEE.

Bio-Compatible Ceramics as Mimetic Material for Bone Tissue Substitution

Zdenek Strnad*, Jaroslav Šesták**

*Laboratory for Glass and Ceramics (LASAK), Papírenská 25,
CZ-16000 Prague 6, Czech Republic
**Division of Solid-State Physics,
Institute of Physics of the Czech Academy of Sciences,
Cukrovarnická 10, CZ-16253 Prague 6, Czech Republic

ABSTRACT

Bone-like apatite formation on the surface of implant is of key importance during the physical and chemical processes leading to the formation of bonds between the implanted material and the newly formed bone tissue. The smartness of such a mimetic process is likely the action of silanole groups (Si-OH) which serve as the nucleation sites for the biocompatible interface formation capable to coexist between the original tissue and the implants which can be made from ceramics, glass-ceramics, composites as well as certain metals (titanium) respecting the condition of suitable surface reactivity. Lasak Co.Ltd., is the leading manufacturer of these materials in the Czech Republic and provides various kinds of bioactive implants, based on calcium phosphate ceramics, apatite wollastonite glass-ceramics and implants with hydroxyapatite surface coatings, permitting differentiated applications in clinical practice. The bioactive materials used as bone substitutes are all the subject of continuing research to attain biological, mechanical and chemical properties as similar as possible to those of the tissue to be replaced – mimetic materials. Clinical applications in orthopaedics, neurosurgery, maxillofacial surgery, auricular surgery, dental surgery and in other fields are demonstrated.

Keywords: biaoctive implants, bone substitutes, glass-ceramics, hydroxyapatite

INTRODUCTION

Degeneration of the skeletal system in time results in dysfunction of bones, teeth and joints. Extensive bone defects left after the removal of tumours, infections or as a result of injuries are ideally replaced by autogenic bone tissue. As the amount of this material for the patient is limited and the use of allogenic bone is accompanied by biological, mechanical and also sociological difficulties, there is a great need for alternate material.

Since discovery of Bioglass in 1971 (1), various kinds of bioactive materials have been found and clinically used. The uniqueness of surface bioactive materials is their high bioactivity, opening qualitatively new application fields, especially for anchoring of the implant in the host tissue, with practical use in orthopedics, stomatology, neurosurgery, oncology, craniofacial surgery and possibly other fields.

LASAK developed and provides three basic kinds of bioactive materials, BAS-O, BAS-HA and BAS-R, permitting differentiated applications in clinical practice. More than 7000 people received these implants as their bone substitutes during last eight years.

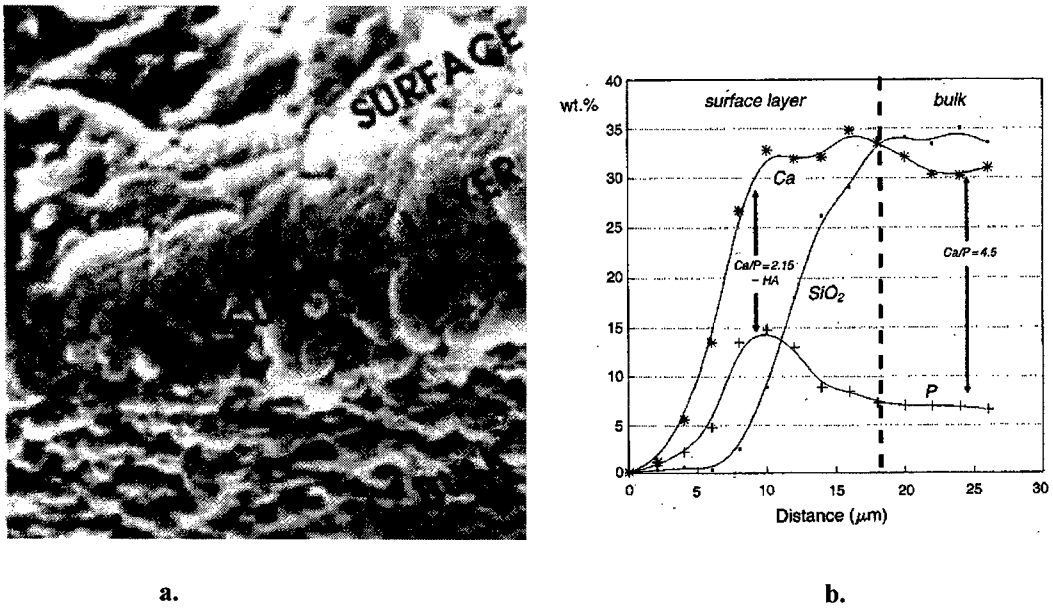
BAS-O GLASS-CERAMICS - BIOACTIVE LONG-TERM STABLE IMPLANT MATERIAL WITH HIGH MECHANICAL STRENGTH

BAS-O is an inorganic, polycrystalline material prepared by controlled crystallization of glass, whose main components are CaO, P205, Si02 MgO, and Al2O3 During the crystallization process, the amorphous material is converted to a glass-ceramic material whose main crystalline phases are apatite and wollastonite (2,3). Controlled crystallization permits not only controlled phase conversion during the process, but also

0-7803-5489-3/99/$10.00 ©1999 IEEE.

control of the chemical composition and structure of the residual glass phase, which are decisive factors in determining the bioactivity of the final material (4).

BAS-O exhibits extraordinary biocompatibility, which has been demonstrated in many experiments and clinical tests. The basic condition for the formation of a bond between the BAS-O implant and the living bone tissue is the formation of a thin layer enriched in Ca and P on the glass-ceramic surface as a result of a reaction between the implant and body fluids (Fig,1).



a. b.

Fig. 1. Surface layer formed on a BAS-O implant after exposure in a simulated body fluid for 28 days.
a. Cross-section through the surface layer (SEM 1000x),
b. Content of elements (P, Ca and SiO2) in the surface layer.

This layer, which is initially amorphous, changes in time to form a polycrystalline layer of apatite agglomerates, into which are incorporated organic components in the interface zone, produced by osteoblasts, such as collagen fibers, with the formation of a tight bond (Fig. 2).

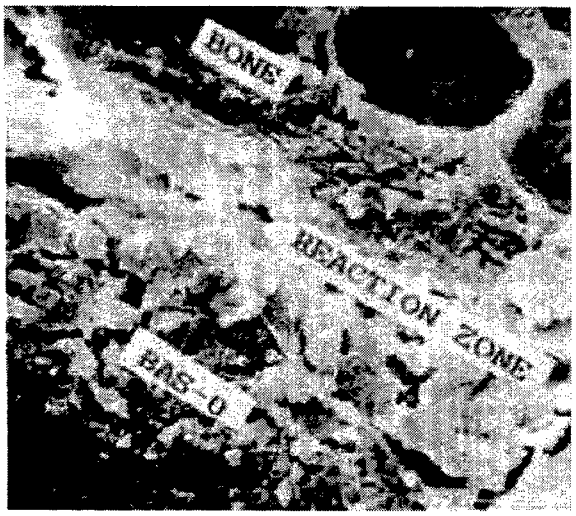


Fig.2: Detail of the interface of the bone tissue with a BAS-O implant 6 months after implantation (SEM).

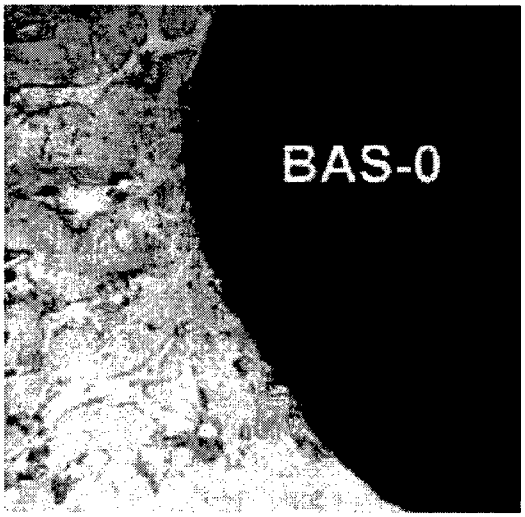


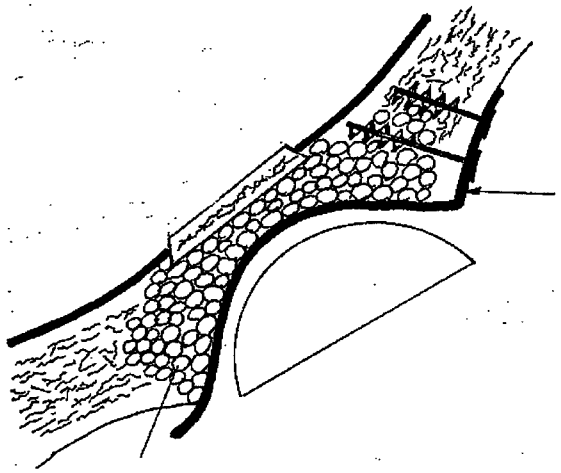
Fig.3: Photomicrograph of a section of BAS-0 granule implant in bone, 2 years after implantation (toluidine blue stain).

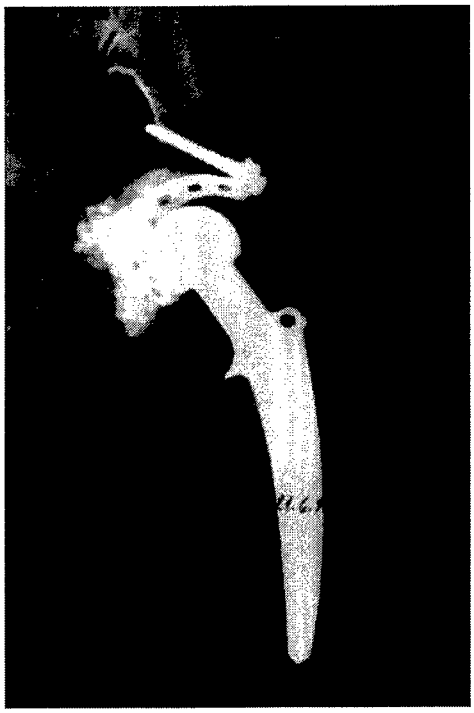
Thus, the implant is not considered to be a foreign body; on the contrary, a strong bond is formed directly between the implant and the bone tissue, without an intermediate layer of soft tissue, in a time period of 4-8 weeks after implantation (Fig. 3).

BAS-O exhibits intense osteoconductive properties and also the ability to form bonds between the individual BAS-O particles in a body fluid medium. BAS-O is a white material with an apparent density of 3000-3100 kg/m3. The material has a similar bending strength to the cortical bone, 170 MPA, and approximately double the compressive strength, > 400 MPa. The strength of the junction of the BAS-O implant with bone tissue, measured by the push-out test (with shear stress) after implantation for 2 months is 15-20 MPa.

Clinical application

BAS-0 granules and ground material are used to fill cysts, defects left by injuries, defects left by excochleation of benign tumors, and to reconstruct extensive acetabular defects (Fig. 4). Compact, wedge-shaped blocks (with various heights and surfaces) can be used, e.g., for condyl elevation. Individually shaped implants can be used in neurosurgery to cover defects left from cranial trepanation and as onlays in plastic surgery.

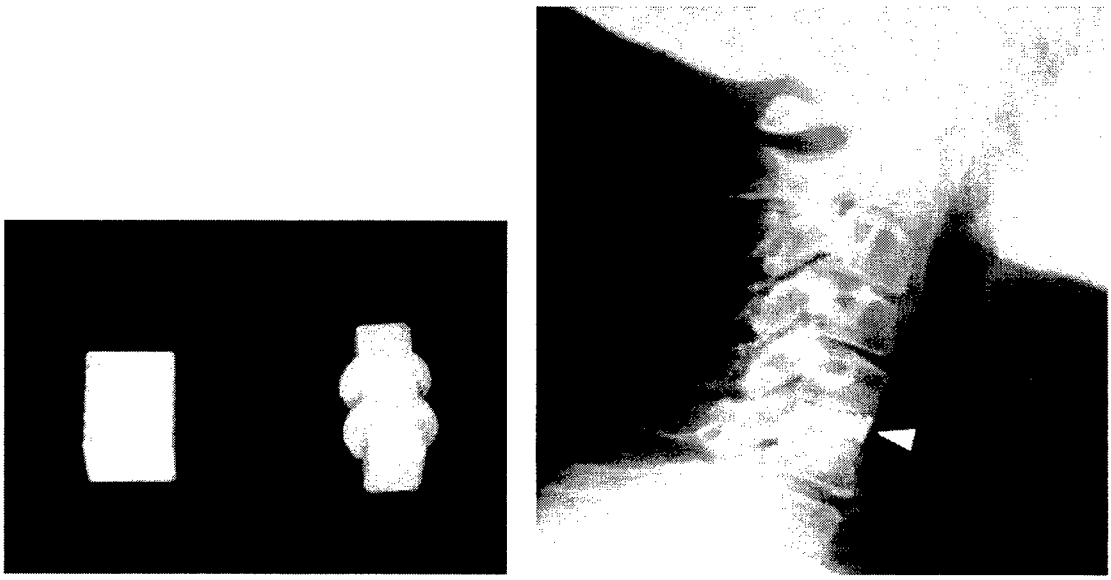




a. **b.**

Fig. 4: Reconstruction of extensive acetabular defects by bioactive glass-ceramics BAS-0 in reoperation of total endoprotheses. **a.** Schematic drawing of implantation. **b.** Radiogram taken 8 months post-operatively. [5]

The special shape of intervertebral prostheses have been developed and successfully used in surgery of spin (Fig. 5). In cranio-facial surgery, the material can be used as plates, blocks, or individually shaped implants to replace bone defects, rebuilding of orbit, for reconstruction of partial mandibular defects. It can be used to enlarge the mandible or for plastic chin and nose profiles.



a. b.

Fig.5: **a.** BAS-0 intervertebral prostheses. **b.** Radiogram taken post-operatively [6].

BAS-HA - BIOACTIVE NONRESORBABLE IMPLANT MATERIAL BASED ON HYDROXYAPATITE $CA_{10}(P0_4)_6(OH)_2$

Hydroxyapatite is synthesized from aqueous solutions under precisely defined pH, temperature and other physical parameters, which ensure reproducible preparation of a highly pure, crystallographically defined product, which does not contain any unwanted calcium phosphates. This product is further processed to yield the final BAS-HA product with defined biophysical properties., Its structure and composition are similar to bio-apatite, which is the main inorganic component of living bone tissue. Implants form a strong: bond between the bone tissue and the implant material without an intermediate fibrous layer (Fig. 6).

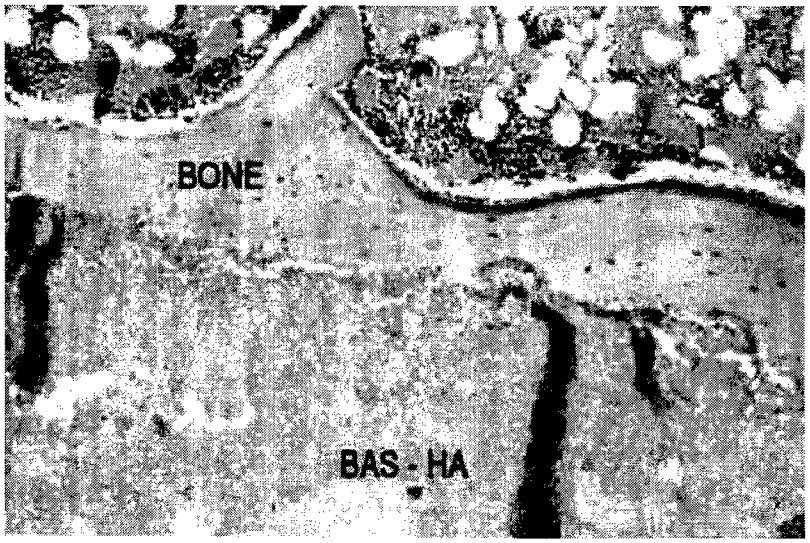


Fig.6: Direct contact between the BAS-HA implant and bone tissue, 2 months after implantation (thin-section, toluidine blue stain)

BAS-HA exhibits high biocompatibility, which has been demonstrated in many preclinical and clinical tests, including tests of cytotoxicity, carcinogenesis and mutagenic effects. The material exhibits osteoconductive properties. After implantation in the defective part of the bone, bone tissue is newly

formed in the space between the granules of this substance. A complex of artificial substances and living bone tissue is formed.

BAS-HA is a very dense ceramic with apparent porosity of 1.7 %. The Ca/P molar ratio is 1.66. The material exhibits a bending strength of 60 MPa and compression strength of 200 MPa. The strength of the junction with the bone tissue measured by the push-out test (shear stress) is equal to 19 MPa two months after implantation and 29 MPa 4 months after implantation.

Clinical application

BAS-HA material is designed for bone grafting especially at sites where only compressive forces are expected to act on the implant. It can be used in dentoalveolar surgery to fill bone defects left after extirpation of cysts, surgical extractions, or to remodel the alveolar ridge. In paradontology, it can be used to treat bone paradontological defects. Bioactive BAS-HA material is also used for production of middle ear implants (Fig. 7) and dental implants with hydroxyapatite coating (Fig. 8) [7, 8].

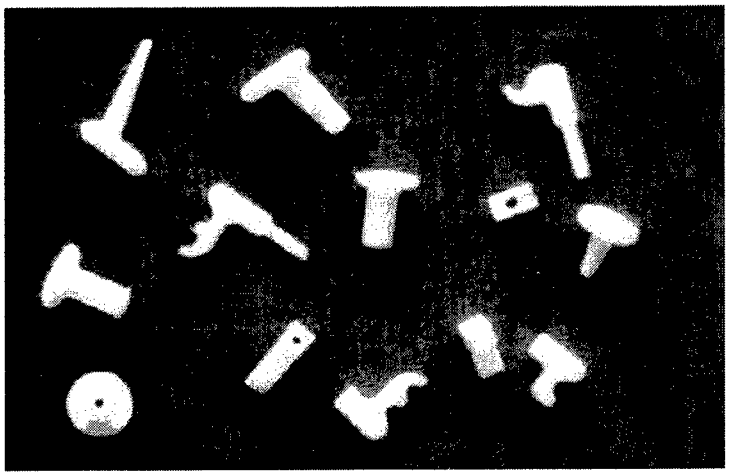


Fig.7: Middle ear implants made of BAS-HA.

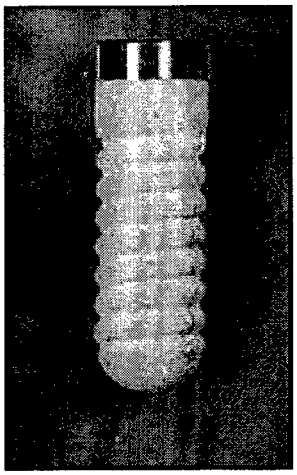


Fig.8: Dental implant (Impladent) with hydroxyapatite coating.

BAS-R - BIOACTIVE RESORBABLE IMPLANT MATERIAL BASED ON TRICALCIUM PHOSPHATE $CA_3(P0_4)_2$

BAS-R is a surface bioactive, resorbable, inorganic, crystalline material based on tricalcium phosphate (β-TCP) .The material is prepared by a special procedure at high temperature by melting and controlled cooling of the melt. BAS-R forms direct bonds with living bone tissue without forming a fibrous interlayer.



Fig. 9. Gradual resorption of granules (- - -) of BAS-R and simultaneous formation of new bone tissue at the edges of the granules; 8 months after implantation (thin-section, toluidine blue stain)

The material greatly stimulates formation of new bone tissue and has osteoconductive properties. The material gradually disintegrates in the body as .a consequence of hydrolytic corrosion and active phagocytosis, accompanied by resorption and replacement with newly formed bone tissue (Fig. 9) BAS-R is white in color and has an apparent density of 2900-3100 kg/m3

Clinical application

It is designed for bone replacement where resorption is required, with gradual replacement by living bone tissue. It is used in paradentology and in dentoalveolar surgery to treat bone defects [10] (see Fig.10).

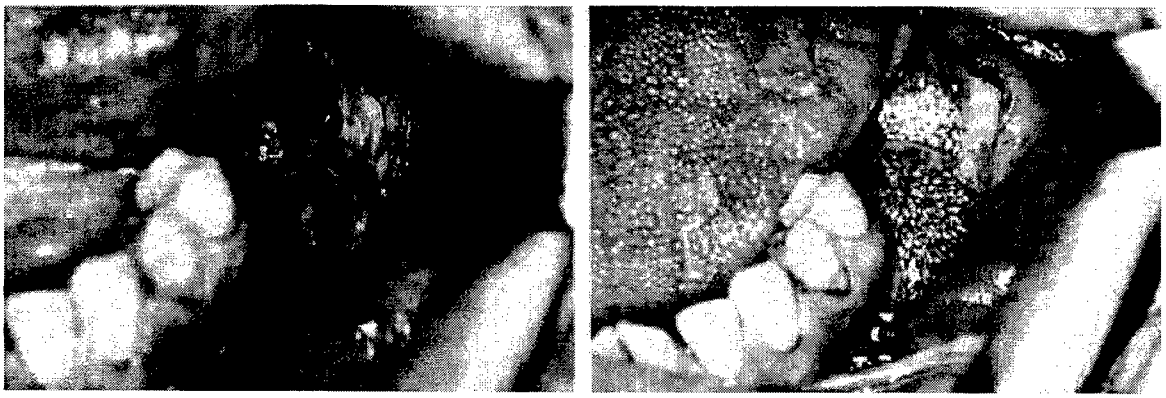


Fig.10: Filling of bone defects left by tooth extraction and extirpation of a radicular cyst a) prior to the operation b) after application of BAS-R

OUTLOOK

Today bioceramics are used in a broad field of devices inside the human body. This is mainly due to their good biocompatibility. Among the ceramic materials used for bone replacement, bioactive ceramics appear particularly promising because of their ability to form stable interface with living host tissue. The major problem of these materials, which inhibits their application on several types of implants, is their poor match of mechanical behavior of the implant with the tissue to be replaced. Principally, the coating, composites, porous structured materials and/or new resorbable materials are promising ways for the next development.

However, no one has succeeded todate, in finding a material, which fully corresponds to bone or other living parts of the body. It is the task of a growing number of researchers and institutions working in the field of biomaterials to further improve performance of these materials. Nature is still the better engineer.

REFERENCES

1. L.L.Hench, R.S.Splinter, W.S.Allen, 1971. Bonding mechanisms at the interface of ceramic prosthetic materials, J.Biomed,Res.Symp. 2, 117.
2. Z.Strnad, 1986. Glass-Ceramic Materials/Liquid Phase Separation, Nucleation and Crystallization in Glasses, Elsevier, Amsterdam.
3. Z.Strnad, K.Urban, 1989. Surface Bioactive Glass-Ceramic Materials, Sklár a keramik, 39, 292.
4. Z.Strnad, 1992. Role of the Glass Phase in Bioactive glass-ceramics, Biomaterials, 13(5), 317.
5. K.Urban, P.Šponer, 1998. Reconstruction of Extensive Acetabular Defects by Bioactive Glass Ceramics in Re-operations of Total Endoprostheses, Acta Chir.Orthop.Traum.Cech., 65, 17.
6. M.Filip, P.Veselský, Z.Strnad, P.Laník, 1995. The Replacement of the Intervertebral Disc by Ceramic Prosthesis in Treatment of Degenerative Diseases of the Spine, Acta Chir.Ortho.Traum. Cech., 62, 226.
7. A. Šimunek, A. Štepánek, V.Zábrodský, Z.Nathanský, Z.Strnad, 1997. A 3-year Multicenter Study on Osseointegrated Implants- Impladent, Quintessenz 6(3).
8. Z.Strnad, J. Strnad, M.Psotová, C.Povýšl, K. Urban, 1998. The Osseoconductive Ability of Plasmatically Deposited Hydroxyapatite and Pure Ti in Vitro and in Vivo, Quintessenz, 7, 5.
9. K.Urban, Z.Strnad, C.Povýšl, P.Šponer, 1996. Tricalcium phosphate as a bone tissue substitute, Acta Chir.Orthop.Traum.Cech, 63, 16.
10. V.Pávek, Z.Novák, Z.Strnad, D.Kudrnová, 1994. Clinical Applications of Bioactive Glass-ceramics BAS-O for Filling Cyst Cavities in Stomatology, Biomaterials, 15(5), 353.

Intelligent Design of GaSb doped Single Crystals

B. Štepánek, J.Šesták, J.J.Mareš, J.Krištofik, V.Šestáková, P.Hubík

Institute of Physics, Academy of Sciences of the Czech Republic, Semiconductor Department, Cukrovarnická 10, 162 53 Praha 6, Czech Republic,
Email: sestak@fzu.cz

ABSTRACT

Various element doping of GaSb crystals was found unsatisfactory in order to achieve desired semiconductor properties until another conception design was introduced providing a better intelligence processing. It was shown that the ionized atmosphere can serve as a passivator in a wider range of tellurium concentration and that the equilibrium between passivated and active donors is created according to the ratio of p- to n-type dopants in the starting melt of GaSb crystals highly doped with tellurium. The Czochralski method without encapsulant in the flowing atmosphere of ionized hydrogen was employed and the resulting intrinsic free carrier concentration was several times lower than that obtained by using simple (molecular) hydrogen.

INTRODUCTION

Gallium antimonide (GaSb) single crystals are promising candidates for a variety of military and civil applications in the 2 - 5 and 8 - 14 μm ranges, among others infrared (IR) imaging sensors for missile and surveillance systems (so-called focal plane arrays), fire detection and monitoring environmental pollution and other light diodes and lasers. In comparison with traditional GaAs, InSb, InP, for which the semi-insulating as well as conductive material is available, GaSb has a disadvantage: its conductivity that is usually very high due to the large amount of p-type natural defects in the lattice, which puts very serious limits on the construction of GaSb-based devices. To develop high-resistive GaSb, intensive optimisation of doping and growth conditions was undertaken [1,2]. Doping by the following elements Cu, Zn, Cd, In, Si, Ge, Sn, N, As, S, Te, Mn was investigated [3-6] systematically using the Czochralski method of growth without encapsulant in a hydrogen flowing atmosphere as well as by diffusion studies [7]. The limit of the doping concentration of each dopant was measured indicating the lowest solubility for S, N, Cu, and the highest for In, Ge, Te, As [8]. Extensive thermodynamic evaluation were also carried out and directed to analyse some binaries and ternaries, such Ga-Sb-S (Te,Cu), etc. [3-5].

However, in spite of big affords, the desired low conductivity material was not obtained. Therefore a special and rather unique method has been developed using the passivation of active donors of n-type (Te-doped) crystals by protons during the inherent growth realised in the ionised hydrogen atmosphere generated in situ by deuterium lamp radiation [9,10]. From a thermodynamic point of view the ionized hydrogen passives a part of donors and shifts equilibrium between passivated and active donors depending on the starting concentration of n- and p-dopants to the intrinsic-like position. The preparation of stable GaSb with sufficiently high resistivity would open unique perspectives in the construction of integrated IR-optoelectronic devices of a new generation.

A major drawback of GaSb substrates is their higher concentration of residual acceptors which reach, in the pure undoped GaSb single crystal, a value [11] of about 1.7×10^{17} cm^{-3}. The acceptors are identified as $V_{Ga}Ga_{Sb}$ complexes (where V is the vacancy) with a double ionized structure [12]. The resulting resistivity of undoped GaSb single crystals is about 10^{-2} Ω.cm. Many researchers have tried to reduce the residual acceptor concentration and to increase the resistivity of GaSb.

The achieved results of growth under the ionized hydrogen atmosphere were sufficiently stimulating to encourage us to continue our study of the GaSb single crystal preparation with higher concentrations of tellurium. The electrical behaviours of such grown crystals were compared with the former measurements of Te-low doped crystals [13,14].

0-7803-5489-3/99/$10.00 ©1999 IEEE.

EXPERIMENT

The Czochralski method without encapsulant in the flowing atmosphere of ionized hydrogen was used for the preparation of GaSb single crystals. The hydrogen atmosphere suppressed creation of an oxide scum on the melt surface [2,15]. In vacuum pre-synthesised GaSb (Ga/Sb = 50/50.05) from elements (6N Ga and 6N Sb) acted as a starting material. Prior the crystal growth, GaSb polycrystalline bowl was cleaned by grinding and etching in an acid solution. Due to evaporation of antimony during the whole growth process, the small amount of antimony (0.1 wt.%) was added into the melt to prevent a nonstoichiometric growth of crystals. It was found that about $1x10^{-3}$ mol antimony could be lost in the gaseous form from the apparatus owing to the flowing hydrogen atmosphere [15].

The axial temperature gradients close to the solidification interface were about 35 $K.cm^{-1}$, which is very low in comparison with other methods; for example with the liquid encapsulated Czochralski method (LEC) the gradients reached about 200 $K.cm^{-1}$. The horizontal gradient on the solid/liquid interface was almost flat. The pulling rate was 12 $mm.h^{-1}$ with the seed rotation [15] of about 20 - 25 rpm. The crystals were grown in the <111> direction, their length was about 70 mm and diameter of about 25 - 30 mm The growth conditions are summarised in the Table 1.

The whole growth procedure, the complete Czochralski apparatus and the gradients profiles were described in detail in our previous papers [2,6,11,15].

RESULTS AND DISCUSSION

The result of electrical measurements of undoped GaSb crystals grown by this method showed that the use of ionized hydrogen caused an increase of resistivity and the free carrier concentration. However, there was a certain asymmetry in acceptor and donor passivation in GaSb, because the Hall concentration increased. It seemed that the residual donors were passivated more than the acceptors [9,13].

Table 1: Growth conditions of the GaSb crystals grown using the Czochralski method without encapsulant in a flowing hydrogen atmosphere.

GaSb charge weight	~ 170 g
Component ratio in charge, wt.%	Ga/Sb = 50.00/50.05
Atmosphere	hydrogen - molecular or ionized
Oxygen impurity content	< 0.1 ppm
Kind of dopants	almost elementary
Hydrogen flow rate	70 cm^3/hour
Pulling rate	12 mm/hour
Rotation speed	20 - 25 rpm
Seed orientation	<111>b(Sb), direction to the melt
Crucible	sand-blasted quartz
Crucible weight	~ 50 g

On the basis of this assumption, we attempted to prepare slightly Te-doped GaSb crystals (3.12×10^{17} $atoms.cm^{-3}$ in the starting melt) using the same conditions as mentioned above [13]. According to the electrical measurements of these crystals, our assumption has been approved (see Table 2.). We believed that the donors were preferentially passivated. It was likely that an equilibrium between the passivated and active donors in the GaSb structure was created depending on the growth length. A fraction of the donors was passivated, as seen in the case of the Te-doped GaSb single crystals, where only a very small amount of active tellurium was incorporated in GaSb, while the rest of tellurium was inactive. The free carrier concentration was almost the same along the whole length of the crystals and although the GaSb bowl was doped by a typical n-type element, such as tellurium, the whole GaSb crystals were of p-type conductivity. As the distribution coefficient ($k_{eff} = 0.32$) of tellurium in GaSb is lower than 1, the tellurium concentration in a crystals should increase during the growth compensating the acceptors until the conductivity of the main part of the crystal bowl became n-type. This did not happen during the growth under ionized hydrogen atmosphere, as indicated by the Hall measurements. We assumed that the amount of passivated donors increased with the donor concentration in such a way that the active donor concentration remained

almost constant during the growth. The slightly Te-doped crystals showed a trend to keep the concentration of active donors equal. In the case of highly Te-doped GaSb crystals, however, it may not be valid.

For this reason the highly doped Te-GaSb crystals were grown under the same conditions as in the case of the above mentioned crystals. The concentration (4.52×10^{18} atoms.cm^{-3}) of tellurium was used and the comparison of electrical properties of crystals grown in molecular hydrogen atmosphere and crystals grown in ionized hydrogen atmosphere was performed. The results have shown that the free carrier concentration was also lower in the crystals grown under ionized atmosphere than in the crystals prepared in molecular hydrogen (see Table 2.). The difference reached several hundreds per cent and we could say that the concentration of active donors (active tellurium concentration) was several times lower in the case of the use of ionized atmosphere than that for the molecular hydrogen. It seemed that our assumption has been confirmed and the ionized atmosphere caused a preferred passivation of donors but not acceptors. The concentration of dislocation density was almost the same for GaSb grown in ionized and molecular hydrogen atmosphere and reached the range of 0 - 100 cm^{-2} in both cases [6]. The quantitative evaluation of the influence of this atmosphere is very difficult now because we have only a few results.

However, from a thermodynamic point of view, the ionized hydrogen atmosphere passivated only a part of the donors and created an equilibrium between passivated and active donors. The state of this equilibrium depends on the starting concentration of n- and p-type dopants. As soon as the concentration of p-type elements is almost the same or higher than that of n-type dopants, n-type dopants are preferentially passivated, which meant the ratio of the concentration of passivated donors to the concentration of active donors approaches unity. For better understanding, it necessary to add, that in the case of heavily Te-doped GaSb crystals (the whole bowl is n-type) the concentration of p-type dopants is very low and therefore the concentration of active donors (n-type dopant) increases along the growth axis almost according to the distribution coefficient of tellurium ($k_{eff} = 0.32$). For this reason, the free carrier concentration and mobility increase as well which is so distinct for the case of p-type crystals (see Table 2.). The value of mobility was very closely connected to the donor concentration in the case of n-type crystals.

Table 2: Comparison of electrical properties of undoped and Te-doped GaSb crystals grown in an ionized and molecular hydrogen atmosphere.

Te Concentration in the start melt [atoms/cm^3]	Kind of Hydrogen Atmosphere	Part of crystal	Fraction [x]	Type of Conductivity	Free carrier concentration [cm^{-3}]	Mobility [cm^2/V.s]	Resistivity [Ω.cm]	Difference in free carrier conc. [%]
Undoped	Molecular Hydrogen	top	0.05	P	1.72×10^{17}	640	0.060	
		bottom	0.95	P	0.96×10^{17}	550	0.062	
	Ionized Hydrogen	top	0.05	P	3.30×10^{17}	300	0.102	+ 190
		bottom	0.95	P	3.50×10^{17}	20	0.807	+ 365
3.12×10^{17}	Molecular Hydrogen	top	0.05	P	0.69×10^{17}	1200	0.0032	
		bottom	0.95	N	6.70×10^{17}	2300	0.0018	
	Ionized Hydrogen	top	0.05	P	0.18×10^{17}	370	0.951	- 380
		bottom	0.95	P	0.23×10^{17}	390	0.705	-3010
4.52×10^{18}	Molecular Hydrogen	top	0.05	N	13.25×10^{17}	2860	0.0012	
		bottom	0.95	N	109.80×10^{17}	3400	0.0010	
	Ionized Hydrogen	top	0.05	N	7.45×10^{17}	2100	0.0028	- 180
		bottom	0.95	N	23.10×10^{17}	2970	0.0013	- 480

Our assumption of the creation of an equilibrium between passivated and active donors is supported by the shapes of free carrier concentration profiles along the growth axis depending on the growth atmosphere. While the profile of the concentration changes in the crystals grown in a molecular hydrogen atmosphere is fully described by the Pfann equation, it means the profile shows the exponential shape (see Figure 1.), the distribution of free carrier concentration in the crystals grown in an ionized hydrogen atmosphere is almost flat, it means, the profile of the curves has a linear character (see Figure 2.). We suppose that the creating equilibrium between passivated and active donors also balances the increasing concentration of acceptors and moderates the influence of a distribution coefficient. There are two factors which act against each other and their influences are compensated. For this reason the free carrier concentration changes linearly along the growth axis and the Pfann equation does not correspond with the Hall measurements.

CONCLUSION

For a satisfactory growth of crystals with the free carrier concentration lower than 10^{15} cm^{-3} (which is the desired goal of scientists working with GaSb substrates) it is necessary to deal with a whole series of crystals with various concentrations of tellurium in the starting melt. According to our preliminary calculation, the optimal concentration should be (6 - 8) x 10^{17} $atoms.cm^{-3}$ of tellurium and such prepared crystals should show the free carrier concentration of about 10^{14} cm^{-3} along the whole crystal bowl (see our predicted profile of the free carrier concentration in such a Te-doped GaSb single crystal, Fig. 3).

ACKNOWLEDGEMENT

The study was carried out under the support of the Grant Agency of the Czech Republic projects numbered as 100/98/0034, 104/97/0589 and 202/99/0410.

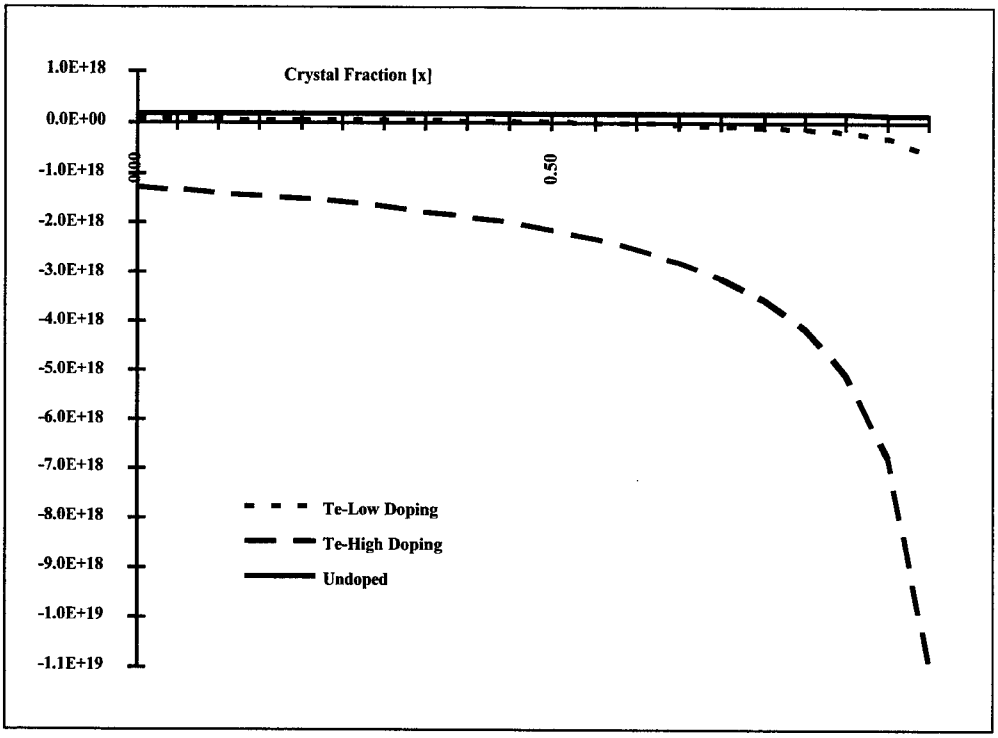


Fig. 1. Free carrier concentration distribution along the growth axis in the GaSb single crystals grown using the Czochralski method without encapsulant in a molecular hydrogen atmosphere.

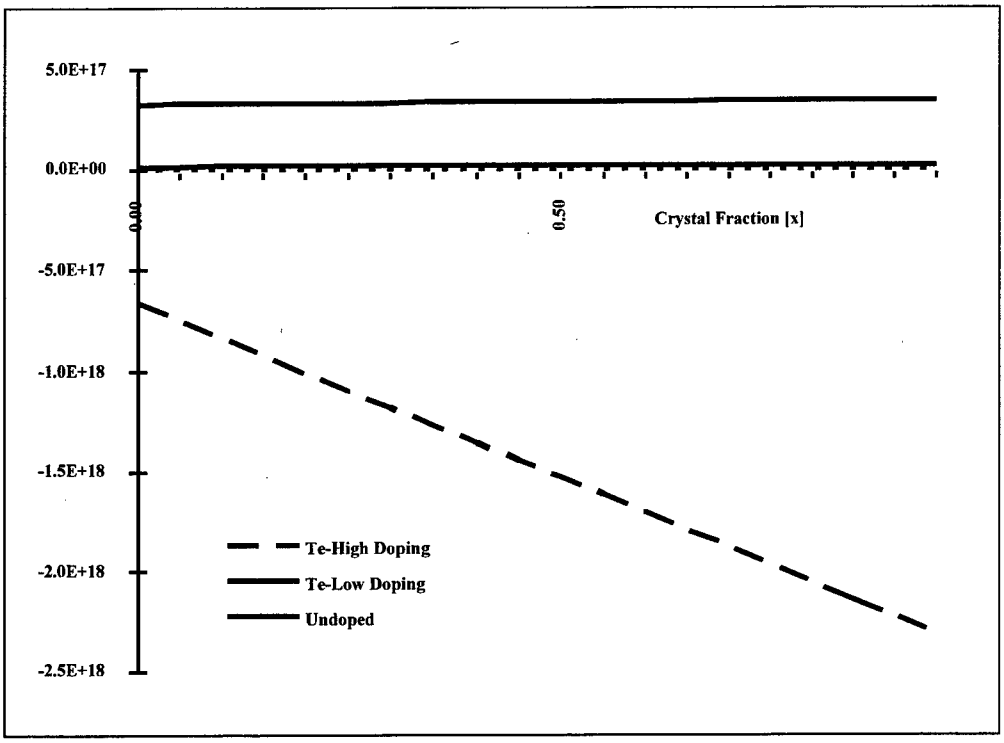


Fig. 2. Free carrier concentration distribution along the growth axis in the GaSb single crystals grown using the Czochralski method without encapsulant in an ionized hydrogen atmosphere.

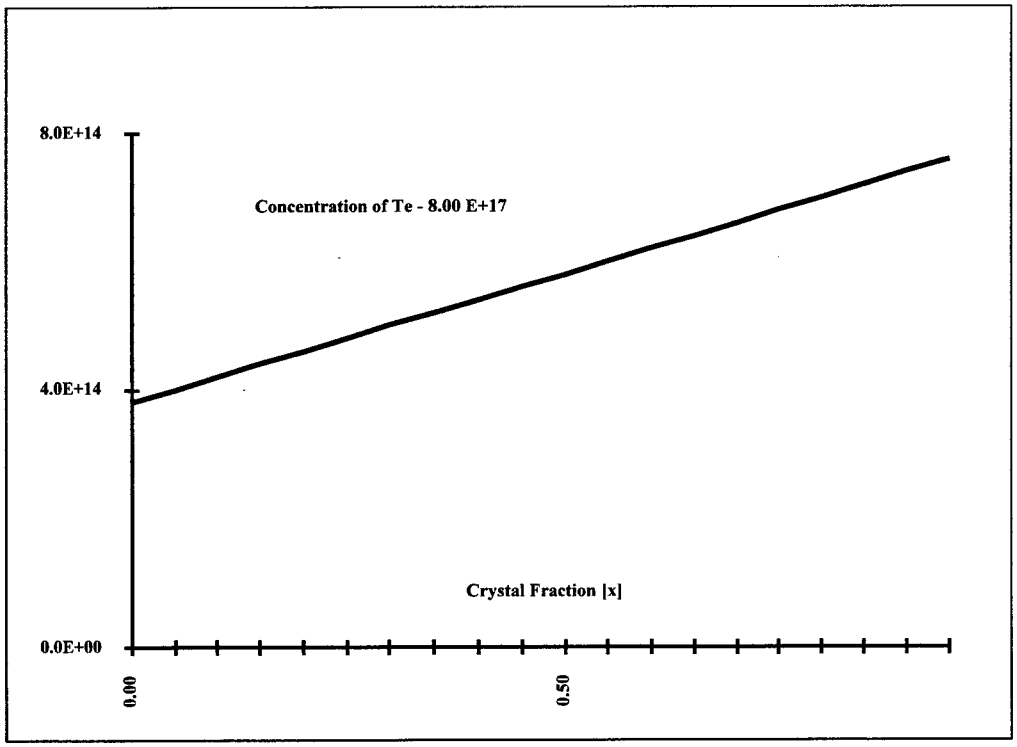


Fig. 3. Predicted distribution of free carrier concentration along the growth axis in the GaSb crystals grown in ionized hydrogen atmosphere.

REFERENCES

1. B. Štepánek, V. Šestáková, J. Šesták, 1993. Comparative analysis of GaSb single crystal growth techniques. Inorganic Mater., 29, 1071-1075.
2. V. Šestáková, B. Štepánek, J. Šesták, 1996. Various methods for the growth of GaSb single crystals. J. Cryst. Growth, 165, 159-162.
3. V. Šestáková, B. Štepánek, J. Šesták, P. Hubík, V. Šmíd, 1993. Thermodynamic aspects of (Te,S)-double-doped GaSb crystal growth. Mater. Sci. Eng., B2, 14-18.
4. J. Šesták, J. Leitner, H. Yokokawa, B. Štepánek, 1994. Thermodynamics and phase equilibria data in the S-Ga-Sb system auxiliary to the growth of doped GaSb single crystals. Thermo. Acta, 245, 189-206.
5. J. Šesták, V. Šestáková, □.□ivkovic, 1995. Estimation of activity data for theGa-Sb-S binaries regarding the doped GaSb semiconductor crystals. Pure Appl.Chem., 67, 1885-1889.
6. V. Šestáková, B. Štepánek, 1995. Doping of GaSb single crystals with various elements. J. Cryst. Growth, 146, 87-91.
7. J. Mimkes, V. Šestáková, K.M. Nassr, M. Lübbers B. Štepánek, 1998. Diffusion mobility and defect analysis in GaSb. J. Cryst. Growth, 187, 355-362.
8. V. Šestáková, B. Štepánek, J. Šesták, 1999. Estimation of doping limit of some elements in GaSb single crystals. Proc. of SPIE, Single Crystal Growth, Characterisation, and Applications. 3724, 125-129.
9. V. Šestáková, B. Štepánek, J.J. Mareš J. Šesták, 1996. Decrease in free carrier concentration in GaSb crystals using an ionized hydrogen atmosphere. Materials Chem. and Phys., 45, 39-42.
10. B. Štepánek, V. Šestáková, J. Šesták, 1996. Growth of GaSb single crystals with low carrier concentration. Proc. SPIE, Solid State Crystals: Growth and Characterisation, 3178, 64-67.
11. B. Štepánek, V. Šestáková, 1992. Czochralski grown concentration profiles in the undoped and Te-doped GaSb single crystals. Thermo. Acta, 209, 285-294.
12. Y.J. Van der Meulen, 1967. Growth properties of GaSb: The structure of the residual acceptor centres. Phys. Chem. Solids, 28, 25-32.
13. V. Šestáková, B. Štepánek, J.J. Mareš J. Šesták, 1994. Hydrogen passivation of residual acceptors in GaSb single crystals, J.Cryst.Growth, 140, 426-428.
14. B. Štepánek, V. Šestáková, J. Šesták, 1994. More progressive technology of GaSb single crystal growth. Cz. J. Phys, 47, 693-697.
15 F. Moravec, V. Šestáková, B. Štepánek, V. Charvát, 1989. Crystal growth and dislocation structure of gallium antimonide. Crystal Res. Technol., 24, 275-281.

Intelligent Image Analysis Applications

Astronomical Image Processing - Applications to Ultra - Faint Imaging of Small, Moving, Solar System Bodies: Comets and Near-Earth-Objects

Karen J. Meech

University of Hawaii, Institute for Astronomy
2680 Woodlawn Drive, Honolulu, 96822, HI, USA
Tel: 808-956-96828 Fax: 808-956-9580 Email: meech@ifa.hawaii.edu

ABSTRACT

Modern electronic detectors, or charge-coupled-devices (CCDs) are being used on large optical ground and space-based telescopes to image ultra-faint astronomical sources, ranging from small, solar system bodies, to diffuse gas and dust in interstellar medium to very distant galaxies. Observations of all these objects are challenging, but the small, solar system bodies create special demands on image processing because of their motion relative to background objects.

Comets are "dirty snowballs" -- archaeological remnants of the birth of the solar system from its primordial cloud of gas and dust. Because many are stored at large distances from the sun and may never have been significantly heated by the sun, they may contain chemical and physical information from this era early in our history. As a cometary orbit brings it into the vicinity of the sun, the surface volatiles heat up and sublimate, dragging the refractory materials from the surface and creating the features we associate with comets. It is when the comets are "active" and close to the sun (and hence bright) that the majority of observations are made. However, in the active phase, comets undergo physical and chemical evolution which makes primordial information difficult to discern from the evolutionary changes. Detecting an inactive comet's nucleus (which may be only a few km in diameter, and which reflects only a few percent of the incident sunlight) at very large distances from the sun is an extremely challenging observation not only because of the faintness of the object, but because of its motion across the detector relative to the field stars. It is even more challenging to attempt to image the first onset or the cessation of activity in the form of a very low surface brightness dust cloud around the comet. The distances at which these processes occur give us information about the chemistry of the comet.

In this paper, techniques for pushing CCD detectors on ground-based and space-based telescopes to the limits of their imaging capabilities to detect objects hundreds to thousands of times fainter than the dark night sky will be discussed. We will also discuss automated techniques for searching the world's largest astronomical CCD mosaics for moving objects. The application of these techniques to understand the early history of our solar system, and toward discovering small fast-moving comets and asteroidal bodies in the near-Earth vicinity will be presented.

0-7803-5489-3/99/$10.00 ©1999 IEEE.

A High Performance Computing Algorithm to Improve In-line Holography

Hesham Eldeib

Computer and System Department
Electronic Research Institute, National Research Center
Tahrir street, Dokki,Giza,Egypt
Email: eldeeb@eri.sci.eg

ABSTRACT

A new holographic algorithm is suggested to reduce the computing time by orders of magnitude in computer generation and reconstruction of holograms, that is called HPCHolo (High Performance Computing Holography). It is proposed to speed up the generation of hologram by ray-tracing technique and the reconstruction of virtual image from that hologram by correlation technique. We applied the new algorithm for two-dimensional (2D) and three-dimensional (3D) objects model on PowerXplorer computer (Multiprocessor message passing machine). We study the relation between the hologram size, the resolution of the reconstruced image and the Computational time for both construction and reconstruction processes and obtain satisfactory results

INTRODUCTION

The concept of holography was proposed and demonstrated by GABOR over forty years ago. The realization of this idea was made possible by the advent of laser light. Since then, a great deal of effort has been exerted on the construction of a holographic system. A considerable interest has arisen in exploring the possibilities of applying the holographic principles of three-dimensional (3D) image storage and reconstruction to digital-computer displays and to other applications, e.g., tomography, nuclear magnetic imaging, astronomy, computer-aided design and 3D communications. With such techniques it is possible to generate holograms capable of displaying 3D images of objects which never existed in reality, since only a mathematical knowledge of the object is necessary .

Most of the computer-generated holograms (CGHs) described in the literature are simply two-dimensional (2D) Fourier transforms of a two-dimensional image plane. Although the fringe pattern on the plate is calculated by a computer, what is calculated is a Fourier transform. In these holograms, the principal mode of reconstruction is Fraunhofer diffraction, which limits low-frequency spatial information to the center of the interference pattern and higher frequency components to the edges. Alternatively, holograms generated via ray tracing distribute information so that different areas of the plate correspond to different perspectives of the object. In the past, however, implementation of this algorithm has not been trivial since the quantity of calculations quickly approached the limits of computing technology. Large holograms, especially those with sizes suitable for display applications, are almost difficult to achieve with present means of single processor [2].Here, we employ an efficient and fast algorithm called HPCHolo(High Performance Computing Holography) algorithm to accelerate the generation of holograms by ray-tracing technique. We will use also the same algorithm to accelerate the reconstruction of virtual image from those holograms by correlation technique, which has been proved to have better image quality than the FFT method [1].

The machine used to generate the hologram and reconstruct the virtual image is a PowerXplorer consisting of 8 nodes; each with 32 Mbytes of memory. The PowerXplorer has no internal disk storage and the only I/O interface is through communication links. It runs in a cross development environment. with a front-end workstation for code development, downloading, and collecting results. The PowerXplorer is an (Multiple Instruction Multiple Data) MIMD parallel computer. Each processor is an autonomous computer that communicates with other processors via message passing [3].

0-7803-5489-3/99/$10.00 ©1999 IEEE.

HIGH PERFORMANCE COMPUTING RAY-TRACING ALGORITHM FOR HOLOGRAM GENERATION

Ray-tracing algorithm

Ray-tracing is a convenient way to model optical systems using a computer. In computer simulations of holograms by ray tracing, the complex amplitudes that reach the plane of the photographic film from different directions are summed up.

The basic equation for hologram generation by ray tracing is [4]:

$$I_\alpha \propto 1+\frac{2}{A_R}\sum_{j=1}^{N}\frac{A_j \exp(ikR_{\alpha j})}{R_{\alpha j}} \qquad 1.$$

where I_α is the hologram intensity at a point α on the hologram plane, i,j,m represent the coordinates of the original objects in 3-D space or the virtual image in 3D space, A is the reflected beams from the object, k is the wave number of beam, and $R_{\alpha j}$ is the distance from an object to the (x,y,z) hologram plane

$$R(x,y,z,\xi,\eta)=[(x-\xi)^2+(y-\eta)^2+z^2]^{1/2} \qquad 2.$$

where (ξ,η) is the coordinate on the hologram plane. The $x-y$ plane is parallel to the $\xi-\eta$ plane, the Z -axis is chosen to be perpendicular to the hologram and the hologram is set at $z=0$.

The term "1" in Equation 1. represents the reference beam. For simplicity, we use a reference beam of normal incidence, as in the in-line holography (GABOR-type), in the following discussion.

HPCHolo algorithm for hologram generation

In this paper we improve the above algorithm to accelerate the calculation of Equation 1. by using HPCHolo algorithm. The flowchart of the HPCHolo algorithm used to generate holograms is shown in Figure 1. The following subsection gives a brief description for this algorithm.

Get node parameters: The processors of Parix partition are arranged as a 2-D or 3-D grid. Identification of a processor's own position within the partition (processor's ID) is necessary for the processor in order to know what to do. A set of global data kept on each node allows this identification.

Link Establishment: The basic communication facility in PARIX is virtual links. Virtual links overcome the restrictions given by the presence of only four physical links per processor that any two processors to communicate directly, even if there is no real link between them.

Reading and broadcasting input data: The main difference between optical holography and CGHs is that the object may not physically exist. Therefore, before starting the generation process, the specification of the desired object should be defined and may be recorded in a file or directly fed via the keyboard.

Hologram generation: At this point each processor has its assigned elements. It will begin to execute the code of the algorithm at the same time with the other processors and generate its assigned part of the hologram.

Broadcasting and Storing hologram data: All Processors will broadcast the output data through the interconnection that already exist to one processor. Then, letting this processor to save the output data to a file opened in the hostcomputer.

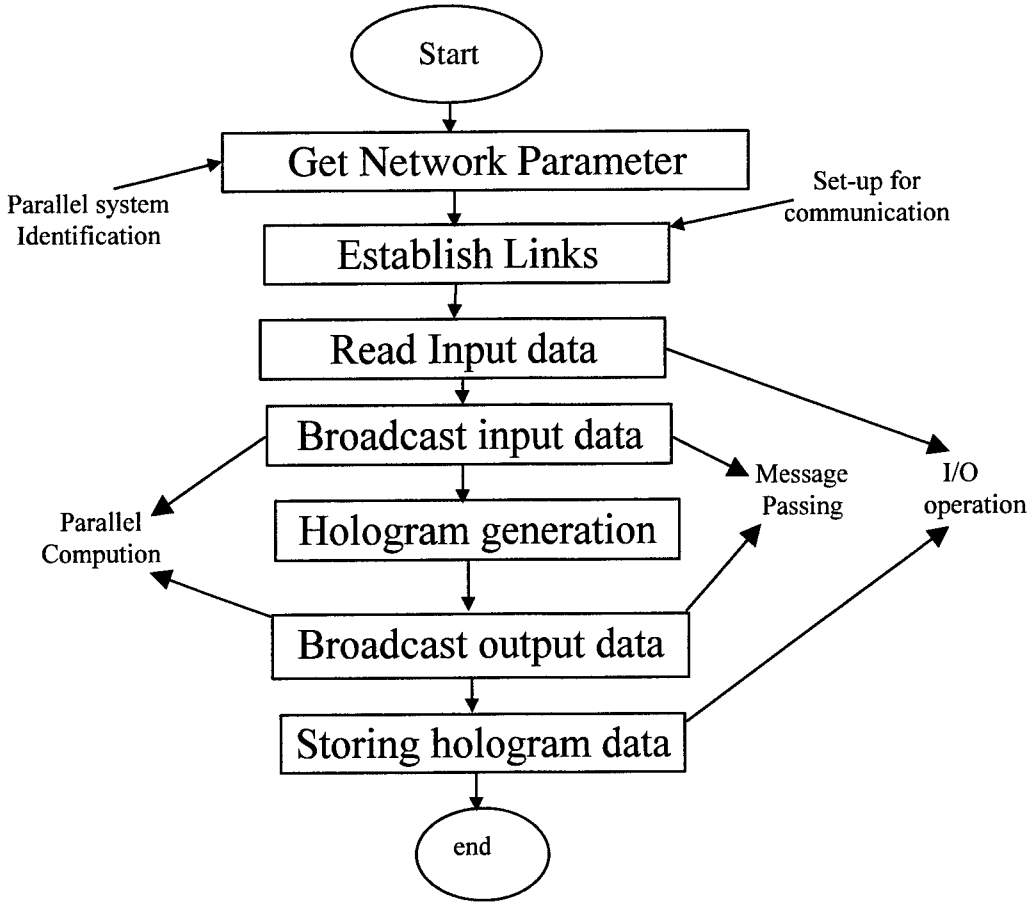


Fig. 1. Flowchart of HPCHolo algorithm for hologram generation

HIGH PERFORMANCE COMPUTING ALGORITHMS FOR VIRTUAL IMAGE RECONSTRUCTION

Correlation method

In previous papers[1,5] we proposed a correlation method to reconstruct the 3D virtual image by computer. The method is based on the correlation between a hologram of a point source and a hologram of real objects and has been proved that it has better virtual image resolution than the methods which use Fast Fourier Transforms (FFT) [1]. But the FFT approach is much faster.

In order to retrieve the 3D pattern $A(x, y, z)$, we perform the calculation

$$\phi_i = \sum_{\alpha} I_{\alpha} \cos(kR_{i\alpha}) / R_{i\alpha}, \qquad 3.$$

where the summation over α is performed on the surface of the hologram. This process can retrieve the image, that is, $A(x, y, z) \approx \varphi_i$. [5]

HPCHolo algorithm for reconstruction of virtual image

In this paper, we improve on the above algorithm to accelerate the calculation of Equation 3 by using the HPCHolo algorithm. The flowchart of the HPCHolo algorithm used to reconstruct the virtual image is the same as shown in Figure 1, except for the step of virtual image reconstruction instead of hologram generation.

In virtual image reconstruction, each processor has its assigned elements. It begins to execute the code of the algorithm simultaneously with other processors to reconstruct its assigned part of the virtual image. Then the output data is broadcast to one processor at the same time. Finally, the algorithm stores this virtual image data to a file on the host computer.

EXPERIMENTAL VERIFICATION OF THE ALGORITHM

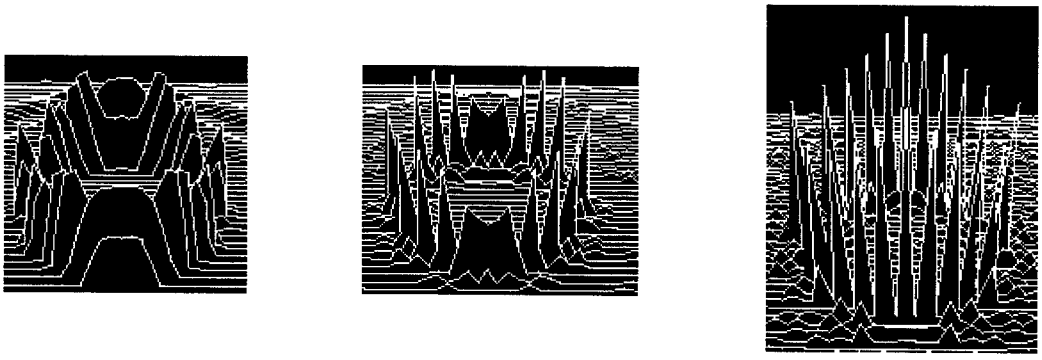
Hologram generation

In 2D case studies, we take a discrete circle consisting of 20 points in space. In 3D case studies, we take an object consisting of five circles situated in different planes at depth to form a cone shape. The radii are 10, 30, 50, 70, 90 pixels, with the smallest circle farthest away from the hologram plan. We generate many holograms for these two objects of (64x64),(128x128),(256x256),(512x512),and (1024x1024) pixels size.

We found that the fringe patterns have more diffraction details with an increase in hologram size. We will show the response of this effect in the reconstructed image in the next subsection.

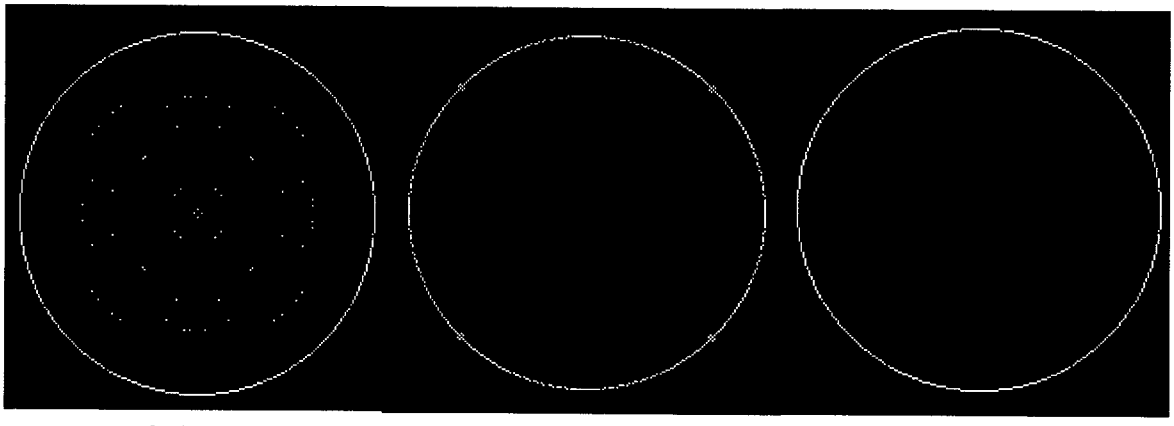
Reconstruction of the virtual image

We have reconstructed the holograms obtained for both the discrete circle and the 3D object. We take the reconstruction area fixed as 64x64 for 2D objects and 256x256 for 3D objects. Figure 3 shows the reconstructed image for a discrete circle with different hologram sizes. Figure 4 shows the reconstructed image for the 3D object with cross-sectional plane at Z=90 with different hologram sizes.



a. 64x64 b. 128x128 c. 256x256

Fig. 3. 3D intensity representation of virtual image for the discrete 2D circle with different hologram sizes.



a. 256x256 b. 512x512 c. 1024x1024

Fig. 4. Tthe virtual image of the 3D object with different hologram size at cross section plane Z=90.

From Figure 4, we found that the appearance (resolution) of the reconstructed image increases with an increase in hologram size. For a 2D object, we found there is no improvement with hologram size above a resolution of 256x256 due to the simple object we have chosen.

PERFORMANCE EVALUATION

In this section, we discuss the two main factors used to evaluate the performance of HPCHolo algorithm. The first factor of these is computation time of the proposed algorithm. The second factor is the resolution of reconstructed image.

Computation time

Figure 5 and Figure 6 show the computation time of hologram generation and reconstruction for different sizes respectively applied on 1, 2, 4 and 8 processors, for the 2D object as a measurable case.

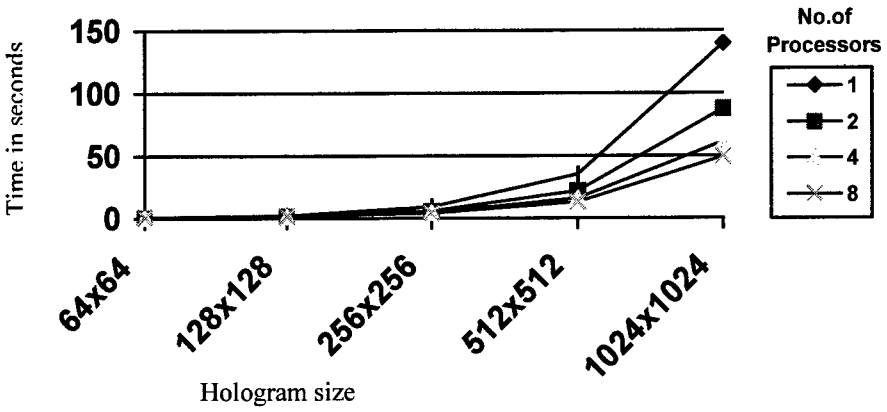


Fig. 5. Computation time of HPCHolo algorithm for hologram generation with different sizes applied to 1, 2, 4 and 8 processors with a 2D object.

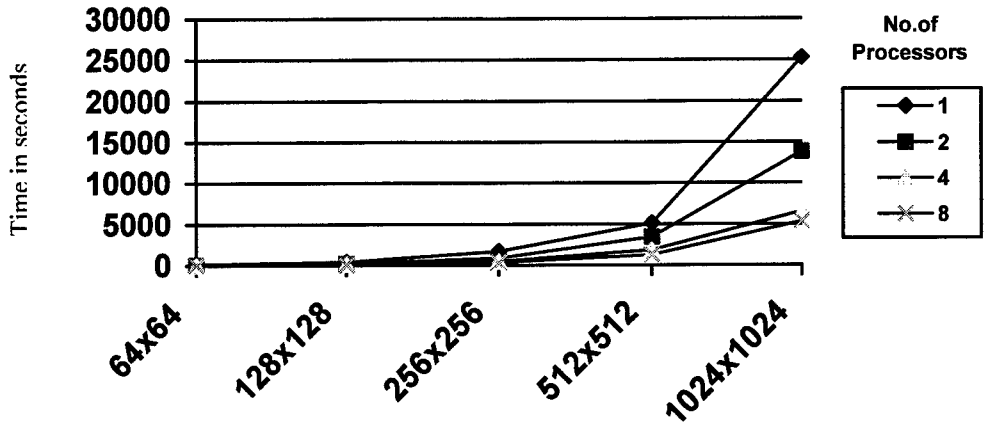


Fig. 6. Computational time of HPCHolo algorithm for reconstruction of virtual image with different sizes applied to 1, 2, 4 and 8 processors with a 2D object.

From Figure 5 and 6, we can see that the maximum gain from the algorithm HPCHolo comes with a size of 1024x1024. Associated with the speed, the HPCHolo algorithm is slower than the conventional algorithm when a hologram of small size is used. However by increasing the size of the hologram, which is suitable for real object applications, the proposed algorithm becomes efficient and fast.

Resolution of the reconstructed image

The results demonstrate that this new computer holography algorithm improves performance. This paper has presented an extensive case study for evaluating the computer generation and reconstruction of holograms. As for the virtual image quality, the HPCHolo algorithm gives excellent results for both types of objects in 2D and 3D. The results show that the larger the hologram size, the much better is the virtual image resolution, but, it is saturated for a certain limit (512x512) as in our case study of 2D objects.

CONCLUSION

We have provided a high-speed algorithm for computer-aided holography for data processing, with a parallel processing machine. Compared with the conventional ray-tracing algorithm, the HPCHolo algorithm is faster, especially with large hologram sizes suitable for display applications, which are almost impossible to achieve using conventional means. In the reconstruction of the virtual image, the HPCHolo algorithm speeds up the calculation time significantly over the full calculation of Equation 3.

The hologram size in the HPCHolo algorithm must be adapted to have comparable image quality with the full calculation scheme and with a large decrease in computation time. In general, the results indicate that this new computer holography algorithm dramatically decreases the computation time of hologram generation, with much better virtual image quality than the conventional method.

REFERENCE

1. Eldeib, H., and Yabe, T., 1996. A Fast Computer Holography System and Its Experimental verification. Journal of Computer Modeling and Simulation in Engineering ,**1**, 251-261.
2. Koren, G., Polack, F., and Joyeux, D., 1993. Iterative algorithms for twin-image elimination in in-line holography using finite-support constraints. J..Optical Soc. Am. A., **10**, 423-433.
3. Parsytec, 1996. Parsytec GC/Power Plus, Power Xplorer and CC-Series Techincal data, Parsytec, Technical Report.
4. Stein, A.D., Wang, Z., and Leigh, J.S., Jr., 1992. Computer-generated holograms: a simplified ray-tracing approach, Computer in Physics **6,** 289-292.York.Tokyo).
5. Yabe, T., Ito T., and Okazaki, M., 1993. Holography Machine HORN-1 for Computer-Aided Retrieval of Virtual three-dimensional images, Japanese J. Appl. Phys. **32**, 261-263.

Human Face Detection System by KenzanNET with Preprocess Analyzing Hyperspectral Image

Takakazu Chashikawa * **, Keizo Fujii * and Yoshiyasu Takefuji *

* Graduate School of Media and Governance,
Keio University 5322 Endo, Fujisawa 252-0816, Japan
** Nittan Co.,Ltd., 1-11-6 Hatagaya, Shibuya, 151-8535, JAPAN

ABSTRACT

This paper proposes a neural network system to detect human faces. Our scheme is composed of a pre-process and KenzanNET. Preprocessing analyzes hyperspectral images by using a hybrid self-organizing classification model to extract skin area and making a facial candidate pattern based on the extracted skin area. KenzanNET discriminate a face from other body parts. KenzanNET is a kind of feed forward neural network and is made from CombNET [1] improved by an additional learning function. Under the various conditions in terms of background and brightness in a room and the distance between people and camera, our system can detect human face with 76.9% accuracy.

INTRODUCTION

Face recognition systems by neural network have been studied for a long time, and many models have been proposed. However, it is difficult to develop a flexible system with high performance and a human ability, because visual processing in the human brain has not yet been fully understood. But even lower animals can detect a target object with flexibility. It is well known that insects with only one millionth of the human brain have flexible recognition abilities because of a special sensor used to detect features of a target object. For example, a bee can sense ultraviolet emissions to detect flower nectar and a mosquito can sense carbon dioxide to detect human skin. We think special sensors help insects to detect objects. If we can install a special sensor to detect features of a human face, the system may have the same flexibility as do humans.

We developed a new camera for human face detection system which camera can capture two image, visible(color) image and infrared image. Infrared image shows thermal patterns of a human and is not affected easily by changes in conditions of the image. Thus, our system analyzes an infrared image and a visible image which we call the hyperspectrum image. Our facial detection process is composed of two schemes, preprocess and neural network. Preprocess analyze hyperspectrum image to make a facial candidate pattern and the neural network discriminates face and other parts of body about the facial candidate pattern. Preprocess convert face detection problem to pattern (like symbol) recognition problem.

In the scheme of the neural network, a conventional feed forward neural network with a back propagation learning model is not so good because of local minimum. We tried to use CombNET [1] in our system [2]. The strategy of CombNET is to divide the problem into several easy problems - we call classified learning. These problems can be solved easily by conventional neural network model. This version of our system has not convergent problem, but the quality of detecting human face is not so good. Because templates should be prepared as a teacher in advance, but it is too difficult in generally.

In this paper, we want to improve our system by adding signal teaching. Thus, we propose a new neural network model, KenzanNET using classified learning and an additional learning strategy. The classified learning strategy is based on CombNET and additional learning strategy is based on refining signal teaching by a quantizing vector. KenzanNET consists of a refining teacher-part, a clustering part and some recognition parts. The refining teacher is added for additional learning and is different fron CombNET. Facial candidate pattern-recognition by including three types of information: skin, hair and background, are fed to KenzanNET. The facial candidate pattern includes many parts of body such as face, hand, leg, and so on. KenzanNET discriminates face and other parts of body.

0-7803-5489-3/99/$10.00 ©1999 IEEE.

SYSTEM DESCRIPTION

An aspect of architecture is shown in Fig. 1. The pre-process is to detect human skin and to decide facial candidate patterns. KenzanNET is to recognize facial candidate patterns.

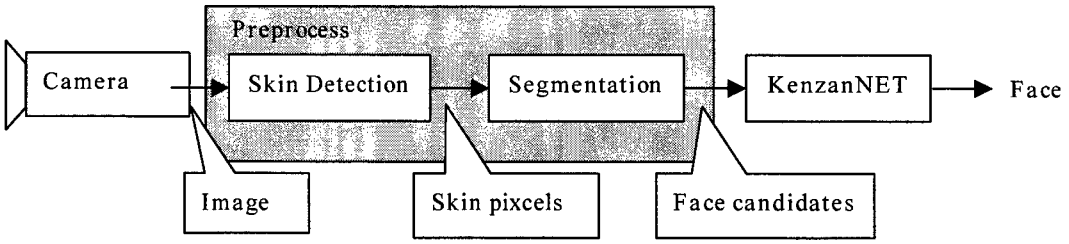


Fig. 1. Overview of proposed system

Hardware

In our system, the camera is composed of a visible camera and an infrared camera as shown in Fig. 2. This camera can obtain a hyperspectral image in the same area simultaneously as shown in Fig. 3.

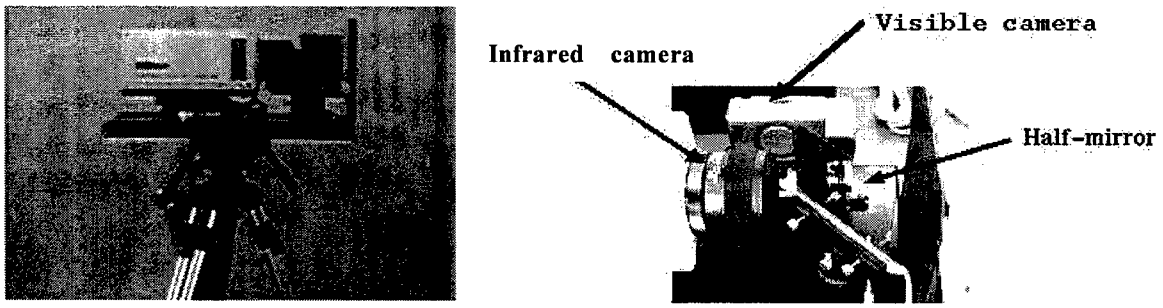


Fig. 2. Hyperspectral camera

Preprocess

An objective of the preprocess is to form facial candidate patterns. Preprocess is composed of two parts: skin detection part, and segmentation part.

Skin detection part uses a hybrid self-organization algorithm where Kohonen's self-organization model and the maximum neuron model are combined [3,4,5,6]. We use the maximum neuron model in the first stage until the state of the system converges to the local-minimum, then the Kohonen's self-organization algorithm is used in order to obtain the solution by escaping from the local minimum in the first stage. The algorithm is able to shorten the computation time without a burden of the parameter tuning. The result of skin detection is shown in Fig. 4. White is assigned to the extracted skin area.

Segmentation part decides head candidate patterns based on skin area as follows: checking criteria, making a pattern including three parts information (skin, hair, and background) and normalizing size into 16×12. The criteria are the size of skin, the ratio of height:width about skin area, the symmetry of skin, and the amount of hair and position from the centered. Outputs that satisfie the criteria are fed to KenzanNET as a facial candidate pattern (Fig. 5).

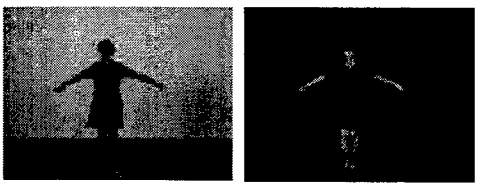


Fig. 3. Input Image

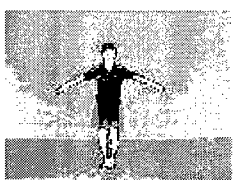


Fig. 4. Result of skin detection



Fig. 5. Head candidate pattern

KenzanNET

KenzanNET uses classified learning strategy and additional learning strategy.KenzanNET consists of three parts: refining teaching part, clustering part and recognition parts as show in **Fig. 6**. Clustering part and recognition parts bear Classified learning strategy and refining teaching part bears additional learning strategy. A number of networks in recognition parts is equivalent to codebook vector of clustering part. KenzanNET is different from CombNET on refining teaching part added and clustering part using maximum neural model.

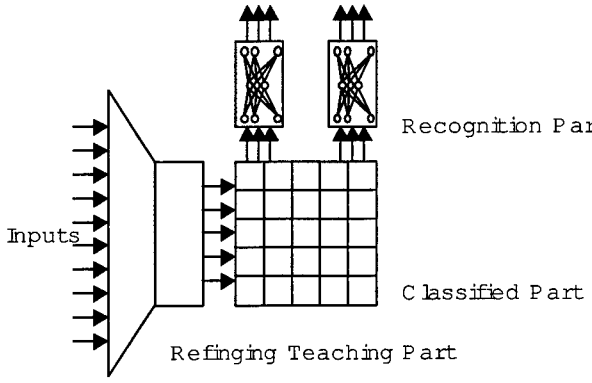


Fig. 6. Structure of KenzanNET

In refining teaching part, maximum neural model (see Appendix) quantizes vector of the teaching signals and trained codebook vectors are used as new teaching signals. The new teaching signals are good enough for training neural network. Because number of teacher is reduce and new teachers still have feature of old teachers statically. In clustering part, input data is divided into several groups. And in the recognition part, three layered hierarchical network is prepared for each group, and back propagation scheme is utilized to train each network. Each neural network doesn't need to have so complex mapping function, so it is easy to train.

A learning process is as follows. In clustering part, refined teaching signals are used for traing. After training the clustering part, all input data is classified into several groups according to the best matching criteria to the codebook vector of neurons. Since the input data that contains similar patterns is assigned into a same group, the output data is fed to a same network in recognition part. The trained clustering part is shown in Fig. 8. And next recognition part is trained for each sub-space to make a mapping function discriminating face from other part of body. And a decision process is as follows. As an input data is given to the clustering network, several neurons which give the smallest distance between the vector of input data and the codebook vector are selected. Then the input data is fed to the networks in recognition part which are connected to the selected neurons in the clustering part. The output of the networks is between 0 and 1. If the output is above 0.6 ,it is recognized as face. And others are recognized as other part of body. If the output indicates face, the system points it's position with rectangle as shown in Fig. 7.

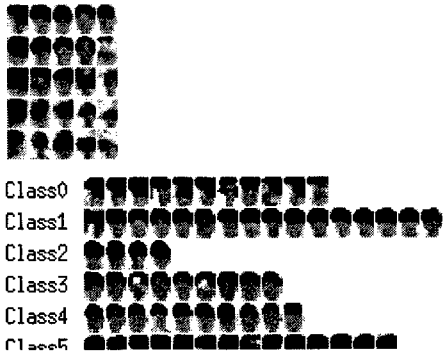


Fig. 8. Result of classified part

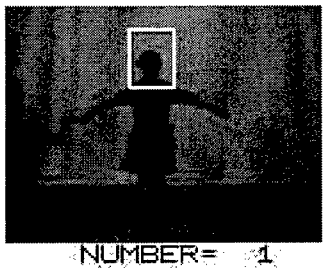


Fig. 7. Output of proposed system

EXPERIMENTS

The experimental data are took in room considering various conditions including background, brightness, and the distance between people and camera. The number of test samples is 431: dark(18lx), bright(500lx), complex background, plane background, big target(1m), and small target(5m).

The KenzanNET should be trained by teaching signals in advance. First we refine teaching signals as follows condition. We generate 3 pattern teaching signals, pattern 1: without refine, pattern 2: refine to 34 (false 9, collect 25) and pattern 3: refine to 52 (false 16, collect 36). The refine procedure is as follows. We divide teachers into collect and false and qantize vector of teacher by using maximum neural model according to pattern 1, 2, and 3. But a codebook vector of class must be false, if no data belong to it. We use codebook vector of each class as new teacher. Second, the classified part is trained, a condition of network is as follows: the number of classes is 25,16,9 and 4, number of neighterhoods is reduced by one per ten iterations. Finally, the each networks in recognition parts are trained. A condition of each network is as follows: the learning rate is 1.0, the criterea to finish the training procedure is that the RMS error decreases less than 0.1, the number of training pattern is 16×12, the number of output units is 1.

We do preprocess all test data and decide facial candidate pattern. And we check facial candidate pattern of all test data by using each trained KenzanNET.

Results and Discussion

Result of preprocess is showed in Table 1. System detects skin over 93.8%, and it means that hyperspectral image contains feature of skin that is not influenced by change of condition of test images, and the feature is extracted in skin detection part. And in this table system detects 402 facial candidates, but other 287 including other part of body, such as hand or leg. Thus, recognition quality is 66.4%. These results mean these test images are much difficult for conventional system.

Table 1: Result of pre-process

Part	Total	Correct	Result[%]
Skin Detection	432	405	93.8
Facial Candidate	432	287*	66.4

* The Number of facial candidates is 402

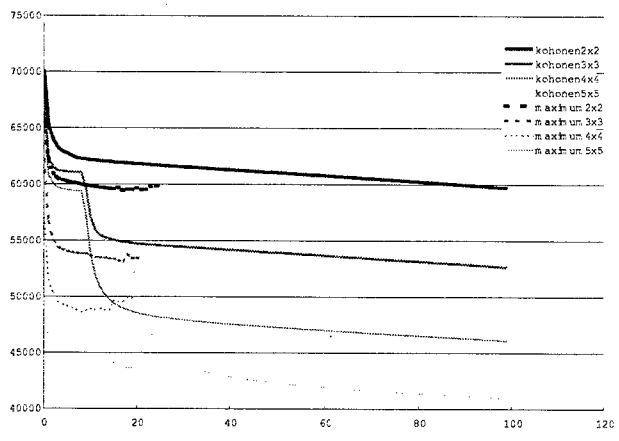


Fig. 9. Result of Classified part

In the process of recognize face, we compare the result of the KenzanNET and CombNET. **Fig. 9** shows result of classified part. This figure shows relationship between energy of clustering and iteration steps, in other words it shows the quality of clustering and computational time. From this figure, we notice that maximum neuron model is faster than Kohonen's model 2 or 5 times, but the quality is not as good as Kohonen's model. In this point it is important that whether quality of classification is important factor for face detection or not. **Table 2** shows relationship between the quality of classification and result of face detection. In this table, we consider the quality of classification is not so important for face detection. It is observed that the maximum neural model is faster than that of Kohonen's model and can classify facial candidate as good as Kohonen's model.

Table 3 shows the quality of detecting human face. From the results, we notice that when the number of additional data is increased, the quality is not always good in CombNET. And the best quality is 76.9% in CombNET (number of class 16(4x4), without additional data) and KenzanNET (refined to 52, with additional data48).

Table 2: Relationship between Kohonen's model and maximum neuron model

Class	Different of Energy	Different of Result[%]
4(2x2)	+861.0	+0.9
9(3x3)	+53328.0	+0.3
16(4x4)	+23034.8	-3.9
25(5x5)	+67223.8	-0.5

Table 3: Quality of detecting human face

Model	Number of Class	Without additional data[%]	With additional data 16[%]	With additional data 48[%]
Using Kohonen model (CombNET)	9(3x3)	72.2	76.0	76.0
	16(4x4)	76.9	74.1	76.4
	25(5x5)	71.0	72.5	74.6
KenzanNET without refine	9(3x3)	72.5	73.4	71.7
	16(4x4)	73.0	72. 0	71.9
	25(5x5)	70.5	72.0	74.9
KenzanNET refined to 34	9(3x3)	72.4	66.3	70.6
	16(4x4)	73.3	73.9	64.5
	25(5x5)	73.4	74.3	76.9
KenzanNET refined to 52	9(3x3)	67.0	70.0	75.3
	16(4x4)	72.1	70.9	75.8
	25(5x5)	72.4	69.1	73.5

CONCLUSION

In this study, we developed face detection system using hyperspectral image. We propose new neural model, where KenzanNET improves CombNET in classification and refining teaching part. We can improve classification time over 2 times, and considering additional learning - our system needs small memory for having teaching signals compared to the CombNET. And our system can detect human face with 76.9%. This result is as good as that of CombNET.

ACKNOWLEDGMENT

Part of this study was work of the Advanced Software Enrichment Project produced by INFORMATION-TECHNOLOGY PROMOTION AGENCY, JAPAN.

REFERENCES

1. A. Iwata, K. Hotta, H. Matsuo, N. Suzumura, 1991. A Large Scaled Neural Network ``CombNET". Proc. of IATSTED. July.
2. T. Chashiakwa, K. Fujii, Y. Ajioka, Y. Takefuji, 1998. Human Detection from Camera-Images by CombNET. Proc. of the fourth International Conference on Engineering Applications of Neural Networks. .47-53, June.
3. T. Kohonen, 1993. Physiological interpretation of the self-organizing map algorithm. Neural Networks. 6, 895-905.
4. S.C. Amartur, D. Piranio, Y. Takefuji, 1992. Optimization Neural Networks for the Segmentation of Magnetic Resonance Images. IEEE Trans. on Medical Imaging. 11(2), 215--220.
5. Y. Takefuji, K.C. Lee, H. Aiso, 1992. An artificial maximum neural network: a winner-take-all neuron model forcing the state of the system in a solution domain. Biological Cybernetics. 67, 243-251.
6. S. Oka, T. Ogawa, T. Oda, Y. Takefuji, 1998. A New Self-Organization Classification Algorithm for Remote-Sensing Images. IEICE Trans.Inf. & Sys., E81-D(1), 132-136.

Appendix. Maximum Neuron Model (MNM)

In classifying P-dimensional N pixels into M clusters, $M \times N$ neurons are required.

U_{nm} is the input to the nm th neuron, and V_{nm} is the output. $V_{nm} = 1$ if the pixel n is assigned to cluster m, and $V_{nm} = 0$ otherwise. x_{sk} is the density of pixel k in the s th image file, X_k the feature vector of pixel k, and $\overline{X_l}$ the feature vector of the centroid of cluster l in the following equation. nl is the number of pixels classified into cluster l.

$$X_k = (x_1, x_2, ..., x_{pk}), X_l = \frac{\left(\sum_{k=1}^{N} X_k V_{kl}\right)}{nl} \quad 1.$$

The distance between pixel k and cluster l based on the square of Euclidean measure is given as R_{kl} in the following equation.

$$R_{kl} = \left(X_k - \overline{X_l}\right)^2 \quad 2.$$

The objective function is determined by the mean square root when each pixel is classified into suitable clusters as follows:

$$E = \sum_{k=1}^{N} \sum_{l=1}^{M} R_{kl} V_{kl} \quad 3.$$

Generally speaking, the lower the value of E, the better the result of image clustering. The purpose of this clustering problem is to reduce the value of E .In order to converge to the optimum solution by reducing the value of E ,the derivatives of input U with respect to time t are given by:

$$\Delta U_{kl} = -R_{kl} \quad 4.$$

The output V of the maximum neuron is determined by:

$$V_{km}(t+1) = 1 \quad if \quad U_{km} = \max[U_{kl}; \forall : l], \\ 0 \quad otherwise \quad 5.$$

Algorithm of MNM

1. Initialize the input of neurons U with uniform-random values.
2. Use the input-output function of eq.(5) to update the new output values.
3. In each clustering, compute the centered (or cluster means) $\overline{X_l}$ using eq.(1).
4. For each neuron, compute the value of R of eq.(2) and derivatives of eq.(4).
5. For each neuron, update input U using the first order Euler's method:

$$U_{kl}(t+1) = U_{kl}(t) + \Delta U_{kl} \quad 6.$$

6. Go to step 2 until the value of E does not change.

Using Image Information and Partial Least Squares Method to Estimate Mineral Concentrations in Mineral Flotation

J. Hätönen[*], H. Hyötyniemi[*], J. Miettunen[**], L.-E. Carlsson[***]

[*]Control Engineering Laboratory, Helsinki University of Technology
P.O. Box 5400, FIN-02015 HUT, Finland
[**]Outokumpu Mining Oy, Pyhäsalmi Mine
P.O. Box 51, FIN-86801 Pyhäsalmi, Finland
[***]Boliden Mineral AB, Mineral Processing Department
P.O. Box 71, SE-93681 Boliden, Sweden

ABSTRACT

In this paper the possibility of predicting mineral concentrations in the flotation froth by the use of real-time acquired image data and Partial Least Squares (PLS) regression method is investigated. This is a straightforward application of utilising image analysis in the control and monitoring of mineral flotation process. For several reasons this approach should also have potential as an industrial application: the price of the measurement unit is relatively inexpensive, and it will quickly supply grade estimates and also important image parameters such as speed, stability, and size of the froth bubbles. However, it will probably not have the long time accuracy of the conventional on-stream analysers. To test the methodology in practise, a reasonable amount of image data was collected together with froth samples from one of the flotation cells at the Pyhäsalmi mine zinc circuit in Finland. The collected images were processed off-line to extract selected features from the images, and then the PLS method was used to construct a model to predict the zinc concentration in the froth as a function of the extracted image features.

INTRODUCTION

Flotation is one of the most difficult and challenging processes in mineral processing industry. The complexity of the process mainly arises from the inherently chaotic nature of the underlying microscopic phenomena. Additional problems are caused by the fact that today's measurement technology is not able to provide a description of the current state of the process that would be accurate and reliable enough.

Thus, most of the chemical reagents that are used to increase the efficiency of flotation are controlled by the human operators. The operators usually determine the suitable levels of the reagents by analysing the visual appearance of the froth. Also the measurement trends of the on-stream X-ray analysers give important information, i.e. the operator can check whether concentration levels are increasing or decreasing, after a control action by the operator has taken place in the process.

The fast development of information technologies, however, has made it possible to automatically acquire images of the froth in real-time and extract features from the froth image that resemble the more or less heuristic features used by the operators. Thus, the limited capacity of the operator to monitor cells continuously (the operator is usually responsible for several circuits each consisting of many cells) could be increased by installing a video camera over critical cells and connecting the camera to a computer that is able to process grabbed images in real-time. This topic has been studied extensively in the mineral processing community, and various research papers have been published on the subject (see [1], [2], and [3]). However, it seems that few applications exist that would deliver useful information for control and monitoring purposes of the flotation process.

When figuring out potential applications of froth images, one application could be to predict mineral concentration(s) in the froth as a function of the extracted image variables. Usually in the process plants the mineral concentrations in the froth are not analysed. One reason for this is that sampling of an unevenly flowing concentrate coming from an individual cell is very difficult, and the concentrate flow from several

0-7803-5489-3/99/$10.00 ©1999 IEEE.

cells has to be combined, before reliable sampling can be achieved. Secondly, the on-stream analysers are relatively expensive. A plant treating sulphide minerals with Cu, Zn and Pb will typically have over 50 flotation cells and the number of streams analysed on-line will be between 12 and 20. So the predicted mineral concentration(s) based on the image variables would offer valuable information, cutting down the uncertainty in determining as well as implementing a suitable control strategy.

Discussions with the plant operators reveal that mainly by using the colour information from the froth, a rough estimate of the main mineral (in this case zinc) can be given. Consequently, practical experience supports the idea presented in this paper.

MEASUREMENT UNIT AND EXPERIMENTS

The measurement unit consisted of an RGB camera placed above the froth in the first rougher cell. The camera was installed inside a metal hood to protect it against dirt. The geometrical shape of the hood was selected so that homogenous illumination of the froth would be obtained for an easy processing of the images. The camera was connected to a frame-grabber inside a PC so that the images could be saved on hard disc and used for off-line analysis.

The actual tests were carried out as a set of factorial experiments. In these experiments the manipulated process variables airflow, xanthate (collector), copper sulphate (activator), oil (frother) and lime (depressant) had three predetermined reference levels, and during the experiments the manipulated process variables were driven to 81 different combinations of these three levels. By using this approach it was secured that both the froth appearance and mineral concentrations in the froth would have enough variation for building reliable regression models, and at the same time useful process data could be obtained for finding statistically significant dependencies between the image features and process variables.

Each test within an experiment consisted of the following phases. First the reference values of the manipulated process variables were set to the predetermined values. By monitoring different measurement trends in the automation system it could be seen when the process reached a steady-state condition. After that the image grabbing was switched on and images were collected approximately for 10 minutes and at the same time the operator took manually a sample from the froth. The main reason for collecting images over a longer period was to filter out small variations around the steady state.

This same procedure was repeated for each test. Finally zinc, copper, iron and lead content, and the percentage of solids were analysed from the froth samples at the process laboratory of the concentrator plant. The experiment design described above resulted in approximately 3240 images and 81 sample points.

EXTRACTION OF THE IMAGE FEATURES

One of the most important decisions when building any regression model is the selection of variables that are used to build the model. Based on the discussions with the operators, the colour of the froth seemed to be the most important variable when trying to give an estimate of the zinc concentration in the froth. Previous experience, on the other hand, had shown that bubble collapse rate and the spatial variance of the froth speed (heterogeneity) can correlate with the zinc concentration. Thus also these variables were included into the model building.

In order to give an accurate numerical description of the colour of the froth, the shape of the intensity histogram of each channel (R, G, and B) was described using the statistical cumulants *mean, standard deviation, skewness* and *kurtosis*, as defined below. To remove the distorting effect caused by the total reflectance points in the bubbles, only pixel values inside a certain intensity range were included in the calculations.

$$mean = \bar{x} = \frac{1}{N}\sum_{i=1}^{N} x_i \qquad 1.$$

$$standard\ deviation = \sigma = \sqrt{\frac{1}{N-1}\sum_{j=1}^{N}\left(x_j - \bar{x}\right)^2}\ , \qquad 2.$$

$$skewness = \frac{1}{N}\sum_{j=1}^{N}\left(\frac{x_j - \bar{x}}{\sigma}\right)^3, \text{ and} \quad 3.$$

$$kurtosis = \left\{\frac{1}{N}\sum_{j=1}^{N}\left(\frac{x_j - \bar{x}}{\sigma}\right)^4\right\} - 3. \quad 4.$$

The bubble collapse rate and spatial speed variance were calculated using image pairs, where the sampling interval between the two images is 20 milliseconds. The bubble collapse rate measure is based on the pixel-wise difference between successive images (translation effect being eliminated). The number of pixels in the difference image whose value is over a certain threshold is calculated, and this number is directly used as an indicator for the bubble collapse rate.

The amount of translation between image pairs can be seen in the cross-correlation matrix of the two images; the indices of the maximum element in the cross-correlation matrix directly give the translation in x and y directions. The fastest and the most robust method for calculating the cross-correlation matrix is by using the 2-dimensional Fourier transform (see [4]).

Further, the spatial speed variance (actually its inverse) is now defined as the value of the maximum element in the cross correlation matrix; this comes from the fact that the more there is similarity between adjacent images (less spatial speed variance), the higher is the value of the maximum element.

As a result the processing of the images resulted in 14 parameters for each image, as shown in Table 1.

Table 1: Extracted image variables.

Variable number	Variable name	Variable number	Variable name
1	Bubble collapse rate	8	Green std
2	Spatial speed variance	9	Green skewness
3	Red mean	10	Green kurtosis
4	Red std	11	Blue mean
5	Red skewness	12	Blue std
6	Red kurtosis	13	Blue skewness
7	Green mean	14	Blue kurtosis

The calculations were carried out inside Labview environment, where each image processing algorithm was implemented as a Microsoft Visual C++ dll. The basic functionality provided by Labview was used to read the images from the hard disc and to save the numerical results of the different image processing algorithms to an Excel chart, so that the results could be easily transferred to other Windows applications.

PARTIAL LEAST SQUARES REGRESSION

The relationships within the data are often represented using *regression models*, where the output variables are expressed in terms of the input variables. The traditional and widely used multilinear regression (MLR) method is not robust: In practical applications, the variables tend to be dependent on each other, and this *collinearity* of data can ruin the regression model altogether. To enhance the robustness of regression, different kinds of schemes can be implemented; the basic idea is to project the data onto a lower dimensional subspace. The compressed data is thereafter mapped onto the output space (see [7] for details).

One approach to selecting the basis vectors of the internal subspace is to maximise the variance of the projected data; this approach results in principal component analysis (PCA) and regression (PCR) – see [5] and [6]. Even though the collinearity problem can efficiently be avoided this way, the regression models may not be good: because only the input data variance is weighted, its relevance with respect to the outputs

cannot be guaranteed. The solution to this dilemma is partial least squares (PLS) regression: the data is projected so that the *correlation* between input and output variables is maximised [8].

CONSTRUCTION AND VALIDATION OF THE PLS PREDICTION MODEL

At the beginning of the model building the data was divided into two sets, the training data set and the validation data set. The division was done randomly, so that the calibration data set consisted of 60 samples and the validation data set of 21 samples. The training data set was scaled to zero mean and unit variance, because variables did not have equal variance.

Because PLS is inherently a linear method, the detection of possible outliers is an important step. The cross-validation approach used here was to leave data samples out one at a time, and construct a PLS model using the rest of the samples (using a fixed number of latent variables, in this case three). Finally the parameters of the regression vector were plotted as functions of the sample number that was left out. If a certain parameter vector differed considerably (checked by visual inspection only) from the rest of the samples, this sample was classified as an outlier and left out from further modelling. In our case, three samples in the training set were considered as outliers and were left out from further model building.

To maximise the prediction power of the PLS method, a "leave-one-out" cross-validation method was used (see [8]) to determine the suitable number of latent variables for the training set. The method suggested that five latent variables is the optimum number for modelling purposes. The amount of variation explained by each latent variable in both X and Y data is shown in Table 2.

Table 2: The amount of variance explained by different latent variables.

Latent variable	Explained variance in X block	Explained variance in X – cumulative	Explained variance in Y	Explained variance in Y – cumulative
1	68.54	68.54	50.57	50.57
2	13.47	82.01	7.48	58.05
3	8.21	90.22	2.18	60.23
4	6.39	96.62	3.08	63.31
5	1.8	98.42	2.68	65.98

It is useful to note that five latent variables are able to explain 98.42% of the variation in X (image) variables, when the original dimension of the data was 14. Thus the presence of large collinearity in the image data is evident, and standard MLR approach would not have worked.

When the regression model has been built, it is always important to verify that it corresponds to the *a priori* information known from the specific domain. When PLS approach is used, the natural way is to analyse the latent vectors; the latent vectors capture the correlation structures in the data.

In our case the sphalerite (ZnS) mineral is reddish-brown, and so, this colour tone should increase in the froth, when the zinc concentration in the froth increases. Previous correlation analyses carried out for different data sets, on the other hand, had shown that low spatial variance of the froth speed and low bubble collapse rate correlate with high zinc concentration and vice versa. When analysing the contribution of the different latent variables to explain the variance in Y variable (zinc concentration), the first latent variable explained over 50% of the total variance. The rest of the latent variables explained considerably smaller amounts of variance in Y. Consequently the first latent variable seems to explain a global relation between image variables and zinc concentrations, and so the *a priori* known relations should be found in it.

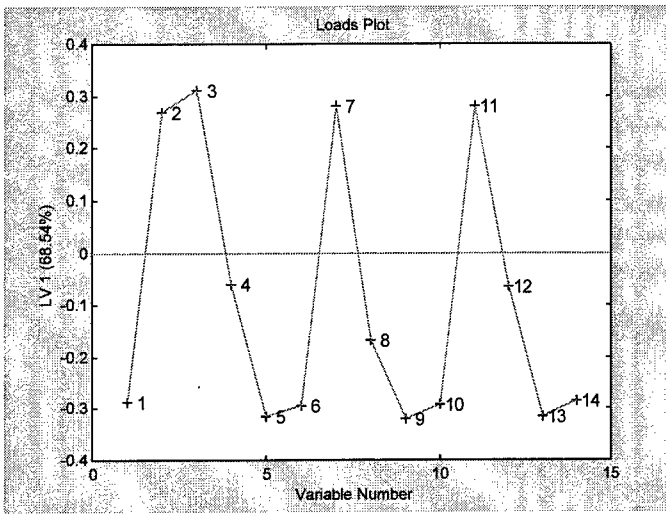


Fig. 1. The first latent variable.

Figure 1 reveals that low bubble collapse rate and low spatial speed variance of the froth are related to high zinc concentration in the froth. The mean value of the red channel seems to play a slightly more important role compared to other channels, which was expected. In addition to this, it seems that also the higher statistical cumulants in each channel have similar behaviour; this suggests that intensity distribution of each channel becomes flatter and skewed to the left, as the froth carries more zinc (this has been further validated in [2]). This result is quite expected, because usually a froth having high zinc concentration tends to have smaller bubbles, and as a consequence there are more dark shadows in the froth compared to a froth having low zinc concentration. Thus, it seems that the model has been able to capture true relations between the image variables and the zinc concentration.

To finally test how well the model is really working, validation data is used. Figure 2 shows how accurately the obtained model can predict samples in the validation data set using five latent vectors.

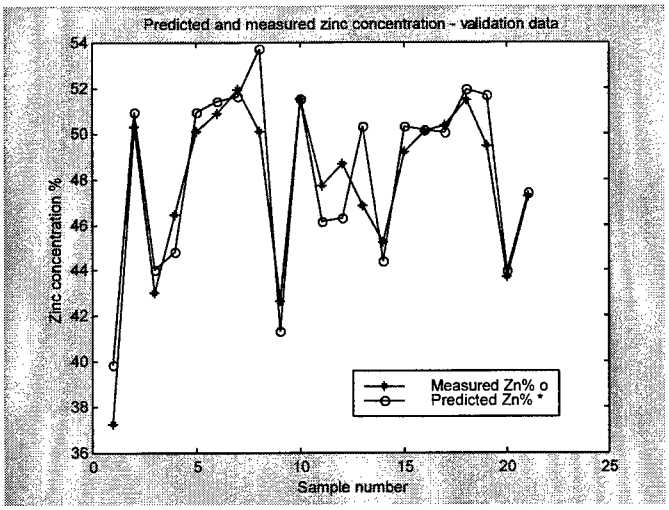


Fig. 2. The actual and predicted zinc concentrations in the validation data set.

The average prediction error is 1.4% Zn and the maximum error is 3.4% Zn in the validation data set. These results can be considered fairly good, because the predictions are made over a very wide range of zinc concentrations. It also seems that the model is able to react to large changes in the zinc concentration, but smaller variations are not predicted so accurately. The main reason could be that colour measurement with a standard RGB camera is not accurate enough, which is also the result obtained in [9].

CONCLUSIONS AND FURTHER WORK

In this paper it has been presented how image data can be used to predict mineral concentrations in the froth by the utilisation of a PLS approach. As a linear method, PLS results in a transparent model that is easy to validate against *a priori* information. It was shown that PLS is an easy and fast method for building linear regression models to predict mineral concentrations in the froth, even when the input data is highly collinear. It turns out that in many cases the linear methods may be *smarter* than the "intelligent" ones!

PLS also includes a variety of different tools for statistical hypothesis testing. For example, when new data arrives, it can be checked whether the model for X data can explain it statistically significantly (so called distance to model approach), and if not, the model is probably no more valid and re-calibration has to be carried out [8]. Thus PLS framework contains a lot of additional functionality that is useful in practical modelling and prediction work.

However, the authors are aware that there are still problems to be solved, before the method can be used for predicting mineral concentrations in the froth in practise. The first problem is the variations in the quality of the incoming ore, which sometimes means that also the colour of the ore changes. Thus, some kind of automatic re-calibration procedure would be needed in order to overcome this problem, resulting in more complex and expensive set-up. The second problem is to guarantee the accurate measurement of the colour. As earlier said it seems that standard RGB camera is not accurate enough for measuring the colour of the froth (see [9]). Accordingly, a more accurate measurement method should be used; for example, a spectrophotometer could be a potential solution. Also the lamp used for illumination causes inaccuracies in colour measurement because the lamp loses its power due to ageing, and some kind of reference measurement should be used in order to eliminate this phenomenon.

ACKNOWLEDGEMENTS

The work described was financially supported within the framework of the ChaCo (*Characterisation of Flotation Froth Structure and Color by Machine Vision*) Esprit Long Term Research Project N.24931.

REFERENCES

1. A. Cipriano, M. Guarini, R. Vidal, A. Soto, C. Sepúlveda, D. Mery, H. Briseño, 1998. A real time visual sensor for supervision of flotation cells. Minerals Engineering, 11 (6), pp. 489–499.
2. A.J. Niemi, R. Ylinen, H. Hyötyniemi, 1997. On characterization of pulp and froth in cells of flotation plant. Int. J. of Mineral Processing, 51, pp. 51–65.
3. D.W. Moolman, C. Aldrich, J.S.J van Deventer, D.B Bradshaw, 1995. The interpretation of flotation froth surfaces by using digital image analysis and neural networks. Chem. Eng. Sci., 50 (22): 3501–3513.
4. E.O. Bringham, 1988. The Fast Fourier Transform and Its Applications. Prentice-Hall, London, UK.
5. A. Basilevsky, 1994. Statistical Factor Analysis and Related Methods. John Wiley & Sons, New York.
6. J. Hätönen., H. Hyötyniemi, G. Bonifazi, S. Serranti, F. Volpe, L.-E. Carlsson, 1999. Using PCA in controller strategy design for a flotation process. Preprints 14th IFAC World Cong., July 5–9, Beijing.
7. H. Hyötyniemi, 1998. Summary – on linear multivariate methods. In Multivariate Statistical Methods in Systems Engineering. Helsinki Univ. of Tech., Control Eng. Lab., Report 112. available on the Internet at http://saato014.hut.fi/Hyotyniemi/publications/98_report112.htm.
8. H. A. Martens, 1985. Multivariable Calibration – Quantitative interpretation of non-selective chemical data. Doctoral Thesis, Technical University of Norway, Trondheim, Norway.
9. A. Siren, 1999. The characterisation of Froth Colour by Machine Vision. Preprints of the EOS/SPIE International Symposia, June 14–18, Munich, Germany.

A Combined Morphological and Color Based Approach to Characterize Flotation Froth Bubbles

Giuseppe Bonifazi, Silvia Serranti, Fabio Volpe, and Riccardo Zuco

Dipartimento di Ingegneria Chimica, dei Materiali, delle Materie Prime e Metallurgia
Università di Roma "La Sapienza", Via Eudossiana 18, 00184 Rome, Italy

ABSTRACT

Flotation process monitoring and control are complex targets due to the highly non-linear behavior of the process and the large number of variables involved. Control is generally achieved by adopting a human based approach. By observing the surface of flotation cells, experienced plant operators suggest, on the basis of their experience, control actions such as changing the cell level set points and/or modifying reagent doses. The main goal of this paper is to demonstrate that with a combined approach based on evaluation of the morphological and morphometrical features of froth bubbles and their color characteristics, it is possible to perform a froth structure analysis. Froth structure modeling permits us to derive useful information about the flotation process behaviour. The structure analysis carried out by means of digital imaging procedures based on color, texture and morphometry enables definition of froth classes that define mineral concentration using estimation models set up from an analysis of froth images. The paper shows that by adopting such an approach, it is possible to identify different froth classes and utilize the results inside estimation models.

INTRODUCTION

It is well known that flotation is a very complex process. Its characteristics are strongly affected by many factors related both to the ore (grade, particles size distribution, particles morphology, degree of liberation of the size classes to float, particle surface properties, etc.) and the process itself (variation in operating conditions). In the past, many attempts with different levels of intervention on the process have been carried out to attempt to control the process by adopting different strategies of data collection. As a result the developed procedures are in many cases insufficient to realize optimal control of the process with the resulting strategies being "too heavy" to be handled by plant operating personnel.

On the other hand very sophisticated control techniques need long periods of tuning and can be set up only by skilled control engineers who are not always "available" in terms of time and costs [1]. Flotation presents intrinsic characteristics that especially in the past, were largely utilized, at a heuristic level by plant operators. According to the behavior of the process, flotation froths present different pictorial aspects. Such aspects are strongly correlated with the grade and recovery of valuable minerals in the concentrate. Woodburn et al. [2] was the first to remark that an optimal froth structure can be recognized visually, and that the image can be quantitatively characterized by image analysis techniques. After these studies several works have been published dealing with image processing/analysis procedures applied to flotation froth characterization. They describe several techniques, different approaches and application, but they were mainly oriented to analyze or to solve a specific target strictly linked with a specific process. For these reasons as well-evidenced by Moolman et al. [3], such work did not analyze in depth the problems arising when a full digital imaging based procedure is applied to complex image samples such as flotation froths. Even though they give a great contribution to the development and application of such an approach, the results obtained demonstrate, one time more, the complexity of the problem and that further research is needed to realize a vision system to perform the required detection and processing. The main issues still to be addressed relate to both the image analysis and flotation sides of the problem. In this paper, we analyze, discuss and critically evaluate problems encountered when an approach is to be developed to analyze flotation froth characteristics at the plant level in terms of bubble shape and color adopting a fully automatic approach based on digital imaging oriented to numerically define and identify froth classes and consequently to formalize numerical models estimating the concentration of valuable minerals inside the froth.

0-7803-5489-3/99/$10.00 ©1999 IEEE.

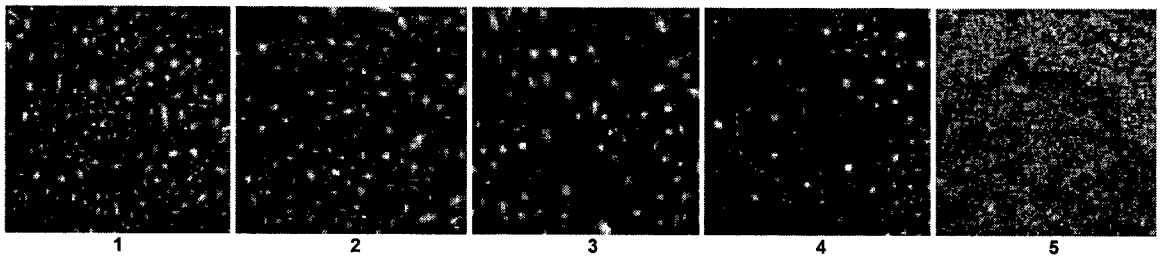


Fig. 1. Pictorial examples of flotation froth classes as they result from "human based" classification. 1: class consisting of quite small bubbles, with an elliptical shape. 2: class consisting of medium sized bubbles, with regular shape. 3: class consisting of regular large bubbles. 4: class consisting of circular bubbles, with both large and small bubbles. 5: class consisting of tiny bubbles. The froth is more like a mud.

DIGITAL IMAGE SAMPLES AND FROTH CLASS DEFINITION

About 1500 digital images of flotation froths have been acquired during 56 experiments made in 1997 in Boliden plant in Garpenberg (Sweden). The camera was placed on the copper-lead circuit on the first scavenger cell. Each experiment was up to 5 minutes long, and produced up to 15 samples. Every sample consisted of two pictures in a pair taken with a delay of 0.2 seconds. A delay time of 20 seconds was adopted between each image pair acquisition. At the same time the pictures were taken, the corresponding froths were sampled and the %Cu, %Zn, %Pb and %MgO concentrations were analyzed. The goal of this first phase was to define froth classes. Since the total number of images was very high, the dataset used for froth class definition was a subset of the original. It must be understood that images belonging to the same experiment have similar macro-features; so, it was possible to take only one image from each experiment in order to assign the images of a specific experiment to one class. The prepared dataset consisted of one image from each experiment. Each image, constituting the reference data, was taken at the same time (60 seconds) from the beginning of each experiment. All acquisitions were made in full color, so RGB (red, green and blue) images with a 24 bit-depth per pixel was processed. The resolution of each image was 288x384 pixels.

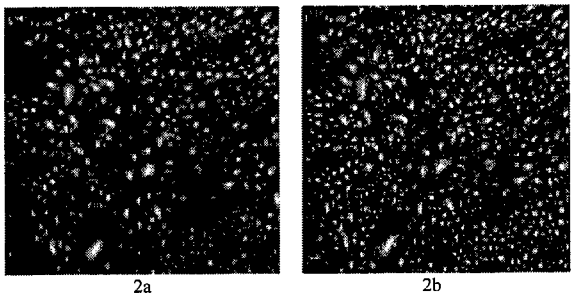
Once the database was created, three people, not expert in image processing, but with good scientific and cultural level, were selected. They were supplied with the images of the database, and they were asked to define some classes and to assign each image of the database to one of the classes. The results were remarkably homogeneous. Four classes were defined according to shape and size of the flotation froth bubbles. The identified classes, defined by non experts, weree then analyzed by experts. As a result of this additional analysis, a new class, based on color characteristics, was added to the original four classes. So a total of five froth classes were identified (Figure 1):

- Class 1: consisting of quite small bubbles, with an elliptical shape.
- Class 2: consisting of medium sized bubbles, with regular shape.
- Class 3: consisting of regular large bubbles.
- Class 4: consisting of circular bubbles, with both large and small bubbles.
- Class 5: consisting of very small bubbles, and the froth is more like a mud.

Assignment of each image to one of the classes gaves varying results according to the "non experts", but the discrepancies were not great. An expert supervised the human-based classification/assignment to solve ambiguous cases. Each image coming from Garpenberg plant was thus assigned to a specific class.

FROTH BUBBLE CHARACTERIZATION

In order to generate a morphological and color characterization of the froth, the first step was to select a method for bubble identification and a method to analyse froth color. In order to segment the froth image to identify and characterize each bubble, morphologically and morphometrically, the watershed technique was applied [4]. Several parameters were identified, computed and averaged for each processed image for morphological characterization of the froths. Froth color characterization is carried out by adopting two different approaches: i) color features analysis applied to the whole image sets in different color spaces and ii) color feature analysis of single bubbles in different color systems.



2a 2b

Fig. 2. Source image (2a) and corresponding segmented image (2b) after applying different enhancement techniques followed by the watershed filter.

Froth Image Segmentation

Image segmentation partitions the spatial domain into mutually exclusive subsets, called regions, each one presenting uniform, homogeneous characteristics with respect to a property such as tone or texture but with one property differing in some way from that of its neighbors. Image segmentation is a crucial step, especially when specific domains of the image (bubbles) must be numerically characterized and classified for recognition. The quality and interpretation of measurements of different parts of an image depend critically on the "quality" of segmentation which assigns pixels to a particular class. Different methods are available:

Region-based Approach (RBA): assign pixels to regions/objects (thresholding or watershed segmentation).
Boundary-based Approach (BBA): locate regional boundaries (boundary-tracking, Laplacian filtering).
Edge-based Approach (EBA): identify edge pixels and link them to form boundaries.

The Watershed Algorithm

In this work a RBA (watershed) was used. The intensity of the froth image was used as a DTM (Digital Terrain Model) with the elevation related to the tone of the pixels in the image. The watershed segmentation algorithm is based on flooding of a landscape or topographic relief with water, on the piercing of the holes at the position of local minima and on the immersion of the landscape into a lake. Basins will fill with water starting at local minima, and at points where water coming from different basins would meet, dams are built. When the water level has reached the highest peak in the landscape, the process is stopped. The set of dams obtained partitions the region into catchment basins. These dams, projected on the horizontal plane, are the watershed lines. A recursive algorithm exists to compute the watershed transform [5]. The basic structure of the algorithm is a loop in which the image is thresholded at successive gray levels. At each iteration, the basins belonging to the minima are extended by their influence zones within the binary image obtained by thresholding at the current gray level. The watershed transform can suffer from severe over-segmentation. This requires preprocessing the images by applying edge detectors and smoothing filters (Figure 2).

The procedure adopted is as follows. The RGB (Red, Green and Blue) source images of froth are first cut with a window of 256x256 pixels to make them comparable and to eliminate black borders, then the intensity channel is extracted. The best image enhancement is accomplished with application of a sharpening filter. Evaluation of the maximum frequency from the gray level histogram of each image is then performed. This value, recalculated as a percentage, is assumed as the threshold value for the watershed filter. With application of the watershed filter to the images, bubble segmentation is obtained [6].

Froth Image Morphological Parameters

For each segmented image, a list of geometrical/morphological parameters (i.e. area, aspect, area/box, box/xy, major and minor axis, min/max diameters, min/max radius, perimeter, roundness, length, width, etc.),which describe a single bubble, is computed. In order to obtain a single value for the whole image morphology, the value of each parameter is averaged over all bubbles with an area exceeding 15 pixels. For each image, 42 output parameters (means and standard deviations) are identified and computed.

Froth Image Color Algorithm

The color algorithms used for the test are based on the color of the froth. They simply computes average values and standard deviations at image level, using the whole image or the segmented images (that is, considering only bubbles with an area exceeding 15 pixels) in the 3 color spaces: RGB (red, green, blue),

HSV (hue, saturation, value) and IHS (intensity, hue, saturation). No significant differences were detected following single domain (bubble) or the full image color approach.

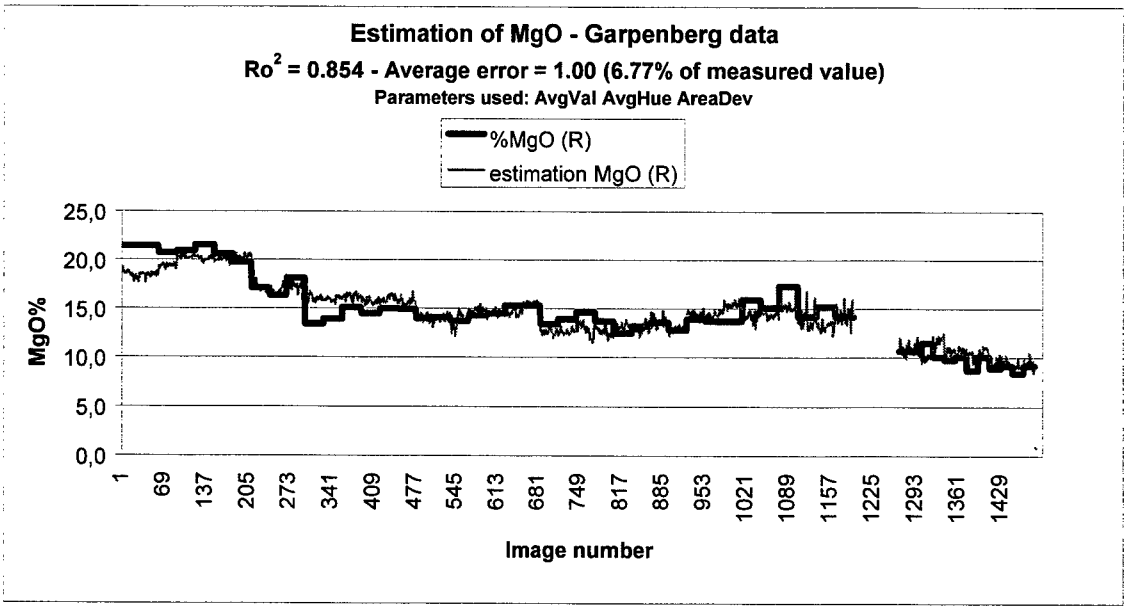


Fig. 3. Relationship between computed %MgO and the same value from lab tests (talc concentration). The parameters used for the estimate are *AverageValue*, *AverageHue* and *AreaDeviation*.

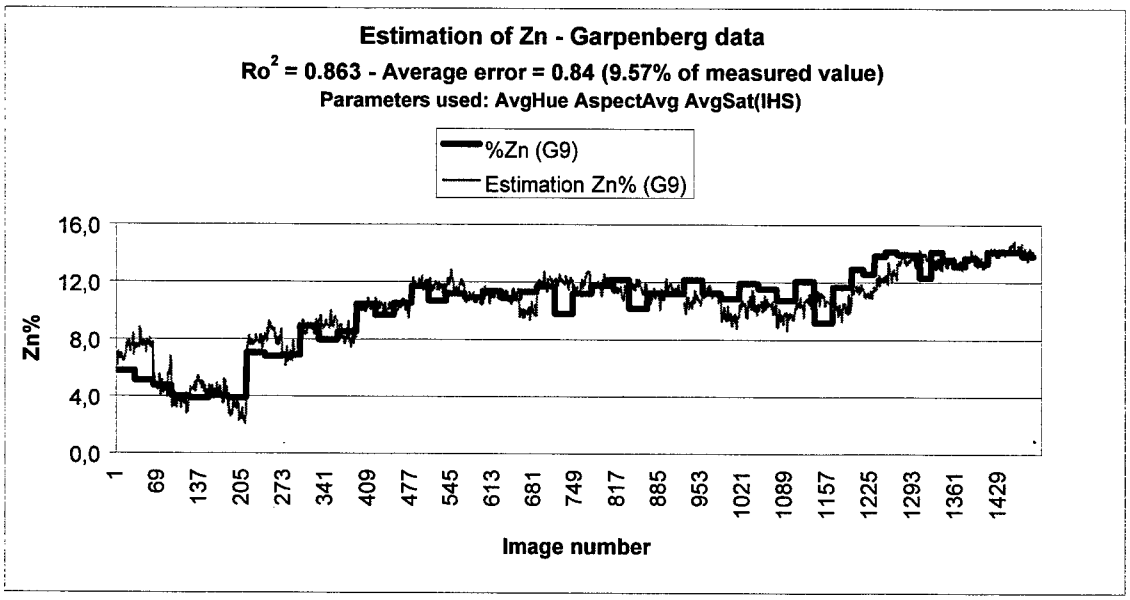


Fig. 4. Relationship between computed %Zn and the same value obtained from laboratory tests. The parameters used for the estimate are *AverageValue*, *AverageAspect* and *AverageSaturation*.

ESTIMATION OF MINERAL CONCENTRATION

Statistical Models

Estimation has been carried out for copper (Cu), zinc (Zn) and talc concentration (MgO). It has been supplied with a satisfactory average error. The quality of the estimation has been quantified by means of regression analysis (the R_o^2 of the distribution, the average and maximum error).

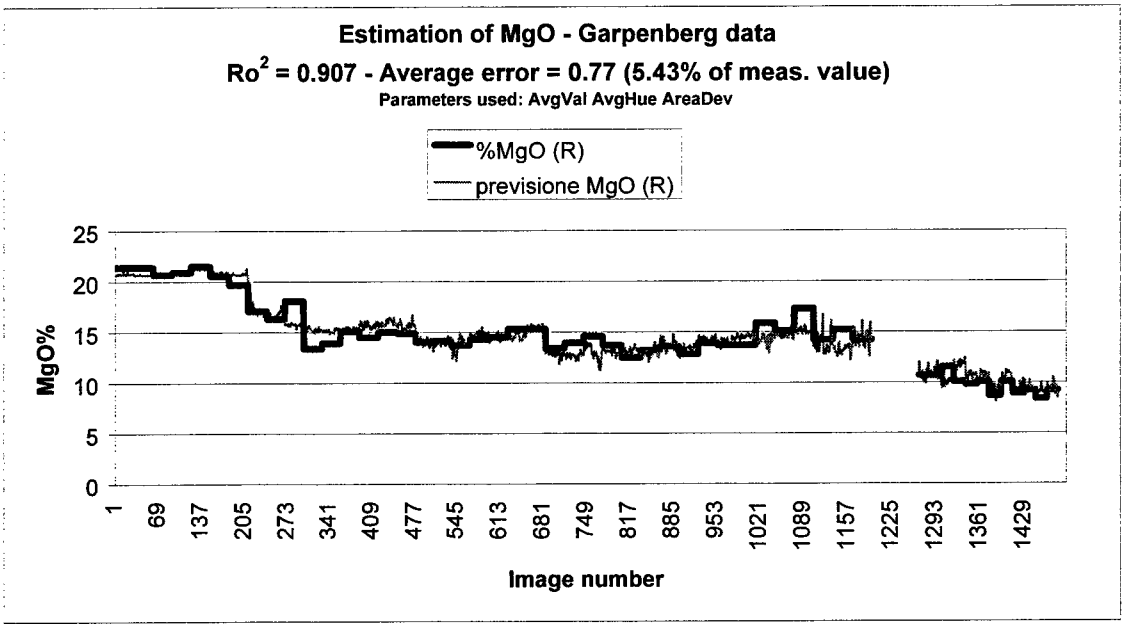


Fig. 5. Relationship between computed %MgO and the same value from laboratory tests. The analyses have been carried out considering the different identified froth classes. The parameters used for the estimate are *AverageValue*, *AverageHue* and *AreaDeviation*.

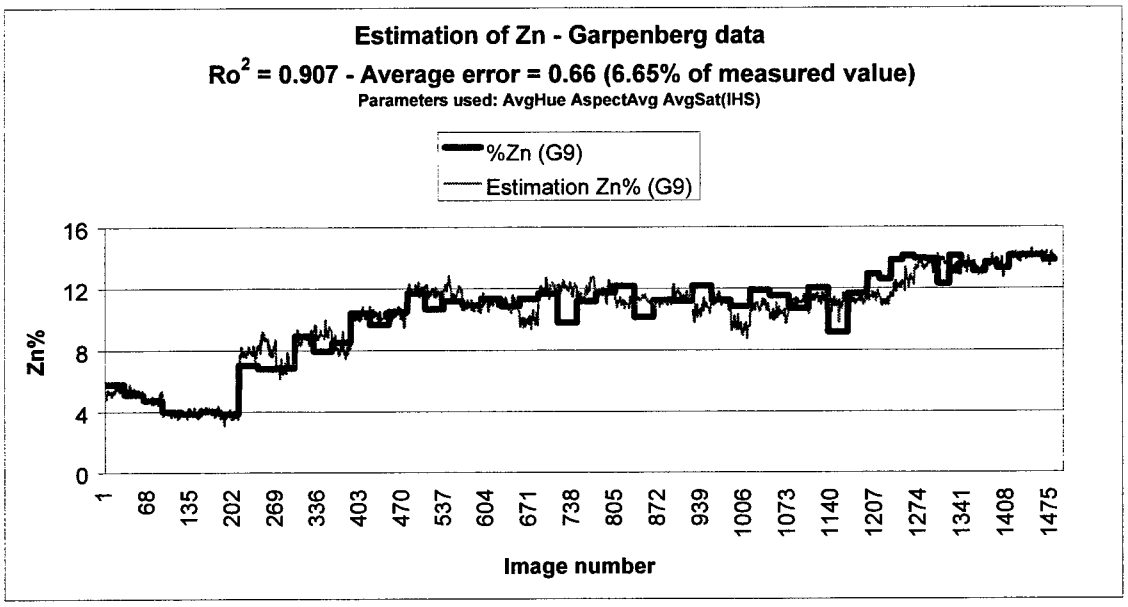


Fig. 6. Relationship between computed %Zn and the same value from laboratory tests. The analyses were carried out considering the different identified froth classes. The parameters used for the estimate are *AverageValue*, *AverageAspect* and *AverageSaturation*.

The analyses applied to the whole set of digitally collected images produce as a result: i) an average error on MgO concentration of about 1.00 %, i.e, 6.8% of the real value, with an R_o^2 of 0.854; ii) an average error on the computed Zn value of about 0.84 %, i.e, 9.6% of the real value, with an R_o^2 of 0.863 and an average error on the computed Cu value of about 0.23 %, i.e., 33.9% of the real value, with an R_o^2 of 0.823. The expressions for the estimated mineral concentration were derived from a subset of the original images, and the resulting correlation was applied to the remaining images. The approach is based on the definition of a single expression that can fit the mineral concentration on all samples (images). From an analysis of Figures 3 and 4 it is evident there are some groups of images (each one belonging to the same experiment, presenting the same

value of concentration in the investigated element) for which the estimation expression gives the worst results. For example, in the case of talc, the average error of 1.00 %, it is possible to see from Figure 3 the error on the first experiment (image number ranging from 1 to 30) is quite high. The same situation is present in at least two or three other experiments (image number ranging from 241 to 298). For zinc, especially in the second experiment (image number ranging from 31 to 60), there are high discrepancies between computed and measured values. If these discrepancies relate to macroscopic froth differences, as it does, the idea of mineral computation expressions depending upon macro-features may be appropriate.

Critical Froth Classes and Statistical Models

In order to improve the estimate of mineral concentration, froth classes are accounted for in the analyses. All images are assigned to one of the five classes previously identified. For each class, the correlation is checked and, if the accuracy is under the global level, it is re-computed. The result is a marked improvement in the estimation correctness (Figures 5 and 6) as compared with the results in Figures 3 and 4 respectively. The estimation of "difficult" experiments has improved, and the R_o^2 of the regression has increased to 0.907 both for talc (from 0.854) and zinc (from 0.863). The average error decreased from 1.00 to 0.77 % for MgO, and from 0.84 to 0.66 % for Zn. The maximum error also decreased from 3.77 to 3.35 % for MgO and from 3.65 to 2.72 % for Zn. In the case of Cu, the R_o^2 increased from 0.823 to 0.894 and the average error decreased from 0.23 to 0.20 %. Introduction of critical froth classes strongly improved the quality of the estimates. The results obtained with "froth classes" must be considered satisfactory; the R_o^2 values are all close to 0.9 and estimation of the concentration value is not far from reality.

CONCLUSION

The adoption of a combined morphological and color based approach to characterize flotation froth bubbles has been demonstrated, with reference to the analyzed digital image sample set, to be quite promising; giving in some cases excellent results and permitting to define procedures suitable to be implemented inside specific control engines. The extensive studies enhanced as the procedures, originally designed and applied, results quite sensitive to i) bubble segmentation algorithms and ii) the definition of critical froth classes to introduce inside the estimation procedures. With reference to this last point it is important the definition of suitable classification procedures in order to operate an “a-priori” assignment of froths to critical classes. The possibility to operate such "a-priori" classification will permit design of "on-line" software architectures to compute to which class a froth belongs and then estimate the unknown mineral concentration by means of algorithms linked to each class. In order to reach this goal, recognition algorithms for classification of the processed froths are under study. The results will be published soon.

ACKNOWLEDGEMENT

This work was financially supported within the framework of ChaCo (Characterization of Flotation Froth Structure and Color by Machine Vision) Esprit long term RP-N.24931 of the EEC. Froth image acquisition and chemical data collection and analyses were carried out by Boliden AB at Garpenberg processing plant.

REFERENCES

1. D.J. McKee, 1991. Automatic flotation control - a review of 20 years of effort. Miner. Eng., 4, 653-66.
2. E.T. Woodburn, J.B.Stockton and D.J. Robbins, 1989. Vision-based characterization of three-phase froths. International Colloquium. Developments in Froth Flotation, South African Inst. of Min. and Met., Gordon's Bay, RSA, 1, 1-20.
3. D.W. Moolman, J.J. Eksteen, C. Aldrich and J.S.J. Van Deventer, 1996. The significance of flotation froth appearance for machine vision control. Int. J. Miner. Process., 48, 135-158.
4. S. Beucher, F. Meyer, 1993. Morphological approach to segmentation: the watershed transformation. In: Math. Morphology and Image Proc. (Ed., Dougherty E.R.), M. Dekker, NY, 433-81.
5. L. Vincent and P. Soille, 1991. Watersheds In Digital Spaces: An Efficient Algorithm Based On Immersion Simulations. IEEE Trans. Pattern Anal. Mach. Intell., 13, 583-598.
6. G. Bonifazi, S.Serranti, F. Volpe, R. Zuco, 1998. Flotation froth characterization by optical-digital sectioning. 4th Inter. Conf. on Quality Control by Artificial Vision. Takamatsu, Japan, 131-137.

A Robust Bubble Delineation Algorithm for Froth Images

Weixing Wang and Ove Stephansson

Engineering Geology, Department of Civil & Environmental Engineering
Royal Institute of Technology, SE-10044 Stockholm, Sweden
E_mail: weixing.wang@imenco.se, ove@aom.kth.se

ABSTRACT

This paper describes a robust segmentation algorithm for froth images from flotation cells in mineral processing. The size, shape, texture and color of bubbles in a froth image is very important information for optimizing flotation. To determine these parameters, the bubbles in a froth image have to be delineated first. Due to the special characteristics of froth images and a large variation of froth image patterns and quality, it is difficult to use classical segmentation algorithms. Therefore, a new segmentation algorithm was developed to delineate every individual bubble in a froth image.

A new segmentation algorithm based on valley-edge detection and edge tracing has been developed. In order to detect bubble edges clearly and disregard the edges of the white spots, the algorithm just detects valley-edges between bubbles in the first step. It detects each image pixel to find if it is the lowest valley point in a certain direction. If it is, the pixel is marked as an edge candidate. Before this procedure, to alleviate noise edges, an image enhancement procedure was added to filter out the noise pixels.

After valley-edge detection, the majority of edges are marked at one time, but some small gap between edges, and noise still exist in the image. To reduce the noise, a clean up procedure was developed. To fill the gaps, an edge tracing algorithm was applied, in which, edges are smoothed into one pixel width. Endpoints and their directions are detected, and edge tracing starts from the detected endpoints. When a new valley-edge pixel is found, the algorithm uses it as a new endpoint, and the valley-edge tracing procedure continues until a contour of a bubble is closed.

The segmentation algorithm has been tested on images from Pyhäsalmi mine in Finland and Garpenberg mine in Sweden. The processing speed of the algorithm is much faster than for normal morphological segmentation algorithms. The processing accuracy is better than that of manual segmentation result.

Keywords: image enhancement, valley-edge detection, segmentation, froth image, bubble delineation.

INTRODUCTION

The project ChaCo (Characterization of Flotation Froth Structure and Color by Machine Vision) is conducted within Esprit-RTD in Information Technologies of the 4th EU - program. The aim of the project is to develop an on-line optical system for monitoring mineral froth and to optimize flotation in mineral processing. The system consists of three parts: (1) illumination system for grabbing high quality froth images; (2) image processing and analysis which will provide the visual information for froth modeling ; and (3) froth modeling for controlling mineral processing. For image processing and analysis, image segmentation is very important for classification and for analyzing bubble mobility, stability, color, texture, size and shape.

In order to recognize the characteristics of froth images, hundreds of images were investigated. The results show: (1) bubbles touch each other and there is no void space (background) between bubbles; (2) the illumination on the bubble surface is uneven; (3) the edges between bubbles are weak, and (4) strong edges exist at the border of specularity regions (white spots). All the characteristics mentioned make segmentation algorithm development of froth images complicated. During the investigation, several commercial software for image segmentation were used. Previous aggregate segmentation algorithms [1-3] were tested too. The segmentation testing results indicated that:

0-7803-5489-3/99/$10.00 ©1999 IEEE.

- It is impossible to use intensity similarity to segment bubbles in a froth image, because the gray value variation between bubbles is too small, and the variation in the interior of a bubble is large. The segmentation results gave both over-segmentation and under-segmentation problem.
- The classical edge detection functions fail to segment froth images [4], the reason is that boundaries between bubbles have a low gradient magnitude value, and the boundaries on the specularity parts (white or light spots) have a high gradient magnitude value.
- The morphological segmentation algorithms (e.g. Watershed) can only be used for froth images where the maxima in a bubble is easy to find. For most cases, this is extremely difficult [4-7].

For forth image investigation and segmentation testing, we developed a new segmentation algorithm based on valley-edge detection and edge tracing. The new algorithm contains: image enhancement and valley-edge detection, and edge smoothing and tracing.

IMAGE ENHANCEMENT AND VALLEY-EDGE DETECTION

In a froth image, the characteristics of surface bubbles are shown in Fig.1. Areas with high gray values are white sports (e.g. areas between lines 2 and 3, 5 and 6, 8 and 9), the boundaries between bubbles are marked at lines 1, 4 and 7, where edge strength is weak. The classical edge detectors cannot be used for this kind of images. The main reasons for this is: (1) white (or light) spots which are on the interion of bubbles affect edge detection results strongly; and (2) the gray value changes at the edges between bubbles are not significant when applying the classic edge detection algorithms.

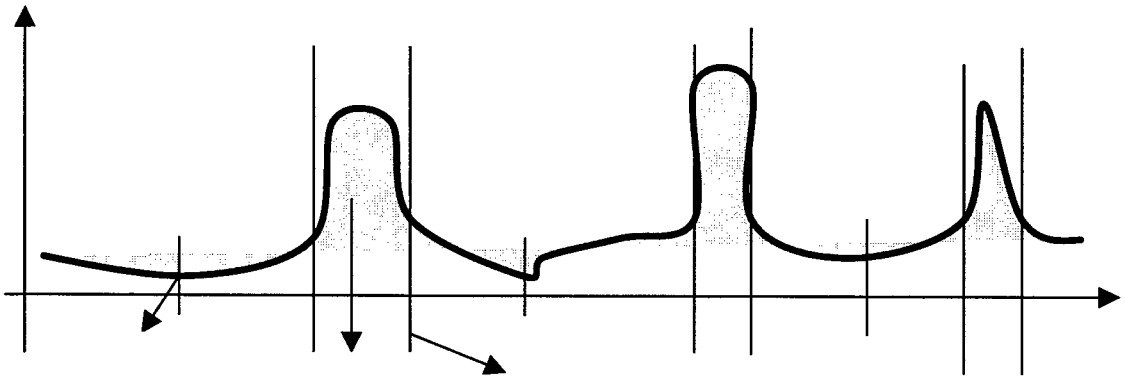


Fig. 1. Gray value versus pixels of a schematic cross-section of a froth image.

Fig. 2a is an example of an original froth image, and Fig. 2b is the gradient magnitude image where high strength edges are located on the boundaries of white spots inside bubbles. The edges between bubbles are very weak.

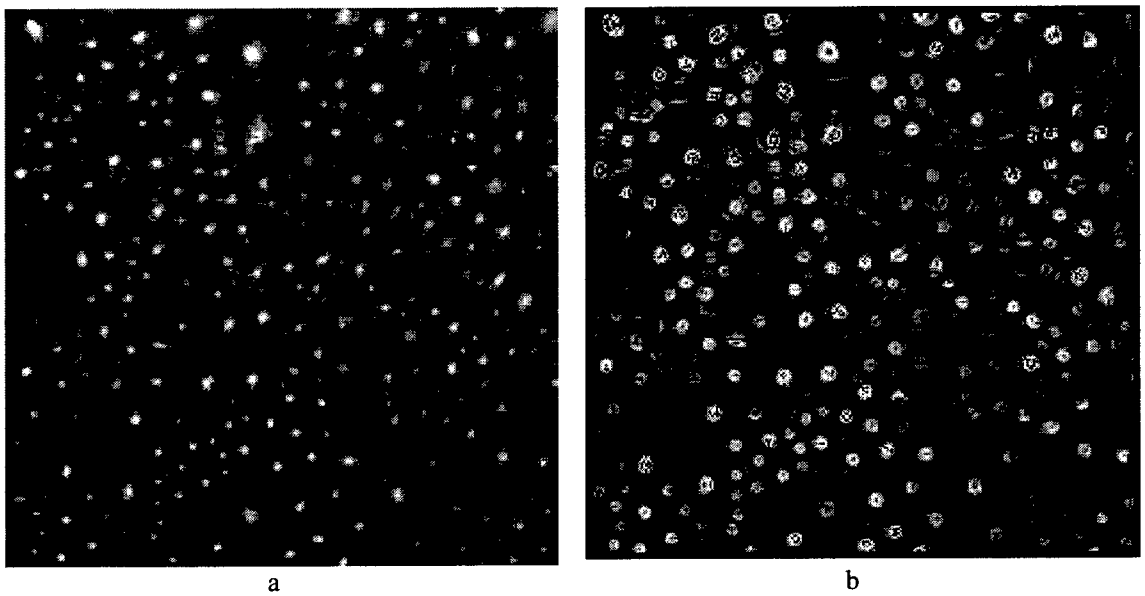
In order to detect bubble edges clearly and disregard the edges of the white spots, a new valley-edge detection algorithm is developed as follows:

The new valley-edge detection algorithm detects each pixel to see if it is the lowest valley point in a certain direction. If it is, the pixel is used as the valley-edge candidate, and its direction and location are marked. In Fig. 3, when detecting pixel p, we check different directions to find out if p is the valley-edge point. If it is, it is marked as a valley-edge candidate. The diameter R is pre-determined on image resolution and quality.

To understand the basic idea, we assume that a froth image is f, at p point, its gray value is $f(i,j)$, and in the α direction, the gray values of five lines on the left side is $l1$, $l2$, $l3$, $l4$ and $l5$, on the right side $r1$, $r2$, $r3$, $r4$ and $r5$, and $l0$ and $r0$ is $f(i,j)$.

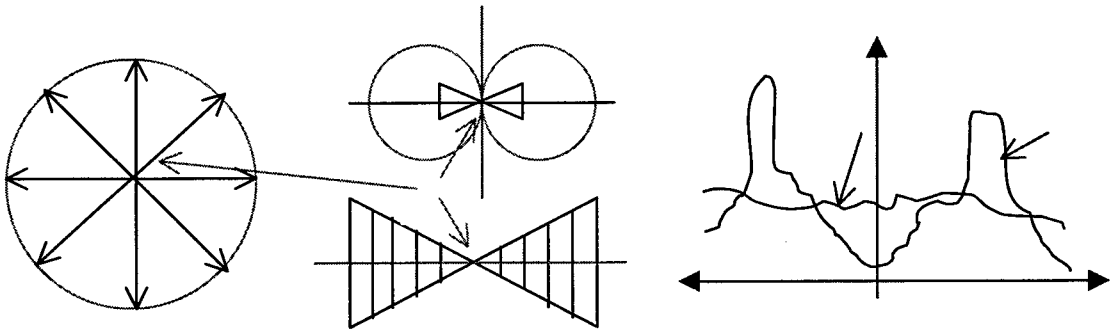
We calculate parameter $V\alpha$ according to Eqs. (1) and (2). If $V\alpha$ is greater than a pre-determined threshold T, the detected point p can be accepted as a valley-edge point.

The gray value for each of the lines in a triangle (see Fig. 3b) can be a weighted average gray value or a median gray value, which is determined based on the number of pixels in each line and image quality. In real applications, the lines can be curves. The number of detecting directions can be decided on the image resolution and bubble size (pixel unit). One question to be resolve in this algorithm is how to select a threshold T, a simple threshold may fail to detect some valley-edges. To increase the detection accuracy, one option is to set up two thresholds $T1$ and $T2$ ($T2 > T1$). When $V\alpha > T2$, the detecting point is accepted as a valley-edge point, but when $T1 < V\alpha < T2$, the detecting point might be a valley-edge point, it is uncertain. For this uncertainty or vague situation, fuzzy mathematics are applied. Detailed discussion and practice of this method will be discussed in a following paper.



a b

Fig. 2. Edge detection result of a froth image. a: Original froth image, b: Gradient magnitude image.



a b c

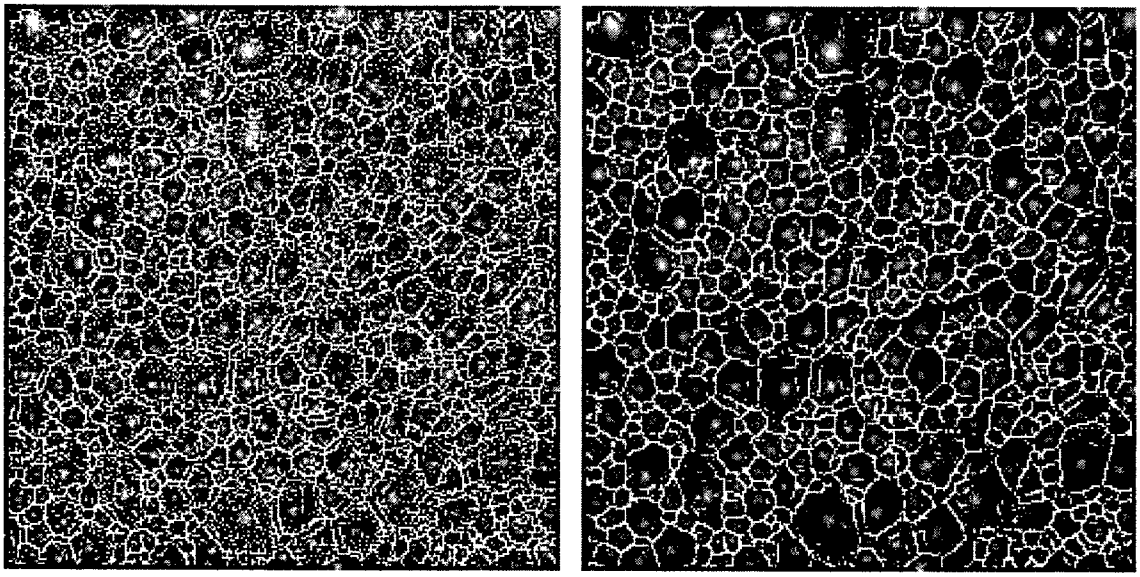
Fig. 3. The diagram for valley-edge detection algorithm. **a:** assuming a circle (diameter R) surrounding the detected point p, with four basic detecting directions (0, 45, 90 and 135 °), **b:** p is a valley point between 2 bubbles in the α-direction, its detecting area is 2 triangles, in each of the triangles, there are 5 lines of pixels, so, the diameter R of the circle in Fig. 3a is 11 pixel units; **c:** curves show that detecting point p is a significant valley-edge point in the α-direction, but not in β-direction .

$$V_{\alpha l} = \sum_{k=1}^{5} w(k) \cdot (l_k - l_{k-1}); \qquad V_{\alpha r} = \sum_{k=1}^{5} w(k) \cdot (r_k - r_{k-1}) \tag{1}$$

where $w(k)$ is a weight function (here k=1,2, ... 5).

$$V_{\alpha} = V_{\alpha l} + V_{\alpha r} \geq T, \quad V_{\alpha l} \geq 0 \quad and \quad V_{\alpha r} \geq 0 \tag{2}$$

Figure 4a shows the detection result from the image in Fig. 2a, where most of the valley points are marked, but there is still much noise in the image. To alleviate the noise, two image enhancement functions are added; one is used prior to valley-edge detection, and another is used as a post-processing function.



a b

Fig. 4. Valley-edge detection results of a froth image.
a: Valley-edge detection directly on an original image (see Fig.2a),
b: Valley-edge detection on smoothed image, in which, an average smoothing filter is used.

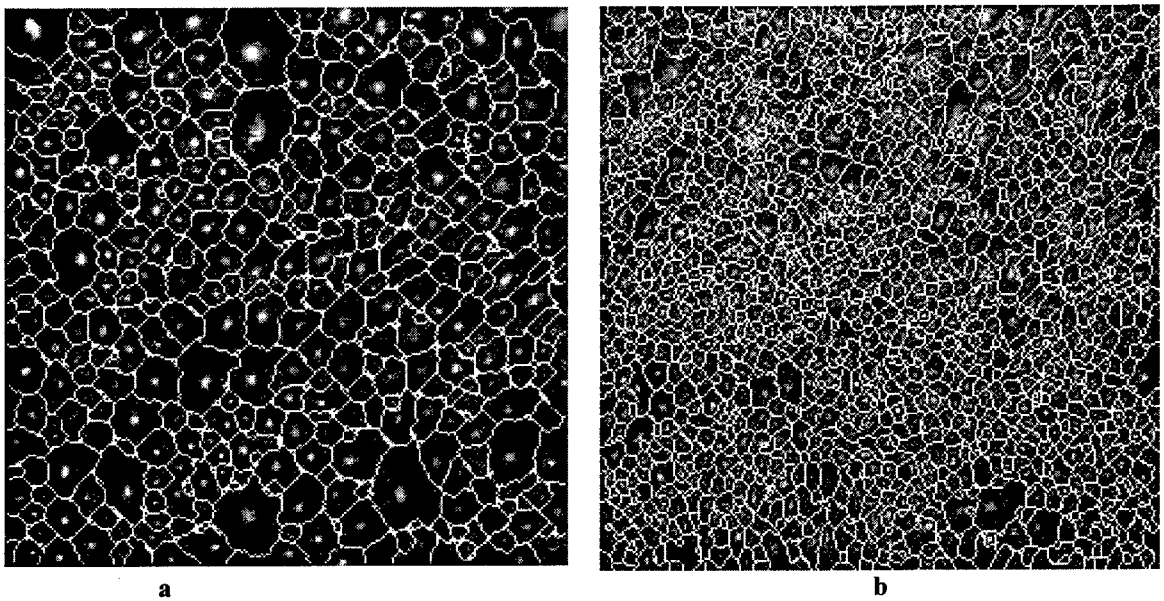
Normally original images include a lot of noise which affect valley-edge detection results. One simple way to reduce noise is to use a smoothing filter such as a Guassian smoothing function. After valley-edge detection, the image is shown in Fig. 4b, where most significant edges exist in the image. As the resulting image is not completely satisfactory, a post-processing subroutine must be added. In post-processing, several functions are used, namely: thinning, small gaps linking, short curve or line removing etc.

EDGE TRACING

After image enhancement and valley-edge detection, the valley-edges are smoothed into one pixel width, but some gaps and noise still exist in the image. To close the contours of bubbles, one must perform edge tracing or contour tracing. To do this, the new algorithm detects significant endpoints of curves (or lines), then estimates the directions for each endpoint based on local valley-edge pixel directions. Finally the algorithm traces contours according to the information of directions of each newly detected pixel (new endpoint) and an intensity cost function, in which, valley-edge tracing starts from the detected endpoints to see which neighborhood has the lowest gray value. When a new pixel is found as a valley-edge point, it is used as a new endpoint. The tracing procedure continues until one of the bubble contours is closed, before it starts to trace from another detected endpoint. When no detected endpoints remain for continuous tracing, the valley-edge tracing procedure stops.

Two image results with the new algorithm are shown in Fig. 5. In Fig. 5a, the original image (Fig.2a) size is 256x256 pixels, and the number of bubbles is about 370. The segmentation result is quite good. In Fig. 5b, the image size is the same as in Fig. 5a, but the number of bubbles is about 1525, and the segmentation result by the new algorithm is reasonable.

To evaluate the new segmentation algorithm, about 10 froth images were segmented manually using interactive image processing and analysis software. The image size is 384x288, the variation in the number of bubbles in an image varies from 300 to 3000. For each of the images, the number of bubbles was counted three times by an operator, or counted by three different operators at the same time. On average, one counting for each image took about two hours. The new algorithm only took about 2-3 seconds in a PC compute with a clock speed of about 200 Mhz. A variation of 20-35% was obtained from the three manual countings of each image. Especially, for the images with more than 1500 bubbles, the variation in number of bubbles is large between countings. When the average number of bubbles counted by manual in an image was compared to the number of bubbles counted by the new algorithm, the difference is about 10%.



a **b**

Fig. 5. Segmentation results on two different types of images, by the new algorithm.
a: Segmentation result of 370 bubbles, **b:** Segmentation result of 1525 bubbles.

CONCLUSIONS

In this contribution, a new segmentation algorithm – based on valley-edge detection and edge tracing has been presented. It was especially designed for froth images from flotation cells in mineral processing. The algorithm first uses a Gaussian filter or average filter to smooth the original image. Then it detects valley-edges between bubbles. Thirdly, it performs valley-edge tracing based on both post-processed valley-edge image and the original image. The segmentation algorithm has been tested on froth images from Pyhäsalmi mine in Finland and Garpenberg mine in Sweden. The processing speed of the algorithm is much faster than normal morphological segmentation algorithms. Accuracy is better than that of manual counting. The test results show that the algorithm works satisfactorily.

ACKNOWLEDGMENT

This contribution is part of the European Commission DG III – Industry, Espri, Project, No. 24931-CHACO. Froth images were provided by Garpenberg mine of Boliden Minerals, Sweden and Pyhäsalmi mine of Outukumpu Oy, Finland. Their contribution is acknowledged.

REFERENCES

1. W.X. Wang, 1999. Image analysis of aggregates. Computers & Geosciences 25, 71-81.
2. O. Stephansson, W.X. Wang and S. Dahlhielm, 1992. Automatic image processing of aggregates. ISRM Symposium: EUROCK '92, Chester, UK, 14-17 September, British Geotechnical Society, London, UK, pp. 31-35.
3. W.X. Wang, F. Bergholm and O. Stephansson, 1996. Program Library for Image Analysis of Aggregates. 20th Conference for Mineral Technique, Luleå, Sweden, 13-14 February,. pp. 159-168.
4. N. Sadr-Kazemi and J. J. Cilliers, 1997. An image processing algorithm for measurement of flotation froth bubble size and shape distributions. Mineral Engineering, 10(10), 1075-1083.
5. P. J. Symonds and G. De Jager, 1992. A technique for automatically segmenting images of the surface froth structures that are prevalent in flotation cells. Proceedings of the 1992 South African Symposium on Communications and Signal Processing. University of Cape Town, Rondebosch, South Africa, 11 September, pp. 111-115.
6. M. Guarini, A. Cipriano, A. Soto, and A. Cuesalaga, 1995. Using image processing techniques to evaluate the quality of mineral flotation process. In Proceedings of the 6th International Conference on Signal Processing, Applications and Technology, Boston, October 24-25, pp. 1227-1231.
7. A. Cipriano, M. Guarini, R. Vidal and A. Soto etc., 1998. A real time visual sensor for supervision of flotation cells. Mineral Engineering, 11(6), 489-499.

The Characterization of Flotation by Colour Information and Selecting the Proper Equipment

A.K. Sirén

VTT Information Technology, Printed Communication,
Tekniikantie 4B, Espoo, 02044 VTT, Otaniemi, Finland
Tel: 358-9-456-5898 Fax: 358-9-455-2839 Email: ari.siren@vtt.fi

ABSTRACT

Flotation is the most common industrial method by which valuable minerals are separated from waste rock, after crushing and grinding the ore. For process control, flotation plants and devices are equipped with conventional and specialized sensors. However certain variables are left to the visual observation of the operator, such as the colour of the froth and the size of the bubbles in the froth.

The ChaCo -project (European Union- project 24931) has been started 1997 November. In this project measuring station was build at Pyhäsalmi flotation plant. System includes RGB- camera and spectral colour measurement instrument for flotation colour inspection. RGB camera or visible spectral range is measured also for comparing the comments of operators for colour of the froth related to sphalerite concentration and process balance.

Different dried mineral (sphalerite) ratios were also studied with iron pyrite to find out the minerals typical spectral features. Sphalerite spectral reflectance over different wavelengths correlation to the sphalerate concentrations are used for selecting proper camera system with filters or for comparing the results with colour information from RGB-camera.

Different machine vision candidate techniques are discussed for this application and the pre-processed information of dried mineral colours is used and adapted to the on-line measuring station.

Moving bubbles of the froth produce total reflections disturbing the colour information. Polarization filters are used and results are reported Also reflectance outside visible light with this application is also studied and reported.

0-7803-5489-3/99/$10.00 ©1999 IEEE.

Intelligence in Environmental Applications

Robust Engineering Approaches to Maximize Results in Business, Cost, Engineering, Human, Quality and System Technologies

Roberto C. Villas Bôas

CYTED - Science and Technology for Development in Iberoamerica,
Mineral Technology Sub-Program, Madrid, Spain
Email: villasboas@cetem.gov.br

ABSTRACT

Robust Engineering is a new branch of engineering techniques developed by Geinichi **Taguchi**, in the early fifties in Japan. It is now in wide use throughout the western world, after the tremendous success of several industrial applications. Theses successes can be grasped with a quick look at the home page of the American Supplier Association: http://www.amsup.com/TAGUCHI.

INTRODUCTION

The basic ideas of Taguchi are well-described in the **Harvard Business Review**, Jan-Feb 1990 edition and elsewhere [1,2]. They consist of taking care of a product or process from the very beginning, i.e., from when the concepts are just being formulated -- well-before production or manufacture starts. The main idea is to avoid selecting a manufacturing route or process development simply to be within certain established tolerances in which you must force yourself to be as narrow as possible to target "the value" instead of "an acceptable range of variation".

A very interesting feature when designing for competitive advantage is that **"value"** is defined as a **measure of choice**; see **Dean, E.B.,** at http://mijuno.larc.nasa.gov/dfc/value.html. Moreover, **robust** products or projects have **"strong signals"**, despite extensive external **"noise"** to which they are subjected. These thoughts are well-illustrated in **every-day** practice, when a given product or process, consisting of several parts (or unit operations for processes), is to be manufactured or run. Every part or unit operation has its own "tolerances" and the couplings of these may result, in the summation of the variances of all the parts or unit operations that results in a product or process of bad performance or failure .

The basis of Robust Engineering is **D.O E. (Design of Experiments)** -- a set of mathematical tools which are well-established in the literature ans which can be thought of as being devised for competitive advantage. The originality of the Taguchi approach was to utilize **fractional factorial design** arrays that could provide the performance or endurance of a product or process, when subjected to both controlled and **uncontrolled** variables that affect such performance and endurance! The utilization of fractional factorial designs for **controlled** variables is not a Taguchi achievement. Rather his main contribution to engineering was the proposal of a specific design plan subject to a set of uncontrolled variables that affect the process or product performance. Such uncontrolled variables might be humidity, temperature, cultural habits in utilizing a given process or product, lack of particular expensive equipment for increased performance of the results, etc. The statistical analysis he proposed which is now being used by engineering users around the world, is very simple, but has been heavily criticized by many statisticians [3,4,5]. Despite the apparent short-comings on strictly statistical grounds, the method of analysis works in the real world and all the supposedly "better" statistical approaches that have been proposed generally achieve the same conclusions!

A discussion on some topics of interest in **Robust Engineering** is fundamental for the reader to understand the overall issue. **DOE Techniques** - Design of Experiments (DOE) involve the application of certain geometric principles to the design space in such a way that an algorithm that indicates the sampling route to be followed is achieved. In the presentation, factorial experiments will be fully described and analyzed through real case-studies; some important fractional factorial designs, such as TAGUCHI's methods, will

0-7803-5489-3/99/$10.00 ©1999 IEEE.

be demonstrated in some real case applications. Several Response Surface designs will be discussed and analyzed. **Taguchi's Orthogonal Arrays** - The utilization of orthogonal arrays has long been known in DOE and several experiments are based on these elements. The innovation that Taguchi brought to the discussion was the establishment of arrays to study controllable, as well as, uncontrollable variables that affect experiments and consequently, the processes and products.

ROBUST DESIGNS

Robust designs are conducted for **optimization** . A mathematical **transform** is utilized to achieve this; the transform being the **signal to noise ratio**, quite arbitrarily selected by Taguchi as **the** transform to be always used. Such a ratio gives an indication of how close the design is to the optimum performance of a given process or product. For a discussion about the measurement of **robustness**, see http://www.amsup.com/TAGUCHI/ROBUST/

The most interesting proposal is that research engineers may choose a variety of designs that best suit the engineering goals. These designs, called Taguchi arrays, are fractional factorials and can be derived by applying the principles of constructing such factorials [6,7]. The literature contains several of these arrays [1,2,8] represented by the letter L, sometimes A, followed by a subscript indicating the number of actual experimental runs. Depending on the source of the plan, there may also be parentheses containing the original basic design that was fractionated. An indication of the number and levels of variables is also given in the plan as an orthogonal array. Computation of the **effect** of each particular variable when subjected to variations in the levels used is very simple.

Taguchi's main contribution to D.O.E. is the introduction of uncontrolled variables within a proposed design. This is done via the following sequence:

a) identify the controlled variables for the process or product ;
b) identify the uncontrolled variables that affect the process or product performance;
c) choose, or construct, arrays for the controlled and uncontrolled variables in such a way that the design plan for the controlled variables is obtained within the design plan for the uncontrolled ones, thus obtaining the desired responses for the problem;
d) analyze the overall design and set new levels for the controlled variables using the mathematical transform, "signal-to-noise ratio", i.e., the performance statistic that estimates the effect of the uncontrolled variables on the response(s);
e) run the experimental design again and check if the new design satisfies the improvements suggested by the mathematical transform, i.e., establish the performance statistics.

The mathematical transform

Here lies one of the major criticisms of Taguchi's approach : the use of the so called signal-to-noise ratio , as **the** sole mathematical transform at all times. (see [3] for a complete review)

There are three cases that the research-engineer can choose for his performance statistic:

a) which specific target value is best
b) minimization, i.e., the smaller , the better
c) maximization, i.e., the larger , the better

AN EXPERIMENT

For the sake of illustration let's perform an experiment according to the sequence suggested. Let's study the production of zinc oxide, where dense pieces are a must in order to enhance the electrical properties of the final product [9]; thus , the response to be examined is the real density of the produced piece. Let's follow the sequence:

a) identify the controlled variables.
1. temperature in °C, at three levels : 1100, 1200 and 1300.
2. time in hours, at three levels : 2, 3 and 4.
3. oxalic acid dispersant in percent , at three levels: 0, 7.5 and 15.
4. polyvinyl alcohol ligand in percent , at three levels: 0, 1, and 2.

b) identify the uncontrolled variable(s).
furnace ventilation, at three levels : ambient , forced ventilation low, forced ventilation high.

c) the array
1. an L9 for the controlled variables was chosen
2. taken at the three settings of the uncontrolled variable
3. obtaining the real density in % as the answer, for every setting defined, in replicates (although unecessary), the **averages** were assessed.
4. these averages were, following an L9:

1 = 92.41
2 = 90.09
3 = 89.92
4 = 91.74
5 = 91.72
6 = 92.17
7 = 91.69
8 = 93.04
9 = 91.88

d) the performance statistics (signal-to-noise ratio)
1.for this specific case study, the selected S/N transform was **the larger ,the better**.
2. the computed S/N ratios were quite near to one another, as follows:

1 = 39.31
2 = 39.09
3 = 39.08
4 = 39.25
5 = 39.25
6 = 39.29
7 = 39.25
8 = 39.37
9 = 39.26

3. so it was decided by the research team to compute the variance for each experiment:

1 = 0.078
2 = 0.031
3 = 0.220
4 = 0.046
5 = 0.083
6 = 0.007
7 = 0.019
8 = 0.013
9 = 0.004

4. and so, the option for analyzing the data was to determine the effect of each variable on the final response (average, S/N and variance), within their levels, instead of referring to the classical ANAVA. In fact, such an analysis gives the controlling levels for each variable to increment the average density , decrease the variance, and maximize the S/N, as follows:

Temperature = 1300 °C (average up by 0.57, variance down by 0.043 and S/N up by 0.054);
Time = 2 hours (average up by 0.32, variance down by 0.008 and S/N up by 0.030);
Dispersant = 0% (average up by 0.91, variance down by 0.023 and S/N up by 0.086);
Ligand = maybe at 0.5 %
since at 0% (average was up, variance was unchanged and S/N was up)
and at 1% (average was down, variance was down alot, and S/N was down)

5. For the uncontrolled variable , furnace ventilation, although Level 2 is indicated as it provided an increase in the average, it also introduced the highest variance and an insignificant change in S/N.

e) run the experimental design again: the experiment was performed with the new conditions suggested by (d) and with no furnace ventilation, with the results showing an improvement in the average with minimum variance and maximum S/N.

CONCLUSION

Thus, the so called Robust Designs are orthogonal arrays formally identified with fractional factorial designs, constituting of a design matrix for the controlled variables and another for the uncontrolled variables in such a way that the response is obtained under the settings of the uncontrolled variables matrix, that will give the variances of the system, and analyzed via the mathematical transform, the "signal-to-noise ratio", for optimization of the controlled variables and their levels.

It is indeed, quite a simple procedure and has the advantage of implementing at the earlier stages of the process/product cycle the robustness of it.

REFERENCES

1. Taguchi, G., 1987. System of Experimental Design : Engineering Methods to Optimize Quality and Minimize Costs , UNIPUB, White Plains, N.Y.
2. Taguchi, G., Yokoyama, Y., 1994. Taguchi Methods : Design of Experiments, ASI, Dearborn, MI.
3. Box , G., 1988. Signal to Noise Ratios, Performance Criteria and Transformations , Technometrics, 30(1), 1-17.
4. Berk, K.N., Picard, R.R., 1991. Significance Tests for Saturated Orthogonal Arrays , J. Qual. Tech., 23(2), 79-89.
5. Lucas, J.M., 1994. How to Achieve a Robust Process Using Response Surface Methodology , J. Qual. Tech., 26(4), 248-260.
6. Kacker, R.N. et al., 1991. Taguchi's Fixed Element Array are Fractional Factorials , Journal of Quality Technology,23,2,pp.107-116 .
7. Villas Bôas, R.C., 1996. Arranjos Ortogonais de Taguchi: os Ln(2k) ; Série Qualidade e Produtividade, 9, 1-14, Rio de Janeiro
8. Fowlkes,W.Y., Creving, C.M., 1995. Engineering Methods for Robust Product Design Using Taguchi Methods in Technology and Product Development , Addison-Wesley Publishing Co., Reading, MA.
9. Duarte, M.V.S. et al., 1998. Zinc Oxide for Varistor Manufacturing ; Class Exercise under Prof. R.C. Villas Bôas, The Federal University of Rio de Janeiro, COPPE, Rio de Janeiro .

Imaging Techniques for Process Optimization and Control in Glass Recycling

Giuseppe Bonifazi, Paolo Massacci

Dipartimento di Ingegneria Chimica, dei Materiali, delle Materie Prime e Metallurgia
Università di Roma "La Sapienza", Via Eudossiana 18 00184 Rome, Italy

ABSTRACT

Glass fragments (cullets) to be recycled present different market values according to their color. Glass recycling plants perform cullets sorting mainly discriminating colored glasses from white and half white glasses; furthermore sorting presents some other technological limits concerning the minimum cullet size, about 4÷5 mm, that is possible to analyze. Cullets which are collected without distinctions of color, can be used primarily for the production of green glass and only in part for the production of yellow glass. The production of white glass requires that only cullets of that color be employed. At present, machines for the separation of cullets according to color are not capable of producing an efficient classification of all the different types. In this paper are analyzed the possibility that could be offered by the adoption of a color imaging based approach to realize cullets sorting, analyzing the textural attributes of the investigated cullets' image field. This study was mainly focused on the effects that cullets surface status and characteristics produce on the detected color-textural characteristics and they can influence the further classification. All the tests have been performed on glass samples as they result after the cleaning stage, impurities removal, of an industrial glass recycling plant.

INTRODUCTION

Glass can be historically considered one of the most recycled materials. Glass recycling can be realized by following different rules according to glass products such as containers (vases and bottles), plates (domestic and industrial), glass works wastes, etc. or according to characteristics and destination of use. Glass can be "easily" recycled thanks to some intrinsic characteristics such as: i) non-absorbent no intrinsic flavor and odor; ii) resistance to temperatures required for cleaning and, finally, iii) strength and mechanical resistance allowing multiple filling and reuse. In some cases it is possible to collect and direct re-use of the "objects", after cleaning without any modification to physical characteristics (i.e., such as comminution). Unfortunately, this strategy can only be applied in limited cases, considering the great amount of glass waste produced. In most cases, glass recycling means to collect and process glass materials usually resulting from differentiated collection of urban waste. In this case, it is necessary to select specific and appropriate processing strategies addressed at "cleaning" glass fragments of all impurities that would compromise re-use of the glass both at melting and final product manufacturing. Together with "cleaning" and other important aspects linked to glass fragment (cullets) recycling, there is the need to realize additional "selection" of the glass according to their destination based of their color characteristics. Successful achievement of these goals together with the intrinsic physical-chemical properties of glass, permit us to reach several positive targets: i) savings of raw materials necessary for production; ii) reduction in energy consumption and iii) reduction in the quantity of solid urban waste. All these aspects push the recycling industry to extensively apply technology in order to recycle glass material.

The setup of efficient and reliable cullet-processing involves defining specific rules addressed at:

- collecting criteria strategies directed at simplifying further processing;
- identifying all "polluting" materials that can reduce processing efficiency and, in some cases, compromise the final correct re-use of cullet materials;
- defining suitable strategies to remove the polluting elements;
- realizing a "final" separation of cullets by sorting according to their color.

0-7803-5489-3/99/$10.00 ©1999 IEEE.

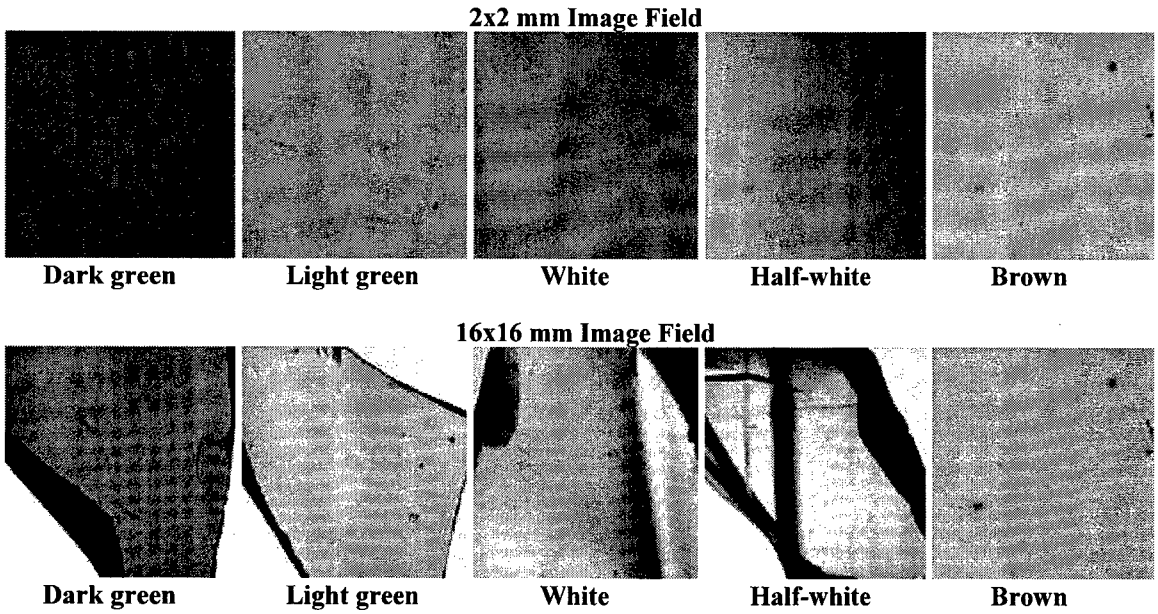


Fig. 1. Dark green, light green, white, half-white and brown cullets (sampled in the plant) and washed with a chromic mixture (1l H_2SO_4 concentrate and 30g $K_2Cr_2O_7$), rinsed with demineralised water and dried at 90°C. Images acquired at: 2x2 mm (high mag) and 16x16 mm (low mag).

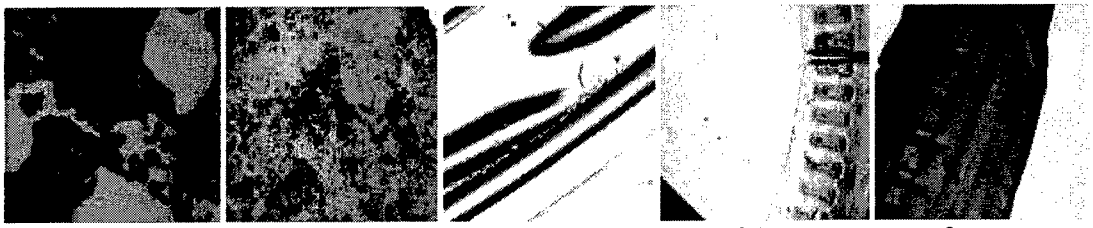
With reference to cullet sorting in recent years, glass works requirements have increased in terms of "acceptable polluting individuals" and as a consequence, stricter rules must be applied for sorting both in terms of "quality control of separation" and "lower size limits" of the cullets. Both the rules, and especially the size criterion, are not so easy to realize. Actually cullets sorting is realized by using as a detector, a laser beam technology-based device. The sorting logic is mainly analogic. An "on-off" logic is applied.

Detection is, in fact, based on an evaluation of the "characteristics" of the energy and spectra received by a detector after the cullets are crossed by a suitable laser beam light. Technological limits can be divided into two classes: those related to the construction characteristics of the equipment and those related to the material (Figure 1). The first are mainly linked with the physical dimension and mechanical arrangement of the optics used to generate signals, and with the pneumatic architecture enabling modification of a cullet trajectory to realize sorting, according to color. Furthermore, flow characteristics can influence selection. To realize efficient optical sorting, the flow must be, in principle, constituted by particles forming a mono-layer. In this condition, cullets can be analyzed one at a time by the laser beam. Recent equipment is so fast in its analysis that the same cullet can be tested several times according to its dimension. As a consequence the larger the cullet, the better its control. The influence of "anomalies" (Figure 2) can be thus reduced since each cullet is analyzed by more than one detector and for more than one time. For smaller pieces, such conditions are difficult to realize since they can pass through, unsorted. As well diffraction/refraction effects can be so strong (presence of marked cleavage or surface anomalies) that detectors are practically unable to analyze them. The establishment of monolayer conditions and effective flowrates are also problematic. All these problems mean that sorting can not be used profitably for the entire size ranges of cullets. Materials of smaller dimensions resulting from the processing-cleaning stages can not be treated and so are usually rejected. This fact represents a double cost: Glass material is lost and money to pay to store such products in a dump must be spent. The aim of this paper is to present the possibilities offered by color digital-imaging to realize the recognition of cullets presenting with an average dimension of about 2 mm, on the basis of their color characteristics starting from an evaluation of their pictorial aspects and moving towards full-control of the quality of the separated products when such strategies are applied.

CULLET CHARACTERIZATION

Cullet sorting is realized on the move. After a "cleaning" stage, the material is fed to a sorting system in order to realize the desired separation. As a consequence, material flow can be considered a complex

domain constituted by several elements (glass particles); each characterized by specific attributes (size, shape, color and degree of dirtiness). Such properties, by directly looking at the bulk material, are not so easy to investigate; especially when the task must be done "on-line" at industrial plant scale.



2a 2b 2c 2d 2e

Fig. 2. The spectral response of the cullets, suitably energized, is based on an evaluation of the transmitted energy received by the detectors. The detected energy is influenced by the status (dirty or clean) and the characteristics (fragments of bottle neck or vase with or without thread, bottle or vase bottom, etc.) of the cullets surface.
2a: 16x16 mm image of dirty light green cullet; **2b:** 16x16 mm image of white dirty cullet; **2c:** 2x2 mm image of white cullet (threaded bottle neck); **2d:** 2x2 mm image of half-white cullet (bottle bottom); and **2e:** 16x16 mm image of dark green cullet (bottle bottom).

Cullets as a Source of Information

A "layered" bulk solid sample [1] presents in general, certain specific pictorial attributes perceived by our senses according to the lighting conditions and, as a consequence, by the spectral response of the surfaces constituted by the particles themselves. The spectral characteristics of each element of the surface is related to the physical characteristics of the constituting particles and the energizing source (lighting). With reference to a digital color image, this is a discrete domain characterized for each constituting element, by a triplet of values representing three base color components (Figure 3). The source of information, for each pixel, is thus represented by the three values of the three corresponding color components [2].

Samples and Sampling

All tests have been carried out by adopting a set of samples (cullets) taken from the feed of an industrial recycling plant. Different sample sets, according to different colored cullets, were identified and collected. The cullets were manually selected, on the basis of their color, into five color classes: light green, dark green, white, half white and brown (Figure 1). Each cullet was classified and stored to be always identifiable in the course of subsequent experiments and measurements.

IMAGING PROCEDURES

Cullet image acquisition was performed by lighting each sample using transmitted light of known wavelength (5000°K). The cullet was lit from below and the transmitted light was registered by an optical system equipped with a colour video-camera (i2s IEC800CC) connected to a RGB frame-grabber (Matrox MVP AT) installed on a standard PC. A randomly investigated image field for each cullet of 2x2 mm was examined using a Leica-Wild M8 stereo microscope. Such a procedure was adopted to analyze and critically evaluate the image fields in terms of the characteristics of the detected colors of the cullet sample and the status of their surfaces (dirty or clean). Furthermore, by adopting such a magnification, it was also possible to evaluate the influence of geometric characteristics (fragment of bottle neck or vase with or without thread, bottle or vase bottom, etc.) on the information collected by imaging. The collected digital image set was analyzed by adopting two different strategies:

- a "simple" color spectra-based approach: each cullet is characterized, analyzed and classified according to its RGB (red, green, blue) spectral distribution [3];
- a texture-based approach (Appendix): each cullet was characterized, analyzed and classified according to textural characteristics (spatial occurrences of color tone on the image) determined with reference to a HSB (hue, saturation, brightness) color reference system [1].

Several procedures can be used to estimate the sensitivity of these two approaches (color- and texture-based), with respect to the possibility to perform complete sorting of the five cullets color classes.

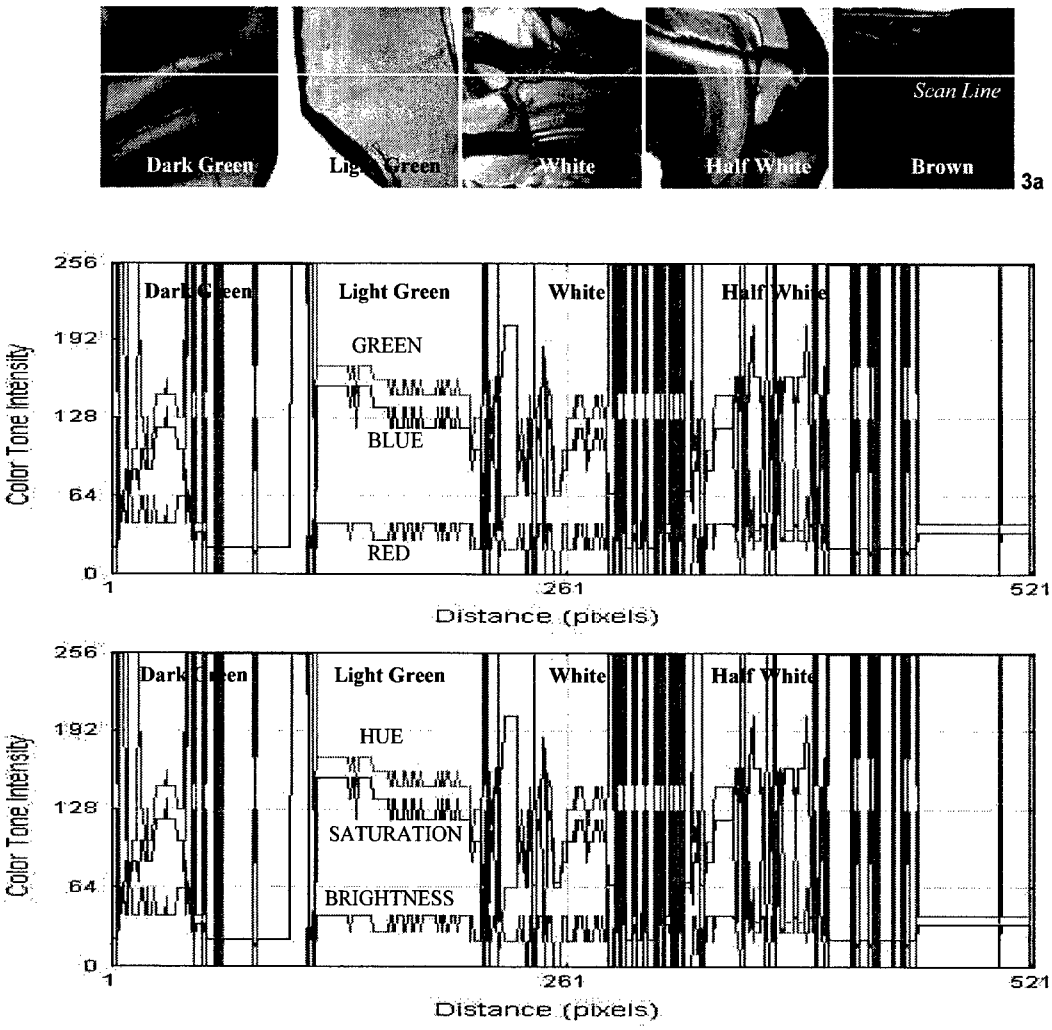


Fig. 3. RGB and HSB color component characteristics along the pre-assigned alignment (scan line) reported on **3a** intercepting five different image windows belonging to cullets with different color and surface characteristics. The presence of such characteristics, or "anomalies", strongly affect the spectral response and quality of the color "signature" for use in further processing.

Statistics or neural nets procedures, widely adopted [4,5] in previous studies, only based on cullets color evaluation, permitted us to achieve quite good results. The limit of these approaches is the computing time and the necessity "to train" the sorting system to recognize the objects (cullets) to sort. This choice was mainly adopted due to the complexity of the available data set, the object of the investigation, and because an intrinsic correlation sometimes exists between the detected parameters. The adoption of a texture-based approach seems quite promising at least in terms of simplification of the data analysis procedures. Textural algorithms, in fact, were demonstrated to be sensitive to some cullets physical parameters not fully recognized and numerically quantified by the "simple" color spectra based approach.

Cullet Classification

Industrial glass recycling sorters classify by looking at one specific cullet attribute per cycle for each cullet. Assuming, the mean color and textural values, for each investigated field of the glass fragment, is representative of the cullet itself, it is possible by evaluating only one cullet attribute per cycle time, to define, for each family of cullets (dark green, light green, white, half-white and brown) a set of Washability Functions (WF) [6], one for each selected attribute, This approach is very easy to plot and analyze. The WF graphs assume the same meaning as used in the field of mineral processing. Such a plot is a cumulative plot.

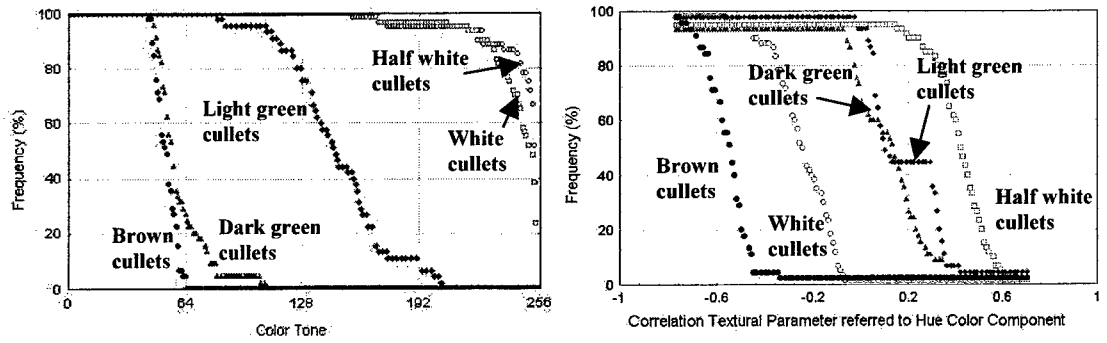


Fig. 4. Color washability curves based on:

4a. the blue mean color value component (RGB color-based approach); and

4b. the correlation value computed on the hue component (texture-based approach) of the different sets of clean cullets examined (mean value from the analyses carried out on each digital image along the four directions: 0°, 45°, 90 and 135°).

Separation functions, based both on color and textural distribution of the investigated sample set, can thus be defined and threshold selection criteria applied.

On the x-axis, the values representative of the physical property investigated are reported, i.e, the value of the cullet colour components or textural parameters as extracted from the image analysis procedures. On the y-axis, the number (normalised frequency) of cullets presenting a value of the colour component or textural parameter equal or less than that of the corresponding abscissa, are reported. Each set of cullets, considered as a whole, can be evaluated in terms of high or low possibilities to be grouped (sorted) on the basis of color. The WF is built with reference to the mean value of the blue color component while the WF is determined for the textural parameter by computing on the hue color component (Figure 4). The system shows that quite good sorting can be realized by adopting a "serial recognition-classification" approach in which detection and separation of the dark green, light green and brown cullets are done only on the basis of their color and separation of the remaining white and half white cullets uses textural characteristics.

CONCLUSION

The adoption of combined digital imaging based approach utilizing both color and textural cullets recognition procedures seems to be quite promising especially in terms of their direct use, adopting simple threshold ("on-off") selection criteria, quite similar to those adopted in the actually utilized sorters (based on laser technology). Further studies to enhance and simplify the procedures, especially in terms of data detection and processing speed, will be addressed to investigate possible improvements: i) adopting specific wavelength to enhance cullets characteristics (light transmittance, color and texture) and ii) identification of other optical-digital characteristics to utilize for the classification (cullets morphology and cleavage).

ACKNOWLEDGEMENTS

The authors wish to thank Mr. E. Weber (WTE, Milan, Italy) for his help during the selection of the glass cullets products examined and Mr. H. Frish (S+S Metallsuchgeräte und Recyclingtechnik, Schönberg, Germany) for his suggestions during the development of the work. Many thanks also to Mr. M. Delfini and Mr. M. Ferrini (technical staff of the Department) for their contribution in testing.

REFERENCES

1. W.K. Pratt, 1991. Digital Image Processing. 2nd edition, John Wiley & Sons Inc., New York.
2. G. Bonifazi, 1997. Imaging Techniques applied to Bulk Handling and Processing. Bulk97 Design Seminars. Materials Handling Engineers'Association. 5.3, 1-7, The Belfry, Sutton Coldfield, UK.
3. G. Bonifazi, P. Massacci, 1998. Cullets (Glass Fragments) Quality Control by Artificial Vision: a Color based Approach. Quality Control by Artificial Vision: QCAV '98. 94-99, Takamatsu, Japan.

4. G. Bonifazi, P. Massacci, G. Patrizi G. Zannoni, 1997. Colour Classification for Glass Recycling. Proceedings of the XX Int. Mineral Processing Congress: IMPC97, 5, 239-252, Aachen, Germany.
5. G. Bonifazi, P. Massacci, 1996. Particle Identification by Image Processing, KONA No. 14, Powder and Particle. Hosokawa Micron Corporation, Osaka, Japan.

APPENDIX

Digital Image Textural Characterization

Textural characterization (Pratt, 1991) of the different glass fragments was carried out evaluating the spatial relationship existing between the different color levels in each component, operating a change of color coordinate system from RGB (red, green, blue) to HSB (Pratt, 1991), presenting these last three components (hue, saturation, brightness) a lower degree of correlation than the red, green and blue. To quantify the "textural" characteristics of the image cullets, the following numerical relationships have been considered and the results of the parameterization evaluated:

Angular Second Moment (ASM): $f_1 = \sum_i \sum_j \frac{1}{R} p(i,j)^2$

Contrast (CON): $f_2 = \sum_{n=0}^{N_g - 1} n^2 \sum_{|i-j|=n} \frac{p(i,j)}{R}$

Correlation (COR): $f_3 = \frac{\sum_i \sum_j [ijp(i,j)/R] - \mu_x \mu_y}{\sigma_x \sigma_y}$

being R number of pairs of contiguous picture elements in the matrix being examined; $p(i,j)$ the element (i,j) in the normalized gray spatial-tone dependence matrix, $[P(i,j)/R]$; Ng the number of gray levels in the image; μ_x, μ_y, the averages of the marginal distribution associated with $p(i,j)$; σ_x, e σ_y the standard deviations in the marginal distribution associated with $p(i,j)$; x, y the coordinates of the generic pixel on the image;

$\sum_i$ and $\sum_j$ respectively $\sum_{i=1}^{N_g}$ and $\sum_{j=1}^{N_g}$ $p_{x+y}(k) = \sum_i \sum_j p(i,j)$ where: $k = 2,3,...,2N_g$ being $i+j = k$

Spatial Tone Dependence Matrix

A spatial-tone dependence matrix describes the relationships existing between the tone level value (H, S, and B for color images or GL for gray-level images) of the pixel at known distances (d pixels) and directions (k). The formulation of these relationships allows one to build a matrix M_k (the spatial-tone dependence matrix), where k is the direction along which the distance d is calculated. If, for example, 0° is assumed as main direction, the corresponding M_k matrix will be defined as:

$M_{0°}(l,m,d) = \#\{[(p,q),(r,s)] \in A\}$ being $A = (L_y L_x)(L_y L_x) \mid p-r = 0, \mid q-s \mid = d, I(p,q) = l, I(r,s) = m$

where: l = row index for matrix M_k, m = column index for matrix M_k, d = distance, along the direction k, defining the spatial relationship of nearby pixels, p: row index of the first pixel considered in the image, q: column index of the first pixel considered in the image, r: row index of the second pixel considered in the image, s: column index of the second pixel considered in the image, L_x: number of pixels in the image along the x axis and L_y: number of pixels in the image along the y axis. The tone (l) (color component or gray level) of the pixel at co-ordinates (p,q) is compared with the tone (m) (color component or gray level) associated with the pixel at co-ordinates (r,s). The symbol # represents the number of pixel pairs that satisfy the required criteria. As regards the matrix, the element $M_{0°}(l,m,d)$ is equal to the set of ordered pixel pairs (p,q), (r,s), whose distance along the y axis is zero and along the x axis is d, and whose tones g(p,q) and g(r,s) have values (l-1) and (m-1), respectively. The matrices are symmetrical, i.e.,: $M_k(l,m,d) = M_k(m,l,d)$.

So, a normalized spatial-tone dependence matrix is one whose generic element equals $M_k(l,m,d) / T_k$ where T_k assumes the following expressions for the main directions 0°, 45°, 90° and 135° : $T_{0°} = 2(N_x - 1)N_y$, $T_{45°} = 2(N_x - 1)(N_y - 1)$, $T_{90°} = 2(N_x(N_y - 1))$ and $T_{135°} = 2(N_x - 1)(N_y - 1)$, respectively.

Application of Heuristics and Fuzzy Logic to Natural Resource Modelling

Steven Mackinson

Fisheries Centre, 2204 Main Mall, University of British Columbia, B.C., Canada
Phone 604-822-2731, Email: smackin@fisheries.com

ABSTRACT

The complexity and dynamics of natural systems poses considerable difficulties for mathematical description. Conventional modelling techniques that rely purely on an analytical, algorithmic approach are poor at capturing non-linear processes, cumulative effects and uncertainties characteristic of such systems. In this respect, heuristic models using the principles of fuzzy logic are well suited for describing and simulating processes and dynamics of natural systems. Currently, there are few examples of fuzzy knowledge-based models in natural resource management and there is significant potential for future development. Demonstrated here, are two recently successful applications; (i) a fuzzy expert system that applies a novel method of defuzzification to predict changes in the structure, dynamics and mesoscale distribution of fish shoals, (ii) a method utilising fuzzy approximation theory to predict the recruitment of young fish to a fishery based on the parent stock size and past recruitment conditions.

INTRODUCTION

Natural resource management demands recognition of the inherent variability of natural processes. In an attempt to satisfy these needs, analytical methods for explicit quantification of variability and uncertainty have pervaded the scientific discipline [1]. However, ecosystem processes in general do not yield well to description by conventional analytical techniques; their complexity, non-stationarity, and non-linear, even chaotic, features defy conformity. Fuzzy knowledge-based systems offer an alternative tool to traditional analytical models. Relationships descriptive of biological and ecological processes can be easily explained and understood by natural language heuristic rules that define them. Use of knowledge-based systems is an admission that our knowledge is incomplete and uncertain, yet through building and testing, it is a move toward practicality, recognising that decisions based on qualitative and sometimes, incomplete knowledge is still better than making decisions without any understanding [2].

Knowledge-based systems have been used in the field of natural resource management for some time [3] although applications in fisheries science are more limited [2]. There is considerable scope for future applications, particularly those utilising fuzzy logic. Two recently successful 'fuzzy' applications are presented here; (i) a fuzzy expert system to predict structure, dynamics and mesoscale distribution of fish shoals [4,5], (ii) a method using fuzzy approximation theory to predict recruitment of young fish to a fishery [6].

PREDICTING STRUCTURE AND DISTRIBUTION OF FISH SHOALS

Despite recent attempts to link cross scale behaviour dynamics and distribution studies on shoaling fish [7], large gaps still exist in our basic scientific understanding. Nonetheless, the knowledge of fishers and fishery managers has not readily been incorporated into scientific analyses, despite the fact that such information is rich in observation since knowledge of fish behaviour and distribution is a prerequisite for their profession. A fuzzy logic expert system is used as a formal framework to combine local knowledge from interviewed fishers, fishery managers and First Nations people (24 interviews), with more conventional scientific information from interviewed fisheries scientists (7 interviews), field work studies (3) and published literature sources (102 references), in an attempt to bridge some gaps in our knowledge. All knowledge contributes equally in building the knowledge base, thus the potential of all data sources is maximised [8].

A 'bottom up' conceptual approach is used in development of the model; heuristic rules defining relationships between ecological, biological and motivational factors and their effect on fish behaviour. Of

0-7803-5489-3/99/$10.00 ©1999 IEEE.

those factors, the key attributes are considered to be food, predation and reproductive state [9]. The dynamic interplay of these attributes combined with temporal changes in the fish's 'life-priorities' result in trade-offs producing behavioural responses that are manifested as changes in shoal structure, dynamics and distribution.

Defining functional relationships using rules

Heuristic rules written in natural language, form relationships between *attributes* that influence fish behaviour and *descriptors* of shoal structure, dynamics and distribution. For example:

IF fish direction facing current
  AND current strength *strong*
THEN mean swimming speed low (item confidence = x)
  AND shoal shape horizontally elongated (item confidence = y)

In the rule above, the variable 'current strength' is designated a fuzzy variable with member sets *strong* and *not strong* (Fig 1). Fuzzy sets allow construction of a model that directly represents knowledge contained in linguistic expressions given by an interviewee.

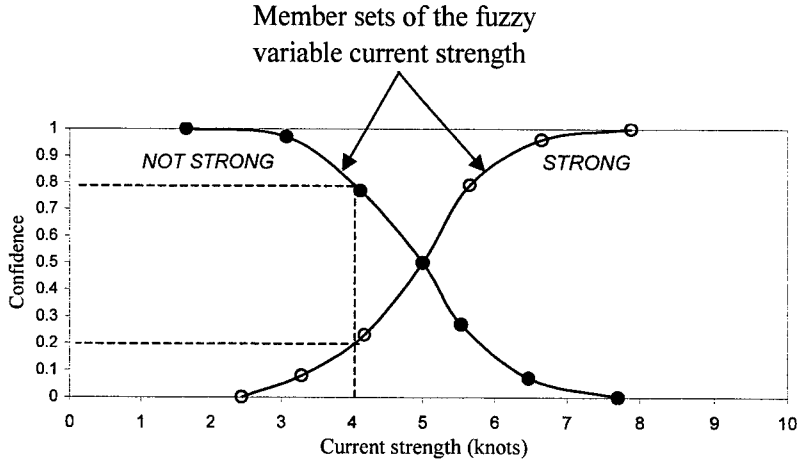


Fig 1. Membership functions of fuzzy sets on the fuzzy variable 'Current strength'. The member sets (also called subsets) are the linguistic concepts: *strong* and *not strong*. The slope and degree of overlapping of the memberships functions is a key element determining the uniqueness or 'fuzziness' of the sets. The confidence on the Y-axis shows our degree of belief in the linguistic concepts. For example, when current strength is 4 knots, we are 0.8 confident that current strength is *not strong* and also 0.2 confident that current strength is *strong*. In an expert system, both pieces of information are used simultaneously to make conclusions, thus avoiding the simplistic notion that something is or is not true, when in fact it may be both to different degrees. Thus, the system implicitly captures uncertainty. The value of current strength whose membership (confidence) is 1, is called the **supremum** value. The range of current strength values contained by a fuzzy set is called the **support.**

Relative influence of attributes - hierarchy, trade-offs and seasonality

A 'weight of evidence' approach is used to impose hierarchy to the degree of influence each attribute has on determining the resulting structure, dynamics and distribution of shoals. The method principle assumes that the more frequently an attribute is mentioned, the higher its importance relative to other contributing factors. Weight is applied by assigning to the THEN statements of each rule, an associated confidence factor that is comprised of the sum of two parts; interviews and literature (each of which are given equal importance). A combined uncertainty of 10% is assumed for all rules, thus the maximum confidence that a THEN statement can achieve is 0.9. During operation, confidence assigned to each THEN statement propagates through the system adding confidence to the output descriptor. Those statements with higher confidence carry more 'weight' and have greater effect. The 'weight of evidence' approach further substitutes as a means to represent behavioural trade-offs that occur when fish balance conflicting forces. For instance, since the effect of predator abundance on packing density has a higher confidence (Conf. =

0.19) than the effect of feeding competition (Conf. = 0.01), predators will have a greater influence on packing density even during competitive interactions.

Operational logic, including rules and commands are also applied to define how the model operates under specific circumstances; in certain scenarios, rules may be ignored whilst others are followed, or variables may be pre-assigned (in particular, when they are deemed of low importance). In addition, the user may be offered placebos (choices that do not lead to any conclusions) or the opportunity to assign low importance to a particular factor. This provides the option of choosing to exclude or reduce the influence of certain attributes. However, if the user answers 'not sure', where knowledge is available, an effort is made to assign a default choice/value.

Temporal changes in motivational state are modelled by assigning a group of 'life-priority' rules that designate behavioural priorities for feeding, avoiding predators, reproduction and energy saving during each life stage. The designations of priority are utilised in a pseudo-weighting method that applies weight to a specific variable used to represent that priority. The effect of the pseudo-weight is manifested through changes in the structure, dynamics and distribution of shoals.

Output descriptors of shoal structure, dynamics and distribution

The weighted-average method of defuzzification is used to obtain a single non-fuzzy value as output for quantitative descriptors. The method is based on a multiplication between the degree of membership in the output fuzzy sets and the supremum value of each set (Fig 2). By applying the same procedure to maximum and minimum ranges associated with each of the output fuzzy sets we also obtain a range around the discrete output value (Fig 2). Using the example in Figure 2, the discrete defuzzified weighted output would be calculated as follows:

Mean = $[(0.2*Small_{sup})+(0.6*Med_{sup})+(0.3*Large_{sup})]$/ sum of confidence (1.1)
Range min. = $[(0.2*Small_{min})+(0.6*Med_{min})+(0.3*Large_{min})]$/ sum of confidence (1.1)
Range max. = $[(0.2*Small_{max})+(0.6*Med_{max})+(0.3*Large_{max})]$/ sum of confidence (1.1)

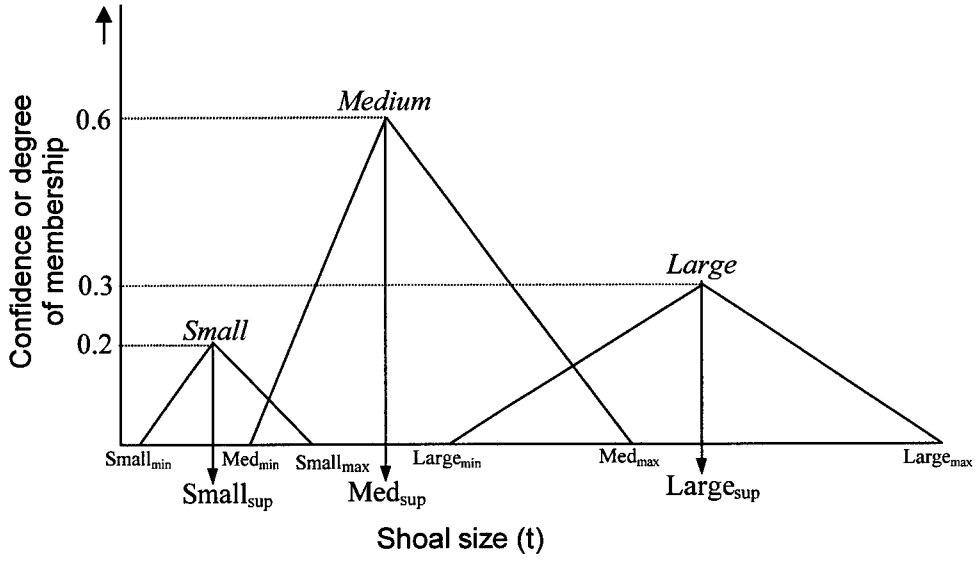


Fig 2. Output fuzzy sets for shoal size used in defuzzification. $Small_{sup}$, represents the supremum value of shoal size for the fuzzy set *small*. Similarly, $Small_{min}$ to $Small_{max}$ represents the support of the fuzzy set *small*. Supremum values used as weights are obtained from an extensive literature review of published values observed in the field.

Results: predicted seasonal dynamics in herring shoal structure

Figure 3 displays predicted changes in shoal size and packing density during 11 different phases of the annual life cycle. Note that the interval between predictions is not related directly to time. Each prediction

is a snapshot in ecological time, since the temporal scale required to capture the necessary changes varies between seasons. The predicted patterns show good correspondence with observations on herring shoals. Overwintering is recognised as a relatively passive phase in the life cycle during which there is little feeding activity and the main priorities are predator avoidance and energy conservation [10]. During this stage, very large shoals, or aggregations of shoals, are commonly found distributed as layers deep in the water column [11]. Increased shoal size and packing density are known to be typical anti-predator strategy for shoaling fish [9]. Prior to spawning, large winter aggregations break down and move to shallower areas where again they may hold for a while forming dense schools immediately over spawning areas [12]. During maturation stage 2-1, large schools tend to break up into smaller, very dense, mobile schools (Mackinson, in prep). Re-aggregation occurs during spawning with large shoals forming on spawning sites. Immediately after, spawned-out fish begin their migration to ocean feeding grounds and rapidly disperse into very small, low density shoals that swim fast and high in the water column [13, 14]. Density and size of ocean feeding shoals is reduced to enhance foraging [15, 7]. Ocean feeding shoals of North Sea herring during summer are observed to be half of overwintering shoals of Norwegian spring spawning herring [16].

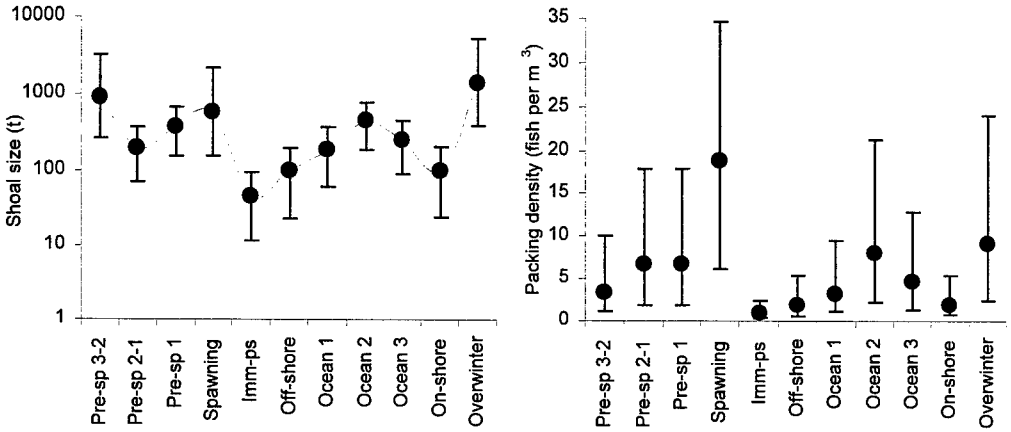


Fig 3. Quantitative predictions of seasonal changes in herring shoal size and packing density. Pre-sp 3-2, 2-1, 1: pre-spawning period divided into 3 maturation stages; Spawning: spawning; Imm-ps: Immediate post spawned; Off-shore: offshore migrating; Ocean 1,2,3: ocean feeding phase during 3 stages of summer with changes in food and predator abundance and distribution of food; On-shore: onshore migrating; Overwinter: overwintering.

MODEL-FREE ESTIMATION OF STOCK-RECRUITMENT RELATIONSHIPS

Within fisheries science, experience has shown that if a stock is fished hard, there is a point at which recruitment drops due to over-fishing [17,18]. Determining the relationship between stock and recruitment is the cornerstone for predicting how much the parent stock can be reduced by fishing without negatively impacting on future productivity. Applying principles and techniques of fuzzy approximation theory [19,20] heuristic reasoning can be used to define stock-recruitment relationships, explicitly characterise vagueness and uncertainty, and provide a functional relationship that combines stock size and past recruitment to predict future recruitment. The approach is termed model-free estimation or approximation.

Simply stated, fuzzy approximation theory demonstrates that any curve can be approximated by covering it with patches. Stock-recruitment relationships are frequently riddled with patches (Fig 4). The model-free approach to stock-recruitment consists of two stages: (1) using previous data to create rules that define the fuzzy system relating stock and past recruitment to future recruitment (Fig 4); (2) predicting recruitment with the fuzzy system. Embedded within stage one are two clustering techniques used to define the fuzzy sets on stock and recruitment. *Visual clustering* relies on the ability to visually define clusters or patches in the data (Fig 4). *Iterative clustering* defines patches or clusters according to an iterative scheme that minimises an objective function. The core element relies on an impartial fuzzy cluster analysis routine [21] that is modified to define supremum and support values of fuzzy sets on stock and recruitment [6].

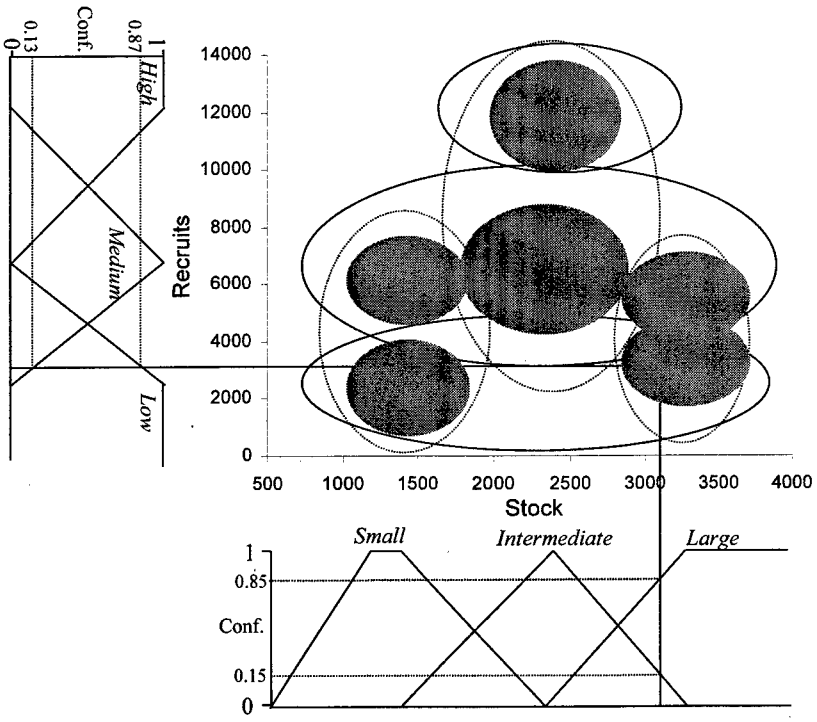


Fig 4. Visual clustering on ICES Plaice VIIe data.
Supremum values are defined according to centre of identified clusters in each plane. Dotted ellipses represent approximate clusters on stock variable, and solid ellipses are approximate clusters on recruit variable. Grey patches identify data clusters which equate to rules that relate stock size (SS) to recruitment (R). Data point **Y** with value of SS=3117 belongs to *intermediate* stock size to a degree of 0.15 and to *large* stock size to a degree of 0.85. Similarly the value R=3062 belongs to *low* recruitment to a degree of 0.87 and *medium* recruitment to a degree of 0.13.

The model-free estimation approach is capable of describing stock-recruitment relationships equally as well as traditional analytical methods (Fig 5). A comparison of residuals between recruitment values predicted by Ricker or Beverton-Holt curves (common analytical functions) and the fuzzy approximations for 8 different fish species revealed no significance difference [6]. The maximum number of sets required to capture the pattern in data on any one of the axes was four. In the majority of cases, 3 sets were sufficient.

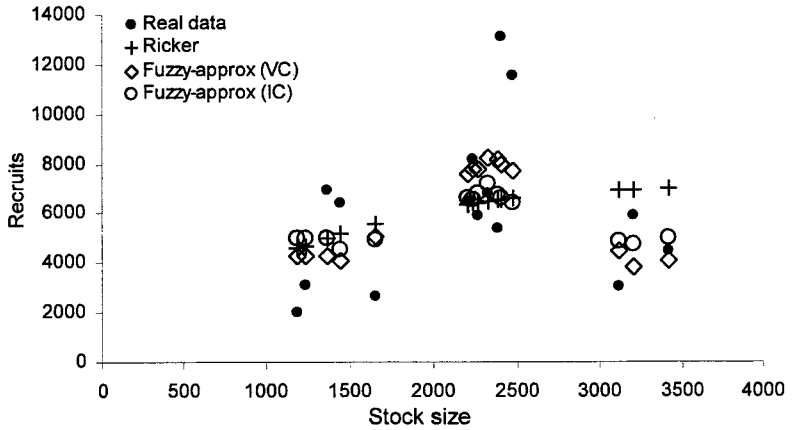


Fig 5. Stock-recruitment data in comparison with the fuzzy approximation approach and traditional analytical method (Ricker). Results for two methods of clustering are displayed; visual clustering (VC) and iterative clustering (IC). Data taken from [18] for ICES division VIIe plaice.

DISCUSSION

The essence of fuzzy logic rests on the truism that all things admit degrees of vagueness. Black and white cases are the exception in a world of gray. Similarly, natural systems do not conform to crisp definitions. Use of heuristics makes it possible to express qualitative information in a series of rules that constitute a knowledge base. Since fuzzy sets are able to model words mathematically, application of fuzzy logic [22,23] takes this one step further, allowing the integration of both qualitative and quantitative information.

Much of our current understanding of fish distribution is largely qualitative and highly uncertain. Such information does not lend itself well to mathematical representation and consequently traditional numerical modelling techniques may be inappropriate [6]. Using input pertaining to the biotic and abiotic environmental conditions, the first example presented here (Herring Shoal Structure and Distribution expert system: HSSDex) uses heuristic rules to predict structure, dynamics and mesoscale distribution of shoals of migratory adult herring during different stages of their annual life cycle. Comprised of more than 35 potential inputs and 23 outputs, the fuzzy expert system uses a 'bottom up' conceptual approach to link multiple causative and inter-related factors. The system is flexible in its predictive ability to forecast shoal structure, dynamics and mesoscale distribution across different temporal scales. Accuracy of prediction is dependent on both the *accuracy* of information captured in rules and the *realism* of the input provided by the user. Several strategies are implemented to avoid predictions breaking down due to inaccurate input by the user. However, even with these safeguards, the onus is ultimately on the user to provide realism in the scenario they develop when providing input. Since the fuzzy rules do not contain high precision, we do not expect highly precise predictions. More important, is the capability to predict general patterns observed in nature. Through the option of changing various weights, the model becomes adaptable and thus can be tuned to particular circumstances.

For many of the world's pelagic fish stocks, structure, dynamics and mesoscale distribution of fish shoals has considerable importance to central issues in fisheries management including; stock structure, stock assessment, resilience and harvest control. Through their incorporation in future models, resolution of the model predictions are at an appropriate scale to address some aspects of these critical issues.

The second example, model-free estimation of stock-recruitment relationships, fulfils the criteria that Hilborn and Mangel [1] define for useful models: "a model is most effective if it provides both understanding (of known patterns) and prediction (about situations not yet encountered)". The approach offers a new and alternative way to express uncertainties about the relationship between stock and recruitment, by means of vagueness in the definition of the variables, the shape of the membership functions and the actual clustering and overlap of the data among the different fuzzy sets. Uncertainties are then expressed in terms of fuzziness rather than probabilities. A fuzzy system lets us guess at the non-linear world and yet does not require us to formulate a mathematical model [19]. Application shows that in comparison to commonly-used analytical stock-recruitment functions, fuzzy approximations fit the observed data at least as well; are robust with respect to the number of sets required to describe the data; and capture some important behaviours of the relationship. The major benefit is that there is no need to form hypotheses, or build a model and determine its parameters prior to fitting the approximation.

In comparison with more conventional modelling techniques that rely on describing relationships with mathematical functions, fuzzy knowledge-based models are similarly able to describe continuous relationships and include feedback effects. In contrast, they do not suffer from the same constraints; when knowledge is incomplete, rules can still be used to describe 'pieces' of relationships without requiring gross assumptions. Moreover, the transparency of the models, both in terms of their intuitive operation and the ability to access expert knowledge when questioning reasoning, contrast with the apparent 'mysteriousness' of typically analytical models. In the field of natural resource science, these techniques are still largely considered novel and in stark contrast to conventional approaches. As a consequence they may not necessarily be readily accepted and may suffer from alienation. Despite this concern, the future holds promise for many applications in natural resource management. Possible areas of application that will prove fruitful include: (1) Descriptive and predictive modelling, (2) Risk assessment and decision analysis, (3) Pattern recognition in data structures, (4) Incorporating local/ traditional ecological knowledge with scientific knowledge for use in assessment and management.

REFERENCES

1. Hilborn, R. and Mangel, M. 1997. The ecological detective: confronting models with data. Princeton University Press, Princeton, New Jersey. 315p.
2. Saila, S.B. 1996. A guide to some computerized artificial intelligence methods. pp.8-40. In: Megrey, B. and E. Moksness (eds.). Computers in Fisheries Research. Chapman and Hall, New York.
3. Davis, J.R. and Clark, J.L. (1989). A selective bibliography of expert systems in natural resource management. AI Applications in Natural Resource Management, 3(3): 1-8.
4. Mackinson, S. and Newlands, N. 1998. Using local and scientific knowledge to predict distribution and structure of herring shoals. ICES CM 1998:J11, 18pp.
5. Mackinson, S. In prep. An adaptive fuzzy expert system for predicting structure, dynamics and distribution of herring shoals.
6. Mackinson, S., Vasconcellos, M., and Newlands, N. 1999. A New Approach to the Analysis of Stock-Recruitment relationships: 'model-free estimation'using fuzzy logic. Can. J. Fish. Aquat. Sci., in press.
7. Mackinson, S., Nøttestad, L, Guénette, S, Pitcher, T.J., Misund, O.A. and Fernö, A.. 1998. Distribution and behavioural dynamics of ocean feeding Norwegian spring spawning herring: observations across spatio-temporal scales. ICES CM 1998:J12
8. Mackinson, S. and Nøttestad, L. 1998 Combining local and scientific knowledge. Rev. Fish Biol. Fish. 8(4): 481-490.
9. Pitcher, T.J., and Parrish J.K. 1993. Functions of schooling behaviour in teleosts. In: The Behaviour of Teleost Fishes, 2nd ed., Ed. by T.J. Pitcher: Croom Helm, London & Sidney, 364-439.
10. Huse I, Ona E (1996) Tilt angle distribution and swimming speed of overwintering Norwegian spring spawning herring. ICES J.mar.Sci 53:863-873
11. Mohr, H. 1971. Behaviour pattern of different herring stocks in relation to ship and midwater trawl. In: Modern fishing gear of the world, 3. pp 368-371. [ed.] H. Kristjonsson. Fishing news books ltd, Farnham, Surrey, England.
12. Hay, D.E. 1985. Reproductive biology of the Pacific herring (Clupea harengus pallasi). Can. J. Fish. Aquat. Sci. 42 (Suppl 1): 111-126.
13. Hourston, A.S. and Haegele, C.W. 1980. Herring on Canada's Pacific coast. Can. Spec. Publ. Fish. Aquat. Sci. 48: 23 p.
14. Nøttestad, L., Aksland, M., Betttestad, A., Fernö, A., Johanessen, A. and Misund, O.A. 1996. 02 27. Schooling dynamics of Norwegian spring spawning herring (Clupea harengus L.) in a coastal spawning area. Sarsia 80, 277-284. Bergen. ISSN 036 - 4827.
15. Robinson, C.M. and Pitcher, T.J. 1989. The influence of hunger and rations on shoal density, polarisation and swimming speed of herring (Clupea harengus L.). J. Fish. Biol., 35:459-60.
16. Misund, O.A. 1990. Sonar observations of schooling herring: school dimensions, swimming behaviour, and avoidance of vessel and purse seine. Rapp P.-v. Réun. Cons. Int. Explor. Mer. 189: 135-146.
17. Cushing, D.H. 1971. The dependence of recruitment on parent stock in different groups of fishes. J. Cons. Int. Explor. Mer. 33: 340-362.
18. Myers, R., Bridson, J. and Barrowman, N.J. 1995. Summary of worldwide spawner and recruitment data. Can. Tech. Rep. Fish. Aquat. Sci. 2020:iv + 327p.
19. Kosko, B. 1993a. Fuzzy systems as universal approximators. IEEE transactions on computers, 1993. Proceedings of the 1992 IEEE conference on fuzzy systems (FUZZ-92), 1153-1162, San Diego, March 1992.
20. Kosko, B. 1993b. Fuzzy thinking: the new science of fuzzy logic. Publ. Hyperion, New York. 318p.
21. Bezdek, J.C., 1981. Pattern recognition with fuzzy objective function algorithms. Advanced applications in pattern recognition. New York: Plenum Press. 256p.
22. Zadeh, L.A 1965. Fuzzy sets. Information and Control. 8 (3): 338-353
23. Zadeh, L.A. 1973. Outline of a new approach to the analysis of complex systems and decision processes. IEEE transactions on systems, man and cybernetics, Vol SMC-3, No. 1. January 1973.

ARDx - A Fuzzy Expert System for ARD Site Remediation

J.V. Balcita, J.A. Meech, M.M. Ghomshei

Department of Mining and Mineral Process Engineering,
University of British Columbia,
Vancouver, B.C., Canada

ABSTRACT

This paper details development of an expert system using fuzzy techniques to design remediation techniques for sites contaminated by Acid-Rock-Drainage. The fuzzy system is able to deal with missing, inaccurate, or heuristic data and still make useful design decisions.

Fuzzy sets are defined using a functional relationship between the degree of belief in a certain qualitative concept and one or more quantitative variables. Rules were developed during interviews with a chosen expert in the field. Using user input site data and characterization, the association of the degree of belief in a concept with that of other concepts come together within these rules to a produce a decision or conclusion.

The development of a fuzzy expert system for ARD is a benefit since it produces a standardized adaptable approach to the problem and provides quick advice to a user looking for a preliminary but detailed analysis.

The work done to this point includes a fuzzy controller, separate control modules for treatment options, cost analysis, and interactive hypertext documents. The controller and control modules work together in an attempt to follow the decision-making process as it chooses an appropriate treatment option for a site with possible or existing ARD. The hypertext documents are set up as user help-resources to provide system output information and to use as a training tool on treatment options for ARD or as a diagnostic tool on the possibility of implementing a treatment system.

BACKGROUND

Acid Rock Drainage (ARD) is contaminated acidic drainage from the spontaneous weathering and oxidation of pyrite and other sulfide minerals [1]. Weathering conditions increase the solubility of heavy metals, radionuclides, sulfate, and acidity; and reduce the pH of the drainage. ARD impacts on watershed characteristics and creates adverse effects in the surrounding ecosystem.

The problem exists in coal as well as metal mines. Once exposed, waste rock and/or tailings dams may continue to generate such acidity and pollution for decades and perhaps, centuries. It is imperative that prediction and prevention be used as a primary method to deal with and control ARD at virtually all mine sites. However, in active or abandoned mine sites where the problem already exists, and as a supplement to preventative measures in new mines; treatment of the contaminated drainage is necessary [2]. This can add appreciably to the on-going operating costs of a mine.

Expertise in the field of ARD is often controversial as fundamental knowledge is lacking, expertise are scarce, and new knowledge is continually being sought and applied. Prediction of weather conditions, surface and ground-water flows, chemistry of reactions in the waste piles and dissolution kinetics are all fraught with significant errors. Data to assess and deal with ARD problems are often missing and so heuristic judgements play an important role in decision-making. A fuzzy system is able to handle and manipulate missing, inaccurate, or heuristic data. [3] A fuzzy expert system thrives on these conditions.

The development of a fuzzy expert system for ARD is of benefit since it produces a standardized adaptable approach to the problem, provides quick advice to a user and is equipped for training and teaching.

0-7803-5489-3/99/$10.00 ©1999 IEEE.

ARDX COMPONENTS

In its entirety, the ARDX system is designed to handle ARD problems ranging from prediction, through to prevention and monitoring for treatment. The scope of the project to date deals with decision-making tactics for prevention and treatment at a mine site in one of three mine stages: planning, operating, or closure. The components of the system come together through a knowledge base and inference engine by using rules and fuzzy concepts; and with an explainer engine providing reasoning, explanations and answers to user questions. Figure 1 shows the components of the ARDX system. The knowledge base is itself made up of a main system module (ARDX "main") and numerous sub-modules.

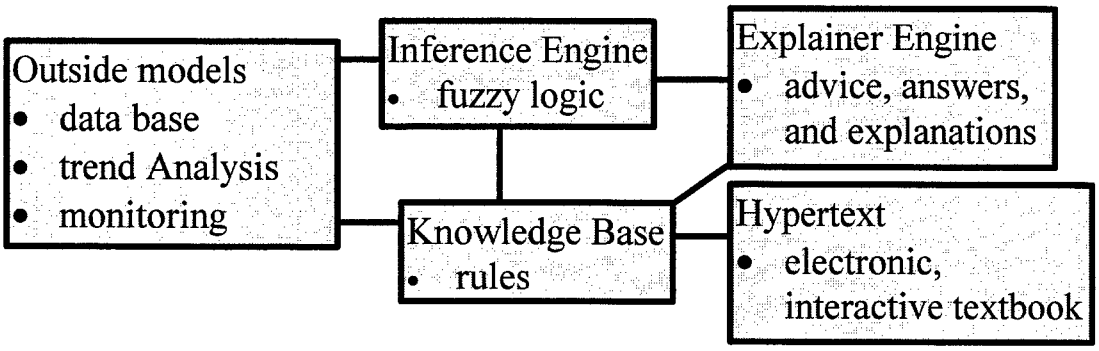


Fig. 1. Basic ARDX configuration flow-chart.

ARDX "main" interacts with the sub-modules and drives the system. It communicates with the user by asking for site specific data input; moves through the appropriate sub-modules; assesses whether an appropriate recommendation has been found; and cycles through again or exits the system as required. Forms pop up when called upon for data input, and hypertext files are used for system output. ARDX "main" decides the final recommended treatment options for the site by assessing the cost of treatment with the probability of success for each treatment option.

DEVELOPMENT PROCEDURE

Development of an expert system requires:

- a clear definition of the problem and domain of the system
- knowledge acquisition
- system development (programming steps)
- testing and verification of the system.

DEFINING THE PROBLEM AND DOMAIN

The first step often poses the most obstacles. In this case the domain of the system was designed to include all treatment possibilities. However, during knowledge acquisition, it became clear that the chosen domain was extremely large. Rather than change the chosen domain of the system, it was decided to focus on two aspects, an overall structure to the decision-making process (developed through ARDX "main") and a more detailed evaluation of separate treatment options (sub-modules). In this way a working system could be developed while separate modules containing further treatment options were added, revised or discarded as seen fit. ARDX "main" has become the seed for development of a larger and more complete system. Figure 2 shows the basic ARDX flow-chart that has become instrumental in organizing and developing the system.

Essentially, the system examines all appropriate methods in terms of their ability to deal with the potential or existing problem. Once a particular method or methods have been evaluated, the system looks for combinations of methods that may improve the solution further. When these have been assessed, the cost of each option is calculated and the recommendations of the least-costly, most-effective options are presented to the user.

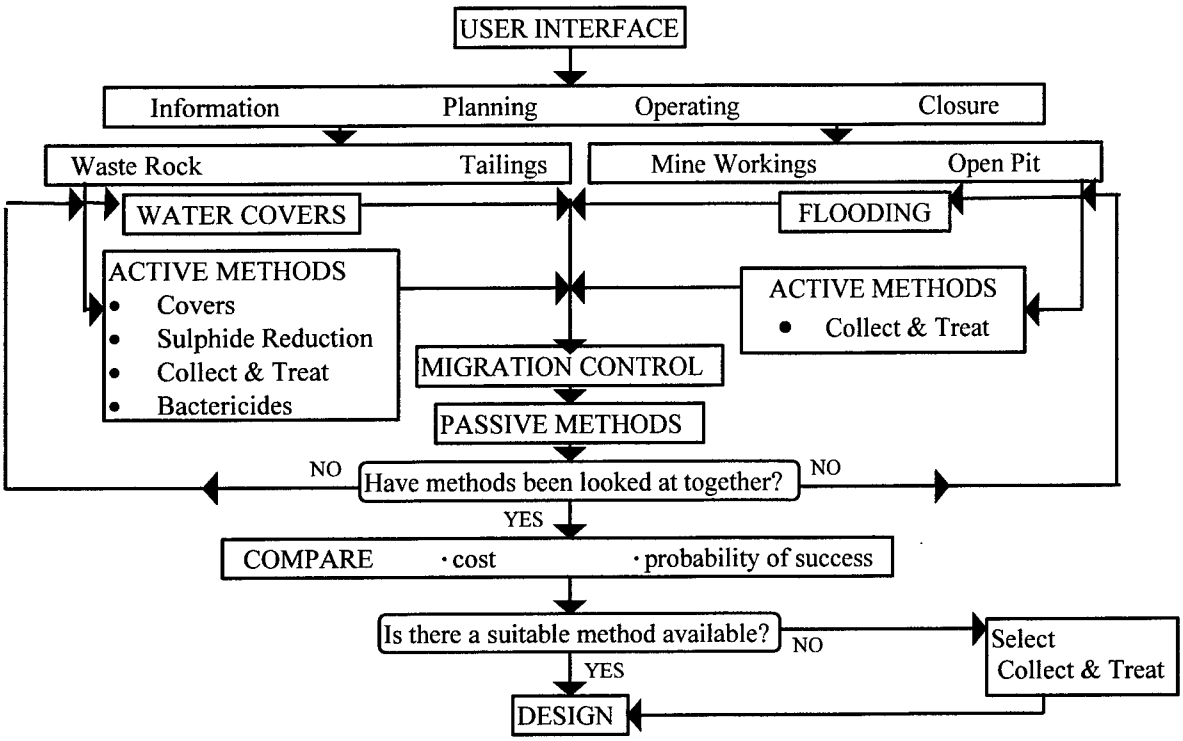


Fig. 2. Basic ARDX Flowsheet.

KNOWLEDGE ACQUISITION

Initially the knowledge acquisition phase included choosing and interviewing the expert as well as extensive literature searches on the topic of ARD treatment. Through interviews with the expert, the framework of the system was established. Expertise was taken from numerous and, sometimes, contradictive published papers on the subject. The challenge of building an expert system for ARD would appear to be in defining rules in a field where many decisions are presently being made by trial and error. Case studies were used to attempt to mimic the actual decision-making process followed by the expert. Acquiring expertise is an ongoing process as the system is developed and expanded.

DEVELOPMENT OF THE SYSTEM

ARDX operates within the COMDALE/X environment. Information is represented using keyword triplets; a method which assigns an attribute and value to each object. Data in a keyword triplet can be stored as strings, floating point numbers, dates, logical fuzzy variables, etc. [4].

The user interface consists of pop up FORMS, text boxes and hypertext documents. Through "forms", data consisting of drainage characteristics and site specifics are input by the user and stored as keyword triplets. The system will communicate with the user in the event of any inconsistency in the input data via text boxes. Once a conclusion has been reached, the output is displayed in a hypertext document.

The first step in successfully developing ARDX "main" was to write a set of preliminary rules to call upon the sub-modules. Output from the sub-modules are based on the concept of "high", "medium", and/or "low" assigned to the probability of successful mitigation or prevention and the capital cost (according to the amount of money available for the project) of the treatment option. Information from each sub-module can be used as inputs to other sub-modules as the system moves through the modules again to review the option of using combinations of the different treatment systems.

Development of the sub-modules is ongoing as new ones are continually being added. The "ACTIVE METHODS" module is itself (like ARDX "main") a smaller driving module that calls upon the various active treatment sub-modules. This secondary smaller driving module was necessary because of the large number of options available. Outputs to each module (probability of success) and the cost (calculated separately), are compared through Fuzzy Associative Memory (FAM) maps and given a Degree of Belief (DoB) in the treatment option.

The "COVERS" sub-module was developed first. This module is part of the extended "ACTIVE METHODS" sub-module and decides on the probability of a cover to be used as an active treatment option. Inputs of site details and characteristics are placed into fuzzy sets. Through these fuzzy sets, inputs are assigned a membership value in a set and a Degree of Belief (DoB) in the concept "low", "medium", and/or "high" [4] [5]. Figure 3 shows the FAM map elements that comprise the "COVERS" module.

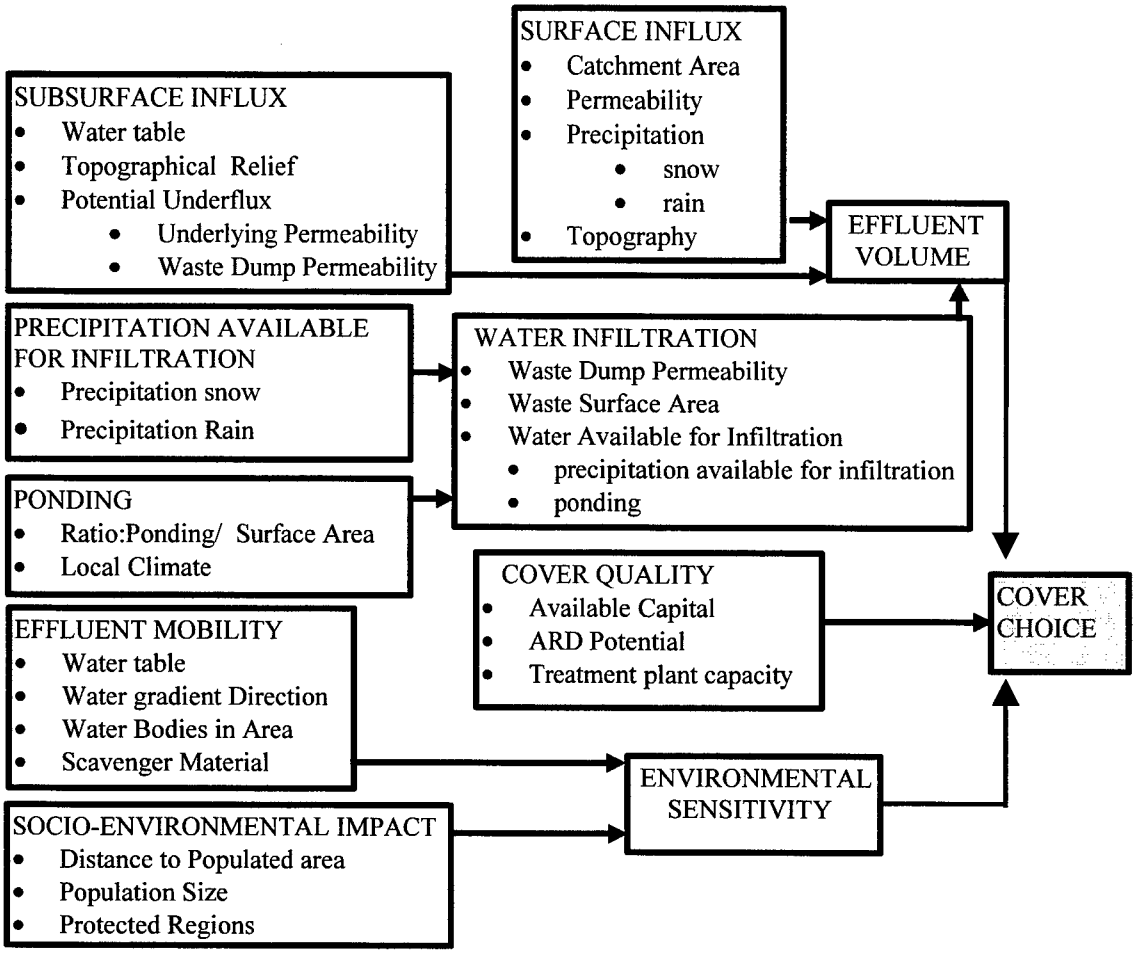


Fig. 3. "COVERS" Module Flowchart

A FAM map is a means to depict rules that combine to determine a degree of belief in a concept from a number of variables [5]. The FAM maps are created through interviews with the expert. They are used within the "COVERS" module to assess input information and decide upon an appropriate cover choice. The FAM map used to acquire a degree of belief in environmental sensitivity from two variables that are themselves determined through other FAM maps is shown in Figure 4. Certainty Factors (CF) of the concepts "sensitive", "slightly sensitive", and "resistant" need not add up to 100 as there may be an overlap in the belief in each concept and can be assigned as indicated within the FAM map.

ENVIRONMENTAL SENSITIVITY FAM		Socio-Environmental Impact		
		L	**M**	**H**
Effluent Mobility	**H**	s = 30 ss = 70 r = 10	s = 70 ss = 40 r = 0	s = 100 ss = 0 r = 0
	M	s = 0 ss = 50 r = 60	s = 20 ss= 90 r = 10	s = 60 ss = 50 r = 0
	L	s = 0 ss = 0 r = 100	s = 0 ss = 40 r = 70	s = 30 ss = 70 r = 10

Fig. 4. FAM map for Environmental Sensitivity of a site.
(ss = slightly sensitive, s = sensitive, r = resistant)

As the number of variables necessary to decide on a concept increases, the size and complexity of the FAM maps also increase resulting in large multi-dimensional maps of the decision-making process. However, by using a two-dimensional FAM map approach as shown above, this complexity can be separated into unique modules which are easy to understand and develop in consultation with the expert.

A separate cost module has been developed and is accessible by all modules as necessary. Calculated costs for an option can be used as inputs to modules. Costs for each remediation option are calculated using unit prices [6] and site-specific information. To account for future cost variability; the module updates all information according to the Marshall & Swift (M&S) index values [7]. The module is able to store input M&S values for future reference and calculations.

The economic evaluation of an treatment option is broken down into capital cost, maintenance and inspection costs; and operating costs due to continued effluent treatment and sludge disposal. The net present value of all on-going maintenance and operating costs are calculated from a user-defined rate of return value (defaulted to 3.5 if unavailable).

Defuzzification is performed using a weighted-average approach for the concepts "no" (an unacceptable treatment option), "no unless" (an acceptable option at a high cost, use if no other is available), "ok" (acceptable option), "good" (acceptable and low-cost), and "very good" (most cost effective) for each treatment option. This becomes the final degree of belief (DoB) in each treatment option recommended.

The output hypertext display provides a list of recommended treatment options, the probability of success and the cost demanded by each option. The user is able to "click" through the document for justification of each recommended treatment option and for information on the decision-making process; and has access to justification of the decision making process within the individual sub-modules.

TESTING

Testing the ARDX system is currently incomplete. Actual mining cases that have used or are using treatment options similar to those investigated by ARDX will be adopted to test the system. It is intended to apply both successful and unsuccessful cases for a comparison of chosen treatment options, their success, and treatment options decided upon by ARDX.

The "COVERS" sub-module has undergone preliminary testing using Samatosum mine data [8]. The data was input by the expert. The resulting output for probable cover treatment options corresponded to one of the options being considered for the mine.

CONCLUSION

Development of a Fuzzy Expert System on the design of ARD remediation plans has been successful. The system has the following benefits:

- a comprehensive, logical organization of the design methodologies has been developed
- a consistent design philosophy can be generated by use of this system
- a training tool has been created to assist in the transfer of ARD technology to the industry
- economic and effective procedures to use for a wide variety of site problems are available

Future expansion of this system will include ARD predictions based on expertise derived from case studies of existing sites. These predictions will be used as inputs to the existing system

ACKOWLEDGEMENT

The authors acknowledge financial support from the National Research Council through IRAP Grant No: 304695. We are also grateful for travel support from the Faculty of Graduate Studies and Research at UBC.

REFERENCES

1. R.W. Lawrence, A. MacG. Robertson, 1994. Acid rock drainage Understanding the problems - finding solutions. CIM District 6 Annual General Meeting, Workshop No. 1.
2. L. Filipek, A. Kirk, W. Schafer, 1996. Control Technologies for ARD. Mining Environment Management, Dec, 4-8.
3. A. Bowen, 1995. Expert systems: Truth and Rumors. Canadian Mining J., Mining Sourcebook, 8-12.
4. J.A. Meech, C.A. Harris, 1992. Expert Systems for Gold Processing Plants. Randol Gold Forum, Vancouver, B.C., 31-39.
5. J.A. Meech, 1995. AI Applications in the Mining Industry into the 21st Century. APCOM XXV Conference, 93-101.
6. MEND, 1995. Economic Evaluation of Acid Mine Drainage Technologies. MEND Report 5.8.1
7. Marshall, Swift, 1999. Marshall & Swift Equipment Cost Index. Chemical Engineering, 106(3), 170.
8. M. Ghomshei, A. Holmes, E. Denholm, R. Lawrence, T. Carriou, 1997. Acid Rock Drainage from the Samatosum Waste Dump, B.C., Canada. Proc. 4th Inter. Conf. on Acid Rock Drainage. 1, 351-366.

Modeling of Gold Heap Leaching for Criteria of Sustainability Targets

Roberto C. Villas-Bôas*, Luiz R. P. de Andrade Lima**

* Center for Mineral Technology, Rua 4, Quadra D, Ilha do Fundão,
Rio de Janeiro, RJ, Brazil, 21941-590
** Polytechnic School, Federal University of Bahia,
Rua Aristides Novis, 2, Salvador, Ba, Brazil, 40210-630

ABSTRACT

Sustainable development principles are forcing proactive approaches from mining and metallurgical process and design engineers to achieve prompt answers to minimize environmental impact, maximize energy utilization throughout processing, reducing materials flows and discards, as well as considering social satisfaction per monetary unit of products and processes. A computational algorithm devised to simulate the temporal evolution of gold ore heap leaching process, in an attempt to better understand the phenomenology behind heap leaching and provide insights into the development of a sustainability indicator is described. The data used in the model include physical-chemical, geometrical and operational data, such as: leachable metals contents, flow rate and cyanide concentration, parameters of passivity, ore size distribution, the average residence time of the solution in the heap, height, irrigated area and tonnage of ore in the heap. The shrinking-core model, describing the solid-fluid reaction under diffusion control, was used to calculate these variables. The simulations show that the number of layers has little effect on results indicating a stable and robust algorithm. The average residence time of the solution in the heap and the effective diffusivity of the cyanide solution through the ore particles have a significant influence on the temporal evolution of gold extraction and its concentration in the pregnant solution, so these parameters may be used to calibrate the model. In applying the algorithm to an industrial case, the results show that the model is able to predict the process performance reasonably, and might be used as a starter for Sustainable Development decision-making indicators, since it reflects changes over time of the analysed problem, and the results are reliable and reproducible.

INTRODUCTION

Criteria of sustainability are been sought in order to devise "green engineering" procedures to reach new targets imposed by society. Environmental constraints are receiving the greatest attention these days, and the effectiveness of cyanide leaching of gold ores in particular, is under question [1]. These criteria are based on indicators that can reflect changes over a period of time, that are reliable and reproducible, and, whenever possible, are calibrated in the same terms as the policy goals or targets linked to them [2].

Heap leaching has been in use for years as an effective method to treat gold ores throughout the world . As is well known, in this process, coarse ore is placed on an impervious surface, so prepared that a small slope relative to the horizontal axis is allowed, to drain-off the pregnant solution. On top of the heap, a leach solution is sprayed to progressively percolate down through the bed of ore. The pregnant solution at the bootom of the heap is then sent to the recovery step.

Column testing or experimental small heaps are utilized to estimate the leaching characteristics of the ore body. However scale-up to industrial heaps is unadvisable from such tests due to poor reproducibility of the geometry of the heap (particle size, heap height, length, width and overall slope) and the hydrodynamics.

These difficulties, associated with the time and costs required to prepare the testing programs, have led to development of phenomenological models to design and analyze heap leaching processes since the 60s and

0-7803-5489-3/99/$10.00 ©1999 IEEE.

throughout the 70s and 80s, in particular, for copper ores and pyrite. These models are based on the material balance of the reactants using a continuity equation applied to the heap and particles using specific kinetic models. In order to solve the complex system of partial differential equations obtained, simplifying hypotheses are introduced without losing the quality of the results.

A brief description of these models and their simplifying hypotheses was presented by De Andrade Lima et al. [3], when reviewing the literature [4,5,6,7,8,9].

THE MODEL

The algorithm is developed based on the hypotheses that: 1. the heap may be represented conveniently by a simplified geometrical shape; 2. the liquid flow through the heap bed is plug flow; 3. the average residence time of the solution in the heap does not vary with time or vertical location; 4. the heap presents an homogeneous grade of leachable metals and size distribution and; 4. the ore/leaching agent reaction is controlled by diffusion of leach solution through the large and weakly porous particles of the ore.

To build the algorithm, the heap is divided into horizontal layers of constant area. The gold recovery from the ore, the residual concentration of cyanide and the enrichment of the leach solution can be calculated from interactions among these layers.

For each heap layer, and for each species of any and every size class, the model equation is solved analytically for each time step. The flow in the heap is considered unidirectional at constant volume flowrate, but the species concentrations is considered to vary with time. Flow dispersion is neglected. Figure 1 illustrates the schematic slicing representation of the heaps.

It is worthwhile to mention that all simplifying assumptions, regarding unidirectional flow, constant volumetric flowrate, neglecting flow dispersion, and neglecting interactions between the main variables will affect the model precision, although not necessarily its robustness, as any model for environmental decision-making should attempt to achieve.

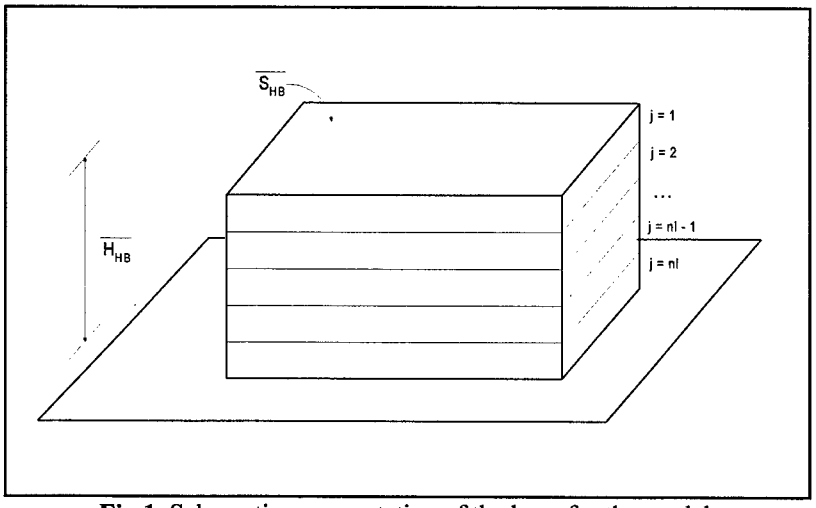


Fig 1. Schematic representation of the heap for the model.

If a division of ***nl*** layers of equal thickness is set in a heap of rectangular shape, as show in Figure 1, the pregnant solution and the leach solution that are flowing through the various layers of the heap are retained at a time equal to $\Delta\tau = \tau / nl$. Since the average residence time of the solution in each layer, is constant, the liquid hold–up of the heap is given by Equation 1.

$$\sigma_{HB}\varepsilon_{HB} = \frac{\tau Q}{\overline{H_{HB}}\,\overline{S_{HB}}} \qquad 1.$$

where ε_{HB} is the heap porosity, σ_{HB} is the heap saturation, τ is the average residence time of the solution in the bed of the heap, Q is the rate of irrigation in the heap, $\overline{H_{HB}}$ is the average heap height and $\overline{S_{HB}}$ is the average heap area.

Due to the coarse nature of the ore in the heap, diffusion control predominates in the reaction of ore/lixiviant so the shrinking core model may be used as in Equation 2. [10]:

$$\frac{d\alpha'_{tjim}}{dt} = \frac{3CCN_{tj}D_{CN}}{\rho lc_T R_i^2\left(1-\alpha'_{tjim}\right)^{-1/3}-1} \qquad 2.$$

where CCN_{tj} is the concentration of the free cyanide in the solution that enters layer ***j*** in time ***t***, D_{CN} is the apparent diffusivity of the cyanide in the ore particles, lc_T is the total lixiviant consumption, R_i is the average radius of the ore particles of the size fraction ***i***, α'_{tjim} is the recovery of the metal ***m*** in the size fraction ***i*** of layer ***j*** in time ***t*** and ρ is the ore density.

Equation 2. may be algebraically transformed into Equation 3. [3], which is analytically solved to give the individual metal (m) recoveries, at time ($t\cdot\Delta\tau$), originating from the particles of size ***i***, located in layer ***j***, when the recoveries at time ($t\text{-}1\cdot\Delta\tau$), the leach solution cyanide concentration from layer ***j-1*** and the individual concentrations of the metal species are known.

$$\alpha'^3_{tjim}+b_{tjim}\alpha'^2_{tjim}+c_{tjim}\alpha'_{tjim}+d_{tjim}=0 \qquad 3.$$

where:

$$b_{tjim}=\left(\frac{3Z_{tjim}}{2}+\frac{27}{8}\right),\ c_{tjim}=\left(\frac{3Z^2_{tjim}-27}{4}\right),\ d_{tjim}=\left(\frac{Z^3_{tjim}+27}{8}\right) \text{ and}$$

$$Z_{tjim}=2K_{tjim}\Delta\tau-3\left(1-\alpha'_{t-1jim}\right)^{2/3}-2\alpha'_{t-1jim}$$

Ore physical constraints, inhibiting the leach solution from diffusing completely through the ore particles; give rise to an attenuation factor (θ_m), as defined by Equation 4. This factor must be determined from laboratory experiments.

$$\alpha_{tjim}=\alpha'_{tjim}\theta_m \qquad 4.$$

On the other hand, knowing the ore size fractions and assuming they are homogeneously distributed within each of the ***nl*** layers, and considering further, that for the time intervals for which Equation 3. is solved, there is no variation in grade of the particles and the metal species contents of each size fraction is known, so the global recovery, at each time increment in each layer is given by Equation 5.

$$\alpha L_{tjm}=\sum_{i=1}^{nf}\alpha_{tjim}f_i \qquad 5.$$

Suppose that each of the ***nl*** layers have the same mass, then the global recoveries of each metal species at each time increment are given by Equation 7.

$$\alpha H_{tm}=\frac{\sum_{j=1}^{nl}\alpha L_{tjm}\gamma_{jm}}{\sum_{j=1}^{nl}\gamma_{jm}} \qquad 6.$$

The residual metal content in each layer of the heap can be calculated from Equation 7 for each instant of time. This is an extremely important feature for developing a Sustainability Development Indicator.

$$\gamma r_{tjm} = \gamma_{ojm}\left(1 - \alpha L_{tjm}\right) \quad 7.$$

where γ_{ojm} is the initial concentration of the metal ***m***, contained in layer ***j***.

The solution cyanide concentration leaving layer **j** is calculated from Equation 8. whereas the concentration of metal species that leave layer **j** are obtained from Equation 9, where CCN_{tj} and CCN_{t-1} are respectively the concentration of free cyanide in solution that enters and leaves layer ***j*** at time ***t***, CM_{tjm} and CM_{tj-1m} are respectively the concentration of metal ***m*** in solution entering and leaving layer ***j*** at time ***t***, αL_{tjm} and $\alpha L_{t\text{-}1jm}$ are the recoveries of metal ***m*** in layer ***j*** at the present and previous times, and M_{HB} is the heap tonnage.

$$CCN_{tj+1} = CCN_{tj} - \left(\frac{M_{HB}\gamma_m}{S_{HB}\ H_{HB}}\right)\sum_{m=1}^{nm}\left[\mathrm{lc_m}\left(\alpha L_{tjm} - \alpha L_{t-1jm}\right)\right] \quad 8.$$

$$CM_{tj+1m} = CM_{tjm} + \left(\frac{M_{HB}\gamma_m}{S_{HB}\ H_{HB}}\right)\left(\alpha L_{tjm} - \alpha L_{t-1jm}\right) \quad 9.$$

The proposed algorithm considers that the lixiviant enters into the first layer (***j***=1) at the top of the heap and remains there for a time $\Delta\tau = \tau / n$. Later on, the solution is transferred to the next layer (***j***=2) and from this to the next until it reaches the last one (***j*** = ***nl***). During the time that the liquid solution remains in layer (***j***) Equation 3. is solved for each metal (***m***) contained in each size-fraction (***i***), taking into account the residuals of the metals (γr) and the composition of the solution (*CCN* and *CM*). Then Equations 4. through 9. are applied to update these concentrations and tenors.

SENSITIVITY ANALYSIS OF THE MODEL

In order to evaluate the effect of the input variables, a numerical design of experiments was performed taking as the measured responses, a set of four that characterizes the time/evolution curve, as shown in Figures 2 to 4. These parameters are: $t_{1/2}$ - half life time of the heap (days), r^o - rate of recovery at the start of process (%/day), Cau_{in} - gold concentration at the first drop of leach liquor (ppm) and t_{ccn} - the time when the non-reacted cyanide solution begins to flow into the heap (day). A 2-level fractional experimental design consisting of 14 variables and 20 numerical experiments were developed. Table 1 shows the values for the high (+) and low (-) levels for each variable chosen to account for the reported ranges in the literature. Table 2 shows the experimental matrix and responses of this arrangement. The results were analysed statistically and by cluster analysis and principal components analysis [11,12, 13].

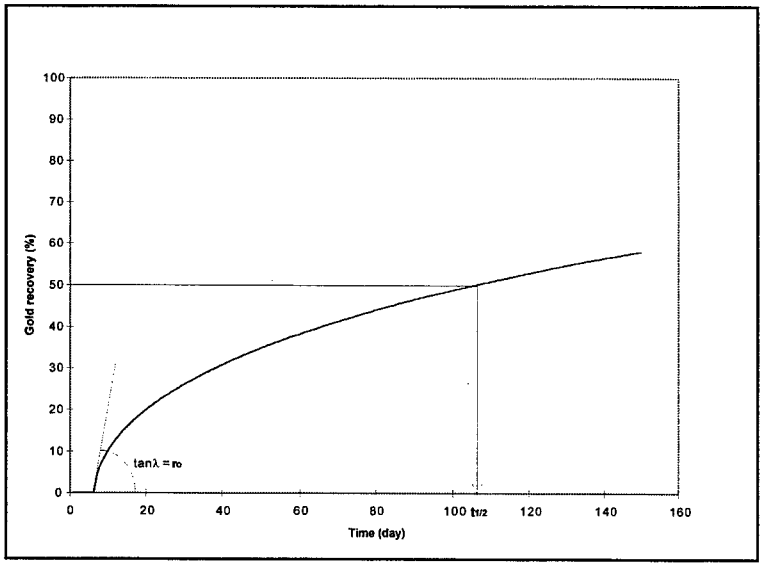


Fig. 2. Parameters utilized to characterize the performance of the process ($t_{1/2}$, r^o).

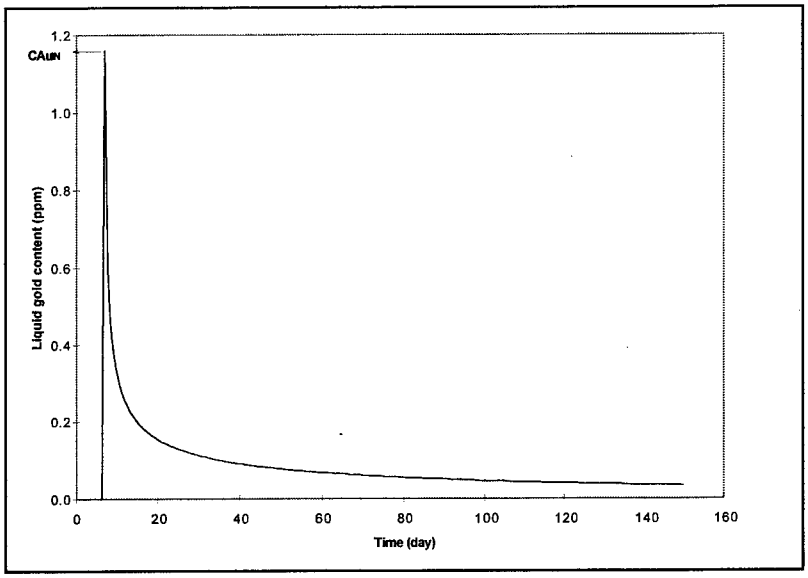


Fig. 3. Parameters utilized to characterize the performance of the process (CAu_{in}).

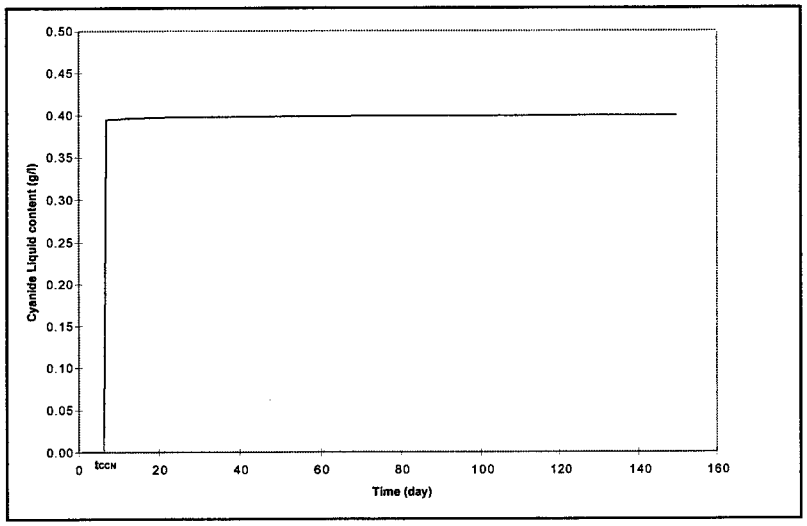


Fig.4. Parameters utilized to characterize the performance of the process (t_{ccn}).

Table 1. Data for the sensitivity analyses.

VARIABLE		LEVEL (-)	LEVEL (+)
β_{CN}	[$m^2 h^{-1}$]	3.5×10^{-7}	7.0×10^{-7}
ρ	[$g\ cm^{-3}$]	2.5	5.0
γ_{Au}	[ppm]	2.0	4.0
θ_{Au}	[%]	80	100
γ_{Ag}	[ppm]	250	500
θ_{Ag}	[%]	70	100
Cl_T	[$g\ kg^{-1}$]	0.5	1.0
H_{HB}	[m]	2.5	5.0
M_{HB}/S_{HB}	[$t\ m^{-2}$]	5.0	10.0
ε_{HB}	[%]	45	75
σ_{HB}	[%]	10	20
C_{CN}	[$g\ l^{-1}$]	0.5	1.0
Q/S_{HB}	[$l\ h^{-1}\ m^{-2}$]	6.5	13.0
R	[mm]	20	40
nl		20	50

Table 2. Design of experiments and numerical results.

	LEVEL OF THE VARIABLES																		RESULTS OF SIMULATION			
TEST	l_{CN}	ρ	γ_{Au}	θ_{Au}	γ_{Ag}	θ_{Ag}	lc_T	H_{HB}	M_{HB}/S_H	ε_{HB}	σ_{HB}	C_{CN}	Q/S_H	nl	R	V_1	V_2	V_3	V_4	$t_{½}$	r^o	CAu_{IN}	t_{CCN}
1	+	+	-	-	+	+	+	+	-	+	-	+	-	-	-	-	+	+	-	6.81	33.28	1.600	2.644
2	-	+	+	-	-	+	+	+	+	-	+	-	+	-	-	-	-	+	+	18.21	13.39	1.600	1.803
3	+	-	+	+	-	-	+	+	+	+	-	+	-	+	-	-	-	-	+	4.97	19.82	4.000	3.990
4	+	+	-	+	+	-	-	+	+	+	+	-	+	-	+	-	-	-	-	12.21	19.50	2.000	2.644
5	-	+	+	-	+	+	-	-	+	+	+	+	-	+	-	+	-	-	-	7.75	15.86	6.400	3.269
6	-	-	+	+	-	+	+	-	-	+	+	+	+	-	+	-	+	-	-	10.46	33.42	4.000	1.262
7	-	-	-	+	+	-	+	+	-	-	+	+	+	+	-	+	-	+	-	3.97	66.78	2.000	1.500
8	-	-	-	-	+	+	-	+	+	-	-	+	+	+	+	-	+	-	+	8.47	75.58	3.115	0.721
9	+	-	-	-	-	+	+	-	+	+	-	-	+	+	+	+	-	+	-	17.17	15.75	0.800	0.829
10	-	+	-	-	-	-	+	+	-	+	+	-	-	+	+	+	+	-	+	67.99	8.15	0.800	5.000
11	+	-	+	-	-	-	-	+	+	-	+	+	-	-	+	+	+	+	-	7.42	26.97	6.400	3.173
12	-	+	-	+	-	-	-	-	+	+	-	+	+	-	-	+	+	+	+	3.05	78.01	4.000	0.661
13	+	-	+	-	+	-	-	-	-	+	+	-	+	+	-	-	+	+	+	3.88	31.73	3.200	1.635
14	+	+	-	+	-	+	-	-	-	-	+	+	-	+	+	-	-	+	+	6.14	65.46	4.000	1.471
15	+	+	+	-	+	-	+	-	-	-	-	+	+	-	+	+	-	-	+	15.63	47.68	2.492	0.361
16	+	+	+	+	-	+	-	+	-	-	-	-	+	+	-	+	+	-	-	3.07	130.93	4.000	0.736
17	-	+	+	+	+	-	+	-	+	-	-	-	-	+	+	-	+	+	-	37.09	16.63	2.000	0.793
18	-	-	+	+	+	+	-	+	-	+	-	-	-	-	+	+	-	+	+	11.60	22.87	3.607	2.404
19	+	-	-	+	+	+	+	-	+	-	+	-	-	-	-	+	+	-	+	7.31	8.29	1.000	6.130
20	-	-	-	-	-	-	-	-	-	-	-	-	-	-	-	-	-	-	-	4.90	54.32	1.600	0.793

Table 3 summarizes the sensitivity analysis for the proposed model. As can be seen, the number of heap subdivisions does not appreciably impact the responses, whereas diffusivity and residence time (represented by porosity and solution saturation) are the variables that most affect response and so, these are the ore parameters that govern the proposed model. These variables can be used to calibrate the model, since they are not easily estimated or measured and yet, they have a substantial effect on the results.

Table 3. Results of the sensitivity analysis

	$t_{½}$		r^o		CAu_{IN}		t_{CCN}	
	SA	PCA-CA	SA	PCA-CA	SA	PCA-CA	SA	PCA-CA
l_{CN}	x	*						
ρ	x							
γ_{Au}		*			x	*		
θ_{Au}		*				*		
γ_{Ag}								
θ_{Ag}								
lc_T	x	*	x	*	x	*		*
H_{HB}								*
M_{HB}/S_{HB}			x			*		*
ε_{HB}			x	*				*
σ_{HB}			x	*			x	*
C_{CN}	x	*	x	*	x	*		
Q/S_{HB}			x	*			x	*
R	x	*		*		*		
nl								

SA : Statistical analysis of the design of experiments
PCA-CA : Principal component analysis and cluster analysis results
x : Significant in the statistical analysis at a confidence level of 90 %
* : Significant in the principal component analysis and cluster analysis

CASE STUDY

The model was tested with published data from the Fazenda Brasileiro Mine operated by Companhia Vale do Rio Doce in the State of Bahia in Brazil [14] (Siqueira et al., 1985). This mine utilizes oxidized ore with gold content of 3.5 ppm. The presence of sulfur and other leachable metals species are negligible. Since no detailed data was available to carry out the simulation, the values of the particle size distributions, the height of the heap and the irrigated area, were taken as nominal ones. Since the effective diffusivity of the cyanide and the average residence time are the variables that most affect the model responses, they were used to perform the model calibration. Table 4 shows the values for the variables used in the simulation.

Table 4. Input data for simulation runs

VARIABLE		Heap P-1A
$\mathcal{D}_{CN}$	[$m^2 h^{-1}$]	5.0×10^{-9} **
ρ	[$g\ cm^{-3}$]	2.7
lc_T	[$g\ kg^{-1}$]	0.50
γ_{Au}	[$g\ t^{-1}$]	3.45
θ_{Au}	[%]	92.2
H_{HB}	[m]	5.0 *
M_{HB}	[t]	31500
S_{HB}	[m^2]	2333 *
τ	[day]	5.84 **
C_{CN}	[g [illegible]$^{-1}$]	1.5
Q/S_{HB}	[[illegible] $h^{-1}\ m^{-2}$]	10.7
R	[mm]	9.525*
nl		25

*nominal values **estimated parameters

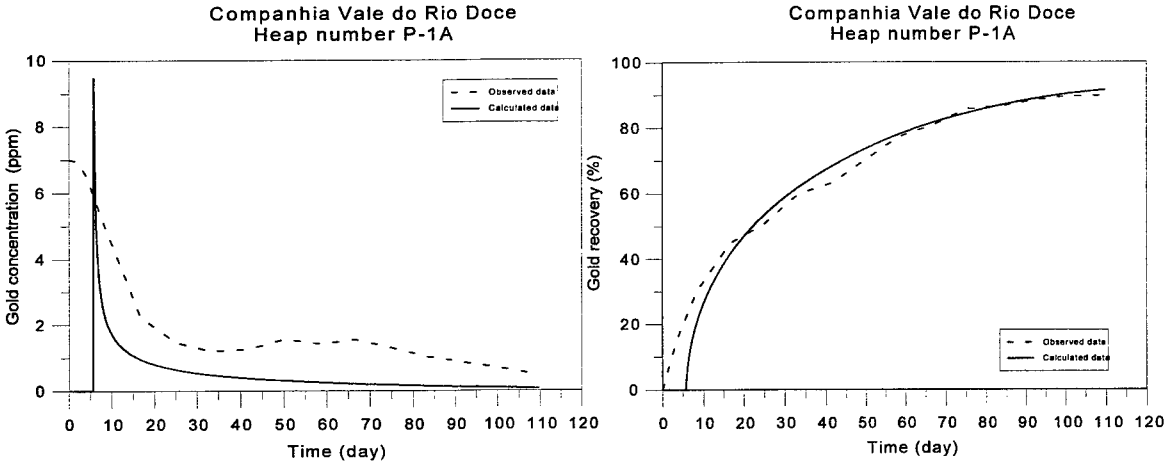


Fig. 5. Comparison between simulated results and experimental data for an industrial heap.

The results of the simulation are shown in Figure 5. As can be seen, there is some nonconformity between the actual and simulated results that may be due to the oversimplifications mentioned above, i.e., neglecting of size distribution, the average surface area, the average height and the radial and axial flow dispersion. However, the simulated curves are relatively close to the real ones, except at the beginning of the leaching process, which may be explained by the limitation of the flow model utilized and to the failure to consider the flow of solution through the impervious surface of the heap. In addition the actual gold concentration values in the leaching solution are maintained on the order of 0.5 to 1 parts per million, by cyanide solution recycle with residual gold.

CONCLUSIONS

1. Heap leaching processes for gold ores may be reasonable described by a model in which plug flow and diffusion control kinetics are considered for the heap and for the ore/cyanide reactions, respectively.
2. The analytical solution at each time interval of the shrinking core model gives robustness to the model.
3. The effective diffusivity of cyanide and the average residence time are calibrating parameters of the model. They also have obvious environmental implications.
4. The development of correlations to relate the average residence time of the solution in the heap to the operational parameters, as well as, the utilization of the real size distribution, the average heap surface, the average heap height and a diffusive flow model definitely improves the precision of the simulation results; however, little is expected in improving its accuracy, due to its robustness per se.
5. The results shown are good indicators to represent the process performance and might, thus, be utilized as a starting point for decision-making procedures targeting maximization of environmental capital represented, in this case, by the heap itself, its chemical species and its solution flow .
6. It is interesting to stress the readily-assessed individual consumption of cyanide, for each metal species of interest, in a given time period, as well as the eventual inhibition of leach solution diffusion, thus resulting in the possibility to build-up individual environmental indicators.

ACKNOWLEDGMENT

One of the authors (L.R.P. De Andrade Lima) thanks the **Conselho Nacional de Desenvolvimento Científico e Tecnologico** of the Brazil (**CNPq**) for the award of a scholarship throughout this project.

REFERENCES

1. R.C. Villas-Bôas ,1994. Materials Production and the Environment. Hydrometallurgy '94 , Chapman & Hall, Suffolk, 107-121.
2. A. Hammond, et al., 1995. Environmental Indicators: A Systematic Approach to Measuring and Reporting on Environmental Policy Performance in the Context of Sustainable Development, World Resources Institute, May, p.11.
3. L.R. De Andrade Lima, R.C. Villas-Bôas, H.M. Kohler, 1998, Mathematical Modeling of Gold Ore Heap Leaching, International Symposium on Gold Recovery, Montreal, Canada, CIM, (in press).
4. R.J. Roman, B.R. Benner, G.W. Becker, 1974. Diffusion model for heap leaching and its application to scale-up, Trans. AIME, 256, 247-256.
5. J.C. Box, R. Yusuf, 1984.Simulation of heap and dump leaching process. Proceedings of the Symposium on Extractive Metallurgy, Melbourne, Australia, 117-124
6. J.C. Box, A.P. Prosser, 1986. A general model for the reaction of several minerals and several reagents in heap and dump leaching. Hydrometallurgy, 16, 77-92.
7. A.P. Prosser, 1988. Simulation of gold heap leaching as an aid to ore-process development, Proceedings of the Precious Metals '89, 121-135.
8. D.G. Dixon, J.L. Hendrix, 1993. A mathematical model for heap leaching of one or more solid reactants from porous ore pellets, Metallurgical Transactions, 24B, 1087-1102.
9. Sanchez-Chacon and Lapidus, 1997. Model for heap leaching of gold ores by cyanidation, Hydrometallurgy, 44, 1-20.
10. G.F. Froment, K.B. Bischoff, 1979. Chemical Reactor Analysis and Design, J. Wiley & Sons, NY, 765pp.
11. L.R.P. De Andrade Lima, R.C. Villas-Bôas, H.M. Kohler, 1995. Análise de sensibilidade de modelos usando as técnicas de cluster analyses e Plackett-Burman, in: XVI Encontro Nacional de Tratamento de Minérios e Hidrometalurgia, Rio de Janeiro, Brazil
12. J.C. Cassa, L.R.P. De Andrade Lima, 1997. Screening variables in complex systems: A comparative study, Proceedings of the XX International Mineral Processing Congress, Aachen, Germany, 1, 433-444.
13. De Andrade Lima, L.R.P., Villas Bôas, R.C. and Kohler, H.M., 1998. Modeling of gold heap leaching for criteria of sustainability targets, in: S.A. Atak, G. Önal & M.S. Çelik (Editors), Innovations in Mineral and Coal Processing, Balkema, Rotterdam. p.541.
14. L.T. Siqueira, R. Madeira, M. Fiuza, S. Nakamura, M.C. Reinhardt, I. Trancosos, 1985, Projeto Ouro Bahia - "Fazenda Brasileiro" (CVRD), In: I Simposio Internacional do Ouro, Rio de Janeiro, 1-22.

Design Optimisation of Aluminum Recycling Process using the Taguchi Approach

A.R. Khoei, D.T. Gethin, I. Masters

Mechanical Engineering Department, University of Wales Swansea, Singleton Park, Swansea, SA2 8PP, U.K.

ABSTRACT

This paper describes an experimental investigation into the process parameter effects on product quality in aluminium recycling. In order to optimise the aluminium recovery process, the factors which have the greatest influence have to be identified and optimum values chosen. In the re-melting of scrap, the ultimate goal is to produce clean aluminium while minimising metal losses. In this project, a Taguchi method is used initially to plan a minimum number of experiments. Orthogonal array experiments are used as these allow the simultaneous variation of several parameters and the investigation of interactions between parameters. Standard *L4* and *L9* orthogonal arrays are employed to evaluate the effects of parameters under changing conditions. Statistical analysis, such as ANOVA, is then employed to determine the relationship between the processing conditions and the yield levels. This investigation has indicated the parameters where process control is important and allowed the elimination of some parameters from the main experimental programme.

INTRODUCTION

Industries are facing not only demands for increased productivity but also stringent legislation involving the release of by products into environment. Both aspects are particularly important for the aluminium recycling industries, who convert aluminium dross and coated scrap into raw material. The role of recycling in the aluminium industry cannot be overstated. Recycling is a critical component of the industry, both from its contribution to the environment and because of the favourable economic impact on production. This dual benefit is probably the reason aluminium beverage cans now account for the total beverage can market in the USA. The demand for used cans is strong and virtually guaranteed. When considering solid waste issues, it's important to remember the aluminium can is solid value, not solid waste.

The melting of aluminium dross and scrap materials to recover aluminium as metal is a simple, yet effective method of recycling a valuable material with a high inherent energy content. There are several processes to recycle aluminium but a viable melting option available to processors of aluminium dross and scrap is to employ a 'rotary furnace', which is commonly used in large-scale aluminium recycling. Once the can has been collected from a collection point, it is crushed, and taken to a recycling plant. The aluminium is then loaded into a hot furnace that is designed to remove all the paint and dirt from them. The furnace is heated until the paint and coatings boil off of the aluminium, and are sucked out of the oven by powerful fans. At the same time furnace melts the aluminium completely, and mixes it to make sure that it is of the right quality to be used again.

Recently, IMCO Recycling Ltd. has sought to introduce a scientific understanding of the process with a view to improving productivity and quality, reduce waste and to develop process models. The purpose of this research is to address aluminium recovery as a manufacturing process and to establish the dominant factors, which need to be controlled, to improve an already efficient process.

The paper presents an application of the Taguchi orthogonal array technique [1] to the aluminium recycling process. A matrix experiment based on an orthogonal array is conducted to change the settings of the various process parameters. The effects of different factors are determined by computing simple averages and indicating the optimum factor. The relative effect of various factors is then calculated using an analysis of variance. This investigation has highlighted key areas of recycling where close control is required to

0-7803-5489-3/99/$10.00 ©1999 IEEE.

improve the consistency of the process. A similar method was recently presented by Wells *et al.* [2] for re-melting of scrap in Reynolds' Reclamation Plants. The Reynolds' Reclamation Plants utilises a reverbatory furnace, but the method appears to hold for both types of operations.

This application of Taguchi methods focuses on how to cost-effectively conduct process control activities during the aluminium recycling process. This method helps to diagnose the health of process, minimise production of defects and achieve an equilibrium between being 'quality conscious' and being 'cost conscious'.

ALUMINIUM RECYCLING PROCESS

The melting process is based on a rotary furnace, which consists of a cylindrical steel drum and a chamber. The furnace is heated by a burner located in the furnace drum. The burner system generates temperatures of over 1700°C inside the refractory lined drum.

At the commencement of 'heat', flux along with a pre-weighted amount of feed material is charged into the furnace. On completion of charging, the burner is ignited and the furnace is rotated. The furnace fume will be collected in the charging chamber, where it will be extracted by the furnace fume gas cleaning system. Once molten, the furnace is stopped and the aluminium is decanted. The molten metal is then discharged from the furnace and directed either to moulds where it will solidify, or into preheated crucibles.

DESIGN OF EXPERIMENTS

The aim of experimental investigation is to more fully understand the aluminium recycling process and its implications for the control of recovery. The orthogonal array technique may be used for experimental design as it reduces the number of experiments required to fully investigate a set of parameters and can be used to indicate interactions between the parameters investigated [3]. It is especially important to minimise time and costs while performing experiments using a production aluminium plant.

At the first stage of this project, a detailed experimental investigation of the existing process was undertaken. Initial brainstorming sessions produced a list of over 100 variables, which are believed to influence the recycling process. These are divided into control parameters and process stability parameters. The first group which can be used and adjusted for the recycling of aluminium, have a significant impact on the process and are used to correct recovery variation while running. The second group are parameters which are either left to vary while the process is running or are adjusted by the operator to obtain optimum running conditions. Establishing which of these are key to maintaining process stability is felt to be essential to the long term success of the project.

In order to investigate the process control and stability factors, experiments need to be undertaken during production. The recycling process is fully instrumented for the measurement of parameters including load weight, melting temperature and speed rotation of furnace. An efficient way to study the effect of several control factors simultaneously is to plan matrix experiments using orthogonal arrays. A series of experiments using a Taguchi-type design are performed during normal production in IMCO Recycling Ltd. This allowed the effects of experiments to be assessed without a serious disruption of production.

Due to the commercially sensitive nature of the process being monitored, the factors are denoted by A, B and C, and the levels are related to standard operating conditions.

Table 1. Test 1 factors and their levels

Factors	Levels	
	1	2
A	*a*	*a + 2*
B	*b*	*b + 60*
C	*c*	*c + 1*

Table 2. Test 1 matrix experiment

Exp. No.	Factors			Recovery (%)
	A	B	C	
1	1	1	1	*r* + 8.1
2	1	2	2	*r* + 6.2
3	2	1	2	*r* + 6.7
4	2	2	1	*r* + 7.7

After creating a Taguchi orthogonal array, the selected process parameters are varied slightly from standard values, which results in varying yield levels. Standard *L4* and *L9* orthogonal arrays are considered to evaluate the optimum level for each factor in the recovery of 'coated' and 'class' scrap materials.

Test 1: An *L4* Orthogonal Array

In the first series of experiments, the simplest orthogonal array, *L4,* is considered in determining the effect of three process parameters in the recycling of 'coated scrap' materials. For each parameter, two levels are chosen to cover the experimental region, as listed in Table 1. The matrix experiment selected for this case is given in Table 2. It consists of four individual experiments corresponding to the four rows. The entries in the matrix represent the levels of the factors. In order to conduct the matrix experiment at different level of temperatures, the furnace has been run by setting up the furnace PID at the indicated temperatures, as shown in Figure 1.

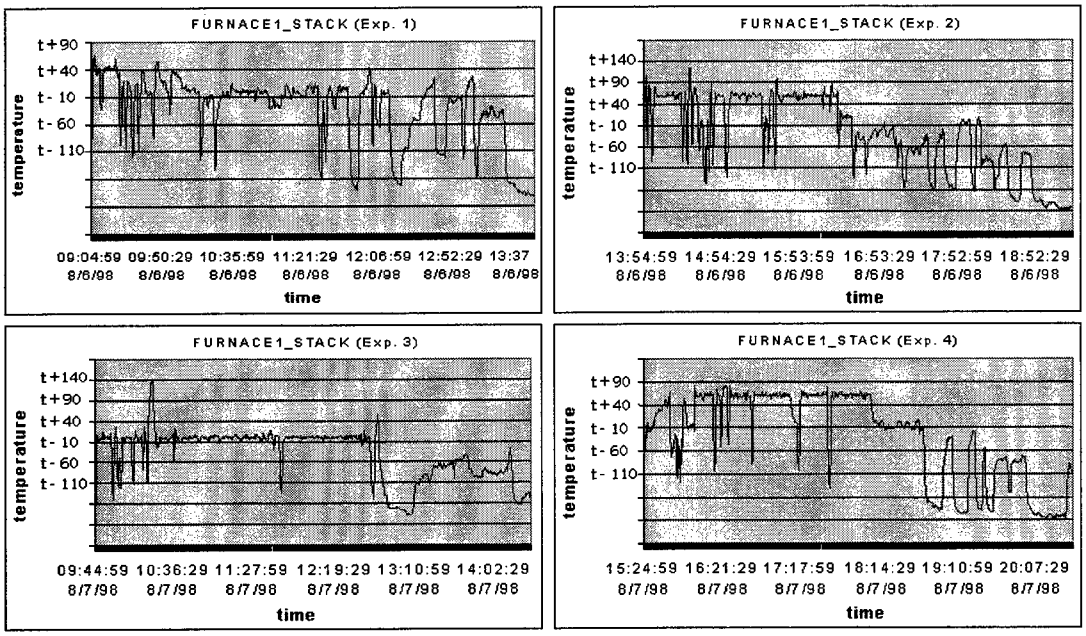


Fig. 1. Variation of temperature with time for different experiments using the furnace PID control

Table 3. Test 1 average of signal-to-noise ratio

Factors	Levels	
	1	2
A	*r* + 7.1	*r* + 7.2 *
B	*r* + 7.4 *	*r* + 6.9
C	*r* + 7.9 *	*r* + 6.4

* indicates the optimum level

Table 4. Test 1 ANOVA analysis for recovery

Factors	Degrees of freedom	Sum of squares	Mean square	Variance Ratio
A	1	0.0025 *	0.0025	
B	1	0.2025 *	0.2025	
C	1	2.1025	2.1025	20.51
Error	0	0	-	
Total	3	2.3075		
(Error)	(2)	(0.205)	(0.1025)	

* indicates sum of squares added together to estimate the pooled error sum of squares indicated by parentheses

A summary static analysis of recovery, called signal-to-noise (S/N) ratio, is employed to find the optimum level [4, 5]. By taking the numerical values of recovery listed in Table 2, the average recovery for each level of the three factors can be obtained as listed in Table 3. The optimum level for each factor is the level that gives the highest value of recovery in the experimental region. Thus, high level of factor A along with low level of factors B and C will make the highest levels of recovery.

The relative magnitude of the effect of different factors can be obtained by the decomposition of variance, called analysis of variance (ANOVA) [4]. An ANOVA analysis for estimating the error variance for the factor effects and variance of the prediction error is given in Table 4. In this Table, the number of independent parameters associated with a matrix experiment or a factor is called 'degrees of freedom'. The matrix experiment with four rows has three degrees of freedom associated with the total sum of square. Each factor with two levels has only one independent parameter and hence, one degree of freedom. Therefore, the degrees of freedom for error comes out to be zero.

The sum of squares values due to various factors, tabulated in Table 4, are a measure of the relative importance of the factors in changing the values of recovery. It can be seen that factor C explains a major portion of the total variation of recovery. In fact, it is responsible for (2.1025/2.3075) x 100 = 91.1 percent of the variation of recovery. Factors B and A together are responsible for only a small portion, namely 8.8 and 0.1 percent, of the variation in recovery. It should be noted that because the error term has no degrees of freedom associated with it, the sum of squares contribution to this term is zero. In Table 4, the mean square for a factor is computed by dividing the sum of squares by the degrees of freedom.

An estimation of the sum of squares for the error term can be obtained by pooling the sum of squares corresponding to the factors having the lowest mean square [4], i.e. factors A and B. These two factors together account for two degrees of freedom and the sum of their sum of squares of 0.205, as indicated by parentheses. Hence, the error variance is 0.1025. The variance ratio can be found using the ratio of the mean square due to a factor and the error mean square. The large value of the variance ratio, 20.51, means the effect of factor C is quite large compared to the error variance.

Table 5: Test 2 factors and their levels

Factors	Levels		
	1	2	3
A	*a - 1.5*	*a*	*a + 1.5*
B	*b*	*b + 20*	*b + 40*
C	*c - 1*	*c*	*c + 1*

Table 6: Test 2 matrix experiment

Exp. No.	Factors *				Recovery (%)
	A	B	C	e	
1	1	1	1	1	*r + 5.3*
2	1	2	2	2	*r + 2.9*
3	1	3	3	3	*r + 9.2*
4	2	1	2	3	*r + 6.1*
5	2	2	3	1	*r + 0.4*
6	2	3	1	2	*r + 1.8*
7	3	1	3	2	*r + 5.2*
8	3	2	1	3	*r + 4.5*
9	3	3	2	1	*r + 6.3*

* empty column is denoted by e.

Test 2: An *L9* Orthogonal Array

In the second series of experiments, an *L9* orthogonal array is employed in recycling of 'class scrap' materials. As in the last test, three control factors A, B and C are selected for process optimisation. For each factor, three levels are chosen to cover the wide region of variation. These factors and their alternate levels are listed in Table 5. The *L9* orthogonal array is given in Table 6, which consists of nine experiments corresponding to the nine rows and four columns. In this matrix, the chosen three factors are assigned to columns 1 through 3 and column 4 is arbitrarily designed as an empty column.

After conducting the experimenter's log given in Table 6, the next step in data analysis is to estimate the effect of each control factor and to perform analysis of variance (ANOVA), as described in the last test. The factor effects for recovery of 'class scrap' materials and the respective ANOVA analysis are given in Table 7. The optimum level for each factor is obtained by the average recovery for each level. From these observations, the optimum setting of factor A is the lowest level. However, for factor B the recovery improves as this factor increases tends to higher level. Also, it suggests that middle level of factor C is most appropriate for higher recovery.

In the analysis of variance (ANOVA), the degrees of freedom are considered eight for a matrix experiment with 9 rows and two for each factor with 3 levels. Thus, the degrees of freedom for the error is two. In order to estimate the relative importance of the factors, the sum of squares value due to different factors is obtained. It can be seen that factors B and A, with 33.7 and 27.9 % respectively, are responsible for a large portion of the total variation of recovery in this type of material. However, an estimation of variance ratio explains that the effect of these two factors is not quite as large as error variance. It should be noted that the error variance, calculated in Table 7, is obtained by pooling the sum of squares corresponding to the factor C taking the lowest mean square. Thus, this factor along with the error account for 4 degrees of freedom, the total of their sum of squares of 21.33 and the error variance of 5.33, as shown by parentheses.

Table 7. Test 2, average of S/N ratio and ANOVA analysis for recovery

Factors	Levels			Degrees of freedom	Sum of squares	Mean square	Variance Ratio
	1	2	3				
A	*r + 5.8* [5]	*r + 2.8*	*r + 5.3*	2	15.5	7.75	1.45
B	*r + 5.5*	*r + 2.6*	*r + 5.8* [5]	2	18.7	9.35	1.75
C	*r + 3.9*	*r + 5.1* [5]	*r + 4.9*	2	2.5 *	1.25	
Error				2	18.8 *	9.4	
Total				8	55.5		
(Error)				(4)	(21.3)	(5.33)	

[5] indicates the optimum level

* indicates sum of squares added together to form the pooled error sum of squares shown by parentheses

CONCLUSION

In this paper a Robust Design is presented for improving productivity during aluminium recycling process and development so that high-quality products can be produced at low cost. A Taguchi method was used to plan a minimum number of experiments. In this method a signal-to-noise ratio which measures quality and an orthogonal array which is used to study design parameters simultaneously were employed. An ANOVA analysis was then applied to evaluate the relative importance of the effect of various factors. A series of orthogonal array experiments was carried out on IMCO Recycling Ltd. with a minimal interruption. The trials on 'coated scrap' material using an *L4* orthogonal array indicated that high level of factor A along with low level of factors B and C give the highest levels of recovery. It was also observed that factor C has the largest contribution to the total sum of squares and correspondingly has a major influence on the total variation of recovery. The experimental on 'class scrap' material employing an *L9* orthogonal array suggested that low level of factor A, high level of factor B and middle level of factor C make the best levels of recovery, in which factors B and A are more effective factors in the total variation of recovery. These results indicated which parameters in the process have a large impact on the product quality during production. In later work, we will show how the interactions between parameters can be effectively used for process optimisation of aluminium recycling.

ACKNOWLEDGMENTS

The authors gratefully acknowledge the support of the EPSRC and IMCO Recycling Ltd., particularly IMCO Recycling Ltd. for assistance in the running of the experimental program.

REFERENCES

1. G. Taguchi, 1988. Introduction to Quality Engineering: Designing Quality into Products and Processes, Asian Productivity Organisation, Japan.
2. M.F.J. Bohan, T.C. Claypole, D.T. Gethin, 1995. 'The application of Taguchi methods to the study of ink transfer in heat set web offset printing', 47th Annual TAGA Tech. Conf., Orlando, Florida.
3. P.A. Wells, R.E. Andreas, T.M. Fox, 1995. 'Metal recovery enhancement using Taguchi style experimentation', In: P.B. Queneau and R.D. Peterson (eds.), 3rd Int. Symp. Recycling of Metals and Engineered Materials, Alabama, 269-281.
4. M.S. Phadke, 1989. Quality Engineering using Robust Design, Prentice Hall, New Jersey.
5. R.K. Roy, 1990. A Primer on the Taguchi method, Society of Manufacturing Engineers, Dearborn, Michigan, USA

Towards a Better Understanding of Fuzzy Sets Applied to Environmental Science

Mory M. Ghomshei and John A. Meech

University of British Columbia, Department of Mining and Mineral Process Engineering,
6350 Stores Road, Vancouver, B.C. V6T 1Z4, Canada
Email: ghomshei@mining.ubc.ca jam@mining.ubc.ca

ABSTRACT

The fuzzy set of a concept is defined by the distribution function of the degree of belief (DoB) in a certain qualitative parameter (the concept), over a range of variation in a quantitative or less-qualitative parameter (the scale). The concept may be expressed with different scaling parameters and each parameter on its own, is not necessarily unique. Therefore the form of a fuzzy set depends on the choice of scale. In the environmental field, regulators, health authorities, epidemiologists, politicians, environmentalists, engineers and the general public often have different definitions for a concept such as contamination. The only term which is more or less unequivocally understood by all interested groups is the final "risk" (often associated with dollar value). Proper definition and scaling of fuzzy sets can provide a common language through which experts from different disciplines can communicate through the entire process of risk assessment. The uncertainty of the input information is propagated (but neither magnified nor dampened) in a fuzzy approach and yet the system output will remain fuzzy which can then be translated into either quantitative risk values or qualitative linguistic terms.

THE PROBLEM

A fuzzy set is defined by the distribution function of the Degree Of Belief (DoB), in a certain qualitative concept, over the range of variation in a quantitative (or less qualitative) parameter which is closely related to that concept. For example, consider the concept "old", which is a qualitative concept closely related to variation in a more quantitative parameter "age" [1]. The distribution of DoB or the membership of a certain age in the concept "old" is a fuzzy set. It should be noted that the parameter used to scale the qualitative concept "old" is not necessarily unique. One can scale the concept "old" with age, health, beauty, hormonal activity, feelings of being old, and so on. Of course, the form of the fuzzy set would be different depending on the choice of scaling parameter.

The DoB distribution over the scaling parameter (i.e., the fuzzy set) depends as well on the definition of the fuzzy concept. For example, in considering "old", the form of the related fuzzy set depends on how this concept is defined (i.e., by functionality, sociological perception or legal definition). The legal definition is usually linear with threshold and, in some contexts, may be a crisp relationship. Sociological perception is more sophisticated, possibly a Laplace-Gaussian distribution, while functionality is possibly the most sophisticated, with an intermediate period of relaxation or maturity (see Fig. 1).

This fuzziness in the very definition of a qualitative concept is often at the origin of miscommunication between different groups of experts collaborating with or confronting each other on a problem. In the area of environmental studies, regulators, health authorities, epidemiologists, politicians, environementalists, engineers and the general public often have different definitions for (or understanding of) a concept such as contamination. Fig. 2 is an example of how different understandings about e meaning of contamination can lead to different fuzzy sets present in the minds of different people. An expert system which tries to communicate with different groups of experts and/or users should therefore accommodate the subtleties existing in the definition or understanding of a concept. Alternatively, one can start with simple or elementary fuzzy sets related to certain primary causes and then adapt the original set to obtain fuzzy sets to represent more complex effects as understanding improves and the definition becomes more focused.

0-7803-5489-3/99/$10.00 ©1999 IEEE.

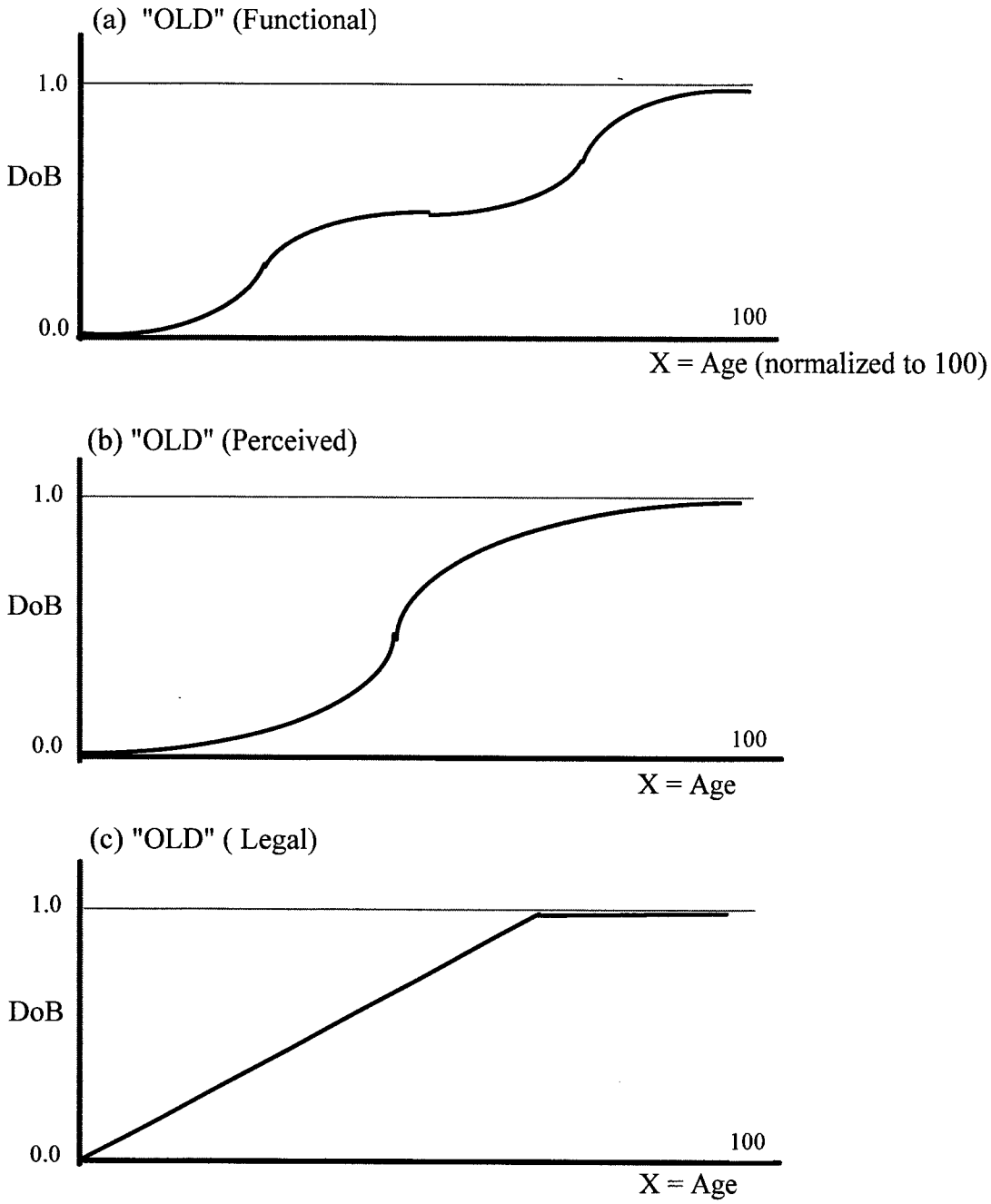


Fig. 1. Scaling the concept of "OLD" against Age.

CAUSE AND EFFECT

Environmental concepts are often scaled against different parameters to relate cause and effect. As an example, consider pollution from two carcinogenic agents such as radon gas and arsenic. The degree of pollution can be scaled against:

1. The concentration of pollutant 1 and 2 in the medium of concern, to define Cause 1 and Cause 2;
2. The individual risk (e.g., cancer) from different causes to define Effect 1-1 and Effect 1-2;
3. The cancer rate in the population to define the Population Risk (Effect 2) from Effects 1-1 and 1-2.
4. The health costs which derive from Effect 2 to derive Effect 3;
5. The overall socio-economic impact from Effect3 and other competing factors to derive Effect 4.

The first scale is the most independent and unbiased one. It is however meaningless if it is not coupled with epidemiological data (the second scale) and human geography (the third scale).

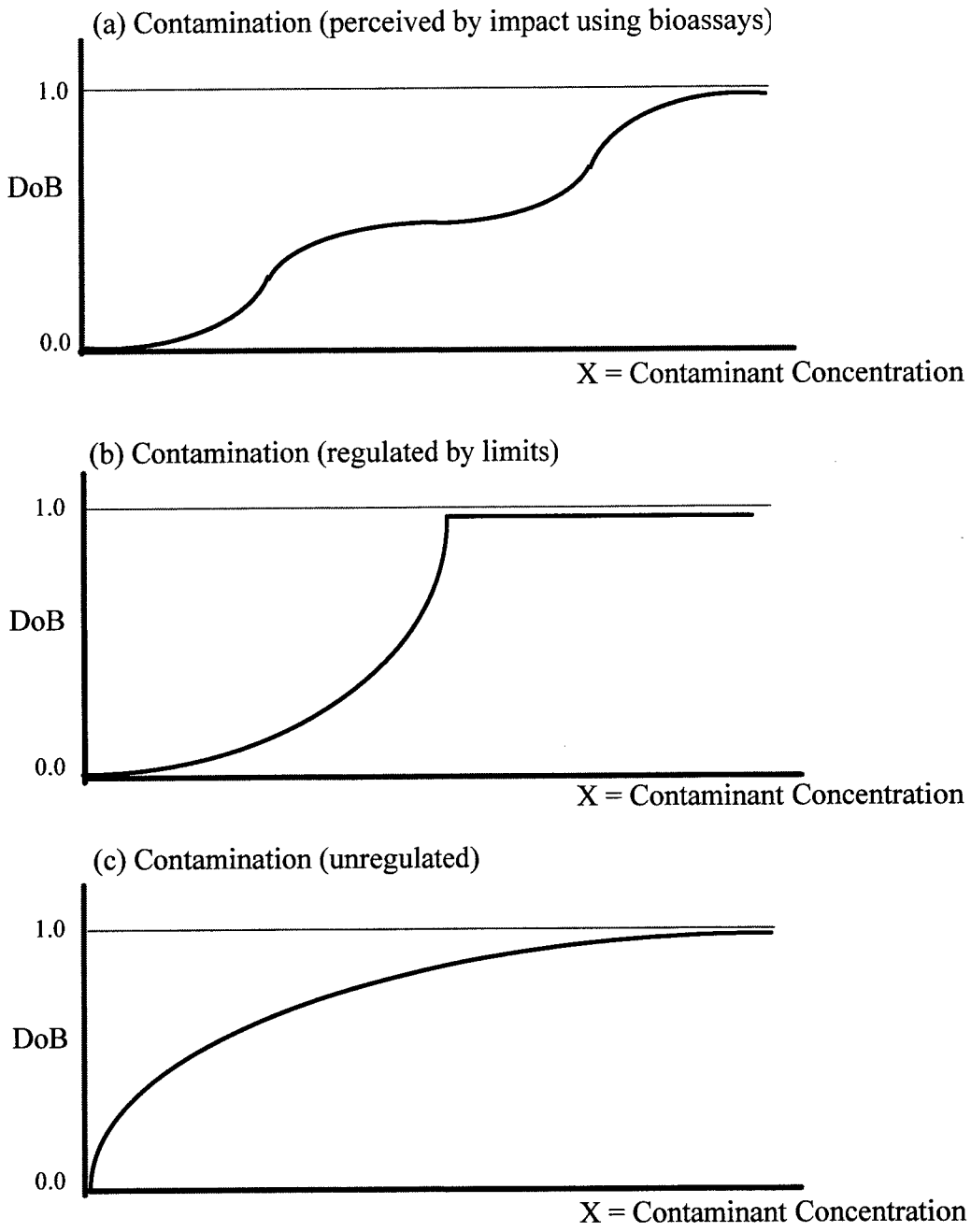


Fig. 2. Scaling the concept of "contamination" against contaminant concentration.

If pollution is scaled against "individual cancer risk" (Effect 1), the distribution function of the DOB (fuzzy set) is likely to be linear (or, at least, assumed to be linear over the range of concern). Both radon and arsenic pollution would therefore have the same "metric" (i.e., cancer risk), allowing their arithmetic combination to yield an overall population risk for cancer (Effect 2). If health costs are used for scaling, the fuzzy sets should have different "metrics", because the cancer related to arsenic is skin cancer (95% benign) [2], while the cancer caused by radon is lung-cancer. One should therefore be cautious about naively combining intermediate effects issuing from different causes. Instead, it would be prudent to treat

each independent cause separately and only combine their effects when they have been scaled against an unambiguously identical "metric" which, in this case, is health dollars.

FUZZY METHOD VERSUS WORST AND BEST

Application of fuzzy logic is especially useful when data are scarce. Consider the case of land contaminated by different agents (e.g., arsenic, lead and/or mercury). A risk assessment study of such land needs extensive data which can be placed into different categories as follow:

1- concentration of the contaminants (chemical agents) in the medium (soil and water)
2- toxicity of each agent (individual risk)
3- land use
4- pathway of each agent for each particular land use
5- health and economic risks

A risk assessment is then conducted based on rigorous statistical treatment and modeling of the data. It must be noted that in most cases the data are actually unreliable. Highly sophisticated numerical models will therefore have to be boiled down to very rough outputs known as worse-case and best-case scenarios. The dilemma, then, is where does the reality stand between the two extreme scenarios? Depending on the spread in the data, the best-case scenario may indicate no risk at all, while the worse-case scenario may suggest extreme hazards, meaning the land is practically unusable. The polarity of such output leaves room for great confusion on the part of regulators, investors and/or adjudicators. In these situations, fuzzy logic can be very helpful to introduce a continuous risk function [3] between the best-case and worse-case scenarios. Such a function is especially useful to those who seek or provide environmental risk insurance.

In fuzzy treatment of risk assessment, the input data are translated into fuzzy numbers and/or sets applicable to fuzzy arithmetic [4]. One can express environmental input as a variety of fuzzy sets. The choice of words or concepts depends on how each fuzzy set absorbs the inaccuracies and biases in the data and still remain meaningful. It is therefore necessary to understand the cause and effect relationships and to begin the process of fuzzification with information about the primary causes and to let the uncertainty propagate through to more complex effects. The input data into such analyses can be expressed as fuzzy functions in which the magnitude of each parameter is coupled with a specific membership value or Degree of Belief [5].

ANATOMY OF RISK (A REAL EXAMPLE)

The average concentration of a contaminant (e.g., arsenic in soil) can be expressed by a fuzzy function to which existing data points are statistically fitted. Suppose we have 9 data points for the concentration of arsenic at site X (Table 1). The simplest fuzzy set would be a curve in which the normalized frequency of each data value is expressed in terms of the DoB as in Fig. 3.

Table 1. Arsenic measurements at site X.

sample	arsenic (ppm)
1	2.5
2	5
3	1.3
4	4
5	3.5
6	2.2
7	3
8	1.7
9	3

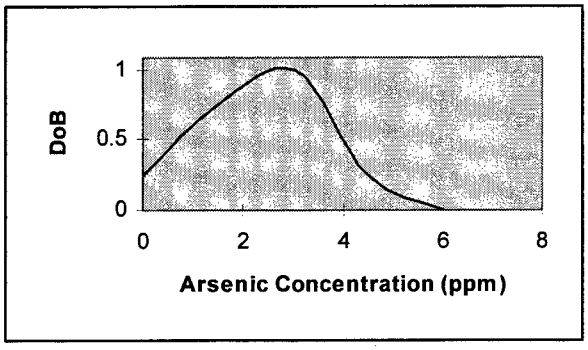


Fig. 3. Probability distribution of arsenic in soil.

The toxicities of the agents are themselves fuzzy numbers or sets and are often defined in relation to the affected biota or human population. Individual risk is often expressed as a range between upper and lower values (thresholds). For the purposes of our example, consider the case of arsenic in which toxicity can be expressed in terms of an individual risk. Each arsenic level is then associated with the probability of cancer in an individual exposed to that concentration in some medium. This is also a fuzzy set which may be linear over the range of interest.

In order to relate the two fuzzy sets (i.e., soil contamination and individual risk), one needs a third function to correlate the arsenic in soil with the arsenic ingested by an individual exposed through a particular pathway. This correlation is based either on epidemiological data or calculated through pathway models. Reliable epidemiological data relating individual risk (e.g., cancer) to the concentration of contaminant in soil is scarce. The individual risk is therefore related to sources (i.e., primary causes) of contamination through a pathway model which defines the process through which a certain contaminant finds its way to an individual at risk [2]. There are usually several pathways associated with each contaminant. For example, for a contaminant in soil, it may be ingested (through hand-to-mouth) by children playing on the ground (pathway 1), or it may be ingested through inhalation of dust arising from the contaminated soil (pathway 2), or by being leached into the hydrological system under low-pH conditions and then ingested through drinking water (pathway 3), to mention a few. In a fuzzy approach to risk assessment, pathways can be modeled by fuzzy functions (instead of assuming maximum and minimum values). Individual risks for each pathway model can then be multiplied by the affected population (itself, a fuzzy number) to calculate the overall population risk and associated costs.

Let's go back to our case of arsenic at site X and consider the two most important pathways:

1. hand-to-mouth (ingestion directly from soil)
2. dust inhalation (ingestion through air)

It is evident that the affected population is not necessarily the same for the two pathways. The individual risk associated with each pathway should therefore be normalized to the size of the affected population before combining the effects. Here we examine the first pathway in detail. Fig. 3 defines the original cause (i.e., arsenic concentration) using a fuzzy set. The hand-to-mouth pathway [6] implies a linear correlation between arsenic in the soil (cause) and ingested arsenic. The slope of the correlation has been determined from epidemiological data and models [7,8]. (see Fig. 4).

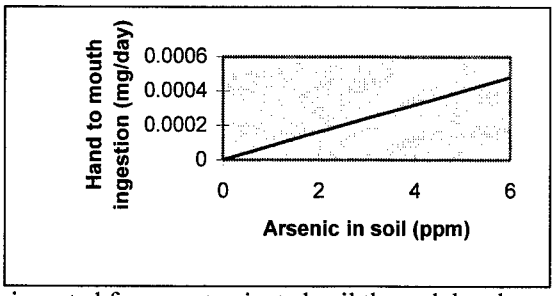


Fig. 4. Arsenic ingested from contaminated soil through hand-to-mouth pathway.

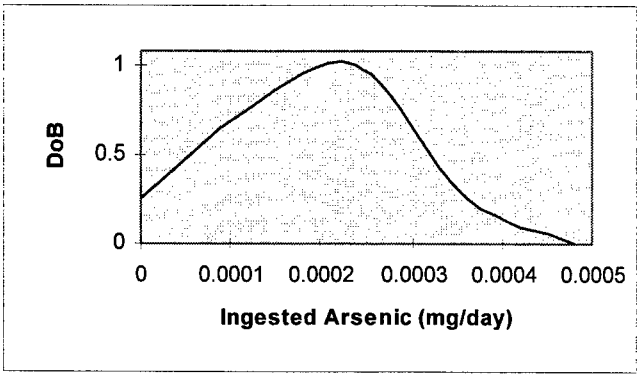


Fig. 5. Probability of arsenic ingestion through hand-to-mouth pathway.

Belief in individual risk can therefore be linearly linked to the original cause [9]. So the fuzzy set of the effect has the same shape as that of the cause. (Fig. 5, 6). Only the "metrics" are different.

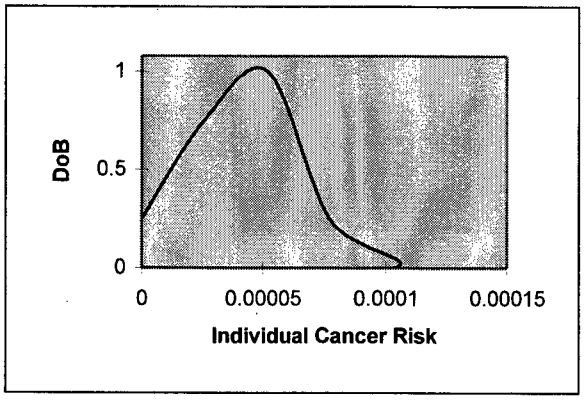


Fig. 6. Degree of Belief that the individual risk of cancer is 0.00005.

The population exposed to the "hand-to-mouth" pathway are children, whose numbers depend on the total residential units and the number of children in each unit. Based on interviews with urban planners, the affected population can be assessed in fuzzy terms (see Fig. 7). Note that conventional risk assessment typically uses the maximum population which leads to overestimation of the total population risk.

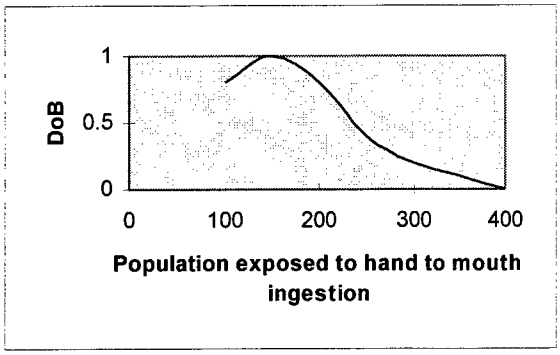


Fig. 7. Degree of Belief that a particular population size is exposed to arsenic by "hand-to-mouth" ingestion.

The total population risk is calculated from multiplication of the individual risk and the exposed population size. Considering that both components are expressed as fuzzy sets, the product is defined as a fuzzy set with 3 dimensions [4], individual risk, population size and DoB. Fig. 8 shows the results of the fuzzy multiplication of individual risk by exposed population size. The outer locus of points basically describes the range of possibilities that a particular total population risk is measured. This envelope can be considered as the location of interest of any specific distribution of population risk measurements.

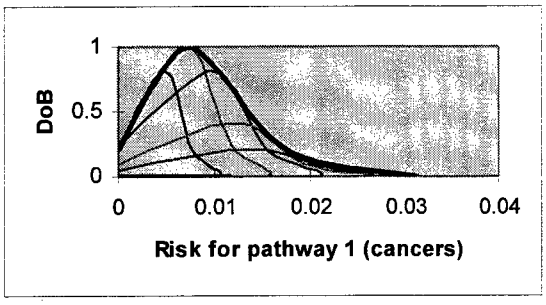


Fig. 8. The population risk distribution for pathway 1 will be located within the envelope defined by the uppermost locus of points (heavy line).

The effect of pathway2 was assessed using the same process. Note that the affected population (adults and children) is significantly larger than that of pathway 1, but countering this is the fact that total ingestion through air is significantly lower that hand-to-mouth. The final risks of the two pathways are therefore comparable in values (Fig. 9).

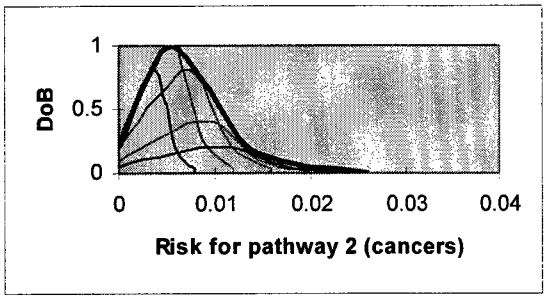


Fig. 8. The population risk distribution for pathway 2 will be located within the envelope defined by the uppermost locus of points (heavy line).

The final population risk is then calculated by simple addition of the two fuzzy sets (Fig. 10).

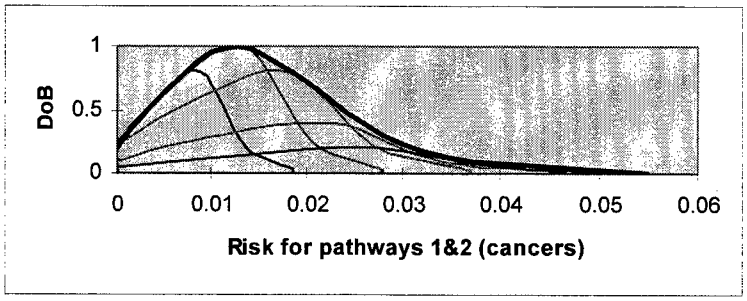


Fig. 10. Total cancer risk distribution associated with arsenic exposure will be located within the envelope defined by the uppermost locus of points (heavy line).

The final population risk related to all pathways can therefore be expressed in a fuzzy set rather than in two extreme values (worse and best) as given in conventional risk assessment. In cases of knowledge about different types of health risks, the population risk for each one should be converted to health costs before combining the effect of all health risks.

DISCUSSION

Definitions and data related to environmental concepts are fuzzy in nature. Risk assessment is a common methodology to quantify (or qualify) the concern. In a fuzzy logic approach to risk assessment, instead of adopting the worse case scenario, all scenarios are given a fair weight by associating a degree of belief (DOB) to each possible scenario. All scenarios are therefore taken into account and uncertainties are propagated through the system, making the output less biased. Fuzzy presentation of the input and output information can provide a simple, yet intelligent, medium of communication.

Contrary to its name, application of fuzzy sets and fuzzy arithmetic to environmental studies can help reduce the fuzziness in both output results and the investigation procedures. It requires defining risk-based fuzzy sets to replace a variety of different fuzzy sets present (but unexpressed) in the minds of the different interested parties as shown in Figure 2. We are continuing our work to examine ways to combine the fuzzy analyses depicted in Figure 2 with the fuzzy arithmetic presented in the example application.

We believe that a fuzzy expression of risk can provide a harmonized baseline for regulations and permits. Causal association of the risks, often reflected in the shape of the fuzziness involved in the process, can facilitate understanding of the system, which otherwise would simply be a black box.

REFERENCES

1. Harris, C.A., and J. Meech, J.A., 1987. "Fuzzy Logic: A Potential Control Technique for Mineral Processing"; CIM Bulletin, 80(905), 51-59.
2. W.H.O. (World Health Organization), 1981. Environmental Health Criteria 18 - ARSENIC. Environmental Health Criteria Series, Geneva, 41-123.
3. Kosco, B., 1994. Fuzzy systems as universal approximators. IEEE Trans. Computers, 43(11), 1329-1333.
4. Kaufmann, A. and Gupta, M.M., 1991. Introduction to fuzzy arithmetic: theory and application. Van Nostrand Reinhold, New York, 361
5. Donato, J.M., Barbieri, E., 1995. Mathematical representation of fuzzy membership functions. IEEE Spectrum, 290 - 294.
6. Binder, S., Forney, D., Kaye, W., Paschal, D., 1987. Arsenic Exposure in Children Living Near a Former Copper Smelter. Bulletin Environmental Contamination, 39: 114 - 121.
7. BCE (British Columbia Ministry of Environment), 1990. Human Exposure Reference Values. Internal report. file 10-9-2.
8. Travis, C.C., Richter, S.A., Crouch, E.A.C., Wilson, R., Klema, E.D., 1987. Cancer Risk Management. Environ. Sci. Tech., 21(5), 415-420.
9. EPA, 1984. Health Assessment Document for Inorganic Arsenic. Washington, D.C.

Intelligence in Rolling Processes

Data Mining and State Monitoring in Hot Rolling

L. Cser*, A.S.Korhonen, J.Gulyás***, P.Mäntylä****,
O. Simula**, Gy. Reiss***, P.Ruha*****

*Bay Zoltan Institute for Logistics and Production Systems,
H3519 Miskolc-Tapolca, Hungary, recently
**Helsinki University of Technology, P.O.Box 6200, FIN-02015 HUT, Finland
***University of Miskolc, H3515 Miskolc-Egyetemváros, Hungary
****University of Oulu, Finland
*****Rautaruukki Steel, Finland

ABSTRACT

An overview of state monitoring in hot rolling is reviewed, and a new concept of state monitoring is shown in the paper. Based on a detailed analysis of all factors a state monitor has been proposed. A system state corresponds to the proper product quality. If the system is leaving the area of required quality in the state space, signal is given with the evaluation of situation. Self-Organising Maps (SOM) are especially suitable in analysing the very complex process of hot rolling. Application of SOM helps to discover hidden dependencies influencing the quality parameters, such as flatness, profile, thickness and width deviation as well as wedge and surface quality. Results from the analysis of more than 70 parameters in 16.000 strips gave the state space used in state monitoring based on on-line data sampling. The coloured visualisation map shows the state space enabling prediction of product quality.

INTRODUCTION

Cutting costs and increasing added-value of steel products using new production methods and advanced control systems are key factors in the competitiveness of European steel producers. Customers require thinner and wider plate with smaller tolerances. Constructions are made lighter and assembled on automatic lines, which can only tolerate minor variations in the spring-back of incoming sheet parts. Short delivery times which reduce the length of rolling campaigns also increase the need for continuous set-ups, adjustments, control and monitoring of the process. To meet the challenge of this steadily-growing pressure to improve product quality, rolling mills employ extensive automation and sophisticated on-line data sampling techniques. However, the sheet quality is influenced by the entire "life history" of the rolled strip.

CONTROL AND MONITORING IN ROLLING MILL

Ten years ago, thickness deviations for 3-5 mm hot rolled strip was usually ~0.05 mm; recently this has decreased to 0.015 mm. The same is true for strip width. Extra-wide strip, trimmed away from the final product was typically 13-15 mm in the 80s. Today it is ~10mm, but the target, representing the world's best practice is 4mm. This progress, experienced only recently, results from very intensive development.

Historical background

In the middle of this century, sheet quality was a product of the teamwork of very highly-skilled labour, so called mill supervisors, or "rollers", led by mill superintendents. Two mill supervisors stayed at the *furnaces*, each on one side, controlling the volume of gas and air supplied to the furnaces, opening the doors, and controlling bar movement on the transfer rolls. In the *roughing train* a "roller" controlled each of the vertical edgers (transfer bar width, speed and direction of the traction motors). Two mill supervisors were located at the roughing stand, one controlling the roll gap and transfer speed; the other handled guidance tasks -- the bar transfer, as well as, the hydraulic descaler. The crop shear machine was also controlled by a skilled worker. The mill superintendents stayed at the *finishing train.* One of them controlled the roll gaps, speed, and tension in the finishing stands #1, #2, #3, the other performed the same operations for stands #4, #5, #6 as well as the cooling line. Dynamic gap control on the drive and change sides of each finishing stand was done by the stand controllers. At the end of the finishing train, a coil supervisor controlled each of the coilers. The main function of automatic rolling mill control took over these tasks, dividing them into four main groups: optimal roll set-up, process monitoring, material flow

0-7803-5489-3/99/$10.00 ©1999 IEEE.

control, data recording and report generation. The tasks are organised into the hierarchy shown in Figure 1 [1].

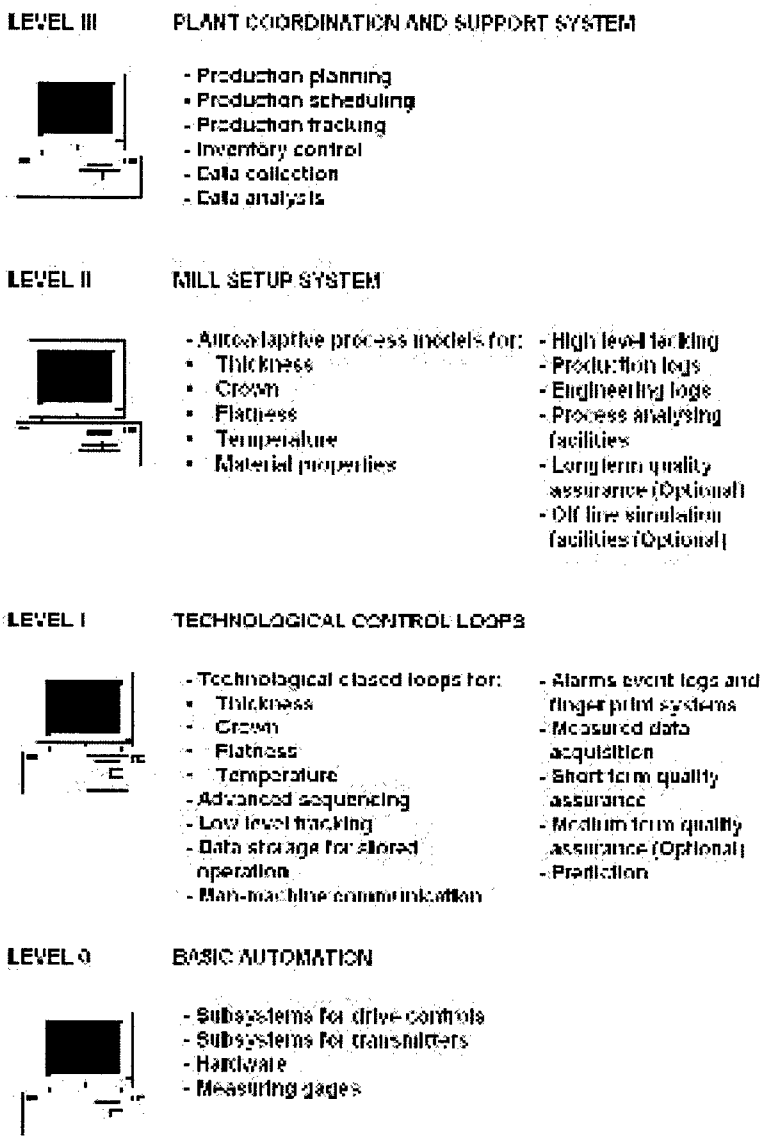


Fig. 1. Hierarchical control of rolling mill [1].

Neural networks in mill control

The use of Artificial Neural Networks (ANN) in rolling started in the beginning of the 1990s and the number of publications is growing rapidly. Reports on successful applications will probably extend the interest in this field as well [2,3,4,5]. Prediction of process variables using measurements from previous process phases has been a common way to utilise ANNs in industrial applications. In the automation and control of strip quality and in the determination of mill settings needed for incoming strip before the strip actually enters the mill, ANNs have been used based on both measured and simulated data. An efficient process model should be able to predict rolling forces, torque, material properties etc. It is sufficient that they be accurate, reliable and adaptable in real time. By using ANNs, these goals can be reached provided, sufficient process data is available. In addition, taking post-calculations into account, which means compensating the pre-calculation error by continuously adapting the models to the real-time situation, neural networks can do both modelling and adaptation and perform them equally well [6].

For control tasks, reasonable task-sharing between mathematical models and neural network-based corrections is necessary [7]:

- The on-line computations should be performed by neural networks, but
- Physically-correct mathematical modelling should be utilised where ever possible.

Validity of a full neural network model is accomplished only with the greatest of difficulties, because the model remains for the engineer as a "black box". The tasks solved by ANN are as follows:

- Prediction of the width in the finishing mill,
- Correction of the strip or plate temperature calculated by analytical models.

Networks used in rolling mill control are trained off-line in development laboratories after which the model can be installed to control or optimise the process and/or used for off-line analysis. In some applications, the ANN model is trained on-line, which is a highly-demanding task, at least in most cases. Currently, ANNs are rather widely and successfully used in rolling mills, as it can be seen in Fig. 2.

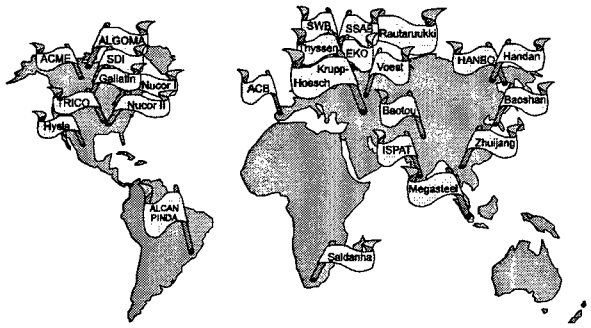


Fig. 2. Rolling mills with neural network control [7]

DATA AND DATA MINING IN HOT ROLLING

In order to set up the models for fine-tuning of rolling mill control, analysis of all influencing factors is necessary. One way to analyse the factors and their influences is by **laboratory experiments**. These are rather expensive, and carry in them all the dangers of physical-modelling (scale-up factors, differences in boundary conditions, etc.). Another approach is to analyse industrial **data, measured on-line** during the actual rolling process, using methods such as *Data Mining*, especially the visualising possibilities of *Self Organising Maps*.

The collected data required by ISO 900X, is a rich source of information about the extremely complex process. The rolling process, consisting of furnaces, transport rolls, rolling stands of the roughing and finishing trains, water-cooling system, lubrication etc. is in itself very complex. In addition to the current state of the mill, the process conditions and product properties are affected by other factors, such as the chemistry of the material to be rolled, the history of each slab before and during rolling, casting, and re-heating, as well. Factors influencing quality have very complex *confluence.* When one of them changes (e.g., temperature), the rolling force is affected, but so is the torque, surface properties, and kinematic boundary conditions. The same is valid for dimensional quality parameters -- thickness, profile, flatness, width, and wedge, as well as, the surface roughness.

As can be seen in Figure 1, in a modern rolling mill each production unit such as furnaces, rolling stands and cooling lines have their own computer control with sensors. The rolling mill automation system forms a hierarchy of computers and programmable controllers. These range in function from simple closed-loop regulators (Level 0) for tasks such as actuator position and motor speed control, through to intermediate controllers (Level 1) for tasks such as sequence management and complex closed loop regulation and finally high level computers (Level 2, often called the optimisation system, and Level 3) for tasks such as material tracking, production unit set-point calculation, quality monitoring and production control. Process and quality critical data are collected from sensors by all levels of the automation system and these measurements flow up this hierarchy from Level 0 to Level 3.Great numbers of controlling and data-sampling computers work together, storing the data for short or long term analysis. For in-bar analysis and modelling, huge amounts of high frequency data must be collected and stored. In uncompressed format, this

would require a huge amount of space, therefore advanced compression and feature extraction methods are needed. In feature extraction, ANNs together with other data mining methods are very promising tools. In a typical modern hot rolling mill, a full temperature map is created in and after the furnace, before the roughing stand, before the first finishing stand, after the first finishing stand, after the last finishing stand, and before the coiler. After the last stand of the finishing train, final dimensional parameters are measured. In each stand the roll separating force, roll bending force, tension, strip bending, and roll shifting values are measured and stored (see Fig. 3). Grain size and mechanical properties will be added later.

The measurements listed above run continuously during rolling of each strip or plate. The data-sampling interval is between 0.2-2 seconds. Temperature is measured across the whole width, before the finishing mill on both upper and lower sides of the strip. This means that millions of measurements are made for each strip. In the specific case of the hot strip mill considered in this study, hundreds of strips are rolled daily.

For the control system, as well as for product records, only some averages, and standard deviations are needed. Other sampled data must be deleted dynamically. Some are deleted immediately after averaging, some are stored for few weeks or months. Data are stored in different computers on different hierarchical levels of the control system. They can be collected by simply using either the strip ID number or according to a timestamp. Since the measurements have been made in different places of the strip at different times, an additional transformation is necessary in order to synchronise the values along the length of the strip.

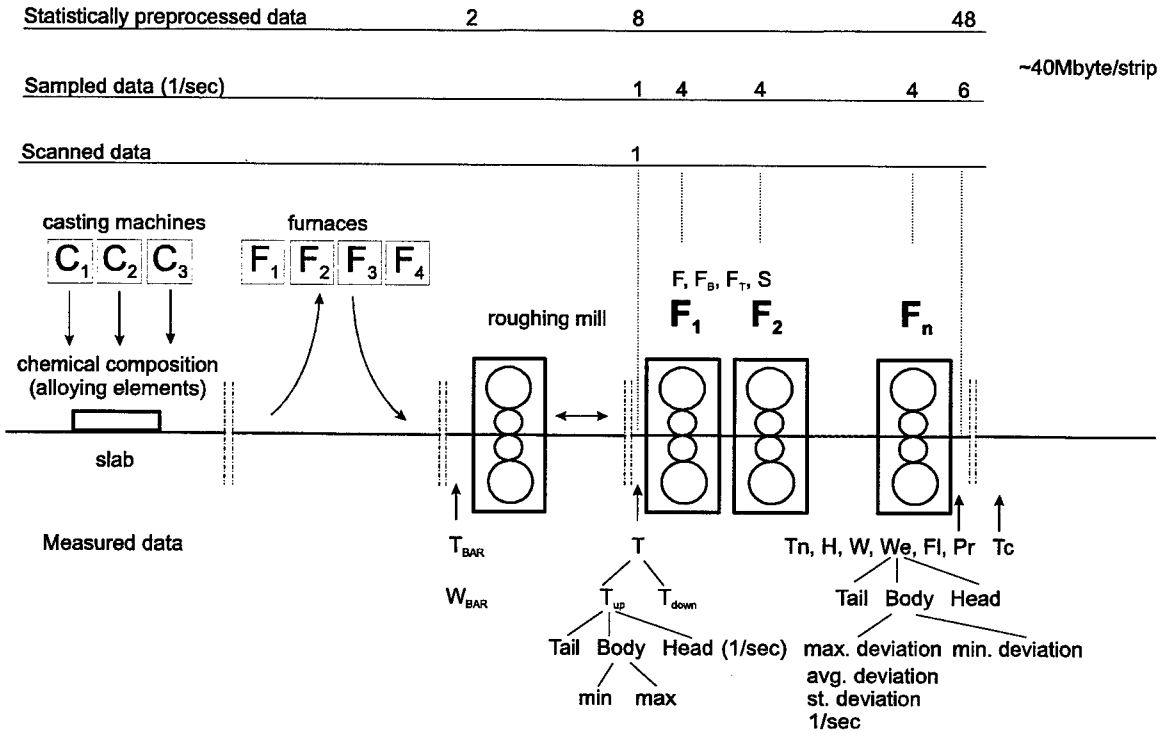


Fig. 3. On-line measurements (data sources) in hot rolling
(C_I - casting machines, F_i - furnaces, T_{bar}, W_{bar} - bar temperature and bar width, T - temperatures of the strip, head, body and tail, $\mathbf{F}_i$ (F, F_b, F_t) - force vector in stand i (roll separating force, roll bending force, strip tension force), T_n - temperature, measured before the stand, H, W, We, Fl, Pr - geometric quality parameters: thickness, width, wedge, flatness, profile, T_c - coiling temperature)

Self-Organising Maps in Hot Rolling

The Self-Organising Map (SOM) [8] is a neural network algorithm based on unsupervised learning. Unlike supervised learning methods, the SOM can be used for clustering data without knowing the class memberships of the input data. It can, thus, be used to detect features inherent to the problem. The projection on the component planes can be interpreted, as slicing the *n*-dimensional model vectors of the map into component planes. Each component plane consists of values of a single vector component in all map units. In case of hot rolling, the measured data characterising the rolling of the strip represent a data

vector. Components of these vectors change from strip to strip. The SOM component planes give the clustering of each component separately.
Component planes can also be used for correlation hunting: discovering hidden *co-incidences*. Correlation between components can be seen as similar patterns in identical positions of component planes. Pattern matching is something that the human eye is very good at, and it is further enhanced by regular shape of the map grid. Using component planes in correlation hunting is easy, selecting the "suspicious" component combinations for further investigations. An advantage of SOM is that it is not necessary to know the character of correlation. It can also be non-linear. The similar patterns do not mean a causal connection! They can be caused by a third factor, as well. The final answer can be done only by human expert.

Results of Analysis
A study of ~16,000 strips covering 70 measured values for each strip could deliver information on the process and the mill. Some interesting and useful co-incidences between the technical parameters, enabling quality improvement have been published [9,10]. Since the dimensional quality parameters have a close connection, the question arose as to the elevated requirements for strip dimensions are not contradictory. *Is it possible to satisfy all elevated requirements by the given rolling mill?*

One of the advantages of the SOM is that it can deal with discrete variables. Figure 4.b shows an attempt to bring all geometric quality parameters into correspondence with the temperature of the last finishing operation. Maps contain the information in binary terms (whether they satisfy the stricter requirements or not). The clear areas of the component plans are those areas corresponding to the goal requirements (width deviation 8 mm $<\Delta W<12$ mm, thickness deviation -0.01 mm $< \Delta H < 0.01$ mm, flatness deviation $-10 < I < 0$, profile deviation $20\ \mu m < \Delta < 100\mu m$). The area corresponding to all elevated quality parameters is shown simultaneously with the white colour on the plan of intersections. The size of the area shows that the investigated rolling mill can produce the required quality rather easily from a technical point of view (the other grey scales correspond to areas, where only some requirements are satisfied). Comparison of the shape of the white area with the pattern of the finishing temperature shows very few similarities. However, it can be seen that achieving the highest dimensional accuracy is *not only a problem of temperature control.*

ON-LINE STATE MONITORING

Using the SOM, after examined the properties of the prototype vectors, new data can be analysed. The term "data" can refer to whole data sets or to single data samples. The main question to be answered is: Which part of the mapped distribution corresponds best to the given data? In other words: where the data samples are located on the map.

The data sets which are the easiest cases of quality analysis are the geometric quality parameters and the intersection of elevated requirements. Figure 4.a shows a typical diagram of on-line geometric quality control measurement. A data set collected from the measured geometric quality parameters in a strip location correspond to a proper system state, described by a point in the state-space. The point can be found in each component map and in the intersection map. By using dynamic seeking for the location of system states in component planes, changes in system-state can be followed. Time series of points corresponding to each sampled data set shows how the system "moves" in state space. Data for each rolled strip require transformation into non-dimensional length co-ordinates. This is done because mill sensors are located in different position along the mill line, and so measurements are recorded at different times in the processing history of the strip and as well, the strip is continually being elongated due to thickness reduction and, hence, the length of the strip in not constant during rolling. Some sampled data points corresponding to the dynamic state-changes of the rolling mill, as a time series in Figure 4.a can be seen in Figure 4.b, indicated by the arrows. Figure 5 shows the position of state monitoring in the set-up and control model of a rolling mill.

CONCLUSION

- Self-Organising Maps are an effective method to discover hidden dependencies among the technique parameters in a fully automated environment. SOM enables separating relevant and irrelevant factors.
- Maps which assess dimensional quality parameters, clearly show system-state-changes during strip-rolling.
- A new method for state-monitoring and prediction of strip quality has been introduced, based on Self-Organising Maps.

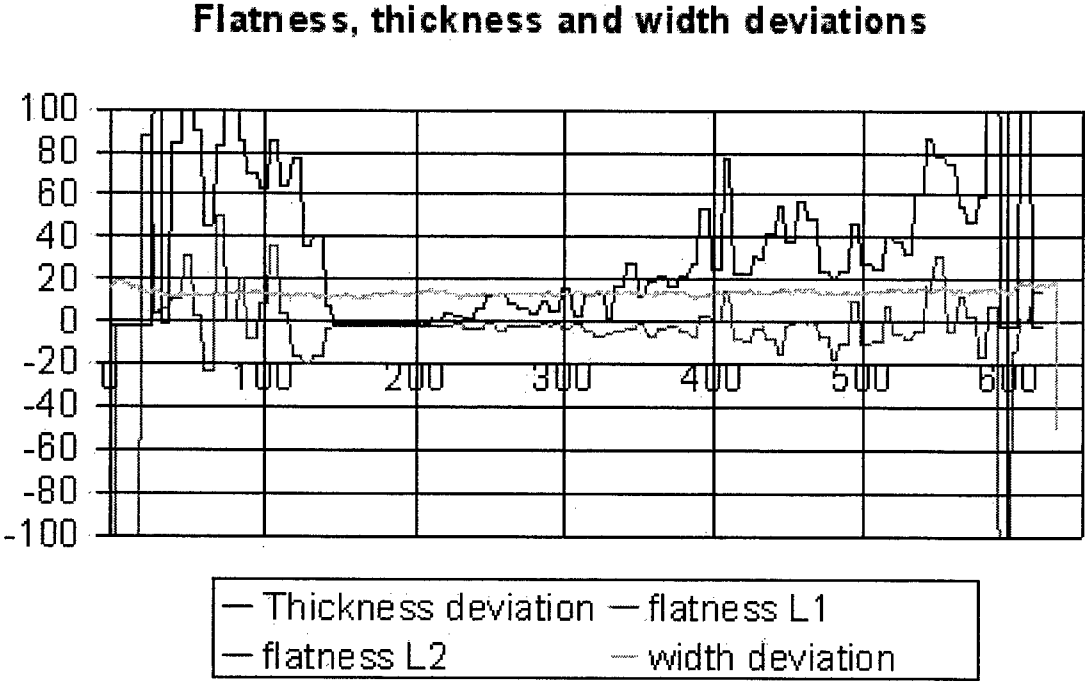


Fig. 4. a. Measured change of geometric quality parameters.

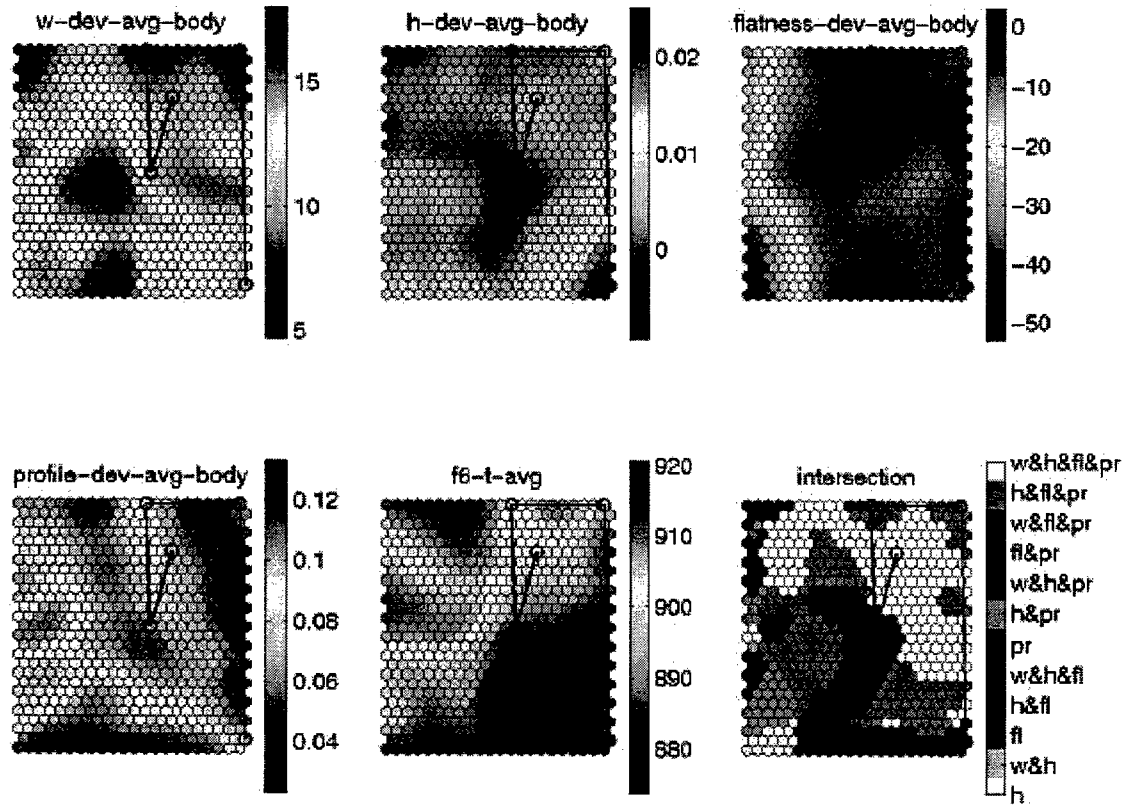


Fig. 4. b. Movement of the system in state space.

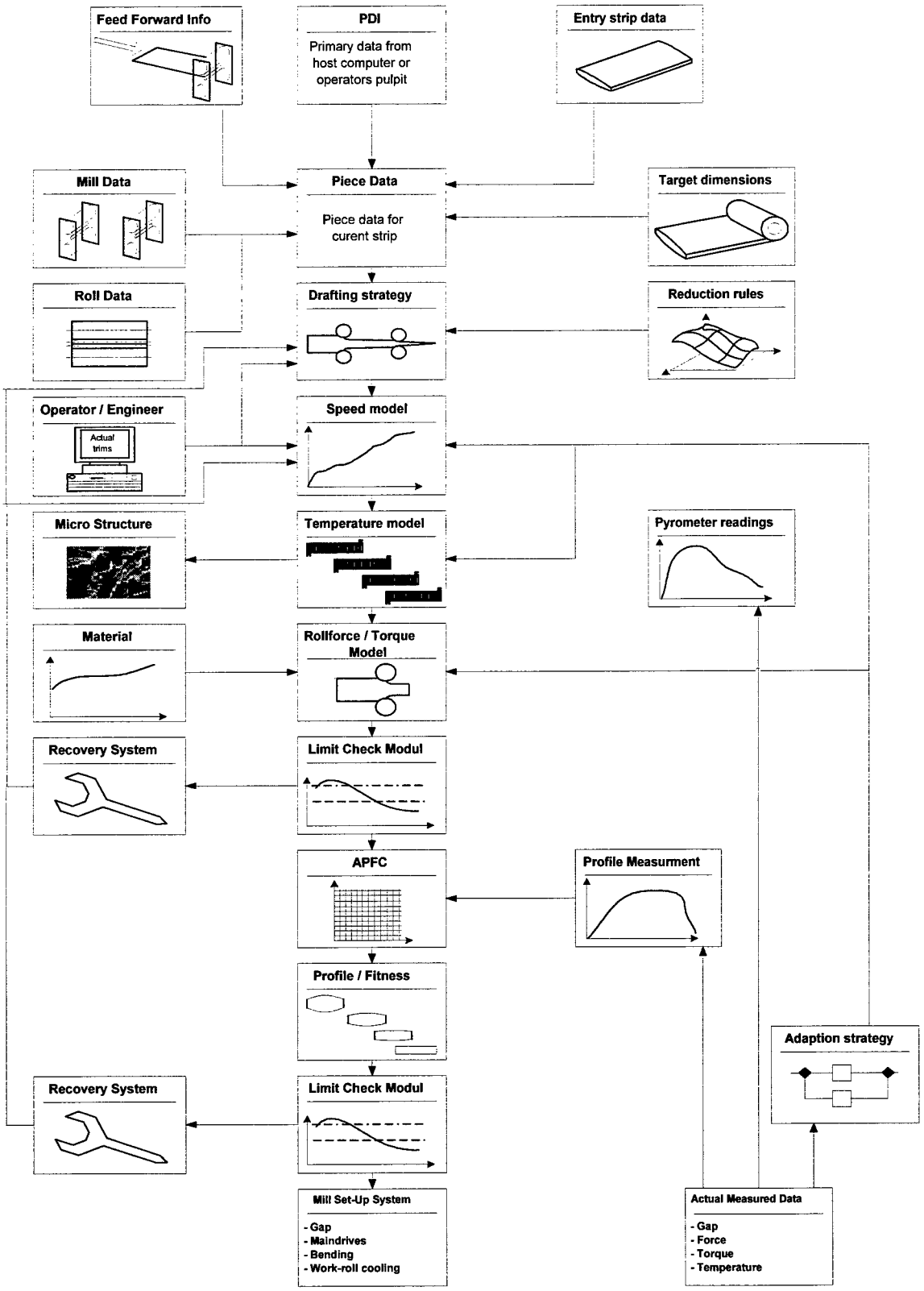


Fig. 5. Mill set-up model with the indication of the expected state [1]

ACKNOWLEDGEMENT

The authors would like to thank the contributors of all partners, especially Dr. J. Larkiola (VTT), Dr. P.Myllykoski, Mr. J.Ahola (Helsinki University of Technology), Mr.L.Árvai and Mr. David C.Martin (University of Oulu).

REFERENCES

1 Schultze, D.: Development and Application of Process Models, *Technologies for the Enhancement of Rolling Mills and Processing Lines,* MANNESMANN DEMAG

2 Korhonen, A.S., Larkiola,J., 1997. *Proceedings of IPMM'97,* Gold Coast, Australia, July, 1997.

3 Montesi, M., Trivella, F. and Brambilla A., 1996. Proc. of EANN'96, 99-102, 17-19 June, London, UK.

4 Myllykoski, P. and Larkiola, J., 1996. Report TKK-MAK-MML 1/96.

5 Cser,L. Korhonen,A.S., Simula,O., Larkiola,J., Myllykoski,P., Ahola,J., 1998. Knowledge Based Methods in Modelling of Hot Rolling of Steel Strip, *Proceeding of the ICME 98,Capri, Italy,* 265-270

6 Portman, F., Lindhoff, D., Sorgel, G., Gramckow, O. 1995., *Iron and Steel Engineer, February,* 33-36.

7 Gramckow,O., Jansen,M., Feldkeller, B., 1998. Anwendung Neuronaler Netze für die Prozeßsteuerung, *Tagungsband MEFORM 98, 25-27 February,* 1-23.

8 T.Kohonen. Self-Organizing Maps, 1995. *Springer, Berlin, Heidelberg,*

9 Myllykoski,P.T., Larkiola,J.E., Korhonen,A.S., Cser,L., 1999. Predicting and Modelling Flatness with Neural Networks, *Proceedings of the 2nd ESAFORM Conference, Guimaraes, Portugal.*

10 Cser,L., Korhonen,a.s., Mäntylä,P., Simula,O., 1999. Data Mining in Improving the Geometric Quality Parameters of Hot Rolled Strips, *Proc. Inter. Conf. on Quality Manuf., Stellenbosch, South Africa,* 8-16.

DETERMINATION OF THE THICKNESS CONTROL PARAMETERS OF THE ROLLING PROCESS THROUGH THE SENSITIVITY METHOD, USING NEURAL NETWORKS

L.E. Zárate*, H. Helman**

*Department of Computer Science,
Pontifical Catholic University of Minas Gerais, Brazil
Email: zarate@brhs.com.br
**Department of Metallurgical and Materials Engineering,
Federal University of Minas Gerais
Email: hhelman@demet.ufmg.br

ABSTRACT

The single stand rolling mill governing equation is a non-linear function on several parameters (entry thickness, front and back tensions, average yield stress and friction coefficient among others). Any alteration on one of them will cause alterations on the rolling load and, consequently, on the outgoing thickness. This paper presents a method for the calculation of the appropriate adjustment on the three control parameters (roll gap, front or back tensions), in which the sensitivity equation of the process, obtained by differentiating a neural network, is used.

INTRODUCTION

The single stand rolling mill governing equation is a non-linear function on several parameters (1). Any alteration on either of them: the entry thickness (h_i), the front (t_f) or back (t_b) tensions, the average yield stress ($\bar{y}$) or the friction coefficient (μ), will cause alterations on the rolling load (P) and, consequently on the outgoing thickness (h_o).

$$h_o = f(P, h_i, t_b, t_f, \mu, \bar{y}, E, R, W, M) \qquad 1.$$

where:
E = Young modulus of the strip material
R = roll radius
W = strip width
M = rigidity rolling mill modulus

When such alterations in the rolling process occur, three control parameters are mainly used to restore the outgoing thickness and so ensuring the $\Delta h_o = 0$ condition: the roll gap and the front and/or back tensions. In the present work, a method for the calculation of the appropriate adjustment of the three control parameters is presented. In this method the sensitivity equation of the process, obtained by differentiating a neural network is used.

The work is organised in five sections. In the first section, the representation of the rolling process operation by means of artificial neural networks (ANN) is presented. In the second section the bases for the calculation of the sensitivity equations through the differentiation of the neural network are described. In the third section, the method for the calculation of the parameter adjustment when alterations on the rolling process occurred is presented and finally, an application to a strip rolling process case, results and discussion are presented.

0-7803-5489-3/99/$10.00 ©1999 IEEE.

REPRESENTATION OF THE ROLLING MILL OPERATION THROUGH ANN

In this case, a back-propagation neural network, with six entries (N=6), two exits (M=2) and one hidden layer with 13 neurons (2N+1), is used. A sigmoid function was selected as the activating function.

$$(h_i, g, \mu, t_b, t_f, \bar{y}) \xrightarrow{\text{Neural Network}} (h_o, P) \qquad 2.$$

Generally, the largest effort to get a neural network trained lies on collecting and pre-processing neural network input data. The pre-processing operation consists in the data normalization in such away that the inputs and outputs values be within the 0 to 1 range.

The following procedure was adopted to normalize the input data before using it in the ANN structure:

- In order to improve convergence of the ANN training process, the normalization interval [0, 1] was reduced to [0.2, 0.8].
- The data was normalized through the following formula:

$$\text{Ln} = (\text{Lo} - \text{Lmin}) / (\text{Lmax} - \text{Lmin}) \qquad 3.$$

  where Ln is the normalized value, Lo value to normalize, Lmin and Lmax are minimum and maximum variable values, respectively.
- Lmin and Lmax were computed as follows:

$$\text{Lmin} = (4 \times \text{LimiteInf.} - \text{LimiteSup}) / 3 \qquad 4.a.$$
$$\text{Lmax} = (\text{LimiteInf.} - 0.8 \times \text{Lmin}) / 0.2 \qquad 4.b.$$

SENSITIVITY EQUATIONS

In this section, the calculation of the sensitivity factors through the differentiation of a general neural net, with N entries, M exits and L neurons in the hidden layer, is presented.

The currently used symbols :

U_i, $i = 0,...,N$ are the net entries and $U_0 = 1$ is a polarization entry

$f_i^a(.)$ $i = 0,...,N$ are the normalization entry functions and $f_0^a(.) = 1$

X_i, $i = 0,...,N$ are the normalized entries $X_0 = U_0$

W_{ij}^h $i = 1,...,L$ e $j = 0,...,N$ is the weight corresponding to the neuron i and entry j

$net_j^h = \sum_{i=0}^{N} W_{ji}^h X_i$ $j = 1,...,L$ product of weights times entries

$f_j^h(net_j^h)$ $j = 0,...,L$ with $f_0^h(net_0^h) = 1$ is the sigmoid function of the hidden layer.

I_j, $j = 0,...,L$ are the corresponding values of the sigmoid function $I_0 = 1$

W_{ij}^o $i = 1,...,M$ e $j = 0,...,L$ is the weight of the neuron i and entry j for the hidden layer.

$net_j^o = \sum_{i=0}^{L} W_{ji}^o I_i$ $j = 1,...,M$ product of the weights times entries for the hidden layer.

$f_j^o(net_j^h)$ $j = 1,...,M$ is the value of the sigmoid function for the exit layer

Y_j, $j = 1,...,M$ are the normalized exits of the net, obtained from the sigmoid function

$f_i^b(.)$ $i = 1,...,M$ are the denormalization functions of the exits

$Z_i,\ \ i=1,...,M$ net exits values

$e\max_k, e\min_k\ \ k=1,..,N$ higher and lower value of the entries

$s\max_k, s\min_k\ \ k=1,..,M$ higher and lower value of the exits

The procedure for obtaining the expressions of the sensitivity of the net:

$$\begin{aligned} Z_1 &= f_1^b(Y_1) \\ Z_2 &= f_2^b(Y_2) \\ &\text{M} \\ Z_{\text{M}} &= f_{\text{M}}^{\text{b}}(Y_{\text{M}}) \end{aligned} \qquad 5.$$

will now be described.

With an appropriate manipulation of the variables, Equation 6., that correlates the entries with the normalised exits of the net is obtained:

$$\begin{aligned} Z_1 &= f_1^b(f_1^o(\sum_{j=0}^{\text{L}} W_{1j}^o f_j^h(\sum_{i=0}^{\text{N}} W_{ji}^h f_i^a(U_i)))) \\ Z_2 &= f_2^b(f_2^o(\sum_{j=0}^{\text{L}} W_{2j}^o f_j^h(\sum_{i=0}^{\text{N}} W_{ji}^h f_i^a(U_i)))) \\ &\text{M} \\ Z_{\text{M}} &= f_{\text{M}}^b(f_{\text{M}}^o(\sum_{j=0}^{\text{L}} W_{\text{M}j}^o f_j^h(\sum_{i=0}^{\text{N}} W_{ji}^h f_i^a(U_i)))) \end{aligned} \qquad 6.$$

By substituting the corresponding values for the functions $f^a(.), f^b(.), f^o(.), f^h(.)$, Equation 7. is obtained:

$$\begin{aligned} Z_1 &= \frac{1}{1+\exp^{-V_1}}[\text{smax}_1 - \text{smin}_1] + \text{smin}_1 \\ Z_2 &= \frac{1}{1+\exp^{-V_2}}[\text{smax}_2 - \text{smin}_2] + \text{smin}_2 \\ &\text{M} \\ Z_{\text{M}} &= \frac{1}{1+\exp^{-V_{\text{M}}}}[\text{smax}_{\text{M}} - \text{smin}_{\text{M}}] + \text{smin}_{\text{M}} \end{aligned} \qquad 7.$$

where :

$$V_k = \sum_{j=0}^{\text{L}} W_{kj}^o f_j^h(\sum_{i=0}^{\text{N}} W_{ji}^h f_i^a(U_i)) \quad \text{para } k=1,...,\text{M} \qquad 8.$$

In a general form, Equation 7. becomes:

$$Z_k = \frac{1}{1+\exp^{-V_k}}[\text{smax}_k - \text{smin}_k] + \text{smin}_k \qquad 9.$$

para k = 1,.., M

The sensitivity factors will be calculated from equation (10):

$$\frac{\partial Z}{\partial U} = \begin{bmatrix} \frac{\partial Z_1}{\partial U_1} & \frac{\partial Z_1}{\partial U_2} & ..... & \frac{\partial Z_1}{\partial U_{\text{N}}} \\ ..... & ..... & ..... & ..... \\ \frac{\partial Z_{\text{M}}}{\partial U_1} & \frac{\partial Z_{\text{M}}}{\partial U_2} & ..... & \frac{\partial Z_{\text{M}}}{\partial U_{\text{N}}} \end{bmatrix} \qquad 10.$$

where each term of the sensitivity matrix is calculated in the form:

$$\frac{\partial Z_k}{\partial U_i} = [\text{smax}_k - \text{smin}_k]\frac{\exp^{-V_k}}{(1+\exp^{-V_k})^2}\frac{\partial V_k}{\partial U_i} \qquad 11.$$

Manipulating the derivative term of Equation 11. and taking into account Equation 8., the following expression is obtained:

$$\frac{\partial V_k}{\partial U_i} = \frac{\partial}{\partial U_i}(W^o_{k0} + \sum_{j=1}^{L} W^o_{kj} f^h_j (\sum_{i=0}^{N} W^h_{ji} f^a_i (U_i))) \qquad 12.$$

By differentiating Equation 12. and substituting the expression in Equation 11., Equation 13. is obtained, which allows the calculation of the sensitivity factors starting from the net:

$$\frac{\partial Z_k}{\partial U_i} = \begin{bmatrix} (\text{smax}_1 - \text{smin}_1)\dfrac{\exp^{-V_1}}{(1+\exp^{-V_1})^2} \\ (\text{smax}_2 - \text{smin}_2)\dfrac{\exp^{-V_2}}{(1+\exp^{-V_2})^2} \\ \text{M} \\ (\text{smax}_M - \text{smin}_M)\dfrac{\exp^{-V_M}}{(1+\exp^{-V_M})^2} \end{bmatrix} o \left\{ W^o x \left\{ \begin{bmatrix} \dfrac{\exp^{-(\sum_{i=0}^{N} W^h_{1i} X_i)}}{(1+\exp^{-(\sum_{i=0}^{N} W^h_{1i} X_i)})^2} \\ \dfrac{\exp^{-(\sum_{i=0}^{N} W^h_{2i} X_i)}}{(1+\exp^{-(\sum_{i=0}^{N} W^h_{2i} X_i)})^2} \\ \text{M} \\ \dfrac{\exp^{-(\sum_{i=0}^{N} W^h_{Li} X_i)}}{(1+\exp^{-(\sum_{i=0}^{N} W^h_{Li} X_i)})^2} \end{bmatrix} o \begin{bmatrix} \dfrac{W^h_{11}}{\text{emax}_1 - \text{emin}_1} & \dfrac{W^h_{12}}{\text{emax}_2 - \text{emin}_2} & \Lambda & \dfrac{W^h_{1N}}{\text{emax}_N - \text{emin}_N} \\ \dfrac{W^h_{21}}{\text{emax}_1 - \text{emin}_1} & \dfrac{W^h_{22}}{\text{emax}_2 - \text{emin}_2} & \Lambda & \dfrac{W^h_{2N}}{\text{emax}_N - \text{emin}_N} \\ \text{M} & \text{M} & \Lambda & \text{M} \\ \dfrac{W^h_{L1}}{\text{emax}_1 - \text{emin}_1} & \dfrac{W^h_{L2}}{\text{emax}_2 - \text{emin}_2} & \Lambda & \dfrac{W^h_{LN}}{\text{emax}_N - \text{emin}_N} \end{bmatrix} \right\} \right\} \qquad 13.$$

The index "o" corresponds to the product of the first value of the column vector by the whole first matrix row, extended to all the rows of the matrix and:

$$W^o = \begin{bmatrix} W^o_{11} & W^o_{12} & \Lambda & W^o_{1L} \\ W^o_{21} & W^o_{22} & \Lambda & W^o_{2L} \\ \text{M} & \text{M} & \text{M} & \text{M} \\ W^o_{M1} & W^o_{M2} & \Lambda & W^o_{ML} \end{bmatrix}$$

DETERMINATION OF ADJUSTMENT IN THE CONTROL PARAMETERS

The necessary steps to determine the adjustments corresponding to the control operation in the rolling process are next described:

I. The entries and nominal exits are contained in the vectors $\overline{X}^* = (h_e^*, g^*, \mu^*, t_r^*, t_f^*, \overline{y})$ and $\overline{Y}^* = (h_S^*, P^*)$ respectively.

II. Through Equation 13. it is possible to calculate the sensitivities for the selected nominal point.

III. After calculating the sensitivity factors it is possible to obtain the linear equations of the process, Equations 14. around the nominal operation point:

$$\Delta h_o = \Delta h_i \frac{\partial h_o}{\partial h_i} + \Delta g \frac{\partial h_o}{\partial g} + \Delta \mu \frac{\partial h_o}{\partial \mu} + \Delta t_b \frac{\partial h_o}{\partial t_b} + \Delta t_f \frac{\partial h_o}{\partial t_f} + \Delta \bar{y} \frac{\partial h_o}{\partial \bar{y}} \qquad 14.$$

being $\Delta X = X^* - X$

If a variation takes place either in one or all the operational parameters $h_e, g, \mu, t_r, t_f, \bar{y}$, an alteration will occur in the h_f value. The existence of a factor *K* such that $\Delta h_f = 0$ may be admitted. That is to say (15):

$$0 = \Delta h_e \frac{\partial h_f}{\partial h_e} + \Delta g \frac{\partial h_f}{\partial g} + \Delta \mu \frac{\partial h_f}{\partial \mu} + \Delta t_r \frac{\partial h_f}{\partial t_r} + \Delta t_f \frac{\partial h_f}{\partial t_f} + \Delta \bar{y} \frac{\partial h_f}{\partial \bar{y}} + K \qquad 15.$$

Equating Equations 14. and 15., we obtain:

$$K = -\Delta h_f \qquad 16.$$

The value of K depends on the selected control parameter: roll gap, front or back tensions and may be defined as:

$$K = \Delta g \frac{\partial h_f}{\partial g} \quad \text{or} \quad K = \Delta t_r \frac{\partial h_f}{\partial t_r} \quad \text{or} \quad K = \Delta t_f \frac{\partial h_f}{\partial t_f} \qquad 17.$$

If control action by means of the roll gap is assumed, the equations would be:

$$K = \Delta g \frac{\partial h_f}{\partial g} = -\Delta h_f \qquad \Delta g = -\frac{\Delta h_f}{\partial h_f / \partial g} \qquad g = g^* + \frac{\Delta h_f}{\partial h_f / \partial g} \qquad 18.$$

Similarly, in terms of the front and back tensions:

$$t_r = t_r^* + \frac{\Delta h_f}{\partial h_f / \partial t_r} \qquad t_f = t_f^* + \frac{\Delta h_f}{\partial h_f / \partial t_f} \qquad 19. \text{ and } 20.$$

APPLICATION, RESULTS AND CONCLUSION

As an example of the possibilities of the method, a numerical application to a rolling process case will be presented. The operation point was chosen as: h_i=5.0 mm; h_o,= 3.6 mm; g=1.846 mm. μ=0.12; t_f =9.098 kgf/mm^2; t_b =0.441 kgf/mm^2; $\bar{y}$ =46.918 kgf/mm^2; W = 500 mm; E=20,400 kgf/mm^2; R= 292.1 mm; M=500,000 kgf/mm^2 and P= 875.31tf.

To obtain the data sets for ANN training, the parameters variations were chosen as: h_i=± 8%; h_o,= ± 3%; μ =± 20%; t_f =± 30%; t_b =± 30% and $\bar{y}$ =± 10%. Three different values were chosen for each parameter resulting in 729 training sets. The load rolling was obtained through Alexander's model [1] and the roll gap by the elastic equations for the rolling mill (Equation 21).

$$h_o = g + P/M \qquad 21.$$

The final weights for the hidden and output layers with its polarization weight are:

$$W^h = \begin{bmatrix} 6.2010 & 9.4161 & -1.7278 & -0.2642 & 1.8475 & 1.3078 \\ -1.5239 & -9.2425 & -2.4238 & 0.0734 & 0.7813 & -6.0229 \\ -11.4365 & -1.7129 & 1.2562 & -0.2171 & -0.6941 & 3.3125 \\ -0.2767 & -8.3214 & -5.5920 & -0.2737 & -3.3595 & -0.8293 \\ 3.3504 & 5.2707 & 3.4006 & 0.0343 & -0.5938 & 4.7363 \\ 8.9832 & 3.9726 & 0.7990 & 9.7730 & 0.9096 & 5.5016 \\ -6.1621 & 3.4810 & 7.4542 & 0.5558 & -7.0447 & -0.9006 \\ -4.8199 & -3.2388 & 6.5208 & -3.4559 & -0.6086 & 8.9722 \\ 0.8914 & -8.2071 & -7.6049 & -0.1518 & -2.2323 & -1.5593 \\ -1.2378 & -10.6099 & -0.0338 & 0.0399 & 0.4850 & -2.1458 \\ 8.3913 & 2.3521 & 5.9967 & -8.1868 & -4.0553 & 1.8826 \\ -1.4947 & -11.9576 & -1.6808 & 0.0733 & 0.7387 & -4.2602 \\ 2.9411 & 4.8319 & -11.5151 & -1.5484 & -4.0985 & -4.2330 \end{bmatrix} \quad W^h_{bias} = \begin{bmatrix} -11.4784 \\ 8.9265 \\ 2.5654 \\ 10.9804 \\ -10.4911 \\ -15.1094 \\ 5.3887 \\ -4.5520 \\ 7.1306 \\ 8.8376 \\ -0.4583 \\ 8.7774 \\ 2.5081 \end{bmatrix}$$

$$W^o = \begin{bmatrix} 0.5503 & 0.4083 \\ -1.7551 & -2.1593 \\ -0.9245 & -0.1960 \\ -0.2976 & 0.2163 \\ 4.2976 & 0.9087 \\ 0.0021 & 0.0045 \\ 0.1479 & 0.1406 \\ 0.1378 & 0.0480 \\ -1.1542 & -0.0074 \\ -6.4508 & 1.0470 \\ -0.0276 & -0.0106 \\ -3.9372 & 2.4463 \\ 0.1814 & 0.0746 \end{bmatrix} \quad W^o_{bias} \begin{bmatrix} 6.4599 \\ -1.4106 \end{bmatrix}$$

The events sequence to determine the control operation adjustments are described next:

I. Define the nominal inputs: $[h_i^*, g^*, \mu^*, t_b^*, t_f^*, \bar{y}]$=[5.00; 1.846; 0.12; 0.441; 9.098; 46.918];

II. Provide the nominal outputs: $[h_o^*, P^*]$=[3.6; 875.31];

III. Calculate through Equation 13 the sensitivity coefficients (Equation 14) for the selected nominal point: $[\frac{\partial h_o}{\partial h_i}, \frac{\partial h_o}{\partial g}, \frac{\partial h_o}{\partial \mu}, \frac{\partial h_o}{\partial t_b}, \frac{\partial h_o}{\partial t_f}, \frac{\partial h_o}{\partial \bar{y}}]$ = [0.3566; 0.6436; 4.7345; -0.0163; -0.011; 0.0327];

IV. In the presence of parameter variation, compute current inputs as: $[h_i, g, \mu, t_b, t_f, \bar{y}]$ = [4.9; 1.846; 0.118; 0.432; 9.098; 46.918];

V. Using an ANN previously trained, determine the current outputs: $[h_o, P]$ = [3.552; 855.527];

VI. Determine the control parameters using Equations 18, 19 and 20:
$[\bar{g}, \bar{t}_b, \bar{t}_f]$=[1.920; –2.504; 4.734]. This corresponds to corrections: +3.8%, -639.9% and -54% respectively;

The smallest correction percentage indicates the best control action. Therefore, the correction of the output thickness deviation should be made through the roll gap. Notice that the value calculated for $\bar{t}_b$ is negative and should be saturated $\bar{t}_b = 0$.

In order to verify the calculated adjustments, the three possible corrections were simulated through an interactive procedure using Alexander's model and equation (21). For the roll gap action ($\bar{g}$=1.920) the value of the output thickness was 3.585 mm with an error of 0.42%. For the back tension action ($\bar{t}_b$ =0) the value of the output thickness was 3.555 mm with an error of 1.25% and for the front tension action ($\bar{t}_f$ =4.734) the value of the output thickness was 3.584 mm with an error of 0.44%.

ACKNOWLEDGEMENT

This work was accomplished with support of the Pontifical Catholic University of Minas Gerais, PUC-MG, SaicSystems and Mechanical Conformation Research Group (UFMG-Brazil).

REFERENCES

1. Alexander, J. M., 1972. On the theory of rolling. *Proc. R. Soc. Lond.* A. 326, pp. 535-563.
2. Zárate, L.E., 1998. Doctoral Thesis, Federal University of Minas Gerais, Belo Horizonte, MG, Brazil.

Artificial Intelligence Approach to The Modeling of Rolling Loads in Technology Design for Cold Rolling Processes

J. Kusiak*, J.G. Lenard, K. Dudek***

*Akademia Gorniczo-Hutnicza, Mickiewicza 30, 30-059 Krakow, Poland
** University of Waterloo, Waterloo, Ont. N2L 3G1, Canada

ABSTRACT

The paper presents an attempt to apply artificial neural networks to the prediction of the influence of various frictional conditions on rolling forces and torques. Training of the network was done using experimental data, which consist of the results of load measurements during cold rolling of aluminum alloys in different lubrication conditions. The properties of the lubricant became the input variables for the neural network. Accurate prediction of the rolling forces and torques during cold rolling under varying frictional conditions is the main ability of the model. The artificial neural network was validated using data, which were not used during the training procedure. Next, the predictions of the artificial neural network were compared with the finite element calculations of rolling under varying friction conditions. This validation confirmed the good predictive ability of the ANN model.

INTRODUCTION

The quality and dimensional accuracy of rolled products can be controlled, provided each parameter of the rolling process is well known. The development of computer techniques create the possibility of calculations of these parameters using numerical methods, based mainly on finite-element models. These methods require large computational time and, therefore cannot be implemented in an on-line control system. An additional difficulty concerns the proper definition of the boundary conditions necessary for numerical calculations. Therefore, alternative techniques, based on artificial intelligence, appear very useful in numerical modeling of complex problems in rolling.

The appropriate modeling of frictional conditions appears to be the main difficulty in the analysis of the cold rolling processes. Therefore, the general goal of the paper is an attempt of the application of artificial neural networks to the prediction of the influence of various frictional conditions on the rolling forces and torques.

Training of the network was done using the experimental data, which consist of the results of load measurements during cold rolling of aluminum alloys using different lubrication conditions. The properties of the lubricant became the input variables for the neural network. The ability of the accurate prediction of the rolling forces and torques during cold rolling in varying frictional conditions is the main facility of the model. Additionally, the predictive capability of the neural network has a great advantage over the classical approach, based on the FEM modeling, due to the speed of the ANN model. Therefore, the ANN model can be easily used in the design of new rolling technology, as well as in on-line control systems of the rolling process.

ALUMINUM COLD ROLLING

Cold, flat rolling of aluminum is usually performed in either the boundary or the mixed lubrication regimes in which some metal-to-metal contact occurs in addition to pockets of lubricants that separated the roll and the rolled metal. In those two regimes control of friction is paramount and this is achieved by the appropriate choice of boundary additives.

Matsui et al. [1] used a paraffin-based oil mixed with lauryl alcohol, lauric acid and methyl laureate, at a 5% (v/v) concentration. In this study, the preferable additive for rolling of aluminum was the alcohol. Kihara [2] evaluated the effects of butyl laureate, lauric acid, and lauryl alcohol, at 5% (v/v), in a low viscosity paraffin-based oil. Friction was lowest with the alcohol. Nautiyal and Schey [3] observed that

0-7803-5489-3/99/$10.00 ©1999 IEEE.

both lauric and oleic acids are ineffective but stearic acid is able to lower friction significantly. Stearyl alcohol, useless at 1%, gave significant improvement at 5%.

Williams [4] writes that in boundary lubrication regimes, where film thickness is only a few molecules deep, viscosity and density of the lubricant have less effect on frictional resistance than either its chemical composition or properties of the rolled metal. The term "oiliness" is used to define the lubricating properties of the film. SAE defines oiliness as signifying, "differences in friction greater than can be accounted for on the basis of viscosity... ". Boundary additives of long chain molecules, typically alcohol or acids, assist base oils in forming films which adsorb on the surface. The additive concentration should be sufficient to cover the necessary surfaces but should not affect the bulk attributes of the base oil.

Material, Equipment and Procedure

Equipment: Experiments were carried out on a two-high rolling mill, with rolls of 254 mm diameter by 100 mm in length. The rolls were made of D2 tool steel, hardened to R_c = 54. Surface roughness was 0.18 μm. The mill was powered by a 30 kW, constant torque, DC motor through a Mack truck transmission, with continuous variable speed. The mill was instrumented with two load cells placed under the bearing blocks of the bottom roll, two torque transducers placed on the drive spindles, one shaft encoder and an LVDT to monitor roll gap.

Material: The strip material was 1100 H14 aluminum, containing 0.05% Mn, 1% Si, 0.05 - 0.2% Cu and 0.1% Zn. The samples were 1 mm x 25 mm x 300 mm long, cut parallel to the original direction of rolling. The plane strain, true stress - true strain curve of the metal is given by $\sigma = 110.9(1 + 100\varepsilon)^{0.11}$, MPa.

Lubricant: Mineral seal oil was used as the base and the effect of increasing concentrations of boundary additives - lauric acid, stearic acid, lauryl alcohol and stearyl alcohol - was examined. The average density was 850 kg/m^3 and the kinematic viscosity was 4.5 mm^2/s, at 40°C. The additive concentration was varied from 1-5%, (v/v). These amounts did not change the effective viscosity or density in a significant manner.

Procedure: Before each pass, the rolls and specimens were degreased with n-heptane, a neutral cleaner,. Ten drops of lubricant were spread uniformly on all surfaces of the specimens. After rolling, the strips were degreased again. The independent variables are the reduction, the rolling speed and the additive concentration.

FEM Simulation

Development of a method to evaluate the friction coefficient for various lubricants was one of the objectives of the project. Comparison of measurements with calculations performed assuming various friction coefficients, has been made. All experiments were simulated using the finite-element technique. Detailed description of the applied finite-element model, is given in [5,6]. Figure 1 shows typical results, which were obtained for 3% stearyl alcohol by volume, with mineral seal oil as lubricant. Numerical results are compared with the measurements performed for various roll velocities.

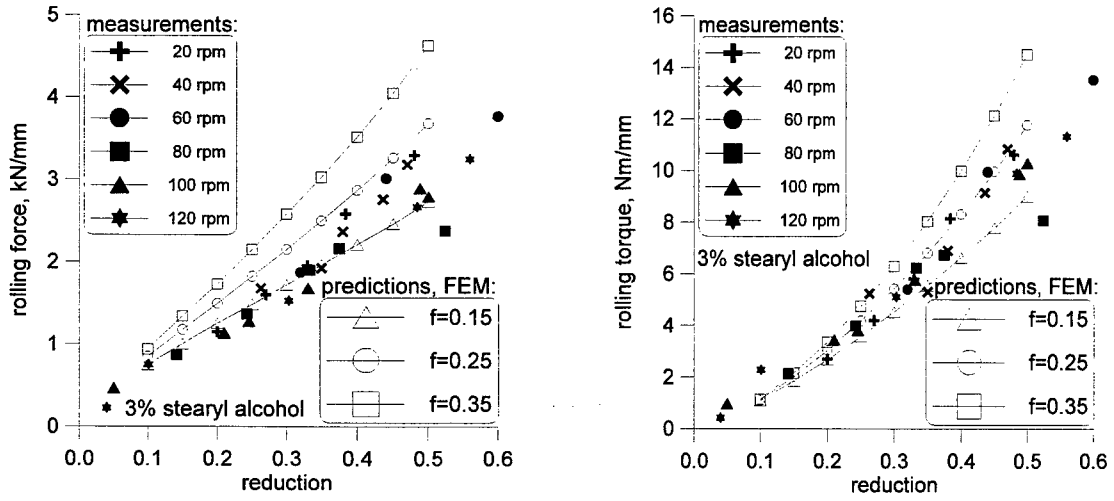


Fig. 1. Calculated rolling force (a) and roll torque (b) compared with the experimental data obtained for various roll velocities; lubricant 3% stearyl alcohol.

Analysis of the results obtained for the four lubricants with different additive concentrations should allow evaluation of the friction coefficient relevant for each particular lubricant. However, scatter of the experimental measurements (see Figure 1) caused problems with interpretation of the results. Therefore, an attempt was undertaken to apply an artificial neural network to overcome these difficulties.

ARTIFICIAL NEURAL NETWORK APPROACH

Artificial neural networks have become powerful tools to simulate and control various processes. Numerous examples of applying ANN to metal forming are found in the scientific literature. Among the many publications, those dealing with control of rolling mills [7,8] as well as with prediction of yield strength in plate mills [9], rolling loads [10,11,12] and plate bending in asymmetrical rolling [13] should be mentioned.

Our main goal was to establish a relation between lubricant additive, its concentration and the rolling conditions. Because there is no mathematical model of such relationships, our aim was to apply an artificial neural network approach to solve the problem. The trained ANN should predict forces and torques during cold rolling under different lubrication conditions. The neural network was trained using experimental data, consisting of load and torque measurements during cold rolling of Al-alloy specimens. The rolling process was performed using different lubrication conditions, as described above. The input variables were:

- the type of lubricant added,
- the lubricant concentration
- the rolling speed
- the reduction.

The training data set included experimental data of all rolling tests with different lubricants and different additive concentrations, except data for rolling with 3% concentration of lubricants. These data were reserved to test the trained network. The outputs of the ANN were:

- rolling force,
- rolling torque.

Different network topologies were tested during training. The best results were obtained for a network with one hidden layer of 20 neurons. Thus, the final network topology was 4-20-2. The trained network was then tested using data from outside the training data set, i.e., results of rolling with 3% concentration of additives.

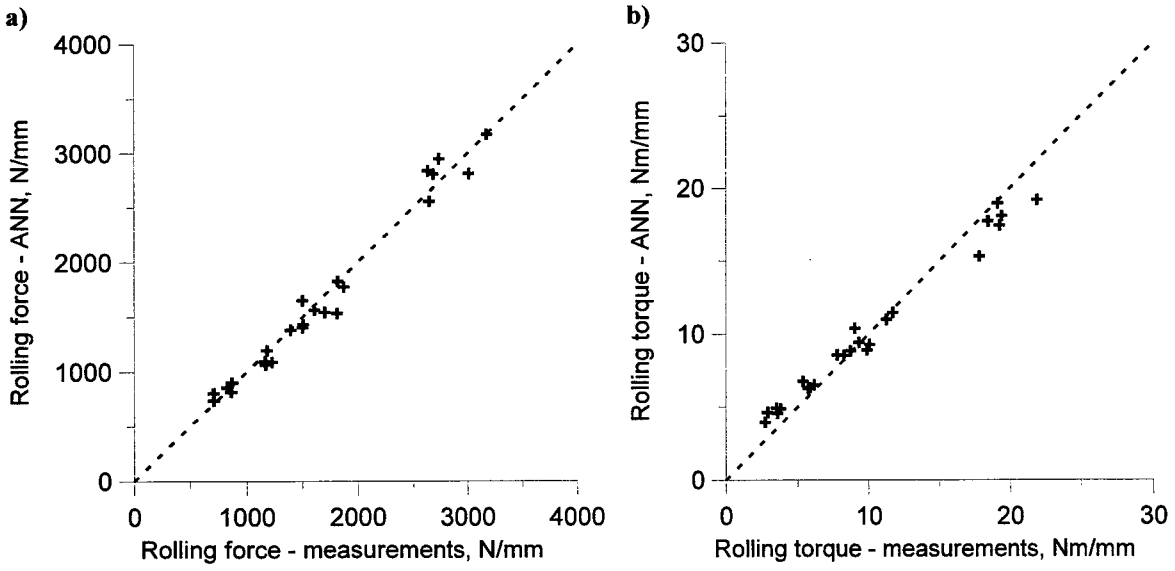


Fig. 2. Comparison of measured and predicted (by ANN) values of forces (a) and torques (b) of rolling with 3% concentration of the stearic acid additive.

The comparison of measured and predicted results by ANN, for values of force and torque of rolling with 3% concentration of stearic acid additive are presented in Figure 2. Good agreement between the measurements and predictions of the artificial neural network is observed. Similar agreement was obtained for rolling with 3% concentration of the other additives, i.e. all of the unseen data showed excellent comparison.

The next step of the validation procedure was to compare the values predicted by the ANN model with the results of FEM calculations. Typical results obtained for the 3% concentration of lauryl alcohol additive are shown in Figure 3. Thick dotted and solid lines in this figure represent predictions of the artificial neural network for 20 rpm and 100 rpm, respectively. The network smoothed the experimental results and allowed the conclusion that an increase in rolling velocity decreases the friction coefficient. This phenomenon was observed for all tested lubricants. Comparison of the predicted curve shapes by the finite element program and by the artificial neural network reveal some differences. The rolling force calculated by the FEM code increases slightly lower than that predicted by the ANN as a function of reduction.

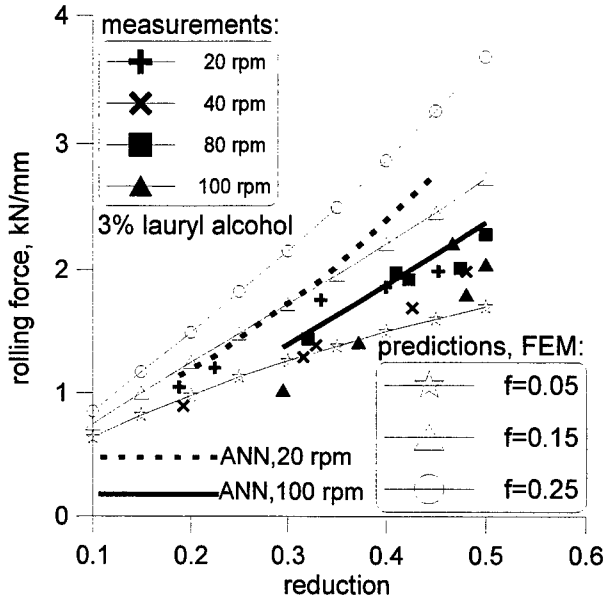


Fig. 3. Results of measurements, FEM calculations and predictions by ANN for 3% lauryl alcohol additive.

Analysis of all results show that a combination of finite element simulation with neural network prediction is a good approach to evaluate the friction coefficient. The neural network eliminates scattering of the experimental results and yields a monotonous relationship between loads and reduction. Comparison of ANN representation of the results with FEM calculations for various friction coefficients allows this coefficient to be chosen more accurately.

CONCLUSIONS

The ability of the accurate prediction of the rolling forces and torques during cold rolling in varying frictional conditions is the main advantage of the model. Additionally, the predictive capability of the neural network has a great advantage over the classical approach based on the FEM modeling, due to the speed of the ANN model. The artificial neural network was validated for the data, which were not used during the training procedure. The validation confirmed the good predictive ability of the model. Therefore, the ANN model can be easily used in the design of new rolling technology, as well as in on-line control systems of the rolling process. The artificial neural network, developed in the present work, was implemented in the computer program, which designs rolling schedules for a reverse four-high mill.

ACKNOWLEDGEMENT

Financial support of KBN (project AGH No 11.11.110.16), NATO and NSERC is gratefully acknowledged.

REFERENCES

1. Matsui, K., Matsushita, T., Takatsuka, K., Yamaguchi, Y., 1984. Advanced Techn. of Plasticity, 1, 247.
2. Kihara, J., 1990. Advanced Techn. of Plasticity, 4, 1693.
3. Nautiyal, P.C., Schey, J.A., 1990. ASME J. Tribol., 112, 282.
4. Williams, J.A., 1994. Engineering Tribology, Oxford University Press, Oxford.
5. Pietrzyk, M., Lenard, J.G., 1991. Thermal-Mechanical Modelling of the Flat Rolling Processes, Springer-Verlag, Berlin.
6. Pietrzyk, M., 1992. Metody numeryczne w przerobce plastycznej metali, skrypt AGH1303, Krakow, (in Polish).
7. Roscheisen, M., Hofmann, R., Tresp, V., 1992. in Advances in Neural Information Processing Systems 4, (M. Kaufman, ed.), 659.
8. Too, J.J.M., Ide, K., Maheral, P., Pussegoda, N., Sherwood, E.G., Gomi, T., 1995. 37th Mechanical Working and Steel Processing Conference, Hamilton, 1995, 555.
9. Tsoi, A.C., 1992. in Advances in Neural Information Processing Systems 4, (M. Kaufman, ed.), 698.
10. Hwu, Y.J., Lenard, J.G., 1995. 37th Mechanical Working and Steel Processing Conf., Hamilton, 549.
11. Larkiola, J, Myllykoski, P., Nylander, J., Korhonen, A.S., 1996. Metal Forming96, (M. Pietrzyk, J. Kusiak, P. Hartley, I. Pillinger, eds), Krakow, J. Material Processing Technology, 60, 381.
12. Wiklund, O., 1996. Steel Strip96, Opava, 136.
13. Kusiak, J., Pietrzyk, M., Wilk, K.,1997. KomPlasTech97, (A. Piela, J. Kusiak, M. Pietrzyk, eds), Ustron-Jaszowiec, 207 (in Polish).

Direct Determination of Sequences of Passes for the Strip Rolling Process by Means of Fuzzy Logic Rules

C.D.M. Pataro.* and H. Helman.**

* Departamento de Engenharia Eletrônica, Escola de Engenharia da UFMG
Av. Antonio Carlos, 6627, Pampulha, Belo Horizonte, MG
** Departamento de Engenharia Metalúrgica, Escola de Engenharia da UFMG
Rua Espírito Santo, 35, Centro, Horizonte, MG, Brazil

ABSTRACT

In this work the direct determination of sequences of passes for the strip rolling process by means of fuzzy logic rules is presented. The variables Rolling Load, Accumulated Deformation and Aimed Deformation are expressed in linguistic terms, such as high, medium and low and their corresponding sublevels. These rules can be established in agreement with data obtained from theoretical models, rolling of samples of the strip or by means of available databases for this particular material and operational conditions. In the last two cases, the procedure becomes independent of the knowledge of mechanical and metallurgical characteristics of the process.

INTRODUCTION

The method to determine sequences of passes for the strip rolling process usually involves an iterative process [1,3,4]. This can be a very time consuming procedure, even if a fast computer is used. A direct determination of the sequences of passes was developed by Pataro, Resende and Helman in 1994, using Neural Networks [8,11], thus speeding up these calculations. As the Neural Network, the Fuzzy Logic [5,6,12,13] also showed to be adequate for the determination of loads and gaps in the rolling process [9,10]. In this work a method for the determination of the sequences of passes based on Fuzzy Logic rules is described. These rules may be derived from a database, as the curves shown in Figure 1.

The relationship "rolling load - deformation" varies significantly with large changes in operational variables such as friction, strip width, yield stress, and entry thickness. These variations are not linear; they not only alter the slope but also cause a displacement of the mention curves. Several theoretical models permit the calculation of this load [3].

Families of curves as a function of logarithmic deformations are produced with that aim. Using the Accumulated Deformation (ε_i) as a parameter, such curves show the relationship between the Rolling Load (P) and Deformation (ε_i). These variables must be obtained for the same material, with a constant width and initial thickness, rolled according to an adequate accumulated deformation schedule. The curve relative to ε_1 should also be plotted for the various desired deformation values, starting at the value of h_1, and according to the accumulated deformation ε_1. These curves can be obtained by using experimental values or theoretical models.

Assuming that $\varepsilon_1 < \varepsilon_2 < \varepsilon_j < \varepsilon_n$ in Figure 1, a curve with a deformation ε_0 represents the behaviour of the strip in the original form, as received to be rolled. This condition can be the result of a full annealing process or an already hardened material, with an unknown history of deformations.

For a direct calculation of the sequence of passes, assuming to be working with logarithmic deformations (that permit to be added up to a final desired deformation) and supposing that the final deformation ε_5 is objectively derived, the following procedure should be carried out:

0-7803-5489-3/99/$10.00 ©1999 IEEE.

1 - Search for the deformation value so that the maximum rolling load is not exceeded. This is achieved looking for the curve with the accumulated deformation, ε_{0},, at the point where the rolling load is at the maximum, $\mathbf{P_{max.}}$ This point defines the logarithmic deformation ε_4 (point B of Figure 1).

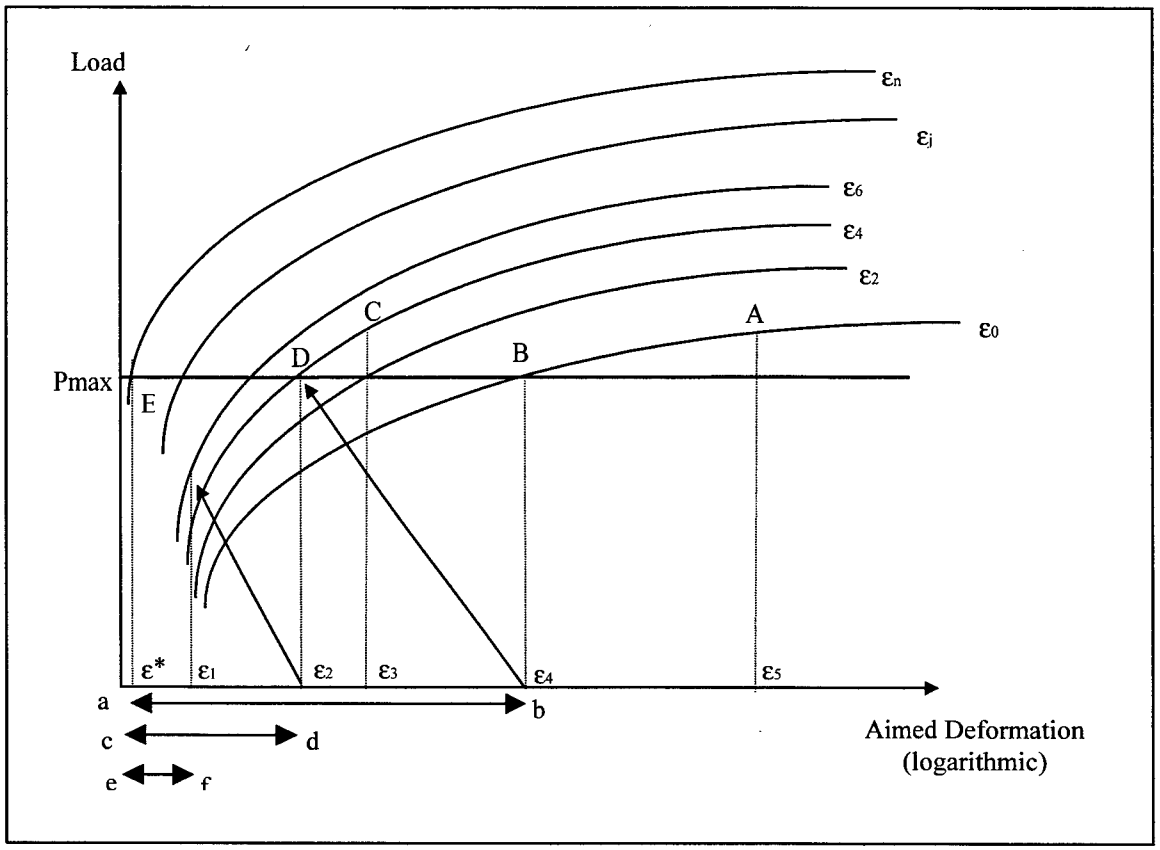


Fig. 1. Typical aspect of a family of curves "Rolling Load – Deformation", using Accumulated Deformation as a parameter .It describes the procedure for the direct calculation of a pass sequence.

2 - Observe the deformation still required to achieve the final objective, or:

$$\varepsilon_r = \varepsilon_3 = \varepsilon_5 - \varepsilon_4$$

3 - Check if it is possible to apply that deformation without exceeding the maximum load. This verification should be done on the curve with an accumulated deformation ε_{4f}, since the material is now in this condition. In this case, point C, which is higher than the acceptable maximum load is found.

4 -Return to step 1, now looking for the desired deformation value corresponding to $\mathbf{P_{max}}$, on the curve with the value of ε_4 for the accumulated deformation.

5 -Repeat the step if the final desired deformation has not achieved. In Figure 3, the steps ε_4, ε_2 e ε_1, which correspond to the sequence of steps necessary to accomplish the final deformation ε_5 are seen. Check that the sum of the segments **ab, cd** and **ef** correspond to the deformation ε_5.

ELABORATION OF PASS SEQUENCES USING FUZZY LOGIC RULES

The rules corresponding to the following example were produced from the data shown in Figure 2, based on Bland-Ford model [2], for a 100mm width steel with the following parameters of Ludwik's equation: A = 9.6 kgf/mm^2; B = 75 kgf/mm^2 and $\eta = 0.3$.

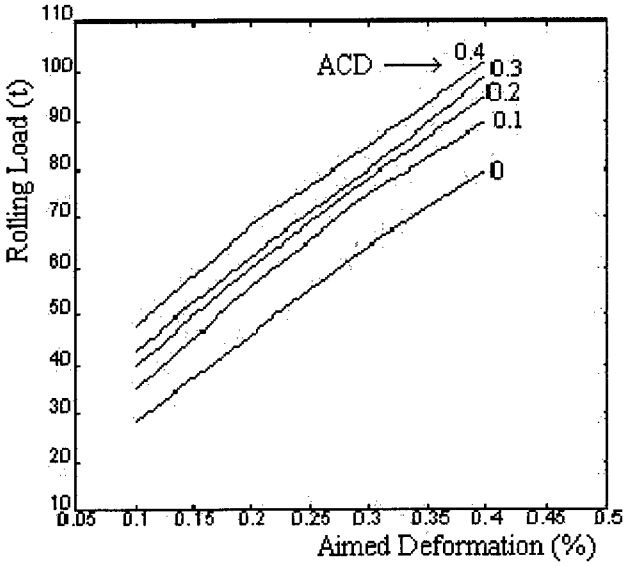


Fig.2. Curves used to establish the fuzzy logic rules for the calculation of sequences of passes.

According with the method of the direct determination for the sequences of passes, described in the first part of this work, the accumulated and aimed deformation will be used to determine the rolling load. The rolling load and the accumulated deformation will be used to obtain the aimed deformation for each pass. The accumulated deformations are classified in linguistic terms, as follow: Super - Low (SL), Low, (L), Medium (M), High (H) and Super- High (SH). The aimed deformations are classified as follows: Super - Low (SL), Medium- Low (ML), Low, (L), Medium-Medium (MM), Medium (M), Medium -High (MH), High (H), High-High (HH) and Super- High (SH). The rolling load received the classification ranging from C1 to C10. Figures 3, 4 and 5 show the membership function (μ) for these variables.

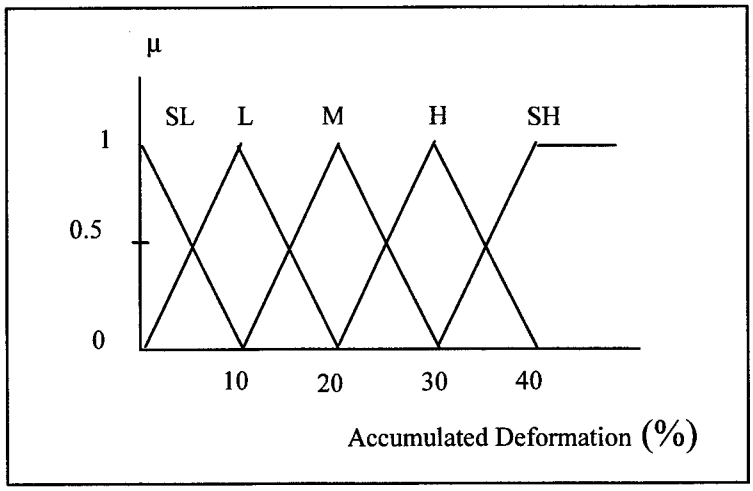


Fig. 3. Membership Functions for accumulated deformation

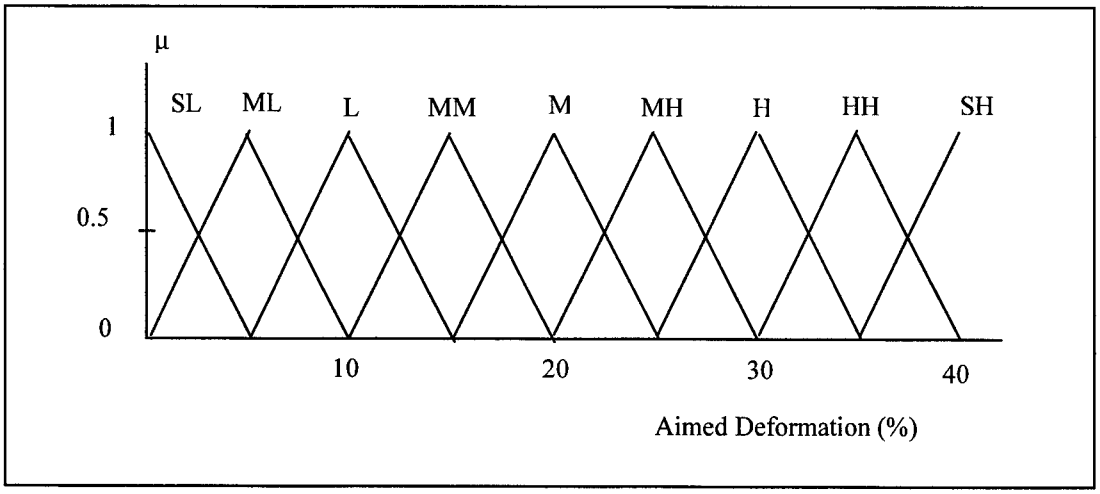


Fig. 4. Membership functions for aimed deformation

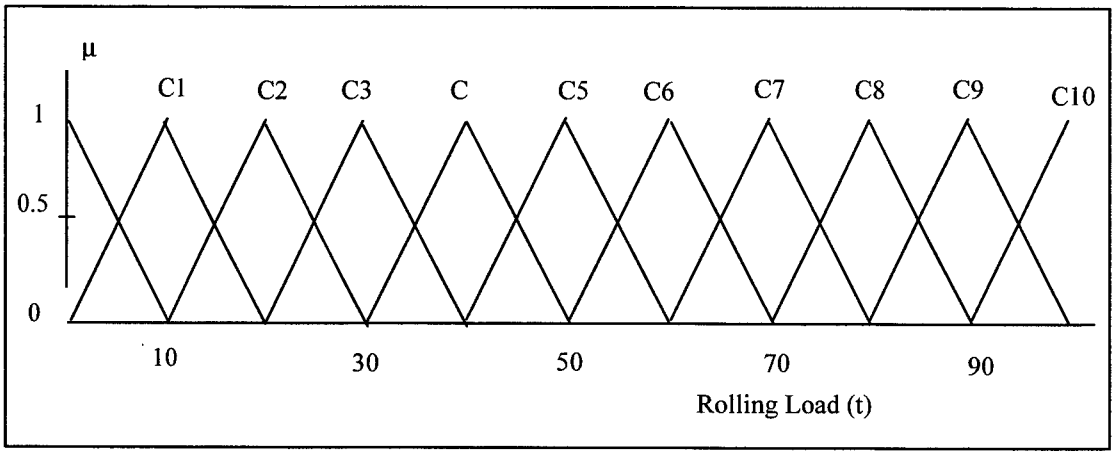


Fig. 5. Membership functions for rolling load

Table 1 describes the rules that determine the rolling load as a function of the accumulated deformation and desired deformation. ACD is the accumulated deformation; AID is the aimed deformation and RLO, the rolling load.

Table 1: Rules used for the determination of the rolling load, as a function of the accumulated deformation and desired deformation.

ACD AID	SL	L	M	H	SH
SL	C1	C2	C2	C3	C3
ML	C2	C3	C3	C4	C4
L	C3	C4	C4	C4	C5
MM	C4	C5	C5	C5	C6
M	C5	C6	C6	C6	C7
MH	C6	C6	C7	C7	C8
H	C7	C7	C8	C8	C9
HH	C7	C8	C9	C9	C10
SH	C8	C9	C9	C10	C10

Table 2 : Rules used for the final deformation, as a function of the accumulated deformation and desired deformation

ACD AID	SL	L	M	H	SH
SL	SB	B	M	A	SA
ML	MB	MM	MA	AA	SA
L	B	M	A	SA	SA
MM	MM	MA	AA	SA	SA
M	M	A	SA	SA	SA
MH	MA	AA	SA	SA	SA
H	A	SA	SA	SA	SA
HH	AA	SA	SA	SA	SA
SH	SA	SA	SA	SA	SA

Table 3: Rules used for the determination of the desired deformation, as a function of accumulated deformation and rolling load

ACD RLO	SL	L	M	H	SH
C2	SL	SL	SL	SL	SL
C3	L	SL	SL	SL	SL
C4	M	MM	L	SL	SL
C5	MH	M	MM	M	L
C6	H	MH	M	M	MM
C7	HH	H	H	MH	MH
C8	SH	HH	HH	HH	H
C9	SH	SH	SH	SH	HH
C10	SH	SH	SH	SH	SH

RESULTS

A computing programme was elaborated in accordance with the exposition made in the previous sections. Several sequences of passes for different desired deformations were simulated. As it was shown, the rules employed are adequate for the given material, with the mechanical characteristics presented in Figure 2, but they can also be used for similar materials.

Table 4: Sequences of passes for maximum rolling load of 60 t, desired deformation of 40%. Obtained deformation: 39%.

Pass	AID(%)	RLO(t)
1	26.0	60
2	13.0	45

Table 5: Sequences of passes for maximum rolling load of 50 t, desired deformation of 30%. Obtained deformation: 29%.

Pass	AID(%)	RLO(t)
1	21.0	50
2	8.0	40

Table 6: Sequences of passes for maximum rolling load of 50 t, desired deformation of 40%. Obtained deformation: 40.6 %.

Pass	AID(%)	RLO(t)
1	21.0	50
2	13.5	50
3	6.1	38

Table 7: Sequences of passes for maximum rolling load of 70 t, desired deformation of 40%. Obtained deformation: 40.6 %.

Pass	AID(%)	RLO(t)
1	33.5	70
2	7.1	40

CONCLUSION

The method developed is suitable to determine sequences of passes in flat rolling, in accordance with the simulation. The maximum error found in the example is less than 3.0%, in the final desired deformation and it can be reduced, by increasing the number of linguistic terms. The application of this procedure in areas where materials with similar characteristics are normally rolled, may be extremely useful.

REFERENCES

1. Avila, A. F., 1998. Otimização da Produtividade de um Laminador Tandem a Frio. Tese de Mestrado. EEUFMG. Depto. de Engenharia Metalúrgica. Belo Horizonte, Novembro.
2. Bland, D.R., Ford, H., 1948. The Calculation of Roll Force and Torque in Cold Strip Rolling with Tensions. Proc. Inst. Mech. Eng., 159, 144-163.
3. Helman, H. et al., 1988. Fundamentos da Laminação – Produtos Planos. Publicação ABM, SP.
4. Helman, H., Cetlin, P.R., 1983. Fundamentos da Conformação Mecânica dos Metais. Guanabara Dois. Rio de Janeiro.
5. Jamshidi, M., Vadiee, N., Ross, T., 1993. Fuzzy Logic and Control - Software and Hardware Applications. PTR,Prentice Hall, Englewood Cliffs, New Jersey
6. Klir, G. J.; Folger, T. A., 1988. Fuzzy Sets, Uncertaint and Information, Prentice-Hall, New York.
7. Pataro, C.D.M., Helman, H., 1997. Determinação Direta de Seqüências de Passes na Laminação de Produtos Planos, Mantendo Constante a Carga de Laminação. Anais do II Congresso Internacional de Tecnologia Metalúrgica e de Materiais. São Paulo, SP.
8. Pataro, C.D.M., 1996. Execução Automática do Processo de Laminação, Utilizando Redes Neurais. Tese de Doutorado, UFMG.
9. Pataro, C.D.M; Resende, P., Helman, H., 1995. Aplicação de Lógica Nebulosa na Laminação de Produtos Planos. Anais do 50° Congresso Anual da ABM. pp. 395-404, São Pedro, São Paulo.
10. Pataro, C.D.M, Helman, H., 1997. Determinação de berturas entre Cilindros de Laminação, Via Lógica Nebulosa. Anais do XIV Congresso Brasileiro de Engenharia Mecânica, Bauru, SP.
11. Pataro, C.D.M; Resende, P., Helman, H., 1994. Geração Automática de uma Seqüências de Passes na Laminação de Produtos Planos. Anais do Congresso Internacional de Tecnologia Metalúrgica São Paulo, SP.
12. Zadeh, L.A., 1965. "Fuzzy sets", Info. & Control., 8, 338-353.
13. Zadeh, L. A., 1973. Outline of a new approach to the analysis of complex systems and decision process, IEEE Trans. Syst., Man, Cybern., 3, 28-44.

Elongation-Control Rolling of H-Shaped Wire

H. Utsunomiya, Y. Saito, M. Shinkawa and F. Shimaya

Division of Materials Science and Engineering,
Graduate School of Engineering, Osaka University,
2-1 Yamada-oka Suita, Osaka, 565-0871, Japan

ABSTRACT

The authors propose a novel technique for size-free rolling, termed *elongation-control rolling*. This technique is characterized by the active use of interstand forces, which, being not only tensile but also compressive, are varied over a wide range. In the present study, H-shaped wires are formed from round wires by elongation-control rolling with grooved rolls. The elongation, i.e. nominal strain in the rolling direction, is controlled over a wide range, from 20% to 80%, where 50% is tension-free rolling. The flange width increases with compressive interstand force, and decreases with tensile force. It is concluded that the rolling of H-shaped wires having an arbitrary flange width is made possible.

INTRODUCTION

In the continuous rolling of bars, rods, and sections, the forces acting on materials between rolling stands (interstand forces) must be negligibly small (tension-free) in order to obtain dimensional accuracy and stable operation. The authors showed that interstand compressive forces promote metal flow and enable effective forming of complicated cross-sections [1,2]. The authors propose a novel rolling technique termed "elongation-control rolling" [3,4]. This method can generate an interstand force with a capacity to vary widely from tensile to compressive. Thus the total elongation or the product size can be controlled, and size-free rolling is made possible. The fundamental characteristics of rolling flat strips were investigated [3]. The width of flat wires can be closely controlled [4]. In the case of square wire, an arbitrary combination of side length and corner radius was obtained by the elongation-control rolling technique [5].

In this study, elongation-control rolling was applied to roll H-shaped wires. H-shaped wires are widely used as piston rings or rails in electric parts. H-shaped wires of arbitrary flange widths were successfully rolled by the proposed method.

PROTOTYPE MILL

A schematic illustration of a constructed prototype elongation-control mill is shown in Figure 1. Details are provided in references [1, 2]. The mill consists of five cassette type stands. Each stand was equipped with two-high 100mm diameter rolls, load cells for roll separating forces, a torque meter, and a tachometer. Each stand was independently driven at a prescribed speed by a 2.2kW servomotor.

All stands were mounted on a pair of slide guides (linear guides) and could move smoothly in the rolling direction. Load cells were inserted between the adjacent stands, so that the interstand force was measured directly and precisely. The stands were all pushed against each other while affording an adequate pre-load from the entrance and exit stays. The distance between adjacent roll axes was 230mm. The pair of guide shoes and side guides were set close to the wire. These guides, by preventing the wire from buckling or meandering, enable stable rolling in the case of large compressive interstand force.

EXPERIMENTAL PROCEDURE

Rolling experiments were performed at ambient temperature using round wires of three different materials, including fully annealed aluminum JIS A1070-O, partially hardened pure C3102, and medium carbon steel S45C. All wires were 5mm in diameter and 2m in length. Prior to rolling, the wires were preformed into round-edged flat wires by one-pass flat rolling. The width of preformed wires was controlled to 5.9 mm, to

0-7803-5489-3/99/$10.00 ©1999 IEEE.

fit the groove on the roll and to prevent meandering. The thickness of the preformed wire was 3.3 mm for aluminum, 3.6mm for copper, and 3.5mm for carbon steel.

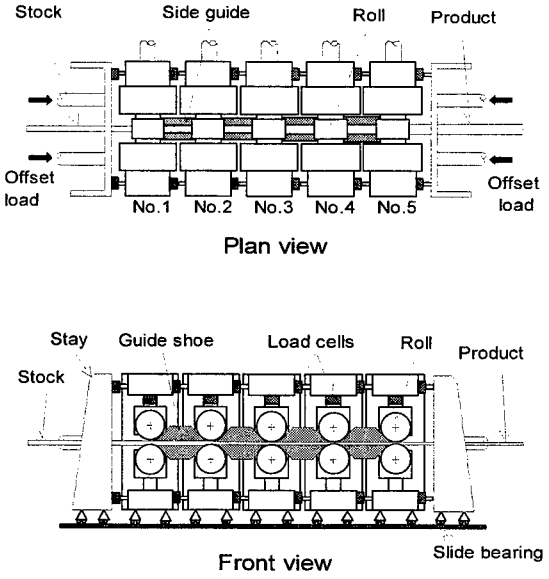


Fig. 1. Schematic illustration of the elongation-control mill.

Rolling stands were set in H-H (horizontal) arrangement. The roll passes used are shown in Figure 2. Closed roll passes were used from the first to the fourth stands. The grooves had a 2 degree draft angle. The reduction in web thickness at each stand was 20% and total reduction was 60%. The fifth stand was used as an edger; the tops of flanges were shaped by symmetrical open pass. Edging draft (the reduced amount of rib height or flange width) was varied 0.25 and 0.5 mm. Rolling experiments were done at ambient temperature under conditions of lubrication with mineral oil (IDEMITSU CU-50).

The interstand forces were generated by prescribing the roll speeds on each stand as follows: first, the roll speed at the first stand, v_1^o, was fixed at 1m/min, and the roll speed at i-th stand, v_i^o (i=2,..5)(which established the tension free rolling), was experimentally determined from upstream stand by stand. For rolling with interstand forces, the roll speed of i-th stand v_i was set as

$$v_i = a^{i-1} v_i^o \qquad (i=1,\ldots,5) \qquad 1.$$

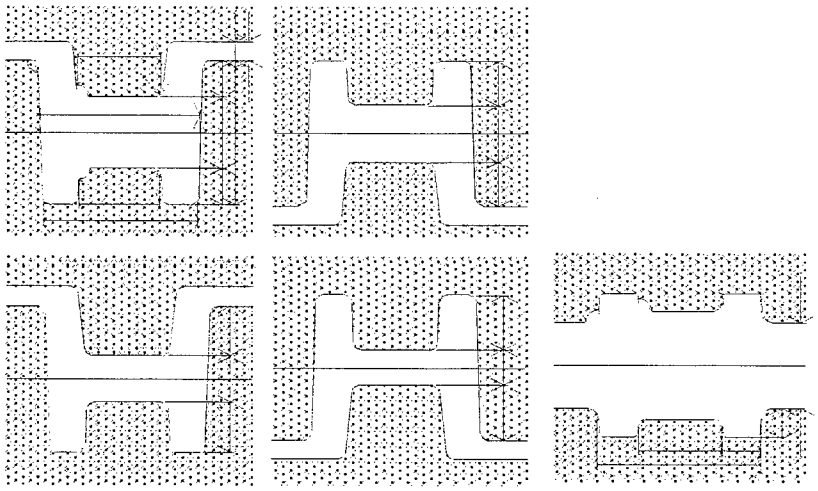


Fig. 2. Roll passes used.

where the parameter a is an arbitrary constant indicating the degree of imbalance of roll speeds which determines interstand forces. This parameter will be referred to as *the roll speed parameter*. When a=1, v_i equals v^0_i, and tension-free rolling is achieved. If a>1, v_i/v_{i-1} is larger than v^0_i/v^0_{i-1}, and tensile forces must be generated between adjacent stands. Conversely, if a<1, compressive forces must be generated. The prescribed speeds in the case of aluminum are shown in Figure 3.

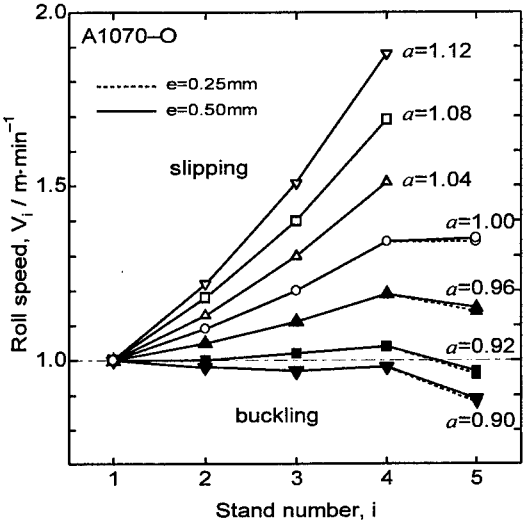


Fig. 3. Roll speeds at each stand.

During the rolling test, the output signals of the interstand forces, the roll forces, and the roll torques were measured at a frequency of 10Hz. The rolling operation was interrupted after a sufficient distance of steady state rolling had been performed. Then the elongation (longitudinal nominal strain) and the cross-section at each stand were measured.

RESULTS AND DISCUSSIONS

The rolling limits

In the case of a>1, rib height was insufficient and edging could not be applied. The results of rolling experiments without the fifth stand were determined in this case. There were upper limits on the roll speed parameter a, which were determined by the slippage between rolls and wires. The upper limit was a=1.14 for aluminum, a=1.12 for copper, and a=1.04 for carbon steel. In the case of a<1, lower limits were determined by the web-buckling of wires. The lower limit was 0.88 for both aluminum and copper, and 0.92 for carbon steel. Therefore, stable rolling conditions were 0.90 - 1.12 for aluminum, 0.90 - 1.10 for copper, and 0.92 - 1.04 for carbon steel.

Cross-sectional profiles

The variation in cross-sections of aluminum wire in the cases of a=0.90, 1.00, and 1.12 respectively are compared in Figure 4. The ribs of wires grow by passing rolling stands. The smaller a causes larger ribs and better filling of the roll grooves. In the case of a=1.12, the edging could not be applied because the rib height was less than the depth of the grooves. In the cases of a=1.00 and 0.90, edging draft e=0.25 resulted in underfilling at corners. Approximately complete filling was achieved in the case of e=0.50, though slight overfilling of flanges was observed. However, the flanges were nearly parallel. As a result, it can be concluded, that elongation-control rolling can closely control the flange width of H-sections.

Elongation

The elongation - roll speed parameter a relationship is shown in Figure 5 in the case of e=0.25. It shows an approximately linear relationship. The elongation was varied over a wide range, from 20 to 80%, where 50% is tension-free rolling. The effects of materials and that of edging on the elongation are less apparent.

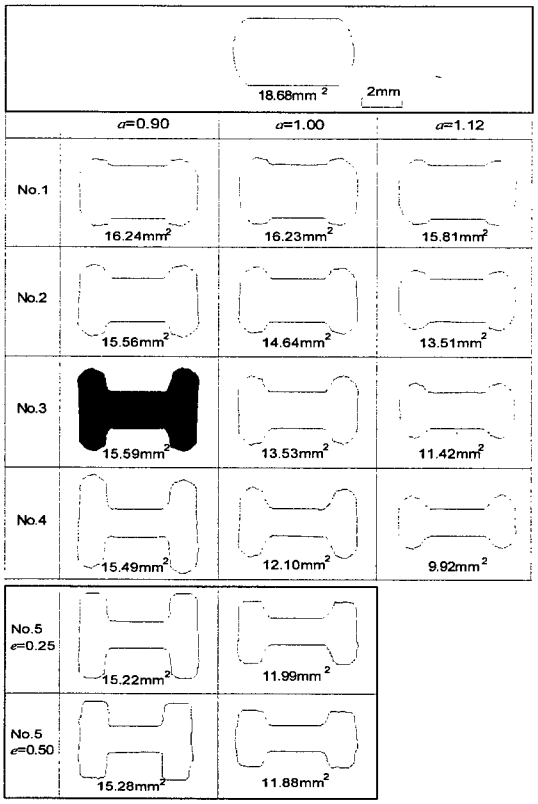


Fig. 4. Variations in cross-sections as a function of roll speed parameter.

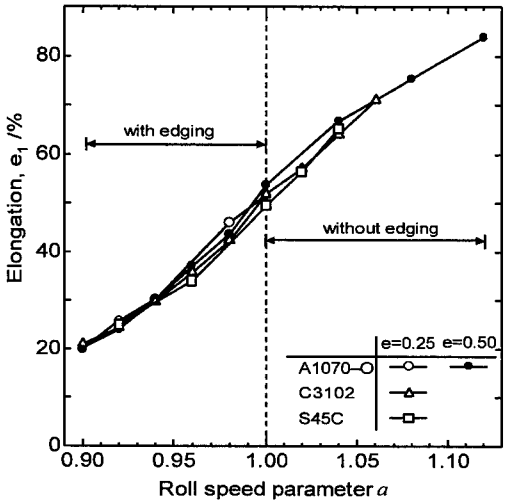


Fig. 5. Relationship between elongation and roll speed parameter.

Interstand forces

The distribution of interstand forces during rolling of aluminum wires is shown in Figure 6. Interstand tensile forces are generated when $a > 1$; compressive forces are generated when $a < 1$. These forces exhibit a concave distribution. Interstand forces at intermediate stands highly depend on the roll speed parameter a. In the case of $a > 1$, interstand force is not generated between the fourth and the fifth stages because the edging is not achieved at the fifth stand. In the case of $a < 1$, the interstand force between the fourth and the fifth stands is generated due to edging, though it does not depend on a. This force may be due to slippage at the fifth stage. It is found that the edging has a negligible effect on the roll forces at upstream stages.

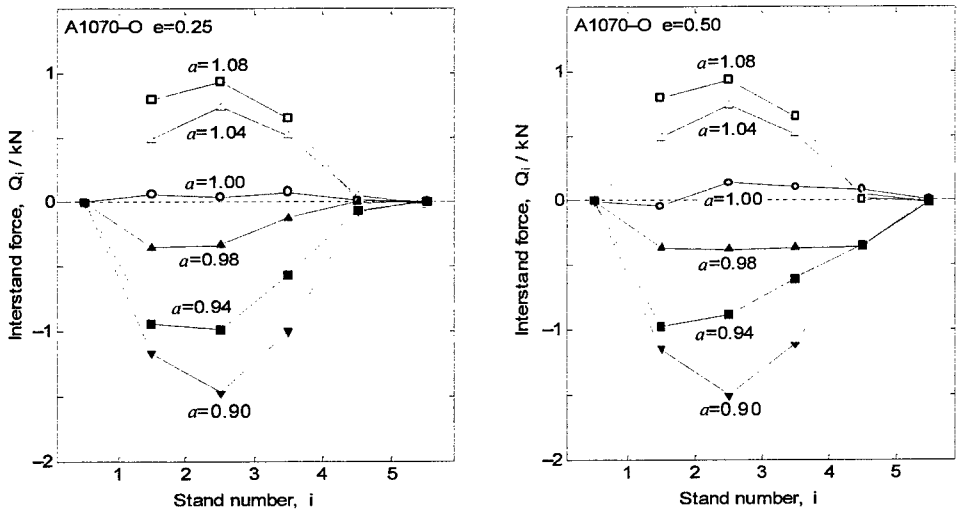


Fig. 6. Interstand forces as a function of roll speed parameter.

CONCLUSION

In this study, elongation-control rolling has been applied to the rolling of H-shaped aluminum, copper, and medium carbon wires, respectively. H-shaped wires were rolled from round wire by five-stand grooved rolling. The elongation varied over a wide range, from 20% to 80%, where 50% was tension free rolling. Flange width increases with compressive interstand force, and decreases with tensile force. It is concluded that the rolling of H-shaped wires that have an arbitrary flange width is made possible by the proposed technique.

ACKNOWLEDGEMENT

This study was supported by the Ministry of Education, Science and Culture of Japan under grant number (A)(2)-07505019.

REFERENCES

1. H. Utsunomiya, Y. Saito, K. Hirata, T. Kawamoto and K. Oka, 1996. Rolling of Profiled wires by the satellite mill, Adv. Tech. of Plasticity, 1, 99-102.
2. H. Utsunomiya, Y. Saito, T. Kawamoto and H. Matsuzawa, 1998. Satellite-mill rolling of U-shaped and H-shaped wires, J. Mat. Proc. Tech., 80-81, 345-350.
3. Y. Saito, H. Utsunomiya, M. Shinkawa and F. Shimaya, 1998, Development of an elongation-control mill, J. Mat. Proc. Tech., 80-81, 351-355.
4. Y. Saito, H. Utsunomiya, M. Shinkawa and K. Oka, 1998. A novel rolling technique for size-free rolling, Proc. 7th Int. Conf. on Steel Rolling, 811-815.
5. H. Utsunomiya, M. Shinkawa and Y. Saito, 1999. Elongation-control rolling of square wire, (to be published in Proc. 6th Int. Conf. on Tech. of Plasticity).

Application of a Neural Network to Speed Up a Mathematical Model to Calculate Strip Profiles in Flat Rolling

Yukio Shigaki, Horacio Helman

Universidade Federal de Minas Gerais, Department of Metallurgy and Materials,
R. Espirito Santo 35, 30160-030 Belo Horizonte, MG, Brazil
Fax: (5531) 238-1815 Email: shigaki@cce.ufmg.br , hhelman@demet.ufmg.br

ABSTRACT

Since the sixties, innumerable mathematical models [1,2,3,4,5] have been developed to simulate flat rolling, specifically, to determine its width-wise profile. These models have great utility in understanding the influence of parameters such as friction, front and back tension, gap, material properties, etc. in the rolling of flat strips. Among these, Pawelski, Rasp and others [4,5] have developed a precise model that accounts for the influence of bending, shearing and flattening of the rolls which are crucial to calculate emergent strip-profiles accurately.

This method divides the strip and roll into many stripes, assuming a plane-strain state. For each stripe of the roll and strip, the load and deformation respectively are calculated using an analytical approach such as the Bland-Ford-Ellis model with Hitchcock's formula for deformed radius of the roll. The effects of bending, shearing and flattening are considered through influence coefficients on the rolls. Though good agreement is achieved between the results of this method and those obtained by experience, the program run-time is so large that it must be considered an off-line system. Since the program works iteratively, and since calculation of the influence coefficient matrix for flattening is time-consuming as (it must be updated nearly every iteration), improvement in program speed can be achieved by *substituting* a trained neural network (inputs: distributed loads; outputs: flattening of the rolls), working as an equal partner in the entire mathematical model.

The neural network can be trained in the inverse direction, making possible very fast "inversion" of the flattening matrix. This is very important for rolling mills operating more than 2 rolls, since calculation of roll contact loads requires inversion of the flattening matrices. This combined model has better acceptance since it doesn't appear as a *black box*, i.e., a model based on neural networks only, and so it can be adapted for on-line process control. Two feed-forward neural networks were designed to cope with the problem of calculating flattening and loading: one for load-to-flattening and the second for inversion. A back-propagation learning rule was used. The training examples were taken from each iteration step for different reduction cases, with a fixed strip width, initially for a two-high mill and subsequently, for a four-high mill. Substantial reduction in processing time is obtained, without loss of precision, since the flattening calculation step is substituted by a simple sum of polynomials with an appropriate activation function.

Keywords: Flat rolling, widthwise profile, neural networks, on-line control.

REFERENCES

1. Bryant, G.F., ed., 1973.. Automation of tandem mills, The Iron and Steel Institute, London,
2. Guo, R.M., 1990. Development of a mathematical model for strip thickness profile, Iron & Steel Eng., 32-39.
3. Ishikawa, T.; Tozawa, Y.; Nakamura, M. Kato, T., 1980. Fundamental study on the profile and shape of the rolled strip, Proc. Int. Conf. on Steel Rolling, Tokyo, 772-783.
4. Pawelski, O., Teutsch, H., 1985. A mathematical model for computing the distribution of loads and thickness in the width direction of a strip rolled in four-high cold-rolling mills, Engineering Fracture Mechanics, 21(4), 853-859.
5. Pawelski, O.; Rasp, W., Rieckmann, J., 1989. A mathematical model for predicting the influence of elastic and plastic deformations on strip profile in six-high cold rolling, 4th Inter. Steel Rolling Conf., 2(E.3.1-E.3.6).

0-7803-5489-3/99/$10.00 ©1999 IEEE.

Intelligent Methods in Metal Forming Processes

A Fundamental Study of Incremental Deep Drawing Process

Susumu Shima, Hidetoshi Kotera and Kei Kamitani

Department of Mechanical Engineering, Kyoto University,
Sakyo-ku, Kyoto 606-8501, Japan

ABSTRACT

This paper deals an investigation into the features of an incremental deep drawing process. On a newly developed incremental deep drawing set-up, aluminium sheets are formed to circular cups of various sizes. Deep-drawing is carried out incrementally with a set of tools with common shapes. Process parameters studied are drawing ratio, formed cup size, the vertical and horizontal displacements of the punch in one step relative to the blank. It is thereby shown that LDR depends on the cup size and that fracture occurs at the blank either near the punch shoulder or die shoulder depending on the forming conditions. A fracture mode diagram is thus obtained, where regions or conditions for successful deep-drawing and for fracture occurrence at either portion of the blank are clearly seen. Strain distributions are measured by a scribed circle method with the aid of a common fabrication process for photo lithography.

INTRODUCTION

Incremental deep-drawing is studied in an attempt to develop a new sheet metal forming process for a small batch production. In our previous work [1], forming was done with a manual operation, while in this work, we built up a new set-up with an automatic control for the movement of the punch and blank.

In recent years, a metal forming system with a large flexibility that is capable of dealing with a small batch production with large varieties has been demanded. Among other attempts, research and development of incremental forming processes have been intensively undertaken [2-8]. Incremental forming is a generalized term of those forming processes where tools of common shapes are used to deform a small portion of the workpiece consecutively next to another to obtain a desired shape, instead of particular die-sets that have been designed exclusively for particular shapes of the products. Although the time required for making one product is much longer than by ordinary press forming, the incremental process may be viable in view of the whole process including design and fabrication of dies.

In previous work [1], we investigated deformation and fracture behaviour of the blank by changing the process parameters involved, drawing ratio, increment in punch displacement, cup diameter to be formed, etc. We have shown as follows:

1. Incremental deep-drawing is successfully performed below a deep-drawing ratio of about 1.5.
2. The counter punch supporting the blank against the main punch, is useful to improve deep-drawability.
3. Strain distribution in the blank and thus, fracture occurrence, depends on the cup-size to be deep-drawn.
4. Fracture occurs near the punch shoulder when the cup is large, while it occurs near the die shoulder when the cup is small.

In this study, we modify the previous set-up so that the operation is done with a sequence controller. We then carry out similar experiments to investigate the effects of the above process parameters on the characteristics of incremental deep-drawing. We also measure strain distributions in the formed cup by a scribed circle method; we put the circles by utilizing a common fabrication process for photo lithography.

INCREMENTAL DEEP-DRAWING

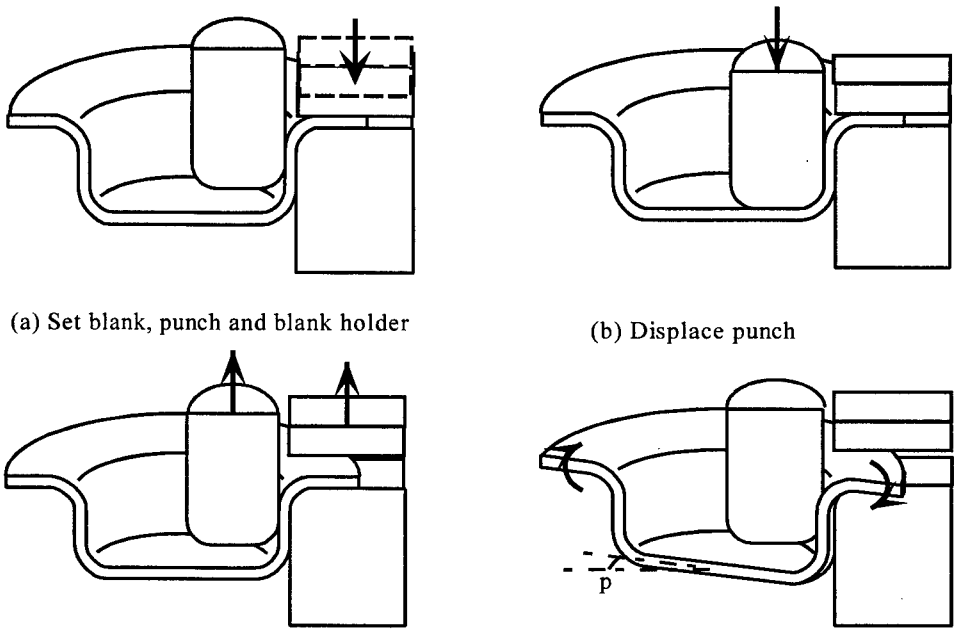
Since the principles and details of the process are written elsewhere [1], we will only describe them briefly. Unlike conventional deep-drawing, we use a few tools of common shapes to produce various shapes. As shown in Figure 1, when we deep-draw a circular cylinder, we use a straight-shaped die and a punch with

0-7803-5489-3/99/$10.00 ©1999 IEEE.

blank holder. We push the punch against one portion of the blank at a small displacement with a blank holding plate pushing against the flange portion. After each displacement of the punch toward the blank, the punch and blank holder are both moved upward to free the blank. The blank is then rotated by a small angle about the vertical axis at the centre of the blank followed by punch displacement for the next step. The punch thus moves in a spiral manner relative to the blank. If n steps are required for one rotation of the blank, pitch p is given by $p = \pi d/n$ and the lead L by $L = ns = \pi ds/p$, where d is the cup diameter, and s the punch stroke in one step. Up to the nth step, the total vertical displacement of the punch measured from the top surface of the initial blank set on the set-up is expressed by

$$S_N = s_0 + (N-1)s$$

where s_0 is the punch displacement at the first step. Deep-drawing is thus performed incrementally and consecutively to produce a desired shape.



(a) Set blank, punch and blank holder

(b) Displace punch

(c) Free blank

(d) Rotate blank

Fig. 1. Process of incremental deep-drawing.

In conventional deep-drawing, LDR (Limit drawing ratio) is a common measure for formability or deep-drawability. Similarly in incremental deep-drawing, we evaluate formability by LDR. As will be shown in a later section, LDR, as well as fracture occurrence, are influenced by the size of the formed cup. We investigate the process by introducing these important measures in addition to DR (drawing ratio=D/d):

a) Specific cup height: h/d.
b) Flange shrinking ratio: D_f/D

where D is the initial blank diameter, D_f is the flange diameter during forming, d is the inner diameter of the formed cup and h is its height. We evaluate the specific cup height and flange shrinking ratio for cases where the cups being formed undergo fracture.

EXPERIMENTAL SET-UP AND PROCESS

The experimental set-up developed for the present study is shown schematically in Figure 2. The main punch is displaced by a ball screw jack that is actuated by a stepping motor. An air cylinder actuates the blank holder. The blank is rotated about its center by three pairs of rollers at a prescribed angle as depicted in Figure 3. These steps are repeated continually one after another, using a sequence controller. Deep-drawing is thus, automatically performed incrementally. For the present process, the diameter of the punch

is 50mm with a shoulder radius of 5mm. We, therefore, deep-draw cylindrical cups with diameters above 50mm.

Circular blanks of commercially-pure aluminium, A1050-O, of ~140mm diameter with 1.0mm thickness were used. Since we had previously confirmed that a counter punch was unnecessary for successful deep drawing, we did not use it in the present set-up. The blank holding force was 430N and was kept constant throughout the experiment. Molybdenum-disulfide was used as a lubricant on both sides of the blank.

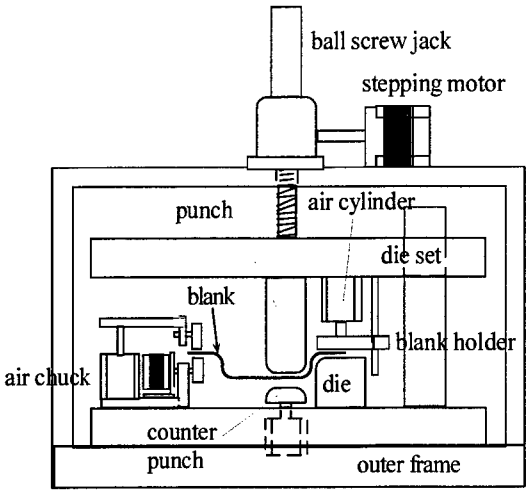


Fig.2. Schematic view of incremental deep-drawing set-up.

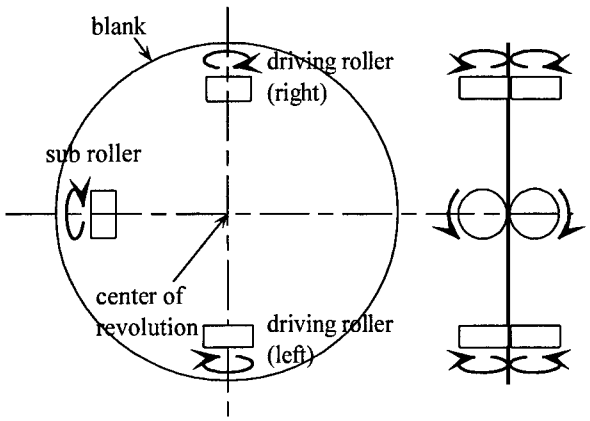


Fig.3. Arrangement of three pairs of rollers.

EXPERIMENTAL RESULTS AND DISCUSSION

Effect of punch stroke, pitch and lead on forming process

In incremental deep-drawing, there are characteristic parameters such as punch stroke s, pitch p and lead L. The effects of these parameters on the specific cup height h/d and flange shrinking ratio D_f/D were first examined with other conditions being fixed; the blank diameter in this case was 138mm. While drawing ratio DR was chosen between 1.408 and 1.438, the punch stroke in one step s was changed from 10.6 to 47.6μm; pitch p from 3.77 to 9.23μm; L was changed from 0.525 to 2.00mm. The results were as follows:

1. For DR=1.422-1.438, and s = 10.6-15.9mm with p = 3.77-9.23mm and L = 0.525-0.848mm, both specific cup height h/d and flange shrinking ratio D_f/D are almost constant; h/d = 0.124 and D_f/D = 0.949.
2. When DR is smaller (DR=1.408), the specific cup height h/d increases to 0.152 and D_f/D decreases to 0.812, while the other parameters above are more or less the same.
3. When the punch stroke in one step s becomes larger at the same drawing ratio DR as in 1) above, deep-drawing is possible, but the surface of the cup becomes bumpy.

If DR is much larger than LDR, the specific height h/d is almost zero and D_f/D is almost unity. If DR decreases to approach LDR, then the former increases, while the latter decreases. From the results above, h/d and D_f/D, and hence, the deep-drawing process, are not influenced by the parameters s, p and L for DR ≅ LDR, although forming with larger s or L may provide products with bumpy surfaces. So in the following, we chose the lead L to be as large as the thickness of the blank.

Fracture mode diagram

As observed in our previous work [1], the LDR in incremental deep-drawing depends on the diameter of the formed cup. To examine this in more detail, we carried out experiments by changing the blank diameter D from 96 to 143mm, and the diameter of the formed cup d from 58 to 109.5mm. For conventional deep-drawing, a size effect on LDR is observed, but for the above conditions, LDR is more or less constant [9]. Figure 4 shows the experimentally derived drawing ratio plotted against cup diameter. In the diagram, J

refers to the case of successful deep-drawing and *I* and *H* refer to fracture occurrence at the cup shoulder and near the die shoulder, respectively. This figure demonstrates that the forming condition can be divided into three regions: the first wherein successful deep-drawing is achieved; the second where fracture occurs in the blank near the punch shoulder; and the third where fracture occurs in the blank near the die shoulder. The first condition refers to the region below LDR. In the region above LDR, fracture occurs in the blank near the cup shoulder for larger cup diameters, while it occurs near the die shoulder for smaller ones. The boundary line between the condition for fracture-at-the-cup and that for fracture-at-the-die may be called the parting line for fracture mode. The diagram shows the main features of incremental deep-drawing and can be called the fracture mode diagram. This is discussed in the next section.

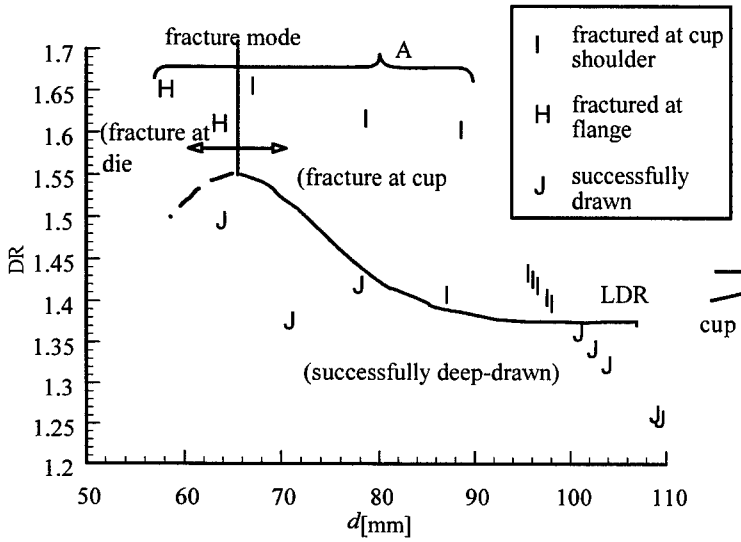


Fig.4. Fracture mode diagram.

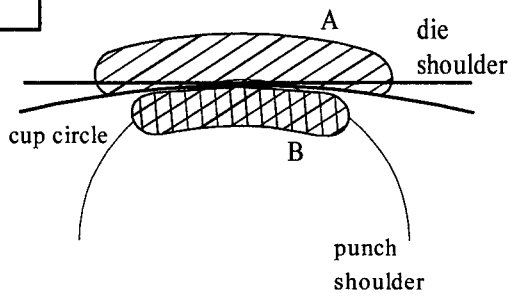


Fig.5. Contact areas between die, blank and punch.

Figure 5 shows an illustration of contact area between the die, blank and punch. The contact area at the die shoulder (area A in Fig. 5) is larger if the formed cup diameter is larger, while the contact area at the punch shoulder (area B) becomes larger as *d* approaches the constant punch diameter. The loads supported by these two contact areas are almost equal to each other during deep-drawing because the friction at the punch/cup interface is negligibly small. If there is a difference between the two areas, the blank portion may undergo fracture at either of the smaller contact areas that result in a larger stress in the blank. This leads to the conclusion that at the condition where the two contact areas are equal to each other, there is a maximum forming limit. Such a cup may be called the optimum cup diameter for a particular punch diameter. Figure 4 demonstrates the phenomena and shows an optimum cup diameter for the present condition of ~65mm. As seen above, we must pay attention to the cup diameter to evaluate formability in incremental deep-drawing. To increase formability, the formed cup must be chosen so that it is near the optimum diameter.

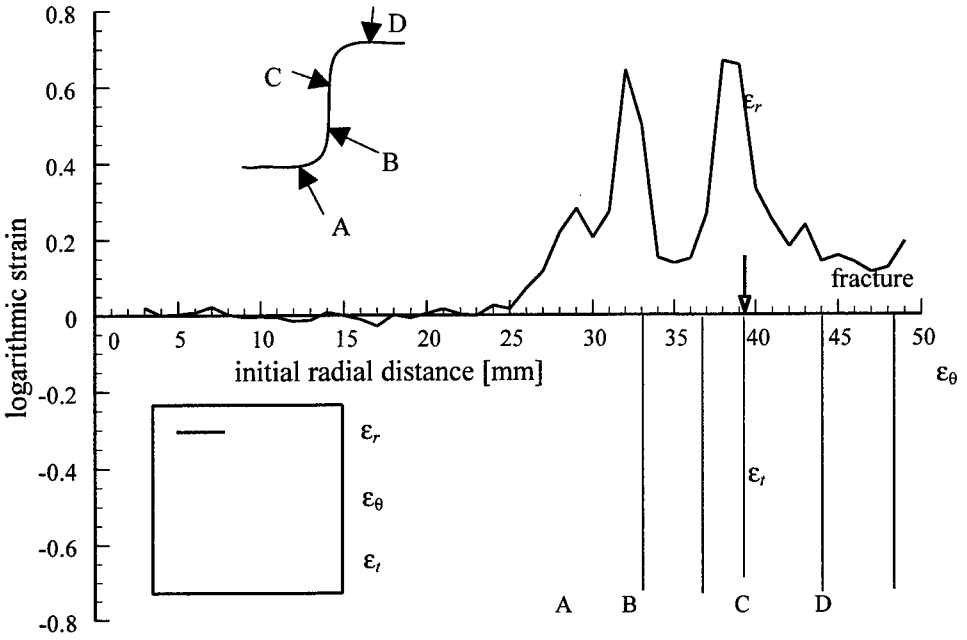
Strain measurement by scribed circle method

While there are various ways to scribe circles on the blank surface, we utilized the photo-resist method commonly used to fabricate semi-conductors. The circles were 1mm in diameter and the process used was:

1. Coat negative-resist liquid on the blank surface on a spin coater so that a thin uniform film is obtained.
2. Pre-bake the blank so that the coated liquid becomes solid.
3. Put a pattern mask that gives scribed circle patterns on the coated surface followed by exposure.
4. Remove the unnecessary resist mask used to develop the scribed circles on the blank surface.
5. Post-bake to fix the circles.

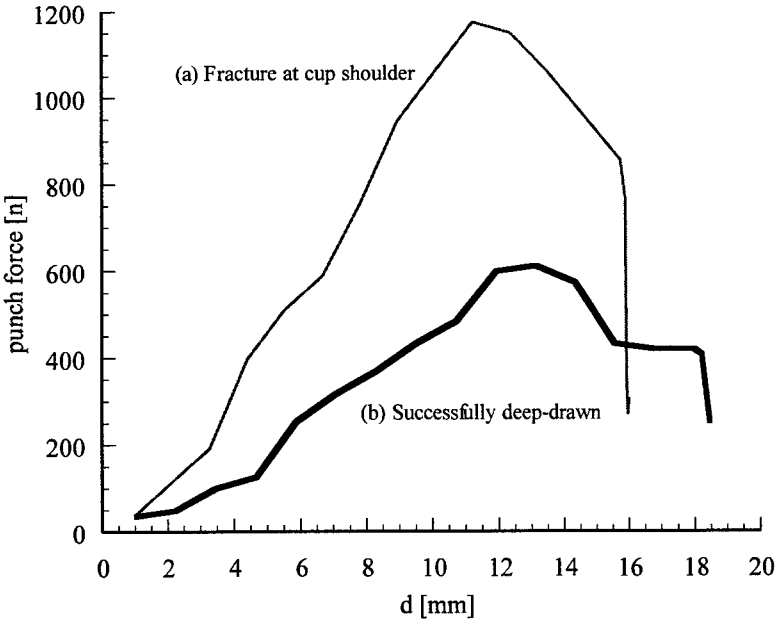
Figure 6 shows measured distribution of radial strain, circumferential strain and thickness strain. The forming condition shown in the figure refers to the case where fracture occurred at the flange near the die shoulder. The diagram shows that strain is concentrated near the cup shoulder and the blank near the die shoulder. Although not shown here, the strain was concentrated more significantly at the cup shoulder for

the case where fracture occurred at this position. The absolute strain values were higher in the former than in the latter. This may be due to the fact that the former condition (referring to Fig.6) was nearly optimum.



d_p [mm]	r_d [mm]	D [mm]	t [mm]	D_f [mm]	d [mm]	h [mm]	DR
50	5	102.5	1.0	96.0	63.5	18.8	1.614

Fig.6. Distributions of radial, circumferential and thickness strains (fracture near die shoulder)



	d_p [mm]	r_d [mm]	D [mm]	t [mm]	D_f [mm]	d [mm]	h [mm]	DR
(a)	50	5	112.0	1.0	106.0	77.5	16.0	1.445
(b)	50	5	96.0	1.0	84.0	64.0	18.9	1.50

Fig.7. Change in punch forces with height of deep-drawn cup.

Forming Load

We measured the forming load by affixing strain gauges on the punch. Figure 7 shows the change in punch force with formed cup height. The conditions shown below the diagram; a) refers to the condition where fracture occurred at the cup shoulder, while b) refers to the case where no fracture occurred. In the present process, forming is done intermittently and the actually recorded curves are a wave with the cycle time required for each forming step; only the peak load in the wave is plotted in the graph. The punch force increases with the progress of incremental deep-drawing, reaches its maximum and then decreases at the end of forming. The peak load is obviously very small but, in case a) is larger than that in case b), although the drawing ratio is smaller. This results in the occurrence of fracture at a lower drawing ratio. The decrease in the punch force after peak load in condition a) refers to the occurrence of necking in the blank at the cup shoulder, while that in b) refers to the decrease in flange width according to the progress of deep-drawing.

CONCLUSIONS

An incremental deep-drawing process was performed on commercially-pure aluminium by using die and punch of common shapes. We were thus able to understand the features of the present process. The results are as follows.

1) Incremental deep-drawing is successfully performed depending on the forming condition. Within the present experiments, the limit of deep-drawing ratio is about 1.5 to 1.6.
2) In evaluating forming, unlike conventional deep-drawing, we must pay attention to the size of the formed cup in relation to the punch size.
3) A forming limit diagram shown on the drawing ratio-cup size diameter plane is thus obtained. The zone in the diagram is divided into three: the first where incremental deep-drawing provides sound products; the second where fracture occurs at the blank near the cup shoulder; the third where fracture takes place near the die shoulder. This can be called the fracture mode diagram.
4) There is an optimum that provides the highest drawing ratio near the boundary between these two fracture conditions.
5) Employing a common fabrication process for semi-conductors, we scribed circles on the blank surface and measured strain distribution after forming. In a successfully formed cup, while strains are larger in the blank near both the cup and die shoulders, the flange undergoes sufficient strain to be deep-drawn.
6) The punch force is obviously very small. It increases with increasing punch stroke and then decreases. The peak force for the case where fracture occurs is larger than in the case of successful drawing, even if the drawing ratio is lower.

REFERENCES

1. S. Shima, H. Kotera, Kamitani, K. and T. Bando, 1998. Development of Incremental Deep Drawing Process. Metals & Materials, 4(3), 404-407.
2. S. Matsubara, 1994. CNC Incremental Forming. J. Japan Soc. Tech. Plasticity, 35(406), 1258-1263.
3. H. Iseki, K. Kato and S. Sakamoto, 1992. Flexible and Incremental Sheet Metal Bulging using a Path-Controlled Spherical Roller. Tr. JSME (C), 58(554), 3147-3152.
4. K. Kitazawa, A. Wakabayashi, K. Murata and J. Seino, 1994. A CNC Incremental Sheet Metal Forming Method Producing the Shell Components Having Sharp Corners. J. Japan Soc. Tech. Plasticity, 35(406), 1348-1353.
5. T. Hasebe and S. Shima, 1994. A Study of Flexible Forming by Hammering. J. Japan Soc. Tech. Plasticity, 35(406), 1323-1329.
6. T. Hasebe, S. Shima and Y. Imaida, 1996. A Study of Flexible Forming by Progressive Hammering. Adv. Tech. Plasticity, Proc. 5th Int. Conf. Tech. Plasticity, Vol.II, 951-954.
7. S. Shima, H. Kotera and H. Murakami, 1997. Development of Flexible Spin-Forming Method. J. Japan Soc. Tech. Plasticity, 38(440), 814-818.
8. S. Shima, H. Kotera, H. Murakami and N. Nakamura, 1996. Development of Flexible Spinning-A Fundamental Study-. Adv. Tech. Plasticity, Proc. 5th Int. Conf. Tech. Plasticity, Vol.II,, 557-560.
9. M. Nakano, Y. Ueno and S. Kanehara, 1972. Size and Shape effect on Sheet Metal Forming. J. Japan Soc. Tech. Plasticity, 13(141), 745-750.

Intelligent Design Architecture for Process Control of Deep-Drawing

K. Manabe*, H. Koyama*, K. Katoh and S. Yoshihara*****

*Tokyo Metropolitan University Department of Mechanical Engineering,
Hachioji-shi, Tokyo 192-0397, Japan
**Integrated Systems Japan, Ltd. Asahi Bank Gotanda Bldg. 1-23-9 Nishi-gotanda,
Shinagawa-ku, Tokyo 141-0031, Japan
***Tokyo National College of Technology Dept. Mechanical Engineering,
Hachioji-shi, Tokyo 193-8610, Japan

ABSTRACT

A concept of design architecture with a database for an intelligent sheet metal forming system was proposed to enable designing of a process control system without experts who are skilled and experienced in the forming process. In this study, the proposed architecture was applied to the variable blank holding force (BHF) control technique for circular-cup deep-drawing. The system is available for three objective functions which are typical process requirements, cup wall uniformity, cup height improvement and energy saving. The availability of this design architecture is confirmed by experiments on aluminum alloy sheets.

INTRODUCTION

Several studies on the optimization of process control in metal forming have been performed in an approach toward intellectualization. For sheet stamping operations, intelligent deep-drawing techniques have been developed to date. One technique is an adaptive control method by means of blank holding force (BHF) with fuzzy inference for circular-cup deep-drawing[1]. Another one is a control approach based on a plastic deformation model involving the material and friction identification process with an artificial neural network (ANN)[2]. Despite their excellent advantages, each control system requires very extensive time and labor for the design and development process, and above all, the design engineer has to be a knowledge expert as well as skilled and experienced engineer on the forming process techniques, or else, the assistance of a craftsman would be essential. Therefore, it is necessary to establish a new concept for process design architecture which obviates the requirement for an expert. In general, the forming cell and system must be efficiently designed during process design and process control. In the former system, as shown in **Fig. 1** (left), the expert plays a number of roles as the core.

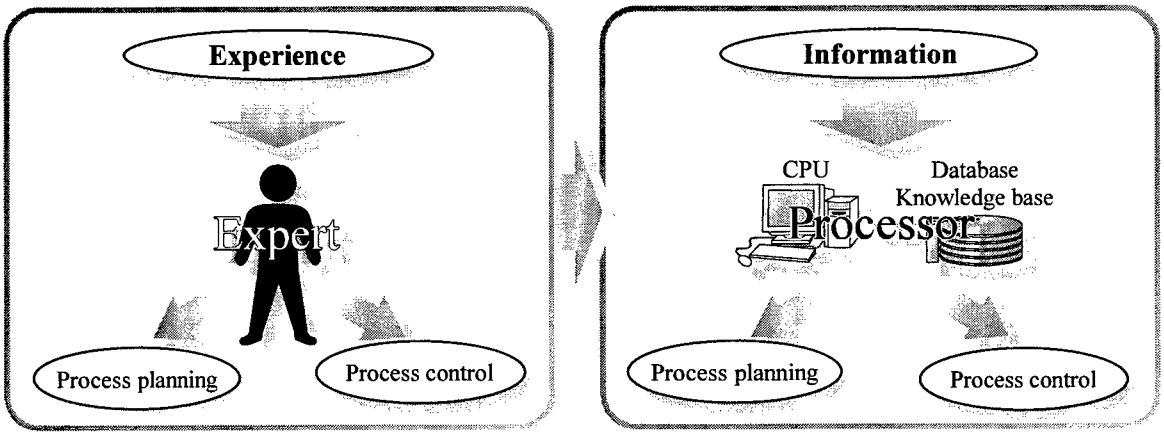


Fig. 1 A new intelligent approach for various design phases on metal forming processes

0-7803-5489-3/99/$10.00 ©1999 IEEE.

He also acquires the required experience and transfers the knowledge to inexperienced engineers. The number of experts has been gradually decreasing over the years. Thus, in the future system, the process conditions must be automatically optimized without the aid of an expert. The purpose of this study is to enable freedom from the dependency on engineering experts in the design phases of process planning and control design and to develop an intelligent design architecture for deep-drawing process control without the aid of a knowledge expert.

OUTLINE OF A NEW INTELLIGENT PROCESS DESIGN AND ITS SYSTEM ARCHITECTURE

Our concept shown in **Fig. 1** (right) involves the replacement of the brain functions of an expert by a processor which contains an analyzer, database and knowledge base. The processor can design and control the process according to a suitable set of rules and algorithm from the database and knowledge base, and stores the sensing information from a forming cell during the process, which is similar to the experience of an expert. In other words, it can grow by acquiring experience in the same manner as an expert. Hence, the proposed system is able to automatically optimize the process and can be operated without any aid from an expert.

Figure 2 shows the outline of the system architecture based on the above concept. It can be broadly divided into two parts. One is a processor and another one is a forming cell and system. The forming cell has several sensors for supplying process information to the processor, and also has actuators to implement the commands from the processor. The processor consists of a database, knowledge base and an analyzer (commercial control design support tool; MatrixX). The database and knowledge base contain the process information under various conditions and the methodology for designing the process, respectively. The processor is capable of not only designing the process using the database and knowledge base but also identifying the material properties of the workpiece and control actuator using sensing information from the sensors. In addition, the system can handle a variety of workpieces as well as the change of workpiece material, tooling conditions and lubricating conditions, by utilizing the database and knowledge base.

APPLICATION OF THE ARCHITECTURE TO DEEP-DRAWING PROCESS

In this study, the circular-cup deep-drawing problem is adopted as a fundamental and important example of the sheet metal forming process. In the deep-drawing process, the forming limit is mainly governed by the fracture at the punch shoulder and the wrinkle at the flange part. Although it is essential to apply the BHF to avoid wrinkles, excessive BHF causes fractures. Therefore, the appropriate amount of BHF is required to carry out the process successfully. So the new design architecture is applied for the adaptive control of BHF in the deep-drawing process in order to verify the availability of the architecture. **Figure 3** shows the design system architecture for an intelligent metal forming process with a database. In the system, fuzzy inference was chosen as an AI tool for process control design.

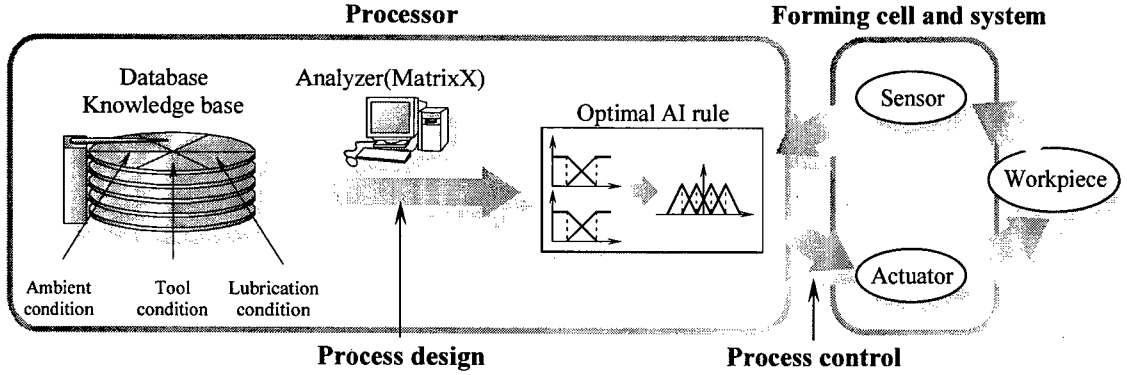


Fig. 2 A concept of intelligent metal forming cell with database

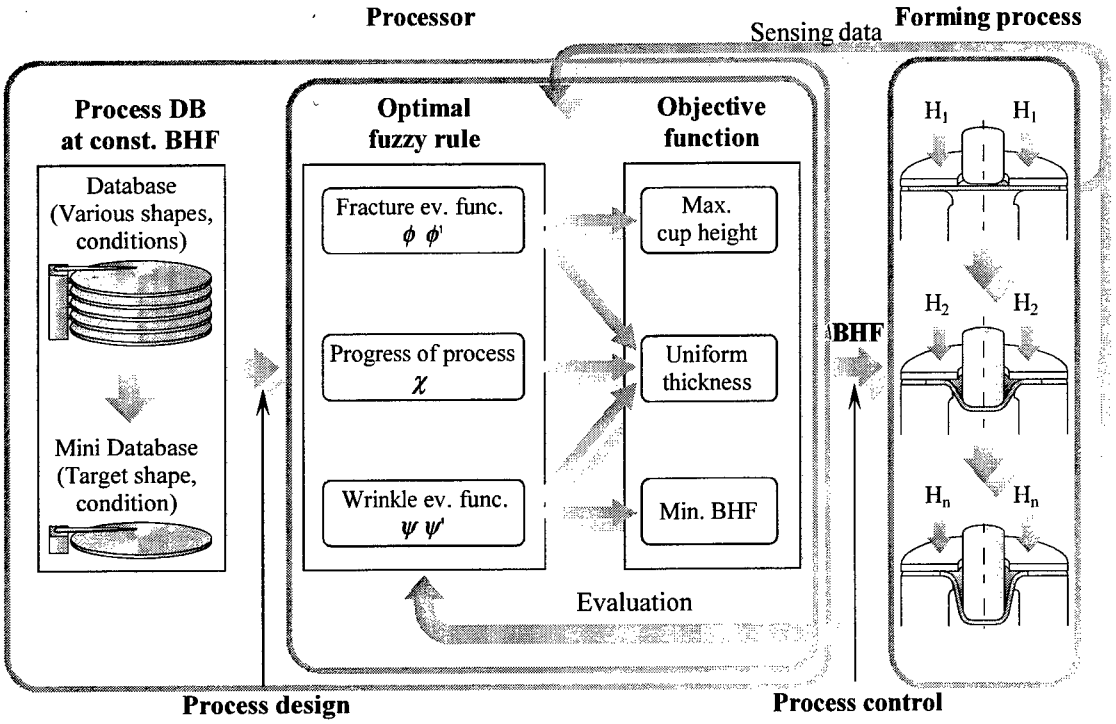


Fig. 3 System architecture of intelligent forming process for deep-drawing process

The evaluation functions should not be influenced by the blank material, tooling conditions, environmental conditions and other factors. For this reason, evaluation functions ϕ and ϕ', obtained from the punch stroke curve and ψ and ψ', from maximum apparent blank thickness curve are used. The evaluation function ϕ is the difference between the actual punch stroke curve and the ideal curve, which can be obtained geometrically by assuming uniform wall thickness. ϕ' is the differential coefficient of ϕ by blank reduction ratio ΔDR^*. A combination of ϕ and ϕ' is used for fracture estimation. The evaluation function ψ is the blank holder displacement which is equal to blank thickness at the flange edge and is used instead of the wall thickness distribution. In the same manner as ϕ, a combination of ψ and ψ' is used to evaluate wrinkle behavior. A constraint function χ is defined as the differential coefficient of the punch load curve to evaluate the progress of the process.

The database in this study is composed of four kinds of process variables, punch stroke, punch load, maximum apparent thickness, and ΔDR^*. The blank reduction ratio ΔDR^* can be obtained from the displacement of the flange edge and is given by

$$\tilde{}DR^* = \frac{s}{R_0}$$

where R_0 is the initial blank radius and s is the displacement of the flange edge.These process data are utilized to design the sets of appropriate membership functions of the evaluation functions so that they have to be accumulated under various material and process conditions (material properties, tooling condition, lubrication condition, ambient condition among others).

In this proposed architecture, three objective functions can be designed. The first is the improvement of the cup height, which can be achieved by applying the maximum BHF below the fracture limit. The second is process energy savings by implementation of the minimum BHF beyond the wrinkle limit. The third is for the wall thickness uniformity, whose control scheme can be achieved by a combination of the above two objective functions.

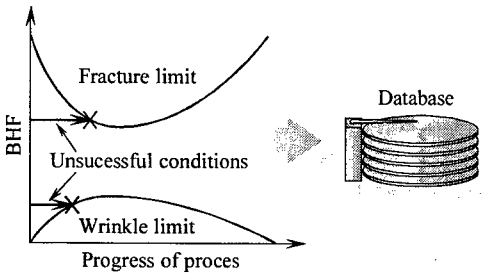


Fig. 4 Requirement of process information contained in the database

Table 1 If-then rule of ϕ, ϕ' and ΔBHF

if(ϕ, ϕ')	Then(ΔBHF)
ϕ is Small and ϕ' is Small	$\Delta BHF = \Delta BHF_{SS}$
ϕ is Small and ϕ' is Large	$\Delta BHF = \Delta BHF_{SL}$
ϕ is Large and ϕ' is Small	$\Delta BHF = \Delta BHF_{LS}$
ϕ is Large and ϕ' is Large	$\Delta BHF = \Delta BHF_{LL}$

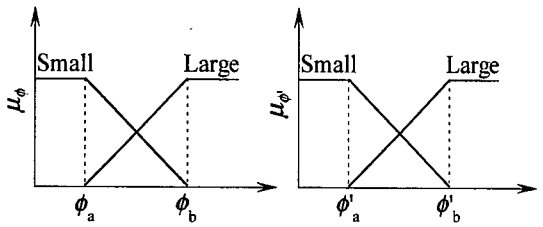


Fig. 5 Sets of input membership functions

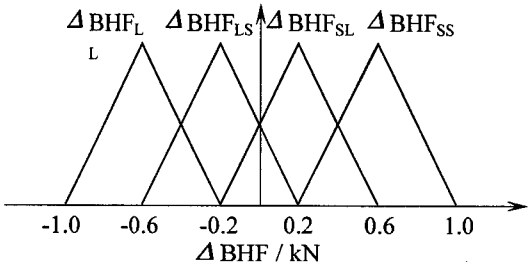


Fig. 6 A set of output membership functions

FUZZY MODEL

Application of the fuzzy model provides a suitable and easy way to optimize process control because the deep-drawing process is not only unsteady and complicated but also has nonlinear forming characteristics.

The sets of membership functions used for the antecedent of the If-then rules are designed through the database. The database must contain at least two typical conditions of the constant BHF. One is a high BHF condition which causes fracture and another one is a low BHF condition which leads to wrinkling as shown in **Fig. 4**. Two membership functions related to ϕ are built from the process data as mentioned in the previous section. The latter data create two membership functions in relation to ψ. In the present study, only two sets of membership functions concerned with ϕ and ϕ' were employed because the objective function is the improvement of cup height as described above. Two maximum values ϕ_b and ϕ'_b in **Fig. 5** should correspond to the state of fracture. Hence each value was decided on the basis of the maximum value retrieved from the database of fracture limit conditions. Meanwhile, ϕ_a and ϕ'_a were decided by substituting the minimum value stored in the database in similar to ϕ and ϕ'.

Figure 6 shows the set of membership functions used for the consequent of If-then rule. This part was decided with the assistance of an expert with experience resulting from trial and error in the previous work [4]. However, the use of this new simplified set of membership functions does not require any experience so that the designer and machine operator need not be skilled and experienced. The initial range of each membership function in Fig.6 can be automatically designed via this system. They only have to provide the multiplier to the value of the system output (ΔBHF),whose value was 0.2, due to the dependency on the forming cell used. **Table 1** shows the If-then rules for BHF control.

Figure 7 shows the fuzzy inference for ΔBHF used in this study. Although the max-min-rule is the most common inference rule, larger membership functions are omitted, when the min-operator is used. However, it is desirable that both membership functions be considered. Therefore, in this work, the areas of the membership functions are used desspite of the use of the min-operator as shown in Fig. 7. Fuzzy outputs of individual fuzzy rules are combined using the max-operator and the centroid of the area is the output.

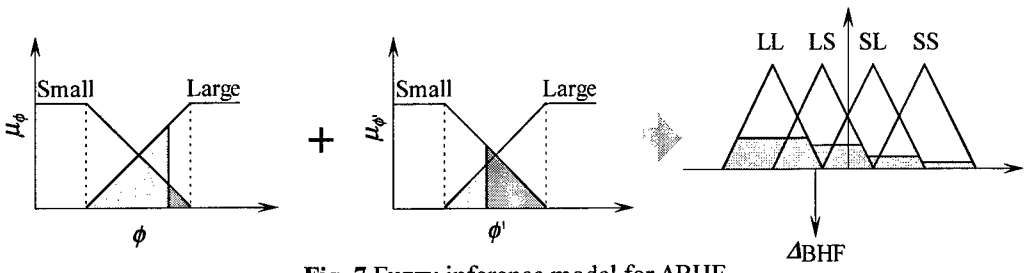


Fig. 7 Fuzzy inference model for ΔBHF

Table 2 Material properties of blank used

Yield Stress σ_S / Nmm^{-2}	Tensile Strength σ_B / Nmm^{-2}	F value / Nmm^{-2}	Elongation / %	N value	R value
117	264	398	30.1	0.28	0.6

Table 3 Experimental conditions

Punch Speed	5 mm/min constant
BHF	0.5~50 kN variable
Lubrication	Lubricating oil (218 mm^{2}s^{-1})
DR	1.98

Table 4 Tooling conditions

Punch shoulder radius r_p / mm	4
Punch diameter D_p / mm	33
Die shoulder radius r_d / mm	3
Die diameter D_d / mm	36.5

EXPERIMENT

Material Used and Experimental Conditions

Aluminum alloy sheet metal (A5182-O) of thickness 1.0mm was used in the deep-drawing experiment. The material properties are listed in **Table 2**. The deep-drawing system used is capable of computerized control of BHF and the punch speed during the process [3]. The system has several sensors: punch stroke, punch load, BHF, radial drawing displacement of the blank flange which was sensed by a displacement transducer and blank holder displacement by an eddy current displacement transducer. **Tables 3** and **4** show the experimental conditions and tooling conditions, respectively.

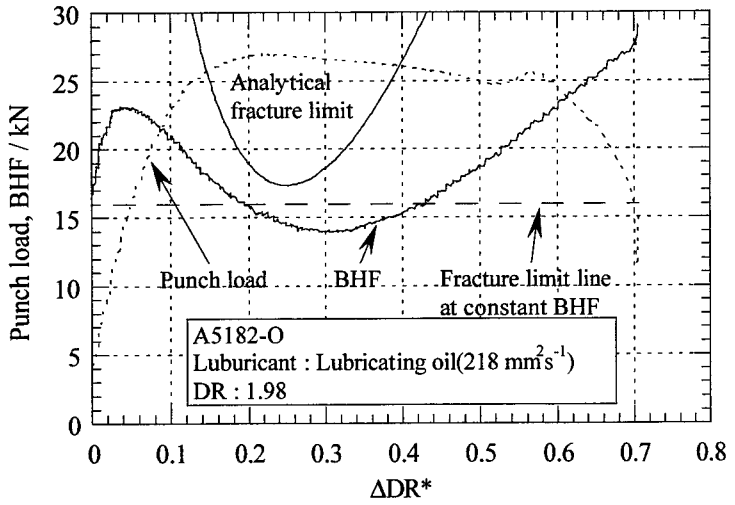


Fig. 8 Punch load and controlled BHF curves during the process.

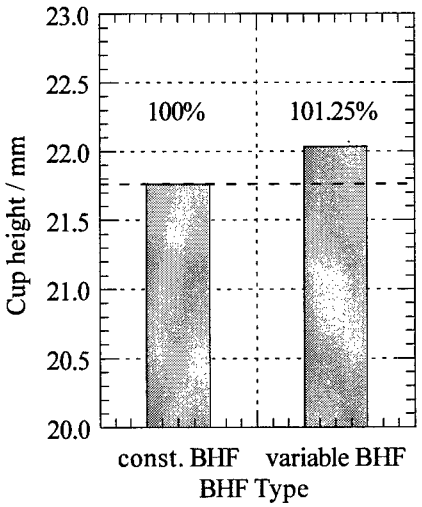


Fig. 9 Comparison of cup height between const. and variable BHF conditions.

Experimental Procedure

CONSTANT BHF DEEP-DRAWING TEST

The first step in the design process is to construct the database from the results of the constant BHF test. In the present architecture, the process information for the fracture and wrinkle limit BHF conditions are essential. However, since this study deals with the improvement of the cup height as the objective function to verify the effectiveness of the design system architecture, process information related to fracture limit BHF condition was collected and stored in the database.

FUZZY CONTROLLED VARIABLE BHF DEEP-DRAWING TEST

The variable BHF deep-drawing test with fuzzy control was conducted on the basis of the above objective function. The details of the procedure are as follows. First, membership functions are produced by using a database constructed from the constant BHF test. Second, initial BHF, blank geometry and punch speed are input into the processor and then the die descends at a constant speed. The BHF is automatically controlled in a closed loop to satisfy the objective function by the obtained fuzzy rule. In this study the initial BHF is set to 1.0kN. For the objective function of the highest cup, the processor basically controls BHF to increase it to the maximum possible value to obtain the highest drawn cup. When the evaluation function indicates a high possibility of fracture, then the BHF can be controlled to decrease it in order to avoid fracture. On the contrary, when the evaluation function shows enough allowance to fracture, then the BHF can be increased.

RESULTS AND DISCUSSION

Figure 8 shows the experimental curves for punch load and BHF which are obtained by a variable BHF control system designed by the new system design architecture with a database. The fracture limit BHF curve obtained from the plastic deformation model [2] is also indicated. Variable BHF path indicates the increase of BHF as high as possible and avoidance of the fracture limit according to the objective function. As a result, an improved drawn cup height was accomplished as shown in **Figure 9.** However the experimental results are still insufficient. At the next stage, is is necessary to feed-back the process information under variable BHF conditions shown in Fig. 8, to optimize the fuzzy rule. Such a routine will enable optimization of the process control.

CONCLUSIONS

1. A new concept of an intelligent design system with a database replacing a knowledge expert, is proposed for intelligent sheet metal forming. A system architecture based on the proposed concept is developed and applied to circular-cup deep-drawing process.

2. The validity of the proposed concept and system is confirmed through the implementation of the system architecture for the fuzzy control variable BHF deep-drawing process.

REFERENCES

1. K.Manabe, S.Yoshihara, M.Yang, and H.Nishimura, 1995. Fuzzy Controlled Variable BHF Technique for Circular-Cup Deep Drawing of Aluminum Alloy Sheet. Technical Papers NAMRI/SME, 41-46.
2. K.Manabe, M.Yang, and S.Yoshihara, 1998. Artificial Intelligence Identification of Process Parameters and Adaptive Control System for Deep-Drawing Process. J. Mater. Process Technol., 80-81, 421-426.
3. K. Soeda, K. Manabe and H. Nishimura, 1993. Process control of Punch Speed and Blank Holding Force on Cylindrical Cup Warm Deep Drawing of Aluminum Alloy Sheets. Proc. 1993 Japanese Spring Conf. Tech. Plasticity (in Japanese), 65-68.
4. S. Yoshihara, K. Manabe, M. Yang, H. Nishimura, 1997. Fuzzy Adaptive Control of Circular-Cup Deep-Drawing Process Using Variable Blank Holder Force Technique. J. JSTP 435 (in Japanese), 46-51

An Iterative Approach to Determine Composition and Heat Treatment from the Mechanical Yield Strength of an Aluminum-Lithium Alloy

J. M. Fragomeni

Department of Mechanical Engineering, Stocker Engineering Center,
Ohio University, Athens, Ohio, USA

ABSTRACT

The development of a model to predict an alloy's microstructure and processing variables from specific mechanical properties or desired mechanical properties was the general emphasis of this investigation. The processing variables included the alloy's overall heat treatment, which involves the aging practice (time and temperature) and the solution heat treatment practice, and also the manufacturing processing of the alloy which involved direct extrusion processing. The particular mechanical property of interest for the aluminum-lithium demonstration alloy was the mechanical tensile strength. The microstructure was used as the basis for determining both the composition and the heat treatment processing requirements for obtaining the desired mechanical property. Specifically, a materials design model was designed to determine microstructural parameters from mechanical properties as the basis for prediction and/or specification of the heat treatment processing parameters. An iterative approach was taken to improve the initial determination of thermal processing and composition. The overall approach will design a precipitation hardened alloy's heat treatment and composition to satisfy the design tensile strength and microstructure requirements of a given materials design and manufacturing program.

BACKGROUND AND INTRODUCTION

The strength of an alloy can considerably vary when going from one heat-treatment to another i.e., say from the underaged to peak-aged condition or from the peak-aged to the overaged condition. Thus, the strength of an alloy is a function of both aging time and aging temperature as well as composition. The strength of a precipitation strengthened alloy is substantially determined from the strengthening precipitates in the microstructure which impede dislocation motion due to plastic deformation. Plastic deformation of a metal or alloy results predominantly by the motion and generation of dislocations. The particles in the microstructure which act as obstacles to dislocation motion are a result of precipitation strengthening or age hardening of an alloy by solution treating and quenching the alloy in which a second phase in solid solution at elevated temperature precipitates out upon quenching and aging at lower temperature. Both strength and hardness of an alloy increases with increasing aging time or increasing aging temperature after rapid cooling from the solution heat treatment. For this age hardening or precipitation strengthening to be possible, the second phase must be soluble in solid solution at an elevated temperature and must exhibit decreasing solid solubility with decreasing temperature.

A considerable amount of energy is required for dislocations to propagate through an array of precipitate particles, either through dislocation particle shearing or dislocation particle looping. The elastic strain energies of dislocations as well as the dislocation particle interaction mechanisms are important considerations. In the underaged heat treatment of an alloy, the precipitates are relatively small in size and therefore easily sheared by dislocations moving under an applied stress. If an alloy is further precipitation hardened with an increased aging time, the precipitate particles will grow in size and provide greater resistance to the motion of dislocations. As a result there is an observed increase in the strength of the alloy. The precipitate particle will continue to increase in size with aging time until a critical particle size is reached where the force of interaction with the dislocation is so high that the particles are no longer sheared but rather are bypassed by the dislocations. The dislocations can no longer shear through the particles so therefore will bypass or may even loop the precipitates via. the Orowan bowing/looping mechanism, which requires a lower shear stress than that required to shear the particles. The dislocations will bow between the

0-7803-5489-3/99/$10.00 ©1999 IEEE.

particles and break away without cutting them. Beyond the critical particle size where the particle are no longer sheared by the dislocations but are rather bypassed by dislocation, the flow stress becomes inversely proportional to the inter-particle separation. When the precipitates continue growing and coarsening at constant volume fraction an overaged material results, the inter-particle separation increases and the strength decreases. There is often a gradual transition between the shearing and looping mechanisms due to the random distribution in sizes of particles and this transition between mechanisms gives the smooth peak of the single-stage aging curve. Thus the influence of both particle shearing and dislocation looping or bypassing results in the classical aging curve, with strength initially increases with increasing particle size followed by the strength decreasing with aging as a result of dislocation particle bypassing or looping.

The strength of a precipitation hardened alloy can be determined in terms of the single crystal strength, often referred to as the critical resolved shear strength (CRSS), which represents the strength of a single grain or crystal of the polycrystalline aggregate. The CRSS is also controlled by the stress necessary for dislocations to glide freely through the matrix of precipitate particles of the single crystal. The single CRSS can be correlated with the yield strength of the polycrystalline alloy. However, a direct comparison between the theoretically determined strength and the experimentally determined strength can be difficult since the experimentally determined strength is usually in terms of polycrystalline behavior. Additional variables must be considered when considering a polycrystalline alloy as compared to a single crystal such texture, and grain boundary effects.

The design approach/model was demonstrated with a precipitation strengthened alloy with a uniform microstructure with one primary strengthening particle phase considering the mechanical property of yield strength as a function of the thermal heat treatment conditions and composition. The precipitation hardened alloy considered was a particle strengthened ternary aluminum-lithium-zirconium alloy containing δ' particles as the strengthening phase. The general approach was successfully demonstrated with this alloy for the mechanical strength, so other mechanical properties and other alloy systems with more complex microstructure can be modeled. Thus the purpose of this study was to provide the foundation for the future research with other more complex alloys and properties. The demonstration Al-Li-Zr alloy, containing approximately 2.6 wt.% lithium and 0.09 wt.% zirconium, was solution heat treated and artificially aged for various aging conditions (times and temperatures) to determine the age hardening curves at different temperatures. For this alloy, the primary microstructural strengthening contribution comes from δ' (Al_3Li) particles that are uniformly distributed throughout the microstructure. These particles act as obstacles and impede the dislocation glide motion during plastic flow deformation. The δ' particle size, distribution, and spacing, which are directly effected by the material processing and composition, are directly responsible for the strength levels achieved.

The aluminum-lithium alloy system has several possible interaction mechanisms whereby coherent, ordered δ' precipitates, which have the Cu_3Au ($L1_2$) crystal structure, can impede dislocation motion. Various deformation mechanisms occur from glide motion of dislocations during plastic flow. When dislocations interact with precipitates, the mechanisms which may contribute to the strengthening include coherency strengthening, chemical strengthening, modulus strengthening, order strengthening, stacking fault strengthening, strengthening from friction stresses in the δ' precipitates, and Orowan strengthening. Order hardening and Orowan hardening are the important controlling strengthening mechanisms with respect to Al-Li alloys, as well as Ni-Al alloys which are strengthened by the ordered γ' phase (Ni_3Al, Ni_3Ti or Ni_3Al,Ti). For the latter of these mechanisms, the dislocations bypass the precipitates, whereas for the others the dislocations shear the precipitates. Thus, the approach taken will be to relate the strengthening of the material through dislocation particle shearing or dislocation particle looping. With respect to particle shearing the strength is roughly proportional to the average particle size squared and with respect to particle looping the strength is inversely proportional to the average particle radius.

The material processing activates and controls the precipitation process which is responsible for the microstructural development. The analytical models which describe the particle strengthening of precipitation hardened alloy systems are usually derived in terms of the single crystal strength i.e., the critical resolved shear strength (CRSS). The CRSS provides the basis for predicting the polycrystalline yield strength. Experimental tensile data for the demonstration alloy was experimentally determined

through performing a series of tensile tests at various aging conditions, for the underaged, peak-aged, and overaged heat treatments, with variations in both aging temperature and aging time. Extrusion processing variables, such as extrusion temperature, extrusion ratio, and extrusion geometry, were also varied as part of this study. However, the extrusion ratio and extrusion temperature were found to have a negligibly small effect on the mechanical strength. Thus, an extensive experimental database of mechanical properties was available to assist in the development of the iterative material design micromechanical approach.

EXPERIMENTAL METHODS

Materials and Processing

The demonstration material that was used for this research was an Al-2.6wt. percent lithium-0.09 wt.% zirconium alloy. The complete composition analysis (see Table 1) was performed by the Aluminum Company of America (ALCOA) using optical emission spectrometric analysis. One large ingot, approximately 2250 kg., was cast by the ALCOA laboratories due to the difficulty in reproducibility of casting several small ingots. The casting was rolled into a slab having dimensions of 30.5 cm. (12 in.) X 96 cm. (38 in.) X 30.5 cm. (12 in.). The ingot was later preheated in a gas fired furnace for a total time of 20 hours. The first 8 hours was in a furnace temperature range of 482-500° C (900-925° F) and the last 12 hours in a furnace temperature range of 527-538° C (980-1000° F). Several billets were then machined from the preheated ingot, having the dimensions of 15.25 cm. (6 in.) in diameter and 25.4 cm. (10 in.) or 50.8 cm. (20 in.) in length, to be used for the extrusion processing of the demonstration alloy. The aluminum-lithium-zirconium billets were direct extruded after being reheated to temperatures of approximately either 466° C (870° F) or 290° C (555° F). Six product geometries were extruded from the billets using an instrumented 2500 ton press in the direct mode. The product geometry used for this investigation was 1.91 cm. (0.75 in.) diameter round extruded rod in the longitudinal grain direction. The extrusion ratio was 73:1 and the corresponding aspect ratio was 1:1 for the round rod geometry. An extrusion temperature of approximately 339° C (642° F) was used for the Al-Li-Zr demonstration alloy.

Heat Treatment

The specimens were first solution heat treated for one hour at 550 °C in a molten sodium nitrate salt solution followed by a cold water quench. Following the solution heat treatment, the specimens were artificially aged for various lengths of time in a molten sodium nitrate ($NaNO_3$) salt bath. The specimens were immediately quenched in cold water after the aging treatment. The specimens were artificially aged for a range of aging times from 0 to 225 hours at temperatures of 185 °C, 193 °C, and 200 °C.

Mechanical Property Characterization

The experimentally determined values for the tensile properties were obtained from mechanically testing the heat treated tensile specimens. The tensile specimens were tested and machined from the extruded product according to the procedures outlined in the American Society for Testing and Materials ASTM standards B557M-84 [1]. Full age-hardening curves were determined for the Al-Li demonstration alloy.

Metallographic Examination

Transmission electron microscopy (TEM) techniques were used to examine and photograph the microstructure from thin foils obtained from samples aged at 185 °C for different aging times ranging from 24 hours to 225 hours. The samples were prepared from 1.91 cm (0.75 in.) diameter round rod (73:0 extrusion ratio) material extruded with an extrusion temperature of 339° C. Disks approximately 3 mm in diameter were obtained from the tin foil specimens. The thin foil disks were then electropolished using a twin jet polisher, with samples submerged in a 3:1 methanol-nitric acid solution (the electrolyte) and cooled by liquid nitrogen to around –20 to –35°C. TEM negatives were taken directly from the thin foils.

Quantitative Measurements

Centered dark field images were used since they gave good contrast between images of the δ'particles and the matrix phase. Particle size measurements of both the Al_3Li precipitates and composite Al_3Li-Al_3Zr precipitates were performed directly from TEM negatives. A semiautomatic eyecom II image analyzing system was used to measure the particle sizes. The average particle size was measured for each aging time. Particle size distributions of over 500 particles were constructed for each aging time. Two particle

diameters were measured for each particle in order to determine as aspect ratio for each particle. The aspect ratios were used to quantitatively describe the spherical morphology of the particle size distributions

OVERALL MATERIALS DESIGN APPROACH

The microstructure provides the medium through which the mechanical properties are related to the material processing and composition. Specifically, the method taken to perform this research was to first evaluate and determine the particle size and size distribution that would be required to achieve a required strengthening contribution. The particle size distribution and average particle size define the microstructure of the demonstration alloy. The microstructure would then be used as the basis to determine the composition and heat treatment processing variables. With respect to the microstructure, the particle size distribution was determined from the Lifshitz-Slyozov-Wagner (LSW) coarsening theory [2,3], in order to determine the growth rate of particles, average particle size of the distribution, and critical radii at the onset of coarsening. An iterative approach was taken to assist in evaluating the particle size and distribution from the mechanical behavior, and the material processing and composition from the microstructure. Based on the LSW coarsening theory for constant volume fraction of precipitates, the aging time can be determined based on the average δ'particle size for a given distribution and is given by:

$$t = r^3/K_c \qquad 1.$$

where t is the aging time, K_c is the particle growth rate constant, and r is the average δ'particle size. The average particle size and growth rate constant for a give alloy system can be evaluated from quantitative measurements using quantitative microscopy from TEM analysis. For the Al-Li demonstration alloy, K_c was equal to 35.1E-24 cm^3/sec based on quantitative measurements of particle sizes. Thus, the heat treatment time or artificial aging time, can be determined from equation 1. The heat treatment temperature can be related to the composition (wt.% Li) of the Al-Li alloy through the expressions given by [4,5]:

$$\ln\{ K_c t \} = -12946.16/T + a \qquad 2.$$

where T is the aging temperature, is the K_c coarsening growth rate, t is the aging time, and where "a" is an empirical constant for the Al-Li alloy system dependent on the composition and given by expression [4,5]:

$$a = 0.52 (\text{wt.\% Li}) - 19.97 \qquad 3.$$

The material processing and composition can be used to directly evaluate/calculate the strength, from a previously developed model, to see how well it compares with the actual experimental value for the strength that was used to determine the first estimate of the material processing and composition. In an alloy system such as aluminum-lithium which contains shearable particles, the single crystal critical resolved shear stress, τ_{crss}, from the interaction of gliding dislocations with the ordered coherent precipitates can represented by an expression of the form [6].

$$\tau_{crss} = c\, f^{0.5}\, r^{0.5} \qquad 4.$$

where τ_{crss} is the single crystal strength, r is the average particle size, f is the volume fraction of the strengthening precipitates, and "c" is strengthening constant for the particular alloy. Based on the LSW theory with constant volume fraction of precipitates, the overall mechanical strength of a precipitation strengthened alloy can be thus directly related to the average particle size from the expression given by:

$$\sigma_o = \sigma_{sss} + C\, r^{0.5} \qquad 5.$$

where σ_o is the proof stress or the total mechanical strength of the material, σ_{sss} is the as-quenched strength which includes the contributions from the solid solution, grain size, and intrinsic lattice strengthening. "C" is a materials constant dependent on the alloy strengthening, crystallographic texture, and microstructure, and r is the average particle size of the intermetallic strengthening precipitates in the microstructure i.e., δ' for the Al-Li alloy. The constant C includes various material parameters/constants such as the antiphase bounday energy, the shear modulus, volume fraction, Burgers vector, the Taylor grain orientation texture factor, etc. For the Al-2.6Li-0.09Zr alloy used in this study the as-quenched strength, ,σ_{sss}, was found to be approximately 140.6 MPa for the solution heat treated only condition. The calibration constant "C" = 76,739,877.3 was determined from fitting a yield tensile data point in the underaged condition (4 hours at 185°C) to the above expressions. Thus, if the yield strength is known in MPa, the average particle size in

Angstroms (1 Angstrom = 10^{-10} meters) can be estimated from equation 4., and thus the heat treatment aging time can then be estimated from equation 1. In the peak-aged condition (48 hours at 185 °C) the yield strength was found to be approximately 449.4 MPa. Using the calibration constant and the as-quenched strength, the average particle size was calculated as 16.1E-11 meters (16.1 angstroms). The aging temperature and composition (wt.% lithium) can then be optimized from equations 2. and 3. based on different average particle sizes corresponding to different heat treatment aging times and temperatures.

DISCUSSION

The microstructure provides the medium through which the mechanical properties are related to the material processing and composition. Specifically, the method to be taken to perform this research will be to first evaluate and determine the particle size and size distribution that would be required to achieve a required strengthening contribution. The particle size distribution and average particle size would define the microstructure of the demonstration alloy. The microstructure would then be used as the basis to determine the composition and heat treatment processing variables. With respect to the microstructure, the particle size distribution can be determined from the Lifshitz-Slyozov-Wagner coarsening theory, in order to determine the growth rate of particles, average particle size of the distribution, and critical radii at the onset of coarsening. Figure 1 shows a computer generated microstructure for the Al-Li alloy which provided a basis for the developing the overall materials design methodology. An iterative approach was taken to assist in evaluating the particle size and distribution from the mechanical behavior, and the material processing and composition from the microstructure. The material processing and composition can then be used to directly evaluate/calculate the strength, from a previously developed model, to see how well it compares with the actual experimental value for the strength that was used to determine the first estimate of the material processing and composition. The process can be iterated a second time by making small adjustments in the composition and/or heat treatment processing (aging temp. and aging time) which would translate in some adjustment to the microstructure through a change average particle size and size distribution. For example, a slight increase in the composition of the minor alloying element of lithium, say from 2.0 to 2.2 wt.%, and/or a small increase in the aging temperature, say from 180°C to 183°C, would result in a increase in the average particle size and distribution which would most likely translate to a some increase in the mechanical strength, unless the alloy was already in the overaged condition which would then continue to decrease in mechanical strength . If necessary, a third or more iteration could be done to improve the computations. The overall approach could be integrated into a computer model for materials design to assist in the calculations. After the materials design methodology has been applied for the mechanical strength property it can then be applied to the other properties, such as fatigue life, fracture toughness, ductility, creep, etc., of the overall materials design approach.

For many alloys, the macrostructural grain size and distribution is an important parameter of the microstructure with respect to controlling the mechanical behavior. The grain size and distribution, as opposed to the particle size and distribution with respect to the Al-Li demonstration alloy, is considerably important in determining the mechanical strength in several alloy systems. However, with respect to the Al-Li alloys, the grain size strengthening effect on the yield strength is very small, and thus the particle strengthening, as previously described, is that which controls the polycrystalline yield strength of a precipitation hardened alloy. The Hall-Petch coefficients for Al-Li alloys are very small, indicating the small grain size strengthening contribution in Al-Li. However, in alloys where the Hall-Petch coefficients are not small, the grain size strengthening is not small and is useful in evaluating the strengthening through the microstructure via. an accurate determination of the size and distribution of the grains. The approach of the micromechanical model with respect to the grain size and distribution would be the same as that with the particle size and distribution in that the mechanical behavior can be related to the microstructure through either the particle size distribution and/or the grain size distribution on the microstructural and macrostructural levels respectively. In some alloys both the grain size and distribution as well as the distribution of precipitate particles within the individual grains would be important microstructural parameters in relating the material processing, composition, and heat treatment to the mechanical behavior via. the microstructure, and thus both would need to be considered.

In general, grain size and the corresponding spatial distribution of grains boundaries in polycrystalline materials, have an important effect for some materials on many physical phenomena in physical

metallurgy. In addition to mechanical strength, properties such as ductility, fracture toughness, creep resistance, fatigue, castability, superplasticity etc. are all influenced by spatial grain size distribution. Various analytical methods exist for calculating the size distribution of grains. These methods are classified into several major categories, according to the type of planar measurements performed. These methods are based on measurements of section diameters, section areas, section chords, and intercept length. The distribution of grain sizes on a given microstructure area plane can be determined and this can be converted to a volume distribution of grain sizes. The volume distribution of grain sizes in an alloy is a more accurate representation of the internal structure and this can be used as a basis to evaluate and determine the mechanical behavior and various properties of materials.

SUMMARY AND CONCLUSIONS

The processing variables included the alloy's overall heat treatment, which involves the aging practice (time and temperature) and the solution heat treatment practice, and also the manufacturing processing of the alloy, such as the extrusion processing, or some other type of mechanical processing method. The mechanical property of interest included the mechanical tensile strength, or yield strength, but some other mechanical properties of interest are necessary as part of the overall approach such as ductility, fracture toughness, and fatigue behavior. Thus, this particular study is a summary of work current in progress on the development of an overall global design procedure to determine thermal and mechanical processing parameters, and alloy composition required for specific mechanical design properties. This communication presents the progress of this effort for the mechanical property of yield strength. Specifically, a materials design model was designed to predict microstructure from mechanical behavior as the basis for prediction and/or specification of the thermal processing parameters. An iterative approach was taken to improve the initial determination of material processing and composition to yield the correct value of the tensile strength. The overall approach will design a precipitation hardened material that can perform according to the design requirements and processing capabilities of a given thermal treating and manufacturing facility.

REFERENCES

1. 1988 Annual Book of ASTM Standards, Section 3: Metals Test Methods and Analytical Procedures, Volume 3.01, American Society for Testing and Materials, Philadelphia, PA, 1988.
2. I.M. Lifshitz, and V.V. Slyozov, 1961, "The Kinetics of Precipitation from Supersaturated Solid Solutions", Journal Physical Chemical Solids, 19, 35-50.
3. C. Wagner, 1931, "Theories Associated with Age Hardening and Overaging During Ostwald Ripening", Zeitschrift fur Elektrochemie, 37, 581-591.
4. K. Mahalingam, B.P. Gu, G.L. Leidl, and T.H. Sanders, Jr., 1987, "The Coarsening of δ'(Al_3Li) Precipitates in Binary Al-Li Alloys", Acta Metallurgicia, 35(2), 483-498.
5. S.C. Jha, G. Liedl, K. Mahaligham, and T.H. Sanders, Jr., 1986, "Coarsening Phenomenon on Aluminum-Lithium Alloys", in Unusual Techniques and New Applications of Metallography, Vol. 24, edited by R.J. Gray and L.R. Cornwell, ASM, Metals Park, Ohio.
6. E.A. Starke, Jr., 1977, "Aluminum Alloys of the 70's: Scientific Solutions to Engineering Problems", Materials Science and Engineering, 29, 99-115.

Table 1: Composition analysis determined by optical emission spectrometric analysis for the Al-2.6wt.%Li-0.09wt.%Zr demonstration alloy.

Al	Li	Zr	Cu	Mg	Si	Fe	Ti	B	Na	Ca
bal	2.59	0.09	0.11	0.07	0.04	0.03	0.01	<0.001	<0.001	<0.001

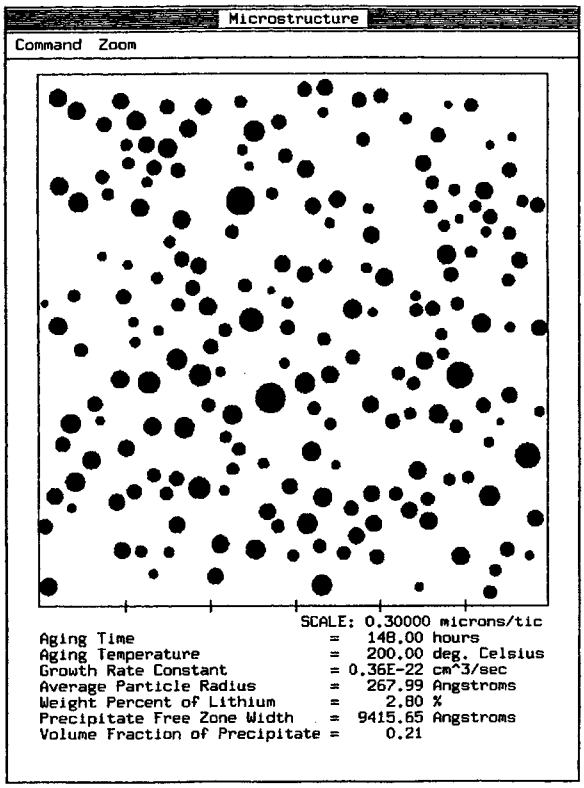


Fig. 1. Computer simulated TEM microstructure for a binary aluminum-lithium (Al-2.8wt.%Li) alloy precipitation age hardened for 148 hours at 200 °C, showing the distribution of Al_3Li (δ') precipitates in the matrix phase of the overall microstructure.

Statistical Approach to Experimental Design to Determine the Effect of Extrusion Variables on the Mechanical Properties of an Al-Li Alloy

J. M. Fragomeni

Department of Mechanical Engineering, Stocker Engineering Center,
Ohio University, Athens, Ohio, USA

ABSTRACT

The objective of this research study was to utilize the statistical design of experiments method to analyze and evaluate the influence of the extrusion process manufacturing parameters on some given mechanical properties for an aluminum-lithium alloy with a given composition and post-extrusion thermal processing. The goal was to analyze and determine if variations in specific extrusion processing variables or parameters had a statistically significant effect on some given mechanical properties such as yield strength, ultimate tensile strength, and ductility. The layout for the design experiment consisted of two extrusion temperatures and two extrusion geometries. The layout also included six cross section areas nested in two extrusion geometries. Thus, the design of the experiment was a mixture of a nested structure and a factorial structure i.e., a nested factorial design. This design included interactions crossed between the extrusion temperature and the extrusion geometry, and the extrusion temperature with the cross sectional area. Thus there was a possibility of twelve different treatment combinations that made up the design of experiments method. It was found that the extrusion geometry was at least 95% statistically significant with respect to the mechanical properties of interest and that the extrusion temperature was not significant at this level.

INTRODUCTION

The emphasis of this investigation was to evaluate what particular extrusion processing parameters from a direct extrusion manufacturing process had a statistically significant effect on mechanical behavior. This was considered important since one may desire to control the mechanical properties through a manufacturing extrusion process for particular design applications. Direct extrusion is a manufacturing process whereby metal or alloy in a billet form is forced through a die under high pressure usually at elevated temperature. The billet is often at elevated temperature since the deformation resistance is low and therefore less force and energy are required to plastically deform the billet through the die orifice by a ram with a dummy block or pressure plate at the end of the ram in direct contact with the billet. The extrusion of a material is a complex process that involves the interaction of various extrusion processing variables to change the shape of the starting billet material and thus substantially change the internal structure and properties of the material. The most common methods of extrusion include direct extrusion, indirect extrusion, and hydrostatic extrusion. The work presented in this investigation involves direct extrusion at elevated temperatures of an aluminum alloy billet containing lithium that was extruded into both round and rectangular cross-sectional geometries by the Aluminum Company of America. Direct extrusion is characterized by the fact that the process occurs in a solid container with the extruded product exiting in the same direction as the ram that is causing the deformation is moving. The relative motion between the billet and the container wall will cause heat to be generated during direct extrusion, and also some plastic deformation. Thus the exit temperature of the extruded product will often be greater than the initial temperature of billet prior to extrusion. The rise in temperature causes the variations in the temperature of material perpendicular to and transverse to the ram travel. Transverse variations in temperature produce variations in structure, and hence in properties, across to extruded geometry. Therefore, in order to accurately represent the extrusion temperature for the given extrusion process, and average equivalent extrusion temperature, developed by Farag and Sellers [1], is often used and expressed as

$$T_{eq} = (2\ T_o\ T_f)/(T_o + T_f) \qquad (1)$$

0-7803-5489-3/99/$10.00 ©1999 IEEE.

Where T_o is the initial billet temperature, T_f is the final billet temperature, and T_{eq} is the average equivalent extrusion temperature. Thus the general rise in temperature during extrusion can cause variations in the internal structure and properties of the extruded product.

EXPERIMENTAL METHODS

Material Processing

An aluminum-lithium-zirconium alloy having a composition of 2.6wt.%Li and 0.09wt.%Zr (see Table 1) was used as the demonstration alloy for this investigation. The complete composition analysis was performed by the Aluminum Company of America (ALCOA) using optical emission spectrometric analysis. One large ingot (2250 kg.) was cast by the ALCOA laboratories due to the difficulty in reproducibility of casting several small ingots. The casting was rolled into a slab having dimensions of 30.5 cm. (12 in.) X 96 cm. (38 in.) X 30.5 cm. (12 in.). The ingot was later preheated in a gas fired furnace for a total time of 20 hours. The first 8 hours was in a furnace temperature range of 482-500° C (900-925° F) and the last 12 hours in a furnace temperature range of 527-538° C (980-1000° F). Several billets were then machined from the preheated ingot, having the dimensions of 15.25 cm. (6 in.) in diameter and 25.4 cm. (10 in.) or 50.8 cm. (20 in.) in length, to be used for the extrusion processing of the Al-Li-Zr demonstration alloy.

Extrusion Processing

The aluminum-lithium-zirconium billets were direct extruded after being reheated to temperatures of approximately either 466° C (870° F) or 290° C (555° F). Six product geometries were extruded from the billets using an instrumented 2500 ton press in the direct mode. The product geometries used for this investigation were 1.91 cm. (0.75 in.), 2.69 cm. (1.06 in.), and 5.3 cm. (2.09 in.) diameter round extruded rod in the longitudinal grain direction. The extrusion ratios were 73:1, 36.5:1, and 9:1 and the corresponding aspect ratio was 1:1 for the round rod geometry. An extrusion temperature of approximately 339° C (642° F) was used for the Al-Li-Zr demonstration alloy.

Extrusion Post-Processing

The Al-Li alloy was machined into tensile samples from the extruded product. The tensile samples were oriented in the longitudinal grain direction. The tensile samples were first solution heat treated (SHT) for one hour at 550° C (1022° F) in a molten sodium nitrate salt solution followed by a cold water quench (CWQ) to room temperature. Following the solution heat treatment, the tensile samples were artificially aged for various lengths of time in a molten sodium nitrate ($NaNO_3$) salt bath. Different aging treatments were utilized by varying both the time and the temperature. The samples were immediately quenched in cold water, at approximately room temperature, after the artificial aging treatment. The samples were aged at temperatures of 185° C (365° F) and 193° C (379° F). The molten salt solution was continuously stirred throughout the solution heat treatment and aging process to insure a uniform temperature distribution throughout the bath.

Monotonic Tensile Tests

The experimentally determined values for the tensile properties along the longitudinal direction were obtained from mechanically testing the heat-treated tensile samples. Tensile testing was performed in accordance with the American Society for Testing and Materials (ASTM) for the ASTM B557M standards [2] test specifications. All the tensile testing was performed at room temperature with the test machine operating in stroke control. The mechanical testing was performed utilizing a +/-22 kip (100 KN) MTS System Corporation electrohydraulic testing system. For the purposes of this investigation, round rod tensile samples were machined from the round geometry extruded product in the longitudinal grain direction. The tensile samples were tested in the longitudinal orientation. It was determined from an extensive tensile database of the demonstration alloy that the tensile strength data was reproducible with no statistical variation in strength for constant aging conditions.

Transmission Electron Microscopy and Particle Size Distribution Statistics

The particle size distribution and particle morphology were examined and photographed using transmission electron microscopy (TEM) from thin foil specimen obtained from samples aged at 185° C for different

aging times ranging from 24 hours to 225 hours. The thin foil specimen were sliced with a diamond blade saw cutter and than polished to foils approximately 0.05 mm thick. Disks approximately 3 mm in diameter were then punched from the thin foils. The thin foil disks were then electropolished using a twin jet polisher, with the disks submerged in a 3:1 methanol-nitric acid solution cooled by liquid nitrogen to around -20 to –35° C. The thin foil disks were observed and photographed using a JEOL-200 CX microscope operating at 200 KV for various specimen inclinations. Figure 1 shows the TEM microstructure of the Al-Li alloy showing the δ' (Al_3Li) precipitates distributed uniformly in the matrix. Particle size measurements of the Al_3Li precipitates were made directly from TEM negatives. A semiautomatic EyeCom II image analyzing system was used to measure particle sizes. The average particle sizes were measured for each aging time. In order to perform the statistical analysis of the particle distributions, particle size distributions consisting of over 500 particles were constructed analyzed for each heat treated aging time. The coefficients of skewness, kurtosis, and variation, as well as the first, second, third, and fourth moments about the mean were evaluated for each of the particle size distributions.

RESULTS

As shown by Table 2, the layout for the experiment consists of the two extrusion temperatures of 320°C and 450°C, and two extrusion geometries. The layout also includes the six cross section areas nested in the two extrusion geometries. Thus, the design of this experiment is a mixture of a nested structure and a factorial structure i.e., a nested factorial design. This design includes interactions crossed between the extrusion temperature and extrusion geometry and the extrusion temperature with the cross section. The nested factorial design was chosen over a completely randomized design, a randomized complete block design, and a nested a design since it best describes the analysis of this experiment. From the layout of the experiment, it can be seen that there are a possibility of twelve different treatment combinations. Once the mechanical testing system has been set up it will take approximately 30 minutes to an hour to perform a single test. Therefore, if no replications are performed i.e., one observation per cell block, then the experiment can be run in a single day. If more than one observation per cell block was desired to be tested, then the entire experiment could be run but more than one day would be necessary. The specimen corresponding to the different treatment combinations would be assigned random numbers one through twelve. The specimen designations could be as shown by Table 3. Equation 2. summarizes the corresponding model for the design of experiments.

$$Y_{ijkl} = \mu + G_i + S_{j(i)} + T_k + GT_{ik} + TS_{jk(i)} + \varepsilon_{(ijk)l} \qquad 2.$$

Where Y_{ijkl} represents the given mechanical property such as the yield strength, elastic modulus, elongation, ultimate tensile strength, etc. μ represents the overall mean, G_i represents the effect of the i^{th} level of the extrusion geometry, $S_{j(i)}$ represents the effect of the j^{th} level of the cross section on the i^{th} level of the extrusion geometry, T_k represents the effect of the k^{th} level of the extrusion temperature, GT_{ik} represents the effect if the interaction of the i^{th} level of extrusion geometry and the k^{th} level of the extrusion temperature, $TS_{jk(i)}$ represents the effect of the interaction of the j^{th} level of the cross section on the i^{th} level of the extrusion geometry and the k^{th} level of the extrusion temperature, and $\varepsilon_{(ijk)l}$ represents the effect of the l^{th} sample within the i^{th} extrusion geometry, the j^{th} cross section, and the k^{th} extrusion temperature. The between sample terms include Gi and $S_{j(i)}$. The within subject terms include T_k, GT_{ik}, $TS_{jk(i)}$, and $\varepsilon_{(ijk)l}$. Using this analysis, the two extrusion geometries could be coded by allowing G to be equal to 1 or 2. The cross section could then be coded by letting S equal to 1, 2, or 3, and the extrusion temperature could be coded by letting T equal to 1 or 2. The numbers 1 through 12 could be randomly drawn and the corresponding treatment combinations run in the exact order that it was drawn.

Table 4 shows the ANOVA for the fixed model which would apply to the tensile specimens that have been mechanically tested to date. However, a future design experiment could be performed with using a random model where all the extrusion variables would be random factors. This is because the mechanical testing system is not constrained by extrusion geometry, extrusion temperature, or extrusion cross section dimensions. The ANOVA table for the random model, where all the extrusion variables would be random factors, is shown by Table 5. However, Table 6 shows the layout of the experimental yield strength tensile data for the Al-2.6wt.%Li-0.09wt.%Zr demonstration alloy in the peak-aged heat treated condition. This layout includes experimental tensile data for the two extrusion temperatures and the six cross section areas nested within the two extrusion geometries. The two missing data points correspond to future tensile test.

DISCUSSION

The design of this experiment produced an interface space for this particular alloy as well as other aluminum-lithium alloys with varying compositions (different weight percents lithium and aluminum). The interface space stated that the experimenter would like to imply that if any of the extrusion processing variables included in the design show up in the experiment, then the same effect on mechanical properties would show up in all tensile specimen that were obtained from the given ingot of material from which the twelve were selected as well as other cast Al-Li ingots with different compositions. All of the mechanical testing was performed with the extrusion variables fixed, and using an MTS Systems Corporation electrohydraulic mechanical testing system. The mechanical tensile data, including both the yield strength and the ultimate tensile strength, the percent elongation, and the elastic modulus was analyzed using the analysis of variance approach. The Student-Neuman Keuls multiple range test was used to analyze the means from the smallest the largest to determine which means are not significantly different. All of the billets used for the extrusion processing were obtained from the same ingot to avoid a possible restriction error, to come from the same ingot processing, and composition. Thus one large ingot was cast instead of several smaller ingots for better reproducibility of the chemical composition of the individual billets. Is addition, billets were cut from the center of the ingot for better chemical homogeneity. This was done to avoid any possible composition variations from the surface to center of the ingot.

SUMMARY AND CONCLUSIONS

The design of the experiment was a mixture of a nested structure and a factorial structure i.e., a nested factorial design. This design included interactions crossed between the extrusion temperature and the extrusion geometry, and the extrusion temperature with the cross sectional area. Thus there was a possibility of twelve different treatment combinations that made up the design of experiments method. It was found that the extrusion geometry was at least 95% statistically significant with respect to the mechanical properties of interest and that the extrusion temperature was not significant at this level.

The design of the experiment produced an interface space for the demonstration alloy as well as other aluminum alloys containing lithium with varying compositions. The interface space proposed that the experimenter would desire to imply that if any of the extrusion processing variables included in the design showed up in the experiment, then the same effect on mechanical properties would show up in all tensile samples that were processed from the given ingot of material from which the twelve were selected as well as other cast Al-Li ingots with varying compositions.

REFERENCES

1. M.M. Farag, and C.M. Sellars, 1973, "Flow Stress in Hot Extrusion of Commercial Purity Aluminum", Journal of the Institute of Metals, 101, 229-238.
2. 1988 Annual Book of ASTM Standards, Section 3: Metals test Methods and Analytical Procedures, Volume 3.01, American Society for Testing and Materials, Philadelphia, PA, 1988.

Table 1: Composition analysis in weight percent determined by optical emission spectrometric analysis for the aluminum-lithium-zirconium demonstration alloy.

Al	Li	Zr	Cu	Mg	Si	Fe	Ti	B	Na	Ca
bal	2.59	0.09	0.11	0.07	0.04	0.03	0.01	<0.001	<0.001	<0.001

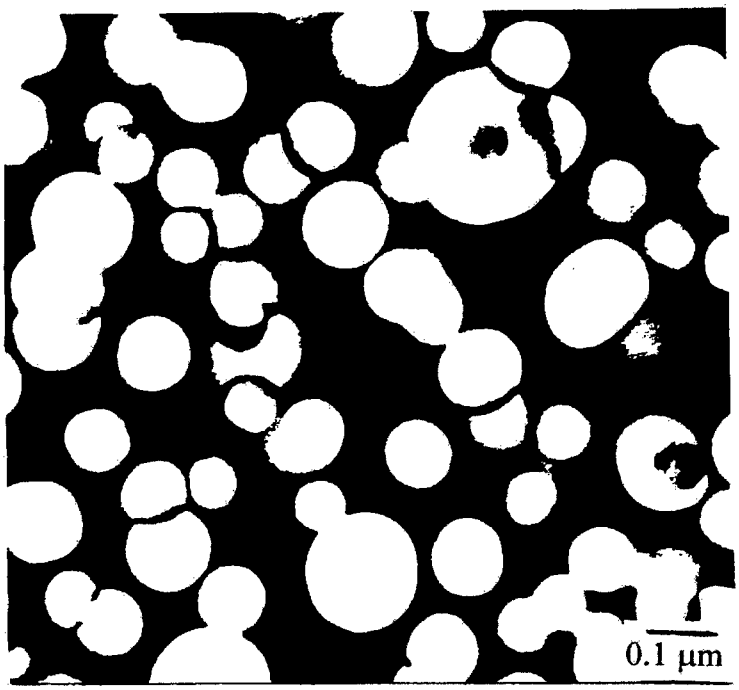


Fig 1. Transmission electron dark field image micrograph showing the TEM microstructure of the Al-2.6wt.%Li-0.09wt.%Zr demonstration alloy heat treated aged at 185°C for 225 hours (186,000X).

Table 2: Layout of the extrusion processing variables showing a nested factorial design.

			EXTRUSION TEMPERATURE	
			320°C	450°C
EXTRUSION GEOMETREY (cm.)	ROUND	5.3 dia O		
		2.69 dia O		
		1.91 dia O		
	RECTANGULAR	2.54 X 8.9 □		
		0.635 X 8.9 □		
		0.318 X 8.9 □		

Table 3: Treatment number designations for different levels.

Treatment #	G_i	$S_{j(i)}$	T_k	Y_{ijk}
1	1	1	1	Y_{111}
2	1	1	2	Y_{112}
3	1	2	1	Y_{121}
4	1	3	1	Y_{131}
5	1	2	2	Y_{122}
6	1	3	2	Y_{132}
7	2	1	1	Y_{211}
8	2	1	2	Y_{212}
9	2	2	1	Y_{221}
10	2	3	1	Y_{231}
11	2	2	2	Y_{222}
12	2	3	2	Y_{232}

Table 4: Analysis of variance table for fixed statistical design model.

Source	df	2 F i	3 F j	2 F k	3 R l	EMS
G_i	1	0	3	2	2	$\sigma_\varepsilon^2 + 12\phi_G$
$S_{j(i)}$	4	1	0	2	2	$\sigma_\varepsilon^2 + 4\phi_S$
T_k	1	2	3	0	2	$\sigma_\varepsilon^2 + 12\phi_T$
GT_{ik}	1	0	3	0	2	$\sigma_\varepsilon^2 + 6\phi_{GT}$
$TS_{jk(i)}$	4	1	0	0	2	$\sigma_\varepsilon^2 + 2\phi_{TS}$
$\varepsilon_{(ijk)l}$	24	1	1	1	1	σ_ε^2

Table 5: Analysis of variance table for random statistical design model.

Source	df	3 R i	3 R j	2 R k	3 R l	EMS
G_i	1	1	3	2	1	$\sigma_\varepsilon^2 + 6\sigma_G^2 + 2\sigma_S^2 + 3\sigma_T^2 + 3\sigma_{TG}^2 + \sigma_{TS}^2$
$S_{j(i)}$	4	1	1	2	1	$\sigma_\varepsilon^2 + 2\sigma_S^2 + 2\sigma_T^2 + \sigma_{TG}^2 + \sigma_{TS}^2$
T_k	1	2	3	1	1	$\sigma_\varepsilon^2 + 6\sigma_T^2 + 3\sigma_{GT}^2 + \sigma_{TS}^2$
GT_{ik}	1	1	3	1	1	$\sigma_\varepsilon^2 + 3\sigma_{GT}^2 + \sigma_{TS}^2$
$TS_{jk(i)}$	4	1	1	1	1	$\sigma_\varepsilon^2 + \sigma_{TS}^2$
$\varepsilon_{(ijk)l}$	24	1	1	1	1	σ_ε^2

Table 6: Layout showing experimental yield strength tensile data for the Al-2.6wt.%Li-0.09wt.%Zr demonstration alloy in the peak-aged heat treated temper, 185°C @ 48 hours; (all tensile data given in ksi).

			EXTRUSION TEMPERATURE	
			320°C	450°C
EXTRUSION GEOMETRY (cm.)	ROUND	5.3 dia. O	66.9, 68.2	62.7, 64.6
		2.69 dia. O	67.1, 67.0	68.4, 67.8
		1.91 dia. O	69.5, 69.2	68.2, 67.8
	RECTANGULAR	2.54 X 8.9 □	--,--	46.0, 45.1
		0.635 X 8.9 □	--,--	46.8, 47.3
		0.318 X 8.9 □	38.9, 40.1	39.1, 39.2

Control of Liquid Segregation of Semi-solid Aluminum Alloys during Intelligent Compression Test

C.G. Kang, K.D. Jung, H.K. Jung

Pusan National University, School of Mechanical Engineering
Pusan, 609-735, Korea

ABSTRACT

Thixoforming is now becoming increasingly popular for manufacturing near-net shape parts and has so many advantages compared with conventional forming technologies that it has spread and been studied worldwide. Components produced by semi-solid forming process have good mechanical properties and less defects such as porosity. A relationship between stress and stain is very important to design a die to avoid defects of products during semi-solid forming process.

Since the liquid will be of eutectic composition in alloys, liquid segregation will result in significant or undesirable situations. The materials used in this experiment are A357, A390, Al2024 alloys that have been fabricated by the electro-magnetic stirring process from Pechiney in France. In the compression test with the semi-solid state materials the liquid phase coexists with globularized solid particles. Billet temperature corresponding to the desired solid fraction is controlled by an induction heating system which was constructed with designed coil dimensions. The intelligent compression test was performed by induction heating and MTS. During compression, specimen temperature were continuously measured.

In order to prevent liquid segregation, the measured temperature is useful to control strain rate during compression. The liquid segregation is controlled by changes in the strain rate and solid fraction during the compression process. The characteristics of flow between solid and liquid phase considering liquid segregation is examined through the above experiments. Generally, it is known that if the applied stress to semi-solid alloys is below the yield stress, the alloys show solid-like behavior but, if the applied stress exceeds the yield stress, the semi-solid alloys flow like liquid. Therefore, it is important to establish the yield point to predict the rheological behavior of semi-solid alloys.

INTRODUCTION

The technology of forming metals to near-net shaped products in partially remelted state satisfies the growing demand for high-strength and lightweight aluminum components in the field of automobile and is gaining attention in the broad field of engineering. For optimization of net shape forging process with semi-solid materials(SSM), it is important to predict the deformation behavior for variation of strain rate, but the rheological behavior of mushy state alloys is not sufficiently known. Usually, the rheological behaviour of alloys in the semi-solid state has been examined by using parallel plate compression. However, for analysis of the thixoforming process, it should be necessary to conduct a formation of stress-strain curve in semi-solid alloys. In particular, important problem is to prevent segregation of liquid component during deformation. When semi-solid aluminum alloys are compressed, or liquid component subjected to compressive forces may be ejected to the outside of the billet surface.

The parts of complex shapes are fabricated by casting and forging. Casting products are limited in their mechanical properties due to microstructural defects such as porosity. However, near-net shape forming holds some promise to improve mechanical properties by removing micro defects in castings by hot forging and hot extrusion from the solid state. However on the other hand, the forming of a precision product is limited due to the higher forming load and so there is a loss in productivity and economic efficiency due to post-processing requirements such as machining. To overcome these problems, a semi-solid forming process for near-net shaped parts from raw materials with semi-solid materials(SSM) is widely studied.

Semi-solid forming is a method to make globular structures, and to deform the near-desired product at temperatures between the solidus and liquidus. A lot of concern is focused on several aspects like saving energy and process efficiency, etc.[1-2]. Since manufacturing technology for semi-solid alloys was

0-7803-5489-3/99/$10.00 ©1999 IEEE.

discovered during studies on hot-tearing phenomena in the early 1970's, Suery et al.[4] have studied compression behavior of Sn-15%Pb alloy in semi-solid state and the effect of strain rate, and Toyosima et al.[5] have studied simple compression, filtering, and rolling processes. They formulated their models by applying compressive visco-plastic models for the solid region of the materials and assuming Darcy's flow for the liquid region. Kang et al.[6] compared experimental data with results of finite-element analysis for compressing semi-solid aluminum(A356) materials using a yield condition for porous material. In the case of SSM forging, Kenny et al.[7] reported the best quality production was obtained at a solid fraction in the billet of 60~70 %. Yoshida et al.[8] reported microstructure and liquid flow state with Al-Cu alloy in semi-solid forging. As a result of casting with rapid velocity, using materials with solid fraction of 60%, it was observed that there is no segregation in the produced specimen. Kang et al.[9] showed the effect of gate shape and forging temperature on mechanical properties in the injection forging process of semi-solid aluminum material. To prevent segregation of liquid in forging, the die should be preheated. It is reported that the lowest temperature in die reheating, depends on billet temperature and compressing die shape, and it was reported that the optimal die temperature is 250 to 300 °C. Chen[10] reported experimental deformation behavior, dividing it into deformation behavior of the liquid region according to mutual contact of the liquid region and solid grains, plastic deformation of the solid grains, and contact of the solid grains, in studying the deformation behavior of SSM.

The curve of stress-strain rate of semi-solid material is different from hot compression phenomenon of established materials for deformation of solid grains in compression forming. It is very important to note that the limiting strain rate does not increase, but decreases, in accordance with the increase in stress in compression experiments of the semi-solid forging process.

Therefore, in this study, compression experiments have been performed to investigate deformation behavior of semi-solid material with variation in processing parameters such as compression velocity and the solid fraction. In order to produce components without defects, the forging condition is controlled to increase stress with increase in strain rate in initial forming at constant velocity. Therefore the relationship of the velocity variation to the continuous increase of stress with increase of strain rate has been designed into the compression experiments.

COMPRESSION EXPERIMENTS

The material used in these experiments are ALTHIX(A357, A390) material, which is fabricated by electro-magnetic stirring, from Pechiney and is Al2024, which is fabricated by hot extrusion at a compression ratio 9.37. The chemical composition of each material is shown Table 1.

Table 1 Chemical composition of A357(ALTHIX), Al2024 and A390(ALTHX)

		Si	Fe	Cu	Mn	Mg	Cr	Zn	Ti	Pb
A357	Min(%)	6.5	-	-	-	0.30	-	-	-	-
	Max(%)	7.5	0.15	0.03	0.03	0.40	-	0.05	0.20	0.03
Al2024	Min(%)	-	-	3.8	0.3	1.2	-	-	-	-
	Max(%)	0.50	0.70	4.9	0.9	1.8	0.10	0.25	0.15	-
A390	Min(%)	16.0	-	4.0	-	0.5	-	-	-	-
	Max(%)	17.0	0.4	5.0	0.1	0.65	-	0.05	0.2	0.03

In forming semi-solid material, compression experiments have been performed to investigate the relationship of flow characteristics with variations in solid fraction and die velocity. The compression test of semi-solid material is performed with specimens of $\varphi \times h = 15 \times 20$ mm at a temperature of 1200 °C with a desired solid fraction using an MTS (Material Test System) with an associated electronic furnace. Fig. 1 is the schematic diagram of the experimental apparatus used for compression of the semi-solid aluminum alloy. Temperature, solid fraction, load, displacement and compression velocity are measured during an SSM compression test. At first, the stress-strain are investigated from load and displacement. Generally, in SSM compression tests, the stress decreases from maximum strain.

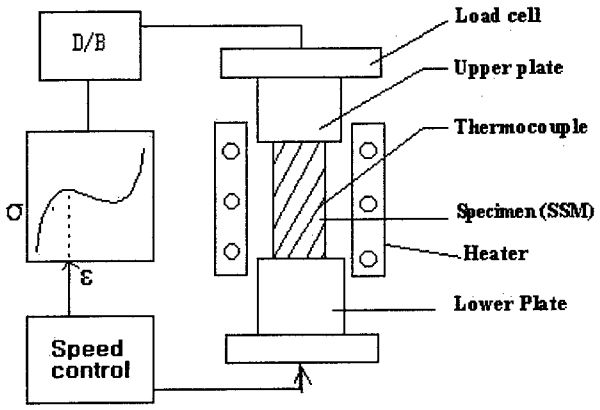


Fig. 1. Schematic diagram of the intelligent compression test apparatus designed to prevent liquid segregation during an SSM experiment.

Then the velocity changes at the displacement correspondent to maximum stress, in order to prevent of liquid segregation. In this obtained stress-strain curve, stress increases according to strain increase. Compression experiments have been performed using A357, A390, Al2024 with compression experiment method of A356. For experiment conditions, solid fractions are 50%(620°C), 70%(599°C) and 90%(556°C), and die velocities are 500, 200, 100, 10, and 1mm s^{-1} in the case of Al2024

EXPERIMENTAL RESULTS AND DISCUSSION

Compression experiments were performed using A357, A390 and Al2024. Fig.2(a)-(e) shows the shape of the specimen at the state of 50%(620°C) solid fraction according to change in V_d. We know the surface of specimen proceeds to fracture with increase in die velocity. Fig. 3(a)-(e) shows the shape of the specimen at the state of 70%(599°C) solid fraction according to the change in die velocity.

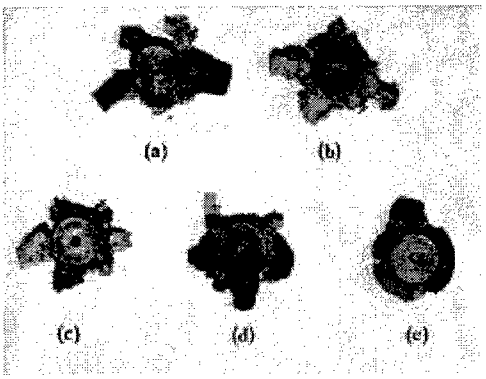


Fig.2. Compression at f_S = 50% (Al2024) where V_d (mm/s) is **a.** 500 **b.** 200 **c.** 100 **d.** 10 **e.** 1

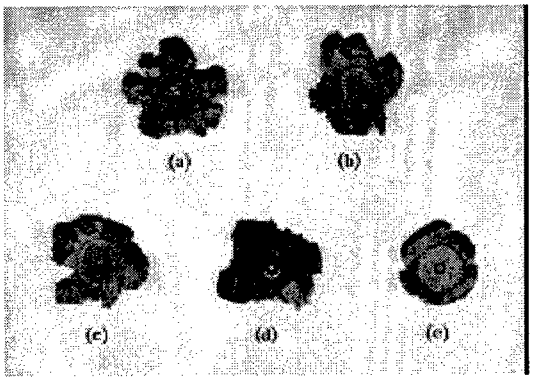


Fig.3. Compression at f_S = 70% (Al2024) where V_d (mm/s) is **a.** 500 **b.** 200 **c.** 100 **d.** 10 **e.** 1

There is only a small difference in the deformation compared to 50%, but the degree of surface fracture is slighty lower. Fig. 4 (a),(b) shows the shape of the specimen at the state of 90%(556°C) solid fraction. The barrel was observed to be similar to that from hot compression with increase in solid fraction.

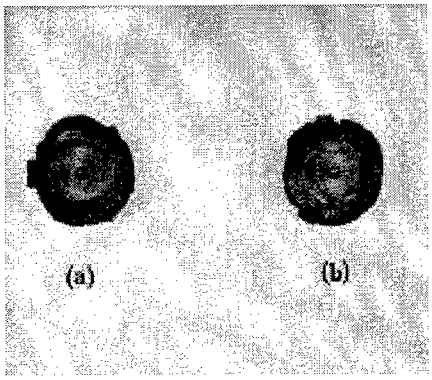


Fig.4. Compression at f_S = 90% (Al2024) where Vd (mm/s) is: **a.** 10 **b.** 1

Figures 5 to7 show curves of true stress-strain rate according to change in die velocity when the solid fractions are f_S = 50%, 70%, and 90%. As shown in Fig. 5 and Fig. 6, the initial stress peak point is observed at strain rates of 0.05 to 0.1. However, from strain $\varepsilon = 0.1$, the stress decreases remarkably and reaches a plateau. This phenomenon is accounted for by liquid flow being activated and transferring to the free surface area at the specific strain rate, even though the stress increases for densification of the structure and stimulation of liquid flow from the very start of the test.

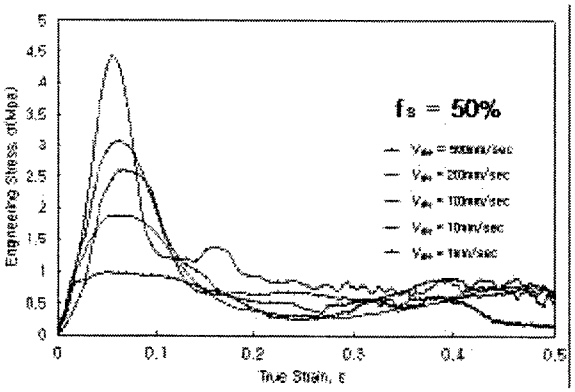


Fig.5. Engineering stress-true strain curve at f_S = 50% (Al2024) (V_d = 500 mm/sec to 1 mm/sec)

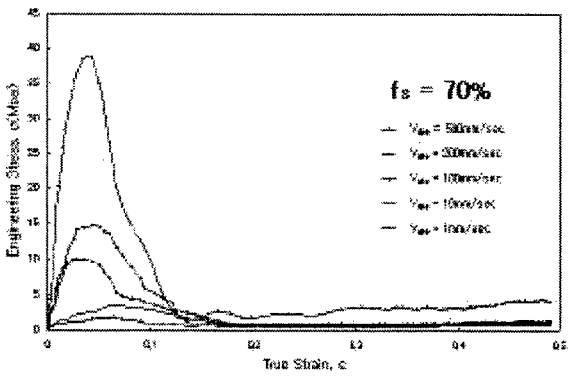


Fig.6. Engineering stress-true strain curve at f_S = 70% (V_d = 500 mm/sec to 1 mm/sec)

In compression forming of semi-solid materials at high temperature, the surface of the specimen brakes away during compression by liquid flow towards the surface of the specimen. Therefore, a forming method for closed forging shapes is needed, since free surface does not exist. Fig. 7 shows the shape of the curve the state of f_S = 90% solid fraction is different from that at 50 and 70 (see Figures 5 and 6). This is because at high temperature, globularity doesn't occurred in the solid fraction, in the direction of extrusion, orientation of the structure doesn't exist and liquid flow does not occur during the early stages of deformation. the stress increases quickly, and as globular microstructure is fractured, stress decreases.

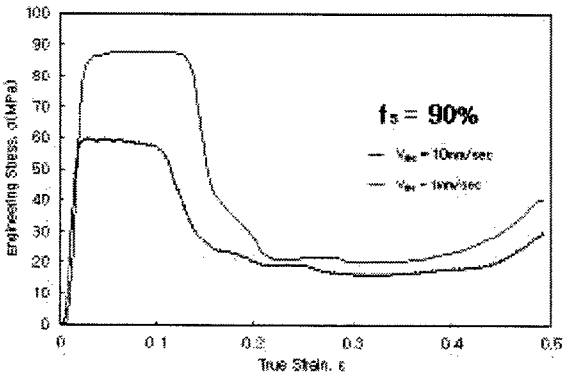


Fig.7. Engineering stress-true strain curve at f_S = 90% (Al2024) (V_d= 10 mm/sec to 1mm/sec)

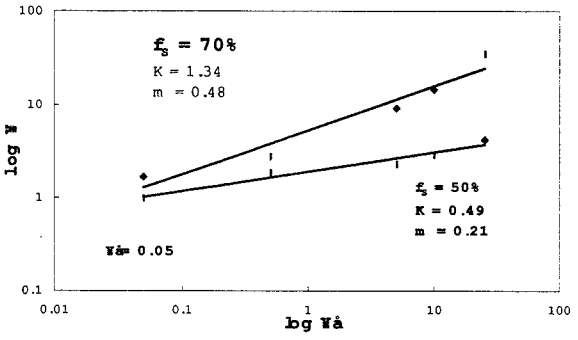


Fig.8. Relationship between logσ and log $\dot{\varepsilon}$ at f_S=50%, f_S=70% (Al2024)

Fig. 8 shows that the relationship of stress-strain rate represents that of algebraic coordinates(log ε-log σ) for compression experiments at solid fractions f_S of 70 and 50%, employing the definition of the coefficients K and m (flow stress equation: $\sigma = K \dot{\varepsilon}^m$). The K and m values are solved with linear regression to give the following:

- Solid fraction f_S = 50%: $\sigma = K \dot{\varepsilon}^m$: K = 0.49, m = 0.21 (Al2024)
- Solid fraction f_S = 70%: $\sigma = K \dot{\varepsilon}^m$: K = 1.34, m = 0.48 (Al2024)

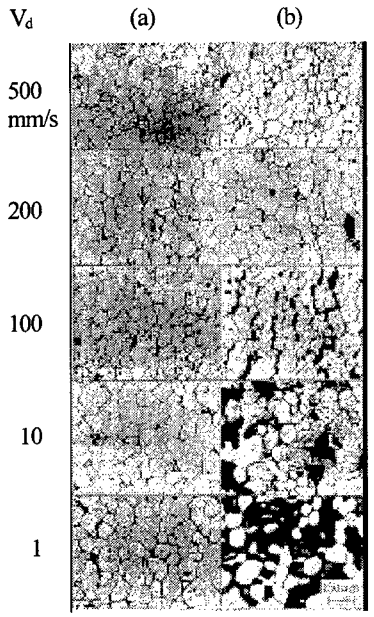
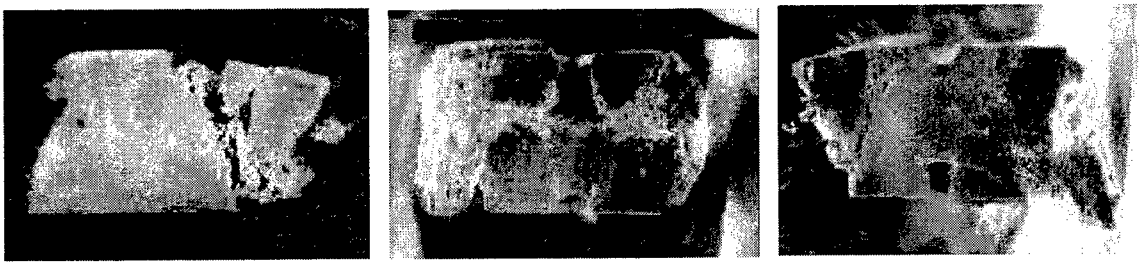


Fig.9. Evolution of the microstructure of semi-solid alloy as a function of variation in die speed (f_S = 50%, 620°C)
a. center **b.** surface

Fig. 9. a. and b. show structural photographs of specimen centers and surfaces compressed at different die velocity in the case of f_S = 50%.When the die velocity is over V_d=100mm s^{-1}, solid grains and liquid phase flow simultaneously, so solid grains are relatively homogeneous over the entire cross section. The compression deformation is observed in the middle part of the material by the sticking of solid grains and the relatively minute structure size.

Fig.10.a.~c. shows the flow state of specimen cross-sections at a height-reduction ratio of 50% for die velocities, V_d of 500mm s^{-1}, 100mm s^{-1}, 1mm s^{-1}. When die velocity, V_d is 500mm s^{-1} (Fig.10.a.), the separation phenomenon of solid and liquid phase is not observed, but when V_d = 1mm s^{-1} (Fig.10.c.), the separation phenomenon of solid and liquid phase is clear, so after deformation, the boundary includes significant porosity and liquid is distributed much around the surface.



a. V_d=500mm/sec b. V_d=100mm/sec c. V_d=1mm/sec

Fig.10. Microphotograph of cross-section compressed at f_S = 50% ,reduction ratio = 50%

Fig.11 shows the relationship between true strain and stress for variation in strain rate with A357 at a solid fraction of 50%. With a high strain rate of 0.588 sec^{-1}, the true strain to obtain maximum stress is 0.1. However, with strain rates below 29.4 sec^{-1}, the maximum stress occurs at a true strain of 0.15. The stress decreases remarkably from the maximum stress when the strain rate increases, as shown in Figures 5 and 6.

Fig12 shows the strain-stress curve for A390 alloy. Except for a strain rate of 0.588 sec^{-1}, the maximum stress is obtained at a true strain of 0.15. In the forming process for SSM, the strain rate should be controlled to increase the stress continuously according to the increase in strain rate at the position shown at the peak point of stress in Figures 5, 6, 11 and 12.

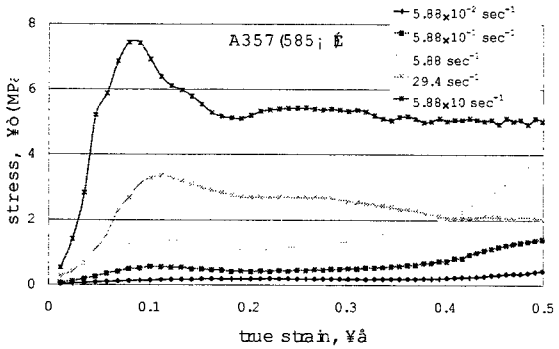


Fig. 11. Engineering stress-true strain curve (A357) for variation of strain rate at f_S = 50%

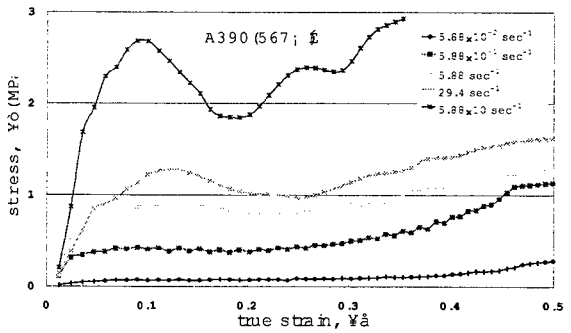


Fig. 12. Engineering stress-true strain curve (A390) for variation of strain rate at fs = 50%

To understand this phenomenon, the continuous increase in stress according to an increase in strain rate is investigated in another compression test. Fig.13 is the curve of stress-strain rate with various compression velocities at a strain, □ = 0.1. As can be seen, the stress increases continually for strain rates of 0.588, 2.353, 7.058, and 29.4 sec^{-1}. Fig.13 is the curve of stress-strain rate with various compression velocities at a strain □=0.1. As shown in Fig13, the stress increases continuously for compression test, when strain rate of , 5.88 $\times 10^{-2}$, 5.88 $\times 10^{-1}$, 2.353 and 7.058 sec^{-1} are to increase of 5.88 $\times 10^{-1}$, 2.353, 7.085 and 29.4 sec^{-1} respectively. When compression velocity changes, discontinuity point is found at strain, 0.17. The sharply decrease of stress is considered as an error of time needed to control velocity with high die speed change in Material Testing System. Fig.14 shows jumping strain rate values to obtain continuously increasing strain-stress curve. When initial strain is 5.88×10^{-2} sec , and first and second jump strain rate is 5.88×10^{-1} and 5.88 sec^{-1} respectively. As shown in Fig.13, the data error at the jumping point is also considered because of sensitivity of MTS due to velocity change.

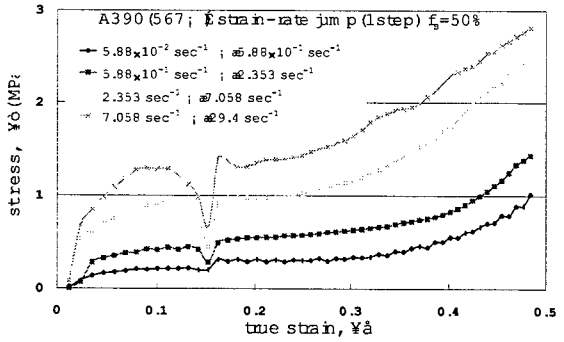


Fig.13. Engineering stress-strain curve obtained by varying the initial compression velocity to prevent liquid segregation.

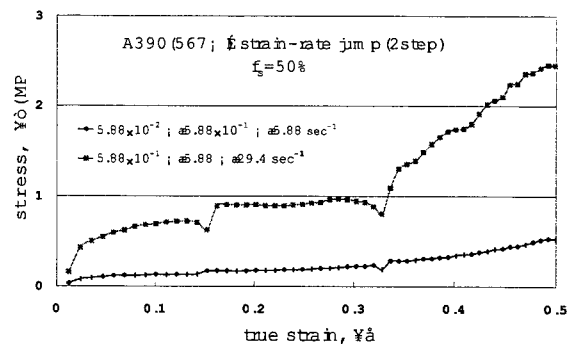


Fig.14. Engineering stress-strain curve obtained by varying the initial compression velocity at 0.588 s^{-1} and 0.0588 s^{-1} to prevent liquid segregation.

According to the above experiment, forming limitations are improved because the lower the solid fraction, the lower the load. It is known that distribution of the solid and liquid phase is homogeneous because of the no distinguished boundary at V_d = 100 mm s^{-1} as shown in Fig. 10.a.~c.

CONCLUSIONS

In the compression test of semi-solid aluminum materials, the following results were obtained from an investigation of the deformation and transformation of the macrostructure, with respect to the strain rate:

1. From the macrostructure change appearing in the compression behavior of SSM, a more homogeneous structure can be obtained with greater compressive velocity.

2. In the compression tests of SSM, macro-separation appears between the solid and the liquid regions because of outflow of the liquid state. Densification of the structure was observed in the center of the column , and reduced porosity at the surface was observed, with greater compressive velocity.

3. After compression forming of Al2024 alloy, the faster the deformation rate, the better the distribution of the solid and liquid phase. The critical rate to distribute solid and liquid phases homogeneously is about $V_d = 100$ mm s^{-1}.

4. From compression experiments using A357, A390 and Al2024, a database of semi-solid materials can be obtained to prevent liquid segregation, in the compression forming process, by changing the strain rate. This technique is suggested as an intelligent way to conduct compression experiments by control of the solid fraction and liquid phase flow conditions.

ACKNOWLEDGEMENT

This work has been supported by the Engineering Research Center for Net Shape and Die Manufacturing (ERC/NSDM) of Pusan National University which is financed jointly by Korean Science and Engineering Foundation(KOSEF)

REFERENCES

1. C.G. Kang, J.S. Choi ,D.W. Kang,1998. A filling analysis of the forging process of semi-solid aluminum materials considering solidification phenomena. *J. Materials Processing Technology*, 73, 289-302.
2. M.C. Flemings, 1991. Behavior of Metal Alloys in the Semi-Solid State. *Metallurgical Transactions*, 27A, 957-981.
3. D.B. Spencer, R. Merabian and M.C. Flemings,1972. "Rheology of Semi-Solid Dendritic Sn-Pb Alloys at Low Strain Rates", *Metall. Trans.*, 3, 1925-1932.
4. M. Suery and M.C. Flemings, 1982. Effect of Strain Rate on Deformation Behavior of Semi-Solid Dendritic Alloys, *Metall. Trans.*, 13(A),1809-1819.
5. S. Toyoshima, 1994. A FEM Simulation of Densification in Forming Processes for Semi-Solid Materials. *Proceedings of the 3rd Int'l Conf. on Processing of Semi-Solid Alloys and Composites*, University of Tokyo, 47-62.
6. C.G. Kang, B.S. Kang, and J.L Kim, 1998. An investigation of the mushy state forging process by the finite element method. *J. Materials Processing Technology*,80(81),444-449
7. M.P. Kenny, J.A. Courtois, R.D. Evans, G.M.Farrior, C.P. Kyonka, A.A. Couch, K.P. Young Semi-Solid Metal Casting and Forming, *Metals Handbook*, 9th Ed., 15, 327-338.
8. C. Yoshida, M. Moritaka, S. Shinya, S. Yahata, K. Takebayashi, A. Nanba,1992. "Semi-Solid Forging Aluminium Alloy", *2nd Int'l Conf. on Processing of Semi-Solid Alloys and Composites*, MIT, 95-102.
9. C.G. Kang, J.S, Choi, 1998. Effect of gate shape and forging temperature on the mechanical properties in the injection forging process of semi-solid aluminum material. *J. Materials Process. Tech.*,73, 251-63
10. C.P. Chen, X-Ya Tsao, 1996. Semi-solid deformation of A356 Al alloys. *Proceedings of the 4th International Conference on Semi-solid Processing of Alloys and Composites*, 16-20.

Adaptability to Frictional Change of Fuzzy Adaptive Blank Holder Control for Deep Drawing

S. Yoshihara*, K. Manabe and H.Nishimura****

*Tokyo National College of Technology, Dept. of Mech. Eng. , 1220-2 Kunugida-machi, Hachioji-shi, Tokyo 193-8610, Japan

**Tokyo Metropolitan University, Dept. of Mech. Eng., 1-1 Minami-ohsawa, Hachioji-shi, Tokyo 192-0397, Japan

ABSTRACT

Validity of the fuzzy adaptive variable blank holder force (BHF) control deep drawing system to frictional change in the process has been studied for steel sheet. The circular-cup deep-drawing experiment has been carried out using steel sheet (SPCD) with high anisotropy (r=1.57). To change the lubrication condition, the partial lubrication method was adopted using fluorine lubricant. The friction coefficient was evaluated by the plastic deformation model. It is confirmed for steel sheet that the BHF was properly controlled corresponding to friction change at the flange part.

INTRODUCTION

Friction between blank and tools in sheet metal forming is a very important process variable governing formability. Many studies on friction coefficient and lubrication conditions have been conducted. For example, the friction coefficient in deep drawing was determined from continuum plastic mechanics, and the effects of the material surface characteristics and the lubrication conditions were studied [1]. Friction coefficient between punch and blank was calculated from plastic deformation model by using the experimental results[2]. The results showed that the lubrication condition varied during the process. From the results, the process characteristics are also considered to vary due to variationin the friction coefficient.

The BHF as well as friction is a very important process variable to improve the product quality. In recent years, the variable BHF technique for suppressing the flange wrinkles was studied for circular-cup deep-drawing [3],[4]. Besides, the variable BHF method based on the fracture limit and a combined method with wrinkle and fracture limit curves were developed [5]. For a rectangular panel stamping, the effects of variable BHF were studied. However, variable BHF control system corresponding to frictional change during the process has not been studied in spite of affecting the drawing limit and the product quality.

In the previous study [6], we developed a fuzzy adaptive BHF control system in order to optimize circular-cup deep-drawing process and to improve the process flexibility coping with frictional change. Two evaluation functions and a constraint function for deciding the progress of deep-drawing process are used in the system. The BHF was calculated and inferred from the membership functions and if-then rule. Meanwhile, the friction coefficient between blank and tools was evaluated from the experimental results of aluminum alloy sheet by a newly proposed formulation based on the plastic deformation model. In the formulation, the following four factors were considered; a die contact angle with the thickness, the lifting-up behavior, the stretching at punch shoulder part and the change of contact boundary at the die hole with the progress of process. The lubrication types of the blank tested were fluorine coating, acetone degreasing and a combination of them for varying the friction state during the process. The calculated results of the friction coefficient agree well with the empirical results under the variable BHF condition as well as under the constant BHF condition. The results of fuzzy adaptive BHF control show that the BHF is adaptively controlled corresponding to the variation in friction for aluminum alloy sheet (A5182-O). By the way,

0-7803-5489-3/99/$10.00 ©1999 IEEE.

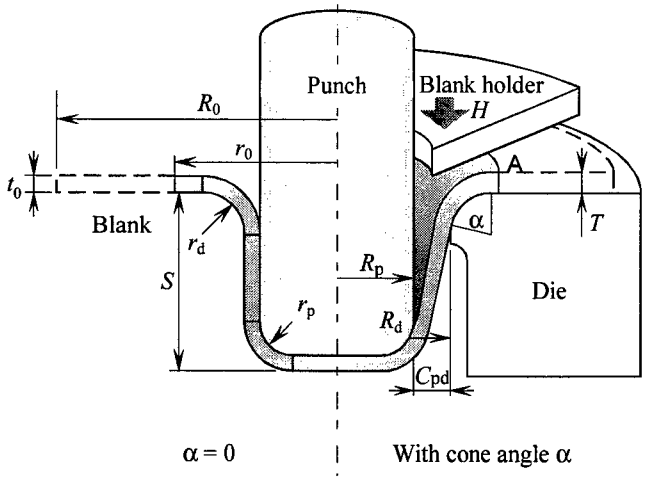


Fig.1 Geometrical shape of deformed blank

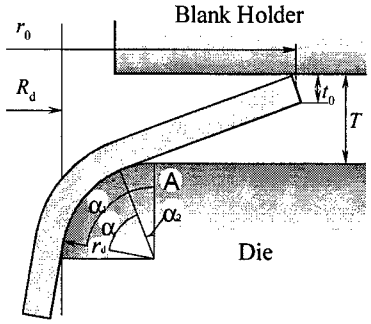


Fig.2 Schematic of blank at die shoulder part

aluminum alloy is a typical face centered cubic lattice (fcc) metal and has low plastic anisotropy (r-value<1). The alternative crystal structure is body centered cubic lattice (bcc) and the typical metal is steel with high plastic anisotropy (r-value >1). The objective of this study is to confirm that the fuzzy adaptive BHF control system achieves high reliability and adaptability to any frictional change for steel sheet with high r-value.

THEORY

In the circular-cup deep-drawing, taking account of the friction resistance at the flange caused by the BHF and the bending/unbending at the die shoulder, the drawing stress(radial stress) on an element at the die throat is given by,

Notation

ΔDR* : blank reduction ratio
DR : drawing ratio
R_0 : initial radius of circular sheet blank
r_0 : current radius of circular sheet blank
r_p : punch shoulder radius
R_p : punch radius
r_d : die shoulder radius
R_d : die hole radius
t_0 : initial blank thickness
t : blank holder displacement
S : punch stroke
α : cone angle body part
σ_{eq} : mean equivalent stress
ε_{eq} : mean equivalent strain
μ : friction coefficient

$$\sigma_{R_d} = e^{(\mu\alpha)}\left\{\sqrt{\frac{2(1+r)}{1+2r}}\bar{\sigma}_{eq}\ln\frac{r_0}{R_0}+\frac{\mu H}{\pi r_0 t}+\frac{\bar{\sigma}_{eq}t}{4r_d}\right\}+\frac{\bar{\sigma}_{eq}t}{4r_d} \quad 1.$$

The constitutive equation of the blank material is,

$$\bar{\sigma}_{eq} = C\bar{\varepsilon}_{eq}^{\,n} \quad 2.$$

The mean equivalent strain in the flange can be written using Mises-Hill 's associated equivalent strain and mean radius of the whole flange.

$$\bar{\varepsilon}_{eq} = \sqrt{\frac{1+r}{2(1+2r)}}\ln\left[\frac{R_0^{\,2}-r_0^{\,2}+\left\{\frac{r_0+R_d}{2}\right\}^2}{\left\{\frac{r_0+R_d}{2}\right\}^2}\right] \quad 3.$$

Punch load by using drawing stress is expressed by,

$$P = 2\pi R_d t\sin\alpha\left[e^{(\mu\alpha)}\left\{\sqrt{\frac{2(1+r)}{1+2r}}\bar{\sigma}_{eq}\ln\frac{r_0}{R_0}+\frac{\mu H}{\pi r_0 t}+\frac{\bar{\sigma}_{eq}t}{4r_d}\right\}+\frac{\bar{\sigma}_{eq}t}{4r_d}\right] \quad 4.$$

The above equation is re-expressed by Taylor expansion,

$$P = 2\pi R_d t\sin\alpha\left[(1+\mu\alpha)\left\{\sqrt{\frac{2(1+r)}{1+2r}}\bar{\sigma}_{eq}\ln\frac{r_0}{R_0}+\frac{\mu H}{\pi r_0 t}+\frac{\bar{\sigma}_{eq}t}{4r_d}\right\}+\frac{\bar{\sigma}_{eq}t}{4r_d}\right] \quad 5.$$

From the above equation, the quadratic equation on friction coefficient can be obtained as

$$\left\{\frac{H\alpha}{\pi r_0 t}\right\}\mu^2+\left\{\frac{\mu H}{\pi r_0 t}+\alpha\left(\sqrt{\frac{2(1+r)}{1+2r}}\bar{\sigma}_{eq}\ln\frac{r_0}{R_0}+\frac{\bar{\sigma}_{eq}t}{4r_d}\right)\right\}\mu+\left\{\sqrt{\frac{2(1+r)}{1+2r}}\bar{\sigma}_{eq}\ln\frac{r_0}{R_0}+\frac{\bar{\sigma}_{eq}t}{2r_d}-\frac{P}{2\pi R_d t\sin\alpha}\right\}=0 \quad 6.$$

Therefore, the friction coefficient can be written by,

$$\mu=\frac{-E+\sqrt{E^2-4DF}}{2D} \quad 7. \qquad D\mu^2+E\mu+F=0 \quad 8.$$

where,

$$D=\frac{H\alpha}{\pi r_0 t} \quad 9.a. \quad E=\frac{\mu H}{\pi r_0 t}+\alpha\left(\sqrt{\frac{2(1+r)}{1+2r}}\bar{\sigma}_{eq}\ln\frac{r_0}{R_0}+\frac{\bar{\sigma}_{eq}t}{4r_d}\right) \quad 9.b. \quad F=\sqrt{\frac{2(1+r)}{1+2r}}\bar{\sigma}_{eq}\ln\frac{r_0}{R_0}+\frac{\bar{\sigma}_{eq}t}{2r_d}-\frac{P}{2\pi R_d t\sin\alpha} \quad 9.c.$$

In **Fig.1**, the die contact angle α_1 can be expressed from the geometrical relationship between the die contact angle and punch stroke as,

$$\alpha_1=\mathrm{Cos}^{-1}\frac{-A_2+\sqrt{A_2^2-4A_1A_3}}{2A_1} \quad 10. \qquad A_1\cos^2\alpha_1+A_2\cos\alpha_1+A_3=0 \quad 11.$$

where

$$A_1=\frac{(S-r_p-r_d-t_0)^2}{(C_{pd}+r_p+r_d)^2}+1 \quad \textbf{12.a.} \quad A_2=\frac{2(r_p+r_d+t_0)(S-r_p-r_d-t_0)}{(C_{pd}+r_p+r_d)^2}+1 \quad 12.b. \quad A_3=\frac{(r_p+r_d+t_0)^2}{(C_{pd}+r_p+r_d)^2}-1 \quad 12.c.$$

Next, when the BHF is low, the die uncontact angle takes place as shown in **Fig.2** as the blank is lifted up by bending at the die shoulder part in a straight shape. The geometrical relationship between blank holder displacement and die uncontact angle is,

$$\tan\alpha_2=\frac{(T-t_0)+r_d(1-\cos\alpha_2)}{r_d\sin\alpha_2+\{r_0-(R_d+r_d)\}} \quad 13.$$

In Fig.2, the die uncontact angle α_2 can be expressed as

$$\cos\alpha_1=\frac{-A_2+\sqrt{A_2^2-4A_1A_3}}{2A_1} \quad 14. \qquad B_1\cos^2\alpha_2+B_2\cos\alpha_2+B_3=0 \quad 15.$$

where

$$B_1=\frac{(T-t_0-r_d)^2}{\{r_0-(R_d+r_d)\}^2}+1 \quad 16.a. \quad B_2=\frac{2(T-t_0-r_d)r_d}{\{r_0-(R_d+r_d)\}^2} \quad 16.b. \quad B_3=\frac{r_d^2}{\{r_0-(R_d+r_d)\}^2}-1 \quad 16.c.$$

The actual contact angle α is expressed by ,

$$\alpha=\alpha_1-\alpha_2 \quad 17.$$

BHF ADAPTIVE CONTROL

Figure 3 shows the block diagram of the fuzzy adaptive BHF control process. The computer can capture online the following five sensing data: punch load, punch stroke, maximum apparent thickness(blank holder displacement), punch speed and blank reduction ratio. The fuzzy rule is constructed by two evaluation functions (punch stroke curve and maximum apparent thickness curve) and one constraint function.

Punch stroke curve

An ideal punch stroke curve can be obtained geometrically by assuming constancy of the wall thickness. The evaluation function ϕ is the difference between actual punch stroke curve and the ideal curve, another evaluation function ϕ' is the differential coefficient of ϕ. An evaluation function ω_s is estimated from the combination of ϕ and ϕ'. When ω_s increases, the BHF has to decrease to minimize the evaluation function.

Maximum apparent blank thickness curve

Blank holder displacement which corresponds to blank thickness at the flange edge (maximum apparent blank thickness) was measured instead of the wall thickness distribution. The difference between maximum apparent blank and initial blank thickness is used as the evaluation function φ, whereas another evaluation function φ', is the differential coefficient of φ regarding to the flange wrinkling. Another evaluation function ω_t is employed from the combination of φ and φ'. When the ω_t increases, the BHF has

to increase to minimize the evaluation function.

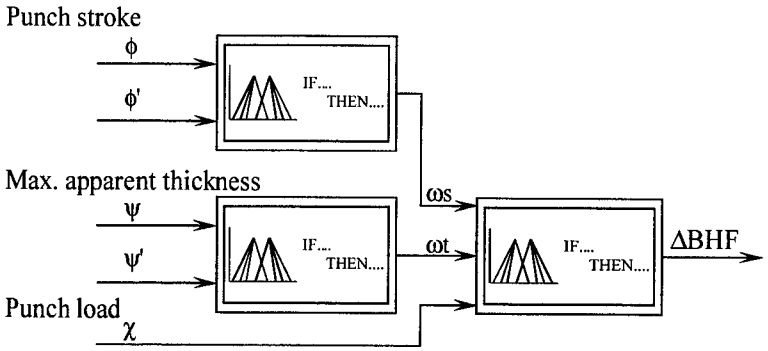


Fig.3 Fuzzy adaptive control block diagram for optimal BHF control system

Table 1 If-then rule for deciding the ΔBHF

IF (χ, ω_s, ω_t)	THEN (ΔBHF_{hij})
χ is PB and ω_s is LA and ω_t is LA	ΔBHF_{PLL}=0
χ is PB and ω_s is LA and ω_t is SM	ΔBHF_{PLS}=1.50
χ is PB and ω_s is SM and ω_t is LA	ΔBHF_{PSL}=-0.25
χ is PB and ω_s is SM and ω_t is SM	ΔBHF_{PSS}=1.00
χ is ZO and ω_s is LA and ω_t is LA	ΔBHF_{ZLL}=0
χ is ZO and ω_s is LA and ω_t is SM	ΔBHF_{ZLS}=0.50
χ is ZO and ω_s is SM and ω_t is LA	ΔBHF_{ZSL}=-0.50
χ is ZO and ω_s is SM and ω_t is SM	ΔBHF_{ZSS}=0
χ is NS and ω_s is LA and ω_t is LA	ΔBHF_{SLL}=0
χ is NS and ω_s is LA and ω_t is SM	ΔBHF_{SLS}=3
χ is NS and ω_s is SM and ω_t is LA	ΔBHF_{SSL}=-0.25
χ is NS and ω_s is SM and ω_t is SM	ΔBHF_{SSS}=2.00
χ is NB and ω_s is LA and ω_t is LA	ΔBHF_{BLL}=0
χ is NB and ω_s is LA and ω_t is SM	ΔBHF_{BLS}=6.00
χ is NB and ω_s is SM and ω_t is LA	ΔBHF_{BSL}=-0.25
χ is NB and ω_s is SM and ω_t is SM	ΔBHF_{BSS}=3.00

Table 2 Mechanical properties of SPCD sheet used

Yield Stress σ_S N/mm^2	Tensile Strength σ_B N/mm^2	Breaking Elongation %	* C value N/mm^2	n value	r value
173	311	51.3	522	0.22	1.57

* see Eq. (2)

Table 3 Lubricating pattems of blank

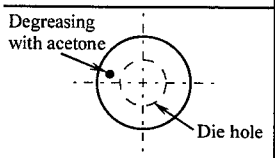
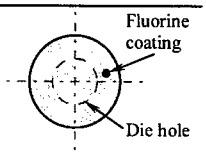
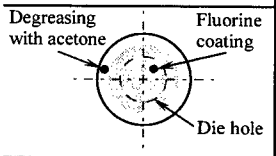
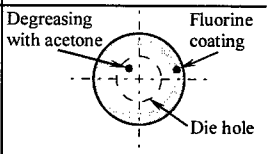
1) Degreasing with acetone(Acetone degreasing)	2) Fluorine coating (Fluorine)
	
3) Inner fluorine (Fluorine/Degreasing)	4) Outer fluorine (Degreasing/Fluorine)
	

Table 4 Specification of punch and die used in the experiment

Punch shoulder radius r_p mm	4
Punch diameter D_p mm	33
Die shoulder radius r_d mm	3
Die diameter D_d mm	36.5

Constraint function

Constraint function decides the progress of deep drawing process. The controlled BHF value was calculated and inferred by the fuzzy logic using above mentioned two evaluation functions and the constraint function in order to achieve optimal control during the process even though the friction changes. The controlled increment of BHF is calculated by the algebraic production-barycenter method from a combination of the membership function and the if-then rule as shown in **Table 1**.

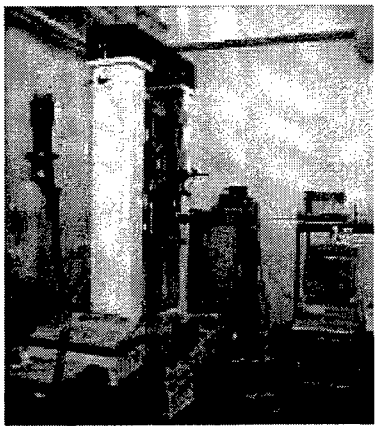


Fig.4 Photograph of deep drawing system

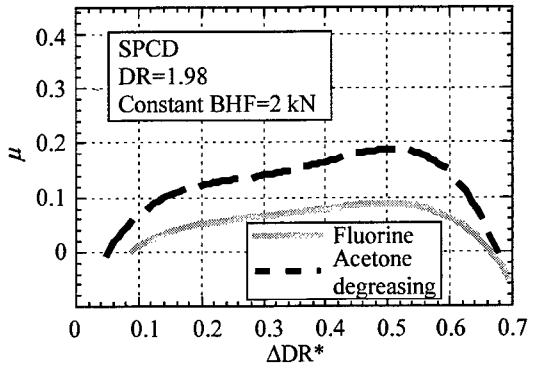


Fig.5 Effect of lubrication conditions of friction coefficient μ-ΔDR* relation (Constant BHF test)

EXPERIMENT

Steel sheet for deep drawing (SPCD) of 1.0 mm thickness was employed in the experiment. The material properties of the blank are listed in **Table 2**. The drawing ratio of the blank used is 1.98. The lubricating patterns used are dry fluorocarbon (spray type) and degreasing with acetone as shown in **Table 3**. The deep drawing apparatus is capable of the computerized control of BHF and punch speed in the deep drawing process, which was already developed by the authors [6]. This system is equipped with several sensors; punch displacement, punch load, blank holding force, blank holder displacement and radial drawing displacement of blank flange. **Figure 4** shows a photograph of the deep drawing control system. The specifications of die and punch used are shown in **Table 4**. All the experiments were conducted under the punch speed of v=5mm/min.

RESULTS AND DISCUSSION

Figure 5 shows the friction coefficient μ estimated in a constant BHF (2kN) test for two different lubrication conditions of the acetone degreasing and fluorine. The mean value of μ in the case of the acetone degreasing is approximately 0.15, while the case of the fluorine 0.05. The relationship between μ and the lubrication proves valuable results because the anisotropy of the steel sheet is taken into consideration. **Figure 6** shows the punch load and BHF-ΔDR* curves, in a fuzzy adaptive BHF control test with three types of lubrication; acetone degreasing, the fluorine and a combination of them (as shown in Table 3). In the combination (degreasing/fluorine), punch load curve is very close to the case of the acetone degreasing type during initial stage (until about ΔDR*=0.2). However, from the middle to the last stage, the punch load curve gradually decreases more than the acetone decreasing type and approaches to the fluorine result. Contrarily, the behavior of the fuzzy adaptive BHF curve is very close to the case of the acetone degreasing in the early stage, but in the middle to the last stages, decreases more than the acetone decreasing and approaches to the fluorine, which is the same as in the case of the punch load curve. As a result, it is confirmed that the adaptive BHF is appropriately controlled to cope with the frictional change. **Figure 7** shows the variation in μ predicted by Eq. (7) for four lubricating types. In the case of acetone degreasing, μ is the highest and fluorine the lowest. Meanwhile, the result of combined lubrication shifts to the alternative state on the way corresponding to the lubricating patterns. From the results, it is confirmed that the fuzzy adaptive BHF control system is valid for steel sheet with high r-value as well as aluminum alloy [7] and possesses high adaptability to friction change during the process.

CONCLUSIONS

1. The fuzzy adaptive BHF control deep drawing system can achieve high reliability and adaptability to any friction condition including frictional change during the process for steel sheet with high r-value.
2. The anisotropy of blank material has to be considered in order to evaluate the friction coefficient.
3. The friction evaluation formula from a simple plastic model is confirmed to be effective for steel sheet, using the partial lubrication combination of acetone degreasing and fluorine.

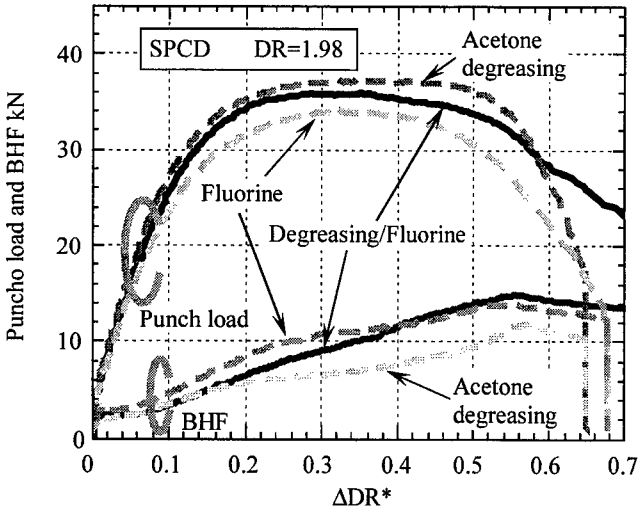


Fig.6 Punch load and BHF vs. ΔDR* curves

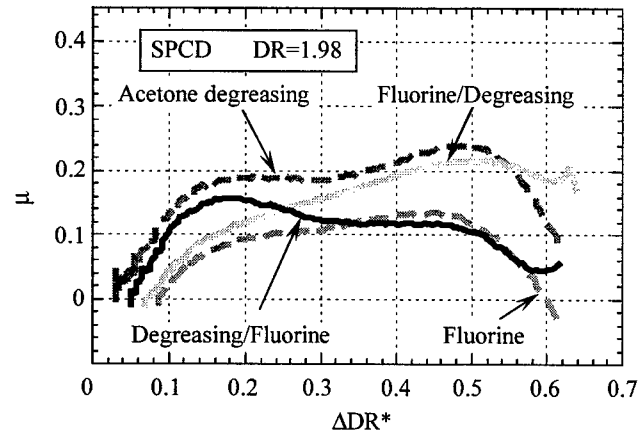


Fig.7 Effect of lubrication conditions on friction coefficient m-DDR* relation (Fuzzy adaptive BHF control test)

REFERENCES

1. B. Kaftanoglu, 1973. Determination of Coefficient of Friction under Conditions of Deep-Drawing and Stretch Forming. *Wear*, 25, 177.
2. S. Rajagopal, 1981. A Deep Drawing Test for Determining the Punch Coefficient of Friction. *Trans. ASME J. Eng. Ind.*, 103, 197.
3. N. Kawai, 1961. Critical Conditions of Wrinkling in Deep Drawing of Sheet Metals. *Reports 1,2 and 3, Bull. J.S.M.E.*, 4, 169.
4. S. Thiruvarudchelvan and J. Gan, 1994. Drawing of Hemispherical Cups with Friction-actuated Blank Holding. *J. Mater. Process. Technol.*, 40, 327.
5. Y.W. Wang and A. Majilessi, 1994. The Design of An Optimum Binder Force System for Improving Sheet Metal Formability. *Proc. 18th IDDRG Biennial Congress*, 491.
6. S. Yoshihara, K. Manabe, M. Yang, and H. Nishimura, 1997. Fuzzy Adaptive Control of Circular-Cup Deep-Drawing Process Using Variable Blank Holder Force Technique. *J. JSTP 38-435 (in Japanese)*, 46.
7. S. Yoshihara, K. Manabe, and H. Nishimura, 1998. Fuzzy Adaptive Control of Blank Holder in Circular-Cup Deep-Drawing (Adaptability to Frictional Change and Simple Evaluation Lubrication). *Trans. JSME 64-624 (in Japanese)*, 3209.

AN AI PROCESS CONTROL SYSTEM WITH SIMULATION DATABASE AND ADAPTIVE FILTER FOR V-BENDING

Ming Yang*+ , Atsushi Katayama*, Ken-ichi Manabe*, Naoyuki Aikawa**

* Department of Mechanical Engineering, Tokyo Metropolitan University,
1-1 Minami-osawa, Hachioji-shi, Tokyo, 192-0397, Japan
+ E-mail yang@mech.metro-u.ac.jp
** Department of Electronics, Faculty of Engineering, Tokyo Engineering University,
1401-1 Katakura, Hachioji-shi, Tokyo 192-8580, Japan

ABSTRACT

In this study, an artificial intelligence (AI) V-bending process control system with a numerical simulation database and adaptive filter was proposed and developed to achieve production with high accuracy and flexibility. The punch force-stroke curve (F-S curve) which includes process information in a compound manner is stored in the database as expertise and applied to evaluate and control the process. An FEM code was used to simulate the V-bending process to obtain the F-S curve during loading and the springback value during unloading of the process. An online adaptive filter was applied to modify the simulated F-S curve and the simulated springback value. Furthermore, the concept of multi-regional filter is proposed to improve filtering accuracy. The modified F-S curves and springback values are stored in the database as pseudo-experimental ones, and used in the V-bending process control with an intelligent process control system. The AI control system of the V-bending process was evaluated using four kinds of materials as workpieces. Results show the FEM simulation database with online adaptive filtering is very effective for precision control. A high accurate V-bending process was achieved without the trial of V-bending tests.

Keywords: V-bending, database, F-S curve, FEM simulation, online adaptive filter, AI process control

INTRODUCTION

In sheet metal forming, the processes which adapt to the production of the variety and small batches of parts are requested. The accuracy is also important for automation of the process. However, in a metal forming process, there may contain errors from unexpected variations in tool characteristics or in the incoming workpiece. The sheet metal forming processes still depend on the manufacturing craftsmen in practical production because of the complexity of metal deformation and the unexpected variations. The craftsmen ponder the correctness of the setup and judge whether changes should be made. During the process, they use the blend of sensory skills that include vision, touch, sensitivity of forces and so on, to measure whether the process is proceeding along according to plan. After a part is made, they measure it and then reevaluate the tools and other process control parameters. In doing so, the craftsmen are learning and relating to the underlying form of the machine and the process [1]. In the V-bending process, setup of the machine and the tool significantly depends on thickness and material properties of the workpiece. In a practical process, the craftsmen adjust tools or control parameters to compensate for variations in the thickness, material properties and other conditions with their skills and expertise. Process control is concerned with monitoring in-process forming states and making adjustments to account for variations.

In this study, an intelligent control system with a simulation database and an online adaptive filter was proposed and developed for precise V-bending process. In addition of the database, an adaptive filter and a fuzzy inference model are included in the control system. Here, the fuzzy inference model with the database corresponding to the craftsmen's skills and expertise. An online adaptive filter was developed to modify the simulated F-S curve and the simulated springback value in-process. Furthermore, a multi-regional filter was proposed to improve the filtering accuracy. The developed control system was evaluated by using bending tests with several kinds of materials and without any trial of V-bending tests.

0-7803-5489-3/99/$10.00 ©1999 IEEE.

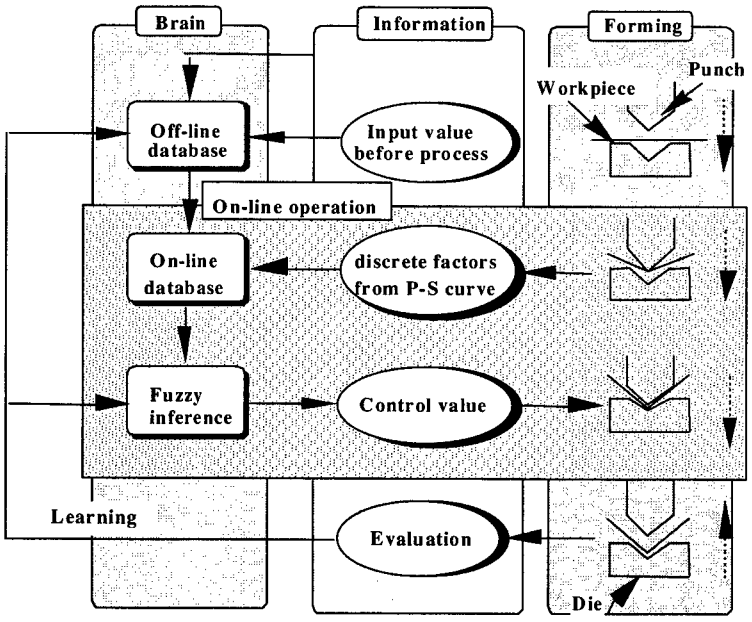


Fig. 1. Concept of intelligent V-bending process control system with database and fuzzy inference model.

INTELLIGENT V-BENDING PROCESS CONTROL SYSTEM WITH SIMULATION DATABASE AND ONLINE ADAPTIVE FILTER

Figure 1 shows an intelligent control system with expertise developed by the authors in order to compensate for variations in thickness and material properties of the workpiece and also in the machine and tool conditions [2]. Here, a database and a fuzzy inference model corresponding to the craftsmen's skills and expertise were applied to on-line process control. In this system, the punch force stroke curves (F-S curves) were measured in-process and stored with other factors, such as bend angle, tool conditions, and ambient temperature, to the database. Figure 2 shows the F-S curves measured for different materials. Discrepancies between the curves correspond to with variations of the geometrical conditions, material and other parameters in a compound manner. The fuzzy inference model for evaluation of the F-S curves corresponds to blend the sensory information synthetically for decision of the process conditions.

For the widely applicable and robust process control, the authors proposed to utilize FEM analysis to simulate the V-bending process in order to construct a simulation database for the control system. Since the FE analysis is widely applied in order to simulate the metal forming processes and its accuracy has significantly been improved in this decade [3], an FEM code is applied to simulate the V-bending process. The concept of the system with the simulation database is shown in Fig.3 [4]. The system consists of an FEM simulator, a simulation database, and an online adaptive filter in addition to the control system as shown in Fig.1. Prior to the V-bending operation, simulation of the process is carried out using a series of the material properties of the workpiece to cope with scattering in the material properties. The simulated results are stored in the simulation database. During the V-bending process, the in-process measured parameters, punch force and stroke, are compared with ones in the database. The discrepancies between the simulated and experimental parameters are evaluated and applied to design an adaptive filter in compensation for the simulation results in the database and then, the filtered simulation results are put in the fuzzy inference model for the process control.

Since the simulated V-bending process only depends on deformation characteristics of the workpiece not on the characteristics of bending machine, it is easy to be applied to various machines by evaluating machine properties and designing an adaptive filter for the particular machine. Figure 4 shows the conceptual adaptive filter for simulation database of V-bending processes with various machines. The signals in the simulation database are converted to the database for each machine by combining with signals of the machinery properties. Conversely, the signals in the database for a particular machine can be also divided to the signals on the deformation of workpiece and on the machine. As a practical application,

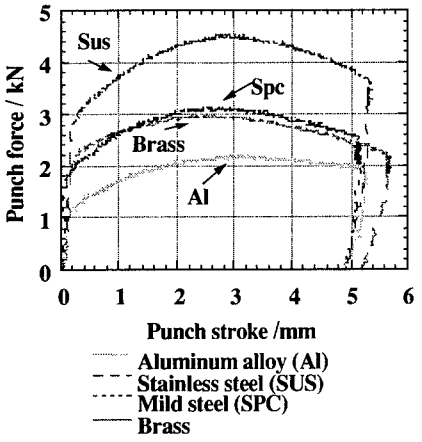


Fig. 2. F-S curve for various materials

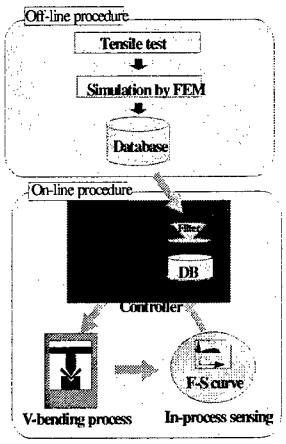


Fig. 3. Concept of intelligent V-bending process control system with simulation database

a database of any old machine can be convert to one for a new machine by abstracting the information from the old machine and then combining with the information about the new machine.

Characteristics of the process control system with simulation database and adaptive filter are as follows:

- All of the information in the database are obtained for the basic material properties by tensile test, and thus trial and error of the V-bending tests are not necessary even for new materials.

- Reliability of the filtered simulation information may become as high as the experimental one.

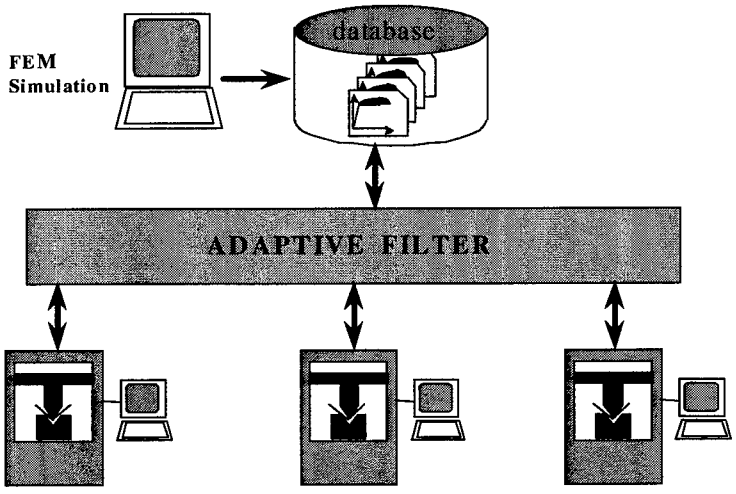


Fig. 4 Application of adaptive filter for different machines

- Since the database are constructed by the FEM simulation, the data distribution corresponding to the scattering range of the material properties and the process conditions can be easily designed and obtained. The information uniformly distributed in the database is important for high accurate process control [5].

- It is easy to convert the simulation database to any bending machine, or convert the database of old machine to the new one for saving resources and time.

COMPENSATION OF SIMULATION RESULTS WITH ONLINE ADAPTIVE FILTER

The authors proposed an online adaptive filter to compensate the process information of the simulation in this study. The proposed online adaptive filter was designed in order to modify the calculated F-S curve and springback value of V-bending process. Figure 5 shows the flow of modification by the adaptive filter. Both calculated and online measured experimental F-S curves are transformed into frequency domain by FFT. The spectrums of the two curves are compared and the differential spectrums are employed to design the filter. A multi-regional filter is newly proposed to improve the accuracy of filtering in this study. The concept of modification of F-S curve with the multi-regional filter is shown in Fig. 6. The F-S curve of V-bending process can be divided to three different areas, which are elastic deformation area, around yielding area and plastic deformation area. The dominant spectrums differ from each other in the different areas. Therefore, applying adaptive filters to the three areas respectively could significantly improve the filtering accuracy. The modified F-S curve is, then, transformed to the pseudo experimental curve by inverse FFT.

Figure 7(a) shows the calculated punch force-stroke curve (F-S curve) in comparison with the experimental one. The figure shows that there are some discrepancies between the two curves, and the discrepancies are not uniform along the curves due to the transition of deformation of the workpiece. Figure 7(b) shows a comparison of a modified (pseudo experimental) F-S curve and corresponding experimental one. It is seen that the pseudo experimental F-S curve completely coincides with the experimental one compared to the unfiltered one. Therefore, the database with the pseudo experimental F-S curve can be used in the process control with accuracy equivalent to the experimental one.

Since the simulated punch strokes for the desired bend angles also include errors, which do not appear on the F-S curve, it is necessary to compensate for the calculated punch stroke for the desired bend angle as well as for the F-S curve. Figure 8 shows the calculated and experimental punch strokes vs. the bend angle around 90 degree. It is due to the same reasons discussed previously about the springback analysis. In this study, both calculated and experimental punch stroke are assumed to be inversely proportional to the bend angle, respectively and the slopes of the two lines to be the same. The coefficients in the filter were applied to compensate the punch stroke and bend angle relationship.

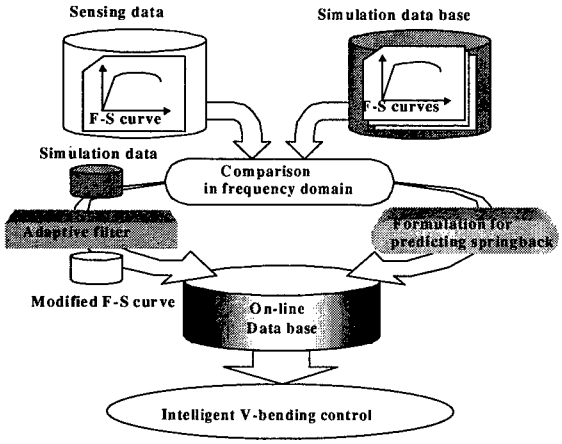


Fig. 5. Configuration of F-S curve modification with online adaptive filter

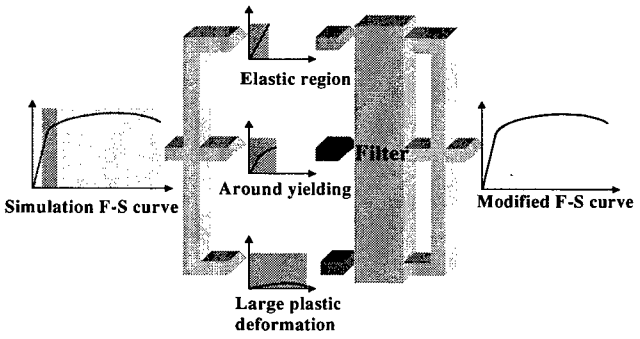


Fig. 6. Modification of F-S curve with multi-regional filter

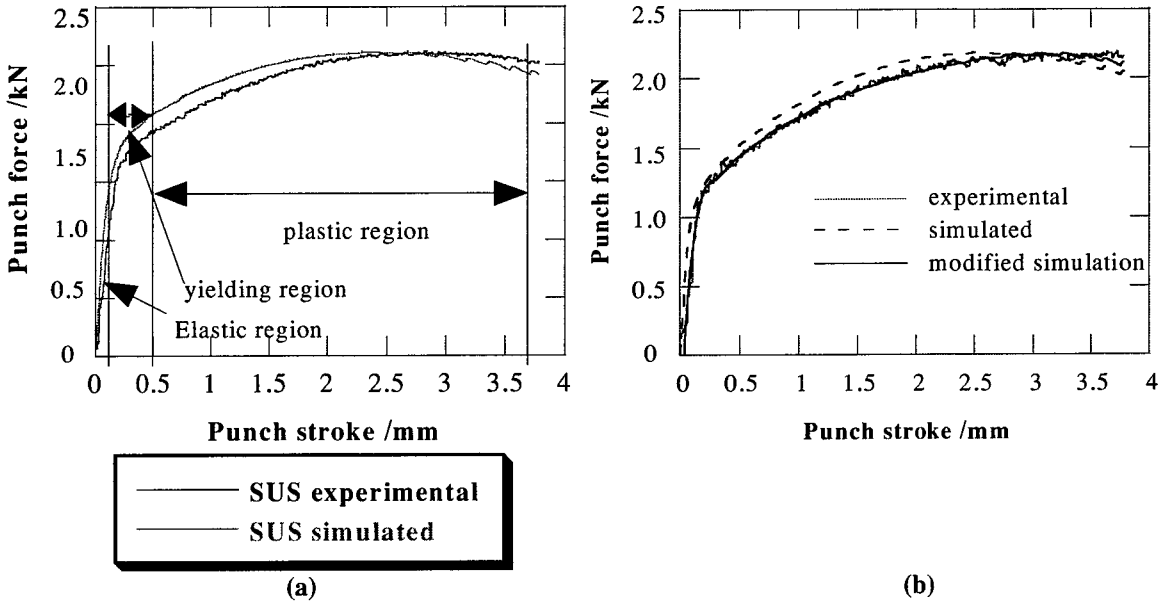


Fig. 7 modification of F-S curve by multi-regional adaptive filter（SUS304）

EVALUATION OF PROCESS CONTROL MODEL

An offline evaluation of the V-bending process control system was implemented by using the experimental results of four kinds of materials as the workpiece. The materials used are aluminum alloy (A5182-O), mild steel (SPCD), brass (C6000-O) and stainless steel (SUS304). **Figure 9** shows the accuracy of the bend angle obtained by the intelligent process control system with the simulation database and the online adaptive filter. The results show that almost of bend angles ranged in 90±0.25 degree and scatters in the workpieces of the same material were very small. A very high accurate V-bending process was achieved although the information in the database was provided only by the simulation without a trial of bending. It is confirmed that the simulation database with the online adaptive filter is very effective for the control system, and the multi-regional filter copes with various materials without reduction of the accuracy. Furthermore, the concept of AI process control with filtered simulation database can be applied to the other metal forming process controls as well.

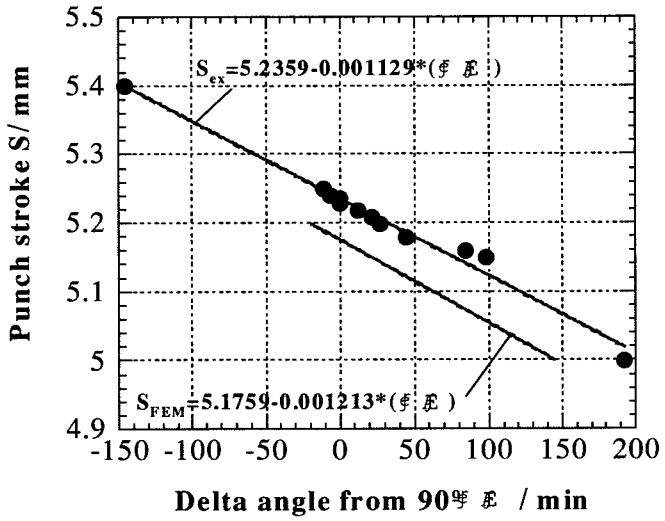


Fig. 8. Comparison of experimental and simulated punch stroke-bend angle relationship around the desired bend angle 90 degree

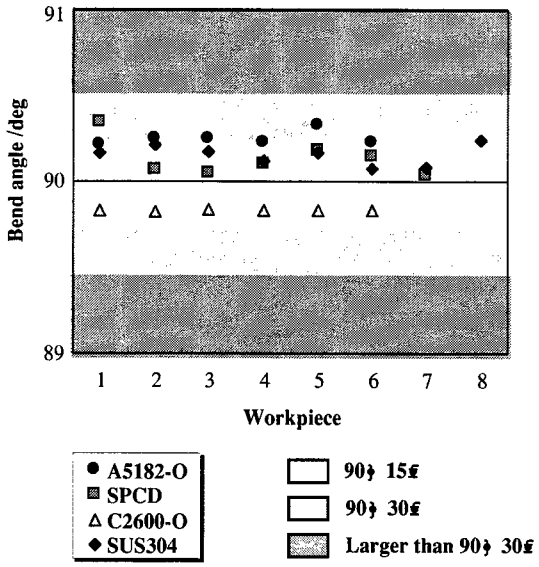


Fig. 9. Offline Evaluation of process accuracy controlled using adaptive filter

CONCLUSION

An intelligent control system with a simulation database and an online adaptive filter was proposed and developed for precise V-bending process. An online adaptive filter was developed to modify the simulated F-S curve and the simulated springback value in-process. Furthermore, a multi-regional filter was applied to improve the filtering accuracy. The evaluation results show that the simulation database with the online adaptive filter is very effective for the precision process control. A high accurate V-bending process was achieved without any trial of V-bending tests.

ACKNOWLEDGEMENTS

The authors would like to thank Amada Foundation for Metal Work Technology for supporting this work. Thanks are also due to Dr. H. Ogawa of Polytechnic University for his kind advice on the FEM simulation.

REFERENCES

1. P. K. Wright, D.A. Bourne, 1988. Manufacturing Intelligence, Addison Wesley.
2. M. Yang, N. Kojima, K. Manabe, H. Nishimura, 1997, JSME int. J. Series C, 40(1), 157-162.
3. A. Makinouchi, 1996, J. Materials Processing Technology, 60, 19-26.
4. M. Yang, K. Manabe, 1998, J. Metals and Materials, 4(3), 315-318.
5. M. Yang, K. Manabe, H. Nishimura, 1996, J. Materials Processing Technology, 60, 249-254.

Intelligent Manufacturing II

The Distributed Intelligent Control of Complex Systems

Wayne J. Davis

Professor of General Engineering,
University of Illinois at Urbana-Champaign,
Urbana, IL 61801

ABSTRACT

This paper begins by discussing the relationship of planning and control, the notion of intelligent control, and the need for the distributed intelligent control of complex systems. The paper then discusses an architecture for the distributed intelligent control architecture. The first step is to define a modeling paradigm that will recursively decompose the overall system into a collection of subsystems where intelligent control exists. Next, the structure of the intelligent controller is defined, focusing on the process of task assignment, planning and execution.

INTRODUCTION AND PROBLEM STATEMENT

Throughout the last fifty years, the engineering/scientific community has witnessed numerous advances in control and planning technologies. In certain cases, these advancements have evolved from new analytical approaches. For example, in the planning area, new interior search algorithms were developed for solving the linear programming problem. In the control field, H^{∞} control procedures represent a new approach in which a rich analytical foundation has been developed. In other cases, however, the new technologies have been more dependent upon computational advances. In planning, genetic and evolutionary programming algorithms are certainly dependent upon such advances. Similarly, artificial neural nets and fuzzy control methods are highly dependent upon the advances of our computational capabilities.

Despite continued improvements in planning and control technologies, these areas continue to be viewed as distinct from each other. Yes, there have been interactions between the two technologies, i.e., mathematical programming procedures have been employed to solve constrained optimal control problems. Similarly, optimal control approaches have been applied in planning. During the 70s, there were embryonic efforts to integrate these technologies through a comprehensive general systems approach. A few authors such as Cannon, Callum and Polak [1] addressed the relationships between planning and control in a direct fashion.

Perhaps, the major reason that planning and control technologies are still viewed as being distinct from each other results from the mindset that the practitioners of these technologies adopt while solving their respective problems. Planners are typically interested in formulating a plan, but seldom specify the manner by which the plan will be implemented. On the other hand, designers of control systems often begin with a desired behavior and then employ control approaches to generate this behavior. In a certain sense, practitioners of each technology are really looking at one half of a problem.

In the last decade, new intelligent control technologies have evolved. The goal of intelligent control is to integrate planning and control in order to permit a system to plan and execute its response in an on-line fashion. The intelligent control approach should be contrasted against the more classical optimal control approach that begins by developing an optimal course of action in an off-line setting and then attempts to implement that action by employing the generated control law. Intelligent control, however, recognizes the fact that the planning problem are dependent upon the current state of the system. The current state of the system, in turn, is influenced by control inputs derived from the application of a control law as well as external inputs into the system. There is often uncertainty in the response of the system. For example, external inputs to the system are often difficult to predict. Usually, one compensates for this uncertainty by employing feedback control techniques. However, in other cases, the current planning problem is modified to such an extent that a new control policy should be sought.

0-7803-5489-3/99/$10.00 ©1999 IEEE.

Bishop, Shirkey and Spong [2] developed an interesting example of intelligent control when they designed a controller that would permit a robot to play air hockey. Using a vision system, the control system first computed the trajectory of the incoming puck. Next, it computed the optimal trajectory for the robotic arm so that it intercepted the incoming puck and returned it toward the opponent's net. It is obvious that each time the robot responded to the incoming puck, it needed a new trajectory to follow. Thus, planning had to be addressed in an on-line fashion and was certainly dependent upon the state of the system (i.e. the trajectory of the incoming puck).

Today, intelligent control is usually employed to supervise or coordinate actions of one or more processes whose state evolution can be described via differential equations. That is, the subordinate processes are continuous state systems. Seldom has more than one level of supervisory control been considered.

On the other hand, modern advancements in computer technology have led to the design or contemplation of far more complex systems such as advanced manufacturing systems, transportation systems and so forth. The complexity of these systems necessitates that the overall supervisory/management function be addressed in a distributed manner. That is, an ensemble of controllers must be defined and coordinated within a comprehensive control architecture. While some of the controllers supervise processes, others supervise other controllers. An effective control architecture should possess the following properties:

- It allows the user to specify high-level tasks, which are then recursively decomposed into more detailed tasks that are eventually executed.
- It considers planning and problems on multiple time scales and at multiple levels of detail. That is, planning and control become multi-resolutional in nature.
- It allows complex functional behaviors to be decomposed into more manageable subfunctions.
- It also permits a given management function to be distributed across several intelligent controllers.

If one looks at each of these properties, one observes that each addresses a different type of decomposition. The first property deals with task decomposition. The second property considers both temporal decomposition as well as aggregation/disaggregation principles. In the third property, functional decomposition is considered. Finally, spatial decompositions are addressed. The important observation is that a well-designed control architecture must address all the above decomposition modes concurrently.

We have also introduced a new element to our planning and control problem with the inclusion of tasks. Although most people easily understand the concept of a task, its consideration within conventional planning and control procedures is not a trivial concern. Most control algorithms presume that the system's dynamics can be described by a set of differential or difference equations. However, when tasks are being considered, the system response includes discrete events where the system state can change abruptly. Examples of events include the start and finish of a task as well as points in time where controllers interact with each other. The resulting discrete-event nature of these systems invalidates the application of conventional control algorithms to these systems.

The inclusion of tasks also complicates planning because there are additional concerns to be addressed.

- Decomposition of high-level tasks into more detailed subtasks requires definition of comprehensive relationships among the tasks.
- Detailed instructions are required to execute each individual task by any process within the managed system.
- Planning must define which processing resource executes each task and then schedule its execution.
- Often, execution of a task by a given process will require additional physical entities and resources to be assembled at the processing resource. That is, the decision to execute a task at a given process may generate additional tasks that must be executed before and after the target task is executed.

The ability to consider all the constraints is well beyond the scope of most current planning procedures. Invariably, simplifications must be made which diminish the ability to specify a feasible plan, i.e, what is planned cannot be implemented. The inherently infeasible nature of the generated plans further contributes to the uncertainty of system response which, in turn, makes control requirements more difficult to address.

Finally, current planning practices seldom consider implementation concerns while formulating the plan. Rather the plan is passed to another control element that attempts to implement the plan until deviations between the planned and actual response become so large that replanning is needed. In reality, planning is constantly trying to catch up to the system response, and the system is never in control.

Not only is there concern about integrating planning and control in a logical manner at a given controller; but there is additional concern to distribute the integrated planning and control function across several intelligent controllers. After the planning and control functions are distributed, the implemented control architecture must provide mechanisms by which the controllers can interact so that a coordinated response is generated. Again, the requirements for distributing planning and/or control in this complex task execution environment are well beyond current technological capabilities.

Perhaps the most troubling issue is that our current simulation capabilities do not permit us to model the behavior of a system while it operates under a given control architecture [3]. So, not only is there little theoretical guidance to specify the required architecture, there is no means to test a particular architecture. Often, the first test of a system's behavior occurs when it becomes operational. It is often too late or too costly to make changes.

Given the current state of affairs, a chasm has developed between the theorist and the practitioner. The need to design and implement complex systems is increasing important. Today, control systems are being designed for complex systems on an ad hoc basis with little or no theoretical guidance. The resulting systems often fail to meet their expectations.

OUR INTEGRATED SOLUTION

Due to the complexity of the current state of affairs, there is no simple fix. Major advancements are needed in the areas of system modeling, planning and control. More importantly, however, there is a need to integrate these historically distinct topics into a unified approach for designing and implementing the distributed intelligent control architectures that are needed to manage these systems. In the remainder of this paper, we will discuss our approach to this problem.

The central element of the integrated solution is a new modeling paradigm. This modeling approach begins with a view of a large scale-system as a system of system. Using object-oriented modeling practices, we define a standard modeling template that can be recursively employed to decompose the overall system into its constituent set of subsystems. The basic modeling template, the coordinated object, is shown in Fig. 1. The coordinated object includes several critical elements. First, we assume that there is a set of processing subsystems, P1 through PN, where processing tasks will occur. We further assume that the processing tasks will be performed upon or with the assistance of other physical entities. These physical entities enter the coordinated object and join the input queue. When they enter, the coordinated object's supervisor specifies a set of tasks to be performed upon the entities. Hence, there are two distinct flows to be considered: the flow of physical entities and the flow of tasks.

Each coordinated object also contains a set of interfacing subsystems that perform tasks supporting implementation of tasks at processing subsystems. For example, a material handling system can move a job entity between processing substations. Each coordinated object also contains an intelligent controller.

The intelligent controller is responsible for receiving the tasks from the coordinated object's supervisor as each entity arrives at the coordinated object. These tasks are then decomposed while additional supporting tasks are defined and then reassigned to the processing and interfacing subsystems for execution.

Several forms of decomposition must be addressed simultaneously. The coordinated object handles those decompositions that deal with physical elements of the system. Particularly, definition of the processing and interfacing subsystems generates both functional and spatial decomposition. Note for example, that the processing subsystems execute processing tasks while the interfacing subsystems execute tasks that support execution of processing tasks. It is obvious that a functional decomposition has been employed. Note that the processing and interfacing subsystems are typically distinct from one other. Hence, a spatial

decomposition occurs as well. The other decompositions include task, aggregation/disaggregation and temporal decompositions. These occur within the intelligent controller that we will discuss shortly.

The modeler can recursively employ the coordinated object to decompose complex systems into its most basic processes. That is, any subsystem within a given coordinated object can also be viewed as a coordinated object. This gives rise to what we have termed the Recursive Object-Oriented Coordination Hierarchy (ROOCH). In Fig. 2, we provide the ROOCH for the Rapid Acquisition of Manufactured Parts flexible manufacturing system operated by the US Army Tobyhanna depot. It is self-evident that the ROOCH captures the system of system nature for these complex systems.

We can cover only briefly the concept of the Coordinated Object and the ROOCH in this paper. The reader is referred to Davis [3] for a more detailed discussion.

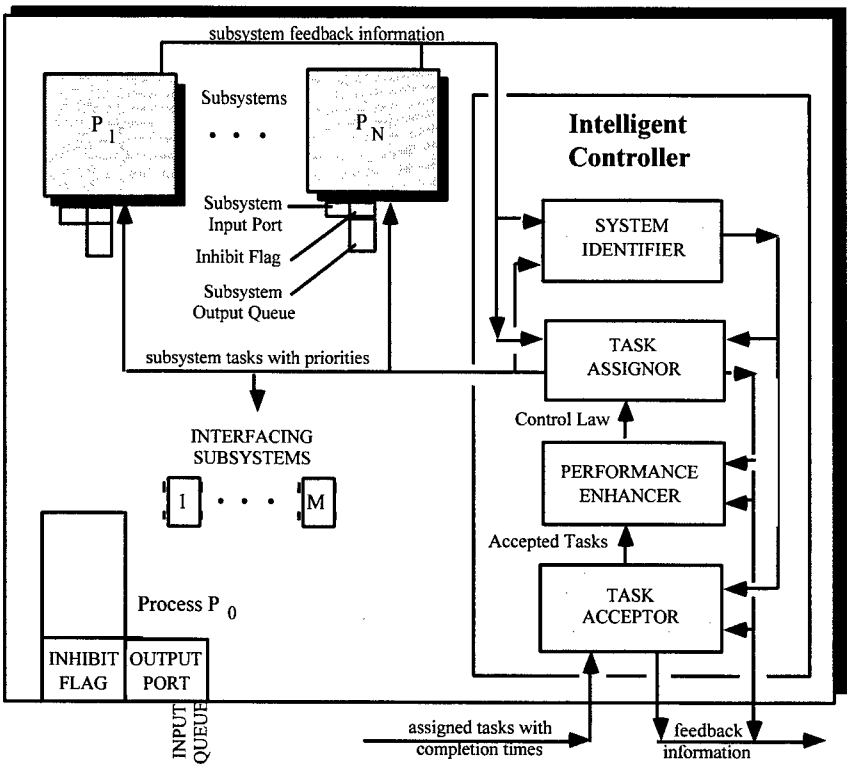


Fig. 1. The Coordinated Object

Unfortunately, the ROOCH is not a sufficient solution in itself. Rather, the ROOCH defines which subsystems comprise the overall system. Essentially, it addresses the physical concerns. One important outcome of the ROOCH is the specification of the hierarchy of controllers that will be needed to manage the system. Note that each coordinated object has its own dedicated intelligent controller. Further, each intelligent controller serves as the supervisor to the intelligent controllers for the subsystems that are contained within the coordinated object. In addition, each intelligent controller also has a supervisor that is the intelligent controller for the coordinated object in which it is a subsystem.

After we have defined this hierarchical relationship, we must then define the mechanisms by which these intelligent controllers will interact. One approach to the interaction among the intelligent controllers is the Real-time Control System, defined by Albus and Meystel [4]. Although this architecture has been employed for several systems, the author believes that it is not the only solution.

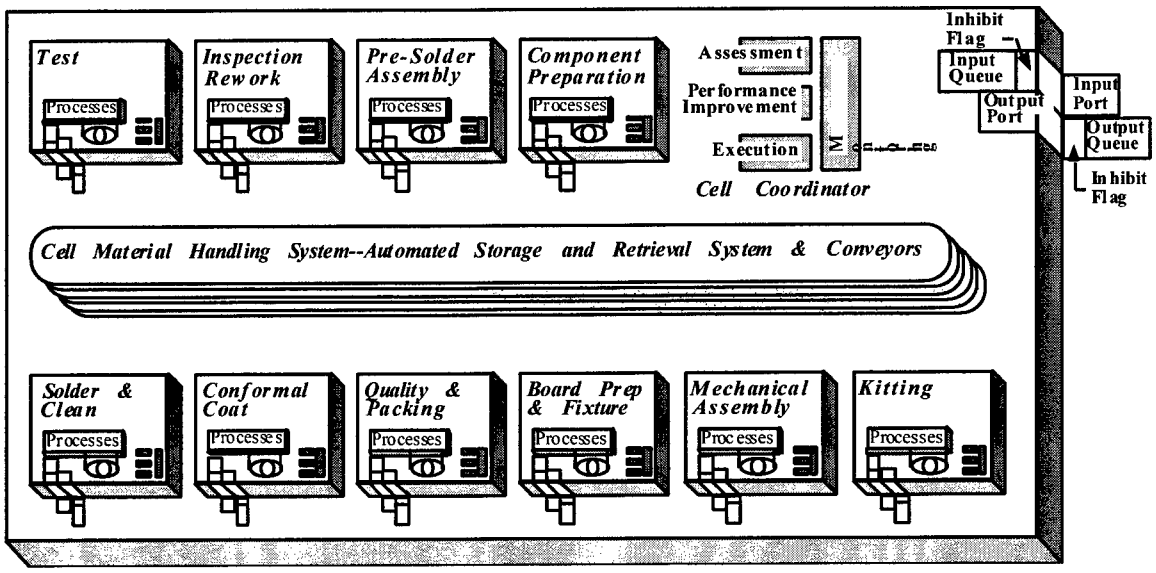


Fig. 2. The Recursive Object-Oriented Coordination Hierarchy.

In Figure 3, we depict our schema for interactions among the intelligent controllers. Each one consists of three primary functions. The Task Acceptor is responsible for accepting new tasks from the supervisor for implementation within the coordinated object where the controller resides. When new tasks are accepted, it is necessary to insure that the coordinated object executes the task in a feasible manner. We can assume that other tasks have already been assigned to the coordinated object and are now being implemented. When each task is assigned, the supervisor typically specifies a task completion time. If the task completion times are improperly specified, there may be no feasible solution. Hence, it is essential that the Task Acceptor within a given coordinated object, negotiate with its supervisor's Task Assignor to establish a meaningful completion time. Finally, it is essential that new tasks are continuously assigned to the coordinated object to prevent it from becoming idle after completing its assigned tasks.

In discussing the Task Assignor, we assume that response of the subsystems is not deterministic. This uncertainty evolves naturally as a consequence of providing intelligent controllers at each of the subordinate subsystems. Because subordinate subsystems can have intelligent controllers, they perform their own planning and their response will depend on the plans they develop. In short, a given intelligent controller cannot or should not perform detailed planning of a subsystem that has its own intelligent controller. Once we accept this principle, behavior of the subordinate subsystem is no longer deterministic.

Given the inherent uncertainty of the subsystems' responses, it is essential that we employ feedback control principles in managing the subsystems. The role of the Task Assignor is to employ the feedback control law that has been selected for implementation. Using this feedback control law, the Task Acceptor monitors feedback information from its subordinate subsystems and then interacts with each subsystem's Task Acceptor to assign new tasks for the subsystem to execute.

The Task Assignor also employs on-line simulation in order to project the future performance of the subsystems as they continue to operate under the current control law given their current state (see Davis [3] for a discussion of on-line simulation). This project response provides feedback information to the Task Assignor that resides within the supervisory intelligent controller. It also provides critical information that will be employed by the other functional elements within the intelligent controller. Using this projected response, the Task Assignor can further employ predictive control techniques. That is, not only can it take control actions based upon the its current state, but also bases actions upon the state that it predicts will occur. In this manner, the controller can look ahead and anticipate what may happen and act accordingly.

The Task Acceptor employs the projected response under the current control law as a baseline trajectory upon which any new tasks must be included. In this manner, the Task Assignor can negotiate a meaningful completion date with its supervisor's Task Assignor in order to insure that a feasible system response exists if the system continues to operate under the current law.

The projected response under the current control law also provides the performance standard against which any other potential control law's performance will be compared. The determination and selection of new control laws is addressed by the Performance Improvement Function. The operations of this function are the most complex. Basically, the function begins by generating new control laws and then performs on-line simulation of its behavior given the system's current state. Then, the performance comparison is made. If the performance of the new control law is better than that of the current control law, then the new control law is sent to the Task Assignor for implementation.

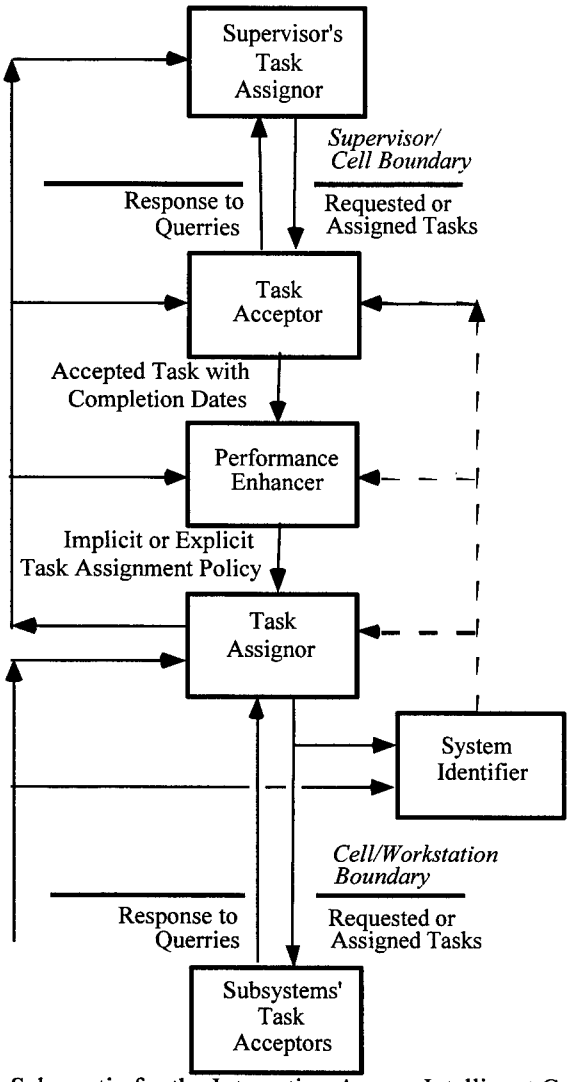


Fig. 3. Schematic for the Interaction Among Intelligent Controllers

There are two important tasks performed by the Performance Improvement Function. The first task is performing the on-line simulation analysis and performance comparisons. The technologies needed to perform this task are still evolving (see Davis [3]). The second task is the generation of the alternative feedback control laws. This is a very important requirement that cannot be discussed here due to space limitations. It is important to state, however, that we have defined means for specifying control laws that will permit our intelligent controller to employ any type of planning algorithm. That is, we will not attempt to specify which planning algorithm should be employed.

We can also assume that the subsystems are time variant, i.e., their behavior changes with time. The role of the System Identifier is to constantly update the system model to reflect the subsystems current behavior. This system model is, in turn, used by the other functions within the intelligent controller in order to perform on-line simulation. Again, the manner by which one performs system identification for this class of systems is a research topic. However, the manner in which we model the system significantly simplifies the identification task. Under our modeling framework, we need only to monitor the time required to complete tasks and the probability of successfully completing a given task.

It is also important to distinguish the above configuration for an intelligent controller from the more conventional approach. Most designers of intelligent controllers separate its function operation into a planning and control (execution). If we are considering a single intelligent controller that is managing a collect of simple dynamic process (they do not have intelligent controllers), then this may be the ideal approach. However, if we consider a control architecture with several hierarchical levels of intelligent controllers, then one should question the separation of the planning and control functions. In such architectures, most researchers recognize the need to distribute planning and control responsibilities among all of the intelligent controllers. However, with an intelligent controller, most researchers try to separate the planning and control responsibilities among the various functional elements. (see Albus and Meystel [4]).

It is our belief that planning and control should be considered in an integrated fashion by every intelligent controller as well as the component functions within the intelligent controller. Our goal is to always consider how the plan will be implemented while we are formulating the plan. We have attempted to define the functional elements within the controller in order to implement the required decomposition. We observe that the Task Acceptor has the longest planning horizon because it is considering tasks that will be assigned to the coordinated object. The Performance Improvement function considers tasks that have already been defined. Finally, the Task Assignor attempts to assign tasks to the subordinate subsystems based upon their current and projected states. Note also that the planning horizon of a subordinate subsystem is less than that of any functional element within its supervisor's intelligent controller.

The intelligent controller is also responsible for performing task decomposition. Here, all the functional elements are able to do task decomposition. The Task Acceptor must define the new subtasks that must be executed under the current control law if the new task is accepted. The Performance Improvement function must consider all tasks when it selects the control law. Note that for flexible systems the employed task decomposition may be dependent upon which control law is selected. Finally, the Task Assignor performs the task decomposition that is needed to execute the control law. Note also that task decomposition inherently implies that the subsystems will consider the planning problems in greater detail than does their supervisor. This further implies that there is aggregation of detail as one moves up the control hierarchy.

SUMMARY AND CONCLUSIONS

Given the space limitations, this paper can only provide the most basic introduction to the control architecture discussed in this paper. There are numerous related details that should be addressed. For example, we can now provide a mathematical justification for our design of the intelligent controller. Entirely new simulation languages are being developed to exploit our modeling paradigm. New technologies are being developed to support on-line simulation analyses. The topic addressed in this paper represents an entirely new area of planning and control research, for which little is now understood.

REFERENCES

1. M.D. Cannon, C.D. Cullum, E. Pokak. 1970. Theory of Optimal Control and Mathematical Programming, McGraw-Hill Book Company, New York.
2. B. Bishop, P. Shirkey, M.W. Spong. 1995. An experimental testbed for intelligent control. Proc. of the American Control Conference, Seattle, WA.
3. W.J. Davis. 1998. Real-time simulation: the need and the evolving research requirement. Simulation Handbook, ed. J. Banks, 465-516, Wiley-Interscience, New York.
4. J.S. Albus, A. Meystel. 1997. Behavior Generation in Intelligent Systems. National Institute of Standards and Technology Internal Report, Gaithersburg, MD.

PDM-based Virtual Enterprises - Bridging the Semantic Gap

Andreas Karcher, Jörg Wirtz

Institute of Information Technology in Mechanical Engineering (itm)
Technical University Munich, Germany

ABSTRACT

This article will describe the experiences which itm has gathered by participating in an European aircraft project. In the first part, the problems of introducing Standards-based integration of PDM (Product Data Management) systems within a Virtual Enterprise will be described. It will be demonstrated that a principle reason for these problems is the *semantic gap* between the interpretations of information objects managed in common by the participants. The second part of the article will introduce a new approach to reducing the *semantic gap* by addressing in a Requirement Engineering process, the specific inter-company aspects of data-sharing and data-exchange.

DESIGN AND MANUFACTURING WITHIN A VIRTUAL ENTERPRISE

An increasing complexity of products and the globalization of markets in mechanical engineering today, has brought the need for the reduction of costs, higher quality and reduction of time-to-market in product development and production [1]. Product design and manufacturing in world-wide networks offer great potentials for the reduction of costs and time-to-market [2]. The concept of a Virtual Enterprise (VE) allows for the integration of the core competencies of companies in a flexible alliance for a defined period of time. But collaboration in Virtual Enterprises requires new communication tools and data exchange concepts to be used by the consortium members [2][3].

First of all, the information for designing and manufacturing the product must be made digitally accessible throughout the Virtual Enterprise in order to establish a CSE (Concurrent/ Simultaneous Engineering) development process between the partner companies.

DATA AND PROCESS INTEGRATION REQUIREMENTS

In order to reduce the time to market of a new product, both in terms of development and production time, the partners within the VE must have access to all relevant product data. However in practice, the information flow parallel to the physical flow of goods between the logistic departments of the partners often takes more time then actually transporting the goods themselves! This often is a consequence of manually manipulating the manufacturing data which is to be exchanged between the different production planning systems (MRP: Material Resource Planning). Problems in exchanging engineering and manufacturing data between different partners of the VE occur due to semantic differences in interpreting the underlying information: None of the known exchange standards like EDIFACT, ANSIx12 or ODETTE can secure the semantic integrity of the data exchange [4]. But in order to achieve improved collaboration between the engineering and manufacturing partners of the VE in a Concurrent/ Simultaneous process it is necessary to distribute information about parts and raw materials in a very early stage of product design.

Increasingly PDM systems are becoming the IT backbone, managing dynamic and ever more complex product development and manufacturing processes. As a consequence of the distributed processes of global VE's new requirements are emerging. These new requirements are specifically related with process integration and data exchange in cross company collaboration. Being this the case we must harmonize the various process related cultures of the partners, thus reaching integration on a data level and process level using IT solutions. A centralized approach controlled and managed by a central database fails to perform adequately due to flexibility requirements, permanently changing VE structures and the required effort to agree upon the contents and mechanisms of the central database [5]. A federalized approach allowing an

0-7803-5489-3/99/$10.00 ©1999 IEEE.

agreement on data integration, process integration, different PDM and IT systems as well as different operating cultures is ultimately required. This integration should however not focus separately on the data level or the process level, however an integrated approach incorporating both data and process aspects is required. Standards such as STEP (STandard for the Exchange of Product Model Data ISO 10303), including the Application Protocols such as AP203 or AP214, can provide a good starting point for data integration, but a remaining *semantic gap* i.e. different interpretations and understanding of "common" information objects and processes needs to be bridged in a conceptual *Integration Layer*. Thus one of the main challenges is to begin on the highest level by using standardized and possibly re-usable models to reach a customized VE specific *Integration Layer*.

Basic methods of data integration

Basically, two different approaches for *Integration Layer*s can be distinguished:

- *Data Exchange Approach*: as a result of an asynchronous exchange of files between the PDM systems, the same (replicated) information is held in the PDM systems of the partners.
- *Data Sharing Approach*: information is distributed among the PDM databases and accessible online via a middleware layer.

To make data transfer possible, defined and agreed interfaces are needed through which the sender and the receiver can access the information. A defined interface consists of a defined notation (representation language) and a defined logical data model. In general, there are two ways to achieve such an interface for an *Integration Layer*:

- Creating a new interface definition from scratch
- Adapting a standardized interface definition

In order to save resources when introducing an *Integration Layer* in a VE, standardized interface definitions should be used.

State of the art approaches for standardized interface definitions

The STEP Standard (ISO 10303) established in 1985 was the first standard with an integrated product model approach which provided semantic data models (defined in Application Protocols such as AP214 and AP203) and mechanisms for PDM data exchange. The formal data specification language EXPRESS is also standardized in Part 11 of ISO 10303 [6].

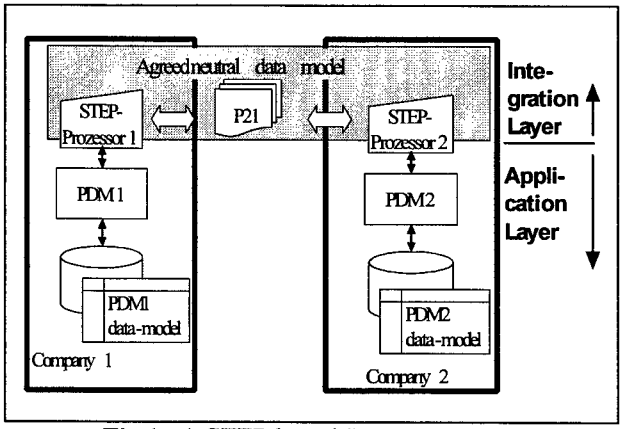


Fig.1. A STEP based *Integration Layer*

The file-based exchange of STEP is based on 'Processors' which transform the data from the PDM systems into files with a standardized format and a standardized data-model (Part 21 ISO 10303) (see Fig.1). The STEP standard also provides mechanisms for data sharing via the Standardized Data Access Interface (SDAI) [8]. Another approach to the data sharing concept is based on the Common Object Request Broker Architecture (CORBA) proposed by the Object Management Group (OMG). The scope of this *Integration Layer* is to access the services of PDM systems of partner companies by sending and receiving requests to object implementations of the PDM systems via the common object broker layer (ORB layer) [9].

Both the proposal of the PDM Enabler group in response to a request of the OMG, and the results of the RISESTEP-project, provide object models for the CORBA-based common use of PDM services (as well as data sharing) between different PDM systems [9][10].

HARMONIZING DATA AND PROCESSES

Customizing a PDM STEP-Processor

Our experience in projects aiming for PDM-based collaboration in VEs is that the agreement to use PDM systems and a certain *Integration Layer* based on a standardized data model such as STEP is a necessary decision in order to achieve standards-based data integration.

However this does not solve all problems. Due to different business processes, companies customize their PDM systems differently [3]. In practice, this means that objects in the data model of the PDM systems are modified, new objects with new behavior are created and/or objects are interpreted in company-specific ways.

The semantic of an information-object can be defined as the description of the intended meaning of it.

Whereas the definitions of semantics and attributes of elements such as points and lines are used almost universally, and the definition of elements such as surfaces and solids is uniform in most CAD systems, the definitions of PDM objects are company-specific.

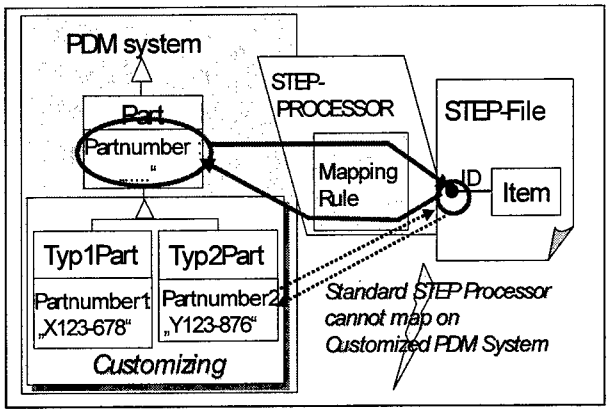


Fig.2. Collision of a standard STEP-Processor and a customized PDM system

Whereas it is possible to agree on a certain data model for CAD data exchange and then buy, install and use an appropriate STEP-Processor between CAD systems, this approach will often not work for PDM. This is due to the mapping rules of the *Integration Layer*, which transform information from the standardized neutral data model that is exchanged, or shared, to the specific data model of the PDM system. Since the PDM system is customized these rules must also be modified according to the customization of the PDM system (see Fig.2). In other words, a customizable *Integration Layer* is required.

"A Semantic mapping' which makes possible bilateral mapping rules, is required...." [11].

So, every partner in the VE must define their mapping rules for their customized PDM, and all partners must map the same information to the same attributes of entities in the data model shared or exchanged.

An example of a *semantic gap*

Experiences within projects with DaimlerChrysler Aerospace showed that the independent definition of mapping rules by partner companies in a VE leads to different results. The different interpretations of the neutral data model to be exchanged or shared led to wrong or senseless populations of the PDM systems' databases and/or errors in the *Integration Layer*. Different interpretations of exchange entities were often not found until the first test-exchange took place. This led to additional effort in the design and development of the *Integration Layer* and can cause project delay.

Figure 3 shows an example of how company-specific interpretations of the agreed data exchange model can give rise to collisions when mapping takes place.

Equivalent information objects of the two companies A and B in the VE, such as a Change Request which identifies a formal proposal for changing the product and causes the engineering action to achieve the change, may be mapped on different entities in AP 214 of STEP. The mapping of a 'Change Request' from company A on the STEP AP214 entity 'activity' would be valid, as would be the mapping on the AP214 entity 'work_request', although the definitions of the two entities are different.

An 'activity' is described as 'a fact of achieving or accomplishing an action' whereas a ' work_request' is described as the 'solicitation for some type of work to be done' [12] (see Fig.3.).

The different interpretation of entities of the standardized data model is called a *semantic gap* between the partners. The reason for this problem is a lack of semantic precision of entities of data models in STEP. Concepts such as 'part' and 'action' are not defined with enough rigor to be shared by different application protocols. Different interpretations are assumed for the same term in different places [13][14]. Clearly then, there must be a common understanding of the semantics of the neutral data model to be exchanged or shared between the partner companies. This is the basis for a correct mapping on the specific PDM data models before any *Integration Layer* should be customized or implemented.

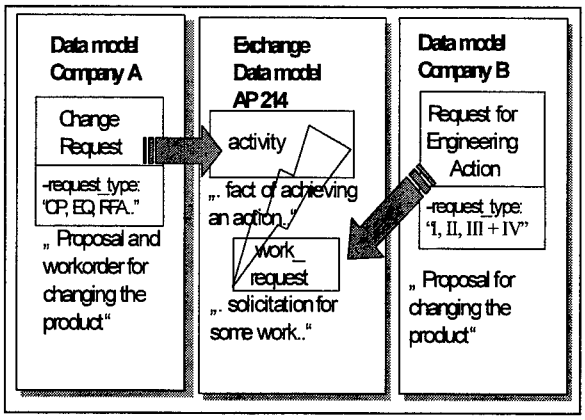


Fig.3. Example of a *semantic gap*

As described above, so are the semantics of the information objects dependant of the process definition steps in which they are created. Therefore, the mentioned trigger events for synchronizing the production information between the partners, needs to be harmonized. Excessive harmonization of the processes between the partner companies may lead to an unacceptable workload, as a result of the specific engagement of the companies with other VE's and their historical backgrounds. Therefore an understanding of the process steps on a general basis between the partners must be reached. Problems in achieving a common understanding on the process level are also included under the term "*semantic gap*". The complexity of the harmonization between the partners increases because data and process harmonization's need to be specified in an integrated way.

The next question is, how do companies in a VE achieve a common understanding and agreement on objects which are often still under definition internally?

Experience in the European aircraft project, in which DaimlerChrysler Aerospace and itm are both participants, showed that the simple approach, in which each company sends the other a list with attributes that they intend to use for exchange, was not successful. As a result, a more systematic approach of achieving a common understanding of the way the VE partners will use the data model to be exchanged or shared is required.

OBJECT-ORIENTED REQUIREMENT ENGINEERING

To reduce the *semantic gap* between the partners, a systematic Requirement Engineering (RE) should be carried out to achieve a common understanding of certain requirements for information content.

According to Pohl [15] RE can be defined as 'a systematic process of developing requirements through an iterative co-operative process of analyzing the problem, documenting the resulting observations in a variety of representation formats and checking the accuracy of the understanding gained'. A four-step generic approach achieves the goals of RE:

- *Requirement Elicitation*: Find out the requirements for the problem to be solved
- *Requirement Negotiation*: Discuss and agree the requirements identified in the elicitation step
- *Requirement Specification*: Derive a formal specification out of the requirements identified and negotiated
- *Requirement Validation*: Certify that the specified requirements are consistent with initial intentions

The four RE steps can be applied to the specific problem to define a VE common *Integration Layer*.

Common Requirement Elicitation
After selection of the appropriate integration approach (data-exchange or data-sharing) and the agreement on a certain standardized data model, the main requirement elicitation process for PDM data exchange can start with the aim of achieving a common understanding of the data model. Common materialization rules for the neutral data model should be defined. The information objects identified and managed in the PDM systems of each partner must be mirrored on suitable objects in the standardized data exchange model.

To avoid a *semantic gap*, the information objects should be identified together with the partners from the very beginning by defining a VE-appropriate interpretation of the standardized neutral data model. The requirements as to which information should be exchanged can be elicited in workshops with users of all participating companies, or by analyzing the information which was exchanged in other consortia or before the digital exchange started in this VE. This can be done by trying to identify and interpret appropriate objects of the chosen standardized data model. As they are used to manage the product structure and the related documents and files, the Bill of Material (BoM) and the Drawing Tree documents are a suitable base for analyzing the information that must be exchanged. The decision, as to whether a certain information object should be exchanged or not, can be influenced by factors such as whether it is necessary for Concurrent/ Simultaneous Engineering (CSE), or if the additional effort to manage the exchange of this object adds value to the cross-company process chain.

On the other hand, trigger points can be determined by analyzing the impact of certain information objects on common processes. These include change requests, work orders and maturity stages of parts to be manufactured. A further process analysis should define precisely what happens on the occurrence of such a triggering event, such as which information should be exchanged on a certain event and which reaction is expected by sending a certain information onto a certain trigger.

Negotiation and Specification
What is the best way to achieve agreement on how the data model should be interpreted and to negotiate how the company-specific interpretations of entities in the data model can be exchanged?

Our experience within the DaimlerChrysler Aerospace aircraft project showed the success of an approach based on exchanging tables of proposals for the semantic definitions of entities - with examples of the populated data model - between the partner companies of the Virtual Enterprise.

As we have seen, both data and process requirements have close interdependencies. Therefore the separated modeling of data and process information bears the danger of inconsistencies between the two specifications. On the other hand the object-oriented paradigm has proven its ability to model reality in a user-friendly way. After modeling preliminary separate data and process models both aspects need to be integrated within one integrated object-oriented model (see Fig4.)

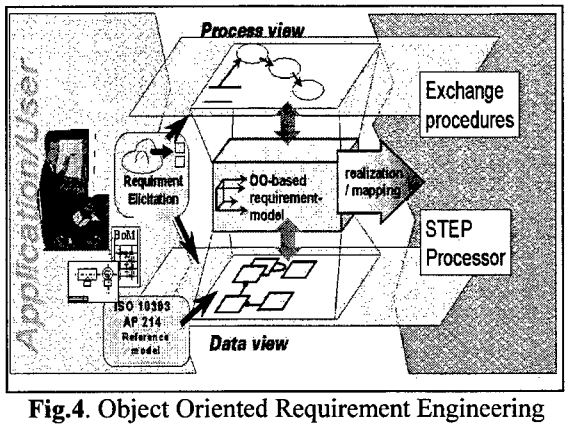


Fig.4. Object Oriented Requirement Engineering

After the neutral data model is defined and agreed, rules must be drawn up to populate it. It is very important to have an agreement on the rules to populate the data model in order to specify the *Integration Layer*. If some identifiers in STEP physical files are missing, or have unexpected values, then the *Integration Layer* will probably not work properly.

Mapping rules are based on a defined set of values. The basis for these rules can only be the vision of what the common product structure should look like. Again, user workshops and the analysis of the Bill of Materials will help to find the requirements for suitable values for the attributes.

Validation

As our experiences in the European aircraft development consortium have revealed, even an integrated RE process was not able to cover all semantic problems and so some of the inconsistencies were not recovered until a final testing and validation process took place. Test scenarios should be defined precisely with the intention of testing all the information content to be exchanged or shared. After the functionality that is relevant for data exchange in each of the individual PDM systems has been tested, a cross-company test should be performed.

CONCLUSION

PDM systems with their ability to manage complex product related data in distributed CSE processes increasingly built up the IT backbone of Virtual Enterprises in the realm of Global Engineering and Manufacturing. On the basis of a federated integration approach, the remaining *semantic gap* resulting from different interpretations and understandings of product and process relevant information objects, has to be balanced in a conceptual *Integration Layer*. The itm approach as a result of its experience in a european aircraft development project allows, on the basis of the object oriented paradigm and under consideration of existing standards a systematic and evolutionary requirement engineering process. This approach leads to a consistent and validated specification of the *Integration Layer*, a prerequisite for a PDM based VE in which different interpretations and understanding of "common" information objects and processes are alleviated.

REFERENCES

1. Krause, F.-L.; Kind, Chr., 1996. "Potentials of information technology for life-cycle-oriented product and process development" in: Krause F.-L.; Jansen, H. : Life Cycle Modeling for Innovative Products and Processes: Chapmann & Hall, London.
2. Eversheim, W., Schuth, S., Bremer, C., Molina, A., 1998. "Globale virtuelle Unternehmen"; ZWF 3/98, 93. Jahrgang; Carl Hanser Verlag.
3. Spur, G.; Krause F.-L., 1997. "Das Virtuelle Produkt – Management der CAD Technik"; Carl Hanser Verlag München Wien.
4. Dangelmeier, W., 1996. "PPS in der virtuellen Fabrik"; proceedings of 'Fortgeschrittene Informationstechnologie in der Produktentwicklung und Fertigung'2. Internationales Heinz Nixdorf Symposium für industrielle Informationstechnologie am 20/21 HNI-Verlagsschriftenreihe, Bd.19 (Rechnerintegrierte Produktion/ Wirtschaftsinformatik).
5. Friedmann, T; Jungfermann, W; Schmid, C., 1998. "Global Engineering – Welchen Beitrag leisten EDM-Systeme und das Internet?"; EDM-Report Nr.4/1998, Dressler Verlag GmbH, Heidelberg.
6. N.N.: ISO/10303-11, "Industrial Automation and Integration –Product Data Representation and Exchange – Part11"; The EXPRESS language reference manual
7. ISO10303-22 (committee draft), 1994. "Industrial automation systems and integration – Product data representation and exchange"; Part22: Standard data access interface specification.
8. Object Management Group (OMG), 1998. "The Common Object Request Broker: Architecture and Specification"; Revision 2.2.
9. N.N., 1997. "Product Data Management Enablers Proposal to the OMG in Response to OMG Manufacturing Domain Task force RFP1"; Initial Submission, OMG Document mfg/97-04-01 , Metaphase Technology, Inc.
10. Behrens, H.; Lotter, N.; Machner, B., 1998. "PDM integration using the CORBA and STEP standards"; Proceedings of the ProSTEP Schience Days '98, Wuppertal.
11. Eigner, M.; Zagel M., 1997. "STEP-Compliant PDM Solutions"; Proceedings of the STEP Forum '97-Development partnerships require compatible product data, 17.4.97, Munich, ProStep GmbH.
12. Hemmelmann, A., 1997. "Entwicklung eines Datenmodells zum Austausch von Produktdaten in der Europäischen Luftfahrtindustrie"; Diploma thesis carried out at the Institute of Information Technology in Mechanical Engineering(itm), TU München.
13. Guarino,N.; Borgo, S.; Masolo, C., 1997. "Logical modelling of product knowledge: towards a well-founded semantics of STEP", Proc. Euro. PDT Days '97, Sophia-Antipolis, PDTAG-AM, ESPRIT 9049.
14. Nowacki, H., 1998. "Scientific issues in product data technology"; Keynote Address at the ProSTEP Science Days '98, Wuppertal.
15. Pohl, K., 1996. "Process-centered requirements engineering"; Research Studies Press Ltd. Taunton, Somerset, England.

A Methodology to Diagnose the Target Cost in a Manufacturing Process

A.Arioti, C. Fantozzi, M.Granchi, E.Vettori

Department of Mechanical, Nuclear and Production Engineering
University of Pisa, Pisa, Italy

ABSTRACT

Techniques of Target Cost Management have been studied to help companies identify the causes of rejected parts because of incorrect design choices. A part of the problem can be removed in the design phase by developing a model to estimate costs. This provides the designer with a tool to carry out cost estimations and make correct choices. The model also permits the determination of the estimated cost of a new component in a direct and rapid way belonging to one of a family of parts well-understood. This study was made for an important Italian company.

INTRODUCTION

Target Costing is essentially a multifunctional activity which employs interdisciplinary groups made up of professionals in charge of various company functions involved in the process of planning manufacturing and commercialisation of a specific product. Its aim is to identify the cost causes and to transfer the knowledge and atudy the problems typical of the production line in the product planning phase in order to remove the cause of anomalous costs even before the beginning of production.

Target Costing was developed in Japan by companies such as NEC, SONY, NISSAN, and above all, TOYOTA as an instrument to plan costs and combine the instruments of Cost Management and Cost Engineering.

By applying the methodology of Target Costing during the planning phase, it has been demonstrated that among the economic characteristics of a product, i.e., selling price, industrial production cost and company profit correlated by the equation: **price – cost = profit**, selling price is imposed by the market, profit is defined by the financial reality of the company, production cost is the only variable which is possible to manipulate so that the true production cost will be less than the one deduced from the equation: **cost = price – profit**.

Estimation of costs by traditional methods first needs to characterise the product according to the functions required and these are determined according to the components needed. Obviously it is better to rely on cost data of the components used with similar products that already exist.

Such an approach does not permit assignment of a cost to the single phase which characterises production of a general component. Such a limitation is the principal cause preventing an effective critical analysis of the planning choices on single components.

Moreover there is a risk to attribute rules to a component's indirect costs which are not relevant. The determination of the real cost is final and therefore a possible reduction generally requesting some changes in the planning or manufacturing cycle in the end may be too expensive.

If we refer to the methodology of Target Costing, the work is developed according to the following phases:

1. Transferring knowledge and manufacturing line problem uderstanding to the planning phase,
2. Identifying the expense threshold of the various aspects which characterise the process in order to make the planner responsible for choices within his competence,
3. Drawing up the "Rules of Design for Manufacturing" to apply in the planning of a new component,

0-7803-5489-3/99/$10.00 ©1999 IEEE.

4. Developing a software system to enable the planner to use the numerical data contained in the graphs and tables on-line without having to write down the necessary operations on paper,
5. Developing a suitable model for the cost-estimate components to give the planner an instrument by which to carry out an economic analytical evaluation of the choices within his competence and, at the same time, to give management an accounting instrument by which it is possible to obtain more precise data in a very short time.

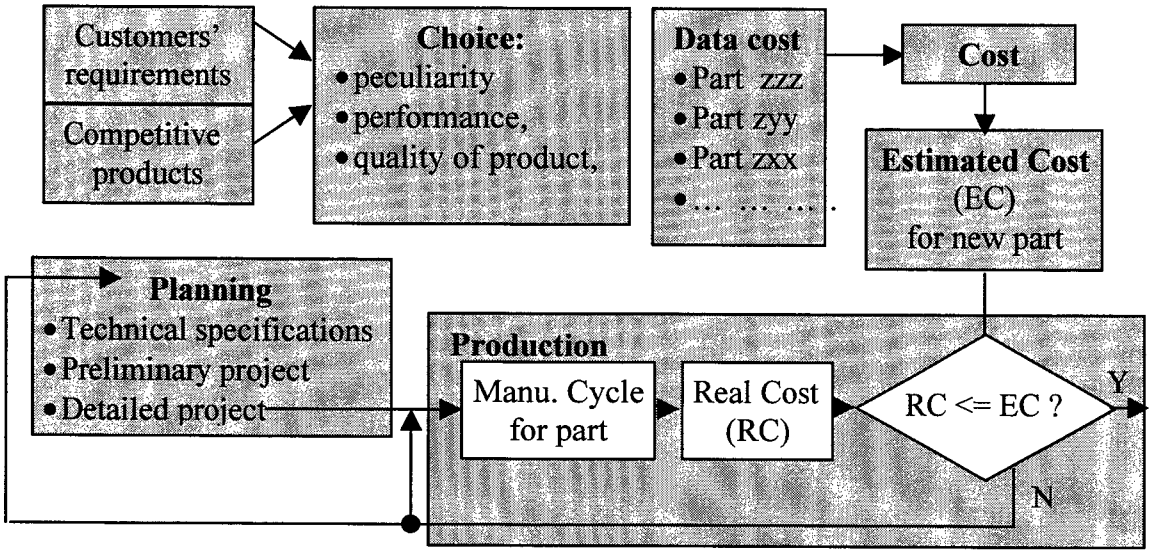


Fig. 1. Traditional approach for costing.

APPLICATION OF THE TARGET COST IN THE PLANNING AREA

The study has been developed in such an area and needs an interdisciplinary group in which each member follows the development of a typology of components which constitute the product.

Among the members of the interdisciplinary groups the planner can have a great influence on the product cost. He must take into account the economic characteristics of the project choices and of the "time to market" to reduce the time between the product planning and its entering the market. The planner therefore must have at his disposal:

1. Exhaustive information about the product materials and existing production technologies not necessarily used by the Company,
2. "Design Rules for Manufacturing" are drawn up by taking into account the problems of the production,
3. Data processing support able to optimise the solutions technically and economically so as to improve the quality of the product without increasing its price.

It will therefore be necessary:

- to transfer the knowledge and fundamental production line problems to the planning phase,
- to determine the economic threshold of the various aspects which characterise the process,
- to draw up "Rules of Design for Manufacturing" to use when planning a new component,
- to develop software which enables the planner to use numeric data contained in graphs and tables on-line so there is no need to write down the required operations on paper.
- to develop a cost estimation model to give planners an economic and critical evaluation of the choices within their competence.

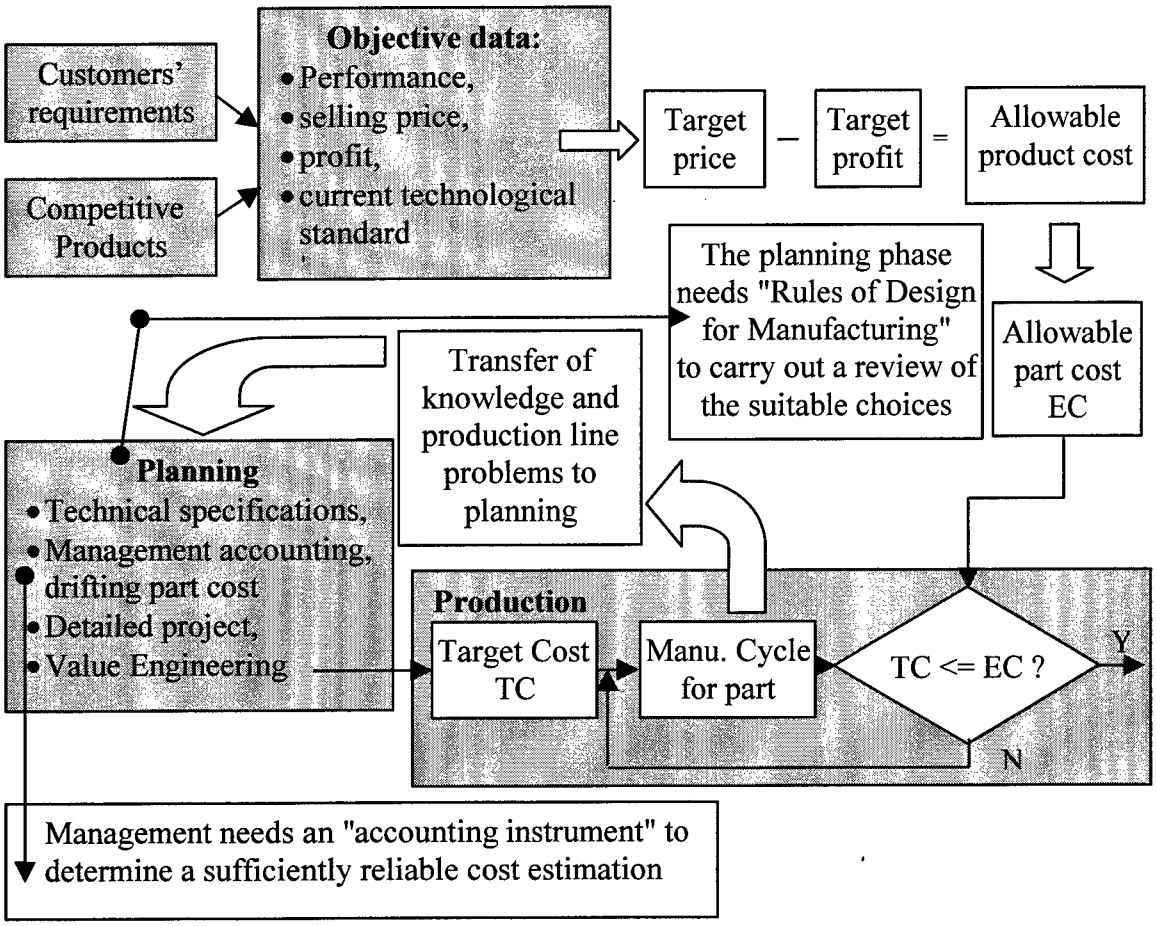


Fig. 2. Target cost methodology.

ASPECTS OF THE STUDY

The activities carried out, have examined the causes for rejection and identified those due to the planning process. A careful analysis has been carried out on the rejected elements in order to determine the planning faults responsible for the rejects.. Planning rules have been studied to take into account the connections within the planning choices.

We have examined the die-casting process of aluminium elements and have studied and developed a suitable software on the basis of "Rules of Design for Manufacturing". The aim has been to give a planner the possibility to work on-line by immediately acquiring the necessary numeric data without requiring long calculations on paper.

The study has been developed for an important Italian Company which manufactures scooters from aluminum alloy die-cast parts.

The software has been developed with the principal interface components shown in Fig. 3. It processes the numeric data contained in graphs and schedules automatically. The numeric values which appear in the software are those recommended for correct planning of the aluminum alloy die-cast parts, in some cases processed to take into account knowledge of company technicians in close contact with the process.

Therefore for problems connected to correct design of a die-cast part, the planning aspects only give the input boxes in which to insert the requested numeric values and the material. Immediately after, the output values for a certain material appear automatically and give the inclinations, tolerances etc.

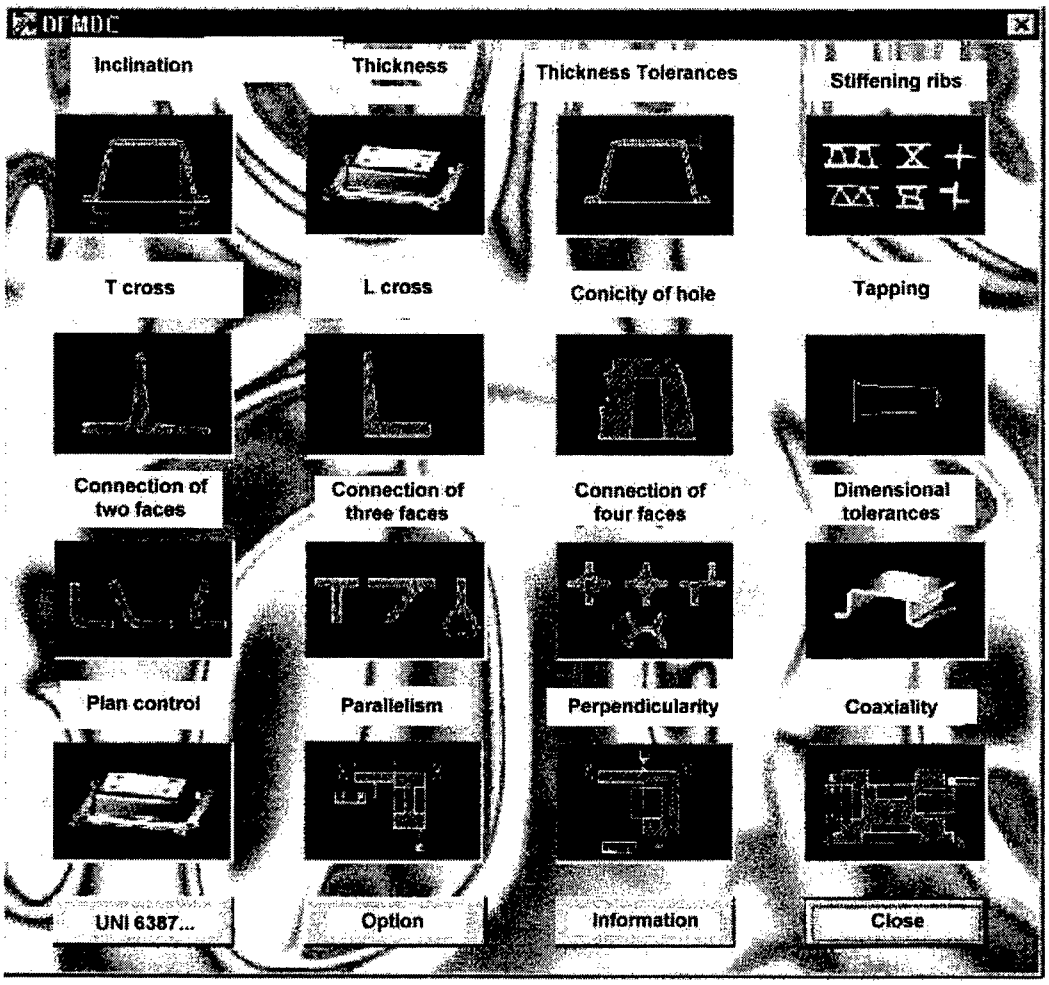


Fig. 3. The principal menu of the program

In order to make a planner's task much easier, we are developing a model of cost estimate in Excel using Visual Basic programming starting from the influence of various factors on the cost of the die-cast part as shown in Fig.4.

CONCLUSIONS

It can be seen that if we refer to the equation **cost = price – profit** by this estimation model, it is possible to choose new components in the planning phase, introductory to mass production, thus intervening in the project when necessary and making changes aimed at controlling real production cost.

In the first application of the software with "Rules of Design for Manufacturing" the following advantages have been achieved:

1. considerable reduction in the time necessary to carry out calculations and make choices while designing the project,
2. considerable reduction in possible errors in numerical calculations,

3. obtaining numeric values on-line giving the possibility to plan based on consideration of the economic limits of the process,
4. standardisation of the technical references of components involved in aluminium die-casting.

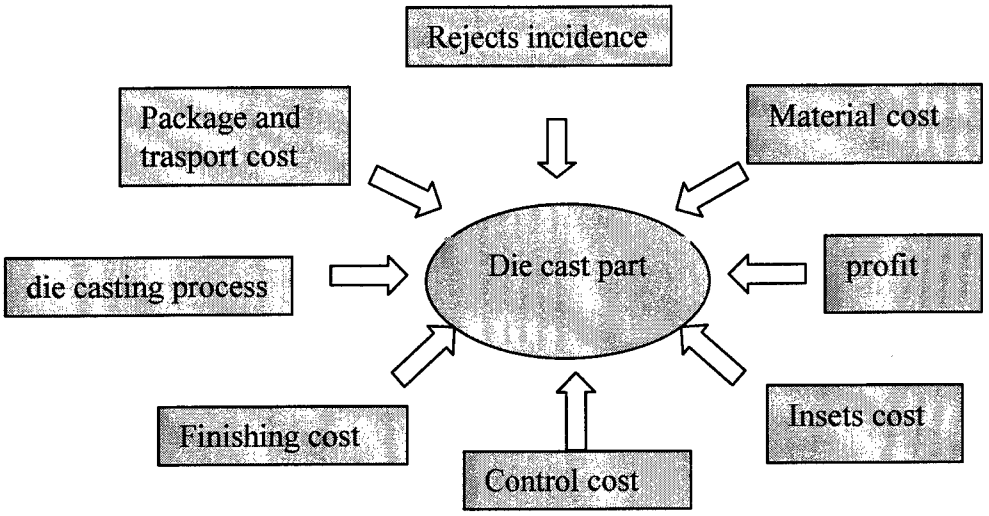


Fig. 4. The influence of various factors on a die-cast part

We are carrying out a subsequent study of the software to estimate cost and are convinced that other advantages can be reached:

1. A considerable reduction in the time necessary to carry out an estimate,
2. Attainment of the estimated costs which are considerably near the real ones,
3. Possibility of different estimates for a new component by simply changing the numeric inputs, by which the planner can carry out an economic and critical evaluation of the choices within his competence.

The detailed disassembling of all the cost causes which characterise a product makes the sessions of value engineering faster and makes it possible to verify the improvements which result from the planning variations aiming at a minimum cost.

REFERENCES

1. Horvath P., 1993. Target Costing a State-Art–Review. ISF International Ltd, pp. 1-64.
2. Tanaka, Yoshikawa. Innes, ed., 1994. Contemporary Cost Management. Chapman & Hall.
3. _____, 1996. FIAT Normative.
4. Parsaei, H.R., Sullivan W.G., 1993. Concurrent Engineering, Chapman & Hall.
5. Halevi, G., 1993. The magic matrix as a smart scheduler. Computers in Industry, 21, 245-253.

Resource Allocation Model for a Fast-Tracked Project

Yassiah Bissiri and Scott Dunbar

Department of Mining and Mineral Process Engineering
University of British Columbia, 6350 Stores Road, Vancouver, B.C., V6T 1Z4, Canada
Email: bissiri@mining.ubc.ca wsd@mining.ubc.ca

ABSTRACT

The concept of fast-tracking a project, although generally economically beneficial, is a risky undertaking. The risks vary from being unable to complete the project in the expected time to higher costs due to excessive compression of the activity duration. This paper describes the variables involved in fast-tracking a project and then demonstrates that risks can be reduced if proper resources are carefully allocated to the project. Reducing the duration of an activity ("crashing") within a project usually requires additional investment and/or resources. These resources can be found within the project's pool of funds such as using overtime for manpower or they are brought into the project as additional items. The success of the fast-tracking approach depends on minimizing the cost of these additional resources. A simulation model is described that allocates resources to project activities in a way so as to minimize the additional cost of resources. The fact that the start time of an activity depends on the completion time of its predecessors makes it a probabilistic problem with respect to completion time.

INTRODUCTION

The decision to fast-track a project is very risky [1] and should be made only after serious analysis of the parameters involved in the process. Fast-tracking a project involves consumption of additional resources that have to be brought into the project at additional cost. Minimizing the cost of fast-tracking a project can be very decisive in reducing risks. The model discussed in this paper analyses the project network and assigns the proper "crashing" time to activities that can be "crashed" in order to fast-track the project.

When a decision is made to fast track, the critical activities are "crashed" based on their "crashability" and their "crash cost" because the critical path defines the project duration. The model is then extended to activities that are "near critical" relative to the amount of time to which the project should be fast-tracked.

An immediate impact of the risks on a plan to fast-track a project is such that although allocating the necessary resources to activities is done, the project may fail to respond and simply adds more expenses to the project cashflow [2]. Figure 1 describes the process of fast-tracking a construction project. Two scenarios appear in the diagram, a traditional approach and a fast-track approach. The traditional approach consists of sequencing design and construction phases, whereas the fast- track approach consists of overlapping and reducing the duration of the design and construction phases. Each phase represents a subproject of the entire project and is formed by a chain of activities such that compressing the duration of each sub-project involves "crashing" activities that are critical to the network representing these subprojects. The process of "crashing" an activity on the network depends on several factors such as:

- The "crashability" (how far can an activity be crashed?)
- The cost of "crashing"
- The type of activity
- The availability of resources

The "crashability" of an activity is defined as the maximum time to which an activity can be compressed and still be economic. The cost of compressing an activity increases exponentially beyond this value [3]. Figure 2 depicts the concept of "crashability" and shows the typical cost behaviour of activity time. As an activity is compressed, the cost decreases, reaching a minimum, and then increases rapidly to an asymptotic value at some minimum activity time. The minimum cost defines the normal cost of an activity.

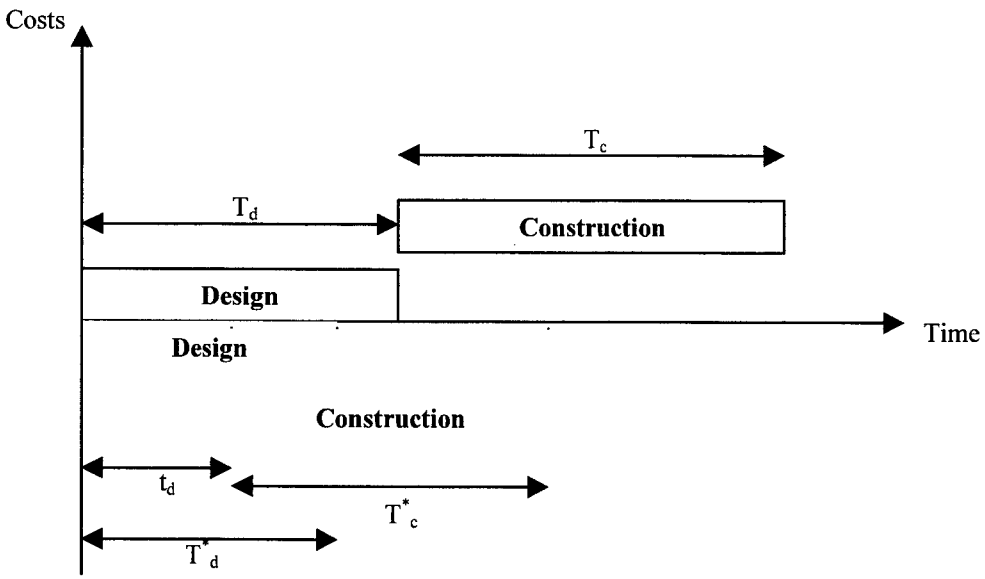


Fig. 1. Model of a fast- tracked construction project
$t_d = xT_d$, $T^*_d = yT_d$ and $T^*_c = zT_c$
where x, y, z are such that $0 < x \leq 1$, $0 < y \leq 1$, and $0 < z \leq 1$.

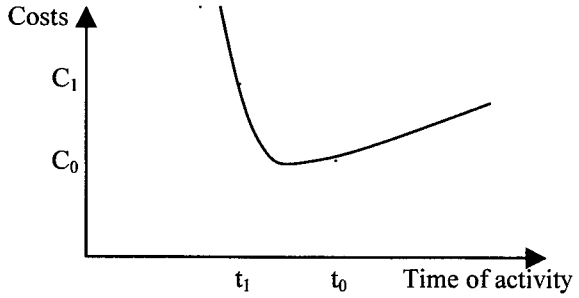


Figure 2. "Crashing" cost as a function of time

The cost of crashing an activity is generally based on data collected from records of past projects that were executed in the same environment and also from Project Managers who have expertise in this domain. Consider a project that has a total of N critical paths (a project can have more that one critical path). The expected total duration of the project is T and a decision is made to reduce the duration to T'.

N = number of critical paths
m_k = number of critical activities on critical path k (two different paths can have common activities).

Path1 = $\{a_{11}, a_{12} \ldots a_{m1}\}$

Path n = $\{a_{n1} \ldots a_{mn}\}$

Critical Path i

Path i = $\{a_{n1} \ldots a_{mi}\}$
d_{ki} = duration of critical activity k on critical path i
c_{ki} = cost per day of crashing critical activity i on critical path k
β_{ki} = upper limit of the number of days critical activity i can be crashed to.
α_{ki} = number of days to "crash" critical activity i on path k
α = T- T' = number of days the project is expected to be fast- tracked

Cost of Crashing Path i
The total cost of crashing the critical path i is the sum of the cost of crashing all critical activities on the path:

$$TC_i = \sum_{k=1}^{mi} \alpha_{ki} \cdot c_{ki} \qquad 1'.$$

Cost of Fast-Tracking the Project
The total cost of fast tracking the project is the sum of the total cost of the n critical paths of the project:

$$TC = \sum_{i=1}^{n} TC_i = \sum_{i=1}^{n} \sum_{k=1}^{mi} \alpha_{ki} \cdot c_{ki} \qquad 2'.$$

Equation 2' represents the additional cost of fast tracking the project. The objective of any project planner who considers fast tracking is to minimize the total cost of using more resources for the project. The problem of allocating the proper "crashing" time becomes an optimization problem.

OPTIMIZATION PROBLEM

Minimize $$\sum_{i=1}^{n} \sum_{k=1}^{mi} \alpha_{ki} \cdot c_{ki} \qquad 3'.$$

Subject to:

$$\sum_{k=1}^{mi} \alpha_{ki} = \alpha \text{ for every i} \qquad 4'.$$

$$\alpha_{ki} \le \beta_{ki}, \text{ for any i, k such that } 1 \le i \le n \text{ and } 1 \le k \le m_i \qquad 5'.$$

For each activity, the proper "crashing" time will determine how much of what type of resources is necessary to complete the work. Construction managers usually keep track of these data in order to use them when needed in the next project. So, when provided with the optimum "crashing" time, they can derive the amount of additional resources required.

It is important to underline the fact that "crashing" critical activities by an amount determined by the optimization problem may not be achieved, creating risks related to uncertainties. A probabilistic approach must therefore be introduced in order to reflect reality. Once again, the probability distribution of the success of "crashing" activities are built-in based on past projects having some common properties in the environment in which they were completed.

Each critical activity will then have a set of possible crashing times to which is assigned a probability distribution. These probabilities will then be simulated to generate more data in order to conduct a statistical analysis. The fast-tracked project completion time becomes probabilistic. An example will illustrate the technique.

A "near critical" path in our model is one that is not critical but has its total duration satisfying the following condition:
If T* is the "near critical" path length, T is the initial project length and T' is the desired fast-tracked project length, then:

$$T' < T^* < T \qquad 6'.$$

Compressing the project length from T to T' will automatically make the "near critical" paths critical activities after the time compression.

N* = number of near critical paths
m_k* = number of activities on a "near critical" path k* (two different paths can have common activities).
Path1 = $\{a^*_{11}, a^*_{12} \ldots a^*_{m1}\}$

Path n* = $\{a^*_{n1} \ldots a^*_{n\,mn}\}$

"Near Critical" Path j

Path j ={a^*_{n1}... $a^*_{n\,mi}$)
d^*_{kj} = duration of "near critical" activity k on critical path j
c^*_{kj} = cost per day of crashing "near critical" activity j on critical path k
β^*_{kj} = upper limit of the number of days to which that a "near critical" activity j can be crashed.
α^*_{kj} = number of day to crash "near critical" activity j
$\alpha^*_j = T_j^* - T'$ where T^*_j = length of "near critical" path j.

The total cost of fast tracking the near critical paths is

$$TC^* = \sum_{p=1}^{n^*} \sum_{l=1}^{m^*_p} (\alpha_{lp}^* \cdot c_{lp}^*) \qquad 7'.$$

A "near critical" path is one whose duration lies between the fast-track time and the expected total duration, i.e., $T' < T^* < T$. Applying Equation 6'. to the model, the optimization problem becomes:

Minimize
$$\sum_{i=1}^{n} \sum_{k=1}^{mi} (\alpha_{ki} \cdot c_{ki}) + \sum_{p=1}^{n^*} \sum_{l=1}^{m^*_p} (\alpha_{lp}^* \cdot c_{lp}^*) \qquad 1.$$

Subject to:
$$\sum_{k=1}^{mi} \alpha_{ki} = \alpha \text{ , for any i} \qquad 2.$$
$$\sum_{l=1}^{m_p^*} \alpha_{lp}^* = \alpha_p^* \qquad 3.$$
$$\alpha = T - T' \qquad 4.$$
$$\alpha_p^* = T_p^* - T' \qquad 5.$$
$$\alpha_{ki} \le \beta_{ki} \text{ , for any i, k such that } 1 \le i \le n \text{ and } 1 \le k \le m_i \qquad 6.$$
$$\alpha_{lp}^* \le \beta_{lp}^* \text{ , for any l, p such that } 1 \le l \le n \text{ and } 1 \le p \le m_l \qquad 7.$$
$$T' < T_p^* < T \qquad 8.$$

APPLICATION

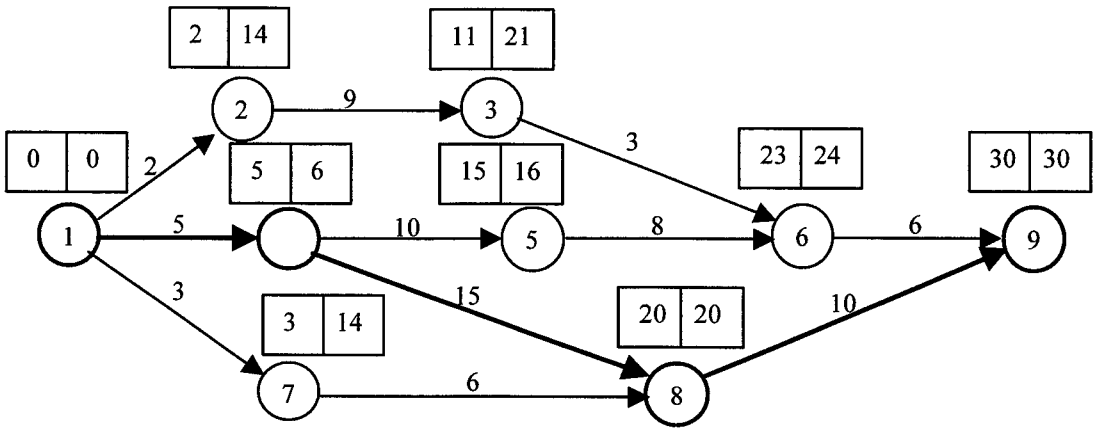


Fig. 3. Arrow on Arrow network of example discussed.

Figure 3 is the scheduled network of a construction project composed of eleven activities. The numbers in the squares represent the earliest and latest times for each activity determined by the backward and forward pass methods respectively. The numbers next to the arrows are the estimated duration of each activity. The critical path of the network (bolded arrows in Figure3) is composed of activities 1-4, 4-8 and 8-9 and has a

length of 30 days, which represents the total duration of the project. Interruption of an activity after having begun the activity is not considered here, although in practice, an activity may be interrupted by, for example, severe weather or other unpredictable factors.

It was decided that the project would be fast-tracked to reduce its total duration from 30 days to 22 days. By doing so, the entire network must be recalculated. The initial critical path will still be critical, but path 1-4-5-6-9 with an initial length of 29 days becomes automatically critical for the new network. The new network will have two critical paths after the "crash". Table 1 is an example of a probability distribution assigned to the completion time of activity 1-2. Initially, the activity was to be completed in 4 days but based on an analysis of the uncertainties, the completion time will now lie between 2 and 5 days. These numbers are usually determined from past project performance.

Table 1. Probability distribution of activity 1-2.

Activity 1-2	
Cumulative Probability	Time
0.00	2
0.10	3
0.35	4
0.70	5

Probability distributions are also determined for all other activities on the network and the notion of critical and "near critical" paths then becomes probabilistic. Usually, there is not enough data to conduct a robust analysis and in order to support a decision, the data (like those presented in Table 1) are generated by simulation to provide sufficient data to conduct a statistical analysis. The simulation results are in fact different scenarios into which the project might fall at a certain time relative to the uncertainties. In Table 2 the results are displayed for the simulation performed on the example network using Microsoft Excel. The numbers 0 and 1 are used to express affirmation (yes) or negation (no) about the criticality and the "near criticality" of the activities. The algorithm also ensures that two different paths cannot be critical and "near critical" at the same time. However, an activity can be critical and "near critical" for the case where two different paths share the same activity such as the case for paths 1-4-8-9 and 1-4-5-6-9 sharing activity 1-4. For simplicity, the following path names are used:

Path # 1 is composed of the chain of activities 1-2-3-6-9 while Path # 2 is composed of the chain of activities 1-4-5-6-9, Path # 3 is composed of the chain of activities 1-4-8-9 and Path # 4 is composed of the chain of activities 1-7-8-9.

Table 2: Results of the simulated network

Simulated		Critical?	Near
Activity	Time		Critical?
1-2	2	0	0
1-4	5	1	0
1-7	3	0	0
2-3	9	0	0
3-6	3	0	0
4-5	10	0	0
4-8	15	1	0
5-6	8	0	0
6-9	6	0	0
7-8	6	0	0
8-9	10	1	0
Total		3	0

Path Information			
Paths	Length	Critical?	Near Critical
1	20	0	0
2	29	0	1
3	30	1	0
4	19	0	0

Critical path length
30

Meet deadline ?
1

The results of the simulation indicate that Path # 2 is "near critical" and Path # 3 is critical and that the activities to be "crashed" lie on these paths. In reality, the simulation is run at least 50 times and the moving average of all these results is considered. Solving the optimization problem with EXCEL using "Solver", we obtained the results shown in Table 3.

Table 3. Solution to the optimization problem.

Path	Critical	Near Critical	Crash	Activities crashed	Crashed cost per day	Upper limit
1	No	No	0	None		
2	No	Yes	7 days	1-4 = 3days	$98	3 days
				4-5 = 2 days	$187	3 days
				6-9 = 2 days	$140	2 days
3	Yes	No	8 days	1-4 = 3days	$98	3 days
				4-8 = 5 days	$70	5 days
4	No	No	0	None		
Objective function	**$ 1592**					

The algorithm recognizes shared activities, as in the case of activity 1-4 which is shared by Path #2 and Path #3. The objective function represents the total additional cost of to compress the network. The results in Table 3 suggest that by compressing activities 1-4, 4-5, 6-9 and 4-8 by 3 days, 2 days, 2 days, and 5 days respectively, the project length can be reduced from 30 days to 22 days Figure 4 is the new Arrow on Arrow network of the "crashed" project. The dashed line arrows represent activities that have been "crashed" as a result of the solution to the optimization problem. The bold and dashed arrows represent the critical path(s) of the new network.

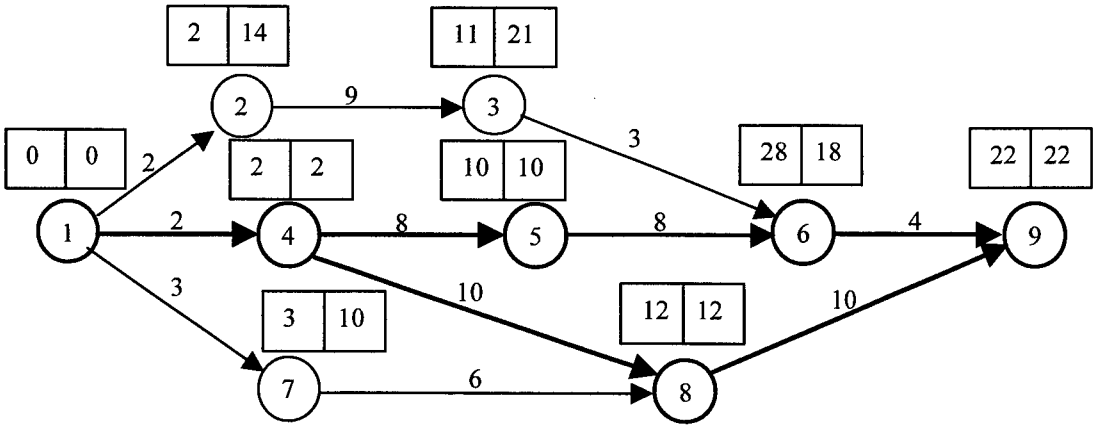


Fig. 4. Arrow on Arrow network of the "crashed" project.

CONCLUSION

Although the model works in theory, it is necessary to first apply different models of resource-leveling to the project before proceeding. Our model does not solve resource-conflict problems but could probably be inserted into resource-leveling models in future research. The model has the following advantages:

- It identifies and analyses activities that are critical or "near critical";
- Based on the upper limits (maximum amount of time an activity can be crashed), it determines the number of days to crash an activity at minimum cost to the overall project.
- The model includes a probabilistic analysis approach related to the uncertainty of estimators and provided by the application of the simulation.

ACKNOWLEDGEMENT

Special thanks to Dr John Meech for his constructive criticism during the elaboration of this paper. His remarks have been very useful in building this model.

REFERENCE:

1. Sproule, J.A., 1992. M.A.Sc. Thesis, University of British Columbia, Civil Engineering.
2. Nahmias, S., 1997. Production and Operations Analysis. 3rd Edition. McGraw- Hill Publishing Co.
3. Burman P.J., 1972. Precedence networks for project planning and control. McGraw-Hill (UK), London.

Hybrid Simulation Objects using Fuzzy Set Theory for Simulation of Innovative Process Chains

T. Menzel, M. Geiger

Chair of Manufacturing Technology, University of Erlangen-Nuremberg,
Egerlandstr. 11, 91058 Erlangen, Germany

ABSTRACT

The purpose of introducing new manufacturing process chains, such as innovative sheet metal processing technologies, is to increase production efficiency. Their success can be quantified by assessing the expected reduction of manufacturing time or costs and the increase in flexibility. Nevertheless, the implementation of new process chains is usually inhibited by the financial effort and the lack of exact knowledge about their real effect on production efficiency. Furthermore, the economic efficiency is mainly dependent on the vaguely known quantity and variety of products which have been planned for future production. Therefore, a hybrid system using dynamic simulation objects and fuzzy set theory is designed to assess its efficiency and flexibility in advance. Its design and application will be explained by the example of the hydroforming process chain of sheet metal pairs, an innovative sheet metal forming technology.

INTRODUCTION

In general, the introduction of innovations into industry involves the implementation or substitution of products or manufacturing techniques [1]. This paper deals with process innovations in sheet metal processing, which are characterized by the new application of manufacturing techniques for the manufacture of products or product groups. Their implementation intends to improve the flexibility and the efficiency of production (manufacturing costs and time). These goals emphasize the economic importance of applying new techniques in ensuring the success of an enterprise in the long term. However, their implementation into industrial production is usually inhibited by the financial effort and the lack of precise information about their capabilities. Moreover, the efficiency depends on the dynamic market demand for workpiece variants and their quantities, which are not exactly known. Therefore, an important task of intelligent production planning is to predict the economic success of applying new manufacturing processes in advance.

In recent years, simulation methods have become increasingly important in the field of production planning (see [2]). The common applications focus primarily on simulations for short term planning. They are applied to optimize the sequencing of products or the layout of production lines. These methods, however, do not evaluate the economic efficiency of applied manufacturing techniques. In order to assess innovations in technology, other approaches aim at assessing technology affected attributes without simulating the innovative production process (e.g. [3]). Therefore, the causes and recommendations for the implementation can not be recognized by the model of the intended process chain. In contrast, the described system simulates the innovative production process taking into account that:

- The criteria for success might be contrary to one another (e.g. the flexibility and the costs),
- the manufacturing process, the products' quantity and variety, and the economic goals interact by complex dependencies,
- the exact quantification of technology affected attributes is hampered by the lack of exact process knowledge.

CASE STUDY: HYDROFORMING OF SHEET METAL PAIRS

The process chain of hydroforming of sheet metal pairs is taken as an example. The process chain consisting of the process steps hydro-preforming, trimming, welding and hydro-calibrating aims at manufacturing metallic hollow structures (Fig. 1). It can be partially substituted for the convertional process chain (consisting of the deep drawing of the upper and the lower shell in multiple stages and the welding of

0-7803-5489-3/99/$10.00 ©1999 IEEE.

them; [4]). A reduction in manufacturing time and workcenter costs is expected due to fewer process steps and less handling and change-over time between the multiple stages of the deep drawing process. In contrast, the process chain causes higher workcenter cost rates because of the investment costs for the complex forming tool, the hydraulic device and the docking system (see [4]). Furthermore, the flexibility might be reduced because of the expensive specialized forming tool. The assessment of the economic efficiency of the hydroforming process chain has to consider the technology as well as the planned spectrum of workpieces.

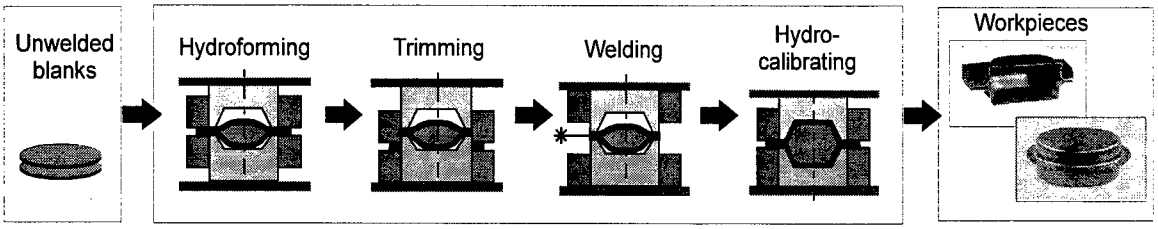


Fig. 1. The process chain of hydroforming of sheet metal pairs.

In order to evaluate the economic consequences of the implementation of the hydroforming technique, a complex network of interdependencies has been taken into consideration (Fig. 2): It contains the attributes of these workpieces which are planned to be produced. They are represented in the example by their quantity and variants. Because of their dependency on changing demand, they are linked to the investigated planning time. The attributes of the process steps, their involved machines, and the tools are depicted in terms of depreciation costs and capacity utilization. As indicated by the arrows, the utilization must take into account its dependency on manufacturing time and the produced quantity. Moreover, the utilization affects the depreciation costs. In turn, the manufacturing cost depends on depreciation costs and manufacturing time. The goals of process chain implementation are in terms of flexibility and efficiency (manufacturing time and costs). Furthermore, the frequency as well as the costs associated with change over time affects the flexibility in sequencing of workpiece variants, keeping in mind that each workpiece variant requires a shape dependent forming tool. Finally, the flexibility and the efficiency influence risks and chances involved in process chain implementation. To highlight the diverse interdependencies, the arrows in Figure 2 are accompanied by plus or minus signs indicating positive and negative effects, respectively.

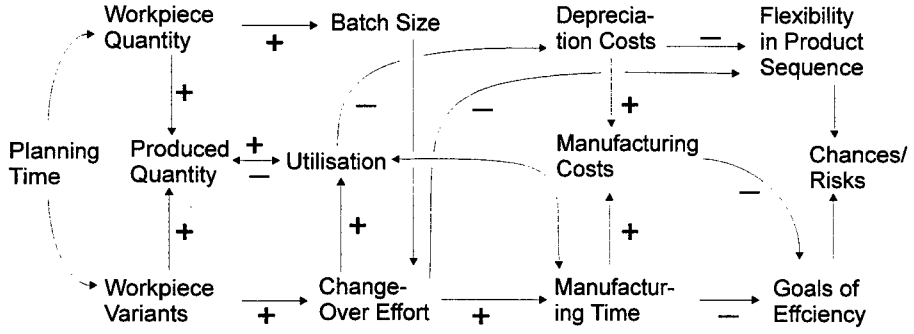


Fig. 2. Effects between the goals and the attributes of product and process chain.

The simplified representation in Figure 2 indicates the complexity of relationships between the attributes of manufacturing process and the intended goals of the innovative process chain. Furthermore, the quantity and variants of products depend on the dynamic behavior of market demand. Therefore, the dependencies have been evaluated with regard to the planning period. It results in a dynamic scenario which has been modeled and simulated to decide whether or not the innovative process chain will satisfy the economic goals. The large number of interdependencies requires a comprehensive, dynamic simulation concept which is capable of modeling all important factors and their mutual interactions.

COMPONENTS OF THE MANUFACTURING PROCESS

In order to cope with complexity, a model structure of the investigated technology defining various simulation objects has been created. These objects define an abstract layer of the system. They are designed to represent separately: the process steps; the machines; the tools; the workpieces; and the human being or operator. For each component, a set of significant attributes is assigned and quantified in order to define their behavior. For example, a tool or a machine is described by its expected utilization, investment and depreciation cost, effective life, etc. The process step is characterized by the flow of workpieces, the associated processing time, the workcenter costs or the effort for flexible changing in product variants etc. The workpiece variations are represented essentially by their quantity and variants. Furthermore, short term planning strategies, such as choice of batch size, are linked to this aspect. The human being, i.e. the operator, can increase efficiency based on experience gained. This effect is described as the learning curve.

In order to design a dynamic simulation scenario, a set of initial attribute values has to be quantified for each component. In contrast to the well researched simulation of existing manufacturing systems, the simulation of innovative, eventually non-implemented process chains, needs a completely different initialization of the scenario. The definition has to take into account that the lack of concrete knowledge obstructs the exact definition of these attributes. Furthermore, a couple of attributes is characterized by a vaguely known dynamic behavior (e.g. quantity of workpieces, utilization of machines).

For example, instead of a well known deep drawing tool, a set of suitable forming tools can be incorporated in the scenario. To define their initial attributes, the lower and upper range as well as the most likely value of cost, e.g. average investment costs, have been identified. This approach results in a fuzzy set defined by the minimal, maximal and the mean values (Fig. 3). The mathematical description of these fuzzy sets is formally given by a *LR fuzzy number* [5]. The steady *membership function* $\mu(x)$ of a fuzzy number determines an uncrisp (non-real) numeric value by the real triple (m,α,β) where m, α, β are the mean value, the left and the right *support* (Fig. 3, [5]). The shape of the fuzzy set can be influenced by choosing a function L(u), R(u) for the left and the right hand side, respectively, such as

$$\mu(x) = \begin{cases} L\left(\dfrac{m-x}{\alpha}\right); & \text{for} \quad x \le m \\ R\left(\dfrac{x-m}{\beta}\right); & \text{for} \quad x > m \end{cases} \qquad 1.$$

$$\text{and } L(u) = R(u) = max(0, 1-u)$$

which leads to a partial linear membership function μ [5, 6]. A membership degree $\mu(x) = 1$ means a high degree of possibility. In contrast, a membership degree $\mu(x) = 0$ indicates that the related values are impossible. The fuzzy numbers are often associated with a linguistic term, such as approximately 30 thousand Euro for the investment costs of the tool.

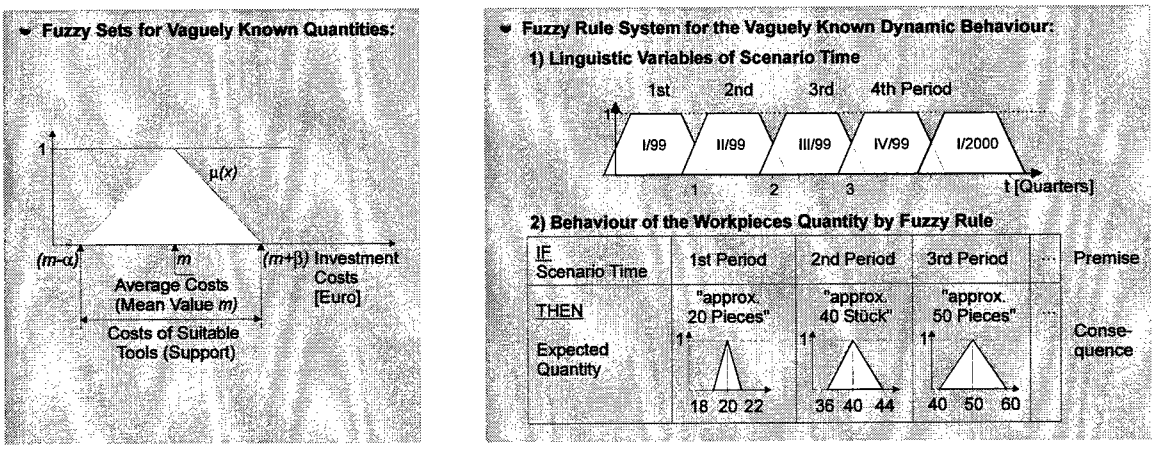


Fig. 4. The use of fuzzy set theory to initialize vaguely known attributes.

A further application of fuzzy set theory occurs with the specification of the vaguely known dynamic behavior of initial features. A good example would be the expected quantity of a workpiece variant (workpiece component). It can be estimated for different planning periods (e.g. quarter of a year,*premise* of the rule system). The planning periods are represented by trapezoidal fuzzy numbers. According to the premise, an uncrisp number of expected demand must be defined for each planning period (*consequence*). The procedure described results in a fuzzy rule system as shown in Figure 4. Fuzzy rules and their evaluation are applied to such simulation quantities which cannot be described using arithmetic functions.

The Modular Concept of the Simulation System

Simulation systems are designed to predict future developments which are described by dependencies of various interacting system variables. In order to assess the economic efficiency of innovative technologies, the complex dependencies between the attributes of manufacturing components and the efficiency goals must be evaluated. A modular concept is designed for representing these dependencies in a formal manner.

Figure 5 shows the objects of the scheme which are designed to represent the components of manufacturing process keeping in mind machines, the tools, the experience of human being (operator), the workpieces, and the process steps. The technology component aims at aggregating the partial effects of efficiency as evaluated by the process steps. The dependencies between these high level components are depicted by arrows. The components and their interfaces define various interacting simulation objects, thus the simulation scheme can be treated as an object oriented simulation [7].

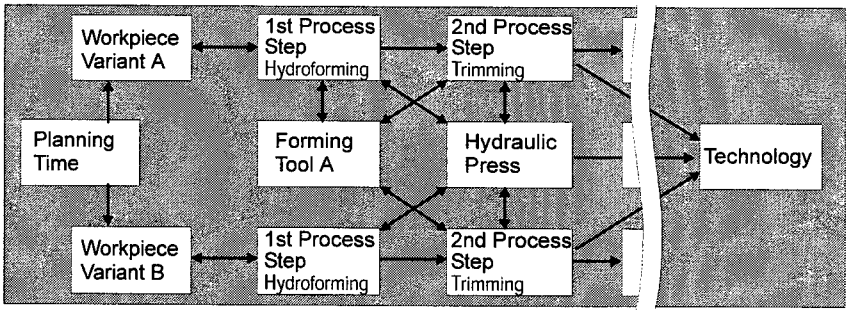


Fig. 5. The objects of the simulation system.

The separate representation of planning periods by planning time and their connection towards the workpiece components must be done for the evaluation of dynamic quantities (fuzzy rule systems), i.e. the quantity of workpieces. The objects of the 1st and 2nd process steps include the flow of workpieces, and the features of manufacturing time and costs regarding the connected workpieces, tools and machines. The components of tools and machines are linked to those process steps which require their capacity and cost features. The object of technology contains quantities of the flexibility, the costs and the efficiency of production. These quantities are derived from cost and time attributes as simulated by the connected objects.

DETAILED DESIGN OF THE SIMULATION OBJECTS

Each of these high level components consists of a set of simulation variables. Their type of design, connection and behavior is similar to *Forrestermodels*, a framework for the simulation of complex dynamic behavior [8]. The system variables are divided into *stocks*, *converters* and *flows* (Fig. 6). The converters have to be calculated for each time step, regardless of their last state. They have to perform an arithmetic operation or the evaluation of a fuzzy rule system. In contrast, stocks act as the memory of the simulation system. Their state at any time depends on their state at the previous time step and on directional *flows*. Flows into a stock are accumulated; the outgoing flow from a stock causes a decrease in the numerical stock value. The value of any flow must be determined using flow regulators, which are described by time-dependent differential equations. Stocks are always zero or greater. *Sources*, depicted in Figure 6 as clouds, act as stocks with unlimited capacity.

The excerpt of the workpiece object is as an example of detailed design (Fig. 6): The simulated variables represent the attributes of the workpiece, designed to model their behavior within the process chain. The conversion of *demanded workpieces per time* has a direct connection with *scenario time*. This is designed to incorporate expected demand modeled by a time-dependent fuzzy rule shown in Figure 4. In turn, the choice of *batch size* may be influenced by the demand. Therefore, a second fuzzy rule system is designed to formalize batch-size strategies as experienced during past production. The required workpieces per time is accumulated in the stock on the left hand side (*demanded workpieces*: x). Its growth is described by the equation $dx/dt=w$ (or $\Delta x/\Delta t=w$) where w represents the current demand. To simulate the quantity of produced workpieces, demand is compared with capacity. So, an input variable (interface to the objects representing the involved process steps) aggregates the manufacturing time, taking into account available capacity. Indeed, the throughput quantity of this workpiece variant is calculated by the lesser of capacity and demand. This is accumulated by the second stock (*produced workpieces*). The variable *workcenter costs* is connected to the involved process steps, from which the *cost per workpiece* is derived. The output variables connect the machines and process steps to utilize their capacity, to relay the frequency of product changing, or to incorporate product specific attributes into a final assessment of the process chain.

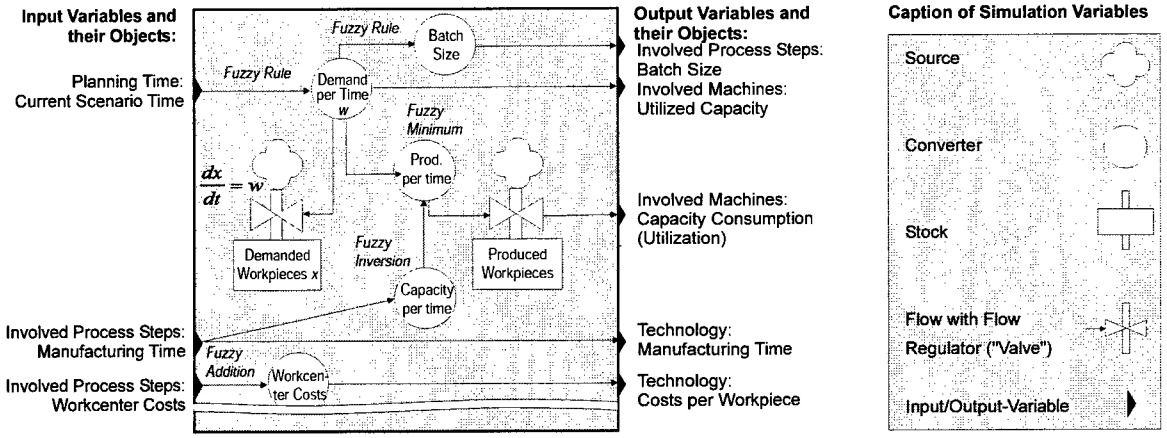


Fig. 6. Excerpt of detailed design of the simulation object *Workpiece variant*.

The basic simulation concept is applied to all other components in the simulation system. Each simulation object must represent its own state and interact with one another by predefined interfaces. Moreover, the object-oriented concept allows the design a set of reference objects for the components of manufacturing process. They might have been incorporated in the scenario in multiple instances depending on workpiece variety and the complexity of the process chain. Therefore, process chains of variable process steps, machines, tools and workpieces could be simulated.

EVALUATION OF A SIMULATION SCENARIO

The simulation variables included in objects (introduced above) are quantified by numerical values for each time step of the dynamic scenario. Because of the scenario initialization by fuzzy numbers and fuzzy rules, the evaluation of a simulation object must be done by fuzzy number-based operations. Fuzzy rules are evaluated by determining the membership degree for each fuzzy set of the premises. The membership degree is assigned to the consequences (Fig. 3. [5]). Finally, the fuzzy sets of the consequence which have a non-zero membership degree are aggregated. This evaluation method does not apply defuzzification to avoid the loss of the fuzzy sets' support.

For further numerical operations (e.g. multiplication, addition, etc.) the *extension principle,* which extends conventional numerical operations into fuzzy quantities, is applied. It is defined for two arguments in terms of membership functions $\mu_a(x)$ and $\mu_b(x)$ [5, 6]:

$$\mu_{a\otimes b}(z) = \sup_{z=x\times y} min\{\mu_a(x), \mu_b(y)\} \qquad 2.$$

In the case of LR fuzzy numbers, there are a set of predefined operators, such as [5, 6]:

$$(m,\alpha,\beta)_{lr} \oplus (n,\gamma,\delta)_{lr} = (m+n,\alpha+\gamma,\beta+\delta)_{lr}$$
$$(m,\alpha,\beta)_{lr} < (n,\gamma,\delta)_{lr} = (mn, m\gamma+n\alpha, m\delta+n\beta)_{lr} \qquad 3.$$

for addition and multiplication, respectively. In order to derive only triangular fuzzy numbers with a linear membership function, the result obtained by the extension principle can be slightly modified [5].

However, application of fuzzy operators can result in unexpected values. These may occur if an *improper function* appears in algebraic terms [6]. These terms contain a variable or a function of this variable more than once. The fuzzy operators try to extend the support as much as possible without accounting for any dependencies between their arguments. The following approaches are taken into account by model design:

- Terms containing a variable more than once should be avoided,
- the use of isotronic functions [6],
- the numeric evaluation by the extension principle incorporating additional conditions [6],
- the value of each stock must be independent of improper functions.

These approaches are often considered by modifying the model structure or the evaluation method, which are basically fixed by predefined components and the interface. These measures attempt to avoid improper functions and/or minimize error propagation during simulation. Although defuzzification generally avoids improper functions, it is not applied here because of the loss of a fuzzy set's support and its information.

A SCENARIO FOR THE HYDROFORMING OF SHEET METAL PAIRS

The concept is applied to the process chain of hydroforming. The scenario evaluates the required components and derives the risk and chances of the process chain implementation. Figure 7 shows the simulation object *technology* (see also Figure 5). The portfolio technique aims to compare risks and chances [9]. Because the scenario is initialized by fuzzy sets, the simulated results are also predicted by fuzzy sets.

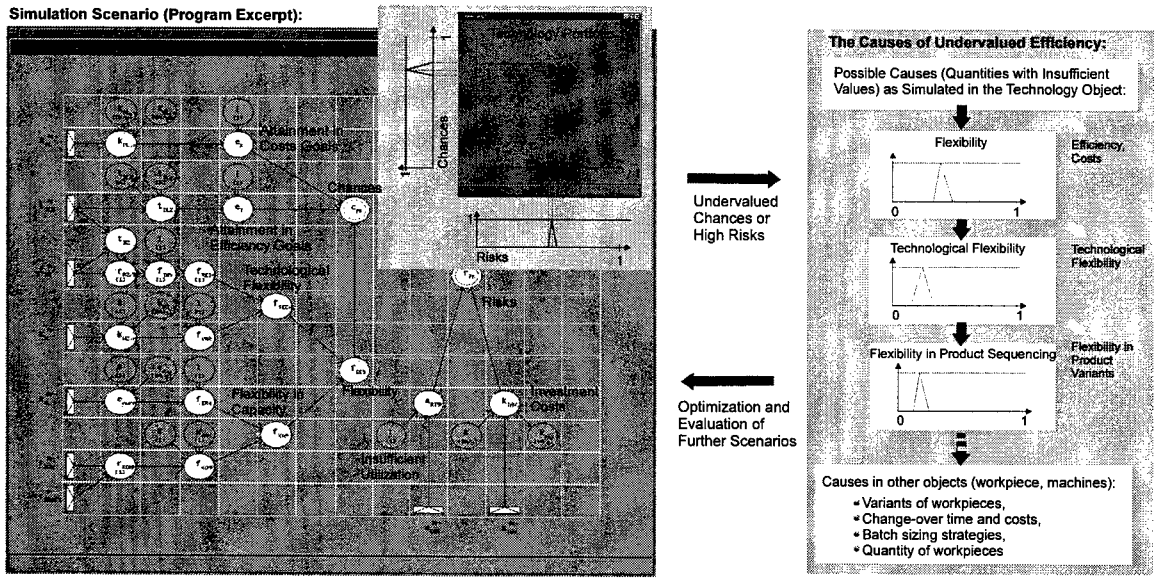


Fig. 7. Predicted risks and chances for hydroforming technology by aggregating the flexibility, the costs and the efficiency of the process chain.

An excerpt of the computer program, shown on the left hand side of Figure 7, is completed by the keywords indicating the sequence of aggregating efficiency goals. It is recognized that the chances are assessed from the predicted flexibility and the attained efficiency in terms of cost and time. Moreover, it can be seen that flexibility includes capacity (capability to adapt to changing product quantity) and technology (capability to adapt to changing variants). Simulation variables are valued with respect to behavior of other simulation

objects, such as process steps, machines, etc. For example, flexibility in sequencing product variants depends on frequency and expense of time and cost to change the product variant keeping in mind that each variant requires its own shape-dependent forming tool. In turn, these quantities are determined by the depreciation cost of machinery, change-over time, and the quantity and variety of products and their batch size. Risk is assessed by the insufficient utilization of expensive process techniques and investment costs.

Comparison of risks and chances by the portfolio technique [9] can yield potential for a process chain. The portfolio identifies behaviors by the relations of chance and risk. Moreover, wide support for the predicted fuzzy set indicates several highly sensitive initial attributes. To optimize the implementation of a process chain, the causes of a simulation result are identified. Concerning the hydroforming process chain in Fig. 7., causes of undervalued chances can be analyzed interactively as follows (Fig. 7.):

Costs, manufacturing time and flexibility have been investigated. It is shown that technological flexibility is, especially undervalued. A more detailed investigation shows that flexibility in product-sequencing is the most undervalued factor involved in technological flexibility, indicating high effort to adapt to product variations. The investigation focuses on the simulation of objects of the process chain and process steps. Small batch sizes, small quantities of workpieces, high frequency and effort in change-over, combined with high investment costs, are the main factors responsible for an undervalued assessment. With this knowledge, a first approach to optimisation is possible: In fact, the quantity of workpieces has increased. Alternatively, an extended batch size may reduce requirements of flexibility. As well, more flexible tool techniques using modular tools or shape-dependent inserts can reduce the effort to adapt to product variations. These approaches can be confirmed and investigated by further scenarios incorporating intended changes in the product spectrum or process technique by modified attributes of manufacturing components.

SUMMARY

The design of hybrid simulation objects using fuzzy set theory to assess implementation of innovative process chains in sheet metal processing has been demonstrated. To cope with complexity, a modular concept is used to represent components of a manufacturing process, their behavior and interdependencies. In particular, integration of uncertain, dynamic behavior of innovative process chains has been considered. Uncertainties in estimating process attributes or vaguely-known dynamic behaviors are accounted for by qualifying the simulation variables as fuzzy sets or fuzzy rules. This allows their specification using membership functions which enclose a variation range dependent on the precision of the knowledge. These uncrisp values are integrated into the simulation by extending dynamic models with algebraic fuzzy operators and fuzzy rule systems. The system predicts the mean efficiency and its sensitivity. Moreover, it supports an analysis of the causes of predicted efficiency to provide starting points for optimisation.

ACKNOWLEDGMENT

The authors are grateful for support from the German Research Society (Deutsche Forschungsgesellschaft, DFG), under the research project "Assessment of the implementation of innovative technologies into industry using simulation" and the activities in hydroforming within the special research topic SFB 396.

REFERENCES

1. J. M. Utterback, 1994. Mastering the dynamics of innovation. Mass. Harvard Business, Boston.
2. J.E. Lenz, 1986. Proc. 2nd International Conference on Simulation in Manufacturing. IFS, Chicago.
3. C. Ullmann, 1995. Methodik zur Verfahrensplanung von innovativen Fertigungstechnologien im Rahmen der technischen Investitionsplanung. Shaker, Aachen.
4. P. Hein, F. Vollertsen, 1998. Hydroforming of sheet metal pairs. J. Mater. Proc. Tech., 87 1-3, 154-164.
5. H.-J. Zimmermann, 1991. Fuzzy Set Theory and Its Applications. Kluwer Academic Publishers, Boston.
6. D. Dubois, H. Prade, 1987. Fuzzy Numbers: An Overview. J. C. Bezdek: Analyses of Fuzzy Information, Vol. 1, CRC Press, Boca Ranton, Florida.
7. B. Schmidt, 1996. Die objektorientierte Modellspezifikation. B. Schmidt: Sim. in Passau, 1996, 1, 4-17.
8. J.W. Forrester, 1972. Industrial dynamics. Mass. MIT Press, Cambridge.
9. H. Wildemann, 1987. Strategische Investitionsplanung. Gabler, Wiesbaden.

Manufacturing Management Improvement through Rapid Production of Budgets

E.J.Colville

School of Engineering, University of Tasmania,
PO Box 252/65, Hobart 7001, Tasmania, Australia
Email: respub@access.net.au

ABSTRACT

This paper explains a method whereby manufacturing control of a firm can be facilitated by rapid preparation of coordinating budgets using simulation. Results of this process applied to a small organisation are reported. By being mathematically integrated, this budgeting system embraces the whole of a firm's activities and allows investigation of alternative policies to obtain an optimum forward plan. The program manual and an outline of the budget support software is explained and its use with a PC is demonstrated.

Use of this mathematical simulation process to produce an overall budget not only provides detailed operating budgets but gives basic data such as cost standards and departmental hourly rates for use in ancillary marketing, costing and production planning programs and input to progressive performance reports. Sales, production, factory overhead and administration budgets for each department are produced in a single run for each proposal. At the same time profit and loss, cash flow predictions, balance sheets and funds movements are all provided using the budget program in addition to cost standards and hourly rates.

A survey of budgeting practice in Australia over a range of manufacturers points to an increasing accent on deriving overall plans as well as input to production planning and calculation of cost standards direct from the budget. Many firms no longer rely solely on production department estimates and the current order position for their detailed planning input. A feature of this procedure is its contribution to communications between board and shop floor and between the marketing, design, production and finance departments with the result that middle management costs are minimised and implementation is expedited. General management, accounting and engineering tend to be consolidated using this approach.

Comments on the application of this budget support system over the past decade are reported and recommendations are given for its use as a coordinating and planning procedure, particularly for small to medium size companies.

INTRODUCTION

From the early days of Gantt charts for direct machine and labour loading to the current production planning schemes such as MRP11, the accent of management has typically been on production standards based on shop-floor experiences and attitudes. In many text books, manufacturing management and manufacturing as a whole has too often been equated only to factory production and mechanical skills.

A new era now opens up in which at last it is being realised that overall management of a manufacturing firm requires managing skills that embrace the shop floor, technology skills and business skills rather than relying solely on just one of these. There is now a global recognition that major improvement can follow an analysis of the whole of an enterprise's activities within the socio-economic background of its industry, both locally and internationally. Far too often we have debated the attributes of MRPII and ERP, for example,[1] without placing sufficient emphasis on the overall input to these programs by the policy makers. We should not rely on production people to fill the gap which top management should define.

The revolution in recent years in computer hardware, software and staff availability with skills in the programming areas needed, now allows immediate calculation of both forward budgets and input to detailed

0-7803-5489-3/99/$10.00 ©1999 IEEE.

production planning programs for the execution of current orders. At the same time the policies agreed by company executives can be incorporated in time for review and allow communication to all who have to participate in, and implement, the budget.

It is more than 30 years since the budget research reported in this paper was initiated. Since that time software improvements and methods of presentation have improved and at the same time the cost of the facilities and speed of system operation have dramatically changed. Original trials ranging from a drilling company to a large cattle and sheep farm have led to regular use in a printing and publishing company as a laboratory to develop the software, in particular for presentation and ease of data entry. The Budget Support program [2] simulates the financial flows of the budget and sets out key plans for marketing, production and financial control. It also provides the standards forlabour and machine loads as well as material purchase requirements to meet current orders and provide a basis for production planning.

This procedure has verified the program's validity. It assists information flow to meet the increasing need for greater communication within firms which have been used to hierarchical management. At the same time economic pressure to reduce middle management while still improving information services requires improved links between top management and factory operations. Clearly the accent in manufacturing management will move towards combining the "general" of overall management, and the "particular" of shop floor activities to process orders involving plans of the MRP, ERP and JIT type as well as simpler production planning procedures. The consequence of this would appear to be that hierarchical management will be modified in many democratic countries to provide a much greater degree of participation and improved team work. This need for two departments to work together has been highlighted in a paper by H.Morino [3], of the Overseas Product Development Division for Toyota, in which he sees the need to overcome the barrier of departmentalisation if we are to attain top quality.

PROGRAM DESCRIPTION

The modelling process and its application described in references [4], [5], [6] and [7] simulates a manufacturing concern from the stage of budget coordination, and trials of alternate policies, to adoption of the budget. The first requirement of integrated manufacturing so clearly outlined by Gerelle and Stark [8] is the definition of the strategy to be adopted. "This cannot be achieved unless it is known where the company's management wants to go, in other words, until the objectives of the company have been defined". These involve the outward looking marketing objectives as concerned with customers and the inward looking innovation objectives concerned with producing products to satisfy customers. The budgets then follow for each of the sales, production and finance departments. Control of liquidity, profit and balance sheet criteria is made possible through regular comparison reports highlighting differences between budget and actual results achieved and analysis of financial ratios.

To achieve this, the dollar value as the common transfer item, is used in equations which define the interacting relationships between the departments of the firm. As an example, sales quantities for the budget period for each subassembly are transferred to sales dollars using multipliers involving price, distribution throughout the budget period, and comparison with prior sales quantities.

Similarly materials required to make each subassembly are calculated using the proportion of each material in each subassembly, the purchasing distribution and the unit material cost. Wages are calculated from expected hours for the staff allocated to each wage department at an expected wage rate. Estimates of supervision for the direct wages is provided using a matrix which proportions the total of direct wages.

Factory overheads are set down in their categories as are administration accounts divisions. Some variable sales expenses are allocated as a proportion of total sales dollars. The actual opening balance sheet is supplied as data so that the simulation can build on it as the budget period progresses. Financial information which affect the costs, the cash flow and the progressive balance sheets is also entered as data together with trading terms which affect cash flow. Changes to capital, depreciation, loans and equity are also entered.

Finally matrices are introduced that distribute overheads where they belong, and allow calculation of hourly rates by departments. The names of the budget components and the periods which a firm wishes to give to its budget and its products/subassemblies as well as its accounts and operating departments can also be entered as data to allow more general application of the simulation to a range of industries.

The pull-down menu of Figure 1, from the manual [2] shows the components of the budget support system made available on the computer screen.

IMPLEMENTATION

First it is necessary to recognise that the initial data entry is a key task requiring:

- detailed investigation of the firm's activities
- clarification of the terms describing the products subassemblies and accounts categories of the firm
- meetings of departmental heads to exchange their needs and the views to be fed into the budget for trials in which the results of their plans will be calculated, and if necessary modified, before adoption as an agreed budget they are prepared to positively implement.
- entering of around 1000 data items describing the budget.
- alignment of company book categories with those of the budget or vice versa.

Next is maintenance and data review in light of new plans and any change in micro and macro-economic conditions. While the five initial installation items above still apply, they usually take far less time and less executive stress as the years of budgeting advance, since in a particular firm certain variables are found to predominate and many of the relationships show only minor variation. It is however necessary to catch up with the opening balance sheet, as well as, new products and changes in emphasis among the product range and potential capital investment and repayment plans. Prices, wage rates and unit material costs may need review. The totals of immediate past actual costs should be compared with those of any new budget.

The most important part of a management procedure of this type is to ensure the desired results are achieved. By the participation of those best able to implement the plan action within the objectives of the company are mostly likely to take place. If people own the plan and believe in it, they are more likely to push it through despite obstacles on the way.

CASE STUDIES

Development of the simulation has taken place as part of the management of a printing, publishing and consulting company. At the same time, there has been the stimulus to provide management education, the encouragement of the University of Melbourne, and the need to grasp the opportunities which the computer hardware and software revolution gives in providing real-time information for decision-makers.

Introduction of the program has highlighted the following:

Advantages

1. The saving in infrastructure costs, such as accounting, estimating and liaison costs between production and supply people and similarly between production and marketing people.
2. Improved participation and the assistance to staff who desire to take responsibility and who desire to take a direct interest in a firm's future.
3. Ability to meet the needs of macro-economic change by testing the effect of radical changes prior to implementation. An example is movement from vertical to horizontal integration should a change from a seller's to a buyer's market justify this.
4. Wise choice of timing for both investment and borrowing to assist the preservation of liquidity and hence the long term security of the company.

5. Easy maintenance and a more profitable business.
6. Incorporates such skills as accounting and industrial psychology which broaden the role of engineers with IT aptitudes, and facilitates their management of technology based enterprises.
7. Applicable to a wide range of industries by simply changing names and data since accounting principles are similar.

Disadvantages

1. Resistance to acceptance can occur due to the fact that this process is one of long term benefit and needs consultation whereas many general managers concentrate on short term returns. This can cause the time taken for initial installation and acceptance to be spread over several months.
2. Firms inculcated with a hierarchical approach to management can be frightened of sharing information and improving communication which is fundamental to the budget support process.
3. The coordinator/facilitator introducing the process needs to have an insight into computer programming as well as management needs.
4. The internal production of budgets involving full coordination may be resented by those external professionals, such as accountants, previously responsible for a more simplified process without input from the key staff responsible for implementation.
5. The problem of the "Our business is different" attitude in many paroch ial firms.

DEVELOPMENT PLANS

While there are always items for technical improvement, the following will be receiving attention in the immediate future in view of the effectiveness of the methods described.

1. Attention to the wider commercial application of the simulation.
2. Reducing the time of installation by setting out proforma procedures for obtaining data, for meeting agendas and to encourage participation.
3. Defining a standard method of adjusting the budgeted balance sheet for any anomaly arising from the difference between the carefully calculated stock figures of the simulation and the sometimes arbitrary estimate in the company's books.
4. Enabling the maintenance of the budget to be expedited by defining, for a particular company, the more important data items to be reviewed regularly rather than be concerned with the statistically less variable data which may only need major change at a time of reconstruction of the company's affairs.

CONCLUSION

It has been shown that the Budget Support program described meets two important needs of current management. First the provision of economic budgets quickly as business climates change. Second, if combined with a high degree of participation by senior executives and their staff, efficient implementation takes place as a result of team work throughout the plant. The procedures outlined shorten the lines of communication within the firm so that flexibility so important for competitiveness in the current global economy is enhanced, particularly for small to medium size companies where economic infrastructure is imperative.

REFERENCES

1. C.Hume, D.Paynter, 1989. An investigative analysis of Just in Time, MRPII, and their integration. University of Melbourne Special Project, 45,113.
2. E.J.Colville, 1997. Budget support - A Management and Development Program. Research Publications, Melbourne.
3. H.Morino, 1999. Total Simultaneous Management through Marketing to Development, Engineering and Production. Proceedings IPC 10 SAE Melbourne.Paper 99056.

4. E.J.Colville, 1992. Mathematical Simulation of a Manufacturing Concern - An Important part of Management Education. ACEME 1 Sydney.
5. E.J.Colville, 1986. A Management Information System for Small Manufacturers. SAE International Conference , Auckland New Zealand.
6. E.J.Colville, 1995. Production Budgets and Costing Standards using Mathematical Simulation from Financial Data. 13th International Conference on Production Research, Jerusalem Israel
7. E.J.Colville, 1998. Computerised Master Planning for a Manufacturing Firm and its Application to Factory and Sales Departments. International Conference on Mechanical Engineering Tehran, Iran.
8. E.G.R. Gervelle, J.Stack, 1988. Integrated Manufacturing . McGraw Hill, 28.

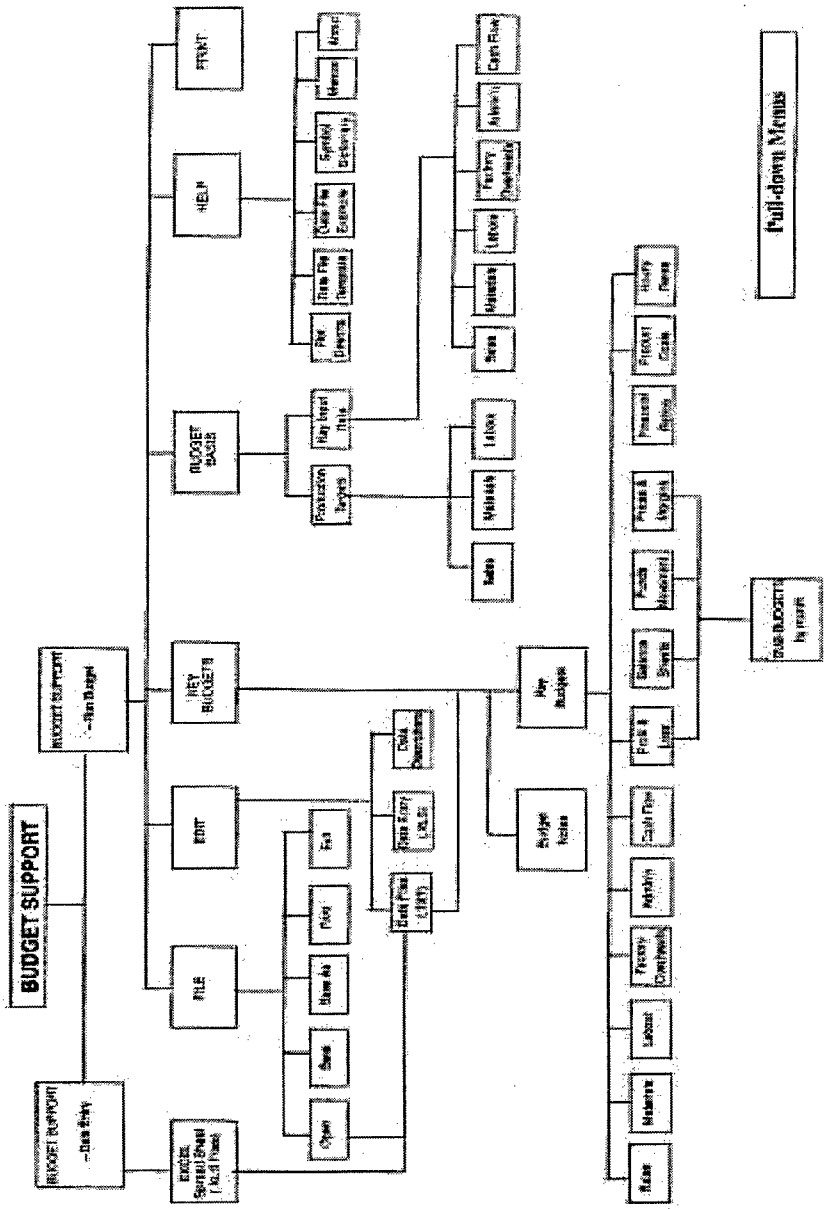


Fig. 1. Pull-down menu of the Budget Support program .

A Connectionist Method to Solve Job Shop Problems

Marko Fabiunke, Gerd Kock

GMD FIRST Berlin
Rudower Chaussee 5, 12489 Berlin
Email: marko@first.gmd.de, gerd@first.gmd.de

ABSTRACT

We propose a novel framework to solve job shop scheduling problems based on connectionist ideas of distributed information processing. In our approach each operation of a given job shop problem is considered to be a simple agent looking for a position in time such that all its time and resource constraints are satisfied. Each agent considers the current time position of its constraint neighbors to gradually change its own position to reach this goal. All agents together form a recurrent dynamical system which either self-organizes after some iterations to a feasible schedule or fails to do so depending on the constraints of the problem. By gradually increasing the constraints through decreasing the allowable overall processing time for a valid schedule, better and better solutions are found up to the point where no further improvements can be made.

INTRODUCTION

In classical job shop scheduling we are given a set of jobs, each of which consists of a chain of operations, and a set of machines being able to process at most one operation at a time. Each operation needs to be processed on a given machine and during an uninterrupted time period of given length. All jobs have to be finished at a given latest completion time. The goal is to find an assignment of operations to starting points (schedule) such that neither the machine capacity constraints nor the job precedence constraints are violated. A schedule is called optimal if it minimizes the overall processing time (makespan) of all jobs.

Job shop problems are known to be NP-hard to be solved to optimality and have the reputation of being one of the most computationally stubborn combinatorial problems. Complete search algorithms are usually unable to solve problems with more than a few operations. For practical reasons it is therefore acceptable to apply heuristic methods to find approximations to the optimal solution which still remains difficult to achieve. Due to [1] it is even NP-hard to find a schedule that is shorter than 5/4 times the optimum. Therefore, schedules generated by enumerative heuristics based on simple dispatching rules are often still far from the optimum.

Currently we distinguish between two major heuristic approaches to solve job shop problems. *Schedule construction* is best done through a combination of classical operation research methods with elaborated global constraint preprocessing techniques to guide the process of construction and to avoid the need of backtracking as much as possible. This idea has found its best expression and most success in the usage of constraint logic programming as a unique framework to combine both methodologies [2, 3]. *Schedule repairing* uses local optimization techniques like simulated annealing, tabu search, guided local search and genetic algorithms to empirically create solutions starting out of some initial found schedule [4, 5]. Those techniques employ the common idea that a given solution may be improved by making small changes. Better and better solutions are found by repeating this process over and over again. Empirically, local search techniques have proven to be very effective in solving large scale combinatorial problems.

The scheduling methodology presented here clearly belongs to the local search group. Starting with some initial assignment for all starting points, a feasible schedule not exceeding a given maximal makespan will be generated, using a self-organizing algorithm based on connectionist ideas. In this algorithm, each operation of a given job shop problem is considered to be a simple agent (or processing unit) looking for a position in time such that all its time and resource constraints are satisfied. To obtain this, each agent considers the current time position of its constraint neighbors (the other agents) to gradually change its own

0-7803-5489-3/99/$10.00 ©1999 IEEE.

position. As distinct from sequential local search methods, all agents are working simultaneously and therefore form a highly recurrent dynamical system of parallel working units, which should self-organize after a while to a feasible schedule but may fail to do so if problem constraints becomes too high.

Decreasing the allowable maximal makespan will gradually increase the degree of constraining and produce better and better schedules as long as the self-organizing algorithm converges.

Compared with the neural network scheduling approach of Zhou et al. [6] and the multi-agent scheduling system of Liu and Sycara [7], our distributed framework shows some kind of hybrid flavor. Our processing units are neither "intelligent" enough to be called agents (in the usual sense), nor do they meet the ordinary definitions of "artificial neurons". Moreover, although information in our framework is distributed much like signals in neural networks, they can't be interpreted simply as unit activations. However, we prefer to call the whole a "connectionist" algorithm since its design has been influenced much by the connectionist idea of simple processing units, where each unit is responsible for one local piece of information and all units act simultaneously, influencing each other to achieve a common global goal.

Accordingly, the algorithm has been implemented using CONNECT, a specification language for connectionist systems, which has been originally designed for the development of artificial neural networks. CONNECT allows for flexible definitions of networks of simple processing units, each of them communicating with the others by sending signals, and can be applied to design neural networks, cellular automata as well as other simple distributed systems. Another interesting feature of CONNECT is that it comes together with a graphical user interface (GUI) library of C++ modules, which easily can be used to visualize the progress in schedule development – for heuristic approaches this is an important point. The complete package of CONNECT and the GUI library is part of the NeuroLution system. For further details see [8, 9].

PROBLEM DESCRIPTION

We start with a formal definition of the classical job shop scheduling problem as used in this paper. Let J be a set of n jobs and R be a set of m resources (machines). Each job $j_i \in J$ consists of a chain of m operations $o_{ij}, \ldots, o_{im}$, such we are given a total of $n \times m$ operations to be scheduled.

Each operation o_{ij} requires for processing a resource $r_{ij} \in R$ and will block this resource for other operations over a period of $d_{ij} \in \mathrm{N}$ time units. Any two different operations belonging to the same job do not require the same resource again, i.e. $r_{ij} \neq r_{ik}$. The operations in one job have to be processed in their given order, defining a precedence relation $\prec$ on the set of all operations O as follows:

$$o_{ij} \prec o_{kl} \Leftrightarrow i = k \wedge j + 1 = l.$$

Our goal is to assign to each operation o_{ij} a discrete starting position in time $x_{ij} \in \mathrm{N}$ out of some given period of possible positions $X_{ij} = [b_{ij}, e_{ij}]$. We call the vector of all starting positions $x = (x_{11}, \ldots, x_{nm})$ a *schedule* and the corresponding domain $X = X_{11} \times \ldots \times X_{nm}$ the set of all schedules. A schedule is called *feasible*, if it satisfies the following constraints:

$$o_{ij} \prec o_{kl} \Rightarrow x_{ij} + d_{ij} \leq x_{kl} \quad 1.$$
$$r_{ij} = r_{kl} \Rightarrow x_{ij} + d_{ij} \leq x_{kl} \vee x_{kl} + d_{kl} \leq x_{ij} \quad 2.$$

The set of all feasible schedules (problem solutions) will be denoted by $L \subseteq X$. The overall processing time (makespan) of a (feasible) schedule is given by the function $\tau(x) = \max_i \{x_{im} + d_{im}\}$. A feasible schedule $\tilde{x}$ is called *optimal* if it minimizes the makespan ($\forall x \in L : \tau(\tilde{x}) \leq \tau(x)$).

SELF-ORGANIZING TO A FEASIBLE SCHEDULE

In our distributed framework each operation o_{ij} of a given problem is considered to be a simple processing unit (agent), trying to find some value for the local variable x_{ij} out of the domain X_{ij} such that constraints 1

and 2 that apply to x_{ij} are satisfied. We start with an initial (possibly random) start position x^o_{ij} for each operation o_{ij}. To evaluate the current position, each agent needs to know the position of the other agents. We therefore have to distribute this information among agents much like distributing activations in neural networks. To be more precise, an agent needs to know just the position of its constraint neighbors, which are its immediate predecessor and successor in the job ($o_{ij-1} \prec o_{ij} \prec o_{ij+1}$) as well as the operations being processed on the same machine ($o_{kl} : r_{ij} = r_{kl}$). This reduces the number of connections since each agent is connected to at most $n + 1$ other agents. For simplicity we denote the constraint neighbors of some agent o_{ij} with $\tilde{O}_{ij}$ and their subrange of time positions with $\tilde{x}_{ij}$.

As we know the positions of our constraint neighbors, we can evaluate our own position. For this purpose we define a constraint violation measure which we call *constraint inconsistency*:

$$\phi_c(x_{ij}, x_{kl}) = \begin{cases} \max(0, \min(x_{ij} + d_{ij}, x_{kl} + d_{kl}) - \max(x_{ij}, x_{kl})) : r_{ij} = r_{kl} \\ \max(0, x_{ij} + d_{ij} - x_{kl}) : o_{ij} \prec o_{kl} \\ \max(0, x_{kl} + d_{kl} - x_{ij}) : o_{kl} \prec o_{ij} \end{cases} \quad 3.$$

It is not difficult to give a descriptive interpretation of the above formula. Assuming that o_{ij} and o_{ij} have to be processed on the same machine ($r_{ij} = r_{kl}$) they block this machine during the time windows $[x_{ij}, x_{ij} + d_{ij})$ and $(x_{kl}, x_{kl} + d_{kl})$. If those windows overlap we have a resource conflict since a machine can process just one operation at a time. We therefore calculate this overlapping as a measure of constraint violation. Something similar is done with precedence constraints $o_{ij} \prec o_{kl}$ or $o_{kl} \prec o_{ij}$ respectively. Here we calculate how many time units we have to shift an operation to the left or to the right, such that there corresponding time windows are in the desired precedence order.

We summarize the individual constraint inconsistencies to form a *local inconsistency* measure for the time position of some operation o_{ij} (Eq. 4.). Similarly we summarize all local inconsistencies to form a *global inconsistency* measure for the schedule formed by the individual time positions (Eq. 5.):

$$\phi_l(\tilde{x}_{ij}, x_{ij}) = \sum_{o_{kl} \in O_{ij}} \phi_c(x_{ij}, x_{kl}) \quad 4.$$

$$\phi(x) = \sum_{i=1}^{n} \sum_{j=1}^{m} \phi_l(x_{ij}, x_{ij}) \quad 5.$$

Note, since the constraint inconsistency is a non-negative function $\phi_c(x_{ij}, x_{kl}) \geq 0$ the same yields for the local and global inconsistency. Moreover, a schedule is feasible iff $\phi(x) = 0$ holds true, which in turn is equivalent to the case that all local inconsistencies are zero. Hence, the local goal each agent has to follow is the minimization of its local inconsistency $\phi_l(x_{ij}, \tilde{x}_{ij})$. This is not easy to achieve since an agent knows about the time positions of its constraint neighbors, but cannot change them. The only thing it can do is to use some local rule $x^{t+1}{}_{ij} = \alpha(x^t_{ij}, \tilde{x}^{\,t}{}_{ij})$ to adjust its own position in time, obtaining a (possibly) better position with respect to the current situation. Since all agents are doing this simultaneously, we end up in a completely new situation which may even be worse then the previous one. But this is not a drawback since strict "hill-climbing" is not a desired feature for any local search method. Instead, we hope that "mistaken" moves are repaired in the following iterations, such that local and global inconsistency minimization is achieved over a longer period of iterations finally ending with a feasible schedule.

The thing we have to do is to choose the local update rule α such that (1) a feasible schedule x, i.e., a schedule with $\phi(x) = 0$, is a fixed point of α and that (2) the recurrent dynamical system $x^{t+1} = \phi(x^t)$ is likely to converge to such a fixed point. Currently there is no simple or analytical way to do so. Of course, we could choose α to be the local conflict minimization rule

$$x^{t+1}{}_{ij} = \arg \min_{\tilde{x}_{ij} \in X_{ij}} \phi_l(\tilde{x}_{ij}, \tilde{x}_{ij})$$

which is used as the basic update rule in the discrete Hopfield neuron model as well as in many sequential local search algorithms. However, we should not expect this to work.

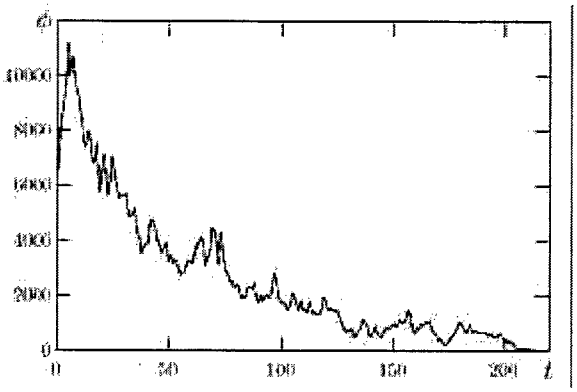


Fig. 1. Progression of ϕ (x^t) using α_1 on a loosely constrained problem.

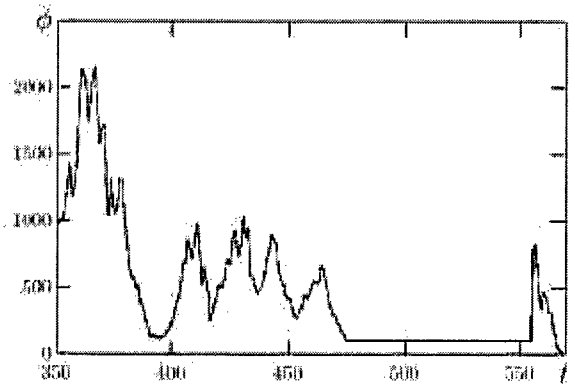


Fig. 2. Progression of ϕ (x^t) using α_1 and α_2 on a tighter constrained problem.

For example, in a similar connectionist approach, applied by the authors to the non-attacking queens problem, applying local conflict minimization simultaneously had the undesired effect that all queens increased the number of conflicts instead of decreasing them. However, with a different update rule we have been able to end up with a conflict-free chess board.

The update rule α for the scheduling problem presented here has been found empirically and should not be assumed to be the only or even the best one. The results obtained with this rule have been promising, but further investigations into the subject may lead to better rules being different from the current one. Our rule α is a combination of two independent rules α_1 and α_2. α_1 is a simple shifting rule. Let o_{kl} be a constraint neighbor of o_{ij}, then we can calculate the minimal shift necessary to obtain a position satisfying the constraint as follows:

$$\delta(x_{ij}, x_{kl}) = \begin{cases} (-\max(0, x_{ij} + dij - x_{kl}) : (o_{ij} \prec o_{kl}) \vee (r_{ij} = r_{kl} \wedge x_{ij} + d_{ij}/2 \le x_{kl} + d_{kl}/2) \\ (\max(0, x_{ij} + dij - x_{kl}) : (o_{ij} \prec o_{kl}) \vee (r_{ij} = r_{kl} \wedge x_{ij} + d_{ij}/2 \le x_{kl} + d_{kl}/2) \end{cases} \quad 6.$$

We summarize all shifts to form a cumulative shift which is finally applied to obtain a new position:

$$\alpha_1(x_{ij}, \tilde{x}_{ij}) = \max(b_{ij}, \min(e_{ij}, x_{ij} + \sum_{o_{kl} \in O_{kl}} \delta(x_{ij}, x_{kl}))) \quad 7.$$

Figure 1 shows the typical progression of ϕ (x) for a loosely constrained problem where all agents apply α_1 simultaneously. Although the function seems to climb up and down unmotivated, we see a clear process of constraint relaxation culminating in finding a feasible schedule. Increasing the degree of constraint on the problem may lead to the undesired effect of getting stuck in a local minimum or a cyclic repetition of infeasible schedules. To escape from this situation we use the second update rule α_2 which is a modified local conflict minimization rule based just on the resource constraints:

$$\alpha_2 = \arg \min_{x_{ij} \in X_{ij}} \left(\sum_{o_{kl}: r_{kl} = r_{ij}} \phi_1(x_{ij}, x_{kl}) \right) \quad 8.$$

Since a local agent cannot detect whether the global algorithm has been trapped in a local minimum or a cycle of infeasible schedules, each agent uses some internal strategy to combine both rules in the intended manner. Update rule α_1 is the preferred one and applied most of the time. However, if an agent detects that it is has reached no conflict-free position for a longer period of iterations, it applies the second rule to jump to another region of the search space to escape from the current trap. More precisely, each time where α_1 is applied the local inconsistency is accumulated, and when the accumulator reaches a threshold $\beta > 0$, instead of α_1 the second rule α_2 is applied once and the accumulator is reset to zero. The effect of this

strategy can be seen in Figure 2. Around iteration 475 the algorithm gets trapped in a local minimum. Some agents can't find a conflict-free position and change their update policy some 80 iterations later, kicking off the relaxation process again which falls into a feasible schedule sometimes later. A smaller β value encourages agents to apply α_2 more often, hence a trap situation can be escaped earlier. On the other hand, a small value for β disturbs the inconsistency relaxation process of α_1 too much, hence β has to be chosen such that a balance between both processes is obtained.

MAKESPAN MINIMIZATION

To obtain schedules with near-optimum makespans we can use the following basic procedure. An initial maximal makespan τ_0 being large enough to ensure that a feasible schedule can easily be found is chosen. The earliest and latest time positions for each operation o_{ij} are calculated according to the following formulas:

$$b_{ij} = \sum_{k=1}^{j-1} d_{ik} \qquad e_{ij} = \tau_0 - \sum_{k=j}^{m} d_{ik} \qquad 9.$$

The position of each operation is initialized with the earliest position possible $x^0_{ij} = b_{ij}$. Our self-organizing algorithm is applied and a first feasible schedule will be found. This schedule can be improved by moving each operation as much as possible to some earlier position without changing the current order of operations on the machines. With the makespan of this improved schedule x_0 a new maximal makespan will be calculated $\tau_1 = \tau(x_0) - \Delta_\tau$ where Δ_τ denotes some constant makespan reduction value. All agents exceeding this new makespan calculate a new position according to update rule α_2. Another run of the self-organizing algorithm is performed and these steps are repeated as long as the self-organizing algorithm converges.

EXPERIMENTAL RESULTS

We applied our method to solve some 10 × 10 benchmark problems taken from the operation research library (http://www.ms.ic.ac.uk/info.html). Our intention was to come as close as possible to the (known) optimum schedule. Since our algorithm is deterministic in its current version, we performed several runs with different parameter settings. We varied the makespan reduction value Δ_τ as well as the parameter β. Table 1 summarizes the results, showing the best and average makespan obtained and the known optimum for each problem.

Each run took about 9 seconds on a 233MHz i686 PC, the best schedule usually emerged after half the time. Taking the best solution found for each benchmark, the generation of schedules differing 3% (on the average) from the optimum seems to be within the reach of our approach.

Table 1. Experimental results on a set of 10 × 10 benchmark problems.

Benchmark problem	abz5	abz6	ft10	la16	la17	la18	la19	la20	orb01
Known optimum	1234	943	930	945	784	848	842	902	1059
Best makespan	1260	976	951	982	794	862	870	922	1121
Average makespan	1295	995	989	1012	826	905	890	932	1171
Benchmark problem	orb02	orb03	orb04	orb05	orb06	orb07	orb08	orb09	orb10
Known optimum	888	1005	1005	887	1010	397	899	934	944
Best makespan	889	1075	1050	916	1033	409	934	971	979
Average makespan	912	1123	1076	954	1056	422	955	1005	1000

In a second experiment we examined whether we can compete with other algorithms. A set of 3000 10 × 10 job shop scheduling problems was generated and solved with a schedule construction algorithm based on constraint logic programming (CLP) known to produce good solutions [3].

Each of the 27 available variable ordering heuristics was applied and the best schedule obtained was compared with the solution generated by our algorithm. We made two runs, one with the parameters Δ_τ and

β proven to be the best to solve the ft10 benchmark problem and a second modified run, additionally allowing repetitions based on random re-initializations after self-organizing has failed.

In the first run we could improve the CLP results in 42% of all cases, whereby on the average we obtained comparable solutions (1.2% deviation towards poorer schedules). In the second run we could improve these values to 65% and -1.25% (towards better schedules), which shows that our search method can still be improved. Note that compared with each individual CLP heuristic our algorithm was superior in terms of robustness and generated solution quality, which has been between 5% to 12% for our set of 3000 test problems.

SUMMARY

We have proposed a novel distributed framework based on connectionist ideas of information processing to solve the classical job shop scheduling problem. Despite its simplicity, our framework seems to be a promising area for further research. Experimental results on standard benchmark problems and large problem test sets have shown that our method can compete with other methods in terms of generated solution quality as well as computational costs. Whereas solution quality is on the average not superior to other methods, the schedules are obtained very fast since a typical run of the algorithm lasts just some seconds. According to the performance comparison in [4], we may well have an algorithm among the fastest local search algorithms currently available.

Since our algorithm is simple, intuitive and easy to implement, it can be seen as a low-cost alternative to other good scheduling methods, based on extensive and expensive software tools (e.g. constraint solvers). Being a connectionist system of simultaneously acting agents there is also room for effective parallelization especially on multi processor systems, making this approach attractive to real-time applications.

REFERENCES

1. D.P. Williamson, L.A. Hall, J.A. Hoogeven, C.A.J. Hurkens, Jan Karel Lenstra, S.V. Sevastjanov, and D.B. Shmoys, 1996. Short shop schedules. Operation Research, 25.
2. S. Breitinger and H.C.R. Lock, 1994. Improving search for job-shop-scheduling with CLP(FD). In M. Hermenegildo and J. Penjam, editors, Programming Language Implementation and LogicProgramming, vol. 844 of Lecture Notes in CS, Springer, 277–291.
3. H.J. Goltz and U. John, 1996. Methods for solving practical problems of job-shop scheduling modelled in CLP(FD). In Proceedings of the Conference on Practical Application of Constraint Technology, London, 73-92.
4. R.J.M. Vaessens, E. H. L. Aarts, and J. K. Lenstra, 1996. Job shop scheduling by local search. INFORMS Journal on Computing, 8(3), 302–317.
5. E. Aarts and J. K. Lenstra, eds., 1997. Local Search in Combinatorial Optimization. John Wiley & Sons.
6. D. N. Zhou, V. Cherkassky, T. R. Baldwin, and D. W. Hong, 1990. Scaling neural network for job-shop scheduling. In Proc. of the Int. Joint Conference on Neural Networks, 3, 889–894, San Diego.
7. J.-S. Liu and K. P. Sycara, 1995. Multiagent coordination in tightly coupled real-time environments. In Victor Lesser, editor, Proc. of the Int. Conference on Multi–Agent Systems. MIT Press.
8. G. Kock and T. Becher, 1997. An integrated environment for the development and acceleration of neuro-fuzzy systems. In Australasia-Pacific Forum on Intelligent Processing and Manufacturing of Materials (IPMM'97).
9. G. Kock and T. Becher, 1998. Flexible neuro-fuzzy simulation based on abstract model and interface definitions. Cybernatics and System: An International Journal (CBS), 29(7), 689–714.

Fuzzy Systems II

Designing in Many-Valued Logic

Antonio Donnarumma; Michele Pappalardo

Department of Mechanical Engineering, University of Salerno
Via Ponte don Melillo, 84084 Fisciano , (Salerno), Italy

ABSTRACT

The analysis followed here is based on the many-valued logic of Lukasiewitcz. It is finalised up to construction of a simple design model when the analysis cannot be based upon a two-valued logic. The reference is to the semantics of Kripke, immersion in a definite possible world, and to the process of verification and confirmation of Carnap. The example is based on the statistics of Dempster and Shafer.

INTRODUCTION

In design, the uncertain of data strongly hinders validation of mathematical models. Many difficulties exist in the recognition of the truth of any proposition.. This study is finalised up to the construction of a simple model to verify data when the analysis cannot be based upon a two-valued logic. The model cannot be based upon two-valued logic since, in many phases of a project, it is unclear from the true-functional point of view and the belief in a concept must often be modified on the basis of new information. We will refer to the semantics of Kripke, immersion in a definite possible world, and to the process of verification and confirmation of Carnap The analysis proposed here is based on the many-valued logic ofLukasiewicz.[1]

According to N. Wiener's model of reasoning [2] it is fundamental to follow information flow about the action in progress, since it is possible to generate feedback. In the choice of the action to take, the principle of feedback means that performance is compared periodically with the desired results, and that the success or failure of this performance modifies future actions. Comparison is founded on the measurement of the information. The information is based on the value of probabilities. In every design, in situations where the information is incomplete and the truth value of proposition is indeterminate we can decide what is possibly true and possibly false and continue to work on basis of plausible reasoning as if theire is no lack of information. Wiener's model of reasoning is coherent with the process of learning developed by Bayes.

Denoting various propositions *A, B, C,* etc., let the propositions $A \cap B$ be true and $\neg A$ be false we have Laplace's mathematical representation of process of learning [3](Bayes Theorem):

$$P(A|B \cap C) = P(A|C)\left(P(B|A \cap C)/P(A|C)\right) \qquad 1.$$

Bayes Theorem is an algorithm for updating results and for acquiring new information. $p(A|C)$ is the prior probability for A when we know only C and $p(A|B \cap C)$ is the posterior information which is updated as a result of acquiring new information B. A represents the hypothesis under analysis and C represents what we know about *A (table of truth)* before getting *B (new data).* The problem is the correct analysis of B in the presence of uncertainty. The learning process is based on probability. It is fundamental to the interpretation of probability. We use Carnap's [4] interpretation: The probability of a statement is the degree of confirmation that the empirical evidence gives to the statement.

DESIGN PROBLEMS

Probability is at the base of the process of learning and its values can be only positive. A process of planning must run in finite time $t_D = \sum \Delta t_i$ equal to the sum of the various phases Δt_i.

0-7803-5489-3/99/$10.00 ©1999 IEEE.

Planning which uses an evolutionary logic, cannot be based on two values (true or false). In two-value logic, the data that cannot be verified during initial planning, would be discarded definitively, but could be used in the next phase. Better results can be obtained using a three-valued logic in which the third logical value is introduced to represent values not verified yet as true or false. The analysis of vague and contradictory data, with any degree of reliability, involves the use of evolutionary methodologies.

To represent possibility or indeterminacy, Lukasiewicz proposed a third value of truth-logic. He wrote [5]:

> *The third logical value may be interpreted as "possibility" and may be symbolised as ½. If we want to formulate a system of three-valued logic, we have to supplement the principle concerning 0 and 1 by the principles concerning ½.*

Table 1: Tables of truth

p	¬p	$p \to q$	q: 1 1/2 0	$p \wedge q$	q: 1 1/2 0	$p \vee q$	q: 1 1/2 0
1	0	p 1	1 1/2 0	p 1	1 1/2 0	p 1	1 1 1
½	½	p 1/2	1 1 1/2	p 1/2	1/2 1/2 0	p 1/2	1 1/2 1/2
1	1	p 0	1 1 1	p 0	0 0 0	p 0	1 1/2 0

In the three-valued logic of $T, \neg T$ and ½ , instead of the two classical truth-values, close to the truth-values of *T*rue and *F*alse, a third indeterminate value ½ is added. The value ½ represent an indeterminate or *possible* value of truth. The truth tables are shown in Table1.

These rules are coherent with all the rules for two values of truth. The objective is to capture truth in the presence of incompleteness and to exclude ambiguity. The data, if true, can be included in a set of true and verified elements. Updating the truth set allows passage from one belief situation to another up to the end of the project.

For our applications we will assume that *"possible propositions"* are such that, in the time interval Δt_D that we have at our disposal, they cannot be verified or falsified.

A proposition is *true* if: it is verified and it is independent of time.	A proposition is *false* if: it has never been true or possible and it is independent of time.
A proposition is *possible* if: in the time interval Δt_D that we have at our disposal, it cannot be verified or falsified.	

Table 2: Propositions

The data $X = \{x_i\}$ can be incomplete or contradictory with beliefs simultaneously true *T(X)* and false *F(X)*. In the presence of contradictory elements *T(X)* and $T(\neg X)$, it is necessary to verify the falsehood of the contradictions $F(X \wedge \neg X)$ otherwise it is necessary to appraise if the data is false *F(X)* or vague $F(X^{\frac{1}{2}})$. From the data we can have

$$\{T(X)\ ,\ T(\neg X)\} \vee \{F(X \wedge \neg X)\} \Rightarrow T(X \wedge \neg X) \qquad 2.$$

The logical procedure of analysis can be defined synthetically as follows:

- Analysis of the data $\{X\}$.
- If the data is false, it doesn't serve in the planning.
- If the data contains contradictions $T(X)$ and $T(\neg X)$), we must analyse the validity of $F(X \wedge \neg X)$. It is necessary to verify the contradictions:

$$If\left(\{T(X), T(\neg X)\} \vee \{F(X \wedge \neg X)\} \Rightarrow T(X \wedge \neg X)\right) \ then \ \ F(X) \ \ vel \ \ F(X^{\frac{1}{2}}) \qquad 3.$$

- If the proposition produces values of truth then data passes to the set of truth-data.

LEARNING USING SHAFERS RULE

For handling truth, in its conventional sense of degree of plausibility and reliability (but also, satisfaction) the rules of Dempster and Shafer combine data coming from different origins. The intersection of sets of information (assuming that the information is, by definition, true) tends towards increasing belief to a degree of reliability for which a hypothesis is definitely confirmed or denied. The lack of convergence of the analysis means that between hypotheses in competition there is not real competition. It will be necessary to retry with another set of hypotheses. This fact is framed in the most general problem that violates both the law of excluded-middle and the law of non-contradiction.

As an example, we mention the process of choice of some town planners in a large Italian city. This concerns the planning program of certain areas of the same city, for use as a tourist zone or as a park or to be simply residential, with all the consequences that every one of these choices involves itself.

For this purpose, some categories of experts and citizens of the zone (tourist operators, industrial workers, etc.) have been called together to express their view, which are held in account by various factors, personal demands, business affairs etc. The results of the investigation have been elaborated with fuzzy techniques [6,7]. The operation, though rather complex, can be performed, in our opinion, using the statistics of Dempter and Shafer (DS theory) [8].

For handling data in the presence of uncertainty, Shafer refined Dempster's theory [9], including Bayesan probability as a special case, and introduced the *belief function* as a lower probability and the *plausibility function* as an upper probability. Evidence theory affords us the opportunity to combine information coming from different origins.

Probabilities are apportioned to subsets and the mass v_i can move over each element. Let the finite non empty set $\Theta = \{x_1, ..x_n\}$ be the frame of discernment. The basic probability is assigned in the range $[0,1]$ to the 2^{Θ} subset of Θ consisting of a singleton or conjunction of singletons of elements x_i. The basic probability is a function which assigns a weight to the subset such that

$$\sum_{A \subseteq \Theta} m(A) = 1 \quad m(\Phi) = 0 \qquad 4.$$

The lower probability $P_*(A_j)$ is defined as

$$P_*(A_j) = \sum_{A_j \subseteq A} m(A_j) \qquad 5.$$

while the upper probability $P^*(A_j)$ is defined as

$$P^*(A_j) = 1 - \sum_{A_j \subseteq A_o} m(A_j) \qquad 6.$$

Without respect to additivity, the $m(A_i)$ values are independent basic values of probability inferred on each subset A_i. The belief function of set M is given by

$$Bel(M) = \sum_{A_i \subseteq M} m(A_i) \qquad 7.$$

If m_1 and m_2 are independent basic probabilities from independent evidence, and $\{A_{1i}\}$ and $\{A_{2j}\}$ are the sets of focal points, then the theorem of Shafer gives the rule of combination. Let m_1 and m_2 be two independent basic probabilities from independent evidence. If $\sum_{A_{1i} \cap A_{2j} \neq \Phi} m_1(A_{1i})\, m_2(A_{2j}) > 0$ then

$$m_1 \oplus m_2 = m(A_k) = \frac{\sum_{A_{1i} \cap A_{2j} = A_k} m_1(A_{1i}) m_2(A_{2j})}{1 - \sum_{A_{1i} \cap A_{2j} = \Phi} m_1(A_{1i}) m_2(A_{2j})}, \qquad A_k \neq \Phi \qquad 8.$$

with $m(\Phi) = 0$, assign the basic probability. In rules $m = m_1 \oplus m_2$ are the combination of basic probabilities.

Let planning of a new area of a city in which there exists three typologies of installation and we want to program an adjoining area with the same typologies using the indication of the citizens.

- Typology x_1 : area destined to park
- Typology x_2 : area destined for sport
- Typology x_3 : area destined for residences

The initial situation is constituted by mixed areas of the type $\{x_1\}$, $\{x_2 x_3\}$ and $\{x_2 x_3 x_3\}$ with the distribution $m_1(\{park\}) = 0.3$, $m_1(\{sport, residence\}) = 0.5$, $m_1(\{park, sport, residence\}) = 0.2$.

Two categories of citizens, consulted for their wishes on the future planning, give these results: First result: $m_2(\{sport, residence\}) = 0.5$, $m_2(park, sport, residence) = 0.6$, in DS theory $m_2(\{x_2, x_3\}) = 0.4$, $m_2(X) = 0.6$
Second result: $m_3(\{residence\}) = 0.7$, $m_3(vpark, sport, residence) = 0.3$, in DS theory $m_3(\{x_1\}) = 0.7$, $m_3(X) = 0.3$

The two results are in clear contradiction since there is much uncertainty. Using DS theory the problem in presence of uncertainty can be analysed as follows:

Let $X = \{x_1, x_2, x_3\}$ be a finite set and consider the basic probability assignment as a table of truth: $m_1(\{x_1\}) = 0.3$, $m_1(\{x_2, x_3\}) = 0.5$, $m_1(X) = 0.2$ with constraint $K = m_1(\{x_1\}) \geq 0.25$.

- Step 1: Let the data from citizens be: $m_2(\{x_2, x_3\}) = 0.4$, $m_2(X) = 0.6$

The distribution of Shafer gives:

$$m_1 \oplus m_2(\{x_1\}) = 0.20\,45,$$
$$m_1 \oplus m_2(\{x_2, x_3\}) = 0.6590 \text{ and}$$
$$m_1 \oplus m_2(X) = 0.1363$$

with a final distribution $m(x_1) = 0.1764, m(x_2) = 0.41176$ *and* $m(x_3) = 0.41176$

The value of $m_1 \oplus m_2(\{x_1\}) < 0.25$ it is not compatible with the constraint K , so in this analysis step, it is not possible to use the data of basic probability $m_2(\{x_2, x_3\}) = 0.5$, $m_2(X) = 0.6$. An analysis of new data is necessary.

- Step-2: Let the data: $m_3(\{x_1\}) = 0.7,\ m_3(X) = 0.3$ and so:

$$m_1 \oplus m_3(\{x_1\}) = 0.6769,$$
$$m_1 \oplus m_3(\{x_2, x_3\}) = 0.23077, \text{ and}$$
$$m_1 \oplus m_3(X) = 0.09231$$

with a final distribution $m(x_1) = 0.5434, m(x_2) = 0.2282$ *and* $m(x_3) = 0.2282$

The value of $m_1 \oplus m_3(\{x_1\})$>0.25 which is compatible with constraint *K*.

- Step-3: Let $m_4(\{x_1\}) = m_1 \oplus m_3(\{x_1\}) = 0.46$, $m_1(\{x_2, x_3\}) = m_1 \oplus m_3(\{x_2, x_3\}) = 0.24$ and $m_4(X) = m_1 \oplus m_3(X) = 0.30$. So now:

$$m_1 \oplus m_4(\{x_1\}) = 0.5581,$$
$$m_1 \oplus m_4(\{x_2, x_3\}) = 0.3661 \text{ and}$$
$$m_1 \oplus m_4(X) = 0.0757$$

with a final distribution $m(x_1) = 0.4172, m(x_2) = 0.29114$ and $m(x_3) = 0.29114$.

The value of $m_1 \oplus m_4(\{x_1\})$>0.33 which is compatible with constraint *K*. So we have been able to rescue the information $m_2(\{x_2, x_3\}) = 0.5,\ m_2(X) = 0.6$ by using an evolutionary technique where the data is not considered to be false but *possible* since we did not have the necessary information to discard it.

CONCLUSION

Models must foresee some choice between different solutions, or adaptation of a present choice for the phenomenon of a following phase. Problems are resolved by induction. There is the possibility of a refusal of an approved choice and of a return to the preceding phase or vice versa. This addresses the insufficiency of classical logic to manage the complete procedure. Different logic have been proposed that foresee violation of the excluded-middle principle and/or that of non-contradiction. A fundamental element is the evaluation of the degree of reliability (the degree of truth) of the information. The trivalent logic of Lukasiewicz has been used. The third value of truth expressed as ½ is used to point out indefinite elements. Between the possible methods to check the truth (verification of Wittgenstein, verification and confirmation of Carnap, falsification of Popper, etc.) the proposal of Carnap appears to be the best.

REFERENCES

1. Lukasiewicz J, 1970. Modal Logic. Polish Scientific Publisher. Warzawa.
2. Wiener N., 1950. Human Use of Human Beings, Houghton Mifflin Company- Boston.
3. Jaynes E.T., 1985. Baysan Methods: General Background. in Proceedings Volume. Maximum Entropy and Methods in Applied Statistics. J.H. Justice , Ed., Cambridge University Press; 1-25.
4. Logic, Language, and the Structure of Scientific Theories: Proc. of Carnap-Reichenbach Centennial, University of Kostanz,, May 1991 Pittsburgh: University of Pittsburgh Press; University of Kostanz.
5. Lukasiewicz J., 1970. On Three-Valued Logic. in L. Boroski Ed., selected Works of Jan Lukasiewcz. Holland Publishing Company Warsaw.
6. Zadeh L.A., 1965. Fuzzy sets . Information and Control 8 , 338-353.
7. Zimmerman H.J., 1985. Fuzzy Sets Theory and its Application, Boston.
8. Shafer G.A , 1976. Mathematical Theory of Evidence -Princeton University Press.
9. Terano T., Asai K., Sugeno M., 1992. Fuzzy System Theory and Applications. Academic Press Inc. San Diego CA.

Modulus Genetic Algorithm and its Application to Fuzzy System Optimization

Sinn-Cheng Lin

Department of Educational Media and Library Sciences,
Tamkang University, Taipei, Taiwan, R.O.C.

ABSTRACT

The conventional genetic algorithm encodes the searched parameters as binary strings. After applying the basic genetic operators such as reproduction, crossover and mutation, a decoding procedure is used to convert the binary strings to the original parameter space. As the result, such an encoding/decoding procedure leads to considerable numeric errors. This paper proposes a new algorithm called modulus genetic algorithm (MGA) that uses the modulus operation to resolve this problem. In the modulus genetic algorithm, the encoding/decoding procedure is not necessary. It has the following advantages: 1) the evolution can be speeded up; 2) the numeric truncation error can be avoided; 3) the precision of solution can be increased.

The proposed MGA is applied to resolve the key problem of fuzzy inference systems – rule acquisition. The fuzzy system with MGA as learning mechanism forms an "intelligent fuzzy system". Based on the proposed approach, the fuzzy rule base can be self-extracted and optimized. Such an intelligent fuzzy system has a general-purpose architecture. It can be applied to many kinds of fields.

INTRODUCTION

Genetic algorithms (GAs) are parallel and global search techniques, which take the concepts from evolution theory and natural genetics. They emulate biological evolution by means of genetic operations such as reproduction, crossover and mutation. Usually, genetic algorithms are used as optimization techniques [1]-[5]. Although there is no necessary and sufficient condition on the functions which are optimizable by genetic algorithms, it has been shown that GAs perform well on multimodal functions (the functions which have multiple local optima). Moreover, various studies have shown that whenever GAs failed to find the optimal solution on a function, other known techniques failed as well [2].

Conventionally, a genetic algorithm works with a set of artificial elements (binary strings, e.g. 10101010), called a population. An individual (string) is referred as a chromosome, and a single bit in the string is called a gene. GA generates a new population (called offspring) by applying the genetic operators to the chromosomes in the old population (called parents). An iteration of genetic operation is referred as a generation. A fitness function, *i.e.* the function to be maximized, is used to evaluate the fitness of an individual. One of the important purposes of GAs is to reserve the better schemata, *i.e.* the patterns of certain genes, so that the offspring may yield higher fitness than their parents. Consequently, the value of fitness function increases from generation to generation. In most of genetic algorithms, mutation is a random-work mechanism to avoid the local optimum trapping problem. As a result, GAs, theoretically, can find the global optimal solution.

The basic disadvantage of the conventional genetic algorithm is that it encodes the searched parameters as binary strings. After applying the basic genetic operators such as reproduction, crossover and mutation, a decoding procedure has to be used to convert the binary strings to the original parameter space. As the result, such an encoding/decoding procedure leads to considerable numeric errors. This paper proposes a new algorithm called modulus genetic algorithm (MGA) that uses the modulus operation to resolve this problem. In the MGA, the encoding/decoding procedure is not necessary. It has the following advantages: 1) the evolution can be speeded up; 2) the numeric truncation error can be avoided; 3) the precision of solution can be increased.

0-7803-5489-3/99/$10.00 ©1999 IEEE.

The MGA is applied to resolve the key problem of fuzzy logic systems – rule acquisition [8]. The fuzzy system with MGA as learning mechanism forms an "intelligent fuzzy system". Based on the proposed approach, the fuzzy rule base can be self-extracted and optimized. Such an intelligent fuzzy system has a general-purpose architecture. It can be applied to many kinds of fields, such as fuzzy control, fuzzy image processing, fuzzy decision making, and fuzzy pattern recognition ... etc.

This paper is organized as follows: Section 1 is an introduction. Section 2 describes the detail of the MGA. In Section 3, the MGA is used to build an intelligent fuzzy inference system. Section 4 applied the MGA-based fuzzy inference system to the field of fuzzy control. Conclusions are drawn in Section 5.

THE MODULUS GENETIC ALGORITHM

Reproduction of MGA

The Darwinian "survival of the fittest" is the underlying spirit of reproduction. This operation, actually, is an artificial version of natural selection.

Let F be the fitness function, and F_i denote the value of fitness function associated with the individual string i in the current population. Reproduction is a process in which individual strings in the current population are copied according to their fitness function values F_i. A higher F value indicates a better fit (or larger benefit). To perform reproduction, first, F_i's are calculated. Next, the current individual strings are probabilistically selected and copied into a mating pool according to their fitness value. The arrangement allows the strings with a higher fitness to have a greater probability of contributing a larger amount of offspring in the new population. The easiest way of implementing a reproduction operator is to create a biased roulette wheel. The slot size of it is proportion to the fitness value of each individual in the current population. Let ps_i denote the probability of selection of the individual i, and M be the population size, then an individual string will get selected with the following probability:

$$ps_i = F_i \Big/ \sum_{j=1}^{M} F_j \qquad 1.$$

Crossover of MGA

Crossover provides a mechanism for individual strings to exchange information via a probabilistic process. Once the reproduction operator is applied, the members in the mating pool are allowed to mate with one another. The binary-coded GA takes the following step to accomplish the crossover: First, two parents are randomly selected from the mating pool. Then, a random crossover point is picked up. Finally, exchange the parents' genetic codes (binary digits) following the crossover point. This random process provides a highly efficient method to search the string space to find a better solution.

In MGA, the parameters lie in the original space rather than binary space. Hence, the crossover operation has to be modified to work with parameters themselves rather than their binary codes.

Let $\{a, b\}$ and $\{a', b'\}$ be the parent and offspring parameter pair, respectively. The search space of them is in the range of $[X_{\min}, X_{\max}] \subseteq R$. The crossover of MGA is proposed as follows:

$$\begin{aligned} a' &= (a - a_0 + b_0) \,\mathrm{MOD}\, \Delta + X_{\min} \\ b' &= (b - b_0 + a_0) \,\mathrm{MOD}\, \Delta + X_{\min} \end{aligned} \qquad 2.$$

where MOD means the modulus operator. It is the reason why the proposed approach called "modulus" genetic algorithm. The meaning of other notations in (2) are: $\Delta = X_{\max} - X_{\min}$, and

$$a_0 = a \,\mathrm{MOD}\, \alpha\Delta$$

$$b_0 = b \,\mathrm{MOD}\, \alpha\Delta$$

in which, $\alpha \in [0,1]$ is called the crossover factor.

Especially, the crossover of a binary-coded GA is a special case of (2) with the following a_0 and b_0:

$$a_0 = a \text{ MOD } 2^c$$

$$b_0 = b \text{ MOD } 2^c$$

where c denotes the bit number of crossover point.

Mutation of MGA

In the genetic algorithm, the mutation operation introduces new genes into the populations such that the problem of trapping in local optimal points may be avoided. The gene of individual is subject to a random change with probability of the pre-assigned mutation rate. In the binary-coded case, a mutation operator changes a bit from 0 to 1 or vice versa. In MGA, mutation is a random work mechanism. It simply replaces a parameter, say a, with an arbitrary value, say a', in the search space $[X_{\min}, X_{\max}]$.

MGA-BASED INTELLIGENT FUZZY SYSTEM DESIGN

Suppose that a fuzzy inference system described by the following rule base [6]:

$$R_j : IF\ x\ is\ X_j(m_j, \sigma_j)\ THEN\ y\ is\ Y_j(\varphi_j) \qquad 3.$$

where $j = 1, 2, \kappa, N$, and N is the number of rules; X_j's and Y_j's are the input and output linguistic labels [10], respectively. Especially, in this paper X_j's are simply assigned as Gaussian-shaped functions, *i.e.*, $\mu_{X_j}(x) = \exp\left(-\left(\frac{x - m_j}{\sigma_j}\right)^2\right)$, and Y_j's are assigned to be fuzzy singletons, *i.e.*, $\mu_{Y_j}(u) = \begin{cases} 1, y = \varphi_j \\ 0, y \neq \varphi_j \end{cases}$.

Suppose that the singleton fuzzification and the weighted average defuzzification methods are applied [8], then the output of (3) is given by:

$$y = \underline{\varphi}^{\mathrm{T}} \underline{\rho}(x) \qquad 4.$$

where $\underline{\varphi} = [\varphi_1, \varphi_2, ..., \varphi_N]^{\mathrm{T}}$ and $\underline{\rho} = [\rho_1, \rho_2, ..., \rho_N]^{\mathrm{T}}$ in which $\rho_j(x) = \frac{\mu_{X_j}(x)}{\sum_{j=1}^{N} \mu_{X_j}(x)}$

Constructing a parameter space to be searched by MGA required transferring the fuzzy rule base (3) to a parameter representation. Clearly, the output of the rule base (3) is uniquely determined by a set of parameters which is unionized by the parameters of IF part and THEN part. Hence, the parameter vector to be learned by genetic algorithm, $\underline{\theta}$, is defined as:

$$\underline{\theta} = [\underline{m}^{\mathrm{T}}\ \underline{\sigma}^{\mathrm{T}}\ \underline{\varphi}^{\mathrm{T}}]^{\mathrm{T}} = [m_1\ m_2 \Lambda\ m_N\ \sigma_1 \sigma_2 \Lambda\ \sigma_N\ \varphi_1 \varphi_2 \Lambda\ \varphi_N]^{\mathrm{T}} \qquad 5.$$

Assume that X_m, X_σ, X_φ are the search space of m_j's, σ_j's, φ_j's, respectively; M is the population size; h is the number of generation. The details of learning procedures of MGA-based fuzzy system are described in the follows.

STEP 1: Initially, set $h = 0$ and randomly generate $3M$ initial parameter vectors,

$$\underline{m}^{(i)}(h) = [m_1^{(i)}(h)\ m_2^{(i)}(h) \Lambda\ m_N^{(i)}(h)]^{\mathrm{T}}$$

$$\underline{\sigma}^{(i)}(h) = [\sigma_1^{(i)}(h) \sigma_2^{(i)}(h) \Lambda\ \sigma_N^{(i)}(h)]^{\mathrm{T}}$$

$$\underline{\varphi}^{(i)}(h) = [\varphi_1^{(i)}(h) \varphi_2^{(i)}(h) \Lambda\ \varphi_N^{(i)}(h)]^{\mathrm{T}}$$

where $m_j^{(i)}(h) \in X_m, \sigma_j^{(i)}(h) \in X_\sigma$ and $\varphi_j^{(i)}(h) \in X_\varphi$ ($i = 1, 2, ..., M, j = 1, 2, ..., N$).

If the i-th candidate of MGA-based fuzzy inference system is denoted by $\mathrm{FIS}^{(i)}$. Then the fuzzy rule base of $\mathrm{FIS}^{(i)}$ can be created as:

$$\mathrm{FIS}^{(i)}:\begin{cases} R_1^{(i)}: \text{IF } x \text{ is } X_1^{(i)}(m_1^{(i)},\sigma_1^{(i)}) \text{ THEN } y \text{ is } Y_1^{(i)}(\varphi_1^{(i)}) \\ R_2^{(i)}: \text{IF } x \text{ is } X_2^{(i)}(m_2^{(i)},\sigma_2^{(i)}) \text{ THEN } y \text{ is } Y_2^{(i)}(\varphi_2^{(i)}) \\ \quad \text{M} \\ R_N^{(i)}: \text{IF } x \text{ is } X_N^{(i)}(m_N^{(i)},\sigma_N^{(i)}) \text{ THEN } y \text{ is } Y_N^{(i)}(\varphi_N^{(i)}) \end{cases}$$

where $X_j^{(i)}$'s and $Y_j^{(i)}$'s are linguistic labels to be learned, and $m_j^{(i)}$'s, $\sigma_j^{(i)}$'s and $\varphi_j^{(i)}$'s are their parameters.

STEP 2: Construct the parameter vector of the *i*-th individual,

$$\begin{aligned} \underline{\theta}^{(i)}(h) &= [\theta_1^{(i)}(h)\ \Lambda\ \theta_N^{(i)}(h)\ \theta_{N+1}^{(i)}(h)\ \Lambda\ \theta_{2N}^{(i)}(h)\ \theta_{2N+1}^{(i)}(h)\ \Lambda\ \theta_{3N}^{(i)}(h)]^T \\ &= [\underline{m}^{(i)T}(h)\ \underline{\sigma}^{(i)T}(h)\ \underline{\varphi}^{(i)T}(h)]^T \end{aligned}$$

STEP 3: Establish the population in the generation *h*, $\boldsymbol{P}(h)$,

$$\boldsymbol{P}(h) = \{\theta^{(1)}(h), \theta^{(2)}(h), \mathrm{K}\ , \theta^{(n)}(h)\}$$

STEP 4: Evaluate the fitness value, $F^{(i)}$, of each individual.

STEP 5: Apply the modulus genetic operators, *i.e.* reproduction of MGA, crossover of MGA and mutation of MGA, to generate a new population $\boldsymbol{P}(h+1)$, which is always known as the offspring of $\boldsymbol{P}(h)$.

STEP 6: Keep the elitist. That is, 1) pick up the best fitted individuals in $\boldsymbol{P}(h)$ and $\boldsymbol{P}(h+1)$; 2) compare their fitness; 3) if the best individual of $\boldsymbol{P}(h)$ has a better fitness value than that of $\boldsymbol{P}(h+1)$, then randomly replace an individual in $\boldsymbol{P}(h+1)$ with the elitist.

STEP 7: Use the parameters to calculate the output y of the fuzzy system.

STEP 8: Set $h = h + 1$; go to Step 2 and repeat the procedure until $F \geq F_M$ or $h \geq H$. Where F_M and H denote an acceptable fitness value and a stop generation number, respectively, as specified by the designer.

AN APPLICATION EXAMPLE

The proposed MGA-based intelligent fuzzy system has a general-purpose architecture. It can be applied to many kinds of fields, such as fuzzy control, fuzzy image processing, fuzzy decision making, and fuzzy pattern recognition ... and so on. In this section, an example of MGA-based fuzzy control system is used to demonstrate its practicability. Consider a class of *n*th order nonlinear systems, which is expressed by the following error dynamics [12]:

$$\begin{cases} \dot{x}_1 = x_2 \\ \dot{x}_2 = x_3 \\ \quad \text{M} \\ \dot{x}_n = f(\underline{x}) + g(\underline{x})u \end{cases} \qquad 6.$$

where $\underline{x} = [x_1\ x_2\ \mathrm{K}\ x_n]^{\mathrm{T}} \in \Re^n$ is the state vector; $u \in \Re$ is the control input; $f(.)$ is an unknown continuous function with known upper bound, *i.e.* $|f| \leq f^U$; $g(.)$ is an unknown positive definite function with known lower bound, *i.e.* $0 < g_L \leq g$. Actually, equation (6) represents a general uncertain nonlinear dynamic system. The chief objectives are:

1) Apply MGA for self-extracting an optimal fuzzy control rule-base, to minimize the following quadratic cost function:

$$J = \frac{1}{2}\int_0^\infty \left(\underline{x}^T(t)\underline{Q}\underline{x}(t) + u^T(t)Ru(t)\right)dt \qquad 7.$$

where $Q \in \Re^{n\times n}$ and $R \in \Re$ are two positive definite weighting matrices.

2) Guarantee the stability of the control system:

$$|x_i| \le \delta_i, i = 1, 2, ..., n \quad 8.$$

To simplify the system design, the fuzzy sliding mode control (FSMC) [12] is adopted as the control scheme. Based on our previous work [14], the control law can be represented as:

$$u = (1-\alpha)u_f + \alpha u_h, \qquad \alpha = \begin{cases} 1, \text{for} |s| \ge \bar{s} \\ 0, \text{for} |s| < \bar{s} \end{cases} \quad 9.$$

where u_f is obtained from the following fuzzy control rule-base:

$$R_j : IF\ s\ is\ S_j(m_j, \sigma_j)\ THEN\ u_f\ is\ U_j(\varphi_j) \quad 10.$$

where $s(x) = \underline{c}^T \underline{x} = \sum_{i=1}^{n} c_i x_i$ is a sliding function and $\underline{c}^T = [c_1\ c_2\ \Lambda\ c_n]^T \in \Re^n$ is the coefficient vector of s. The optimal coefficients of sliding function can be determined by the criterion we proposed in [14].

Notice that the rule base (10) is in the form of (3). Therefore, the approach described in the previous section can be directly applied to find the parameter vector of (10), that is $[m_1\ m_2 \Lambda\ m_N \sigma_1 \sigma_2 \Lambda\ \sigma_N \varphi_1 \varphi_2 \Lambda\ \varphi_N]^T$. To minimize the quadratic cost function (7), the fitness function can be defined as:

$$F = 1/(J_s + \varepsilon_0)$$

in which $J_s = t_s + \sum_{k=1}^{K} (s^2 + Ru^2)$. Where t_s denotes the reach time of sliding mode; $k = \text{int}(t/\Delta t)$ denotes the iteration instance; Δt is the sampling period; int(.) is the round-off operator; $K = \text{int}(t_{\max}/\Delta t)$ denotes the number of iterations in each run; $t_{\max}$ is the running time in one run.

Moreover, the hitting control law in (9), u_h, is designed to guarantee system stability. If u_h given by [13]:

$$u_h = -sign(s)[g_L^{-1}(f^U + |\bar{c}^T \bar{x}| + \eta)] \quad 11.$$

in which $\bar{c} = [c_1\ c_2\ \Lambda\ c_{n-1}]^T$ and $\bar{x} = [x_1\ x_2\ \Lambda\ x_{n-1}]^T$. Then the sliding condition, $s\dot{s} \le -\eta |s|$, is satisfied as $|s| \ge \bar{s}$, and the control system is stable in the sense that all system states x_i (i = 1, 2,..., n) are bounded by:

$$|x_i(t)| \le \left(2^{i-1} \Big/ \prod_{j=1}^{n-i} \lambda_j \right) \bar{s} \equiv \delta_i$$

For example, consider an underwater vehicle whose simplified model is represented as [11]:

$$\begin{cases} \dot{x}_1 = x_2 \\ \dot{x}_2 = -\frac{d}{m} x_2 |x_2| + \frac{1}{m} u \end{cases}$$

where x_1, x_2 represent the position error and velocity error of the vehicle, respectively; u is the control force; m is the mass of the vehicle; d denotes the drag coefficient. The parameter values that used in [11] are also adopted in the following simulations, *i.e.* $m = 3 + 1.5\sin(|x_2|t)$ and $d = 1.2 + 0.2\sin(|x_2|t)$.

Suppose that the weighting matrices are selected as $\underline{Q} = \begin{bmatrix} 2 & 0.5 \\ 0.5 & 1 \end{bmatrix}$, $R = 0.1$; the population size, the crossover rate and the mutation rate are selected as 10, 0.8 and 0.03, respectively. Based on [14], the optimal coefficients of sliding function can be derived as $\underline{c} = [1.4142\ \ 1]^T$. Six fuzzy rules are created in this simulation. Fig. 1 shows the evaluation result of cost function and Fig. 2 shows the final state space response after learning.

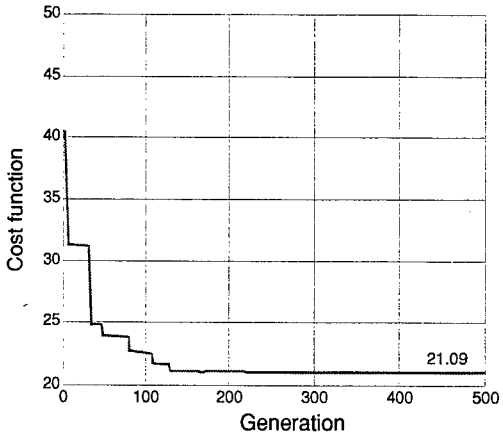


Fig. 1. The cost function

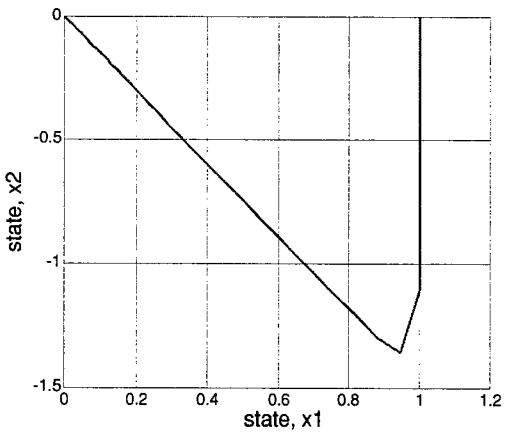


Fig. 2. The final state space response

CONCLUSION

In this paper, a new approach called modulus genetic algorithm was described. The numeric error, which arisen by the encoding/decoding procedure in conventional GAs, was avoided. In the modulus genetic algorithm, the encoding/decoding procedure is not necessary. It has the following advantages: 1) the evolution can be speeded up; 2) the numeric truncation error can be avoided; 3) the precision of solution can be increased.

The MGA was applied to resolve the key problem of fuzzy logic systems – rule acquisition. The fuzzy system with MGA forms an "intelligent fuzzy system". Based on the proposed learning step, the fuzzy rule base can be self-extracted and optimized. Such an intelligent fuzzy system has a general-purpose architecture. It can be applied to many kinds of fields, such as fuzzy control, fuzzy image processing, fuzzy decision making, and fuzzy pattern recognition, etc.

REFERENCES

1. Back, T., 1993. Optimal mutation rates in genetic search, Proc. 5th Int. Conf. on GAs, 2-8.
2. Goldberg, D.E., 1989. Genetic Algorithms in Search, Optimization, and Machine learning, Addison-Wesley.
3. Goldberg, D.E., 1991. Real-coded genetic algorithms, virtual alphabets, and blocking, Complex Systems, 5, 129-167.
4. Karr, C.L., 1991. Applying genetics to fuzzy logic, AI Expert, March, 38-43.
5. Karr, C.L., 1991. Genetic algorithms for fuzzy controller, AI Expert, February, 26-33.
6. Lin, S.C., Chen, Y.Y., 1997. Design of self-learning fuzzy sliding mode controller based on genetic algorithms, Fuzzy Sets and Systems, 86, 139-153.
7. Tate, D.M., Smith, A.E., 1993. Expected allele coverage and the role of mutation in genetic algorithms, Int. Conf. on Genetic Algorithms, 31-37.
8. Wang, L.X., 1994. Adaptive Fuzzy Systems and Control, Englewood Cliffs, NJ: Prentice Hall.
9. Zadeh, L.A., 1965. Fuzzy sets, Information and Control, 8, 338-353.
10. Zadeh, L.A., 1973. Outline of a new approach to the analysis of complex systems and decision processes," IEEE Trans. on Systems, Man and Cybernetics, (SMC3), 28-44.
11. Lewis, F.L., 1992. Applied Optimal Control and Estimation, Englewood Cliffs, NJ: Prentice Hall.
12. Lin, S.C., Chen, Y.Y., 1997. Design of self-learning fuzzy sliding mode controller based on genetic algorithms, Fuzzy Sets and Systems, 86(2).
13. Lin, S.C., Chen, Y.Y., 1995. Design a hitting controller to stabilize the fuzzy sliding mode control systems, Proc. Int. Joint Conf. CFSA/IFIS/SOFT'95 - Fuzzy Theory and Apps., Taipei, 374-379.
14. Lin, S.C., 1997. Stable Self-Learning Optimal Fuzzy Control System Design and Application, Ph.D. Dissertation, National Taiwan University.

FUZZY EVOLUTIONARY PROGRAMMING FOR PORTFOLIO SELECTION IN INVESTMENT

Tu Van Le

School of Computing
University of Canberra, ACT 2601 Australia
Email: vanle@ise.canberra.edu.au

ABSTRACT

The problem of portfolio selection in investment is concerned with minimizing the risk for a prespecified level of return. In this paper, the constraint on the level of return is fuzzified and the technique of fuzzy evolutionary programming is used to select an optimal portfolio of securities with low risk and a highly acceptable level of total return. Experimental results show the method is highly effective. The problem to select a portfolio with low risk and high probability of expected return is resolved in the same manner.

INTRODUCTION

Portfolio selection is a crucial task in investment. An investor is faced with a choice from among an enormous number of securities. The decisions on which securities to invest in and on the proportions of investment in those securities are highly complicated. The two principal factors that concern a portfolio selection are its risk and its expected total return. As broadly acknowledged, most investors hold strong aversion to risk and would rather accept a modest return for low risk. Therefore, Markowitz [4] has formulated the problem of portfolio selection into minimizing the risk provided that its expected total return is above some prespecified threshold.

So, portfolio selection is a constrained optimization problem. Theoretically, this problem can be resolved mathematically by solving systems of quadratic equations. In practice, however, due to the large number of securities, a mathematical approach requires a great deal of programming computation [2, 5]. Recently, Watanabe et al. [6] employed a Boltzmann machine to solve the portfolio selection problem by maximizing the energy function: Expected Return - Risk. In reality, for most investors, the constraint on expected total return is tolerable, particularly in the case where investment risk is unexpectedly too high and needs to be lowered. Thus, one may relax the constraint and allow it to be satisfied to a certain degree in order to find a compromised optimal solution. In [3], I have presented an evolutionary approach to solve this type of constrained optimization problem based on a combination of fuzzy logic and evolutionary programming. In this paper, the method of fuzzy evolutionary programming is employed to solve the portfolio selection problem, according to which the degree of satisfying the total return expectation is used as a weight factor for potential solutions.

PORTFOLIO SELECTION IN INVESTMENT

Consider N securities having expected returns r_i with variances σ_i and covariances σ_{ij}, $0 \le i, j \le N$. The portfolio selection problem is expressed as

$$\text{Minimize} \quad \sum_{i=1}^{N} x_i^2 \sigma_i^2 + \sum_{i=1}^{N} \sum_{j=1, i \neq j}^{N} x_i x_j \sigma_{ij}$$

$$\text{Subject to} \quad \sum_{i=1}^{N} x_i = 1, \qquad 1.$$

$$\sum_{i=1}^{N} x_i r_i \ge E, \qquad 2.$$

$$x_i \ge 0, i = 1, \ldots, N \qquad 3.$$

0-7803-5489-3/99/$10.00 ©1999 IEEE.

where x_i is the fraction of funds invested in the ith security, and E is a prespecified expected total return.

Here, we consider the constraint on the expected total return as tolerable. That is, the investor would be completely happy if the total return is greater than or equal to E, but it is still acceptable to some degree if this total return is below the expectation E. Thus, condition 2. on the previous page is replaced with a fuzzy constraint

$$\mu_{\phi(E,\varepsilon)}(\textstyle\sum_{i=1}^{N} x_i r_i)$$

where the fuzzy set $\phi(a,\varepsilon)$ is defined by

$$\mu_{\phi(a,\varepsilon)}(x)=\begin{cases} 1 & \text{if } x \geq a \\ \dfrac{e^{-p\left(\frac{x-a}{\varepsilon}\right)^2}-e^{-p}}{1-e^{-p}} & \text{if } a-\varepsilon \leq x \leq a \\ 0 & \text{otherwise} \end{cases}$$

where, p is a parameter used to control the shape of the membership function. Intuitively, we allow a high degree of tolerance if $\sum_{i=1}^{N} x_i r_i$ is smaller than E, but close to E, and we make this tolerance decrease rapidly as the gap increases.

The portfolio selection problem is now redefined as follows, where for simplicity we use the notation σ_{ii} to denote the variance σ_i^2.

$$\text{Maximize} \quad (1-\sum_{i=1}^{N}\sum_{j=1}^{N} x_i x_j \sigma_{ij})\mu_{\phi(E,\varepsilon)}(\sum_{i=1}^{N} x_i r_i)$$

$$\text{Subject to} \quad \sum_{i=1}^{N} x_i = 1,$$

$$x_i \geq 0, i = 1,\ldots,N$$

Thus, the degrees of constraint satisfaction are used as weight factors of potential solutions. As the objective function in this problem is not differentiable everywhere, the mathematical method is inapplicable. A fuzzy evolutionary programming approach to solving this problem is presented in the next section to deal with this problem.

FUZZY EVOLUTIONARY PROGRAMMING FOR PORTFOLIO SELECTION

Consider the constrained optimization problem of portfolio selection as presented in the previous section. The following evolutionary algorithm is employed to solve the problem. In this algorithm, ρ denotes a sigmoid function that compresses the positive real line into the interval [0,1], and the expression $\frac{1}{4}\sqrt{\ln\left(\frac{1}{r^{1-\rho(f^k)}}\right)}$ represents a random number between 0 and 1, with rather high probability to be close to 0 when f^k is large.

Algorithm 1 (*Fuzzy evolutionary programming for portfolio selection*)

Generate a population of m vectors $\tilde{x}^k = (x_1^k,\ldots,x_N^k)$, $k = 1,\ldots m$, where each x_i^k is randomly taken from the interval [0,1], $i = 1,\ldots N$, such that $\sum_{i=1}^{N} x_i^k = 1$.

For $k = 1,\ldots m$, compute the objective value:

$$f^k = (1-\sum_{i=1}^{N}\sum_{j=1}^{N} x_i^k x_j^k \sigma_{ij})\mu_{\phi(E,\varepsilon)}(\sum_{i=1}^{N} x_i^k r_i) \qquad 4.$$

Repeat

For each $k = 1,\ldots m$, generate the offspring $\tilde{x}^{m+k}$ by letting, for $i = 1,\ldots N$,

$s_i^k = x_i^k$ if the sign – is chosen, and $1 - x_i^k$ if the sign + is chosen;

$$\delta x_i^k = \begin{cases} \dfrac{s_i^k}{4}\sqrt{\ln\left(\dfrac{1}{r^{1-\rho(f^k)}}\right)} & \text{if } r^{1-\rho(f^k)} > 10^{-6} \\ s_i^k & \text{otherwise} \end{cases}$$

$x_i^{m+k} = x_i^k \pm \delta x_i^k$, (+ or − is chosen at random)

and compute the corresponding objective value f^{m+k}, using Equation 4.

For each $k = 1,\ldots, 2m$, select a random set U of c indices from 1 to $2m$, and record the number w^k of $h \in U$ such that $f^h \le f^k$.

Select m vectors from the set $\{\tilde{x}^k : k = 1,\ldots,2m\}$ that have highest scores w^k to form the next generation of population.

Until $|f^0 - f^m| < \varepsilon$ or the time allowed is exhausted.

The above algorithm was used to select an optimal portfolio of forty securities from the Australian stock market. The experimental results are discussed in the next section.

EXPERIMENTAL RESULTS

We chose forty securities currently available on the Australian stock market, the names of which are listed below. Henceforth, for convenience we will refer to these securities by their listed numbers.

1. AGL
2. ANZ
3. Amcor
4. Amwy Asia
5. Blackmore
6. Boral
7. Burswood
8. Cadbury
9. Caltex
10. Coles Myer
11. Comalco
12. Email
13. Fairfax
14. GIO Aust
15. GPT unit
16. Greens
17. Hancock
18. I Drug Tc
19. Incitec
20. Just Jeans
21. Lang Corp
22. Leighton
23. Linden
24. Nat Foods
25. News Corp
26. OPSM Pr
27. Oldfields
28. POSN
29. Petaluma
30. Prime TV
31. QBE
32. Rock Blg
33. Rothmans
34. Seaworld
35. Seven Net
36. UO Aust
37. WA News
38. Wfield Hl
39. Woolworths
40. Yates A

The monthly yields from 1994 to 1998 of the above listed securities were obtained from the business section of the Canberra Times, then the expected returns and variances of individual securities and the covariances of pairs of securities were computed accordingly. The securities' expected returns and variances are shown in Table 1.

Table 1: Expected returns and variances of the listed securities

	r_i	σ^2_i		r_i	σ^2_i		r_i	σ^2_i		r_i	σ^2_i
1:	4.472000	0.497816	11:	1.991000	0.758129	21:	3.086000	0.773664	31:	3.903000	0.601921
2:	5.089000	0.383469	12:	5.771000	1.676289	22:	3.823000	0.882741	32:	6.909999	2.348640
3:	4.199000	0.581369	13:	2.964000	0.313804	23:	1.819000	0.029649	33:	7.669000	14.347868
4:	2.557000	2.035761	14:	5.223000	2.753821	24:	3.942000	0.774856	34:	8.295000	4.453125
5:	5.898000	4.174596	15:	8.168000	0.341396	25:	0.397000	0.008901	35:	4.077001	0.688021
6:	5.205999	0.910164	16:	2.940000	2.629520	26:	5.092000	0.662936	36:	7.208000	5.864076
7:	6.870000	3.892480	17:	5.169000	0.336229	27:	5.109000	0.620929	37:	6.461000	3.793409
8:	2.908000	0.810956	18:	2.623000	0.548481	28:	4.881001	1.007369	38:	1.798000	0.167956
9:	3.921000	2.580169	19:	5.043000	0.600441	29:	2.375000	0.612125	39:	4.390000	2.174800
10:	4.162000	0.522016	20:	4.615000	1.322225	30:	3.733000	1.030001	40:	5.101000	1.827329

Algorithm 1 was used to select an optimal portfolio of the above forty securities. The expected total return was set at 5.25, which is 1.5% higher than the government bond interest. For the fuzzy membership function representing the constraint on expected total return, we let $p = 1$ and $\varepsilon = 0.6$. The program results are recorded in Figure 1, where the continuous line represents the fitness of the best candidate, and the dotted line shows that of the worst candidate. We observe that the fitness of both candidates converge rapidly. An optimal portfolio was found and is shown in Table 2.

Table 2. An optimal portfolio obtained by fuzzy evolutionary programming.

0.000563	0.023234	0.007975	0.000545	0.002791	0.004772	0.069821	0.000270
0.000869	0.002115	0.027605	0.000056	0.000646	0.002880	0.105348	0.062290
0.000495	0.046219	0.099688	0.102540	0.067659	0.004849	0.000521	0.001846
0.000895	0.000007	0.002513	0.043807	0.000003	0.001972	0.048508	0.000150
0.012759	0.067761	0.000717	0.006255	0.069103	0.000565	0.072669	0.036720

The optimal portfolio shown in Table 2 corresponds to a risk value of 0.160 with a degree of confidence 0.998 of producing the prespecified expected total return. This solution attains a fitness of 0.838.

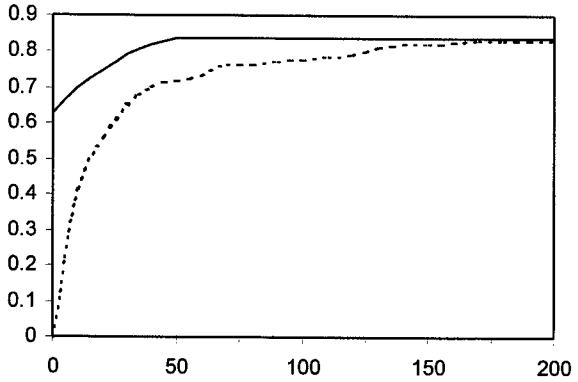


Fig. 1: Convergence of fitness in portfolio selection

Note that the optimal portfolio level of risk is less than one tenth of the average risk of all securities. It is interesting that the prespecified expected return at 5.25 can also be attained (with a degree of confidence of 1) with the price of a slightly higher level of risk, i.e., 0.164. This portfolio is shown in Table 3.

Table 3. A portfolio attaining the expected total return with slightly higher risk

0.001641	0.021828	0.025770	0.001682	0.009418	0.014278	0.065408	0.000935
0.002860	0.006620	0.021164	0.000186	0.002185	0.009830	0.104936	0.049695
0.001464	0.042652	0.081119	0.085430	0.061873	0.015389	0.001613	0.006067
0.002955	0.000024	0.008586	0.044122	0.000009	0.007517	0.038231	0.000482
0.011672	0.064489	0.002329	0.021459	0.063397	0.001885	0.068075	0.030726

The portfolio shown in Table 3 is not recommended by our program, however, as its fitness is only 0.836, which is lower than that of the optimal portfolio shown in Table 2. From Table 2, we observe also that the securities numbered 0, 3, 7, 8, 11, 12, 16, 22, 24, 25, 28, 31, 34, 37 have fairly low rates of investment. This suggests that no money should be invested in those securities. A check of the table of variances confirms that the listed securities have rather high risks. Therefore, we excluded those securities from the original list and reran Algorithm 1 to select an optimal portfolio of the remaining securities. The result shows a new optimal portfolio is obtained with a level of risk of 0.107, and with the expected total return fully achievable (with a confidence degree of 1). This suggests that we may expect a higher total return than that previously specified. In fact, when we ran the program again with a new expected total return of 5.84, the optimal portfolio found achieved this expected return with a confidence degree of 0.998 and with a risk level of 0.181, which is still far below the average risk of all securities.

FUZZY EVOLUTIONARY PROGRAMMING FOR STOCHASTIC PORTFOLIO SELECTION

In the problem of portfolio selection, the constraint on expected total return may be expressed differently as follows. The investor may be interested in the likelihood that the expected total return will be above some prespecified threshold. That is, the probability that the expected total return is higher than the prespecified threshold must be greater than some predetermined level. So, the portfolio selection problem is redefined as

$$\text{Minimize} \quad \sum_{i=1}^{N} x_i^2 \sigma_i^2 + \sum_{i=1}^{N} \sum_{j=1, i \neq j}^{N} x_i x_j \sigma_{ij}$$

$$\text{Subject to} \quad \sum_{i=1}^{N} x_i = 1,$$

$$P\left(\sum_{i=1}^{N} x_i r_i \geq E\right) \geq 1 - \alpha \qquad 5.$$

$$x_i \geq 0, i = 1, \ldots, N$$

Suppose that the expected returns r_i have normal distributions with mean $\bar{r}_i$ and standard deviation σ_{r_i}. Then $h = \sum_{i=1}^{N} x_i r_i$ has mean $\bar{h} = \sum_{i=1}^{N} x_i \bar{r}_i$ and variance $\sigma_h^2 = \sum_{i=1}^{N} x_i^2 \sigma_{r_i}^2$. Also let K_α be such that $P(X < K_\alpha) = \alpha$. Then $P(h \geq E) \geq 1 - \alpha$ if and only if

$$\frac{E - \bar{h}}{\sigma_h} \leq K_\alpha .$$

It follows that constraint 5. is equivalent to

$$\sum_{i=1}^{N} x_i \bar{r}_i + K_\alpha \sqrt{\sum_{i=1}^{N} x_i^2 \sigma_{r_i}^2} \geq E \qquad 6.$$

Thus, the stochastic portfolio selection problem is reduced to a standard portfolio selection problem, which can be solved by the technique of fuzzy evolutionary programming as discussed in the previous section.

REFERENCES

1. E.J. Elton and M.J. Gruber, 1995. Modern Portfolio Theory and Investment Analysis. John Wiley & Sons, New York.
2. H. Konno and K. Suzuki, 1992. A fast algorithm for solving large scale mean-variance model by compact factorization of covariance matrices. J. Operations Research Society of Japan, 35, 93-104.
3. T.V. Le, 1996. A fuzzy evolutionary approach to constrained optimization problems. Proc. IEEE Int. Conf. On Evolutionary Computation, Nagoya, Japan, May, 274-278.
4. H.M. Markowitz, 1987. Mean-Variance Analysis in Portfolio Choice and Capital Markets, Blackell.
5. A. Perold, 1984. Large scale portfolio optimization. Management Science, 30, 1143-1160.
6. T. Watanabe, K. Oda, J. Watada, 1998. Strategic decision of investment by a Boltzmann machine. Proc. of VJFuzzy'98, HaLong Bay, Oct., 201-208.

Design of a Region-Wise Fuzzy Sliding Mode Controller with Fuzzy Tuner

Chung-Chun Kung and Wei-Chi Lai

Department of Electrical Engineering, Tatung Institute of Technology,
40 Chungshan North Road, 3rd Sec., Taipei, Taiwan, R. O. C.
Tel: (886)-2-25925252 Ext. 3473
E-mail: cckung@ctr3.ee.ttit.edu.tw

ABSTRACT

In this paper, a region-wise fuzzy sliding mode controller (**RFSMC**) is proposed. In the process of designing the **RFSMC**, we firstly employ the sliding mode control techniques to design the fuzzy control rules, and to obtain the fuzzy sliding mode controller (**FSMC**). Secondly, we will adopt the concepts of region-wise linear fuzzy controller to design the **FSMC**, namely the region-wise fuzzy sliding mode controller (**RFSMC**). Then based on the state values of the controlled plant, a fuzzy tuner (**FT**) is used to tune the output scaling factors for the **RFSMC**. Finally, a genetic algorithm (**GA**) is applied to search the optimal parameters of the **RFSMC**. The simulation results show that the proposed **RFSMC** has the following advantages: (1) the fuzzy control rules of the **RFSMC** are efficiently reduced. (2) It exhibits better performance than that of **FSMC**.

INTRODUCTION

The fuzzy logical controller (**FLC**) has been successfully applied in the complex ill-defined processes with better performance than that of the conventional controller [1-3]. However, there are several difficulties still exist in **FLC** design, such as: (1) fuzzy control rules are experience oriented. (2) Characteristics of the fuzzy control systems cannot be pre-specified. (3) It is difficult to find an optimal fuzzy controller.

In [4-8], **FSMC** has been presented to overcome the above mentioned difficulties (1) and (2). The **FSMC** derives the control signal to force the states of the controlled plant converge to the sliding surface and then stay on it. Thus, the characteristics of the closed-loop control system can be specified by a pre-defined sliding surface.

Although the **FSMC** is a good solution for designing the fuzzy logic control systems, it has two input variables and it will lead the number of rules in a complete fuzzy rule base equals to m^2 (where m is the number of input linguistic labels). Thus the number of fuzzy rules in the **FSMC** will go up exponentially as m increase. In this paper, we will adopt the concepts of region-wise linear fuzzy controller [9] to design the **FSMC**, namely the region-wise fuzzy sliding mode controller (**RFSMC**). We combine the two input variables of **FSMC** as a new one input variable for the **RFSMC**. Thus, the number of fuzzy control rules in the **RFSMC** will be equal to m^*(where m^* is the number of linguistic labels of the new one input variable). Then, a fuzzy tuner (**FT**) is utilized to tune the scaling factors of the **RFSMC**. Finally, a **GA** is applied to search the optimal parameters of **RFSMC** and **FT**. The simulation results show the **RFSMC** with **FT** has better performance than that of **FSMC**.

ELITIST GENETIC ALGORITHM

GA's are global search algorithms based on the mechanics of natural genetics and natural selection [11,12]. Unlike many classical optimization techniques, **GA's** do not rely on computing local derivatives to guide the search process. **GA's** also include random elements, which help to avoid being trapped in local optimum. So **GA's** can provide a mean to search poorly understood and irregular space. They have been used mainly as function optimizers and have been proved to be

0-7803-5489-3/99/$10.00 ©1999 IEEE.

effective global optimization tools, especially for multimodel and non-continuous functions. In this paper, we will use the elitist **GA** to find the optimal values of the fuzzy controller. The elite selection procedure will ensure the survival of the fittest individual in each generation.

THE REGION-WISE FSMC WITH FUZZY TUNER

SLIDING MODE CONTROLLER

Consider a class of MIMO nonlinear system of the form:

$$x_j^{(n_j)}(t) = f_j(X_1,...,X_p;t) + b_j(X_1,...,X_p;t)u(t) + d_j(t), \quad j = 1,2,...,p \qquad 1.$$

where

$$X_i = \left[x_i, \dot{x}_i, ..., x_i^{(n_i-1)}\right]^T, \ i = 1,2,...,p,$$
$$b_j = [b_{j1}, b_{j2}, \cdots, b_{jq}], \quad u = [u_1, u_2, \cdots, u_q]^T,$$

and p and q are the numbers of input and output variables. It is assumed that all the f_j, b_j and d_j are unknown but bounded functions.

CONTROL OBJECTIVE: For a system given by Eq. (1), design a controller so that the state $X_j(t)$ of the system will track the desired trajectory $X_{dj}(t)$, for all $j = 1,...,p$.

Let $X_{dj} = \left[x_{dj}(t), \dot{x}_{dj}(t), \cdots, x_{dj}^{(n_j-1)}(t)\right]^T$ and $\left|x_{dj}^{(n_j)}(t)\right| \le v_j(t)$.

Then the tracking error vector can be written as follows:

$$X_j - X_{dj} = \left[e_j, \dot{e}_j, \cdots, e_j^{(n_j-1)}\right]^T$$

Let us define a set of sliding surface $H_j(t)$ in the state space R^{n_j} as

$$\mathbf{H}_j(t): \left\{ X_j \middle| s_j(X_j,t) \equiv \left(\frac{d}{dt} + \lambda\right)^{(n_j-1)} e_j = 0 \right\}, \quad j = 1, \cdots, p.$$

It is known that if there exists a positive constant η_j, such that [13-14]

$$\frac{1}{2}\frac{d}{dt} s_j(X_j,t)^2 \le -\eta_j s_j(X_j,t)^2, \qquad 2.$$

then the states trajectories will reach the sliding surface $\mathbf{H}_j(t)$ and then remain on the surface $s_j(X_j,t) = 0$, for all $t > 0$. In the sliding region, the system error will converge to zero asymptotically.

THE FUZZY SLIDING MODE CONTROLLER DESIGN

The **FSMC** for the system of Eq. 1 is shown in Fig. 1 and its linguistic rule base can be summed up as in Table 1, where

$$S(KT) = s(KT) * GS,$$
$$\dot{S}(KT) = \dot{s}(KT) * GCS,$$
$$\Delta U(KT+T) = FSMC\,[S(KT),\ \dot{S}(KT)],$$
$$\Delta u(KT+T) = \Delta U(KT+T) * GU,$$

and the associated fuzzy subsets involved in the **FSMC** are as follows: NL = Negative Large, NM = Negative Medium, NS = Negative Small, Z = Zero, PS = Positive Small, PM = Positive Medium, PL = Positive Large and are shown in Fig. 2.

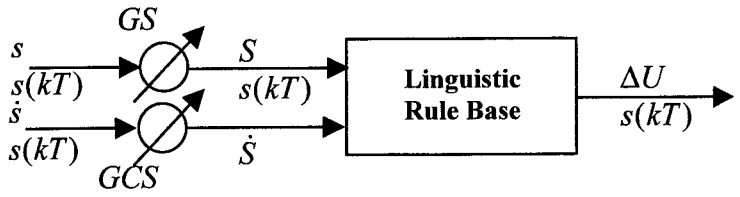


Fig. 1. The block diagram of the **FSMC**.

Table 1: The linguistic rule base of **FSMC**

$\dot{S}$ \ S	NL	NS	Z	PS	PL
NL	PL	PL	PM	PS	Z
NS	PL	PM	PS	Z	NS
Z	PM	PS	Z	NS	NM
PS	PS	Z	NS	NM	NL
PL	Z	NS	NM	NL	NL

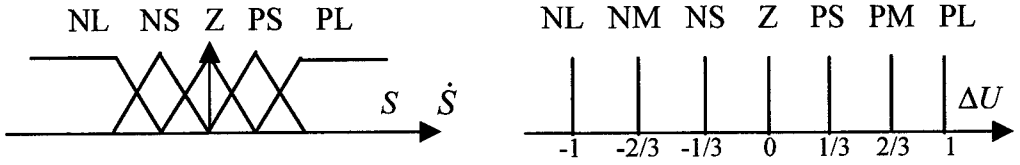


Fig. 2. Membership functions of the fuzzy variable S, $\dot{S}$ and ΔU.

REGION-WISE FUZZY SLIDING MODE CONTROLLER

Since the **FSMC** has two input variables, S and $\dot{S}$, the number of fuzzy control rules in a complete rule base of the **FSMC** equals to m^2 (m is the number of fuzzy sets for S and $\dot{S}$). Thus, the complexity of the **FSMC** will go up exponentially as m increases. To reduce the number of fuzzy control rules in the **FSMC**, we will adopt the concepts of region-wise linear fuzzy controller [9] to design the **FSMC**, namely the region-wise fuzzy sliding mode controller (**RFSMC**).

To design the **RFSMC**, we define

$$S^* = 2(S + \dot{S})/3 \qquad 3.$$

as the input to the **RFSMC**, whose structure is shown in Fig. 3. Let the input and output fuzzy variables of **RFSMC** have seven linguistic labels which are denoted by PL, PM, PS, Z, NS, NM, and NL as shown in Fig. 4. The relationship between S^*, S and $\dot{S}$ is listed in Table 2. Based on Table 2, the rule base shown in Table 1 for the **FSMC** will be equivalent to the rule base shown in Table 3 for the **RFSMC**. Since the **RFSMC** has only seven fuzzy if-then rules in its rule base, it is much simpler than **FSMC**. The change of the control signal for the **RFSMC** can be calculated by

$$\Delta u(kT + T) = RFSMC\left[S^*(kT + T)\right] * GU \qquad 4.$$

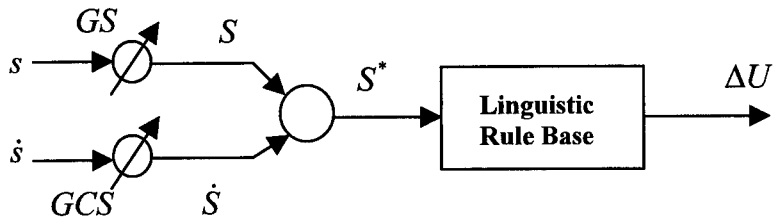


Fig. 3. The block diagram of **RFSMC.**

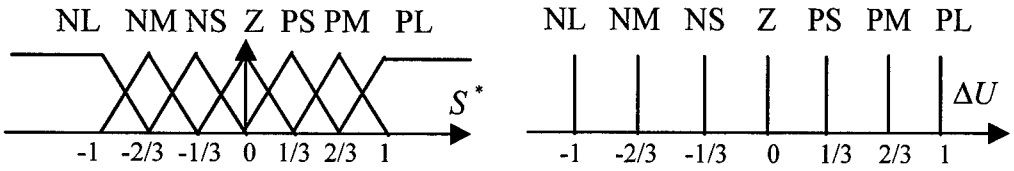


Fig. 4. Membership functions of the fuzzy variable S^* and ΔU for **RFSMC.**

Table 2: The relationship between S^*, S and $\dot{S}$

$\dot{S}$ \ S	NL	NS	Z	PS	PL
NL	NL	NL	NM	NS	Z
NS	NL	NM	NS	Z	PS
Z	NM	NS	Z	PS	PM
PS	NS	Z	PS	PM	PL
PL	Z	PS	PM	PL	PL

Table 3: The rule base for the **RFSMC**.

S^*	NL	NM	NS	Z	PS	PM	PL
ΔU	PL	PM	PS	Z	NS	NM	NL

RFSMC WITH FUZZY TUNER

In designing the fuzzy control system, the choice of suitable scaling factor for the output of the fuzzy controller is an important task [10]. A large scaling factor is needed for the output to enlarge the change of control signal so that the control signal can fast converge to the desired value. While a small scaling factor is needed for the control signal to shrink the change of control signal so that the control signal can smooth converge to its desired value. In this section, we design a fuzzy tuner (**FT**) to offer a suitable scaling factor for the output of the **RFSMC**. The structure of the **FT** is shown in Fig. 5.

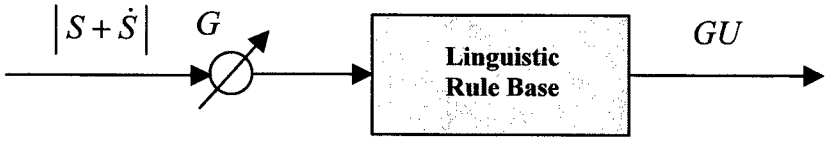


Fig. 5. The block diagram of the **FT**

From Eq. 2, we must design the control signal so that

$$s\dot{s} \le -\eta s^2 \qquad 5.$$

A sufficient condition for Eq. (5) to be satisfied is that $\dot{s}+\eta s=0$, or equivalently,

$$\dot{s}+\eta s = \dot{S}/_{GS} + \eta S/_{GCS} = 0 \qquad 6.$$

By multiplying GS on both sides of Eq. (6) and letting $\eta = \dfrac{GS}{GCS}$,

Eq. 6 becomes:

$$\dot{S}+S=0 \qquad 7.$$

Let $G^*|S+\dot{S}|$ be the input variable of **FT** (which is bound in [0,1]) and GU the output of **FT**. In order to satisfy Eq. (7), we can design the fuzzy rule of the **FT** as shown in Table 4, and membership functions as shown in Fig. 6.

Table 4: The fuzzy rule base of the **FT**

$G^*\|S+\dot{S}\|$	S	M	L
GU	ϕ_1	ϕ_2	ϕ_3

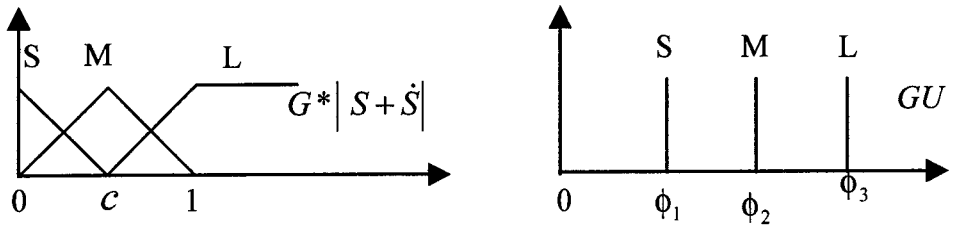


Fig. 6. Membership functions of the fuzzy variable $G^*|S+\dot{S}|$ and GU.

To obtain the optimal **RFSMC** and **FT**, we will apply the elitist **GA** to search the optimal values of c, ϕ_1, ϕ_2, ϕ_3, G, GS and GCS. The change of control signal derived by the **RFSMC** with a **FT** is then given by

$$\Delta u(kT+T) = RFSMC\left[S(kT+T)^*\right] * GU(kT+T)$$

where

$$GU(kT+T) = FT\left[G^*\left|S(kT+T)+\dot{S}(kT+T)\right|\right]$$

SIMULATION RESULTS

To compare performances of the proposed **RFSMC** with **FSMC**, an inverted pendulum was simulated. Consider an inverted pendulum system described by the following differential equations [15]:

$$\dot{\theta}_1 = \theta_2$$

$$\dot{\theta}_2 = \frac{g\sin\theta_1 - \cos\theta_1\left(\frac{mL}{M+m}\theta_2^2\sin\theta_1 + \frac{1}{M+m}u\right)}{\frac{4}{3}L - \frac{mL}{M+m}\cos^2\theta_1}$$

We set the parameters in this system as $M = 1$ kg, $m = 0.1$ kg, $L = 0.5$ m, $g = 9.8$ m/s^2, and sampling time = 0.005 sec. The control objective is to design a fuzzy controller so that the output angle θ can track the desired trajectory θ_d.

In order to meet the control objective, we define the sliding surface as follows:

$$\mathbf{H}: \left\{X \mid s(X;t) = \dot{e} + 20e = 0\right\}, \text{ where } e = \theta - \theta_d$$

The following two cases are controlled to compare the performances of the **RFSMC** with **FSMC**.

CASE 1: $\theta(0) = 1.0$ radius, $\dot{\theta}(0) = 0$ radius/sec, and $\theta_d(t) = 0$ radius.

CASE 2: $\theta(0) = 1.0$ radius, $\dot{\theta}(0) = 0$ radius/sec, and $\theta_d(t) = \sin(t)$ radius.

To compare the performance of **RFSMC** with **FSMC**, we define the cost function as follows:

$$J = \sum_{k=1}^{800} kT * \left|s(kT)\right| + 0.05\left|u(kT)\right|$$

We adopt the resulting data of case 1 as training data for the **GA** to search the optimal **RFSMC** and **FSMC**. The fitness function for the **GA** is defined by:

$$F = 2{,}000 \Big/ \left(\sum_{k=1}^{800}\left(\left|kT * s(kT)\right| + 0.05\left|u(kT)\right|\right)\right)$$

The resulting optimal controllers are then respectively applied to control the system of case 2. The simulation results are shown in Table 5, where t_s is defined as the settling time of s.

Table 5: The simulation results

	FSMS with FT		RFSMC with FT	
	J	t_s	J	t_s
Case 1	167.54	0.505	150.11	0.48
Case 2	1272.5	0.52	1115.6	0.475

CONCLUSIONS

In this paper, we have proposed a **RFSMC** with a **FT** and then uses a **GA** to search for optimal parameters. By combining the two input variables of **FSMC** as a new one input variable, the fuzzy control rules of **RFSMC** only increase linearly rather than exponentially when the input fuzzy labels increase. Hence the complexity of the fuzzy rule base is reduced. To improve the performance of **RFSMC** further, we combine the **RFSMC** with a **FT**, which uses three rules to tune the scaling factor for the output of the **RFSMC**. Finally, the elitist **GA** is applied to search for optimal parameters for **RFSMC** and **FT**. The simulation results show that the **RFSMC** with **FT** exhibits better performance than that of a conventional **FSMC**.

ACKNOWLEDGEMENT

The authors would like to thank National Science Council for providing financial support for this research under Grant NSC88-2213-E-036-020

REFERENCES

1. C.C. Fuh, P.C. Tung, 1997. "Robust stability analysis of fuzzy control systems", Fuzzy Sets and Systems, 88, 289-298.
2. G. Feng, S.G. Cao, N.W. Rees, C.K. Chak, 1997. "Design of fuzzy control systems with guaranteed stability", Fuzzy Sets and Systems, 85, 1-10.
3. J.A. Johnson, H.B. Smartt, 1995. "Advantages of an alternative form fuzzy logic", IEEE Trans. Fuzzy Systems, 3(2), 149-157.
4. C.L. Chen, M.H. Chang, 1998. "Optimal design of fuzzy sliding-mode control: A comparative study", Fuzzy Sets and Systems, 93, 37-48.
5. H.X. Li, H.B. Gayland, A.W. Green, 1997. "Fuzzy Variable Structure Control", IEEE SMC, 27(2), 306-312.
6. C.C. Kung, C.C. Liao, 1994. "Fuzzy-sliding mode control of nonlinear system", R. O. C. Automatic Control Conference, 259-264.
7. C.C. Kung, S.C. Lin, 1992. "A fuzzy-sliding mode controller design", IEEE International Conference on System Engineering, 1904-1905.
8. G.C. Hwang, S.C. Lin, 1992. "A stability approach to fuzzy control design for nonlinear systems", Fuzzy Sets and Systems, 48, 279-287.
9. J.S. Taur, C.W. Tao, 1997. "Design and Analysis of Region-Wise Linear Fuzzy Controllers", IEEE SMC Trans., 27(3).
10. H.Y. Chung, B.C. Chen, J.J. Lin, 1998. "A PI-type fuzzy controller with self-tuning scaling factors", Fuzzy Sets and Systems, 93, 23-28.
11. J.H. Holland, 1975. Adaptation in Natural and Artificial Systems. Ann Arbor, Univ. Mich. Press.
12. D.E. Goldberg, 1989. Genetic Algorithms in Search, Optimization and Machine Learning. Reading, MA, Addison-Wesley.
13. J.J. Slotine, 1984. "Sliding controller design for non-linear systems", Int. J. Contr., 40(2), 421-434.
14. J.J. Slotine, S.S. Sastry, 1983. "Tracking control of non-linear systems using sliding surfaces with application to robot manipulators", Int. J. Control, 38(2), 465-492.
15. M. Fliess, 1989. "Nonlinear control theory and differential algebra", in Modeling and Adaptive Control, Ch. I., Byrnes and A. Khurzhansky, Eds., New York, Springer-Verlag.

A MULTI-INPUT CURRENT-MODE FUZZY INTEGRATED CIRCUIT FOR PATTERN RECOGNITION

Gu Lin, Bingxue Shi

Institute of Microelectronics, Tsinghua University, Beijing, 100084, China

ABSTRACT

A multi-input current-mode fuzzy recognition integrated circuit is proposed in this paper, which is amenable to many pattern recognition applications. It can accept multiple inputs that represent multiple features of an unknown pattern in time-shared way. The principle of the fuzzy circuit is based on "Sum - Sorting" rule. In the fuzzy circuit, membership function generators employs current-mode circuit to generate memberships corresponding to each standard pattern according to the input features. Switched-current accumulators are adopted to realize the Sum function to get synthetic memberships. Sorting circuit sorts all of synthetic memberships based on their magnitudes , and finally recognition results are outputted. The fuzzy integrated circuit has been successfully manufactured in 2μm N-well standard digital CMOS process. It has been applied to speaker-independent Chinese digits speech recognition with the high recognition speed of 1.7×10^5 digits per second and the high recognition rate(the first recognition rate is more than 90% , the second recognition rate is more than 98%).

INTRODUCTION

Since fuzzy mathematics was established, it has found applications in expert system, pattern recognition, robotics, and industry control, etc. There are two ways to implement fuzzy processes. One is completed by software using digital computer, but it is difficult to work by this way in real-time. The other is completed directly using hardware system, it could implement high-speed process.Fuzzy hardware can be implemented in analog or digital circuits. Digital fuzzy system is a special computer system, it takes advantage of mature digital VLSI technology, but its scale is large [1]. Analog fuzzy system is composed of multiple-valued logic (MVL) circuit elements. MVL circuits have two kinds of mode, current-mode and voltage-mode. Comparing with the voltage-mode circuit, current-mode circuit is easy to realize sum and difference operation, has large current range and high integration density , especially, current-mode circuit is able to be implemented in a standard CMOS technology. So current-mode circuits are employed in many fuzzy systems[2,3,4].

In this paper, a fuzzy integrated circuit for Chinese-digit speech recognition is proposed. Its structure is amenable to other many pattern recognition applications. Experimental results show that the circuit can correctly realize the recognition function and has the advantages of high recognition speed and high recognition rate .

PRINCIPLE OF FUZZY PATTERN RECOGNITION

The feature of objective things often has some ambiguity. It is demonstrated with fuzzy set characterized by a membership function. The fundamental of fuzzy pattern recognition is the principle of maximum membership. In fact, a standard pattern has often multiple fuzzy features. Let each of N standard patterns have M fuzzy features. $\tilde{A}_{ij}$, $i=1,2,\ldots,N$; $j=1,2,\ldots,M$, represents the jth fuzzy feature of the ith standard pattern. Then, each standard pattern becomes a fuzzy vector (or multifactorial fuzzy set)

0-7803-5489-3/99/$10.00 ©1999 IEEE.

$\tilde{A}_i = \tilde{A}_i = \langle \tilde{A}_{i1}, \tilde{A}_{i2}, \ldots, \tilde{A}_{iM} \rangle$, $1 \le i \le N$. Assuming that $u_0 = (u_1^0, u_2^0, \ldots, u_M^0)$ is the unknown pattern to be recognized, its each element u_j^0 corresponds to a fuzzy feature. If there exits $k \in \{1,2,\ldots,N\}$ to make

$$\mu_{\tilde{A}_k}(u_0) = \max\{\mu_{\tilde{A}_1}(u_0), \mu_{\tilde{A}_2}(u_0), \ldots, \mu_{\tilde{A}_N}(u_0)\} \quad 1.$$

then, it is decided that u_0 relatively belongs to $\tilde{A}_k$, in which, assuming that

$$\mu_{\tilde{A}_i}(u_0) = M_m(\mu_{\tilde{A}_{i1}}(u_1^0), \mu_{\tilde{A}_{i2}}(u_2^0), \ldots, \mu_{\tilde{A}_{iM}}(u_M^0)) \quad 2.$$

$M_m(\bullet)$is defined as a multifactorial synthetic function.

Equation (1) is the classical rule for multifactorial fuzzy pattern recognition. At present, almost of fuzzy recognition integrated circuits are implemented based on the rule.According to this rule, these fuzzy processors only find the standard pattern closest to unknown pattern as the recognition result, that is, the standard pattern having the largest synthetic membership is chosen as the result. However, with the increase of the system complexity and the number N of standard patterns, especially the improvement of the multi-stage cascade system , the above method can not further meet the requirement of system. To develop the performances of system, it is necessary that the system is able to find two or more standard patterns closer to unknown pattern based on the magnitudes of synthetic memberships. To this end, the proposed fuzzy recognition integrated circuit employs sorting operation based on magnitude in the judgment part of fuzzy recognition process. This fuzzy processor can find h ($1 \le h \le N$) standard patterns closer to unknown pattern. That is, if there exits $k_1, k_2, \ldots, k_h \in \{1,2,..,N\}$ to make

$$\mu_{\tilde{A}_{k_1}}(u_0) = \max_{i=1}^{N} \mu_{\tilde{A}_i}(u_0) \quad 3.$$

$$\mu_{\tilde{A}_{k_2}}(u_0) = \max_{i=1, i \ne k_1}^{N} \mu_{\tilde{A}_i}(u_0) \quad 4.$$

$$\mu_{\tilde{A}_{k_h}}(u_0) = \max_{i=1, i \ne k_1, k_2, \ldots, k_{h-1}}^{N} \mu_{\tilde{A}_i}(u_0) \quad 5.$$

then, it is decided that h ($1 \le h \le N$) standard patterns closer to unknown pattern u_0 will be $\tilde{A}_{k_1}$, $\tilde{A}_{k_2}$, ..., $\tilde{A}_{k_h}$ respectively.

Generally, the synthetic function is defined in two kinds of way: minimum function and sum function. Comparing with the minimum function , the sum function has better generalization ability which means better recognition performance can be achieved for untrained data. So the sum function is employed in the proposed fuzzy processor.

DESIGN OF FUZZY INTEGRATED CIRCUIT

The structure diagram of the fuzzy integrated circuit is shown in Fig. 1. The fuzzy integrated circuit consists of membership function generators (MFG), switched-current accumulators(SIA),a sorting circuit , feature decoder and clock circuit. Assuming that feature code is K bit, every feature could have 2^K value. In order to decrease pad number on the chip and share a feature decoder, M features are inputted to the processor in a time-shared way.

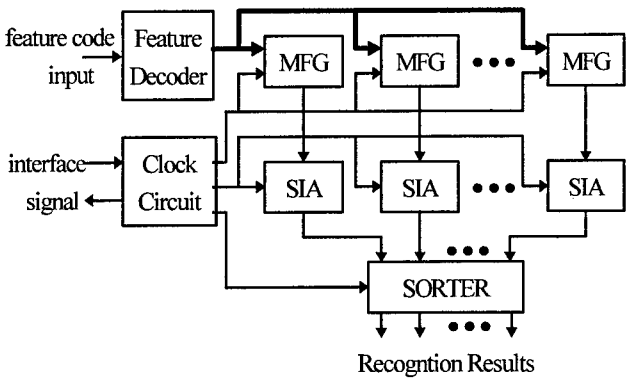


Fig.1 The strcture of Fuzzy Processor

When the processor is started, feature code is firstly inputted and decoded by the feature decoder. The outputs of the feature decoder enter membership function generators, and memberships of the feature belonging to N standard patterns are gotten. Then memberships are accumulated by accumulators to get synthetic memberships in time-shared way. Finally, the sorting circuit sorts synthetic memberships based on their magnitudes and outputs recognition results.

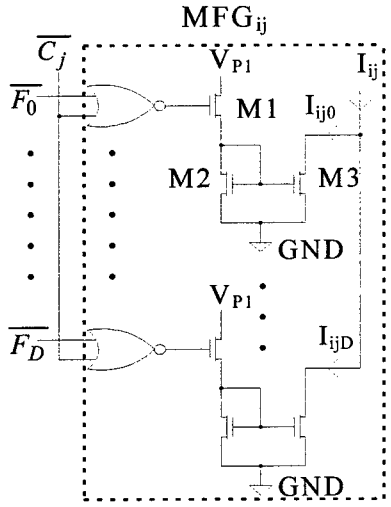


Fig.2 The circuit diagram of MFG

Membership Function Generator (MFG)

MFG is shown in Fig.2. MFG_{ij} ($1 \le i \le N, 1 \le j \le M$)is the membership function generator of the *j*th fuzzy feature of the *i*th standard pattern. I_{ij} ($1 \le i \le N, 1 \le j \le M$) represents the membership value of the *j*th fuzzy feature of the *i*th standard pattern. I_{ij} is composed of I_{ijl} ($0 \le l \le D$, $D=2^K-1$) that represents the *l*th membership value of the *j*th fuzzy feature of the *i*th standard pattern. The current-mode MFG employs a scaled current mirror. It is mainly composed of NMOS mirror transistors M2 and M3. The scaled output current according to shape ratio of M3 to M4 corresponds to one membership value. Analog switched transistor M1 is controlled by output F_l ($0 \le l \le D$) of the feature decoder and timing signals C_j ($1 \le j \le M$), in which C_j ($1 \le j \le M$)are some neighboring and non-overlapping pulses, each of which matches one input feature. In Fig.2, $\overline{C}_j$ ($1 \le j \le M$) is the inverted signal ofC_j. $\overline{F_l}$ ($0 \le l \le D$) is the inverted signal of F_l .

Switched-Current Accumulator (SIA)

Accumulator adopted to perform accumulation of memberships is implemented by using second-generation RGC(Regulated-Gate Cascode) switched-current integrator. Switched-current circuits are able to be directly fabricated in standard digital CMOS technology, and is easily to be integrated in mixed analog-digital system and implemented in VLSI. At present, switched-current circuits have been employed in many fields[5,6,7]. Fig.3 shows the diagram of the switched-current accumulator. In Fig.3, RGC1,RGC2 and RGC3 are fully identical RGC unit. SW0,SW1 and SW3 are analog switches which are controlled by nonoverlapping clock signals CL_1 and CL_2 respectively. I_{out} is the output current of the integrator in the accumulator. $I_{out} \sim I_{in}$ in z transformation is

$$I_{out} = (I_{in} \times z^{-1}) / (1 - z^{-1}) \qquad 6.$$

From above equation, the circuit shown in Fig.3 is able to perform the function of integrator, that is, it can implement the function of accumulation.

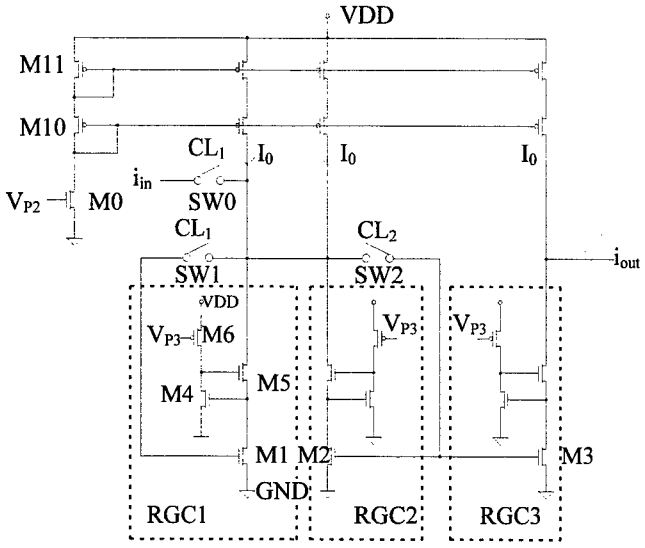


Fig.3 The circuit diagram of SIA

Sorting Circuit

The current-mode sorting circuit is employed to sort synthetic memberships based on their magnitudes and find out standard patterns closer to unknown pattern [8]. For simplicity, a current-mode sorting circuit based on magnitude is discussed by taking three input currents for example. The structure and timing diagram of the sorting circuit is shown in Fig.4. Fig.5 shows the circuit diagram of TRANS unit in the sorting circuit.

Here, the operation principle of the sorting circuit is discussed. Referring to the circuit and timing diagram shown in Fig.4, firstly, the signal Reset increases from low level to high level , this causes the level at the node CT_k (k=0,1,2) in block3 to go to high , and the level at the node $Vout_k$(k=0,1,2) to go to low . Because the level at the node CT_k(k=0,1,2) is high, I_k(k=0,1,2)=Iin_k(k=0,1,2) in block1. In the sorting circuit shown in Fig.4, Block2 mainly consists of a current-mode winner-take-all(WTA) circuit network which is a laterally inhibitory interconnected network with high resolution and high speed. In the WTA circuit, all of NMOS transistors corresponding to M_{21}~M_{23} have same W/l ratio. For the convenience of description, herein Iin_0 is assumed as the maximum input current,that is,Iin_0 =max(Iin_0, Iin_1, Iin_2) and I_0 =max(I_0, I_1, I_2). When the WTA circuit works, it finds the maximum input current by lateral inhibitory effect. This causes the level at node $VSout_0$ to be high and the levels at node $VSout_1$ and $VSout_2$ to be low . At the instant T_1 , the clock signal CK goes to high. It is clear that the $Vout_0$ becomes high since the level at the node $VSout_0$ is high, while $Vout_1$ and $Vout_2$ become low since the levels at the node $VSout_1$ and $VSout_2$ are low. When

the clock signal Ck goes to low at the instant T_2, the level at the node CT_0 becomes low , and $Vout_0$ becomes low, so that a high voltage pulse is generated on the $Vout_0$ terminal. While CT_1 and CT_2 are still high,$Vout_1$ and $Vout_2$ are still low. Among $Vout_0$,$Vout_2$ and $Vout_2$, only $Vout_0$ outputs one high level pulse, this shows the terminal of input current Iin_0 has the maximum input current value.

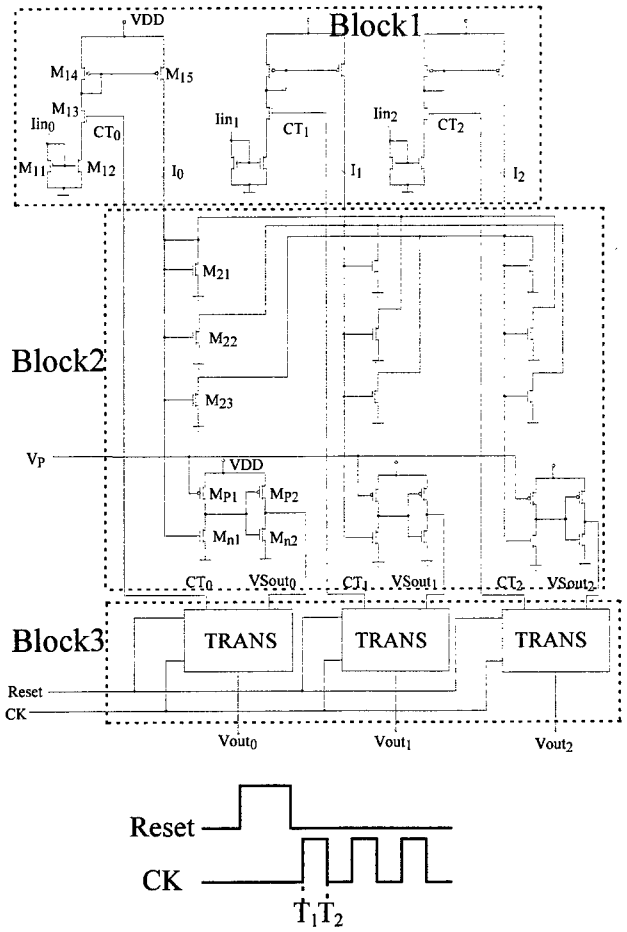


Fig.4 The circuit and timing diagram of the sorting circuit

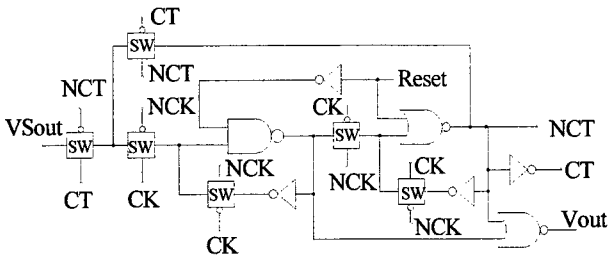


Fig.5 The circuit diagram of TRANS unit

Since the level at the node CT_0 is low, the voltage at the node $VSout_0$ can not be inputted to the block3 so that the level at the node CT_0 and $Vout_0$ will hold zero until the next reset signal is activated. On the other hand, the levels at the node CT_0 being low makes the current I_0 become zero in block1, so that I_0 will not influence the sequential comparison operation. In this manner, Iin_1 and Iin_2 are compared and the maximum one between them will be determined by the process described above. A high voltage pulse is generated on the corresponding Vout terminal. The remaining operations can be deduced accordingly. Finally, the sorted

results can be obtained. In fuzzy integrated circuit shown in Fig.4, the sorted results are outputted as recognition results.

In the sorting circuit, the pulse number h of signal CK can be chosen to meet different requirements. For example, when h is equal to 1, the sorting circuit only executes the MAX function; when h is equal to N which is the number of input currents, the sorting circuit sorts all of input currents.

From above discussion, it is clear that the fuzzy integrated circuit is able to find h ($1 \leq h \leq N$) standard patterns closer to unknown pattern based on magnitudes of synthetic memberships. This will greatly improve the performances of the fuzzy system.

Table 1. Measured results for the fuzzy processor

chip area	$5.4 \times 5.8 mm^2$
chip core area	$3.6 \times 4.1 mm^2$
pin number	40
transistors number	about 4100
pattern number N	11
frequency	2MHz
recognition rate	1.7×10^5 patterns /second
power supply	5V
lowest power supply	3.5V
power consumption in the state of recognition	about 80mW
power consumption in the state of wait	about 20mW

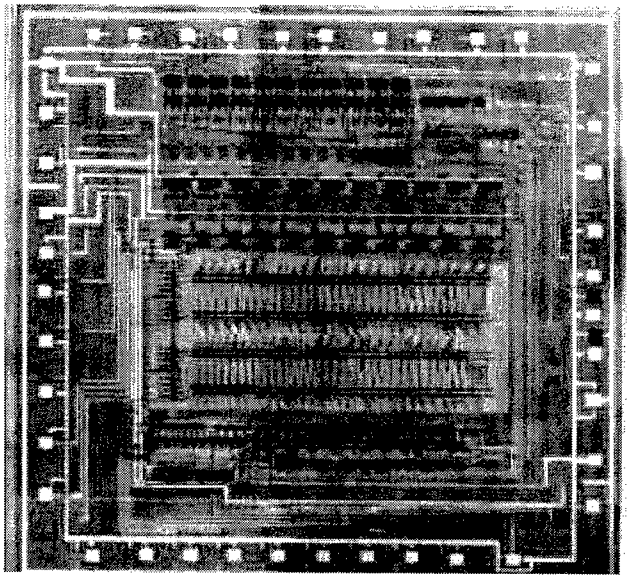


Fig.6 The microphotograph of the fuzzy processor chip

EXPERIMENTAL RESULTS

The fuzzy integrated circuit has been manufactured in 2μm N-well standard digital CMOS technology. The microphotograph of the fuzzy processor chip is shown in Fig.6. The fuzzy processor has been successfully measured . The measured results are shown in Table.1.

This fuzzy processor has been successfully applied to speaker-independent Chinese digits speech recognition including 11 digits. Recognition experimental results show that the fuzzy processor has high recognition speed of 1.7×10^5 digits per second , and high recognition rate (the first recognition rate is more than 90%, the second recognition rate is more than 98%).

SUMMARY

A multi-inputs current-mode fuzzy integrated circuit is proposed in this paper,which can accept multiple inputs that represent multiple features of an unknown pattern in time-shared way. In this fuzzy system, the Sum-Sorting operation is used. The structure of the fuzzy processor is amenable to many pattern recognition applications. The fuzzy processor has been successfully manufactured in 2μm N-well standard digital CMOS process. It has been applied to speaker-independent Chinese digits speech recognition with the recognition speed of 1.7×10^5 digits per second and the high recognition rate(the first recognition rate is more than 90%, the second recognition rate is more than 98%).

ACKNOWLEDGMENT

This project(69636030) is supported by National Natural Science Foundation of China

REFERENCE

1. Togai, H., Watanabe, 1986, A VLSI implementation of a fuzzy inference engine: toward an expert system on a chip, Information Sciences, .38(2), 147–164.
2. Yamakawa, 1985. The design and fabrication of the current mode fuzzy logic semi-custom IC in the standard CMOS IC Technology. Proc. 15th ISMVL, 76-82.
3. W. Current, 1994. Current-mode CMOS multiple-valued logic circuits. IEEE J. of Solid-State Circuits, 29(2), 95-107.
4. Gu Lin, Bingxue Shi, 1997. Novel switched-current fuzzy processor for pattern recognition . .J. Tsinghua University (Science and Technology), 37(9), 86-89.
5. Terri, S , Guojin, L., David, J., 1991. Switched-current circuit design issues . IEEE Solid-State Circuit, 26(3), 192 -201.
6. Gu Lin, Bingxue Shi, 1998. A novel high resolution switched-current sorter based on magnitude, Chinese Journal of Semiconductors,19(2),144-150.
7. Rajaesh H , David, J , Terri, S., 1993. Fully balanced CMOS current-mode circuits . IEEE Solid-State Circuit, 28(5) ,569 -575.
8. Gu Lin, Bingxue Shi, 1999. A current-mode sorting circuit for pattern recognition, Proc. Second International Conference on Intelligent Processing and Manufacturing of Materials (IPMM'99), Honolulu, Hawaii.

A Framework for Intelligent Systems based on Vector Annotated Logic Programs

K. Nakamatsu*, Y. Hasegawa*, J. Minoro Abe, A. Suzuki*****

* School of Humanity of Environment Policy and Technology.,
Himeji Institute of Technology, Himeji, Japan
Email: nakamatu@hept.himeji-tech.ac.jp; , yumi}@hept.himeji-tech.ac.jp
** Department of Informatics (ICET), Paulista University, Sao Paulo, Brazil
Email: jmabe@lsi.usp.br
*** Faculty of Information, Shizuoka University, Hamamatsu, Japan

ABSTRACT

This paper presents a framework of intelligent reasoning systems. It is based on a logic programming system called VALPSN (Vector Annotated Logic Program with Strong Negation) and its stable model computing system. We introduce an overview of the framework and describe the three kinds of nonmonotonic theories, default theory, defeasible theory, and default fuzzy theory that can be translated into VALPSNs. We also show that these three kinds of nonmonotonic reasoning can be achieved by computing the stable models of the VALPSNs.

Keywords
annotated logic program, stable model, intelligent system, default reasoning, defeasible reasoning, fuzzy reasoning

INTRODUCTION

Annotated logics are a family of paraconsistent logics and multi-valued logics that are appropriate for dealing with inconsistency or conflicts[3]. Generally, each atomic formula of annotated logics is explicitly attached a truth value called an annotation. For example, let p be an atomic formula, μ be an annotation, then, $p : \mu$ is an annotated atomic formula. There are two kinds of negation , an epistemic negation and an ontological negation, in annotated logics. The ontological negation is a strong negation and we have proposed ALPSN (Annotated Logic Program with Strong Negation) that can deal with nonmonotonic reasoning in [7,8].

In this paper, we introduce a new extended version of the ALPSN called VALPSN (Vector Annotated Logic Program with Strong Negation) in order to formalize some intelligent reasonings. In VALPSN, an annotation of a literal is a 2-dimensional vector such that the first and second components of the vector indicate the amount of positive and negative knowledge in terms of the literal, respectively, and the epistemic negation is defined as the exchange of each component. For example, let q be a literal and (2, 1) a vector annotation. Then , a vector annotated literal $q : (2, 1)$ is intuitively interpreted as "the literal q is known to be true strength 2 and false strength 1", and $\neg q : (2, 1) = q : (1, 2)$. The details of VALPSN are formally described in the following sections.

We have shown that VALPSN can represent three kinds of reasonings, defeasible reasoning, default reasoning, and fuzzy reasoning [6]. There fore, we propose a framework for intelligent reasoning systems based on VALPSN and its stable model computation, which can deal with the three kinds of reasonings. We introduce the overview of the framework in the following section.

OVERVIEW OF THE FRAMEWORK

The framework consists of two modules, the knowledge translation module and the inference module, as shown in Figure 1. The inference engine of this system is a stable model computing system. In the

framework, it is assumed that all input knowledge are represented in the three kinds of theories, defeasible theories, default theories, and fuzzy theories. Each theory is translated into a VALPSN in the knowledge translation module and the model of each theory is computed as the stable models of the VALPSNs in the inference module. These stable models represent the inference results of the three nonmonotonic reasonings, default one, defeasible one, and default fuzzy one.

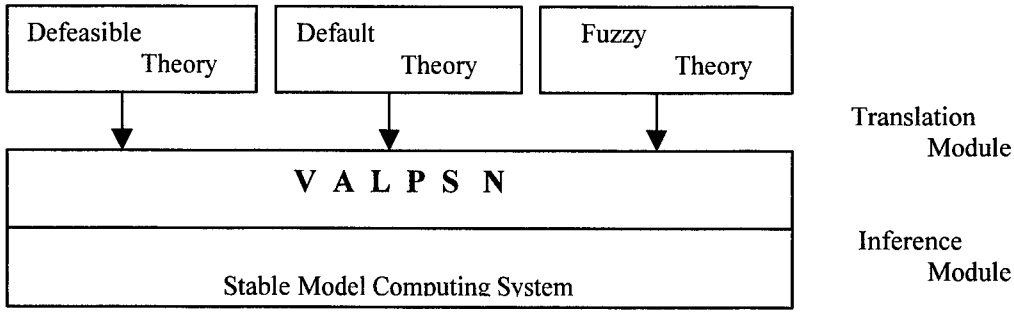


Fig. 1. A Framework for Intelligent Systems.

We describe the details of the translation process and the inference process by presenting some examples after introducing VALPSN.

VALPSN

In this section, we introduce ALPSN and its extended version, VALPSN. Generally, the set of truth values T in annotated logics has an arbitrary complete lattice structure. ALPSN has a well known the 4–valued lattice, *Lattice-4*, as the lattice of truth values. The ordering of the lattice is denoted by $=$ as usual

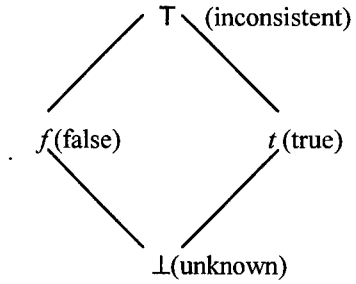


Fig. 2. 4-valued Lattice Structure.

Let A be a lattice. $A : \mu$ is called an *annotated literal* and μ is called an *annotation,* where $\mu \in T$. Generally, annotated literals can be interpreted epistemically. For example, an annotated literal $p : t$ is interpreted as p is known to be true(t), and $p : \mathsf{T}$ is interpreted as p is known to be both true(t) and false(f). In annotated logics, there are two kinds of negations, an epistemic negation($\neg$) and an ontological one($\sim$). The epistemic negation is defined as a mapping from annotations to annotations. For example, $\neg(\bot) = \bot$, $\neg(t) = f$, $\neg(f) = t$, $\neg(\mathsf{T}) = \mathsf{T}$.

Definition 1.
The (well formed) formulas of annotated logics are defined as :

1. Any annotated literal is a formula.
2. If F_1, F_2, and F are formulas, then, $F_1 \wedge F_2, F_1 \vee F_2, F_1 \rightarrow F_2$, $\forall x F$, and $\exists x F$ are formulas.

The ontological negation $\sim$ can be defined by the epistemic negation $\neg$. This ontological negation is a strong negation that has all properties that classical negations contain.

Definition 2. (Strong Negation)[3]
Let A be any formula. $\sim A =_{def} (A \rightarrow ((A \rightarrow A) \wedge \neg(A \rightarrow A)))$.

The epistemic negation followed by $(A \rightarrow A)$ is not interpreted as a mapping between annotations, or rather , a negation in the sense of classical logics.

Definition 3. [2,7]
Let $L_0, \cdot, L_n$ be any annotated literals. $L_1 \wedge \cdot \wedge L_n \rightarrow L_0$ is called an *annotated clause(a-clause)*, and $L_1 \wedge \cdot L_i \wedge \sim L_{i+1} \wedge \cdot \wedge \sim L_n \rightarrow L_0$ is called an *annotated clause with strong negation(asn-clause).* An ALP (Annotated Logic Program) and an ALPSN (Annotated Logic Program with Strong Negation) are finite sets of a-clauses and asn-clauses, respectively.

We now address the semantics for ALPSN and assume that all interpretations have a Herbrand base Bp as their domain of interpretation. Since T is a complete lattice, the Herbrand interpretation I of an ALPSN P over T may be considered to be a mapping $I : Bp \rightarrow T$. Usually, the interpretation I is denoted by the set $\{(p : ?\mu_i) \mid I \models (p : \mu_1) \wedge \cdot \wedge (p : \mu_n)\}$, where $?\mu_i$ is used to denote the least upper bound of $\{\mu_1, \cdot, \mu_n\}$ and so is it in the rest of this paper. We assume that every interpretation of annotated logic programs is a Herbrand interpretation. The ordering $\leq$ on T is extended to interpretations in a natural way and the notion of satisfaction is defined.

Definition 4. [2]
Let I_1 and I_2 be any interpretations and A be an annotated atom. $I_1 \leq I_2 =_{def} (\forall A \in Bp)(I_1(A) \leq I_2(A))$, where $I_1(A), I_2(A) \in T$. An interpretation I is said to satisfy

- a formula F *iff* it satisfies every closed instance of F,
- a ground annotated atom $(A : \mu)$ *iff* $I(A) \geq \mu$,
- a ground annotated literal $(\neg A : \mu)$ *iff* $I(A) \leq \neg(\mu)$,
- a complex formula $\neg F$ *iff* I does not satisfy F.

The satisfaction of the other formulas, $F_1 \wedge F_2$, $F_1 \vee F_2$, $F_1 \rightarrow F_2$, $\forall x F$, and $\exists x F$, are the same as classical logics.

The satisfaction is denoted by the usual symbol $\models$. We obtain that, for any formula F, $\models \sim F$ *iff* $\not\models F$ from the above definition.

Definition 5.
Associated with every ALPSN P, a function Tp from Herbrand interpretations to themselves and an upward iteration of it. For any ground instance, $B_1 \wedge \cdot \wedge Bm \wedge \sim C_1 \wedge \cdot \wedge \sim C_n \rightarrow (A : \mu)$, of an asn-clause in an ALPSN P, $Tp(I)(A) = ?\{\mu \mid I \models B_1 \wedge \cdot \wedge B_m \wedge \sim C_1 \wedge \cdot \wedge C_n\}$.
Let $?$ be a special interpretation that assigns the truth value $\perp$ to all members of a Herbrand Base Bp. Then, the upward iteration of Tp is defined as: $Tp \uparrow 0 = ?$, $Tp \uparrow \lambda = \bigcup_{\alpha<\lambda} Tp(Tp \uparrow \alpha)$, for any ordinals α, λ.

Then the following propositions hold (The proofs are in [2]) : If a program P is an ALP, then ,

- Tp is a monotonic function,
- P has the unique least model that is identical to the least fixed point of Tp,
- $Tp \uparrow \omega$ is identical to the least fixed point of Tp.

We describe the stable model[4] of an ALPSN P taking account into propositions. Let I be any interpretation. P^I, the *Gelfond – Lifschitz transformation* of P with respect I, is an ALP obtained from P by deleting.

(1) each clause that has a literal $\sim (C : \mu)$ in its body with $I \models (C : \mu)$ and
(2) all strongly negated literals in the bodies of the remaining clauses.

Since P^I has no strong negation, it has the unique least model that is given by $Tp_I \uparrow \omega$ [2,4].

Definition 6. (Stable Model of ALPSN) [4,7,8]
If I is a Herbrand interpretation of an ALPSN P, then , I is called a stable model of P *iff* $I = Tp_1 \uparrow \omega$.

Example 7.
Let an ALPSN $P = \{\sim (b : t) \rightarrow (a : t), \sim(a : t) \rightarrow (b : t), (a : t) \rightarrow (p : t), (b : t) \rightarrow (p : f)\}$.
If $I_1 = \{(a : t), (b : \perp), (p : t)\}$, then, $P^{I1} = \{(a : t), (a : t) \rightarrow (p : t), (b : t) \rightarrow (p : f)\}$ and $Tp^{I1} \uparrow \omega = I_1$. Therefore, I_1 is a stable model of the ALPSN P. If $I_2 = \{(a : \perp), (b : t), (p : f)\}$,then, $P^{I2} = \{(b : t), (a : t) \rightarrow (p : t), (b : t) \rightarrow (p : f)\}$ and $TP^{I2} \uparrow \omega = I_2$. Therefore, I_2 is also a stable model of the ALPSN P.

The primary difference between ALPSN and VALPSN is in their annotations. In the case of ALPSN, the annotations are usually some symbols expressing some meanings such as $\perp$(*unknown*), *f*(*false*), *t*(*true*), T(*inconsistent*). On the other hand, in the case of VALPSN, the annotation is a vector called a *vector annotation*. The vector annotation is a 2-dimentional vector (i , j) such that i and j are non-negative integers, and the lattice T_v of vector annotations is defined as : $T_v = \{(i, j) \mid 0 = i = n,\ 0 = j = n,\ i, j$ and n are non-negative integers$\}$. Moreover, we define the ordering $\leq$ on T_v. Let $v_1 = (x_1, y_1)$ and $v_2 = (x_2, y_2)$, then , $v_1 = v_2$ *iff* $x_1 = x_2$ and $y_1 = y_2$, where, x_1 , x_2 , y_1 , and y_2 are non-negative integers. Roughly speaking , if the first component of a vector annotation can be regarded as representing the strength of truth while the second component represents the strength of falseness, we can provide epistemic interpretations for vector annotated literals as well as the case of ordinary annotated literals. If p is a literal and i , j are non-negative integers, $p : (i, j)$ is interpreted as p is known to be true of strength i and false of strength j. This interpretation provides a definition of the epistemic negation in vector annotated logics. The epistemic negation can be defined as the exchange of each component of vector annotations. Let (i , j) be a vector annotation. Then , $\neg(i, j) = (j, i)$. A vector annotated literal $p : (i , j)$ may be regarded as implying both a conflict and defeasibility. The vector annotation, (i , j) , is the least upper bound of the vector annotations, $(i , 0)$ and $(0, j)$, and it can be regarded as containing both meanings, "true of strength i " and "false of strength j". Moreover, if the integer i is larger than the integer j, then the literal p may be interpreted as being relatively true, in the sense of that "true of strength i " defeats "false of strength j". Therefore, VALPSN can be obtained by replacing the terms, annotated and **annotated** and **annotation**, in ALPSN by the terms, **vector annotated** and **vector annotation**, respectively.

DEFAULT REASONING

Generally, it is well-known that logic programs with strong negation can formalize a default reasoning. Actually, we have already shown that a default reasoning can be translated into ALPSNs in [7,8]. Generally, a default theory[9] $T = (D, W)$ consists of a set of facts, W, which are closed first order formulas, and of a set of defaults, D, which are specific inference rules having the form $u : v/w$, where u, v and w are first order formulas. However, in order to deal with the default theories in our framework, we restrict W to be a set of generalized Horn clauses(that are allowed to contain negative literals in their heads or bodies), and D, to be a set of defaults having the following form : $p_1 \wedge \cdot \wedge p_m : j_1, \cdot , j_k / C$, where p_1 ,$\cdot$, p_m , j_1 , $\cdot$, j_k ,C are literals. $p_1 \wedge \cdot \wedge p_m$ is the *prerequisite*, j_i ($1 = i = k$) the *justification* and C the consequent of the default. An informal interpretation of the default is that it is allowed to add C to the current knowledge databases whenever $p_1 \wedge \cdot \wedge p_m$ belong to that database and j_1 , $\cdot$, j_k are consistent with that database(i.e., $\neg j_1$, $\cdot$, $\neg jk$ do not belong to that database) If $T = (D, W)$ is a default theory,

(1) for any $d \in D$ such that $d = p_1 \wedge \cdot \wedge p_m : j_1, \cdot , j_k / C$,
$tr(d) = (p_1 : t) \wedge \cdot \wedge (p_m : t) \wedge \sim(j_i : f) \wedge \cdot \wedge \sim(j_k : f) \rightarrow (C : t)$ and
$tr(D) = \{tr(d_1), \ldots tr(d_n)\}$ such that $di \in D$ ($1 = i = n$),

(2) for any $w \in W$ such that $w = A_1 \wedge \cdot \wedge A_l \rightarrow A_0$,
$tr(w) = (A_1 : t) \wedge \cdot \wedge (A_l : t) \rightarrow (A_0 : t)$ and
$tr(W) = \{tr(w_1), \ldots tr(w_k)\}$ such that $wi \in W$ ($1 = i = k$).

In order to demonstrate that VALPSN can deal with default reasoning , we propose a mapping from the set T of annotations into the set T_v of vector annotations. Let $T_v = \{(0,0),(0,1),(1,0),(1,1)\}$. Then the mapping : $\perp \rightarrow (0,0), f \rightarrow (0,1), t \rightarrow (1,0)$, T$\rightarrow(1,1)$. We take the example, **Pennsylvania-Dutch** , whish has been used as an example of defeasible theories in [1], as an example of default theories in this section.

Example 8. (Pennsylvania-Dutch) [1]
This example consists of one fact, **F1**, two default rules, **R1**, **R2**, and two normal rules, **R3**, **R4**, and can be formalized in a default theory[8].

F1 : Hans$\{h\}$ is a native speaker of Pennsylvania-Dutch (PD), $\{nspd(h)\}$.
R1 : native speakers of PD are usually born in Pennsylvania, $\{nspd(h) : bp(h)/bp(h)\}$.
R2 : people born in Pennsylvania are born in the USA, $\{ bp(h) \rightarrow busa(h)\}$.
R3 : native speakers of PD are native speakers of German, $\{ nspd(h) \rightarrow nsg(h)\}$.
R4 : native speakers of German are usually not born in the USA, $\{nsg(h) : \neg busa(h)/\neg busa(h)\}$.

First, the above default theory is translated into an ALPSN in the way as described in [6], and next, the ALPSN is translated into a VALPSN P based on the mapping from the T into the T_v defined above. Then , we obtain the following VALPSN P.

$P = \{nspd(h) : (1,0),\ nspd(h) : (1,0) \wedge \sim bp(h):(0,1) \rightarrow bp(h) : (1,0),$
$bp(h) : (1,0) \rightarrow busa(h)(1,0),\ nspd(h):(1,0) \rightarrow nsg(h) : (1,0),$
$nspd(h) : (1,0) \wedge \sim nsg(h) : (1,0) \rightarrow busa(h) : (0,1)\}.$

This VALPSN P has two stable models I_1 and I_2.

$I_1 = \{ nspd(h) : (1,0),\ nsg(h) : (1,0),\ bp(h): (1,0),\ busa(h):(1,0)\},$
$I_2 = \{ nspd(h): (1,0),\ nsg(h):(1,0),\ bp(h): (0,1),\ busa(h): (0,0) \}.$

I_1 indicates that Hans is known to be born in Pennsylvania and in the USA. I_2 indicates that Hans is known not to be born in Pennsylvania and it is unknown whether he was born in the USA or not.

VALPSN can formalize default theories and the stable models of VALPSN represent the results of the default reasoning as shown in the above example. The example is cited in the following section from the viewpoint of defeasible reasoning. There is a conflict in terms of the question, " Where was Hans born ?" between the stable models, I_1 and I_2. We consider defeasible reasoning to resolve the conflict in the following section.

DEFEASIBLE REASONING

We have shown that there is the relation between the defeasible logic[1] and VALPSN shown in Figure 3. Based on the relation, we show that the defeasible theories can be translated into VALPSNs taking the same example, **Pennsylvania-Dutch**.

The defeasible logic[1] contains three kinds of rules, strict rules, defeasible rules and defeaters. Conflicts between defeasible rules with incompatible cnseoquents are resolved by using explicit superior relations on rules. The defeasible logic is defined as the set of conditions on nodes of proof trees. The alphabet is the union of the following four pairwise disjoint sets of symbols.

- A nonempty countable set of proposition symbols.
- The set $\{\neg,\rightarrow,\Rightarrow,\approx\}$ of connectives.
- The set $\{+,-,?,?\}$ of positive, negative, definite, and defeasible proof symbols.
- The set of punctuation marks consisting of the comma, braces and parentheses.

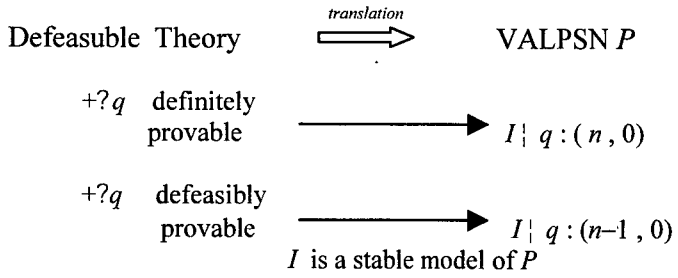


Fig. 3. Defeasible Theory and VALPSN.

The negation of the proposition P is denoted by $\neg p$. The complement of the proposition p is $\neg p$ and the complement of $\neg p$ is p. If q is any literal then the complement of the q is denoted by Q. The positive proof symbol + indicates that the following literal has been proved. The negative proof symbol – indicates that the following literal has been proved to be unprovable. The definite proof symbol ? indicates that the proof of the following literal cannot be defeated by more information. The defeasible proof symbol ? indicates that the proof of the following literal can be defeated by more information. A *rule* has three parts : a finite set of literals on the the left , an arrow in the middle, and a literal on the right. A rule which contains the *strict arrow* $\rightarrow$, for example $\mathbf{A} \rightarrow q$, is called a *strict rule.* The intuition is that whenever all the literals in **A** are accepted then q must be accepted. A rule which contains the *defeasible arrow* $\Rightarrow$, for example $\mathbf{A} \Rightarrow q$, is called a *defeasible rule.* If all the literals in **A** are accepted then q is accepted provided that there is an insufficient evidence against q. A rule which contains the *defeater arrow* $\approx$, for example $\mathbf{A} \approx Q$, is called a *defeating rule* or a *defeater*. If all the literals in **A** are accepted then $\mathbf{A} \rightarrow q$ is an evidence against q, but not for Q. It should be noted that the antecedent of a rule can be empty set.

The defeasible logic has the four inference conditions, $+?$, $-?$, $+?$, and $-?$. We comment about the notations in the conditions before describing them. Let q be a literal. In a proof, $+?q$ indicates that q is proved definitely, $-?q$ indicates that it is proved that q can not be proved definitely, $+?q$ indicates that q is proved defeasibly, and $-?q$ indicates that is proved that q can not be proved defeasibly. Let R be any set of rules. The set of strict rules in R denoted by R_s, and the union of R_s and the set of defeasible rules in R by R_{sd}. The antecedent of any rule r is denoted by $A(r)$ and its consequent is denoted by $C(r)$. The set of consequents of rules in R is denoted by $C(R) = \{C(r) \mid r \in R\}$.$R[q] =_{def} \{r \mid r \in R \text{ and } q = C(r)\}$. The superiority relation on R is any symmetric binary relation $>$ on R. A finite sequence $P = (P(1), \cdot, P(\mid P \mid))$ of tagged literals$(+?q, -?q, +?q, -?q)$is called a proof. An element of a proof is called a line of the proof. $P(i+1)$ indicates the $i+1$th line of a proof. $P(1..i)$ indicates the proof lines from the first one to the ith one. The four conditions of inference in the defeasible logic are :

+ ?) If $P(i+1) = +?q$, for some literal q, then either
.1) $q \in F$; or
.2) $\exists r \in R_s[q] \forall a \in A(r), +?a \in P(1..i)$.

– ?) If $P(i+1) = -?q$, for some literal q, then
.1) $q \notin F$, and
.2) $\forall r \in R_s[q] \exists a \in A(r), -?a \in P(1...i)$.

+?) If $P(i+1) = +?q$, for some literal q, then either
.1) $+?q \in P(1..i)$; or
.2) All three of the following conditions hold.
.1) $\exists r \in R_{sd}[q] \forall a \in A(r), +?a \in P(1..i)$,
.2) $-?Q \in P(1..i)$, and
.3) $\forall s \in R[Q]$ either
.1) $\exists a \in A(s), -?a \in P(1..i)$; or
.2) $\exists t \in R_{sd}[q]$ such that
.1) $\forall a \in A(t), +?a \in P(1..i)$, and
.2) $t > s$.

$-?$) If $P(i+1) = -?q$, for some literal q, then either
.1) $-?q \in P(1..i)$;or
.2) either
.1) $\forall r \in R_{sd}[q] \exists a \in A(r), -?a \in P(1..i)$,
.2) $+?Q \in P(1..i)$, or
.3) $\exists s \in R[Q]$ such that
.1) $\forall a \in A(s), +?a \in P(1..i)$; and
.2) $\forall t \in R_{sd}[q]$ either
.1) $\exists a \in A(t), -?a \in P(1..i)$, or
.2) not $(t > s)$.

Example 9.
We take the same **Pennsylvania-Dutch in Example 8** as an example of defeasible theories . The VALPSN in **Example 8** has two stable models and there is a conflict when the question " Was Hans born in the USA ?" is asked. The generally agreed answer for the question is "defeasibly yes". In order to obtain the desirable answer, a formalization of **Pennsylvania-Dutch** by the defeasible logic contains the superiority relation **R1** > **R4**. The details of the formalization are found in [1].

F1 : $nspd(h)$, **R1** : $nspd(h) \Rightarrow bp(h)$, **R2** : $bp(h) \rightarrow busa(h)$,
R3 : $nspd(h) \rightarrow nsg(h)$, **R4** : $nsg(h) \Rightarrow \neg busa(h)$.

This defeasible theory derives $+\partial busa(h)$ that indicates that " Hans was born in the USA "is defeasibly provable, and it is translated into a VALPSN P. Basically, there are proof procedures on both cases in which conflicting literals(q and $\neg q$) are derived and not derived in the defeasible logic. Therefore, since we have to take into account the both cases as the translation, the translation rule from the defeasible theory into a VALPSN is complicated. We omit the formal definition and the details of the rule for the sake of space restriction. Let $T_v = \{(i, j) \mid 0 = i = 3,\ 0 = j = 3,\ i, j$ are integers$\}$. Then , we can formalize the defeasible theory, **Pennsylvania-Dutch**, in VALPSN based on the translation.

F1 is translated into $\{nspd(h) : (3,0)\}$.
R1 is translated into $\{nspd(h)$: $(2,0) \wedge nsg(h) : (2,0) \wedge \sim bp(h) : (0,3) \rightarrow bp(h) : (2,0)$,
$nspd(h)$: $(2,0) \wedge \sim nsg(h) : (2,0) \wedge \sim bp(h) : (0,3) \rightarrow bp(h) : (2,0)\}$.
R2 is translated into $\{bp(h) : (3,0) \wedge busa(h) : (3,0),\ bp(h) : (2,0) \wedge busa(h) : (2,0)\}$.
R3 is translated into $\{nspd(h) : (3,0) \rightarrow nsg(h) : (3,0), nspd(h) : (2,0) \rightarrow nsg(h) : (2,0)\}$.
R4 is translated into $\{ nsg(h) : (2,0) \wedge nspd(h) : (2,0) \wedge \sim busa(h) : (3,0) \rightarrow busa(h) : (0,1)$,
$nsg(h) : (2,0) \wedge \sim nspd(h) : (2,0) \wedge \sim busa(h) : (3,0) \rightarrow busa(h) : (0,2)\}$.

Then, the VALPSN P has the unique stable model,
$I = \{ nspd(h) : (3,0),\ nsg(h) : (3,0),\ bp(h) : (2,0),\ busa(h) : (2,1)\}$.
Since $busa(h) : (2, 1)$ implies $busa(h) : (2,0)$, we have $busa(h) : (2,0)$ which measns that "Hans was born in the USA" is defeasibly true as well as the original defeasible theory.

DEFAULT FUZZY REASONING

VALPSN can deal with not only defeasible reasoning but also fuzzy reasoning . In order to implement default fuzzy reasoning in the framework of VALPSN, the set of vector annotations is required to be redenfined as $T_v = \{ (x, y) \mid x, y \in [0,1]\}$. The first component x indicates the degree of belief and the second component y indicates the degree of disbelief. If $x + y > 1$, then, it indicates a kind of conflict, if $x + y < 1$, then it in indicates uncertainty due to lack of information, and if $x + y = 1$ then it indicates normal belief[10]. For example , p :(0.7, 0.3) is interpreted informally as " p is 70% believed and 30% disbelieved". We show the default fuzzy reasoning based on VALPSN by using the following modified **Penguin-Triangle** as an example.

Example 10(modified **Penguin-Triangle**)[9]

This example consists of one fact,

F1: "Tweety(t) is a penguin" is 100% believed, $\{p(t) : (1,0, 0.0)\}$,

two fuzzy rules,

R1: If "Tweety is a penguin" is 100% believed, then "Tweety is a bird" is 80% believed and 10% disbelieved, $\{p(t) : (1,0, 0.0) \rightarrow \neg b(t) : (0.8, 0.1)\}$,

R2: If "Tweety is a penguin" is 100% believed, then "Tweety can not fly" is 80% believed and 20% disbelieved, $\{p(t) : (1.0, 0.0) \rightarrow \neg f(t) : (0.8, 0.2)\}$,

and one default fuzzy rule,

R3: If "Tweety is a bird" is more than 80% believed and "Tweety can not fly" is not more than 70% believed, then "Tweety can fly" is 70% believed.

$$\{b(t) : (0.8,0.0) \wedge \neg f(t) : (0.7, 0.0) \rightarrow f(t) : (0.7,0.0)\}.$$

Taking the **R1** rule as an example and comparing the vector annotation, (1.0, 0.0), of the antecedent with one, (0.8, 0.1), of the consequents of **R1** from the viewpoint of knowledge amount, it is realized that the inference by **R1** reduces the amount of knowledge, which means **R1** contains uncertainty. Intuitively, it can be regarded that "a penguin is a bird" is not 100% believed. The intuitive reasoning process of this example is as follows: from **F1** and **R1**, we have $\{b(t) : (0.8, 0.1)\}$, from **F1** and **R2**, we have $\{\neg f(t) : (0.8, 0.2)\}$, however, we can not have consequent, $\{f(t) : (0.7, 0.0)\}$,since$\{\neg f(t) : (0.8, 0.2)\}$ conflicts with $\{\sim \neg f(t) : (0.7, 0.0)\}$. Then, this VALPSN has only one stable model, $I = \{ p(t) : (1.0,0.0), b(t) : (0.8,0.1), f(t) : (0.2,0.8)\}$, which means that "Tweety is a penguin" is 100% believed, "Tweety is a bird" is 80% believed and 10% disbelieved, however, "Tweety can fly""is 20% believed and 80% disbelieved.

CONCLUSION

In this paper, we have proposed a framework for intelligent reasoning systems that can deal with three kinds of nonmonotonic reasoning: default, defeasible, and fuzzy. The framework consists of two modules , knowledge translation and inferencing. The inference module is a stable model computing system.

We have implemented the two modules as PROLOG programs. However, there are some problems in the implementation. The efficiency of the stable model computing system is not good. Generally, it takes a long time to compute the stable models of VALPSNs. Translation from defeasible theories into VALPSNs is so complicated that it also takes a long time to translate. So the efficiency of these speed issues should be improved in future work.

REFERENCES

1. Billington, D., 1997. "Conflicting Literals and Defeasible Logic", Proc.2nd Australian Workshop on Commonsense Reasoning , 1-14.
2. Blair, H.A., Subrahmanian, V.S., 1989. "Paraconsistent Logic Programming", Theoretical Computer Science, 68, 135-154.
3. da Costa, N.C.A., Subrahmanian, V.S., Vago, C., 1989. "The Paraconsistent Logics PT", Zeitschrift für Mathematische Logik und Grundlangen der Mathematik , 37, 139-148.
4. Gelfond , M., Lifschits, V., 1988. "The Stable Model Semantics for Logic Programming", Proc. 5th Inter. Conf. on Logic Programming , 1070-1080.
5. Lloyd, J.W., 1987. "Foundations of Logic programming", (2nd edition), Springer-Verlag.
6. Nakamatsu, K., Abe, J.M., 1999. "Reasonings Based on Vector Annotated Logic Programs", Proc. Intl Conf. on Computa. Intelligence for Modeling, Control, and Automation, IOS Press., Vienna, Austria.
7. Nakamatsu, K., Suzuki, A., 1994. "Annotated Semantics for Default Reasoning", Proc. 3rd Pacific Rim Inter. Conf. on AI, 180-186.
8. Nakamatsu, K. and Suzuki, A., "A Nonmonotonic ATMS Based on Annotated Logic Programs", in Agents and Multi-Agent Systems , LNAI 1441, Springer-Verlag, 1998.
9. Reiter, R., 1980. "A Logic for Default Reasoning", Artificial Intelligence, 13, 81-132.
10. Turksen, I.B., 1986. "Interval Valued Fuzzy Sets Based on Normal Forms", Fuzzy Sets and Systems, 20(2), 191-210.

A Fuzzy Logic Assisted Electrodynamic Balance for Unit Operations on Single Levitated Particles

M. Pappalardo*, A. Pellegrino*, M. d'Amore, P. Giordano** and P. Russo****

* Department of Mechanical Engineering, University of Salerno, Fisciano, Italy
** Department of Chemical and Food Engineering, University of Salerno, Fisciano, Italy
**Email: damore@dica.unisa.it

ABSTRACT

An electrodynamic balance (EDB) as a tool for unit operations on single sub-millimeter particles is described. Fine control of the particle position is designed and realized using either fuzzy logic concepts or traditional PID schemes. Precision and efficacy of the two methods are compared. A simple application to the drying of a droplet is shown.

INTRODUCTION

Unit operations are the core of chemical engineering. Distillation, evaporation, absorption, extraction, crystallization, drying are of a basic importance. Howbeit, these operations often involve bed of particles, whose density and size distribution are sometimes difficult even to estimate. The lack of experimental data strongly hinders the validation of mathematical models developed with the aim of investigating the role of operating parameters in industrial processes. As a matter of fact, a number of plants of industrial size in the field of particle treatments are designed basing on data from pilot or bench scale apparatuses.

The electrodynamic balance appears to be an intriguing tool for analysis of momentum and mass transfer phenomena between gas and particles or drops in crucial conditions, since it is able to hold, by means of an electric field, a single submillimeter particle suspended in space in controlled atmosphere ([1], [2]). Some features make it a unique apparatus: i) it operates on a single particle, so problems arising from interactions between particles are inexistent; ii) as the boundary layer surrounding one particle can be clearly defined, heat and mass transfer phenomena are easy to approach; iii) very fast heating via a power laser, or quenching, are possible when working with a single particle due to the very high surface to volume ratio; iv) measurements of particle characteristics and their evolution during the run (mass, density, surface area, composition, etc.) are in principle at the hand; v) discrimination between homogeneous and heterogeneous phenomena is allowed for when considering that gaseous products quenched in a cold boundary layer are representative of what happens on the solid surface; vi) direct observation of what is going on makes optical diagnostics and other facilities easy to apply and to study. d'Amore et al. [3] used the tool to measure the apparent density of individual synthetic char particles known as "Spherocarb". Dudek et al. [4] performed oxidation rate measurements on single char particles at various temperatures. Davis and Ray [5] measured the evaporation rates of single droplets of dibutyl-sebacate. Cohen et al. [6] obtained pure crystallization letting single levitated droplets of a salty solution evaporate undisturbed.

Nevertheless, use of the balance requires some special care as the reference point for any measurement is the chamber center and, in turn, the particle can be kept stable, levitated in the center only by a continuous balancing of gravity, electrical and aerodynamic drag forces. If the forces are constant or slowly changing, manual adjustment of the electrical fields are enough for fairly good control. Fast changes require, of course, automatic devices. In the past [7], position control systems were based on conventional concepts and offered fast but, sometimes not quite accurate, controls. It must be outlined that fast movement of the particle may produce alteration of the boundary layer, which would cause misleading results if delicate measurements are made, as for instance, drying of droplets, drag, even combustion studies.

Whatever the technique used (either photo-multiplier or photo-diodes as detecting units, and proportional, integral, derivative or a combination of them as controller), knowledge of the physics of the phenomenon is

0-7803-5489-3/99/$10.00 ©1999 IEEE.

necessary. In fact, as the motion equations of a particle suspended in the balance are highly non linear, their handling in designing a conventional position control may be quite complicated. Fuzzy logic appears to offer a wise way to overcome this difficulty ([8], [9], [10]). Actually, the Fuzzy strategy does not require any knowledge of the mathematical models describing the process to be controlled. It is, in fact, based on a qualitative description of the phenomenon, refined step by step. Very often, control systems based on Fuzzy logic present a better stability than PID do, with an increased tolerance in the control variables range. Independence on mathematical models and flexibility make fuzzy control a subject of an increasing interest, with many applications in engineering from NASA space controls to cameras handling.

In this work, Fuzzy Logic is applied to design position control of a particle levitated in an electrodyamic balance, with the aim to increase the potential of the balance in the field of chemical engineering.

THE APPARATUS

The electrodynamic chamber consists of three electrodes in an hyperboloidal configuration. A schematic view of the balance is shown in Fig. 1.

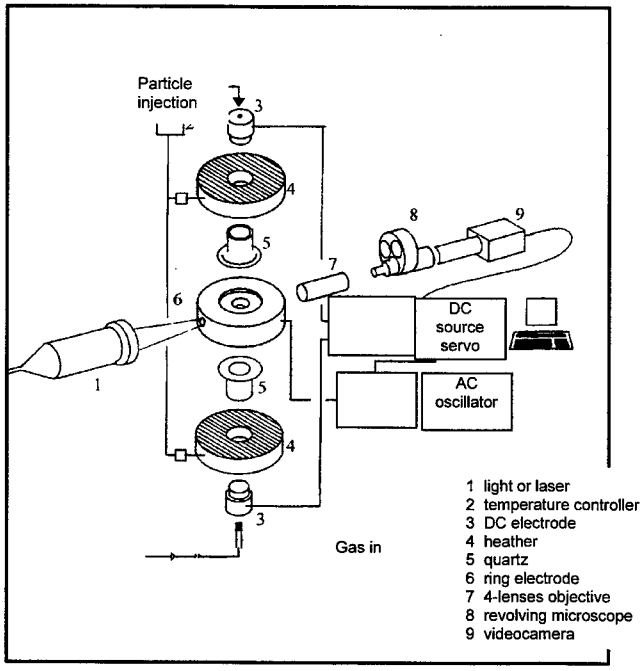


Fig. 1. Schematic of the electrodynamic balance.

The chamber creates a dynamic electric field capable of suspending a single, charged particle. The AC or ring electrode provides lateral stability to the particle through an imposed AC field V_{ac} oscillating sinusoidally ± 3000 volts at variable pulsation Ω. The DC top and bottom electrodes provide vertical stability balancing by means of a DC field V_{dc} the gravitational and drag forces, thus stable suspension of the charged particle at the chamber center. Changes in particle mass or charge are counterbalanced by proportional changes in the imposed V_{dc} to keep the particle centered. Solid particles are charged in the chamber simply injecting them by a syringe, electrical charges coming by tribo-electricity. Single droplets are generated via a piezoelectric crystal and charged by an induction copper ring kept at 400 volts (UNIPHOTON). A specially designed microscope, a video camera, and an image processing system purposely setup for the balance allow for sizing and position monitoring of the levitated particle. Due to the particle size, which is in the order of the tenth of microns, a large magnification is required (up to 2000X on the PC monitor). The particle must be back-lit to have enough light for observation by microscope. The algorithm developed for the image analysis takes this into account. A vertical strip of 512 pixels is considered. Starting from the top, position of the first black pixel is recorded. After having verified

that the pixel belongs to the particle by checking that the following ones are black too, analysis proceeds from the bottom in the same way until another black pixel is found and checked [11]. The particle diameter is evaluated as the difference between the two black pixels in the strip. Particle center comes as a consequence, while chamber center is a fixed point in the graphic plan. Information are then sent to a virtual controller based on either conventional or fuzzy logic, as discussed in details later.

Mass flow controllers and special electric heaters make possible to operate the balance in controlled atmosphere. An Ar-ion laser (Coherent, Innova 90, 4W nominal power) coupled to an optical and electronic group (Dantec, Flow Velocity Analyser) allows for the characterization of the gas flow field inside the chamber.

PARTICLE STABILITY

The balance works as follows. A local minimum in the energy field has to be generated to keep an electrically charged particle in stable equilibrium. In a real system, a saddle point can be generated at most. If the direction of the field lines is continuously and rapidly reversed, then the particle can be kept in proximity to the saddle point. A stability analysis will then give the conditions the system parameters will have to satisfy to let a particle stay levitated in the balance.

The theory is fully described by Wuerker et al. [1], Frickel et al. [2], Davis and Ray [5]. The electric field produced by V_{dc} is:

$$E_{dc} = \frac{V_{dc}}{z_0}\vec{k} \qquad 1.$$

where $\vec{k}$ is the unit vector of the vertical direction. The electric field generated by the ring electrode with a $V(t) = V_{ac}\cos(\omega t)$ applied is:

$$E_r = -V_{ac}\frac{r}{z_0^2}\cos(\omega t)\vec{r} \qquad 2.$$

$$E_\phi = 0 \qquad 3.$$

$$E_z = 2V_{ac}\frac{z}{z_0^2}\cos(\omega t)\vec{k} \qquad 4.$$

where z_0 is the distance of the endcap electrode from the geometrical center of the chamber and r , ϕ and z the polar coordinates.

The continuous field E_{dc} allows for balancing the gravity force ($qE_{dc}=mg$), whereas the E_{ac} field generates a saddle point in the chamber center. Intensity and sign of the related field lines vary with time according to a synusoidal law. Since the saddle point above is not a point of stable equilibrium, the forces acting on the particle, and consequently all the related parameters (i.e. V_{ac}, ω, V_{dc}, q, m) cannot arbitrarily vary without affecting the particle equilibrium if the only constraint were

$$V_{dc} = z_0\frac{mg}{q}. \qquad 5.$$

It is thus necessary to identify all the constraints the parameters above must respect to guarantee stable equilibrium conditions.

If the differential equations of the motion of a charged particle in the chamber are considered [5], then:

(1) a charged particle can be stably kept in the balance if the following conditions are satisfied:

$$0 < q_z = \frac{4V_{ac}q}{\omega^2 z_0 m} \le 0.908 \qquad 6.$$

$$z_0 > \frac{8\left(1+b^2\right)}{\omega^2 q_z^2}\left(g - \frac{qV_{dc}}{z_0 m}\right) \qquad 7.$$

(2) in a stability region a charged particle is always radially centered.

Relations above are actually more useful to our purposes if transformed as follows:

$$\nu > 16.55\sqrt{\frac{V_{ac}}{V_{dc}^{eq}}} \qquad 8.$$

$$\nu < \frac{1}{2\pi}\sqrt{4905\left(\frac{V_{ac}}{V_{dc}}\right)^2 - \frac{65.6}{\rho^2}\left(\frac{200}{D_{\mu m}}\right)^4} \qquad 9.$$

where

$$\nu = \frac{\omega}{2\pi} \qquad 10.$$

These latter give the range of the frequency values at which the particle is stably kept in the chamber center, as a function of either measurable or known variables. It has to be noted that, since the relations above are inequalities, the number of degrees of freedom of the system does not decrease.

Howbeit, solving for the stability equations allows for the particle levitation, but does not guarantee that the particle will occupy the center of the chamber. On the other hand, the chamber center is the only point of the field where the equilibrium of all the forces acting is satisfied and the balance equations can be solved. It is now evident the need for a particle position control system.

POSITIONING CONTROL

Aim of the control it is to determine the V_{dc} equilibrium value necessary to bring the particle in the stability position. The distance h of the particle from the center has been selected as the measured variable, while V_{dc} is the manipulated variable used to keep the particle in the center by counterbalancing, with the electrical force any change in the other forces possibly acting. Both the image analyzer and the AD/DA interface computer/equipment have been purposely chosen as they work in the same programming language. It has thus been possible to write a single algorithm for sizing and positioning of the particle, evaluating the stability parameters, and control the particle position. A virtual digital controller has been adopted via Pascal programming. In the following are described the two different kind of control realized for operating the balance: i. e. a classic PID, as a reference tool, and a Fuzzy-Logic based control.

PID control

A proportional integral derivative control (PID) in velocity form, which is particularly proper with unknown or variable set-points [12], has been designed for the system. Being the controller a non continuous one (sampling rate 30 s^{-1}), the system stability is a function of K, T/I, D/T, where T is the sampling time, and K, I D are the time constants of the proportional, integral and derivative controller, respectively. The last three particle positions are required for this controller.

By a force balance along the vertical axis, it is:

$$m^1\frac{d^2z^1}{dt^2} = -3\mu\pi D\frac{dz^1}{dt} - m^1 g + q\frac{V_{dc}}{z_0} + q\frac{2V_{ac}z^1\cos(\omega t)}{z_0^2} \qquad 11.$$

where z^1 and m^1 are the deviation variables for particles position and mass, respectively. Thus, for a given particle there will be a set of values of K, T/I, D/T which can control the position, by adjusting the V_{dc} to the equilibrium value. The control law is:

$$\Delta V_{dc}=K*((1+T/I+D/T)*(Ai)-(1+2*D/T)*(Bi)+(Ci)*D/T))*Diam \qquad 12.$$

where Ai, Bi, Ci are the last three positions and Diam is the particle diameter.

The system equations of the acting forces are at variable coefficients and thus difficult to handle. The values of the three parameters have therefore to be evaluated experimentally. However, the system is highly

non linear and the PID controller is thus not easily optimized. It will not be able to perfectly control the system in a constant way as the disturb varies.

Adoption of Fuzzy Control has been actually stimulated by the non linearity of the system and by the perspective of improving particle position control in the presence of changes in the force field.

The FUZZY controller

Designing a Fuzzy control requires 4 well-defined steps:

i) verbally modeling the system to be controlled
ii) identifying the control laws which relate DC variations to particle position
iii) formulating the fuzzy rules which constitute the control
iv) validating the fuzzy controller

We define an algorithm which exhaustively enumerates all rules consistent with the qualitative model, having defined a rule as a structure:

$$\text{"If } T_h \text{ is } \ldots \text{ then} \Delta V_{dc} \text{ is } \ldots \text{ "} \qquad 13.$$

where each T_h is a test on the observable parameter P_i and P_{i-1} (testing either $P_i>k$ or $P_i<k$ with $P_i-P_{i-1}>k^1$ or $P_i-P_{i-1}<k^1$, where k and k^1 are constant). Differently from above, the two last particle position (P_i and P_{i-1}) are enough for controlling the particle.

29 rules (T_i) are determined; the tests $P_i>k$ (0 is equilibrium position) and $P_i-P_{i-1}>k^1$ are identified by the adjective *greater than, much greater than, less than, much less than*. Basing on this approach and on trivial physical considerations, ΔV_{dc} is given for each of the above rules.

An example of the Turbo-Pascal algorithm is:

```
if Ai > (gy)
  then begin
      if (Bi-Ai) > (hy)
      then ΔVdc:=-my
      else if (Bi-Ai) >= 0
         then ΔVdc:=-ny
         else if ((Bi-Ai) < 0) and (Bi >= 0)
            then ΔVdc:=-ty
            else if Bi < 0
               then ΔVdc:=-ry
    end
  else ... ... ... ..
```

where *gy, hy* are distances while *my, ny, ty, ry*, are positive ΔV_{dc}.

The ΔV_{dc} values are then optimized according to experimental results.

RESULTS

The effectiveness of both the position control realized has been tested by inducing variations in the drag forces acting on levitated glass spheres < 200 micron. The flow rate of the gas entering the balance through the bottom electrode was varied via a computer-driven flow controller so as to have linear variations in the gas-to-particle slip velocity.

Figures 2(a) and 2(b) show the deviation from the center position as a function of time for a 110 μm glass sphere undergoing a variable drag force, and controlled by a PID and a Fuzzy system, respectively.

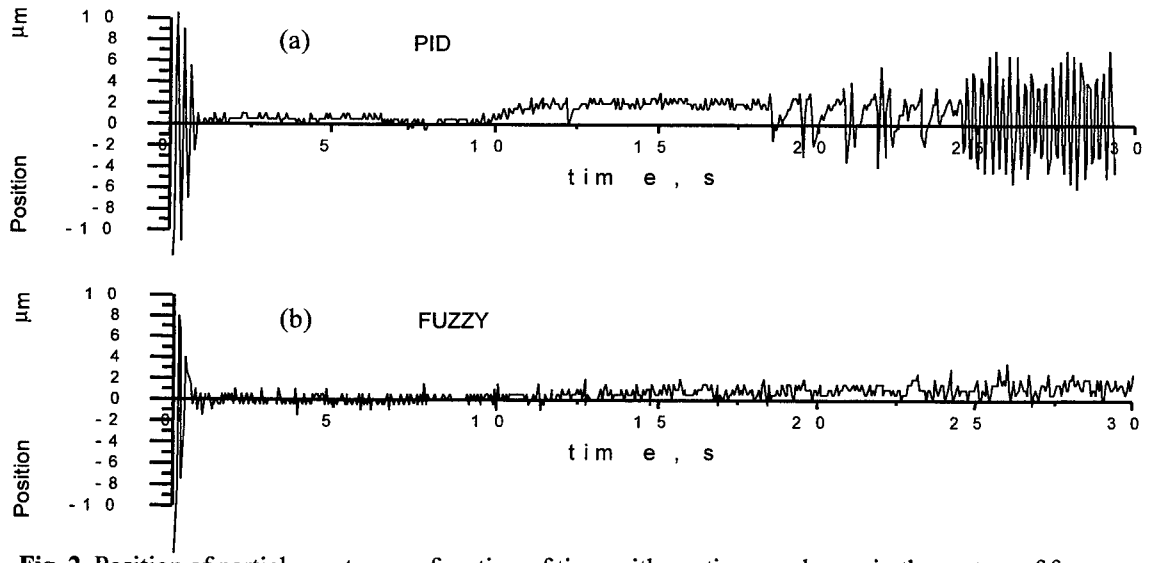


Fig. 2. Position of particle center as a function of time with continuous change in the system of forces. Particle diameter = 110 µm.

It can be seen that particle movement is limited to the order of ± 2 µm at most, i.e. 1% of the particle diameter, when fuzzy control is used. The PID controller, in spite of good control in the first ten seconds of the run, seems unable to keep the particle in the center as the drag force increases. The particle is kept some microns far from the chamber center, then begins to oscillate by ± 6 µm around the center. Note that in the absence of any position control, the particle is lost within the first second of applying the drag force.

From the comparison it appears that fuzzy control more rapidly restores particle equilibrium and better reacts to system instabilities. In Figures 3(a) and 3(b), the results obtained with the two controls on a glass sphere of 60 microns, are compared, with the drag force increased according to a power law, to balance the particle weight.

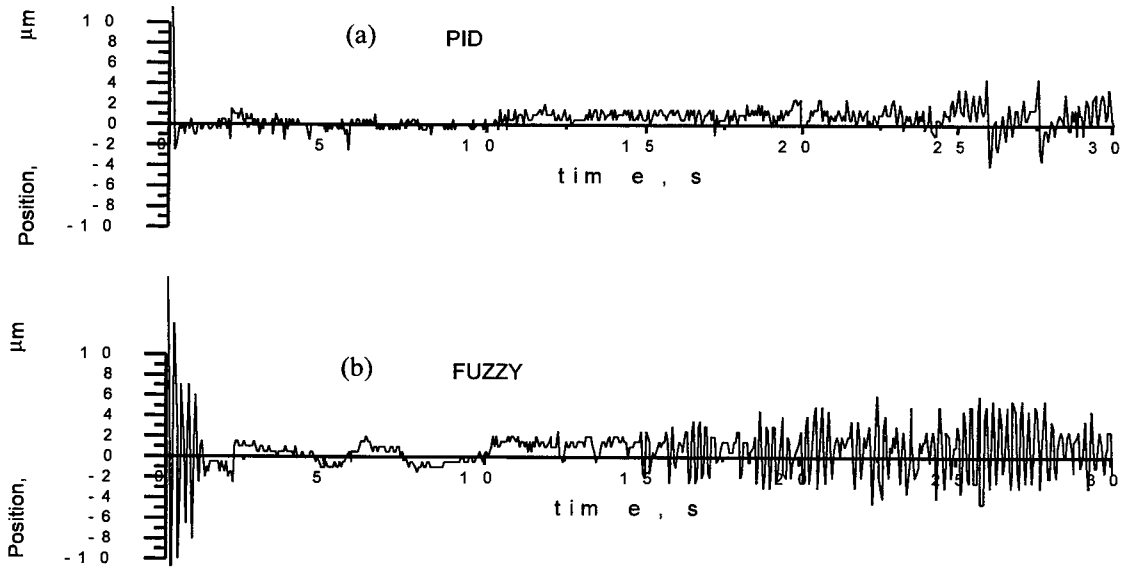


Fig. 3. Position of particle center as a function of time with a continuous change in the system of forces. Particle diameter = 60 µm.

The Fuzzy controller gives once again a better answer. In fact, it rapidly brings the particle back to the equilibrium position and compensates well for changes in the external forces without showing the oscillations evidenced by the PID controller in Fig. 3(a). Nevertheless, a certain difficulty appears when the imposed drag force is very high and the equilibrium is reached with increased difficulty.

It is noteworthy that Fuzzy Control shows better behavior even at the beginning of the run when the particle undergoes a sort of shock. Particle position deviations from the center in the case of PID control are significant. The amplitude and kind of deviations seem to be independent of particle size. For Fuzzy control, some minor deviations appear at high values of the imposed changes in the drag force. As an example of the efficacy of the control realized, Fig. 4 shows the evolution of the results of an evaporation test performed at room temperature on a milk droplet levitated in the balance using Fuzzy position control.

In the Figure the droplet diameter is reported as a function of time. Some interesting features are shown. The smoothness of the drying curve is a direct witness of the quality of the fuzzy control realized, as it means that the particle is quietly drying in the chamber center. Then, it is definitely intriguing a so well defined inflection point. The curve is actually of a great help in modeling the drying of milk .

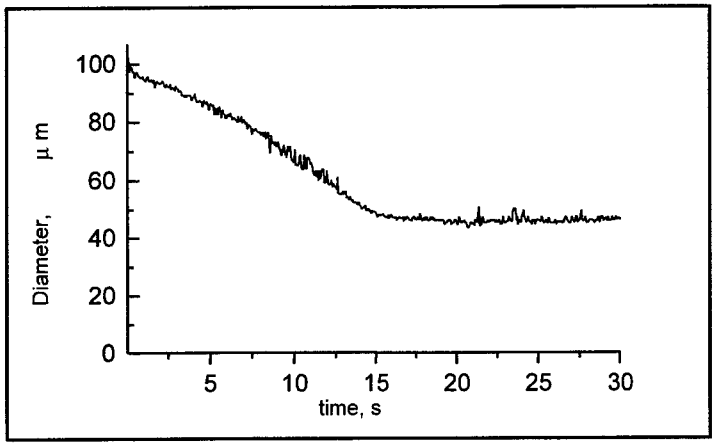


Fig. 4. Diameter of an evaporating milk droplet as a function of time

CONCLUSIONS

The Fuzzy Logic-based position control realized appears to offer remarkable advantages with respect to traditional systems, as it can be set up without knowing in the deepest the phenomenon to be controlled. Moreover, the control appears to be more rapid and accurate. The balance in this arrangement is suitable for fundamental studies on mass transfer on single solid or liquid particles, like for instance spray-drying, or on measurements of the aerodynamic drag forces acting on solid particles in both cold or hot gases.

REFERENCES

1. R.F. Wuerker, H. Shelton, R.V. Langmuir, 1959. Electrodynamic Containment of Charged Particles. .J. Appl. Phys.30,342
2. R.H. Frickel, R.E. Shaffer, J.B. Stamatoff, 1978. Techn Rep.. ARCEL-TR77041, U.S., Command, Aberdeen, Maryland.
3. M. d'Amore, R.D. Dudek, A.F. Sarofim, J.P. Longwell, 1988. Apparent Particle Density of a Fine Particle. Powder Technology, 129-134.
4. E. Bar-Ziv, D. Jones, R. Spjut, D. Dudek, A. Sarofim, J. Longwell, 1989. Combust. & Flame, 75-81.
5. E.J. Davis, A.K., Ray, 1980. Single aerosol particle size and mass measurements using an electrodynamic balance. J. Colloid Interface Sci., 566-576.
6. M.D. Cohen, R.C. Flagan, J.H. Seinfeld, 1987. Studies of Concentrated Electrolyte Solutions Using the Elecxtrodynamic Balance. 3. Solute Nucleation. J. Phys. Chem. 91, 4583-4590.
7. R.E. Spjut, E. Bar-Ziv, A.F. Sarofim, J.P. Longwell, 1986. Electrodynamic Thermogravimetric Analyzer. Rev. Sci. Instrum. 57, 1604
8. L. A. Zadeh, 1965. Fuzzy sets. Information and Control, 8, 338-353.
9. L. A. Zadeh, 1992. The calculus of fuzzy if-then rules. AI Expert., March
10. B. Kosko,1992. Neural Network and Fuzzy Systems. Prentice Hall Inter. Ed., Englewood Cliffs N.J..
11. M. d'Amore, P. Giordano, P. Russo, 1998. Mass transfer measurements from single levitated droplets in electrodynamic balance, Proc of SIMAI IV, Catania, Italy, June 1998, II, 308-315
12. G., Stephanopoulos ,1984. Chemical process control. Prentice Hall International.

AUTHOR'S INDEX

M.F. Abbod 215
S.M. Adballah 1017
S. Ahn 1047
J.M. Abe 695
A. Akhtar 417
J. Ahola 531
N. Aikawa 607
J.D. Allen, Jr. 961, 989
K. Ameyama 1041
W. Andreoni 1397
A. Arioti 629
J.F. Atkinson 347

G. Baiden 53
T.J. Bailey 921
J. Balcita 499
P. Barr 111
R. Barton 269
O.A. Bascur 829
D. Bassi 975
M. Benedict 1185
R.R. Biggers 1258, 1317
Y. Bissiri 635
H. Bode 339
G. Bonifazi 465, 485
B.M. Brasfield 347
J.C. Bressiani 797
R.T. Bui 749
J.D. Busbee 1258, 1317

T.L. Calton 347
J.J. Campbell 939
N. Cappetti 185
M.J. Cardew-Hall 1017
L.-E. Carlsson 459
J.C. Cassa 291, 381
O. Castillo 151, 855
A.C.D. Chaklader 797
T. Chandra 105
T. Chashikawa 453
C.C. Chang 789
J.Y. Chen 901
L.S. Chen 805
M.Y. Chen 395
N. Chen 1381
N. Chen 1419
R. Chen 1419
Y.-M. Chen 1061
D. Cheung 1079
C.-C. Chiang 1131
D.J. Choo 947
C.Y. Chung 1023
S. Cierpisz 933
D.J. Clancy 871
E.J. Colville 649
J.A. Cooper 191
C.S. Cornelius 325
L. Cser 531
C. Curtis 317

J. Daams 1339
M. d'Amore 703
D. Dasgupta 257
W.J. Davis 615
L.R.P. De Andrade Lima 505
D.V. Dempsey 1258, 1317
S. Dessureault 145
R.J. Dippenaar 75
S. Dolinšek 847
A. Donnarumma 185, 663
R. Doraiswami 735
B.F. Duan 1361
M. Duarte 975
K. Dudek 543
S. Dunbar 145, 635
M.N. Durakbasa 927

S.A. Ehikioya 139
H. Eldeib 447
J. Endou 817
J.R. Esslinger 331
R.N. Evans 331

M. Fabiunke 655
C. Fantozzi 629
N. Farmer 879
P. Farrington 157
M. Fathi-Torbaghan 1011

F. Ferguson 317
R. Felix 299
M. Ferry 105
G. Floridia 291, 381
G.A. Fodor 895
S. Forouzi 967
S. Forrest 257
J.M. Fragomeni 577, 585
W.G. Frazier 1139
K. Fujii 453
S. Fuks 1123
M. Furukawa 1115
Y. Furukawa 21
Y. Fukuhara 743

M. Geiger 641
L.M Geng 91
R. Gerth 1151
D.T. Gethin 513, 1035
M.M. Ghomshei 519
H. Ghulman 1151
D.A. Gibson 325
P. Giordano 703
Z. Gomolka 813
G.D. González 59
M. Granchi 629
J.L. Grantner 895
R.W. Grimes 1197
W.A. Gruver 839
A. Grzech 823
C. Guist 339
S.R. Gunn 361
M.J. Guo 779
Y.M. Guo 861
M. Gupta 119

A. Hambaba 1073
S. Hanada 429
R.D. Harrell 157, 347
J. Hart 879
Y. Hasegawa 695
J. Hätönen 459
H. Helman 537, 549, 561
L. Hildebrand 1011
T. Hirasawa 221
T. Hirasawa 245
S. Hirose 233
B. Hlavácek 403
C.T.T. Ho 1061
P.D. Hodgson 389, 953
D.A. Holder 157
D.A. Holder 347
R.-Q. Hsu 1029
C.-C. Hu 1131
H.M. Huang 285
I.B. Huang 423
W. Huang 1277
P. Hubík 437
G. Huh 947
Y.S. Hwang 879
H. Hyötyniemi 11, 179, 459

B. Igelnik 367
K. Ishida 373
K. Ishino 1093
N. Ivezic 961, 989
S. Iwata 1323, 1399

A.G. Jackson 1185
J. Jang 947
H-G. Jeong 429
P.D. Jero 1241
L Jin 805
J.G. Jones 1241, 1258, 1317
H.K. Jung 593
K.D. Jung 593

B. Kádár 131
R. Kainuma 373
K. Kamitani 565
J.S. Kandola 361
C.G. Kang 593
S. Kang 1047
A. Karcher 623
A. Katayama 607
M. Kato 373
K.Katoh 571
Y. Kawazoe ..355
A.R. Khoei 513, 1035
H.S. Kim 429
J. Kim 1263
N.N. Kiselyova 1387

M. Kitabata 995
Gerd Kock 655
T. Kohonen 27
N. Koga 403
L.X. Kong 389, 953
J. Kopac 847
A.S. Korhonen 531
H. Kotera 221, 245, 565
H.Koyama 571
G. Kozlowski 1258, 1317
J. Krištofik 437
C. Kropas-Hughes 1305
C.C. Kung 681
J.A. Kurien 871
A. Kusiak 887
J. Kusiak 543, 773
D-W. Kum 429
T. Kurita 239
K. Kyuma 1297

W.C. Lai 681
K.C. Lau 1023
S.R. LeClair 367, 1235, 1263, 1361, 1399
E.S. Lee 1047
J.Y.Lee 947
P.D. Lee 1197
R.S. Lee 1061
Y.J. Lee 1285
Y.K. Lee 947
J.G. Lenard 543
J. Leopold 227
P.L. Leung 285
R.W. Lewis 1035
J.Y. Li 765
K.P Li 91
Y.P. Li 867
G. Lin 687, 1003
L. Lin 953
S.-C. Lin 669
Y. Liu 939
D.A. Linkens 215, 395, 755, 921
H.R. Liu 765
R.S. Liu 765
W. Lu 1419
Y. Luo 867

P. Ma 867
S. Mackinson 491
J.F. Maguire 1235
J.T. Malin 1179
K. Manabe 571, 601, 607
P.A. Manohar 105
A. Mansour 1103
P.Mäntylä 531
J.J.Mareš 437
P. Massacci 485
I. Masters 513
E. Medina 1157
J.A. Meech 111, 309, 499, 519, 975
K.J. Meech 445
G. Meghabghab 729
B. Mehta 1151
P. Melin 151, 855
T. Menzel 641
S. Messimer 157
J. Metcalfe 215
J. Miettunen 459
L. Miller-Tait 983
L. Monostori 131, 847
C. Mui 111
H. Munekata 233

Y. Nagasaka 85
S. Nagatomo 565
K. Nakamatsu 695
K. Nakanishi 861
G. Nasr 729
G.M. Nicoletti 713, 1087
A.J. Niemi 11
H. Nishimura 601
D.H. Norrie 887
B. Novak 201
B. Nichols 215

H. Ohtani 373
S. Oka 1277
R.T. Oliveira 291, 381
N. Ono 373
T. Ono 239
C. Orlowski 195
P.H. Osanna 927
M. Oxley 1371

E.P. Paladini 165
R. Pakalnis 983
Y.-H. Pao 367, 1361
M. Pappalardo 185, 663, 703
Z. Pawlak 37
G.H. Park 1285
G.R. Park 1263
J. H. Park 1285
S.H. Park 947
P.E. Parker 895
C.D.M. Pataro 549
A. Pellegrino 703
J. Perron 749
M. Pietrzyk 773
J. Poindexter 1163

P. Qin 1419
M.V. Quintella-Cury 1123

C. Reidsema 1055
S. Reimann 1103
S. Rajan 735
P.A.S. Reed 361
D.A. Ress 1225
D. Rochoviak 157
J. Rogers 157
B.F. Rolfe 1017
J.A. Romagnoli 947
D. Roy 281
P. Russo 703
D. Russell 157

Y. Sahai 119
T. Saito 723
Y. Saito 555
Y. Sakamoto 221, 245
G. Samadi Hosseinali 417
I.V. Samarasekera 73
S. Sändig 251
E. Santoro 185
M. Sato-Ilic 207
M. Scoble 145
H.-J. Sebastian ..163
S. Serranti 465
J. Šesták 403, 431, 437
V.Šestáková 437
B. Shi 687, 1003
Y. Shigaki 561
S. Shima 221, 245, 563
F. Shimaya 555
M. Shinkawa 555
S.S. Shivathaya 105
G.R. Shumaker 1163
O. Simula 531
I. Sinclair 361
A.K. Sirén 477
M.H. Smith 839
G.W. Snyder 331
S.J. Spencer 939
B. Štepánek 437
O. Stephansson 471
M. Stevenson 735
A.R. Souza 291, 381
Z. Strnad 431
B.A. Stucke 1163
A. Suárez 975
Y. Suehiro 1041
S. Sugiyama 909
A. Suzuki 695
H. Szczerbicka 269
3 E. Szczerbicki 813, 1055

M. Tabib-Azar 367, 1249
Y. Takefuji 453, 723, 743, 995, 1109, 1271, 1277
A. Talaie 947
J. Tenner 921
L. Tikasz 749
K.M. Tiwari 281
S.K. Tiwari 281
A. Torres 309
V. Torres 309
T.T. Tran 139
D. Tromans 411
E.G. Truelove 139
U.-B. Tsai 1029
H.-L. Tsoi 1079
I.B. Turksen 173

O. Unold 277
T. Ushio 299
H. Utsunomiya 555

T. Van Le 675
M.M. Veiga 797
S.M.B.Veiga 797
E. Vettori 629
N.K. Vidyarthi 281
Z.J. Viharos 847
P. Villars 1339
P. Villars 1399
R.C. Villas Bôas 481, 505
F. Volpe 465

R.H. Wagoner 91
B. Wang 953
D. Wang 805
W.X. Wang 471
Z. Wang 1067
M. Watanabe 1115
K.R. Weller 939
G.A.W. West 1017
P. Wiesner 251
M. Willams 785
J. Wirtz 623
C.-W. Wu 1029

L Xie 1067
Y. Xu 805

T. Yamamoto 221
M. Yamaura 233
M. Yang 607
Y.Y. Yang 755
S.K. Yen 423, 779, 789
R. Ylinen 11
A. Yoshida 221
S. Yoshihara 571, 601
N. Yoshiike 1109
G.T. Yu 785
W.S. Yu 1125

M.O. Zacate 1197
L.A. Zadeh 3
T. Zacharia 961, 989
H.Z. Zan 779
L.E. Zárate 537
B.L.Zhang 867
T. Zhang 839
X. Zhang 887
Y.L. Zhao 1361
B.S. Zhu 867
D.D. Zhu 1381
H.J. Zimmermann 45
R. Zuco 465